Advanced Structured Materials

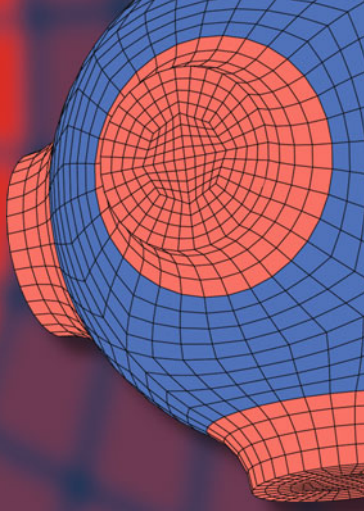

Holm Altenbach
Jacek Chróścielewski
Victor A. Eremeyev
Krzysztof Wiśniewski *Editors*

Recent Developments in the Theory of Shells

Springer

Advanced Structured Materials

Volume 110

Common engineering materials reach in many applications their limits and new developments are required to fulfil increasing demands on engineering materials. The performance of materials can be increased by combining different materials to achieve better properties than a single constituent or by shaping the material or constituents in a specific structure. The interaction between material and structure may arise on different length scales, such as micro-, meso- or macroscale, and offers possible applications in quite diverse fields.

This book series addresses the fundamental relationship between materials and their structure on the overall properties (e.g. mechanical, thermal, chemical or magnetic etc) and applications.

The topics of *Advanced Structured Materials* include but are not limited to

- classical fibre-reinforced composites (e.g. glass, carbon or Aramid reinforced plastics)
- metal matrix composites (MMCs)
- micro porous composites
- micro channel materials
- multilayered materials
- cellular materials (e.g., metallic or polymer foams, sponges, hollow sphere structures)
- porous materials
- truss structures
- nanocomposite materials
- biomaterials
- nanoporous metals
- concrete
- coated materials
- smart materials

Advanced Structured Materials is indexed in Google Scholar and Scopus.

More information about this series at http://www.springer.com/series/8611

Holm Altenbach · Jacek Chróścielewski ·
Victor A. Eremeyev · Krzysztof Wiśniewski
Editors

Recent Developments in the Theory of Shells

Springer

Editors
Holm Altenbach
Faculty of Mechanical Engineering
Otto-von-Guericke-Universität Magdeburg
Magdeburg, Germany

Victor A. Eremeyev
Faculty of Civil and Environmental Engineering
Gdańsk University of Technology
Gdańsk, Poland

Jacek Chróścielewski
Faculty of Civil and Environmental Engineering
Gdańsk University of Technology
Gdańsk, Poland

Krzysztof Wiśniewski
Institute of Fundamental Technological Research
Polish Academy of Sciences
Warsaw, Poland

ISSN 1869-8433 ISSN 1869-8441 (electronic)
Advanced Structured Materials
ISBN 978-3-030-17746-1 ISBN 978-3-030-17747-8 (eBook)
https://doi.org/10.1007/978-3-030-17747-8

This Springer imprint is published by the registered company Springer Nature Switzerland AG
The registered company address is: Gewerbestrasse 11, 6330 Cham, Switzerland

This book is dedicated to a truly outstanding scientist and person, our dear friend and teacher Prof. Wojciech Pietraszkiewicz on the occasion of his 80th birthday.

Preface

Professor Wojciech Pietraszkiewicz is one of the leading Polish scientists in the theory of shells (thin-walled structures) and in continuum mechanics. His scientific contribution covers several areas, such as:

- Statics and dynamics of classical and non-classical theory of shells, including six-parameter theory of shells;
- Mechanics of classical and Cosserat continua;
- Finite rotations in mechanics of solids and structures;
- Non-linear mechanics and FE analysis of multi-fold shell structures;
- Intrinsic non-linear theory of thin shells;
- Non-linear phase transitions in shells;
- Refined thermomechanics of shells;
- Differential geometry of surface in 3D space.

This volume of the Advanced Structured Materials Series is dedicated to Prof. W. Pietraszkiewicz on the occasion of his 80th birthday, and it contains papers on beams, plates and shells prepared by his friends and colleagues from Austria, Belarus, France, Germany, India, Italy, Mexico, Poland, Russia, Slovenia, UK, Ukraine and USA.

Prof. W. Pietraszkiewicz was born on January 23rd 1939 in Wilno (then in Poland; currently Vilnius, the capital of Lithuania). He received a MSc degree in 1961 and a PhD degree in 1966 from the Department of Civil Engineering of the Gdańsk University of Technology. The same department honored him with a DSc degree (habilitation) in 1977. He became the Extraordinary Professor in 1983 and received the title of Full Professor from the President of Poland in 1990.

In the period 1961–1966 he worked in the Gdańsk University of Technology. Next he moved to the Institute of Fluid-Flow Machinery of the Polish Academy of Sciences in Gdańsk, where in the years 1966–2009 he held the positions of a Head of Division, a Deputy Director, a Director, and a Head of the Department of Mechanics of Structures and Materials. He retired in 2010, and, since 2016, he is a Full Professor at the Gdańsk University of Technology.

Wojciech Pietraszkiewicz

From the beginning of his scientific carrier Prof. W. Pietraszkiewicz was internationally active. He was a visiting professor in 1971–1972 at the University of Illinois Urbana-Champaign (USA) on the Fulbright Scholarship. In the years 1976–

Wojciech Pietraszkiewicz with Leonid Zubov and Victor Berdichevski, during IUTAM symposium, Tbilisi, (1978)

1997, he had several appointments as a visiting professor at the Ruhr-Universität Bochum (Germany), where he spent in total over 5 years. In 2001 he was a visiting professor at RWTH Aachen (Germany). In 2000–2007, he visited several times the Université de Poitiers (France). During his carrier, he lectured in over 30 scientific institutions in Germany, USA, Netherlands, Switzerland, Italy, Belgium, France, UK, Hungary, Czech Republic, Brazil, China, Russia and Ukraine.

Prof. W. Pietraszkiewicz organized several international conferences: *Shell Structures: Theory and Applications (SSTA)* (many times since 1986), Euromech Colloquium 197 *Finite Rotations in Structural Mechanics* (Jabłonna, 1985), and 3rd Meeting *Scientific Foundations of Mechanics of Materials, Machinery, Structures and Technological Processes* (Gdańsk, 1984). Especially famous is the large international SSTA conference; Prof. Pietraszkiewicz chaired the International

With Philippe Ciarlet (on the left) and Satya Atluri (on the right), ICCES'11, Nanjing (2011)

Advisory Board of its seven editions: Szklarska Poręba (1986), Jurata (1998, 2002, 2005, 2009) and Gdańsk (2013, 2017). Four volumes of post-conference papers were published by Balkema as a follow-up of the last four editions of the SSTA conference. In the years 2006–2016, he co-chaired the session on shells and plates within the Solid Mechanics (SOLMECH) conference, which is organized biennially by the Institute of Fundamental Technological Research of the Polish Academy of Sciences (IPPT PAN).

Ireneusz Kreja, Jacek Chróścielewski, J.N. Reddy, Wojciech Pietraszkiewicz, and Victor Eremeyev, at the SSTA conference, Jurata, (2009)

He co-edited special issues of several international journals, such as: *Archives of Civil Engineering* (1999, 2003), *Journal of Theoretical and Applied Mechanics* (2003), *ZAMM* (2014) and *Mathematics and Mechanics of Solids* (2015).

Prof. Pietraszkiewicz received several awards for outstanding research achievements from the Polish Academy of Sciences (1975, 1979, 1982) and an award of the Polish Ministry of National Education (2002). Since 2005 he is the Honorary Member of the Polish Society of Theoretical and Applied Mechanics. In 2011 he obtained *The Wei-Zhang Chien Award* at the ICCES'11 in Nanjing, China, for his "*fundamental contributions in the intrinsic theory of shells*".

Prof. W. Pietraszkiewicz published 5 monographs, 4 textbooks and lecture notes, 178 original refereed papers in journals and books, presented 174 lectures at scientific meetings (most published in Proceedings), edited 17 volumes of collected papers, and supervised 11 PhD dissertations. It is also worth to mention, that he served as a section editor and wrote several entries for the section *Shells* in *Encyclopedia of Continuum Mechanics* (Springer, Berlin, Heidelberg, 2019).

The 80th birthday of Prof. W. Pietraszkiewicz is a good occasion to thank Him not only for his excellent and well known papers on shells but also for his friendly and supportive attitude, which helped many of us to stay in science and work on shells. On behalf of ourselves and all the contributors to this volume,

Best wishes Prof. Pietraszkiewicz on the occasion of your 80th birthday !

Selected publications of Prof. Wojciech Pietraszkiewicz

(A list of publications with full texts are available at http://www.imp.gda.pl/en/wpietraszkiewicz/.)

Books

1. Pietraszkiewicz, W.: Elastic Materials (in Polish). Bulletin No. 652, Institute of Fluid-Flow Machinery of PASci., Gdańsk (1969)
2. Pietraszkiewicz, W.: Introduction to the Non-Linear Theory of Shells. Mitt. Inst. f. Mech., Nr. 10 Ruhr-Universität Bochum, Bochum (1977)
3. Pietraszkiewicz, W.: Finite Rotations and Lagrangean Description in the Non-linear Theory of Shells. Polish Scientific Publishers, Warszawa—Poznań (1979)
4. Pietraszkiewicz, W.: Finite rotations in the non-linear theory of thin shells. In: Olszak, W. (ed.) Thin Shell Theory, New Trends and Applications, CISM Courses and Lectures, vol 240, Springer, Wien, pp 153–208 (1980)

5. Pietraszkiewicz, W.: Geometrically non-linear theories of thin elastic shells (published also in Mitt. Inst. f. Mech. Nr 55, Ruhr-Universität Bochum, Bochum, 1988). Adv. Mech. **12**(1):51–130 (1989)
6. Pietraszkiewicz, W.: Non-linear theories of shells (in Polish). In: Woźniak, Cz. (ed.) Mechanics of Elastic Plates and Shells, pp. 424–497. Polish Scientific Publishers, Warszawa (2001)
7. Makowski, J., Pietraszkiewicz, W.: Thermomechanics of Shells with Singular Curves. Zeszyty Naukowe, vol 528/1487. IMP PAN, Gdańsk (2002)
8. Chróścielewski, J., Makowski, J., Pietraszkiewicz, W.: Statics and Dynamics of Multyfolded Shells. Nonlinear Theory and Finite Elelement Method (in Polish). Wydawnictwo IPPT PAN, Warszawa (2004)

Edited Books

1. Pietraszkiewicz, W. (ed.): Finite Rotations in Structural Mechanics, Proc. Euromech Colloquium 197, Jabłonna (Poland), 1985, Lecture Notes in Engineering, vol 19. Springer, Berlin (1986)
2. Pietraszkiewicz, W., Szymczak, C. (eds.): Shell Structures: Theory and Applications — Proceedings of the 8th SSTA Conference. CRC Press, Boca Raton (2005)
3. Pietraszkiewicz, W., Kreja, I. (eds.): Shell Structures: Theory and Applications — Proceedings of the 9th SSTA Conference, vol 2. CRC Press, Boca Raton (2010)
4. Pietraszkiewicz, W., Górski, J.: (eds) Shell Structures: Theory and Applications —Proceedings of the 10th SSTA 2013 Conference, vol 3. CRC Press, Boca Raton (2014)
5. Pietraszkiewicz, W., Witkowski, W. (eds.): Shell Structures: Theory and Applications — Proceedings of the 11th SSTA 2017 Conference, vol 4. CRC Press, Boca Raton (2018)

Selected Papers

1. Bielewicz, Eu., Pietraszkiewicz, W.: Design of cylindrical shell roofs. Confrontation of folded plate methods and Schorer's approximation (in Polish). Arch. Inż. Ląd. **9**(1):89–105
2. Bouby, C., Fortuné, D., Pietraszkiewicz, W., Vallée, C.: Direct determination of the rotation in the polar decomposition of the deformation gradient by maximizing a Rayleigh quotient. ZAMM **85**(3):155–162 (2005)

3. Chróścielewski, J., Makowski, J., Pietraszkiewicz, W.: Non-linear dynamics of flexible shell structures. Comput. Assist. Mech. Eng. Sci. **9**(3):341–357 (2002)
4. Chróścielewski, J., Pietraszkiewicz, W., Witkowski, W.: On shear correction factors in the non-linear theory of elastic shells. Int. J. Solids Struct. **47**(25–26):3537–3545 (2010)
5. Chróścielewski, J., Konopinska, V., Pietraszkiewicz, W.: On modelling and non-linear elasto-plastic analysis of thin shells with deformable junctions. ZAMM **91**(6):477–484 (2011)
6. Eremeyev, V.A., Pietraszkiewicz, W.: The nonlinear theory of elastic shells with phase transitions. J. Elast. **74**(1):67–86 (2004)
7. Eremeyev, V.A., Pietraszkiewicz, W.: Local symmetry group in the general theory of elastic shells. J. Elast. **85**(2):125–152 (2006)
8. Eremeyev, V.A., Pietraszkiewicz, W.: Phase transitions in thermoelastic and thermoviscoelastic shells. Arch. Mech. **61**(1):41–67 (2009)
9. Eremeyev, V.A., Pietraszkiewicz, W.: Thermomechanics of shells undergoing phase transition. J. Mech. Phys. Solids **59**(7):1395–1412 (2011)
10. Eremeyev, V.A., Pietraszkiewicz, W.: Material symmetry group of the non-linear polarelastic continuum. Int. J. Solids Struct. **49**(14):1993–2005 (2012)
11. Eremeyev, V.A., Pietraszkiewicz, W.: Editorial: Refined theories of plates and shells. ZAMM **94**(1–2):5–6 (2014)
12. Eremeyev, V.A., Pietraszkiewicz, W.: (2016) Material symmetry group and constitutive equations of micropolar anisotropic elastic solids. Math. Mech. Solids **21**(2):210–221
13. Górski, J., Pietraszkiewicz, W.: The 10th jubillee conference "Shell Structures: Theory and Applications", SSTA2013, Oct. 16-18, 2013, Gdansk (Poland). Arch. Civ. Eng. **59**(4):579–581 (2013)
14. Konopinska, V., Pietraszkiewicz, W.: Exact resultant equilibrium conditions in the nonlinear theory of branching and self-intersecting shells. Int. J. Solids Struct. **44**(1):352–369 (2007)
15. Makowski, J., Pietraszkiewicz, W.: Incremental formulation of the non-linear theory of thin shells in the total Lagrangian description. ZAMM **64**(4):T65–T67 (1984)
16. Makowski, J., Pietraszkiewicz, W.: Work-conjugate boundary conditions in the nonlinear theory of thin shells. J. Appl. Mech. Trans. ASME **56**(2):395–402 (1989)
17. Makowski, J., Pietraszkiewicz, W., Stumpf, H.: On the general form of jump conditions for thin irregular shells. Arch. Mech. **50**(3):483–495 (1998)
18. Makowski, J., Pietraszkiewicz, W., Stumpf, H.: Jump conditions in the non-linear theory of thin irregular shells. J. Elast. **54**(1):1–26 (1999)
19. Opoka, S., Pietraszkiewicz, W.: Intrinsic equations for non-linear deformation and stability of thin elastic shells. Int. J. Solids Struct. **41**(11–12):3275–3292 (2004)
20. Opoka, S., Pietraszkiewicz, W.: On modified displacement version of the non-linear theory of thin shells. Int. J. Solids Struct. **46**(17):3103–3110 (2009)

21. Opoka, S., Pietraszkiewicz, W.: On refined analysis of bifurcation buckling for the axially compressed circular cylinder. Int. J. Solids Struct. **46**(17):3111–3123 (2009)
22. Pietraszkiewicz, W.: The case of axial symmetry of shallow shells (in Polish). Rozpr. Inż. **14**(2):241–262 (1966)
23. Pietraszkiewicz, W.: On a solving equation for shallow shells. Bull. Acad. Polon. Sci., Serie. sci. techn. **15**(5):265–270 (1967)
24. Pietraszkiewicz, W.: On the linear theory of shallow shells (in Polish). Rozpr. Inż. **15**(2):349–358 (1967)
25. Pietraszkiewicz, W.: On the multivaluedness of solutions of shallow shells. Bull. Acad. Polon. Sci., Serie. sci. techn. **15**(10):877–881 (1967)
26. Pietraszkiewicz, W.: On the multivaluedness of stress functions in the linear theory of shells. Bull. Acad. Polon. Sci., Serie. sci. techn. **15**(10):871–876 (1967)
27. Pietraszkiewicz, W.: Multivalued stress functions in the linear theory of shells. Arch. Mech. Stos. **20**(1):37–45 (1968)
28. Pietraszkiewicz, W.: Multivalued solutions for shallow shells. Arch. Mech. Stos. **20**(1):3–10 (1968)
29. Pietraszkiewicz, W.: Stresses in an isotropic elastic solid after successive superposition of two small deformations (in Polish). Trans. Inst. Fluid-Flow Mach. **52**:129–141 (1971)
30. Pietraszkiewicz, W.: Material equations of motion for nonlinear theory of shells. Bull. Acad. Polon. Sci., Serie. sci. techn. **19**(6):261–266 (1971)
31. Pietraszkiewicz, W.: On the elasticity tensors of deformed isotropic solids. Bull. Acad. Polon. Sci., Serie. sci. techn. **19**(9):641–646 (1971)
32. Pietraszkiewicz, W.: On the Lagrangean non-linear theory of moving shells. Trans. Ins. Fluid-Flow Mach. **64**:91–103 (1974)
33. Pietraszkiewicz, W.: Lagrangian non-linear theory of shells. Arch. Mech.—Arch. Mech. Stos. **26**(2):221–228 (1974)
34. Pietraszkiewicz, W.: Stress in isotropic elastic solid under superposed deformations. Arch. Mech.—Arch. Mech. Stos. **26**(5):871–884 (1974)
35. Pietraszkiewicz, W.: Some exact reduction of the non-linear shell compatibility conditions. ZAMM **57**(5):T133–T134 (1977)
36. Pietraszkiewicz, W.: Simplified equations for the geometrically non-linear thin elastic shells. Pol. Akad. Nauk. Pr. Inst. Masz. Przeplyw. **75**:165–173 (1978)
37. Pietraszkiewicz, W.: Some relations of the non-linear theory of Reissner type shells (in Russian), Vestnik Leningradskogo Un-ta, Seriia Mat., Mech. Astr. **1**:115–124 (1979)
38. Pietraszkiewicz, W.: Consistent second approximation to the elastic strain energy of a shell. ZAMM **59**(5):T206–T208 (1979)
39. Pietraszkiewicz, W.: Finite rotations in shells. In: Koiter, W.T., Mikhailov, G. K. (eds.) Theory of Shells, pp. 445–471. North-Holland P.Co., Amsterdam (1980)
40. Pietraszkiewicz, W.: Certain problems of nonlinear shell theory (in Polish). Mech. Theoret. Stos. **18**(2):169–192 (1980)

41. Pietraszkiewicz, W.: Three forms of geometrically non-linear bending shell equations. Works Inst. Fluid-Flow Mach. **81**:79–92 (1981)
42. Pietraszkiewicz, W.: On consistent approximations in the geometrically non-linear theory of shells. Ruhr-Universität Bochum., Mitt. Inst. f. Mech. Nr. **26**:1–43 (1981)
43. Pietraszkiewicz, W.: Determination of displacements from given strains in the non-linear continuum mechanics. ZAMM **62**(3–4):T154–T156 (1982)
44. Pietraszkiewicz, W.: A simplest consistent version of the geometrically non-linear theory of shells undergoing large/small rotations. ZAMM **63**(5): T200–T202 (1983)
45. Pietraszkiewicz, W.: Lagrangian description and incremental formulation in the nonlinear theory of thin shells. Int. J. Nonlin. Mech. **19**(2):115–140 (1984)
46. Pietraszkiewicz, W.: Addendum to: Bibliography of monographs and surveys on shells. Appl. Mech. Rev. **45**(6):249–250 (1992)
47. Pietraszkiewicz, W.: Unified Lagrangian displacement formulation of the non-linear theory of thin shells. R. BCM—J. Braz. Soc. Mech. Sci. **14**(4): 327–345 (1992)
48. Pietraszkiewicz, W.: Explicit Lagrangian incremental and buckling equations for the non-linear theory of thin shells. Int. J. Nonlin. Mech. **28**(2):209–220 (1993)
49. Pietraszkiewicz, W.: Work-conjugate boundary conditions associated with the total rotation angle of the shell boundary. J. Appl. Mech., Transact. ASME **60** (3):785–786 (1993)
50. Pietraszkiewicz, W.: On the vector of change of boundary curvature in the non-linear T-R type theory of shells. Trans. St-Petersburg Acad. Sci. Strength Prob. **1**:140–148 (1997)
51. Pietraszkiewicz, W.: On deformational boundary quantities in the nonlinear theory of shear-deformable shells. ZAMM **77**(S1):S265–S266 (1997)
52. Pietraszkiewicz, W.: Deformational boundary quantities in the nonlinear theory of shells with transverse shears. International J. Solids Struct. **35**(7–8):687–699 (1998)
53. Pietraszkiewicz, W.: Bernoulli numbers and rotational kinematics. J. Appl. Mech., Transact. ASME **66**(2):576 (1999)
54. Pietraszkiewicz, W.: On the Alumäe type non-linear theory of thin irregular shells. Izvestiya VUZov, Severo-Kavkazskii Region, Yestestvennye Nauki, Spetzvypusk, 127–136 (2000)
55. Pietraszkiewicz, W.: Development of intrinsic formulation of W.-Z. Chien of the geometrically nonlinear theory of thin elastic shells. CMES—Comput. Model. Eng. Sci. **70**(2):153–190 (2010)
56. Pietraszkiewicz, W.: On constitutive restrictions in the resultant thermomechanics of shells with interstitial working. Advanced Structured Materials **15**:251–260 (2011)
57. Pietraszkiewicz, W.: Refined resultant thermomechanics of shells. Int. J. Eng. Sci. **49**(10):1112–1124 (2011)

58. Pietraszkiewicz, W.: On exact expressions of the bending tensor in the non-linear theory of thin shells. Appl. Math. Model. **36**(4):1821–1824 (2012)
59. Pietraszkiewicz, W.: On a description of deformable junction in the resultant nonlinear shell theory. Advanced Structured Materials **60**:457–468 (2016)
60. Pietraszkiewicz, W.: The resultant linear six-field theory of elastic shells: What it brings to the classical linear shell models? ZAMM **96**(8):899–915 (2016)
61. Pietraszkiewicz, W., Badur, J.: Finite rotations in the description of continuum deformation. Int. J. Eng. Sci. **21**(9):1097–1115 (1983)
62. Pietraszkiewicz, W., Eremeyev, V.: On natural strain measures of the non-linear micropolar continuum. Int. J. Solids Struct. **46**(3–4):774–787 (2009)
63. Pietraszkiewicz, W., Eremeyev, V.: On vectorially parameterized natural strain measures of the non-linear Cosserat continuum. Int. J. Solids Struct. **46**(11–12):2477–2480 (2009)
64. Pietraszkiewicz, W., Górski, J.: Foreword. Math. Mech. Solids **20**(7):789 (2015)
65. Pietraszkiewicz, W., Konopinska, V.: On unique kinematics for the branching shells. Int. J. Solids Struct. **48**(14–15):2238–2244 (2011)
66. Pietraszkiewicz, W., Konopinska, V.: Drilling couples and refined constitutive equations in the resultant geometrically non-linear theory of elastic shells. Int. J. Solids Struct. **51**(11–12):2133–2143 (2014)
67. Pietraszkiewicz, W., Konopinska, V.: Singular curves in the resultant thermomechanics of shells. Int. J. Eng. Sci. **80**:21–31 (2014)
68. Pietraszkiewicz, W., Konopinska, V.: Junctions in shell structures: A review. Thin-Wall. Struct. **95**:310–334 (2015)
69. Pietraszkiewicz, W., Kreja, I.: The 9th Conference "Shell Structures: Theory and Applications", SSTA2009, Oct. 14–16, 2009, Jurata (Poland). Arch. Civ. Eng. **55**(4):449–451 (2009)
70. Pietraszkiewicz, W., Szwabowicz, M.: Determination of the midsurface of a deformed shell from prescribed fields of surface strains and bendings. Int. J. Solids Struct. **44**(18–19):6163–6172 (2007)
71. Pietraszkiewicz, W., Vallée, C.: A method of shell theory in determination of the surface from components of its two fundamental forms. ZAMM **87**(8–9):603–615 (2007)
72. Pietraszkiewicz, W., Eremeyev, V., Konopinska, V.: Extended non-linear relations of elastic shells undergoing phase transitions. ZAMM **87**(2):150–159 (2007)
73. Pietraszkiewicz, W., Szwabowicz, M.: Entirely Lagrangian non-linear theory of thin shells. Arch. Mech. **33**(2):273–288 (1981)
74. Pietraszkiewicz, W., Szwabowicz, M.: Hu-Washizu variational functional for the Lagrangian geometrically non-linear theory of thin elastic shells. ZAMM **62**(4):T156–T158 (1982)
75. Pietraszkiewicz, W., Szwabowicz, M., Vallée, C.: Determination of the midsurface of a deformed shell from prescribed surface strains and bendings via the polar decomposition. Int. J. Nonlin Mech. **43**(7):579–587 (2008)

76. Schieck, B., Pietraszkiewicz, W., Stumpf, H.: Theory and numerical analysis of shells undergoing large elastic strains. Int. J. Solids Struct. **29**(6):689–709 (1992)
77. Schmidt, R., Pietraszkiewicz, W.: Variational principles in the geometrically non-linear theory of shells undergoing moderate rotations. Ing.-Arch. **50** (3):187–201 (1981)
78. Szwabowicz, M.L., Pietraszkiewicz, W.: Determination of the deformed position of a thin shell from surface strains and height function. Int. J. Nonlin. Mech. **39**(8):1251–1263 (2004)
79. Szwabowicz, M.L., Pietraszkiewicz, W.: Erratum: Determination of the deformed position of a thin shell from surface strains and height function (international journal of non-linear mechanics (2004) 39(1251–1263). Int. J. Nonlin. Mech. **39**(10):1737 (2004)
80. Visarius, H., Nolte, L.P., Pietraszkiewicz, W.: Closed-form force-elongation relations for the uniaxial viscoelastic behavior of biological soft tissues. Mech. Res. Commun. **24**(5):575–581 (1997)

Magdeburg, Germany/ Lublin, Poland — Holm Altenbach
Gdańsk, Poland — Jacek Chróścielewski
Gdańsk, Poland/ Rostov on Don, Russia — Victor A. Eremeyev
Warsaw, Poland — Krzysztof Wiśniewski
September, 2019

Contents

Tribute to Professor Wojciech Pietraszkiewicz

Igor V. Andrianov

Abstract This short paper is devoted to analysis of contribution by Professor Pietraszkiewicz to the Theory of Shells.

I met Professor Pietraszkiewicz in 1992 at SSTA92 in Janovice. I was familiar with his work before, but I consider personal acquaintance with this remarkable scientist and man as a great success. I was impressed by the erudition of Prof. Pietraszkiewicz, and not only in the Theory of Shells.

It must be said that at that time Polish scientists were in a very favorable position—fluent in both English and Russian, they could use the achievements of both Western and Soviet science. Although some scientific journals of the USSR were translated into English, the quality of these translations was usually very low. In addition, the style of writing papers in the USSR did not help spread the achievements of Soviet scientists in the West.

The Soviet Theory of Shells was strong WRT theoretical achievements, in the West, more attention was paid to applications, and the exchange of ideas at that time was limited. In recent years, I regretted that the achievements of the Soviet Theory of Shells are little known and often "the wheel reinvented" occurs in the West, and in a significantly weakened form.

On many key issues my opinion coincided with Prof. Pietraszkiewicz' ones. In 1992, FEM codes were just beginning their winning march. The enthusiasm was incredible, it seemed that all problems could be solved. The analytical methods were recalled with a smile. Paying tribute to FEM codes, Prof. Pietraszkiewicz called for a harmonious combination of numerical and analytical (especially asymptotic) methods.

I. V. Andrianov (✉)
Institute of General Mechanics, RWTH Aachen University, Templergraben 64, 52056 Aachen, Germany
e-mail: igor.andrianov@gmail.com

H. Altenbach et al. (eds.), *Recent Developments in the Theory of Shells*,
Advanced Structured Materials 110, https://doi.org/10.1007/978-3-030-17747-8_1

At the suggestion of Prof. Pietraszkiewicz at SSTA–2005 I made a review report on the application of asymptotic methods in the Theory of Shells (see [1]). I insisted that asymptotic, numerical, and rigorous mathematical methods are not competing, but mutually complementary approaches. This report was met with understanding by the computer community, which is not surprizing—by this time, both the strengths and weaknesses of FEM codes were well-understood [4]. Not all experts of the mathematical Theory of Shells agreed with my opinion, but it was strongly supported by Prof. Pietraszkiewicz. It makes sense to dwell on this point.

In a some sense, Theory of Shells can be separated into Physical, Computational, Asymptotical and Mathematical subtheories. Representatives of the Mathematical subtheory made a significant contribution to Theory of Shells, justifying and sometimes corrected the results initially obtained at a low level of mathematical rigor, see, e.g., [5]. However, on this way it is difficult not to be carried away with purely mathematical generalizations that go far beyond real physical problems.

As John von Neumann mentioned: "At a great distance from its empirical source, or after much "abstract" inbreeding, a mathematical subject is in danger of degeneration. At the inception, the style is usually classical; when it shows signs of becoming baroque, then the danger signal is up. ... In any event, whenever this stage is reached, the only remedy seems to me to be the rejuvenating return to the source: the reinjection of more or less directly empirical ideas" [3].

Of course, the separation of Theory of Shells into several subtheories should not be taken too literally. SSTA conferences (initiated by Prof. Pietraszkiewich) greatly contributed to the fruitful exchange of ideas from representatives of different communities.

Modern Civil and Industrial Engineering widely used composite and other artificially created materials with complicated properties. The shape and structure of thin-walled structures are also becoming more complex. This means that unemployment is not threat the Theory of Shells experts. Just look at the terms in the headlines of leading scientific journals: architected, functionally graded, active, dynamic, smart, phononic materials; meta-, nano-, graphene materials, etc. Shell systems are also becoming more complex: morphing shell structures, multifunctional material systems, etc. Some authors even see this as the renaissance of continuum mechanics, see [2]. "Probably, this is not a renaissance of the old continual mechanics, based on its classical models, but the birth of new areas. On the one hand, models of new materials were needed, and on the other hand, it made sense to construct them, thanks to new possibilities of numerical analysis and modern computers" (V.N. Pilipchuk, private message).

Analysis of the existing literature allows us to conclude: many authors try to use automatically the existing classical theories to describe new objects. "But new wine must be put into new bottles" (Luke 5: 36–39, KJV). For example, to develop a theory of nanotubes, it is necessary to take into account a number of specific effects (discreteness, surface tension) and to work in close cooperation with experimenters. Unfortunately, one can observe the disunity of the communities of physicists and mechanicians. For example, in some physical papers, devoted to the nanotubes, the results of the Theory of Shells, well known to mechanicians, are being rediscovered.

A detailed overview of the books and papers written by Prof. Pietraszkiewicz is not my task. I note only an interesting aspect of the current state of the art. The main results obtained by Prof. Pietraszkiewicz constitute the derivation of refined nonlinear equations Theory of Shells and their analysis. Now that the solution of complex nonlinear problems does not present unsolvable difficulties, the value of such theoretical studies increases.

Last but not least. The number of bad papers is multiplying. Probably the tendency is winning, but a new, dramatic problem arises: how to select in the mud the papers conveying innovative ideas? [6]. Of course, this is a serious problem, especially for beginners. I offer a simple and natural solution: read books and articles that have stood the test of time. Books and papers by Prof. Pietraszkiewicz belong to this category.

References

1. Andrianov, I.V., Awrejcewicz, J.: Asymptotic solution of the theory of shells boundary value problem. Math. Prob. Eng. 1–25 (2007). Article ID 82348
2. Chen, W.Q.: The renaissance of continuum mechanics. J. Zhejiang Univ. Sci. A **15**(4), 231–240 (2014)
3. von Neumann, J.: The mathematician. In: Heywood, R.B. (ed.) The Works of the Mind, pp. 180–196. The University of Chicago Press, Chicago (1947)
4. Ramm, E., Wall, W.A.: Shell structures—a sensitive interrelation between physics and numerics. Int. J. Numer. Methods Eng. **60**(1), 381–427 (2004)
5. Sanchez-Palencia, E., Millet, O., Béchet, F.: Singular Problems in Shell Theory: Computing and Asymptotics. Lecture Notes in Applied and Computational Mechanics, vol. 54. Springer, Berlin (2010)
6. Villaggio, P.: Crisis of mechanics literature? Meccanica **48**, 765–767 (2013)

Computer Modeling of Nonlinear Deformation and Loss of Stability of Composite Shell Structures Under a Combined Effect of Quasi-static and Pulsed Loads

N. A. Abrosimov, L. A. Igumnov, S. M. Aizikovich and A. V. Elesin

Abstract The formulation and solution method of problems of nonlinear dynamic deformation, loss of stability and supercritical behavior of composite spatial shell structures under combined loading by quasistatic and pulsed effects is considered. The structure is assumed to be made up by rigidly joining plates and shells of revolution along the lines coinciding with the coordinate directions of the joined elements. Separate elements of the structure can be made of both composite and conventional isotropic materials. A kinematic model of deformation of the structural elements is based on the hypothesis of the applied theory of shells. This approach is aimed at analyzing nonstationary deformation processes in composite structures with small deformations but with large displacements and rotation angles and is implemented in the framework of a simplified version of the geometrically nonlinear shell theory. Physical relations in composite structural elements are established based on the theory of effective moduli for the entire package as a whole, and in metallic ones in the framework of the plastic flow theory. Equations of motion of a composite shell structure are derived using the virtual displacement principle with additional provisions providing joint operation of the structural elements. To solve the formulated initial boundary-value problems, an effective numerical approach has been developed, which is based on the finite-difference discretization of variational equations of motion for spatial variables and an explicit second-order accuracy time integration scheme. The admissible time integration step is determined using Neumann's spectral criterion. In doing so, the quasistatic loading regime is modeled by assigning an external factor in the form of a linearly increasing time function attaining a stationary value during three periods of the lowest-form vibrations of the composite structure. This method is especially resultative in analyzing thin-walled shells, as well as the structural element is affected by local loads, which necessitates condensation of the grid in the zones of quickly changing solutions for spatial variables. The reliability of the developed approach is corroborated by comparing the computational results with experimental data. The characteristic forms of dynamic loss of strength and critical loads of smooth composite and isotropic cylindrical shells as well as of shells

N. A. Abrosimov · L. A. Igumnov (✉) · S. M. Aizikovich · A. V. Elesin
Research Institute for Mechanics, Nizhniy Novgorod Lobachevski National Research State University, Nizhniy Novgorod, Russia
e-mail: lgumnov@mech.unn.ru

H. Altenbach et al. (eds.), *Recent Developments in the Theory of Shells*,
Advanced Structured Materials 110, https://doi.org/10.1007/978-3-030-17747-8_2

stiffened by a system of discrete ribs under combined loading by axial compression and external pressure have been analyzed.

Keywords Composite and isotropic materials · Plates · Shells of revolution · Nonlinear deformation · Stability · Numerical methods · Quasistatic and dynamic loading

1 Introduction

Due to high strength and stiffness characteristics, composite materials open new possibilities in constructing rational structures in various fields of modern technology. In a number of cases, structural elements of composite materials can be subjected to combined effects of pulsed and static loading, leading to significant changes of form and loss of stability of these structural elements. To use the potential of composite materials more effectively, comprehensive study of dynamic deformation and loss of stability of composite shell structures under hybrid quasistatic and dynamic effects is required.

The analysis of publications on nonlinear nonstationary deformation and loss of stability of shell structures shows that the overwhelming majority of the papers tackle axisymmetric problems for smooth structural elements, such as cylindrical, conical and spherical shells, made, as a rule, of conventional materials [1–5]. Only a small range of nonlinear problems of dynamics and stability for composite shells of revolution under non-axisymmetric pulsed effects has been analyzed [6–15]. Thus, in [10], the results of experimental-numerical investigation of the instability region of a steel cylindrical shell under pulsed loading by external pressure in combination with external (or internal) static pressure are presented. In [11], the results of experimentally studying the effect of internal static pressure and rate of loading on the stability of aluminum cylindrical shells of under pulsed loading by external pressure are given. In [15], a methodology of numerically analyzing nonlinear nonstationary deformation and loss of stability of cylindrical shells made of composite materials under combined quasistatic and pulsed effects is presented. There are significantly fewer works on analyzing nonstationary dynamic problems of shell structures. Problems of dynamic deformation and stability of stiffened cylindrical shells have mostly been analyzed. In [16], the linear problems of dynamic deformation and strength of orthotropic cylindrical shells stiffened by circular ribs, loaded by axial compression and external pressure were analyzed. To describe the deformation of the skin, the Kirchhoff-Love hypothesis was used, whereas the deformation of ribs was described based on the Kirchhoff-Klebsh technical theory. The solution is constructed with Bubnov-Galerkin's method, using polynomial approximation of displacements. In [17], a similar formulation is used for analyzing a nonlinear problem of dynamic buckling of layered cylindrical shells stiffened with frames and loaded by uniform external pressure (with a monomial approximation of deflection). Dynamic problems of stiffened shells with various approximations were also studied in [18–21].

In [12], experimental analysis of buckling of thin-walled cylindrical shells under local pulsed loading by external pressure and different values of axial static compression is presented. Dynamic stability of stiffened cylindrical shells is experimentally studied in [20]. In [21, 22], the results of investigating the stability of cylindrical shells under the effect of axial static loading and a pressure wave incident in the direction of the longitudinal axis are given. It was found in the experiments that, depending on the rigidity of stiffening ribs and their location, local ('arch') or general form of loss of stability takes place. This fact necessitates taking into account the discrete character of stiffening elements.

A concise analysis of the above works testifies to the fact that the issues of theoretically analyzing nonlinear problems of dynamic behavior and loss of stability of composite shell structures, accounting for discrete location of stiffening elements and effects of interconnection of buckling forms under a combined effect of quasistatic and pulsed loading, have not been studied well enough.

The present paper is aimed at numerically modeling nonlinear nonstationary deformation and loss of stability of shell structures under combined quasistatic and pulsed effects.

2 Constructing the Resolving Equation Set

It is assumed that the shell structure is formed by rigidly joining plates and shells made of composite and (or) conventional isotropic materials along the lines coinciding with the coordinate directions of the joined elements. Elements of structures (substructures or their parts) are joined along the lines of intersection of their internal surfaces. Thus, a composite part of the structure is formed by stacking adjacent symmetrical layers with reinforcement angles $\pm\phi^k\left(k = \overline{1, K}\right)$. Structural elements can have variable thickness.

Each substructure is analyzed in an orthogonal curvilinear coordinate system α_i $(i = \overline{1, 3})$ coinciding with the main curvature lines and the outer normal to the internal surface of the shell.

Lame coefficients defining the metric properties of the shell element are:

$$H_1 = A_1 Z_1, \;\; H_2 = A_2 Z_2, \;\; H_3 = 1, \tag{1}$$

where $Z_1 = (1 + k_1\alpha_3)$; $Z_2 = (1 + k_2\alpha_3)$; A_1, A_2, k_1, k_2 are coefficients of the first quadratic form and main curvatures of internal surface S.

In what follows, it is assumed that geometric and mechanical characteristics of the shell structure and the loading effects acting on it are such that linear distribution of tangential components of the displacement vector through the thickness of the package holds, and normal displacement is constant through the thickness [23]

$$U_j(\alpha_1, \alpha_2, \alpha_3, t) = u_j(\alpha_1, \alpha_2, t) + \alpha_3\phi_j(\alpha_1, \alpha_2, t), \;\; (j = \overline{1, 2}),$$

$$U_3(\alpha_1, \alpha_2, \alpha_3, t) = u_3(\alpha_1, \alpha_2, t). \tag{2}$$

In the above expression, $u_i(\alpha_1, \alpha_2, t)$ are displacements of the coordinate surface in directions α_i $(i = \overline{1,3})$, respectively; $\phi_j(\alpha_1, \alpha_2, t)$ $(j = \overline{1,2})$ are angles of rotation of the normal to the internal surface.

In constructing geometrical relations, expressions of the quadratic version of the nonlinear elasticity theory will be used [24], which, taking into account non-deformability of the material of the shell in the direction of coordinate α_3 and the averaging of the shear deformation through the shell thickness, can be written as [23]

$$\begin{aligned}
e_{11} &= \frac{1}{Z_1}\left(\varepsilon_{11} + \varepsilon_{13}^2/2 + \alpha_3\chi_{11}\right), \quad (1 \to 2),\\
e_{12} &= \frac{1}{Z_1}(\varepsilon_{12} + \varepsilon_{13}\varepsilon_{23}/2 + \alpha_3\chi_{12}) + \frac{1}{Z_2}(\varepsilon_{21} + \varepsilon_{13}\varepsilon_{23}/2 + \alpha_3\chi_{21}), \quad (1 \to 2),\\
e_{13} &= \frac{1}{Z_1}(\phi_1 + \varepsilon_{13}), \quad (1 \to 2),
\end{aligned} \tag{3}$$

where

$$\begin{aligned}
\varepsilon_{11} &= \frac{1}{A_1}\frac{\partial u_1}{\partial \alpha_1} + \frac{u_2}{A_1A_2}\frac{\partial A_1}{\partial \alpha_2} + k_1u_3, \qquad (1 \to 2),\\
\chi_{11} &= \frac{1}{A_1}\frac{\partial \phi_1}{\partial \alpha_1} + \frac{\phi_2}{A_1A_2}\frac{\partial A_1}{\partial \alpha_2}, \qquad (1 \to 2),\\
\varepsilon_{12} &= \frac{1}{A_1}\frac{\partial u_2}{\partial \alpha_1} - \frac{u_1}{A_1A_2}\frac{\partial A_1}{\partial \alpha_2}, \quad (1 \to 2),\\
\chi_{12} &= \frac{1}{A_1}\frac{\partial \phi_2}{\partial \alpha_1} + \frac{\phi_1}{A_1A_2}\frac{\partial A_1}{\partial \alpha_2}, \qquad (1 \to 2),\\
\varepsilon_{13} &= \frac{1}{A_1}\frac{\partial u_3}{\partial \alpha_1} - k_1u_1, \quad (1 \to 2).
\end{aligned}$$

It is assumed that the composite element of the structure is formed by cross-stacking $\pm\phi^k\left(k = \overline{1,K}\right)$ a large enough number of composite layers. Keeping in mind the assumed hypotheses, physical relations for the cross-reinforced composite material of the shell can be written as

$$\begin{aligned}
&\sigma_{11} = A_{11}e_{11} + A_{12}e_{22}, \quad \sigma_{22} = A_{21}e_{11} + A_{22}e_{22},\\
&\sigma_{12} = A_{33}e_{12}, \quad \sigma_{13} = A_{44}e_{13}, \quad \sigma_{23} = A_{55}e_{23}.
\end{aligned} \tag{4}$$

It is assumed here that coefficients A_{mn} are certain smooth or stepped (for a layered material) functions of variable α_3. After substituting strains (3) into relations (4), stresses σ_{11}, σ_{22}, σ_{12}, σ_{13}, σ_{23} can be expressed through certain generalized deformational characteristics ε_{11}, ε_{22}, ε_{12}, ε_{21}, ε_{13}, ε_{23}, χ_{11}, χ_{22}, χ_{12}, χ_{21}. However, it is more natural to describe the stressed state of composite shells of revolution by formulating defining relations, using generalized force factors—forces and moments.

$$(N_{11}, N_{12}, M_{11}, M_{12}, Q_{13}) = \int_0^h (\sigma_{11}, \sigma_{12}, \alpha_3\sigma_{11}, \alpha_3\sigma_{12}, \sigma_{13}) Z_2 d\alpha_3, \quad (1 \to 2). \tag{5}$$

After integrating relation (5) through the thickness of the shell, keeping in mind (3), (4), $H_1 \approx A_1$, $H_2 \approx A_2$ be expressed as [23]

$$\begin{aligned}
N_{11} &= B_{11}\overline{\varepsilon}_{11} + B_{12}\overline{\varepsilon}_{22} + C_{11}\chi_{11} + C_{12}\chi_{22}, \quad (1 \to 2),\\
N_{12} &= B_{33}^{11}\overline{\varepsilon}_{12} + B_{33}^{12}\overline{\varepsilon}_{21} + C_{33}^{11}\chi_{12} + C_{33}^{12}\chi_{21}, \quad (1 \to 2),\\
M_{11} &= C_{11}\overline{\varepsilon}_{11} + C_{12}\overline{\varepsilon}_{22} + D_{11}\chi_{11} + D_{12}\chi_{22}, \quad (1 \to 2),\\
M_{12} &= C_{33}^{11}\overline{\varepsilon}_{12} + C_{33}^{12}\overline{\varepsilon}_{21} + D_{33}^{11}\chi_{12} + D_{33}^{12}\chi_{21}, \quad (1 \to 2),\\
Q_{13} &= K_1(\varepsilon_{13} + \phi_1), \quad (1 \to 2),
\end{aligned} \tag{6}$$

where

$$\begin{aligned}
&\bar{\varepsilon}_{11} = \varepsilon_{11} + \varepsilon_{13}^2/2, \qquad (1 \to 2),\\
&\bar{\varepsilon}_{12} = \varepsilon_{12} + \varepsilon_{13}\varepsilon_{23}/2,\\
&B_{jj} = I_{jj}^{(0)}, \qquad B_{12} = B_{21} = J_{12}^{(0)}, \qquad C_{jj} = I_{jj}^{(1)}, \qquad C_{12} = C_{21} = J_{12}^{(1)},\\
&B_{33}^{jj} = I_{33,jj}^{(0)}, \qquad B_{33}^{12} = B_{33}^{21} = J_{33}^{(0)}, \quad C_{33}^{jj} = I_{33,jj}^{(1)}, \qquad C_{33}^{12} = C_{33}^{21} = J_{33}^{(1)},\\
&D_{jj} = I_{jj}^{(2)}, \quad D_{12} = D_{21} = J_{12}^{(2)}, \quad D_{33}^{jj} = I_{33,jj}^{(2)}, \qquad D_{33}^{12} = D_{33}^{21} = J_{33}^{(2)},\\
&K_j = h^2\left[\sum_{k=1}^{K} \frac{H_j^{(k)} h_k}{A_{j+3\,j+3}^{(k)}}\right]^{-1}, \quad H_1^{(k)} = \frac{\left(1 + \overline{h}_k k_1\right)}{\left(1 + \overline{h}_k k_2\right)}, \quad (1 \to 2) \quad (j = 1, 2),\\
&h_k = z_k - z_{k-1}, \quad \overline{h}_k = (z_k + z_{k-1})\big/2,
\end{aligned}$$

$$\begin{aligned}
I_{11}^{(i)} &= \frac{1}{i+1}\sum_{\kappa=1}^{K} A_{11}^{(\kappa)} H_2^{(\kappa)} (z_\kappa^{i+1} - z_{\kappa-1}^{i+1}), \quad (i = 0,\ 1,\ 2) \qquad (1 \to 2),\\
I_{33,11}^{(i)} &= \frac{1}{i+1}\sum_{\kappa=1}^{K} A_{33}^{(\kappa)} H_2^{(\kappa)} (z_\kappa^{i+1} - z_{\kappa-1}^{i+1}),\\
J_{12}^{(i)} &= \frac{1}{i+1}\sum_{\kappa=1}^{K} A_{12}^{(\kappa)} (z_\kappa^{i+1} - z_{\kappa-1}^{i+1}),\\
J_{33}^{(i)} &= \frac{1}{i+1}\sum_{\kappa=1}^{K} A_{33}^{(\kappa)} (z_\kappa^{i+1} - z_{\kappa-1}^{i+1}), \quad (i = 0,\ 1,\ 2).
\end{aligned}$$

$A_{ij}^{(\kappa)}$ are effective stiffness characteristics of the layer, which are expressed through elasticity moduli $E_{jj}^{(\kappa)}$, $G_{12}^{(\kappa)}$, $G_{j3}^{(\kappa)}$ and Poisson's ratios $\nu_{12}^{(k)}$ in the axes of orthotropy

of the layer, using known relations [23]; z_κ are coordinates of the layers counted from the internal surface of the shell.

Total strains e_{ij} of the isotropic parts of the structure will be represented as a sum of elastic e'_{ij} and plastic e''_{ij} components. Elastic strains are related with stresses through Hook's law

$$\sigma_{ij} = \lambda e \delta_{ij} + 2\mu\, e'_{ij}, \tag{7}$$

where $e = \sum_{i=1}^{3} e_{ii}$; λ, μ are Lame parameters; δ_{ij} is Kronecker delta. Plastic components of the strain are defined by relations of the flow theory with linear kinematic hardening [25]

$$e''_{ij} = \int_0^t \dot{e}''_{ij} dt;\ \sum_{i=1}^{3} e''_{ii} = 0;\ \dot{e}''_{ij} = \dot{\gamma} S_{ij};\ \sum_{i,\,j=1}^{3} S_{ij} S_{ij} - \frac{2}{3}\sigma_*^2 = 0;$$
$$S_{ij} = \sigma_{ij} - \sigma\delta_{ij} - \rho_{ij};\ \sigma = (\sigma_{11} + \sigma_{22})/3;\ \rho_{ij} = 2g e''_{ij}; \tag{8}$$

ρ_{ij} is tensor of residual micro-strains; g is modulus of linear hardening of the material; $\dot{\gamma}$ is scalar parameter; σ_* is yield strength; S_{ij} is deviator of effective stresses; the upper dot indicates time derivative.

One of the important properties of the applied theory is its being energy-consistent, that is, the ability to obtain initial equations as conditions of a steady state of a certain energy functional. Thus, to derive equations of motion of a shell structure of revolution, the virtual displacement principle [24] will be used, which, taking into account (1)–(8), will be written for each element of the structure as [26]

$$\begin{aligned}
&\iint_S \Bigg[\frac{N_{11}}{A_1}\frac{\partial(\delta u_1)}{\partial\alpha_1} + \frac{N_{21}}{A_2}\frac{\partial(\delta u_1)}{\partial\alpha_2} + \frac{N_{22}}{A_1A_2}\frac{\partial A_2}{\partial\alpha_1}\delta u_1 - \frac{N_{12}}{A_1A_2}\frac{\partial A_1}{\partial\alpha_2}\delta u_1 \\
&- (Q_{13} + N_{11}\varepsilon_{13} + N_{12}\varepsilon_{23})k_1\delta u_1 + \frac{N_{22}}{A_2}\frac{\partial(\delta u_2)}{\partial\alpha_2} + \frac{N_{12}}{A_1}\frac{\partial(\delta u_2)}{\partial\alpha_1} + \frac{N_{11}}{A_1A_2}\frac{\partial A_1}{\partial\alpha_2}\delta u_2 \\
&- \frac{N_{21}}{A_1A_2}\frac{\partial A_2}{\partial\alpha_1}\delta u_2 - (Q_{23} + N_{22}\varepsilon_{23} + N_{21}\varepsilon_{13})k_2\delta u_2 \\
&+ \frac{(Q_{13} + N_{11}\varepsilon_{13} + N_{12}\varepsilon_{23})}{A_1}\frac{\partial(\delta u_3)}{\partial\alpha_1} + \frac{(Q_{23} + N_{22}\varepsilon_{23} + N_{21}\varepsilon_{13})}{A_2}\frac{\partial(\delta u_3)}{\partial\alpha_2} \\
&+ N_{11}k_1\delta u_3 + N_{22}k_2\delta u_3 + \frac{M_{11}}{A_1}\frac{\partial(\delta\phi_1)}{\partial\alpha_1} + \frac{M_{21}}{A_2}\frac{\partial(\delta\phi_1)}{\partial\alpha_2} \\
&+ \left(\frac{M_{22}}{A_1A_2}\frac{\partial A_2}{\partial\alpha_1} - \frac{M_{12}}{A_1A_2}\frac{\partial A_1}{\partial\alpha_2}\right)\delta\phi_1 + Q_{13}\delta\phi_1 + \frac{M_{22}}{A_2}\frac{\partial(\delta\phi_2)}{\partial\alpha_2} + \frac{M_{12}}{A_1}\frac{\partial(\delta\phi_2)}{\partial\alpha_1} \\
&+ \left(\frac{M_{11}}{A_1A_2}\frac{\partial A_1}{\partial\alpha_2} - \frac{M_{21}}{A_1A_2}\frac{\partial A_2}{\partial\alpha_1}\right)\delta\phi_2 + Q_{23}\delta\phi_2\Bigg]\, A_1A_2 d\alpha_1 d\alpha_2 \\
&+ \iint_S \Big[\big(B_{11}\ddot{u}_1 + B_{12}\ddot{\phi}_1\big)\delta u_1 + \big(B_{11}\ddot{u}_2 + B_{12}\ddot{\phi}_2\big)\delta u_2 + B_{11}\ddot{u}_3\delta u_3 \\
&+ \big(B_{22}\ddot{\phi}_1 + B_{21}\ddot{u}_1\big)\delta\phi_1 + \big(B_{22}\ddot{\phi}_2 + B_{21}\ddot{u}_2\big)\delta\phi_2\Big]\, A_1A_2 d\alpha_1 d\alpha_2
\end{aligned}$$

$$
\begin{aligned}
&- \iint\limits_S \left(\sum_{i=1}^{3} F_i \delta u_i + \sum_{j=1}^{2} M_j \delta \phi_j \right) d\alpha_1 d\alpha_2 - \sum_{i=1}^{2} \int\limits_{\Gamma_i^0} \left(N_{11}^0 \delta u_1^0 + N_{12}^0 \delta u_2^0 + Q_1^0 \delta u_3^0 \right. \\
&+ \left. M_{11}^0 \delta \phi_1^0 + M_{12}^0 \delta \phi_2^0 \right) A_2 d\alpha_2 - \sum_{i=3}^{4} \int\limits_{\Gamma_i^0} \left(N_{22}^0 \delta u_2^0 + N_{21}^0 \delta u_1^0 + Q_2^0 \delta u_3^0 \right. \\
&+ \left. M_{21}^0 \delta \phi_1^0 + M_{22}^0 \delta \phi_2^0 \right) A_1 d\alpha_1 - \sum_{i=1}^{2} \int\limits_{\Gamma_i^*} \left(N_{11}^* \delta u_1^* + N_{12}^* \delta u_2^* + Q_1^* \delta u_3^* \right. \\
&+ \left. M_{11}^* \delta \phi_1^* + M_{12}^* \delta \phi_2^* \right) A_2 d\alpha_2 - \sum_{i=3}^{4} \int\limits_{\Gamma_i^*} \left(N_{21}^* \delta u_1^* + N_{22}^* \delta u_2^* + Q_2^* \delta u_3^* \right. \\
&+ \left. M_{21}^* \delta \phi_1^* + M_{22}^* \delta \phi_2^* \right) A_1 d\alpha_1 = 0, \qquad (9)
\end{aligned}
$$

where

$$
\begin{aligned}
&(B_{11},\ B_{12} = B_{21},\ B_{22}) = \int\limits_0^h \left(\rho,\ \alpha_3 \rho,\ \alpha_3^2 \rho \right) Z_1 Z_2 \, d\alpha_3, \\
&F_1 = A_2 p_1 + B_1 B_2 \left(q_1 + q \frac{1}{B_1} \frac{\partial h}{\partial \alpha_1} \right), \quad (1 \to 2), \\
&F_3 = A_1 A_2 p - B_1 B_2 \left(q - q_1 \frac{1}{B_1} \frac{\partial h}{\partial \alpha_1} - q_2 \frac{1}{B_2} \frac{\partial h}{\partial \alpha_2} \right), \\
&M_1 = h B_1 B_2 \left(q_1 + q \frac{1}{B_1} \frac{\partial h}{\partial \alpha_1} \right), \quad (1 \to 2).
\end{aligned}
$$

ρ is density; q, p are external and internal pressures; q_j, p_j $(j = 1, 2)$ are tangential loads in the directions of coordinate axes α_i; S is integration region on the internal surface; B_j $(j = 1, 2)$ are coefficients of the first quadratic form of external surface; Γ_i^0, Γ_i^* $\left(i = \overline{1, 4}\right)$ are boundary and joining lines of region S, N_{ij}^0, Q_j^0, M_{ij}^0; N_{ij}^*, Q_j^*, M_{ij}^* are forces and moments applied to the corresponding boundary and joining lines.

After applying to (9) a well-known integral transform procedure, the system of equations of motion of a part of a composite shell will have the following form:

$$
\begin{aligned}
&L_1(N) + Q_{11} A_1 A_2 k_1 + F_1 = A_1 A_2 \left(B_{11} \ddot{u}_1 + B_{12} \ddot{\phi}_1 \right), \\
&L_2(N) + Q_{22} A_1 A_2 k_2 + F_2 = A_1 A_2 \left(B_{11} \ddot{u}_2 + B_{12} \ddot{\phi}_2 \right), \\
&\left[\frac{\partial (A_2 Q_{11})}{\partial \alpha_1} + \frac{\partial (A_1 Q_{22})}{\partial \alpha_2} \right] - A_1 A_2 (k_1 N_{11} + k_2 N_{22}) + F_3 = A_1 A_2 B_{11} \ddot{u}_3 \qquad (10) \\
&L_1(M) - Q_{13} A_1 A_2 + M_1 = A_1 A_2 \left(B_{22} \ddot{\phi}_1 + B_{21} \ddot{u}_1 \right),
\end{aligned}
$$

$$L_2(M) - Q_{23}A_1A_2 + M_2 = A_1A_2\left(B_{22}\ddot{\phi}_2 + B_{21}\ddot{u}_2\right),$$
$$L_1(T) = \frac{\partial(A_2T_{11})}{\partial\alpha_1} - T_{22}\frac{\partial A_2}{\partial\alpha_1} + \frac{\partial(A_1T_{21})}{\partial\alpha_2} + T_{12}\frac{\partial A_1}{\partial\alpha_2}, \quad (1 \to 2),$$
$$Q_{11} = Q_{13} + N_{11}\varepsilon_{13} + N_{12}\varepsilon_{23}, \quad (1 \to 2),$$

and the natural boundary conditions on contour Γ_i^0 $\left(i = \overline{1,4}\right)$ and (or) joining Γ_i^* $\left(i = \overline{1,4}\right)$ lines will be

$$\begin{aligned} &N_{11} = N_{11}^0; \quad N_{12} = N_{12}^0; \quad Q_{11} = Q_1^0; \quad M_{11} = M_{11}^0; \quad M_{12} = M_{12}^0, \quad (1 \to 2),\\ &N_{11} = N_{11}^*; \quad N_{12} = N_{12}^*; \quad Q_{11} = Q_1^*; \quad M_{11} = M_{11}^*; \quad M_{12} = M_{12}^*, \quad (1 \to 2). \end{aligned} \tag{11}$$

Equipping relations (1)–(11) with a required number of initial conditions

$$\begin{aligned} &u_i(\alpha_1,\alpha_2,0) = U_i^0(\alpha_1,\alpha_2), \quad \phi_j(\alpha_1,\alpha_2,0) = \phi_j^0(\alpha_1,\alpha_2),\\ &\dot{u}_i(\alpha_1,\alpha_2,0) = \dot{U}_i^0(\alpha_1,\alpha_2), \quad \dot{\phi}_j(\alpha_1,\alpha_2,0) = \dot{\phi}_j^0(\alpha_1,\alpha_2) \quad \left(i = \overline{1,3},\ j = 1,2\right), \end{aligned} \tag{12}$$

and assigning initial camber, one obtains a complete equation system for analyzing nonlinear processes of deformation and loss of stability of composite plate-shell structures under combined quasistatic and pulsed loading. In doing so, the quasistatic loading mode is modeled by assigning an external effect in the form of a linearly increasing function in time, which attains a stationary value during three lowest-form oscillation periods of the composite structure.

It noteworthy that in basis α_i^* $(i = \overline{1,3})$, which is assumed to be common for all the structural elements along joining lines Γ_i^* $\left(i = \overline{1,4}\right)$, conditions of rigid gluing must be fulfilled.

A critical load of loss of stability is identified by a characteristic kink on the curve of maximal loading amplitude—maximal deflection.

3 The Numerical Method of Analyzing the Initial Boundary-Value Problem

The numerical method of analyzing the formulated problem us based on an explicit variational-difference scheme [26]. The internal surface of each of the plate-shell elements of the structure is covered by a grid of triangular and (or) quadrangular meshes. The discretization is done in such a way that the nodes of the grid coincide along the joining lines.

Approximating with operators

$$f \approx d_0 f = \sum_{k=1}^{n} \beta_k f_k, \ \sum_{k=1}^{n} \beta_k = 1, \ \beta_k = \frac{1}{n} \ (k = \overline{1,n}),$$

$$\frac{\partial f}{\partial \alpha_j} \approx d_j f = \sum_{k=1}^{n} \beta_k^j f_k = (-1)^j \frac{\sum\limits_{k=1}^{n} \left(\alpha_{3-j}^{k+1} - \alpha_{3-j}^{k-1}\right) f_k}{\sum\limits_{k=1}^{n} \left(\alpha_1^{k+1} - \alpha_1^{k-1}\right)\alpha_2^k} \ (j = 1, 2) \qquad (13)$$

functions and derivatives contained in variational Eq. (9), and using summation of virtual works over the elementary areas and sides of the grid meshes instead of integrating over the internal surfaces and contours, yields a system of grid equations of the second order in time, defining the motion of internal, boundary and joining nods:

$$L_{d_1}(N) + d_0(Q_{11}k_1) + \frac{F_1}{\langle A_1\rangle\langle A_2\rangle} = B_{11}\ddot{u}_1 + B_{12}\ddot{\phi}_1,$$
$$L_{d_2}(N) + d_0(Q_{22}k_2) + \frac{F_2}{\langle A_1\rangle\langle A_2\rangle} = B_{11}\ddot{u}_2 + B_{12}\ddot{\phi}_2,$$
$$d_1\left(\frac{Q_{11}}{\langle A_1\rangle}\right) + d_2\left(\frac{Q_{22}}{\langle A_2\rangle}\right) - d_0(N_{11}k_1 + N_{22}k_2) + \frac{F_3}{\langle A_1\rangle\langle A_2\rangle} +$$
$$+ \left(Q_1^0\Delta\Gamma_{\alpha_2^0} + Q_2^0\Delta\Gamma_{\alpha_1^0} + Q_1^*\Delta\Gamma_{\alpha_2^*} + Q_2^*\Delta\Gamma_{\alpha_1^*}\right)/\Delta S_* = B_{22}\ddot{u}_3, \qquad (14)$$

$$L_{d_1}(M) + d_0(Q_{13}) + \frac{M_1}{\langle A_1\rangle\langle A_2\rangle} = B_{22}\ddot{\phi}_1 + B_{21}\ddot{u}_1,$$
$$L_{d_2}(M) + d_0(Q_{23}) + \frac{M_2}{\langle A_1\rangle\langle A_2\rangle} = B_{22}\ddot{\phi}_2 + B_{21}\ddot{u}_2,$$
$$L_{d_1}(T) = d_1\left(\frac{T_{11}}{\langle A_1\rangle}\right) - d_0\left(\frac{T_{22}d_1A_2}{\langle A_1\rangle\langle A_2\rangle}\right) + d_2\left(\frac{T_{21}}{\langle A_2\rangle}\right) + d_0\left(\frac{T_{12}d_2A_1}{\langle A_1\rangle\langle A_2\rangle}\right) +$$
$$+ \left(T_{21}^0\Delta\Gamma_{\alpha_1^0} + T_{11}^0\Delta\Gamma_{\alpha_2^0} + T_{21}^*\Delta\Gamma_{\alpha_1^*} + T_{11}^*\Delta\Gamma_{\alpha_2^*}\right)/\Delta S_*, \quad (1 \to 2),$$

$\Delta S_*, \Delta\Gamma_{\alpha_j^0}, \Delta\Gamma_{\alpha_j^*}$ are areas and side lengths of all the meshes adjacent to the analyzed nod; the angle brackets designate an average value.

The obtained semi-discrete system has the same structure as initial system of equations of motion (10), and is solved using an explicit scheme of the second-order accuracy relative to time step:

$$\dot{u}_j\left(t^{k+1/2}\right) = \dot{u}_j\left(t^{k-1/2}\right) + \frac{\Delta t}{B_{11}B_{22} - B_{12}B_{21}}\left(F_{u_j}B_{22} - F_{\phi_j}B_{\cdot 12}\right),$$
$$\dot{u}_3\left(t^{k+1/2}\right) = \dot{u}_3\left(t^{k-1/2}\right) + \frac{\Delta t}{B_{11}}\left(F_{u_3}\right),$$
$$\dot{\phi}_i\left(t^{k+1/2}\right) = \dot{\phi}_i\left(t^{k-1/2}\right) + \frac{\Delta t}{B_{11}B_{22} - B_{12}B_{21}}\left(F_{\phi_i}B_{11} - F_{u_i}B_{21}\right),$$

$$u_i\left(t^{k+1}\right) = u_i\left(t^k\right) + \Delta t \dot{u}_i\left(t^{k+1/2}\right), \quad \left(i = \overline{1,3};\ j - 1,2\right), \quad \left(k = \overline{0,\infty}\right),$$
$$\phi_j\left(t^{k+1}\right) = \phi_j\left(t^k\right) + \Delta t \dot{\phi}_j\left(t^{k+1/2}\right),$$

where generalized forces and moments F_{u_i}, F_{ϕ_j} are defined by the left-hand sides of system (14). Time integration step Δt is defined using Neumann's spectral feature [27], which yields condition:

$$\Delta t \leq 2/\omega_{max}, \tag{15}$$

where ω_{max} is maximal eigenfrequency of semi-discrete system (14).

The concretization of evaluation (15) for linear bending equations of motion of composite bars, which follow from (10) for $u_2 = \phi_2 = 0$ and from the dependence of the rest of the grid functions on the single coordinate α_1, will be written in the following form:

$$\Delta t = \begin{cases} \Delta\alpha_1, & \frac{\Delta\alpha_1}{\eta} \leq \left(\frac{\alpha-1}{3}\right)^{1/2} \\ \frac{\eta\sqrt{\alpha}}{\sqrt{3}}, & \frac{\Delta\alpha_1}{\eta} \geq \left(\frac{\alpha+1}{3}\right)^{1/2} \\ 2/\omega(\beta_0), & \left(\frac{\alpha+1}{3}\right)^{1/2} < \frac{\Delta\alpha_1}{\eta} < \left(\frac{\alpha-1}{3}\right)^{1/2} \end{cases} \tag{16}$$

$$\omega(\beta) = \left\{ \frac{6}{\alpha\eta^2}(1-\beta) + \frac{2(\alpha+1)}{\alpha}\frac{\beta}{\Delta\alpha_1^2} + \left[\left(\frac{6}{\alpha\eta^2}(1-\beta) + \frac{2(\alpha+1)}{\alpha}\frac{\beta}{\Delta\alpha_1^2} \right)^2 - \frac{16\beta^2}{\alpha\Delta\alpha_1^4} \right]^{1/2} \right\}^{1/2},$$

$$\beta_0 = \frac{\frac{12}{\alpha}\left(\frac{\Delta\alpha_1}{\eta}\right)^2\left[\frac{3}{\alpha}\left(\frac{\Delta\alpha_1}{\eta}\right)^2 - \frac{1}{\alpha} - 1\right]}{\left[\frac{3}{\alpha}\left(\frac{\Delta\alpha_1}{\eta}\right)^2 - \frac{1}{\alpha} - 1\right]^2 - \frac{4}{\alpha}}, \quad \alpha = \frac{E_{11}}{G_{13}},$$

where $\Delta\alpha_1$ is dimensionless step of the grid; η is dimensionless thickness of the bar; E_{11}, G_{13} are longitudinal and shear moduli.

Evaluation (16) is also applicable to the integration of system (14). In doing so, it is assumed that $\Delta\alpha_1$ means minimal linear dimension of a two-dimensional mesh.

The above methodology of numerically integrating equations of motion of shell structures can lead on quadrangular meshes to 'sand-glass' instability [28], which, although not accompanied by exponentially increasing computational inaccuracy, can contribute to the accumulation of inaccuracies in computations, resulting in the distortion of displacement fields. This phenomenon is caused by incompleteness of difference operators (13), defined on quadrangular meshes. To overcome this undesirable effect, it is suggested to define generalized forces and moments F_{u_i}, F_{ϕ_j} in (14) as a sum of respective generalized forces obtained for difference grids on quadrangular and triangular meshes. The approximation on triangular meshes is done

with a small coefficient. Modernized in this way, the difference scheme becomes free from the "sand-glass' instability.

4 Investigation Results

4.1 Numerical Analysis of Loss of Stability of Cylindrical Shells, Accounting for Quasistatic Preloading

To corroborate the reliability and accuracy of the suggested approach, the numerical results were compared with experimental data [11] on dynamic stability of isotropic cylindrical shells preloaded by internal pressure followed by a pulse of external pressure of various rates.

The geometric and physical-mechanical parameters of the material of the shell were as follows: R/h = 104; $h = 0.0005$ m; L/R = 1.9; $E = 73$ GPa; $\nu = 0.3$, $\rho = 2700$ kg/m^3, $\sigma_* = 0.37$ GPa; $g = 0.6$ GPa, L is length of the generatrix of the shell.

Static internal pressure was applied by compressed air, whereas pulsed pressure resulted from an electro-hydraulic discharge resulting from the explosion of calibrated copper wires [11]. The edges of the shell were secured in the way close to rigid clamping.

Figure 1 compares experimental and numerical results for dynamic amplification factor $K = F_3^*/F_3^0$ as a function of the rate loading by a pulse of external pressure $\dot{F}_3^+$ (F_3^*, F_3^0—are critical loss of stability loads under dynamic and static external pressure, respectively). The given results were obtained for static internal pressure F_3^-, which in a dimensionless is defined by expression $\dot{F}_3^- = \frac{F_3^-}{E}\left(\frac{R}{h}\right)^2$ and, in this particular case, is equal to $\dot{F}_3^- = 0.07$.

The obtained results testify to good agreement between the numerical and experimental data.

Figure 2 presents characteristic forms of loss of stability under static and dynamic loading with various rates of the external pressure, accounting for the preloading by internal pressure $\dot{F}_3^- = 0.42$.

It follows from the present results that increasing the rate of external pressure leads to substantially increasing the dynamic overload factor, and that there is a trend of

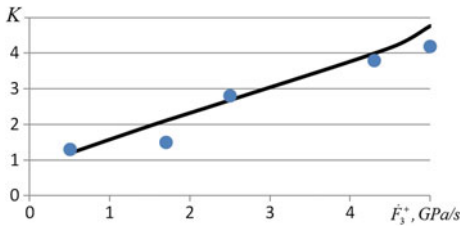

Fig. 1 Dynamic overload factor as a function of loading rate (the dots correspond to the experimental data [2], the curve shows numerical results using the present methodology)

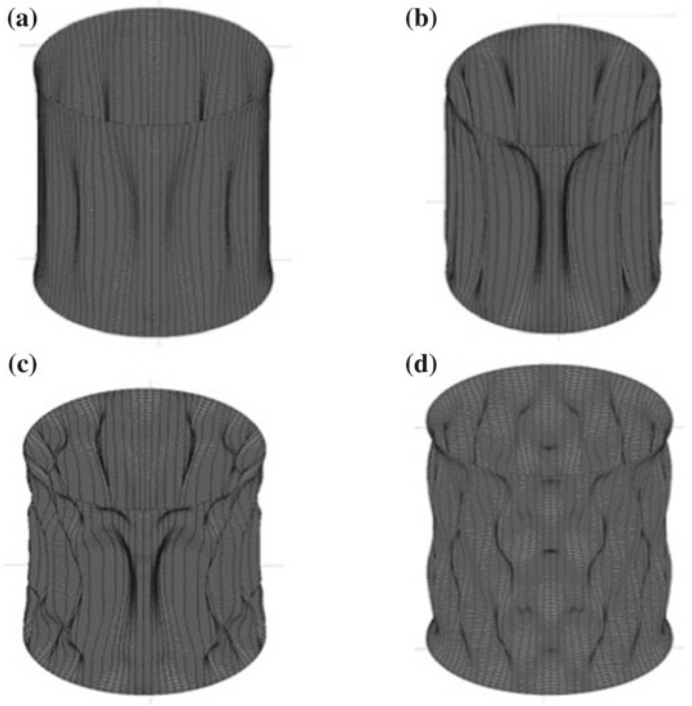

Fig. 2 Characteristic forms of waveformation in isotropic cylindrical shells under various rates of the pressure pulse: **a** static loading by external pressure; **b**, **c**, **d** dynamic loading by external pressure with the rates of 10, 30, 50 GPa/s

the increase of the number of waves along both the circumference and length of the shell with the increasing loading rate, which was noted in [11].

Further on, a cylindrical shell was considered, which was made of a composite material with the following geometric and physical mechanical parameters: $R = 0.072$ m; R/h = 112, L/R = 2.22; $E_1 = 200$ GPa; $E_2 = E_1/30$; $G_{12} = G_{13} = G_{23} = E_2/2$; $\nu_{12} = 0.25$, $\rho = 1800$ kg/m^3.

The results of analyzing the effect of the reinforcement angle and static preloading by internal pressure on the loss of stability process of the shell during subsequent loading by a pulse of external pressure with various rates are presented in Figs. 3, 4, 5 and 6.

Figure 3 shows a time history of absolute values of maximal deflections U_3^* of the shell for various reinforcement angles and rates of the external pressure pulse, preloaded by internal static pressure $\dot{F}_3^- = \frac{F_3^-}{E_{11}}\left(\frac{R}{h}\right)^2$.

The deformed configurations of the shells observed at the moment of loss of stability and computed for different reinforcement patterns in a wide range of external pressure rates, accounting for static internal pressure $\dot{F}_3^- = 0.1$, are presented in Fig. 4.

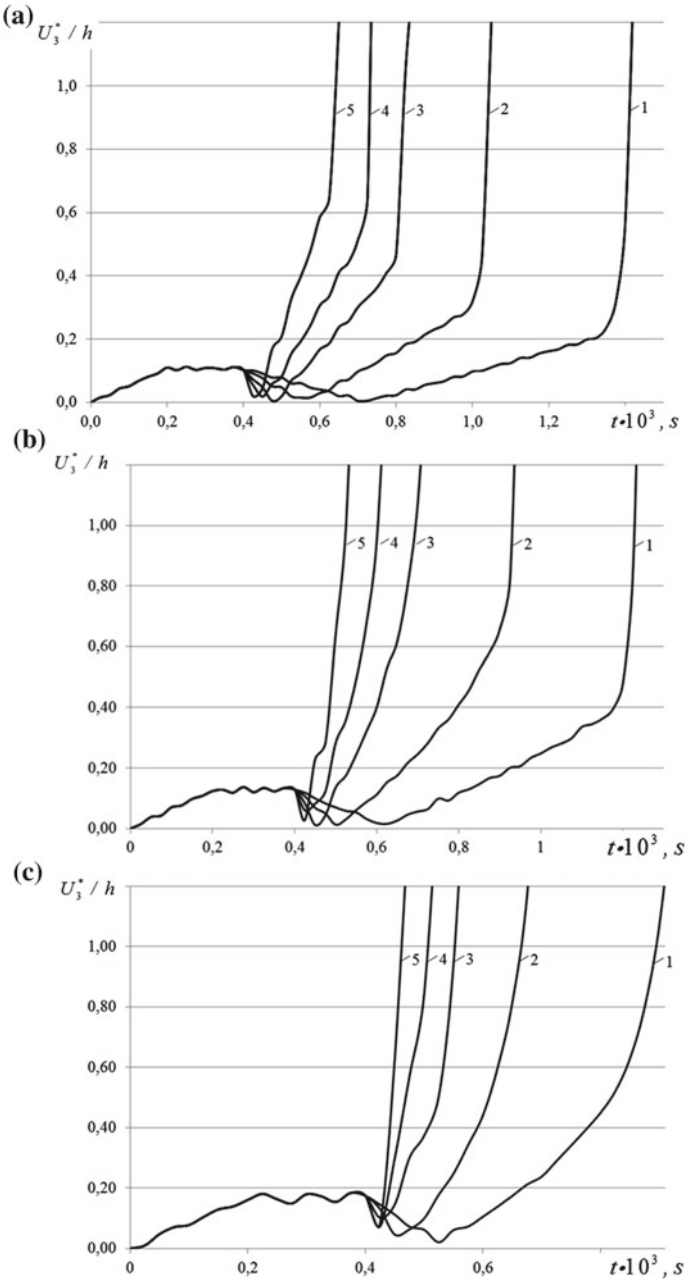

Fig. 3 Absolute values of the maximum deflection of the shell as a function of time, accounting for the preloading by internal static pressure $\dot{P}_3^- = 0.1$ for the external pressure pulse rates of: 5 GPa/s (1); 10 GPa/S (2); 20 GPa/s (3); 30 GPa/s (4); 50 GPa/s (5) and reinforcement angles of: 90°(**a**); 60°(**b**); 45°(**c**); 30°(**d**) relative to the generatrix of the shell, respectively

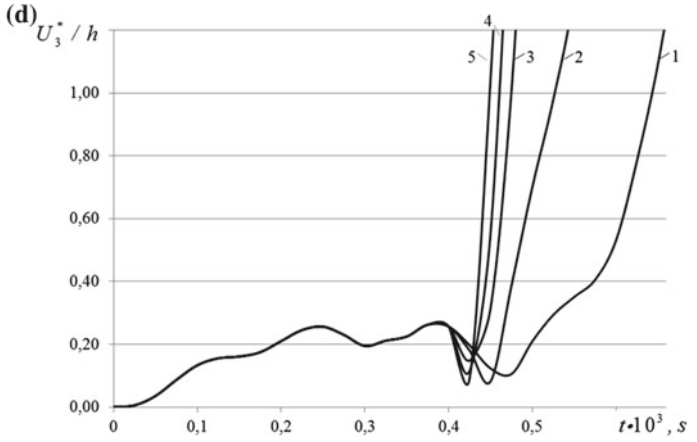

Fig. 3 (continued)

It is evident from Figs. 3, and 4 that the reinforcement angle and the external pressure pulse rate significantly affect both the critical value of the loss of stability load and the characteristic forms of waveformation of the composite cylindrical shells.

In the process of loss of stability, the shells with the reinforcement angle close to 90°, exhibit localization of the bulges along the generatrix, their number increasing with the loading rate, and the axisymmetric buckling forms tending to transform into non-axisymmetric ones. The process for the shells with the reinforcement angle of 60° is characterized by changing the deformation configuration with the increasing pressure pulse rate from the bulges along the generatrix to a corrugated form of loss of stability. The shells with the reinforcement angle of 45° lose their stability with a clearly pronounced corrugated configuration, the number of corrugations increasing with the pressure pulse rate. For the shells with the 30°-reinforcement angle, the form of loss of stability is characterized by practically retaining the initial cylindrical geometry except for the zone of boundary effects.

Figure 5 depicts the results of analyzing the effect of loading rates on the dynamic overload factor for different reinforcement patterns.

It is evident that the dynamic factor grows with the pressure pulse rate, this relation being more pronounced in the shells with higher anisotropy.

The deformed geometries of the shells illustrating the effect of reinforcement angle on the character of loss of stability under quasistatic and dynamic loading with the pulse rate of 5 GPa/s, both with and without preloading, are shown in Fig. 6.

Shells with strongly pronounced anisotropy lose their stability in the process of quasistatic deformation with forming dimples along the generatrix, whereas loss of stability of shells with the reinforcement angle of 45° is in the form of corrugation, the corrugating level being higher along the clamped edges.

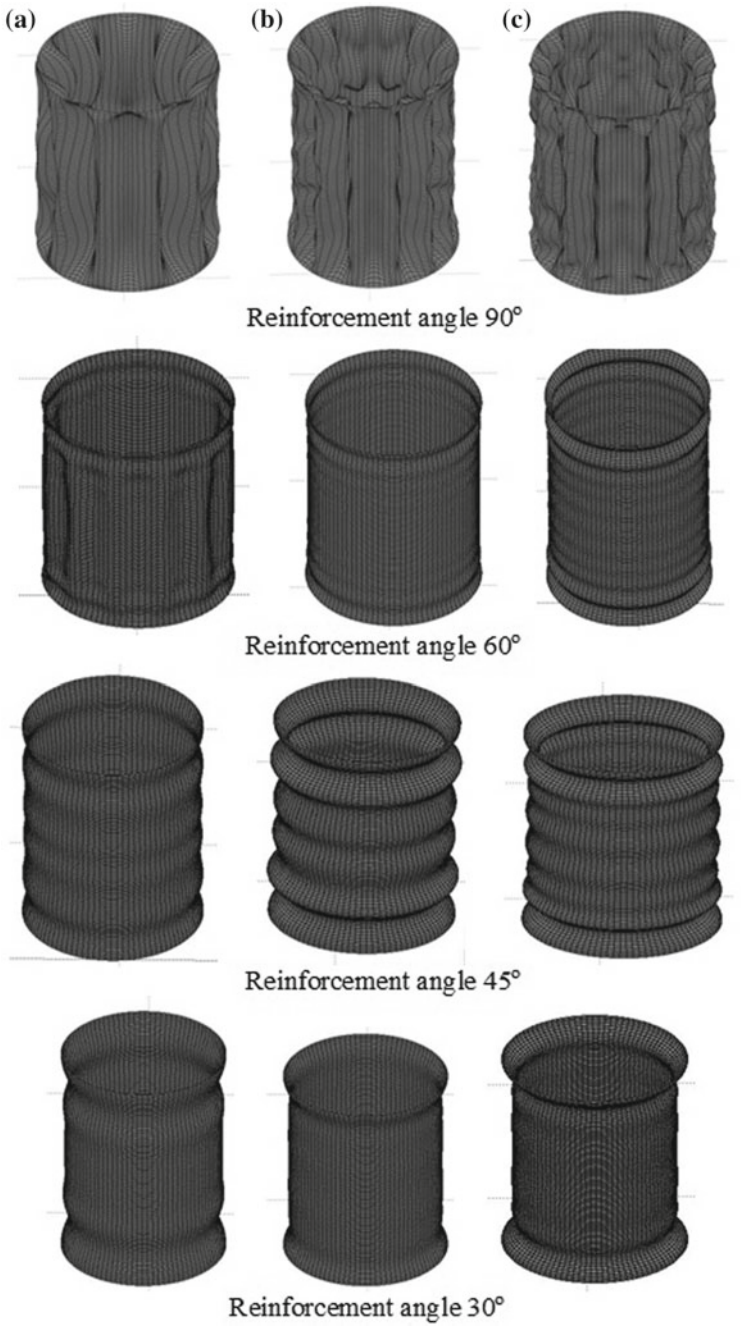

Fig. 4 Characteristic forms of loss of stability of composite cylindrical shells loaded by an external pressure pulse with the rates of: 10 (**a**); 30 (**b**); 50 (**c**) GPa/s

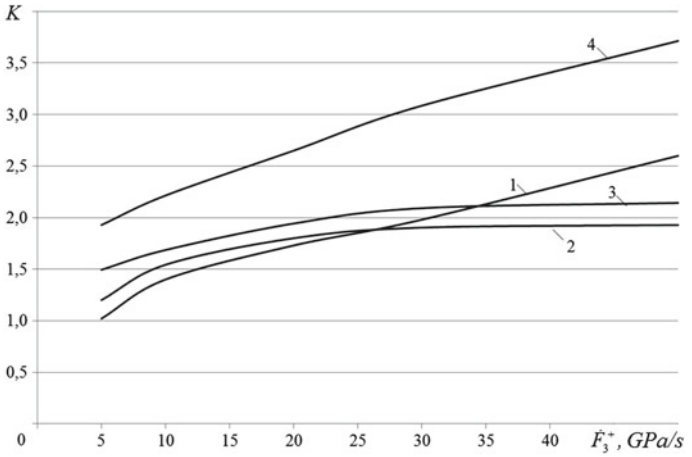

Fig. 5 Dynamic overload factor as a function of pressure pulse rate for different reinforcement angles: 90°(1); 60°(2); 45°(3); 30°(4) relative to the generatrix of the shell

Loss of stability of a dynamically loaded shell with the reinforcement angle of 90° is characterized by the formation of two rows of dimples along the generatrix and the stiffening rib in the middle part of the shell.

Loss of stability of the shells with 60°- and 45°-reinforcement angles is caused by dimples along the entire generatrix of the shell and by increasing their number along the circumference of the shell with the 45°-reinforcement angle. The shell with the 30°-reinforcement angle loses its stability by corrugating.

The shells with the 90° reinforcement angle lose their stability under a combined effect of quasistatic and dynamic loading by forming two or three rows of dimples for the internal pressures of $\dot{F}_3^- = 0.1$ and $\dot{F}_3^- = 0.35$, respectively. The shells with the reinforcement angle of 60° lose their stability by forming dimples along the generatrix of the shell. The characteristic form of loss of stability of the shells with the 45°-reinforcement angle is by corrugating, the number of corrugations increasing with the internal static pressure. The shells with the 30°-reinforcement angle lose their stability by forming ring-shaped wrinkles near the clamped edges of the shell.

A comparative analysis if the deformed geometries of the shells in the process of loss of stability revealed their qualitative differences under static and dynamic loading. Varying the reinforcement angle results in the transformation of characteristic forms of loss of stability of the shell, from the configurations with elongated dimples along the generatrix of the shell to corrugated forms.

The increase in the rate of growth of the external pressure pulse in dynamically loaded composite cylindrical shells results in the increase of the number of waves both in the circumferential and longitudinal directions.

It follows from the obtained results that the loading rate, the level of static preloading and the reinforcement level significantly affect both the value of the dynamic

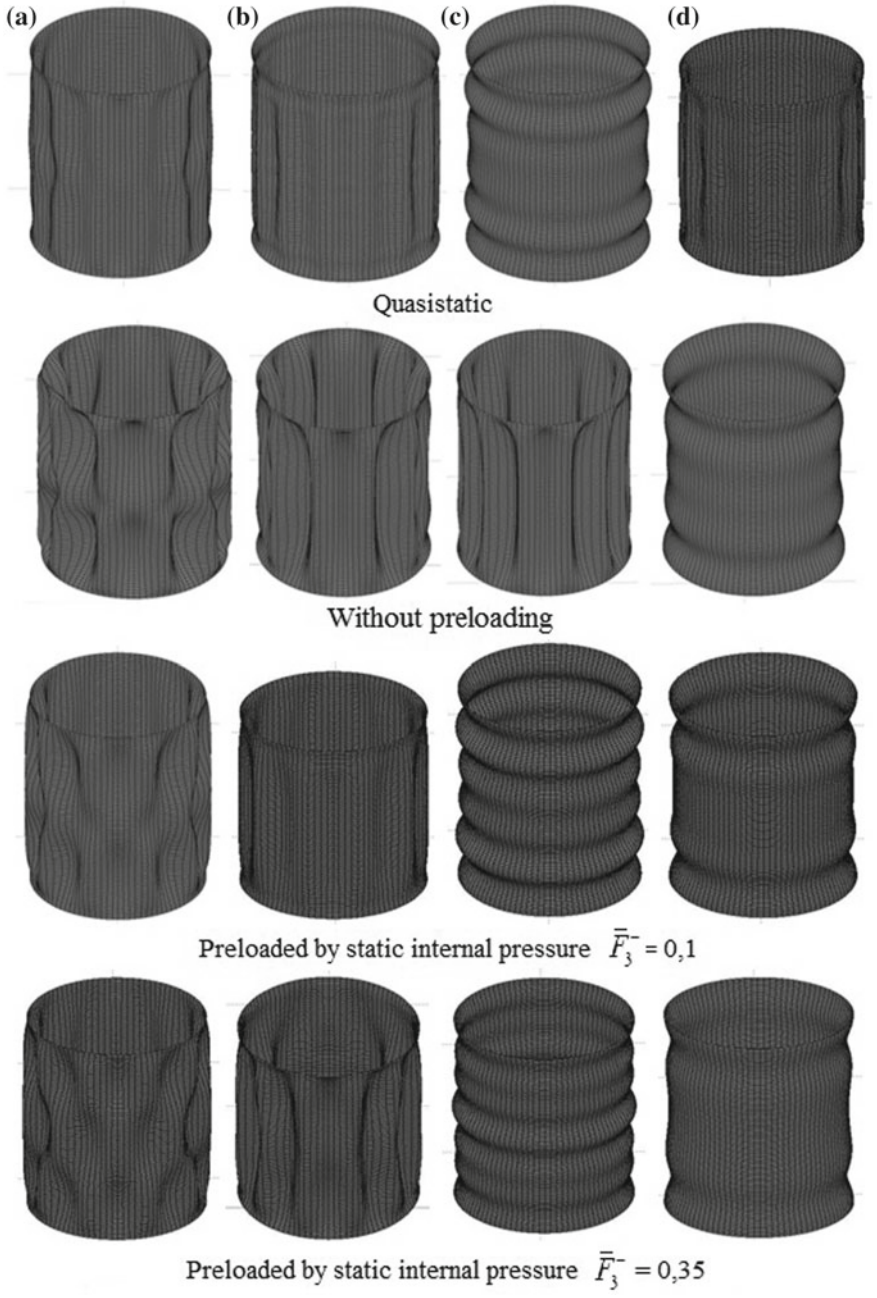

Fig. 6 Characteristic forms of loss of stability of composite cylindrical shells for different reinforcement angles (90°(**a**); 60°(**b**); 45°(**c**); 30°(**d**)) relative to the generatrix of the shell

overload factor and the characteristic forms of waveformation in the process of loss of stability of composite cylindrical shells.

4.2 Numerical Analysis of Loss of Stability of Isotropic and Composite Cylindrical Shells Under Dynamic External Pressure and (or) Axial Compression

The reliability of the introduced methodology was corroborated by comparing the theoretical results with the experimental data on dynamic stability of cylindrical shells loaded by an internal pressure pulse [13]. The shells lost stability by forming six bulges in the circumferential direction. The critical pulse value was computed to be $I_*^T = 1.4 \times 10^3$ Pa·s, while the corresponding experimental value was $I_* = 1.72 \times 10^3$ Pa·s, which testifies to satisfactory agreement between the numerical results and the experimental data. The quantitative difference is evidently due to the imperfections in the measuring scheme (as it is noted in [13]) incomplete adequacy between the numerical scheme and the experimental conditions.

Then, dynamic behavior and loss of stability of a cylindrical shell ($R = 0.072$ m, $R/h = 100$, $L/R = 2$) under uniform compression was considered. The shell was made of aluminum: $E = 77.5$ GPa, $\rho = 2700$ kg/m^3, $\nu = 0.3$, $\sigma_* = 0.16$ GPa, $g = 1$ GPa.

The results of the analysis of elastic and elastoplastic loss of stability of a shell with free ends, loaded by a combination of external pressure and axial compression pulses are given in Figs. 7, and 8.

The curves with odd numbers correspond to the elastoplastic behavior of the shell material and the even ones to the ideally elastic behavior. Curves 1, 2 were computed for purely axial loading with the rate of growth of pressure $V_1 = 1.1 \times 10^3$ GPa/s, curves 3, 4 for loading by external pressure with the rate of $V_3 = 10$ GPa/s, and curves 5, 6 for loading by a combination of pulses of axial compression and external pressure of a triangular form, with the rates of growth of the pressure on the 'ascending' parts being the same as in the case of pure axial compression and external pressure, and the rates on the 'descending' ones being 36 times bigger, and the loading attained its maximum value in $t_* = 3.6 \times 10^{-4}$ s.

It follows from the above results that under combined loading, in the case of elastic deformation, the process of loss of stability starts from the edges of the shell by forming twelve dimples facing the center of the curvature, and then, as the process develops, a belt of twelve dimples is formed in the middle part of the shell, which are shifted a quarter of a wave relative to the edge ones.

In the case of elastoplastic behavior, the process begins with forming ring wrinkles at the edges of the shell; then the number of wrinkles grows, and they shift to the central cross-section of the shell. Later, a belt in the form of a dodecahedral prism is formed in the region of the central cross-section.

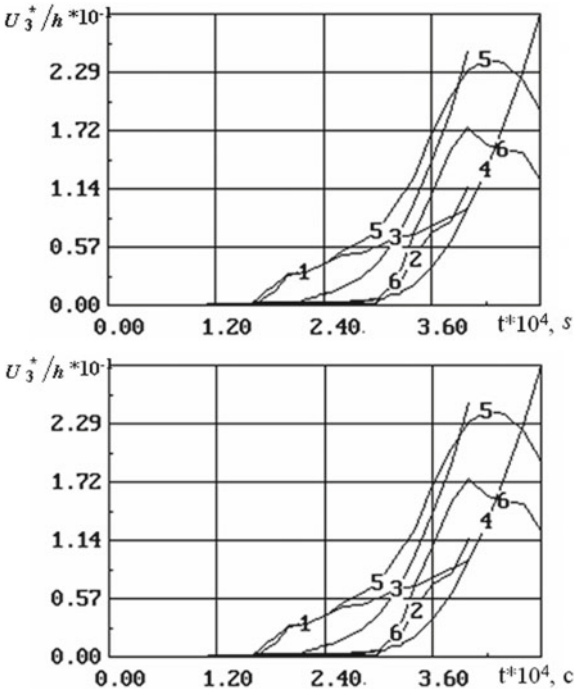

Fig. 7 Time history of the absolute values of maximal deflection of a shell for elastic and elastoplastic behavior of the shell material

From the analysis of the curves depicted in Fig. 7 it follows that accounting for physical nonlinearity results in substantially lower critical values of loading, this effect being more pronounced in the case of combined loading.

Further on, composite cylindrical shells secured on the ends by rigid discs, loaded by linearly increasing radial pressure or axial compression, were considered. The effect of the reinforcement pattern and the shell thickness on the critical value of the load and the character of initial supercritical behavior. The shell had the following geometrical parameters: R = 0.072 m; R/h = 112; L/R = 2.2. The physical-mechanical properties of the shell varied in the following limits: $E_1 = 200$ GPa; $E_2 = E_1/2 \div E_1/30$; $G_{12} = G_{13} = G_{23} = E_2/2$; $\nu_{12} = 0.25$; $\rho = 1800$ kg/m^3 (Figs. 9 and 10).

In the case of circumferential reinforcement, a large number of rhomb-shaped dimples are clearly observed, as compared with the longitudinal reinforcement. An analogous effect is observed for the shells with strongly pronounced anisotropy, reinforced along the generatrix (Fig. 11).

The analysis of the waveformation showed that in this case loss of stability takes place by forming eight elongated dimples along the generatrix for the both reinforcement patterns and is practically independent of the degree of anisotropy of the shell material (Fig. 12).

It is seen that the decrease in the circumferential modulus results in the substantial drop of the critical loads of axial compression and external pressure. With the

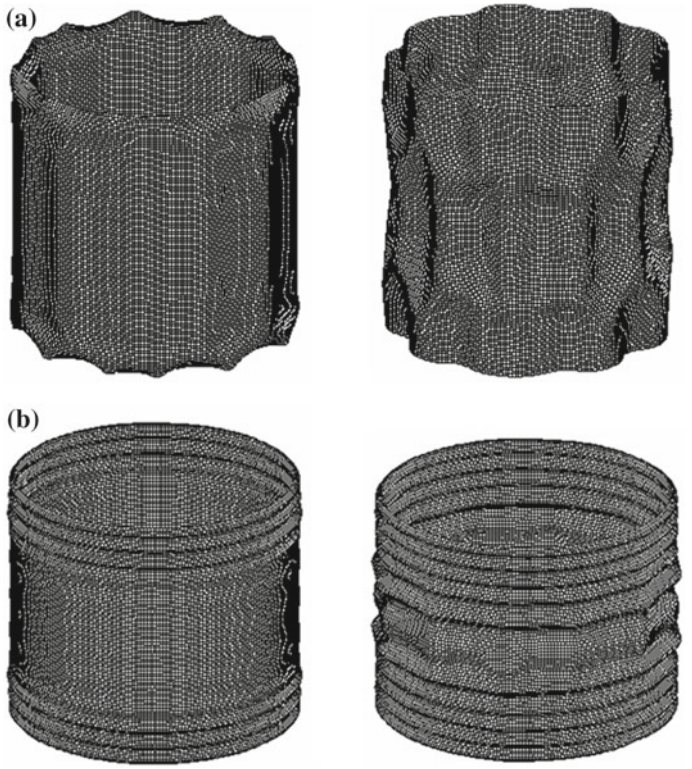

Fig. 8 Characteristic forms of loss of stability under combined loading: for elastic (**a**) and elasto-plastic (**b**) behavior of the shell material

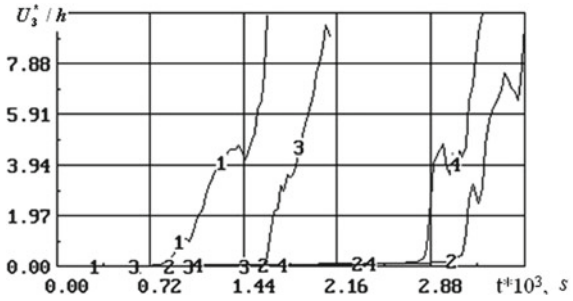

Fig. 9 Time history of maximal deflections for the case of axial loading at a rate of $V_1 = 8$ GPa/s. Curves 1, 2 correspond to longitudinal reinforcement, and curves 3, 4 to the circumferential one; curves 2, 4 were computed for $E_1/E_2 = 2$, and curves 1, 3 for $E_1/E_2 = 30$

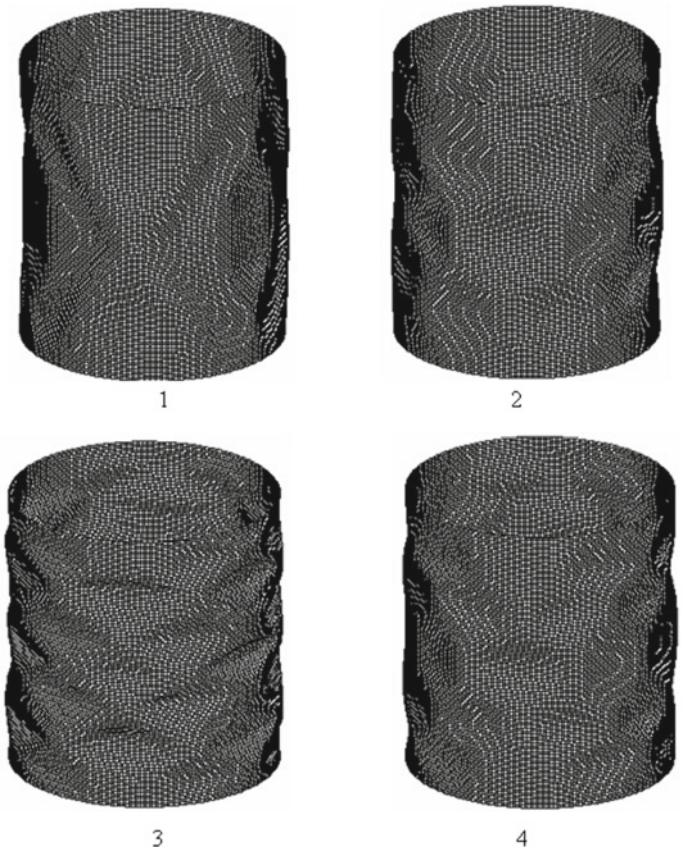

Fig. 10 Characteristic forms of waveformation as a result of loss of stability under axial loading (the numbering of the pictures in the same as that of the curves in Fig. 9)

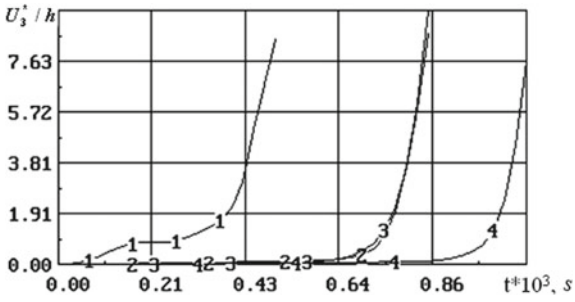

Fig. 11 Time histories of maximal deflections for the case of loading by external pressure at a rate of $V_3 =$ 2 GPa/s (the numbering of the curves is the same as in Fig. 9)

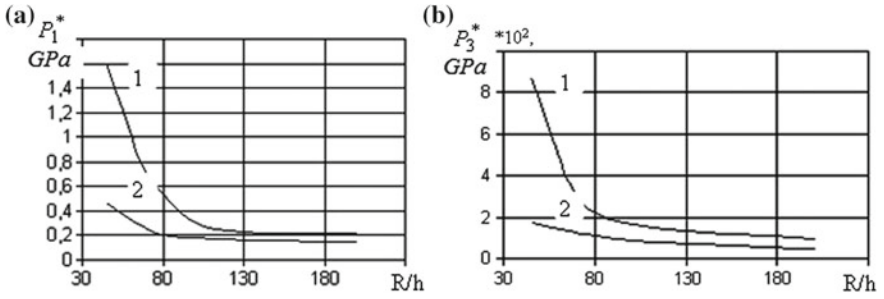

Fig. 12 Critical loads of axial compression (**a**) and external pressure (**b**) as a function of the thickness of the shell reinforced along the generatrix. Curves 1 correspond to $E_1/E_2 = 2$, and curves 2 to $E_1/E_2 = 30$

increasing shell thickness, the effect of the degree of anisotropy of the shell material on the value of the critical load becomes less pronounced.

4.3 Numerical Analysis of Dynamic Buckling of Discretely Stiffened Cylindrical Shells Loaded by Axial Compression and External Pressure

The reliability of the introduced methodology was corroborated by comparing the theoretical results with experimental data on dynamic stability of stiffened cylindrical shells loaded by an external pressure pulse [13]. A comparative analysis was done for elastoplastic shells stiffened by circumferential ribs. The process of loss of stability of the stiffened shells consisted of two stages. First, local loss of stability between the stiffening ribs was observed, then total loss of stability took place, with the formation of waves covering the circumferential ribs. The computed value of the critical pulse for the stiffened shells was equal to $I_*^T = 2.2 \times 10^3$ Pa·s, with the corresponding experimental value being $I_* = 2.52 \times 10^3$ Pa·s. The computational results and the experimental data show satisfactory agreement. The quantitative difference between the numerical and experimental results may be due to inaccuracies in the measuring scheme (as it was noted in [13]) and not complete correspondence between the numerical scheme and the experimental conditions.

The dynamic behavior and loss of stability of a stringer cylindrical section ($R = 0.072$ m, $L/R = 2$, stringers with the cross-section dimensions of $1.6 \cdot 10^{-3}$ m $\times$ $3 \cdot 10^{-3}$ m) with free ends, loaded by linearly increasing external pressure. The structure was made of aluminum: $E = 77.5$ GPa; $\rho = 2700$ kg/m^3; $\nu = 0.3$; $\sigma_* = 0.16$ GPa; $g = 1$ GPa.

The results of analyzing the elastic and elastoplastic deformation of a cylindrical shell stiffened by twenty-four stringers, loaded by external pressure at a rate of $V_3 = 10$ GPa/s, are presented in Figs. 13, 14 and 15.

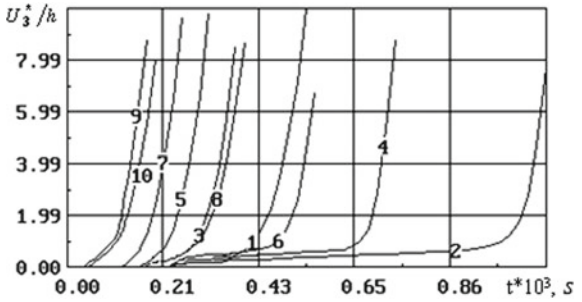

Fig. 13 Time histories of maximal deflections for different thicknesses of the shell of the stringer section. The curves with odd numbers 1, 3, 5, 7, 9 correspond to elastoplastic behavior of the shell and the stiffening elements, calculated for R/h = 50, 75, 100, 125, 250, respectively; the analogous curves with even numbers 2, 4, 6, 8, 10 correspond to elastic deformation of the structure

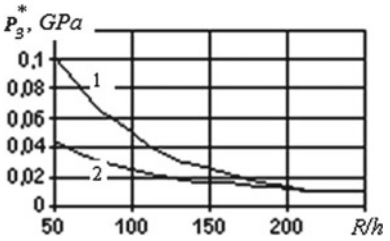

Fig. 14 Values of critical pressure for elastic (curve 1) and elastoplastic (curve 2) behavior of the material of the structure as a function of the shell thickness

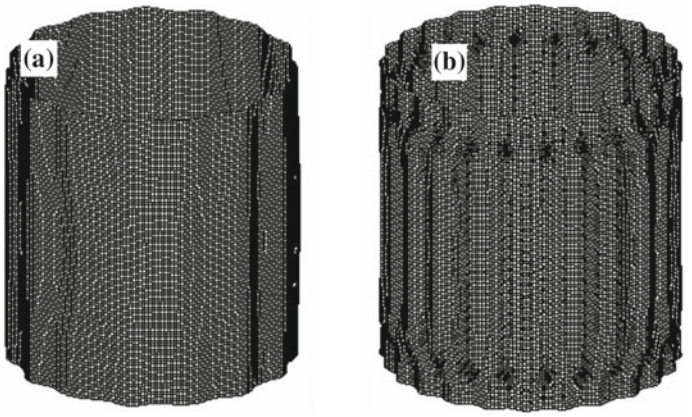

Fig. 15 Characteristic forms of loss of stability for elastic (**a**) and elastoplastic (**b**) deformation of the structures with the shell thickness of R/h = 100

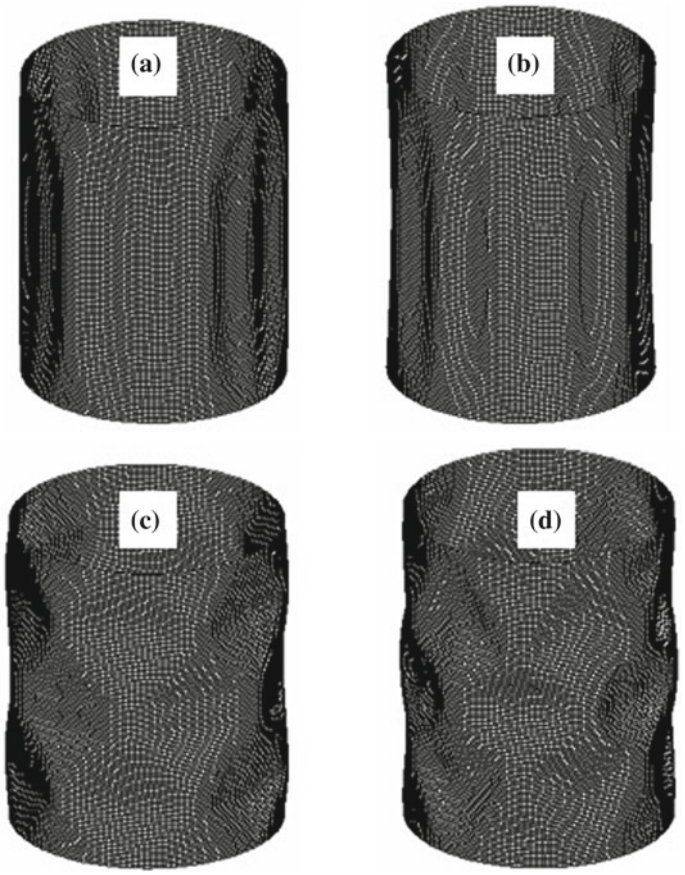

Fig. 16 Characteristic forms of loss of stability of a shell stiffened with six stringers: **a**, **b** after loading by external pressure at a rate of $V_3 = 2$ GPa/s, **c**, **d** after loading by axial compression at a rate of $V_1 = 36$ GPa/s; **a**, **c** computed using the model with discrete spacing of stringers, **b**, **d** using the structurally orthotropic theory

The analysis of loss of stability shows that, in the case of elastic deformation of the material of the structure, loss of stability results in the formation of elongated bulges along the generatrix of the cylinder. For $R/h = 50$, the stringer section transforms into a regular hexagonal prism, while with the decreasing shell thickness the number of the form of loss of stability increases and, beginning with $R/h \geq 150$, the structure loses its stability by arching, the stiffening stringers acting as intermediate supports.

In the case of elastoplastic behavior of the structural material, loss of stability by arching is characteristic both for the shells of medium thickness $R/h \leq 75$, and for the thin enough ones, $R/h \geq 125$. In the intermediate range of shell thicknesses, $125 \leq R/h \leq 75$, loss of stability takes place in the form of the 'Chinese lantern' (see Fig. 15 б). In the case of loading with high rates of growth of external pressure, the

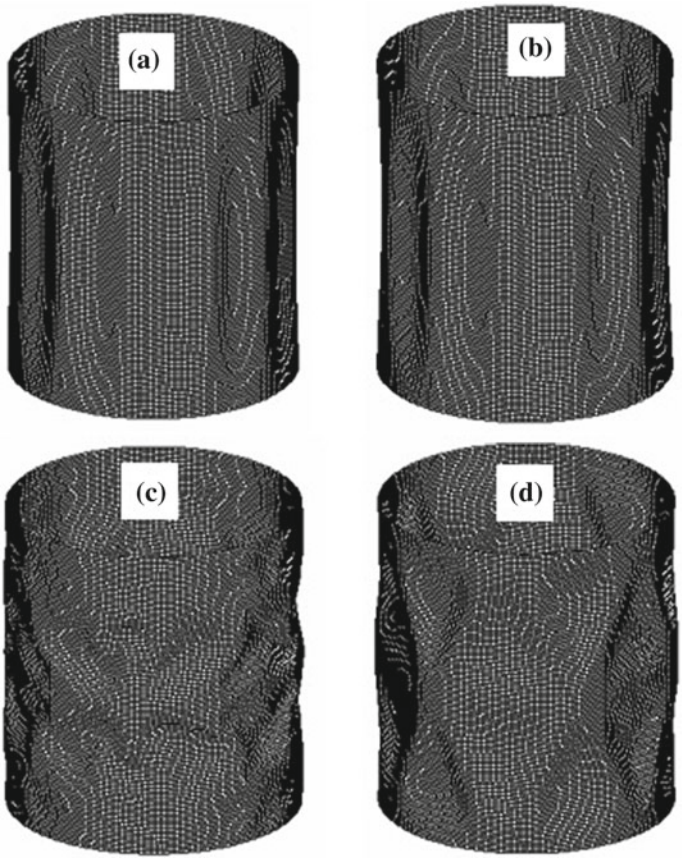

Fig. 17 Characteristic forms of loss of stability of a shell stiffened with twenty-four stringers: **a**, **b** after loading by external pressure at a rate of $V_3 = 2$ GPa/s, **c**, **d** after loading by axial compression at a rate of $V_1 = 36$ GPa/s; **a**, **c** computed using the model with discrete spacing of stringers, **b**, **d** using the structurally orthotropic theory

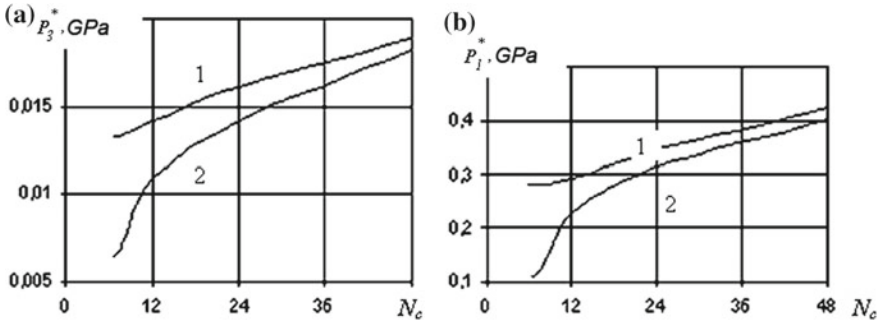

Fig. 18 Critical values of external pressure (**a**) and axial compression (**b**) as a function of stiffening stringers (curve 1 corresponds to the discrete model, curve 2—to the structurally orthotropic theory)

length of the bulges in the middle part of the 'Chinese lantern' decreases, and three rows of dimples are formed. It follows from the obtained results that, in computing critical values of external pressure on a stringer-stiffened cylindrical shell, taking account of the physical nonlinearity becomes necessary beginning with R/h $\leq$ 200.

The conducted investigations and the experimental results [13, 20] on dynamic stability of rib-stiffened cylindrical shells under nonstationary external pressure testify to the fact that spacing between the stiffening elements, as well as their stiffness, affect the process of dynamic buckling and, in particular, the dominating form of loss of stability (general or local), in a rather complex way. However, by now, the overwhelming majority of theoretical results have been obtained when analyzing ribbed shells according to a structurally orthotropic model. The scope of such approach, as a rule, remains unidentified.

In what follows, a comparative analysis of the loss of stability forms and critical values of axial compression and external pressure is given for a stringer cylindrical shell, computed in the framework of the structurally orthotropic theory and a model with discrete spacing of stringers. The geometrical parameters of a stringer cylindrical section were as follows: R = 0.072 m; R/h = 100; L/R = 2; the cross-sectional dimensions of the stringers were $1.6 \cdot 10^{-3} \times 3 \cdot 10^{-3}$ m. The structure was made of aluminum: $E = 77.5$ GPa; $\rho = 2700$ kg/m^3; $\nu = 0.3$; $\sigma_* = 0.16$ GPa;. $g = 1$ GPa. On its ends, the structure was secured with rigid discs (Figs. 16, 17 and 18).

It follows from the results obtained that, when the number of stringers is less that twenty four, the structurally orthotropic scheme not only yields qualitatively different forms of loss of stability as compared with the discrete model, but also substantially underestimates critical loading values.

5 Conclusion

Based on the results of the conducted studies, the following can be concluded. Internal static pressure results in substantially increasing the critical load of loss of stability of cylindrical shells. The number of waves both in the circumferential and longitudinal directions of the shell tends to increase with the loading rate. The characteristic form of the deformed configuration in the process of loss of stability strongly depends on the reinforcement angle.

The analysis of stability of isotropic shells has shown that taking into account physical nonlinearities leads to substantially decreasing critical loads, this effect being more pronounced in the case of combined loading.

It was concluded from the analysis of stability of composite shells that decreasing the circumferential modulus leads to a considerable drop of critical values of axial compression and external pressure. The effect of the degree of anisotropy of the shell material on the critical loading value increases with the shell thickness.

In analyzing critical values of external pressure for stringer-stiffened cylindrical shells, accounting for physical nonlinearities becomes necessary beginning with R/h

≤ 200. The structurally orthotropic scheme not only yields qualitatively different forms of loss of stability, as compared with the discrete model, but also substantially underestimates critical loading values.

Acknowledgements The work was done with financial support from the Federal Program 'Researches and developments in the priority directions of developing the scientific-technological complex in Russia in the years of 2014-2020' under the Contract № 14.578.21.0246 (unique identification No RFMEFI57817X0246).

References

1. Volmir, A.S.: Nelineynaya dinamika plastinok i obolochek. (in Rus.). Nauka, 432 (1972)
2. Grigolyuk, E.I., Selezov, I.T.: Mehanika tverdyh deformiruemyh tel. (in Rus.). 5. Neklassicheskiye teorii kolebaniya sterzhney, plastin i obolochek. Itogi nauki i tehn. VINITI AN SSSR. Nauka (1973)
3. Pertsev, A.K., Platonov, E.G.: Dinamika obolochek i plastin. (in Rus.) L.: Sudostroyeniye, 317 (1987)
4. Lugovoy, P.Z.: Dinamika obolochechnyh konstruktsyi pri impulsnyh nagruzkah (obzor) (in Rus.). Prikladnaya Mehanika. 26. № 8, 3–20 (1990)
5. Amiro, I.Y., Zarutskiy, V.A., Palamarchuk, V.G.: Dinamika rebristyh obolochek. (in Rus.) Kiyev: Naukova dumka, 204 (1983)
6. Dudchenko, A.A., Lurye, S.A., Obraztsov, I.F.: Anizotropnye mnogosloynye plastiny i obolochki (in Rus.). Itogi nauki n tehn. Ser. Mehanika deformiruyemogo tverdogo tela. VINITI. 15. 3–68 (1983)
7. Bogdanovich, A.E.: Helineynye zadachi dinamiki tsilindricheskih kompozitnyh obolochek. (in Rus.) – Riga: Zinatne, 295 (1987)
8. Abrosimov, N.A., Bazhenov, V.G., Elesin, A.V.: Chislennyi analiz dinamicheskogo deformirovaniya I poteri ustoichivosti kompozitnyh obolochek vrasheniya pri impulsnom hagruzhenii (in Rus.). Mehanika kompozitnyh materialov. 31. № 1. 65–71 (1995)
9. Christoforou, A.P., Swanson, S.R.: Analysis of Simply-Supported Ortotropic Cylindrical Shells Subject to Lateral Impact Loads. Transaction of the ASME. J. Appl. Mech. **57**, 376–382 (1990)
10. Manevich, L.I., Mihailov, G.V., Pavlenko, I.D., Prokopalo, E.F.: Issledovaniye ustoychivosti obolochek pri sovmestnom deystvii staticheskih i dinamicheskih nagruzok (in Rus.). Prikladnaya mehanika. XIII. № 1, 27–32 (1977)
11. Baskakov, V.N., Kostoglotov, A.I., Shvetsova, L.A.: Issledovaniye dinamicheskoy ustoycivosti gladkih tsilindricheskih obolochek. (in Rus.) Problemy prochnosti. № 5, 31–33 (1982)
12. Bendyukov, V.V., Deryushev, V.V.: Dinamicheskaya korotkovolnovaya neustiychivost tonkostennyh tsilindricheskih obolochek pri lokalnom deystvii impulse vneshnego davleniya (in Rus.). Problemy prochnosti. № 4, 36–43 (1995)
13. Andreyev, L.V., Krushelnitskiy, I.N., Pavlenko, I.D., Privarnikov, Y.K., Prokopalo, E.F.: Dinamicheskaya ustoychivost podkreplennyh tsilindricheskih obolochek pri nagruzhenii impulsom vneshnego davleniya (in Rus.). Izv. AN SSSR. Mehanika tverdogo tela. № 1, 118–125 (1974)
14. Kostoglotov, A.I., Bendyukov, V.V., Deryushev, V.V., Shevtsova, L.A.: Issledovaniye protsessa poteri ustoychivosti gladkih tonkostennyh tsilindricheskih obolochek pri lokalnom deystvii impulse izlucheniya (in Rus.). Problemy prochnosti. № 5, 56–62 (2004)
15. Abrosimov, N.A., Elesin, A.V.: Chisslennyi analiz dinamicheskogo deformirovaniya i poteri ustoychivosti predvaritelno napryazhennyh kompozitnyh tsilindricheskih obolochek (in Rus.). Problemy prochnosti I plastichnosti. 79. № 4, 375–386 (2017)

16. Bogdanovich, A.E., Koshkina, T.B.: Deformirovaniye i prochnost ortotropnyh tsilindricheskih obolochek, podkreplennyh prodolnymi rebrami zhestkosti, pri dinamicheskih szhimayushih nagruzkah (in Rus.). Mehanika kompozit. materialov. № 5, 866–876 (1984)
17. Bogdanovich, A.E.: Resheniye nelineynyh zadach dinamicheskogo vypuchivaniya podkreplennyh sloistyh tsilindricheskih obolochek (in Rus.). Prikl. Mehanika. 22. № 8, 57–66 (1986)
18. Myshonkov, A.K.: Dinamicheskoye povedeniye rebristoy obolochki pri deystvii bokovoy impulsnoy nagruzki (in Rus.). Prikl. mehanika. 22. № 7, 49–53 (1986)
19. Meysh, V.F.: Nelineynoye deformirovaniye prodolno podkreplennyh orto-tropnyh tsilindricheskih obolochek pri nestatsionarnyh nagruzkah (in Rus.). Mehanika kompozitnyh materialov. 29. № 2, 184–190 (1993)
20. Andreev, L.V., Dubovik, O.N., Dyshko, A.L., Pavlenko, I.D.: Priblizhyonnye otsenki kriticheskogo impulse tsilindricheskoy obolochki, podkreplennoy prodol-nymi diskretnymi rebrami. Problemy prochnosti. № 3, 66–69 (1978)
21. Skurlatov, E.D.: Eksperimentalnoye issledovaniye povedeniya tsilindricheskih obolochek pri dinamicheskih nagruzkah (in Rus.). Problemy prochnosti. № 9, 79–83 (1972)
22. Skurlatov, E.D.: Eksperimentalnoye issledovaniye ustoychivosti tsilindricheskih obolochek pri deystvii podvizhnyh nagruzok (in Rus.). Rudy vsesoyuznoy konferentsii po teorii plastin i obolochek. Nauka, 565–568 (1973)
23. Vasilyev, V.V.: Mehanika konstruktsyi iz kompozitnyh materialov. (in Rus.). Mashinostroyenie, 272 (1988)
24. Novozhilov, V.V.: Osnovy nelineynoy teorii obolochek. (in Rus.), L.: Gostehizdat, 212 (1948)
25. Ishlinskiy, A.Y.: Obshaya teoriya plastichnosti s lineynym uprochneniyem (in Rus.). Ukr. mat. Zhurn. № 6, 314–325 (1954)
26. Abrosimov, N.A., Bazhenov, V.G.: Nelineynye zadachi dinamiki kompozitnyh konstrukstyi. (in Rus.). N.Novgorod: Izd-vo NNGU, 400 (2002)
27. Marchuk, G.I.: Metody vychislitelnoy matematiki. (in Rus.) Nauka (1980)
28. Flanagan, D.P., Belytschko, T.: A uniform strain hexahedron and quadrilateral with orthogonal hourglass control. Int. J. Num. Meth. Eng. **17**(5), 679–706 (1981)

Analytical Buckling Analysis of Cylindrical Shells with Elliptic Cross Section Subjected to External Pressure

Igor I. Andrianov and Alexander A. Diskovsky

Abstract An analytical algorithm for studying the stability of a cylindrical shells with elliptic cross section subjected to external pressure is proposed. It is based on perturbation procedure. The mentioned buckling problem can be solved using FEM. However, FEM solutions may be less manageable, for instance, in terms of optimal design, than the associated approximate analytical models. The approximate formulas obtained are sufficiently accurate and can be used in engineering practice.

1 Introduction

Cylindrical shells with elliptic cross section (ECSh) are frequently used in the manufacturing of aircrafts, missiles, boilers, pipelines, automobiles, and some submarine structures [1]. We can mention fuselage or tank of hypersonic aircraft [2]. Elliptic steel hollow sections are used as element of modern building façade [3]. In recent years, hot-rolled elliptical hollow sections have attracted significant attention from engineers and architects owing to their complementary qualities of aesthetic appearance and structural efficiency. Hot-rolled and cold-formed structural steel tubular members of elliptical cross-section are widely used in the civil engineering [4, 5]. In addition, it often occurs that shells designed to be circular cylindrical deviate measurably from perfect circularity once they are fabricated. Laterally loaded cylindrical clusters have been effectively employed as energy dissipators in impact attenuation devices [6]. ECSh can be made from composite, sandwich or functionally graded materials and reinforced by ribs [1, 7–10].

Numerical studies of ECSh use variational methods: Bubnov-Galerkin [8, 11], Kantorovich with trigonometrical basis functions in axial [12–14] or circumferential

I. I. Andrianov (✉)
RheinEnergie AG, Parkgürtel 24, 50823 Cologne, Germany
e-mail: i.andrianov@rheinenergie.com

A. A. Diskovsky
Dnipro State University of Internal Affairs, Gagarina Ave 26, Dnepr 49005, Ukraine
e-mail: alex_diskovskiy@ukr.net

H. Altenbach et al. (eds.), *Recent Developments in the Theory of Shells*,
Advanced Structured Materials 110, https://doi.org/10.1007/978-3-030-17747-8_3

direction [2, 9, 15], FEM [3]. The finite-difference method is also used [16–18], in [17] it is used in conjunction with energy minimization.

The mentioned buckling problem can be solved using FEM. However, FEM solutions may be less manageable, for instance, in terms of optimal design, than the associated approximate analytical models. An analytical study of the stability of ECSh was carried out by Babenko on the basis of Pogorelov's geometric method [19–21]. In these papers it is shown how a regular classical buckling mode becomes local in the circumferential direction for the load less than the classical buckling load. It leads to the localization of the postbuckling behavior in the vicinity of the weak generatrix of the middle surface. On the basis of this result it is proposed to calculate the stability of ECSh replacing it with a circular cylindrical shell of the maximum radius of curvature. Numerically and experimentally, this approach has been confirmed in [12–14] and [14, 22] respectively.

Theoretical and experimental research showed two mechanisms of buckling: bifurcation and collapse. It can be concluded that nonlinear effects are important for this type of shell and that a linear bifurcation type of analysis should be used with caution for shells with a radius of curvature to thickness ratio R_0/h less than 270 [18]. It would appear that for $R_0/h < 270$, a bifurcation buckling should give good results and for $R_0/h > 270$ a nonlinear analysis should be used. With the use of bifurcation buckling analysis, the assumption of membrane prebuckling state gives good results [11, 14, 18].

Many studies [23, 24] showed, that ECSh are much less sensitive to imperfections, a sentence that was in sharp contrast to the significant imperfection sensitivity of circular cylindrical shells.

Experimental results are described in [9, 11, 14, 15, 22]. As a rule, the experimental values of buckling pressure are lower than theoretical ones. It is noted that the elliptical cross section tends under the action of the pressure to the circular one, and the critical load for ECSh is higher than for the circle cylindrical shell with the same cross section perimeter.

In this paper perturbation procedure is used for construction of simple expressions, described a linear bifurcation type of buckling of cylindrical shells with elliptic cross section. The remainder of the paper is organized as follows. In Sect. 2 we analyse characteristics of the elliptic cross section. Semimembrane theory is applied in Sect. 3. In Sect. 4 we use perturbation procedure. Comparison with known numerical and experimental results is given in Sect. 5. Finally, concluding remarks are presented in Sect. 6.

2 Characteristics of the Elliptic Cross Section

It is well known that the ellipse radius $R(\alpha)$ and curvature $\kappa(\alpha)$ are given by [3]

$$R(\alpha) = \frac{A}{b}(\sin^2\alpha + b^2\cos^2\alpha)^{3/2}; \kappa(\alpha) = 1/R(\alpha),$$

where $b = B/A; A$ and B are the major and minor axis width values, respectively, and α is the angle from the ellipse centre.

Instead of considering the ellipse centre angle α, one may use the tangential angle θ between the normal at any given point, for instance P and the major axis $\theta = \arctan(b \tan \alpha)$. One can easily express the exact radius $R(\theta)$ and curvature $\kappa(\theta)$ by means of the following Fourier cosine series

$$R(\theta) = R_0[1 + \sum_1 r_{2k} \cos(2k\theta)]; \kappa(\theta) = \kappa_0[1 + \sum_1 \lambda_{2k} \cos(2k\theta)];$$
$$R_0 = \frac{1}{2\pi} \int_0^{2\pi} R(\theta) d\theta; r_{2k} = \frac{1}{2\pi R_0} \int_0^{2\pi} R(\theta) \cos(2k\theta) d\theta;$$
$$\kappa_0 = \frac{1}{2\pi} \int_0^{2\pi} \kappa(\theta) d\theta; \lambda_{2k} = \frac{1}{2\pi \kappa_0} \int_0^{2\pi} \kappa(\theta) \cos(2k\theta) d\theta, k = 1, 2, \ldots \quad (1)$$

It can be mentioned fast decrease of the coefficients in the Fourier series. E.g., for $A/B = 1.5$ one obtains [3]

$$R(\theta) = R_0[1 - 0.59 \cos(2\theta) + 0.15 \cos(4\theta) - 0.034 \cos(6\theta) + 0.0077 \cos(8\theta) - \ldots]. \quad (2)$$

It is obvious that (2) are alternating series with rapidly decreasing terms.

3 Semimembrane Theory

The prebuckling state is assumed to be momentless, which is completely justified for a sufficiently long shell [25], viz.

$$L \gg \sqrt{hR_0}, \quad (3)$$

where h, L are the shell thickness and length.

The circumferential stress is [25].

$$\sigma_\theta = \frac{QR(\theta)}{h}. \quad (4)$$

For simplification of stability equation semimembrane theory is used. It can be obtained using Vlasov assumptions [26] and justified due asymptotic procedure [27]. Semimomentous stability equation can be written as follows [26]:

$$\frac{Eh^2}{12(1-\nu^2)}\frac{\partial^8 W}{\partial s^8}+\frac{QR(\theta)}{h}\frac{\partial^6 W}{\partial s^6}+E\kappa^2(\theta)\frac{\partial^4 W}{\partial x^4}=0,$$
$$s=\int_0^\theta R(\theta)d\theta, \tag{5}$$

where W is the normal displacement, E, v are the Young modulus and the Poisson coefficient of the shell material, Q is the lateral external pressure, x is the longitudinal coordinate.

In addition to simplifying the original shell equation, it is necessary to simplify the boundary conditions. The splitting of the boundary conditions, given in [27], leads to an important conclusion: in the first approximation, the edge effect for sufficiently long shell does not affect the magnitude of the buckling load. For simply supported shell

$$\text{at } x=0, L \quad T_1=0, V(T_{12})=0, W=0, \frac{\partial^2 W}{\partial x^2}=0 \tag{6}$$

boundary conditions for Eq. (5) take the form [27]:

$$\text{at } x=0, L \quad W=0, \frac{\partial^2 W}{\partial x^2}=0. \tag{7}$$

In (6) T_1, T_{12} are the membrane forces, V is the circumferential displacement.

4 Perturbation Solution of Eigenvalue Problem

Eigenvalue problem (5), (7) allows separation of variables

$$W=w(s)\sin(\frac{\pi x}{L}). \tag{8}$$

Then one obtains

$$\frac{Eh^2}{12(1-\nu^2)}\frac{d^8 w}{ds^8}+\frac{QR_0[1+\sum_1 r_{2k}\cos(2k\theta)]}{h}\frac{d^6 w}{ds^6}+\frac{E\pi^4}{L^4R_0^2}[1+2\sum_1\lambda_{2k}\cos(2k\theta)]w=0,$$
$$w(s)=w(s+2\pi R_0). \tag{9}$$

Let us introduce homotopy small parameter ε and represent the eigenfunction w and eigenvalue Q in the following form

$$w = w_0 + \varepsilon w_1 + \varepsilon^2 w_2 + \ldots; \; Q = Q_0 + \varepsilon Q_1 + \varepsilon^2 Q_2 + \ldots \tag{10}$$

In recent years the so-called homotopy perturbation method has received large attention (the term "method of artificial small parameters" is also used). Its essence is as follows. In the boundary value problem (BVP) the parameter is introduced so that for $\varepsilon = 0$ one obtains a BVP which admits a simple solution, and for $\varepsilon = 1$ one obtains the governing BVP. Then the perturbation method regarding ε is apllied and we put $\varepsilon = 1$ in the final formula [28].

Now regular perturbation procedure for eigenvalue problems [29, 31] is used. After substitution Ansatz (10) in eigenvalue problem (9) and splitting with respect to powers of ε one obtains:

$$\frac{Eh^2}{12(1-\nu^2)}\frac{d^8 w_0}{ds^8} + \frac{Q_0 R_0}{h}\frac{d^6 w_0}{ds^6} + \frac{E\pi^4}{L^4 R_0^2} w_0 = 0, \tag{11}$$

$$\frac{Eh^2}{12(1-\nu^2)}\frac{d^8 w_1}{ds^8} + \frac{Q_0 R_0}{h}\frac{d^6 w_1}{ds^6} + \frac{Q_1 R_0}{h}\frac{d^6 w_0}{ds^6} + \frac{E\pi^4}{L^4 R_0^2} w_1$$
$$= -[\frac{Q_0 R_0}{h}\frac{d^6 w_0}{ds^6}\sum_1 r_{2k}\cos(2k\theta) + \frac{2E\pi^4}{L^4 R_0^2} w_0 \sum_1 \lambda_{2k}\cos(2k\theta)],$$
$$\ldots \tag{12}$$

$$w_i(s) = w_i(s + 2\pi R_0), \qquad i = 0, 1, 2, \ldots \tag{13}$$

The eigenvalue problem (11), (13) is self-adjoint, which solution can be found in the following form:

$$w_0(s) = C \; \sin(\frac{ns}{R_0}), \tag{14}$$

$$\frac{Q_0^{(n)}}{E\delta} = \frac{\delta^2 n^2}{12(1-\nu^2)} + \frac{\pi^4}{n^6 l^4}, \tag{15}$$

where $\delta = h/R_0, l = L/R_0$.

The minimal eigenvalue is determined by the expression

$$Q_{0\min} = Q_0^{(n^*)} = \min_{n \subset \mathbb{N}} Q_0^{(n)}. \tag{16}$$

For practically important cases $n^* >> 1$, this allows for a minimization analytically and the familie Southwell-Papkovich formula [31] is obtained

$$\frac{Q_0}{E\delta} = \frac{\sqrt{6}\pi\delta^{1.5}}{9l(1-\nu^2)^{3/4}}, \quad n = \left[\sqrt[4]{6\pi^2\sqrt{1-\nu^2}l^{-2}\delta^{-1}}\right]. \tag{17}$$

Here […] denotes integer part of (…).

In accordance with the regular perturbation procedure for eigenvalue problems [29, 30], the equation of the first approximation (12) is multiplied by $w_0(s)$ and is integrated in respect to s from 0 to $2\pi R_0$. Taking into account that eigenvalue problem (12), (13) is self-adjoint, one obtains

$$\frac{Q_1^{(n)}}{E\delta} = \frac{Q_0^{(n)} r_{2n}}{4E\delta} - \frac{\pi^4 \lambda_{2n}}{2l^4 n^6}. \tag{18}$$

We note an important circumstance. In the first approximation, the correction to the eigenvalue is determined by the resonant harmonic of the Fourier series with the number $2n$. Using the expressions of the zero (15) and first (18) approximations and suppose $\varepsilon = 1$, we obtain a simple approximate formula for calculating the buckling load of a cylindrical shell with the elliptic cross section subjected to external pressure.

$$Q \approx \min_{n \subset \mathbb{N}} (Q_0^{(n)} + Q_1^{(n)}). \tag{19}$$

As is known, semimembrane equations are not very accurate for very long shells, when shell can be treated as ring [31]. Stability equation for ring can be written in the following form

$$\frac{Eh^2}{12(1-\nu^2)} \left(\frac{d^2}{ds^2} + \frac{1}{R^2} \right)^2 \frac{d^4 W}{ds^4} + \frac{QR}{h} \left(\frac{d^2}{ds^2} + \frac{1}{R^2} \right)^2 \frac{d^2 W}{ds^2} = 0. \tag{20}$$

Using above explained perturbation procedure one obtains buckling load for elliptic ring

$$\frac{Q}{E\delta} = (1 + \frac{r_4}{4}) \frac{\delta^2}{3(1-\nu^2)}, n = 2. \tag{21}$$

5 Proof of Accuracy

To verify the obtained formulas, let us compare our calculations with experimental results (ER) [11], the Bubnov-Galerkin approach (BGA) [11], and finite-difference method (FD) [17].

Yao and Jenkins obtained buckling pressures from tests on simply supported polyvinyl chloride shells [11]. They compared the test results with a theory in which the prebuckled state is calculated from linear membrane theory. Buckling pressures are obtained from an eigenvalue problem based on the Bubnov-Galerkin method. By virtue of known theorems of the calculus of variations, this method gives upper bounds for the first eigenvalue.

Table 1 A/B = 1.5

δ	l	q ER [11]	q BGA [11]	q FD [17]	(18)
0.00282	1.485	1.28	1.21	1.46	1.30
0.00728	0.00728	1.188	5.29	5.67	5.65
0.0134	1.485	11.83	14.30	13.86	14.40

Bushnell used BOSOR3 code based on FD approximation [17]. It was shown that the prebuckling stress distributions are very similar to those predicted by membrane theory. Cross section shape changing also does not play any significant role.

We calculate nondimensional quantity $q = 10^4(1-\nu^2)lQ$ and suppose, in accordance with experiment [11], $\nu = 0.37$. Numerical results are presented in Table 1 (for A/B = 1.5).

One can see sufficient accuracy of obtained approximate solution.

6 Concluding Remarks

Modern codes using FEM make it possible to easily obtain numerical solutions to problems of buckling of a cylindrical shell with elliptic cross section subjected to external pressure. However, FEM solutions may be less manageable, for instance, in terms of optimal design, than the associated approximate analytical models. These analytical models must be simple, informative and accurate. Formula (19) satisfies these requirements. Of course, one must remember the limitations imposed by the approximate model used: $L >> \sqrt{hR_0}$, $1 >> h/R_0$.

References

1. Soldatos, K.P.: Mechanics of cylindrical shells with non-circular cross-section: a survey. Appl. Mech. Rev. **52**, 237–274 (1999)
2. García, J.G., Albus, J., Reimerdes, H.-G.: Static and stability behaviour of elliptical cylindrical shells under combined mechanical and thermal loads. In: Spacecraft Structures, Materials and Mechanical Engineering, Proceedings of the Conference held by ESA, CNES and DARA in Noordwijk, 27–29 March 1996. Edited by W.R. Burke. ESA SP-386. Paris: European Space Agency (ESA), 1996, pp. 295–303 (1996)
3. Silvestre, N.: Buckling behaviour of elliptical cylindrical shells and tubes under compression. Int. J. Solids Struct. **45**, 4427–4447 (2008)
4. Ruiz-Teran, A.M., Gardner, L.: Elastic buckling of elliptical tubes. Thin-Walled Struct. **46**, 1304–1318 (2008)
5. Chan, T.M., Gardner, L., Law, K.H.: Structural design of elliptical hollow sections: a review. Proc. Inst. Civil Eng. Struct. Build. **163**(6), 391–402 (2010)

6. Wu, L., Carney, J.F.: Initial collapse of braced elliptical tubes under lateral compression. Int. J. Mech. Sci. **39**(9), 1023–1036 (1997)
7. Allakhverdiev, Dzh.É., Amenzade, R.Yu., Shikhlinskaya, G.T.: Numerical analysis of problems of loss of stability of transversely inhomogeneous cylindrical shells with noncircular contour and its comparison with the asymptotic solution. Mech. Comp. Mat. **26**, 94–97 (1990)
8. Slepov, B.I.: Vibrations and stability of anisotropic and sandwich cylindrical shells of arbitrary cross section. In: Theory of Shells and Plates: Proceedings of the 4th All-Union Conference on Shells and Plates, Erevan, 24–31.10.1962. Jerusalem, Israel Program for Scientific Translations, pp. 826–834 (1966)
9. Meyers, C.A., Hyer, M.W.: Response of elliptical composite cylinders to internal pressure loading. Mech. Compos. Mater. Struct. **4**, 317–343 (1997)
10. Duc, N.D., Tuan, N.D., Tran, P., Cong, P.H., Nguyen, P.D.: Nonlinear stability of eccentrically stiffened S-FGM elliptical cylindrical shells in thermal environment. Thin-Walled Struct. **108**, 280–290 (2016)
11. Jenkins, W.C., Yao, J.C.: Buckling of elliptic cylinders under normal pressure. AIAA J. **8**(1), 22–27 (1970)
12. Andreev, L.V., Obodan, N.I., Lebedev, A.G.: Shell Stability under Non-Axisymmetric Loading. Nauka, Moscow (1988). (in Russian)
13. Obodan, N.I., Lebedev, O.G., Gromov, V.A.: Nonlinear Behaviour and Stability of Thin-Walled Shells. Springer, Berlin (2013)
14. Andreev, L.V., Andrianov, I.V., Lebedev, A.G., Kucherenko, V.M., Obodan, N.I.: Non-linear deformation of elliptic cylinders under uniform external pressure. Mech. Solids **14**(2), 119–123 (1979)
15. Albus, J., Miermeister, M., Friese, H., Öry, H.: Stress and stability analysis of shells with elliptic cross-section. Z. Flugwiss. Weltraumforschung **20**, 117–127 (1996)
16. Koroleva, E.M.: Stability of cylindrical shells of oval cross section in the bending state of stress. J. Appl. Math. Mech. **37**(5), 901–904 (1973)
17. Bushnell, D.: Stress, buckling, and vibration of prismatic shells. AIAA J. **9**(10), 2004–2013 (1971)
18. Marlowe, M.B., Brogan, F.A.: Collapse of elliptic cylinders under uniform external pressure. AIAA J. **9**, 2264–2266 (1971)
19. Babenko, V.I.: On the stability loss of cylindrical shells under external pressure. Dopovidi AN USSR Ser. A **3**, 222–225 (1977). (in Ukrainian)
20. Babenko, V.I.: Initial postbuckling behaviour of cylindrical shells under external pressure. Mech. Solids **14**(1), 155–162 (1979)
21. Pogorelov, A.V., Babenko, V.I.: Geometric methods in the theory of stability of thin shells (review). Soviet Appl. Mech. **28**(1), 1–17 (1992)
22. Andreev, L.V., Antsiferov, A.V., Kucherenko, V.M., Pavlenko, I.D.: Regions of stability of elliptical cylinders under loading by static and impulsive external pressure. Strength Mater. **17**, 1606–1609 (1985)
23. Feinstein, G., Erickson, B., Kempner, J.: Stability of oval cylindrical shells. J. Exp. Mech. **11**(11), 514–520 (1971)
24. Kempner, J., Chen, Y.N.: Buckling and postbuckling of an axially compressed oval cylindrical shell. In: Symposium on the Theory of Shells to Honor Lloyd H. Donnell, McCuthan Publishers Co., pp. 141–183 (1967)
25. Romano, F., Kempner, J.: Stresses in short noncircular cylindrical shells under lateral pressure. J. Appl. Mech. **29**, 669–674 (1962)
26. Axelrad, E.L.: Theory of Flexible Shells. North Holland, Amsterdam (1987)
27. Andrianov, I.V., Awrejcewicz, J., Manevitch, L.I.: Asymptotical Mechanics of Thin-Walled Structures: A Handbook. Springer, Berlin (2004)
28. Andrianov, I.V., Awrejcewicz, J., Danishevs'kyy, V.V., Ivankov, A.O.: Asymptotic Methods in the Theory of Plates with Mixed Boundary Conditions. Wiley, Chichester (2014)

29. Nayfeh, A.H.: Perturbation Methods. Wiley, New York (2000)
30. Andrianov, I.I.: Analytical investigation of buckling of a cylindrical shell subjected to nonuniform external pressure. Math. Mech. Solids. **24**(3), 874–883 (2019). https://doi.org/10.1177/1081286518756179
31. Alfutov, N.A.: Stability of Elastic Structures. Springer, Berlin (2000)

Subclasses of Mechanical Problems Arising from the Direct Approach for Homogeneous Plates

Marcus Aßmus, Konstantin Naumenko and Holm Altenbach

Abstract Pavel Andreevich Zhilin proposed a theory for deformable directed surfaces which builds a generalized framework in context of linear engineering theories of plates. We introduce this theory axiomatically, delineate the basic ideas and formalize the governing equations. In doing so we present a self-contained set of equations for time-invariant problems. Thereof, subclasses of mechanical problems can be deduced, whereby in present context the main existing theories are derived. These are in-plane and out-of-plane loaded plate problems. Next to the in-plane loaded plate problem, we also distinguish between transverse shear-deformable and transverse shear-rigid out-of-plane loaded plates. Typical representatives are the plate theories by Kirchhoff, Reissner, and Mindlin.

Keywords Generalized plate theory · In-plane · Out-of-plane · Transverse shear

1 Introduction

1.1 Motivation

Our intention is to present a framework to treat mechanical problems on slender structures with uniform thickness. Hereby we reduce our concern to initially flat structures, i.e. uncurved in the reference placement. The treatment of such theories has a long tradition, since their original beginnings date back more than 150 years. All attempts associated can be considered as theories for dimensionally-reduced

M. Aßmus (✉) · K. Naumenko · H. Altenbach
Otto von Guericke University, Universitätsplatz 2, 39106 Magdeburg, Germany
e-mail: marcus.assmus@ovgu.de

K. Naumenko
e-mail: konstantin.naumenko@ovgu.de

H. Altenbach
e-mail: holm.altenbach@ovgu.de

H. Altenbach et al. (eds.), *Recent Developments in the Theory of Shells*,
Advanced Structured Materials 110, https://doi.org/10.1007/978-3-030-17747-8_4

continua. However, engineers usually have a pragmatic perception, so that we have to divide our introduction.

Let us start with more abstract considerations in context of generalized continua. A modern notion to the direct approach for plates is based on the treatise of Ericksen and Truesdell [11] which was revitalizing a topic associated with continua which exhibit independent rotational degrees of freedom. Hereby, the Cosserat brothers [10] were the godfathers since their ideas were used as parent model. For further attempts, Green [15] introduced the so called Cosserat surface. Such surface is kinematically equivalent to the 6-parameter plate theory. Zhilin [44] proposed a physically motivated theory with only five parameters as sufficient. Therein, drilling rotations are neglected. This rotation about the normal to the surface is not considered as independent variable since the structural rigidity is much higher than resistance against the out-of-plane rotations.

Turning to the historical developments of engineering applications, we have to leave the pathway of such non-classical approaches connected with Cosserat-type theories of plates, or more general, Cosserat-type shells, cf. [4]. First efforts to predict the structural mechanics of plates were done by Germain [14]. Lagrange [21] delivered corrections to this attempts. Also Navier [30] and Poisson [34] participated in this early endeavors. A completed plate theory was delivered by Kirchhoff [19] for the first time, who also revealed flaws of the latter ones. This theory retains valid for shear rigid plates. It is also known as Kirchhoff-Love plate theory (or Kirchhoff-Love shell theory) in english-speaking regions, while the achievement of Love [23] was an extension to initially curved surfaces what was already shown by Aron [5], what however, was unnoticed during that time. Improvements to Kirchhoff's theory were proposed only about 100 years later. Reissner [36, 37] and Mindlin [24] contemplated extensions to shear-deformable plates which was broaden the scope of application of plate theories drastically. However, these improvements were originally ignited approximately 30 years earlier by Timoshenko [39, 40], who incorporated first-order transverse shear effects at beams. It is worth to mention that Mindlin [24] and Reissner [37] used different approaches to derive a plate theory incorporating transverse shear effects.

The research area of plate theories has gained an overwhelming variety of approaches and directions, so that it is almost impossible to get an overview of all branches. This includes developments with six- or seven-parameter theories to incorporate thickness distortion (extensible director) [8], approaches to consider moderate deflections [12, 17], higher order approaches to transverse shear deformations [35], whereby all developments are derived mathematically consistent or not [3]. Nowadays, these theoretical advances are often correlated to developments of finite elements since numerical solutions gained therewith are liberated from severely restricted boundary conditions of closed-form solutions.

However, since a dimensional reduction cannot be fully reconciled with classical 3D Cauchy continuum theory [20], we take the quest by introducing a planar elastic surface ab initio. This is called direct approach. A deformable plane surface is introduced, and two-dimensional field equations are formulated in analogy to three-dimensional continuum theory. Thereby, it is our intention to represent the governing

equations in a modern spirit where we adopt tensor notation for a rational representation. In the sequel we will operate on the two-dimensional body mid surface while restrictions are made for the thin-walled spatial systems considered. To be exact, these are as follows:

- the mid surface, that is the surface which halves the thickness of the plate at each point, is a plane
- the plate thickness is small compared to the dimensions of the mid surface
- the outer surfaces surfaces of the plate enclose a homogeneous and continuous, i.e. continuously connected, material

Naturally the direct approach claims for a delicate interplay between physics and mathematics. Based on this concept, engineering theories for plates can be introduced in a natural way, as we will present here. Our journey will thus take us from a five-parameter theory to a two-parameter, a three-parameter and a one-parameter theory.

1.2 Frame of Reference

We reduce ourselves to the mid surface of slender bodies with uniform thickness $h(X_\alpha) = h \; \forall \alpha \in \{1, 2\}$. For what follows, we refer to this two-dimensional body manifold $\mathfrak{S}$, which is henceforth introduced as primitive concept. In context of the original volume V of the three-dimensional body manifold $\mathfrak{B}$, following relation hold.

$$V = \left\{(X_1, X_2, X_3) \in \mathfrak{B} \subset \mathbb{E}^3 : (X_1, X_2) \in \mathfrak{S} \subset \mathbb{E}^2, X_3 \in [-h/2, +h/2]\right\} \tag{1}$$

Herein, $\mathbb{E}^n$ is the n-dimensional Euclidean space. A visualization of the choice of $\mathfrak{S}$ is given in Fig. 1. For the sake of clarity we designate the outer surface of the three-dimensional body $\mathfrak{B}$ with $\mathfrak{S}^\pm$. To be exact, these are defined as follows.

$$\mathfrak{S}^+ : -\frac{h}{2}\Big|_{X_\alpha=0}^{X_\alpha=L_\alpha} \qquad\qquad \mathfrak{S}^- : +\frac{h}{2}\Big|_{X_\alpha=0}^{X_\alpha=L_\alpha} \tag{2}$$

We introduce an orthonormal basis $\{\boldsymbol{e}_\alpha, \boldsymbol{n}\} \; \forall \alpha \in \{1, 2\}$ of a right-handed coordinate system with the Euclidean norm $|\boldsymbol{e}_\alpha| = |\boldsymbol{n}| = 1$, while following relation holds.

$$\boldsymbol{n} = \frac{\boldsymbol{e}_1 \times \boldsymbol{e}_2}{|\boldsymbol{e}_1 \times \boldsymbol{e}_2|} = \boldsymbol{e}_1 \times \boldsymbol{e}_2 \tag{3}$$

For what follows, it is also beneficial to introduce the first metric tensor $\boldsymbol{P} = \boldsymbol{e}_\alpha \otimes \boldsymbol{e}_\alpha$. The surface considered features a boundary $\partial\mathfrak{S}$. At this boundary we introduce outward normals $\boldsymbol{\nu}$, whereby we do not distinguish between different directions. The normals introduced are related as follows.

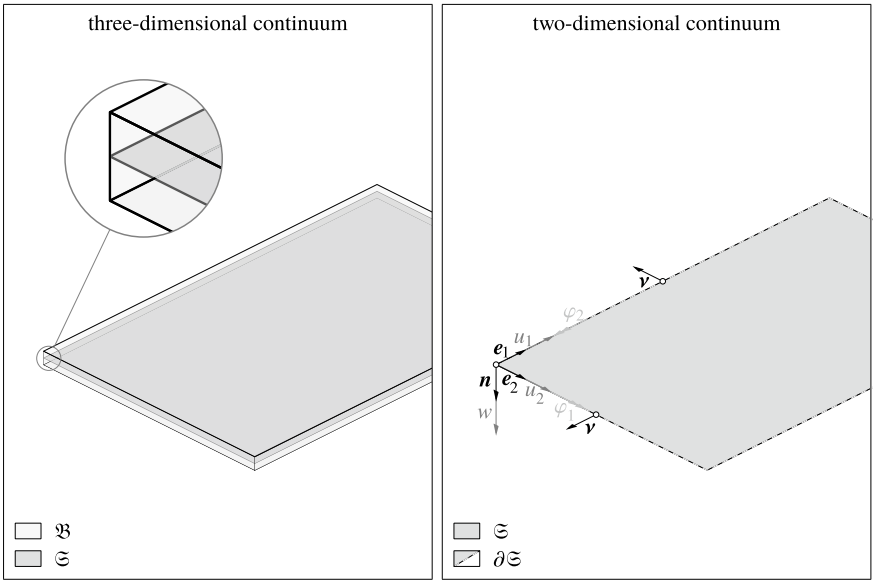

Fig. 1 Reference surface in context of a slender body and the degrees of freedom endowed

$$\boldsymbol{v} \cdot \boldsymbol{n} = 0 \tag{4}$$

The position vector r of a material point on $\mathfrak{S}$ can be written as follows.

$$\boldsymbol{r} = \boldsymbol{r}_0 + \boldsymbol{v} + w\boldsymbol{n} \tag{5}$$

Herein, $\boldsymbol{r}_0 = X_\alpha \boldsymbol{e}_\alpha$ is the position in the reference placement, $\boldsymbol{v} = v_\alpha \boldsymbol{e}_\alpha$ is the in-plane displacement vector and w is the deflection. Furthermore, we introduce rotations of a material point, characterized by the vector $\boldsymbol{\psi} = -\varphi_2 \boldsymbol{e}_1 + \varphi_1 \boldsymbol{e}_2$. To sum up, the degrees of freedom possessed by the surface continuum can be written in a rational spirit.

$$\boldsymbol{a} = v_1 \boldsymbol{e}_1 + v_2 \boldsymbol{e}_2 + w\boldsymbol{n} \tag{6}$$

$$\boldsymbol{\varphi} = \varphi_1 \boldsymbol{e}_1 + \varphi_2 \boldsymbol{e}_2 \tag{7}$$

Herein, $\boldsymbol{a}$ is the vector of translational degrees of freedom and $\boldsymbol{\varphi} = \varphi_\alpha \boldsymbol{e}_\alpha$ is the vector of rotational degrees of freedom. Furthermore, the relations $\boldsymbol{\varphi} = \boldsymbol{\psi} \times \boldsymbol{n}$ and $\boldsymbol{\psi} = -\boldsymbol{\varphi} \times \boldsymbol{n}$ hold.

We limit ourselves to the static case and restrict our concern to the derivation of classical engineering theories in this field. This is highlighted by Eqs. (6) and (7), resulting in a so called five-parameter theory. Such a theory is a special case of the Cosserat surface, cf. [31]. However, following restrictions are introduced.

- kinematics
  - displacements, deflections, and rotations remain small
  - strains (in-plane and transverse shear strains) and curvature changes are small
  - i.e. a linear differential correlation of displacements/deflections/rotations and strains/curvature changes can be assumed
- material properties
  - homogeneous and isotropic
  - purely elastic and scleronomous

Preceding restrictions result in geometrical and physical linear theories, i.e. so called 1st order structural theories.

1.3 Preliminaries

In this paper we apply a direct notation for tensors, whenever possible. Tensors of zeroth order (or scalars) are symbolised by italic letters (e.g. a), italic lowercase bold letters denote first-order tensors (or monads) (e.g. $\boldsymbol{a} = a_i\, \boldsymbol{e}_i$ or $\boldsymbol{b} = b_j\, \boldsymbol{e}_j$), second-order tensors (or dyads) are designated by italic uppercase bold letters (e.g. $\boldsymbol{A} = A_{lm}\, \boldsymbol{e}_l \otimes \boldsymbol{e}_m$ or $\boldsymbol{B} = B_{no}\, \boldsymbol{e}_n \otimes \boldsymbol{e}_o$), third-order tensors (or triads) by italic lowercase bold calligraphic letters (e.g. $\boldsymbol{\mathscr{a}} = a_{pqr}\, \boldsymbol{e}_p \otimes \boldsymbol{e}_q \otimes \boldsymbol{e}_r$), and fourth-order tensors (or tetrads) are symbolised by italic uppercase bold calligraphic letters (e.g. $\boldsymbol{\mathscr{A}} = A_{stuv}\, \boldsymbol{e}_s \otimes \boldsymbol{e}_t \otimes \boldsymbol{e}_u \otimes \boldsymbol{e}_v$), whereas Einstein sum convention is applied. Latin indices run through the values 1, 2, and 3, while Greek indices run through the values 1 and 2.

In the following, essential operations for tensors used in this paper are introduced based on a Cartesian coordinate system and orthonormal bases, e.g. $\{\boldsymbol{e}_i\}$:

- the scalar product

$$\boldsymbol{a} \cdot \boldsymbol{b} = a_i\, b_j\, \boldsymbol{e}_i \cdot \boldsymbol{e}_j = a_i\, b_i = \alpha \qquad \alpha \in \mathbb{R}\,, \tag{8}$$

- the cross product

$$\boldsymbol{a} \times \boldsymbol{b} = a_i\, b_j\, \boldsymbol{e}_i \times \boldsymbol{e}_j = a_i\, b_j\, \epsilon_{ijk}\, \boldsymbol{e}_k = \boldsymbol{c}\,, \tag{9}$$

- the dyadic product

$$\boldsymbol{a} \otimes \boldsymbol{b} = a_i\, b_j\, \boldsymbol{e}_i \otimes \boldsymbol{e}_j = \boldsymbol{C}\,, \tag{10}$$

- the composition of a second and a first-order tensor

$$\boldsymbol{A} \cdot \boldsymbol{a} = A_{lm}\, a_i\, \boldsymbol{e}_l \otimes \boldsymbol{e}_m \cdot \boldsymbol{e}_i = A_{li}\, a_i\, \boldsymbol{e}_l = \boldsymbol{d}\,, \tag{11}$$

- the composition of two second-order tensors

$$\boldsymbol{A}\cdot\boldsymbol{B}=A_{lm}\,B_{no}\,\boldsymbol{e}_l\otimes\boldsymbol{e}_m\cdot\boldsymbol{e}_n\otimes\boldsymbol{e}_o=A_{lm}\,B_{mo}\,\boldsymbol{e}_l\otimes\boldsymbol{e}_o=\boldsymbol{D}\,, \tag{12}$$

- the cross product between a second and a first-order tensor

$$\boldsymbol{A}\times\boldsymbol{b}=A_{lm}\,b_j\,\boldsymbol{e}_l\otimes\boldsymbol{e}_m\times\boldsymbol{e}_j=A_{lm}\,b_j\,\epsilon_{mjk}\,\boldsymbol{e}_l\otimes\boldsymbol{e}_k=\boldsymbol{G}\,, \tag{13}$$

- the double scalar product between two second-order tensors

$$\begin{aligned}\boldsymbol{A}:\boldsymbol{B}&=A_{lm}\,B_{no}\,\boldsymbol{e}_l\otimes\boldsymbol{e}_m:\boldsymbol{e}_n\otimes\boldsymbol{e}_o\\&=A_{lm}\,B_{mo}\end{aligned} \tag{14}$$

- the double scalar product between a fourth and a second-order tensor

$$\begin{aligned}\boldsymbol{\mathcal{A}}:\boldsymbol{B}&=A_{pqrs}\,B_{no}\,\boldsymbol{e}_p\otimes\boldsymbol{e}_q\otimes\boldsymbol{e}_r\otimes\boldsymbol{e}_s:\boldsymbol{e}_n\otimes\boldsymbol{e}_o\\&=A_{pqrs}\,B_{sr}\boldsymbol{e}_p\otimes\boldsymbol{e}_q=\boldsymbol{F}\,.\end{aligned} \tag{15}$$

As previously applied, ϵ_{ijk} is the permutation symbol

$$\epsilon_{ijk}=\begin{cases}+1 & \text{if } (i,j,k) \text{ is an even permutation of } (1,2,3)\\ -1 & \text{if } (i,j,k) \text{ is an odd permutation of } (1,2,3)\\ \;\;0 & \text{if } (i,j,k) \text{ is not a permutation of } (1,2,3)\end{cases}\,. \tag{16}$$

Each tensor $\boldsymbol{A}$ can be decomposed in its symmetric $\boldsymbol{A}^{\mathrm{sym}}$ ($\boldsymbol{A}=\boldsymbol{A}^T$ or $\boldsymbol{b}\cdot\boldsymbol{A}=\boldsymbol{A}\cdot\boldsymbol{b}$) and antimetric part $\boldsymbol{A}^{\mathrm{skw}}$ ($\boldsymbol{A}=-\boldsymbol{A}^{\top}$ or $\boldsymbol{b}\cdot\boldsymbol{A}=-\boldsymbol{A}\cdot\boldsymbol{b}$).

$$\begin{aligned}\boldsymbol{A}&=\boldsymbol{A}^{\mathrm{sym}}+\boldsymbol{A}^{\mathrm{skw}}\\ \boldsymbol{A}^{\mathrm{sym}}&=\tfrac{1}{2}\left[\boldsymbol{A}+\boldsymbol{A}^{\top}\right]\\ \boldsymbol{A}^{\mathrm{skw}}&=\tfrac{1}{2}\left[\boldsymbol{A}-\boldsymbol{A}^{\top}\right]\end{aligned} \tag{17}$$

The norm of a vector $\boldsymbol{a}$ is defined as $|\boldsymbol{a}|=[\boldsymbol{a}\cdot\boldsymbol{a}]^{1/2}$. The Nabla operator $\boldsymbol{\nabla}$ is defined as $\boldsymbol{\nabla}_2=\boldsymbol{e}_\alpha\,\partial/\partial x_\alpha$ for two-dimensional considerations and $\boldsymbol{\nabla}_3=\boldsymbol{e}_i\,\partial/\partial x_i$ in three dimensions. $\boldsymbol{\nabla}\cdot\square$ is the divergence, and $\boldsymbol{\nabla}\square$ is the gradient of a tensor. $\boldsymbol{\nabla}^{\mathrm{sym}}\square=1/2[\boldsymbol{\nabla}\square+\boldsymbol{\nabla}^{\top}\square]$ is the symmetric part of the associated gradient, where $\square$ holds true for every differentiable tensor field. The transposed gradient is defined as $\boldsymbol{\nabla}^{\top}\square=[\boldsymbol{\nabla}\square]^{\top}$ where $\square$ holds for all first-order tensors.

2 The Original Problem

In the present treatise we follow the perspective of Zhilin [44]. As already mentioned, this is driven by a more pragmatic viewpoint since we neglect drilling rotations at deformable directed surfaces. In context of engineering applications this is justifiable

since the rigidity against wrinkling is considerably bigger than against bending and torsion of the surface. In the sequel we delineate the tenets of this theory. Thereby we use a more appropriate notation for representation. The theory is expected to find applications in the treatment of mechanics of thin walled structural elements with arbitrary loadings and stiffnesses.

2.1 Kinematics

We introduce deformations measures associated with three distinct deformation states. Thereby we neglect terms of higher order for the in-plane displacement gradient and the rotational gradient.

$$\boldsymbol{G} = \nabla_2^{\mathrm{sym}} \boldsymbol{v} \tag{18}$$

$$\boldsymbol{K} = \nabla_2^{\mathrm{sym}} \boldsymbol{\varphi} \tag{19}$$

$$\boldsymbol{g} = \nabla_2 w + \boldsymbol{\varphi} \tag{20}$$

Herein, $\boldsymbol{G} = G_{\alpha\beta} \boldsymbol{e}_\alpha \otimes \boldsymbol{e}_\beta$ is the second-order in-plane strain tensor, $\boldsymbol{K} = K_{\alpha\beta} \boldsymbol{e}_\alpha \otimes \boldsymbol{e}_\beta$ is the second-order curvature change tensor, and $\boldsymbol{g} = g_\alpha \boldsymbol{e}_\alpha$ is the first-order transverse shear strain tensor. The tensors $\boldsymbol{G}$ and $\boldsymbol{K}$ are symmetric. In the sequel we will introduce dual measures to these deformation tensors.

2.2 Kinetics

Analogous to Cauchys theorem, boundary quantities are defined by forces and moments acting at the surface which is the starting point of Zhilin's approach. Thereby we make use of tangential forces $\boldsymbol{s}_{\mathfrak{S}}$, orthogonal forces $p_{\mathfrak{S}}$, and out-of-plane moments $\boldsymbol{m}_{\mathfrak{S}}$ acting at the surface.

$$\boldsymbol{n}_{\boldsymbol{\nu}} = \lim_{\Delta L \to 0} \frac{\Delta \boldsymbol{s}_{\mathfrak{S}}}{\Delta L} \qquad \boldsymbol{m}_{\boldsymbol{\nu}} = \lim_{\Delta L \to 0} \frac{\Delta (\boldsymbol{m}_{\mathfrak{S}} \times \boldsymbol{n})}{\Delta L} \qquad q_{\boldsymbol{\nu}} = \lim_{\Delta L \to 0} \frac{\Delta p_{\mathfrak{S}}}{\Delta L} \tag{21}$$

Herein L is a length measure. The vectors and the scalar of the left hand sides indicate the boundary resultants of the in-plane state $\boldsymbol{n}_{\boldsymbol{\nu}}$, the out-of-plane state $\boldsymbol{m}_{\boldsymbol{\nu}}$ and the transverse shear state $q_{\boldsymbol{\nu}}$. The orientation of the cut is defined by the corresponding normal. Thereby we make use of the boundary normals $\boldsymbol{n}$ and $\boldsymbol{\nu}$, introduced in Sect. 1.2. Following Cauchy [9], a tensor field exists to the boundary resultants introduced in Eq. (21). The following applies to boundaries with normals $\boldsymbol{n}$.

$$\boldsymbol{n} \cdot \boldsymbol{N} = \boldsymbol{o} \qquad \boldsymbol{n} \cdot \boldsymbol{L} = \boldsymbol{o} \qquad \boldsymbol{n} \cdot \boldsymbol{q} = 0 \tag{22}$$

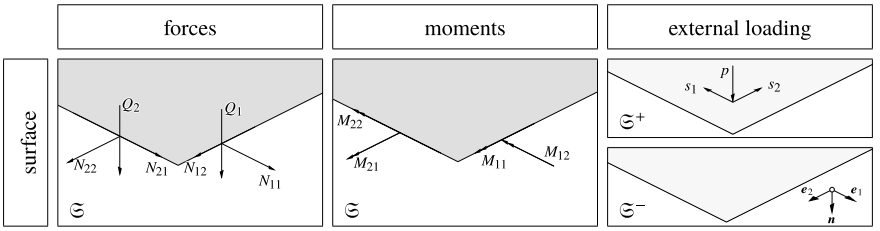

Fig. 2 Forces and moments at the surface as well as exemplary loading at the outer faces

However, with the boundary normal $\boldsymbol{\nu}$, which points along the plane directions, the following boundary loads result.

$$\boldsymbol{\nu}\cdot\boldsymbol{N}=\boldsymbol{n}_{\boldsymbol{\nu}} \qquad \boldsymbol{\nu}\cdot\boldsymbol{L}=\boldsymbol{m}_{\boldsymbol{\nu}} \qquad \boldsymbol{\nu}\cdot\boldsymbol{q}=q_{\boldsymbol{\nu}} \tag{23}$$

As with Cauchy's Lemma, the resultants at opposite edges are equal in magnitude, but opposite.

$$\boldsymbol{n}_{\boldsymbol{\nu}}(-\boldsymbol{\nu})=-\boldsymbol{n}_{\boldsymbol{\nu}}(\boldsymbol{\nu}) \qquad \boldsymbol{m}_{\boldsymbol{\nu}}(-\boldsymbol{\nu})=-\boldsymbol{m}_{\boldsymbol{\nu}}(\boldsymbol{\nu}) \qquad q_{\boldsymbol{\nu}}(-\boldsymbol{\nu})=-q_{\boldsymbol{\nu}}(\boldsymbol{\nu}) \tag{24}$$

Tensors for the stress resultants arise from Eqs. (22) and (23). Here $\boldsymbol{N}=N_{\alpha\beta}\boldsymbol{e}_\alpha\otimes\boldsymbol{e}_\beta$ is the in-plane force tensor, $\boldsymbol{L}=M_{\alpha\beta}\boldsymbol{e}_\alpha\otimes\boldsymbol{e}_\beta$ is the polar tensor of moments, and $\boldsymbol{q}=Q_\alpha\boldsymbol{e}_\alpha$ [32] is the transverse shear force vector. Components of these measures are visualized in Fig. 2. It is worth to mention that the tensors $\boldsymbol{N}$ and $\boldsymbol{L}$ are symmetric.

2.3 Equilibria

In present context we here built the local forms of the equilibrium of forces and the equilibrium of moments. This results in the so called Euler's laws of motion whereby we neglect acceleration terms for the sake of brevity. Thereby forces acting at the outer faces $\mathfrak{S}^{\pm}$ are summarized by means of the overall surface force vector $\boldsymbol{f}$.

$$\boldsymbol{f}=\mathcal{G}(\boldsymbol{s},p) \qquad \boldsymbol{f}=\boldsymbol{s}+p\boldsymbol{n} \tag{25}$$

Herein $\boldsymbol{s}=s_\alpha\boldsymbol{e}_\alpha$ is tangential and $p\boldsymbol{n}$ the orthogonal portion. We furthermore introduce moments $\boldsymbol{m}=-m_2\boldsymbol{e}_1+m_1\boldsymbol{e}_2$. The local forms of force and moment equilibrium are given as follows.

$$\nabla_3\cdot\,(\boldsymbol{N}+\boldsymbol{q}\otimes\boldsymbol{n}) \qquad +\boldsymbol{f}=\boldsymbol{o} \tag{26}$$

$$\nabla_2\cdot\,(-\boldsymbol{L}\times\boldsymbol{n})+\boldsymbol{q}\times\boldsymbol{n}+\boldsymbol{m}=\boldsymbol{o} \tag{27}$$

Obviously the overall force tensor $\boldsymbol{F}=F_{\alpha i}\,\boldsymbol{e}_\alpha\otimes\boldsymbol{e}_i=\boldsymbol{N}+\boldsymbol{q}\otimes\boldsymbol{n}=N_{\alpha\beta}\,\boldsymbol{e}_\alpha\otimes\boldsymbol{e}_\beta+Q_\alpha\boldsymbol{e}_\alpha\otimes\boldsymbol{n}$ and the axial tensor of moments $\boldsymbol{M}=-\boldsymbol{L}\times\boldsymbol{n}=M_{\alpha\beta}\boldsymbol{e}_\alpha\otimes\boldsymbol{n}\times\boldsymbol{e}_\beta$ are

both not symmetric. Alternatively one can introduce a representation where all shares are clearly distinguished.

$$\nabla_2 \cdot \boldsymbol{N} \quad + \boldsymbol{s} \quad = \mathbf{o} \tag{28}$$

$$\nabla_2 \cdot \boldsymbol{q} \quad + p \quad = 0 \tag{29}$$

$$\nabla_2 \cdot \boldsymbol{L} - \boldsymbol{q} + \boldsymbol{m} \times \boldsymbol{n} = \mathbf{o} \tag{30}$$

Therein we have splitted the force equilibrium into an in-plane [Eq. (26)$\cdot \boldsymbol{P}$] and an out-of-plane part [Eq. (26)$\cdot \boldsymbol{n}$]. We have furthermore rewritten the moment equilibrium for the sake of clarity. Apparently this presentation offers the advantage to operate with the symmetric measures $\boldsymbol{N}$ and $\boldsymbol{L}$, while the transverse shear measure $\boldsymbol{q} \otimes \boldsymbol{n}$ is reduced to the tensor of first order $\boldsymbol{q}$.

In context of engineering applications we assume that moments are resulting from forces acting at the outer faces solely, i.e. independent moments do not exist. Therefore, we can write the moments as functions of the tangential forces.

$$\boldsymbol{m} = \mathcal{K}(\boldsymbol{s}) \qquad\qquad \boldsymbol{m} \times \boldsymbol{n} = \frac{h}{2}\boldsymbol{s} \tag{31}$$

However, by no means our theoretical framework is restricted to the constrain introduced in Eq. (31).

2.4 Boundary Conditions

The following boundary conditions are required to solve the field equations introduced above. Thereby we distinguish between so called Dirichlet $\partial\mathfrak{S}_\mathrm{D}$ and Neumann boundaries $\partial\mathfrak{S}_\mathrm{N}$, which are defined as follows at the boundary $\partial\mathfrak{S}$ of the two-dimensional body manifold.

$$\partial\mathfrak{S} = \partial\mathfrak{S}_\mathrm{D} \cup \partial\mathfrak{S}_\mathrm{N} \qquad\qquad \partial\mathfrak{S}_\mathrm{D} \cap \partial\mathfrak{S}_\mathrm{N} = \emptyset \tag{32}$$

In the sequel, prescribed quantities are designated with a superscript star.

2.4.1 Dirichlet Boundary Conditions

The Dirichlet boundary conditions are constraints in the form of given translations and rotations.

$$\begin{aligned} \boldsymbol{v}(\boldsymbol{r}_0) &= \boldsymbol{v}^\star(\boldsymbol{r}_0) \\ \boldsymbol{\varphi}(\boldsymbol{r}_0) &= \boldsymbol{\varphi}^\star(\boldsymbol{r}_0) \\ w(\boldsymbol{r}_0) &= w^\star(\boldsymbol{r}_0) \end{aligned} \qquad \forall\, \boldsymbol{r}_0 \in \partial\mathfrak{S}_\mathrm{D} \tag{33}$$

Homogeneous Dirichlet boundary conditions can also be specified.

2.4.2 Neumann Boundary Conditions

The Neumann boundary conditions link forces and moments that can act as loads on the boundary of the surface continuum with the stress resultants.

$$\boldsymbol{v}\cdot\boldsymbol{N}=\boldsymbol{n}_{\boldsymbol{v}}^{\star}\qquad \boldsymbol{v}\cdot\boldsymbol{L}=\boldsymbol{m}_{\boldsymbol{v}}^{\star}\qquad \boldsymbol{v}\cdot\boldsymbol{q}=q_{v}^{\star}\qquad \forall\,\boldsymbol{r}_0\in\partial\mathfrak{S}_{\mathrm{N}} \tag{34}$$

2.4.3 Initial Conditions

On the other hand it is possible to introduce translations and rotations and velocity fields thereof at time $t=t_0$, representing the initial state. Since we restrict our concern to the scleronomous case, we drop the description of $\square(\boldsymbol{r}_0,t_0)\ \forall\,\square\in\{\boldsymbol{v},\dot{\boldsymbol{v}},\boldsymbol{\varphi},\dot{\boldsymbol{\varphi}},w,\dot{w}\}$.

2.5 Constitutive Relations

In present treatise we assume linear elastic material behavior. In context of engineering applications we can presuppose this. In this case, the kinetic measures depend on the first gradient of the degrees of freedom in maximum. So, the measures introduced in Eqs. (22) and (23) depend on the measures given in Eqs. (18), (19), and (20) solely. In generalized form, the constitutive equations can be given as follows.

$$\boldsymbol{N}=\boldsymbol{\mathcal{A}}:\boldsymbol{G}+\boldsymbol{\mathcal{B}}:\boldsymbol{K}+\boldsymbol{\mathcal{C}}\cdot\boldsymbol{g} \tag{35}$$

$$\boldsymbol{L}=\boldsymbol{\mathcal{B}}:\boldsymbol{G}+\boldsymbol{\mathcal{D}}:\boldsymbol{K}+\boldsymbol{\mathcal{d}}\cdot\boldsymbol{g} \tag{36}$$

$$\boldsymbol{q}=\boldsymbol{\mathcal{C}}:\boldsymbol{G}+\boldsymbol{\mathcal{d}}:\boldsymbol{g}+\boldsymbol{Z}\cdot\boldsymbol{g} \tag{37}$$

Herein $\boldsymbol{\mathcal{A}}$ and $\boldsymbol{\mathcal{D}}$ are fourth-order stiffness tensors, $\boldsymbol{\mathcal{B}}$ is a fourth-order coupling stiffness tensor, $\boldsymbol{\mathcal{C}}$ and $\boldsymbol{\mathcal{d}}$ are third-order coupling stiffness tensors, and $\boldsymbol{Z}$ is a second-order stiffness tensor. When reducing to the mid surface of a homogeneous plate with isotropic material behavior, the coupling stiffness tensors vanish.

$$\text{in-plane–out-of-plane coupling: } \boldsymbol{\mathcal{B}}=\boldsymbol{\mathcal{O}} \tag{38}$$

$$\text{in-plane–transverse shear coupling: } \boldsymbol{\mathcal{C}}=\boldsymbol{\mathcal{o}} \tag{39}$$

$$\text{out-of-plane–transverse shear coupling: } \boldsymbol{\mathcal{d}}=\boldsymbol{\mathcal{o}} \tag{40}$$

For completely decoupled deformation states the constitutive equations can be considerably simplified.

$$\boldsymbol{N} = \boldsymbol{\mathcal{A}} : \boldsymbol{G} \tag{41}$$

$$\boldsymbol{L} = \boldsymbol{\mathcal{D}} : \boldsymbol{K} \tag{42}$$

$$\boldsymbol{q} = \boldsymbol{Z} \cdot \boldsymbol{g} \tag{43}$$

To be exact, $\boldsymbol{\mathcal{A}}$ is the in-plane stiffness, $\boldsymbol{\mathcal{D}}$ is the out-of-plane stiffness, and $\boldsymbol{Z}$ is the transverse shear stiffness. These linear mappings are in accordance with Hooke's law in linear elasticity of three-dimensional Cauchy continua [9]. In the case of isotropy, these constitutive tensors read as follows.

$$\boldsymbol{\mathcal{A}} = D_{\mathrm{ip}}\, \nu\, \boldsymbol{P} \otimes \boldsymbol{P} + 0.5 D_{\mathrm{ip}}\, (1-\nu)\ (\boldsymbol{P} \boxtimes \boldsymbol{P} + \boldsymbol{P} \boxplus \boldsymbol{P}) \tag{44}$$

$$\boldsymbol{\mathcal{D}} = D_{\mathrm{op}}\, \nu\, \boldsymbol{P} \otimes \boldsymbol{P} + 0.5 D_{\mathrm{op}}\, (1-\nu)\ (\boldsymbol{P} \boxtimes \boldsymbol{P} + \boldsymbol{P} \boxplus \boldsymbol{P}) \tag{45}$$

$$\boldsymbol{Z} = D_{\mathrm{ts}} \boldsymbol{P} \tag{46}$$

Herein we have introduced three engineering interpretations. These are the in-plane stiffness D_{ip}, the out-of-plane stiffness D_{op}, and the transverse shear stiffness D_{ts}.

$$D_{\mathrm{ip}} = \frac{Y\, h}{1-\nu^2} \qquad D_{\mathrm{op}} = \frac{Y\, h^3}{12\left(1-\nu^2\right)} \qquad D_{\mathrm{ts}} = \kappa\, \frac{Y\, h}{2\,(1+\nu)} \tag{47}$$

Herein, Y is Young's modulus and ν is Poisson's ratio. The parameter κ is a tuning parameter to account for the shear energy contribution. Furthermore we make use of the following metric tensors where $\boxtimes$ and $\boxplus$ are conjugation products [33].

$$\boldsymbol{P} \otimes \boldsymbol{P} = \boldsymbol{e}_\alpha \otimes \boldsymbol{e}_\alpha \otimes \boldsymbol{e}_\beta \otimes \boldsymbol{e}_\beta$$

$$\boldsymbol{P} \boxtimes \boldsymbol{P} = \boldsymbol{e}_\alpha \otimes \boldsymbol{e}_\beta \otimes \boldsymbol{e}_\beta \otimes \boldsymbol{e}_\alpha \qquad \boldsymbol{P} \boxplus \boldsymbol{P} = \boldsymbol{e}_\alpha \otimes \boldsymbol{e}_\beta \otimes \boldsymbol{e}_\alpha \otimes \boldsymbol{e}_\beta$$

We can identify the following relations of the constitutive measures introduced above.

$$D_{\mathrm{op}} = \frac{h^2}{12} D_{\mathrm{ip}} \qquad \wedge \qquad \boldsymbol{\mathcal{D}} = \frac{h^2}{12} \boldsymbol{\mathcal{A}} \tag{48}$$

However, in context of isotropy, the stiffness tensors possess two material parameters, one geometry parameter and one tuning parameter. Restrictions on these coefficients are as follows which result for reasons of stability (Y, h), physical interpretation (h), and consistency (κ).

$$Y > 0 \qquad -1 < \nu < \frac{1}{2} \qquad h > 0 \qquad 0 < \kappa \leq 1 \tag{49}$$

Alternative representation forms of Eqs. (44)–(46) were given by, e.g. Naumenko and Eremeyev [29], Aßmus et al. [7], or Altenbach [2]. However, following properties apply to the constitutive tensors $\boldsymbol{\mathcal{H}} \in \{\boldsymbol{\mathcal{A}}, \boldsymbol{\mathcal{D}}\}$.

$$\boldsymbol{B}:\boldsymbol{\mathcal{H}}:\boldsymbol{A} = \boldsymbol{A}:\boldsymbol{\mathcal{H}}:\boldsymbol{B} \tag{50}$$

$$\boldsymbol{A}:\boldsymbol{\mathcal{H}} = \boldsymbol{A}^{\top}:\boldsymbol{\mathcal{H}} \tag{51}$$

$$\boldsymbol{\mathcal{H}}:\boldsymbol{A} = \boldsymbol{\mathcal{H}}:\boldsymbol{A}^{\top} \tag{52}$$

$$\boldsymbol{A}:\boldsymbol{\mathcal{H}}:\boldsymbol{A} \geq 0 \tag{53}$$

$$\boldsymbol{\mathcal{H}}:\boldsymbol{A}^{\mathrm{skw}} = \boldsymbol{0} \tag{54}$$

Herein $\boldsymbol{A}$ and $\boldsymbol{B}$ are chosen arbitrary. For the second-order constitutive tensor $\boldsymbol{Z}$, the following applies.

$$\boldsymbol{Z}\cdot\boldsymbol{a} = \boldsymbol{a}\cdot\boldsymbol{Z} \tag{55}$$

$$\boldsymbol{a}\cdot\boldsymbol{Z}\cdot\boldsymbol{a} \geq 0 \tag{56}$$

Herein $\boldsymbol{a}$ is chosen arbitrary.

2.6 Variational Principle

Exact solutions in closed-form are only available for a small family of problems. For the formulation of approximation methods it is helpful to use equivalent variational statements instead of equilibrium conditions. Variational principles provide information on the extremal properties of functionals. A typical representative is the principle of virtual work. The principle of virtual work for present generalized problem can be formulated as follows.

$$\delta W_{\mathrm{int}} = \delta W_{\mathrm{ext}} \tag{57}$$

with

$$\delta W_{\mathrm{int}} = \int_{\mathfrak{S}} (\boldsymbol{N}:\delta\boldsymbol{G} + \boldsymbol{L}:\delta\boldsymbol{K} + \boldsymbol{q}\cdot\delta\boldsymbol{g})\,\mathrm{d}\mathfrak{S} \tag{58}$$

$$\delta W_{\mathrm{ext}} = \int_{\delta\mathfrak{S}} (\boldsymbol{n}_{\boldsymbol{v}}\cdot\delta\boldsymbol{v} + \boldsymbol{m}_{\boldsymbol{v}}\cdot\delta\boldsymbol{\varphi} + q_{\boldsymbol{v}}\delta w)\,\mathrm{d}(\partial\mathfrak{S}) + \int_{\mathfrak{S}} (p\delta w + \boldsymbol{s}\cdot\delta\boldsymbol{v})\,\mathrm{d}\mathfrak{S} \tag{59}$$

The equilibrium equations introduced in preceding sections are fulfilled for the deformable plane surface if and only if Eq. (57) holds for all virtual fields $\delta\boldsymbol{v}$, $\delta\boldsymbol{\varphi}$, and δw.

2.7 Classification and Formalization

As apparent in the splitted representation of the equlibrium equations, we can identify three different states. The first one is the in-plane state [Eq. (28)], the second is the transverse shear state [Eq. (29)], and the third one is the out-of-plane state [Eq. (30)]. In progress, this also becomes apparent in the constitutive equations (41), (42), and (43) whereby reasons for simplification due to decoupling are clearly stated. However, we herein use the designation 'superposed' in the sense that all three states are uncoupled but heterodyne. This is reasonable in context of linearity, as presupposed in present treatise. For coupled deformation states, it is not possible to decompose the original problem into various subproblems. However, it turns out that the direct approach results in a generalized framework for the treatment of slender structures like thin plates.

Based on the boundary value problem presented in the previous sections, a structured overview is developed, which is graphically presented in form of a Tonti diagram [41]. The left column records the equilibria as a function of the field variables, their flux and their production terms. The right column contains the field variables including their temporal and spatial derivatives. These measures result in the driving forces which are connected to the field variables via constitutive laws (Fig. 3).

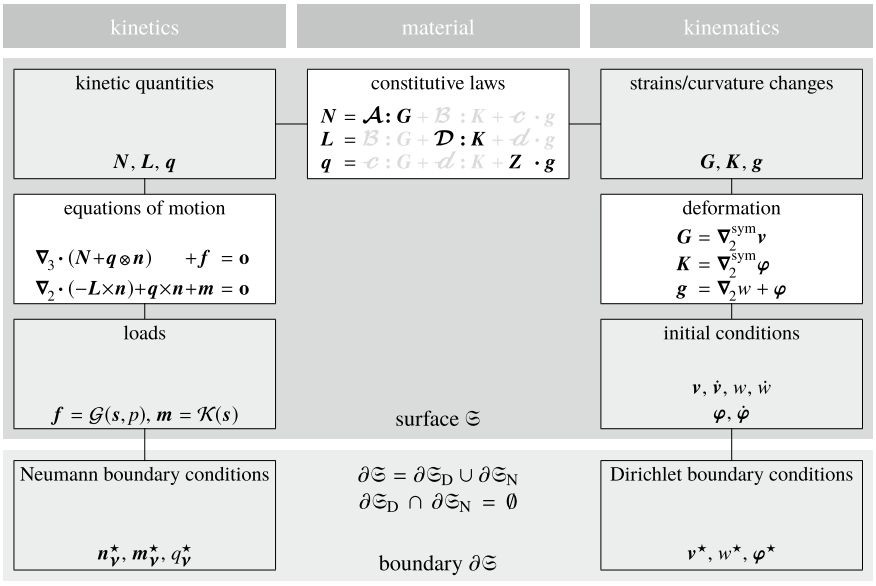

Fig. 3 Tonti diagram for the five parameter deformable plane surface problem, adapted from [6]

3 Subclasses

3.1 In-Plane Loaded Plate Problem

Present problem is concerned with the subproblem where all forces and deformations acting in-plane. This case is often referred to as membrane state, causing some confusion since we will also consider compression, what is not the case for membranes. Of course, the treatment of membranes is a separate problem. Therefore, others coined the state considered as 'disc' state or 'disc' problem [18]. Obviously this choice has also shortcomings. That is the reason why we call it in-plane loaded plate problem. Following restrictions are introduced in the context of the theory introduced in Sect. 2:

- The surface is only loaded in-plane.
- The surface is stretched and sheared, but not bent.
- All normals to the surface shift parallel.

These restrictions induce various consequences. The kinematics are reduced to the translational degrees of freedom

$$\boldsymbol{v} = v_1 \boldsymbol{e}_1 + v_2 \boldsymbol{e}_2 \tag{60}$$

Therefore, the in-plane strain tensor is sufficient to describe deformation measures.

$$\boldsymbol{G} = \nabla_2^{\mathrm{sym}} \boldsymbol{v} = G_{\alpha\beta}\, \boldsymbol{e}_\alpha \otimes \boldsymbol{e}_\beta \tag{61}$$

Since only tangential loads are acting, kinetics are defined through forces $\boldsymbol{n}_{\boldsymbol{v}}$.

$$\boldsymbol{n}_{\boldsymbol{v}} = \lim_{\Delta L \to 0} \frac{\Delta \boldsymbol{s}_{\mathfrak{S}}}{\Delta L} \tag{62}$$

So, the in-plane force tensor results.

$$\boldsymbol{n} \cdot \boldsymbol{N} = \boldsymbol{0} \qquad\qquad \boldsymbol{v} \cdot \boldsymbol{N} = \boldsymbol{n}_{\boldsymbol{v}} \tag{63}$$

The analogy of Cauchy's lemma remains with the following part.

$$\boldsymbol{n}_{\boldsymbol{v}}(-\boldsymbol{v}) = -\boldsymbol{n}_{\boldsymbol{v}}(\boldsymbol{v}) \tag{64}$$

For boundary conditions, only in-plane portions remain.

$$\boldsymbol{v}(\boldsymbol{r}_0) = \boldsymbol{v}^\star(\boldsymbol{r}_0) \qquad \forall\, \boldsymbol{r}_0 \in \partial\mathfrak{S}_{\mathrm{D}} \tag{65}$$

$$\boldsymbol{v} \cdot \boldsymbol{N} = \boldsymbol{n}_{\boldsymbol{v}}^\star \qquad \forall\, \boldsymbol{r}_0 \in \partial\mathfrak{S}_{\mathrm{N}} \tag{66}$$

The equilibrium equations reduces to the following in-plane portion.

$$\boldsymbol{\nabla}_2 \cdot \boldsymbol{N} + \boldsymbol{s} = \boldsymbol{o} \tag{67}$$

The material behavior is solely determined by the in-plane relations

$$\boldsymbol{N} = \boldsymbol{\mathcal{A}} : \boldsymbol{G} \tag{68}$$

with the in-plane stiffness tensor.

$$\boldsymbol{\mathcal{A}} = D_{\mathrm{ip}}\, \nu\, \boldsymbol{P} \otimes \boldsymbol{P} + 0.5 D_{\mathrm{ip}}\, (1-\nu)\ (\boldsymbol{P} \boxtimes \boldsymbol{P} + \boldsymbol{P} \boxplus \boldsymbol{P}) \tag{69}$$

In context of Eq. (57) we can reduce the terms of internal and external work for the in-plane loaded problem to the following expressions.

$$\delta W_{\mathrm{int}} = \int_{\mathfrak{S}} (\boldsymbol{N} : \delta \boldsymbol{G})\, \mathrm{d}\mathfrak{S} \tag{70}$$

$$\delta W_{\mathrm{ext}} = \int_{\delta\mathfrak{S}} (\boldsymbol{n}_{\boldsymbol{v}} \cdot \delta \boldsymbol{v})\, \mathrm{d}(\partial\mathfrak{S}) + \int_{\mathfrak{S}} (\boldsymbol{s} \cdot \delta \boldsymbol{v})\, \mathrm{d}\mathfrak{S} \tag{71}$$

3.2 Out-of-Plane Loaded Plate Problems

Present problem is concerned with the subproblems where all forces and deformations acting out-of-plane. In present treatise we assume that moments acting at the surface arise from tangential loads at the surface solely. Since tangential loads are unconsidered in the out-of-plane loaded case, these moments remain zero ($\boldsymbol{m} = \boldsymbol{o}$, $\boldsymbol{m} \times \boldsymbol{n} = \boldsymbol{o}$). This is also in the sense of Mindlin [24] and Kirchhoff [19].

3.2.1 Shear-Deformable Plate

First we want to treat the problem of shear-flexible (also shear-deformable or shear-soft) plate problem. This problem is associated with the names Reissner [36, 37] and Mindlin [24]. We introduce following restrictions in context of the overall problem:

- The surface is loaded out-of-plane only, i.e. only orthogonal portions of the load vector.
- The surface is bent, bot not stretched and strained.
- The deflection is unequal zero.

Thus, the degrees of freedom are reduced to deflections $w\boldsymbol{n}$ and rotations $\boldsymbol{\varphi}$. Therefore, deformation measures considered are the curvature change tensor and the transverse shear strain vector.

$$\boldsymbol{K} = \nabla_2^{\mathrm{sym}} \boldsymbol{\varphi} \tag{72}$$

$$\boldsymbol{g} = \nabla_2 w + \boldsymbol{\varphi} \tag{73}$$

Since only orthogonal loads are acting, kinetics are defined through forces $q_{\boldsymbol{\nu}}$.

$$\boldsymbol{m}_{\boldsymbol{\nu}} = \lim_{\Delta L \to 0} \frac{\Delta(\boldsymbol{m}_{\mathfrak{S}} \times \boldsymbol{n})}{\Delta L} \qquad q_{\boldsymbol{\nu}} = \lim_{\Delta L \to 0} \frac{\Delta p_{\mathfrak{S}}}{\Delta L} \tag{74}$$

For boundary conditions, only moment and transverse shear portions remain.

$$\boldsymbol{n} \cdot \boldsymbol{L} = \boldsymbol{o} \qquad \boldsymbol{\nu} \cdot \boldsymbol{L} = \boldsymbol{m}_{\boldsymbol{\nu}} \tag{75}$$

$$\boldsymbol{n} \cdot \boldsymbol{q} = 0 \qquad \boldsymbol{\nu} \cdot \boldsymbol{q} = q_{\boldsymbol{\nu}} \tag{76}$$

Cauchy's Lemma for residually moments and forces remain.

$$\boldsymbol{m}_{\boldsymbol{\nu}}(-\boldsymbol{\nu}) = -\boldsymbol{m}_{\boldsymbol{\nu}}(\boldsymbol{\nu}) \qquad q_{\boldsymbol{\nu}}(-\boldsymbol{\nu}) = -q_{\boldsymbol{\nu}}(\boldsymbol{\nu}) \tag{77}$$

In terms of boundary conditions, we can now define out-of-plane rotations and out-of-plane forces.

$$\boldsymbol{\varphi}(\boldsymbol{r}_0) = \boldsymbol{\varphi}^\star(\boldsymbol{r}_0) \qquad \forall\, \boldsymbol{r}_0 \in \partial\mathfrak{S}_{\mathrm{D}} \tag{78}$$

$$w(\boldsymbol{r}_0) = w^\star(\boldsymbol{r}_0) \qquad \forall\, \boldsymbol{r}_0 \in \partial\mathfrak{S}_{\mathrm{D}} \tag{79}$$

$$\boldsymbol{\nu} \cdot \boldsymbol{L} = \boldsymbol{m}_{\boldsymbol{\nu}}^\star \qquad \forall\, \boldsymbol{r}_0 \in \partial\mathfrak{S}_{\mathrm{N}} \tag{80}$$

$$\boldsymbol{\nu} \cdot \boldsymbol{q} = q_{\boldsymbol{\nu}}^\star \qquad \forall\, \boldsymbol{r}_0 \in \partial\mathfrak{S}_{\mathrm{N}} \tag{81}$$

The equilibria are reduced to terms for the out-of-plane deformation.

$$\nabla_2 \cdot \boldsymbol{L} - \boldsymbol{q} = \boldsymbol{o} \tag{82}$$

$$\nabla_2 \cdot \boldsymbol{q} + p = 0 \tag{83}$$

The material behaviour is described by the constitutive tensors for the out-of-plane state while considering transverse shear deformations separately.

$$\boldsymbol{L} = \boldsymbol{\mathcal{D}} : \boldsymbol{K} \tag{84}$$

$$\boldsymbol{q} = \boldsymbol{Z} \cdot \boldsymbol{g} \tag{85}$$

Herein, the out-of-plane and transverse shear relations for the stiffness tensors

$$\boldsymbol{\mathcal{D}} = D_{\mathrm{op}}\, \nu \boldsymbol{P} \otimes \boldsymbol{P} + 0.5 D_{\mathrm{op}}\, (1-\nu)\, (\boldsymbol{P} \boxtimes \boldsymbol{P} + \boldsymbol{P} \boxplus \boldsymbol{P}) \tag{86}$$

$$\boldsymbol{Z} = D_{\mathrm{ts}} \boldsymbol{P} \tag{87}$$

are used. Considering the principle of virtual work, we can reduce the required terms to the following.

$$\delta W_{\text{int}} = \int_{\mathfrak{S}} (\boldsymbol{L} : \delta \boldsymbol{K} + \boldsymbol{q} \cdot \delta \boldsymbol{g}) \, \mathrm{d}\mathfrak{S} \tag{88}$$

$$\delta W_{\text{ext}} = \int_{\delta\mathfrak{S}} (\boldsymbol{m}_{\boldsymbol{\nu}} \cdot \delta \boldsymbol{\varphi} + q_{\nu} \delta w) \, \mathrm{d}(\partial\mathfrak{S}) + \int_{\mathfrak{S}} (p \delta w) \, \mathrm{d}\mathfrak{S} \tag{89}$$

3.2.2 Shear-Rigid Plate

As a last point we want to derive the shear rigid problem which is widely used in engineering sciences as it is probably the simplest approach to treat mechanical problems at slender structures. This problem is associated with the name Kirchhoff [19]. Assumptions:

- The surface is loaded out-of-plane only, i.e. only orthogonal portions of the load vector.
- The surface is bent, bot not stretched and strained.
- All normals to the surface remain orthogonal for arbitrary deformations, i.e. rotations of material points are no longer independent.

This last key point is related to the transverse shear stiffness. In the shear-rigid case, the shear stiffness tends to infinity ($D_{\text{ts}} \to \infty$). While considering this case, we can substitute the rotation-curvature-change relation (19) since

$$\boldsymbol{\varphi} = -\nabla_2 w \tag{90}$$

holds true now. This induces, that only one degree of freedom remains. so that $\boldsymbol{K} = -\nabla_2^{\text{sym}} \left[\nabla_2 w\right]$ results. Furthermore, $\boldsymbol{g} = \nabla_2 w - \nabla_2 w = \boldsymbol{0}$ holds true. Due to this relation, the system is adequately described by a unknown function for the deflection w, the only remaining independent degree of freedom. Within this context, we can reformulate Eq. (30) to $\nabla \cdot \boldsymbol{L} = \boldsymbol{q}$ and insert this expression in Eq. (29). As becomes apparent, the set of governing equations depends on the moments and their dual measures solely.

$$\nabla_2 \cdot [\nabla_2 \cdot \boldsymbol{L}] + p = 0 \tag{91}$$

$$L = \boldsymbol{\mathcal{D}} : \boldsymbol{K} \tag{92}$$

$$K = -\nabla_2^{\text{sym}} \left[\nabla_2 w\right] \tag{93}$$

The transverse shear stresses $\boldsymbol{q}$ are unequal zero and can be determined through equilibrium equations since there is no separate constitutive relation. The only constitutive measure remaining is the out-of-plane stiffness tensor.

$$\boldsymbol{\mathcal{D}} = D_{\text{op}} \, \nu \boldsymbol{P} \otimes \boldsymbol{P} + 0.5 D_{\text{op}} \, (1 - \nu) \, (\boldsymbol{P} \boxtimes \boldsymbol{P} + \boldsymbol{P} \boxplus \boldsymbol{P}) \tag{94}$$

However, concerning the boundary conditions kinetic measures and boundary conditions, Eqs. (74)–(81) hold true. The terms of virtual work are reduced as follows.

$$\delta W_{\text{int}} = \int_{\mathfrak{S}} (\boldsymbol{L} : \delta \boldsymbol{K}) \, \mathrm{d}\mathfrak{S} \tag{95}$$

$$\delta W_{\text{ext}} = \int_{\delta\mathfrak{S}} (\boldsymbol{m}_{\nu} \cdot \delta \left[-\nabla_2 w \right] + q_{\nu} \delta w) \, \mathrm{d}(\partial\mathfrak{S}) + \int_{\mathfrak{S}} (p \delta w) \, \mathrm{d}\mathfrak{S} \tag{96}$$

4 Conclusion

We have introduced a plane surface with its kinematic degrees of freedom, the geometry of deformation, strain and curvature change measures, compatibility conditions, external and internal loads and equlibria. The constitutive equations are streamlined by the smart choice of the position of $\mathfrak{S}$ in $\mathfrak{B}$. Boundary conditions are introduced which are important for the practical implementation of the local forms of the equilibria introduced. Finally, a variational principle is exploited to generate a solution approach for displacement, deflection, and rotation fields of lesser smoothness. In this sense we may conclude that the direct approach results in a geometrically exact, elegant, and concise description of the governing equations. However, since our starting point was reduced to a fully linear framework it is unfeasible to derive the membrane problem thereof.

Based on the representation introduced we distinguish three basic subproblems. A visualization of these sets is given in Fig. 4. Through typical engineering assumptions that are clearly formulated we have derived classical theories for plates. Hereby we have shown, that the direct approach for plates is in fact applicable for a wide class of problems - all subproblems fit into this framework without conceptual problems. Thereby this gives it conceptual and methodological clearness. The considerations presented can be enlarged when terms of inertia are taken into account. We have furthermore omitted to decay in special cases of the these subclasses. Such depictions in scalar representation will occasionally be associated with special loading scenarios or boundary conditions, respectively.

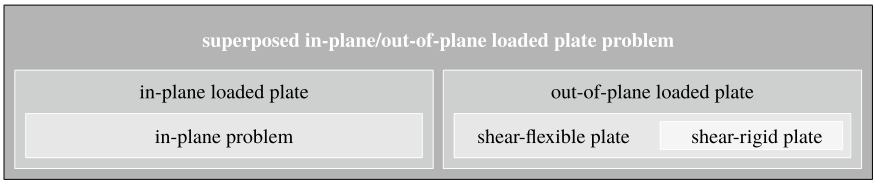

Fig. 4 Euler diagram with subclass problems designating special cases of the superposed problem

Popular computation approaches for closed-form solutions of the problems presented are delivered by, e.g. Navier [30], Nádai [25], and Levy [22]. Approximation methods are given by Ritz [38], Galerkin [13], Wlassow [42, 43], and Kantorowitsch [16]. Hereby, the use of Airys stress function [1] is advantageous. Practical implementations are presented in, e.g. [26–28].

Acknowledgements The authors acknowledge support by the German Research Foundation (DFG) within the framework of the Research Training Group *Micro-Macro-Interactions of Structured Media and Particle Systems* (RTG 1554, grant no. 83477795).

References

1. Airy, G.B.: On the strains in the interior of beams. Philos. Trans. R. Soc. **153**, 49–80 (1863). https://doi.org/10.1098/rstl.1863.0004
2. Altenbach, H.: The direct approach in the theory of viscoelastic shells. Habilitation thesis, Leningrad Polytechnic Institute (1987) (in Russia)
3. Altenbach, H., Meenen, J.: On the different possibilities to derive plate and shell theories. In: Jaiani, G., Podio-Guidugli, P. (eds.) IUTAM Symposium on Relations of Shell Plate Beam and 3D Models, pp. 37–47. Springer Berlin, Dordrecht (2008). https://doi.org/10.1007/978-1-4020-8774-5_3
4. Altenbach, J., Altenbach, H., Eremeyev, V.A.: On generalized Cosserat-type theories of plates and shells: a short review and bibliography. Arch. Appl. Mech. **80**(1), 73–92 (2010). https://doi.org/10.1007/s00419-009-0365-3
5. Aron, H.: Das Gleichgewicht und die Bewegung einer unendlich dünnen, beliebig gekrümmten elastischen Schale. Crelles Journal für die reine und angewandte Mathematik **78**, 136–174 (1874). https://doi.org/10.1515/crll.1874.78.136
6. Aßmus, M.: Structural mechanics of anti-sandwiches: an introduction. In: SpringerBriefs in Continuum Mechanics. Springer, Berlin (2019). https://doi.org/10.1007/978-3-030-04354-4
7. Aßmus, M., Eisenträger, J., Altenbach, H.: Projector representation of isotropic linear elastic material laws for directed surfaces. Zeitschrift für Angewandte Mathematik und Mechanik **97**(12), 1625–1634 (2017). https://doi.org/10.1002/zamm.201700122
8. Carrera, E.: Theories and finite elements for multilayered, anisotropic, composite plates and shells. Arch. Comput. Methods Eng. **9**(2), 87–140 (2002). https://doi.org/10.1007/BF02736649
9. Cauchy, A.L.: Recherches sur l'équilibre et le mouvement intérieur des corps solides ou fluides. élastiques ou non élastiques. Bulletin de la Societé Philomathique **3**(10), 9–13 (1823). https://doi.org/10.1017/CBO9780511702518.038
10. Cosserat, E., Cosserat, F.: Théorie des corps déformables. A. Hermann et fils, Paris (1909). http://jhir.library.jhu.edu/handle/1774.2/34209
11. Ericksen, J.L., Truesdell, C.: Exact theory of stress and strain in rods and shells. Arch. Ration. Mech. Anal. **1**(1), 295–323 (1957). https://doi.org/10.1007/BF00298012
12. Föppl, A.: Vorlesungen über technische Mechanik. B.G. Teubner, Leipzig (1907)
13. Galerkin, B.G.: Rods and plates. Using series for some problems in the elastic equilibrium of rods and plates. Engineers Bulletin (Vestnik Inzhenerov), Petrograd **19**, 897–908 (1915) (in Russia)
14. Germain, S.: Recherches sur la théorie des surfaces élastiques. Veuve Courtier, Paris (1821). www.cambridge.org/9781108050371
15. Green, A.E., Naghdi, P.M., Wainwright, W.L.: A general theory of a Cosserat surface. Arch. Ration. Mech. Anal. **20**(4), 287–308 (1965). https://doi.org/10.1007/BF00253138

16. Kantorowitsch, S.B., Krylow, W.I.: Näherungsmethoden der höheren Analysis. Deutscher Verlag der Wissenschaften, Berlin (1956)
17. von Kármán, T.: Festigkeitsprobleme im Maschinenbau. Encyklopädie der mathematischen Wissenschaften IV **311–384**, (1910)
18. Kienzler, R., Schneider, P.: Consistent theories of isotropic and anisotropic plates. J. Theor. Appl. Mech. **50**(3), 755–768 (2012). http://www.ptmts.org.pl/jtam/index.php/jtam/article/view/v50n3p755
19. Kirchhoff, G.R.: Über das Gleichgewicht und die Bewegung einer elastischen Scheibe. Journal für die reine und angewandte Mathematik (Crelle's Journal) **40**, 51–88 (1850). https://doi.org/10.1515/crll.1850.40.51
20. Koiter, W.: Theory of thin shells. Foundations and basic equations of shell theory: a survey of recent progress. In: IUTAM Symposium Copenhagen 1967, pp. 93–105. Springer, Berlin (1969). http://www.springer.com/gp/book/9783642884788
21. Lagrange, J.L.: Annales de Chimie **39**(149), 207 (1828)
22. Levy, M.: Mémoire sur la théorie des plaques élastiques planes. Journal de Mathématiques Pures et Appliquées **3**(3), 219–306 (1877). http://eudml.org/doc/235159
23. Love, A.E.H.: The small free vibrations and deformation of a thin elastic shell. Philos. Trans. R. Soc. London, Ser. A Math. Phys. Eng. Sci. **179**, 491–546 (1888). https://doi.org/10.1098/rsta.1888.0016
24. Mindlin, R.D.: Influence of rotatory inertia and shear on flexural motions of isotropic, elastic plates. Trans. Am. Soc. Mech. Eng. J. Appl. Mech. **18**, 31–38 (1951)
25. Nádai, A.: Die elastischen Platten—Die Grundlagen und Verfahren zur Berechnung ihrer Formänderungen und Spannungen, sowie die Anwendungen der Theorie der ebenen zweidimensionalen elastischen Systeme auf praktische Aufgaben. Springer, Berlin (1925). https://doi.org/10.1007/978-3-662-11487-2
26. Naumenko, K., Altenbach, J., Altenbach, H.: Variationslösungen für schubstarre Platten (I). Technische Mechanik **19**(2), 161–174 (1999)
27. Naumenko, K., Altenbach, J., Altenbach, H.: Variationslösungen für schubstarre Platten (II). Technische Mechanik **19**(3), 177–185 (1999)
28. Naumenko, K., Altenbach, J., Altenbach, H., Naumenko, V.K.: Closed and approximate analytical solutions for rectangular Mindlin plates. Acta Mech. **147**(1), 153–172 (2001). https://doi.org/10.1007/BF01182359
29. Naumenko, K., Eremeyev, V.A.: A layer-wise theory for laminated glass and photovoltaic panels. Compos. Struct. **112**, 283–291 (2014). https://doi.org/10.1016/j.compstruct.2014.02.009
30. Navier, M.: Mémoire sur les lois de l'équilibre et du mouvement des corps solides élastiques. Bulletin de la Société Philomathique de Paris, pp. 177–181 (1823)
31. Neff, P., Hong, K.I., Jeong, J.: The Reissner-Mindlin plate is the Γ-limit of Cosserat elasticity. Math. Models Methods Appl. Sci. **20**(9), 1553–1590 (2010). https://doi.org/10.1142/S0218202510004763
32. Palmow, W.A., Altenbach, H.: Über eine Cosseratsche Theorie für elastische Platten. Technische Mechanik **3**(3), 5–9 (1982). http://www.uni-magdeburg.de/ifme/zeitschrift_tm/1982_Heft3/Palmow_Altenbach.pdf
33. Podio-Guidugli, P.: A primer in elasticity. J. Elast. Phys. Sci. Solids **58**(1), 1–104 (2000). https://doi.org/10.1023/A:1007672721487
34. Poisson, S.D.: Sur l'équilibre et mouvement des corps élastiques. Mémoires de l'Académie des Sciences **VIII** (1829)
35. Reddy, J.N.: A simple higher-order theory for laminated composite plates. Trans. Am. Soc. Mech. Eng. J. Appl. Mech. **51**(4), 745–752 (1984). https://doi.org/10.1115/1.3167719
36. Reissner, E.: On the theory of bending of elastic plates. J. Math. Phys. **23**(1–4), 184–191 (1944). https://doi.org/10.1002/sapm1944231184
37. Reissner, E.: The effect of transverse shear deformation on the bending of elastic plates. Trans. Am. Soc. Mech. Eng. J. Appl. Mech. **12**, 69–77 (1945)

38. Ritz, W.: Über eine neue Methode zur Lösung gewisser Variationsprobleme der mathematischen Physik. Journal für die reine und angewandte Mathematik (Crelle's Journal) **135**, 1–61 (1909). https://doi.org/10.1515/crll.1909.135.1
39. Timoshenko, S.P.: On the correction for shear of the differential equation for transverse vibrations of prismatic bars. Philos. Mag. Ser. 6 **41**(245), 744–746 (1921). https://doi.org/10.1080/14786442108636264
40. Timoshenko, S.P.: On the transverse vibrations of bars of uniform cross-section. Philos. Mag. **43**(253), 125–131 (1922). https://doi.org/10.1080/14786442208633855
41. Tonti, E.: On the mathematical structure of a large class of physical theories. Accademia Nazionale Dei Lincei **52**(1), 48–56 (1972)
42. Vlasov, V.Z.: General theory of shells and its application in engineering. NASA Technical Translation, Washington, D.C. (1964)
43. Wlassow, W.S.: Allgemeine Theorie der Schalen und ihre Anwendung in der Technik. Staatsverlag technisch theoretische Literatur, Moskau (1949)
44. Zhilin, P.A.: Mechanics of deformable directed surfaces. Int. J. Solids Struct. **12**(9), 635–648 (1976). https://doi.org/10.1016/0020-7683(76)90010-X

Large Oscillations Around Curled Equilibrium Configurations of Uniformly Loaded Euler–Bernoulli Beams: Numerical and Experimental Evidences

D. Baroudi, I. Giorgio and E. Turco

Abstract In this paper, we show that equilibrium configurations of a clamped beam under distributed load, resembling a curled pending wire—whose existence has been mathematically established—can be obtained experimentally using 'soft' beams, i.e. beams for which the ratio between amplitude of the load and bending stiffness is large enough. Moreover, we introduce a Hencky-type discrete model, i.e. a finite dimensional Lagrangian model, for the 'soft' *Elastica* and build a numerical code for determining its motion, in the most general nonlinear regime. This code is able to qualitatively describe observed nonlinear dynamical behavior.

Keywords Nonlinear beam · Hencky bar-chain · Discrete modelling

1 Introduction

Since the introduction of the *Elastica* by Bernoulli and Euler [15, 27], beam theory has attracted the attention of various scientists due to its importance both from the mathematical point of view [17] and in its applications to structural mechanics. The

D. Baroudi
Aalto University School of Engineering, Aalto University, 00076 Aalto, Finland
e-mail: djebar.baroudi@aalto.fi

I. Giorgio (✉)
Department of Mechanical and Aerospace Engineering, SAPIENZA Università di Roma, 00184 Rome, Italy
e-mail: ivan.giorgio@uniroma1.it

I. Giorgio · E. Turco
International Research Center for the Mathematics and Mechanics of Complex Systems, Università degli studi dell'Aquila, 67100 L'Aquila, Italy
e-mail: emilio.turco@uniss.it

E. Turco
Department of Architecture, Design and Urban Planning, University of Sassari, 07041 Alghero, Italy

H. Altenbach et al. (eds.), *Recent Developments in the Theory of Shells*,
Advanced Structured Materials 110, https://doi.org/10.1007/978-3-030-17747-8_5

literature on the subject is huge and many relevant problems have been studied with sufficient completeness [7, 9, 26, 29, 37, 43, 45]. However, the richness of the model is such that there are still interesting and practically significant problems, that lack a complete study, especially in case of a beam in large deformation under distributed load—which leads to non-autonomous variational problems/Euler-Lagrange equations. In the paper [19] the existence of non-trivial (curled) equilibrium shapes of a clamped Euler beam under uniformly distributed dead load orthogonal to the straight reference configuration has been shown and a study of the properties of the global and local minimizers of the total energy has been performed. The last years have been characterized by a rediscovery of old models conjectured to study, with very simple tools, classical mechanical problems such as, one example for all, the computation of the buckling load of a beam. Hencky, in his work [30] which dates back to 1920, proposed a very simple, but extremely sharp, road to compute the buckling load of a rectilinear planar beam.[1] The keynote was to consider the beam as an assemblage of rigid links and elastic joints. In this way the equilibrium equations, or the stationarity condition of the potential energy, allow to estimate the buckling load quickly. The accuracy of such an estimate improves by increasing the number of elastic joints and rigid links. One of the more attractive point of Hencky's concept is that of avoiding the necessity of a continuum model since the problem naturally arises in a discrete environment. Moreover, recent Γ-convergence results have shown that Hencky's model is a fully reliable approximation of continuous inextensible [4] and extensible [3] Euler beams. Of note, this discrete model is intrinsically nonlinear and for this reason naturally avoids issues related to the objectivity of the energy when a linearization (around a given deformed configuration) is performed.

Limiting us to mechanical problems, the application of Hencky's idea can be seen in a series of recent works which treat beams, see [24, 31, 40, 41, 46], assemblage of beams, see [25, 47, 52], and specifically designed materials, see [5, 14, 16, 50]. This last research line, fairly trend in last decades, is the additional reason which suggests to take into consideration Hencky's models. Indeed, this kind of problems are characterized by a very large number of structural elements, therefore, the use of models as simple as possible is a forced road to follow. On the other hand, the study of complex metamaterials [8, 12, 28, 33, 44], such as pantographic structures, based on models which can be seen as generalization of that proposed by Hencky have proven to be fairly effective for predicting the mechanical behavior in static problems in large displacements, see [47, 49], and also the onset of failure phenomena [48]. The importance of studying nonlinear beam under distributed load has become clear in the recent past. Let us cite for instance the very active field of microstructured continua and in particular its significant branch in which the fundamental element constituting the microstructure is represented by a beam. In particular, in pantographic continua [2, 10, 21, 22] the single fiber, in a first approximation, can be modeled as a beam interacting with the other fibers, in the homogenized limit, a distributed load.

[1] It has to be remarked that an outline of Hencky's idea can also be found in the work of Gabrio Piola almost one century before, see [20, 23].

Some examples of studies which consider the nonlinear dynamics of beams described by simple discrete models are [25, 31, 52]. The present work aims at contributing in this direction. Indeed, we consider some very simple physical experiments reproducible without expensive tools concerning the curled equilibrium shape of a highly flexible beam under a gravity load. We also investigate the planar nonlinear motion in the neighborhood of this configuration.

We assume the same hypotheses characterizing the continuous beam model: (i) the elastic stored energy depends quadratically (a more general dependence could easily be considered) upon the curvature; (ii) the axis of the beam is inextensible; (iii) the shear deformation of the cross-section with respect to the axis is negligible; (iv) the cross-section is assumed undeformable. As we will see Hencky's model is consistent with these usual assumptions.

The paper, after this brief introduction, describes the main ingredients necessary to build the discrete model in Sect. 2. Successively, in Sect. 3, are reported firstly a complete description of two physical experiments along with the estimated data and successively the comparison between physical and numerical experiments both for static and dynamic cases. Section 4 closes the paper discussing the main results along with possible extensions of this work.

2 Naturally Discrete Model of *Elastica*

In order to describe the behavior of a 'soft' cantilever beam under gravity load, we follow the Hencky technique of discretization [39, 51, 53] and consider a discrete system which consists of an articulated chain of N_e rigid rods of length η connected each other by means of zero-torque hinges. Each joint is equipped by a rotational spring in order to model the resistance to be bent of the system (see Fig. 1). The configurations of the introduced system are completely defined by specifying the evolution of N_e Lagrangian coordinates, $\Phi_i(t)$, which represent the orientation of the rigid rods with respect to the x-axis pointing along the horizontal direction while the y-axis is directed vertically upwards. The system prior to deformation is straight and disposed along the x-axis. Each rigid segment is characterized by a mass, m_i, and a moment of inertia, J_i with respect to an axis orthogonal to the plane of the motion and passing through the mass center. Therefore, the position of the mass center for each segment can be easily written as

$$\begin{cases} x_i(t) = \sum_{k=1}^{i} \eta \left(1 - \frac{\delta_{ik}}{2}\right) \cos(\Phi_k(t)) \\ y_i(t) = \sum_{k=1}^{i} \eta \left(1 - \frac{\delta_{ik}}{2}\right) \sin(\Phi_k(t)) \end{cases} \tag{1}$$

where δ_{ik} is the Kronecker delta and, by a differentiation with respect to time, the velocities of the mass centers are evaluated as follows

$$\begin{cases} \dot{x}_i(t) = -\sum_{k=1}^{i} \eta \left(1 - \frac{\delta_{ik}}{2}\right) \dot{\Phi}_k(t) \sin(\Phi_k(t)) \\ \dot{y}_i(t) = \sum_{k=1}^{i} \eta \left(1 - \frac{\delta_{ik}}{2}\right) \dot{\Phi}_k(t) \cos(\Phi_k(t)) \end{cases} \tag{2}$$

The adopted kinematic description of the discrete beam leads to a convenient formulation of the motion equations derived from the following Lagrangian

$$\mathcal{L} = \mathcal{K} - \Psi \tag{3}$$

where $\mathcal{K}$ and Ψ are the kinetic and potential energies of the system, respectively. Specifically, the kinetic energy, using König's theorem and after some algebraic manipulations, assumes the form

$$\mathcal{K} = \sum_{i=1}^{N_e} \frac{1}{2} m_i \left\{ \left[\sum_{k=1}^{i} \eta \left(1 - \frac{\delta_{ik}}{2}\right) \dot{\Phi}_k \sin(\Phi_k) \right]^2 + \left[\sum_{k=1}^{i} \eta \left(1 - \frac{\delta_{ik}}{2}\right) \dot{\Phi}_k \cos(\Phi_k) \right]^2 \right\} + \frac{1}{2} J_i \dot{\Phi}_i^2 \tag{4}$$

The potential energy Ψ consists of two contributions, namely an elastic term Ψ_{el} which is assumed to be

$$\Psi_{el} = \sum_{i=1}^{N_e} \kappa_{b\,i} \left[\cosh(\phi_i) - 1\right] \tag{5}$$

where we introduce the relative angles between rods, i.e. $\phi_1 = \Phi_1$ (due to the clamping constraint) and $\phi_i = \Phi_i - \Phi_{i-1}$ for $i \geq 2$ and a uniform lumped bending stiffness $\kappa_{b\,i}$ related to the rotational springs [22, 47], and a gravitational term Ψ_{wg} which is

$$\Psi_{wg} = \sum_{i=1}^{N_e} g\, m_i \left[\sum_{k=1}^{i} \eta \left(1 - \frac{\delta_{ik}}{2}\right) \sin(\Phi_k) \right] \tag{6}$$

being g the magnitude of the gravity acceleration. We remark that the potential energy in Eq. (5) should be only positive definite, hence, any convex function can be employed for this purpose, not necessarily a simple quadratic function. It is also worth noting that the first relevant term in a Taylor expansion of each addend of the assumed potential Eq. (5) is the classical quadratic form expressed in terms of the relative angle.

In order to take into account also a possible viscous dissipation (for a more general framework, see e.g. [6, 18]) occurring during the motion due to the interaction of the 'soft' beam with the air, we introduce, as a first approximation, the Rayleigh dissipation function as follows

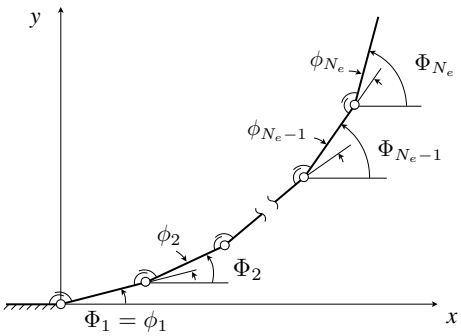

Fig. 1 Hencky-type discrete model for a highly flexible cantilever beam

$$\mathcal{R} = \sum_{i=1}^{N_e} \frac{1}{2} c_{b\,i}\, \dot{\phi}_i^2 \tag{7}$$

The Euler-Lagrange equations of motion, thus, can be deduced as

$$\frac{\partial}{\partial t}\left(\frac{\partial \mathcal{K}}{\partial \dot{\Phi}_i}\right) - \frac{\partial \mathcal{K}}{\partial \Phi_i} + \frac{\partial \Psi_{el}}{\partial \Phi_i} + \frac{\partial \Psi_{wg}}{\partial \Phi_i} + \frac{\partial \mathcal{R}}{\partial \dot{\Phi}_i} = 0 \quad \text{for } i = 1 \ldots N_e \tag{8}$$

Equation (8) is solved numerically by means of the computing system Wolfram Mathematica with a differential-algebraic system of equations (DAEs) solver after a proper transformation to a standard form.

3 Physical Experiments and Numerical Simulations

The previously introduced Lagrangian model is tested in this section with two relevant experimental cases. Specifically, we consider two samples made up of two different materials and sizes to reproduce the equilibrium configurations related to a local minimum for the energy, and we investigate also the dynamic behavior of such specimens in a regime of large oscillation around the curled stable equilibrium configurations found out. In the first case, we examine a paper strip of size 329 × 20 mm, whose thickness is about 0.17 mm and its mass is 0.62 ± 0.02 g. The second case involves a similar strip of a thin isotropic sheet of polyethylene terephthalate, namely PET, of size 220 × 20 mm and thickness about 0.15 mm. The mass of the strip is 0.91 ± 0.02 g; moreover, we add at the free end of the specimen a further mass, i.e. a ‘paper clip’ of 0.41 ± 0.02 g (see Fig. 2).

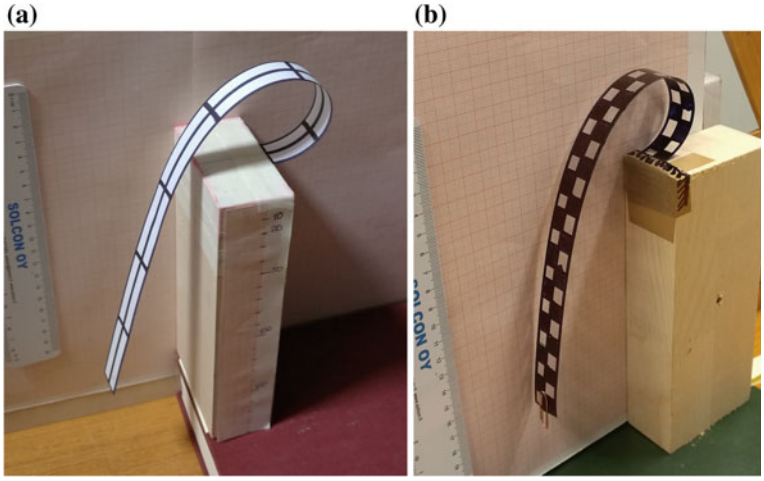

Fig. 2 Curled stable equilibrium configurations: paper beam **a**; PET beam with a tip mass **b**

3.1 Using the Curled Static Configuration to Estimate Mechanical Parameters

First of all, let us consider the local-minimum energy configurations for the two specimens under test (see Fig. 2). Figure 3 shows the pictures of the equilibrium shapes for the beams and also the equilibrium configurations obtained by finding the

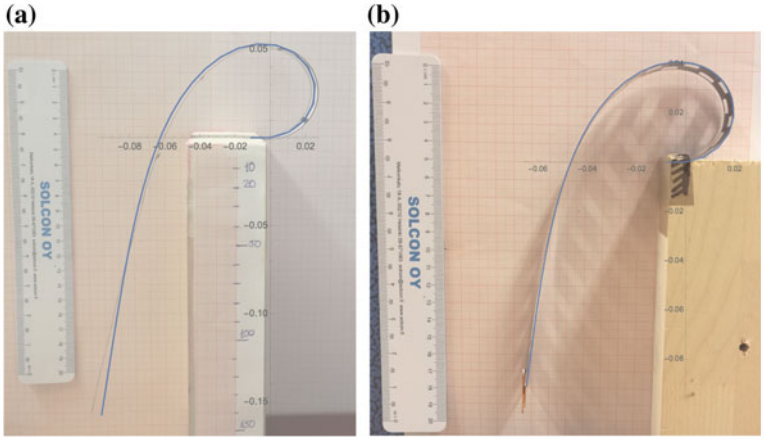

Fig. 3 Comparison between measured and simulated equilibrium configurations: paper beam **a**; PET beam with a mass on the tip **b**

corresponding local minimum of the potential energy Ψ in the examined cases for $N_e = 30$.

In order to obtain the agreement exhibit in Fig. 3, we use for the lumped bending stiffness the following expression

$$\kappa_{bi} = Y_b j_b / \eta \tag{9}$$

where j_b is the second moment of area of the beam cross section and Y_b, i.e. the Young modulus of the material, is used as a material parameter which we identify to fit the 'measured' shape. Particularly, we found for the paper beam that $Y_b = 1.25$ GPa and for the PET beam that $Y_b = 2.5$ GPa, starting from an initial guess near to the known values of the elastic moduli of the considered materials.

3.2 *Large Oscillations Around Curled Stable Equilibrium Configurations*

As illustrative examples of the foregoing, we consider some in-plane oscillating motions around the curled equilibrium configurations which are presented before. From the experiments, we evaluate the Lagrangian coordinates of the effective initial configurations (see Fig. 4 with the overlap between the computed piecewise linear curve and the picture of the beam for both the specimens treated) and then, specifying these values and zero angular velocities as initial conditions, we solve the Eqs. (8) to obtain the motions that originate from those. The evolutions in terms of orientations $\Phi_i(t)$ and angular velocities $\dot{\Phi}_i(t)$ are shown in Fig. 5 and Fig. 6, respectively, for the two cases examined of the paper and the PET beam. Figure 6 also displays a zoom of the initial part of the motion. Since the initial shapes and the equilibrium

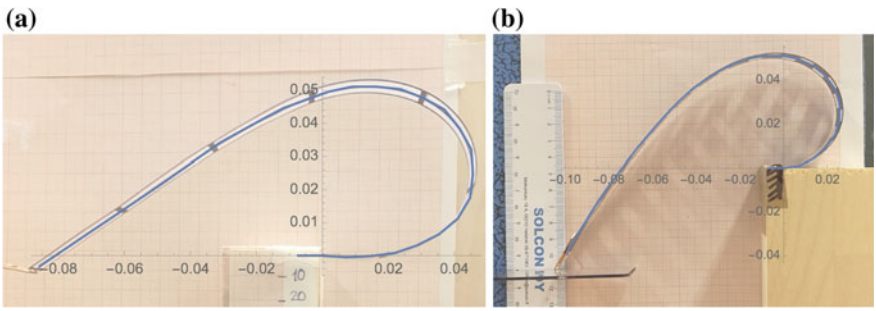

Fig. 4 Initial configurations: paper beam **a**; PET beam with a mass on the tip **b**

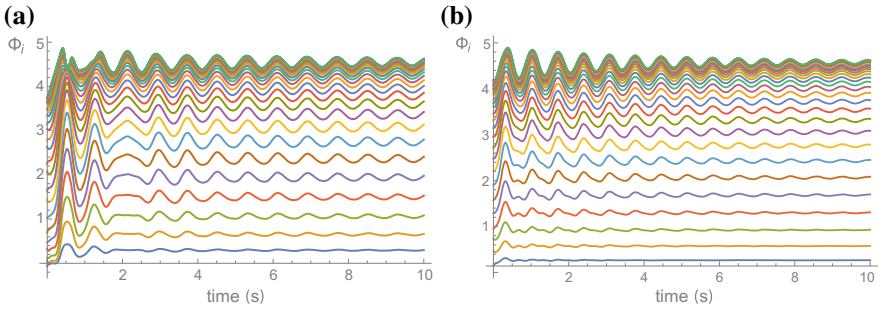

Fig. 5 Large oscillations, $\Phi_i(t)$, around the equilibrium configurations: paper beam **a**; PET beam with a mass on the tip **b**. The plots of Lagrangian coordinates result in an increasing order from the $\Phi_1(t)$ to $\Phi_{Ne}(t)$

configurations, towards which the evolutions approach, are both curves where the curvature never changes its sign (i.e. the curve never crosses its tangent, and therefore the coordinates $\Phi_i(t)$ for a given instant do not decrease with the index i), we note that the plots of Lagrangian coordinates, in Fig. 5, result in an almost increasing order from $\Phi_1(t)$ to $\Phi_{Ne}(t)$ and tend to compact each other for the last part of the beam. Indeed, this terminal part remains almost undeformed. As shown in Fig. 6, the same sequence in the disposition of the plots disappears for the angular velocities. These last exhibit a maximum value around less than a quarter of the beam length at the very beginning of the motion and subsequently the trend of all the histories is governed by the dissipation (the curves are neatly superimposed on top of each other by the lowest index, and hence it is possible to see which segment presents the velocity peak). In the performed simulations, the viscous coefficients are roughly estimated to fit the dissipative behavior of the real 'soft' beams. Specifically, we found $c_n = 10^{-5}$ N m s for the beam made up of paper and $c_n = 5 \times 10^{-5}$ N m s in the case of the PET. In Fig. 7 are plotted the evolution, along the motion, of the kinetic and potential energy for the paper and for the PET beam. Their trends are almost counter-phase and consistent with what we expected; indeed, the kinetic energy tends to vanish because of the dissipation while the potential energy approaches the value related to the local minimum around which the beams oscillate. For the sake of brevity, Fig. 8 shows the trajectory in phase space of the Lagrangian coordinate $\Phi_{Ne}(t)$ for both the cases investigated, since the qualitative behavior of the trajectories related to the other coordinates is very similar. In the initial part of the motion the nonlinear behavior is remarkable while towards the end, for the effect of viscous dissipation, the system becomes almost linear and a point of stable equilibrium is easily detectable.

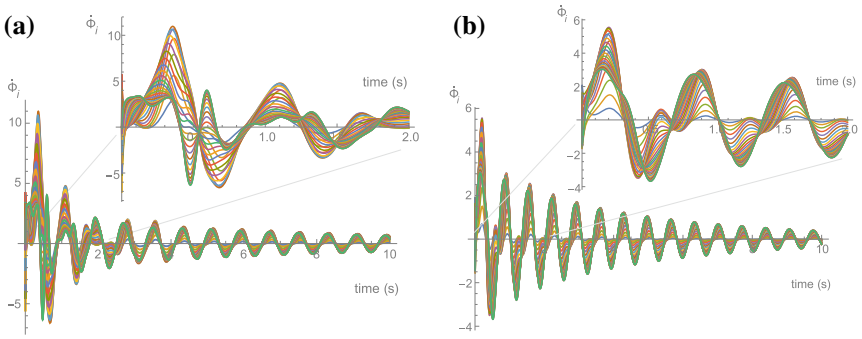

Fig. 6 Histories of the angular velocities, $\dot{\Phi}_i(t)$ with a zoomed initial part: paper beam **a**; PET beam with a mass on the tip **b**

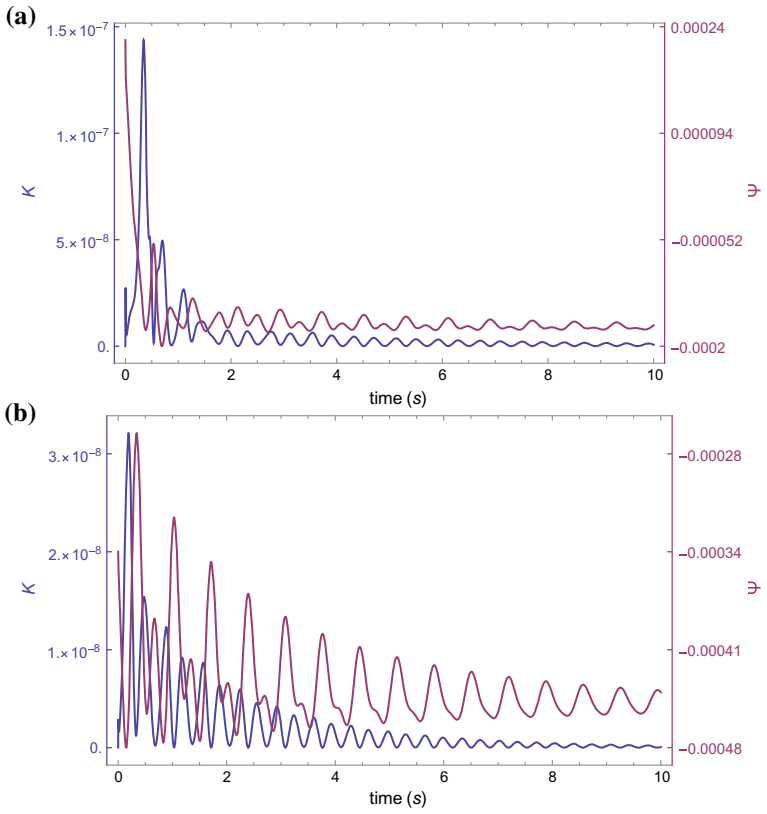

Fig. 7 Histories of the kinetic energy $\mathcal{K}$ (blue solid line) and potential energy Ψ (purple solid line): paper beam **a**; PET beam with a mass on the tip **b**

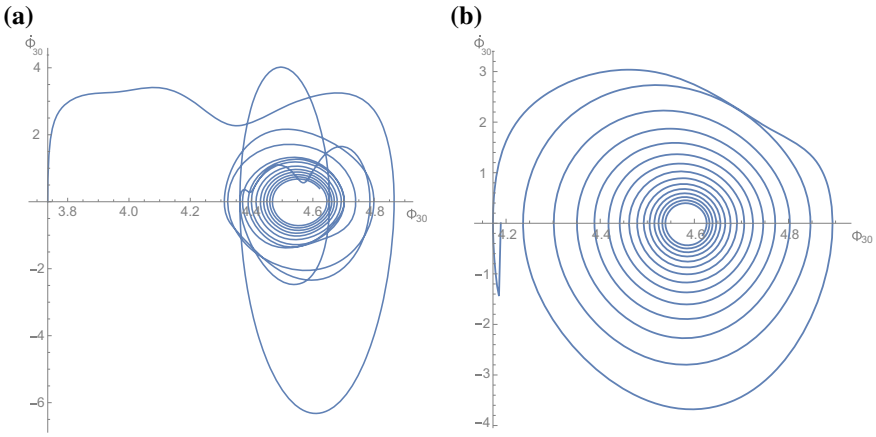

Fig. 8 Phase path of the Lagrangian coordinate related to the last rigid segment: paper beam **a**; PET beam with a mass on the tip **b**

4 Concluding Remarks and Future Challenges

Herein, the local minimum configurations for highly flexible beams predicted in [19] and characterized by curled shapes are shown experimentally and predicted numerically. Besides, using a Hencky-type discrete model for describing such mechanical systems, we adopt a Lagrangian formulation, which is computationally efficient for determining the motion in the most general nonlinear regime, and compare the solutions of the obtained differential equations with experimental tests with a good qualitative agreement. We expect, therefore, that when a more accurate measurement campaign will be performed and when the lumped parameters in the considered Lagrangian functions will be suitably fitted a perfect quantitative agreement will become possible (see e.g. [1, 34, 36, 38]). Considered their great efficiency, we also expect that similar codes will be useful in the study of the nonlinear dynamics of Timoshenko beams [13] and lattice systems including many beams in large deformations as pantographic metamaterials [11, 32, 35, 42, 49].

It is worth noting that, in case of PET beam, the presence of the point mass, i.e. the paper clip, at the end of the beam makes stable the 'curled equilibrium'. Of course, we can add length to the strip to achieve the stable configuration under the distributed own weight but, on the other hand, removing the tip mass and hence, reducing the gravity load, we can show that the only minimum is, in this circumstance, the global one. Indeed, it can be proven that below a critical value of the external load the only minimum for the energy is related to the classical equilibrium configuration which resembles the pending wire shape of a cantilever beam. Specifically, Fig. 9 exhibits, for the PET beam without tip mass, a stroboscopic motion sampled at the

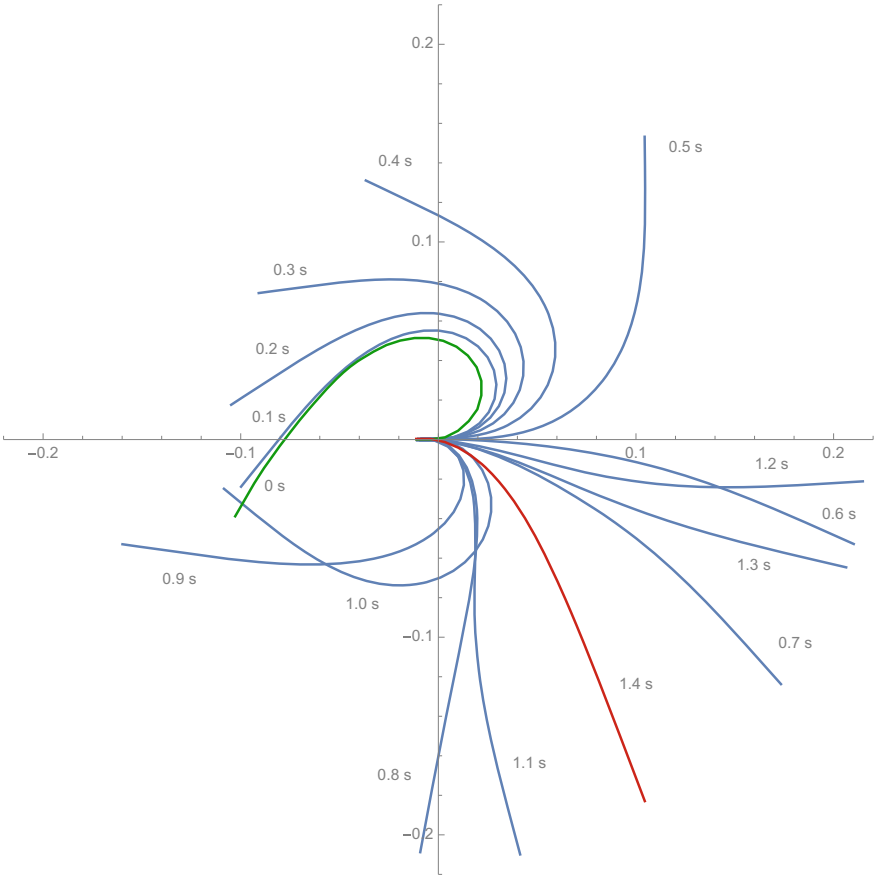

Fig. 9 Stroboscopic motion of the PET beam without mass on the tip. The initial shape is highlighted in green, while the final configuration is red. Near each configuration is specified the corresponding time

rate of 10 images per second from the initial configuration (green solid line), the same displayed also in Fig. 4b, to the image of the current configuration captured at 1.4 s (red solid line).

References

1. Abali, B.E., Wu, C.C., Müller, W.H.: An energy-based method to determine material constants in nonlinear rheology with applications. Contin. Mech. Thermodyn. **28**(5), 1221–1246 (2016)
2. Alibert, J.J., Seppecher, P., dell'Isola, F.: Truss modular beams with deformation energy depending on higher displacement gradients. Math. Mech. Solids **8**(1), 51–73 (2003)
3. Alibert, J.J., Della Corte, A., Giorgio, I., Battista, A.: Extensional elastica in large deformation as Γ-limit of a discrete 1D mechanical system. Zeitschrift für angewandte Mathematik und Physik **68**(2), 19 (2017)

4. Alibert, J.J., Della Corte, A., Seppecher, P.: Convergence of Hencky-type discrete beam model to Euler inextensible elastica in large deformation: rigorous proof. In: Mathematical Modelling in Solid Mechanics, pp. 1–12. Springer (2017)
5. Altenbach, H., Eremeyev, V.A.: Generalized Continua-from the Theory to Engineering Applications, vol. 541. Springer (2012)
6. Altenbach, H., Eremeyev, V.A.: On the constitutive equations of viscoelastic micropolar plates and shells of differential type. Math. Mech. Complex Syst. **3**(3), 273–283 (2015)
7. Altenbach, H., Bîrsan, M., Eremeyev, V.A.: Cosserat-type rods. In: Generalized Continua from the Theory to Engineering Applications, pp. 179–248. Springer (2013)
8. Andreaus, U., Spagnuolo, M., Lekszycki, T., Eugster, S.R.: A Ritz approach for the static analysis of planar pantographic structures modeled with nonlinear Euler–Bernoulli beams. Contin. Mech. Thermodyn., 1–21 (2018)
9. Antman, S.S.: Kirchhoff's problem for nonlinearly elastic rods. Q. Appl. Math. **32**(3), 221–240 (1974)
10. Barchiesi, E., Dell'Isola, F., Laudato, M., Placidi, L., Seppecher, P.: A 1D continuum model for beams with pantographic microstructure: asymptotic micro-macro identification and numerical results. In: Advances in Mechanics of Microstructured Media and Structures, pp. 43–74. Springer (2018)
11. Barchiesi, E., Ganzosch, G., Liebold, C., Placidi, L., Grygoruk, R., Müller, W.H.: Out-of-plane buckling of pantographic fabrics in displacement-controlled shear tests: experimental results and model validation. Contin. Mech. Thermodyn., 1–13 (2018)
12. Barchiesi, E., Spagnuolo, M., Placidi, L.: Mechanical metamaterials: a state of the art. Math. Mech. Solids **24**(1), 212–234 (2019)
13. Battista, A., Della Corte, A., dell'Isola, F., Seppecher, P.: Large deformations of 1D microstructured systems modeled as generalized Timoshenko beams. Zeitschrift für angewandte Mathematik und Physik **69**, 22 (2018)
14. Berezovski, A., Yildizdag, M.E., Scerrato, D.: On the wave dispersion in microstructured solids. Contin. Mech. Thermodyn., 1–20 (2018)
15. Bernoulli, D.: Letter from Daniel Bernoulli to Euler, 20 Oct 1742. http://eulerarchive.maa.org/correspondence/letters/OO0147.pdf
16. Bîrsan, M., Altenbach, H., Sadowski, T., Eremeyev, V.A., Pietras, D.: Deformation analysis of functionally graded beams by the direct approach. Compos. Part B: Eng. **43**(3), 1315–1328 (2012)
17. Born, M.: Untersuchungen über die stabilität der elastischen linie in ebene und raum, unter verschiedenen grenzbedingungen. Ph.D. thesis, University of University of Gottingen (1906)
18. Cuomo, M.: Forms of the dissipation function for a class of viscoplastic models. Math. Mech. Complex Syst. **5**(3), 217–237 (2017)
19. Della Corte, A., dell'Isola, F., Esposito, R., Pulvirenti, M.: Equilibria of a clamped Euler beam (Elastica) with distributed load: large deformations. Math. Model. Methods Appl. Sci. **27**(08), 1391–1421 (2017)
20. dell'Isola, F., Maier, G., Perego, U., Andreaus, U., Esposito, R., Forest, S.: The complete works of Gabrio Piola: Volume I Commented English Translation. Springer Publishing Company, Incorporated (2014)
21. dell'Isola, F., Lekszycki, T., Pawlikowski, M., Grygoruk, R., Greco, L.: Designing a light fabric metamaterial being highly macroscopically tough under directional extension: first experimental evidence. Zeitschrift für angewandte Mathematik und Physik **66**(6), 3473–3498 (2015)
22. dell'Isola, F., Giorgio, I., Pawlikowski, M., Rizzi, N.L.: Large deformations of planar extensible beams and pantographic lattices: heuristic homogenization, experimental and numerical examples of equilibrium. Proc. R. Soc. A **472**(2185), 23 (2016)
23. dell'Isola, F., Andreaus, U., Cazzani, A., Esposito, R., Placidi, L., Perego, U., Maier, G., Seppecher, P.: The Complete works of Gabrio Piola: Volume II Commented English Translation. Springer Publishing Company, Incorporated (2019)
24. Duncan, W.J.: A critical examination of the representation of massive and elastic bodies by systems of rigid masses elastically connected. Q. J. Mech. Appl. Math. **5**(1), 97–108 (1952)

25. Dupac, M., Marghitu, D.B.: Nonlinear dynamics of a flexible mechanism with impact. J. Sound Vib. **289**(4–5), 952–966 (2006)
26. Eugster, S.R., Hesch, C., Betsch, P., Glocker, C.: Director-based beam finite elements relying on the geometrically exact beam theory formulated in skew coordinates. Int. J. Numer. Methods Eng. **97**(2), 111–129 (2014)
27. Euler, L.: De curvis elasticis, Additamentum I to his Methodus inveniendi lineas curvas maximi minimive proprietate gaudentes. Lausanne and Geneva (1744)
28. Franciosi, P., Spagnuolo, M., Salman, O.U.: Mean green operators of deformable fiber networks embedded in a compliant matrix and property estimates. Contin. Mech. Thermodyn., 1–32 (2018)
29. Greco, L., Cuomo, M.: Consistent tangent operator for an exact Kirchhoff rod model. Contin. Mech. Thermodyn. **27**(4–5), 861–877 (2015)
30. Hencky, H.: Über die angenäherte lösung von stabilitätsproblemen im raum mittels der elastischen gelenkkette. Der Eisenbau **11**, 437–452 (1920)
31. Leckie, F.A., Lindberg, G.M.: The effect of lumped parameters on beam frequencies. Aeronaut. Q. **14**(3), 224–240 (1963)
32. Maurin, F., Greco, F., Desmet, W.: Isogeometric analysis for nonlinear planar pantographic lattice: discrete and continuum models. Contin. Mech. Thermodyn., 1–14 (2018)
33. Milton, G.W., Briane, M., Harutyunyan, D.: On the possible effective elasticity tensors of 2-dimensional and 3-dimensional printed materials. Math. Mech. Complex Syst. **5**(1), 41–94 (2017)
34. Misra, A., Poorsolhjouy, P.: Identification of higher-order elastic constants for grain assemblies based upon granular micromechanics. Math. Mech. Complex Syst. **3**(3), 285–308 (2015)
35. Placidi, L., Barchiesi, E., Turco, E., Rizzi, N.L.: A review on 2D models for the description of pantographic fabrics. Zeitschrift für angewandte Mathematik und Physik **67**(5), 121 (2016)
36. Placidi, L., Barchiesi, E., Battista, A.: An inverse method to get further analytical solutions for a class of metamaterials aimed to validate numerical integrations. In: Mathematical Modelling in Solid Mechanics, pp. 193–210. Springer (2017)
37. Reissner, E.: On one-dimensional finite-strain beam theory: the plane problem. Zeitschrift für angewandte Mathematik und Physik ZAMP **23**(5), 795–804 (1972)
38. Rosi, G., Placidi, L., Auffray, N.: On the validity range of strain-gradient elasticity: a mixed static-dynamic identification procedure. Eur. J. Mech.-A/Solids **69**, 179–191 (2018)
39. Rubinstein, D.: Dynamics of a flexible beam and a system of rigid rods, with fully inverse (one-sided) boundary conditions. Comput. Methods Appl. Mech. Eng. **175**(1–2), 87–97 (1999)
40. Ruocco, E., Zhang, H., Wang, C.M.: Hencky bar-chain model for buckling analysis of non-uniform columns. Structures **6**, 73–84 (2016)
41. Šalinić, S.: An improved variant of Hencky bar-chain model for buckling and bending vibration of beams with end masses and springs. Mech. Syst. Signal Process. **90**, 30–43 (2017)
42. Scerrato, D., Zhurba Eremeeva, I.A., Lekszycki, T., Rizzi, N.L.: On the effect of shear stiffness on the plane deformation of linear second gradient pantographic sheets. ZAMM - Zeitschrift für Angewandte Mathematik und Mechanik **96**(11), 1268–1279 (2016)
43. Spagnuolo, M., Andreaus, U.: A targeted review on large deformations of planar elastic beams: extensibility, distributed loads, buckling and post-buckling. Math. Mech. Solids **24**(1), 258–280 (2019)
44. Spagnuolo, M., Barcz, K., Pfaff, A., dell'Isola, F., Franciosi, P.: Qualitative pivot damage analysis in aluminum printed pantographic sheets: numerics and experiments. Mech. Res. Commun. **83**, 47–52 (2017)
45. Steigmann, D.J., Faulkner, M.G.: Variational theory for spatial rods. J. Elast. **33**(1), 1–26 (1993)
46. Turco, E.: Discrete is it enough? The revival of Piola-Hencky keynotes to analyze three-dimensional Elastica. Contin. Mech. Thermodyn. (2018). https://doi.org/10.1007/s00161-018-0656-4:1-19
47. Turco, E., dell'Isola, F., Cazzani, A., Rizzi, N.L.: Hencky-type discrete model for pantographic structures: numerical comparison with second gradient continuum models. Zeitschrift für angewandte Mathematik und Physik **67**(4), 28 (2016). https://doi.org/10.1007/s00033-016-0681-8

48. Turco, E., dell'Isola, F., Rizzi, N.L., Grygoruk, R., Müller, W.H., Liebold, C.: Fiber rupture in sheared planar pantographic sheets: numerical and experimental evidence. Mech. Res. Commun. **76**, 86–90 (2016b)
49. Turco, E., Golaszewski, M., Cazzani, A., Rizzi, N.L.: Large deformations induced in planar pantographic sheets by loads applied on fibers: experimental validation of a discrete lagrangian model. Mech. Res. Commun. **76**, 51–56 (2016c)
50. Turco, E., Giorgio, I., Misra, A., dell'Isola, F.: King post truss as a motif for internal structure of (meta) material with controlled elastic properties. R. Soc. Open Sci. **4**(10), 20 (2017)
51. Wang, C.M., Zhang, H., Gao, R.P., Duan, W.H., Challamel, N.: Hencky bar-chain model for buckling and vibration of beams with elastic end restraints. Int. J. Struct. Stab. Dyn. **15**(07), 16 (2015)
52. Wang, Y., Huston, R.L.: A lumped parameter method in the nonlinear analysis of flexible multibody systems. Comput. Struct. **50**(3), 421–432 (1994)
53. Zhang, H., Wang, C.M., Challamel, N.: Buckling and vibration of Hencky bar-chain with internal elastic springs. Int. J. Mech. Sci. **119**, 383–395 (2016)

Unsymmetrical Wrinkling of Nonuniform Annular Plates and Spherical Caps Under Internal Pressure

Svetlana M. Bauer and Eva B. Voronkova

Abstract Unsymmetrical buckling of inhomogeneous annular plates and spherical shallow shells subjected to internal pressure is studied. The effect of material heterogeneity, shallowness and ratio of inner to outer radii on the buckling load is examined. The unsymmetric part of the solution is sought in terms of multiples of the harmonics of the angular coordinate. A numerical method is employed to obtain the lowest load value, which leads to the appearance of waves in the circumferential direction. It is shown that if the elasticity modulus decreases away from the center of a plate, the critical pressure for unsymmetric buckling is sufficiently lower than for a plate with constant mechanical properties.

1 Introduction

The possibility of unsymmetrical buckling of internally pressurised spherical, torispherical, ellipsoidal shells has been discussed by many authors (e.g., [1, 2, 5, 13, 15]). Bushnell emphasized that nonlinearity of the prebuckling state is significant in such problems. Sufficiently precise approximation of the prebuckling state is crucial in predicting of buckling load and mode shape [5, 11].

Panov and Feodos'ev were the first who analyzed unsymmetrical buckling of the thin circular isotropic plates under normal pressure [15]. They suggested that under sufficiently large load an unsymmetric state branched from the axisymmetric one and waves developed near the edge of the plates. Panov and Feodos'ev represented nonaxisymmetric displacement in the form $w = (1 - r^2)^2(A + Br^4 \cos n\theta)$ and examined the bending problem by Galerkin procedure.

In this approach the prebuckling axisymmetric state was approximated by function with only one unknown parameter. Later, Feodos'ev showed that the elastic surface

S. M. Bauer (✉) · E. B. Voronkova
St. Petersburg State University, 7/9 Universitetskaya nab., St. Petersburg, Russia
e-mail: s.bauer@spbu.ru

E. B. Voronkova
e-mail: e.voronkova@spbu.ru

H. Altenbach et al. (eds.), *Recent Developments in the Theory of Shells*,
Advanced Structured Materials 110, https://doi.org/10.1007/978-3-030-17747-8_6

of plates or shells under large deformations could not be described by one or two unknown parameters in approximating functions [11]. Existence of unsymmetric equilibrium states for a simply supported circular plate was showed by Morozov [14], and Piechocki proved the uniqueness theorem [16].

Cheo and Reiss studied axially unsymmetric equilibrium states of a clamped circular plate subjected to a surface load [6]. They confirmed that a ring of large circumferential compressive stress develops near the edge of the plate and indicates possibility of wrinkling near the edge. Cheo and Reiss suspected that Panov and Feodos'ev had found unstable unsymmetric state in [15], and underlined the approximation function with two unknown parameters was "too inaccurate to adequately describe the wrinkling of the plate".

The postbuckling asymmetrical behaviour of annular plates was considered in [17]. The critical load and number of waves depended on the boundary conditions, the ratio between the inner and outer radii and the loads applied. Experiments on uniform heating of thin circular plates with fixed edges and formation of waves near plate's edge are discussed in [12].

Coman investigated the wrinkling of a uniformly stretched circular plate under transverse pressure [7]. He showed that the critical load increases with the background tension. Comparisons of the asymptotic approximations with numerical calculations was reported in [9, 10].

The asymmetric bifurcation for a shallow spherical cap subjected to either external or internal pressure was treated in [8]. Two-term asymptotic predictions for the buckling pressure and one-term approximations of the corresponding wave number were derived.

This paper deals with buckling of an annular plates and spherical caps with nonuniform mechanical characteristics. Such a plate or a cap can be used as the simplest model of Lamina Cribrosa (LC) in the human eye [3]. Buckling of the LC in a non-axisymmetric state in the neighborhood of the edge could cause edamas and folds at the periphery of the LC and loss of sight.

2 Problem Formulation

Consider a shallow spherical elastic shell of uniform thickness $h > 0$, subjected to uniformly distributed inner pressure p, as shown in Fig. 1. The equation of the shell middle surface is given by $z = H\left(1 - r^2/a^2\right)$, where a is the base radius, H is the rise of the mid-surface at the center. The cap is thin and shallow, which means that the ratio of its thickness to the radius of curvature $R = a^2/(2H)$ is much less than unity ($h/R \ll 1$), and that the apex rise is much less that the curvature radius ($H \ll R$). A spherical shell may also be named as shallow if $H/a < 1/8$.

We assume meridional material inhomogeneity for the shell, i.e. Young's modulus E is spatially dependent. For a shallow spherical shell we may set the modulus of elasticity $E = E(r)$.

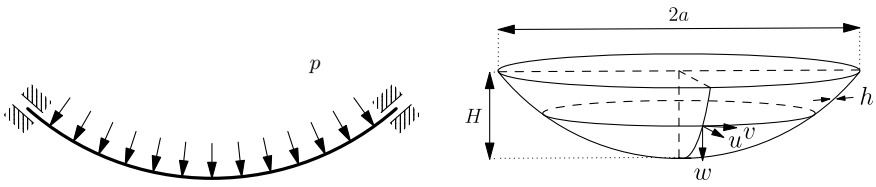

Fig. 1 Geometry of the spherical cap

For a spherical cap with meridional inhomogeneity under inner pressure the well-known Donnell-Mushtari-Vlasov equations can be written in the form

$$\begin{aligned} &D\Delta\Delta w + \frac{\partial D}{\partial r}L_1^+(w) + \frac{\partial^2 D}{\partial r^2}L_2^+(w) = P + L(w,F) - \frac{1}{R}\Delta F, \\ &\frac{\Delta\Delta F}{E} + \frac{\partial}{\partial r}\left(\frac{1}{E}\right)L_1^-(F) + \frac{\partial^2}{\partial r^2}\left(\frac{1}{E}\right)L_2^-(F) = -\frac{h}{2}L(w,w) + \frac{1}{R}\Delta w, \end{aligned} \tag{1}$$

where r and θ are polar coordinates in the base plane, $w(r,\theta)$ is the displacement in the direction of z, $F(r,\theta)$ is the Airy stress function, $D(r) = E(r)h^3/12(1-\nu^2)$ is the bending stiffness, and ν is Poisson's coefficient. The Laplacian is defined as

$$\Delta = \frac{\partial^2}{\partial r^2} + \frac{1}{r}\frac{\partial}{\partial r} + \frac{1}{r^2}\frac{\partial^2}{\partial\theta^2}.$$

We shall further use the notations $(\,)' = \partial(\,)/\partial r$, $\dot{(\,)} = \partial(\,)/\partial\theta$. The differential operators that appear in (1) are listed in Appendix.

Let us introduce the following dimensionless quantities

$$\begin{aligned} &r^* = \frac{r}{a}, \quad w^* = \beta\frac{w}{h}, \quad P^* = \beta^3\frac{Pa^4}{E_{av}h^4}, \quad F^* = \beta^2\frac{F}{E_{av}h^3}, \\ &A = \beta\frac{a^2}{Rh}, \quad \beta^2 = 12(1-\nu^2). \end{aligned} \tag{2}$$

Here E_{av} is an average value of Young's modulus in the radial direction

$$E_{av} = \frac{1}{S}\iint_S E(r)r\,dr\,d\theta, \quad E(r) = E_0 f(r), \tag{3}$$

where $f(r)$ is a smooth position function, S denotes the area of the shell mid-surface.

The dimensionless forms of Eqs. (1) are (with the asterisks being omitted)

$$
\begin{aligned}
g_1(r)\Delta\Delta w + g_1'(r)L_1^+(w) + g_1''(r)L_2^+(w) &= P + L(w,F) - A\Delta F,\\
g_2(r)\Delta\Delta F + g_2'(r)L_1^-(F) + g_2''(r)L_2^-(F) &= -L(w,w)/2 + A\Delta w,\\
g_1(r) = E_0 f(r)/E_{av}, \quad g_2(r) &= 1/g_1(r).
\end{aligned} \tag{4}
$$

We remark here that the deformation of the externally pressurised spherical shell can be described by the same system of Eqs. (4) after reversing signs before the last terms on the right-hand site. By taking $A = 0$ in Eqs. (4) one can obtain the governing equations for the inhomogeneous circular plate subjected to normal pressure.

The boundary conditions for the problem are the following. The outer edge of the shell is clamped but can move freely in the radial direction without rotation. In addition, all sought-for functions must fulfil the boundedness condition at the apex of the shell. In this case the system (4) are completed by the set of conditions

$$
w = w' = \frac{F'}{r} + \frac{\ddot{F}}{r^2} = -\left(\frac{\dot{F}}{r}\right)' = 0 \quad \text{at} \quad r = 1, \tag{5}
$$

$$
w' = \dot{w} = F' = \dot{F} = 0 \quad \text{at} \quad r = 0. \tag{6}
$$

We also consider a truncated spherical shell—a shell with a circular opening at the top. For this situation the inner edge of the shell can be assumed to be supported by roller which can slide along a vertical wall. This constrain can be written as

$$
w' = 0, \quad N_{r\theta} = 0, \quad (rM_r)' - M_\theta + 2\dot{M}_{r\theta} = 0, \quad u = 0 \quad \text{at} \quad r = \delta. \tag{7}
$$

Here $r = \delta = a_{in}/a$ is a dimensionless radial coordinate of the inner edge, u denotes the horizontal radial components of displacement, M_r, M_θ, $M_{r\theta}$ are meridional, circumferential and twisting moments, respectively, and $N_{r\theta}$ is tangential stress resultant.

In the terms of the displacement component w and stress function F, the boundary conditions (7) are equivalent to

$$
\begin{aligned}
&w' = 0, \quad \frac{\dot{F}}{r^2} - \frac{\dot{F}'}{r} = 0,\\
&g_1(r)\left((\Delta w)' + \frac{1-\nu}{r}\left(\frac{\ddot{w}}{r}\right)'\right) + g_1'(r)L_2^+(w) = 0,\\
&g_2(r)\left((\Delta F)' + \frac{\Delta F}{r} - \frac{1+\nu}{r^2}\left(\ddot{F} + F\right)'\right) + g_2'(r)L_2^-(F) = -A\frac{w}{r}.
\end{aligned} \tag{8}
$$

Setting $A = 0$ in (8) we arrive at set of boundary conditions for an annular plate.

2.1 Axisymmetric Behavior

The governing equations of the symmetrical problem can be obtain from Eqs. (4). For the shell closed at the top we have

$$\begin{aligned} g_1\left(\Theta_0'' + \frac{\Theta_0'}{r} - \frac{\Theta_0}{r^2}\right) + g_1'\left(\Theta_0' + \nu\frac{\Theta_0}{r}\right) &= \frac{Pr}{2} + \frac{\Theta_0\Phi_0}{r} - A\Phi_0, \\ g_2\left(\Phi_0'' + \frac{\Phi_0'}{r} - \frac{\Phi_0}{r^2}\right) + g_2'\left(\Phi_0' - \nu\frac{\Phi_0}{r}\right) &= -\frac{\Theta_0^2}{2r} + A\Theta_0, \end{aligned} \tag{9}$$

where $\Theta_0 = w_s'$ and $\Phi_0 = F_0'$ and boundary conditions

$$\Theta_0 = \Phi_0 = 0 \quad \text{at} \quad r = 0,\ 1. \tag{10}$$

2.1.1 Equations for Truncated Shell

For the the truncated spherical shell Eqs. (4) become

$$\begin{aligned} g_1\left(w''' + \frac{w''}{r} - \frac{w'}{r^2}\right) + g_1'\left(w'' + \nu\frac{w'}{r}\right) &= \frac{Pr}{2} + \frac{w'\Phi_0}{r} - A\Phi_0 + \frac{C}{r}, \\ g_2\left(\Phi_0'' + \frac{\Phi_0'}{r} - \frac{\Phi_0}{r^2}\right) + g_2'\left(\Phi_0' - \nu\frac{\Phi_0}{r}\right) &= -\frac{\Theta_0^2}{2r} + A\Theta_0, \end{aligned} \tag{11}$$

and the boundary conditions are

$$\begin{aligned} w = w' = \Phi_0 = 0 \quad &\text{at} \quad r = 1, \\ w' = 0, \quad \Phi_0' - \frac{\nu}{r}\Phi_0 + Aw = 0 \quad &\text{at} \quad r = \delta, \end{aligned} \tag{12}$$

and

$$C = -p\delta^2/2 - w'(\delta)\Phi_0(\delta) + A\delta\Phi_0(\delta).$$

3 Equations for Buckling

Asymmetrical solutions of problem (4) with appropriate boundary conditions branch from a solution of axisymmetric states. To detect the occurrence of wrinkling we seek for a solution of Eqs. (4) in the form

$$w(r,\theta) = w_s(r) + \varepsilon w_{ns}\cos(n\theta), \quad F(r,\theta) = F_s(r) + \varepsilon F_{ns}\cos(n\theta), \tag{13}$$

where $w_s(r)$, $F_s(r)$ describe prebuckling axisymmetric state, ε is infinitesimal parameter, n is a mode number and $w_n(r)$, $F_n(r)$ are the non-symmetrical components.

After substitution of (13) in (4), using Eqs. (9) (or (11)), and linearization with respect to ε we obtain

$$\begin{aligned} g_1\Delta_n\Delta_n w_n + \mathcal{L}_1(g_1, w_n) &= -A\Delta_n F_n + \frac{w_n''}{r}\Phi_0 + \frac{F_n''}{r}\Theta_0 + \\ &+ \Theta_0'\left(\frac{F_n'}{r} - \frac{n^2}{r^2}F_n\right) - \Phi_0'\left(\frac{w_n'}{r} - \frac{n^2}{r^2}w_n\right), \\ g_2\Delta_n\Delta_n F_n + \mathcal{L}_2(g_2, F_n) &= A\Delta_n w_n - \frac{w_n''}{r}\Theta_0 - \Theta_0'\left(\frac{w_n'}{r} - \frac{n^2}{r^2}w_n\right). \end{aligned} \tag{14}$$

The definitions of the operators $\mathcal{L}_1$, $\mathcal{L}_2$ are listed in Appendix.

Boundary conditions (5) and (6) are reduced to

$$w_n = w_n' = F_n = F_n' = 0 \quad \text{at} \quad r = 0,\ 1. \tag{15}$$

For the truncated shell we replace the constrain at the shell apex by

$$\begin{aligned} &w_n' = 0, \quad F_n' - rF_n = 0, \\ &g_1\left((\Delta_n w_n)' - \frac{n^2}{r}(1-\nu)\left(\frac{w_n}{r}\right)'\right) + g_1' L_{2n}^{+}(w_n) = 0, \\ &g_2\left((\Delta_n F_n)' + \frac{\Delta_n F_n}{r} + \frac{1+\nu}{r^2}(n^2-1)F'\right) + g_2' L_{2n}^{-}(F_n) = -A\frac{w_n}{r} \end{aligned} \tag{16}$$

for $r = \delta$.

4 Numerical Results and Discussion

Buckling equation (14) with boundary conditions (15) or (16) constitute an eigenvalue problem, in which the parameter p is implicit and appears in the equations through the functions Θ_0 and Φ_0.

We use standard MATLAB functions to solve nonlinear axisymmetric problem (9) together with (10) or (12). The value of P, for which (14) with (15) or (16), have nontrivial solution, was found by using the finite difference method [6, 13]. We regard the smallest of these eigenvalues as the buckling load.

Figure 2 illustrates behaviour of the normalized critical load P^{cr} and the critical mode number m for a homogeneous shallow spherical shell. P_{pl}^{cr} corresponds to the buckling load of axisymmetric equilibrium state of an isotropic homogeneous circular

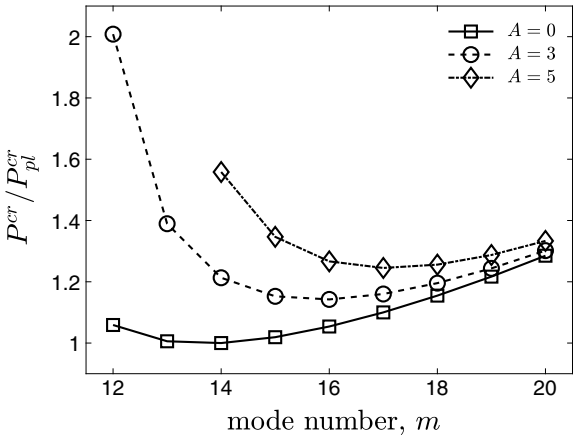

Fig. 2 Dependence of the normalized critical load P^{cr} on the mode number m for a uniform shallow spherical shell. Solid line corresponds to a circular plate ($A = 0$), dashed and dash-dotted lines—to a shell with $A = 3$ and $A = 5$, respectively. P^{cr}_{pl} denotes the buckling pressure for a uniform circular plate

Table 1 Normalized buckling load (P^{cr}/P^{cr}_{pl}) and corresponding wave numbers for the heterogenous plate and shallow shells

	$q = 0$	$q = 1$	$q = 3$
$A = 0$			
P^{cr}/P^{cr}_{pl}	1	0.76	0.41
Mode number, m	14	14	15
$A = 5$			
P^{cr}/P^{cr}_{pl}	1.25	0.96	0.5
Mode number, m	17	17	18
$A = 10$			
P^{cr}/P^{cr}_{pl}	1.51	1.16	0.59
Mode number, m	20	20	21

plate ($P^{cr}_{pl} = 64453$). The critical load P^{cr} increases as the shallowness parameter A increases.

To study the effect of the varying rate of inhomogeneity on the critical load and buckling mode, we assume exponential law for material inhomogeneity: $E = E_0 e^{-qr}$. The buckling load for unsymmetrical buckling was calculated numerically over a large range of parameters E_0, q, but for constant average value of the elastic modulus (3). The results are summarized in Table 1 and Fig. 3. The parameter value $q = 0$ corresponds to uniform plate with constant Young's modulus.

The normalized buckling pressure P^{cr}/P^{cr}_{pl} decreases as the rate of inhomogeneity $|q|$ increases, whereas the buckling mode m increases with $|q|$ (see Table 1). Similar results we reported in [4].

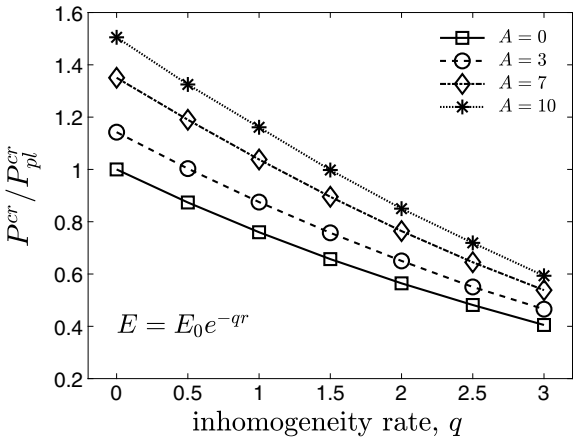

Fig. 3 Change of the normalized buckling pressure P^{cr} when the degree of heterogeneity of the shell q changes for different values of the curvature parameter A. P^{cr}_{pl} denotes the buckling pressure for a uniform circular plate

Table 2 Normalized buckling load (P^{cr}/P^{cr}_{pl}) for the homogenous annular plate and truncated shells

	$\delta = 0$	$\delta = 0.1$	$\delta = 0.15$	$\delta = 0.2$	$\delta = 0.25$
$A = 0$					
P^{cr}/P^{cr}_{pl}	1	1.08	1.14	1.25	1.37
Mode number, m	14	13	12	11	11
$A = 5$					
P^{cr}/P^{cr}_{pl}	1.25	1.35	1.43	1.55	1.7
Mode number, m	17	16	15	14	14
$A = 10$					
P^{cr}/P^{cr}_{pl}	1.51	1.64	1.74	1.88	1.6
Mode number, m	20	18	18	17	16

The results for an annular plate and truncated shell are presented in Table 2, Figs. 4 and 5. The normalized buckling pressure P^{cr}/P^{cr}_{pl} increases as the radius of the opening δ increases, while the buckling mode m has opposite behavior: it decreases when δ increases.

We note closely adjacent values of the critical load for the consecutive wave number, e.g. for the uniform spherical shell with $A = 7$ the critical loads differ between each other by less than 1% ($P^{cr} = 87044$ for $m = 18$ and $P^{cr} = 87415$ for $m = 19$). The truncated shell (with $A = 7$ and radius of the opening $\delta = 0.1$) wrinkles at $P^{cr} = 94296$, and the buckling mode has 17 waves, while for 16 waves the critical load is 95316. Thus, the considered plates and shells are sensitive to initial imperfections of form or to initial stresses.

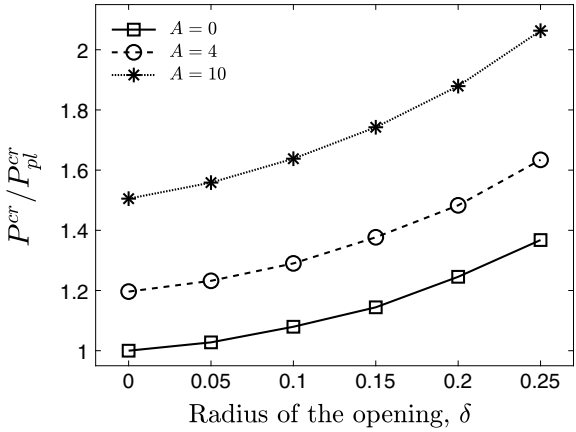

Fig. 4 Dependence of the normalized buckling pressure P^{cr} on the radius of the opening δ for different values of the curvature parameter A. P^{cr}_{pl} denotes the buckling pressure for a uniform circular plate

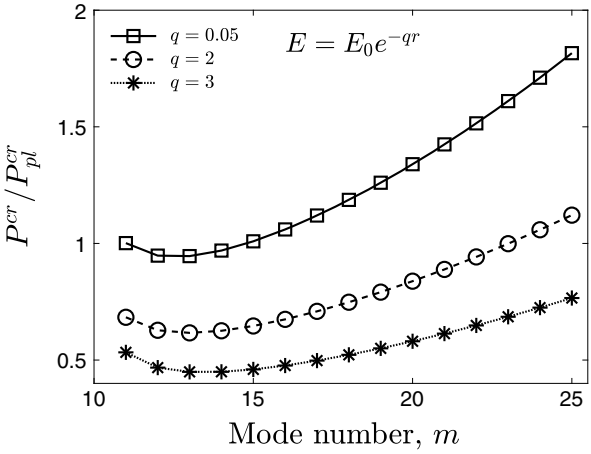

Fig. 5 Dependence of the normalized critical load P^{cr} of an annular plate ($\delta = 0.1$) on the mode number m for different values of the inhomogeneity rate q. P^{cr}_{pl} denotes the buckling pressure for a uniform circular plate

The axisymmetrical stability for the internally pressurized shell was studied in [8]. Authors came to conclusion that the dimensionless critical load $\lambda \to 0$ as shallowness parameter $\mu = 2(3(1-\nu^2))^{1/4}(H/h)^{1/2}$ grows. We report here the opposite behavior: the non-dimensionless pressure P^* grows as parameter A increases. After matching dimensionless variables employed in [8] and in the current paper (2)

$$\mu = A^{1/2}, \quad \lambda = P^*/(4\mu^4) = P^*/(4A^2)$$

we can conclude that the results of the both studies are in good agreement.

5 Conclusion

The wrinkling of the annular plates and shallow spherical shells under subjected to internal pressure has been studied in this work. Prebuckling stress-state in a narrow zone near the shells edge makes a major contribution to the unsymmetrical buckling mode and the value of the critical load. It is shown that if the elasticity modulus decreases away from the center of a plate, the critical pressure for unsymmetric buckling is sufficiently lower than for a plate with constant mechanical properties. Number of waves in the circumferential direction increases with the degree of nonuniformity. The buckling load and corresponding mode number increase as the shallowness parameter grows. For a truncated shallow shell the wrinkling pressure increases as the radius of the opening increases, while the buckling mode decreases.

Acknowledgements This research was supported by the Russian Foundation for Basic Research (project no. 18-01-00832).

Appendix

The differential operators that appear in (1) are defined by

$$L(x,y) = x''\left(\frac{y'}{r} + \frac{\ddot{y}}{r^2}\right) + y''\left(\frac{x'}{r} + \frac{\ddot{x}}{r^2}\right) - 2\left(\frac{\dot{x}}{r}\right)'\left(\frac{\dot{y}}{r}\right)',$$
$$L_1^{\pm}(y) = 2y''' + (2 \pm \nu)\frac{y''}{r} + 2\frac{(\ddot{y})'}{r^2} - \frac{y'}{r^2} - 3\frac{\ddot{y}}{r^3},$$
$$L_2^{\pm}(y) = y'' \pm \nu\left(\frac{y'}{r} + \frac{\ddot{y}}{r^2}\right).$$

The differential operators introduced in (13) are given by

$$\mathcal{L}_1(g_1, w_n) = g_1' L_{1n}^{+}(w_n) + g_1'' L_{2n}^{+}(w_n),$$
$$\mathcal{L}_2(g_2, F_n) = g_2' L_{1n}^{-}(F_n) + g_2'' L_{2n}^{-}(F_n),$$

where

$$L_1^{\pm}(y) = 2y''' + \frac{2 \pm \nu}{r}y'' - \frac{2n^2+1}{r^2}\ddot{y} + \frac{3n^2}{r^3}\ddot{y},$$
$$L_2^{\pm}(y) = y'' \pm \nu\left(\frac{y'}{r} - \frac{n^2}{r^2}\ddot{y}\right).$$

References

1. Adachi, J.: Stresses and buckling in thin domes under internal pressure. Tech. Rep. MS68–01, U.S. Army Materials and Mechanics Research Center, Watertown (1968)
2. Adachi, J., Benicek, M.: Buckling of torispherical shells under internal pressure. Exp. Mech. **4**(8), 217–222 (1964). https://doi.org/10.1007/BF02322954
3. Bauer, S.M., Voronkova, E.B.: Models of shells and plates in the problems of ophthalmology. Vestnik St. Petersburg University: Mathematics **47**(3), 123–139 (2014). https://doi.org/10.3103/S1063454114030029
4. Bauer, S.M., Voronkova, E.B., Ignateva, K.: Unsymmetric equilibrium states of inhomogeneous circular plates under normal pressure. In: Pietraszkiewicz, W., Górski, J. (eds.) Shell structures, vol. 3. CRC Press, Taylor & Francis Group, Boca Raton (2014)
5. Bushnell, D.: Buckling of shells-pitfall for designers. AIAA J. **19**(9), 1183–1226 (1981). https://doi.org/10.2514/3.60058
6. Cheo, L.S., Reiss, E.L.: Unsymmetric wrinkling of circular plates. Q. Appl. Math. **31**(1), 75–91 (1973). https://doi.org/10.1090/qam/99710
7. Coman, C.D.: Asymmetric bifurcations in a pressurised circular thin plate under initial tension. Mech. Res. Commun. **47**, 11–17 (2013). https://doi.org/10.1016/j.mechrescom.2012.09.005
8. Coman, C.D., Bassom, A.P.: Asymptotic limits and wrinkling patterns in a pressurised shallow spherical cap. Int. J. Non Linear Mech. **81**, 8–18 (2016). https://doi.org/10.1016/j.ijnonlinmec.2015.12.004
9. Coman, C.D., Bassom, A.P.: On the nonlinear membrane approximation and edge-wrinkling. Int. J. Solids Struct. **82**, 85–94 (2016). https://doi.org/10.1016/j.ijsolstr.2015.11.011
10. Coman, C.D., Bassom, A.P.: Wrinkling structures at the rim of an initially stretched circular thin plate subjected to transverse pressure. SIAM J. Appl. Math. **78**(2), 1009–1029 (2018). https://doi.org/10.1137/17M1155193
11. Feodos'ev, V.I.: On a method of solution of the nonlinear problems of stability of deformable systems. J. Appl. Math. Mech. **27**(2), 392–404 (1963). https://doi.org/10.1016/0021-8928(63)90008-X
12. Goldstein, R., Popov, A., Kozintsev, V., Chelyubeev, D.: Non-axisymmetric edge buckling of circular plates when heated. PNRPU Mech. Bull. **1**, 45–53 (2016). https://doi.org/10.15593/perm.mech/2016.2.04
13. Huang, N.C.: Unsymmetrical buckling of shallow spherical shells. AIAA J. **1**(4), 945 (1963). https://doi.org/10.2514/3.1690
14. Morozov, N.F.: On the existence of a non-symmetric solution in the problem of large deflections of a circular plate with a symmetric load. Izv. Vyssh. Uchebn. Zaved. Mat. **2**, 126–129 (1961)
15. Panov, D.Y., Feodosiev, V.I.: On the equilibrium and loss of stability of shallow shells in the case of large displacement. Prikladnaya matematika mekhanika. Prikladnaya Matematika Mekhanika **12**, 389–406 (1948)
16. Piechocki, W.: On the nonlinear theory of thin elastic spherical shells: Nonlinear partial differential equations solutions in theory of thin elastic spherical shells subjected to temperature fields and external loading. Archiwum mechaniki stosowanej **21**(1), 81–102 (1969)
17. Radwańska, M., Waszczyszyn, Z.: Numerical analysis of nonsymmetric postbuckling behaviour of elastic annular plates. Comput. Methods Appl. Mech. Eng. **23**(3), 341–353 (1980). https://doi.org/10.1016/0045-7825(80)90014-6

Two-Dimensional Model of a Plate, Made of Material with the General Anisotropy

A. K. Belyaev, N. F. Morozov, P. E. Tovstik, T. P. Tovstik and A. V. Zelinskaya

Abstract A new two-dimensional linear model of the second order accuracy describing deformations of an anisotropic heterogeneous in the thickness direction plate is proposed. The case of the general anisotropy with 21 elastic modules is studied. The asymptotic expansions of solutions of 3D equations of the theory of elasticity in power series with small thickness parameter are used. The zero asymptotic approximation was constructed earlier and it is similar to the Kirchhoff–Love model. Also earlier the models of the second order accuracy were built for an isotropic material and for partial cases of anisotropy (for transversely isotropic and for monoclinic materials). In this work the general case is studied. A peculiarity of the proposed model is that the model includes the zero, the first, and the second approximations in contrary to the more simple models where summands of the first asymptotic order are absent. The proposed model may be applied to multi-layered and to functionally graded plates. The model may be used to solve various static and vibration problems. A 2D system of three PDE with the constant coefficients is obtained. The harmonic solution is investigated more detailed, and in this case the problem is reduced to a linear algebraic system.

Keywords Anisotropic heterogeneous plate · Two-dimensional model · The second order accuracy · Bending · Vibrations · Waves propagation.

A. K. Belyaev · T. P. Tovstik
Institute for Problems in Mechanical Engineering RAS, Bolshoy pr. V. O., 61, 199178 St. Petersburg, Russia
e-mail: 13augen@mail.ru

T. P. Tovstik
e-mail: tovstik_t@mail.ru

N. F. Morozov · P. E. Tovstik (✉) · A. V. Zelinskaya
St. Petersburg State University, Universitetsky prospekt, 28, 198504 St. Petersburg, Russia
e-mail: peter.tovstik@mail.ru

N. F. Morozov
e-mail: morozov@nm1016.spb.edu

A. V. Zelinskaya
e-mail: anna_zelinskaya@inbox.ru

H. Altenbach et al. (eds.), *Recent Developments in the Theory of Shells*,
Advanced Structured Materials 110, https://doi.org/10.1007/978-3-030-17747-8_7

1 Introduction

Derivation of two-dimensional approximate models of thin plates and shells is one of the classic problems of mechanics [1–6]. The equation of bending and vibrations of a plate can be obtained from three-dimensional equations of the elasticity theory by applying the Kirchhoff–Love (KL) hypotheses [1, 2]. The more complex and more accurate equations accounting for transversal shear are derived by means of the Timoshenko–Reissner (TR) hypotheses [3, 7]. The two-dimensional equations can also be obtained by expansions of the plate quantities in series of Legendre polynomials in the thickness direction [8, 9]. Similarly, the two-dimensional shell equations can be written directly as an equilibrium equation for a two-dimensional elastic media [10].

The numerous investigations are devoted to delivering of 2D approximate models of thin plates and shells made of anisotropic materials (we mention the books [9, 11–13], containing an extensive bibliography).

For a transversely isotropic material the 2D equations of the second order accuracy (SOA) are delivered and investigated in [14–19]. The SOA of 2D models is important for the multi-layered plates with the alternating hard and soft layers because the models based on the classic KL and TR models lead to the large errors.

An analysis of multi-layered orthotropic plates with the arbitrary orientation of the main directions of orthotropy is reduced to investigation of heterogeneous in the thickness direction monoclinic plates. Asymptotic analysis of monoclinic plates is performed in [20], and in [21] 2D equations of SOA are delivered.

In the case of the general anisotropy (with 21 elastic modules) the classic KL and TR models also are unacceptable. In [22] for anisotropic plates and in [23] for shells the generalized TR model is proposed. These models are obtained by using kinematic hypotheses and lead to equations of 10th differential order. Among the solutions, following from these models, there are the boundary layers. It is desirable to exclude the boundary layers from solutions (see [23]) because they describe stress states with the very large variability that are not typical for shell theories. The shell theory is based on the assumption that the typical length of picture of deformations is larger than the shell thickness, and the boundary layer does not satisfy this assumption.

In [24] based on the asymptotic expansions, elaborated in [15–17], the 2D model of a multi-layered plate with the general anisotropy is delivered. This model leads to equations of 8th differential order and it is similar to the KL model with the equivalent elastic modules. This model is of the zero order of accuracy and it is not acceptable for a multi-layered plate with the alternating hard and soft layers.

In this work we consider an anisotropic heterogeneous plate of the general anisotropy (with 21 elastic modules) and construct the higher asymptotic approximations. For the general anisotropy the asymptotic solution is essentially more difficult and bulky compared with the monoclinic material. To construct a model of the SOA for a material with the general anisotropy it is necessary to built asymptotic solutions of the zero, the first, and the second approximations, and for a monoclinic material the first approximation is absent.

As a result a PDE system with constant coefficients is obtained. The differential order of this system is the same as the order of the TR model, but this system essentially more complex. For a heterogeneous in the thickness direction plate to find coefficients it is necessary to calculate repeated integrals of elastic modules. Closed solutions of the boundary value problems for a finite plate do not exist because a separation of variables is impossible. A harmonic solution for an infinite plate is considered for that the problem is reduced to a system of linear algebraic equations. The harmonic bending and vibration problems are considered.

2 The Main Equations and Assumptions

Consider a thin elastic plate of the constant thickness h. In the main Cartesian co-ordinate system x_1, x_2, x_3 the equilibrium equations read as:

$$\sum_{j=1}^{3} \frac{\partial \sigma_{ij}}{\partial x_j} + f_i = 0, \quad i = 1, 2, 3, \qquad -\frac{h}{2} \le x_3 = z \le \frac{h}{2}, \tag{2.1}$$

where σ_{ij} are the stresses, and f_i are the intensities of the external forces.

In the case of the general anisotropy of material the stresses σ_{ij} are expressed through the strains γ_{kl} as follows

$$\sigma_{ij} = C_{ijkl}\gamma_{kl}, \quad \gamma_{kl} = \frac{1}{2}\left(\frac{\partial u_k}{\partial x_l} + \frac{\partial u_l}{\partial x_k}\right), \tag{2.2}$$

where $\mathbf{C} = \{C_{ijkl}\}$ is the elastic tensor of the 4th rank with 21 independent components, and $u_k(x_1, x_2, z)$ are the deflections.

Here the tensor designations are not used, and strains ε_{ij} are as follows:

$$\varepsilon_{ii} = \gamma_{ii} = \frac{\partial u_i}{\partial x_i}, \quad \varepsilon_{ij} = 2\gamma_{ij} = \frac{\partial u_i}{\partial x_j} + \frac{\partial u_j}{\partial x_i}, \quad i \neq j, \quad i, j = 1, 2, 3. \tag{2.3}$$

We write strains and stresses as 6D vectors. Then the elasticity relation (2.2) read as [13]:

$$\begin{gathered} \sigma = \mathbf{E}\cdot\varepsilon, \quad \mathbf{E} = \left(E_{ij}\right)_{i,j=1,\ldots,6}, \\ \sigma = (\sigma_{11}, \sigma_{22}, \sigma_{33}, \sigma_{23}, \sigma_{13}, \sigma_{12})^T, \quad \varepsilon = (\varepsilon_{11}, \varepsilon_{22}, \varepsilon_{33}, \varepsilon_{23}, \varepsilon_{13}, \varepsilon_{12})^T. \end{gathered} \tag{2.4}$$

Here and later ^{T} denotes transposition, the bold letters are used for vectors, for matrices and for operators, the product of vectors and matrices is denoted by dot(). The matrix $\mathbf{E}$ is symmetric and positively definite. It is assumed that elastic modules E_{ij} do not depend on tangential co-ordinates x_1, x_2, and they may depend on $x_3 = z$.

A dependence on z has place for functionally graded plates, and for multilayered plates modules $E_{i,j}$ are piece-wise functions of z.

As in [17] for an asymptotic analysis we divide stresses σ_{ij} and strains ε_{ij} in the groups of tangential $\sigma_t,\ \varepsilon_t$ and transversal $\sigma_n,\ \varepsilon_n$ stresses and strains and put

$$\begin{aligned} \sigma_t &= (\sigma_{11},\ \sigma_{22},\ \sigma_{12})^T\ ,\ \sigma_n = (\sigma_{13},\ \sigma_{23},\ \sigma_{33})^T\ , \\ \varepsilon_t &= (\varepsilon_{11},\ \varepsilon_{22},\ \varepsilon_{12})^T\ ,\ \ \varepsilon_n = (\varepsilon_{13},\ \varepsilon_{23},\ \varepsilon_{33})^T\ , \end{aligned} \tag{2.5}$$

where

$$\begin{aligned} \mathbf{A} = \{A_{ij}\} = \begin{pmatrix} E_{11} & E_{12} & E_{16} \\ E_{12} & E_{22} & E_{26} \\ E_{16} & E_{26} & E_{66} \end{pmatrix},\quad \mathbf{B} = \{B_{ij}\} = \begin{pmatrix} E_{15} & E_{25} & E_{56} \\ E_{14} & E_{24} & E_{46} \\ E_{13} & E_{23} & E_{36} \end{pmatrix}, \\ \mathbf{C} = \{C_{ij}\} = \begin{pmatrix} E_{55} & E_{45} & E_{35} \\ E_{45} & E_{44} & E_{34} \\ E_{35} & E_{34} & E_{33} \end{pmatrix}. \end{aligned} \tag{2.6}$$

Then elasticity relations (2.4) accept the form:

$$\sigma_t = \mathbf{A}\cdot\varepsilon_t + \mathbf{B}\cdot\varepsilon_n,\quad \sigma_n = \mathbf{B}^T\cdot\varepsilon_t + \mathbf{C}\cdot\varepsilon_n, \tag{2.7}$$

Excluding small transversal strains ε_n we obtain

$$\sigma_t = \mathbf{A}^*\cdot\varepsilon_t + \mathbf{B}\cdot\mathbf{C}^{-1}\cdot\sigma_n,\qquad \varepsilon_n = \mathbf{C}^{-1}\cdot\sigma_n - \mathbf{C}^{-1}\cdot\mathbf{B}^T\cdot\varepsilon_t \tag{2.8}$$

where

$$\mathbf{A}^* = \mathbf{A} - \mathbf{B}\cdot\mathbf{C}^{-1}\cdot\mathbf{B}^T. \tag{2.9}$$

We suppose that the planes $z = -h/2$ and $z = h/2$ are free that yields the boundary conditions

$$\sigma_{13} = \sigma_{23} = \sigma_{33} = 0,\qquad z = \pm h/2,\quad z = h. \tag{2.10}$$

The external surface forces may be included in the body forces by using the Dirac delta-function.

Introduce dimensionless variables (with the sign$\hat{}$) by relations

$$\begin{aligned} &\{x_1, x_2, u_1, u_2, u_3\} = l\{\hat{x}_1, \hat{x}_2, \hat{u}_1, \hat{u}_2, w\},\quad z = l\hat{z},\quad \mu = h/l, \\ &\{A_{ij}, B_{ij}, C_{ij}, \sigma_{ij}\} = E\{\hat{A}_{ij}, \hat{B}_{ij}, \hat{C}_{ij}, \hat{\sigma}_{ij}\},\quad \{f_i\} = (E/l)\{\hat{f}_i\},\quad i, j = 1, 2, 3, \end{aligned} \tag{2.11}$$

where l is the typical length of waves in tangential directions, E is the typical value of elastic modules, μ is the small parameter. Further the sign$\hat{}$ is omitted. As a result we get a system of 6th order with the small parameter μ

$$\begin{aligned}
&\frac{\partial w}{\partial z} = \mu\varepsilon_{33},\\
&\frac{\partial u_i}{\partial z} = -\mu(p_i w - \varepsilon_{i3}), \quad i = 1, 2,\\
&\frac{\partial \sigma_{i3}}{\partial z} = -\mu(p_1\sigma_{1i} + p_2\sigma_{2i} + f_i) \equiv g_i, \quad i = 1, 2,\\
&\frac{\partial \sigma_{33}}{\partial z} = -\mu(p_1\sigma_{13} + p_2\sigma_{23} + f_3) \equiv g_3,
\end{aligned} \tag{2.12}$$

where $p_1 = \partial(\,)/\partial x_1,\ p_2 = \partial(\,)/\partial x_2$.

3 Transformation of System (2.12)

We introduce the 2D vectors

$$\mathbf{u} = (u_1, u_2)^T, \quad \sigma_s = (\sigma_{13}, \sigma_{23})^T, \quad \varepsilon_s = (\varepsilon_{13}, \varepsilon_{23})^T, \quad \mathbf{f}_t = (f_1, f_2)^T, \tag{3.1}$$

the differential operators

$$\mathbf{p} = (p_1, p_2)^T, \qquad \mathbf{P} = \begin{pmatrix} p_1 & 0 & p_2 \\ 0 & p_2 & p_1 \end{pmatrix}^T, \tag{3.2}$$

and the integral operators

$$\mathbf{I}_a(Z) \equiv \int_{-1/2}^{1/2} Z dz, \quad \mathbf{I}(Z) \equiv \int_{-1/2}^{z} Z(z)\, dz, \quad \mathbf{I}_0(Z) \equiv \int_{0}^{z} Z(z)\, dz. \tag{3.3}$$

In these designations Eqs. (2.12) may be written as a system of integral equations

$$\begin{aligned}
&w = w_0 + \mu\mathbf{I}_0(\varepsilon_{33}),\\
&\mathbf{u} = \mu\mathbf{u}_0 - \mu\,\mathbf{I}_0(\mathbf{p}\,w - \varepsilon_s),\\
&\sigma_s = -\mu\,\mathbf{I}(\mathbf{P}^T\cdot\sigma_t + \mu\mathbf{f}_t),\\
&\sigma_{33} = -\mu\,\mathbf{I}(\mathbf{p}^T\cdot\sigma_s + \mu^2 f_3),
\end{aligned} \tag{3.4}$$

where

$$\begin{aligned}
&\varepsilon_n = (\varepsilon_s^T, \varepsilon_{33})^T = \mathbf{C}^{-1}\cdot(\sigma_n - \mathbf{B}^T\varepsilon_t),\ \varepsilon_t = \mathbf{P}\cdot\mathbf{u},\\
&\sigma_t = \mathbf{A}^*\cdot\mathbf{P}\cdot\mathbf{u} + \mathbf{B}\cdot\mathbf{C}^{-1}\cdot\sigma_n, \qquad \sigma_n = (\sigma_s^T, \sigma_{33})^T.
\end{aligned} \tag{3.5}$$

In Eqs. (3.4) $w_0(x_1, x_2),\ \mathbf{u}_0(x, 1, x_2)$ are the arbitrary functions that are to be found from boundary conditions $\sigma_n(1/2) = 0$. The boundary conditions $\sigma_n(-1/2) = 0$ are satisfied due to designation of operator $\mathbf{I}$ (see Eq. (3.3)).

Equations (3.4) *are* the main system for the following analysis. The values $u_1, u_2, w, \sigma_{13}, \sigma_{23}, \sigma_{33}$ are the main unknowns of Eqs. (3.4). The rest unknowns containing in the right sides of Eqs. (3.4) are expressed through the main unknowns by Eqs. (3.5).

We assume that all elastic modules have the identical orders, and the variability of unknowns is moderate, $p_1, p_2 \sim 1$. Let $\sigma_t,\ \sigma_s,\ \sigma_n$ be the typical values of the tangential stresses $\sigma_{11}, \sigma_{12}, \sigma_{22}$, of the transversal shear stresses σ_{13}, σ_{23}, and of the normal stresses σ_{33}, respectively. From Eqs. (2.1) in the dimensionless variables (2.11) the following asymptotic estimates

$$\sigma_s \sim \mu\sigma_t, \quad \sigma_n \sim \mu\sigma_s \sim \mu^2\sigma_t. \tag{3.6}$$

are valid.

Accepting that the transversal stresses are neglected ($\sigma_s = \sigma_n = 0$), we get the classic KL model based on the elasticity relations

$$\sigma_t = \mathbf{A}^* \cdot \varepsilon_t \tag{3.7}$$

with the equivalent elastic modules $\mathbf{A}^*$. The equations of this model coincide with the zero approximation of the asymptotic solution of Eqs. (3.4), constructed in [24] (see the next Sect. 4).

The orders of functions σ_s and σ_{33} are different, and we re-write Eqs. (3.5) introducing the block-structure of matrices $\mathbf{C}^{-1} = \{G_{ij}\}$ and $\mathbf{C}^{-1}\cdot\mathbf{B}^T = \{S_{ij}\}$ as follows:

$$\begin{aligned}
&\mathbf{C}^{-1} = \begin{pmatrix} \mathbf{G} & \mathbf{g} \\ \mathbf{g}^T & c_3 \end{pmatrix}, \qquad \mathbf{G} = \begin{pmatrix} G_{11} & G_{12} \\ G_{12} & G_{22} \end{pmatrix}, \quad \mathbf{g} = (G_{13}, G_{23})^T, \quad c_3 = G_{33}, \\
&\mathbf{C}^{-1}\cdot\mathbf{B}^T = \begin{pmatrix} \mathbf{S} \\ \mathbf{s} \end{pmatrix}, \qquad \mathbf{S} = \begin{pmatrix} S_{11} & S_{12} & S_{13} \\ S_{21} & S_{22} & S_{23} \end{pmatrix}, \quad \mathbf{s} = (S_{31}, S_{32}, S_{33}).
\end{aligned} \tag{3.8}$$

Then Eqs. (3.5) read as:

$$\begin{aligned}
\sigma_t &= \mathbf{A}^*\cdot\mathbf{P}\cdot\mathbf{u} + \mathbf{S}^T\cdot\sigma_s + \mathbf{s}^T\sigma_{33}, \\
\varepsilon_s &= \mathbf{G}\cdot\sigma_s + \mathbf{g}\,\sigma_{33} - \mathbf{S}\cdot\mathbf{P}\cdot\mathbf{u}, \\
\varepsilon_{33} &= \mathbf{g}^T\cdot\sigma_s + c_3\,\sigma_{33} - \mathbf{s}\cdot\mathbf{P}\cdot\mathbf{u}.
\end{aligned} \tag{3.9}$$

As a result the right sides of Eqs. (3.4) are expressed through the main unknowns.

4 Asymptotic Solution of Eqs. (3.4). The Zero Approximation

We change a scale of unknown functions according with their orders and put:

$$\mathbf{u} = \mu\hat{\mathbf{u}}, \quad \sigma_s = \mu^2\hat{\sigma}_s, \quad \sigma_{33} = \mu^3\hat{\sigma}_{33}, \quad \mathbf{f}_t = \mu\hat{\mathbf{f}}_t, \quad f_3 = \mu^2\hat{f}_3. \tag{4.1}$$

Omitting the sign ˆ we re-write Eqs. (3.4) as follows:

$$\begin{aligned} &w = w_0 - \mu^2 \mathbf{I}_0(\mathbf{s}_P \cdot \mathbf{u})) + \mu^3 \mathbf{I}_0(\mathbf{g}^T \cdot \sigma_s) + \mu^4 \mathbf{I}_0(c_3\, \sigma_{33}), \\ &\mathbf{u} = \mathbf{u}_0 - \mathbf{I}_0(\mathbf{p}\, w) - \mu \mathbf{I}_0(\mathbf{S}_P \cdot \mathbf{u}) + \mu^2 \mathbf{I}_0(\mathbf{G} \cdot \sigma_s) + \mu^3 \mathbf{I}_0(\mathbf{g}\, \sigma_{33}), \\ &\sigma_s = -\mathbf{I}(\mathbf{L} \cdot \mathbf{u}) - \mu \mathbf{I}(\mathbf{S}_P^T \cdot \sigma_s) - \mu^2 \mathbf{I}(\mathbf{s}_P^T \sigma_{33}) - \mathbf{I}(\mathbf{f}_t), \\ &\sigma_{33} = -\mathbf{I}(\mathbf{p}^T \cdot \sigma_s) - \mathbf{I}(f_3), \end{aligned} \tag{4.2}$$

where we use the following designations

$$\mathbf{L}(z) = \mathbf{P}^T \cdot \mathbf{A}^*(z) \cdot \mathbf{P}, \quad \mathbf{S}_P(z) = \mathbf{S}(z) \cdot \mathbf{P}, \quad \mathbf{s}_P(z) = \mathbf{s}(z) \cdot \mathbf{P}. \tag{4.3}$$

All unknowns in Eqs. (4.2) are of the order of *the* unit. System (4.2) is exact and it is convenient to construct a solution by using the method of iterations. In the next sections the solution of the SOA with respect to the small thickness parameter μ will be constructed. Therefore for a simplicity the small summands of the orders of μ^3 and of μ^4 may be omitted in the first two Eqs. (4.2).

In the zero approximation we put $\mu = 0$ in Eqs. (4.2) and sequently obtain [24]

$$\begin{aligned} &w^{(0)}(x_1, x_2, z) = w_0(x_1, x_2), \\ &\mathbf{u}^{(0)}(x_1, x_2, z) = \mathbf{u}_0(x_1, x_2) - z\, \mathbf{p}\, w_0(x_1, x_2)), \\ &\sigma_s^{(0)}(x_1, x_2, z) = -\mathbf{I}(\mathbf{L}(z) \cdot \mathbf{u}^{(0)}) - \mathbf{I}(\mathbf{f}_t), \\ &\sigma_{33}^{(0)}(x_1, x_2, z) = \mathbf{II}(\mathbf{p}^T \cdot \mathbf{L}(z) \cdot \mathbf{u}^{(0)}) + \mathbf{I}(\mathbf{p}^T \cdot \mathbf{f}_t) - \mathbf{I}(f_3). \end{aligned} \tag{4.4}$$

The boundary conditions $\sigma_s^{(0)}(1/2) = \sigma_{33}^{(0)}(1/2) = 0$ give equations

$$\begin{aligned} &\sigma_s^{(0)}(x_1, x_2, 1/2) = -\mathbf{I}_a(\mathbf{L}(z) \cdot \mathbf{u}^{(0)}) - \mathbf{I}_a(\mathbf{f}_t) = 0, \\ &\sigma_{33}^{0}(x_1, x_2, 1/2) = \mathbf{I}_a \mathbf{I}(\mathbf{p}^T \cdot \mathbf{L}(z) \cdot \mathbf{u}^{(0)}) + \mathbf{I}_a(\mathbf{p}^T \cdot \mathbf{f}_t) - \mathbf{I}_a(f_3) = 0. \end{aligned} \tag{4.5}$$

By using equality

$$\mathbf{I}_a \mathbf{I}(Z(z)) = (1/2)\mathbf{I}_a(Z(z)) - \mathbf{I}_a(z\, Z(z)) \tag{4.6}$$

and taking into account that $\mathbf{u}^{(0)} = \mathbf{u}_0 - z\, \mathbf{p}\, w_0$, we write equations of the zero approximation as follows [24]:

$$\begin{aligned} &\mathbf{L}_0 \cdot \mathbf{u}_0 - \mathbf{N}_1 w_0 + \mathbf{F}_t = \mathbf{0}, \\ &\mathbf{N}_1^T \cdot \mathbf{u}_0 - Q_2 w_0 + m + F_3 = 0, \end{aligned} \tag{4.7}$$

where

$$\begin{aligned} &\mathbf{L}_0 = \mathbf{P}^T \cdot \mathbf{I}_a(\mathbf{A}^*(z)) \cdot \mathbf{P}, \quad \mathbf{N}_1 = \mathbf{P}^T \cdot \mathbf{I}_a(z\, \mathbf{A}^*(z)) \cdot \mathbf{P} \cdot \mathbf{p}, \quad \mathbf{F}_t = \mathbf{I}_a(\mathbf{f}_t), \\ &Q = \mathbf{p}^T \cdot \mathbf{P}^T \cdot \mathbf{I}_a(z^2\, \mathbf{A}^*(z)) \cdot \mathbf{P} \cdot \mathbf{p}, \quad F_3 = \mathbf{I}_a(f_3), \quad m = \mathbf{I}_a(\mathbf{p}^T \cdot \mathbf{f}_t). \end{aligned} \tag{4.8}$$

The detailed expressions of operators in Eqs. (4.7) read as [24]:

$$\mathbf{L}_0 = \begin{pmatrix} L_{11} & L_{12} \\ L_{12} & L_{22} \end{pmatrix}, \qquad \begin{aligned} L_{11} &= a_{11}^{(0)} p_1^2 + 2a_{13}^{(0)} p_1 p_2 + a_{33}^{(0)} p_2^2, \\ L_{12} &= a_{13}^{(0)} p_1^2 + (a_{12}^{(0)} + a_{33}^{(0)}) p_1 p_2 + a_{23}^{(0)} p_2^2, \\ L_{22} &= a_{33}^{(0)} p_1^2 + 2a_{23}^{(0)} p_1 p_2 + a_{22}^{(0)} p_2^2, \end{aligned}$$

$$\mathbf{N}_1 = \begin{pmatrix} N_1 \\ N_2 \end{pmatrix}, \qquad \begin{aligned} N_1 &= a_{11}^{(1)} p_1^3 + 3a_{13}^{(1)} p_1^2 p_2 + (a_{12}^{(1)} + 2a_{33}^{(1)}) p_1 p_2^2 + a_{23}^{(1)} p_2^3, \\ N_2 &= a_{13}^{(1)} p_1^3 + (a_{12}^{(1)} + 2a_{33}^{(1)}) p_1^2 p_2 + 3a_{23}^{(1)} p_1 p_2^2 + a_{22}^{(1)} p_2^3, \end{aligned} \tag{4.9}$$

$$Q = a_{11}^{(2)} p_1^4 + a_{13}^{(2)} p_1^3 p_2 + 2(a_{12}^{(2)} + 2a_{33}^{(2)}) p_1^2 p_2^2 + 4a_{23}^{(2)} p_1 p_2^3 + a_{22}^{(2)} p_2^4,$$

where the coefficients $a_{ij}^{(k)}$ depend *at* the moments of the zero, of the first, and of the second orders of elements of matrix $\mathbf{A}^*(z)$:

$$a_{ij}^{(k)} = \mathbf{I}(z^k A_{ij}^*(z)) = \int_{-1/2}^{1/2} z^k A_{ij}^*(z)\, dz, \quad i, j = 1, 2, 3, \quad k = 0, 1, 2. \tag{4.10}$$

Equations (4.7) describe approximately bending deformations of an anisotropic plate in frames of the KL hypotheses.

We call a plate with symmetric in z elastic modules ($E_{ij}(-z) = E_{ij}(z)$) as a symmetric (in the thickness direction) plate. For a symmetric plate $\mathbf{N}_1 = \mathbf{0}$, and the bending and the tangential deformations may be investigated separately. In the zero approximation for a symmetric plate all unknown functions are symmetric or anti-symmetric functions in z. We mark that in the higher approximation the last state is correct not in all cases (see Sect. 5).

It is shown [17] that in the case if all elastic modules are of the identical orders then the zero approximation gives an acceptable exactness for approximate calculations. If some elements of matrix $\mathbf{C}$ in the denominator of Eqs. (3.7) are small, then *exactness* of the zero approximation is not enough, and it is necessary to construct the higher approximations. Some important effects of the second order are not described by Eq. (4.7). The main of these effects is a transversal shear that may be essential for multi-layered plates with hard and soft alternating layers.

5 The Higher Approximations

The first approximation takes into account the summands of the order of μ in Eqs. (4.2). IF $\mathbf{S} = \mathbf{0}$ the summands of the order of μ in Eqs. (4.2) are absent. We construct here the first approximation for an anisotropic material with $\mathbf{S} \neq \mathbf{0}$. Such anisotropy we name as an inclined anisotropy, because it may be obtained at a composite plate, consisting of an orthotropic matrix reinforced by a system of fibres, inclined to a plane of plate [25] (see also Sect. 6).

For an inclined anisotropy the first approximation read as:

$$
\begin{aligned}
&w^{(1)} = w_0,\\
&\mathbf{u}^{(1)} = \mathbf{u}_0 - \mathbf{I}_0(\mathbf{p}\, w^{(1)}) - \mu\mathbf{I}_0(\mathbf{S}_P\cdot\mathbf{u}^{(0)}) = \mathbf{u}^{(0)} - \mu\mathbf{I}_0(\mathbf{S}_P\cdot\mathbf{u}^{(0)}),\\
&\sigma_s^{(1)} = -\mathbf{I}(\mathbf{L}\cdot\mathbf{u}^{(1)}) - \mu\mathbf{I}(\mathbf{S}_P^T\cdot\sigma_s^{(0)}) - \mathbf{I}(\mathbf{f}_t) =\\
&\quad = -\mathbf{I}(\mathbf{L}\cdot\mathbf{u}^{(0)}) + \mu\mathbf{I}(\mathbf{L}\cdot\mathbf{I}_0(\mathbf{S}_P\cdot\mathbf{u}^{(0)})) + \mu\mathbf{I}(\mathbf{S}_P^T\cdot\mathbf{I}(\mathbf{L}\cdot\mathbf{u}^{(0)} + \mathbf{f}_t)) - \mathbf{I}(\mathbf{f}_t),\\
&\sigma_{33}^{(1)} = -\mathbf{I}(\mathbf{p}^T\cdot\sigma_s^{(1)}) - \mathbf{I}(f_3) =\\
&\quad = \mathbf{II}(\mathbf{p}^T\cdot\mathbf{L}\cdot\mathbf{u}^{(0)}) - \mu\mathbf{II}\left(\mathbf{p}\cdot\mathbf{L}\cdot\mathbf{I}_0(\mathbf{S}_P\cdot\mathbf{u}^{(0)}) + \mathbf{p}\cdot\mathbf{S}_P^T\cdot\mathbf{I}(\mathbf{L}\cdot\mathbf{u}^{(0)})\right) +\\
&\quad + \mathbf{II}(\mathbf{p}^T\cdot\mathbf{f}_t) - \mathbf{I}(f_3).
\end{aligned}
\tag{5.1}
$$

Here the normal deflection $w^{(1)}$ is the same, as in the zero approximation, and the tangential deflections $\mathbf{u}^{(1)}$ and stresses $\sigma_s^{(1)}$, $\sigma_{33}^{(1)}$ are changed.

The second approximation is very bulky:

$$
\begin{aligned}
&w^{(2)} = w_0 + \mu^2\mathbf{I}_0(\sigma_{33}^{(0)}) = w_0 - \mu^2\mathbf{I}_0(\mathbf{s}_P\cdot\mathbf{u}^{(0)})),\\
&\mathbf{u}^{(2)} = \mathbf{u}_0 - \mathbf{I}_0(\mathbf{p}\, w^{(2)}) - \mu\mathbf{I}_0(\mathbf{S}_P\cdot\mathbf{u}^{(1)}) + \mu^2\mathbf{I}_0(\mathbf{G}\cdot\sigma_s^{(0)}) =\\
&\quad = \mathbf{u}^{(0)} - \mu\mathbf{I}_0(\mathbf{S}_P\cdot\mathbf{u}^{(0)}) + \mu^2\mathbf{I}_0\mathbf{I}_0(\mathbf{p}\cdot\mathbf{s}_P\cdot\mathbf{u}^{(0)}) +\\
&\quad + \mu^2\mathbf{I}_0(\mathbf{S}_P\cdot\mathbf{I}_0(\mathbf{S}_P\cdot\mathbf{u}^{(0)})) - \mu^2\mathbf{I}_0(\mathbf{G}\cdot\mathbf{I}(\mathbf{L}\cdot\mathbf{u}^{(0)})) - \mu^2\mathbf{I}_0(\mathbf{G}\cdot\mathbf{I}(\mathbf{f}_t)),\\
&\sigma_s^{(2)} = -\mathbf{I}(\mathbf{L}\cdot\mathbf{u}^{(2)}) - \mu\mathbf{I}(\mathbf{S}_P^T\cdot\sigma_s^{(1)}) - \mu^2\mathbf{I}(\mathbf{s}_P^T\sigma_{33}^{(0)}) - \mathbf{I}(\mathbf{f}_t),\\
&\sigma_{33}^{(2)} = -\mathbf{I}(\mathbf{p}^T\cdot\sigma_s^{(2)}) - \mathbf{I}(f_3).
\end{aligned}
\tag{5.2}
$$

To obtain the final expressions, it is necessary to substitute the values $\mathbf{u}^{(1)}$ and $\sigma_s^{(1)}$ from Eq. (5.1) and the values $\mathbf{u}^{(2)}$ and $\sigma_s^{(2)}$ from Eqs. (5.2).

We write the value $\sigma_s^{(2)}$ as follows:

$$
\sigma_s^{(2)} = -\mathbf{I}(\mathbf{L}^*\cdot\mathbf{u}^{(0)} + \mathbf{f}^*), \quad \mathbf{L}^* = \mathbf{L}_0^* + \mu\mathbf{L}_1^* + \mu^2\mathbf{L}_2^*,
\tag{5.3}
$$

with

$$
\begin{aligned}
&\mathbf{L}_0^* = \mathbf{L} = \mathbf{P}^T\cdot\mathbf{A}^*(z)\cdot\mathbf{P}, \qquad \mathbf{L}_1^* = -\mathbf{L}\cdot\mathbf{I}_0(\mathbf{S}_P) - \mathbf{S}_P^T\cdot\mathbf{I}(\mathbf{L}),\\
&\mathbf{L}_2^* = \mathbf{L}\cdot\mathbf{I}_0\mathbf{I}_0(\mathbf{p}\cdot\mathbf{s}_P) + \mathbf{L}\cdot\mathbf{I}_0(\mathbf{S}_P\cdot\mathbf{I}_0(\mathbf{S}_P)) - \mathbf{L}\cdot\mathbf{I}_0(\mathbf{G}\cdot\mathbf{I}(\mathbf{L})) +\\
&\quad + \mathbf{S}_P^T\cdot\mathbf{I}(\mathbf{L}\cdot\mathbf{I}_0(\mathbf{S}_P)) + \mathbf{S}_P^T\cdot\mathbf{I}(\mathbf{S}_P^T\cdot\mathbf{I}(\mathbf{L})) + \mathbf{s}_P^T\cdot\mathbf{II}(\mathbf{p}^T\cdot\mathbf{L})],\\
&\mathbf{f}^* = \mathbf{f}_t - \mu\mathbf{S}_P^T\cdot\mathbf{I}(\mathbf{f}_t) - \mu^2[\mathbf{L}\cdot\mathbf{I}_0(\mathbf{G}\cdot\mathbf{I}(\mathbf{f}_t)) + \mathbf{s}_P^T\cdot\mathbf{p}^T\cdot\mathbf{I}(\mathbf{f}_t) - \mathbf{s}_P^T\,\mathbf{I}(f_3)].
\end{aligned}
\tag{5.4}
$$

Then the forth Eq. (5.2) yields

$$
\sigma_{33}^{(2)} = \mathbf{II}(\mathbf{L}^*\cdot\mathbf{u}^{(0)} + \mathbf{f}^*) - \mathbf{I}(f_3).
\tag{5.5}
$$

The boundary conditions $\sigma_s^{(2)} = \sigma_{33}^{(2)} = 0$ at $z = 1/2$ lead to equations for $\mathbf{u}_0\, w_0$:

$$
\begin{aligned}
&\mathbf{I}_a(\mathbf{L}^*\cdot\mathbf{u}^{(0)} + \mathbf{f}^*) = 0, \qquad \mathbf{u}^{(0)} = \mathbf{u}_0 - \mathbf{p}\, z\, w_0\\
&\mathbf{I}_a\mathbf{I}(\mathbf{p}^T\cdot(\mathbf{L}^*\cdot\mathbf{u}^{(0)} + \mathbf{f}^*)) - \mathbf{I}_a(f_3) = 0.
\end{aligned}
\tag{5.6}
$$

By using equality (4.6) at $Z = \sigma^*\cdot\mathbf{u}^{(0)} + \mathbf{f}^*$ with $\mathbf{I}_a(Z) = 0$, we present Eqs. (5.6) in the form:

$$\begin{aligned}&\mathbf{I}_a(\mathbf{L}^*)\cdot\mathbf{u}_0 - \mathbf{I}_a(\mathbf{L}^*\cdot\mathbf{p}\,z)\,w_0 + \mathbf{I}_a(\mathbf{f}^*) = 0,\\ &\mathbf{I}_a(z\,\mathbf{p}^T\cdot\mathbf{L}^*)\cdot\mathbf{u}_0 - \mathbf{I}_a(z\,\mathbf{p}^T\cdot\mathbf{L}^*\cdot\mathbf{p}\,z)\,w_0 + \mathbf{I}_a(z\,\mathbf{p}^T\cdot\mathbf{f}^*) + F_3 = 0.\end{aligned} \tag{5.7}$$

Therefore, the model of the SOA is built. Equation (5.7) are a PDE system with constant coefficients with respect to unknown functions $\mathbf{u}_0 = (u_{10}, u_{20})$, w_0. The differential orders of the operators $\mathbf{p}$, $\mathbf{P}$, $\mathbf{S}_P$, $\mathbf{s}_P$ are equal to *the* unit, the operator $\mathbf{L}$ is of the second order, and the differential orders of operators $\mathbf{L}_k^*$ are equal to 2+k. The presence of $\mathbf{p}$ or $\mathbf{p}^T$ in Eqs. (5.7) lead to a growth of the differential orders of corresponding summands by *the* unit. The differential order of system (5.7) is the same as the order of the TR model, but the system (5.7) is essentially more complex.

If the elastic modules depend on z then to find coefficients in Eqs. (5.7) it is necessary to calculate repeated integrals. If the elastic modules are constant then the numerical coefficients appear instead of integral operators $\mathbf{I}_a$, $\mathbf{I}$, $\mathbf{I}_0$ and multipliers z according the following relations:

$$\begin{array}{llll}
\mathbf{I}_a \to 1, & \mathbf{I}_a(z) \to 0, & & \mathbf{I}_a(z^2) \to 1/12,\\
\mathbf{I}_a\mathbf{I}_0 \to 0, & \mathbf{I}_a\mathbf{I}_0(z) \to 1/12, & \mathbf{I}_a(z\mathbf{I}_0) \to 1/12, & \mathbf{I}_a(z\mathbf{I}_0(z)) \to 0,\\
\mathbf{I}_a\mathbf{I} \to 1/2, & \mathbf{I}_a\mathbf{I}(z) \to -1/2, & \mathbf{I}_a(z\mathbf{I}) \to 1/12, & \mathbf{I}_a(z\mathbf{I}(z)) \to 0,\\
\mathbf{I}_a\mathbf{I}_0\mathbf{I}_0 \to 1/24, & \mathbf{I}_a\mathbf{I}_0\mathbf{I}_0(z) \to 0, & \mathbf{I}_a(z\mathbf{I}_0\mathbf{I}_0) \to 0, & \mathbf{I}_a(z\mathbf{I}_0\mathbf{I}_0(z)) \to 1/480,\\
\mathbf{I}_a\mathbf{I}_0\mathbf{I} \to 1/24, & \mathbf{I}_a\mathbf{I}_0\mathbf{I}(z) \to 0, & \mathbf{I}_a(z\mathbf{I}_0\mathbf{I}) \to 1/24, & \mathbf{I}_a(z\mathbf{I}_0\mathbf{I}(z)) \to -1/120,\\
\mathbf{I}_a\mathbf{I}\mathbf{I}_0 \to -1/12, & \mathbf{I}_a\mathbf{I}\mathbf{I}_0(z) \to 1/48, & \mathbf{I}_a(z\mathbf{I}\mathbf{I}_0) \to 0, & \mathbf{I}_a(z\mathbf{I}\mathbf{I}_0(z)) \to 1/480,\\
\mathbf{I}_a\mathbf{I}\mathbf{I} \to 1/6, & \mathbf{I}_a\mathbf{I}\mathbf{I}(z) \to -1/24, & \mathbf{I}_a(z\mathbf{I}\mathbf{I}) \to 1/24, & \mathbf{I}_a(z\mathbf{I}\mathbf{I}(z)) \to -1/120.
\end{array} \tag{5.8}$$

For a symmetric in the thickness direction plate the tangential and the transversal deflections my be investigated separately only in the zero approximations. In the higher approximations these deflections may be tied by small terms. For an inclined anisotropy this connection is of the order of μ and for a monoclinic material it is of the order of μ^2 (see examples in Sect. 7).

6 Two Examples of Elasticity Relations

We consider a plate, consisting of a homogeneous orthotropic matrix, reinforced by a system of hard fibers, inclined to axes Ox and Oz by angles α and β (see Fig. 1).

We present elastic modules (2.4) as a sum of modules of a matrix E_{ij}^m and an additional modules of fibers E_{ij}^f:

$$E_{ij} = E_{ij}^m + E_{ij}^f, \quad i, j = 1, \ldots, 6, \tag{6.1}$$

where the modules E_{ij}^f are obtained in [25] an assumption, that there is a full contact between a matrix and fibers, and only an extension of fibers is taken into account. The potential energy density of fibers is equal

Fig. 1 A direction of fibers

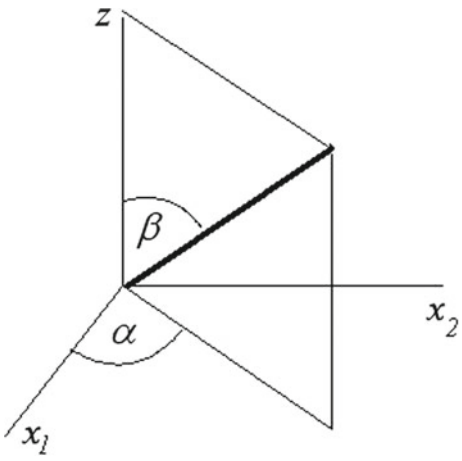

$$\begin{aligned} &\Pi_f = \frac{1}{2} E_f \varepsilon_f^2, \qquad \varepsilon_f = a_1^2\varepsilon_{11} + a_2^2\varepsilon_{22} + a_3^2\varepsilon_{33} + a_1a_2\varepsilon_{12} + a_1a_3\varepsilon_{13} + a_2a_3\varepsilon_{23}, \\ &E_f = E_0\delta_f, \qquad a_1 = \cos\alpha\sin\beta,\ a_2 = \sin\alpha\sin\beta,\ a_3 = \cos\beta, \end{aligned} \tag{6.2}$$

where ε_f is the deformation of fiber extension, E_0 is the Young modulus of fibers, and δ is the part of volume, occupied by fibers.

Then elastic modules E_{ij}^f may be found from the equality $\sigma_{ij} = \partial\Pi_f/\partial\varepsilon_{ij}$:

$$\begin{aligned} &E_{11}^f = E_f a_1^4, && E_{12}^f = E_f a_1^2 a_2^2, && E_{13}^f = E_f a_1^2 a_3^2, \\ &E_{16}^f = E_f a_1^3 a_2, && E_{14}^f = E_f a_1^2 a_2 a_3, && E_{15}^f = E_f a_1^3 a_3, \\ &E_{22}^f = E_f a_2^4, && E_{23}^f = E_f a_2^2 a_3^2, && E_{26}^f = E_f a_1 a_2^3, \\ &E_{24}^f = E_f a_2^3 a_3, && E_{25}^f = E_f a_1 a_2^2 a_3, && E_{33}^f = E_f a_3^4, \\ &E_{36}^f = E_f a_1 a_2 a_3^2, && E_{34}^f = E_f a_2 a_3^3, && E_{35}^f = E_f a_1 a_3^3, \\ &E_{66}^f = E_f a_1^2 a_2^2, && E_{46}^f = E_f a_1 a_2^2 a_3, && E_{56}^f = E_f a_1^2 a_2 a_3, \\ &E_{44}^f = E_f a_2^2 a_3^2, && E_{45}^f = E_f a_1 a_2 a_3^2, && E_{55}^f = E_f a_1^2 a_3^2. \end{aligned} \tag{6.3}$$

By the same way several systems of fibers may be considered.

We consider a multi-layered plate with n orthotropic layers of the constant thickness h_k, $k = 1, \ldots, n$, $\sum h_k = 1$. Let the k-th layer lies in $z_{k-1} \le z \le z_k$ with $z_0 = -1/2$, $z_k = z_{k-1} + h_k$. For the k-th layer the elasticity relations, connected with the orthotropic directions, in the matrix form (instead of Eqs. (2.4)) read as [13]:

$$\hat{\sigma}^{(k)} = \hat{\mathbf{E}}^{(k)} \cdot \hat{\varepsilon}^{(k)}, \quad z_{k-1} \le z \le z_k, \tag{6.4}$$

with

$$\hat{\sigma}^{(k)} = (\hat{\sigma}_{11}^{(k)}, \hat{\sigma}_{22}^{(k)}, \hat{\sigma}_{33}^{(k)}, \hat{\sigma}_{23}^{(k)}, \hat{\sigma}_{13}^{(k)}, \hat{\sigma}_{12}^{(k)})^T, \qquad \hat{\varepsilon}^{(k)} = (\hat{\varepsilon}_{11}^{(k)}, \hat{\varepsilon}_{22}^{(k)}, \hat{\varepsilon}_{33}^{(k)}, \hat{\varepsilon}_{23}^{(k)}, \hat{\varepsilon}_{13}^{(k)}, \hat{\varepsilon}_{12}^{(k)})^T,$$

$$\hat{\mathbf{E}}^{(k)} = \begin{pmatrix} \hat{E}_{11}^{(k)} & \hat{E}_{12}^{(k)} & \hat{E}_{13}^{(k)} & 0 & 0 & 0 \\ \hat{E}_{12}^{(k)} & \hat{E}_{22}^{(k)} & \hat{E}_{23}^{(k)} & 0 & 0 & 0 \\ \hat{E}_{13}^{(k)} & \hat{E}_{23}^{(k)} & \hat{E}_{33}^{(k)} & 0 & 0 & 0 \\ 0 & 0 & 0 & \hat{E}_{44}^{(k)} & 0 & 0 \\ 0 & 0 & 0 & 0 & \hat{E}_{55}^{(k)} & 0 \\ 0 & 0 & 0 & 0 & 0 & \hat{E}_{66}^{(k)} \end{pmatrix}. \tag{6.5}$$

Here the sign ˆ marks that the relations (6.4) are written in the auxiliary co-ordinate system connected with the orthotropic directions of the layer.

Let the angle between axes X of the main and the auxiliary systems be α_k. Then the elasticity relations (2.4) in the main co-ordinate system read as

$$\sigma^{(k)} = \mathbf{E}^{(k)} \cdot \varepsilon^{(k)}, \quad z_{k-1} \le x_3 \le z_k \tag{6.6}$$

where the matrix $\mathbf{E}^{(k)}$ corresponds to a monoclinic material

$$\mathbf{E}^{(k)} = \begin{pmatrix} E_{11}^{(k)} & E_{12}^{(k)} & E_{13}^{(k)} & 0 & 0 & E_{16}^{(k)} \\ E_{12}^{(k)} & E_{22}^{(k)} & E_{23}^{(k)} & 0 & 0 & E_{26}^{(k)} \\ E_{13}^{(k)} & E_{23}^{(k)} & E_{33}^{(k)} & 0 & 0 & E_{36}^{(k)} \\ 0 & 0 & 0 & E_{44}^{(k)} & E_{45}^{(k)} & 0 \\ 0 & 0 & 0 & E_{45}^{(k)} & E_{55}^{(k)} & 0 \\ E_{16}^{(k)} & E_{26}^{(k)} & E_{36}^{(k)} & 0 & 0 & E_{66}^{(k)}, \end{pmatrix} \tag{6.7}$$

and the modules $E_{ij}^{(k)}$ are expressed by $\hat{E}_{ij}^{(k)}$ as follows [13]:

$$\begin{aligned}
E_{11}^{(k)} &= \hat{E}_{11}^{(k)} c_k^4 + 2\left(\hat{E}_{12}^{(k)} + 2\hat{E}_{66}^{(k)}\right) c_k^2 s_k^2 + \hat{E}_{22}^{(k)} s_k^4, \\
E_{12}^{(k)} &= \hat{E}_{12}^{(k)} c_k^4 + \left(\hat{E}_{11}^{(k)} + \hat{E}_{22}^{(k)} - 4\hat{E}_{66}^{(k)}\right) c_k^2 s_k^2 + \hat{E}_{12}^{(k)} s_k^4, \quad E_{13}^{(k)} = \hat{E}_{13}^{(k)} c_k^2 + \hat{E}_{23}^{(k)} s_k^2, \\
E_{16}^{(k)} &= \left(\hat{E}_{11}^{(k)} - \hat{E}_{12}^{(k)} - 2\hat{E}_{66}^{(k)}\right) c_k^3 s_k + \left(2\hat{E}_{66}^{(k)} + \hat{E}_{12}^{(k)} - \hat{E}_{22}^{(k)}\right) c_k s_k^3, \\
E_{22}^{(k)} &= \hat{E}_{22}^{(k)} c_k^4 + 2\left(\hat{E}_{12}^{(k)} + 2\hat{E}_{66}^{(k)}\right) c_k^2 s_k^2 + \hat{E}_{11}^{(k)} s_k^4, \quad E_{23}^{(k)} = \hat{E}_{23}^{(k)} c_k^2 + \hat{E}_{13}^{(k)} s_k^2, \\
E_{26}^{(k)} &= \left(\hat{E}_{12}^{(k)} - \hat{E}_{22}^{(k)} + 2\hat{E}_{66}^{(k)}\right) c_k^3 s_k + \left(\hat{E}_{11}^{(k)} - \hat{E}_{12}^{(k)} - 2\hat{E}_{66}^{(k)}\right) c_k s_k^3, \quad E_{33}^{(k)} = \hat{E}_{33}^{(k)}, \\
E_{36}^{(k)} &= \left(\hat{E}_{13}^{(k)} - \hat{E}_{23}^{(k)}\right) c_k s_k, \quad E_{44}^{(k)} = \hat{E}_{44}^{(k)} c_k^2 + \hat{E}_{55}^{(k)} s_k^2, \quad E_{45}^{(k)} = \left(\hat{E}_{55}^{(k)} - \hat{E}_{44}^{(k)}\right) c_k s_k, \\
E_{55}^{(k)} &= \hat{E}_{55}^{(k)} c_k^2 + \hat{E}_{44}^{(k)} s_k^2, \quad E_{66}^{(k)} = \left(\hat{E}_{11}^{(k)} + \hat{E}_{22}^{(k)} - 2\hat{E}_{12}^{(k)} - 2\hat{E}_{66}^{(k)}\right) c_k^2 s_k^2 + \hat{E}_{66}^{(k)} (c_k^4 + s_k^4),
\end{aligned} \tag{6.8}$$

with $c_k = \cos\alpha_k$, $s_k = \sin\alpha_k$.

Therefore, we get a monoclinic material with piece-vice constant elastic modules E_{ij}.

7 Harmonic Solution

The main difficulty in obtaining a closed-form solution of Eq. (5.7) for a finite plate (for example, for a rectangular plate) consists in satisfying boundary conditions. The same difficulty arises for the rectangular KL plate with clamped edges. However for a rectangular plate with two opposite simply supported edges (the Navier conditions) the separation of variables ($w(x_1, x_2) = w(x_1) \sin \alpha x_2$) is possible and the problem is reduced to the one-dimensional one. A peculiarity of a plate made of the material with the general anisotropy (with 21 elastic modules) or of a monoclinic plate (with 13 elastic modules) is that there do not exist boundary conditions that admit the separation of variables. Therefore, only approximate variation methods may be used. A lot of boundary value problems for laminated plates are solved in book [13]. In [26] vibrations of a multi-layered rectangular plate with free edges are investigated by the variation method, and deflection is expanded into a product of Legendre polynomials.

Further, we consider an infinite plate and investigate the harmonic solutions admitting closed-form solutions.

Firstly, we consider a static harmonic problem. Let the external forces be

$$\mathbf{f}_t(x_1, x_2, z) = \mathbf{f}_t(z) e^{i(x_1 q_1 + x_2 q_2)}, \quad f_3(x_1, x_2, z) = f_3(z) e^{i(x_1 q_1 + x_2 q_2)}, \quad i = \sqrt{-1}, \tag{7.1}$$

where q_1, q_2 are the real-valued wave numbers. We seek the solution of three-dimensional Eqs. (2.12) in the same harmonic form

$$\{w, \mathbf{u}, \sigma_t, \sigma_{33}\}(x_1, x_2, z) = \{w, \mathbf{u}, \sigma_t, \sigma_{33}\}(z) e^{i(x_1 q_1 + x_2 q_2)} \tag{7.2}$$

and the solution of two-dimensional Eqs. (5.7)

$$w(x_1, x_2) = W e^{i(x_1 q_1 + x_2 q_2)}, \quad \mathbf{u}(x_1, x_2) = \mathbf{U} e^{i(x_1 q_1 + x_2 q_2)}, \quad \mathbf{U} = (U_1, U_2)^T, \tag{7.3}$$

where $\mathbf{U}$, W are the unknown amplitudes of deflection.

Inserting Eqs. (7.1) and (7.3) into Eqs. (5.7) yields to the linear algebraic system the for unknown variables $\mathbf{U}$, W:

$$\begin{aligned} &\mathbf{I}_a(\mathbf{L}^*) \cdot \mathbf{U} - \mathbf{I}_a(\mathbf{L}^* \cdot \mathbf{p}\, z)\, W + \mathbf{I}_a(\mathbf{f}^*) = 0, \\ &\mathbf{I}_a(z\, \mathbf{p}^T \cdot \mathbf{L}^*) \cdot \mathbf{U} - \mathbf{I}_a(z\, \mathbf{p}^T \cdot \mathbf{L}^* \cdot \mathbf{p}\, z)\, W + \mathbf{I}_a(z\, \mathbf{p}^T \cdot \mathbf{f}^*) + F_3 = 0. \end{aligned} \tag{7.4}$$

Here the differential operators $\mathbf{p}$ and $\mathbf{P}$ in Eqs. (7.4) and (5.8) are to be formally replaced by

$$\mathbf{p} = i\mathbf{q} = i\,(q_1, q_2)^T, \qquad \mathbf{P} = i\mathbf{Q} = i \begin{pmatrix} q_1 & 0 & q_2 \\ 0 & q_2 & q_1 \end{pmatrix}^T. \tag{7.5}$$

We consider a bending of a plate with constant elastic modules under action of a periodic compression applied to a lower plane:

$$\mathbf{f}_t = 0, \quad f_3(x_1, x_2, z) = F_3\delta(z + 1/2)e^{i(x_1q_1+x_2q_2)}. \tag{7.6}$$

At these assumptions Eqs. (7.4) read as:

$$\begin{array}{l}(\mathbf{l}_{11}^{(0)} + \mu\,\mathbf{l}_{11}^{(1)} + \mu^2\mathbf{l}_{11}^{(2)})\mathbf{U} + (\mathbf{l}_{12}^{(0)} + \mu\,\mathbf{l}_{12}^{(1)} + \mu^2\mathbf{l}_{12}^{(2)})W + i\,\mu^2\mathbf{s}_Q\,F_3 = 0,\\ (\mathbf{l}_{21}^{(0)} + \mu\,\mathbf{l}_{21}^{(1)} + \mu^2\mathbf{l}_{21}^{(2)})\mathbf{U} + (l_{22}^{(0)} + \mu\,l_{22}^{(1)} + \mu^2 l_{22}^{(2)})W + F_3 = 0\end{array} \tag{7.7}$$

with the coefficients that are calculated by using Eqs. (5.3), (5.4), and (5.8):

$$\begin{array}{l}\mathbf{l}_{11}^{(0)} = -\mathbf{l}, \qquad \mathbf{l}_{11}^{(1)} = (i/2)\,\mathbf{S}_Q\cdot\mathbf{l},\\ \mathbf{l}_{11}^{(2)} = -(1/24)\,\mathbf{l}\cdot\mathbf{G}\cdot\mathbf{l} - (1/24)\,\mathbf{l}\cdot\mathbf{q}\cdot\mathbf{s}_Q + (1/6)\,\mathbf{s}_Q^T\cdot\mathbf{q}^T\cdot\mathbf{l} +\\ \quad (1/24)\,\mathbf{l}\cdot\mathbf{S}_Q\cdot\mathbf{S}_Q - (1/12)\,\mathbf{S}_Q\cdot\mathbf{l}\cdot\mathbf{S}_Q + (1/6)\,\mathbf{S}_Q^T\cdot\mathbf{S}_Q^T\cdot\mathbf{l},\\ \mathbf{l}_{12}^{(0)} = 0, \qquad \mathbf{l}_{12}^{(1)} = (1/12)\,\mathbf{l}\cdot\mathbf{S}_Q\cdot\mathbf{q} - (1/2)\,\mathbf{S}_Q\cdot\mathbf{l}\cdot\mathbf{q},\\ \mathbf{l}_{12}^{(2)} = -(i/24)\,\mathbf{s}_Q^T\cdot\mathbf{q}^T\cdot\mathbf{l}\cdot\mathbf{q} + (i/48)\,\mathbf{S}_Q\cdot\mathbf{l}\cdot\mathbf{S}_Q - (i/24)\,\mathbf{S}_Q^T\cdot\mathbf{S}_Q^T\cdot\mathbf{l}\cdot\mathbf{q},\\ \mathbf{l}_{21}^{(0)} = 0, \qquad \mathbf{l}_{21}^{(1)} = -(1/12)\,\mathbf{q}^T\cdot\mathbf{l}\cdot\mathbf{S}_Q - (1/12)\,\mathbf{q}^T\cdot\mathbf{S}_Q\cdot\mathbf{l},\\ \mathbf{l}_{21}^{(2)} = -(i/24)\,\mathbf{q}^T\cdot\mathbf{l}\cdot\mathbf{G}\cdot\mathbf{l} + (i/24)\,\mathbf{q}^T\cdot\mathbf{s}_Q^T\cdot\mathbf{q}^T\cdot\mathbf{l} + (i/24)\,\mathbf{q}^T\cdot\mathbf{S}_Q^T\cdot\mathbf{S}_Q^T\cdot\mathbf{l},\\ l_{22}^{(0)} = -(1/12)\,\mathbf{q}^T\cdot\mathbf{l}\cdot\mathbf{q}, \qquad l_{22}^{(1)} = 0,\\ l_{22}^{(2)} = (1/120)\,\mathbf{q}^T\cdot\mathbf{l}\cdot\mathbf{G}\cdot\mathbf{l}\cdot\mathbf{q} + (1/480)\,\mathbf{q}^T\cdot\mathbf{l}\cdot\mathbf{q}\cdot\mathbf{s}_Q\cdot\mathbf{q} - (1/120)\,\mathbf{q}^T\cdot\mathbf{s}_Q^T\cdot\mathbf{q}^T\cdot\mathbf{l}\cdot\mathbf{q} +\\ \quad (1/480)\,\mathbf{q}^T\cdot\mathbf{l}\cdot\mathbf{S}_Q\cdot\mathbf{S}_Q\cdot\mathbf{q} + (1/480)\,\mathbf{q}^T\cdot\mathbf{S}_Q\cdot\mathbf{l}\cdot\mathbf{S}_Q\cdot\mathbf{q} - (1/120)\,\mathbf{q}^T\cdot\mathbf{S}_Q^T\cdot\mathbf{S}_Q^T\cdot\mathbf{l}\cdot\mathbf{q},\end{array} \tag{7.8}$$

where $\mathbf{l} = \mathbf{Q}^T\cdot\mathbf{A}^*\cdot\mathbf{Q}$, $\mathbf{S}_Q = \mathbf{S}\cdot\mathbf{Q}$, $\mathbf{s}_Q = \mathbf{s}\cdot\mathbf{Q}$.

We present the solutions Eqs. (7.7) as expansions in power series in μ:

$$W = W_0 + \mu\,W_1 + \mu^2 W_2, \quad \mathbf{U} = \mathbf{U}_0 + \mu\,\mathbf{U}_1 + \mu^2\mathbf{U}_2. \tag{7.9}$$

In the zero approximation independently of the kind of elastic modules we obtain

$$W_0 = -\frac{F_3}{l_{22}^{(0)}} = \frac{12\,F_3}{Q}, \qquad \mathbf{U}_0 = 0, \tag{7.10}$$

where Q is given in Eqs. (4.9). In the first approximation

$$W_1 = 0, \qquad \mathbf{U}_1 = -\left(\mathbf{l}_{11}^{(0)}\right)^{-1}\cdot\mathbf{l}_{12}^{(1)}\,W_0. \tag{7.11}$$

The second approximation is bulky:

$$W_2 = -\frac{\mathbf{l}_{21}^{(1)}\cdot\mathbf{U}_1 + l_{22}^{(2)}\,W_0}{l_{22}^{(0)}}, \quad \mathbf{U}_2 = -(\mathbf{l}_{11}^{(0)})^{-1}\cdot\left(\left(\mathbf{l}_{11}^{(0)}\right)^{-1}\cdot\mathbf{l}_{11}^{(1)}\cdot\mathbf{U}_1 + \mathbf{l}_{12}^{(2)}W_0 + i\,\mathbf{s}_Q\,F_3\right). \tag{7.12}$$

If we want to find only a normal deflection W with the SOA then instead of Eqs. (7.7) we may use the more simple system

$$\mathbf{l}_{11}^{(0)}\mathbf{U} + \mathbf{l}_{12}^{(0)} W = 0, \qquad \mu\,\mathbf{l}_{21}^{(1)}\mathbf{U} + (l_{22}^{(0)} + \mu^2 l_{22}^{(2)})W + F_3 = 0 \tag{7.13}$$

and some coefficients (7.8) are not included in Eqs. (7.12) and (7.13).The value W_2 includes three effects of the second order:

(i) the effect of a transversal shear that is described by a summand with $\mathbf{G}$ in $l_{22}^{(2)}$,
(ii) the effect of an inclined anisotropy that disappear for a monoclinic material with $\mathbf{S} = \mathbf{0}$, and
(iii) the effect of normal fibers extension that is described by a summands with $\mathbf{s}_Q$ in $l_{22}^{(2)}$.

The effect of normal fibers extension is always small compared with the zero approximation W_0, and two corresponding summands in $l_{22}^{(2)}$ may be omitted.

For a monoclinic material $\mathbf{S} = \mathbf{0}$ the effect of transversal shear may be essential for a plate with a small transversal shear stiffness. Really, Eqs. (3.8) and (3.9) yield $\varepsilon_s = \mathbf{G}\cdot\sigma_s$ where

$$\mathbf{G} = \hat{\mathbf{G}}^{-1}, \qquad \hat{\mathbf{G}} = \begin{pmatrix} E_{44} & E_{45} \\ E_{45} & E_{55} \end{pmatrix} \tag{7.14}$$

is the inverse matrix of a transversal shear stiffness, and elements of $\mathbf{G}$ are large. For a transversely isotropic material the generalized TR model taking into account a transversal shear is built [16].

Calculations show that for a plate made of a material with the inclined anisotropy ($\mathbf{S} \neq \mathbf{0}$) the small transversal compliance $\hat{\mathbf{G}}$ does not lead to a growth of deflections.

8 Harmonic Vibrations

We consider free vibrations of an infinite anisotropic plate and seek solutions of the 3D and of the 2D equations in the same forms (7.2) and (7.3), respectively, after changing the factor $e^{i(x_1q_1+x_2q_2)}$ by $e^{i(x_1q_1+x_2q_2+\omega t)}$ where ω is the natural frequency. According to Eqs. (2.4) and (4.1) the external (inertia) forces in the dimensionless form read as:

$$\mathbf{f}_t(x_1, x_2, z) = \lambda\,\hat{\rho}(z)\mathbf{u}(z)\,e^{i(x_1q_1+x_2q_2)}, \quad f_3(x_1, x_2, z) = \frac{\lambda}{\mu^2}\hat{\rho}(z)w(z)\,e^{i(x_1q_1+x_2q_2)} \tag{8.1}$$

with

$$\lambda = \frac{\rho_0\, l^2\omega^2}{E}, \quad \hat{\rho}(z) = \frac{\rho(z)}{\rho_0}, \quad \rho_0 = \mathbf{I}_a(\rho(z)), \tag{8.2}$$

where λ is the unknown frequency parameter, and $\rho(z)$ is the density, ρ_0 is the average density. The sign $\hat{}$ again is omitted.

For a homogeneous in the thickness direction plate the elastic modules are constant and $\rho = 1$, and the dynamic equations instead of Eqs. (7.7) are as follows:

$$
\begin{aligned}
&(\mathbf{l}_{11}^{(0)} + \mu\,\mathbf{l}_{11}^{(1)} + \mu^2\mathbf{l}_{11}^{(2)})\mathbf{U} + (\mu\,\mathbf{l}_{12}^{(1)} + \mu^2\mathbf{l}_{12}^{(2)})W + \lambda\,(\mathbf{U} + \mu\mathbf{a}_1 W) = 0,\\
&(\mu\,\mathbf{l}_{21}^{(1)} + \mu^2\mathbf{l}_{21}^{(2)})\mathbf{U} + (l_{22}^{(0)} + \mu^2 l_{22}^{(2)})W + \lambda\left(\mu a_2 U + \left(\frac{1}{\mu^2} + \frac{\mathbf{q}^T\cdot\mathbf{q}}{12}\right)W\right) = 0,
\end{aligned}
\tag{8.3}
$$

where the coefficients $\mathbf{l}_{ij}^{(k)}$ are given in Eqs. (7.8). In Eqs. (8.3) only the main inertia summands are hold.

The determinant of Eqs. (8.3) give an equation:

$$
\Delta(\lambda, q_1, q_2, \mu) = 0. \tag{8.4}
$$

This equation is cubic in λ with complex coefficients. It is easy to prove that the roots of Eq. (8.4) are the real positive numbers, $\lambda_j > 0$. For this aim we write Eqs. (4.2) in the differential form:

$$
\begin{aligned}
&\frac{dw}{dz} = H_1 = -\mu^2\mathbf{s}_P\cdot\mathbf{u} + \mu^3\mathbf{g}^T\cdot\sigma_s + \mu^4 c_3\,\sigma_{33},\\
&\frac{d\mathbf{u}}{dz} = \mathbf{H}_2 = \mathbf{p}\,w - \mu\mathbf{S}_P\cdot\mathbf{u} + \mu^2\mathbf{G}\cdot\sigma_s + \mu^3\mathbf{g}\,\sigma_{33},\\
&\frac{d\sigma_s}{dz} = \mathbf{H}_3 - \lambda\,\rho\,\mathbf{u}, \quad \mathbf{H}_3 = -\mathbf{L}\cdot\mathbf{u} - \mu\mathbf{S}_P^T\cdot\sigma_s - \mu^2\mathbf{s}_P^T, \sigma_{33}\\
&\frac{d\sigma_{33}}{dz} = H_4 - \frac{\lambda}{\mu^2}\rho\,w, \quad H_4 = -\mathbf{p}^T\cdot\sigma_s,
\end{aligned}
\tag{8.5}
$$

From the two last Eqs. (8.5) it follows:

$$
\lambda\,\mathbf{I}_a(\rho\overline{\mathbf{u}}^T\cdot\mathbf{u} + \mu^{-2}\rho\overline{w}\,w) = \mathbf{I}_a\left(\overline{\mathbf{u}}^T\cdot\left(\mathbf{H}_3 - \frac{d\sigma_s}{dz}\right) + \overline{w}\left(H_4 - \frac{d\sigma_{33}}{dz}\right)\right) = r. \tag{8.6}
$$

After integrating by part and using two first Eqs. (8.5) we get

$$
r = I_a\left(\overline{\mathbf{u}}^T\cdot\mathbf{Q}^T\cdot\mathbf{A}^*\cdot\mathbf{Q}\cdot\mathbf{u} + \mu^2\,\overline{\sigma}_s^T\cdot\mathbf{G}\cdot\sigma_s + +2\mu^3\,Re(\sigma_{33}\,\mathbf{g}^T\cdot\overline{\sigma}_s) + \mu^4 c_3|\sigma_{33}|^2\right) > 0. \tag{8.7}
$$

Therefore, inequality $\lambda_j > 0$ is proved.

The small root of Eq. (8.4), $\lambda_1 = \mu^2 Q/12 + O(\mu^4)$, corresponds to the bending vibrations, and two rest roots, $\lambda_{2,3} = O(1)$, correspond to the tangential vibrations.

Equation (8.4) *is* a dispersion equation because it describes a harmonic wave propagation according to the factor $e^{i(x_1q_1+x_2q_2+\omega t)}$. If we take $q_1^2 + q_2^2 = 1$ then the velocity of wave is $v = -\omega$ and the direction of wave propagation is described by the vector $\mathbf{q}$.

To obtain a stationary bending vibration mode $w(x_1, x_2, t) = W\sin q_1x_1\sin q_2x_2\sin\omega t$ we ought to consider a sum $We^{i(q_1x_1-q_2x_2)}\sin\omega t - We^{i(q_1x_1+q_2x_2)}\sin\omega t$.

9 Conclusions

The 2D linear model (7.5) of the SOA describing deformations of a heterogeneous plate in the case of the general anisotropy (with 21 elastic modules) is constructed. It is necessary to continue investigations of the studied problem. It is desirable to investigate the peculiarities that appears in the case of plates with inclined anisotropy. It is interesting to estimate errors for test examples of the 2D models compared with the exact solutions of 3D equations of the theory of elasticity. The obtained model is bulky, and it is desirable to propose in the partial cases of plates parameters the more simple but the exact enough models.

The next step is to solve some static, vibration, and buckling problems for partial kinds of anisotropy and heterogeneity.

The used algorithm is based on the Cartesian co-ordinate system. It is interesting to apply the obtained results for heterogeneous anisotropic shells, in partial, for shallow shells for that the metric is close to the Cartesian metric.

Acknowledgements The study is supported by Russian Foundation of Basic Researches, grants 16.01.00580-a, 16.51.52025 MHT-a.

References

1. Kirchhoff, G.: Vorlesungen uber Matematische Physik. Mechanik, Leipzig (1876). [in German]
2. Love, A.E.H.: A Treatise on the Mathematical Theory Elasticity. Cambridge University Press (1927)
3. Timoshenko, S.P.: Strength of Materials. Van Vistrand, New York (1956)
4. Donnell, L.H.: Beams. McGraw-Hill, Plates and Shells (1976)
5. Novozhilov, V.: Theory of Thin Shells. Wolters-Noordhoff, Groningen (1970)
6. Goldenweizer, A.L.: Theory of Elastic Thin Shells. Nauka, Moscow (1976). [in Russian]
7. Reissner, E.: The effect of transverse shear deformation on the bending of elastic plates. Trans. ASME J. Appl. Mech. **12**, 69–77 (1945)
8. Vekua, I.N.: On one method of calculating prismatic shells. Trudy Tbilis. Mat. Inst. **21**, 191–259 (1955). [in Russian]
9. Chernykh, K.F., Rodionova, V.A., Titaev, B.F.: Applied Theory of Anisotropic Plates and Shells. St. Petersburg University Press (1996). [in Russian]
10. Eremeev, V.A., Zubov, L.M.: Mechanics of Elastic Shells. Nauka, Moscow (2008). [in Russian]
11. Ambartsumyan, S.A.: General Theory of Anisotropic Shells. Nauka, Moscow (1974). [in Russian]
12. Agolovyan, L.A.: Asymptotic Theory of Anisotropic Plates and Shells, 414 p. Nauka, Moscow (1997). [in Russian]
13. Reddy, J.N.: Mechanics of Laminated Composite Plates and Shells, 831 p. CRC Press (2004)
14. Kienzler, R., Shneider, P.: Comparison of various linear plate theories in the light of a consistent second order approximation. Shell Struct. Theory Appl. **3**, 109–112 (2014). Proceedings of the 10th SSTA 2013 Conference
15. Tovstik, P.E., Tovstik, T.P.: A thin-plate bending equation of second-order accuracy. Dokl. Phys. **59**(8), 389–392 (2014)
16. Tovstik, P.E., Tovstik, T.P.: Generalized Timoshenko–Reissner models for beams and plates, strongly heterogeneous in the thickness direction. ZAMM **97**(3), 296–308 (2017)

17. Tovstik, P.E., Tovstik, T.P.: An elastic plate bending equation of second-order accuracy. Acta Mech. **228**(10), 3403–3419 (2017)
18. Morozov, N.F., Tovstik, P.E., Tovstik, T.P.: Generalized Timoshenko–Reissner model for a multilayer plate. Mech. Solids **51**(5), 527–537 (2016)
19. Morozov, N.F., Tovstik, P.E., Tovstik, T.P.: A continuum model of a multilayer nanosheet. Dokl. Phys. **61**(11), 567–570 (2016)
20. Schneider, P., Kienzler, R.: A Reissner-type plate theory for monoclinic material derived by extending the uniform-approximation technique by orthogonal tensor decompositions of nth-order gradients. Meccanica **52**, 21432167 (2017). https://doi.org/10.1007/s11012-016-0573-1
21. Morozov, N.F., Belyaev, A.K., Tovstik, P.E., Tovstik, T.P.: Two-dimensional equations of second order accuracy for a multilayered plate with orthotropic layers. Dokl. Phys. **63**(11), 471–475 (2018). ISSN 1028-3358
22. Tovstik, P.E.: Two-dimensional models of plate made of an anisotropic material. Dokl. Phys. **425**(4), 487–491 (2009)
23. Tovstik, P.E., Tovstik, T.P.: Two-dimensional models of shells made of an anisotropic material. Acta Mech. **225**(3), 647–661 (2014)
24. Tovstik, P.E., Tovstik, T.P.: Two-dimensional model of a plate made of an anisotropic inhomogeneous material. Mech. Solids **52**(2), 144–154 (2017)
25. Tovstik, P.E., Tovstik, T.P.: Two-dimensional model of a plate made of an anisotropic inhomogeneous material. Trudy seminara "Komputernye metody v mekhanike sploshnoi sredy", vol. 3, pp. 4–16. St. Petersburg Publishing (2008)
26. Parshina, L.V., Ryabov, V.M., Yartsev, B.A.: Energy dissipation during vibrations of nonuniform composite structures. 1. Formulation of the Problem. 2. Method of Solution. 3. Numerical Experiment. Vestn. St. Petersburg Univ. Math. **51**(2–4) (2018)

An Alternative Approach to the Buckling Resistance Assessment of Steel, Pressurised Spherical Shells

Paweł Błażejewski and Jakub Marcinowski

Abstract Provisions leading to the assessment of the buckling resistance of pressurised spherical shells are available since 2008 when they were published first time as the European Design Recommendations (EDR) (cf. Rotter and Schmidt in Buckling of Steel Shells: European Design Recommendations. ECCS, 2008 [13], Rotter and Schmidt in Buckling of Steel Shells: European Design Recommendations. ECCS, 2013 [14]). This collection of recommendations comprises rules which refer to the buckling resistance of steel shells of different shapes. In the first step of the general procedure, the calculation of two reference quantities: the elastic critical buckling reference p_{Rcr} and the plastic reference resistance p_{Rpl} is required. These quantities should be determined in the linear buckling analysis (LBA) and in the materially nonlinear analysis (MNA) respectively. Only in the case of spherical shells the existing procedure has exceptional character. It is based on the geometrically nonlinear analysis (GNA) and on the geometrically and materially nonlinear analysis (GMNA), respectively. From this reason, in this particular case there was a need to change the existing provisions. The first version of a new procedure was presented in the work of Błażejewski and Marcinowski (Buckling capacity curves for pressurized spherical shells. Taylor & Francis Group, London, pp. 401–406, 2016 [4]). All steps of the procedure leading to the assessment of buckling resistance of pressurized steel, spherical shells were presented in that work. The elaborated procedure is consistent with provisions of Eurocode EN1993-1-6 (cf. Błażejewski and Marcinowski in The worst geometrical imperfections of steel spherical shells, pp. 219–226, 2014 [3]) and with general recommendations inserted in Europeans Design Recommendations. In the present work the proposed capacity curves were compared with the existing provisions of ECCS for three different fabrication quality classes predicted. Comparisons of the author's proposal with some experimental results obtained by other authors are presented as well. They have confirmed that the proposed procedure is less conservative than the existing one but it is still safe.

P. Błażejewski · J. Marcinowski (✉)
Institute of Civil Engineering, University of Zielona Góra, Licealna 9, 65-417 Zielona Góra, Poland
e-mail: J.Marcinowski@ib.uz.zgora.pl

P. Błażejewski
e-mail: P.Blazejewski@ib.uz.zgora.pl

H. Altenbach et al. (eds.), *Recent Developments in the Theory of Shells*,
Advanced Structured Materials 110, https://doi.org/10.1007/978-3-030-17747-8_8

Keywords Steel spherical shell · Buckling resistance · Buckling curve · External pressure · Clamped edge · Numerical simulations · Design recommendations

1 Introduction

Steel, spherical shells subjected to the action of external pressure p are usually very slender and internal forces which are generated within their domain are compressive. For this reason they are exposed to local or global buckling, probably the most important reasons for failures of such shells. An accurate assessment of the buckling resistance, as the maximum pressure p which can be safely sustained, is very important from the engineering point of view. The buckling limit state (LS3 according to EN 1993-1-6) is usually the decisive criterion among all design criteria.

Existing designing provisions define precisely procedures leading to the buckling resistance assessment of steel shells (cf. EN 1993-1-6). The approach based on the MNA analysis and LBA analysis is a commonly accepted approach as far as the plastic reference resistance p_{Rpl} and elastic critical buckling reference p_{Rcr} are concerned. These are two reference quantities on the basis of which buckling capacity curves for particular cases of shells are created. EDR 5th includes provisions which refer to several cases of shells exposed to buckling. In the existing chapter dedicated to spherical shells the different approach was adopted. Reference quantities of the whole procedure p_{Rcr} and p_{Rpl} are determined on the basis of the GNA (geometrically nonlinear analysis) and the GMNA (geometrically and materially nonlinear analysis) respectively and it is a single exception in these recommendations.

In this paper an alternative approach was presented, the approach consistent with the general approach recommended in EN 1993-1-6 (cf. [9]) and in EDR 5th. All steps of the proposed approach were presented by Błażejewski and Marcinowski [2, 4]. All parameters defining capacity curves were obtained as a result of many numerical analyses carried out for spherical shells of different geometry and different material parameters. Spherical caps of semi-angles $\varphi = 10°, 20°, 30°, 45°, 60°, 90°$ and of following R/t ratios: $R/t = 300, 400, 500, 600, 750, 1000$ were considered. Seven different imperfection modes were taken into account and three fabrication quality classes were considered. Only one case of boundary condition was taken into account: the fully clamped basic circle of considered caps (see Fig. 1). All calculations were performed by means of COSMOS/M system (cf. [6]) based on FEM.

In this work also comparison of the proposed approach with experimental results of other authors was presented and this comparison is a valuable verification test for buckling capacity curves elaborated by authors.

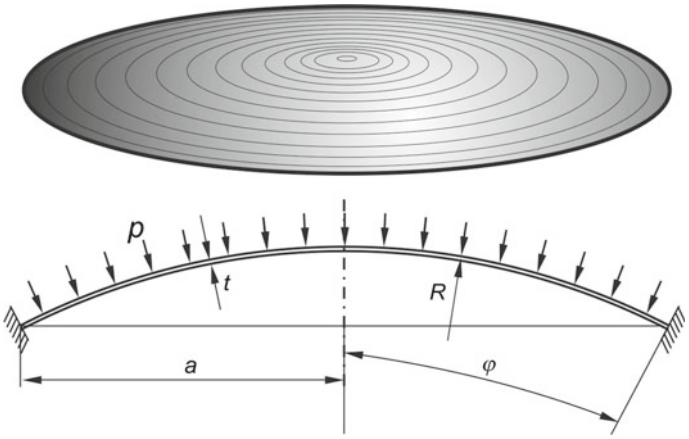

Fig. 1 Pressurised, spherical shell

2 Elastic Critical Buckling Resistance and Plastic Reference Resistance

The elastic critical buckling resistance p_{Rcr} and the plastic reference resistance p_{Rpl} are principal quantities required in the buckling resistance assessment procedure. An attempt of derivation of the simple formulae on p_{Rcr} and p_{Rpl} was undertaken by Authors earlier (cf. [3]).

To find this formulae many numerical analyses (LBA—the linear buckling analysis in reference to p_{Rcr} and MNA—the materially nonlinear analysis in a case of p_{Rpl}) were carried out for a huge range of R/t ratios and for a great diversity of semiangles φ defining the rise of spherical shells. Details of this stage of the research were presented in [3]. After some supplementary numerical simulations carried out on very dense mesh the following formulae defining two reference quantities were obtained:

$$p_{\mathrm{Rcr(LBA)}} = 1.21E\left(\frac{t}{R}\right)^2 \tag{1}$$

$$p_{\mathrm{Rpl(MNA)}} = 2.0\, f_{\mathrm{yk}}\frac{t}{R} \tag{2}$$

in which E—Young's modulus, f_{yk}—characteristic value of the yield stress, both expressed in [MPa].

The formula (1) is identical as critical buckling pressure for the pressurised, full sphere and is called Zoelly-Leibenson formula (cf. [11, 18]). The formula (2) is the same as the membrane pressure causing plastification of the whole section of the pressurised, full sphere.

The determination of the critical pressure p_{Rcr} and the plastic reference pressure p_{Rpl} according to EDR 5th (cf. [13, 14]) are done in a very similar way. These quantities are determined from the following formulae:

$$p_{\mathrm{Rcr(GNA)}} = 0.97E\left(\frac{t}{R}\right)^2 \tag{3}$$

$$p_{\mathrm{Rpl(GMNA)}} = 1.80\, f_{\mathrm{yk}}\frac{t}{R} \tag{4}$$

Coefficients used in these formulae are different than their counterparts in formulae (1) and (2) and it follows from different approaches used in both cases.

The summary of curves presenting the critical pressure due to formulae (1) and (3) and (2) and (4) respectively are shown in Figs. 2 and 3 as a function of R/t ratio. Differences between both proposals are easily visible.

Having both reference quantities defined above, and namely p_{Rcr} and p_{Rpl}, one can calculate the dimensionless relative slenderness defined in the standard way

$$\lambda = \sqrt{p_{\mathrm{Rpl(MNA)}}/p_{\mathrm{Rcr(LBA)}}} \tag{5}$$

and respectively:

$$\lambda = \sqrt{p_{\mathrm{Rpl(GMNA)}}/p_{\mathrm{Rcr(GNA)}}} \tag{6}$$

The calculation of relative slenderness is a very easy task due to the fact that all quantities appearing under the square root symbols are described by formulae.

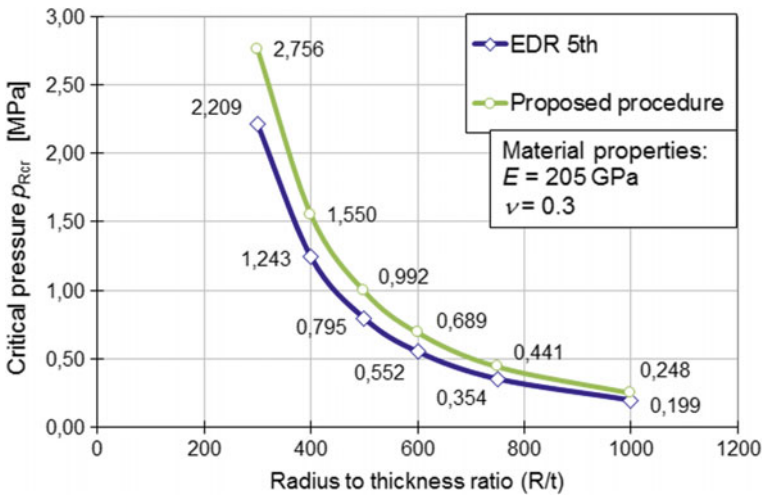

Fig. 2 Critical pressure p_{Rcr} according to the proposed procedure and due to EDR 5th provisions

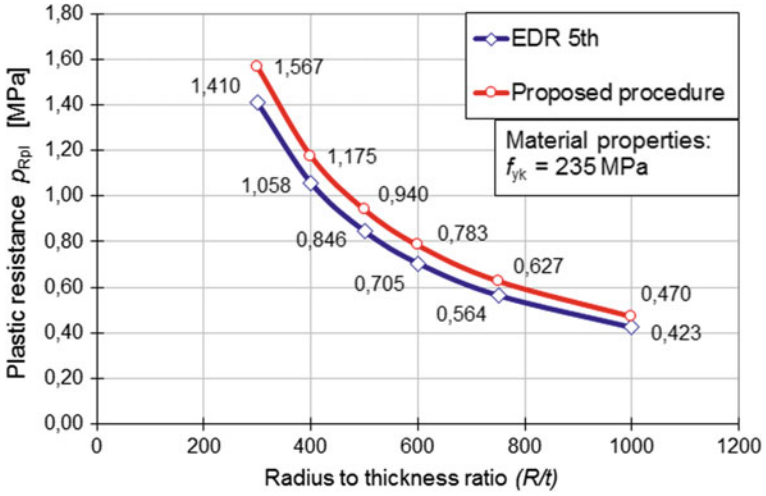

Fig. 3 Plastic resistance p_{Rpl} according to the proposed procedure and due to EDR 5th provisions

3 Modified Capacity Curves—Buckling Parameters

To assess the buckling resistance of a pressurised spherical shell one should know all the buckling parameters λ_0, α, β and η describing the standard capacity curve (cf. EDR 5th and EN 1993-1-6). The dimensionless relative slenderness λ is defined according to Eq. (5) and the buckling strength reduction factor χ is equal to the p_{Rk}/p_{Rpl} ratio, where p_{Rk} is the characteristic value of the buckling resistance.

Values of buckling parameters can be effectively determined by means of the approach proposed by Doerich and Rotter [7]. According to this approach a modified capacity curve should be calculated. This curve is determined for an assumed mode of imperfection and for the adopted amplitude of this imperfection mode. Particular points on this curve are obtained for different values of relative slenderness. This can be achieved by means of artificially changed yield stress and this approach was adopted in this work.

Seven different modes of imperfections were considered. Detailed considerations relating to the selection and generation of these imperfection modes were presented by Błażejewski and Marcinowski [3].

Similarly as in EDR 5th the amplitudes of imperfections were defined as follows

$$\Delta w_k = \frac{1}{Q}\sqrt{Rt} \tag{7}$$

where Q—is the fabrication quality parameter corresponding to the specified fabrication tolerance quality. For three different fabrication quality classes A, B and C (excellent, high and normal) the quality parameter Q adopts values 40, 25 and 16 respectively.

Figure 4 presents the example of modified capacity curve obtained as a results of many numerical analyses carried out for a particular geometry (cf. [3]), for a specific imperfection mode and adopted quality class. On the abscissa of this plot the ratio $p_{R(GMNIA)}/p_{Rcr(LBA)}$ are depicted while the ordinates of this plot present the ratio $p_{R(GMNIA)}/p_{Rpl(MNA)}$. The squash limit relative slenderness is defined by the last point on the horizontal segment of the plot. At this point $p_{R(GMNIA)}$ is equal to $p_{Rpl(MNA)}$ (the ordinate equal to 1.0) and at the same time the ratio $p_{Rpl(MNA)}/p_{Rcr(LBA)}$/is equal to λ_0^2.

Precise determination of the elastic imperfection reduction factor α is very easy if the modified capacity curve is plotted. For very slender shells $p_{R(GMNIA)}$ can be identified as a product of α and p_{Rcr}. This means that the value of α is determined by the final vertical segment of the plot (see Fig. 4).

Transition from the elastic-plastic range into purely elastic range is accomplished at the point at which the vertical segment starts. At this point $\lambda = \lambda_p$ and $\chi = 1 - \beta$.

Analysing all obtained results and comparing them with existing proposal for cylindrical, and spherical shells (comp. [13]) it was assumed that the λ_0 value is constant and equal 0.2. Parameters α and β were determined from all modified capacity curves quite accurately due to the fact that they can be detected very distinctly. Figure 5 presents the "cloud" of calculated alfas for different values of the $\Delta w_k/t$ ratio. Calculation points depicted in Fig. 5 were obtained from modified capacity curves determined for spherical shells of different R/t ratios, different semi-angles φ and for different imperfection modes (seven imperfection modes were considered). Amplitudes of imperfections were dependent on Q parameter according to relationship (7).

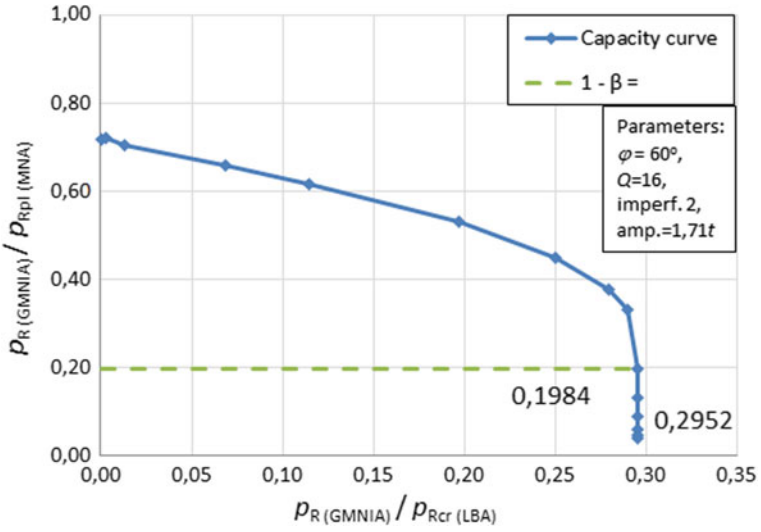

Fig. 4 The modified capacity curve

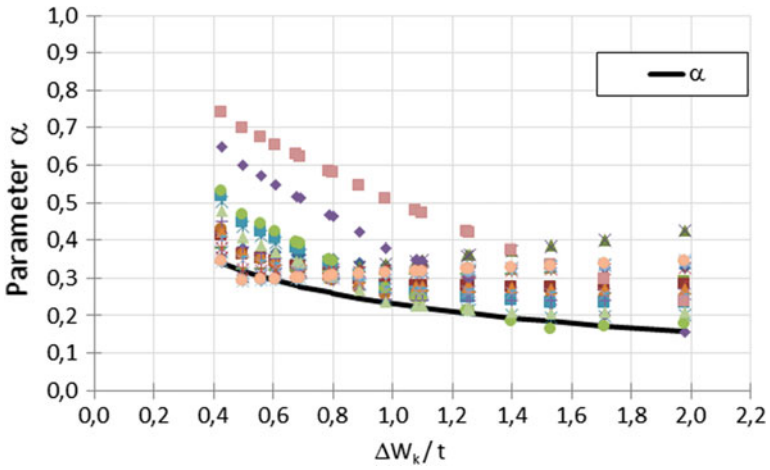

Fig. 5 Calculations points defining α as a function of the $\Delta w_k/t$ ratio

To guarantee the safety in all possible circumstances α was approximated as a lower bound of all points depicted in Fig. 5. As a result the following function was obtained:

$$\alpha(\Delta w_k/t) = \frac{0.65}{1 + 1.8(\Delta w_k/t)^{0.8}} \tag{8}$$

The other parameter describing the final shape of the capacity curve, the β parameter, was determined on the basis of all registered results as a weighted curve approximating points shown in Fig. 6. Also in this case particular points were obtained for spherical shells of different R/t ratios, different semi-angles φ and for different imperfection modes (seven imperfection modes were considered). Amplitudes of imperfections were dependent on Q parameter according to relationship (7).

The proposed formula expressing the dependence of the β parameter as a function of the $\Delta w_k/t$ ratio has the following form:

$$\beta(\Delta w_k/t) = 0.87\left(\frac{\Delta w_k}{t}\right)^{0.026} \tag{9}$$

It is worth noting that both determined parameters depend not only on geometrical characteristics R, t, and φ but also on fabrication quality class due to the fact that the $\Delta w_k/t$ ratio is expressed by Q. Figures 7 and 8 show plots of α and β parameters as functions of R/t ratios for different values of the Q parameter. In the same figure proposals of EDR 5th were presented as well.

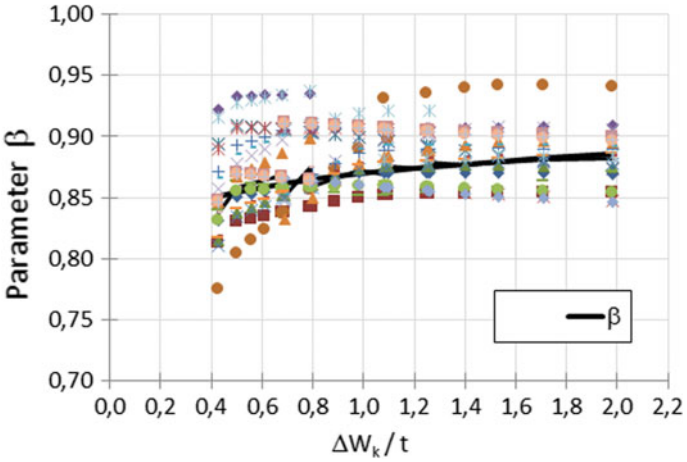

Fig. 6 Calculations points defining β as a function of the $\Delta w_k/t$ ratio

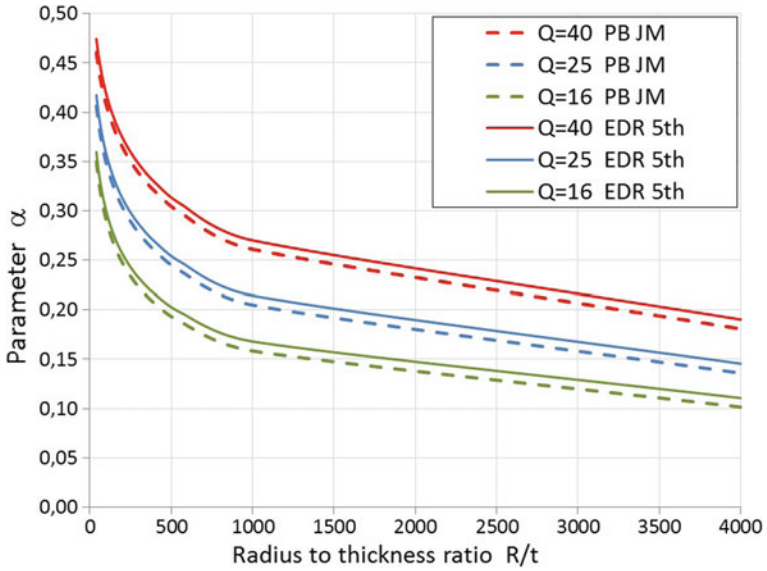

Fig. 7 Function $\alpha(R/t)$ for different values of the Q parameter

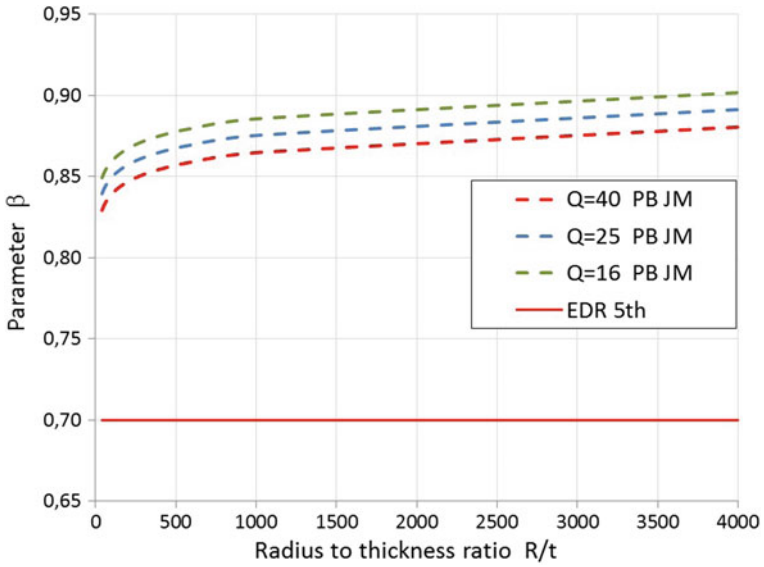

Fig. 8 Function $\beta(R/t)$ for different values of the Q parameter

The comparison of presented proposals with those proposed in EDR 5th shows that elastic buckling reduction factor α is smaller than its counterpart from EDR 5th. It means that the buckling strength reduction factor χ will be smaller within the elastic interval. On the other hand the greater values of the plastic range factor β mean that the elastic-plastic range will be enlarged in comparison to the previous proposal of EDR 5th in which β does not depend on R/t ratio.

The knowledge of α and β parameters allows to determine the plastic limit relative slenderness λ_p from the formula

$$\lambda_p = \sqrt{\frac{\alpha}{1-\beta}} \tag{10}$$

4 Buckling Capacity Curves

The standard form of the buckling capacity curve consistent with proposals of Schmidt [15, 16] and Rotter [12] was presented in Fig. 9a.

Due to some significant difficulties arising in the reference to the exact evaluation of the interaction exponent η defining the capacity curve within the elastic-plastic range, Authors have proposed a modification of this standard capacity curve within this range. In place of the function shown in Fig. 9a the polynomial of the second order was proposed, and namely

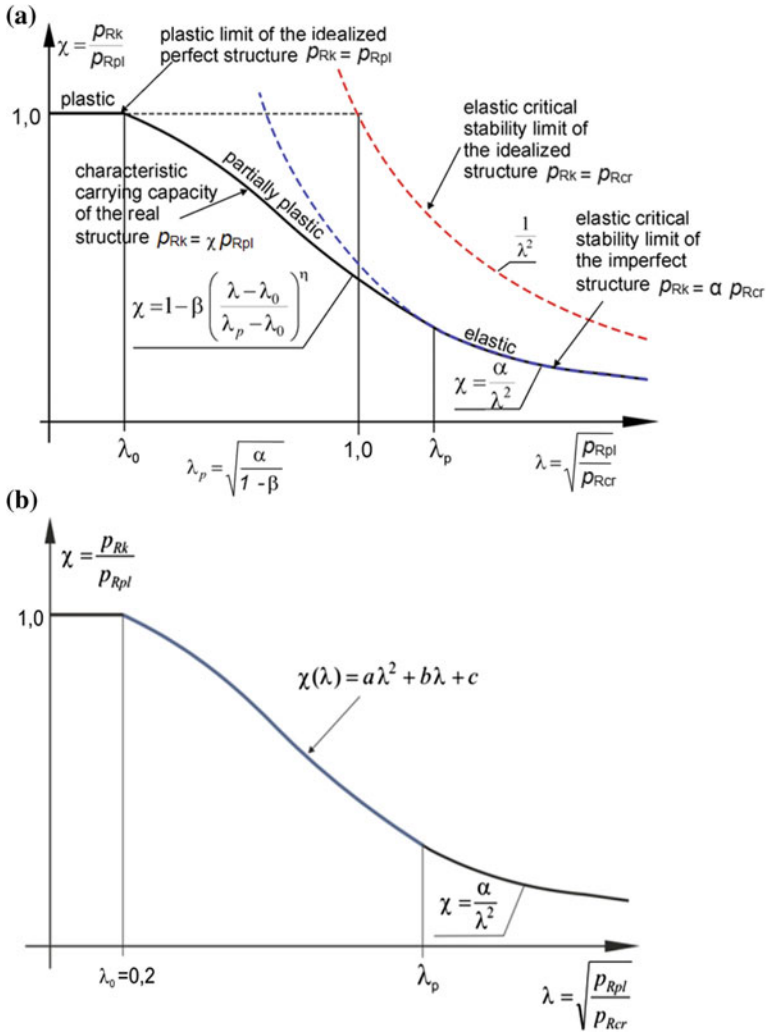

Fig. 9 **a** The standard buckling capacity curve. **b** The modified buckling capacity curve

$$\chi(\lambda) = a\lambda^2 + b\lambda + c, \quad \text{for } \lambda_0 \le \lambda \le \lambda_p \tag{11}$$

This function was shown in Fig. 9b and its coefficients were determined from continuity conditions at λ_0 and λ_p points. They adopt the following form:

$$a = \frac{\alpha(0.4 - 3\lambda_p) + \lambda_p^3}{\lambda_p^3(0.04 - 0.4\lambda_p + \lambda_p^2)}, \tag{12a}$$

$$b = \frac{-2\lambda_p^4 + \alpha\left(4\lambda_p^2 - 0.08\right)}{\lambda_p^3\left(0.04 - 0.4\lambda_p + \lambda_p^2\right)}, \tag{12b}$$

$$c = \frac{\alpha\left(0.12 - 0.8\lambda_p\right) + \lambda_p^4}{\lambda_p^2\left(0.04 - 0.4\lambda_p + \lambda_p^2\right)}. \tag{12c}$$

It is worth mentioning that in the existing EDR5th provisions the η parameter defining $\chi(\lambda)$ in elastic-plastic range (comp. Fig. 8) is constant and equals 1. It means that within elastic-plastic range $\chi(\lambda)$ characteristics is linear and do not fulfils smooth continuity conditions at point of transition to the elastic range. Author's proposal is free from this drawback.

Using the approach presented above the capacity curves can be generated for the spherical shell of specific geometrical and material characteristics and for three fabrication quality classes. The example of such capacity curves were presented in Fig. 10. In this figure the transition from the purely elastic range to the elastic-plastic range was clearly marked.

In the proposed procedure the buckling parameter β is variable and defined by the Formula (9). In the existing provisions of EDR5th the buckling parameter β is constant and equals 0.7 (comp. [13]). It means that at the point $\lambda = \lambda_0$ the buckling resistance parameter χ is equal 0.3 for all three fabrication quality parameters Q (comp. Fig. 11).

Figure 12 shows the comparison of the present proposal with existing provisions of EDR 5th. In this case capacity curves are plotted as the function of the characteristic value of the buckling resistance $p_{\mathrm{Rk}}(R/t)$. It is visible that existing provisions provide slightly lower assessment of the buckling resistance, it means that they are more conservative.

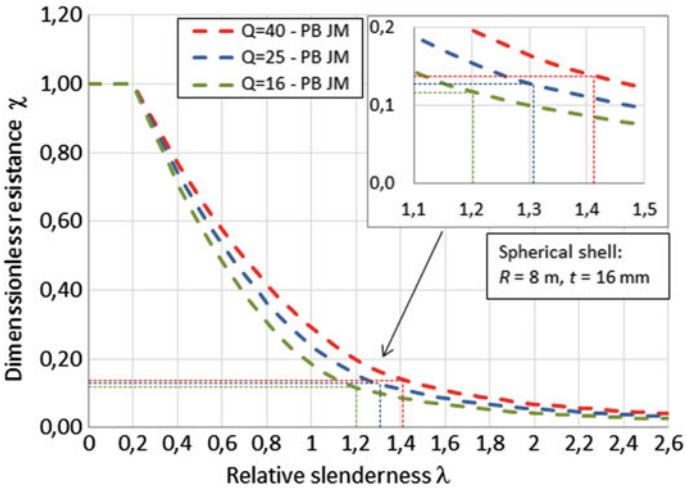

Fig. 10 Buckling capacity curves for different values of the Q parameter

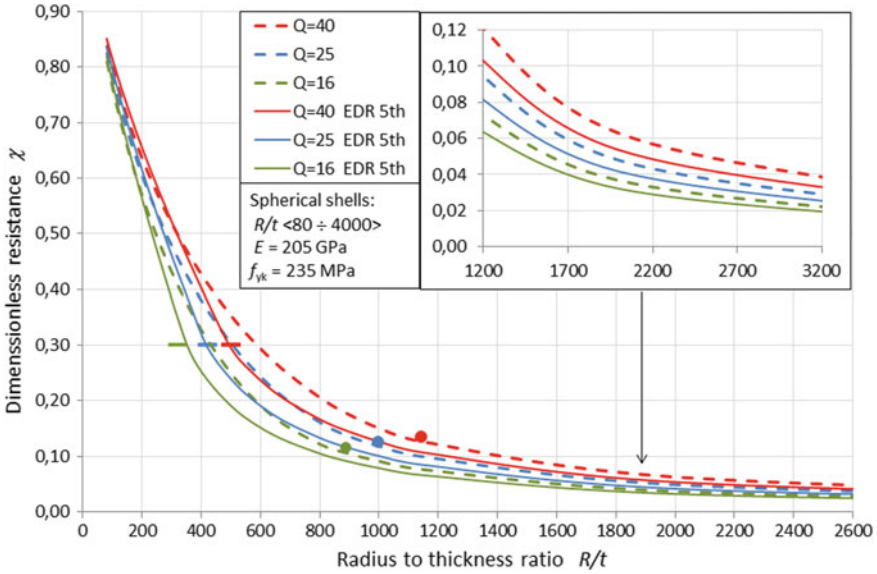

Fig. 11 Dimensionless buckling capacity χ for different parameters Q according to author's proposal and due to EDR 5th

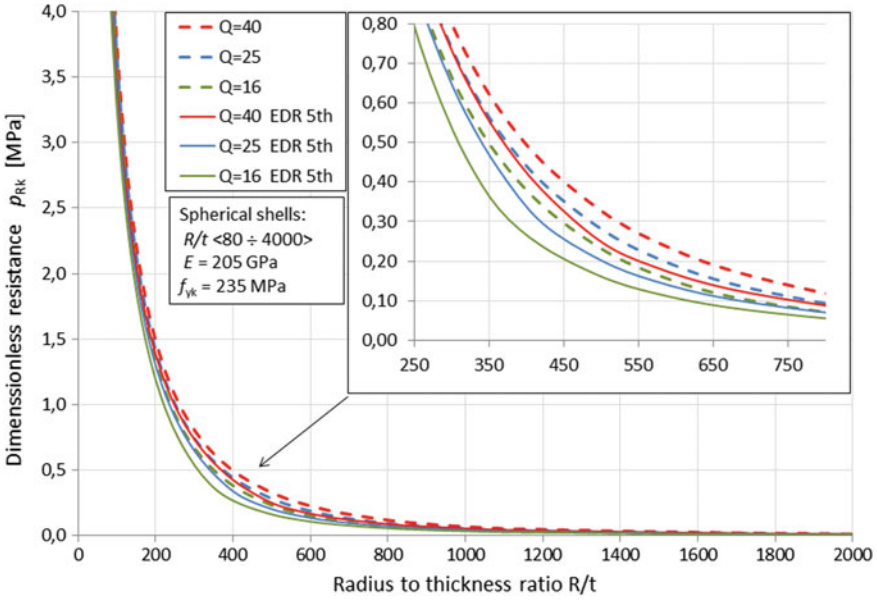

Fig. 12 The comparison with existing provisions of EDR 5th

Analysing results presented in Fig. 12 one can distinguish two intervals. Within the first interval defined by R/t for <80÷420>, differences are smaller than 19%, 35% and 43% for Q parameters 16, 25 and 40 respectively. These differences decrease for smaller R/t ratios and it is due to the fact that in both approaches all capacity curves tend to the same point $\chi = 1.0$ and $\lambda = \lambda_0 = 0.2$. This fact is well visible in Fig. 12.

Within the other interval defined by R/t for <420÷560>, differences between both approaches are greater and oscillates between 35% ÷ 44%. Discrepancies decrease for higher R/t ratios and for $R/t = 2400$ reach the values 20÷28% for different values of Q parameter, 16, 25 and 40 respectively.

The complete flow chart of the buckling resistance assessment of pressurised spherical shells is presented below. This flow chart can be helpful for designers of tanks, silos and pressure vessel in which spherical shells loaded by external pressure occur.

5 Determination of the Buckling Resistance—The Flow Chart

Step 1. Adoption of principal design data: E, f_{yk}, R, t

Step 2. Calculation of reference quantities and determination of the dimensionless, relative slenderness λ

$$\left.\begin{aligned} p_{\mathrm{Rcr(LBA)}} &= 1.21E\left(\tfrac{t}{R}\right)^2 \\ p_{\mathrm{Rpl(MNA)}} &= 2.0\, f_{\mathrm{yk}}\tfrac{t}{R} \end{aligned}\right\} \Rightarrow \lambda = \sqrt{p_{\mathrm{Rpl(MNA)}}/p_{\mathrm{Rcr(LBA)}}}$$

Step 3. Specification of the fabrication quality class and calculation of the characteristic value of imperfection amplitude.

$$\begin{aligned} &\text{Class } A \rightarrow Q = 40 \\ &\text{Class } B \rightarrow Q = 25 \\ &\text{Class } C \rightarrow Q = 16 \end{aligned} \Rightarrow \Delta w_k = \frac{1}{Q}\sqrt{Rt}$$

Step 4. Determination of buckling parameters α and β. Calculation of the plastic limit relative slenderness λ_{p}

$$\left.\begin{aligned} \alpha(\Delta w_k/t) &= \tfrac{0.65}{1+1.8(\Delta w_k/t)^{0.8}} \\ \beta(\Delta w_k/t) &= 0.87\left(\tfrac{\Delta w_k}{t}\right)^{0.026} \end{aligned}\right\} \Rightarrow \lambda_p = \sqrt{\frac{\alpha}{1-\beta}}$$

Step 5. The buckling strength reduction factor χ for different intervals of λ (cf. Fig. 7).

$$\begin{aligned}
&\chi(\lambda) = 1, && \text{for} \quad \lambda < \lambda_0 \\
&\chi(\lambda) = a\lambda^2 + b\lambda + c, && \text{for} \quad \lambda_0 < \lambda < \lambda_p, \quad \text{where } \lambda_0 = 0.2 \\
&\chi(\lambda) = \alpha/\lambda^2, && \text{for} \quad \lambda > \lambda_p
\end{aligned}$$

Step 6. Determination of the polynomial coefficients in the case of elastic-plastic range.

$$a = \frac{\alpha\left(0.4 - 3\lambda_p\right) + \lambda_p^3}{\lambda_p^3\left(0.04 - 0.4\lambda_p + \lambda_p^2\right)}$$

$$b = \frac{-2\lambda_p^4 + \alpha\left(4\lambda_p^2 - 0.08\right)}{\lambda_p^3\left(0.04 - 0.4\lambda_p + \lambda_p^2\right)}$$

$$c = \frac{\alpha\left(0.12 - 0.8\lambda_p\right) + \lambda_p^4}{\lambda_p^2\left(0.04 - 0.4\lambda_p + \lambda_p^2\right)}$$

Step 7. Characteristic value of the buckling resistance of the considered spherical shell

$$p_{Rk} = \chi \cdot p_{Rpl}$$

6 Illustrative Examples

To show differences between both considered approaches two calculation examples were presented in which buckling resistances for particular spherical shells were determined. It is worth noting that presented provisions refer to spherical caps of semiangles φ in the range 10–90 degrees.

6.1 Calculation Example No. 1

Determine the buckling resistance of pressurised spherical shell of given geometrical parameters and material properties:

- Radius: $R = 8000$ mm
- Shell thickness: $t = 16$ mm
- Ratio $R/t = 500$
- Steel grade S235–$f_{yk} = 235$ MPa, $E = 205$ GPa, $v = 0.3$
- Fabrication quality class: C (normal), hence $Q = 16$
- Shell clamped along its supporting edge, case BC2, hence $C_c = 0.8$, $C_{pl} = 0.9$

6.1.1 Buckling Resistance Assessment Procedure According to EDR5th

1. Elastic, critical buckling pressure

$$p_{\mathrm{Rcr}} = \frac{2}{\sqrt{3(1-v^2)}} C_c E \left(\frac{t}{R}\right)^2 = \frac{2}{\sqrt{3\left(1-0.3^2\right)}} \cdot 0.8 \cdot 205000 \cdot \left(\frac{0.016}{8.0}\right)^2 = 0.794\,\mathrm{MPa}$$

2. Plastic reference resistance

$$p_{\mathrm{Rpl}} = f_{y,k} \cdot C_{pl} \cdot \frac{2 \cdot t}{R} = 235 \cdot 0.9 \cdot \frac{2 \cdot 0.016}{8.0} = 0.846\,\mathrm{MPa}$$

3. Dimensionless relative slenderness

$$\lambda = \sqrt{p_{\mathrm{Rpl}}/p_{\mathrm{Rcr}}} = \sqrt{0.846/0.794} = 1.032$$

4. Characteristic imperfection amplitude and elastic imperfection factor α

$$\Delta w_k = \frac{1}{Q}\sqrt{Rt} = \frac{1}{16}\sqrt{8.0 \cdot 0.016} = 0.022\,\mathrm{m}$$

$$\alpha = \frac{0.7}{1 + 1.9 \cdot (\Delta w_k/t)^{0.75}} = \frac{0.7}{1 + 1.9 \cdot (0.022/0.016)^{0.75}} = 0.205$$

5. Buckling parameters and the plastic limit relative slenderness λ_{p}

$$\beta = 0.70;\ \eta = 1.0;\ \lambda_0 = 0.20$$

$$\lambda_p = \sqrt{\frac{\alpha}{1-\beta}} = \sqrt{\frac{0.205}{1-0.7}} = 0.827$$

6. Determination of the interval on the buckling curve

$$\lambda \geq \lambda_p \rightarrow \lambda = 1.032 > \lambda_p = 0.827$$

Because it is the case of purely elastic buckling the buckling reduction factor χ should be determined from the formula:

$$\chi = \frac{\alpha}{\lambda^2} = \frac{0.205}{1.032^2} = 0.192$$

7. The characteristic value of the buckling resistance

$$p_{\mathrm{Rk}} = \chi \cdot p_{\mathrm{Rpl}} = 0.192 \cdot 0.846 = 0.162\,\mathrm{MPa}$$

8. The design value of the buckling resistance

$$p_{\mathrm{Rd}} = p_{\mathrm{Rk}}/\gamma_{\mathrm{M1}} = 0.162/1.1 = 0.147\,\mathrm{MPa}$$

where the safety factor γ_{M1} is taken from EN 1993-1-1 and is equal 1.1 (cf. [8]).

6.1.2 The Proposed Procedure Based on Assumptions of EN 1993-1-6

1. Elastic, critical buckling pressure

$$p_{\mathrm{Rcr(LBA)}} = 1.21E\left(\frac{t}{R}\right)^2 = 1.21 \cdot 205000 \cdot \left(\frac{0.016}{8.0}\right)^2 = 0.992\,\mathrm{MPa}$$

2. Plastic reference resistance

$$p_{\mathrm{Rpl(MNA)}} = 2.0\, f_{yk}\frac{t}{R} = 2.0 \cdot 235 \cdot \frac{0.016}{8.0} = 0.940\,\mathrm{MPa}$$

3. Dimensionless relative slenderness

$$\lambda = \sqrt{p_{\mathrm{Rpl(MNA)}}/p_{\mathrm{Rcr(LBA)}}} = \sqrt{0.940/0.992} = 0.973$$

4. Characteristic imperfection amplitude and elastic imperfection factor α and the plastic range factor β

$$\Delta w_k = \frac{1}{Q}\sqrt{Rt} = \frac{1}{16}\sqrt{8.0 \cdot 0.016} = 0.022\,\mathrm{m}$$

$$\alpha(\Delta w_k/t) = \frac{0.65}{1 + 1.8(\Delta w_k/t)^{0.8}} = \frac{0.65}{1 + 1.8(0.022/0.016)^{0.8}} = 0.196$$

$$\beta(\Delta w_k/t) = 0.87\left(\frac{\Delta w_k}{t}\right)^{0.026} = 0.87\left(\frac{0.022}{0.016}\right)^{0.026} = 0.877$$

5. The plastic limit relative slenderness λ_{p}

$$\lambda_p = \sqrt{\frac{\alpha}{1-\beta}} = \sqrt{\frac{0.196}{1 - 0.877}} = 1.262$$

6. Determination of the interval on the buckling curve

$$\lambda_0 = 0.2 < \lambda = 0.940 < \lambda_p = 1.262$$

Because it is the case of elastic-plastic buckling the buckling reduction factor χ should be determined from the formula:

$$\chi(\lambda) = a\lambda^2 + b\lambda + c,$$

where:

$$a = \frac{\alpha\left(0.4 - 3\lambda_p\right) + \lambda_p^3}{\lambda_p^3\left(0.04 - 0.4\lambda_p + \lambda_p^2\right)} = \frac{0.196(0.4 - 3 \cdot 1.262) + 1.262^3}{1.262^3\left(0.04 - 0.4 \cdot 1.262 + 1.262^2\right)} = 0.594$$

$$b = \frac{-2\lambda_p^4 + \alpha\left(4\lambda_p^2 - 0.08\right)}{\lambda_p^3\left(0.04 - 0.4\lambda_p + \lambda_p^2\right)} = \frac{-2 \cdot 1.262^4 + 0.196\left(4 \cdot 1.262^2 - 0.08\right)}{1.262^3\left(0.04 - 0.4 \cdot 1.262 + 1.262^2\right)} = -1.694$$

$$c = \frac{\alpha\left(0.12 - 0.8\lambda_p\right) + \lambda_p^4}{\lambda_p^2\left(0.04 - 0.4\lambda_p + \lambda_p^2\right)} = \frac{0.196(0.12 - 0.8 \cdot 1.262) + 1.262^4}{1.262^2\left(0.04 - 0.4 \cdot 1.262 + 1.262^2\right)} = 1.315$$

$$\chi(\lambda) = 0.594 \cdot 0.934^2 - 1.694 \cdot 0.934 + 1.315 = 0.251$$

7. The characteristic value of the buckling resistance

$$p_{\mathrm{Rk}} = \chi \cdot p_{\mathrm{Rpl}} = 0.251 \cdot 0.940 = 0.236\,\mathrm{MPa}$$

8. The design value of the buckling resistance

$$p_{\mathrm{Rd}} = p_{\mathrm{Rk}}/\gamma_{\mathrm{M1}} = 0.236/1.1 = 0.214\,\mathrm{MPa}$$

It is the value higher by 45% than their counterparts obtained according to EDR5th provisions.

6.2 Calculation Example No. 2

Determine the buckling resistance of pressurised spherical shell of given geometrical parameters and material properties:

- Radius: $R = 8000$ mm
- Shell thickness: $t = 4$ mm
- Ratio $R/t = 2000$
- Steel grade S235–$f_{\mathrm{yk}} = 235$ MPa, $E = 205$ GPa, $v = 0.3$
- Fabrication quality class: A (excellent), hence $Q = 40$
- Shell clamped along its supporting edge, case BC2, hence $\mathrm{C_c} = 0.8$, $\mathrm{C_{pl}} = 0.9$

6.2.1 Buckling Resistance Assessment Procedure According to EDR5th

1. Elastic, critical buckling pressure

$$p_{\mathrm{Rcr}} = \frac{2}{\sqrt{3(1-v^2)}} C_c E \left(\frac{t}{R}\right)^2 = \frac{2}{\sqrt{3(1-0.3^2)}} \cdot 0.8 \cdot 205000 \cdot \left(\frac{0.004}{8.0}\right)^2 = 0.049\,\mathrm{MPa}$$

2. Plastic reference resistance

$$p_{\mathrm{Rpl}} = f_{y,k} \cdot C_{pl} \cdot \frac{2 \cdot t}{R} = 235 \cdot 0.9 \cdot \frac{2 \cdot 0.004}{8.0} = 0.211\,\mathrm{MPa}$$

3. Dimensionless relative slenderness

$$\lambda = \sqrt{p_{\mathrm{Rpl}}/p_{\mathrm{Rcr}}} = \sqrt{0.211/0.049} = 2.075$$

4. Characteristic imperfection amplitude and elastic imperfection factor α

$$\Delta w_k = \frac{1}{Q}\sqrt{Rt} = \frac{1}{40}\sqrt{8.0 \cdot 0.004} = 0.0045\,\mathrm{m}$$

$$\alpha = \frac{0.7}{1 + 1.9 \cdot (\Delta w_k/t)^{0.75}} = \frac{0.7}{1 + 1.9 \cdot (0.0045/0.004)^{0.75}} = 0.2276$$

5. Buckling parameters and the plastic limit relative slenderness λ_{p}

$$\beta = 0.70;\ \eta = 1.0;\ \lambda_0 = 0.20$$

$$\lambda_p = \sqrt{\frac{\alpha}{1-\beta}} = \sqrt{\frac{0.2276}{1-0.7}} = 0.871$$

6. Determination of the interval on the buckling curve

$$\lambda \geq \lambda_p \rightarrow \lambda = 2.075 > \lambda_p = 0.871$$

Because it is the case of purely elastic buckling the buckling reduction factor χ should be determined from the formula:

$$\chi = \frac{\alpha}{\lambda^2} = \frac{0.2276}{2.075^2} = 0.053$$

7. The characteristic value of the buckling resistance

$$p_{\mathrm{Rk}} = \chi \cdot p_{\mathrm{Rpl}} = 0.053 \cdot 0.211 = 0.0112\,\mathrm{MPa}$$

8. The design value of the buckling resistance

$$p_{\mathrm{Rd}} = p_{\mathrm{Rk}}/\chi_{\mathrm{M1}} = 0.0112/1.1 = 0.0102\,\mathrm{MPa}$$

where the safety factor γ_{M1} is taken from EN 1993-1-1 and is equal 1.1.

6.2.2 The Proposed Procedure Based on Assumptions of EN 1993-1-6

1. Elastic, critical buckling pressure

$$p_{\mathrm{Rcr(LBA)}} = 1.21E\left(\frac{t}{R}\right)^2 = 1.21 \cdot 205000 \cdot \left(\frac{0.004}{8.0}\right)^2 = 0.062\,\mathrm{MPa}$$

2. Plastic reference resistance

$$p_{\mathrm{Rpl(MNA)}} = 2.0\, f_{yk}\frac{t}{R} = 2.0 \cdot 235 \cdot \frac{0.004}{8.0} = 0.235\,\mathrm{MPa}$$

3. Dimensionless relative slenderness

$$\lambda = \sqrt{p_{\mathrm{Rpl(MNA)}}/p_{\mathrm{Rcr(LBA)}}} = \sqrt{0.235/0.062} = 1.947$$

4. Characteristic imperfection amplitude and elastic imperfection factor α and the plastic range factor β

$$\Delta w_k = \frac{1}{Q}\sqrt{Rt} = \frac{1}{40}\sqrt{8.0 \cdot 0.004} = 0.0045\,\mathrm{m}$$

$$\alpha(\Delta w_k/t) = \frac{0.65}{1 + 1.8(\Delta w_k/t)^{0.8}} = \frac{0.65}{1 + 1.8(0.0045/0.004)^{0.8}} = 0.2183$$

$$\beta(\Delta w_k/t) = 0.87\left(\frac{\Delta w_k}{t}\right)^{0.026} = 0.87\left(\frac{0.0045}{0.004}\right)^{0.026} = 0.8727$$

5. The plastic limit relative slenderness λ_{p}

$$\lambda_p = \sqrt{\frac{\alpha}{1-\beta}} = \sqrt{\frac{0.2183}{1 - 0.8727}} = 1.3095$$

6. Determination of the interval on the buckling curve

$$\lambda \geq \lambda_p \rightarrow \lambda = 1.947 > \lambda_p = 1.3095$$

Because it is the case of purely elastic buckling the buckling reduction factor χ should be determined from the formula:

$$\chi = \frac{\alpha}{\lambda^2} = \frac{0.2183}{1.947^2} = 0.057$$

7. The characteristic value of the buckling resistance

$$p_{\mathrm{Rk}} = \chi \cdot p_{\mathrm{Rpl}} = 0.057 \cdot 0.235 = 0.0134\,\mathrm{MPa}$$

8. The design value of the buckling resistance

$$p_{\mathrm{Rd}} = p_{\mathrm{Rk}}/\gamma_{\mathrm{M1}} = 0.0134/1.1 = 0.0122\,\mathrm{MPa}$$

It is the value higher by 31% than their counterparts obtained according to EDR5th provisions.

Results obtained in presented above computational examples make it possible to draw the following conclusions. In both approaches the course of procedures is comparatively easy and very similar. The similarities between both proposals are only apparent. The main difference refers to the kind of analyses used to determine two reference quantities and namely p_{Rcr} and p_{Rpl}. In existing provisions they were determined as results of GNA and GMNA analyses respectively. In presented alternative approach these quantities were determined as results of LBA and MNA analyses respectively and such approach is consistent with general recommendations of EN 1993-1-6.

The remaining steps of both approaches are analogous. Knowing both reference quantities p_{Rcr} and p_{Rpl} then the dimensionless slenderness λ is determined. After that the amplitude of geometric imperfections is established and required buckling parameters are determined from appropriate formulae, different for both approaches. Parameters λ_0 and λ_P define three parts of the buckling curve. Knowing the part in which the calculated slenderness λ occurs, the buckling reduction factor χ is determined from the appropriate formula. The characteristic value of the buckling resistance is calculated from the formula

$$p_{\mathrm{Rk}} = \chi \cdot p_{\mathrm{Rpl}} \tag{13}$$

and finally, the design value of the buckling resistance is obtained from the formula

$$p_{\mathrm{Rd}} = p_{\mathrm{Rk}}/\gamma_{\mathrm{M1}} \tag{14}$$

where the partial safety factor γ_{M1} is taken from EN 1993-1-1 and is equal 1.1.

Despite apparently large similarity between both proposals final differences in results are significant. Two examples presented above show that in some cases buckling resistances determined according to the new proposal is nearly 50% higher than their counterparts calculated according to the existing procedure.

7 Comparison with Experimental Results

The procedure inserted in EDR5th and the procedure proposed by authors were compared with three series of experimental results. As a source of comparative analysis were chosen experiments which had comprised comparatively large number of examined specimens. The other criterion of the selection was the R/t ratio of the examined shells. Experiments in which examined caps had R/t ratio corresponding to R/t ratio of domes encountered in engineering practice were selected to the comparative procedure.

7.1 Experimental Research by Kaplan and Fung [10]

Results of the first comparative series were presented in the paper entitled: "A nonlinear theory of bending and buckling of thin elastic shallow spherical shells" by Abner Kaplan and Yuan-Cheng Fung in August 1954 as the Technical Note 3212 of NACA (comp. [10]). In this work not only theoretical considerations but also results of experimental results were presented.

An experimental program was carried out on a series of shallow spherical caps having a base diameter of 8 inches, nominal radii of curvature of 20 and 30 inches, and nominal thicknesses varying from 0.032 to 0.102 inch. The edges of the specimens were held between two rings which were bolted to a circular plate thus providing a clamped edge support.

The specimens were made by spinning from flat sheet. The magnesium alloy QQ-M-44 was selected because of its favorable ratio of yield stress to Young's modulus us compared with other non-heat treated metals. Material parameters were as follows: Young's modulus: $E = 6.5\ 10^6$ psi $= 44815.92$ MPa, the yield stress: $f_{\mathrm{yk}} = 29900$ psi $= 206.15$ MPa; Poisson's ratio $\nu = 0.32$.

Pressure measurements were made using a Bourdon tube for pressure over 20 psi and a mercury manometer for pressures under 20 psi. More details referring to experimental procedures can be found in [10].

Capacity curves generated for geometrical and material parameters the same as those from experiments were presented in Fig. 13. Three different fabrication quality classes defined by parameters Q (comp. EN 1993-1-6, [13, 15]) were taken into account. Markers in a form of circles shown in Fig. 13 refers to results obtained by Kaplan and Fung and presented in [10]. Characteristic values of the critical pressure p_{Rk} were expressed in MPa.

Looking at Fig. 13 one can observe that critical pressures obtained in experiments of Kaplan and Fung are always above all three capacity curves proposed in EN 1993-1-6 and [13]. It means that limits defined by capacity curves obtained by means of the new procedure are generally conservative as it should be. Only in two cases experimental results are little bit lower than the capacity curve for the $Q = 40$ corresponding to the best fabrication quality class. This comparison indicates that

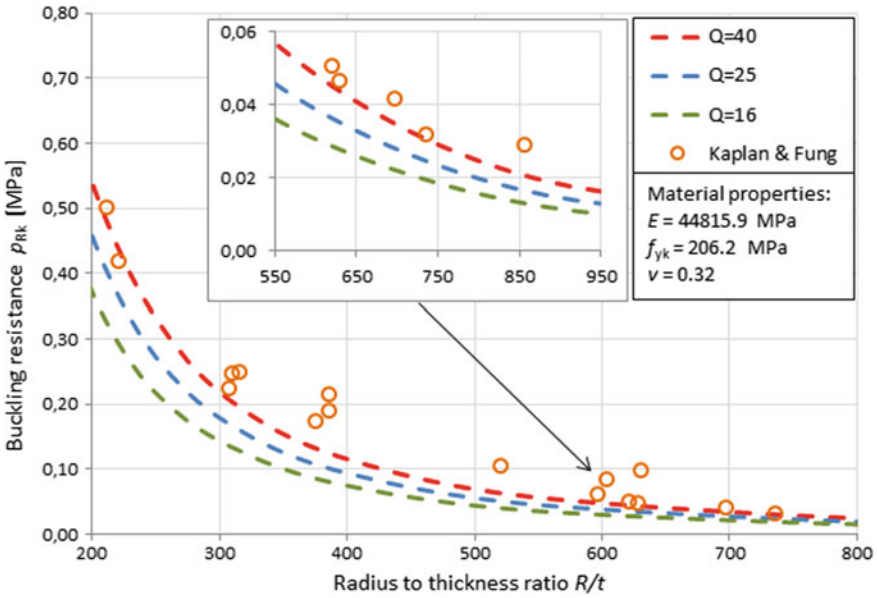

Fig. 13 The test results of Kaplan and Fung compared with new predictions

the new proposals are conservative relative to these tests. No information is available on the actual imperfections in these tests, so no judgement can be made concerning the appropriate fabrication quality class. Probably in these two cases geometrical imperfections were higher than those predicted for the best admissible class defined by $Q = 40$.

7.2 Experimental Research by Seaman [17]

The second series of experimental results which was the basis of comparative analysis was published in the paper entitled: "The nature of buckling in thin spherical shells" (cf. [17]). This work was the part of PhD thesis of Lynn Seaman. The paper included not only theoretical considerations related to buckling resistance of spherical shells but also the wide part in which results of experimental investigations were presented. Experiments were conducted on a big series of specimens counting 40 pieces.

A plastic was chosen as the shell material rather than aluminum or other light metals which have usually been used by other authors in experimental investigations. The particular plastic chosen was a polyvinyl chloride which was available in thicknesses from 0.010 to 0.080 inch.

The shell segments were formed from polyvinyl chloride (P.V.C.) sheets by a process known as vacuum drawing. In this method a single mold, the female, was required. The plastic sheet was heated, drawn into the mold, and allowed to cool in

the new shape. Since the shells were to have five different radii—15, 25, 35, 45 and 80 inches, five molds were manufactured from aluminium.

After forming the shells it was necessary to find the thickness and radius to which the shell actually conformed. Thicknesses were read to the nearest ten thousandth of an inch with an dial gage at five positions in the shell—one at the apex of the shell, and the other four at points halfway between the apex and the edge. An average of the five readings was taken as the shell thickness. The thickness variation was about 1% except for the very thin shells where variations were 10–12%.

The radius of the spherical shell can be found if the rise in the center is known. The rise was measured to the nearest thousandth of an inch. The radius was then computed from the easy derived formula

$$R = \frac{H^2 + r^2}{2H} \tag{15}$$

where H is the rise in the center, r is the radius of the supported circular edge used in this measurement and $r = 5.25$ inch.

All other details of the adopted measurement procedures used in conducted experiments were described in [17].

There were two basically different types of tests used. The constant volume test was the most important and it was of the controlled displacement type. A certain strain or displacement was applied to the shell and the pressure which was required to make the shell stay in that position was read. The other type, the constant pressure test, was carried out by increasing the load until buckling occurred and hence the control was on the load, not on the displacement.

Capacity curves generated for geometrical and material parameters the same as those from experiments were presented in Fig. 14. The following material parameters specified in [17] were used: $E = 498{\cdot}10^3$ psi $= 3433.6$ MPa; $f_{yk} = 4500$ psi $= 33.0$ MPa; $\nu = 0.41$. Three different fabrication quality classes defined by parameters Q (comp. EN 1993-1-6, [4, 13]) were taken into account. Markers in a form of circles shown in Fig. 14 refer to results obtained by Seaman and presented in [17]. Characteristic values of the critical pressure p_{Rk} were expressed in MPa.

Looking at Fig. 14 one can observe that critical pressures obtained in experiments of Seaman are generally above all three capacity curves proposed in [3, 4]. It means that limits defined by proposed capacity curves are generally conservative as it should be. Only in two cases experimental results are little bit lower than the capacity curve for the $Q = 16$ corresponding to the worst fabrication quality class. It can be assumed that in these two cases geometrical imperfections were higher than those predicted for the worst admissible class defined by $Q = 16$.

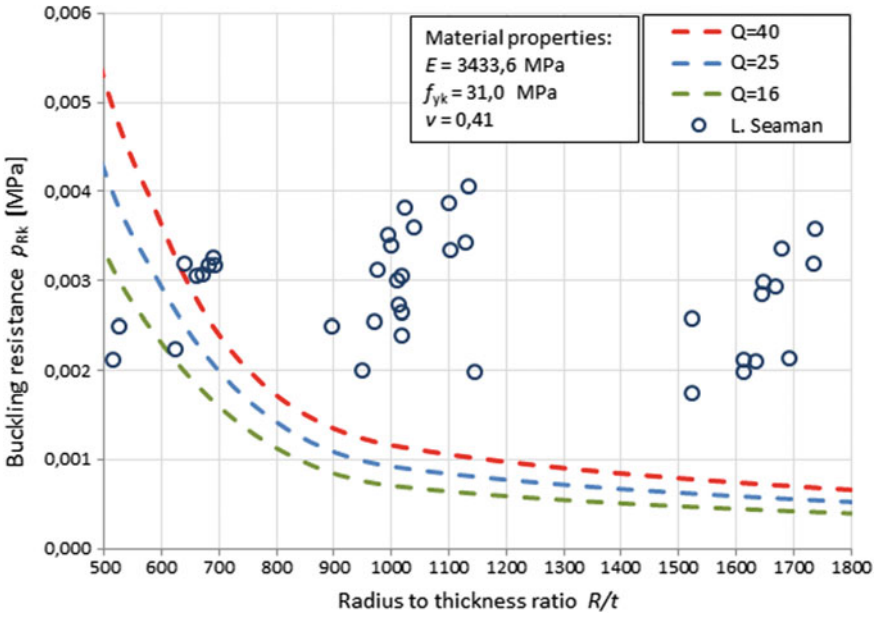

Fig. 14 The test results of Seaman compared with new predictions

7.3 Experimental Research by Błachut [1]

The third series of experimental results was a series of six metal dome tests which was reported by Błachut [1]. These domes were CNC-machined from 245 mm diameter mild steel billet. The shells had a heavy edge ring, integral with the wall, used to model a fully clamped boundary condition. The shallowness parameter, λ, was chosen to be between 3.5 and 5.5. After final machining, these domes were stress-relieved in a vacuum furnace, followed by shape and wall thickness measurements using an (XYZ) coordinate measuring table (cf. [1]). Measurements were made along 14 equally spaced meridians and at 10 mm arc-length intervals. The height-to-wall thickness ratio varied approximately from 2.5 to 4.0 and the radius-to-thickness ratio from 300 to 1800. Examining the scatter of wall thickness, and radial deviations from perfect geometry it was concluded that they all were, geometrically, nearly-perfect. The average mechanical properties of the mild steel were measured as: Young's modulus $E = 207.0$ GPa, yield stress $f_{yk} = 303.5$ MPa and Poisson's ratio $\nu = 0.28$. Other details of this experimental work can be found in [1].

The test results of Błachut [1] are compared with the new proposals in Fig. 15. All have buckling resistances far above the predictions of Błażejewski and Marcinowski [3, 4], which is not surprising because they were very precisely manufactured.

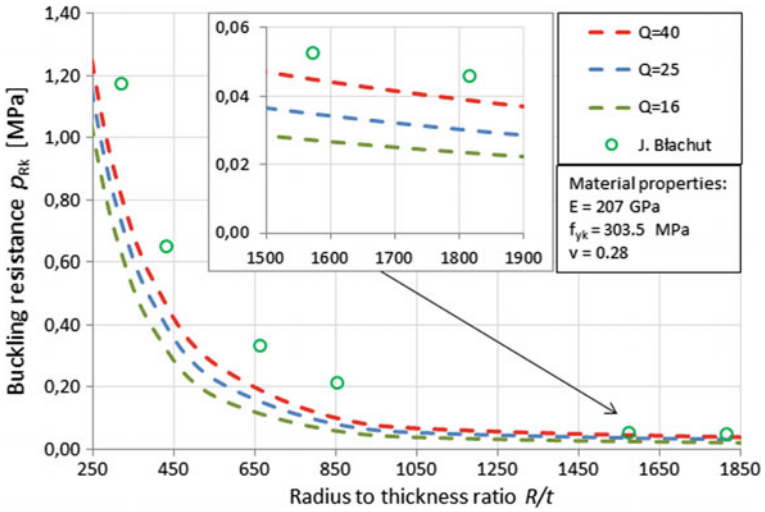

Fig. 15 The test results of Błachut compared with new predictions

8 Conclusions

The buckling resistance of steel, spherical, pressurised shells can be assessed according to the existing since 2008 EDR5th provisions (cf. [13, 14]). Authors of the present paper have elaborated the alternative approach (cf. [3, 4]) which is consistent with general provisions of EN1993-1-6. These two approaches were compared in this work. They are relatively simple, clear and does not require an engineer to have special skills. Presented calculation examples have shown details of both procedures. They revealed the general tendency: EDR5th provisions give too conservative assessments of buckling resistances. In some domains of R/t ratio differences in buckling resistances have exceeded value of 40%.

The comparison of the new procedure with chosen experimental results published by other authors was presented in this work as well. Buckling resistance predictions are generally lower than their counterparts obtained experimentally. In single cases one or two test results fell into the lower fabrication quality classes but none lay below the lowest class prediction. These comparative analyses and those presented in [5] do confirm that the current new proposal is well supported by experiments conducted in the past. Hence it follows that the proposed procedure deserves a recommendation.

References

1. Błachut, J.: Buckling of shallow spherical caps subjected to external pressure. J. Appl. Mech. Trans. ASME **72**, 803–806 (2005)
2. Błażejewski, P., Marcinowski, J.: A new approach to the buckling resistance assessment of pressurized spherical shells, SSTA. In: Proceedings of the 10th Conference, Gdańsk, Polska, pp. 179–182. Taylor & Francis Group, London (2013)
3. Błażejewski, P., Marcinowski, J.: Najbardziej niekorzystne imperfekcje geometryczne stalowych powłok sferycznych. The worst geometrical imperfections of steel spherical shells. Budownictwo i Architektura **13**(3), 219–226 (2014). (in Polish)
4. Błażejewski, P., Marcinowski, J.: Buckling capacity curves for pressurized spherical shells. In: Recent Progress in Steel and Composite Structures: Proceedings of the XIII International Conference on Metal Structures—ICMS 2016, Zielona Góra, Poland, pp. 401–406. Taylor & Francis Group, London (2016)
5. Błażejewski, P., Marcinowski, J., Rotter, M.: Buckling of externally pressurised spherical shells. Experimental results compared with recent design recommendations. Presented in EUROSTEEL 2017, September 13–15, 2017, Copenhagen, Denmark (2017)
6. COSMOS/M: Finite element analysis system, version 2.5, Structural Research and Analysis Corporation, Los Angeles, California (1999)
7. Doerich, C., Rotter, J.M.: Generalised capacity curves for stability and plasticity: application and limitations. Thin Walled Struct. **49**(9), 1132–1140 (2011)
8. EN1993-1-1: Eurocode 3: design of steel structures, part 1.1: general rules and rules for buildings, CEN (2005)
9. EN1993-1-6: Eurocode 3: design of steel structures, part 1.6: strength and stability of shell structures, CEN (2006)
10. Kaplan, A., Fung, Y.C.: A nonlinear theory of bending and buckling of thin elastic shallow spherical shells. U.S.N.A.C.A. Technical Note 3112 (1954)
11. Leibenson, L.S.: About an adoption of harmonic functions of Thompson to stability problems of spherical and cylindrical shells (in Russian). Reports of Jurovskovo University, No. 5, pp. 1–47 (1917)
12. Rotter, J.M.: Shell buckling and collapse analysis for structural design: the new framework of the European standard. In: Drew, H.R., Pellegrino, S. (eds.) New Approaches to Structural Mechanics, Shells and Biological Structures, pp. 355–378. Kluwer Academic Publishers, London (2002)
13. Rotter, J.M., Schmidt, H. (eds.): Buckling of Steel Shells: European Design Recommendations, 5th edn. Published by ECCS (2008)
14. Rotter, J.M., Schmidt, H. (eds.): Buckling of Steel Shells: European Design Recommendations, 5th edn. Revised Second Impression, Published by ECCS (2013)
15. Schmidt, H.: The German code DIN 18800 Part 4: stability of shell-type steel structures, design philosophy and practical applications, International Colloquium on Buckling of Shell Structures on Land, in the Sea and in the Air, Villeurbanne, Lyon, France, 17–19 Sept., pp. 265–269 (1991)
16. Schmidt, H.: Stability of shells, CEN TC250 SC3 PT 3 (Masts, Chimneys, Pipelines) Report, August, 12 (1994)
17. Seaman, L.: The nature of buckling in thin spherical shells. Watertown Arsenal Laboratories, Monograph Series No 46 (1962)
18. Zoelly, R.: Über ein Knickungsproblem an der Kugelschale (“About a buckling problem of spherical shell”—in German). Thesis, Zürich (1915)

Asymptotically-Accurate Nonlinear Hyperelastic Shell Constitutive Model Using Variational Asymptotic Method

Ramesh Gupta Burela and Dineshkumar Harursampath

Abstract The focus of this work is on the development of asymptotically-accurate nonlinear hyperelastic constitutive model for thin shell structures using Variational Asymptotic Method (VAM). In this work, these structures are analyzed for both geometric and material nonlinearities. The geometric nonlinearity is handled by allowing finite deformations and generalized warping functions through Green strain, while the material nonlinearity is incorporated through strain energy density function of hyperelastic material model. Using the inherent small parameters (moderate strains, very small thickness-to-wavelength ratio and very small thickness-to-initial radius of curvature) for the application of VAM, the process begins with three-dimensional nonlinear hyperelasticity and it weakly decouples the analysis into a one-dimensional through-the-thickness nonlinear analysis and a two-dimensional nonlinear shell analysis. Through-the-thickness analysis is analytical work, providing 3-D warping functions and two-dimensional nonlinear constitutive relation for Nonlinear Finite Element Analysis of shells. Current theory and code are demonstrated through standard test cases and validated with literature.

1 Introduction

Current work focuses on development of asymptotically-accurate nonlinear hyperelastic constitutive model for thin shell structures using Variational Asymptotic Method (VAM). In general shell structures are three-dimensional (3-D) in nature.

R. G. Burela (✉)
MFC Lab, Mechanical Engineering Department, School of Engineering, Shiv Nadar University, Greater Noida 201314, Uttar Pradesh, India
e-mail: rameshgupta.iisc@gmail.com

D. Harursampath
NMCAD Lab, Department of Aerospace Engineering, Indian Institute of Science, Bengaluru 560012, India
e-mail: dineshkumar@iisc.ac.in

H. Altenbach et al. (eds.), *Recent Developments in the Theory of Shells*,
Advanced Structured Materials 110, https://doi.org/10.1007/978-3-030-17747-8_9

Their relative geometric dimensions between thickness (h) to planner dimensions and/or initial radius of curvature enable them to be reduced to two-dimensional (2-D) smooth reference surfaces. Analysis of 2-D structures is computationally efficient as compared to 3-D finite element analysis especially in case of combined nonlinear analysis. In the current work, systematic dimensional reduction is carried out using Variational Asymptotic Method (VAM) [1] with moderate strains, very small thickness to shortest wavelength of the deformation along the shell reference surface, and thickness to initial radius of curvatures as small parameters without making use of any ad hoc kinematic assumptions. The development starts with 3-D nonlinear shell problem and mathematically splits the analysis into a nonlinear one-dimensional (1-D) through-the-thickness analysis, and a nonlinear (2-D) shell analysis. Through-the-thickness analysis provides a 2-D nonlinear constitutive law for the shell analysis. These structures are analyzed for both geometric and material nonlinearities. The geometric nonlinearity is handled by allowing finite deformations and generalized warping functions [2, 3] through the Green strain while the material nonlinearity is incorporated through hyperelastic material model [4]. Analytical development of shell modeling (consist of 2-D nonlinear constitutive law and warping functions) is an extension of plate model [5]. Current work is the first to provide analysis of shell reference surface with asymptotically-accurate shell nonlinear constitutive law using VAM. Integration of nonlinear FEA and asymptotically accurate nonlinear constitutive model has led to reliable analysis of shell structures and finds its application in the design and manufacturing of shell surfaces of aircrafts, cars, ships, deployable structures, etc. Validation of present theory is carried out with two standard test cases. Current analysis results match well with the literature.

2 Analysis

3-D combined nonlinear hyperelastic problem can be weakly decoupled into one-dimensional (1-D) through-the-thickness (along the normal of shell) nonlinear analysis, and a 2-D nonlinear analysis of reference surface of shell. This dimensional reduction process is carried out using the mathematical methodology, VAM. The starting point of the application of the VAM is 3-D potential energy function. In the current work compressible neo-Hookean model [4] is chosen (because of its applicability of material model for moderate strains) with the following expression for the 3-D strain energy density, ψ:

- Compressible neo-Hookean model (NH model)

$$\psi = \frac{\lambda}{2}(\ln J)^2 + \frac{\mu}{2}(\mathrm{tr}\mathbf{C} - 3) - \mu \ln J \tag{1}$$

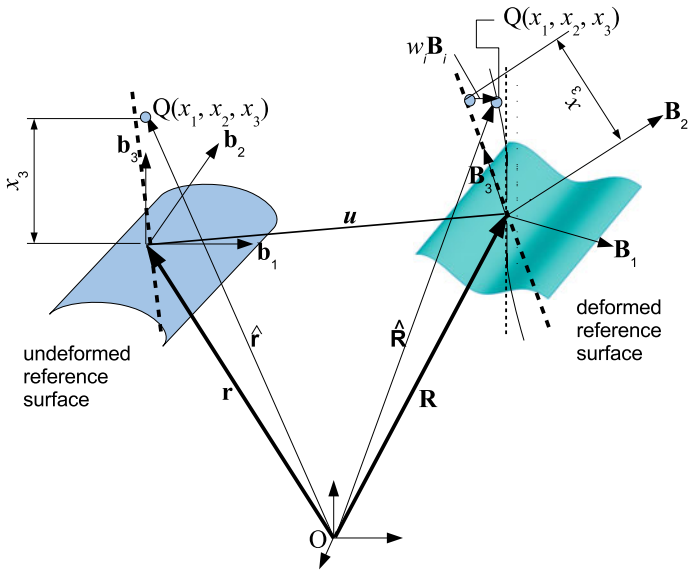

Fig. 1 Shell deformation

where λ and μ are isotropic hyperelastic material parameters (Lamé constants), are related to Young's modulus and Poisson's ratio, $\lambda = \frac{E\nu}{(1+\nu)(1-2\nu)}$, $\mu = \frac{E}{2(1+\nu)}$), $J = \det(\mathbf{F})$ and $\mathbf{C} = \mathbf{F}^{\mathrm{T}}\,\mathbf{F}$.

2.1 Kinematics

Figure 1 represents schematic representation of shell deformation. Shell reference surface usually chosen to be the mid-surface, in its undeformed state, is mathematically represented by a set of arbitrary but independent curvilinear coordinates, x_α while x_3 is the shell normal coordinate (Here and throughout the formulation, Greek indices assume values 1 and 2 while Latin indices assume 1, 2, and 3. Dummy indices are summed over their range except where explicitly indicated.) In order to simplify the formulation, lines of curvatures are assumed to be the curvilinear coordinate curves. Unit vectors along x_i in the undeformed and deformed configurations are denoted by $\mathbf{b}_i$ and $\mathbf{B}_i$, respectively. Any material point $\mathrm{Q}(x_1, x_2, x_3)$ in the undeformed and deformed configurations are described by the position vectors, $\hat{\mathbf{r}}$ and $\hat{\mathbf{R}}$, respectively, from any point O, which is fixed in a reference frame whose motion itself is inertial and/or known, such that

$$\hat{\mathbf{r}}(x_1, x_2, x_3) = \mathbf{r}(x_1, x_2) + x_3\mathbf{b}_3(x_1, x_2) \tag{2}$$

$$\hat{\mathbf{R}}(x_1, x_2, x_3) = \mathbf{R}(x_1, x_2) + x_3\mathbf{B}_3(x_1, x_2) + w_i(x_1, x_2, x_3)\mathbf{B}_i(x_1, x_2). \tag{3}$$

where $\mathbf{r}$ and $\mathbf{R}$ are position vectors of any material point on the reference surface of undeformed and deformed configurations respectively and $w_i(x_1, x_2, x_3)$ are 3-D warping field components. Here, w_1 and w_2 are in-plane warpings (due to local rotations of line elements normal to the reference surface) and w_3 is out-of-plane warping (stretching or contraction of the normal line elements). Thus the formulation accounts for the contraction or extension of the normal through-the-thickness. The covariant and contravariant base vectors in the undeformed state are, $\mathbf{g}_i = \frac{\partial \hat{\mathbf{r}}}{\partial x_i}$ and $\mathbf{g}^i = \frac{1}{2\sqrt{g}}\epsilon_{ijk}\mathbf{g}_j \times \mathbf{g}_k$, respectively, where $g = \det\left(\mathbf{g}_i.\mathbf{g}_j\right)$ is determinant of the metric tensor for the undeformed configuration and ϵ_{ijk} are measure numbers of permutation tensor. In the same way, the covariant base vectors for the deformed configuration are given by $\mathbf{G}_i = \frac{\partial \hat{\mathbf{R}}}{\partial x_i}$. The relation between the two set of unit vectors, $\mathbf{b}_i$ and $\mathbf{B}_i$ can be prescribed by an arbitrarily large rotation specified in terms of the matrix of direction cosines $\Theta(x_1, x_2)$ so that $\mathbf{B}_i = \Theta_{ij}\mathbf{b}_j$ and $\Theta_{ij} = \mathbf{B}_i.\mathbf{b}_j$. In the present scheme, all possible deformations (large displacements and rotations) are allowed and the corresponding 3-D strains are Green strain (Γ) whose Lagrangian components are

$$\Gamma_{ij} = \frac{1}{2}({F_{ik}}^T F_{kj} - I_{ij}) \tag{4}$$

where F_{ij} are mixed bases components of the deformation gradient tensor, given by $F_{ij} = \mathbf{B}_i.\mathbf{G}_k\mathbf{g}^k.\mathbf{b}_j$ and I_{ij} are elements of the 3×3 identity matrix.

2.2 Potential Due to Load

Specific work done by the loads acting on the top and bottom surfaces of the shell and by the body force distribution on the normal are

$$P_L = \tau^T w^+ + \beta^T w^- + \langle \phi^T w \rangle \tag{5}$$

where, through-out the text, $\langle\ \rangle$ symbolizes definite integral (of the enclosures within the angular brackets) through-the-thickness of the shell. τ and β are 3×1 column matrices representing the traction forces acting on the top and bottom surfaces respectively of the shell; w^+ and w^- are 3×1 column matrices containing the warping functions corresponding to top and bottom surfaces of the shell; and ϕ is a 3×1 column matrix of body forces.

2.3 Total Potential Energy

The total potential energy per unit mid-surface area of the shell is given by $\Pi = \langle \psi \rangle - P_L$. The stationary point of the functional, Π, with respect to the 3-D warping components, w_i, subjected to constraints ($\langle w_i(x_1, x_2, x_3) \rangle = 0$ and $\langle x_3 w_\alpha(x_1, x_2, x_3) \rangle = 0$ because, Eq. (3) is 6 times redundant and thus requires 6 equations; 5 constraints with respect to warping functions and another one to specify the deformed surface as provided by [3]) is obtained by setting the first variation equal to zero.

2.4 Zeroth-Order Approximation

Application of usual calculus of variation in order to find unknown 3-D warping functions is not feasible because of the resulting set of differential equations and associated boundary conditions. VAM can be applied as an alternative to find unknown functions in an asymptotic form. Application of VAM requires inherent small parameters; these identifiable small parameters are of two kinds. The first are geometric small parameters, where thickness is much smaller than planner dimensions or radius of curvatures. Thus, we can represent the geometric small parameters as $h/l \ll 1$ and/or $h/r \ll 1$ [6], where h, l, r are the thickness, characteristic length and characteristic radius of curvatures. Second, we can identify the strains $\varepsilon < 1$ as moderately small parameters. By taking advantage of these small parameters, 3-D potential energy can be classified into different orders of energies such that major contribution of energy is referred as the zeroth order energy and subsequent energy contributions are termed as the first order and higher order energies. Solution of zeroth order energy results in unknown warping functions that are substituted back into the strain energy expression followed by integration along the shell normal (through the thickness) to result in 2-D energy (zeroth order energy), followed by first and higher order energy contributions. Thus, 3-D energy is represented as a series of 2-D energies. Hence, dimensional reduction leads to a computational efficiency that is achieved as a byproduct while targeting asymptotic accuracy.

In order to proceed with dimensional reduction process of shells, one has to assess and keep track of the orders [5, 7] of all the quantities affecting the formulation. ε is the order of the maximum strain (moderate) anywhere and at any time in the shell and μ is the order of the 3-D material stiffness (all of which are assumed to be of the same order i.e., isotropic). Orders of magnitude of the 2-D generalized strain components can be estimated based on their contribution to the moderate 3-D strains. Thus $\varepsilon_{\alpha\beta} \sim O(\epsilon)$, $x_3\kappa_{\alpha\beta} \sim O(\epsilon)$ and $x_3 k_{\alpha\beta} \sim O(\epsilon)$ where ε_{11} and ε_{22} are the 2-D in-plane strains along x_1 and x_2 respectively, γ_{12} is the in-plane shear strain, κ_{11} and κ_{22} are the deformed reference surface bending curvatures about coordinate curves x_1 and x_2 respectively, ω is the deformed reference surface twisting curvature, $\omega = \frac{\kappa_{12}+\kappa_{21}}{2}$ and γ_{13} and γ_{23} are the transverse shear strains, k_{11} and k_{22} are the undeformed reference surface curvatures about coordinate curves x_1 and x_2 respectively, and k_{12} and k_{21}

are the undeformed reference surface twisting curvatures. And, the relative order of magnitude of the small parameters are taken as $\varepsilon_{\alpha\beta} \sim O(\epsilon)$, h/l and $h/r \sim O(\epsilon^2)$, VAM requires one to find the leading terms of the functional to be minimized based on the estimated orders. For the first approximation, these leading terms are denoted by Π_0 which corresponds to energy of order $\mu\epsilon^2$. The leading asymptotically accurate solutions, for the unknown 3-D warping functions are found by minimizing the functional subject to constraints: $\langle w_i(x_1, x_2, x_3)\rangle = 0$ and $x_3 w_\alpha(x_1, x_2, x_3)\rangle = 0$.

- Warping Functions: Zeroth-Order Approximation

$$w_\alpha = \gamma_{\alpha 3}\left(\frac{x_3}{4} - \frac{5x_3^3}{3h^2}\right) \tag{6}$$

$$w_3 = \frac{\lambda}{\lambda + 2\mu}\left[\frac{h^2}{24}(\kappa_{11} + \kappa_{22}) - x_3(\varepsilon_{11} + \varepsilon_{22}) - \frac{x_3^2}{2}(\kappa_{11} + \kappa_{22})\right] \tag{7}$$

Zeroth-order warping functions doesn't have any contribution from initial curvatures of shell which are same as plate [5]. These warping functions are substituted back into the zeroth-order energy expression Π_0, and integrated over the thickness to get the 2-D energy. The first approximation to the energy functional coincides with that of classical plate theory. However, we do not use ad hoc kinematic assumptions such as the Kirchhoff assumption to obtain this result. Zeroth-order 2-D stiffness matrix is derived as double derivative of 2-D energy with respect to strain vector, $e = \{\varepsilon_{11}\ \ \varepsilon_{22}\ \ \gamma_{12}\ \ \kappa_{11}\ \ \kappa_{22}\ \ \omega\ \ \gamma_{13}\ \ \gamma_{23}\}^T$, and is given below (non-zero stiffness elements).

$$\mathscr{C}_{11} = \mathscr{C}_{22} = \frac{4h\mu(\lambda+\mu)}{\lambda+2\mu}, \mathscr{C}_{33} = h\mu, \mathscr{C}_{44} = \mathscr{C}_{55} = \frac{h^3\mu(\lambda+\mu)}{3(\lambda+2\mu)}, \mathscr{C}_{66} = \frac{h^3\mu}{12}, \mathscr{C}_{77} = \mathscr{C}_{88} = \frac{5h\mu}{6},$$
$$\mathscr{C}_{12} = \frac{2h\lambda\mu}{\lambda+2\mu}, \mathscr{C}_{45} = \frac{h^3\lambda\mu}{6(\lambda+2\mu)} \tag{8}$$

The elements of zeroth-order stiffness matrix $\mathscr{C}$ are a constant part of first-order stiffness matrix to be introduced later in this section.

2.5 First-Order Approximation

Perturbed warping functions can be found by minimizing the energy Π_1 of order $\mu\epsilon^2\frac{h}{l}$ with perturbed warping functions, such that $v_i(x_1, x_2, x_3, t) < w_i(x_1, x_2, x_3, t)$ where Π_1 is subjected to corresponding constraints

$$\langle v_i(x_1, x_2, x_3)\rangle = 0 \text{ and } \langle x_3 v_\alpha(x_1, x_2, x_3)\rangle = 0 \tag{9}$$

- Warping Functions: First-Order Perturbation

$$
\begin{aligned}
v_1 = &-\frac{h^2}{24}\left[\frac{11\lambda+10\mu}{6(\lambda+2\mu)}\gamma_{13}\kappa_{11}+\frac{\lambda}{\lambda+2\mu}\gamma_{13}\kappa_{22}+\frac{5}{12}\gamma_{23}\omega+\frac{5}{6}\gamma_{13}k_{11}+\frac{9}{8}\gamma_{23}k_{12}-\frac{7}{24}\gamma_{23}k_{21}\right]\\
&-x_3\left[\frac{\lambda+\mu}{2(\lambda+2\mu)}\gamma_{13}\varepsilon_{11}+\frac{\lambda}{4(\lambda+2\mu)}\gamma_{13}\varepsilon_{22}+\frac{1}{8}\gamma_{23}\gamma_{12}\right]\\
&+x_3^2\left[\frac{11\lambda+10\mu}{12(\lambda+2\mu)}\gamma_{13}\kappa_{11}+\frac{\lambda}{2(\lambda+2\mu)}\gamma_{13}\kappa_{22}+\frac{5}{24}\gamma_{23}\omega+\frac{5}{12}\gamma_{13}k_{11}+\frac{5}{8}\gamma_{13}k_{12}-\frac{5}{24}\gamma_{13}k_{21}\right]\\
&+x_3^3\left[\frac{10(\lambda+\mu)}{3h^2(\lambda+2\mu)}\gamma_{13}\varepsilon_{11}+\frac{5\lambda}{3h^2(\lambda+2\mu)}\gamma_{13}\varepsilon_{22}+\frac{5}{6h^2}\gamma_{23}\gamma_{12}\right]\\
&-x_3^4\left[\frac{5\left(k_{12}-k_{21}\right)}{12h^2}\gamma_{23}\right]
\end{aligned}
\tag{10}
$$

$$
\begin{aligned}
v_2 = &-\frac{h^2}{24}\left[\frac{\lambda}{\lambda+2\mu}\gamma_{23}\kappa_{11}+\frac{11\lambda+10\mu}{6(\lambda+2\mu)}\gamma_{23}\kappa_{22}+\frac{5}{12}\gamma_{13}\omega+\frac{5}{6}\gamma_{23}k_{22}-\frac{7}{24}\gamma_{13}k_{12}+\frac{9}{8}\gamma_{13}k_{21}\right]\\
&-x_3\left[\frac{\lambda}{4(\lambda+2\mu)}\gamma_{23}\varepsilon_{11}+\frac{\lambda+\mu}{2(\lambda+2\mu)}\gamma_{23}\varepsilon_{22}+\frac{1}{8}\gamma_{13}\gamma_{12}\right]\\
&+x_3^2\left[\frac{\lambda}{2(\lambda+2\mu)}\gamma_{23}\kappa_{11}+\frac{11\lambda+10\mu}{12(\lambda+2\mu)}\gamma_{23}\kappa_{22}+\frac{5}{24}\gamma_{13}\omega+\frac{5}{12}\gamma_{23}k_{22}-\frac{5}{24}\gamma_{13}k_{12}+\frac{5}{8}\gamma_{13}k_{21}\right]\\
&+x_3^3\left[\frac{5\lambda}{3h^2(\lambda+2\mu)}\gamma_{23}\varepsilon_{11}+\frac{10(\lambda+\mu)}{3h^2(\lambda+2\mu)}\gamma_{23}\varepsilon_{22}+\frac{5}{6h^2}\gamma_{13}\gamma_{12}\right]\\
&+x_3^4\left[\frac{5\left(k_{12}-k_{21}\right)}{12h^2}\gamma_{13}\right]
\end{aligned}
\tag{11}
$$

$$
\begin{aligned}
v_3 = &-\frac{h^2}{24}\left[\frac{3\lambda^3+4\lambda^2\mu-44\lambda\mu^2-32\mu^3}{(\lambda+2\mu)^3}\left(\varepsilon_{11}\kappa_{11}+\varepsilon_{22}\kappa_{22}\right)+\right.\\
&\qquad\left.\frac{2\left(\lambda^3-24\lambda\mu^2-16\mu^3\right)}{(\lambda+2\mu)^3}\left(\varepsilon_{11}\kappa_{22}+\varepsilon_{22}\kappa_{11}\right)-\frac{\lambda}{2(\lambda+2\mu)}\omega\gamma_{12}\right]\\
&-\frac{h^2}{24}\left[k_{11}\frac{\varepsilon_{22}\lambda^2+2\varepsilon_{11}\lambda\left(\lambda+\mu\right)}{(\lambda+2\mu)^2}+k_{22}\frac{\varepsilon_{11}\lambda^2+2\varepsilon_{22}\lambda\left(\lambda+\mu\right)}{(\lambda+2\mu)^2}+\left(k_{12}+k_{21}\right)\frac{\gamma_{12}\lambda}{2\left(\lambda+2\mu\right)}\right]\\
&+x_3\left[\frac{\lambda^3+\lambda^2\mu-22\lambda\mu^2-16\mu^3}{(\lambda+2\mu)^3}\left(\varepsilon_{11}^2+\varepsilon_{22}^2\right)+\frac{\lambda}{4(\lambda+2\mu)}\gamma_{12}^2-\frac{h^2\mu}{8(\lambda+2\mu)}\omega^2-\right.\\
&\qquad\frac{h^2\left(\lambda^2+12\lambda\mu+12\mu^2\right)}{24(\lambda+2\mu)^2}\left(\kappa_{11}^2+\kappa_{22}^2\right)-\frac{h^2\left(\lambda^2+6\lambda\mu\right)}{12(\lambda+2\mu)^2}\kappa_{11}\kappa_{22}+\\
&\qquad\left.\frac{\lambda^3-2\lambda^2\mu-48\lambda\mu^2-32\mu^3}{(\lambda+2\mu)^3}\varepsilon_{11}\varepsilon_{22}\right]\\
&-x_3\left[\frac{h^2\left(\lambda^2+12\lambda\mu+12\mu^2\right)}{24(\lambda+2\mu)^2}\left(k_{22}\kappa_{22}+k_{11}\kappa_{11}\right)+\frac{h^2\left(\lambda^2+6\lambda\mu\right)}{24(\lambda+2\mu)^2}\left(k_{22}\kappa_{11}+k_{11}\kappa_{22}\right)\right]\\
&+x_3\frac{\lambda+\mu}{4(\lambda+2\mu)}\left(\gamma_{13}^2+\gamma_{23}^2\right)\\
&+x_3^2\left[\frac{3\lambda^3+4\lambda^2\mu-44\lambda\mu^2-32\mu^3}{2(\lambda+2\mu)^3}\left(\varepsilon_{11}\kappa_{11}+\varepsilon_{22}\kappa_{22}\right)+\right.\\
&\qquad\left.\frac{\lambda^3-24\lambda\mu^2-16\mu^3}{(\lambda+2\mu)^2}\left(\varepsilon_{11}\kappa_{22}+\varepsilon_{22}\kappa_{11}\right)+\frac{\lambda}{4(\lambda+2\mu)}\omega\gamma_{12}\right]\\
&+x_3^2\left[k_{11}\frac{\varepsilon_{22}\lambda^2+2\varepsilon_{11}\lambda\left(\lambda+\mu\right)}{2\left(\lambda+2\mu\right)^2}+k_{22}\frac{\varepsilon_{11}\lambda^2+2\varepsilon_{22}\lambda\left(\lambda+\mu\right)}{2\left(\lambda+2\mu\right)^2}+\left(k_{12}+k_{21}\right)\frac{\gamma_{12}\lambda}{4\left(\lambda+2\mu\right)}\right]
\end{aligned}
$$

$$+x_3^3\left[\frac{\omega^2}{12}+\frac{2\left(\lambda^3+\lambda^2\mu-22\lambda\mu^2-16\mu^3\right)}{3(\lambda+2\mu)^3}\kappa_{11}\kappa_{22}+\frac{\left(3\lambda^3+8\lambda^2\mu-32\lambda\mu^2-24\mu^3\right)}{6(\lambda+2\mu)^3}\left(\kappa_{11}^2+\kappa_{22}^2\right)\right]$$
$$+x_3^3\left[(k_{11}\kappa_{11}+k_{22}\kappa_{22})\frac{3\lambda+2\mu}{6(\lambda+2\mu)}+(k_{11}\kappa_{22}+k_{22}\kappa_{11})\frac{\lambda}{6(\lambda+2\mu)}+(k_{12}+k_{21})\frac{\omega(\lambda+\mu)}{6(\lambda+2\mu)}\right]$$
$$-x_3^3\frac{5(\lambda+\mu)}{3h^2(\lambda+2\mu)}\left(\gamma_{13}^2+\gamma_{23}^2\right) \tag{12}$$

Thus, perturbed warping functions are derived in terms of 2-D generalized strains and initial/undeformed curvatures. These are substituted back into the original energy density function and integrated through the thickness to derive the 2-D nonlinear constitutive law, which is input to the 2-D nonlinear shell analysis. Present theory is implemented using a symbolic manipulator, *Mathematica.*®

2.6 Shell Stiffness Matrix

Dimensionally reduced form of shell stiffness matrix is derived from the double derivative of ψ_{2D} (2-D strain energy) with respect to a 2-D generalized strain vector, e. This constitutive law will be given as an input to the 2-D nonlinear finite element analysis of the shell's reference surface. Derived constitutive law is represented as a summation of constant, linear and quadratic parts of generalized strain vector.

$$\mathscr{S}_{ij}=\mathscr{C}_{ij}+\mathscr{L}_{ij}^{k}e_k+\mathscr{Q}_{ij}^{kl}e_ke_l\quad(i,j,k,l=1,2,...,8) \tag{13}$$

where $e = 8 \times 1$ column matrix of 2-D strains; $\mathscr{C}$ is the 8×8 constant part of stiffness matrix due to initial curvature (excluding the constant part corresponding to zeroth order energy); $\mathscr{L}$ represents the linear part and is a $8\times8\times8$ 3-D matrix; and $\mathscr{Q}$ represents the quadratic part and is a $8\times8\times8\times8$ 4-D matrix symmetric about its superscripted 3rd and 4th indices. Note that $\mathscr{S}$, $\mathscr{C}$, $\mathscr{L}$ and $\mathscr{Q}$ are all symmetric about their subscripted 1st and 2nd indices. Initial curvature contribution is appended to plate stiffness elements [5] accordingly. For completeness all the nonzero stiffness coefficients of matrices $\mathscr{C}$, $\mathscr{L}$ and $\mathscr{Q}$ are presented in Appendix.

3 Nonlinear Shell Theory

Consistent with 2-D nonlinear constitutive law, a set of equations (compatibility equations, kinematics and equilibrium equations) are developed (similar to those in [5, 8] such that they form the governing equations for 2-D nonlinear shell theory. Compact form of 2-D strain-displacement relations provided by [8] are

$$\delta_\alpha+\gamma_\alpha=\Theta\mathbf{r}_{,\alpha}+\mathbf{u}_{,\alpha}+\tilde{k}_\alpha(\mathbf{r}+\mathbf{u}) \tag{14}$$

where $\gamma_1 = \left[\varepsilon_{11}, \varepsilon_{12}, 2\gamma_{13}\right]^T$, $\gamma_2 = \left[\varepsilon_{21}, \varepsilon_{22}, 2\gamma_{23}\right]^T$, $\delta_1 = [1, 0, 0]^T$ and $\delta_2 = [0, 1, 0]^T$ and Θ is the matrix of direction cosines. Expressions for components of the total curvature in the deformed configuration can be found in terms of the direction cosine matrix Θ [9] as

$$\tilde{K}_\alpha = -\frac{\Theta_{,\alpha}\Theta^T}{A_\alpha} + \Theta\tilde{k}_\alpha\Theta^T \tag{15}$$

where $K_\alpha = [-k_{\alpha 2}\ k_{\alpha 1}\ k_{\alpha 3}]^T + [-\kappa_{\alpha 2}\ \kappa_{\alpha 1}\ \kappa_{\alpha 3}]^T$ with the first term on the right hand side being initial curvature of the shell reference surface and the second term being load-induced additional elastic curvature.

3.1 Nonlinear Finite Element Analysis

Finite Element Analysis (FEA) is a versatile numerical technique that can be used for reference surface (2-D) analysis. Thus, 2-D nonlinear FEA is more reliable analysis for complex geometric, boundary and loading conditions with the combination of asymptotically accurate nonlinear constitutive law (derived in the previous section) for the combined nonlinear analysis of shell structures. This is the first attempt to integrate NFEA and asymptotically accurate nonlinear shell constitutive law using VAM.

4 Numerical Results

An in-house unified module has been developed in Mathematica for the analysis of thin hyperelastic shells, which is to be part of VAMNLM (Variational Asymptotic Method for Non-Linear Material models) software utilizing the nonlinear constitutive law developed in Sect. 2.6, and nonlinear shell theory described in the Sect. 3. This program incorporates the Newton-Raphson iteration procedure [10] to solve all nonlinear equations. Loads are applied gradually in an incremental form. For each load step, iterations are carried out to obtain a converged equilibrium position of the shell reference surface in the form of 2-D displacements. Overall procedure of the combined geometrically and materially nonlinear analysis of shells is given in Fig. 2. Validation of current development and code is demonstrated through two standard test cases that are available in literature [11, 12]. Both these test cases are modeled using dimensionally reduced form of neo-Hookean hyperelastic constitutive law.

First test case is thin cylinder having open ends on both sides as shown in Fig. 3, is subjected to uniform line load, 34 (total line load) and rests on a rigid line support. Because of the symmetry of load and structure only one quarter of the model is analyzed and modeled by a uniform 8×4 mesh. Geometric and material properties used are: Length, $l = 30$, arc radius, $r = 9$, thickness, $h = 0.2$, Lamé constants,

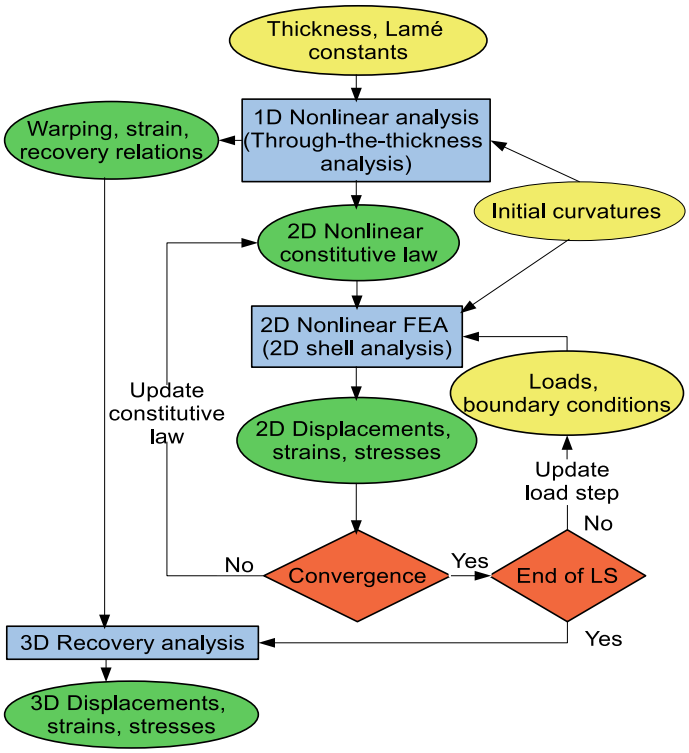

Fig. 2 Overview of non-linear hyperelastic shell analysis

Table 1 Thin cylinder subjected to line load

Details	Literature [12]	Current
Deflection at A	15.5	15.6

$\lambda = 24000$ and $\mu = 6000$. Four-noded isoparametric elements, with reduced Gauss quadrature (1×1), are used for the analysis. Comparison of displacement at point A is carried out with literature [12] as observed in Table 1, results matches well.

Pinched hemispherical shell subjected to two alternating radial point loads is used as a second test case. Geometric and material properties are: Radius, $r = 10$, thickness, $h = 0.04$, Lamé constants, $\lambda = 3.9375 \times 10^7$ and $\mu = 2.625 \times 10^7$. Here also due to symmetry of the load and structures only one-eight of the model is analyzed and modeled by 6×8 mesh as shown in Fig. 4. Four-noded isoparametric elements, with reduced Gauss quadrature (1×1), are used for the analysis. Deflection due to load of 100 (consistent units) from the current analysis and code matches well with literature [11] and shown in Table 2.

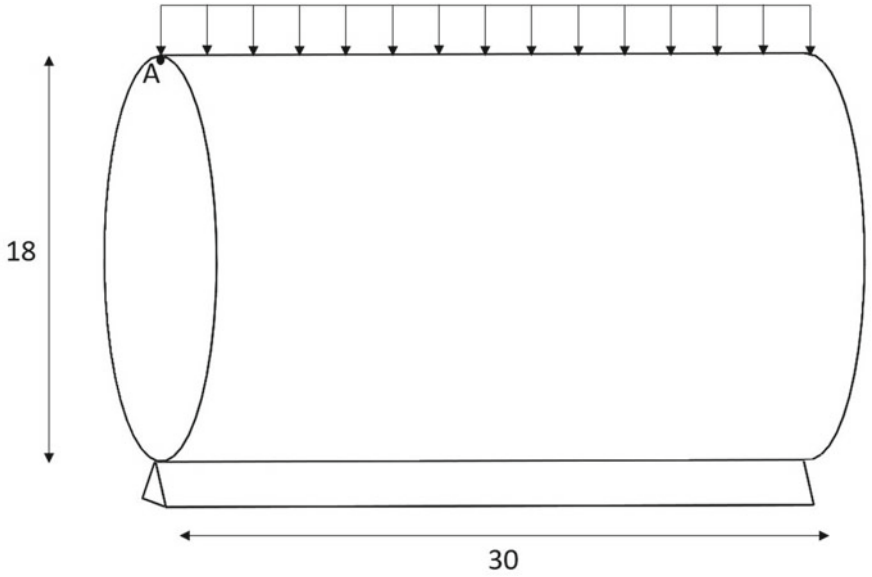

Fig. 3 Thin cylinder subjected to lined load and support

Fig. 4 A quarter of pinched hemispherical shell mesh with alternative radial loads

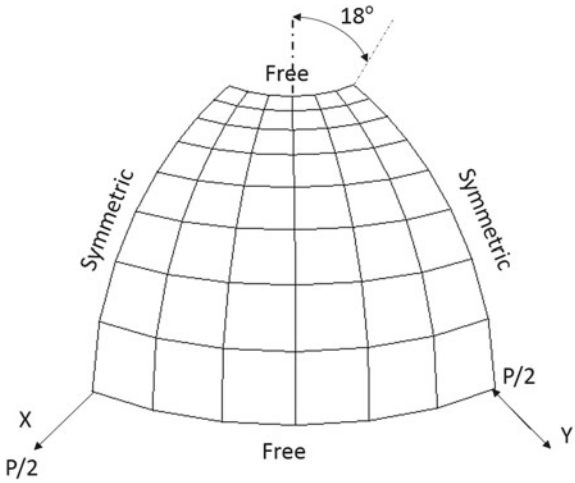

Table 2 Pinched hemispherical shell with a 18° hole subjected to radially alternating point forces

Details	Literature [11]	Current
Displacement, Ux	3.2	3.21
Displacement, Uy	5.8	5.78

5 Conclusions

An asymptotically-accurate 2-D nonlinear hyperelastic constitutive model and 3-D warping functions for shell structures using Variational Asymptotic Method (VAM) based on moderate strains, very small thickness-to-wavelength ratio and thickness-to-radius of curvatures as small parameters were derived. An intrinsic formulation of 2-D nonlinear shell theory consistent with the 2-D nonlinear constitutive law was developed and corresponding numerical tool nonlinear finite element analysis was developed. Current development is demonstrated with standard test cases made of hyperelastic material model and present results show good agreement with literature. Derivation of recovery relations (by product of 1-D analysis) to represent 3-D displacements, strains and stresses along the shell normal are at the final stage for near future publication.

Acknowledgements The authors are grateful to Jagath Kamineni for his support to simulate the test cases.

Appendix

$$\mathscr{L}^1_{11} = \mathscr{L}^2_{22} = \frac{12h\mu\left(4\mu^3 + 4\mu^2\lambda - 3\mu\lambda^2 - \lambda^3\right)}{(\lambda + 2\mu)^3}$$

$$\mathscr{L}^2_{11} = \mathscr{L}^1_{22} = \frac{2h\mu\left(32\mu^3 + 44\mu^2\lambda - 4\mu\lambda^2 - 3\lambda^3\right)}{(\lambda + 2\mu)^3}$$

$$\mathscr{L}^1_{33} = \mathscr{L}^2_{33} = \mathscr{L}^3_{23} = \mathscr{L}^3_{13} = -\frac{h\mu(3\lambda + 2\mu)}{2(\lambda + 2\mu)}$$

$$\mathscr{L}^1_{44} = \mathscr{L}^2_{55} = \mathscr{L}^4_{14} = \mathscr{L}^5_{25} = -\frac{h^3\mu\left(5\lambda^3 + 15\mu\lambda^2 - 8\mu^2\lambda - 12\mu^3\right)}{3(\lambda + 2\mu)^3}$$

$$\mathscr{L}^2_{44} = \mathscr{L}^1_{55} = \mathscr{L}^5_{15} = \mathscr{L}^4_{24} = -\frac{h^3\mu\left(7\lambda^3 + 16\mu\lambda^2 - 36\mu^2\lambda - 32\mu^3\right)}{6(\lambda + 2\mu)^3}$$

$$\mathscr{L}^1_{66} = \mathscr{L}^2_{66} = \mathscr{L}^6_{16} = \mathscr{L}^6_{26} = -\frac{h^3\mu(7\lambda + 2\mu)}{24(\lambda + 2\mu)}$$

$$\mathscr{L}^1_{77} = \mathscr{L}^1_{88} = \mathscr{L}^7_{17} = \mathscr{L}^8_{28} = \frac{2h\mu(\lambda + \mu)}{3(\lambda + 2\mu)}$$

$$\mathscr{L}^2_{77} = \mathscr{L}^2_{88} = \mathscr{L}^8_{18} = \mathscr{L}^7_{27} = \frac{h\lambda\mu}{3\lambda + 6\mu}$$

$$\mathscr{L}^5_{14} = \mathscr{L}^4_{15} = \mathscr{L}^5_{24} = \mathscr{L}^4_{25} = \frac{h^3\mu\left(-5\lambda^3 - 8\mu\lambda^2 + 44\mu^2\lambda + 32\mu^3\right)}{6(\lambda + 2\mu)^3}$$

$$\mathscr{L}^6_{34} = \mathscr{L}^6_{35} = \mathscr{L}^4_{36} = \mathscr{L}^5_{36} = \mathscr{L}^3_{46} = \mathscr{L}^1_{56} = -\frac{h^3\mu(3\lambda + 2\mu)}{24(\lambda + 2\mu)}$$

$$\mathscr{L}^8_{37} = \mathscr{L}^7_{38} = \mathscr{L}^3_{78} = \frac{\mathscr{C}_{88}}{5}$$

$$\mathscr{L}^1_{45} = \mathscr{L}^2_{45} = \frac{h^3\mu\left(-5\lambda^3 - 8\mu\lambda^2 + 44\mu^2\lambda + 32\mu^3\right)}{6(\lambda + 2\mu)^3}$$

$$\mathscr{Q}_{11}^{11} = \mathscr{Q}_{22}^{22} = \frac{6h\mu\left(5\lambda^5 + 25\mu\lambda^4 - 72\mu^2\lambda^3 - 632\mu^3\lambda^2 - 688\mu^4\lambda - 240\mu^5\right)}{(\lambda+2\mu)^5},$$

$$\mathscr{Q}_{11}^{12} = \mathscr{Q}_{22}^{12} = 2\mathscr{Q}_{12}^{11} = \mathscr{Q}_{12}^{22} = \frac{24h\mu\left(\lambda^5 + 2\mu\lambda^4 - 54\mu^2\lambda^3 - 304\mu^3\lambda^2 - 296\mu^4\lambda - 96\mu^5\right)}{(\lambda+2\mu)^5},$$

$$\mathscr{Q}_{77}^{77} = \mathscr{Q}_{88}^{77} = 3\mathscr{Q}_{77}^{88} = 3\mathscr{Q}_{88}^{88} = \frac{3\mathscr{Q}_{78}^{78}}{2} = \frac{\mathscr{C}_{11}}{4},$$

$$\mathscr{Q}_{11}^{22} = \mathscr{Q}_{22}^{11} = \frac{\mathscr{Q}_{12}^{12}}{2} = \frac{h\mu\left(9\lambda^5 + 8\mu\lambda^4 - 632\mu^2\lambda^3 - 3456\mu^3\lambda^2 - 3248\mu^4\lambda - 1024\mu^5\right)}{(\lambda+2\mu)^5},$$

$$\mathscr{Q}_{11}^{33} = \mathscr{Q}_{22}^{33} = \mathscr{Q}_{33}^{11} = \mathscr{Q}_{33}^{22} = \frac{\mathscr{Q}_{13}^{13}}{2} = \frac{\mathscr{Q}_{23}^{23}}{2} = \frac{3h\mu\left(\lambda^3 + 3\mu\lambda^2 - 4\mu^2\lambda - 4\mu^3\right)}{(\lambda+2\mu)^3},$$

$$\mathscr{Q}_{11}^{44} = \mathscr{Q}_{22}^{55} = \mathscr{Q}_{44}^{11} = \mathscr{Q}_{55}^{22} = 2\mathscr{Q}_{14}^{14} = \frac{\mathscr{Q}_{25}^{25}}{2}$$
$$= \frac{h^3\mu\left(33\lambda^5 + 161\mu\lambda^4 - 244\mu^2\lambda^3 - 2352\mu^3\lambda^2 - 2528\mu^4\lambda - 848\mu^5\right)}{6(\lambda+2\mu)^5},$$

$$\mathscr{Q}_{11}^{45} = \mathscr{Q}_{22}^{45} = \mathscr{Q}_{14}^{15} = \mathscr{Q}_{15}^{14} = \mathscr{Q}_{24}^{25} = \mathscr{Q}_{25}^{24} = 2\mathscr{Q}_{45}^{11} = \frac{\mathscr{Q}_{45}^{22}}{2}$$
$$= \frac{h^3\mu\left(5\lambda^5 + 14\mu\lambda^4 - 144\mu^2\lambda^3 - 728\mu^3\lambda^2 - 656\mu^4\lambda - 192\mu^5\right)}{(\lambda+2\mu)^5},$$

$$\mathscr{Q}_{11}^{55} = \mathscr{Q}_{22}^{44} = \mathscr{Q}_{44}^{22} = \mathscr{Q}_{55}^{11} = \frac{\mathscr{Q}_{15}^{15}}{2} = \frac{\mathscr{Q}_{24}^{24}}{2}$$
$$= \frac{h^3\mu\left(33\lambda^5 + 100\mu\lambda^4 - 880\mu^2\lambda^3 - 4560\mu^3\lambda^2 - 4240\mu^4\lambda - 1280\mu^5\right)}{12(\lambda+2\mu)^5},$$

$$\mathscr{Q}_{11}^{66} = \mathscr{Q}_{22}^{66} = \mathscr{Q}_{66}^{11} = \mathscr{Q}_{66}^{22} = \mathscr{Q}_{16}^{16} = 2\mathscr{Q}_{26}^{26} = \frac{h^3\mu\left(9\lambda^3 + 21\mu\lambda^2 - 52\mu^2\lambda - 44\mu^3\right)}{12(\lambda+2\mu)^3},$$

$$\mathscr{Q}_{11}^{77} = \mathscr{Q}_{22}^{88} = \mathscr{Q}_{77}^{11} = \mathscr{Q}_{88}^{11} = \frac{\mathscr{Q}_{17}^{17}}{2} = \frac{\mathscr{Q}_{28}^{28}}{2} = \frac{h\mu\left(4\mu^3 - 4\mu^2\lambda - 19\mu\lambda^2 - 5\lambda^3\right)}{3(\lambda+2\mu)^3},$$

$$\mathscr{Q}_{11}^{88} = \mathscr{Q}_{22}^{77} = \mathscr{Q}_{77}^{22} = \mathscr{Q}_{88}^{22} = \mathscr{Q}_{18}^{18} = \frac{\mathscr{Q}_{27}^{27}}{2} = \frac{h\mu\left(32\mu^3 + 44\mu^2\lambda - 4\mu\lambda^2 - 3\lambda^3\right)}{6(\lambda+2\mu)^3},$$

$$\mathscr{Q}_{33}^{12} = \mathscr{Q}_{12}^{33} = 2\mathscr{Q}_{13}^{23} = \mathscr{Q}_{23}^{13} = \frac{h\mu\left(9\lambda^3 + 22\mu\lambda^2 - 68\mu^2\lambda - 56\mu^3\right)}{2(\lambda+2\mu)^3},$$

$$\mathscr{Q}_{33}^{44} = \mathscr{Q}_{33}^{55} = \mathscr{Q}_{44}^{33} = \mathscr{Q}_{55}^{33} = \mathscr{Q}_{34}^{34} = \mathscr{Q}_{35}^{35} = \frac{h^3(\lambda-\mu)\mu\left(5\lambda^2 + 20\mu\lambda + 12\mu^2\right)}{12(\lambda+2\mu)^3},$$

$$\mathscr{Q}_{33}^{45} = \mathscr{Q}_{34}^{35} = \mathscr{Q}_{35}^{34} = 2\mathscr{Q}_{45}^{33} = \frac{h^3\mu\left(13\lambda^3 + 30\mu\lambda^2 - 68\mu^2\lambda - 56\mu^3\right)}{24(\lambda+2\mu)^3},$$

$$\mathscr{Q}_{33}^{66} = \mathscr{Q}_{66}^{33} = 2\mathscr{Q}_{36}^{36} = \frac{h^3\mu(13\lambda+6\mu)}{96(\lambda+2\mu)},$$

$$\mathscr{Q}_{33}^{77} = \mathscr{Q}_{33}^{88} = \mathscr{Q}_{77}^{33} = \mathscr{Q}_{88}^{33} = \frac{\mathscr{Q}_{37}^{37}}{2} = 2\mathscr{Q}_{38}^{38} = -\frac{h\mu(5\lambda+6\mu)}{24(\lambda+2\mu)},$$

$$\mathscr{Q}_{44}^{12} = \mathscr{Q}_{55}^{12} = 2\mathscr{Q}_{12}^{44} = \mathscr{Q}_{12}^{55} = \mathscr{Q}_{14}^{24} = \mathscr{Q}_{15}^{25} = \mathscr{Q}_{24}^{14} = \mathscr{Q}_{25}^{15}$$
$$= \frac{h^3\mu\left(19\lambda^5 + 64\mu\lambda^4 - 436\mu^2\lambda^3 - 2368\mu^3\lambda^2 - 2272\mu^4\lambda - 704\mu^5\right)}{3(\lambda+2\mu)^5},$$

$$\mathscr{D}_{44}^{44} = \mathscr{D}_{55}^{55} = \frac{h^5\mu\left(89\lambda^5 + 325\mu\lambda^4 - 1616\mu^2\lambda^3 - 9160\mu^3\lambda^2 - 9744\mu^4\lambda - 3312\mu^5\right)}{120(\lambda+2\mu)^5},$$

$$\mathscr{D}_{44}^{45} = \mathscr{D}_{55}^{45} = 2\mathscr{D}_{45}^{44} = \frac{\mathscr{D}_{45}^{55}}{2}$$
$$= \frac{h^5\mu\left(21\lambda^5 + 29\mu\lambda^4 - 880\mu^2\lambda^3 - 3868\mu^3\lambda^2 - 3552\mu^4\lambda - 1056\mu^5\right)}{30(\lambda+2\mu)^5},$$

$$\mathscr{D}_{44}^{66} = \mathscr{D}_{55}^{66} = \mathscr{D}_{66}^{44} = \mathscr{D}_{66}^{55} = \frac{\mathscr{D}_{46}^{46}}{2} = \frac{\mathscr{D}_{56}^{56}}{2} = \frac{h^5\mu\left(47\lambda^3 + 79\mu\lambda^2 - 360\mu^2\lambda - 300\mu^3\right)}{720(\lambda+2\mu)^3},$$

$$\mathscr{D}_{44}^{77} = \mathscr{D}_{55}^{88} = \mathscr{D}_{77}^{44} = \mathscr{D}_{88}^{44} = \mathscr{D}_{47}^{47} = 2\mathscr{D}_{58}^{58} = \frac{h^3\mu\left(196\mu^3 - 570\mu^2\lambda - 1578\mu\lambda^2 - 433\lambda^3\right)}{756(\lambda+2\mu)^3},$$

$$\mathscr{D}_{44}^{88} = \mathscr{D}_{55}^{77} = \mathscr{D}_{77}^{55} = \mathscr{D}_{88}^{55} = \frac{\mathscr{D}_{48}^{48}}{2} = \frac{\mathscr{D}_{57}^{57}}{2} = \frac{h^3\mu\left(48\mu^3 + 66\mu^2\lambda - 11\mu\lambda^2 - 7\lambda^3\right)}{36(\lambda+2\mu)^3},$$

$$\mathscr{D}_{66}^{12} = 2\mathscr{D}_{12}^{66} = \mathscr{D}_{16}^{16} = \mathscr{D}_{26}^{16} = \frac{h^3\mu\left(29\lambda^3 + 54\mu\lambda^2 - 244\mu^2\lambda - 184\mu^3\right)}{24(\lambda+2\mu)^3},$$

$$\mathscr{D}_{66}^{45} = 2\mathscr{D}_{45}^{66} = \frac{\mathscr{D}_{46}^{56}}{2} = \mathscr{D}_{56}^{46} = \frac{h^5\mu\left(137\lambda^3 + 190\mu\lambda^2 - 1332\mu^2\lambda - 888\mu^3\right)}{1440(\lambda+2\mu)^3},$$

$$\mathscr{D}_{66}^{66} = \frac{h^5(17\lambda - 26\mu)\mu}{640(\lambda+2\mu)},\ \mathscr{D}_{66}^{77} = \mathscr{D}_{66}^{88} = \mathscr{D}_{77}^{66} = \mathscr{D}_{88}^{66} = \frac{\mathscr{D}_{67}^{67}}{2} = \frac{\mathscr{D}_{68}^{68}}{2} = \frac{-h^3\mu(47\lambda + 58\mu)}{864(\lambda+2\mu)},$$

$$\mathscr{D}_{77}^{12} = \mathscr{D}_{88}^{12} = 2\mathscr{D}_{12}^{77} = \frac{\mathscr{D}_{12}^{88}}{2} = \mathscr{D}_{17}^{27} = \mathscr{D}_{18}^{28} = \mathscr{D}_{27}^{17} = \mathscr{D}_{28}^{18} = \frac{4h\mu(\lambda+4\mu)\left(2\mu^2 + 2\mu\lambda - \lambda^2\right)}{3(\lambda+2\mu)^3},$$

$$\mathscr{D}_{77}^{45} = \mathscr{D}_{88}^{45} = 2\mathscr{D}_{45}^{77} = \frac{\mathscr{D}_{45}^{88}}{2} = \mathscr{D}_{47}^{57} = \mathscr{D}_{48}^{58} = \mathscr{D}_{57}^{47} = \mathscr{D}_{58}^{48}$$
$$= \frac{h^3\mu\left(1344\mu^3 + 1524\mu^2\lambda - 632\mu\lambda^2 - 277\lambda^3\right)}{504(\lambda+2\mu)^3},$$

$$\mathscr{D}_{12}^{45} = \mathscr{D}_{14}^{25} = \mathscr{D}_{15}^{25} = \mathscr{D}_{24}^{15} = \mathscr{D}_{25}^{14} = \mathscr{D}_{45}^{12}$$
$$= \frac{h^3\mu\left(25\lambda^5 + 56\mu\lambda^4 - 872\mu^2\lambda^3 - 4192\mu^3\lambda^2 - 3632\mu^4\lambda - 1024\mu^5\right)}{6(\lambda+2\mu)^5},$$

$$\mathscr{D}_{13}^{46} = \mathscr{D}_{14}^{36} = \mathscr{D}_{16}^{34} = \mathscr{D}_{23}^{56} = \mathscr{D}_{25}^{36} = \mathscr{D}_{26}^{34} = \mathscr{D}_{34}^{16} = \mathscr{D}_{35}^{26} = \mathscr{D}_{36}^{14} = \mathscr{D}_{36}^{25}$$
$$= \mathscr{D}_{46}^{13} = \mathscr{D}_{56}^{23} = \frac{h^3\mu\left(9\lambda^3 + 26\mu\lambda^2 - 20\mu^2\lambda - 24\mu^3\right)}{12(\lambda+2\mu)^3},$$

$$\mathscr{D}_{13}^{56} = \mathscr{D}_{15}^{36} = \mathscr{D}_{23}^{46} = \mathscr{D}_{24}^{36} = \mathscr{D}_{26}^{34} = \mathscr{D}_{34}^{26} = \mathscr{D}_{35}^{16} = \mathscr{D}_{36}^{24} = \mathscr{D}_{36}^{15} = \mathscr{D}_{46}^{23}$$
$$= \mathscr{D}_{56}^{13} = \frac{h^3\mu\left(15\lambda^3 + 38\mu\lambda^2 - 60\mu^2\lambda - 56\mu^3\right)}{24(\lambda+2\mu)^3}$$

$$\mathscr{C}_{11} = k_{11}^2\frac{4h^3\mu(\lambda+\mu)^2(2\lambda+3\mu)}{3(\lambda+2\mu)^3} + k_{22}^2\frac{h^3\lambda^2\mu(2\lambda+3\mu)}{3(\lambda+2\mu)^3} + k_{12}^2\frac{h^3\lambda^2\mu}{12(\lambda+2\mu)^2} + k_{21}^2\frac{h^3\mu(\lambda+\mu)^2}{3(\lambda+2\mu)^2}$$
$$+ k_{12}k_{21}\frac{h^3\mu\left(6\lambda^2 + 9\lambda\mu + 4\mu^2\right)}{3(\lambda+2\mu)^2} + k_{11}k_{22}\frac{2h^3\lambda^2\mu(\lambda+\mu)}{3(\lambda+2\mu)^3}$$

$$\mathscr{C}_{22} = k_{11}^2\frac{h^3\lambda^2\mu(2\lambda+3\mu)}{3(\lambda+2\mu)^3} + k_{22}^2\frac{4h^3\mu(\lambda+\mu)^2(2\lambda+3\mu)}{3(\lambda+2\mu)^3} + k_{12}^2\frac{h^3\mu(\lambda+\mu)^2}{3(\lambda+2\mu)^2} + k_{21}^2\frac{h^3\lambda^2\mu}{12(\lambda+2\mu)^2}$$
$$+ k_{12}k_{21}\frac{h^3\mu\left(6\lambda^2 + 9\lambda\mu + 4\mu^2\right)}{3(\lambda+2\mu)^2} + k_{11}k_{22}\frac{2h^3\lambda^2\mu(\lambda+\mu)}{3(\lambda+2\mu)^3}$$

$$\mathscr{C}_{33} = (k_{11}^2 + k_{22}^2)\frac{5h^3\mu}{48} + (k_{12}^2 + k_{21}^2)\frac{h^3\mu(\lambda+\mu)}{12(\lambda+2\mu)} + k_{12}k_{21}\frac{h^3\mu(3\lambda+4\mu)}{12(\lambda+2\mu)} + k_{11}k_{22}\frac{h^3\mu}{24}$$

$$\mathscr{C}_{44} = k_{11}^2\frac{h^5\mu\left(10\lambda^3+38\lambda^2\mu+49\lambda\mu^2+21\mu^3\right)}{45(\lambda+2\mu)^3} + k_{12}^2\frac{h^5\lambda^2\mu}{720(\lambda+2\mu)^2} + k_{21}^2\frac{h^5\mu\left(7\lambda^2+22\lambda\mu+18\mu^2\right)}{360(\lambda+2\mu)^2}$$
$$+ k_{12}k_{21}\frac{h^5\mu\left(17\lambda^2+40\lambda\mu+24\mu^2\right)}{120(\lambda+2\mu)^2} + k_{11}k_{22}\frac{h^5\lambda\mu\left(3\lambda^2-16\lambda\mu-24\mu^2\right)}{180(\lambda+2\mu)^3} + k_{22}^2\frac{h^5\lambda^2\mu(2\lambda-\mu)}{180(\lambda+2\mu)^3}$$

$$\mathscr{C}_{55} = k_{22}^2\frac{h^5\mu\left(10\lambda^3+38\lambda^2\mu+49\lambda\mu^2+21\mu^3\right)}{45(\lambda+2\mu)^3} + k_{21}^2\frac{h^5\lambda^2\mu}{720(\lambda+2\mu)^2} + k_{12}^2\frac{h^5\mu\left(7\lambda^2+22\lambda\mu+18\mu^2\right)}{360(\lambda+2\mu)^2}$$
$$+ k_{12}k_{21}\frac{h^5\mu\left(17\lambda^2+40\lambda\mu+24\mu^2\right)}{120(\lambda+2\mu)^2} + k_{11}k_{22}\frac{h^5\lambda\mu\left(3\lambda^2-16\lambda\mu-24\mu^2\right)}{180(\lambda+2\mu)^3} + k_{11}^2\frac{h^5\lambda^2\mu(2\lambda-\mu)}{180(\lambda+2\mu)^3}$$

$$\mathscr{C}_{66} = (k_{11}^2 + k_{22}^2)\frac{h^5\mu}{64} + (k_{12}^2 + k_{21}^2)\frac{h^5\mu(4\lambda+\mu)}{240(\lambda+2\mu)} + k_{12}k_{21}\frac{h^5\mu(11\lambda+8\mu)}{240(\lambda+2\mu)} + k_{11}k_{22}\frac{h^5\mu}{160}$$

$$\mathscr{C}_{77} = k_{11}^2\frac{25h^3\mu}{216} - k_{12}^2\frac{5h^3\mu}{1512} + k_{12}k_{21}\frac{5h^3\mu}{42}$$

$$\mathscr{C}_{88} = k_{22}^2\frac{25h^3\mu}{216} - k_{21}^2\frac{5h^3\mu}{1512} + k_{12}k_{21}\frac{5h^3\mu}{42}$$

$$\mathscr{C}_{12} = (k_{11}^2 + k_{22}^2)\frac{2h^3\lambda\mu\left(2\lambda^2+5\lambda\mu+3\mu^2\right)}{3(\lambda+2\mu)^3} + (k_{12}^2 + k_{21}^2)\frac{h^3\lambda\mu(\lambda+\mu)}{6(\lambda+2\mu)^2}$$
$$+ k_{12}k_{21}\frac{h^3\mu\left(21\lambda^2+24\lambda\mu+4\mu^2\right)}{12(\lambda+2\mu)^2} + k_{11}k_{22}\frac{h^3\lambda\mu\left(5\lambda^2+8\lambda\mu+4\mu^2\right)}{6(\lambda+2\mu)^3}$$

$$\mathscr{C}_{13} = (k_{11}k_{21} + k_{22}k_{21})\frac{h^3\mu(3\lambda+2\mu)(2\lambda+3\mu)}{12(\lambda+2\mu)^2} + k_{11}k_{12}\frac{h^3\mu(3\lambda+2\mu)(5\lambda+8\mu)}{24(\lambda+2\mu)^2}$$
$$+ k_{22}k_{12}\frac{h^3\mu(3\lambda+2\mu)(3\lambda+4\mu)}{24(\lambda+2\mu)^2}$$

$$\mathscr{C}_{14} = -k_{11}\frac{h^3\mu\left(3\lambda^2+7\lambda\mu+4\mu^2\right)}{3(\lambda+2\mu)^2} - k_{22}\frac{h^3\lambda^2\mu}{6(\lambda+2\mu)^2}$$

$$\mathscr{C}_{15} = -k_{11}\frac{h^3\lambda\mu(\lambda+\mu)}{3(\lambda+2\mu)^2} - k_{22}\frac{h^3\lambda\mu(3\lambda+4\mu)}{6(\lambda+2\mu)^2}$$

$$\mathscr{C}_{16} = \mathscr{C}_{26} = -(k_{12}+k_{21})\frac{h^3\mu(3\lambda+2\mu)}{12(\lambda+2\mu)}$$

$$\mathscr{C}_{23} = (k_{11}k_{12} + k_{22}k_{12})\frac{h^3\mu(3\lambda+2\mu)(2\lambda+3\mu)}{12(\lambda+2\mu)^2} + k_{11}k_{21}\frac{h^3\mu(3\lambda+2\mu)(3\lambda+4\mu)}{24(\lambda+2\mu)^2}$$
$$+ k_{22}k_{21}\frac{h^3\mu(3\lambda+2\mu)(5\lambda+8\mu)}{24(\lambda+2\mu)^2}$$

$$\mathscr{C}_{24} = -k_{11}\frac{h^3\lambda\mu(3\lambda+4\mu)}{6(\lambda+2\mu)^2} - k_{22}\frac{h^3\lambda\mu(\lambda+\mu)}{3(\lambda+2\mu)^2}$$

$$\mathscr{C}_{25} = -k_{11}\frac{h^3\lambda^2\mu}{6(\lambda+2\mu)^2} - k_{22}\frac{h^3\mu\left(3\lambda^2+7\lambda\mu+4\mu^2\right)}{3(\lambda+2\mu)^2}$$

$$\mathscr{C}_{34} = \mathscr{C}_{35} = -(k_{12}+k_{21})\frac{h^3\mu(\lambda+\mu)}{6(\lambda+2\mu)}$$

$$\mathscr{C}_{36} = -(k_{11}+k_{22})\frac{h^3\mu}{12}$$

$$\mathscr{C}_{45} = (k_{11}^2 + k_{22}^2)\frac{h^5\lambda\mu\left(21\lambda^2+46\lambda\mu+28\mu^2\right)}{360(\lambda+2\mu)^3} + (k_{12}^2 + k_{21}^2)\frac{h^5\lambda\mu(3\lambda+4\mu)}{720(\lambda+2\mu)^2}$$
$$+ k_{12}k_{21}\frac{h^5\mu\left(25\lambda^2+44\lambda\mu+12\mu^2\right)}{240(\lambda+2\mu)^2} + k_{11}k_{22}\frac{h^5\mu\left(21\lambda^3+16\lambda^2\mu-36\lambda\mu^2-48\mu^3\right)}{360(\lambda+2\mu)^3}$$

$$
\begin{aligned}
\mathscr{C}_{46} &= k_{11}k_{12}\frac{h^5\mu\left(51\lambda^2+106\lambda\mu+48\mu^2\right)}{720(\lambda+2\mu)^2}+k_{11}k_{21}\frac{h^5\mu\left(89\lambda^2+168\lambda\mu+60\mu^2\right)}{1440(\lambda+2\mu)^2}\\
&\quad+k_{22}k_{12}\frac{h^5\mu\left(25\lambda^2+48\lambda\mu+36\mu^2\right)}{720(\lambda+2\mu)^2}+k_{22}k_{21}\frac{h^5\mu\left(63\lambda^2+140\lambda\mu+108\mu^2\right)}{1440(\lambda+2\mu)^2}\\
\mathscr{C}_{56} &= k_{11}k_{12}\frac{h^5\mu\left(63\lambda^2+140\lambda\mu+108\mu^2\right)}{1440(\lambda+2\mu)^2}+k_{11}k_{21}\frac{h^5\mu\left(25\lambda^2+48\lambda\mu+36\mu^2\right)}{720(\lambda+2\mu)^2}\\
&\quad+k_{22}k_{12}\frac{h^5\mu\left(89\lambda^2+168\lambda\mu+60\mu^2\right)}{1440(\lambda+2\mu)^2}+k_{22}k_{21}\frac{h^5\mu\left(51\lambda^2+106\lambda\mu+48\mu^2\right)}{720(\lambda+2\mu)^2}\\
\mathscr{C}_{78} &= (k_{11}k_{12}+k_{22}k_{21})\frac{5h^3\mu}{84}+(k_{11}k_{21}+k_{22}k_{12})\frac{85h^3\mu}{1512}
\end{aligned}
\tag{16}
$$

$$
\begin{aligned}
\mathscr{L}_{11}^{1} &= \frac{12h\mu\left(4\mu^3+4\mu^2\lambda-3\mu\lambda^2-\lambda^3\right)}{(\lambda+2\mu)^3}\\
\mathscr{L}_{11}^{4} &= k_{11}\frac{h^3\mu\left(23\lambda^4+93\lambda^3\mu-12\lambda^2\mu^2-192\lambda\mu^3-104\mu^4\right)}{3(\lambda+2\mu)^4}\\
&\quad+k_{22}\frac{h^3\lambda\mu\left(5\lambda^3+7\lambda^2\mu-66\lambda\mu^2-48\mu^3\right)}{3(\lambda+2\mu)^4}\\
\mathscr{L}_{11}^{5} &= \mathscr{L}_{15}^{1} = k_{11}\frac{h^3\mu\left(9\lambda^4+21\lambda^3\mu-98\lambda^2\mu^2-168\lambda\mu^3-64\mu^4\right)}{3(\lambda+2\mu)^4}\\
&\quad+k_{22}\frac{h^3\mu\left(19\lambda^4+46\lambda^3\mu-192\lambda^2\mu^2-336\lambda\mu^3-128\mu^4\right)}{6(\lambda+2\mu)^4}\\
\mathscr{L}_{11}^{6} &= \mathscr{L}_{22}^{6} = (k_{12}+k_{21})\frac{h^3\mu\left(17\lambda^3+44\lambda^2\mu-56\lambda\mu^2-56\mu^3\right)}{12(\lambda+2\mu)^3}\\
\mathscr{L}_{22}^{4} &= \mathscr{L}_{24}^{2} = k_{11}\frac{h^3\mu\left(19\lambda^4+46\lambda^3\mu-192\lambda^2\mu^2-336\lambda\mu^3-128\mu^4\right)}{6(\lambda+2\mu)^4}\\
&\quad+k_{22}\frac{h^3\mu\left(9\lambda^4+21\lambda^3\mu-98\lambda^2\mu^2-168\lambda\mu^3-64\mu^4\right)}{3(\lambda+2\mu)^4}\\
\mathscr{L}_{22}^{5} &= k_{11}\frac{h^3\lambda\mu\left(5\lambda^3+7\lambda^2\mu-66\lambda\mu^2-48\mu^3\right)}{3(\lambda+2\mu)^4}\\
&\quad+k_{22}\frac{h^3\mu\left(23\lambda^4+93\lambda^3\mu-12\lambda^2\mu^2-192\lambda\mu^3-104\mu^4\right)}{3(\lambda+2\mu)^4}\\
\mathscr{L}_{33}^{4} &= k_{11}\frac{h^3\mu\left(5\lambda^2+10\lambda\mu+4\mu^2\right)}{12(\lambda+2\mu)^2}+k_{22}\frac{h^3\mu\left(5\lambda^2+8\lambda\mu+4\mu^2\right)}{24(\lambda+2\mu)^2}\\
\mathscr{L}_{33}^{5} &= k_{11}\frac{h^3\mu\left(5\lambda^2+8\lambda\mu+4\mu^2\right)}{24(\lambda+2\mu)^2}+k_{22}\frac{h^3\mu\left(5\lambda^2+10\lambda\mu+4\mu^2\right)}{12(\lambda+2\mu)^2}
\end{aligned}
$$

$$\mathscr{L}^6_{33} = \mathscr{L}^3_{36} = (k_{12}+k_{21})\frac{h^3\mu(11\lambda+6\mu)}{48(\lambda+2\mu)}$$

$$\mathscr{L}^4_{44} = k_{11}\frac{h^5\mu\left(51\lambda^4+181\lambda^3\mu-180\lambda^2\mu^2-760\lambda\mu^3-408\mu^4\right)}{60(\lambda+2\mu)^4} + k_{22}\frac{h^5\lambda\mu\left(4\lambda^3-23\lambda^2\mu-186\lambda\mu^2-128\mu^3\right)}{60(\lambda+2\mu)^4}$$

$$\mathscr{L}^5_{44} = k_{11}\frac{h^5\mu\left(62\lambda^4+111\lambda^3\mu-918\lambda^2\mu^2-1808\lambda\mu^3-768\mu^4\right)}{180(\lambda+2\mu)^4} + k_{22}\frac{h^5\mu\left(25\lambda^4+18\lambda^3\mu-496\lambda^2\mu^2-784\lambda\mu^3-320\mu^4\right)}{120(\lambda+2\mu)^4}$$

$$\mathscr{L}^6_{44} = \mathscr{L}^6_{55} = (k_{12}+k_{21})\frac{h^5\mu\left(47\lambda^3+110\lambda^2\mu-214\lambda\mu^2-204\mu^3\right)}{360(\lambda+2\mu)^3}$$

$$\mathscr{L}^4_{55} = k_{11}\frac{h^5\mu\left(25\lambda^4+18\mu\lambda^3-496\mu^2\lambda^2-784\mu^3\lambda-320\mu^4\right)}{120(\lambda+2\mu)^4} + k_{22}\frac{h^5\mu\left(62\lambda^4+111\mu\lambda^3-918\mu^2\lambda^2-1808\mu^3\lambda-768\mu^4\right)}{180(\lambda+2\mu)^4}$$

$$\mathscr{L}^5_{55} = k_{11}\frac{h^5\lambda\mu\left(4\lambda^3-23\mu\lambda^2-186\mu^2\lambda-128\mu^3\right)}{60(\lambda+2\mu)^4} + k_{22}\frac{h^5\mu\left(51\lambda^4+181\mu\lambda^3-180\mu^2\lambda^2-760\mu^3\lambda-408\mu^4\right)}{60(\lambda+2\mu)^4}$$

$$\mathscr{L}^4_{66} = k_{11}\frac{h^5\mu\left(11\lambda^2+13\mu\lambda-3\mu^2\right)}{180(\lambda+2\mu)^2} + k_{22}\frac{h^5\mu\left(43\lambda^2+44\mu\lambda+36\mu^2\right)}{1440(\lambda+2\mu)^2}$$

$$\mathscr{L}^5_{66} = k_{11}\frac{h^5\mu\left(43\lambda^2+44\mu\lambda+36\mu^2\right)}{1440(\lambda+2\mu)^2} + k_{22}\frac{h^5\mu\left(11\lambda^2+13\mu\lambda-3\mu^2\right)}{180(\lambda+2\mu)^2}$$

$$\mathscr{L}^6_{66} = (k_{12}+k_{21})\frac{h^5(3\lambda-2\mu)\mu}{64(\lambda+2\mu)}$$

$$\mathscr{L}^4_{77} = -k_{11}\frac{h^3\mu\left(943\lambda^2+2614\mu\lambda+1624\mu^2\right)}{1512(\lambda+2\mu)^2} - k_{22}\frac{h^3\lambda^2\mu}{36(\lambda+2\mu)^2}$$

$$\mathscr{L}^5_{77} = -k_{11}\frac{h^3\lambda\mu(137\lambda+246\mu)}{504(\lambda+2\mu)^2} - k_{22}\frac{h^3\lambda\mu(2\lambda+3\mu)}{18(\lambda+2\mu)^2}$$

$$\mathscr{L}^6_{77} = -k_{12}\frac{h^3\mu(52\lambda+41\mu)}{756(\lambda+2\mu)} - k_{21}\frac{h^3\mu(25\lambda+36\mu)}{168(\lambda+2\mu)}$$

$$\mathscr{L}^4_{88} = -k_{11}\frac{h^3\lambda\mu(2\lambda+3\mu)}{18(\lambda+2\mu)^2} - k_{22}\frac{h^3\lambda\mu(137\lambda+246\mu)}{504(\lambda+2\mu)^2}$$

$$\mathscr{L}_{88}^{5} = -k_{11}\frac{h^3\lambda^2\mu}{36(\lambda+2\mu)^2} - k_{22}\frac{h^3\mu\left(943\lambda^2+2614\mu\lambda+1624\mu^2\right)}{1512(\lambda+2\mu)^2}$$

$$\mathscr{L}_{88}^{6} = -k_{12}\frac{h^3\mu(25\lambda+36\mu)}{168(\lambda+2\mu)} - k_{21}\frac{h^3\mu(52\lambda+41\mu)}{756(\lambda+2\mu)}$$

$$\mathscr{L}_{12}^{4} = -k_{11}\frac{h^3\mu\left(13\lambda^4+38\mu\lambda^3-98\mu^2\lambda^2-220\mu^3\lambda-96\mu^4\right)}{3(\lambda+2\mu)^4} - k_{22}\frac{h^3\mu\left(13\lambda^4+24\mu\lambda^3-168\mu^2\lambda^2-216\mu^3\lambda-64\mu^4\right)}{6(\lambda+2\mu)^4}$$

$$\mathscr{L}_{12}^{5} = -k_{11}\frac{h^3\mu\left(13\lambda^4+24\mu\lambda^3-168\mu^2\lambda^2-216\mu^3\lambda-64\mu^4\right)}{6(\lambda+2\mu)^4} - k_{22}\frac{h^3\mu\left(13\lambda^4+38\mu\lambda^3-98\mu^2\lambda^2-220\mu^3\lambda-96\mu^4\right)}{3(\lambda+2\mu)^4}$$

$$\mathscr{L}_{12}^{6} = (k_{12}+k_{21})\frac{h^3\mu\left(29\lambda^3+66\mu\lambda^2-140\mu^2\lambda-120\mu^3\right)}{24(\lambda+2\mu)^3}$$

$$\mathscr{L}_{13}^{4} = (k_{12}+k_{21})\frac{h^3\mu\left(19\lambda^3+56\mu\lambda^2-36\mu^2\lambda-48\mu^3\right)}{24(\lambda+2\mu)^3}$$

$$\mathscr{L}_{13}^{5} = (k_{12}+k_{21})\frac{h^3\mu\left(8\lambda^3+21\mu\lambda^2-28\mu^2\lambda-28\mu^3\right)}{12(\lambda+2\mu)^3}$$

$$\mathscr{L}_{13}^{6} = k_{11}\frac{h^3\mu\left(11\lambda^2+22\mu\lambda+8\mu^2\right)}{24(\lambda+2\mu)^2} + k_{22}\frac{h^3\mu\left(4\lambda^2+7\mu\lambda+2\mu^2\right)}{12(\lambda+2\mu)^2}$$

$$\mathscr{L}_{14}^{1} = k_{11}\frac{h^3\mu\left(23\lambda^4+93\mu\lambda^3-12\mu^2\lambda^2-192\mu^3\lambda-104\mu^4\right)}{3(\lambda+2\mu)^4} + k_{22}\frac{h^3\lambda\mu\left(5\lambda^3+7\mu\lambda^2-66\mu^2\lambda-48\mu^3\right)}{3(\lambda+2\mu)^4}$$

$$\mathscr{L}_{14}^{2} = k_{11}\frac{h^3\mu\left(13\lambda^4+38\mu\lambda^3-98\mu^2\lambda^2-220\mu^3\lambda-96\mu^4\right)}{3(\lambda+2\mu)^4} + k_{22}\frac{h^3\mu\left(13\lambda^4+24\mu\lambda^3-168\mu^2\lambda^2-216\mu^3\lambda-64\mu^4\right)}{6(\lambda+2\mu)^4}$$

$$\mathscr{L}_{14}^{3} = (k_{12}+k_{21})\frac{h^3\mu\left(19\lambda^3+56\mu\lambda^2-36\mu^2\lambda-48\mu^3\right)}{24(\lambda+2\mu)^3}$$

$$\mathscr{L}_{15}^{2} = k_{11}\frac{h^3\mu\left(13\lambda^4+24\mu\lambda^3-168\mu^2\lambda^2-216\mu^3\lambda-64\mu^4\right)}{6(\lambda+2\mu)^4} + K_{22}\frac{h^3\mu\left(13\lambda^4+38\mu\lambda^3-98\mu^2\lambda^2-220\mu^3\lambda-96\mu^4\right)}{3(\lambda+2\mu)^4}$$

$$\mathscr{L}_{15}^{3} = (k_{12}+k_{21})\frac{h^3\mu\left(8\lambda^3+21\mu\lambda^2-28\mu^2\lambda-28\mu^3\right)}{12(\lambda+2\mu)^3}$$

$$\mathscr{L}_{16}^{1} = (k_{12}+k_{21})\frac{h^3\mu\left(17\lambda^3+44\mu\lambda^2-56\mu^2\lambda-56\mu^3\right)}{12(\lambda+2\mu)^3}$$

$$\mathscr{L}_{16}^{2} = (k_{12}+k_{21})\frac{h^3\mu\left(29\lambda^3+66\mu\lambda^2-140\mu^2\lambda-120\mu^3\right)}{24(\lambda+2\mu)^3}$$

$$\mathscr{L}_{16}^{3} = k_{11}\frac{h^3\mu\left(11\lambda^2+22\mu\lambda+8\mu^2\right)}{24(\lambda+2\mu)^2}+k_{22}\frac{h^3\mu\left(4\lambda^2+7\mu\lambda+2\mu^2\right)}{12(\lambda+2\mu)^2}$$

$$\mathscr{L}_{23}^{4} = (k_{12}+k_{21})\frac{h^3\mu\left(8\lambda^3+21\mu\lambda^2-28\mu^2\lambda-28\mu^3\right)}{12(\lambda+2\mu)^3}$$

$$\mathscr{L}_{23}^{5} = (k_{12}+k_{21})\frac{h^3\mu\left(19\lambda^3+56\mu\lambda^2-36\mu^2\lambda-48\mu^3\right)}{24(\lambda+2\mu)^3}$$

$$\mathscr{L}_{23}^{6} = k_{11}\frac{h^3\mu\left(4\lambda^2+7\mu\lambda+2\mu^2\right)}{12(\lambda+2\mu)^2}+k_{22}\frac{h^3\mu\left(11\lambda^2+22\mu\lambda+8\mu^2\right)}{24(\lambda+2\mu)^2}$$

$$\mathscr{L}_{24}^{1} = k_{11}\frac{h^3\mu\left(13\lambda^4+38\mu\lambda^3-98\mu^2\lambda^2-220\mu^3\lambda-96\mu^4\right)}{3(\lambda+2\mu)^4}$$
$$+k_{22}\frac{h^3\mu\left(13\lambda^4+24\mu\lambda^3-168\mu^2\lambda^2-216\mu^3\lambda-64\mu^4\right)}{6(\lambda+2\mu)^4}$$

$$\mathscr{L}_{24}^{3} = (k_{12}+k_{21})\frac{h^3\mu\left(8\lambda^3+21\mu\lambda^2-28\mu^2\lambda-28\mu^3\right)}{12(\lambda+2\mu)^3}$$

$$\mathscr{L}_{25}^{1} = k_{11}\frac{h^3\mu\left(13\lambda^4+24\mu\lambda^3-168\mu^2\lambda^2-216\mu^3\lambda-64\mu^4\right)}{6(\lambda+2\mu)^4}$$
$$+k_{22}\frac{h^3\mu\left(13\lambda^4+38\mu\lambda^3-98\mu^2\lambda^2-220\mu^3\lambda-96\mu^4\right)}{3(\lambda+2\mu)^4}$$

$$\mathscr{L}_{25}^{2} = k_{11}\frac{h^3\lambda\mu\left(5\lambda^3+7\mu\lambda^2-66\mu^2\lambda-48\mu^3\right)}{3(\lambda+2\mu)^4}$$
$$+k_{22}\frac{h^3\mu\left(23\lambda^4+93\mu\lambda^3-12\mu^2\lambda^2-192\mu^3\lambda-104\mu^4\right)}{3(\lambda+2\mu)^4}$$

$$\mathscr{L}_{25}^{3} = \mathscr{L}_{34}^{1} = \mathscr{L}_{35}^{2} = (k_{12}+k_{21})\frac{h^3\mu\left(19\lambda^3+56\mu\lambda^2-36\mu^2\lambda-48\mu^3\right)}{24(\lambda+2\mu)^3}$$

$$\mathscr{L}_{26}^{1} = (k_{12}+k_{21})\frac{h^3\mu\left(29\lambda^3+66\mu\lambda^2-140\mu^2\lambda-120\mu^3\right)}{24(\lambda+2\mu)^3}$$

$$\mathscr{L}_{26}^{2} = (k_{12}+k_{21})\frac{h^3\mu\left(17\lambda^3+44\mu\lambda^2-56\mu^2\lambda-56\mu^3\right)}{12(\lambda+2\mu)^3}$$

$$\mathscr{L}_{26}^{3} = k_{11}\frac{h^3\mu\left(4\lambda^2+7\mu\lambda+2\mu^2\right)}{12(\lambda+2\mu)^2}+k_{22}\frac{h^3\mu\left(11\lambda^2+22\mu\lambda+8\mu^2\right)}{24(\lambda+2\mu)^2}$$

$$\mathscr{L}_{34}^{2} = (k_{12}+k_{21})\frac{h^3\mu\left(8\lambda^3+21\mu\lambda^2-28\mu^2\lambda-28\mu^3\right)}{12(\lambda+2\mu)^3}$$

$$\mathscr{L}_{34}^{3} = k_{11}\frac{h^3\mu\left(5\lambda^2+10\mu\lambda+4\mu^2\right)}{12(\lambda+2\mu)^2}+k_{22}\frac{h^3\mu\left(5\lambda^2+8\mu\lambda+4\mu^2\right)}{24(\lambda+2\mu)^2}$$

$$\mathscr{L}_{35}^{1} = (k_{12}+k_{21})\frac{h^3\mu\left(8\lambda^3+21\mu\lambda^2-28\mu^2\lambda-28\mu^3\right)}{12(\lambda+2\mu)^3}$$

$$\mathscr{L}_{35}^{3} = k_{11}\frac{h^3\mu\left(5\lambda^2+8\mu\lambda+4\mu^2\right)}{24(\lambda+2\mu)^2}+k_{22}\frac{h^3\mu\left(5\lambda^2+10\mu\lambda+4\mu^2\right)}{12(\lambda+2\mu)^2}$$

$$\mathscr{L}_{36}^{1} = k_{11}\frac{h^3\mu\left(11\lambda^2+22\mu\lambda+8\mu^2\right)}{24(\lambda+2\mu)^2}+k_{22}\frac{h^3\mu\left(4\lambda^2+7\mu\lambda+2\mu^2\right)}{12(\lambda+2\mu)^2}$$

$$\mathscr{L}_{36}^{2} = k_{11}\frac{h^3\mu\left(4\lambda^2+7\mu\lambda+2\mu^2\right)}{12(\lambda+2\mu)^2}+k_{22}\frac{h^3\mu\left(11\lambda^2+22\mu\lambda+8\mu^2\right)}{24(\lambda+2\mu)^2}$$

$$\mathscr{L}_{45}^{4} = k_{11}\frac{h^5\mu\left(62\lambda^4+111\mu\lambda^3-918\mu^2\lambda^2-1808\mu^3\lambda-768\mu^4\right)}{180(\lambda+2\mu)^4}+k_{22}\frac{h^5\mu\left(25\lambda^4+18\mu\lambda^3-496\mu^2\lambda^2-784\mu^3\lambda-320\mu^4\right)}{120(\lambda+2\mu)^4}$$

$$\mathscr{L}_{45}^{5} = k_{11}\frac{h^5\mu\left(25\lambda^4+18\mu\lambda^3-496\mu^2\lambda^2-784\mu^3\lambda-320\mu^4\right)}{120(\lambda+2\mu)^4}+k_{22}\frac{h^5\mu\left(62\lambda^4+111\mu\lambda^3-918\mu^2\lambda^2-1808\mu^3\lambda-768\mu^4\right)}{180(\lambda+2\mu)^4}$$

$$\mathscr{L}_{45}^{6} = \mathscr{L}_{46}^{5} = \mathscr{L}_{56}^{4} = (k_{12}+k_{21})\frac{h^5\mu\left(143\lambda^3+290\mu\lambda^2-916\mu^2\lambda-696\mu^3\right)}{1440(\lambda+2\mu)^3}$$

$$\mathscr{L}_{46}^{4} = \mathscr{L}_{56}^{5} = (k_{12}+k_{21})\frac{h^5\mu\left(47\lambda^3+110\mu\lambda^2-214\mu^2\lambda-204\mu^3\right)}{360(\lambda+2\mu)^3}$$

$$\mathscr{L}_{46}^{6} = k_{11}\frac{h^5\mu\left(11\lambda^2+13\mu\lambda-3\mu^2\right)}{180(\lambda+2\mu)^2}+k_{22}\frac{h^5\mu\left(43\lambda^2+44\mu\lambda+36\mu^2\right)}{1440(\lambda+2\mu)^2}$$

$$\mathscr{L}_{47}^{7} = -k_{11}\frac{h^3\mu\left(943\lambda^2+2614\mu\lambda+1624\mu^2\right)}{1512(\lambda+2\mu)^2}-k_{22}\frac{h^3\lambda^2\mu}{36(\lambda+2\mu)^2}$$

$$\mathscr{L}_{47}^{8} = \mathscr{L}_{48}^{7} = -k_{12}\frac{h^3\mu(77\lambda+72\mu)}{336(\lambda+2\mu)}-k_{21}\frac{41h^3\mu(11\lambda+4\mu)}{3024(\lambda+2\mu)}$$

$$\mathscr{L}_{48}^{8} = -k_{11}\frac{h^3\lambda\mu(2\lambda+3\mu)}{18(\lambda+2\mu)^2} - k_{22}\frac{h^3\lambda\mu(137\lambda+246\mu)}{504(\lambda+2\mu)^2}$$

$$\mathscr{L}_{56}^{6} = k_{11}\frac{h^5\mu\left(43\lambda^2+44\mu\lambda+36\mu^2\right)}{1440(\lambda+2\mu)^2} k_{22}\frac{h^5\mu\left(11\lambda^2+13\mu\lambda-3\mu^2\right)}{180(\lambda+2\mu)^2}$$

$$\mathscr{L}_{57}^{7} = -k_{11}\frac{h^3\lambda\mu(137\lambda+246\mu)}{504(\lambda+2\mu)^2} - k_{22}\frac{h^3\lambda\mu(2\lambda+3\mu)}{18(\lambda+2\mu)^2}$$

$$\mathscr{L}_{57}^{8} = \mathscr{L}_{58}^{7} = -k_{12}\frac{41h^3\mu(11\lambda+4\mu)}{3024(\lambda+2\mu)} - k_{21}\frac{h^3\mu(77\lambda+72\mu)}{336(\lambda+2\mu)}$$

$$\mathscr{L}_{58}^{8} = -k_{11}\frac{h^3\lambda^2\mu}{36(\lambda+2\mu)^2} - k_{22}\frac{h^3\mu\left(943\lambda^2+2614\mu\lambda+1624\mu^2\right)}{1512(\lambda+2\mu)^2}$$

$$\mathscr{L}_{67}^{7} = -k_{12}\frac{h^3\mu(52\lambda+41\mu)}{756(\lambda+2\mu)} - k_{21}\frac{h^3\mu(25\lambda+36\mu)}{168(\lambda+2\mu)}$$

$$\mathscr{L}_{67}^{8} = \mathscr{L}_{68}^{7} = \mathscr{L}_{78}^{6} = -(k_{11}+k_{22})\frac{29h^3\mu}{432}$$

$$\mathscr{L}_{68}^{8} = -k_{12}\frac{h^3\mu(25\lambda+36\mu)}{168(\lambda+2\mu)} - k_{21}\frac{h^3\mu(52\lambda+41\mu)}{756(\lambda+2\mu)}$$

$$\mathscr{L}_{78}^{4} = -k_{12}\frac{h^3\mu(77\lambda+72\mu)}{336(\lambda+2\mu)} - k_{21}\frac{41h^3\mu(11\lambda+4\mu)}{3024(\lambda+2\mu)}$$

$$\mathscr{L}_{78}^{5} = -k_{12}\frac{41h^3\mu(11\lambda+4\mu)}{3024(\lambda+2\mu)} - k_{21}\frac{h^3\mu(77\lambda+72\mu)}{336(\lambda+2\mu)}$$

References

1. Berdichevsky, V.L.: Variational-asymptotic method of constructing a theory of shells. Prikladnaya Matematika i Mekhanika (PMM) **43**, 664–687 (1979)
2. Atilgan, A.R., Hodges, D.H.: On the strain energy of laminated composite plates. Int. J. Solids Struct. **29**(20), 2527–2543 (1992)
3. Yu, W.: Variational asymptotic modeling of composite dimensionally reducible structures. Ph.D Thesis, Aerospace Engineering, Georgia Institute of Technology, Georgia, U.S.A (2002)
4. Bouzidi, R.: Numerical solution of hyperelastic membranes by energy minimization. Comput. Struct. **82**, 1961–1969 (2004)
5. Burela, R.G., Harursampath, D.: VAM applied to dimensional reduction of non-linear hyperelastic plates. Int. J. Eng. Sci. **59**, 90–102 (2012)
6. Pietraszkiewicz, W.: Geometrically non-linear theories of thin elastic shells. Ruhr-Universitat Bochum, Mitt. Inst. fur Mechanik (1988)
7. Hodges, D.H., Harursampath, D., Volovoi, V.V., Cesnik, C.E.S.: Non-classical effects in nonlinear analysis of pretwisted anisotropic strips. Int. J. Non-Linear Mech. **34**, 259–277 (1999)
8. Hodges, D.H., Atilgan, A.R., Danielson, D.A.: A geometrically nonlinear theory of elastic plates. J. Appl. Mech. **60**(1), 109–116 (1993)
9. Yu, W., Hodges, D.H., Volovoi, V.V.: Asymptotic generalization of Reissner-Mindlin theory: accurate three-dimensional recovery for composite shells. Comput. Methods Appl. Mech. Eng. **191**(44), 5087–5109 (2002)

10. Javier Bonet, R.D.W.: Nonlinear continuum mechanics for finite element analysis. Cambridge University Press (1997)
11. Toscano, R., Dvorkin, E.: A shell element for finite strain analyses: hyperelastic material models. Eng. Comput. Int. J. Comput. Aided Eng. Softw. **24**(07), 514–535 (2007)
12. Sze, K., Zheng, S.-J., Lo, S.: A stabilized eighteen-node solid element for hyperelastic analysis of shells. Finite Elem. Anal. Design **40**(3), 319–340 (2004)

Three-Dimensional Finite Element Modelling of Free Vibrations of Functionally Graded Sandwich Panels

Vyacheslav N. Burlayenko, Tomasz Sadowski, Holm Altenbach and Svetlana Dimitrova

Abstract A three-dimensional modelling of free vibrations of functionally graded material (FGM) sandwich plates is presented. Natural frequencies and mode shapes are determined by using the finite element method within the ABAQUS code. The three-dimensional (3-D) brick graded finite element is programmed and incorporated into the code via the user-defined material subroutine UMAT. The results of modal analysis are demonstrated for square metal–ceramic functionally graded simply supported plates with a power-law through-the-thickness variation of the volume fractions of the material constituents. The through-the-thickness distributions of effective material properties at a point are defined based on the Mori–Tanaka scheme. First, exact values of natural frequencies, displacements and stresses available in the literature are used to estimate the accuracy of the developed 3-D graded finite element for FGM sandwich plates. Then, parametric studies are carried out for the frequency analysis by varying the volume fraction profile and the length-to-thickness ratio.

Keywords Functionally graded material · Sandwich panels · 3-D brick graded element · Modal analysis

V. N. Burlayenko (✉) · T. Sadowski
Department of Solid Mechanics, Lublin University of Technology,
40 Nadbystrzycka str., 20-618 Lublin, Poland
e-mail: burlayenko@yahoo.com

T. Sadowski
e-mail: t.sadowski@pollub.pl

V. N. Burlayenko
Department of Applied Mathematics, National Technical University KhPI,
2 Kyrpychova str., Kharkiv 61002, Ukraine

H. Altenbach
Institut für Mechanik, Otto-von-Guericke-Universität Magdeburg, Universitätsplatz 2,
39106 Magdeburg, Germany
e-mail: holm.altenbach@ovgu.de

S. Dimitrova
Department of Higher Mathematics, National Technical University KhPI,
2 Kyrpychova str., Kharkiv 61002, Ukraine
e-mail: s.dimitrovaburlayenko@gmail.com

H. Altenbach et al. (eds.), *Recent Developments in the Theory of Shells*,
Advanced Structured Materials 110, https://doi.org/10.1007/978-3-030-17747-8_10

1 Introduction

Composite materials such as the sandwich panels have found a widespread use in many modern engineering applications due to their excellent strength-to-weight and stiffness-to-weight ratios, acoustic and thermal insulation, corrosion and wear resistance, and the possibility of tailoring their properties for optimizing their structural responses. A conventional sandwich composite looks like as a tri-layer material consisting of two thin, stiff and strength face sheets (skins) and a thick, lightweight and soft core [1]. Such layered structure with high mismatch in material and geometrical properties between the constitutive layers leads to an inter-laminar stress concentration at the face sheet-to-core interface and, as a result, sandwich composites often suffer from premature failure caused by debonding the face sheet from the core. This issue has become one of major topics being extensively studied in sandwich constructions involving static, dynamic and fracture problems over the past two decades, e.g. in some recent papers [2–13].

FGMs combine two or more material phases with a desired grading in elastic and thermal properties achieved by changing in a controlled manner the volume fraction of the constituents. This new type of composites was originally developed as thermal barrier coatings for minimizing thermal and residual stresses and to prevent large deflections under high temperature in aerospace structures and fusion reactors [14]. In this respect, many studies have been performed to analyse the thermal mechanical behaviour of FGMs, e.g. [15–25] among of the latest. The modelling techniques used in the thermal analysis of FGMs have recently been reviewed in [26, 27]. However, since the use of FGMs is increasingly spreading on new engineering applications such as sandwich composites, which are often subjected to dynamic loads in-service time, the dynamic analysis of FGM sandwich panels is to be developed to provide their reliable exploitation. Approaches, existing in the literature for studying plates and shells made up of FGMs, use techniques and methodologies incorporated into already known methods with minimal modifications, if needed.

The problem of free vibrations of FGM sandwich panels have been solved by analytical (or semi-analytical) and numerical methods. The former ones are used the through-the-thickness assumptions of well-known plate/shell theories with a defined variation of elastic modulus along the thickness direction to obtain the solutions. As concluded in [28], a material gradient along the thickness direction leads to more complex deformations of the core as a result the use of higher order shear deformation plate/shell theories is required for accurate predictions. So-called quasi-3-D theories, accounting for the effect of both shear and normal deformations in the thickness direction, have been developed as an improvement of the 2-D theories of FGM panels, [29]. Various higher-order shear and normal deformable theories have been proposed by many researchers to analyse FG sandwich plates, e.g. [30] among the latest ones. An alternative six-field linear plate/shell model, based on a modified polar decomposition of shell deformation gradient and a vector of deviation from the linear displacement distribution, has been developed in [31, 32]. This model seems to be very useful for developing new 2-D theories accounting for stretch and

bending measures. Also, in addition to known mathematical approaches like power series expansions or asymptotic integration techniques applied for formulation of 2-D theories, a conceptually new consideration is connected with the direct approach in the theory of FGM plates and shells, as demonstrated in the series of papers [33–35]. Analytical 3-D solutions for FGM sandwich plates have also been developed, e.g. in [36, 37]. Although such approaches are associated with the complexity and require much efforts, they accurately describe complicating effects and are usually used as a benchmarks for 2-D solutions and numerical results. Besides, the complexity of analytic solutions for FGM plates which is associated with their geometry different from rectangular, can be successfully overcome by using semi-analytic approaches. For instance, a numerical-analytical approach based on R-functions theory and the Ritz method has been worked out for studying geometrically nonlinear vibrations of functionally graded shallow shells of complex planform in [38]. An approach implementing the differential transform method for free vibration analysis of non-uniform cross-section and axially functionally graded Euler-Bernoulli beams has been presented in [39].

Nevertheless, the analysis of more general FGM panel shapes and loading and boundary conditions requires the use of numerical tools such as the finite element method (FEM). Conventional finite elements are typically formulated assuming constant elastic properties over the whole element. Modelling a FGM structure with such elements, requires a fine enough mesh discretization to accurately capture the gradients in materials properties as well as the gradients in calculated strain and stress fields. As a result, such models are quite cumbersome in preparation of the input data and lead to excessive computational costs, especially in the case of 3-D modelling. To improve the efficiency of FEM, new finite elements that include the gradient in material properties at the element level have been proposed. In some of them, the element material properties have been approximated by using interpolation functions identical to those used for the displacement field as done in [40], whereas in the others the material parameters have been sampled at the Gauss points of the element, e.g. in [41].

In recent years, commercially available finite element codes such as ABAQUS, ANSYS, MSC Marc, and others have become popular among engineers and researchers due to their versatility, sufficient accuracy and their ease in use. However, all those packages present a difficulty in implementation of a spatial variation of material properties into FE models. In the present work, a 3-D brick finite element available in ABAQUS [42] is coded to carry out the 3-D analysis to model free vibrations of FGM sandwich plates. To assign a material gradient within the element, a user-defined material subroutine UMAT is exploited. A similar approach for implementation of varying material properties has been reported for 2-D plane strain elements available in ABAQUS in [43, 44], where the strain-stress state of FGM pavement and the thermomechanical behaviour of FGM plate have been analysed, respectively. Here, this idea is extended on the case of 3-D models to determine natural frequencies and mode shapes of metal–ceramic FGM sandwich plates. Simply supported rectangular FGM plates with a power-law through-the-thickness variation of the volume fractions of the material constituents are considered. The effective material properties at a point

across the thickness direction are defined based on the Mori–Tanaka approach. Exact values of natural frequencies, displacements and stresses, available in the literature for the FGM sandwich plates, are used to validate the developed 3-D graded finite element and to estimate its accuracy in the finite element predictions. Then, parametric studies are carried out to find out the effect of varying volume fraction profiles and the length-to-thickness ratio on natural frequencies and associated mode shapes.

2 Problem Statement

For the sake of completeness, the standard mechanical initial boundary value problem is briefly summarized in this section. Throughout the section we adopt the notations usual in most of the books on Continuum Mechanics, to which we address the reader for more details.

2.1 Equations of Motion

Let us consider a flat FGM sandwich panel as a 3-D deformable medium occupying the domain $\Omega \in [0, a] \times [0, b] \times [-\frac{h}{2}, +\frac{h}{2}]$ bonded by the surface $\partial\Omega \subset \Omega$ at an instant of time $t \in [0, T]$. The panel is defined in an unstressed reference configuration with respect to a rectangular Cartesian co-ordinate system $x_i = (x, y, z)$ with the z-axis aligned along the panel thickness and with the plane $z = 0$ coinciding with the mid-plane of the sandwich panel. Also, the planes $z = \pm h/2$ refer to the bottom $\partial\Omega^-$ and the top $\partial\Omega^+$ panel surfaces, respectively, where $\partial\Omega \backslash (\partial\Omega^- \cup \partial\Omega^+) = [-\frac{h}{2}, +\frac{h}{2}]$, as shown in Fig. 1a.

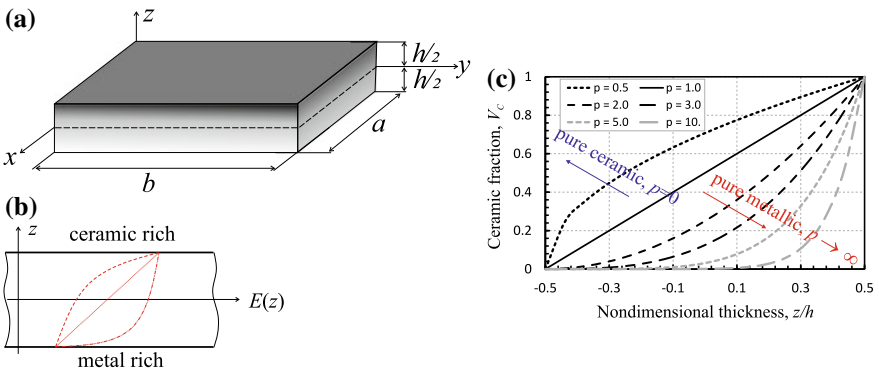

Fig. 1 Sketches of: **a** geometry of a FGM sandwich panel; **b** gradation profile across the plate thickness; and **c** variation of volume fraction function across the thickness for various values of the power-law index p

The motion of the panel is described by a displacement field $\mathbf{u}$ at time $t \in [0, T]$. Assume that during the motion the panel experiences only infinitesimal deformations with a strain measure defined by a tensor $\boldsymbol{\varepsilon} = \frac{1}{2}\left(\nabla\mathbf{u} + (\nabla\mathbf{u})^T\right)$, and the stress state associated with the deformations is described by the Cauchy stress tensor $\boldsymbol{\sigma}$. Also, the panel is subjected to prescribed displacements $\bar{\mathbf{u}}$ on the boundary $\partial\Omega_u$ and prescribed surface traction $\bar{\mathbf{t}}$ on the boundary $\partial\Omega_t$, the boundaries are such that $\partial\Omega_t \cup \partial\Omega_u = \partial\Omega$ and $\partial\Omega_t \cap \partial\Omega_u = \oslash$. Neglecting the body forces, the deformations of the sandwich panel during its motion have to obey the following system of equations [45]:

$$\begin{aligned} &\nabla \cdot \boldsymbol{\sigma} = \rho\ddot{\mathbf{u}}, && \text{in } \Omega \times [0, T] \\ &\boldsymbol{\sigma} \cdot \mathbf{n} = \bar{\mathbf{t}}, && \text{on } \partial\Omega_t \times [0, T] \\ &\mathbf{u} = \bar{\mathbf{u}}, && \text{on } \partial\Omega_u \times [0, T] \\ &\mathbf{u}(\mathbf{x}, 0) = \mathbf{u}_0(\mathbf{x}), && \text{in } \Omega \\ &\dot{\mathbf{u}}(\mathbf{x}, 0) = \dot{\mathbf{u}}_0(\mathbf{x}), && \text{in } \Omega \end{aligned} \tag{1}$$

where ρ is the density of material, and the superscript dot means a time derivative, i.e. $\dot{\mathbf{u}}$ and $\ddot{\mathbf{u}}$ stand for a velocity and an acceleration, respectively, $\mathbf{n}$ is an outward unit normal to the surface $\partial\Omega$.

Using the dynamic principle of virtual work, the system of Eqs. (1) can be rewritten in weak form as follows:

$$\int_{\Omega} (\boldsymbol{\sigma} : \nabla\delta\mathbf{u} + \rho\ddot{\mathbf{u}} \cdot \delta\mathbf{u})\, dV - \int_{\partial\Omega_t} \bar{\mathbf{t}} \cdot \delta\mathbf{u} dA = 0 \tag{2}$$

for all virtual (kinematically admissible) displacement fields $\delta\mathbf{u}$.

2.2 Constitutive Equations and FGM

Let the panel be made of a functionally graded material, which, without loss of generality, is a mixture of two material phases such as metal and ceramic. The composite material is assumed to be linearly isotropic with smoothly varying mechanical properties in the z-direction only, Fig. 1b. The constitutive equation of the linear isotropic FGM material is defined by the generalized Hooke's law:

$$\boldsymbol{\sigma} = \lambda(z)\mathrm{tr}(\boldsymbol{\varepsilon})\mathbf{I} + 2\mu(z)\boldsymbol{\varepsilon} = \mathbb{C} : \boldsymbol{\varepsilon}, \tag{3}$$

where the Lamé constants $\lambda(z)$ and $\mu(z)$ composing the elasticity tensor $\mathbb{C}$ are pointwise functions of location along the panel thickness direction. In the Voigt notation the material tensor reads as [45]:

$$\boldsymbol{C}(z) = \begin{bmatrix} 2\mu(z)+\lambda(z) & \lambda(z) & \lambda(z) & & \\ \lambda(z) & 2\mu(z)+\lambda(z) & \lambda(z) & \boldsymbol{0} & \\ \lambda(z) & \lambda(z) & 2\mu(z)+\lambda(z) & & \\ & & & \mu(z) & \\ & \boldsymbol{0} & & & \mu(z) \\ & & & & & \mu(z) \end{bmatrix} \tag{4}$$

Further, we replace the two-constituent microscopically inhomogeneous composite material by an equivalent macroscopically homogeneous FGM with effective material properties. The effective mechanical parameters of the FGM are usually evaluated based on the volume fraction distribution and the approximate shape of the dispersed phase [36]. It is assumed that the gradation of the volume fraction of ceramic phase from the bottom to top panel surfaces is determined by a power-law function as follows:

$$V_c = V_c^- + (V_c^+ - V_c^-)\left(\frac{1}{2} + \frac{z}{h}\right)^p, \tag{5}$$

where V_c^- and V_c^+ are the volume fraction of ceramic on the panel bottom and top surfaces, respectively. The case of $V_c^- = 0$ and $V_c^+ = 1$ refers to the gradation profile from pure metal on the bottom surface ($z = -h/2$) to pure ceramic on the top surface ($z = +h/2$).

There exist different approaches to estimate the effective properties of such equivalent FGM. The Mori–Tanaka homogenization method is the most popular among others in literature. In this scheme, the effective Lamé constants are computed from corresponding effective bulk modulus K and shear modulus μ as follows:

$$\begin{aligned} \frac{K-K_m}{K_c-K_m} &= V_c \Big/ \left(1 + (1-V_c)\frac{K_c-K_m}{K_m+(4/3)\mu_m}\right) \\ \frac{\mu-\mu_m}{\mu_c-\mu_m} &= V_c \Big/ \left(1 + (1-V_c)\frac{\mu_c-\mu_m}{\mu_m+f_m}\right), \end{aligned} \tag{6}$$

where $f_m = \mu_m(9K_m + 8\mu_m)/6(K_m + 2\mu_m)$; the subscripts '$m$' and '$c$' stand for the metallic and ceramic phases, respectively, and $V_m + V_c = 1$. From (5) it follows that the FGM is ceramic rich when the parameter $p < 1$ and metal rich when the parameter $p > 1$. Figure 1c shows the volume fraction variation of the ceramic phase along the panel thickness for various values of the power-law index p.

Finally, the effective mass density at a point of the FGM is calculated using the 'rule of mixture' in the form:

$$\rho(z) = \rho_m + (\rho_c - \rho_m)V_c \tag{7}$$

2.3 Finite Element Solution Procedure

A displacement-based FEM framework is used for solving the problem formulated above. Then, the actual continuous model of the sandwich panel is idealized as an assemblage of arbitrary non-overlapping finite elements $\Omega = \bigcup_{e=1}^{N} \Omega^{(e)}$ interconnected at nodal points. In each a base element the components of the displacement field are approximated by suitable interpolation functions, thus, a vector of the displacement field $\boldsymbol{u}$ at an arbitrary point of the element can be written in the matrix form as follows:

$$\boldsymbol{u}(\mathbf{x}, t) = \boldsymbol{N}(\mathbf{x})\boldsymbol{U}^{(e)}(t), \tag{8}$$

Here, the summation over all nodal points of the base element is intended. Also, $\boldsymbol{N} = [N_I(\mathbf{x})]$ is a matrix of the shape functions N_I for the displacements associated with a certain node I and $\boldsymbol{U}^{(e)}$ is a vector of the nodal unknowns.

With the adopted displacement approximation (8), the strain-displacement relations can be rewritten through the nodal unknowns in the matrix notation as the following: $\boldsymbol{\varepsilon} = \boldsymbol{B}\boldsymbol{U}$, where $\boldsymbol{B} = [B_I]$ is the matrix of gradients of the shape functions, i.e. $B_I = N_{I,\mathbf{x}}$. Inserting all these matrix relations into the variational equality (2) and taking into account a linear elastic material definition (4), we arrive at the system of semi-discrete equations of motion at the element level as:

$$\boldsymbol{M}^{(e)}\ddot{\boldsymbol{U}}^{(e)} + \boldsymbol{K}^{(e)}\boldsymbol{U}^{(e)} = \boldsymbol{F}^{(e)}, \tag{9}$$

where $\boldsymbol{M}^{(e)}$, $\boldsymbol{K}^{(e)}$ and $\boldsymbol{F}^{(e)}$ are the mass matrix, the stiffness matrix and the force vector, defined by the expressions:

$$\begin{aligned} &\boldsymbol{M}^{(e)} = \int_{\Omega^{(e)}} \rho(\mathbf{x})\boldsymbol{N}^T\boldsymbol{N}dV^{(e)}, \boldsymbol{K}^{(e)} = \int_{\Omega^{(e)}} \boldsymbol{B}^T\boldsymbol{C}(\mathbf{x})\boldsymbol{B}dV^{(e)}, \\ &\boldsymbol{F}^{(e)} = \int_{\partial\Omega^{(e)}} \boldsymbol{N}^T\bar{\mathbf{t}}dA^{(e)} \end{aligned} \tag{10}$$

Thereafter, an assembly operation $(\bullet) = \mathbb{A}_{e=1}^{N}(\circ)^{(e)}$ over all finite elements leads us to the global system of finite element semi-discrete equations of motion:

$$\boldsymbol{M}\ddot{\boldsymbol{U}} + \boldsymbol{K}\boldsymbol{U} = \boldsymbol{F}, \tag{11}$$

It should be noted that damping is not included in the dynamic system of Eq. (11). Moreover, this system still needs to be discretized in time, i.e. $[0, T] = \bigcup_n [t_n, t_{n+1}]$, where $\triangle t = t_{n+1} - t_n$ is a time increment. The governing system of Eq. (11) can be employed to study the static and free vibrations by excluding the appropriate terms. For the static (or quasi-static) analysis, the problem reduces to the system of algebraic equations:

$$\boldsymbol{K}\boldsymbol{U} = \boldsymbol{F}, \tag{12}$$

where the time t is a formal monotonically increasing parameter. In the case of free vibration analysis, the solution of the eigenvalue problem is required as follows:

$$\left(\boldsymbol{K} - \omega^2 \boldsymbol{M}\right)\boldsymbol{\phi} = 0, \tag{13}$$

where ω is an undamped circular frequency and $\boldsymbol{\phi}$ is a vector of mode shape associated with found ω. The n unknown uncoupled solutions of (13) can be rearranged into the form convenient for the frequency extraction as [46]:

$$\boldsymbol{K\Phi} = \boldsymbol{\Omega}^2 \boldsymbol{M\Phi}, \tag{14}$$

wherein the columns of the matrix $\boldsymbol{\Phi}$ are orthogonal mass-normalized eigenvectors ($\boldsymbol{\phi}_1 \ldots \boldsymbol{\phi}_n$) and $\boldsymbol{\Omega}^2 = \mathrm{diag}(\omega_1^2 \ldots \omega_n^2)$ is a diagonal matrix containing squared eigenfrequencies.

3 Three-Dimensional Graded Finite Element

The modal analysis for extraction of natural frequencies and associated mode shapes of FGM sandwich flat panels is carried out with the ABAQUS/Standard code using three-dimensional models. Conventional 3-D finite elements available in the ABAQUS finite element library do not enable to model variation of mechanical properties within the element volume. To eliminate this inconvenience, we have developed within the package environment a graded 3-D finite element incorporating gradients of material properties. For this purpose, we used as a base element either eight-node linear `C3D8` or twenty-node quadratic `C3D20` brick isoparametric finite elements, Fig. 2. Isoparametric interpolation is defined in terms of the natural coordinates (ξ, η, ζ) each spanning the range from -1 to $+1$, as shown in Fig. 2a. The node numbering convention used for these elements with either full or reduced integration is also demonstrated in Fig. 2b and c. The shape functions of both the 8-node and 20-node brick elements can be presented as follows:

$$\begin{aligned}
&N_i^{(8)} = \tfrac{1}{8}(1-\xi_i)(1-\eta_i)(1-\zeta_i), \quad \text{for } i = 1 \ldots 8 \\
&\text{and} \\
&N_i^{(20)} = -(2+\xi_i+\eta_i+\zeta_i)N_i^{(8)}, \quad \text{for } i = 1 \ldots 8, \\
&N_i^{(20)} = 2(1+\xi_i)N_i^{(8)}, \quad \text{for } i = 9, 11, 13, 15, \\
&N_i^{(20)} = 2(1+\eta_i)N_i^{(8)}, \quad \text{for } i = 10, 12, 14, 16, \\
&N_i^{(20)} = 2(1+\zeta_i)N_i^{(8)}, \quad \text{for } i = 17 \ldots 20
\end{aligned} \tag{15}$$

The spatial variation of the material parameters have been achieved by coding the user-defined material subroutine UMAT. The routine evaluates the increments of strain and stress vectors and the material Jacobian to provide an implementation of the incremental form of a defined mechanical constitutive law into the code solver. At the

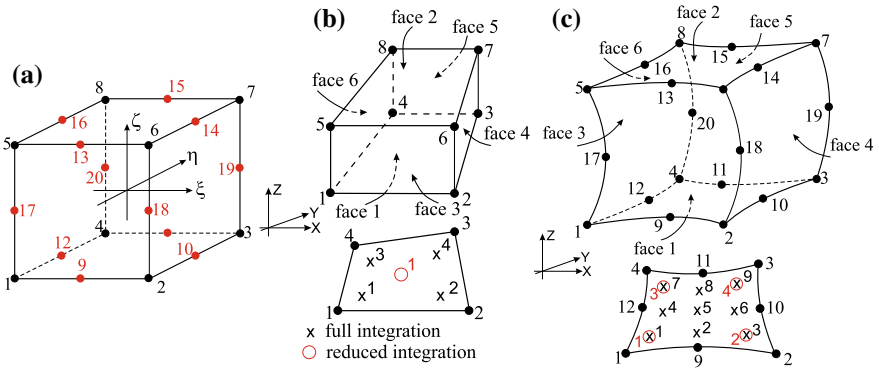

Fig. 2 Isoparametric 3-D brick finite elements after [42]: **a** master elements; **b** 8-node linear element with reduced and full integration schemes[1]; and **c** 20-node quadratic element with reduced and full integration schemes[1]. [1]Numbering of integration points for output is shown in the element layer closest to the face 1, and the integration points in the second (and third for the quadratic element) layers are numbered consecutively

end, it updates the stress and strain vectors, and other solution dependent variables over the element volume at the Gauss points, [42]. Since the material constants depend on the position within the element, the calculations of the constitutive material relation will assign the material parameters directly at different integration points of the element. Finally, by means of numerical integration of the tangential stiffness matrix of the finite element,

$$\boldsymbol{K}^{(e)} = \sum_{i=1}^{N}\sum_{j=1}^{N}\sum_{k=1}^{N} \boldsymbol{B}^T \boldsymbol{C}\boldsymbol{B} |J_{ijk}| w_i w_j w_k \tag{16}$$

the actual gradient of material properties is specified within the element. In this expression, i, j and k are the Gauss points, $|J_{ijk}|$ is the determinant of the Jacobian matrix and w_i are the Gaussian weights. The matrix $\boldsymbol{C}$ contains the material constants λ and μ depending on the position as given in (7).

To complete the development of the graded finite element, the mass density, which is also a function of position for the FGM plate, should be incorporated into the element formulation. However, there is a complication in terms of formulating the element mass matrix with sampling the density values at the Gauss points similar to (15). The frequency extraction procedure is a linear perturbation analysis in ABAQUS. The perturbations are assumed to be about the base state of a model and they ignore any inelastic effects and any parametric dependencies of the model on temperature or other field variables [42]. The code does not also provide a direct access to the elements of the mass matrix. If the latter is formed by conventional elements, the element volume is simply multiplied by a given constant mass density.

In the case of graded finite element, a constant value of the mass density is assumed to be obtained by averaging an actual density distribution over the whole volume of the FGM plate, V as follows:

$$\rho_{avg} = \frac{1}{V}\int_V \rho(\mathbf{x})dV \tag{17}$$

Thus, an effective density averaged over the plate volume is used in the free vibration analysis.

4 Numerical Results

In this section numerical results for studying the free vibration behaviour of two-constituent metallic-ceramic functionally graded sandwich plates are presented. The computer simulations have been performed on an Intel®Core™ i7-7700 CUP@3.60 GHz desktop PC with 16 GB memory and 64 bit Windows 10 operating system. In each the analysis presented below, first, convergence studies with mesh refinement have been conducted. An optimal mesh was selected from the conditions that difference between fundamental frequencies of the current and finer meshes is small enough, but from the other hand, the result should be the best compromise between computational cost and solution accuracy.

4.1 Static Analysis

The accuracy of the 3-D graded finite element programmed via UMAT in the ABAQUS environment is verified, first, performing the static analysis of a FGM sandwich plate. A simply supported Al/SiC square sandwich plate subjected to a normal pressure given by $q_0 \sin\frac{\pi x}{a}\sin\frac{\pi y}{b}$ on the top surface was considered. We accepted the parameters of (5) as $V_c^- = 0$, $V_c^+ = 1$ and $p = 2$, the plane dimensions and the thickness-to-length ratio as $a = b = 100$ and $\frac{h}{a} = 0.2$, respectively, and $q_0 = 1$ MPa. The material constants used in the calculations are listed in Table 1. The numerically calculated results are compared with those obtained analytically as reported in [36].

Table 1 Material properties of the FGM sandwich plates

FG material	Material constants
Al/SiC	$E_m = 70$ GPa; $E_c = 427$ GPa; $\nu_m = 0.3$; $\nu_c = 0.17$; $\rho_m = 2702$ kgm^{-3}; $\rho_c = 3100$ kgm^{-3}
Al/ZrO_2	$E_m = 70$ GPa; $E_c = 200$ GPa; $\nu_m = \nu_c = 0.3$; $\rho_m = 2702$ kgm^{-3}; $\rho_c = 5700$ kgm^{-3}

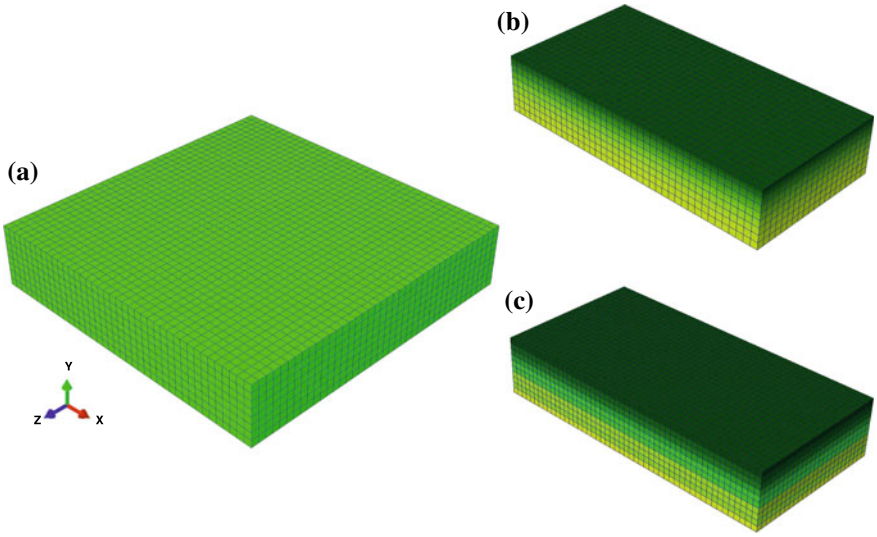

Fig. 3 Finite element model of the FGM sandwich plate: **a** general mesh; **b** half of model discretized with FGM elements; and **c** half of model discretized with homogeneous elements

A 3-D finite element model of the FGM sandwich plates, which is used in the present work, is illustrated in Fig. 3. For the sake of comparison, the mesh generated by both the developed 3-D FGM elements and the conventional homogeneous 3-D elements available in ABAQUS are also shown in Fig. 3b and c, respectively. The latter model explicitly exhibits a layered structure.

The physical quantities compared with the solutions of [36] are presented in a dimensionless form as follows:

$$\bar{u} = \frac{100E_m h^2}{q_0 a^3} u, \qquad \bar{w} = \frac{100E_m h^3}{q_0 a^4} w$$
$$(\bar{\sigma}_{xx}, \bar{\sigma}_{xy}) = \frac{10h^2}{q_0 a^2}(\sigma_{xx}, \sigma_{xy}),\ \bar{\sigma}_{xz} = \frac{10h}{q_0 a}\sigma_{xz},\ \bar{\sigma}_{zz} = \frac{\sigma_{zz}}{q_0}$$

The results of the static analysis are summarized in Table 2. A good agreement with the analytic solutions in [36] can be seen. The minor discrepancies (a relative error, Δ, %) between the results of the model with FGM elements and the reference values may relate to the problem of non-equivalency between the ways of applying boundary conditions to the plate edges in 3-D analytic and FEM models, as discussed elsewhere in literature, e.g. in [47].

The distributions of the dimensionless deflection, and longitudinal σ_{xx} and transverse normal σ_{zz} stresses through-the-thickness of the FGM sandwich plate, computed at a point $(\frac{a}{2}, \frac{b}{2}, z)$ using both the FGM elements in the continuous model and the homogeneous elements in the layered model, in comparison with the known analytic values given in [36] are shown in Fig. 4. One can see that the numerical models have very close results. While, the layered model is a bit stiffer and leads to the stepwise change of the longitudinal stress, but the transverse normal stress in

Table 2 The comparison of the results of static analysis between the present calculations and the analytic solution in [36]

	$\bar{u}$	$\bar{w}$	$\bar{\sigma}_{xx}$		$\bar{\sigma}_{xy}$	$\bar{\sigma}_{xz}$	$\bar{\sigma}_{zz}$
	$(0, \frac{b}{2}, +\frac{h}{2})$	$(\frac{a}{2}, \frac{b}{2}, 0)$	$(\frac{a}{2}, \frac{b}{2}, +\frac{h}{2})$	$(\frac{a}{2}, \frac{b}{2}, +\frac{h}{2})$	$(0, 0, +\frac{h}{2})$	$(0, \frac{b}{2}, 0)$	$(\frac{a}{2}, \frac{b}{2}, +\frac{h}{4})$
[36]	−1.7421	1.8699	1.8767	4.1042	−2.8534	2.1805	0.7623
Present							
– Graded model	−1.7051	1.8299	1.8338	3.8989	−2.6378	2.2541	0.7645
– Layered model	−1.6624	1.8198	1.7292	3.8449	−2.6142	2.2514	0.8327
Δ, %	2.13	2.14	2.29	5.0	7.56	3.38	0.29

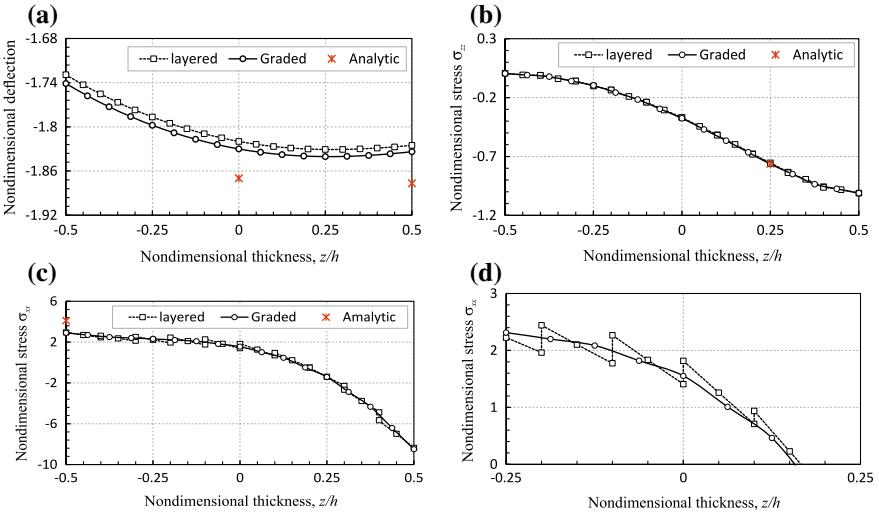

Fig. 4 The distributions of the dimensionless quantities through-the-thickness of the FGM sandwich plate at a point $(\frac{a}{2}, \frac{b}{2}, z)$: **a** deflection; **b** transverse normal stress σ_{zz}; **c** longitudinal stress σ_{xx}; and **d** zoom of the longitudinal stress σ_{xx}

the two models is indistinguishable and coincides with the analytic result. From the illustrations it is clearly seen that the deflections of the FGM sandwich plates are not symmetrical with respect to the plate midplane and the stresses have nonlinear patterns across the thickness. These conclusions are in a compliance with the results presented in [29, 37].

4.2 Free Vibration Analysis

The correctness of the developed 3-D graded finite element in conjunction with the proposed procedure of the mass density averaging for finite element modelling of free vibrations has been verified by comparing the fundamental frequency, displacements

Table 3 The comparison of the results of free vibration analysis between the present calculations and the analytic solution in [37]

	$\bar{\omega}$	$\bar{u}(0, \frac{b}{2}, +\frac{h}{2})$	$\sigma_{xx}(\frac{a}{2}, \frac{b}{2}, +\frac{h}{2})$	$\sigma_{xz}(0, \frac{b}{2}, 0)$	$\sigma_{zz}(\frac{a}{2}, \frac{b}{2}, 0)$
[37]	5.1915	−1.0099	1.2950	0.8235	1.3597
Present					
– Graded model	5.6547	−1.0788	1.3679	0.9572	1.5920
– Layered model	5.6558	−1.0637	1.3645	0.8683	1.5703
Δ, %	8.92	6.82	5.63	16.2	15.7

and stresses of a simply supported square Al/ZrO_2 sandwich plate with the results of the paper [37]. The material properties of the FGM plate are listed in Table 1. The dimensions and the parameters of the power-law material distribution given by (5) for the FGM sandwich plate are taken identical to the previous static analysis. Table 3 shows the comparisons between the reference values and the results obtained with the 3-D FGM elements and the layered model with the conventional homogeneous 3-D elements. All the represent quantities have been nondimensionalized by the formulae as [37]:

$$\bar{\omega} = \omega \frac{a^2}{h}\sqrt{\frac{\rho_m}{E_m}}, \qquad \bar{u}(z) = \frac{a}{w(\frac{a}{2}, \frac{b}{2}, 0)h}u, \quad \bar{\sigma}_{xx} = \frac{a^2}{10E_m w(\frac{a}{2}, \frac{b}{2}, 0)h}\sigma_{xx},$$
$$\bar{\sigma}_{xz} = \frac{a^3}{10E_m w(\frac{a}{2}, \frac{b}{2}, 0)h^2}\sigma_{xz}, \; \bar{\sigma}_{zz} = \frac{a^4}{10E_m w(\frac{a}{2}, \frac{b}{2}, 0)h^3}\sigma_{zz}$$

A glance at the values in Table 3 reveals that the computed results are in satisfactory agreement with those presented in [37]. The finite element solutions of the both models with FGM and homogeneous elements are almost the same, and they a bit overestimate the analytical reference values. The sources of these discrepancies could be, first, the normalization formulae involve a deflection which is not exact value itself, but being calculated. Second, not actual distribution of the mass density is implemented into the model. Finally, because of an incompatibility between the ways of applying boundary conditions in the FEM and analytical techniques. In the latter case, by assigning the boundary constraints not over the whole face of the plate edges, but using MPC constraints with node by node settings, the values of the frequency and stresses fall into a better agreement with the analytic data. Such calculations are not presented here, however, it confirms the sensitivity of the 3-D numerical results to the realization of the boundary conditions. Nevertheless, for the sake of simplicity, the calculations carried out in the present research used constraints of the nodal displacements over the whole face of each plate edge.

Also, the finite element frequency analysis revealed the existence of peculiar mode shapes associated with the natural frequencies of the thick sandwich plate. Besides usual bending or flexural shapes, the pumping or thickness-stretching modes, where the deflections are predominant and symmetric with respect to the mid-plane, in-plane or extensional modes, where one of longitudinal displacements prevails and

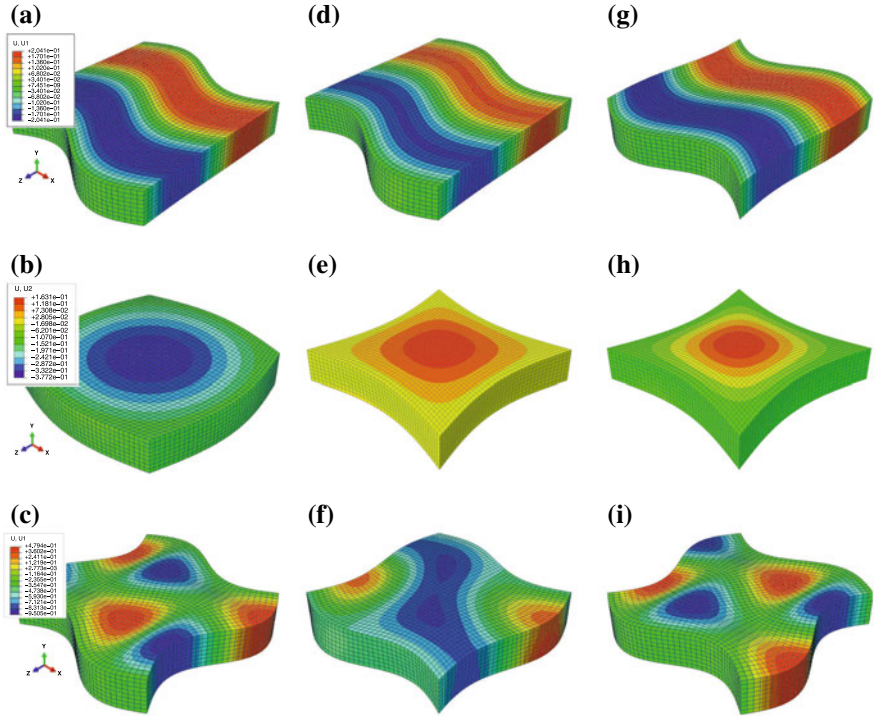

Fig. 5 In-plane, pumping and bi-inplane mode shapes of square thick: **a–c** metallic plate; **d–f** Al/ZrO_2 sandwich plate; and **g–i** ceramic plate

so-called bi-inplane modes or extensional modes, where two longitudinal displacements act simultaneously, either symmetrically or anti-symmetrically, have been observed. These types of the mode shapes and the differences between them for pure metallic, Al/ZrO_2 sandwich and pure ceramic plates are illustrated in Fig. 5.

The ability of the developed 3-D graded element to properly capture the gradation profile across the plate thickness for the frequency analysis has also been examined. The fundamental frequency of the simply supported Al/ZrO_2 square thick sandwich plate considered above is calculated for different values of the power index p. The results of calculations are compared with those known in literature, e.g. [29]. The values of the frequencies normalized by $\bar{\omega} = \omega h\sqrt{\rho_m / E_m}$ are exhibited in Table 4, where the numerical results obtained by using both the FGM elements and the homogeneous elements in the layered model are compared with the analytic solutions.

The numerical results are in a very good agreement with the analytic solutions that may confirm the accurate performance of the developed 3-D graded finite element. Moreover, it should be mentioned that due to the convergence requirement, the element size of the layered model was smaller than the graded elements as 1 mm and 2.5 mm, respectively. As a result, the total CPU time of calculations with homogeneous elements was about 3 times longer than the computations with graded elements

Table 4 The comparison of the dimensionless fundamental frequencies of the Al/ZrO_2 simply supported thick square sandwich plate for different p between the present calculations and the solutions in [29]

Power Index, p	[29]	Layered	Graded	Δ,%	
0.5		0.2293	0.2341		
1.0	0.2192	0.2268	0.2282	3.46	4.11
2.0	0.2197	0.2262	0.2262	2.97	2.95
3.0	0.2211	0.2273	0.2269	2.81	2.63
5.0	0.2225	0.2291	0.2281	2.98	2.52
10.0		0.2304	0.2273		

Table 5 The dimensionless natural frequencies of the Al/ZrO_2 simply supported thick square sandwich plate ($h/a = 0.2$) depending on the power index p

Mode	Ceramic	FGM						Metallic
		$p = 0.5$	$p = 1.0$	$p = 2.0$	$p = 3.0$	$p = 5.0$	$p = 10.0$	
(1,1)	0.2469	0.2339	0.2282	0.2262	0.2269	0.2281	0.2283	0.2121
2×In-plane	0.4535	0.4417	0.4333	0.4227	0.4162	0.4089	0.4011	0.3897
(1,2)/(2,1)	0.5421	0.5165	0.5038	0.4961	0.4947	0.4940	0.4951	0.4658
Bi-inplane	0.6413	0.6242	0.6118	0.5963	0.5873	0.5772	0.5697	0.5511
(2,2)	0.7859	0.7516	0.7331	0.7192	0.7144	0.7105	0.7097	0.6753
2×In-plane	0.9070	0.8815	0.8624	0.8394	0.8267	0.8134	0.8050	0.7793
(3,1)/(1,3)	0.9297	0.8908	0.8690	0.8510	0.8437	0.8374	0.8311	0.7989
2×Bi-inplane	1.0140	0.9848	0.9627	0.9364	0.9222	0.9078	0.8937	0.8713
Pumping	1.0770	1.0473	1.0241	0.9954	0.9795	0.9631	0.9546	0.9255
(3,2)/(2,3)	1.1251	1.0806	1.0543	1.0303	1.0193	1.0091	1.0047	0.9668

model. This demonstrates the efficiency of the 3-D graded element in the finite element predictions. The first sixteen dimensionless natural frequencies of this FGM sandwich plate depending on the power index p are computed and summarized in Table 5.

For the sake of better illustration of the power-index dependence of the natural frequencies of the Al/ZrO_2 sandwich plate, the evolutions of four frequencies with increasing the metal phase are depicted in Fig. 6. One can see that, first, quantitatively the natural frequencies of the FGM sandwich plate are between those of the same metallic and ceramic plates. Second, the power-index or an assumption about the material phase distribution through-the-thickness of the FGM sandwich plate affects its natural frequencies such that with increasing p the frequencies tend to the values close to those of the metallic plate. However, the rate of this trend is different for the lower frequencies, as illustrated in Fig. 6a and b and for the higher ones, as shown in Fig. 6c and d. The former are slightly changed at the small p and, then, slowly reduce to the frequencies of the metallic plate with growing the exponent to infinity.

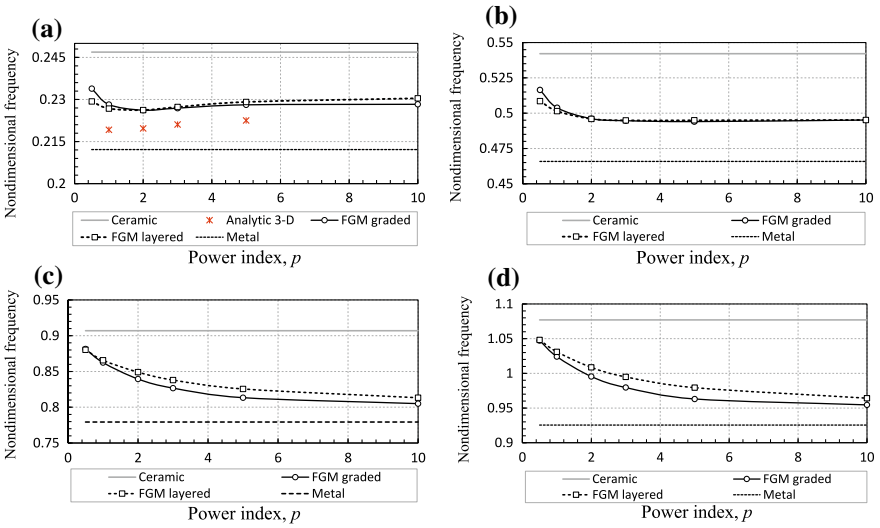

Fig. 6 The variations of the dimensionless natural frequencies of the Al/ZrO_2 square thick sandwich plate with increasing the power-index p: **a** mode (1,1); **b** mode (1, 2); **c** in-plane mode no. 9; and **d** symmetric (pumping) mode no. 14

Table 6 The comparison of the first nine dimensionless natural frequencies of the Al/ZrO_2 simply supported thin square sandwich plate ($h/a = 0.05$) between the present calculations and the analytic solution in [37]

Mode no.	1	2	3	4	5	6	7	8	9
[37]	0.0149	0.0377	0.0377	0.0593	0.0747	0.0747	0.0912	0.0913	0.1029
Present	0.0154	0.0381	0.0381	0.0603	0.0748	0.0748	0.0961	0.0961	0.1056
Δ, %	3.52	1.07	1.07	1.62	0.08	0.08	5.40	5.40	2.63

In contrast to this, the latter decrease quickly enough with increasing the metal phase and tend to the frequencies of the metal plate.

Finally, to demonstrate the influence of the side-to-thickness ratio on the free vibrations of FGM sandwich plates, we have examined a relatively thin FGM sandwich plate. A simply supported Al/ZrO_2 square sandwich plate with the ratio of $h/a = 0.05$ and with material constants identical to the thick FGM plate from the previous analysis was considered. The accuracy of the developed 3-D graded element to properly model such thin plate was verified by comparing the present results with those available in [37]. The comparisons of the first nine nondimensional natural frequencies for the exponent $p = 1$ are shown in Table 6. A good compliance between the both solutions can be seen.

It should also be noted that unlike the thick sandwich plate, the thin plate does not exhibit symmetric (pumping) modes, only flexural and extensional (in-plane and

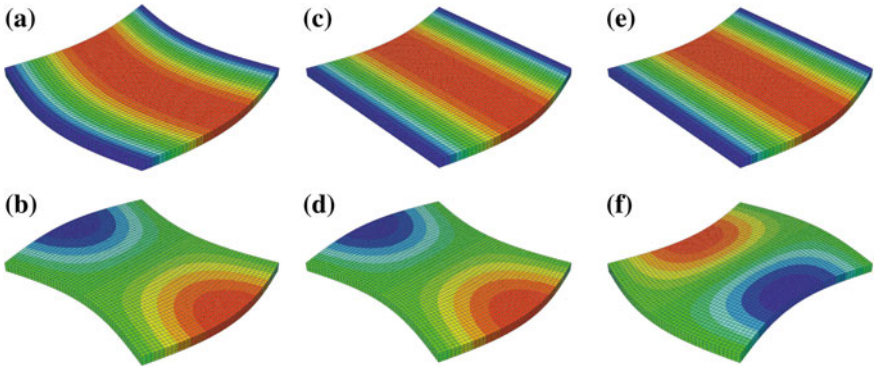

Fig. 7 In-plane and bi-inplane mode shapes of square thin: **a–b** metallic plate; **c–d** Al/ZrO_2 sandwich plate; and **e–f** ceramic plate

Table 7 The dimensionless natural frequencies of the Al/ZrO_2 simply supported thin square sandwich plate $h/a = 0.05$ depending on the power index p

Mode	Ceramic	FGM						Metallic
		$p = 0.5$	$p = 1.0$	$p = 2.0$	$p = 3.0$	$p = 5.0$	$p = 10$	
(1,1)	0.0173	0.0159	0.0154	0.0158	0.0163	0.0170	0.0169	0.0148
(1,2)/(2,1)	0.0426	0.0392	0.0381	0.0391	0.0401	0.0419	0.0417	0.0366
(2,2)	0.0673	0.0619	0.0603	0.0618	0.0634	0.0660	0.0657	0.0578
(3,1)/(1,3)	0.0835	0.07684	0.0748	0.0766	0.0785	0.0818	0.0814	0.0717
(3,2)/(2,3)	0.1073	0.0988	0.0961	0.0984	0.1008	0.1049	0.1044	0.0922
2×In-plane	0.1135	0.1079	0.1056	0.1060	0.1062	0.1076	0.1052	0.0975
(1,4)/(4,1)	0.1382	0.1274	0.1239	0.1267	0.1297	0.1349	0.1342	0.1187
(3,3)	0.1458	0.1345	0.1308	0.1337	0.1368	0.1423	0.1415	0.1253
Bi-inplane	0.1605	0.1484	0.1443	0.1474	0.1502	0.1521	0.1488	0.1379
(2,4)/(4,2)	0.1608	0.1527	0.1493	0.1499	0.1508	0.1568	0.1560	0.1382

bi-inplane) modes exist. The mode shapes corresponding to the in-plane and bi-inplane modes of the simply supported metallic, ceramic and Al/ZrO_2 thin square plates are shown in Fig. 7.

In Table 7 the first sixteen normalized natural frequencies of the Al/ZrO_2 square thin sandwich plate for different values of the exponent p are summarized. A graphical representation of the effect of the gradation profile on the four selected natural frequencies of the thin FGM sandwich plate is illustrated in Fig. 8. It is seen that the two lower frequencies are more sensitive to the gradation profile than the two higher ones. However, for the values of $p > 5$ the index-dependence is not much different for them. Moreover, comparing the changes of the frequencies with increasing p between the thick (Fig. 6) and thin (Fig. 8) simply supported Al/ZrO_2 square sandwich plates, one can conclude that the sandwich plates exhibit different dependencies

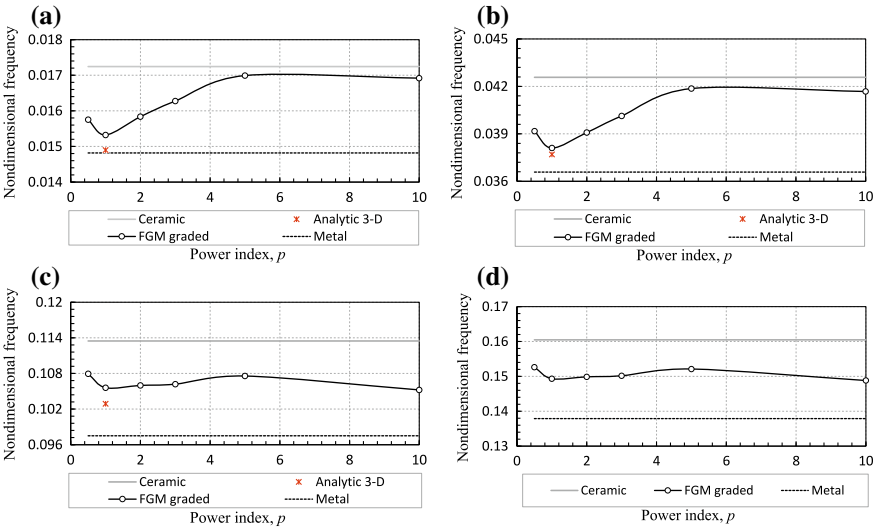

Fig. 8 The variations of the dimensionless natural frequencies of the Al/ZrO_2 square thin sandwich plate with increasing the power-index p: **a** mode (1, 1); **b** mode (1, 2); **c** in-plane mode no. 9; and **d** bi-inplane mode no. 16

on the gradation profile. Thus, the side-to-thickness ratio is an important factor for the dynamic design of FGM sandwich plates. More detailed studies of this problem are still needed, but they are out of the scope of this work.

5 Conclusions

The static response and free vibrations of simply supported thick square FGM metal–ceramic sandwich plates have been analyzed by using the three-dimensional finite element modelling with the ABAQUS code. The effective material properties at a plate point were defined based on the Mori–Tanaka scheme. A power-law variation of the volume fraction of the ceramic phase through-the-thickness of the sandwich plate was assumed. The 3-D brick graded finite element incorporating the variation of material properties in direction of the plate thickness was programmed and, then, was implemented into ABAQUS via the user-defined material subroutine UMAT. A simple procedure was proposed to estimate an average constant value of the mass density within the graded element. The use of this element in finite element predictions turned out to be very efficient since the graded element unlike the layered model with conventional homogeneous elements neither requires extensive procedure of input data preparation nor fine enough mesh, but it allowed one using the whole power of the ABAQUS code.

With the 3-D graded finite element developed and implemented into the ABAQUS code, the calculated displacements and stresses in the static analysis and the computed natural frequencies in the free vibration analysis of the FGM sandwich plates have been found to match well the analytic solutions reported in literature. The minor discrepancies between the results of the finite element models and the reference values could be addressed to the problem of non-equivalency of boundary conditions applied to the plate edges between analytic and numerical 3-D modelling procedures. Also, the predictions showed that the deflections and the values of natural frequencies of the FGM sandwich plates are between those for pure ceramic and pure metallic plates. The gradients in the material properties affect the natural frequencies of a simply supported square FGM sandwich plate. The values of the natural frequencies tend to be closer to those of a pure metallic plate. However, the lower frequencies are less sensitive to the power-law index than the higher ones. It was also found that the mode shapes associated with the frequencies of the thick sandwich plates exhibit not only flexural dominant deformations, but thickness-stretching dominant and extensional dominant deformations as well. Yet, it was found out that the side-to-thickness ratio is an important factor for the dynamic design of FGM sandwich plates. The thin FGM sandwich plate examined in the present work demonstrated the gradation profile dependency different from that of the same FGM thick plate. Finally, it needs to mention that although the present results are demonstrated only for the simply supported square metallic-ceramic FGM sandwich plate, the graded 3-D element developed here can be used for 3-D modelling sandwich plates with any other geometry, gradation profile and boundary conditions. Thus, the results presented in the paper may provide a benchmark for studying static deformation and modal dynamics of the FGM sandwich plate by other methods and models.

Acknowledgements The authors would like to mention that this research has been done within the POLONEZ 2 Project, Grant Agreement No. UMO-2016/21/P/ST8/00790, supported by the National Science Centre of Poland at the Lublin University of Technology within the European Union's Horizon 2020 research and innovation programme under the Marie Skłodowska-Curie Grant Agreement No. 665778. The third author (H. Altenbach) also would like to acknowledge the financial support of the Foundation for Polish Science for his stay at the Lublin University of Technology.

References

1. Altenbach, H., Altenbach, J., Kissing, W.: Mechanics of Composite Structural Elements, 2nd edn. Springer Nature, Singapore Pte Ltd (2018)
2. Burlayenko, VN, Sadowski, T.: Post-impact dynamic response of sandwich plates with foam and non-metallic honeycomb cores. In: Bernardini, D., Rega, G., Romeo, F. (eds.) Proceedings of the 7th European Nonlinear Dynamics Conference ENOC 2011, July 24–29, Rome, Italy, 6pp (2011)
3. Burlayenko, V.N., Sadowski, T.: Dynamic analysis of debonded sandwich plates with flexible core-Numerical aspects and simulation. In: Altenbach, H., Eremeyev, V.A. (eds.) Shell-like Structures, Advanced Structured Materials 15, pp. 415–440. Springer, Berlin, Heidelberg (2011)

4. Rinker, M., Ratcliffe, J.G., Adams, D.O., Kruger, R.: Characterizing facesheet/core disbonding in honeycomb core sandwich structure. NASA/CR-2013-217959, Langley Research Center, Hampton, Virginia (2013)
5. Burlayenko, VN, Altenbach, H, Sadowski, T.: Dynamic fracture analysis of sandwich composites with face sheet/core debond by the finite element method. In: Altenbach, H., Belyaev, A., Eremeyev, V., Krivtsov, A., Porubov A. (eds.) Dynamical Processes in Generalized Continua and Structures, Advanced Structured Materials 103, pp. 163–194. Springer, Cham (2019)
6. Burlayenko, V.N., Sadowski, T.: Simulations of post-impact skin/core debond growth in sandwich plates under impulsive loading. J. Appl. Nonlinear Dyn. **3**(4), 369–379 (2014)
7. Elmalich, D., Rabinovitch, O.: On the effect of inter-laminar contact on the dynamics of locally delaminated FRP strengthened walls. Int. J. Non-Linear Mech. **77**, 141–157 (2015)
8. Qu, Y., Meng, G.: Nonlinear vibro-acoustic analysis of composite sandwich plates with skin-core debondings. AIAA J. **55**(5), 1723–1733 (2017)
9. Idriss, M., El Mahi, A.: Effects of debonding length on the fatigue and vibration behaviour of sandwich composite. J. Compos. Mater. **51**(13), 1839–1847 (2017)
10. Burlayenko, V.N., Sadowski, T.: Linear and nonlinear dynamic analyses of sandwich panels with face sheet-to-core debonding. Shock Vib 2018, Article ID 5715863 (2018)
11. Szekrényes, A.: The role of transverse stretching in the delamination fracture of soft core sandwich plates. Appl. Math. Model. **63**, 611–632 (2018)
12. Funari, M.F., Greco, F., Lonetti, P.: Sandwich panels under interfacial debonding mechanisms. Compos. Struct. **203**, 310–320 (2018)
13. Seguel, F., Meruane, V.: Damage assessment in a sandwich panel based on full-field vibration measurements. J. Sound Vib. **417**(17), 1–18 (2018)
14. Miyamoto, Y., Kaysser, W.A., Rabin, B.H., Kawasaki, A., Ford, R.G.: Functionally Graded Materials Design, Processing and Applications. Springer, New York (1999)
15. Sadowski, T., Golewski, P.: The analysis of heat transfer and thermal stresses in thermal barrier coatings under exploitation. Defect Diffus. Forum **326–328**, 530–535 (2012)
16. Sadowski, T., Golewski, P.: Cracks path growth in turbine blades with TBC under thermo-mechanical cyclic loadings. Frattura Integr. Strutt. **10**(35), 492–499 (2016)
17. Petrova, V., Schmauder, S.: Modelling of thermal fracture of functionally graded/homogeneous bimaterial structures under thermo-mechanical loading. Key Eng. Mater. **592–593**, 145–148 (2014)
18. Burlayenko, V.N., Altenbach, H., Sadowski, T., Dimitrova, S.D.: Computational simulations of thermal shock cracking by the virtual crack closure technique in a functionally graded plate. Comput. Mater. Sci. **116**, 11–21 (2016)
19. Singh, A., Das, S., Craciun E.-M.: Effect of thermomechanical loading on an edge crack of finite length in an infinite orthotropic strip. Mech. Compos. Mater. **55**(3), 285–296 (2019)
20. Burlayenko, V.N.: Modelling thermal shock in functionally graded plates with finite element method. Adv. Mater. Sci. Eng. Article ID 7514638 (2016)
21. Gömze, L.A., Gömze, L.N.: Rheological principles of development hetero-modulus and hetero-viscous complex materials with extreme dynamic strength. IOP Conf. Ser. Mater. Sci. Eng. **175**(1), 012001 (2017)
22. Ciarletta, M., Sellitto, A., Tibullo, V.: Heat-pulse propagation in functionally graded thin layers. Int. J. Eng. Sci. **119**, 78–92 (2017)
23. Pathak, H.: Three-dimensional quasi-static fatigue crack growth analysis in functionally graded materials (FGMs) using coupled FE-XEFG approach. Theor. Appl. Fract. Mech. **92**, 59–75 (2017)
24. Zhang, H.H., Han, S.Y., Fan, L.F., Huang, D.: The numerical manifold method for 2D transient heat conduction problems in functionally graded materials. Eng. Anal. Bound Elem. **88**, 145–155 (2018)
25. Gömze, L.A., Kurovics, E.: Influence of compacting times and pressures on rheological properties of alumina and quartz ceramic powder mixtures. J. Phys. Conf. Ser. **1045**(1), 012011 (2018)

26. Swaminathan, K., Sangeetha, D.M.: Thermal analysis of FGM plates-a critical review of various modelling techniques and solution methods. Compos. Struct. **160**, 43–60 (2017)
27. Petrova, V.E., Schmauder, S.: Fracture of functionally graded thermal barrier coating on a homogeneous substrate: models, methods, analysis. J. Phys. Conf. Ser. **973**(1), 012017 (2018)
28. Zenkour, A.M.: A comprehensive analysis of functionally graded sandwich plates: part 2-Buckling and free vibration. Int. J. Solids Struct. **42**, 5244–5258 (2005)
29. Qian, L.F., Batra, R.C., Chen, L.M.: Static and dynamic deformations of thick functionally graded elastic plates by using higher-order shear and normal deformable plate theory and meshless local Petrov-Galerkin method. Compos. Part B Eng. **35**, 685–697 (2004)
30. Van Do, V.N., Lee, C.-H.: Quasi-3D higher-order shear deformation theory for thermal buckling analysis of FGM plates based on a meshless method. Aerosp. Sci. Technol. (2018) (In press)
31. Pietraszkiewicz, W., Konopińska, V.: Drilling couples and refined constitutive equations in the resultant geometrically non-linear theory of elastic shells. Int. J. Solids Struct. **51**(11–12), 2133–2143 (2014)
32. Pietraszkiewicz, W.: The resultant linear six-field theory of elastic shells: what it brings to the classical linear shell models? ZAMM-Z Angew Math Me **96**(8), 899–915 (2016)
33. Altenbach, H., Eremeyev, V.A.: Direct approach based analysis of plates composed of functionally graded materials. Arch. Appl. Mech. **78**(10), 775–794 (2008)
34. Altenbach, H., Eremeyev, V.A.: Eigen-vibrations of plates made of functionally graded material. CMC: Comput. Mater. Contin. **9**(2), 153–178 (2009)
35. Bîrsan, M., Altenbach, H.: Analysis of the deformation of multi-layered orthotropic cylindrical elastic shells using the direct approach. In: Altenbach, H., Eremeyev, V. (eds.) Shell-like Structures. Advanced Structured Materials 15, pp. 29–52. Springer, Berlin, Heidelberg (2011)
36. Vel, S.S., Batra, R.C.: Exact solution for thermoelastic deformations of functionally graded thick rectangular plates. AIAA J. **40**(7) (2002)
37. Vel, S.S., Batra, R.C.: Three-dimensional exact solution for the vibration of functionally graded rectangular plates. J. Sound Vib. **272**, 703–730 (2004)
38. Awrejcewicz, J., Kurpa, L., Shmatko, T.: Analysis of geometrically nonlinear vibrations of functionally graded shallow shells of a complex shape. Lat. Am. J. Solids Struct. **14**, 1648–1668 (2017)
39. Ghazaryan, D., Burlayenko, V.N., Avetisyan, A., Bhaskar, A.: Free vibration analysis of functionally graded beams with non-uniform cross-section using the differential transform method. J. Eng. Math. **110**, 97–121 (2018)
40. Kim, J.H., Paulino, G.H.: Isoparametric graded finite elements for nonhomogeneous isotropic and orthotropic materials. J. Appl. Mech. **69**, 502–514 (2002)
41. Santare, M.H., Lambros, J.: Use of graded finite elements to model the behavior of nonhomogeneous materials. J. Appl. Mech. **67**(4), 819–822 (2000)
42. ABAQUS User's manual, ver. 2016: Dassault Systémes Simulia Corp., Providence, RI, USA (2016)
43. Buttlar, W.G., Paulino, G.H., Song, S.H.: Application of graded finite elements for asphalt pavements. J. Eng. Mech. **132**(3), 240–248 (2006)
44. Burlayenko, V.N., Altenbach, H., Sadowski, T., Dimitrova, S.D., Bhaskar, A.: Modelling functionally graded materials in heat transfer and thermal stress analysis by means of graded finite elements. Appl. Math. Model. **45**, 422–438 (2017)
45. Timoshenko, S., Goodier, J.N.: Theory of Elasticity. McGraw-Hill, New York (1970)
46. Bathe, K.J., Wilson, E.L.: Numerical Methods in Finite Element Analysis. Prentice-Hall, Englewood Cliffs (1977)
47. Naumenko, K., Altenbach, H., Huang, C.-X., Burlayenko, V.: Influence of the element type on the accuracy of creep–damage predictions in thin-walled structures. In: Proceedings of the European Conference on Computational Mechanics (ECCM-3) June 26–29, 2001, Cracow, Poland (2001)

Recent Achievements in Constitutive Equations of Laminates and Functionally Graded Structures Formulated in the Resultant Nonlinear Shell Theory

Stanisław Burzyński, Jacek Chróścielewski, Karol Daszkiewicz, Agnieszka Sabik, Bartosz Sobczyk and Wojciech Witkowski

Abstract The development of constitutive equations formulated in the resultant nonlinear shell theory is presented. The specific features of the present shell theory are drilling rotation naturally included in the formulation and asymmetric measures of strains and stress resultants. The special attention in the chapter is given to recent achievements: progressive failure analysis of laminated shells and elastoplastic constitutive relation for shells made of functionally graded material (FGM). The modified Hashin criterion is used to estimate failure initiation in laminates and stiffness degradation approach in the last ply failure computations. The numerical results obtained for axially compressed C-shaped column are compared with experimental load-deflection curve. The Cosserat plane stress assumption, Tamura-Tomota-Ozawa (TTO) model and improved method of shear correction factor calculation are applied in the elastoplastic constitutive relation for FGM shell. The proposed formulation is tested in numerical examples: rectangular compressed plate and channel section clamped beam. The influence of TTO model parameters and Cosserat characteristic length is investigated.

1 Introduction

The resultant nonlinear shell theory was proposed in [1] and described in detail in monographs [2, 3]. In contradiction to the direct approach and the derived approach, a mixed approach was used to formulate the present shell theory. In this approach, the two dimensional (2D) equations of the shell-like body are obtained as a result of the exact through-the-thickness integration of generic equations of the three dimensional (3D) continuum mechanics. Only the constitutive relations and the Conservation of Energy, that are not exact in three dimensions, are postulated in two dimensions. In this way, all approximations in the present theory of elastic shells are thrown

S. Burzyński · J. Chróścielewski · K. Daszkiewicz (✉) · A. Sabik · B. Sobczyk · W. Witkowski
Faculty of Civil and Environmental Engineering, Department of Mechanics of Materials and Structures, Gdansk University of Technology, Narutowicza 11/12, 80-233 Gdańsk, Poland
e-mail: kardaszk@pg.edu.pl

H. Altenbach et al. (eds.), *Recent Developments in the Theory of Shells*,
Advanced Structured Materials 110, https://doi.org/10.1007/978-3-030-17747-8_11

into the constitutive equations that are approximate by nature, because they must be determined in experiments.

The 2D shell kinematics is uniquely defined on the shell reference surface M by translation vector $\boldsymbol{u}$ and rotation tensor $\boldsymbol{Q}$. Consequently, the present shell theory is also called the 6-parameter (6p) or six-field shell theory, because the deformation of any material particle is described by six independent scalar variables. The characteristic features of 6p shell model are: independent drilling rotation (about normal to the reference surface) and two work-conjugate drilling components of 2D stress and strain vectors. Hence, the drilling rotation is naturally included in the formulation and the kinematic model of the shell base surface is equivalent to the Cosserat surface [4, 5]. The measures of strains are defined on M as work-conjugate fields to the 2D stress resultants and couples obtained in through-the-thickness integration.

Brief review of what has been done in the field of constitutive relations in framework of the resultant shell theory is presented below. The linear elastic constitutive equations for thin shells were proposed in [6] and then applied in the majority of numerical studies. These equations result from the first approximation to the strain energy density [3]. The constitutive equations for the isotropic elastic shells undergoing small strains were described in [7, 8]. They were obtained from the consistent second approximation to the 2D complementary energy density. Especially, the constitutive relation expressed in orthogonal lines of principal curvatures of M and formula for the drilling bendings were derived in [7]. The constitutive model for rubber-like shells made of incompressible hyperelastic material was described in [6, 9]. The invariant properties of the strain energy density of orthotropic, hemitropic and isotropic shells were introduced in [10] based on the local symmetry group of the 6p shell theory.

The comparison of constitutive relations for the linear elastic micropolar plates proposed by Altenbach and Eremeyev [11] with the constitutive equations [6] for the resultant shell theory was presented in [12, 13]. The bounds for values of micropolar material parameters for the Cosserat plates were determined in [13]. The new elastic constitutive law for 6p shell theory was derived in the course of through-the-thickness integration of the Cosserat plane stress in [14, 15] using the Reissner-Mindlin kinematics. Two additional parameters: micropolar modulus and micropolar characteristic length were introduced into the constitutive relation. Their influence on the results was evaluated in the nonlinear numerical examples. The same approach was used in [15, 16] to obtain J_2-type elastoplastic constitutive equations. The implementation of chosen plasticity algorithm within the nonlinear resultant shell theory was described in [16]. The elastic constitutive relation for functionally graded shells was formulated with respect to the middle [17] and neutral [18] reference surface based on the assumption of 2D Cosserat plane stress in each shell lamina. The influence of the micropolar parameters and choice of the reference surface on the equilibrium paths was studied also in papers [17, 18]. Then, the material law for the functionally graded shells was extended into the elastoplastic range using Tamura-Tomota-Ozawa

(TTO) [19] mixture model. The initial results were shown in [8], while the complete description of the formulation and its verification in demanding numerical tests were presented in [20]. Recently, the 2D Cosserat type orthotropic constitutive relation for laminated shells was formulated in the 6p shell theory in [21] using the equivalent single layer (ESL) approach. The generalized orthotropic plane stress state of Cosserat type with additional transverse shear components was assumed in each layer. The effect of Cosserat parameters on First Ply Failure (FPF) onset was shown in numerical examples employing the Hashin criterion.

Another method of modeling of thin elastic composite shells in the 6p shell theory was proposed earlier in paper [22]. The orthotropic plane stress constitutive relation was generalized for strain measures of Cosserat type using only five engineering constants of classical anisotropic material. Then Tsai-Wu and Hashin failure initiation criteria were modified in [23, 24] to enable estimation of FPF load capacity of composite laminates in the nonlinear resultant shell theory. In further study [25] modified Hashin hypothesis was used in the model of progressive failure of composite shells. The elastic-brittle material behaviour with specific degradation scheme was assumed within the 6p shell theory.

In this chapter elastoplastic analysis of FGM shells and progressive failure analysis of laminated shells are presented as recent achievements in formulation of constitutive equations in the nonlinear resultant shell theory.

2 Failure Analysis of Multilayered Shells

2.1 Introduction

All engineers face a problem, which material should be chosen for the efficient design of a structure under the given design circumstances. One can select from conventional materials like steel or concrete. On the other hand, many modern and hi-tech solutions are available, as for instance: textiles, foams, functionally graded materials, fibre metal laminates, fibre reinforced plastics (FRP), etc. The new materials have a lot of benefits, they are light, robust, durable, environmental friendly, etc., if compared with the traditional ones. Although still a big number of structures to be seen in the real-life are the conventional ones, the application of the modern approaches in civil engineering has remarkably increased in the recent years. For instance in the case of laminated composites, one can find a lot of papers that confirm this trend, see [26–35].

The analysis of multi-layered shells behaviour requires selection of a method of the laminate layer stiffness description. According to [36], it is possible to use equivalent single layer 2D theories, 3D continuum approaches, or a combination of them.

We use the first one, as thin shells are considered. The stiffness of the whole laminate is described by statically equivalent single-layer shell, which macromechanical properties are calculated as a weighted average of the homogenized mechanical properties of each lamina [36].

The main aspect that we focus on is the failure of laminated shells. One can distinguish two methods of laminates damage description: the FPF and the Last Ply Failure (LPF) [37]. The moment of failure onset in the whole structure is described as FPF. The LPF occurs after FPF, when the structure is not able to sustain more loads. In order to estimate the beginning of failure appropriate criteria are used. A lot of them were formulated, for example: maximum stress/strain, Tsai-Hill, Tsai-Wu, Hashin, Puck, Cuntze, LaRC. Their validity and applicability was discussed in many papers [38–42]. For the purpose of further progressive damage calculations, that end when LPF is observed, some damage evolution descriptions need to be incorporated, as for example in [43–49].

An important thing to notice is that in most of cases the failure initiation criteria and damage evolution approaches are considered for the continuum with symmetric strain and stress measures. However, here we use the nonlinear 6p shell theory. The material law for this type of theory is specific, as asymmetric strain and stress measures appear. Therefore, the criteria and damage descriptions need to be modified to enable application of the 6p theory, see for instance [23, 25]. In the next paragraph the aspects of FPF and LPF in the 6p theory are described in more details. A numerical example to show the validity of the approach is presented as well, where we use the Hashin criterion to estimate failure initiation and stiffness degradation approach for further LPF calculations.

2.2 Progressive Failure Analysis

It is assumed that each single layer k of the laminate is a transversely isotropic medium. In the progressive failure analysis it is presumed that the failure of the layer is a brittle mechanism and that up to the failure the material response is linear elastic. Thus, following constitutive law in the material axes a-b is valid [22]:

$$\left\{\begin{array}{c}\sigma_{aa}\\ \sigma_{bb}\\ \sigma_{ab}\\ \sigma_{ba}\\ \hline \sigma_{a}\\ \sigma_{b}\end{array}\right\}_k = \left[\begin{array}{cccc|cc} \frac{E_a}{1-\nu_{ab}\nu_{ba}} & \frac{\nu_{ab}E_b}{1-\nu_{ab}\nu_{ba}} & 0 & 0 & 0 & 0 \\ \frac{\nu_{ba}E_a}{1-\nu_{ab}\nu_{ba}} & \frac{E_b}{1-\nu_{ab}\nu_{ba}} & 0 & 0 & 0 & 0 \\ 0 & 0 & 2G_{ab} & 0 & 0 & 0 \\ 0 & 0 & 0 & 2G_{ab} & 0 & 0 \\ \hline 0 & 0 & 0 & 0 & \alpha_s G_{ac} & 0 \\ 0 & 0 & 0 & 0 & 0 & \alpha_s G_{bc} \end{array}\right] \left\{\begin{array}{c}\varepsilon^{aa}\\ \varepsilon^{bb}\\ \varepsilon^{ab}\\ \varepsilon^{ba}\\ \hline \varepsilon^{a}\\ \varepsilon^{b}\end{array}\right\}_k, \tag{1}$$

or in general form:

$$\boldsymbol{\sigma}_k = \mathbf{C}_0 \boldsymbol{\varepsilon}_k$$

$$\left\{\begin{array}{c} \sigma_{aa} \\ \sigma_{bb} \\ \sigma_{ab} \\ \sigma_{ba} \\ \hline \sigma_a \\ \sigma_b \end{array}\right\}_k = \left[\begin{array}{cccc|cc} C_{11} & C_{12} & 0 & 0 & 0 & 0 \\ C_{21} & C_{22} & 0 & 0 & 0 & 0 \\ 0 & 0 & C_{33} & 0 & 0 & 0 \\ 0 & 0 & 0 & C_{44} & 0 & 0 \\ \hline 0 & 0 & 0 & 0 & C_{55} & 0 \\ 0 & 0 & 0 & 0 & 0 & C_{66} \end{array}\right] \left\{\begin{array}{c} \varepsilon^{aa} \\ \varepsilon^{bb} \\ \varepsilon^{ab} \\ \varepsilon^{ba} \\ \hline \varepsilon^{a} \\ \varepsilon^{b} \end{array}\right\}_k . \tag{2}$$

In (1) σ_{aa}, σ_{bb}, σ_{ab}, σ_{ba} and ε^{aa}, ε^{bb}, ε^{ab}, ε^{ba} are, correspondingly, in-plane stress and strain components, while σ_a, σ_b and ε^a, ε^b are the transverse shear stresses and strains. E_a and E_b stand for the longitudinal and transverse Young's moduli, ν_{ab} and ν_{ba} indicate the Poisson ratios and G_{ab}, G_{ac}, G_{bc} are the shear moduli of the material, α_s denotes the shear correction factor. In the present study α_s is equal to 5/6. As stated previously in the 6p theory σ_{ab}, σ_{ba} and ε^{ab}, ε^{ba} are in general asymmetric due to the presence of the drilling couples, which are not included in Eq. (1). In the present approach they are taken into account only in 2D balance equation [6, 7]. At the layer level only force-stresses arise, thus the constitutive law can be expressed in terms of well-known engineering constants, as proposed in [22]. This is in opposite to the approach published recently in [21], where the drilling couples together with the additional Cosserat constants are introduced into the layer constitutive equation.

The failure mechanisms, namely fiber breakage and matrix cracking, are detected with the use of the modified Hashin criterion [23, 25], which takes into account the asymmetry of stresses. The failure arises, if appropriate failure variables: F_f (fiber failure), F_m (matrix failure) approach the value 1.0. Accordingly, the fiber damage is recognized if following conditions are satisfied:

$$F_f^t = \left(\frac{\sigma_{aa}}{X_t}\right)^2 = 1.0 \quad if \quad \sigma_{aa} \geq 0, \tag{3}$$

$$F_f^c = \left(\frac{\sigma_{aa}}{X_c}\right)^2 = 1.0 \quad if \quad \sigma_{aa} < 0. \tag{4}$$

On the other hand the crack in the matrix direction is identified, if:

$$F_m^t = \left(\frac{\sigma_{bb}}{Y_t}\right)^2 + \left(\frac{\sigma_{ba}}{S_l}\right)^2 = 1.0 \quad if \quad \sigma_{bb} \geq 0. \tag{5}$$

$$F_m^c = \left(\frac{\sigma_{bb}}{2S_t}\right)^2 + \left[\left(\frac{Y_c}{2S_t}\right)^2 - 1\right]\frac{\sigma_{bb}}{Y_c} + \left(\frac{\sigma_{ba}}{S_l}\right)^2 = 1.0 \quad if \quad \sigma_{bb} < 0. \tag{6}$$

In conditions (3)–(6) X_t and X_c indicate the tensile and compressive strengths in the fiber direction, Y_t and Y_c are the tensile and compressive strengths in the matrix direction, S_l and S_t denote, respectively, the in-plane and the transverse shear strength of the layer. According to the recognized failure mechanisms the resultant components

Table 1 Stiffness degradation scheme

Failure mechanism	C_{11}	C_{22}	C_{12}	C_{21}	C_{33}	C_{44}	C_{55}	C_{66}
Fiber	0	1	0	0	1	1	0	0
Matrix	1	0	0	0	1	1	1	1
Fiber and Matrix	0	0	0	0	0	0	0	0

$\mathbf{C}_{ij}$ of the elasticity matrix (2) are rapidly reduced by making use of the following general formula

$$\mathbf{C}_{ij} = SRC \cdot \mathbf{C}_{0,ij}, \tag{7}$$

where $\mathbf{C}_{0,ij}$ are the initial values and *SRC* is a Stiffness Reduction Coefficient, taking small values, i.e. 0.01 or less. The reduction is performed according to the type of the arising failure mode. The adopted scheme of the degradation is included in Table 1, whereas 0 and 1 demonstrate, respectively, reduced and unchanged component. If both failure mechanisms occur, all in-plane as well as the transverse shear components are decreased [25]. The details of the adopted numerical algorithm are described in [25].

2.3 Numerical Example

As a representative example the analysis of axially compressed C-shaped column is presented. The problem was investigated experimentally and numerically in [50]. Figure 1 depicts the geometrical data and boundary conditions of the shell. All nodes along the top edge are kinematically coupled with respect to the displacement *v*, which

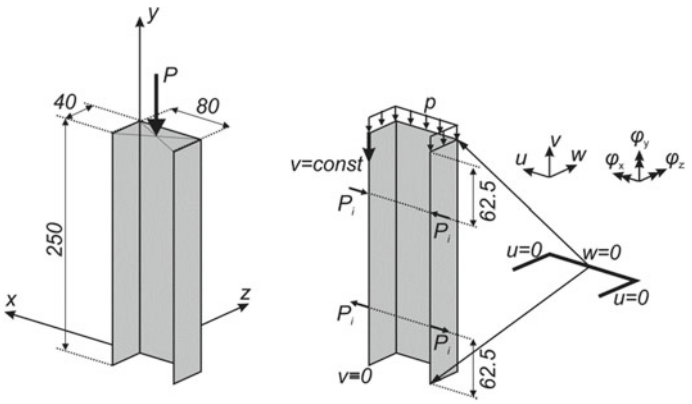

Fig. 1 C-shaped column—geometry and boundary conditions

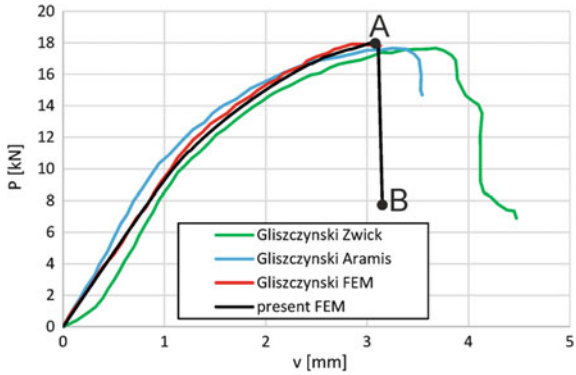

Fig. 2 C-shaped column—results

is chosen as the control parameter during the computations. The structure is made of multilayered GFRP composite with lamination scheme: $[45°/-45°/+45°/-45°]_s$, whereas the fibers orientation is measured with reference to the y–axis (Fig. 1). The layers are 0.26 mm thick and are characterized by following stiffness and strength properties: $E_a = 38.5$ GPa, $E_b = 8.1$ GPa, $G_{ab} = 2$ GPa, $v_{ab} = 0.27$, $X_t = 792$ MPa, $X_c = 679$ MPa, $Y_t = 39$ MPa, $Y_c = 71$ MPa, $S_L = 108$ MPa. In the computations it is assumed that $S_t = 0.5\ Y_c$ [25]. The value of the stiffness reduction parameter is equal to 0.01. Regular mesh of 16 FI (fully integrated) shell elements is adopted: 30 elements in the column's height direction, 6 elements along the width of the flanges and 12 elements along the web's width. In the FEM model additional small perturbation forces ($P_i = 0.002\ P$) are employed (Fig. 1), with the purpose to impose the experimentally obtained buckling mode [50].

Figure 2 illustrates the equilibrium path of the axial displacement obtained in the present analysis compared with the experimental and numerical solutions reported in [50].

Additionally in Figs. 3, and 4 the qualitative distribution of the displacements and failure variables NLF1 and NLFT are shown. The displayed contours correspond, respectively, to point A and B, see Fig. 2. NLF1 indicates the number of layers in which at least one failure mechanism is detected, whereas NLFT stands for the number of totally damaged layers. On the basis of appropriate numerical results corresponding to the presented NLFT variable distribution it can be stated, that before the collapse the maximum number of totally failed layers reaches 4, whereas after the collapse this value increases rapidly to 7–8, indicating, that in some points open cracks occur.

2.4 Conclusions

The obtained failure mode is in good agreement with the experimental one reported in [50]. It is observed, that the numerically estimated limit load of the shell agrees

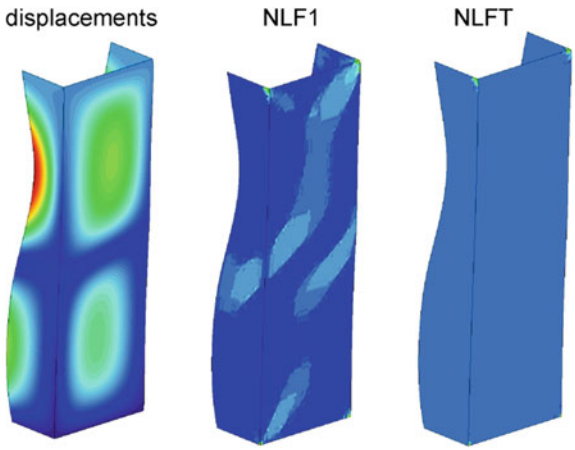

Fig. 3 Displacements, NLF1 and NLFT variable distribution before the collapse (point A)

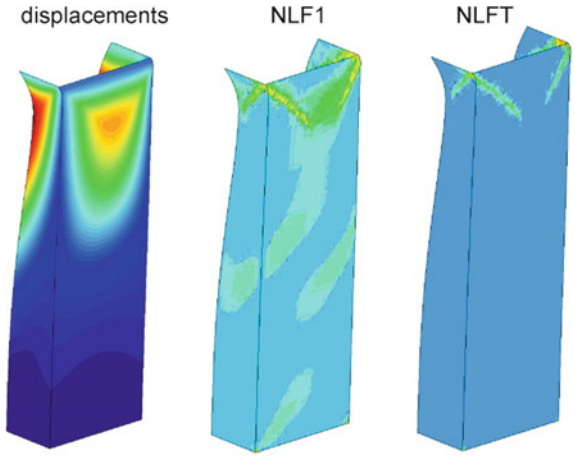

Fig. 4 Displacements, NLF1 and NLFT variable distribution after the collapse (point B)

with the experimental results, see Fig. 2. However, the collapse in the FEM model arises at slightly lower shortening of the column. It can be supposed, that it is due to the neglect of the in-plane shear nonlinearity effect [51] in the numerical model. This phenomenon can be pronounced in the case of the analyzed angle-ply lamination arrangement. Unfortunately, owing to the lack of the data concerning the nonlinear in-plane shear behavior of the considered material, there is no possibility to take it into account in the numerical model.

3 Elastoplastic Analysis of FGM Shells

3.1 Introduction

The idea of functionally graded materials (FGMs) characterized by continuous change in composition of constituents materials in the given direction was introduced in [52]. Here the gradient of material properties is assumed along the shell thickness. The national projects performed by Japanese scientists in the 80s and 90s started intensive development of FGMs. The characteristic for composite laminates problems of delamination and stress concentration on the material interfaces almost disappear in the case of FGMs. The advantage of the most popular ceramic-metal combination is connection of high mechanical strength, toughness with high resistance to heat, oxidation and corrosion. The functionally graded materials are used in different sectors of industry, e.g. aerospace, manufacturing, energy and defense. The review of what has been done in stress, vibration and stability analyses of FGM plates is presented in [53, 54].

The elastoplastic analysis is necessary to determine approximate load capacity of FGM structures. The first analyses of functionally graded ceramic-metal interlayer in the elastoplastic range were performed in [55, 56]. The FGM constitutive parameters were computed using modified rule of mixtures—TTO model [19] in papers [55, 56] and the majority of further studies. The extension of TTO model taking into account exponential hardening of metal constituent was proposed and tested in [57]. The further studies concentrated on elastoplastic behavior of functionally graded: circular plates [58, 59], rectangular plates [60, 61], cylindrical shells [62, 63], spherical vessels [64, 65], hemispherical and hyperboloidal shells [66]. Recently the size effect for FGMs in the elastoplastic range was evaluated in [67]. In our previous work [20] new results for example of irregular shell—box section were shown.

3.2 Elastoplastic Constitutive Relation

The formulation of elastoplastic constitutive equations of functionally graded shells of Cosserat type was described in detail in [20]. Here, a brief description of the constitutive relation and necessary aspects to present numerical results are presented below.

Cosserat plane stress

The Cosserat plane stress is assumed in each lamina of the shell section during formulation of the constitutive equations. The plane stress relation between the vectors of the generalized strains $\mathbf{e}$ and stresses $\boldsymbol{\sigma}$ takes the following form in the present shell theory, see e.g. [14, 18]

$$\boldsymbol{\sigma} = \begin{Bmatrix} \sigma_{11} \\ \sigma_{22} \\ \sigma_{12} \\ \sigma_{21} \\ m_1 \\ m_2 \end{Bmatrix} = \left[\begin{array}{c|c} \mathbf{C}_{mm} & \mathbf{C}_{md} \\ \hline \mathbf{C}_{dm} & \mathbf{C}_{dd} \end{array}\right] \mathbf{e} = \left[\begin{array}{cccc|cc} Ea_1 & Ea_2 & 0 & 0 & 0 & 0 \\ Ea_2 & Ea_1 & 0 & 0 & 0 & 0 \\ 0 & 0 & G\mu_1 & G\mu_2 & 0 & 0 \\ 0 & 0 & G\mu_2 & G\mu_1 & 0 & 0 \\ \hline 0 & 0 & 0 & 0 & 2Gl^2 & 0 \\ 0 & 0 & 0 & 0 & 0 & 2Gl^2 \end{array}\right] \begin{Bmatrix} \varepsilon_{11} \\ \varepsilon_{22} \\ \varepsilon_{12} \\ \varepsilon_{21} \\ \varepsilon_1 \\ \varepsilon_2 \end{Bmatrix}, \tag{8}$$

where $a_1 = \frac{1}{1-\nu^2}$, $a_2 = \nu a_1$, $\mu_1 = \frac{1}{1-N^2}$, $\mu_2 = \frac{1-2N^2}{1-N^2}$. Two Cosserat parameters are introduced in (8): the micropolar characteristic length l and the Cosserat coupling number N, see e.g. [68].

TTO formulation

In the paper the variation of the material through the shell thickness is described by the power law

$$V_{\mathrm{c}} = (z/h_0 + 0.5)^n, \quad V_{\mathrm{m}} = 1 - V_{\mathrm{c}}, \quad n \geq 0, \tag{9}$$

where V_{c} and V_{m} denote the volume fraction of ceramic (c) and metal (m) constituents, respectively. Here the shell reference surface is assumed on the middle surface, thus thickness coordinate $z \in \langle -h^-, h^+ \rangle$, where $h^- = h^+ = 0.5h_0$.

The Tamura-Tomota-Ozawa model (see e.g. [19, 62, 63]) is used to compute the material properties distribution through the shell thickness. The elastic properties are given by the equations

$$E(z) = \left(\frac{q + E_c}{q + E_m} E_m V_m + E_c V_c\right) / \left(\frac{q + E_c}{q + E_m} V_m + V_c\right), \tag{10}$$

$$\nu(z) = \nu_c V_c + \nu_m V_m, \; G(z) = \frac{E(z)}{2(1 + \nu(z))}, \tag{11}$$

where q denotes the so-called [62, 69] ratio of stress to strain transfer. The micropolar characteristic length is determined in the same way as the Poisson's ratio

$$l(z) = l_c V_c + l_m V_m. \tag{12}$$

The constant value of the Cosserat parameter N is assumed along the thickness. The effective yield stress σ_Y^0 and the multilinear hardening modulus H are calculated as follows

$$\sigma_Y^0(z) = \sigma_{Ym}^0 \left(\frac{q + E_m}{q + E_c} \frac{E_c}{E_m} V_c + V_m\right), \tag{13}$$

$$H(z) = \left(\frac{q + E_c}{q + H_m} H_m V_m + E_c V_c\right) / \left(\frac{q + E_c}{q + H_m} V_m + V_c\right). \tag{14}$$

Elastic constitutive relation of FGM shell

The relation between the strain vector $\boldsymbol{\varepsilon} = \{\boldsymbol{\varepsilon}_m \mid \boldsymbol{\varepsilon}_s \mid\mid \boldsymbol{\varepsilon}_b \mid \boldsymbol{\varepsilon}_d\}^{\mathrm{T}}$ at the shell reference surface and the membrane components of strains $\mathbf{e}_m$ at the shell lamina is assumed in the following form

$$\mathbf{e}_m = \boldsymbol{\varepsilon}_m + z\boldsymbol{\varepsilon}_b. \tag{15}$$

based on the First Order Shear Deformation Theory (FOSDT). The constant value of the drilling components of strains $\mathbf{e}_d$ is presumed in the shell section $\mathbf{e}_d = \boldsymbol{\varepsilon}_d$.

The stress and couple resultants $\mathbf{s}$ are derived by numerical integration of stresses through the shell thickness. The Gauss-Legendre quadrature rule was used in the computations. The following form of elastic constitutive matrix $\mathbf{C}^e$ was obtained in [20]

$$\mathbf{s} = \begin{Bmatrix} \mathbf{s}_m \\ \mathbf{s}_s \\ \mathbf{s}_b \\ \mathbf{s}_d \end{Bmatrix} = \mathbf{C}^e\boldsymbol{\varepsilon} = \begin{bmatrix} \mathbf{A}_{mm} & \mathbf{0} & \mathbf{B}_{mb} & \mathbf{0} \\ \mathbf{0} & \mathbf{D}_{ss} & \mathbf{0} & \mathbf{0} \\ \mathbf{B}_{bm} & \mathbf{0} & \mathbf{E}_{bb} & \mathbf{0} \\ \mathbf{0} & \mathbf{0} & \mathbf{0} & \mathbf{H}_{dd} \end{bmatrix} \begin{Bmatrix} \boldsymbol{\varepsilon}_m \\ \boldsymbol{\varepsilon}_s \\ \boldsymbol{\varepsilon}_b \\ \boldsymbol{\varepsilon}_d \end{Bmatrix}, \tag{16}$$

where the matrices $\mathbf{A}_{mm}, \mathbf{B}_{mb}, \mathbf{B}_{bm}, \mathbf{E}_{bb}, \mathbf{H}_{dd}$ are defined as

$$\mathbf{A}_{mm} = \int_{-h^-}^{+h^+} \mathbf{C}_{mm}\, dz, \mathbf{B}_{mb} = \mathbf{B}_{bm}^T = \int_{-h^-}^{+h^+} \mathbf{C}_{mm}\, z\, dz, \tag{17}$$

$$\mathbf{E}_{bb} = \int_{-h^-}^{+h^+} \mathbf{C}_{mm} z^2\, dz,\ \mathbf{H}_{dd} = \int_{-h^-}^{+h^+} \mathbf{C}_{dd} dz. \tag{18}$$

The shear components are treated as purely elastic in the present shell theory and the constitutive matrix for these components is computed as

$$\mathbf{D}_{ss} = \alpha_s \int_{-h^-}^{+h^+} \mathbf{C}_{ss}\, dz\,,\ \mathbf{C}_{ss} = \begin{bmatrix} G(z) & 0 \\ 0 & G(z) \end{bmatrix}, \tag{19}$$

where α_s is the shear correction factor. In our previous papers [8, 18, 20] the value 5/6 or 1 was assumed for α_s. Here improved approach (see e.g. [70, 71]) that takes into account asymmetric distribution of the transverse shear strains $\gamma_{\alpha 3}$ ($\alpha = 1, 2$) is employed. The state of cylindrical bending of the FGM shell is assumed in the following derivations. The transverse strain energy due to the non-uniform distribution of shear stress $\tau_{\alpha 3}$ is given by formula

$$U_\alpha = \frac{1}{2}\int_{-h^-}^{+h^+} \tau_{\alpha 3}(z)\gamma_{\alpha 3}(z)dz = \frac{1}{2}\int_{-h^-}^{+h^+} \frac{\tau_{\alpha 3}^2(z)}{G(z)}dz. \tag{20}$$

The transverse shear stress may be computed as follows

$$\tau_{\alpha 3}(z) = \frac{Q^{\alpha}}{D^{n}_{FGM}} f(z),\ f(z) = \int_{-h^{-}}^{z} \frac{E(\zeta)}{1-\nu(\zeta)^2}(\zeta - \zeta_0)d\zeta, \tag{21}$$

where Q^{α} is shear force, ζ_0 the distance between the middle and neutral surface [18, 72] and D^{n}_{FGM} bending stiffness computed with respect to the neutral surface

$$D^{n}_{FGM} = \int_{-h^{-}}^{+h^{+}} \frac{E(z)}{1-\nu(z)^2}(z-\zeta_0)^2 dz. \tag{22}$$

The substitution of (21) into (20) gives

$$U_{\alpha} = \frac{1}{2}\int_{-h^{-}}^{+h^{+}} \frac{\tau^2_{\alpha 3}(z)}{G(z)}dz = \frac{1}{2}\left(\frac{Q^{\alpha}}{D^{n}_{FGM}}\right)^2 \int_{-h^{-}}^{+h^{+}} \frac{[f(z)]^2}{G(z)}dz. \tag{23}$$

The transverse strain energy may be also expressed by average shear strain $\bar{\gamma}_{\alpha 3}$

$$\bar{U}_{\alpha} = \frac{1}{2}Q^{\alpha}\bar{\gamma}_{\alpha 3} = \frac{(Q^{\alpha})^2}{2\alpha_s \bar{G}},\ \bar{G} = \int_{-h^{-}}^{+h^{+}} G(z)dz. \tag{24}$$

Equality $U_{\alpha} = \bar{U}_{\alpha}$ yields the following formula for the shear correction factor

$$\alpha_s = \frac{\left(D^{n}_{FGM}\right)^2}{\bar{G}\int_{-h^{-}}^{+h^{+}} \frac{[f(z)]^2}{G(z)}dz}. \tag{25}$$

The integrals in (25) were computed numerically using the Gauss-Legendre quadrature. The integrals D^{n}_{FGM}, $f(z)$, $\bar{G}$ for FGM section with properties computed based on rule of mixture ($q = \infty$) may be calculated analytically, see [72].

Plasticity with linear isotropic hardening for FGM shell of Cosserat type

The yield function based on J_2 flow theory is assumed in the form

$$f = \sqrt{3J_2} - \sigma_Y(\bar{\dot{\varepsilon}}^{\mathrm{p}}), \tag{26}$$

where J_2 is the second invariant of deviatoric stress tensor. The generalized form of J_2 for the Cosserat plane stress may be written as (see e.g. [16, 20, 73])

$$J_2 = \frac{1}{3}\left(\sigma^2_{11} + \sigma^2_{22} - \sigma_{11}\sigma_{22} + \frac{3}{4}\left(\sigma^2_{12} + \sigma^2_{21}\right) + \frac{3}{2}\sigma_{12}\sigma_{21} + \frac{3}{2l^2}\left(m^2_1 + m^2_2\right)\right). \tag{27}$$

The effective plastic strain is defined as

$$\bar{\dot{\varepsilon}}^{\mathrm{p}} = \left[\frac{2}{3}\left((\dot{e}^{p}_{11})^2 + (\dot{e}^{p}_{22})^2\right) + \frac{1}{3}(\dot{e}^{p}_{12})^2 + \frac{2}{3}\dot{e}^{p}_{12}\dot{e}^{p}_{21} + \frac{1}{3}(\dot{e}^{p}_{21})^2 + \frac{2}{3}\left((\dot{\kappa}^{p}_{1})^2 + (\dot{\kappa}^{p}_{2})^2\right)\right]^{1/2}, \tag{28}$$

where the dot denotes the time derivative and $\dot{e}_{ij} = \dot{\varepsilon}_{ij} - \frac{1}{3}\delta_{ij}\dot{\varepsilon}_{kk}$ is the deviatoric strain.

Associated plastic flow rule and isotropic linear hardening are employed in the current formulation

$$\dot{\boldsymbol{\varepsilon}}^{\mathrm{p}} = \dot{\gamma}\frac{\partial f}{\partial \boldsymbol{\sigma}},\ \sigma_Y(\bar{\varepsilon}^{\mathrm{p}}) = \sigma_Y^0 + H\bar{\varepsilon}^{\mathrm{p}},\ H = \frac{\partial f}{\partial \Delta\dot{\gamma}}. \tag{29}$$

In the computations the consistent elastoplastic modulus $\mathbf{C}^{ep}$ is used in the form proposed by De Borst [73]

$$\dot{\boldsymbol{\sigma}} = \left[\mathbf{H} - \frac{\mathbf{N}^{\mathrm{T}}\mathbf{H}\mathbf{H}\mathbf{N}}{\mathbf{N}^{\mathrm{T}}\mathbf{H}\mathbf{N} - H}\right]\dot{\boldsymbol{\varepsilon}} = \mathbf{C}^{ep}\dot{\boldsymbol{\varepsilon}},\ \mathbf{a} = \frac{\partial f}{\partial \boldsymbol{\sigma}}, \tag{30}$$

where

$$\mathbf{N} = \frac{\partial f}{\partial \boldsymbol{\sigma}}, \mathbf{H} = \left[\mathbf{1} + \Delta\gamma\mathbf{C}^e\frac{\partial \mathbf{N}}{\partial \boldsymbol{\sigma}}\right]^{-1}\mathbf{C}^e,\ \Delta\gamma = \bar{\varepsilon}^{\mathrm{p}}. \tag{31}$$

The closest point projection (CPP) algorithm (see, e.g. [74, 75]) is used in numerical integration of the elastoplastic constitutive relations. The system of incremental equations is solved using the Newton method. The application of CPP procedure in the framework of the present shell theory is described in detail in [16].

3.3 Numerical Examples

The computations for nonlinear benchmark problems were performed with the own FEM code CGM, written in Fortran. The 16-node shell elements (CAMe16) [6] with full 4×4 Gauss-Legendre integration scheme were used in the numerical analyses.

Rectangular plate under in-plane compression

The first test is an example of rectangular plate subjected to a uniform axial compression, supported on the whole edge. This test for FGM plate was analyzed in papers [20, 61] for six variants which differ in assumed ratios of plate dimensions and thickness. In the present paper, the variant F ($b/h_0 = 80$, $a/b = 2.625$) with complex nonlinear behavior is analyzed. In comparison to paper [20], where the present shell theory and numerical code were used, following changes are introduced: factor α_s is calculated for each n individually and initial imperfection is calculated as

$$w_0 = w_0^{\max}\sin\frac{\pi x}{a}\sin\frac{\pi y}{b},\ w_0^{\max} = 0.001b, \tag{32}$$

not as static solution obtained for imperfection imposed at middle point of the plate [20]. Main goal of current study is to give insight into plate's limit force and post-buckling deformation for different values of imperfection amplitude.

The boundary conditions, uniform load, geometry and mesh 24×8 of CAMe16 elements are presented in Fig. 5. Only the quarter of the plate is analyzed, due to assumed double symmetry of the task. The material parameters are set as follows: $E_c = 340\,\text{GPa}$, $E_m = 206.2\,\text{GPa}$, $v_c = 0.35$, $v_m = 0.3$, $l_c = l_m = 0.0001\,\text{mm}$, $N = \sqrt{2}/2$, $H_m = 0, \sigma^0_{Ym} = 250\,\text{MPa}, q = 4.5\,\text{GPa}$. Load is defined as $p = \lambda \cdot p_{ref}$, where $p_{ref} = \sigma^0_{Ym} \cdot h_0$. Here 7-point Gauss-Legendre quadrature was used in the through-the-thickness integration.

The comparison of current and reference solutions is presented in Fig. 6. The limit load of FGM plate becomes lower with the increase of parameter n, because of greater volume fraction of the weaker metal constituent. Very good agreement for most curves is observed. For three cases ($n = 5.0$, purely ceramic and metallic plates) agreement is not perfect, what can be explained by path drawn with respect to w_B displacement (Fig. 6, right graph). In those cases, initial imperfection deepens while loading proceeds in the reference solution, while in current solution middle point deflection tends to revers it's direction.

In further study, cases $n = 0.5$ and $n = \text{inf.}$ (metallic plate) are investigated. Their behavior change with respect to initial deformation amplitude value is analyzed, namely initial value of $w_0^{\max}$ is varied in range from $0.001b$ to $0.02b$. Figure 7 presents equilibrium curves with respect to the deflection at point B in series of analysis. In both series, in case $w_0^{\max} = 0.01b$ the highest limit load is achieved. For $n = \text{inf.}$ limit load is 14% higher than for $w_0^{\max} = 0.001b$ case and for $n = 0.5$ this increase equals 11%. Figure 8 shows final achieved configurations for different

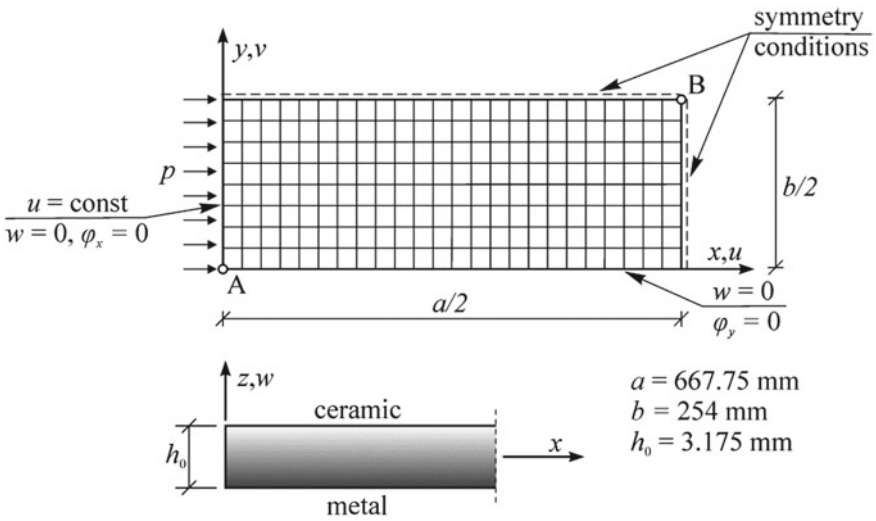

Fig. 5 Rectangular compressed plate: geometry, mesh, boundary conditions and load

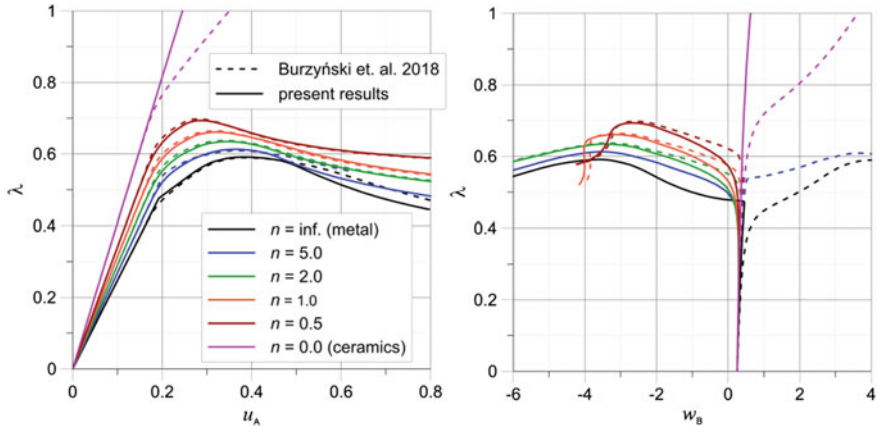

Fig. 6 Rectangular compressed plate: influence of power law exponent n on equilibrium paths, comparison of reference solution [20] with present results

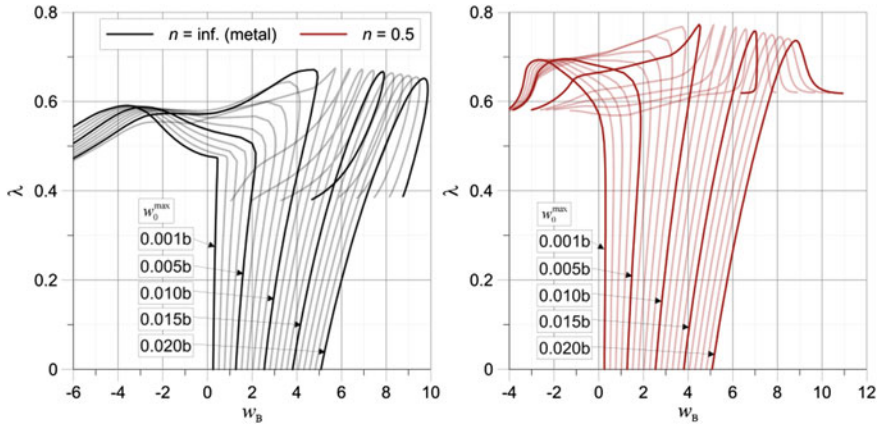

Fig. 7 Rectangular compressed plate: influence of initial deformation amplitude value on load-deflection curves

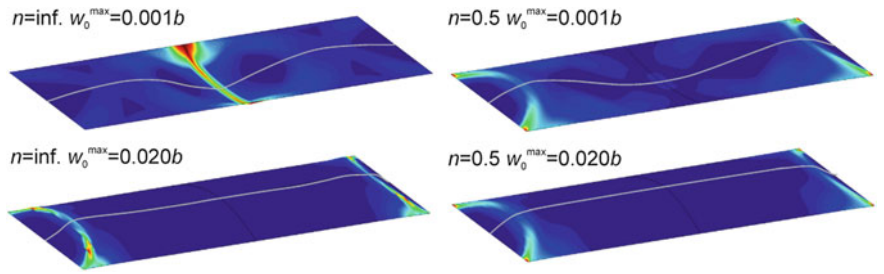

Fig. 8 Rectangular compressed plate: deformation and contour plot of $\dot{\bar{\varepsilon}}^{p}$ at the end of analysis

analysis, with contour plots of $\dot{\bar{\varepsilon}}^{p}$ (through-the-thickness envelopes). Plastic zones in every case cover almost whole plates, but some narrow zones of the highest values of effective plastic strain could be recognized. Symmetry line deformation, distinguished with grey color, reveals different mid-point (B) deflection in showed cases.

Channel section clamped beam

The nonlinear resultant shell theory is especially dedicated to the analysis of multifold shell structures containing branches and orthogonal intersections due to the problem of the drilling degree of freedom. The example of such structure is fully clamped short channel section beam loaded by concentrated force P at point A, see Fig. 9. This benchmark was originally proposed in paper [6] for homogenous isotropic shell. Then it was analyzed in the elastoplastic range in [16, 76, 77]. The nonlinear elastic analysis of FGM channel section clamped beam was performed in [17]. Here for the first time this example is investigated in the elastoplastic range for FGM section.

The material properties for ceramic and metal constituents $E_c = 3.75 \times 10^5$, $E_m = 1.07 \times 10^5$, $\nu_c = 0.14$, $\nu_m = 0.34$, $H_m = 4600$, $\sigma_{Ym} = 450$, $q = 4500$ are assumed taking into consideration data from paper [57]. The computations are performed for the following default values of Cosserat parameters $N = \sqrt{2}\Big/2$, $l_m = l_c = 1.5 \cdot 10^{-4}$. Ten times greater in-plane dimensions (Fig. 9) and thirty times greater shell thickness $h_0 = 1.5$ than in the original version of test are assumed to obtain coupling of local and global loss of stability with the plastic deformation. The regular $(4 + 8 + 4) \times 36$ mesh of CAMe16 elements, shown in Fig. 9, was used in the Author's code CGM. The corresponding discretization $(6 + 12 + 6) \times 54$ of eight-node shell elements S8R with reduced integration of matrices was generated in the commercial code Abaqus [78]. The FGM section was modelled in Abaqus by laminate section consisting of 30 layers of equal thickness with 3 integration points per layer. The material properties were computed in the centre of each layer

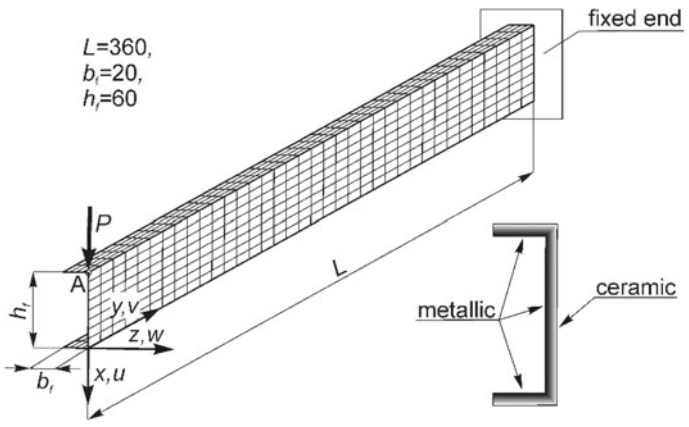

Fig. 9 Channel section beam: geometry, mesh $(4 + 8 + 4) \times 36$, boundary conditions and load

according to formulas (10)–(14). Integration of constitutive equations in Author's FEM code was performed using 9-point Gauss-Legendre quadrature. The relatively big number of integration points was used to obtain converged solution.

The equilibrium paths were obtained using displacement control method with the control deflection u_A of point A (Fig. 9). The influence of the power-law exponent n on the load-deflection curves was investigated in the Author's and Abaqus code. The very good agreement between our equilibrium paths and reference curves is observed in Fig. 10. In the case of FGM sections the loss of stability occurs for greater value of u_A than for metallic section.

Further computations were performed for $n = 2.0$. The influence of ratio of stress to strain transfer q on the equilibrium paths is shown in Fig. 11. It is visible that with increase of the parameter q the shell section becomes stiffer and has larger load capacity. Similar as in previous papers [16–18] the influence of characteristic length on the results is observed for values greater than shell thickness, see Fig. 12. For $l_m = l_c = 10h_0$ more than two times bigger limit load was obtained than for default value of l. Moreover, increase of the parameter l changes shape of the equilibrium path, because limit load point is observed for significantly lower value of deflection u_A. Change of characteristic length for only one constituent material shows that the parameter l_m affects the shape of the load-deflection curve. The parameter N has very limited influence on the results, thus it is not presented here.

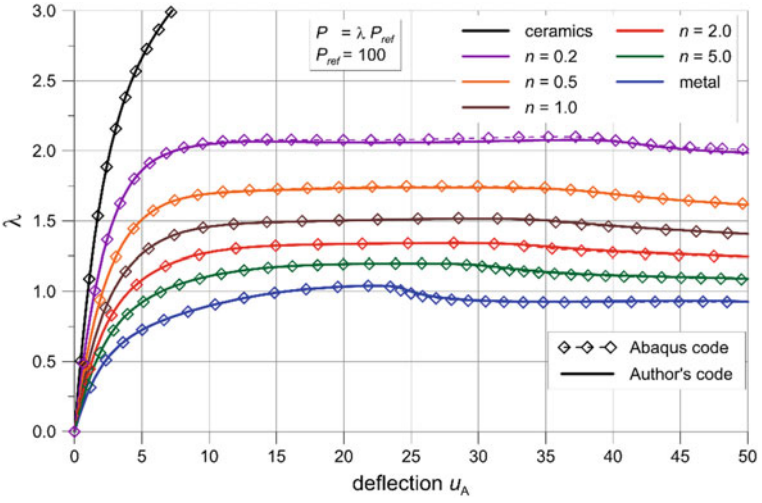

Fig. 10 Channel section beam: influence of the power law exponent n on load-deflection curves

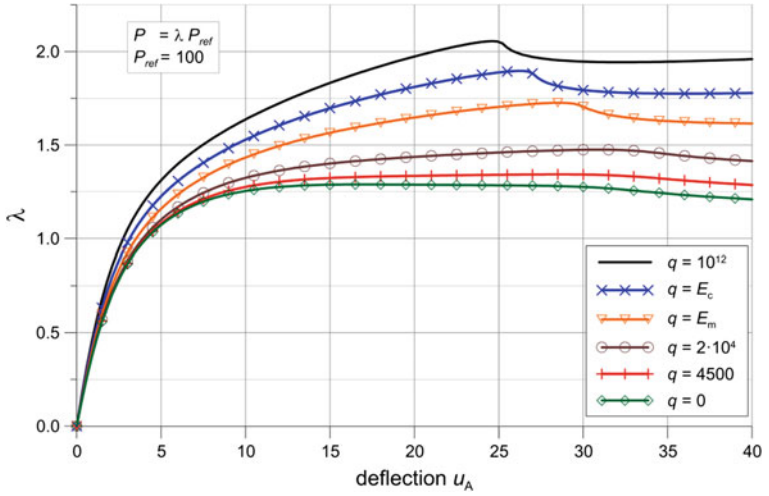

Fig. 11 Channel section beam: influence of parameter q on load-deflection curves

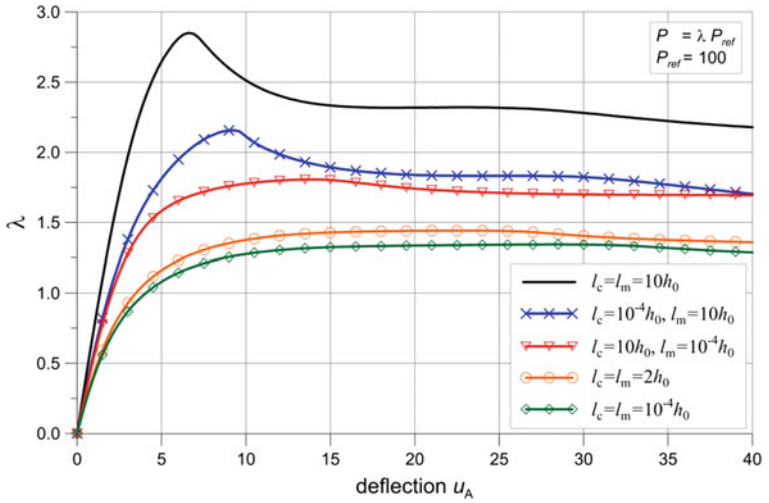

Fig. 12 Channel section beam: comparison of load-deflection curves for different values of characteristic length l_c, l_m of ceramic and metal constituents, respectively

4 Conclusions

The main features of elastoplastic constitutive relation for FGM shell are presented within the nonlinear resultant shell theory. In comparison to the previous paper [20], where $\alpha_s = 5/6$ was assumed, here shear correction factor was computed using formula (25). Moreover, the response of clamped FGM channel section beam is for the first time analyzed in the elastoplastic range. The very good agreement between our results and reference solutions (own Abaqus computations) confirms correctness of the proposed constitutive equations. Our results show that the stiffness of the FGM structures decreases with the growth of the power law exponent also in the elastoplastic range. The effect of increased load capacity for $l > h_0$ may be helpful in modelling of complex materials with microstructure such as e.g. foams, beam lattices. The significant influence of the parameter q on the load-deflection curves is observed. Taking into consideration that the value of q was assumed based on the value proposed for mixture of metals in paper [69] accurate determination of this parameter should be area of further experimental and numerical studies.

Acknowledgements The research reported in this paper was supported by the National Science Centre, Poland with the grant UMO-2015/17/B/ST8/02190. Parallel solver for CAM elements is developed on the basis of HSL, a collection of Fortran codes for large-scale scientific computation. http://www.hsl.rl.ac.uk. Abaqus calculations were carried out at the Academic Computer Centre in Gdańsk.

References

1. Reissner, E.: Linear and nonlinear theory of shells. In: Fung, Y.C., Sechler, E.E. (eds.) Thin Shell Structures, pp. 29–44. Prentice-Hall, Englewood Cliffs (1974)
2. Libai, A., Simmonds, J.G.: The Nonlinear Theory of Elastic Shells. Cambridge University Press, Cambridge (1998)
3. Chróścielewski, J., Makowski, J., Pietraszkiewicz, W.: Statyka i Dynamika Powłok Wielopłatowych: Nieliniowa teoria i metoda elementów skończonych (Statics and Dynamics of Multifold Shells: Nonlinear Theory and Finite Element Method). Wydawnictwo IPPT PAN, Warszawa (2004)
4. Altenbach, J., Altenbach, H., Eremeyev, V.A.: On generalized Cosserat-type theories of plates and shells: a short review and bibliography. Arch. Appl. Mech. **80**, 73–92 (2010). https://doi.org/10.1007/s00419-009-0365-3
5. Neff, P.: A geometrically exact Cosserat shell-model including size effects, avoiding degeneracy in the thin shell limit. Part I: Formal dimensional reduction for elastic plates and existence of minimizers for positive Cosserat couple modulus. Contin. Mech. Thermodyn. **16**, 577–628 (2004). https://doi.org/10.1007/s00161-004-0182-4
6. Chróścielewski, J., Makowski, J., Stumpf, H.: Genuinely resultant shell finite elements accounting for geometric and material non-linearity. Int. J. Numer. Methods Eng. **35**, 63–94 (1992). https://doi.org/10.1002/nme.1620350105
7. Pietraszkiewicz, W., Konopińska, V.: Drilling couples and refined constitutive equations in the resultant geometrically non-linear theory of elastic shells. Int. J. Solids Struct. **51**, 2133–2143 (2014). https://doi.org/10.1016/j.ijsolstr.2014.02.022

8. Burzyński, S., Chróścielewski, J., Daszkiewicz, K., Pietraszkiewicz, W., Sabik, A., Sobczyk, B., Witkowski, W.: On constitutive relations in the resultant non-linear theory of shells. In: Kołakowski, Z., Mania, R.J. (eds.) Statics, Dynamics and Stability of Structures. Selected Problems of Solid Mechanics, pp. 298–318. Lodz University of Technology, Lodz (2016)
9. Makowski, J., Stumpf, H.: Finite strains and rotations in shells. In: Pietraszkiewicz, W. (ed.) Finite Rotations in Structural Mechanics. Lecture Notes in Engineering, vol. 19, pp. 175–194. Springer, Berlin (1986)
10. Eremeyev, V.A., Pietraszkiewicz, W.: Local symmetry group in the general theory of elastic shells. J. Elast. **85**, 125–152 (2006). https://doi.org/10.1007/s10659-006-9075-z
11. Altenbach, H., Eremeyev, V.A.: On the linear theory of micropolar plates. ZAMM Zeitschrift fur Angew. Math. und Mech. **89**, 242–256 (2009). https://doi.org/10.1002/zamm.200800207
12. Chróścielewski, J., Witkowski, W.: On some constitutive equations for micropolar plates. ZAMM Zeitschrift fur Angew. Math. und Mech. **90**, 53–64 (2010). https://doi.org/10.1002/zamm.200900366
13. Chróścielewski, J., Witkowski, W.: FEM analysis of Cosserat plates and shells based on some constitutive relations. ZAMM Zeitschrift fur Angew. Math. und Mech. **91**, 400–412 (2011). https://doi.org/10.1002/zamm.201000090
14. Burzyński, S., Chróścielewski, J., Witkowski, W.: Geometrically nonlinear FEM analysis of 6-parameter resultant shell theory based on 2-D Cosserat constitutive model. ZAMM - J. Appl. Math. Mech. Zeitschrift für Angew. Math. und Mech. **96**, 191–204 (2016). https://doi.org/10.1002/zamm.201400092
15. Burzyński, S., Chróścielewski, J., Witkowski, W.: Elastoplastic material law in 6-parameter nonlinear shell theory. In: Pietraszkiewicz, W., Górski, J. (eds.) 10th Jubilee Conference on Shell Structures—Theory and Applications (SSTA), pp. 377–380. CRC Press, London (2014)
16. Burzyński, S., Chróścielewski, J., Witkowski, W.: Elastoplastic law of Cosserat type in shell theory with drilling rotation. Math. Mech. Solids. **20**, 790–805 (2015). https://doi.org/10.1177/1081286514554351
17. Daszkiewicz, K., Chróścielewski, J., Witkowski, W.: Geometrically nonlinear analysis of functionally graded shells based on 2-D Cosserat constitutive model. Eng. Trans. **62**, 109–130 (2014)
18. Burzyński, S., Chróścielewski, J., Daszkiewicz, K., Witkowski, W.: Geometrically nonlinear FEM analysis of FGM shells based on neutral physical surface approach in 6-parameter shell theory. Compos. Part B Eng. **107**, 203–213 (2016). https://doi.org/10.1016/j.compositesb.2016.09.015
19. Tamura, I., Tomota, Y., Ozawa, M.: Strength and ductility of Iron-Nickel-Carbon alloys composed of austenite and martensite with various strength. In: 3rd International Conference on Strength of Metals and Alloys, pp. 611–615. Institute of Metal and Iron, Cambridge (1973)
20. Burzyński, S., Chróścielewski, J., Daszkiewicz, K., Witkowski, W.: Elastoplastic nonlinear FEM analysis of FGM shells of Cosserat type. Compos. Part B Eng. **154**, 478–491 (2018). https://doi.org/10.1016/j.compositesb.2018.07.055
21. Chróścielewski, J., Sabik, A., Sobczyk, B., Witkowski, W.: 2-D constitutive equations for orthotropic Cosserat type laminated shells in finite element analysis. Compos. Part B Eng. **165**, 335–353 (2019). https://doi.org/10.1016/j.compositesb.2018.11.101
22. Chróścielewski, J., Kreja, I., Sabik, A., Witkowski, W.: Modeling of composite shells in 6-parameter nonlinear theory with drilling degree of freedom. Mech. Adv. Mater. Struct. **18**, 403–419 (2011). https://doi.org/10.1080/15376494.2010.524972
23. Chróścielewski, J., Sabik, A., Sobczyk, B., Witkowski, W.: Nonlinear FEM 2D failure onset prediction of composite shells based on 6-parameter shell theory. Thin-Walled Struct. **105**, 207–219 (2016). https://doi.org/10.1016/j.tws.2016.03.024
24. Sobczyk, B.: FEM analysis of composite materials failure in nonlinear six field shell theory. Doctoral Thesis (2016)
25. Sabik, A.: Progressive failure analysis of laminates in the framework of 6-field non-linear shell theory. Compos. Struct. **200**, 195–203 (2018). https://doi.org/10.1016/j.compstruct.2018.05.069

26. Debski, H., Teter, A.: Effect of load eccentricity on the buckling and post-buckling states of short laminated Z-columns. Compos. Struct. **210**, 134–144 (2019). https://doi.org/10.1016/j.compstruct.2018.11.044
27. Kim, Y.J.: State of the practice of FRP composites in highway bridges. Eng. Struct. **179**, 1–8 (2019). https://doi.org/10.1016/j.engstruct.2018.10.067
28. Siwowski, T., Kulpa, M., Rajchel, M., Poneta, P.: Design, manufacturing and structural testing of all-composite FRP bridge girder. Compos. Struct. **206**, 814–827 (2018). https://doi.org/10.1016/j.compstruct.2018.08.048
29. Birman, V., Kardomateas, G.A.: Review of current trends in research and applications of sandwich structures. Compos. Part B Eng. **142**, 221–240 (2018). https://doi.org/10.1016/j.compositesb.2018.01.027
30. Amaro, A.M., Pinto, M.I.M., Reis, P.N.B., Neto, M.A., Lopes, S.M.R.: Structural integrity of glass/epoxy composites embedded in cement or geopolymer mortars. Compos. Struct. **206**, 509–516 (2018). https://doi.org/10.1016/j.compstruct.2018.08.060
31. Zhang, X., Shi, Y., Li, Z.-X.: Experimental study on the tensile behavior of unidirectional and plain weave CFRP laminates under different strain rates. Compos. Part B Eng. **164**, 524–536 (2019). https://doi.org/10.1016/j.compositesb.2019.01.067
32. Zhang, Z., He, M., Liu, A., Singh, H.K., Ramakrishnan, K.R., Hui, D., Shankar, K., Morozov, E.V.: Vibration-based assessment of delaminations in FRP composite plates. Compos. Part B Eng. **144**, 254–266 (2018). https://doi.org/10.1016/j.compositesb.2018.03.003
33. Gliszczynski, A., Kubiak, T., Borkowski, L.: Experimental investigation of pre-damaged thin-walled channel section column subjected to compression. Compos. Part B Eng. **147**, 56–68 (2018). https://doi.org/10.1016/j.compositesb.2018.04.022
34. Altaee, M., Cunningham, L.S., Gillie, M.: Practical application of CFRP strengthening to steel floor beams with web openings: a numerical investigation. J. Constr. Steel Res. **155**, 395–408 (2019). https://doi.org/10.1016/j.jcsr.2019.01.006
35. Chróścielewski, J., Miśkiewicz, M., Pyrzowski, Ł., Rucka, M., Sobczyk, B., Wilde, K.: Modal properties identification of a novel sandwich footbridge—comparison of measured dynamic response and FEA. Compos. Part B Eng. **151**, 245–255 (2018). https://doi.org/10.1016/j.compositesb.2018.06.016
36. Reddy, J.N.: Mechanics of Laminated Composite Plates and Shells, Theory and Analysis, 2nd edn. CRC Press, Boca Raton, London, New York, Washington.C (2004)
37. Kaw, A.: Mechanics of Composite Materials, 2nd edn. Taylor & Francis Group, Boca Raton, London, New York (2006)
38. Davila, C.G., Camanho, P.P., Rose, C.A.: Failure criteria for FRP laminates. J. Compos. Mater. **39**, 323–345 (2005). https://doi.org/10.1177/0021998305046452
39. Hinton, M., Kaddour, A., Soden, P.: A further assessment of the predictive capabilities of current failure theories for composite laminates: comparison with experimental evidence. Compos. Sci. Technol. **64**, 549–588 (2004). https://doi.org/10.1016/S0266-3538(03)00227-6
40. Kaddour, A.S., Hinton, M.J., Soden, P.D.: A comparison of the predictive capabilities of current failure theories for composite laminates: additional contributions. Compos. Sci. Technol. **64**, 449–476 (2004). https://doi.org/10.1016/S0266-3538(03)00226-4
41. Soden, P., Kaddour, A., Hinton, M.: Recommendations for designers and researchers resulting from the world-wide failure exercise. Compos. Sci. Technol. **64**, 589–604 (2004). https://doi.org/10.1016/S0266-3538(03)00228-8
42. Puck, A., Schürmann, H.: Failure analysis of FRP laminates by means of physically based phenomenological models. Compos. Sci. Technol. **62**, 1633–1662 (2002). https://doi.org/10.1016/S0266-3538(01)00208-1
43. Reddy, Y.S.N., Dakshina Moorthy, C.M., Reddy, J.N.: Non-linear progressive failure analysis of laminated composite plates. Int. J. Non. Linear. Mech. **30**, 629–649 (1995). https://doi.org/10.1016/0020-7462(94)00041-8
44. Xie, D., Biggers, S.B.: Postbuckling analysis with progressive damage modeling in tailored laminated plates and shells with a cutout. Compos. Struct. **59**, 199–216 (2003). https://doi.org/10.1016/S0263-8223(02)00233-7

45. Ambur, D.R., Jaunky, N., Hilburger, M., Dávila, C.G.: Progressive failure analyses of compression-loaded composite curved panels with and without cutouts. Compos. Struct. **65**, 143–155 (2004). https://doi.org/10.1016/S0263-8223(03)00184-3
46. Bai, J.B., Shenoi, R.A., Yun, X.Y., Xiong, J.J.: Progressive damage modelling of hybrid RTM-made composite Π-joint under four-point flexure using mixed failure criteria. Compos. Struct. **159**, 327–334 (2017). https://doi.org/10.1016/j.compstruct.2016.09.083
47. Matzenmiller, A., Lubliner, J., Taylor, R.L.: A constitutive model for anisotropic damage in fiber-composites. Mech. Mater. **20**, 125–152 (1995). https://doi.org/10.1016/0167-6636(94)00053-0
48. Lee, C.S., Kim, J.H., Kim, S.K., Ryu, D.M., Lee, J.M.: Initial and progressive failure analyses for composite laminates using Puck failure criterion and damage-coupled finite element method. Compos. Struct. **121**, 406–419 (2015). https://doi.org/10.1016/j.compstruct.2014.11.011
49. Lopes, C.S., Camanho, P.P., Gürdal, Z., Tatting, B.F.: Progressive failure analysis of tow-placed, variable-stiffness composite panels. Int. J. Solids Struct. **44**, 8493–8516 (2007). https://doi.org/10.1016/j.ijsolstr.2007.06.029
50. Gliszczynski, A., Kubiak, T.: Progressive failure analysis of thin-walled composite columns subjected to uniaxial compression. Compos. Struct. **169**, 52–61 (2017). https://doi.org/10.1016/j.compstruct.2016.10.029
51. Sabik, A.: Direct shear stress vs strain relation for fiber reinforced composites. Compos. Part B Eng. **139**, 24–30 (2018). https://doi.org/10.1016/j.compositesb.2017.11.057
52. Shen, M., Bever, M.B.: Gradients in polymeric materials. J. Mater. Sci. **7**, 741–746 (1972). https://doi.org/10.1007/BF00549902
53. Jha, D.K., Kant, T., Singh, R.K.: A critical review of recent research on functionally graded plates. Compos. Struct. **96**, 833–849 (2013). https://doi.org/10.1016/j.compstruct.2012.09.001
54. Swaminathan, K., Naveenkumar, D.T., Zenkour, A.M., Carrera, E.: Stress, vibration and buckling analyses of FGM plates—a state- of-the-art review. Compos. Struct. **120**, 10–31 (2015). https://doi.org/10.1016/j.compstruct.2014.09.070
55. Williamson, R.L., Rabin, B.H., Drake, J.T.: Finite element analysis of thermal residual stresses at graded ceramic-metal interfaces. Part I. Model description and geometrical effects. J. Appl. Phys. **74**, 1310–1320 (1993). https://doi.org/10.1063/1.354910
56. Drake, J.T., Williamson, R.L., Rabin, B.H.: Finite element analysis of thermal residual stresses at graded ceramic-metal interfaces. Part II. Interface optimization for residual stress reduction. J. Appl. Phys. **74**, 1321–1326 (1993). https://doi.org/10.1063/1.354911
57. Jin, Z.H., Paulino, G.H., Dodds, R.H.: Cohesive fracture modeling of elastic-plastic crack growth in functionally graded materials. Eng. Fract. Mech. **70**, 1885–1912 (2003). https://doi.org/10.1016/S0013-7944(03)00130-9
58. Baghani, M., Fereidoonnezhad, B.: Limit analysis of FGM circular plates subjected to arbitrary rotational symmetric loads using von-Mises yield criterion. Acta Mech. **224**, 1601–1608 (2013). https://doi.org/10.1007/s00707-013-0828-z
59. Gunes, R., Aydin, M., Kemal Apalak, M., Reddy, J.N.: Experimental and numerical investigations of low velocity impact on functionally graded circular plates. Compos. Part B Eng. **59**, 21–32 (2014). https://doi.org/10.1016/j.compositesb.2013.11.022
60. Xu, G., Huang, H., Chen, B., Chen, F.: Buckling and postbuckling of elastoplastic FGM plates under inplane loads. Compos. Struct. **176**, 225–233 (2017). https://doi.org/10.1016/j.compstruct.2017.04.061
61. Kleiber, M., Taczała, M., Buczkowski, R.: Elasto-plastic response of thick plates built in functionally graded material using the third order plate theory. In: Advances in Computational Plasticity, pp. 185–199 (2018)
62. Huang, H., Han, Q.: Elastoplastic buckling of axially loaded functionally graded material cylindrical shells. Compos. Struct. **117**, 135–142 (2014). https://doi.org/10.1016/j.compstruct.2014.06.018
63. Zhang, Y., Huang, H., Han, Q.: Buckling of elastoplastic functionally graded cylindrical shells under combined compression and pressure. Compos. Part B Eng. **69**, 120–126 (2015). https://doi.org/10.1016/j.compositesb.2014.09.024

64. Kalali, A.T., Hassani, B., Hadidi-Moud, S.: Elastic-plastic analysis of pressure vessels and rotating disks made of functionally graded materials using the isogeometric approach. J. Theor. Appl. Mech. **113** (2016). https://doi.org/10.15632/jtam-pl.54.1.113
65. Akis, T.: Elastoplastic analysis of functionally graded spherical pressure vessels. Comput. Mater. Sci. **46**, 545–554 (2009). https://doi.org/10.1016/j.commatsci.2009.04.017
66. Jrad, H., Mars, J., Wali, M., Dammak, F.: Geometrically nonlinear analysis of elastoplastic behavior of functionally graded shells. Eng. Comput. (2018). https://doi.org/10.1007/s00366-018-0633-3
67. Mathew, T.V., Natarajan, S., Martínez-Pañeda, E.: Size effects in elastic-plastic functionally graded materials. Compos. Struct. **204**, 43–51 (2018). https://doi.org/10.1016/j.compstruct.2018.07.048
68. Jeong, J., Ramezani, H., Münch, I., Neff, P.: A numerical study for linear isotropic Cosserat elasticity with conformally invariant curvature. ZAMM Zeitschrift fur Angew. Math. und Mech. **89**, 552–569 (2009). https://doi.org/10.1002/zamm.200800218
69. Fischmeister, H., Karlsson, B.: Plastizitatseigenschaften Grob-Zweiphasiger Werkstoffe. Zeitschrift für Met. **68**, 311–327 (1977)
70. Nguyen, T.K., Sab, K., Bonnet, G.: First-order shear deformation plate models for functionally graded materials. Compos. Struct. **83**, 25–36 (2008). https://doi.org/10.1016/j.compstruct.2007.03.004
71. Singha, M.K., Prakash, T., Ganapathi, M.: Finite element analysis of functionally graded plates under transverse load. Finite Elem. Anal. Des. **47**, 453–460 (2011). https://doi.org/10.1016/j.finel.2010.12.001
72. Daszkiewicz, K.: A family of hybrid mixed elements in 6-parameter shell theory, geometrically nonlinear analysis of functionally graded shells. Doctoral Thesis (in Polish) (2017)
73. de Borst, R.: Simulation of strain localization: a reappraisal of the Cosserat continuum. Eng. Comput. **8**, 317–332 (1991)
74. de Souza Neto, E.A., Peric, D., Owen, D.R.: Computational Methods for Plasticity: Theory and Applications (2009)
75. Simo, J.C., Hughes, T.J.R.: Computational Inelasticity. Springer New York, Inc. (1998)
76. Eberlein, R., Wriggers, P.: Finite element concepts for finite elastoplastic strains and isotropic stress response in shells: theoretical and computational analysis. Comput. Methods Appl. Mech. Eng. **171**, 243–279 (1999). https://doi.org/10.1016/S0045-7825(98)00212-6
77. Tan, X.G., Vu-Quoc, L.: Efficient and accurate multilayer solid-shell element: non-linear materials at finite strain. Int. J. Numer. Methods Eng. **63**, 2124–2170 (2005). https://doi.org/10.1002/nme.1360
78. Abaqus 6.14-2 User Manual. Dassault Systemes Simulia Corp., Providence, RI, USA (2014)

On Optimal Archgrids

R. Czubacki and T. Lewiński

Abstract The aim of the paper is twofold. The first part deals with the optimum design of fully stressed planar funiculars of least volume. The problem turns out to be reducible either to a transverse shear force based minimization problem or to a displacement based maximization problem. In the second part of the paper a proof is given that the similar optimum design problem of archgrids proposed by W. Prager and G.I.N. Rozvany in 1970s can be reduced to two mutually dual problems expressed in terms of a vector stress field or in terms of scalar displacements. The both formulations are new and deliver the tools for the setting and solving the problem of optimal archgrids effectively. The method is illustrated by the example concerning the optimal roof over a square domain.

1 Introduction

Planar pin-supported arches subject to vertical transmissible loads can be formed in a manner which assures vanishing of the bending moments. Such arches, called funiculars, are not subject to shear and the only non zero stresses act along the arch axis. By appropriate choice of the cross section areas the axial stress can be made uniform in the whole arch body. Let this stress reach the limit value $-\sigma_C$. Among such uniformly stressed arches one can find the arch of the least volume. This arch cannot be too shallow and cannot be too high. It turns out that the least volume arch satisfies the *mean square slope condition*, cf. [18, 20]. In particular, the least volume arch under a uniform load assumes the shape of a parabola inscribed into an equilateral triangle; its rise is equal the half of the height of the triangle.

R. Czubacki · T. Lewiński (✉)
Faculty of Civil Engineering, Department of Structural Mechanics and Computer Aided Engineering, Warsaw University of Technology, al. Armii Ludowej 16, 00-637 Warsaw, Poland
e-mail: t.lewinski@il.pw.edu.pl

R. Czubacki
e-mail: r.czubacki@il.pw.edu.pl

H. Altenbach et al. (eds.), *Recent Developments in the Theory of Shells*,
Advanced Structured Materials 110, https://doi.org/10.1007/978-3-030-17747-8_12

The theory of optimal funiculars is outlined in the two first sections of the present paper. The optimization problem is expressed by two mutually dual problems, both in two variants. The first problem is a minimization of the L^2 norm (or its square - in the second variant) of the transverse shear force over the set of statically admissible shear forces.

The second problem reduces to maximization of the virtual work over the set of vertical displacements v such that L^2 norm of slope dv/dx is bounded from the upper side (or—reduces to maximization of an elastic potential—in the second variant).

This variational setting of the problem of optimum design of funiculars paves the way towards a correct setting of optimum design of archgrids. The fundamental paper on the archgrids has been written by Rozvany and Prager [20]. In papers by Rozvany et al. [21], Rozvany and Wang [22], Wang and Rozvany [23], Darwich et al. [10] the funiculars and archgrids are treated as Michell structures and are discussed within the approach called now the theory of optimal layout, cf. Jiang et al. [15]. In the present paper the methods of the general theory of optimal layout will not be invoked. The theory of archgrids will be constructed with using the tools of the paper by Rozvany and Prager [20]—the unknown fields will be defined on the structure and not on the design domain in which the structure is embedded.

We consider the problem in which a given vertical load of intensity $q(x, y)$ is transmitted to the contour Γ of a convex domain Ω along the planar arches in the planes: $y = \text{const}$ and $x = \text{const}$; x, y are Cartesian coordinates parametrizing Ω lying on the $z = 0$ plane. If q represents a distributed load the arches will be infinitely thin; they form two surfaces: $z_x(x, y)$, $z_y(x, y)$. Their shapes are chosen such that the arches are not subject to bending and transverse shearing. The arches are uniformly stressed up to $\sigma = -\sigma_C$, σ being the axial stress.

Rozvany and Prager [20] proved that the condition of minimum volume implies $z_x(x, y) = z_y(x, y) = z(x, y)$, hence the optimal archgrid becomes a gridwork on a single shell. The present paper confirms this result. The optimum design problem is reduced to an auxiliary problem of minimization of a functional $\wp(\boldsymbol{T})$, $\boldsymbol{T} = (T_x, T_y)$, whose argument is subject to the condition: $\text{div}\boldsymbol{T} + q = 0$. The functional $\wp(\cdot)$ has the properties of a norm, hence is convex and of linear growth. This auxiliary problem determines possible numerical approaches to solve the initial problem. The fields T_x, T_y represent transverse shear forces in the simply supported effective beams along x and y directions. Upon computing T_x, T_y one can recover the loads $q_x = -\partial T_x/\partial x$, $q_y = -\partial T_y/\partial y$ acting on the arches in the planes: $y = \text{const}$, $x = \text{const}$, as well as - find the optimal areas of cross sections. The minimizer (T_x,T_y) can vanish on a certain subdomain of Ω and there the roof will not be designed, being unnecessary.

The problem of minimization of the functional $\wp(\boldsymbol{T})$ is then reformulated to the dual form. In this new problem the virtual work of the load q is maximized over the vertical displacements which along each sections: $y = \text{const}$, $x = \text{const}$ satisfy the *mean square slope conditions*. The solution $z(x, y)$ of this problem represents the elevation function of the archgrid. One can prove that ∇z is determined by $\boldsymbol{T}$ but the relation cannot be inverted.

The optimal archgrids are not shells, they are only formed on a single surface. From the dense family of arches of an optimal archgrid one can select the main

arches and replace the grid structure between them by a shell. The *structural shell* thus constructed is rationally designed such that the bending is minimized. By using the theory of *structural shells* developed in Sects. 3.6 and 3.7 of Chróścielewski et al. [1] the final statical analysis can be performed leading to the final process of dimensioning.

2 Optimal Pin-Supported Planar Arches—The Direct Construction

We consider the problem of optimum design of a three hinges planar arch subject to a vertical load of intensity $q(\bar{x})$ referred to the horizontal line linking the supports. The pin supports are at points A and B; the ordinate $\bar{x}$ runs along the x axis, cf. Fig. 1.

We assume that the load follows the arch if it is redesigned and does not change its intensity $q(\bar{x})$; such loads are called transmissible, see Fuchs and Moses [13] where this term has been introduced for the first time.

For any load distribution $q(\bar{x})$ one can choose the shape of the arch: $z = z(x)$, $0 \leq x \leq l$, for which the bending is absent. The construction of such a shape is well-known; we follow the paper by Hetmański and Lewiński [14], Lewiński and Sokół [16]. In the first step we consider a simply supported beam subject to the same load $q(\bar{x})$, see Fig. 2.

The load q causes the bending moment in the effective beam:

$$\hat{M}(x) = \hat{V}_A \, x - \int_0^x (x - \bar{x}) \, q(\bar{x}) \, \mathrm{d}\bar{x} \, , \tag{1}$$

where

$$\hat{V}_A = \frac{1}{l} \int_0^l (l - \bar{x}) \, q(\bar{x}) \, \mathrm{d}\bar{x} \, . \tag{2}$$

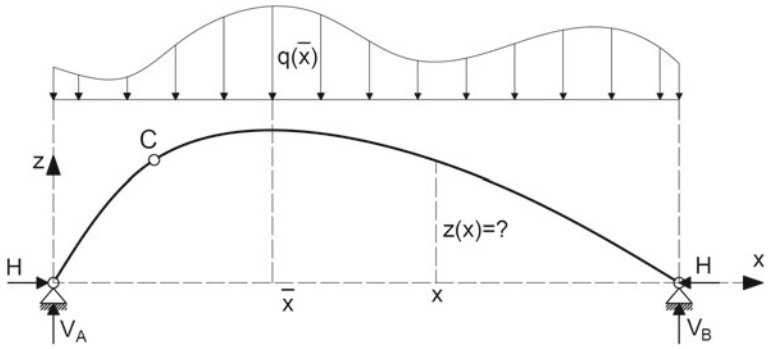

Fig. 1 The funicular problem

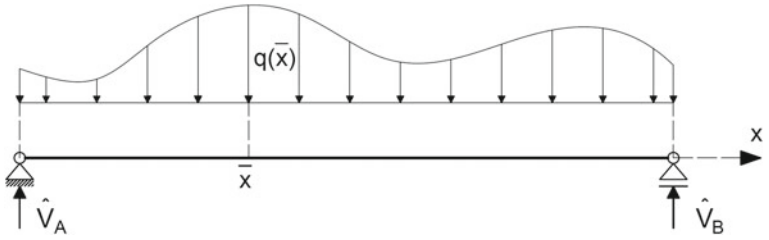

Fig. 2 The effective simply supported beam

Let us come back now to the problem of the arch, Fig. 1. The bending moment in the section over the ordinate x is expressed by

$$M(x) = V_A\, x - Hz(x) - \int_0^x (x - \bar{x})\, q(\bar{x})\, \mathrm{d}\bar{\mathrm{x}}\ . \tag{3}$$

We note that $V_A = \hat{V}_A$ and

$$M(x) = \hat{M}(x) - Hz(x)\ . \tag{4}$$

Now we require: $M(x) = 0$ for each $0 \le x \le l$, which leads to the formula for the optimal shape of the arch

$$z(x) = \frac{1}{H}\hat{M}(x)\ . \tag{5}$$

By differentiating we get

$$\frac{dz}{dx} = \frac{1}{H}\hat{T}(x)\ , \tag{6}$$

where

$$\hat{T}(x) = \hat{V}_A - \int_0^x q(\bar{x})\, \mathrm{d}\bar{\mathrm{x}} \tag{7}$$

represents the transverse shear force in the effective beam. We differentiate (6) and come across

$$H\frac{d^2z}{dx^2} + q(x) = 0\ , \tag{8}$$

which is the funicular equation, see Rozvany [18].

The arch thus constructed is also free of transverse shear; for the proof the reader is referred to Hetmański and Lewiński [14].

Let us assume the areas $A(x)$ of the cross sections such that the axial stress in the arch is made uniform. This condition is achieved by taking

$$A(x) = \frac{H}{\sigma_C \cos\varphi(x)} , \tag{9}$$

where $\varphi(x) = \arctan\left(\frac{dz}{dx}\right)$. The volume of such an arch is expressed by

$$V = \frac{H}{\sigma_C} \int_0^l \left[1 + \left(\frac{dz}{dx}\right)^2\right] \mathrm{dx} , \tag{10}$$

and substitution of (6) gives

$$V = \frac{1}{\sigma_C}\left[H\, l + \frac{1}{H}\|\hat{T}\|^2\right] , \tag{11}$$

with

$$\|\hat{T}\| = \left(\int_0^l (\hat{T}(x))^2 \,\mathrm{dx}\right)^{1/2} \tag{12}$$

being the $L^2(0, l)$ norm of $\hat{T}$.

Minimization of V over H leads to the optimum value of the horizontal force

$$\check{H} = \frac{1}{\sqrt{l}}\|\hat{T}\| , \tag{13}$$

and to the formula for the volume of the optimal arch

$$\check{V} = \frac{2\sqrt{l}}{\sigma_C}\|\hat{T}\| . \tag{14}$$

The optimal shape of the arch is given by

$$\check{z}(x) = \frac{\sqrt{l}}{\|\hat{T}\|}\hat{M}(x) , \quad \frac{d\check{z}}{dx} = \sqrt{l}\,\frac{\hat{T}(x)}{\|\hat{T}\|} . \tag{15}$$

We note that the function $\frac{d\check{z}}{dx}$ satisfies the condition $\|\frac{d\check{z}}{dx}\| = \sqrt{l}$ or

$$\frac{1}{l}\int_0^l \left(\frac{d\check{z}}{dx}\right)^2 \mathrm{dx} = 1 . \tag{16}$$

This is just the *mean square slope condition* discovered by Rozvany and Prager [20].

Summing up, the direct construction of the optimal arch is as follows. We solve the problem of the effective simply supported beam under the load $q(x)$. We find the diagrams of $\hat{M}(x)$ and $\hat{T}(x)$. The optimal arch is a three-hinge structure, the hinge can be placed anywhere. Its shape is given by $\check{z}(x)$ which is proportional to $\hat{M}(x)$,

see (15). The level function $\check{z}(x)$ satisfies the mean square slope condition (16). The optimal area of the cross section is determined by (9) or

$$\check{A}(x) = \frac{1}{\sigma_C \sqrt{l}} \left[\|\hat{T}\|^2 + l\,(\hat{T}(x))^2 \right]^{1/2} . \tag{17}$$

It is seen that $\check{A} \geq \frac{1}{\sigma_C \sqrt{l}} \|\hat{T}\|$. The cross section area cannot degenerate to zero.

3 The Variational Construction of the Optimal Arch

Let us note that the volume $\check{V}$ of the optimal arch can be directly expressed by the level function $\check{z}(x)$:

$$\check{V} = \frac{2}{\sigma_C} \int_0^l q(\bar{x}) \check{z}(\bar{x})\, \mathrm{d}\bar{x} . \tag{18}$$

The proof of this formula is as follows. We start from recalling that the field $\hat{T}(x)$ given by (7) satisfies the variational equation

$$\int_0^l \hat{T} \frac{d\tilde{v}}{dx}\, \mathrm{dx} = \int_0^l q\tilde{v}\, \mathrm{dx} \quad \forall\, \tilde{v} \text{ such that } \tilde{v}(0) = \tilde{v}(l) = 0 . \tag{19}$$

The function $\check{z}$ satisfies, $\check{z}(0) = \check{z}(l) = 0$, hence one can choose $\tilde{v} = \check{z}$ and, by using the second equation of (15) we arrive at

$$\int_0^l q\, \check{z}\, \mathrm{dx} = \int_0^l \hat{T}\, \frac{d\check{z}}{dx}\, \mathrm{dx} = \sqrt{l}\, \|\hat{T}\| , \tag{20}$$

and, due to (14), we confirm (18).

Thus, we have derived two alternative formulae for $\check{V}$: (14) and (18). We shall see below that this fact has deeper theoretical reasons. Consider two problems of variational calculus

$$Z_1 = \max \left\{ \int_0^l qv\mathrm{dx} \mid v \text{ such that : } \int_0^l \left(\frac{dv}{dx} \right)^2 \mathrm{dx} \leq 1 \text{ and } v(0) = v(l) = 0 \right\} , \tag{21}$$

$$Z_2 = \min \left\{ \left(\int_0^l Q^2(x)\, \mathrm{dx} \right)^{1/2} \mid Q \text{ such that : } \frac{dQ}{dx} + q = 0 \right\} . \tag{22}$$

We show below that the above problems are mutually dual and their solutions are: $v = \frac{1}{\sqrt{l}} \check{z}$ and $Q = \hat{T}$. Moreover, the duality gap is zero, or $Z_1 = Z_2 = Z$.

Let us introduce the notation

$$< u, v >= \int_0^l u\, v \, \mathrm{dx} \ . \tag{23}$$

The differential condition nested in (22) can be written in the form (19) or

$$< Q, \frac{dv}{dx} >=< q, v > \tag{24}$$

for each v vanishing for $x = 0$ and $x = l$.

We write (22) with using the Lagrangian multipliers:

$$Z_2 = \min_{Q} \max_{\substack{v \\ v(0)=v(l)=0}} \left\{ \|Q\| + < q, v > - < Q, \frac{dv}{dx} > \right\} \ , \tag{25}$$

where now Q does not obey the differential constraints nested in (22), Q is arbitrary, except for regularity conditions omitted here. We interchange the "min" and "max" operations to get

$$Z_2 = \max_{\substack{v \\ v(0)=v(l)=0}} \left\{ < q, v > -F(\frac{dv}{dx}) \right\} \ , \tag{26}$$

with

$$F(p) = \max_{Q} \{ < Q, p > -\|Q\| \} \tag{27}$$

being the Fenchel transform of: $Q \to \|Q\|$. The result of "max" operation in (27) is known, see Duvaut and Lions [11]

$$F(p) = \begin{cases} 0 & \text{if } \|p\| \le 1 \\ +\infty & \text{otherwise} \end{cases} \ . \tag{28}$$

Let us outline the proof of (28). Let $Q(x) = \|Q\|\eta(x)$, $\|\eta\| = 1$. We compute

$$< Q, p > -\|Q\| = \|Q\|(< \eta, p > -1) \ . \tag{29}$$

To maximize the r.h.s. of (29) over η one should take $\eta = p/\|p\|$, which gives

$$< Q, p > -\|Q\| = \|Q\|(\underline{\|p\| - 1}) \ . \tag{30}$$

We proceed now to maximizing the r.h.s. of (29) over $\|Q\|$. If the underlined factor in (30) is equal or smaller than 0, then the operation "max" over $\|Q\|$ gives the 0 value. Otherwise the expression at the r.h.s. of (30) may be arbitrarily big, which proves (28).

Substitution of (28) into (26) gives (21). Hence $Z_1 = Z_2$. Moreover, the substitution of $v = \frac{1}{\sqrt{l}}\check{z}$ into (21), with taking into account (20), leads to the equality

$$Z_1 = \frac{1}{\sqrt{l}} \int_0^l q(x)\, \check{z}(x)\, \mathrm{dx} = \|\hat{T}\|. \tag{31}$$

We shall show now that $Q = \hat{T}$ is the minimizer of (22). The field Q must satisfy the equilibrium equation nested in (22), hence Q may be represented by

$$Q(x) = \hat{T}(x) + c\ , \tag{32}$$

where c is an arbitrary constant. Moreover,

$$\int_0^l \hat{T}(x)\, \mathrm{dx} = \int_0^l \frac{d\hat{M}}{dx}\, \mathrm{dx} = 0\ , \tag{33}$$

since $\hat{M}(0) = \hat{M}(l) = 0$. Therefore

$$\int_0^l (Q(x))^2\ \mathrm{dx} = \|\hat{T}\|^2 + l\, c^2\ , \tag{34}$$

or

$$Z_2 = \min_{c\in\mathbb{R}} \left[\|\hat{T}\|^2 + l\, c^2\right]^{1/2} = \|\hat{T}\|\ , \tag{35}$$

which confirms the equality $Z_1 = Z_2$, see (31) and determines the minimizer of (22) and the maximizer of (21). In the discussion above we have found the solution to the problem (22), but we have not shown the construction of the problem (21). This construction can be done by noting that the solution v of the problem (21) is also the stationary point of the functional

$$J_2(u) = \int_0^l q\, u\, \mathrm{dx} + \lambda \int_0^l \left(\frac{du}{dx}\right)^2\ \mathrm{dx}\ . \tag{36}$$

The condtion $\delta J_2 = 0$ leads to

$$-2\lambda \frac{d^2u}{dx^2} + q = 0\ , \tag{37}$$

see (8), and since $u(0) = u(l) = 0$, we find $u = -\frac{1}{2\lambda}\hat{M}$. Thus, the maximizer of problem (21) has the form: $v = \alpha\hat{M}$ and the constant α is determined by (16), or

$$\alpha^2 \int_0^l \left(\frac{d\hat{M}}{dx}\right)^2\ \mathrm{dx} = 1\ , \tag{38}$$

hence $\alpha = \frac{1}{\|\hat{T}\|}$. Thus, $v = \frac{\hat{M}(x)}{\|\hat{T}\|}$ while by the equation: $\check{z}(x) = \sqrt{l}\, v(x)$ we find the level function $\check{z}$ given previously by (15).

We see that the maximizer $\check{z}$ of problem (21) and the minimizer $\hat{T}$ of problem (22) are linked by (15). This formula cannot be inverted. Having $\hat{T}$ one can find $d\check{z}/dx$, but not vice versa.

The problem (22) is equivalent to the problem

$$\tilde{Z}_2 = \min \left\{ \int_0^l (Q(x))^2 \, \mathrm{dx} \mid Q \text{ such that : } \frac{dQ}{dx} + q = 0 \right\} , \tag{39}$$

since the function $x \to \sqrt{x}$ is increasing. We shall show that the problem dual to (39) reads

$$\tilde{Z}_1 = \max \left\{ \int_0^l q\, v \, \mathrm{dx} - \frac{1}{4} \int_0^l \left(\frac{dv}{dx} \right)^2 \mathrm{dx} \mid v(0) = v(l) = 0 \right\} , \tag{40}$$

and $\tilde{Z}_1 = \tilde{Z}_2$. Moreover, if $v = \hat{v}$ is the maximizer of (40) and $Q = \hat{T}$ is the minimizer of (39) then

$$\hat{v} = 2\hat{M}, \ \frac{d\hat{M}}{dx} = \hat{T}, \ \hat{M}(0) = \hat{M}(l) = 0, \ \tilde{Z}_1 = \tilde{Z}_2 = \|\hat{T}\|^2 . \tag{41}$$

Let us re-write (39) as follows

$$\tilde{Z}_2 = \min_{Q} \max_{\substack{v \\ v(0)=v(l)=0}} \left\{ \int_0^l Q^2 \, \mathrm{dx} + \int_0^l q\, v \, \mathrm{dx} - \int_0^l Q \frac{dv}{dx} \, \mathrm{dx} \right\} , \tag{42}$$

hence

$$\tilde{Z}_2 = \max_{\substack{v \\ v(0)=v(l)=0}} \left\{ \int_0^l q\, v \, \mathrm{dx} - F_1\left(\frac{dv}{dx}\right) \right\} , \tag{43}$$

where

$$F_1(p) = \max_{Q} \int_0^l \left(Qp - Q^2 \right) \mathrm{dx} . \tag{44}$$

We compute

$$F_1(p) = \frac{1}{4} \int_0^l p^2 \, \mathrm{dx} . \tag{45}$$

Substitution of this result into (43) gives (40). Now we proceed to derive (41). We know that the minimizer of (39) is $Q = \hat{T}$, where $\hat{T}$ is the shear force in the effective beam. The maximizer $v = \hat{v}$ of (40) satisfies the Euler-Lagrange equation for the functional (40) or

$$\frac{d^2\hat{v}}{dx^2} + 2q = 0 \,, \tag{46}$$

with $\hat{v}(0) = \hat{v}(l) = 0$. Hence $\hat{v} = 2\hat{M}$ where $\hat{M}$ is the bending moment in the effective beam. Let us note that

$$\int_0^l q\,\hat{M}\,\mathrm{dx} = -\int_0^l \frac{d\hat{T}}{dx}\hat{M}\,\mathrm{dx} = -\int_0^l \left[\frac{d}{dx}(\hat{T}\hat{M}) - \hat{T}\frac{d\hat{M}}{dx}\right]\mathrm{dx} = \int_0^l (\hat{T})^2\,\mathrm{dx} = \|\hat{T}\|^2 \,. \tag{47}$$

We compute

$$\tilde{Z}_1 = \int_0^l q\,(2\hat{M})\,\mathrm{dx} - \frac{1}{4}\int_0^l \left(2\frac{d\hat{M}}{dx}\right)^2 \mathrm{dx} = 2\|\hat{T}\|^2 - \|\hat{T}\|^2 = \|\hat{T}\|^2 \,, \tag{48}$$

which confirms: $\tilde{Z}_1 = \tilde{Z}_2$.

In the simplest case of $q = \text{const}$ the level function of the optimal arch is given by

$$\check{z}(x) = \sqrt{3}\,l\left(\frac{x}{l}\right)\left(1 - \frac{x}{l}\right) \,. \tag{49}$$

The parabola is inscribed into an equilateral triangle. The volume of the optimal arch equals

$$\hat{V} = \frac{\sqrt{3}}{3}\frac{ql^2}{\sigma_C} \,. \tag{50}$$

4 Optimal Archgrids

4.1 Setting of the Optimization Problem

The subject of the discussion is a rational design of canopies (or roofs) over plane domains. The roofs are to be formed of two families of planar arches with the planes being mutually orthogonal. The arches are packed densely, they are infinitely thin thus forming two roofs of level functions $z_x(x, y)$, $z_y(x, y)$, where the net (x, y) is Cartesian. The roof is supported on the level $z = 0$, z being orthogonal to the (x, y) plane.

We confine our attention to the case of the roof being designed over a convex plane domain Ω. Thus, the lines $x = \text{const}$ cut the contour Γ of Ω at least at two points: $(x, y_1(x))$, $(x, y_2(x))$, $y_1(x) \le y_2(x)$, where $a \le x \le b$. Similarly, the lines $y = \text{const}$ cut the contour Γ at least at two points: $(x_1(y), y)$, $(x_2(y), y)$, $x_1(y) \le x_2(y)$; $c \le y \le d$, see Fig. 3.

The roof is subject to the vertical transmissible load of intensity $q(x, y)$ measured per a unit area of the (x, y) plane. The load of density $q_x(x, y)$ is carried by the

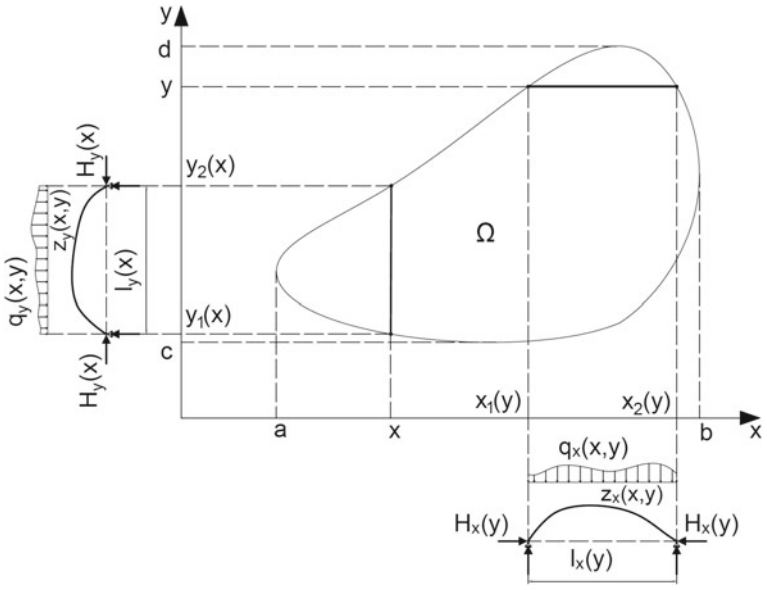

Fig. 3 Description of the archgrid problem

arches lying in the planes $y = \text{const}$ and the arches lying in the planes $x = \text{const}$ are subject to the load $q_y(x, y)$. Thus, $q(x, y) = q_x(x, y) + q_y(x, y)$.

Thus, the arches supported at points $(x_1(y), y)$, $(x_2(y), y)$ are subject to the load $q_x(x, y)$. The arches supported at points $(x, y_1(x))$, $(x, y_2(x))$ are subject to the load $q_y(x, y)$. The horizontal reactions are denoted by $H_x(y)$, $H_y(x)$, respectively. The shapes of the arches are chosen such that the bending does not occur, see Sect. 2. The areas of the cross-sections $A_x(x, y)$, $A_y(x, y)$ are designed in a way to make the stress distribution uniform. The axial stress $\sigma = -\sigma_C$, σ_C being the permissible stress in compression. This assumption determines the volume of the roof. The aim of the optimum design is to choose the elevation functions z_x, z_y corresponding to the least volume design.

The problem stated is a natural extension of the problem posed in Sects. 2, 3 concerning the optimum design of a single arch. Like in Sect. 2 we introduce the effective beams simply supported at the ends: $(x_1(y), y)$, $(x_2(y), y)$ and of length $l_x(y) = x_2(y) - x_1(y)$ and the effective beams supported at the ends: $(x, y_1(x))$, $(x, y_2(x))$ and of length $l_y(x) = y_2(x) - y_1(x)$.

The beams are subject to the loads of intensities $q_x(x, y)$, $q_y(x, y)$, respectively. There appear the transverse shear forces $\hat{T}_x(x, y)$, $\hat{T}_y(x, y)$ and bending moments $\hat{M}_x(x, y)$, $\hat{M}_y(x, y)$ linked with the load by the equilibrium equations

$$\frac{\partial \hat{T}_x}{\partial x} + q_x = 0, \quad \hat{T}_x = \frac{\partial \hat{M}_x}{\partial x}, \tag{51}$$

$$\frac{\partial \hat{T}_y}{\partial y} + q_y = 0, \quad \hat{T}_y = \frac{\partial \hat{M}_y}{\partial y} \,. \tag{52}$$

In order to eliminate bending we assume

$$z_x = \frac{1}{H_x(y)} \hat{M}_x(x, y), \quad z_y = \frac{1}{H_y(x)} \hat{M}_y(x, y) \,. \tag{53}$$

The angles of slopes φ_x, φ_y of the level functions are determined by

$$\tan \varphi_x = \frac{\partial z_x}{\partial x}, \quad \tan \varphi_y = \frac{\partial z_y}{\partial y} \,. \tag{54}$$

In order to make the axial stress uniform we assume the areas of the cross sections according to (9) or

$$A_x = \frac{H_x}{\sigma_C \cos \varphi_x}, \quad A_y = \frac{H_y}{\sigma_C \cos \varphi_y} \,. \tag{55}$$

The elementary lengths of the neutral axes of the arches are

$$ds_x = \frac{dx}{\cos \varphi_x}, \quad ds_y = \frac{dy}{\cos \varphi_y} \,. \tag{56}$$

The volume of all the arches in the planes $y = \text{const}$ is given by

$$V_x = \int_c^d \int_{x_1(y)}^{x_2(y)} A_x \, \mathrm{ds_x dy} \,, \tag{57}$$

hence

$$\sigma_C \, V_x = \int_c^d \int_{x_1(y)}^{x_2(y)} \frac{H_x(x)}{\cos^2 \varphi_x(x, y)} \, \mathrm{dxdy} \,. \tag{58}$$

By using the formulae (51)–(56) we rearrange this formula as below

$$\sigma_C \, V_x = \int_c^d l_x(y) \, H_x(y) \, \mathrm{dy} + \int_c^d \frac{1}{H_x(y)} \int_{x_1(y)}^{x_2(y)} \left(\hat{T}_x \right)^2 \mathrm{dxdy} \,. \tag{59}$$

By analogy, the volume of all the arches in the $x = \text{const}$ planes is given by

$$\sigma_C \, V_y = \int_a^b l_y(x) \, H_y(x) \, \mathrm{dx} + \int_a^b \frac{1}{H_y(x)} \int_{y_1(x)}^{y_2(x)} \left(\hat{T}_y \right)^2 \mathrm{dydx} \,. \tag{60}$$

The total volume of the archgrid is $V = V_x + V_y$. The transverse forces are linked by

$$\frac{\partial \hat{T}_x}{\partial x} + \frac{\partial \hat{T}_y}{\partial y} + q = 0 \,, \tag{61}$$

since $q_x + q_y = q$. Thus, the transverse forces satisfy the variational equation

$$G(\tilde{v}) = 0 \quad \text{for each } \tilde{v} = 0 \text{ on } \Gamma \,, \tag{62}$$

where

$$G(v) = \int_\Omega q\, v \,\mathrm{dxdy} - \int_\Omega \left(\hat{T}_x \frac{\partial v}{\partial x} + \hat{T}_y \frac{\partial v}{\partial y} \right) \mathrm{dxdy} \,. \tag{63}$$

The aim is to find the least volume archgrid, hence $V = V_x + V_y$ is to be minimized over admissible $\hat{T}_x(x, y)$, $\hat{T}_y(x, y)$, $H_x(y)$, $H_y(x)$. The transverse forces are subject to (62), (63) and H_x, H_y are non-negative.

4.2 Analysis of the Optimization Problem

Before proceeding further we define the operations

$$\begin{aligned} \rho_x(f; a(x), b(x)) &= \left(\int_{a(x)}^{b(x)} (f(x, y))^2 \,\mathrm{dy} \right)^{1/2} , \\ \rho_y(f; a(y), b(y)) &= \left(\int_{a(y)}^{b(y)} (f(x, y))^2 \,\mathrm{dx} \right)^{1/2} , \end{aligned} \tag{64}$$

where $a(x) < b(x)$ are given functions.

Note that for given x the functional $\rho_x(\cdot; a(x), b(x))$ is a norm and, similarly, for given y the functional $\rho_y(\cdot; a(y), b(y))$ is a norm.

Let us introduce the Lagrangian

$$\mathfrak{L} = \sigma_C \left[V_x + V_y + 2G(v) \right] \,. \tag{65}$$

We require $\delta\mathfrak{L} = 0$ for arbitrary $\delta\hat{T}_x$, $\delta\hat{T}_y$, δH_x, δH_y , δv, which results in

$$\begin{aligned} H_x(y) &= \frac{1}{\sqrt{l_x(y)}} \rho_y(\hat{T}_x; x_1(y), x_2(y)), \\ H_y(x) &= \frac{1}{\sqrt{l_y(x)}} \rho_x(\hat{T}_y; y_1(x), y_2(x)), \end{aligned} \tag{66}$$

and

$$\frac{\partial v}{\partial x} = \frac{1}{H_x(y)} \hat{T}_x, \quad \frac{\partial v}{\partial y} = \frac{1}{H_y(x)} \hat{T}_y \,. \tag{67}$$

Similar equations have been found in Sect. 2 concerning planar funiculars: compare (13) with (66) and (6) with (67).

Assume now that $H_x(y) > 0$ and $H_y(x) > 0$. On combining (63) and (67) one arrives at the variational problem: find v vanishing on Γ such that

$$a_H(v, \tilde{v}) = \int_\Omega q\, \tilde{v}\, \mathrm{dxdy} \tag{68}$$

for each $\tilde{v}$ vanishing on Γ, the bilinear form at the l.h.s. of (68) being

$$a_H(v, \tilde{v}) = \int_\Omega \left[H_x(y) \frac{\partial v}{\partial x} \frac{\partial \tilde{v}}{\partial x} + H_y(x) \frac{\partial v}{\partial y} \frac{\partial \tilde{v}}{\partial y} \right] \mathrm{dxdy} \,. \tag{69}$$

This bilinear form is elliptic, since $H_x(y) > 0$ and $H_y(x) > 0$. The problem (68) is uniquely solvable.

The Eqs. (51), (52), (53), (67) imply

$$H_x(y) \frac{\partial}{\partial x}(z_x - v) = 0, \quad H_y(x) \frac{\partial}{\partial y}(z_y - v) = 0 \,. \tag{70}$$

Let $\mathscr{A} = \{y \mid H_x(y) > 0\}$. Then for $y \in \mathscr{A}$ the first equation of (70) implies

$$z_x(x, y) - v(x, y) = f_1(y) \,.$$

Let us note that for each $y \in \mathscr{A}$ there exists x such that $(x, y) \in \Gamma$ and then

$$f_1(y) = 0 \,,$$

since z_x and v vanish on Γ. Thus

$$z_x(x, y) - v(x, y) = 0 \quad \text{for } y \in \mathscr{A} \,.$$

If $H_x(y) = 0$ then from (55) we get $A_x = 0$, which indicates that the arch for $y =$ const. does not exist and the functions z_x and v are not linked. Similarly,

$$z_y(x, y) - v(x, y) = 0$$

for those x for which $H_y(x) > 0$. Hence

$$z_x(x, y) = v(x, y), \quad z_y(x, y) = v(x, y) \tag{71}$$

for x such that $H_y(x) > 0$ and for y such that $H_x(y) > 0$.

We see that $z = v$ is the solution to (68). Its local form reads

$$H_x(y)\frac{\partial^2 z}{\partial x^2} + H_y(x)\frac{\partial^2 z}{\partial y^2} + q(x, y) = 0 \ . \tag{72}$$

This is the archgrid equation, a counterpart of the funicular equation (8). The identities (71) link the level functions of optimal arches in the x and y directions, thus forming a grid shell over the given domain Ω. Thus, from now onward the division of q into q_x and q_y becomes irrelevant, since the final equations involve the initial load only. The identities (71) have been first noted by Rozvany and Prager [20], Rozvany et al. [19, 21].

Let $\boldsymbol{w} = (u(x, y), v(x, y))$ and

$$\wp(\boldsymbol{w}) = \int_a^b \sqrt{l_y(x)}\, \rho_x(v; y_1(x), y_2(x))\, \mathrm{dx} + \int_c^d \sqrt{l_x(y)}\rho_y(u; x_1(y), x_2(y))\, \mathrm{dy} \ . \tag{73}$$

This functional satisfies: $\wp(\lambda \boldsymbol{w}) = |\lambda|\wp(\boldsymbol{w})$, $\lambda \in \mathbb{R}$, $\wp(\boldsymbol{w}_1 + \boldsymbol{w}_2) \leq \wp(\boldsymbol{w}_1) + \wp(\boldsymbol{w}_2)$, $\wp(\boldsymbol{w}) \geq 0$ and $\wp(\boldsymbol{w}) = 0 \implies \boldsymbol{w} = \boldsymbol{0}$. Note that $\wp(\cdot)$ is convex and of linear growth.

The above functional is helpful in expressing the total volume $V = V_x + V_y$ of the archgrid in terms of the transverse force vector $\hat{\boldsymbol{T}} = (\hat{T}_x, \hat{T}_y)$. Indeed, by substituting the results (66) into (59) and (60) one obtains

$$V = \frac{2}{\sigma_C}\wp(\hat{\boldsymbol{T}}) \ . \tag{74}$$

According to (61) the vector $\hat{\boldsymbol{T}}$ satisfies $\mathrm{div}\hat{\boldsymbol{T}} + q = 0$. The set of such vectors is rich, in contrast to the case of planar funiculars. The problem of minimal volume of the archgrid reduces to solving

$$Z_2 = \min\{\wp(\boldsymbol{Q}) \mid \boldsymbol{Q} \text{ such that : } \mathrm{div}\,\boldsymbol{Q} + q = 0\} \ , \tag{75}$$

where $\boldsymbol{Q} = (Q_x, Q_y)$ is a trial vector of transverse shear forces in the effective beams. The problem (75) is solvable. The minimizer $\check{\boldsymbol{Q}}$ may vanish in a subdomain of Ω. The effective domain of $\check{\boldsymbol{Q}}$ is denoted by Ω_m.

Assume that $\check{\boldsymbol{Q}}$ is the minimizer of (75). Then we can compute the horizontal forces by (66) and then solve the problem (68) to find the elevation function $v = z(x, y)$.

By substituting

$$\check{Q}_x = H_x(y)\frac{\partial z}{\partial x}, \quad \check{Q}_y = H_y(x)\frac{\partial z}{\partial y} \ , \tag{76}$$

into (66) one finds the equations

$$\rho_y(\frac{\partial z}{\partial x}; x_1(y), x_2(y)) = \sqrt{l_x(y)},$$
$$\rho_x(\frac{\partial z}{\partial y}; y_1(x), y_2(x)) = \sqrt{l_y(x)}, \tag{77}$$

to hold there, where $\hat{Q}_x \neq 0$ and $\hat{Q}_y \neq 0$, respectively. The Eq. (77) express the *mean square slope conditions* for the arches in x and y directions, cf. (16).

The problem dual to (75) reads

$$Z_1 = \max \left\{ \int_\Omega q\, v \,\mathrm{dxdy} \mid \rho_y \left(\frac{\partial v}{\partial x}; x_1(y), x_2(y) \right) \leq \sqrt{l_x(y)} \text{ for } c \leq y \leq d; \right.$$
$$\rho_x \left(\frac{\partial v}{\partial y}; y_1(x), y_2(x) \right) \leq \sqrt{l_y(x)} \text{ for } a \leq x \leq b,$$
$$\left. v = 0 \text{ on } \Gamma \right\}. \tag{78}$$

Let us outline the proof of the equality $Z_1 = Z_2$. We re-write problem (75) as

$$Z_2 = \min_{\boldsymbol{T}} \max_{\substack{v \\ v=0 \text{ on } \Gamma}} \{\wp(\boldsymbol{T}) + < q, v > - < \boldsymbol{T}, \nabla v >\}\ , \tag{79}$$

where

$$< \boldsymbol{u}, \boldsymbol{v} >= \int_\Omega \boldsymbol{u} \cdot \boldsymbol{v} \,\mathrm{dxdy}, \quad < q, v >= \int_\Omega q\, v \,\mathrm{dxdy}\ , \tag{80}$$

and interchange the order of the operations: min and max to find

$$Z_2 = \max_{\substack{v \\ v=0 \text{ on } \Gamma}} \{< q, v > - F(\nabla v)\}\ , \tag{81}$$

where

$$F(\boldsymbol{p}) = \max_{\boldsymbol{T}} \{< \boldsymbol{T}, \boldsymbol{p} > - \wp(\boldsymbol{T})\}\ , \tag{82}$$

is the Fenchel transform of $\wp(\boldsymbol{T})$.

We compute F for $\boldsymbol{p} = (p_x, p_y)$

$$F(\boldsymbol{p}) = \max_{T_y} \left\{ \int_a^b \int_{y_1(x)}^{y_2(x)} T_y\, p_y \,\mathrm{dydx} - \int_a^b \sqrt{l_y(x)} \rho_x(T_y; y_1(x), y_2(x))\,\mathrm{dx} \right\} +$$
$$\max_{T_x} \left\{ \int_c^d \int_{x_1(y)}^{x_2(y)} T_x\, p_x \,\mathrm{dxdy} - \int_c^d \sqrt{l_x(y)} \rho_y(T_x; x_1(y), x_2(y))\,\mathrm{dy} \right\}. \tag{83}$$

The first term can be expressed as below

$$F_1 = \max_{T_y} \int_a^b \left[\int_{y_1(x)}^{y_2(x)} T_y \, p_y \, \mathrm{d}y - \sqrt{l_y(x)} \rho_x(T_y; y_1(x), y_2(x)) \right] \mathrm{d}x \, . \tag{84}$$

We represent $T_y(x, y)$ as follows

$$T_y(x, y) = \rho_x(T_y; y_1(x), y_2(x)) \phi(x, y) \, , \tag{85}$$

where

$$\rho_x(\phi; y_1(x), y_2(x)) = 1 \, , \tag{86}$$

and substitute into (84) to get

$$F_1 = \max_{T_y} \int_a^b \left[\rho_x(T_y; y_1(x), y_2(x)) \left[\int_{y_1(x)}^{y_2(x)} \phi \, p_y \, \mathrm{d}y - \sqrt{l_y(x)} \right] \right] \mathrm{d}x \, . \tag{87}$$

By using Schwarz inequality and (86) one can estimate

$$\int_{y_1(x)}^{y_2(x)} \phi \, p_y \, \mathrm{d}y \le \rho_x(\phi; y_1(x), y_2(x)) \rho_x(p_y; y_1(x), y_2(x)) = \rho_x(p_y; y_1(x), y_2(x)). \tag{88}$$

Thus,

$$F_1 = \max_{T_y} \int_a^b \rho_x(T_y; y_1(x), y_2(x)) \left[\rho_x(p_y; y_1(x), y_2(x)) - \sqrt{l_y(x)} \right] \mathrm{d}x \, , \tag{89}$$

or

$$F_1 = \begin{cases} 0 & \text{if } \rho_x(p_y; y_1(x), y_2(x)) \le \sqrt{l_y(x)} \\ +\infty & \text{otherwise} \end{cases} \, . \tag{90}$$

Similar arguments can be applied to the second term of (83).

We eventually find

$$F(\boldsymbol{p}) = \begin{cases} 0 & \text{if } \rho_x(p_y; y_1(x), y_2(x)) \le \sqrt{l_y(x)} \\ & \text{and} \\ & \rho_y(p_x; x_1(y), x_2(y)) \le \sqrt{l_x(y)} \\ +\infty & \text{otherwise} \end{cases} \, . \tag{91}$$

Substitution of this result into (81) confirms (78) and the equality $Z_1 = Z_2$. The maximizer $v = \check{z}(x, y)$ satisfies the first condition of (77) there, where $\check{Q}_x \neq 0$ and it satisfies the second condition of (77) there, where $\check{Q}_y \neq 0$. On the other hand the conditions nested in (78) are satisfied everywhere in Ω, even there, where $\check{\boldsymbol{Q}} = \boldsymbol{0}$. Thus, the function $v = \check{z}$ which solves (78) must be constructed in Ω and not only in Ω_m being the effective domain of $\check{\boldsymbol{Q}}$.

The maximizer $v = \check{z}$ of problem (78) and the minimizer $\boldsymbol{Q} = \check{\boldsymbol{Q}}$ of problem (75) are linked by (66), (67) or

$$\frac{\partial \check{z}}{\partial x} = \sqrt{l_x(y)}\frac{\check{Q}_x}{\rho_y(\check{Q}_x; x_1(y), x_2(y))},$$
$$\frac{\partial \check{z}}{\partial y} = \sqrt{l_y(x)}\frac{\check{Q}_y}{\rho_x(\check{Q}_y; y_1(x), y_2(x))}. \tag{92}$$

These equations are non-invertible. Having $\check{\boldsymbol{Q}}$ one can compute $\nabla\check{z}$, but not vice versa. Moreover, by putting $\check{\boldsymbol{T}} = \check{\boldsymbol{Q}}$ in (66) we can compute the optimal values of the horizontal forces $\check{H}_x(y)$, $\check{H}_y(x)$, which determine the bilinear form $a_{\check{H}}(\cdot,\cdot)$, see (69). The maximizer $\check{z}$ of problem (78) is the solution to the elliptic problem (68) and satisfies the local Eq. (72) for $H_x = \check{H}_x$, $H_y = \check{H}_y$.

The areas of the cross-sections of the arches in the planes $y = \text{const}$, $x = \text{const}$ forming the optimal archgrid are given by (55), or

$$\check{A}_x = \frac{1}{\sigma_C\sqrt{l_x(y)}}\left[\left(\rho_y(\check{Q}_x; x_1(y), x_2(y))\right)^2 + l_x(y)\left(\check{Q}_x\right)^2\right]^{1/2},$$
$$\check{A}_y = \frac{1}{\sigma_C\sqrt{l_y(x)}}\left[\left(\rho_x(\check{Q}_y; y_1(x), y_2(x))\right)^2 + l_y(x)\left(\check{Q}_y\right)^2\right]^{1/2}. \tag{93}$$

Remark 4.1 The results (93) refer to the case of $\check{Q}_x \neq 0$, $\check{Q}_y \neq 0$ and then $\check{H}_x > 0$, $\check{H}_y > 0$. However, for some loads q there could be $\check{Q}_x = 0$ and $\check{Q}_y \neq 0$ and vice versa. Then over this subdomain $\check{H}_x = 0$ and the problem reduces to that of Sect. 2. If both $\check{Q}_x$, $\check{Q}_y$ vanish then the roof is not necessary. The roof is constructed only in the effective domain of $(Q_x)^2 + (Q_y)^2$.

5 Optimal Roof for a Uniform Vertical Load over a Square Domain

Consider the problem of optimum design of an archgrid over a square domain Ω of sides $2L \times 2L$, cf. Fig. 4. The load is assumed as transmissible and uniformly distributed of an intensity $q = \text{const}$, acting along the z axes orthogonal to Ω. Here $l_x(y) = 2L$, $l_y(x) = 2L$.

Both the problems (75), (78) will be solved by using the Fourier series expansions.

Fig. 4 Problem formulation

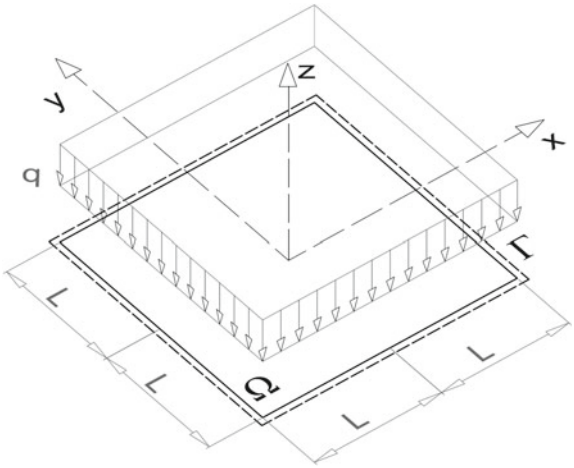

5.1 Solution to the Problem (78)

The trial function v in (78) is expressed by the double cosine series truncated as below:

$$v(x, y) = \sum_{m=1,3,5,\ldots}^{M} \sum_{n=1,3,5,\ldots}^{M} v_{mn} \cos(\alpha_m x) \cos(\alpha_n y) \ , \tag{94}$$

where $\alpha_m = (m\pi)/(2L)$, the kinematic boundary conditions being satisfied identically. The computations have been performed for $M = 99$. The inequality conditions involved in (78) are satisfied for the selected sections: $y = \frac{i}{200}L$, $i = 0, \ldots, 199$; $x = \frac{j}{200}L$, $j = 0, \ldots, 199$. Thus, the problem (78) reduces to the maximization problem with a linear objective function and 400 non-linear inequality constraints. This problem has been solved with the help of the available optimization tools in *Mathematica* software. We note that the optimal roof forms the non-convex surface, see Fig. 5. This property of non-convexity is well seen while analysing the shape of the cross sections $x = \text{const}$, see Fig. 6. These results show that the arches close to the edges are partly loaded upward, while the arches within the central part of the roof are subject to the load directed downward. Yet, let us stress that all the arches are in compression.

The method discussed delivers the volume $V_{(78)} = 3.681V_0$, $V_0 = qL^3/\sigma_C$. The maximal elevation (at the center) of Ω turns out to be: $0.8275L$.

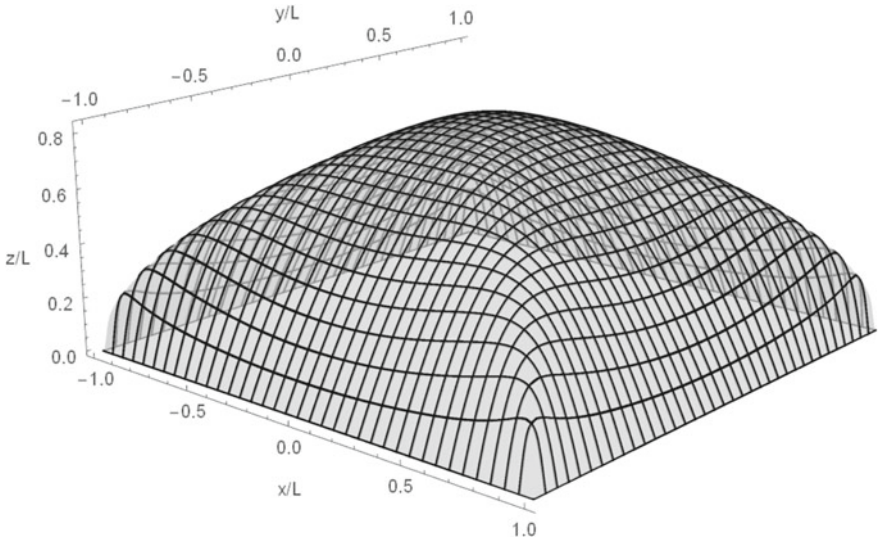

Fig. 5 The shape of the optimal archgrid found by solving the problem (78)

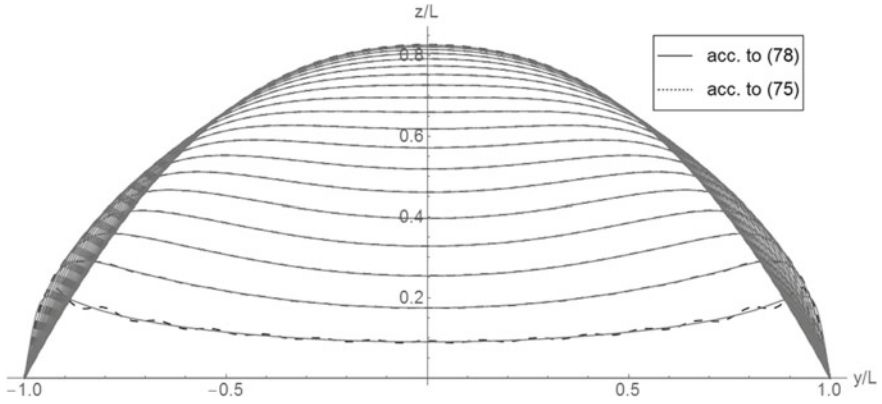

Fig. 6 The cross sections of the level function z for $x = 0 + \frac{i}{20}L,\ i = 0, ..., 19$. The solid lines represent the solutions to the problem (78), the results of the problem (75) are denoted by the dashed lines

5.2 Solution to the Problem (75)

The components of the test vector **Q** are expanded as below:

$$Q_x(x, y) = \sum_{m=1}^{N} \sum_{n=1}^{N} Q^x_{mn} \cos(\alpha_m \tilde{x}) \sin(\alpha_n \tilde{y}) \ ,$$
$$Q_y(x, y) = \sum_{m=1}^{N} \sum_{n=1}^{N} Q^y_{mn} \sin(\alpha_m \tilde{x}) \cos(\alpha_n \tilde{y}) \ , \tag{95}$$

where $\tilde{x} = x + L$ and $\tilde{y} = y + L$, while the load will be expressed by the double sine series:

$$q(x, y) = \sum_{m=1}^{N} \sum_{n=1}^{N} q_{mn} \sin(\alpha_m \tilde{x}) \sin(\alpha_n \tilde{y}) \ . \tag{96}$$

The equilibrium constraint nested in (75) implies

$$Q^y_{mn} = \frac{-\alpha_m Q^x_{mn} + q_{mn}}{\alpha_n} \ . \tag{97}$$

The minimization operation in (75) is replaced by minimization over the unknown independent coefficients Q^x_{mn}. This operation is performed with the help of the built in optimization tool in *Mathematica* software. The results presented correspond to $N = 29$. Having the distribution of the transverse shear forces we can reconstruct the shapes of the arches by numerical integration of the Eq. (92). The shapes thus constructed compare favourably with the shapes obtained previously by performing maximization in problem (78). The method used here delivers the optimal volume: $V_{(75)} = 3.681 V_0$. The maximal elevation turns out to be: $0.8275L$

The same optimization problem has been the subject of the paper by Rozvany and Prager [20], where theory of the optimal archgrids has been put forward yet not reduced to the problems (75), (78). An updating scheme has been there constructed to arrive at the optimal solution. By this method similar results have been found, in particular the optimal volume has been assessed to be $V = 3.665 V_0$ and the maximal elevation has been predicted as equal $0.8281L$.

6 Final Remarks

The problems of optimal funiculars and optimal archgrids reduce to two mutually dual auxiliary problems. The minimization problem determines the transverse forces in the effective beams, while the maximization problem determines the elevation function of the roof. These solutions are linked by relations which express the gradient of the elevation function by the transverse forces of the effective beams. These equations cannot be inverted.

The paper shows that the problems of optimal funicular and optimal archgrids fall within the known mathematical framework encompassing: the theory of Michell

structures, theory of Prager-Rozvany grillages and the free material design in its extended version, as elaborated in Czarnecki and Lewiński [3–7], Czarnecki [2], Czubacki and Lewiński [9], Czarnecki and Wawruch [8], Dzierżanowski and Lewiński [12], cf. Lewiński et al. [17], Chap. 6.

Thus, the solutions to the auxiliary problems (78), (75) determine the subdomain Ω_m over which the roof should be constructed. Therefore, not only the elevation function is constructed, but also a subdomain of the planar domain Ω is indicated over which the roof should be built. This feature links this theory with the methods of optimization of structural topology.

On the other hand, the method imposes that the arches are directed along the x and y axes. It seems that this limitation of the method cannot be removed by new theoretical approaches. Instead, a direct numerical approach based on the ground structure concept should be applied.

To extend the approach used in the present paper towards archgrids composed of arches within arbitrary planes orthogonal to the domain Ω, i.e. not necessarily designed in the $x = \text{const}$ and $y = \text{const}$ planes, one should treat the archgrids as Michell structures under transmissible loads. This approach will be the subject of the forthcoming papers.

References

1. Chróścielewski, J., Makowski, J., Pietraszkiewicz, W.: Statics and Dynamics of Multifolded Shells. The Nonlinear Theory and the Finite Element Method, IPPT PAN, Warsaw (In Polish) (2004)
2. Czarnecki, S.: Isotropic material design. Comput. Meth Sci. Technol. **21**, 49–64 (2015)
3. Czarnecki, S., Lewiński, T.: A stress-based formulation of the free material design problem with the trace constraint and single loading condition. Bull. Pol. Acad. Sci. Tech. Sci. **60**(2), 191–204 (2012)
4. Czarnecki, S., Lewiński, T.: A stress-based formulation of the free material design problem with the trace constraint and multiple load conditions. Struct. Multidiscip. Optim. **49**(5), 707–731 (2014)
5. Czarnecki, S., Lewiński, T.: The free material design in linear elasticity. In: Rozvany, G.I.N., Lewiński, T. (eds.) Topology Optimization in Structural and Continuum Mechanics. CISM International Centre for Mechanical Sciences. Courses and Lectures, vol. 549, pp. 213–257. Springer, Wien, Heidelberg, New York, Dordrecht London, CISM, Udine (2014)
6. Czarnecki, S., Lewiński, T.: On material design by the optimal choice of Young's modulus distribution. Int. J. Solids Struct. **110–111**, 315–331 (2017)
7. Czarnecki, S., Lewiński, T.: Pareto optimal design of non-homogeneous isotropic material properties for the multiple loading conditions. Phys. Status Solidi B Basic Solids State Phys. **254**(1600821), 1–14 (2017)
8. Czarnecki, S., Wawruch, P.: The emergence of auxetic material as a result of optimal isotropic design. Phys. Status Solidi B **252**, 1–11 (2015)
9. Czubacki, R., Lewiński, T.: Topology optimization of spatial continuum structures made of non-homogeneous material of cubic symmetry. J. Mech. Mater. Struct. **10**(4), 519–535 (2015)
10. Darwich, W., Gilbert, M., Tyas, A.: Optimum structure to carry a uniform load between pinned supports. Struct. Multidiscip. Optim. **42**, 33–42 (2010)
11. Duvaut, G., Lions, J.-L.: Inequalities in Mechanics and Physics. Springer-Verlag, Berlin (1976)

12. Dzierżanowski, G., Lewiński, T.: Young's modulus control in material and topology optimization. In: Schumacher, A., Vietor, Th., Fiebig, S., Bletzinger, K.-U., Maute, K. (eds.) Advances in Structural and Multidisciplinary Optimization. Proceedings of the 12th World Congress of Structural and Multidisciplinary Optimization (WCSMO12), pp 1374–1385. Springer International Publishing AG, Cham (2018)
13. Fuchs, M.B., Moses, E.: Optimal structural topologies with transmissible loads. Struct. Multidiscip. Optim. **19**, 263–273 (2000)
14. Hetmański, K., Lewiński, T.: Forming the frames and arches which do not undergo bending. In: Szcześniak, W. (ed.) Theoretical Foundations of Civil Engineering-XV. Proceedings of Polish-Ukrainian-Lithuanian Transactions, pp. 231–246. Oficyna Wydawnicza PW, Warszawa (2007). (in Polish)
15. Jiang, Y., Zegard, T., Baker, W.F., Paulino, G.H.: Form finding of grid-shells using the ground structure and potential energy methods: a comparative study and assessment. Struct. Multidiscip. Optim. **57**, 1187–1211 (2018)
16. Lewiński, T., Sokół, T.: On plane funicular structures. In: Kamiński, M., Obrębski, J.B. (eds.) Lightweight Structures in Civil Engineering. Contemporary problems. International Seminar of IASS Polish Chapters. Łódź December 2, 2011, JBO MP Wydawnictwo Naukowe, pp. 78–82 (2011)
17. Lewiński, T., Sokół, T., Graczykowski, C.: Michell Structures. Springer, Cham (2019)
18. Rozvany, G.I.N.: Structural Design via Optimality Criteria. Kluwer Academic Publishers, Dordrecht, The Netherlands (1989)
19. Rozvany, G.I.N., Nakamura, H., Kuhnell, B.T.: Optimal archgrids: allowance for self-weight. Comput. Meth. Appl. Mech. Eng. **24**, 287–304 (1980)
20. Rozvany, G.I.N., Prager, W.: A new class of structural optimization problems: optimal archgrids. Comput. Meth. Appl. Mech. Eng. **19**, 127–150 (1979)
21. Rozvany, G.I.N., Wang, C.-M., Dow, M.: Prager-structures: archgrids and cable networks of optimal layout. Comput. Meth. Appl. Mech. Eng. **31**, 91–113 (1982)
22. Rozvany, G.I.N., Wang, C.-M.: On plane Prager-structures- I. Int. J. Mech. Sci. **25**, 519–527 (1983)
23. Wang, C.-M., Rozvany, G.I.N.: On plane Prager-structures- II. Non-parallel external loads and allowances for selfweight. Int. J. Mech. Sci. **25**, 529–541 (1983)

Cylindrical Shell Model of Helical Type Wire Structures Accounting for Layers' Interaction

Alexander N. Danilin and Sergey I. Zhavoronok

Abstract Analysis of overhead power transmission lines (OPL) involves the simulation of statics and dynamics of conductors and cables together with spiral accessories, vibration dampers, and other devices accounting for internal conductors' structures. As a typical conductor is formed by wire layers wound on each other at different angles, known issues arise in the estimates of stiffness, bearing capacity, and other properties of such structure. Indeed, the bending stiffness of the conductor depends considerably on its deformation and vary along the conductor axis as well as in time since the wire layers may slip relative to each other, and a separate wire is movable within the wire layer. On the other hand, each wire layer could be considered as an equivalent elastic anisotropic cylindrical shell on the basis of energy averaging, therefore a conductor or a spiral clamp could be modeled as a system of shells nested into each other and interacting by means of pressure and friction. This method allows one to obtain the formulae for the flexibility and stiffness of spiral structures. Some simulation results for two-layer connecting clamps with conductors including the estimates for the bearing clamp capacity limits are shown below.

1 Introduction

The wire structures such as overhead power line conductors are usually modeled by cables or uniform flexible roads by averaging mechanical properties. This engineering approach was widely used in dynamics to simulate oscillations of conductors loaded by wind flows [2, 4, 5, 12, 14, 20]. At the same time neglecting of internal

A. N. Danilin · S. I. Zhavoronok (✉)
Institute of Applied Mechanics of Russian Academy of Sciences, 125040 Leningradskiy prosp. 7, Moscow, Russia
e-mail: Zhavoronok@iam.ras.ru

Moscow Aviation Institute, National Research University, 125993 Volokolamskoie Shosse 4, A-80, GSP-3, Moscow, Russia

H. Altenbach et al. (eds.), *Recent Developments in the Theory of Shells*,
Advanced Structured Materials 110, https://doi.org/10.1007/978-3-030-17747-8_13

structures of conductors does not allow one to account properly various effects of their deformation [3, 5, 8, 12, 13, 15, 16, 19, 20], results in uncertainties in estimates of properties of wired structures and leads to severe errors as it was shown by Papailiou [19]. Use of detailed finite element modeling of typical wire structures [11, 18] remains extremely resource consuming, therefore it seems to be almost unacceptable in problems of wired conductors' dynamics. On the other hand the determination of multiple contact interfaces between wires and wire layers depending on computing algorithms effects significantly on simulation results, thus, the use of the direct finite element simulation in 3D for structural optimization of wires may become inefficient, and the appropriate simplified modeling is required.

Two different assumptions about the deforming of wired structures that could be interpreted as "opposite" in meaning result in lower and upper analytical estimates for bending and torsional stiffness of conductors. These approaches assume ideally independent behavior of wires or, vice versa, their ideal coupling, i.e. the rigid connection of wires. Both approaches lead to simple models, however, Vinogradov [28] has shown that such estimates obtained for one cable can differ by more than 70 times. The inaccuracy of such models and the inefficiency of detailed finite element simulations lead to the development of various "intermediate" approaches, e.g. based on the energy averaging of the properties of wire spirals in each wire layer of a conductor's structure. For instance, [3, 5, 12, 13, 15, 16, 22–24] considered the deformation of an arbitrary spiral wire, and then the coupling of all wires in the layer of in the whole conductor was assumed. At the same time the adequate modeling of the adjacent layers' interaction by the pressure and the friction forces may be too difficult, and wrong hypotheses could demolish entirely the integrity of the wire model and result in unacceptable errors.

An improved approach of Shalashilin et al. [27], Danilin [7], Danilin et al. [6] treats each wire layer as an equivalent anisotropic cylindrical shell using energy averaging. Conductors are interpreted hence as systems of cylindrical shells embedded into each other and interacting through the pressure and friction. The further development of this method is presented below. Indeed, one of the features of the shell-based approach consists in the possibility of modeling of such complex systems as spiral type clamps that are used for conductors suspending, tension, connecting, protecting and repairing in the modern engineering practice (e.g. see [1, 6, 9, 10, 17, 25, 26, 29, 30]). The high flexibility of typical spiral clamps consisting in one or several wired layers of limited length allows one to combine them with different conductors, moreover a spiral clamp integrated with a conductor after installation forms an almost monolithic structure. Thus, the layers of such a clamp mounted on a conductor could be considered within the presented modeling strategy as additional limited-length layers os wire structures. As the optimal design of clamps requires its geometry parameters, i.e. the clamping length, direction, and angle of rise of spirals as well as the load capacity to be estimated accurately, the appropriate models accounting properly the pressure and friction must be constructed. Some estimates based on the equivalent laminate shell models of wire structures of OPL's conductors with integrated spiral clamps are shown below.

2 Reduction of a Helix Layer to An Equivalent Cylindrical Shell

Let us consider the cross-section of a helical rod by an osculating plane (Fig. 1). Let $\rho = r/\cos^2\alpha$ be the curvature radius, where α is the ascent angle, $d\Theta = ds/\rho$:

The equilibrium of the forces in the rod can be formulated hence as follows:

$$\frac{dN}{ds} - \frac{Q}{\rho} + t = 0; \quad \frac{dQ}{ds} + \frac{N}{\rho} - q = 0 \tag{1}$$

while the equilibrium of couples results in the well known equation

$$dM/ds = Q$$

Let L be the turn pitch length measured along the conductor axis, and let S denote the helix length along its own longitudinal axis:

$$S = \frac{2\pi r}{\cos\alpha}; \quad L = S|\sin\alpha| = 2\pi r\frac{|\sin\alpha|}{\cos\alpha} \tag{2}$$

Let us consider the equilibrium of the helix rod assuming the internal forces be constant along the rod length. First, let us neglect the effect of the shear force Q. Second, let us introduce the longitudinal force P (Fig. 2a); the resultant reaction couple arising in the cross-section could be decomposed in the sum of the bending couple $M_b(P)$ and torque $M_t(P)$:

$$M_b(P) = Pr\sin\alpha, \quad M_t(P) = Pr\cos\alpha \tag{3}$$

whereas the longitudinal force in the wire cross-section is defined as

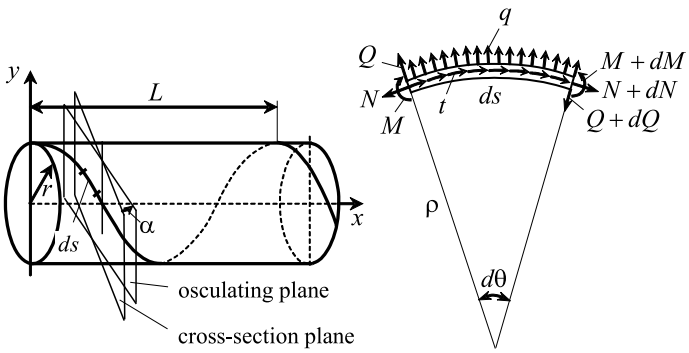

Fig. 1 The equilibrium of the differential element of the helical rod in the osculating plane

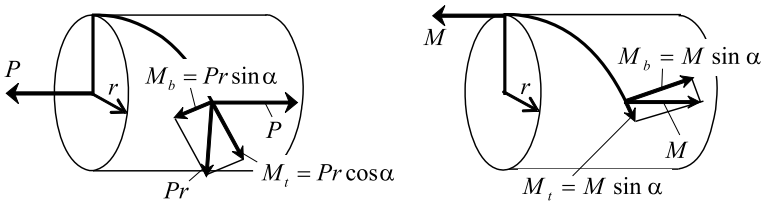

(a) Couples induced by the longitudinal force

(b) Couples induced by the torque

Fig. 2 Couples in the cross section of the helical rod from the action of external force factors

$$N(P) = P\sin\alpha \tag{4}$$

Let the transverse load q act along the curvature radius $\rho = r/\cos^2\alpha$ in the osculating plane. Assuming that only the translation w along the curvature radius appears as a result of loading by q, moreover it remains constant along the rod, we obtain the longitudinal force $N(q)$ accordingly to the Eq. (1):

$$N(q) = q\rho = \frac{qr}{\cos^2\alpha} \tag{5}$$

Finally, let us consider the external torque M acting along the rod longitudinal axis as it is shown on the Fig. 2b and equilibrated by the internal torque $M_t(M)$ and the corresponding bending couple $M_b(M)$:

$$M_b(M) = -M\cos\alpha, \quad M_t(M) = M\sin\alpha \tag{6}$$

As a result, we could define the summary bending, torsional, and longitudinal internal reactions in the cross-section of the rod as functions of the external force P, the torque M, and the transverse load q:

$$\begin{aligned} M_b &= M_b(P) + M_b(M) = Pr\sin\alpha - M\cos\alpha \\ M_t &= M_t(P) + M_t(M) = Pr\cos\alpha + M\sin\alpha \\ N &= N(P) + N(q) = P\sin\alpha + qr/\cos^2\alpha \end{aligned} \tag{7}$$

Taking into account (7), we can represent the strain energy of the helix as follows:

$$U = \frac{1}{2}\int_0^S \left(\frac{M_b^2}{EJ_z} + \frac{M_t^2}{GJ_t} + \frac{N^2}{EF}\right) ds \tag{8}$$

$$= \frac{S}{2}\left[\frac{(Pr\sin\alpha - M\cos\alpha)^2}{EJ_z} + \frac{(Pr\cos\alpha + M\sin\alpha)^2}{GJ_t} + \frac{\left(P\sin\alpha + qr\sec^2\alpha\right)^2}{EF}\right] \tag{9}$$

EJ_z, GJ_t, and EF are bending, torsional, and longitudinal stiffness of the helical rod.

Let us introduce the following conjugated generalized forces:

$$P^* = P + N(q)\sin\alpha = P + qr\sin\alpha = P + qr\frac{\sin\alpha}{\cos^2\alpha},$$
$$M^* = M + N(q)r\cos\alpha = M + qr^2\frac{1}{\cos^2\alpha} \tag{10}$$

The work of the external force q on the displacement w can be defined as follows:

$$A_q = \int_0^S qw\,ds$$

As $w = \text{Const}$ within a coil of length S, we obtain $A_q = qSw$, therefore the quantity Sw defines the generalized displacement being work-conjugated to the force q.

Expressing the force P and torque M through the conjugated ones P^*, M^*, and the load q, and substituting them into (9) accordingly to (10) gives the final formulation for the strain energy U:

$$U = \frac{S}{2}\left\{\frac{1}{EJ_z}\left[P^*r\sin\alpha - M^*\cos\alpha - qr^2\left(\tan^2\alpha - 1\right)\right]^2\right.$$
$$\left. + \frac{1}{GJ_t}\left(P^*r\cos\alpha + M^*\sin\alpha - 2qr^2\tan\alpha\right)^2 + \frac{1}{EF}\left(P^*\sin\alpha + qr\right)\right\} \tag{11}$$

Thus, we can define the generalized displacements introduced by the differentiation of the strain energy (11) with respect to P^*, M^*, and q as provided by the Castigliano theorem:

$$\Delta = \frac{\partial U}{\partial P^*}; \quad \varphi = \frac{\partial U}{\partial M^*}; \quad Sw = \frac{\partial U}{\partial q}$$

here Δ denotes the elongation of the helical rod along the axis x, and φ is the angle twisting of the rod around the longitudinal axis. The obtained constitutive equations have the following matrix formulation:

$$[\Delta \quad \varphi \quad Sw]^T = A\left[P^* \quad M^* \quad q\right]^T, \quad A = \left(a_{ij}\right) = \left(a_{ji}\right), \quad i, j = 1, 2, 3$$

where the elements of the matrix A are introduced below:

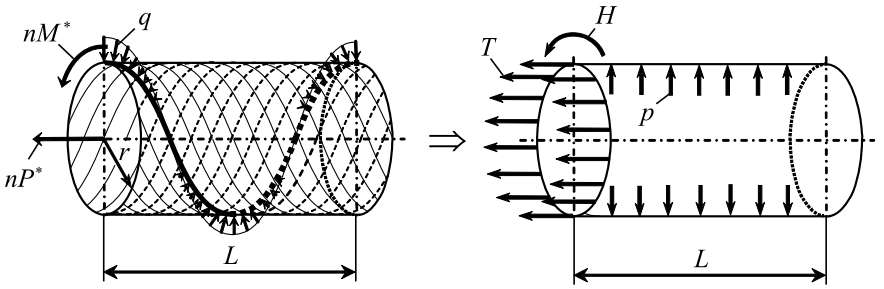

Fig. 3 The reduction of the conductor layer to an equivalent shell

$$
\begin{aligned}
a_{11} &= Sr^2\left(\frac{1+\psi}{EJ_z}\sin^2\alpha+\frac{\cos^2\alpha}{GJ_t}\right);\quad a_{12}=Sr\left(\frac{1}{GJ_t}-\frac{1}{EJ_z}\right)\sin\alpha\cos\alpha\\
a_{22} &= S\left(\frac{\sin^2\alpha}{GJ_t}+\frac{\cos^2\alpha}{EJ_z}\right);\quad a_{33}=Sr^4\left[\frac{(1-\mathrm{tg}^2\alpha)^2+\psi}{EJ_z}+\frac{4\mathrm{tg}^2\alpha}{GJ_t}\right]\\
a_{13} &= -Sr^3\left(\frac{\tan^2\alpha-(1+\psi)}{EJ_z}+\frac{2}{GJ_t}\right)\sin\alpha\\
a_{23} &= -Sr^2\left(\frac{2\tan^2\alpha}{GJ_t}+\frac{1-\tan^2\alpha}{EJ_z}\right)\cos\alpha
\end{aligned}
\tag{12}
$$

here $\psi = J_z/Fr^2$ is the dimensionless factor.

Let us consider the cylindrical shell of radius r and length L, loaded at its ends by the longitudinal force T, the torque H, and the internal pressure p (see Fig. 3):

As provided by the proposed modeling concept, the shell should be elastically equivalent to the conductor layer. First, the loads p_1, M_1, q_1 acting on the separate rod of the system should be related with the loads T, H, and q acting on the shell:

$$
P_1 = T\frac{2\pi r}{n};\quad M_1=\frac{H}{n};\quad q_1=p\frac{2\pi rL}{nS} \tag{13}
$$

where n denotes the rods number. Thus, the constitutive equations for the relative elongation ε, the relative twist angle θ, and the deflection w for the equivalent cylindrical shell could be introduced accounting for (13) in the matrix representation:

$$
[\varepsilon\quad\theta\quad w]^T = B\,[T\quad H\quad p]^T\quad B=\left(b_{ij}\right),\quad i,j=1,2,3 \tag{14}
$$

The elements of the matrix B are defined as follows:

$$
\begin{aligned}
b_{11} &= \frac{2\pi r^3}{n|\sin\alpha|}\left(\frac{1+\psi}{EJ_z}\sin^2\alpha + \frac{\cos^2\alpha}{GJ_t}\right)\\
b_{12} &= \frac{r}{n}\left(\frac{1}{GJ_t} - \frac{1}{EJ_z}\right)\operatorname{sgn}\alpha\cos\alpha, \quad b_{21} = 2\pi r b_{12}\\
b_{13} &= -\frac{2\pi r^4}{n}\left[\frac{\tan^2\alpha - (1+\psi)}{EJ_z} + \frac{2}{GJ_t}\right]\sin\alpha, \quad b_{31} = b_{13}\\
b_{22} &= \frac{1}{n|\sin\alpha|}\left(\frac{\sin^2\alpha}{GJ_t} + \frac{\cos^2\alpha}{EJ_z}\right)\\
b_{23} &= -\frac{2\pi r^3}{n}\left(\frac{2\tan^2\alpha}{GJ_t} + \frac{1-\tan^2\alpha}{EJ_z}\right)\cos\alpha, \quad b_{32} = \frac{b_{23}}{2\pi r}\\
b_{33} &= \frac{2\pi r^5}{n}|\sin\alpha|\left[\frac{(1-\tan^2\alpha)^2+\psi}{EJ_z} + \frac{4\tan^2\alpha}{GJ_t}\right]
\end{aligned}
\tag{15}
$$

3 Stiffness of a Conductor

As a conductor is modeled by an elastic rod with corresponding mechanical properties, the constitutive equations can be introduced accordingly to the Hookean law:

$$
(\varepsilon\ \theta\ \kappa)^T = B\,(N\ H\ M)^T \quad \text{or} \quad (N\ H\ M)^T = R\,(\varepsilon\ \theta\ \kappa)^T \tag{16}
$$

here ε, θ, and κ are the longitudinal strain, the relative twisting angle, and the curvature change of the rod axis, respectively; N, H, M denote the longitudinal force, the torque, and the bending couple in the rod; finally, B and R are the compliance and stiffness matrices, i.e. $R = B^{-1}$. The definition of the tensile, torsional, and bending stiffness for an usual isotropic beam referred to the principal central axes follows from (16) by considering the diagonal stiffness and compliance matrices R and B.

As the considered conductor consists of a central wire (so-called core) and several wire layers interpreted here as anisotropic cylindrical shells defined within the constitutive equations (14), (15). Let the conductor layers be numbered from 1 to n, while the core is indexed by 0. Thus, the constitutive equation (14) formulated for the i-th layer the takes the following form:

$$
\left(\varepsilon^{(i)}\ \theta^{(i)}\ 0\right)^T = B^{(i)}\left(T^{(i)}\ H^{(i)}\ p^{(i)}\right)^T \tag{17}
$$

Here the tangent force in the midsurface of the i-th shell referred hereinafter as $T^{(i)}$ is related to the longitudinal force $N^{(i)}$ acting on the shell by the equation (18):

$$
N^{(i)} = 2\pi r^{(i)} T^{(i)} \tag{18}
$$

where $r^{(i)}$ denotes the radius of the i-th layer midsurface.

Let us express $p^{(i)}$ through $T^{(i)}$ and $H^{(i)}$, therefore the constitutive equations (17) can be reduced to the following form:

$$\left(\varepsilon^{(i)}\ \theta^{(i)}\right)^T = \bar{B}^{(i)}\left(T^{(i)}\ H^{(i)}\right)^T \tag{19}$$

$$\bar{B}^{(i)} = \left(\bar{b}_{kl}\right) = \begin{pmatrix} b_{11}^{(i)} - \dfrac{b_{13}^{(i)} b_{31}^{(i)}}{b_{33}^{(i)}} & b_{12}^{(i)} - \dfrac{b_{13}^{(i)} b_{32}^{(i)}}{b_{33}^{(i)}} \\ b_{21}^{(i)} - \dfrac{b_{23}^{(i)} b_{31}^{(i)}}{b_{33}^{(i)}} & b_{22}^{(i)} - \dfrac{b_{23}^{(i)} b_{32}^{(i)}}{b_{33}^{(i)}} \end{pmatrix}, \quad k, l = 1, 2 \tag{20}$$

Inversion of the matrix $B^{(i)}$ allows one to express the forces $T^{(i)}$, $H^{(i)}$:

$$\left(T^{(i)}\ H^{(i)}\right)^T = C^{(i)}\left(\varepsilon^{(i)}\ \theta^{(i)}\right)^T; \quad C^{(i)} = \left(c_{pq}\right) = \left(\bar{B}^{(i)}\right)^{-1}; \quad p, q = 1, 2 \tag{21}$$

The longitudinal force N and the torque H for the whole conductor can be introduced by the summation of the forces and torques acting on the core and layers:

$$N = N^{(0)} + \sum_{i=1}^{n} N^{(i)} = N^{(0)} + 2\pi \sum_{i=1}^{n} r^{(i)} T^{(i)}; \quad H = H^{(0)} + \sum_{i=1}^{n} H^{(i)} \tag{22}$$

Let us assume the conductor layers lie without gaps, interference fits, and let their contacts be ideal with no relative sliding. As a result, we can assume equality of the deformations of all the layers of the conductor:

$$\varepsilon^{(i)} = \varepsilon; \quad \theta^{(i)} = \theta, \quad i = 0, 1 \ldots n \tag{23}$$

and, accounting for (22), we can obtain the following internal forces:

$$\begin{pmatrix} N \\ H \end{pmatrix} = \begin{pmatrix} N^{(0)} \\ H^{(0)} \end{pmatrix} + \sum_{i=1}^{n} \begin{pmatrix} 2\pi r^{(i)} & 0 \\ 0 & 1 \end{pmatrix} \begin{pmatrix} T^{(i)} \\ H^{(i)} \end{pmatrix} \tag{24}$$

Let us introduce hence the area $F^{(0)}$ and the polar moment of inertia $J_t^{(0)}$ for the core:

$$F^{(0)} = \pi \frac{\left(d^{(0)}\right)^2}{4}, \quad J_t^{(0)} = \pi \frac{\left(d^{(0)}\right)^4}{32}$$

here $d^{(0)}$ is the core wire diameter while its tension and shear moduli are denoted as $E^{(0)}$ and $G^{(0)}$. Thus, the substitution of (21) into (24) and accounting for (23) give

$$\begin{pmatrix} N \\ H \end{pmatrix}^T = R \begin{pmatrix} \varepsilon \\ \theta \end{pmatrix}^T; \quad R = \begin{pmatrix} E^{(0)} F^{(0)} & 0 \\ 0 & G^{(0)} J_t^{(0)} \end{pmatrix} + \sum_{i=1}^{n} \begin{pmatrix} 2\pi r^{(i)} & 0 \\ 0 & 1 \end{pmatrix} C^{(i)}$$

The obtained stiffness matrix R corresponds to the coupled stretching and twisting of the conductor. It could be expected that the elements $R_{12} = R_{21}$ are in any case relatively small as compared to the diagonal ones, R_{11} and R_{22}, as a result of the counter winding of conductor layers. Thus, as the angles of winding layers can be selected to secure vanishing out-of-diagonal elements of the stiffness matrix, R_{11} and R_{22} can be interpreted as traditional longitudinal and torsional stiffness of the conductor, therefore the constitutive equations (19), (20) allow one to determine both bending and torsional stiffness of the wire structure.

Indeed, let us consider the pure torsion. At $T = 0$ it follows from (19) that

$$\theta^{(i)} = \bar{b}_{22}^{(i)} H^{(i)} \tag{25}$$

Let the wire be twisted by the angle θ, thus, accounting for (22) and (23), we define the torque H as follows:

$$H = \sum_{i=0}^{n} \theta^{(i)} c_{22}^{(i)} = \theta \sum_{i=0}^{n} c_{22}^{(i)} \tag{26}$$

As the torsional stiffness of the conductor is denoted as GJ_t, where G is some shear modulus, we have

$$\theta = \frac{H}{GJ_t}$$

As a result, we obtain the summary torsion stiffness on the background of (26):

$$GJ_t = \sum_{i=0}^{n} c_{22}^{(i)} \tag{27}$$

Let us define the compliance for the core

$$b_{22}^{(0)} = \frac{1}{G^{(0)} J_t^{(0)}} \approx \frac{10}{G^{(0)} \left(d^{(0)}\right)^4}$$

as well as for the i-th layer:

$$J_t^{(i)} \approx 0.1 \left(d^{(i)}\right)^4 \quad J_b^{(i)} \approx 0.05 \left(d^{(i)}\right)^4; \quad G^{(i)} = \frac{E^{(i)}}{2(1+\nu^{(i)})}$$

where $E^{(i)}$, $\nu^{(i)}$ are Young moduli and Poisson ratios of layers' materials. Thus, we obtain the final expression for the torsion siffness of the conductor:

$$GJ_t = 0.1 G^{(0)} J_t^{(0)} + \sum_{i=1}^{n} c_{22}^{(i)} \tag{28}$$

Let us consider hence the conductor bending stiffness. Let the bending couple be expressed through the longitudinal stress as follows:

$$M_b = \int_F y\sigma dF \tag{29}$$

The curvature change of the rod axis κ is related with the current curvature radius ρ and with the bending couple M_b by the following known formula:

$$\kappa = \frac{1}{\rho} = \frac{M_b}{EJ_b} \tag{30}$$

As we assume the flat cross-sections condition be fulfilled, the elementary fiber elongation corresponding to the curvature radius ρ can be defined by (31):

$$\varepsilon = \frac{y}{\rho} \tag{31}$$

On the other hand the i-th layer is interpreted as a shell consisting of longitudinal fibers with the stresses $\sigma^{(i)} = T^{(i)}/d^{(i)}$, therefore the constitutive equation for longitudinal fibers follows from (19), (20):

$$\varepsilon^{(i)} = \bar{b}_{11}^{(i)} T^{(i)} = \bar{b}_{11}^{(i)} d^{(i)} \sigma^{(i)}$$

Accounting for (30) as well as for (31), we obtain

$$E^{(i)} J_b^{(i)} = M_b^{(i)} \rho^{(i)} = \rho \int_F y \frac{\varepsilon^{(i)}}{\bar{b}_{11}^{(i)} d^{(i)}} dF = \frac{1}{\bar{b}_{11}^{(i)} d^{(i)}} \int_{F^{(i)}} y^2 dF^{(i)}$$

Typical wire has circular cross-sections. Thus, assuming the radius $r^{(i)}$ and thickness $d^{(i)}$ be known, we have

$$\int_{F^{(i)}} y^2 dF^{(i)} = \pi \left(r^{(i)}\right)^3 d^{(i)}$$

and the bending stiffness of the i-th layer can be defined as follows:

$$E^{(i)} J_b^{(i)} = \frac{\pi \left(r^{(i)}\right)^3}{\bar{b}_{11}^{(i)}} \tag{32}$$

Assuming hence the axes curvature of all the layers as well as the one of the conductor be equal, we determine the bending couple by summation:

$$M_b = \sum_{i=0}^{n} M_b^{(i)}$$

Finally, accounting for (32), the bending stiffness of a whole conductor can be computed:

$$EJ_b = M_b\rho = \rho \sum_{i=0}^{n} M_b^{(i)} = \rho \sum_{i=0}^{n} \frac{E^{(i)} J_b^{(i)}}{\rho}$$
$$\approx 0.05 \left(d^{(0)}\right)^4 E^{(0)} + \pi \sum_{i=1}^{n} \left(r^{(i)}\right)^3 c_{11}^{(i)} \tag{33}$$

4 Modeling of Aluminum-Steel Conductors

The typical cross-section of an Aluminum-Steel conductor (AS) is shown on Fig.4. The aluminum conductive layers are referred hereinafter as 1 and 2 while the steel core is formed by the layer 3 and the central wire 4.

The torsional and bending stiffness for such conductors (AS series, Russia) were computed earlier by Boshnyakovich [2], Glazunov [14]. The data used for our further modeling are shown below in the Table 1. The first column contains the conductors marks given by the ratio of nominal cross-section areas of aluminum and steel parts (mm^2) while in the second column the outer conductor diameter (mm) is presented. The third column gives the sums of the wires numbers in layers; the value of each term of the sum represents the number of wires in the layer whereas the number of terms corresponds to the layers number. The nominal wire diameters and the lay ratios defined by the formula $m = L/(2r + d)$ are presented in the fourth column. Here L is the twist step, r is the radius of the layer (i.e. radius of the circle on which the centers of wires' cross sections lie), and d is the wire diameter. Thus, $L = m(2r + d)$, and finally $\alpha = \arctan[L/(2\pi r)]$ accordingly to the second formula (2). The fifth column shows the lay ratios for aluminum and steel parts.

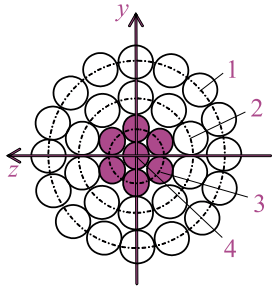

Fig. 4 Structure of an AC conductor

Table 1 Parameters of aluminum and steel parts of the conductor cross-sections

AS conductor	Outer diameter, mm	Number of wires in the layers		Wire diameter, mm		Lay ratio	
1	2	3		4		5	
Alum/Steel	Alum+Steel	Alum	Steel	Alum	Steel	Alum	Steel
120/19	15,15	10+16	1+6	2,40	1,85	15, 12	20
120/27	15,40	12+18	1+6	2,20	2,20	15, 12	20
150/19	16,75	9+15	1+6	2,80	1,85	15, 12	20
150/34	17,50	12+18	1+6	2,50	2,50	15, 12	20
185/24	18,90	9+15	1+6	3,15	2,10	15, 12	20
240/39	21,55	10+16	1+6	3,40	2,65	15, 12	20
185/128	23,10	24+30	1+6+12+18	2,10	2,10	15, 12	25, 20, 15
300/39	23,95	9+15	1+6	4,00	2,65	15, 12	20
300/66	24,50	12+18	1+6+12	3,50	2,10	15, 12	25, 20
330/30	24,78	10+16+22	1+6	2,98	2,30	15, 12, 10	20
330/43	25,20	12+18+24	1+6	2,80	2,80	15, 12, 10	20
400/22	26,56	10+16+22+28	1+6	2,57	2,00	18, 15, 13, 11	20
400/64	27,68	10+16	1+6	4,37	3,40	15, 12	20
400/93	29,10	12+18	1+6+12	4,15	2,50	15, 12	25, 20
300/204	29,15	24+30	1+6+12+18	2,65	2,65	15, 12	25, 20, 18
500/26	30,00	8+14+20	1+6	3,90	2,20	15, 12, 10	20
500/64	30,60	12+18+24	1+6	3,40	3,40	15, 12, 10	20
550/71	32,40	12+18+24	1+6	3,60	3,60	15, 12, 10	20
600/72	33,20	12+18+24	1+6+12	3,70	2,20	15, 12, 10	25, 20
650/79	34,70	15+21+27+33	1+6+12	2,90	2,30	18, 15, 12, 10	25, 20

The results of the computing are presented on the Fig. 5 where the markers indicate the values of torsional (left) and flexural (right) conductor stiffness obtained on the background of the formulae (28) and (33) and depending on the external wire diameter d (see the second column of the Table 1). For comparison, the left figure shows the dependence curve

$$GJ_t = 0.00027d^4 \tag{34}$$

where the outer diameter of the wire is given in millimeters and the numerical coefficient dimension is $\mathrm{N} \times \mathrm{m}^2/\mathrm{mm}^4$. The formula (34) was obtained at the Montefiore Institute (Belgium, University of Liège) [8] after the extensive analysis of the results of the experimental measurements. The comparison of the values given by (28) and (34) shows the good correlation of the torsional stiffness predicted by the proposed shell model of a wire and the known experimental data.

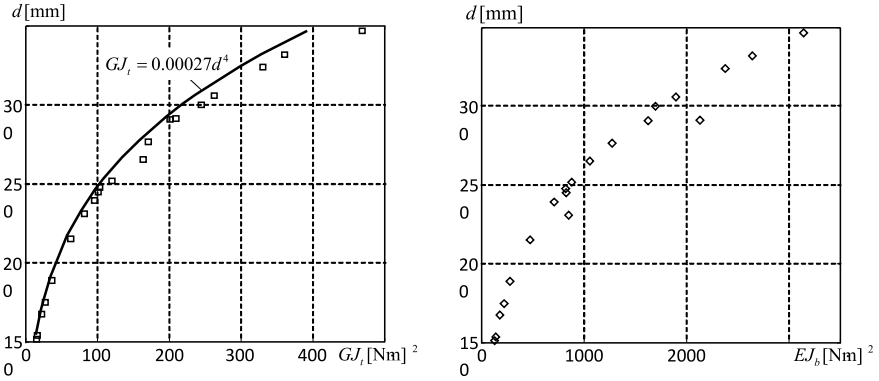

Fig. 5 Torsional (left) and bending (right) stiffness depending on external conductor diameters: shell model (squares) and experimental results' interpolation of [8] (solid line)

5 Modeling of Spiral Reinforcements

Spiral reinforcement used in OPL systems is a relatively new and very promising type of devices which can also be referred to as spiral clamps, fittings or spiral-type clamps; more strictly, there are products from factory formed helices (FFH). Their design is formed of wire spirals that come into contact directly with the conductor (ground wire, cable, etc.), covering it. A variety of applications forms various types of spiral reinforcement. Works related to the creation, production and use of spiral-type fittings for OPL, self-supporting optical communication cables, and lightning protection cables with an integrated optical cable have been carried out in a number of countries for quite a long time [1, 9, 10, 17, 21]. To date, quite a lot of spiral-type designs (spiral clamps) have been developed, which used for a wide variety of purposes and working conditions.

The purpose of spiral reinforcement is suspension, tension, connection, protection, repair and restoration of OPL conductors and cables. The simple manufacturing technology allows producing piece products for individual applications. Figure 6 shows three spiral clamp variants, which are widely used on OPL.

Next, we consider a particular problem of computing the parameters and the bearing capacity of a two-layer connecting tension clamp. Example demonstrates the capabilities of the mathematical model based on an equivalent shell method. Let us note that calculations of more complex spiral type structures will only require complication of algorithms without changing the general approach.

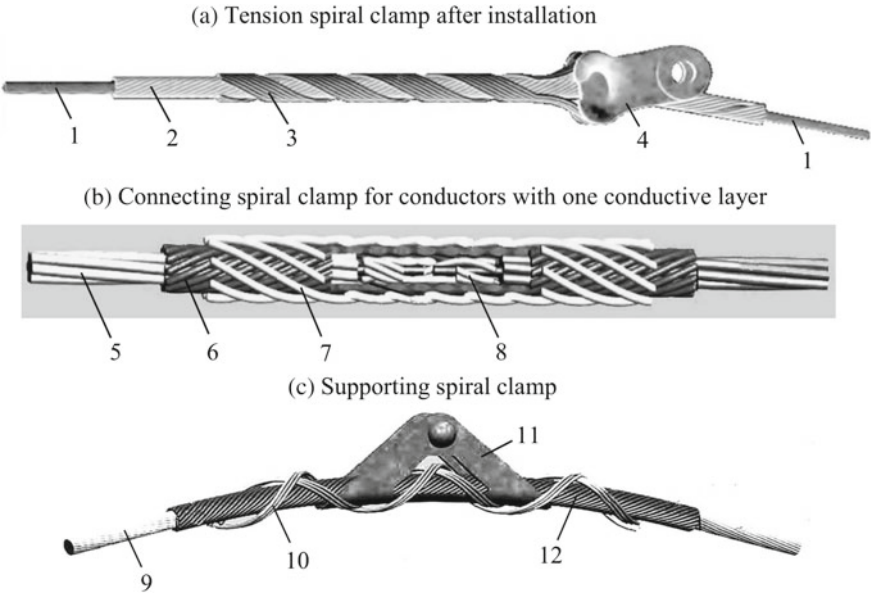

Fig. 6 Spiral clamps: 1—conductor; 2—protector; 3—power strand of spirals; 4—thimble; 5—conductor; 6—protector-retainer; 7—conductive layer; 8—connector; 9—conductor; 10—load-bearing spiral strands; 11—supporting boat; 12—protector

6 Extension of the Connecting Clamp

The connecting clamp and its model are shown on Fig. 7. The clamp consists of an external steel wire layer (i.e. a protector) and an aluminum conductive one.

Let us consider the particular case of the external and conductive clamp layers of equal lengths. We neglect the difference between the average radii of the layers, i.e.

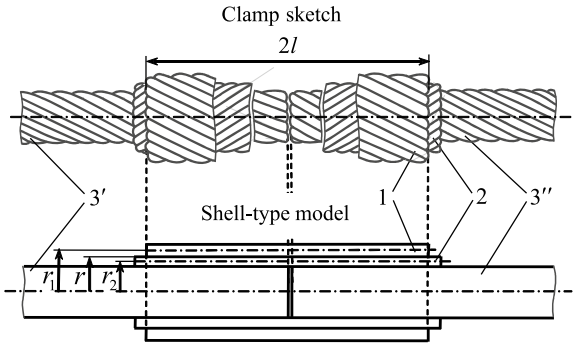

Fig. 7 The connecting spiral clamp: 1 external steel layer; 2 conductive layer; 3, 3 parts of the conductor

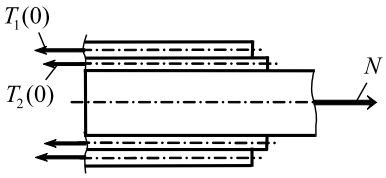

Fig. 8 The distribution of forces between the clamp layers when system extension

$r_1 = r_2 = r = 0.5(r_1 + r_2)$ is assumed below. It is clear that the extending force N is resisted by the forces in the external layer T_1 and the conductive layer T_2 (Fig. 8).

Placing the origin of the longitudinal coordinate axis in the break section (see Fig. 8), from the equilibrium condition we get

$$N = 2\pi r\,[T_1(0) + T_2(0)] = 2\pi r T(0), \quad T = T_1 + T_2$$

Let us consider hence two possible variants of reaching the bearing capacity of the connecting clamp:

- The sliding (pulling) of the clamp occurs along the contact surface between the conductive layer and the conductor itself, and the upper and conductive layers of the clamp are deformed as a whole.
- Sliding occurs first along the surface between the external and conductive layers, and further, as the load increases, the clamp slips along the contact surface between the conductive layers and the conductor.

6.1 The External and Conductive Layers are Deformed as a Whole

This case occurs when the magnitude of the friction factor $k^{(1)}$ at the interface of the upper and conductive surfaces is large enough to ensure their joint deformation without slipping relative to each other. At the same time, it is believed that slipping occurs on the interface between the conductive sheet and the wire. The constitutive relation for external ($i = 1$) and conductive layers ($i = 2$) follows from (14):

$$\left[\varepsilon^{(i)}\ \theta^{(i)}\ w^{(i)}\right]^T = B^{(i)}\left[T^{(i)}\ H^{(i)}\ p^{(i)}\right]^T, \tag{35}$$

where the elements of the matrix $B^{(i)}$ are given by the formulae (15). Here the following notation is used for an arbitrary wire of the i-th clamp layer: $E^{(i)}$, $G^{(i)}$ are elastic tension and shear moduli; $J_z^{(i)}$, $J_t^{(i)}$ are the bending and torsion inertia moments of the cross-section; $n^{(i)}$ is the number of wires in the i-th layer; $\psi^{(i)} = J_z^{(i)}/(F^{(i)}r^2)$ is the dimensionless factor, $F^{(i)}$ denotes the cross-sectional area, and finally $\alpha^{(i)}$ is the angle of inclination of the tangent line to the wire axis measured counterclockwise from the vertical.

The relations (35) could be hence inverted and presented as follows:

$$\begin{pmatrix} T^{(i)} \\ H^{(i)} \\ p^{(i)} \end{pmatrix} = D^{(i)} \begin{pmatrix} \varepsilon^{(i)} \\ \theta^{(i)} \\ w^{(i)} \end{pmatrix} = \begin{pmatrix} D_1^{(i)} & D_3^{(i)} \\ D_2^{(i)} & d_{33}^{(i)} \end{pmatrix} \begin{pmatrix} \varepsilon^{(i)} \\ \theta^{(i)} \\ w^{(i)} \end{pmatrix}; \quad i = 1,\ 2. \tag{36}$$

$$D^{(i)} = \left(d_{mn}^{(i)}\right) = \left(B^{(i)}\right)^{-1}; \quad m, n = 1, 2, 3$$

$$D_1^{(i)} = \begin{pmatrix} d_{11}^{(i)} & d_{12}^{(i)} \\ d_{21}^{(i)} & d_{22}^{(i)} \end{pmatrix}, \quad D_2^{(i)} = \begin{pmatrix} d_{31}^{(i)} & d_{32}^{(i)} \end{pmatrix}, \quad D_3^{(i)} = \begin{pmatrix} d_{13}^{(i)} \\ d_{23}^{(i)} \end{pmatrix} \tag{37}$$

It is considered that the external and conductive layers have the preloads $w_0^{(1)}$ and $w_0^{(2)}$ which are selected at installation. Together clamp layers deform when extension, so that

$$\left(\varepsilon^{(1)}\ \theta^{(1)}\right)^T = \left(\varepsilon^{(2)}\ \theta^{(2)}\right)^T = (\varepsilon\ \theta)^T; \quad w^{(1)} = w_0^{(1)}, \quad w^{(2)} = w_0^{(2)} \tag{38}$$

Taking into account (37), (38) we obtain on the background of the relation (36)

$$\begin{pmatrix} T^{(1)} \\ H^{(1)} \end{pmatrix} = D_1^{(1)} \begin{pmatrix} \varepsilon \\ \theta \end{pmatrix} + w_0^{(1)} D_3^{(1)}, \quad \begin{pmatrix} T^{(2)} \\ H^{(2)} \end{pmatrix} = D_1^{(2)} \begin{pmatrix} \varepsilon \\ \theta \end{pmatrix} + w_0^{(2)} D_3^{(2)}$$

$$p^{(1)} = D_2^{(1)} \begin{pmatrix} \varepsilon \\ \theta \end{pmatrix} + d_{33}^{(1)} w_0^{(1)}, \quad p^{(2)} = D_2^{(2)} \begin{pmatrix} \varepsilon \\ \theta \end{pmatrix} + d_{33}^{(2)} w_0^{(2)}$$

Adding these equations in pairs, we have finally

$$\begin{pmatrix} T \\ H \end{pmatrix} = \begin{pmatrix} T^{(1)} + T^{(2)} \\ H^{(1)} + H^{(2)} \end{pmatrix} = \left(D_1^{(1)} + D_1^{(2)}\right) \begin{pmatrix} \varepsilon \\ \theta \end{pmatrix} + w_0^{(1)} D_3^{(1)} + w_0^{(2)} D_3^{(2)} \tag{39}$$

$$p = p^{(1)} + p^{(2)} = \left(D_2^{(1)} + D_2^{(2)}\right) \begin{pmatrix} \varepsilon \\ \theta \end{pmatrix} + d_{33}^{(1)} w_0^{(1)} + d_{33}^{(2)} w_0^{(2)} \tag{40}$$

Let us exclude hence $(\varepsilon\theta)^T$ from (40) by means of (39). As a result, we obtain

$$p = \left(D_2^{(1)} + D_2^{(2)}\right) \left(D_1^{(1)} + D_1^{(2)}\right)^{-1} \left[\begin{pmatrix} T \\ H \end{pmatrix} - w_0^{(1)} D_3^{(1)} - w_0^{(2)} D_3^{(2)} \right]$$
$$+ d_{33}^{(1)} w_0^{(1)} + d_{33}^{(2)} w_0^{(2)} = a_0 + a_1 T + a_2 H$$

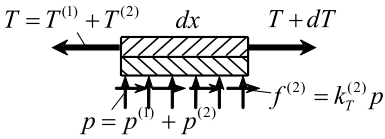

Fig. 9 The equilibrium of a clamp element

$$a_0 = d_{33}^{(1)} w_0^{(1)} + d_{33}^{(2)} w_0^{(2)} - \left(D_2^{(1)} + D_2^{(2)}\right)\left(D_1^{(1)} + D_1^{(2)}\right)^{-1}\left(w_0^{(1)} D_3^{(1)} + w_0^{(2)} D_3^{(2)}\right)$$

$$a_1 = \left(D_2^{(1)} + D_2^{(2)}\right)\left(D_1^{(1)} + D_1^{(2)}\right)^{-1}\begin{pmatrix}1\\0\end{pmatrix}$$

$$a_2 = \left(D_2^{(1)} + D_2^{(2)}\right)\left(D_1^{(1)} + D_1^{(2)}\right)^{-1}\begin{pmatrix}0\\1\end{pmatrix}$$

We assume that circumferential friction forces do not arise when slipping in the limit state, then it follows from the equilibrium of the ring element of length dx which unites the clamp layers (Fig. 9) that $H = 0$. As a result, we could obtain the following Cauchy problem:

$$\frac{dT}{dx} = -k^{(2)} p = -k^{(2)}\left(a_0 + a_1 T\right), \quad T(0) = T_0 \tag{41}$$

The solution of the problem given by (41) could be represented in the form

$$T(x) = T_\infty + (T_0 - T_\infty)\, e^{-k^{(2)} a_1 x}, \quad T_\infty = -a_0/a_1$$

The limit value of the force $T_0 = T(0)$ is reached at $T(l) = 0$:

$$T_{\text{lim}} = T_\infty\left(1 - e^{k^{(2)} a_1 l}\right) = \frac{a_0}{a_1}\left(e^{k^{(2)} a_1 l} - 1\right) \tag{42}$$

The obtained value of the limiting extension force T_{lim} and a half-length l of a clamp allows one to estimate the friction coefficient $k^{(2)}$ on the interface between the conductive surface layer and the wire itself on the basis of experimental measurements of the pulling forces of the clamp from the conductor. Indeed, it follows from (42) that

$$e^{k^{(2)} a_1 l} = 1 - \frac{T_{\text{lim}}}{T_\infty}$$

therefore we obtain the friction coefficient:

$$k^{(2)} = \frac{1}{a_1 l} \ln\left(1 - \frac{T_{\text{lim}}}{T_\infty}\right) \tag{43}$$

6.2 The External Layer Slides on the Conductive Layer

If the value of the friction coefficient $k^{(1)}$ on the interface between the external and conductive layers is not large enough, then the limit value of the force in the external layer $T^{(1)}_{\text{lim}}$ is first reached. It is defined as after solving the following Cauchy problem:

$$\frac{dT^{(1)}}{dx} = -k^{(1)} p^{(1)}, \quad T^{(1)}(0) = T_0^{(1)} \tag{44}$$

Here $p^{(1)}$ is the pressure between the external and conductive layers, which, as follows from (35), is introduced as

$$p^{(1)} = \frac{w_0^{(1)} - b_{31}^{(1)} T^{(1)}}{b_{33}^{(1)}} = a_0^{(1)} + a_1^{(1)} T^{(1)}, \quad a_0^{(1)} = \frac{w_0^{(1)}}{b_{33}^{(1)}}, \quad a_1^{(1)} = -\frac{b_{31}^{(1)}}{b_{33}^{(1)}} \tag{45}$$

The problem given by (44), (45), up to notation, coincides with problem (41). Therefore, in the limiting case, by analogy with (42), we obtain

$$T^{(1)}_{\text{lim}} = T^{(1)}_{\infty} \left(1 - e^{k^{(1)} a_1^{(1)} l}\right); \quad T^{(1)}_{\infty} = -\frac{a_0^{(1)}}{a_1^{(1)}} \tag{46}$$

For this particular case, the pressure distribution $p^{(1)}(x)$ along the clamp length on the conductive layer is determined by the formula (47) accordingly to (45), (46):

$$p^{(1)}(x) = a_0^{(1)} e^{k^{(1)} a_1^{(1)} (l-x)} \tag{47}$$

Let us consider a conductive layer under the action of longitudinal forces, pressure, and friction forces from the external layer and the actual conductor (Fig. 10). Then for the conductive layer we get the following Cauchy problem:

$$\frac{dT^{(2)}}{dx} = f^{(1)} - f^{(2)} = k^{(1)} p^{(1)} - k^{(2)} p, \quad T^{(2)}(0) = T_0^{(2)} \tag{48}$$

here $p = p^{(1)} + p^{(2)}$, where $p^{(2)}$ is the pressure that causes the conductive layer deflection that equals to its pre-load $w_0^{(2)}$.

In accordance with (35), we could obtain the contact pressure $p^{(2)}$:

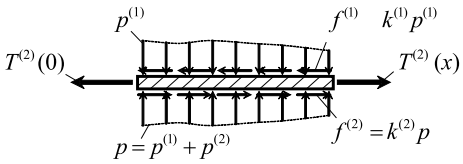

Fig. 10 The conductive layer and the forces acting on it

$$p^{(2)} = \frac{w_0^{(2)} - b_{31}^{(2)} T^{(2)}}{b_{33}^{(2)}} = a_0^{(2)} + a_1^{(2)} T^{(2)}, \quad a_0^{(2)} = \frac{w_0^{(2)}}{b_{33}^{(2)}}, \quad a_1^{(2)} = -\frac{b_{31}^{(2)}}{b_{33}^{(2)}}$$

Thus, the problem (48) can be reduced to the following formulation:

$$\frac{dT^{(2)}}{dx} = \left(k^{(1)} - k^{(2)}\right) p^{(1)} - k^{(2)} \left(a_0^{(2)} + a_1^{(2)} T^{(2)}\right), \quad T^{(2)}(0) = T_0^{(2)}$$

or, taking into account the expression (47) for $p^{(1)}$, to (49):

$$\begin{aligned} &\frac{dT^{(2)}}{dx} = \left(k^{(1)} - k^{(2)}\right) a_0^{(1)} e^{k^{(1)} a_1^{(1)} (l-x)} - k^{(2)} \left(a_0^{(2)} + a_1^{(2)} T^{(2)}\right), \\ &T^{(2)}(0) = T_0^{(2)} \end{aligned} \tag{49}$$

The general solution for the equation (49) can be represented as

$$T^{(2)}(x) = C e^{-k^{(2)} a_1^{(2)} x} + T_\infty^{(2)} - \frac{k^{(1)} - k^{(2)}}{k^{(1)} a_1^{(1)} - k^{(2)} a_1^{(2)}} a_0^{(1)} e^{k^{(1)} a_1^{(1)} (l-x)}, \tag{50}$$

$$T_\infty^{(2)} = -\frac{a_0^{(2)}}{a_1^{(2)}}$$

The integration constant C could be found from the condition $T^{(2)}(0) = T_0^{(2)}$. From (50) we get

$$C = T_0^{(2)} - T_\infty^{(2)} + \frac{k^{(1)} - k^{(2)}}{k^{(1)} a_1^{(1)} - k^{(2)} a_1^{(2)}} a_0^{(1)} e^{k^{(1)} a_1^{(1)} l} \tag{51}$$

The force $T_0^{(2)}$ will take the limit value at $T^{(2)}(l) = 0$:

$$C e^{k^{(2)} a_1^{(2)} l} + T_\infty^{(2)} - \frac{k^{(1)} - k^{(2)}}{k^{(1)} a_1^{(1)} - k^{(2)} a_1^{(2)}} a_0^{(1)} = 0$$

Taking into account the expression (51), we obtain hence

$$T_{\text{lim}}^{(2)} = T_\infty^{(2)} \left(1 - e^{k^{(2)} a_1^{(2)} l}\right) + \frac{k^{(1)} - k^{(2)}}{k^{(1)} a_1^{(1)} - k^{(2)} a_1^{(2)}} a_0^{(1)} \left(e^{k^{(2)} a_1^{(2)} l} - e^{k^{(1)} a_1^{(1)} l}\right) \tag{52}$$

The expressions for the limit values of the forces for the external and current-conducting layers make it possible to calculate the total limiting force

$$N_{\text{lim}} = 2\pi r \left(T_{\text{lim}}^{(1)} + T_{\text{lim}}^{(2)}\right)$$

that the clamp withstands. As a result, accounting for (46) and (52), we get

$$N_{\lim} = 2\pi r \left[T_{\infty}^{(1)} \left(1 - e^{k^{(1)} a_1^{(1)} l} \right) + T_{\infty}^{(2)} \left(1 - e^{k^{(2)} a_1^{(2)} l} \right) \right] + \frac{k^{(1)} - k^{(2)}}{k^{(1)} a_1^{(1)} - k^{(2)} a_1^{(2)}} a_0^{(1)} \left(e^{k^{(2)} a_1^{(2)} l} - e^{k^{(1)} a_1^{(1)} l} \right)$$

7 Example of a Connecting Clamp

Let us consider a connecting clamp ShS-15,2-01 (Russia) with an outer diameter of 15.2 mm [9] used for connecting conductors AS 120/19. Clamp half-length is assumed to be 350 mm. The main parameters of clamping patterns are given in Table 2. The pre-load coefficient, i.e. the ratio of the initial helix diameter to the diameter of the core (conductor) on which the layer is mounted, is equal to 0.91 for the protector and 0.9 for the conductive layer.

Mode 1. In this case the sliding (pulling) of the clamp occurs on the contact interface between the conductive layer and the conductor itself. For this clamp type the value of the sliding force acting on the clamp from the given conductor is experimentally established as $N_{\lim} = 23\,\text{kN}$. This value allows one to estimate the coefficient of friction on the interface between the shells modeling the conductive layer and the external layer of the conductor itself. According to (43) we find $k^{(2)} = 0.13$.

Using the pre-load factors we compute the pre-load of the protector-retainer when it is mounted on the conductive layer of the conductor: $w_0^{(1)} = 0.954\text{mm}$, and the pre-load of the conductive layer when it is mounted on the conductor $w_0^{(2)} = 0.76\text{mm}$. Using the clamp parameters, we obtain the limit value of the extension force that the clamp can withstand, $N_{\lim} = 23\,\text{kN}$, that is consistent with the friction coefficient value as provided by the formula (43). The Fig. 11 shows the distribution of the total extension force along the clamp length as well as the pressure of the conductive layer on the conductor corresponding to the first mode of the clamp carrying capacity exhaustion.

Mode 2. In this case, the sliding occurs first on the interface between the upper and conductive layers, and then, when the load increases, on the contact interface between

Table 2 Connecting clamp ShS-15,2-01

Parameters of clamp layers	Protector	Conductive layer
Wire diameter, mm	3.8	3.0
Outer diameter of the spiral, mm	27.1	19.9
Winding direction	Right	Left
Winding angle, measured from the axis of the wire, deg.	35.5	34.4
Number of spirals	4	15

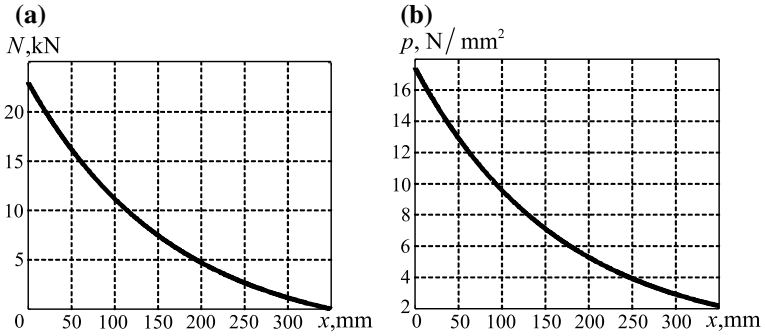

Fig. 11 The distribution of the total extension force in the clamp (**a**) and the clamping pressure on the conductor (**b**) along its length for the first mode of exhaustion of the clamp carrying capacity

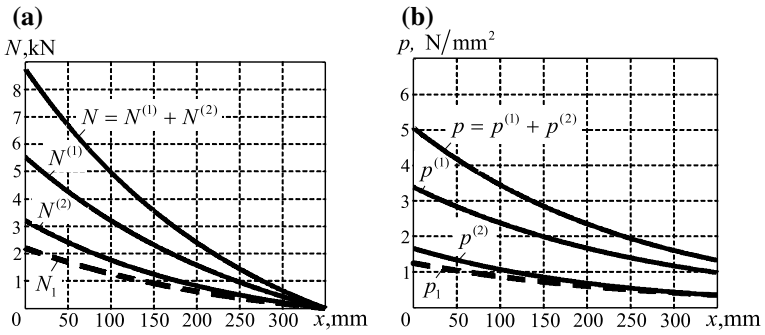

Fig. 12 Distribution of extension forces in the layers (**a**) and pressure between the layers (**b**) along the clamp length for the second mode of exhaustion of its bearing capacity

the conductive layer and the conductor. The friction factor on the contact interface between the protector-retainer and the conductive layer is assumed to be 0.12, and the friction coefficient on the interface between the conductive layer and the conductor is equal to 0.13. The pre-load is assumed to be the same as for the Mode 1. The limiting values of extension forces that can withstand the protector and conductive layer are calculated on the background of the formula $N_{\text{lim}}^{(i)} = 2\pi r T_{\text{lim}}^{(i)}\, i = 1, 2$ taking into account (46), (52). The obtained force values are equal to $N_{\text{lim}}^{(1)} \approx 5.55\,\text{kN}$, $N_{\text{lim}}^{(2)} \approx 3.22\,\text{kN}$. Finally, the total value of the limiting extension force is then equal $N_{\text{lim}} = N_{\text{lim}}^{(1)} + N_{\text{lim}}^{(2)} \approx 8.77\,\text{kN}$.

The Fig. 12a shows the distributions of the longitudinal forces and the total extension force along the clamp layers. The Fig. 12b shows the pressure distribution between the protector and the conductive layer, as well as between the conductive layer and the conductor itself. For comparison, the distribution of longitudinal forces N_1 and pressure p_1 along the clamp axis, consisting of only one aluminum layer, is also shown in Fig. 12 by dashed lines.

Thus, the limit load for the second mode of exhaustion of the bearing capacity of the connecting clamp is significantly lower as compared with the limit load for the first mode. Therefore, it is necessary to ensure contact between the layers of the clamp without slippage to increase the load-bearing clamp capacity. It can be achieved by increasing the pre-load of the external layer on the conductive layer put on the wire, as well as the friction coefficient on the interface between the external and conductive layers of the connecting clamp.

8 Conclusion

Modeling of multilayer wire structures of regular structure is considered on the basis of a new continuum model. The proposed improved approach that offers the possibility to take into account the interaction of wire layers by the pressure and friction forces consists in interpreting each layer as an equivalent anisotropic cylindrical shell on the background of energy averaging, and the whole wire structure is represented as a system of cylindrical shells enclosed into each other and interacting with possible relative sliding. The formulae for the stiffness and compliance matrices allowing one to evaluate the torsion and bending stiffness of conductors accounting their internal structures are obtained on the basis of the developed approach. Such a continuum model is significantly simpler and less consuming than the three-dimensional finite element one, nevertheless it is sufficiently accurate for the engineering practice, moreover it could result in several analytical estimates not provided by more detailed approaches. The efficiency of the equivalent shell model of a wired structure is shown on the example of the Overhead Power transmission Line conductor with the tension spiral clamp. The computation of the bearing capacity and the structural efficiency of the considered spiral clamps is presented.

Acknowledgements The work was financially supported by the Russian Ministry of Education and Science (Project ID RFMEFI60417X0188).

References

1. APRESA: Accesorios preformados. Catalog APRESA, Parcella-155, Sevilla, Spain (2005)
2. Boshnyakovich, A.D.: Mechanical Modeling of Conductors and Cables of Power Lines. Energy, Leningrad (1971). (in Russian)
3. Cardou, A., Jolicoeur, C.: Mechanical models of helical strands. Appl. Mech. Rev. **50**(1), 1–14 (1997)
4. Cloutier, L., Goudreau, S., Cardou, A.: EPRI. Transmission Line Reference Book: Wind Induced Conductor Motion, 2nd edn, CA: Electric Power Research Institute, Paolo Alto, chap Fatigue of overhead electrical conductors, pp. 3–1, 3–56 (2006, 2009)
5. Costello, G.A.: Theory of Wire Rope, 2nd edn. Springer, New York (1997)

6. Danilin, A.N., Zakharov, A.P., Kuznetsova, E.L., Kurdyumov, N.N., Tarasov, S.S.: Deformation of helical clamps for overhead power lines conductors (in rus.). Nelineiny Mir. **11**(4), 234–242 (2010)
7. Danilin, A.N., RLTS Kuznetsova, E.L.: New deformation model of the wire spiral structures (in rus.). Nelineiny Mir. **9**(10), 635–645 (2011)
8. Dubois, H., Lilien, J., Dal Maso, F.: A new theory for frequencies computation of overhead lines with bundle conductors. In: Rev. AIM, 1, Liege, pp. 46–62 (1991)
9. Electrosetstroyprorkt: Spiral linear reinforcement for suspension and repair of overhead power lines. multi-frequency vibration dampers. accessories and devices for installation works on opl (in rus.). catalogue. Catalog. Issue 14, Moscow (2004)
10. Elektrosetstroyproekt: Spiral line fittings for suspension and repair of conductors and ground wires of overhead lines. mounting devices and accessories. catalog. Issue 18, Moscow (2011)
11. Fekr, M.R.F.M., McClure, G.: Application of adina to stress analysis of an optical ground wire. Comput. Struct. **72**, 301–316 (1999)
12. Feyrer, K.: Wire Ropes: Tension, Endurance, Reliability. Springer, Berlin, New York (2007)
13. Foti, F., Martinelli, L.: A model for the cyclic biaxial bending of stranded ropes. In: Proceedings 20th Congress AIMETA, Bologna, p. 240 (2011)
14. Glazunov, A.A.: Basics of the mechanical part of overhead power lines, vol. 1. Work and computing of conductors and cables, Gosenergoizdat, Moscow-Leningrad (1956). (in Russian)
15. Goudreau, S., Lévesque, F., Cardou, A., Cloutier, L.: Strain measurements on acsr conductors during fatigue tests ii—stress fatigue indicators. IEEE Trans. Power Deliv. **25**(4), 2997–3006 (2010)
16. Hong, K.J., Der Kiuregian, A., Sackman, J.L.: Bending behavior of helically wrapped cables. ASCE J. Eng. Mech. **131**(5), 500–511 (2005)
17. JSC: Spiral fittings for overhead power lines. Technical requirements. The standard of the organization of JSC Federal Grid Company of Unified Energy System, Moscow (2010)
18. Lévesque, F., Goudreau, S., Cloutier, L., Cardou, A.: Finite element model of the contact between a vibrating conductor and a suspension clamp. Tribol. Int. **44**(9), 1014–1023 (2011)
19. Papailiou, K.: On the bending stiffness of transmission line conductors. IEEE Trans. Power Deliv. **12**(4), 1576–1588 (1997)
20. Pilkey, W.D.: Analysis and Design of Elastic. Beams Computational Methods. Wiley, New York (2002)
21. PLP: Preformed line products. Energy Product Catalog (2007)
22. Rawlins, C.B.: Analytical Elements of Overhead Conductor Fabrication. Fultus Corp (2005a)
23. Rawlins, C.B.: Flexure of a single-layer tensioned cable at a rigid support. In: Proceedings 6th International Symposium on Cable Dynamics, Charleston, USA, pp. 363–370 (2005b)
24. Rawlins, C.B.: Flexural self-damping in overhead electrical transmission conductors. J. Sound Vib. **323**(1–2), 232–256 (2009)
25. Ryzhov, S., Tsvetkov, Y.: Application experience of spiral-type fitting on overhead transmission lines (in rus.). Elektro **2**, 32–36 (2005)
26. Ryzhov, S.V.: Method of calculating the technological parameters of spiral-type tension clamps electrical stations (in rus.). Electr. Stat. **1**, 8–11 (1998)
27. Shalashilin, V., Danilin, A., Volkov-Bogorodskiy, D.: Model of overhead line conductor with interaction of layers. In: Proceedings 6th International Symposium on Cable Dynamics, Charleston, USA, pp. 371–377 (2005)
28. Vinogradov, A.: Vibrations of conductors of overhead power lines under wind. Educational and reference manual. Part 1. Fatigue strength. Vibration. (in Rus.). Publishing house CJSC. Elektrosetstroyproekt, Moscow (2005)
29. Vinogradov, A., Ryzhov, S., Shtelmakh, A.: On the development of methods for calculating tension spiral clamps. Energ. Pag. **3**, 60–61 (1994)
30. Vinogradov, A., Ryzhov, S., Tishchenko, A.: Development and promotion of industrial production of spiral-type fittings for conductor suspension (in rus.). Electr. Stat. **1**, 3–7 (1998)

Buckling of Cylindrical Shell Stiffened by Annular Plate Under External Pressure

S. B. Filippov and V. S. Sabaneev

Abstract The critical external pressure and buckling modes of a closed circular cylindrical shell joined at an edge with an annular plate are obtained by means of asymptotic methods. Two tipe of buckling, corresponding to narrow and wide rings, are analyzed. In both cases approximate solution of shell equations is represented as a sum of slowly varying functions and edge effect integrals. It is shown that a narrow ring can be considered as circular beam. For a wide ring joined with a cylindrical shell the couple buckling problem in the first approximation is reduced to the eigenvalue problem describing the plate buckling. An approximate solution of the last problem is obtained with the help of the perturbation approach. The asymptotic results are in good agreement with the numerical ones obtained by finite element analysis.

1 Introduction

Ring-stiffened shells are applied in engineering such as pressure vessel, aircraft fuselages and submarine hulls. Almost in all numerous studies of ring-stiffened shells, including [2, 3, 5, 12, 15, 16], the rings have been considered as circular beams.

In [3, 5] an algorithm for the evaluation of the optimal parameters corresponding to the maximum critical external pressure of the ring-stiffened shell with a given mass was developed. If the ring cross-section is a rectangle, then the critical pressure increases monotonically with the increase in the ratio $k = b/a$, where b and a are the non-dimensional width and the thickness of the ring. However, for large values of k, the ring must be considered as a annular plate (plate model).

S. B. Filippov (✉) · V. S. Sabaneev
St. Petersburg State University, 7/9 University Embankment, St. Petersburg 199034, Russia
e-mail: s_b_filippov@mail.ru

V. S. Sabaneev
e-mail: lesha@westcall.spb.ru

H. Altenbach et al. (eds.), *Recent Developments in the Theory of Shells*,
Advanced Structured Materials 110, https://doi.org/10.1007/978-3-030-17747-8_14

There are, at least, two reasons to use plate model for the wide ring. First, the flexural stiffness of the beam in its plane c_b increases rapidly with ring width b. However, for the wide ring its stress-strain state localizes near the inner boundary of the ring, which is attached to cylindrical shell [6]. Therefore, in reality, change in b almost have no influence upon the stiffness c of the wide ring in its plane. To catch this effect one should consider the wide ring as an annular plate. It is especially important because in the buckling problem the stiffness c has an determinative influence on the critical external pressure.

In the work [6] for $b \gg 1$ the approximate formula $c \simeq c_p$ was obtained, where c_p do not depends on b. In the first part of this paper the continuity condition for the shell joined at an edge with an annular plate are developed and by means of asymptotic methods the dependence of c on b is analyzed. In the case $b \ll h^{1/2}$, where h is dimensionless shell thickness, the stiffness of the ring $c \simeq c_b$. If $b \gg h^{-1/4}$ then the formula $c \simeq c_p$ takes place.

Secondly, the buckling of the shell stiffened at an edge by an narrow ring differs very much from the buckling of the shell stiffened at an edge by a wide ring. If the width of the ring is sufficiently small, then the buckling mode is similar to the buckling mode of the shell without rings, and the shell surface is covered by a series of pits stretched along the generatrix of a cylinder. In this case it is possible consider the ring as a circular beam. Such buckling we call the buckling of the first type.

At increase in width of a ring the critical pressure grows until the buckling of the first type replaces with the buckling of the second type. The buckling mode of the second type consists of many small pits formed on the surface of the ring. The cylindrical shell itself does not actually deform. After the buckling changed, the further increase in width of a ring leads to reduction of critical pressure. For studying the buckling of the second type the beam model can not be used, and one must consider the ring as an annular plate [7].

In the case of the second type buckling the eigenvalue problem for a cylindrical shell joined at an edge with an annular plate in the first asymptotic approximation can be split into the four separated problems. The main of them is the eigenvalue problem, describing the buckling of the annular plate. In [7] this problem was solved with the help of asymptotic method. In assumption that the ratio of the plate width to the radius of its inner edge is small, an approximate formula for the critical pressure was obtained. In the second part of this paper the formulation of other three problem are presented.

The equations describing the thin shells buckling contain the dimensionless shell thickness h as a small parameter. To get the approximate solutions the Vishik-Lyusternik algorithm [1, 18] is applied. We seek solutions of shell equations as a sum of slowly varying functions and edge effect integrals. Thus the initial singularly perturbed system of differential equations is reduced to an approximate system of the smaller order [17].

The major problem in the asymptotic analyses of the ring-stiffened shell buckling is a separation of the continuity conditions on main and additional conditions. The main conditions we use as boundary conditions for the approximate system. From additional conditions one can find arbitrary constants in the edge effect functions.

Fig. 1 Shell and ring

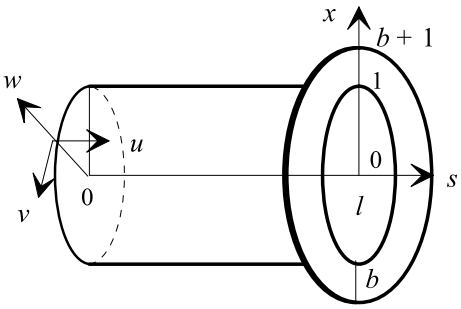

To get the main and additional conditions, as a rule, it is necessary to make linear combinations of the continuity conditions. The general continuity conditions are presented in [10, 13, 14].

The Vishik-Lyusternik algorithm was used in [4, 9] for the asymptotic analyses of low-frequency vibrations of the cylindrical shell stiffened at an edge by the annular plate.

2 Basic Equations

We consider buckling under uniform external pressure p of a thin cylindrical shell stiffened at one edge by a ring of rectangular cross-section (see Fig. 1).

We assume that the ring and the shell are made from the same material and take the radius of the cylindrical shell as the characteristic size. The non-dimensional equations describing the buckling of the cylindrical shell can be written as [17]

$$\begin{gathered} T_1' + mS = 0, \quad S' - mT_2 + Q_2 + 2H' = 0, \quad Q_1' + mQ_2 - T_2 + \lambda m\vartheta_2 = 0, \\ Q_1 = M_1' + 2mH, \quad Q_2 = -mM_2, \quad M_1 = \mu^4(\vartheta_1' + \nu m\vartheta_2), \\ M_2 = \mu^4(m\vartheta_2 + \nu\vartheta_1'), \quad H = \mu^4(1-\nu)\vartheta_2', \quad 2S = (1-\nu)(v' - mu), \\ T_1 = u' + \nu(w + mv), \quad T_2 = w + mv + \nu u', \quad \vartheta_1 = -w', \quad \vartheta_2 = mw + v, \end{gathered} \tag{1}$$

where $(')$ denotes the derivative with respect to the axial coordinate, $s \in [0, l]$, l is the dimensionless shell length, m is the circumferential wave number, $\lambda = \sigma p/(Eh)$ is the loading parameter, $\sigma = 1 - \nu^2$, ν is Poisson's ratio, E is Young's modulus, u, v and w are the components of the displacement, T_1, T_2, S, Q_1, Q_2, M_1, M_2, H are the dimensionless stress-resultants and stress-couples, ϑ_1 and ϑ_2 are the angles of rotation of the normal, $\mu^4 = h^2/12$ is a small parameter, h is the dimensionless shell thickness.

The ring is considered as the annular plate. The equations describing the transverse flexural deformation of the plate have the form [6]

$$
\begin{gathered}
(xQ_{1p})' + mQ_{2p} = xT_{1p}w_p'' + T_{2p}(w_p' - x^{-1}m^2 w_p), \\
xQ_{1p} = (xM_{1p})' - M_{2p}, \quad xQ_{2p} = -mM_{2p} + 2H_p, \\
xM_{1p} = \mu_p^4[x\vartheta_{1p}' + \nu(m\vartheta_{2p} + \vartheta_{1p})], \quad xM_{2p} = \mu_p^4(m\vartheta_{2p} + \vartheta_{1p} + \nu x\vartheta_{1p}'), \\
H_p = \mu_p^4 x(1-\nu)\vartheta_{2p}', \quad \vartheta_{1p} = -w_p', \quad x\vartheta_{2p} = mw_p.
\end{gathered}
\tag{2}
$$

Here $(')$ denotes the derivative with respect to the radial coordinate, $x \in [1, 1+b]$, b is the dimensionless plate width, w_p is the transverse deflection, Q_{1p}, Q_{2p}, M_{1p}, M_{2p}, H_p are the dimensionless stress-resultants and stress-couples, T_{1p} and T_{2p} are pre-buckling stress-resultants, ϑ_{1p} and ϑ_{2p} are the angles of rotation of the normal, $\mu_p^4 = a^2/12$ is a small parameter, a is the dimensionless plate thickness.

The tangential (in plane) deformation of the plate is described by the following equations [6]:

$$
\begin{gathered}
(xT_{1p})' - T_{2p} + S_p x = 0, \quad xS_p' + 2S_p - mT_{2p} = 0, \\
xT_{1p} = xu_p' + \nu(mv_p + u_p), \quad xT_{2p} = u_p + mv_p + \nu x u_p', \\
2xS_p = (1-\nu)(xv_p' - mu_p - v_p),
\end{gathered}
\tag{3}
$$

where u_p and v_p are the tangential components of the displacement, T_{1p}, T_{2p}, S_p are the dimensionless stress-resultants.

At the circumference $s = l$, $x = 1$, the continuity conditions

$$
\begin{gathered}
u = -w_p, \quad \vartheta_1 = \vartheta_{1p}, \quad hT_1 = -aQ_{1p}, \quad hM_1 = aM_{1p}, \\
w = u_p, \quad v = v_p, \quad hQ_1 = aT_{1p}, \quad hS = aS_p
\end{gathered}
\tag{4}
$$

have to be satisfied. We assume the left shell edge is clamped, i.e.

$$
u = v = w = \vartheta_1 = 0 \quad \text{for} \quad s = 0 \tag{5}
$$

and that the outer plate edge is free, i.e.

$$
T_{1p} = S_p = M_{1p} = Q_{1p} - T_{1p}w_p = 0 \quad \text{for} \quad x = 1 + b. \tag{6}
$$

3 Buckling of the First Type

3.1 Analysis of Boundary Conditions

Let us seek the buckling mode of the first type which is similar to the buckling mode of the shell without a ring.

The transverse flexural stiffness of the plate is more less than its tangential stiffness in plane. Neglecting the flexural stiffness of the plate we obtain from (4) two following

boundary conditions at the shell edge $s = l$:

$$T_1 = 0, \quad M_1 = 0 \quad \text{for} \quad s = l. \tag{7}$$

Sometimes there is a reason to believe that the tangential stiffness of the plate in plane is infinitely large. Then $v_p = u_p = 0$ and it follows from (4) that

$$v = 0, \quad w = 0 \quad \text{for} \quad s = l. \tag{8}$$

Conditions (7) and (8) corresponding to the freely supported shell edge, are the most simple approximate connection conditions between shell and plate.

If the ratio a/h is large then one should not to ignore the flexural stiffness of the plate and conditions (7) need an revision. On the contrary, for the small ratio a/h it is unjustified to suppose that the tangential stiffness is very large and use conditions (8). Since the ratio a/h is usually not too large for ring-stiffened shells, we assume that conditions (7) are valid. To correct conditions (8) we have to solve Eq. (3).

The change of variable $x = e^t$ reduces Eq. (3) to equations with constant coefficients:

$$\begin{aligned} &\frac{d^2u_p}{dt^2} - u_p - \gamma m^2 u_p + \delta m \frac{dv_p}{dt} - (1+\gamma) m v_p = 0, \\ &\gamma \frac{d^2v_p}{dt^2} - \gamma v_p - m^2 v_p + \delta m \frac{du}{dt} - (1+\gamma) m u_p = 0, \end{aligned} \tag{9}$$

where $\gamma = (1-\nu)/2, \delta = (1+\nu)/2$. The general solution of Eq. (9) have the form

$$\begin{aligned} u_p &= C_1 x^{m-1} + a_1 C_2 x^{m+1} + C_3 x^{-m-1} + a_2 C_4 x^{-m+1}, \\ v_p &= -C_1 x^{m-1} + b_1 C_2 x^{m+1} + C_3 x^{-m-1} + b_2 C_4 x^{-m+1}. \end{aligned} \tag{10}$$

Here $C_k, k = 1, 2, 3, 4$ are arbitrate constants,

$$a_1 = 2\gamma/(\delta m) - 1, \quad a_2 = 2\gamma/(\delta m) + 1, \quad b_1 = 2/(\delta m) + 1, \quad b_2 = 1 - 2/(\delta m).$$

From Eq. (3) we obtain the following formulas

$$\begin{aligned} T_{1p} = {} & 2C_1\gamma(m-1)x^{m-2} - 2C_2\gamma(m+1)(m-2)m^{-1}x^m - \\ & -2\gamma(m+1)C_3x^{-m-2} - 2C_4\gamma(m-1)(m+2)m^{-1}x^{-m}, \\ S_p = {} & -2C_1\gamma(m-1)x^{m-2} + 2C_2\gamma(m+1)x^m - \\ & - 2\gamma(m+1)C_3x^{-m-2} - 2C_4\gamma(m-1)x^{-m}. \end{aligned} \tag{11}$$

On the free edge of the plate $x = 1 + b$

$$T_{1p} = S_p = 0. \tag{12}$$

The substitution solutions (10) and (11) into conditions $w(l) = u_p(1)$, $v(l) = v_p(1)$ and (12) get the equations

$$\begin{gathered} C_1 + a_1 C_2 + C_3 + a_2 C_4 = w(l), \quad -C_1 + b_1 C_2 + C_3 + b_2 C_4 = v(l), \\ (m-1)[m\beta^m C_1 - (m+2)\beta C_4] - (m+1)[(m-2)\beta^{m+1} C_2 + mC_3] = 0, \\ (m-1)(\beta^m C_1 + \beta C_4) - (m+1)(\beta^{m+1} C_2 - C_3) = 0, \end{gathered} \tag{13}$$

where $\beta = (1+b)^2$.

Determine the expressions for the arbitrary constants C_k from Eq. (13) and substitute them into formulas (11). Then we obtain

$$\begin{aligned} S_p &= -2\gamma\delta[(B_1 + mB_2)w + (D_1 + mD_2)v]/D, \\ T_{1p} &= -2\gamma\delta[(mB_1 + B_2)w + (mD_1 + D_2)v]/D. \end{aligned} \tag{14}$$

Here

$$\begin{aligned} B_1 &= \beta(\beta^{2m} - 1) - 2mb(b+2)\beta^m, \\ B_2 &= \beta(\beta^m + 1)^2 - 4\beta^m - \delta\beta(\beta^m - 1)^2 + \delta m^2 b^2 (b+2)^2 \beta^m, \\ D_1 &= \gamma\beta(\beta^m - 1)^2 + \delta m^2 b^2 (b+2)^2 \beta^m, \\ D_2 &= \beta(\beta^{2m} - 1) + 2mb(b+2)\beta^m, \\ D &= \gamma[4\beta^m + \delta\beta(\beta^m - 1)^2] + \delta[\beta(\beta^m + 1)^2 + \delta m^2 b^2 (b+2)^2 \beta^m]. \end{aligned} \tag{15}$$

From the last two formulas (4) we get the two boundary conditions at the shell edge $s = l$:

$$\begin{aligned} S &= -2a\gamma\delta[(B_1 + mB_2)w + (D_1 + mD_2)v]/(hD), \\ Q_1 &= -2a\gamma\delta[(mB_1 + B_2)w + (mD_1 + D_2)v]/(hD). \end{aligned} \tag{16}$$

In boundary conditions (16) the tangential stiffness of the plate is taken into account therefore conditions (7) and (16) generalize conditions (7) and (8) corresponding to the freely supported shell edge.

3.2 *The Asymptotic Approach for a Shell with Freely Supported Edge*

Consider the buckling under uniform external pressure of a thin cylindrical shell with the boundary conditions (5), (7) and (8). In the problem under consideration

$$\lambda = m^{-6}\lambda_0, \quad \lambda_0 \sim 1, \quad m \sim \mu^{-1/2} \gg 1.$$

Table 1 Intensity indices for the buckling mode of the first type

	Functions							
Indices	u	v	w	ϑ	T_1	S	M_1	Q_1
I	-2	-1	0	0	-2	-3	-6	-6
$I_1 = I_2$	-4	-5	-2	0	-4	-3	-6	-4

We seek the approximate asymptotic solution of system (1) as a sum of the semi-membrane solution and the edge effect functions [17]:

$$y = m^{I(y)} y_0 + m^{I_1(y)} y_1 + m^{I_2(y)} y_2.$$

Here y denotes any unknown function, $I(y)$, $I_1(y)$ and $I_2(y)$ are the intensity indices. Table 1 lists values of the intensity indices for the problem under consideration

The function v_0 satisfy the semi-membrane equation

$$\frac{d^4 v_0}{ds^4} - \alpha^4 v_0 = 0, \quad \alpha^4 = \frac{\lambda m^6 - \mu^4 m^8}{\sigma}, \tag{17}$$

and

$$w_0 = -v_0, \quad u_0 = \frac{dv_0}{ds}, \quad T_{10} = \frac{d^2 v_0}{ds^2}, \quad S_0 = -\sigma \frac{d^3 v_0}{ds^3}. \tag{18}$$

The edge effect functions have the form

$$y_1 = \sum_{j=1}^{2} \hat{D}_j \hat{y}_j \exp(r_j s/\mu), \quad y_2 = \sum_{j=3}^{4} \hat{D}_j \hat{y}_j \exp[r_j (s-l)/\mu]. \tag{19}$$

Here $\hat{D}_j \sim 1$ are arbitrary constants,

$$r_{1,2} = g(-1 \pm i), \quad r_{3,4} = g(1 \pm i), \quad g = \sigma^{1/4}/\sqrt{2}, \quad i^2 = -1.$$

In particular $\hat{w}_j = 1$, $j = 1, 2, 3, 4$. The functions y_1 decrease rapidly away from the shell edge $s = 0$ and the functions y_2 are very small in the entire domain except the neighborhood of the edge $s = l$. Assume that $l \sim 1$. Then the following approximate equalities are valid

$$y(0) \simeq y_0(0) + y_1(0), \quad y(l) \simeq y_0(l) + y_2(l).$$

Boundary conditions for the Eq. (17) can be determine after a separation of the boundary conditions on main and additional conditions. From the two main conditions by neglecting of small terms we obtain boundary conditions for the Eq. (17).

Let Δ be the difference between maximal values intensity indices of semi-membrane solutions and the edge effect functions. Then

(1) For the main boundary conditions the value Δ must be strict more, than for the additional boundary conditions.

(2) The both semi-membrane solutions included in the main boundary conditions and the edge effect solutions included in the additional boundary conditions must be independent.

In order to satisfy this condition, as a rule, it is necessary to use linear combinations of boundary conditions.

Taking into account that at the edge $s = 0$

$$u = m^{-2}u_0 + m^{-4}u_1, \quad v = m^{-1}v_0 + m^{-5}v_1, \quad w = w_0 + m^{-2}w_1, \quad \vartheta_1 = \vartheta_{10} + \vartheta_{11},$$

for boundary conditions (5) we obtain

$$\Delta_1 = 2, \quad \Delta_2 = 4, \quad \Delta_3 = 2, \quad \Delta_4 = 0,$$

where Δ_k corresponds to k-th Eq. (5). It is impossible to separate boundary conditions (5) on main and additional conditions so that the condition 1 has been fulfilled. However, for linear combinations of second and third conditions $w + mv = 0$ we have $\Delta = 0$. Therefore main and additional conditions are $u = v = 0$ and $w + mv = \vartheta_1 = 0$. The boundary conditions for the equation (17) at the edge $s = 0$ have the form $u_0 = v_0 = 0$ or

$$v_0 = \frac{dv_0}{ds} = 0, \quad s = 0. \tag{20}$$

Substituting the relations

$$T_1 = m^{-2}T_{10} + m^{-4}T_{12}, \quad M_1 = m^{-6}(M_{10} + M_{12}),$$
$$v = m^{-1}v_0 + m^{-5}v_2, \quad w = w_0 + m^{-2}w_2,$$

into boundary conditions (7) and (8) we can see, that the main and additional conditions at the edge $s = l$ are $T_1 = v = 0$ and $w + mv = M_1 = 0$. Hence, the solution of Eq. (17) satisfy boundary conditions

$$v_0 = \frac{d^2v_0}{ds^2} = 0, \quad s = l. \tag{21}$$

A nontrivial solution of eigenvalue problem (17), (20) and (21) exists on the assumption that

$$\lambda = \frac{\sigma z^4}{l^4 m^6} + \mu^4 m^2,$$

where $z = \alpha l$ is the root of the equation

$$\tan z = \tanh z. \tag{22}$$

The minimal value λ_c of the loading parameter λ corresponds to the critical pressure p_c. Hence

$$\lambda_c = \min_m \left(\frac{\sigma z_1^4}{l^4 m^6} + \mu^4 m^2 \right) \simeq \frac{4\sigma^{1/4} z_1 \mu^3}{3^{3/4} l}, \tag{23}$$

where $z_1 \simeq 3.927$ is the minimal positive root of Eq. (22). For the critical pressure p_c we get the following approximate formula

$$p_c = \frac{Eh}{\sigma}\lambda_c = \frac{4Ez_1 h^{5/2}}{\sigma^{3/4} 6^{3/2} l}. \tag{24}$$

For the shell with the free supported edges instead Eq. (22) we have the equation $\sin z = 0$, $z_1 = \pi$ and relation (24) is transformed into the Southwell-Papkovich formula [17].

3.3 Approximate Solutions in the Case of Generalized Boundary Conditions

Let us separate the generalized boundary conditions (7) and (16) on main and additional conditions. One of the two main boundary conditions is $T_1(l) = 0$. To obtain the second one we substitute the relations

$$S = m^{-3}(S_0 + S_2), \quad Q_1 = m^{-6} Q_{10} + m^{-4} Q_{12},$$
$$w = w_0 + m^{-2} w_2, \quad v = m^{-1} v_0 + m^{-5} v_2, \quad M_1 = m^{-6}(M_{10} + M_{12}).$$

into conditions (16) and $M_1 = 0$. Taking the formulas

$$w_2(l) = \hat{C}_3, \quad M_{12}(l) = -2g^2 K^2 \hat{C}_4,$$
$$M_{10}(l) = -\nu K^4 w_0, \quad S_2(l) = Q_{12}(l) = 2g^3 K(\hat{C}_3 - \hat{C}_4),$$

where

$$\hat{C}_3 = \hat{D}_3 + \hat{D}_4, \quad \hat{C}_4 = i(\hat{D}_3 - \hat{D}_4), \quad K = \mu m^2,$$

into account and neglecting of small terms, we obtain

$$\begin{aligned} 2Ag^3 K(\hat{C}_3 - \hat{C}_4) + AS_0 &= mD_2 w_0 - B_2(\hat{C}_3 + m^2 w_0), \\ AS_0 &= mB_1 \hat{C}_3 + m^3 B_1 w_0 - m^2 D_1 w_0, \quad 2g^2 K^2 \hat{C}_4 = \nu K^4 w_0. \end{aligned} \tag{25}$$

Here

$$A = \frac{hD}{2a\gamma\delta m^2}.$$

The linear combination of boundary conditions (25), which do not contains the arbitrary constants $\hat{C}_3$ and $\hat{C}_4$ can be written as

$$S_0 + cv_0 = 0, \quad s = l, \tag{26}$$

where

$$c = \frac{2m^2g^3KA(mB_1 - D_1) + m^2(B_1D_2 - D_1B_2) + vmgK^3AB_1}{A(2g^3KA + mB_1 + B_2)}. \tag{27}$$

Boundary condition (26) is the second main condition.

Assume that

$$a = a_0m^{-\xi}, \quad b = b_0m^{-\eta}, \quad a_0 \sim b_0 \sim 1.$$

where a and b are the non-dimensional thickness and the width of the plate. Consider the case $\eta > 2$, i. e. $bm^2 \ll 1$ (the narrow ring). Substituting the approximate relation

$$\beta^m \simeq 1 + 2mb + \frac{2m(2m-1)b^2}{2} + \frac{2m(2m-1)(2m-2)b^3}{6}$$

into formulas (15) and neglecting of small terms, we obtain

$$\begin{aligned} B_1 &\simeq 4mb^2 + 8m^3b^3/3, \quad D_1 \simeq 4m^2b^2, \\ B_2 &\simeq 8b + 4m^2b^2, \quad D_2 \simeq 8mb, \quad D \simeq 4. \end{aligned} \tag{28}$$

If we substitute formulas (28) into relation (27) then we obtain

$$c \simeq c_b = m^8\left(J_x + \frac{e^2F_c}{1+d}\right), \tag{29}$$

where

$$d = \frac{m^2F_c}{2g^3K}, \quad e = \frac{b}{2}, \quad F_c = \frac{\sigma ab}{h}, \quad J_x = \frac{\sigma ab^3}{12h}.$$

The condition

$$S_0 + c_bv_0 = 0, \quad s = l$$

is the main continuity conditions of a cylindrical shell and a beam of the rectangular cross-section [3].

In the case $\eta < 1$, i. e. $bm \gg 1$ (the wide ring), when $\beta^m \gg 1$, using the approximate relations

$$A \simeq A_0\beta^{2m+1}, \quad A_0 = \frac{h(1+\gamma)}{2am^2\gamma}, \quad B_1 \simeq D_2 \simeq \beta^{2m+1}, \quad B_2 \simeq D_1 \simeq \gamma\beta^{2m+1},$$

we obtain

$$c \simeq c_p = \frac{m^2(2g^3mKA_0 + 1 - \gamma^2)}{A_0(2g^3KA_0 + m)}.$$

The value c_p do not depends on the width of the ring b, but depends on its thickness $a \sim m^{-\xi}$. If $\xi = 9$ then $c_p \sim 1$ and neglecting of small terms, we obtain

$$c_p \simeq \frac{2am^5\gamma}{h(1+\gamma)}, \tag{30}$$

Formula (30) was derived in [6] by means of an another approach.

For the thin ring $\xi > 9$, $c_p \ll 1$, and condition (26) can be replaced by the approximate relation $S_0(l) = 0$. The boundary conditions $T_{10}(l) = S_0(l) = 0$ correspond to free shell edge $s = l$. The shell "does not notice" the thin ring.

For the thick ring $\xi > 9$, $c_p \gg 1$, and condition (27) can be transformed into the approximate relation $v_0(l) = 0$. The boundary conditions $T_{10}(l) = v_0(l) = 0$ correspond to conditions (7) and (8) on the free supported shell edge $s = l$.

Equation (17) has nontrivial solution satisfying boundary conditions (20) and the conditions

$$\frac{d^2v_0}{ds^2} = 0, \quad \sigma\frac{d^3v_0}{ds^3} = cv_0$$

if $\lambda = \sigma z^4/l^4m^6 + \mu^4m^2$, where z is the root of the equation

$$cl^3(\tanh z \cos z - \sin z) = \sigma z^3(\cos z + \cosh^{-1} z). \tag{31}$$

Hence the minimal value λ_c of the loading parameter λ is

$$\lambda_c = \min_m \left(\frac{\sigma z_1^4}{l^4m^6} + \mu^4m^2\right). \tag{32}$$

Here z_1 is the minimal positive root of Eq. (31).

3.4 Example

Consider the cylindrical shell of the length $l = 3$ and the thickness $h = 0.01$ joint with the ring of thickness $a = 0.001$. Assume that the Poisson's ratio of the materials is $\nu = 0.3$. The dependence of $\Lambda = 10^4\lambda_c$ on the ring width b for this case is shown in Fig. 2. Curve 1 was obtained by means of formulas (32) and (27) (plate model). Curve 2 plots the results which are found using formula (29) (beam model). Straight line 3

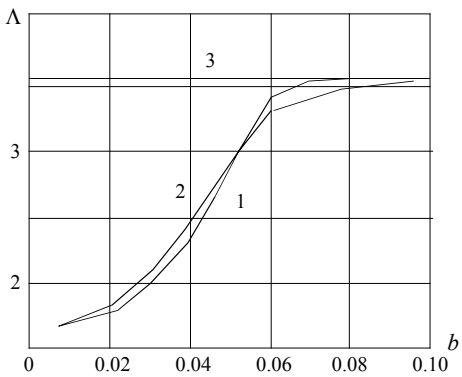

Fig. 2 Loading parameter Λ versus the ring width b

corresponds to the value of c calculated by formulas $c \simeq c_p$ and (30) (wide ring). The points of inflection appear on curves 1 and 2 at the changing of circumferential wave number m corresponding to λ_c.

While the ring is sufficiently narrow, the using of the beam model gives good results, which differ a little from the results obtained on the basis of plate model. However, for sufficiently large b (in the current example for $b > 0.06$) the buckling mode changed, and the asymptotic approach developed in this section do not allow to find critical pressure.

4 Buckling of the Second Type

4.1 Asymptotic Analysis of Boundary Conditions

To the buckling mode of the second type corresponds the dimensionless critical pressure $\lambda_p \sim \mu_p^4$. Asssume that $\mu_p \sim \mu$, i.e. the thickness of the plate a and the thickness of the shell h have the same orders. In this case $\lambda_p \ll \lambda_c$, where $\lambda_c \sim \mu^3$ corresponds to the buckling mode of the first type.

Let us seek the approximate solution of system (1) as a sum of the membrane solutions and the edge effect functions:

$$y = \mu^{I(y)} y_0 + \mu^{I_1(y)} y_1 + \mu^{I_2(y)} y_2. \tag{33}$$

The intensity indices are given in Table 2. The functions u_0, v_0, T_{10} and S_0 satisfy the membrane equations:

$$T_{10}' + mS_0 = 0, \quad S_0' = 0, \quad 2S_0 = (1-\nu)(v_0' - mu_0), \quad T_{10} = \sigma u_0'. \tag{34}$$

Table 2 Intensity indices for the buckling mode of the second type

	Functions							
Indices	u	v	w	ϑ	T_1	S	M_1	Q_1
I	4	4	4	4	4	4	8	8
I_1	5	6	4	3	6	5	6	5
I_2	3	4	2	1	4	3	4	3

Membrane equations (34) are derived from Eq. (1) assuming $\mu = 0$ and neglecting the small term $\lambda m \vartheta_2$. The edge effect functions y_1 and y_2 have the form (19).

We suppose that

$$w_p \sim \vartheta_{1p} \sim 1, \quad M_{1p} \sim Q_{1p} \sim \mu^4, \quad u_p \sim v_p \sim T_{1p} \sim S_p \sim \mu^3. \tag{35}$$

After the substitution the solutions (33) and (35) into Eqs. (1–3), continuity conditions (4) and boundary conditions (5–6) the eigenvalue problem (1–6) in the first approximation can be split into the following four separated problems:

(1) The eigenvalue problem for Eq. (2), describing the transverse flexural deformation of the plate with the boundary conditions

$$w_p = \vartheta_{1p} = 0, \quad x = 1, \quad M_{1p} = Q_{1p} - T_{1p} w_p = 0, \quad x = 1 + b. \tag{36}$$

(2) Non-homogeneous boundary value problem for membrane shell equations (34) with the boundary conditions

$$u_0 = v_0 = 0, \quad s = 0, \quad hT_{10}(l) = aQ_{1p}(1), \quad hS_0(l) = aS_p(1). \tag{37}$$

(3) The linear algebraic equations

$$w_1 = w_0, \quad \vartheta_{11} = 0, \quad x = 0 \tag{38}$$

for the unknown constants $\hat{D}_1$ and $\hat{D}_2$ and

$$w_2(l) = 0, \quad hM_{12}(l) = aM_{1p}(1) \tag{39}$$

for the unknown constants $\hat{D}_3$ and $\hat{D}_4$.

(4) Non-homogeneous boundary value problem for plate equations (3) with the boundary conditions

$$v_p(1) = 0, \quad aT_{1p}(1) = hQ_{12}(l), \quad T_{1p} = S_p = 0, \quad x = 1 + b.$$

Thus, the approximate solution of the the eigenvalue problem (1–6) is reduced to the step-by-step solution of the four more simple problems. First we have to solve the

buckling problem 1 for the plate. Then one can obtain the solution of the membrane problem 2, using boundary conditions (37) and find from (38) and (39) the boundary effect functions near the parallel $s = 0$ and $s = l$. Finally it is possible to solve the boundary value problem 4, describing tangential deformation of the plate.

We consider only the problem 1, since the displacements of the cylindrical shell and the tangential displacement of the plate are very small in comparison with the transverse plate deflection (see Table 2 and relations (35)).

4.2 Pre-buckling Stress-Resultants

Let us analyzed the buckling of the annular plate, attached to an edge of a cylindrical shell, under the radial and hoop stress-resultants T_{1p} and T_{2p}, caused by the external uniform pressure p applied on the shell (see Fig. 2). To find T_{1p} and T_{2p} determine the axisymmetric deformation of the annular plate joined with the cylindrical shell.

The non-dimensional equations

$$\begin{gathered} T_1' = 0, \quad Q_1' - T_2 = \lambda, \quad Q_1 = M_1', \\ T_1 = u' + \nu w, \quad T_2 = \nu u' + w, \quad M_1 = -\mu^4 w'', \end{gathered} \tag{40}$$

describing the axisymmetric deformation of the cylindrical shell, can be obtain from Eq. (1) assuming $m = 0$, $v = 0$ and replacing the term $\lambda m \vartheta_2$ with $\lambda = \sigma p/(Eh)$.

The equations

$$(xT_{1p})' - T_{2p} = 0, \quad xT_{1p} = xu_p' + \nu u_p, \quad xT_{2p} = u_p + \nu x u_p', \tag{41}$$

following from Eq. (3), describe tangential axisymmetric deformation of the plate.

We do not take into account the transverse bending stiffness of the plate since it is much less than its tangential stiffness. In this case continuity conditions (4) at the circle $s = l$, $x = 1$ take the form

$$w(l) = u_p(1), \quad M_1(l) = 0, \quad hQ_1(l) = aT_{1p}(1), \quad T_1(l) = 0. \tag{42}$$

We assume that the shell edge $s = 0$ is clamped and the plate edge $x = 1 + b$ is free, i.e.

$$u(0) = w(0) = w'(0) = 0, \quad T_{1p}(r) = 0, \tag{43}$$

where $r = 1 + b$ is the dimensionless outer radius of the plate.

Let us seek the approximate solution of Eq. (40) as a sum of the membrane solutions and the edge effect functions [1]:

$$y = \mu^{I(y)} y_0 + \mu^{I_1(y)} y_1 + \mu^{I_2(y)} y_2. \tag{44}$$

Table 3 lists values of the intensity indices for the axisymmetric deformation.

Table 3 Intensity indices for the axisymmetric deformation

	Functions					
Indices	u	w	ϑ	T_1	M_1	Q_1
I	0	0	0	0	4	4
$I_1 = I_2$	1	0	-1	2	2	1

The solution of the membrane system

$$T_1' = 0, \quad T_2 + \lambda = 0, \quad T_1 = u' + \nu w, \quad T_2 = \nu u' + w,$$

satisfying boundary conditions $u(0) = 0$ and $T_1(l) = 0$, is

$$w_0 = -\frac{\lambda}{\sigma}, \quad u_0 = \frac{\nu\lambda s}{\sigma}, \quad T_{10} = 0.$$

The edge effect functions y_1, y_2 may be determined from formulas (19).

The general solution of system (41)

$$u = C_1 x + C_2/x, \quad T_{1p,2p} = (1+\nu)C_1 \mp (1-\nu)C_2/x^2 \tag{45}$$

contains the two arbitrary constants C_1 and C_2.

To find C_1 and C_2 we substitute solution (45) and approximate relations

$$w(l) = w_0(l) + w_2(l) = -\frac{\lambda}{\sigma} + \hat{D}_3 + \hat{D}_4,$$
$$M_1(l) = \mu^2 M_{12}(l) = -\mu^2(r_3^2\hat{D}_3 + r_4^2\hat{D}_4), \quad Q_1(l) = \mu Q_{12}(l) = -\mu(r_3^3\hat{D}_3 + r_4^3\hat{D}_4)$$

into the last condition (43) and the three first conditions (42) and get the following system of equations

$$\begin{aligned} r^2(1+\nu)C_1 = (1-\nu)C_2, \quad r_3^2\hat{D}_3 + r_4^2\hat{D}_4 = 0, \\ \sigma(C_1 + C_2 - \hat{D}_3 - \hat{D}_4) + \lambda = 0, \\ h\mu^4(r_3^3\hat{D}_3 + r_4^3\hat{D}_4) + a[(1+\nu)C_1 - (1-\nu)C_2] = 0. \end{aligned} \tag{46}$$

It follows from the first two Eq. (46) that

$$C_2 = \frac{r^2(1+\nu)}{(1-\nu)}C_1, \quad \hat{D}_3 = \hat{D}_4.$$

From the last two Eq. (46) we obtain

$$C_1 = -\frac{\lambda}{A}, \quad A = (1-\nu)[1-\nu+(1+\nu)r^2] + \frac{2ga(1+\nu)(r^2-1)}{\mu h}. \tag{47}$$

Substituting the expressions for C_1 and C_2 into last formulas (45), we find the pre-buckling stress-resultants in the annular plate:

$$T_{1p} = \frac{r^2-x^2}{x^2}A(1+\nu)\lambda, \quad T_{2p} = -\frac{r^2+x^2}{x^2}A(1+\nu)\lambda. \tag{48}$$

4.3 Buckling of the Plate

Buckling plate Eq. (2) can be reduced to the following equation

$$\frac{d^4w_p}{dx^4} + \frac{2}{x}\frac{d^3w_p}{dx^3} - \frac{m_2+\beta t_1}{x^2}\frac{d^2w_p}{dx^2} + \frac{m_2-\beta t_2}{x^3}\frac{dw_p}{dx} + \frac{m^2(m^2-4+\beta t_2)}{x^4}w_p = 0, \tag{49}$$

where $m_2 = 2m^2+1$,

$$\beta = \frac{12T_{1p}(1)}{a^2}, \quad t_k = \frac{x^2T_{kp}(x)}{T_{1p}(1)}, \quad k = 1, 2. \tag{50}$$

If we find the least positive eigenvalue β_p for eigenvalue problem (49), (36) then, using the first formula (48), we obtain the dimensionless critical pressure

$$\lambda_p = \frac{\mu_p^4\beta_p}{(1+\nu)(b^2+2b)}, \tag{51}$$

corresponding to the buckling of the second type.

Equation (49) does not have an analytical solution. The analytical solution of this equation was obtained by Mansfild [11] for specific pre-buckling stress-resultants $t_1 = 1$ and $t_2 = -1$. However one can get an approximate analytical solution assuming that the plate is narrow, i.e. $b \ll 1$ [7]. Usually this assumption is valid for ring-stiffened shells.

Let us suppose that the circumferential wave number $m \sim 1$. In this case replacing variable $x = 1 + b\xi$ in Eqs. (49), (36) and neglecting small terms leads to the boundary-value problem

$$d^4w/d\xi^4 - \beta b^2[(1-\xi)w'' + w'] = 0, \quad w(0) = w'(0) = w''(1) = w'''(1) = 0,$$

which does not have positive eigenvalues since

$$\beta b^2 = -\frac{\int_0^1 (w'')^2 d\xi}{\int_0^1 (1-\xi)(w')^2 d\xi} < 0.$$

Here $w' = dw/d\xi$.

Replace variable $x = 1 + b\xi$ in (49) and (36) assuming $m \sim 1/b$. Keeping only main terms, we get the approximate equation

$$d^4w/d\xi^4 - 2m_0^2 w'' + m_0^4(1-\beta_0^2)w = 0 \tag{52}$$

and the boundary conditions

$$w(0) = w'(0) = 0, \quad w''(1) - \nu m_0^2 w(1) = 0, \quad w'''(1) - m_0^2(2-\nu)w'(1) = 0, \tag{53}$$

where $\beta_0 = \sqrt{\beta}/(m\sqrt{b})$, $m_0 = bm$.

If $\beta_0 \le 1$ then eigenvalue problem (52), (53) does not have nontrivial solutions. In the case $\beta_0 > 1$ the solution of Eq. (52) has the form

$$w = C_1 \sin\alpha_0 x + C_2 \cos\alpha_0 x + C_3 \sinh\gamma_0 x + C_4 \cosh\gamma_0 x, \tag{54}$$

where C_k are arbitrary constants and

$$\alpha_0 = m_0\sqrt{\beta_0 - 1}, \quad \gamma_0 = m_0\sqrt{\beta_0 + 1}.$$

Substituting (54) into conditions (53) we obtain four linear homogeneous algebraic equations for unknowns C_1, C_2, C_3, and C_4. These equations have nontrivial solutions if the characteristic determinant is equal to zero:

$$F \sinh\gamma_0 \sin\alpha_0 + G \cosh\gamma_0 \cos\alpha_0 + H = 0, \tag{55}$$

where

$$F = \beta_0^2(1-2\nu) - (1-\nu)^2, \quad G = [\beta_0^2 + (1-\nu)^2]\sqrt{\beta_0^2 - 1},$$
$$H = [\beta_0^2 - (1-\nu)^2]\sqrt{\beta_0^2 - 1}.$$

The approximate value of least positive eigenvalue β_p may be found as

$$\beta_p = \frac{\eta_p}{b}, \quad \eta_p = \min_{m_0}[m_0^2\beta_0^2(m_0)], \tag{56}$$

where β_0 is the least positive root of Eq. (55). The error of formula (56) appears whereas $m = m_0/b$ is not integer. This error is small for $b \ll 1$ since then $m \gg 1$. The function η_p depends only on Poisson's ratio ν. Figure 3 shows graphs of this function

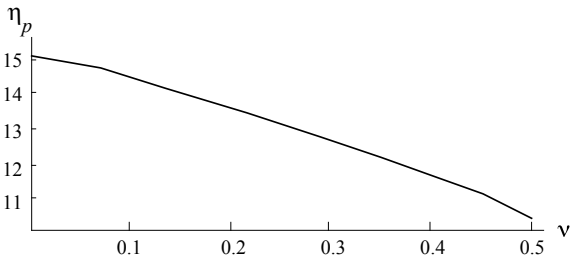

Fig. 3 Plot of the function $\eta_p(\nu)$

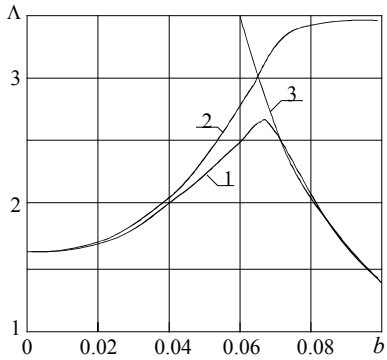

Fig. 4 Loading parameter Λ versus ring width b

In particular, for $\nu = 0.3$ from the numerical solution of Eq. (55) it follows that $\eta_c = 12.6$ corresponds $m_0 = 1.92$. Hence, in this case $\beta_c \simeq 12.6/b$ and $m \simeq 1.92/b$.

Substituting (56) into (51) we obtain the following approximate formula for the dimensionless critical pressure

$$\lambda_p = \frac{\eta_p a^2}{12b}\left(\frac{2(1+b)}{b(2+b)} + \frac{2ag}{\mu h} + \nu\right). \tag{57}$$

Formula (57) show that the critical pressure goes up as the width of ring b increases.

As an example consider the buckling of the cylindrical shell stiffened by an edge with the annular plate, assuming that parameter of this structure are the same as in Sect. 3.4. The dependence of $\Lambda = 10^4\lambda_p$ on the ring width b, is shown in Fig. 4.

Curve 1 has been obtained by FEA. Curve 2 plots the asymptotic results which are found in 3.4 by using the beam model of the ring. Curve 3 corresponds to the value of Λ calculated by formula (57).

For small b the beam model gives the values of Λ that are slightly different from the FEA results. For sufficiently large b the numerical results and the asymptotic results obtained by (57) practically coincide. The error of the asymptotic methods attains its maximum at the point $b = b_* = 0.07$ where the type of the buckling mode changes.

The non-dimensional critical pressure Λ attains the maximum value for $b = b_*$. To maximize the critical pressure, we take b_* as the optimal value for b. This optimal value does not differ significantly from the value corresponding to the intersection point of curves 2 and 3 Therefore, the asymptotic methods can be used for the evaluation of the approximate optimal plate width.

5 Conclusions

The application of asymptotic method to the buckling problem of cylindrical shell joined with an annular plate permits to obtain simple approximate formulas for evaluation of the critical external pressure. The different approaches were used for narrow and wide plates. In the both cases the solutions of shell equations were represented as a sums of slowly varying functions and edge effect integrals. To get the first approximation of the solutions of eigenvalue problems the separation of the boundary conditions on main and additional conditions was fulfilled.

The same asymptotic approaches can be used for a shell stiffened by plates located on internal parallels. The some results in this direction are presented in [8]. It is also possible with the help of approximate formulas evaluate optimal parameters, corresponding to the maximum critical pressure for the stiffened shell with given mass.

Acknowledgements This work was supported by RFBR (grant 16-01-00580) which is gratefully acknowledged.

References

1. Bauer, S.M., Filippov, S.B., Smirnov, A.L., Tovstik, P.E., Vaillancourt, R.: Asymptotic Methods in Mechanics of Solids. Springer International Publishing, Switzerland (2015)
2. Dai, H.L., Qi, L.L., Zheng, H.Y.: Buckling analysis for a ring-stiffened FGM cylindrical shell under hydrostatic pressure and thermal loads. J. Mech. **30**, 403–410 (2014)
3. Filippov, S.B.: Theory of Connected and Stiffened Shells. St. Petersburg State University Press, St. Petersburg (1999). (in Russian)
4. Filippov, S.B.: Optimal design of stiffened cylindrical shells based on an asymptotic approach. Technishe Mechanik **24**, 221–230 (2004)
5. Filippov, S.B.: Buckling, vibrations and optimal design of ring-stiffened thin cylindrical shells. In: Advances in Mechanics of Solids, pp. 17–48. World Scientific Publishing Co Ltd. (2006)
6. Filippov, S.B.: Buckling of cylindrical shell joint with annular plate. In: Pietraszkiewicz, W., Szymczak, C. (Eds.) Shell Structures: Theory and Applications. Proceedings of the 8th SSTA Conference, Jurata, 2005, pp. 211–214. Taylor & Francis, London (2006)
7. Filippov, S.B.: Buckling of circular ring joint with cylindrical shell. In: Pietraszkiewicz, W., Kreja, I. (Eds.) Shell Structures: Theory and Applications. Proceedings of the 9th SSTA Conference, Gdansk-Jurata, 2009, pp. 109–112. CRC Press/Balkema, London (2010)

8. Filippov, S.B.: Buckling and optimal design of ring-stiffened thin cylindrical shell. In: Pietraszkiewicz, W., Witkowski, W. (Eds.) Shell Structures: Theory and Applications. Proceedings of the 11th SSTA Conference, Gdansk, 2017, pp. 219–222. CRC Press/Balkema, London (2018)
9. Filippov, S.B., Haseganu, E.: Low-frequency vibrations of a thin cylindrical shell joined with an annular thin plate. Trans. CSME **27**, 169–178 (2003)
10. Konopinska, V., Pietraszkiewicz, W.: On exact dynamic continuity conditions in the theory of branched shells. In: Pietraszkiewicz, W., Szymczak, C. (Eds.) Shell Structures: Theory and Applications, Proc 8th SSTA Conf, Jurata, October 2005, pp. 135–138. Taylor & Francis, London (2006)
11. Mansfield, E.H.: On the buckling of an annular plate. Quart. J. Mech. Appl. Math. **13**, 16–23 (1960)
12. Mao, J.F., Bao, S.Y.: Comparative studies on buckling behaviors of T joint and pipe by varying geometric parameters and analysis methods. Int. J. Mech. Sci. **90**, 113–121 (2015)
13. Pietraszkiewicz, W., Konopinska, V.: On unique kinematics for the branching shells. Int. J. Solids Struct. **48**, 2238–2244 (2011)
14. Pietraszkiewicz, W., Konopinska, V.: Junctions in shell structures: a review. Thin-Walled Struct. **95**, 310–334 (2015)
15. Teng, J.G., Rotter, J.M.: Buckling of Thin Metal Shells. CRC Press (2003)
16. Tian, J., Wang, C.M., Swaddiwudhipohg, S.: Elastic buckling analysis of ring-stiffened cylindrical shell under general pressure loading via the Ritz method. Thin-Walled Struct. **35**, 1–24 (1999)
17. Tovstik, P.E., Smirnov, A.L.: Asymptotic Methods in The Buckling Theory of Elastic Shells. World Scientific Publishing Co Ltd., Singapore, New Jersey, London, Hong Kong (2001)
18. Vishik, M.I., Lyusternik, L.A.: Regular degeneration and boundary layer for linear differential equations with small parameter. Russian Math. Surveys **12**, 3–122 (1957)

2D Theory of Shell-like Tensegrity Structures

Wojciech Gilewski, Paulina Obara and Anna Al Sabouni-Zawadzka

Abstract Six-parameter shell theory is proposed for tensegrity-like structures. Continuum model to describe mechanical properties of tensegrity lattices is based on the equivalence of the strain energy with discrete model. Parametric analysis is presented to describe the influence of geometrical properties and the level of self-equilibrated normal forces to the static response of the structure.

Keywords Six-parameter shell theory · Tensegrity

1 Introduction

The works of Professor Wojciech Pietraszkawicz regarding the six-parameter theory of shells, initiated in the second half of the 1970s [1, 2], resulted in numerous publications and were an inspiration for scientific research. Research and papers mainly concern non-linear theory in terms of statics and dynamics (e.g. [3–7]) with applications of the finite element method (e.g. [5, 8, 9]). Linearized equations were also used for the construction of finite elements with the so-called physical shape functions [10, 11] and the theory of shells built of tensegrity lattices [12, 13]. The aim of this paper is to present the general theory of tensegrity-like shells, taking into account self-equilibrated states of normal forces in struts and cables. Parametric study is presented for two closed-form boundary value solutions.

W. Gilewski (✉) · A. Al Sabouni-Zawadzka
Warsaw University of Technology, Warsaw, Poland
e-mail: w.gilewski@il.pw.edu.pl

A. Al Sabouni-Zawadzka
e-mail: a.sabouni@il.pw.edu.pl

P. Obara
Kielce University of Technology, Kielce, Poland
e-mail: paula@tu.kielce.pl

H. Altenbach et al. (eds.), *Recent Developments in the Theory of Shells*,
Advanced Structured Materials 110, https://doi.org/10.1007/978-3-030-17747-8_15

2 The Concept of Tensegrity

An interesting type of structures are tensegrities. The term "tensegrity" was first introduced in the third decade of the XXth century. Several definitions of this concept can be found in the literature [14–16]. For the purpose of this paper, a tensegrity structure is defined as a pin-jointed system with a particular configuration of cables and struts that form a statically indeterminate structure in a stable equilibrium. Tensegrities consist of a discontinuous set of compressed elements inside a continuous net of tensioned members, which have no compressive stiffness. Selected typical tensegrity modules are presented in Fig. 1. Infinitesimal mechanisms, that occur in tensegrity structures, are balanced with self-stress states [15]. Occurrence of a self-stress state in a structure indicates that there is a certain set of internal forces in structural members, which are independent from external loading and boundary conditions because they are in self-equilibrium.

To major advantages of tensegrity systems belong: large stiffness-to-mass ratio, deployability, reliability and controllability. Moreover, tensegrities have some unique features that result from the infinitesimal mechanisms, which are stabilized by self-stress forces. It is possible to control their static and dynamic properties by adjusting the pre-stressing forces [17].

There are: self-control, self-diagnosis, self-repair and self-adjustment (active control). Self-control of tensegrity systems consists in self-stiffening of the structures under the applied load that causes displacements consistent with the infinitesimal mechanism mode. External loading acts similarly to the self-stress—it eliminates singularity of the problem, additionally pre-stresses the structure and stiffens it. Self-diagnosis relates to the possibility of damage detection and identification by measuring internal forces in active members. Damage of one structural element affects the distribution and level of self-stress in the whole structure. Self-repair of tensegrity structures is realized by adjusting self-stress forces. A proper change of pre-stressing level can compensate the damaged element and restore the values of structural displacements from before damage. Self-adjustment (active control) in regard to tensegrity systems is related with the ability of self-adjustment through self-stress forces. Both the pre-stressing of the whole structure and its part causes stiffening of the system and reduction of its displacements. Therefore, active control

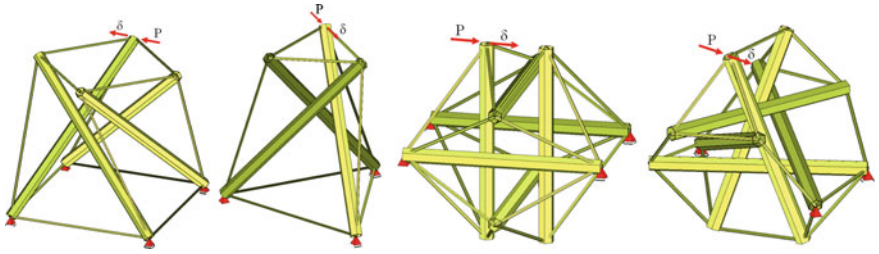

Fig. 1 Typical tensegrity modules

of tensegrities can be realized by adjusting the level of self-stress in only one selected part of the structure.

An interesting area of the applications of tensegrities are plate and shell lattices composed as a combination of the basic modules (Figs. 2 and 3).

Tensegrity lattices are complicated regarding both their geometry and mechanical properties. In order to describe their actual properties and identify features of the structure as a whole, a shell continuum model is considered within the six-parameter theory. The shell parameters are calibrated with the use of discrete model based on algebraic equations of the problem.

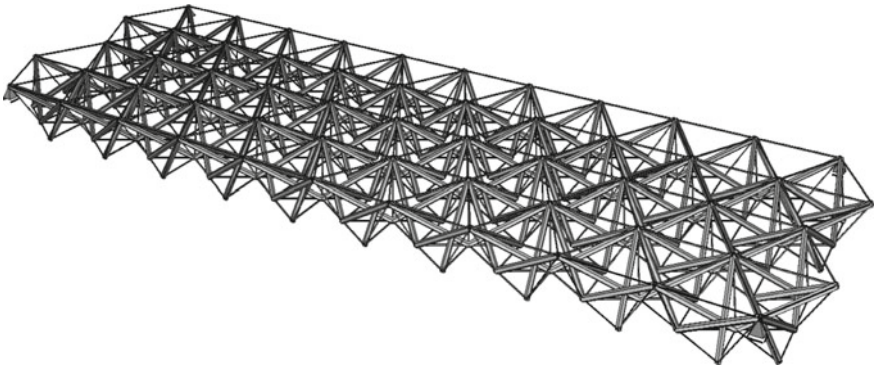

Fig. 2 Tensegrity-like plate

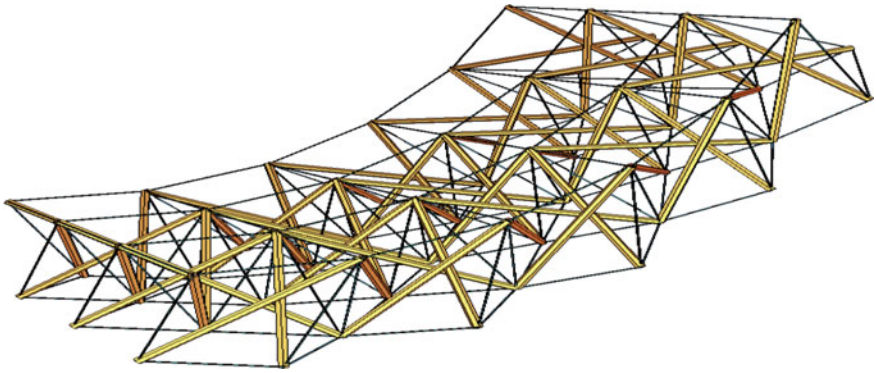

Fig. 3 Tensegrity-like shell

3 Mechanical Properties of Tensegrity Shell-like Structures

Discrete model of the tensegrity pin-joined truss structure is composed of e straight and prismatic bars of the lengths l_k, cross sections A_k and Young's modulus E_k. The bars are connected in nodes in which the number of s nodal displacements q_j and nodal forces Q_i are defined (see [19, 20] for details). Axial forces N_k can be expressed by the extensions of bars Δ_k in the form $N_k = E_k A_k \Delta_k / l_k$. The extensions Δ_k are a combination of nodal displacements $\Delta_k = \sum_{j=1}^{s} B_{kj} q_j$, $j = 1, 2, \ldots, s$. Additionally the self-equilibrated system of axial forces S_k which satisfy the homogeneous set of equilibrium equations $\sum_{k=1}^{e} B_{jk} S_k = 0$ is considered. If one consider equations of equilibrium in the actual configuration then moment $M_k = S_k l_k \psi_k$ is acting on each bar. Angles of bar rotations ψ_k can be expressed as a combination of nodal displacements $\psi_k = \frac{1}{l_k} \sum_{j=1}^{s} C_{kj} q_j$. The above formalism leads to the linear system of algebraic equations $\sum_{j=1}^{s} (k_{ij} + k_{ij}^G) q_j = Q_i$, in which the linear stiffness matrix k_{ij} and geometric stiffness matrix k_{ij}^G can be expressed in algebraic form $k_{ij} = \sum_{k=1}^{e} B_{ki} \frac{E_k A_k}{l_k} B_{kj}$, $k_{ij}^G = \sum_{k=1}^{e} C_{ki} \frac{S_k}{l_k} C_{kj}$ (see [20, 21] for further details). The approach is not dependent on any approximation typical for the finite element method.

The continuum model proposed by [18] is based on the comparison of the strain energy of a tensegrity structure defined using a discrete model and the strain energy of a solid determined according to the symmetric 3D elasticity theory.

In a discrete model (DM), the strain energy of a tensegrity truss can be expressed as a quadratic form of nodal displacements $\mathbf{q}$:

$$E_{\mathrm{s}}^{\mathrm{DM}} = \frac{1}{2} \mathbf{q}^{\mathrm{T}} \mathbf{K} \mathbf{q}, \tag{1}$$

where:

$\mathbf{K} = \mathbf{K}_{\mathrm{L}} + \mathbf{K}_{\mathrm{G}}$, $\mathbf{K}_{\mathrm{L}}$—global linear stiffness matrix, $\mathbf{K}_{\mathrm{G}}$—global geometric stiffness matrix.

The self-stress of the structure is represented by the geometric stiffness matrix. The strain energy of a solid according to the symmetric linear 3D elasticity theory (ET) can be expressed as:

$$E_{\mathrm{s}}^{\mathrm{ET}} = \frac{1}{2} \int_V \boldsymbol{\varepsilon}^{\mathrm{T}} \mathbf{E} \, \boldsymbol{\varepsilon} \, dV, \tag{2}$$

where: $\boldsymbol{\varepsilon}$—vector of strain components, $\mathbf{E}$—elasticity matrix.

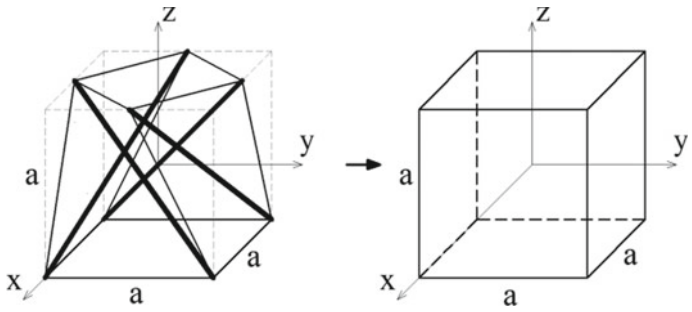

Fig. 4 Tensegrity module and continuum

In order to analyse mechanical properties of the material, it is proposed to compare the strain energy of an unsupported tensegrity to the strain energy of a cube, with an assumption that the strain energy of the cube is constant in its whole volume. In a general case both the analysed structure and the solid can have arbitrary dimensions. However, in order to show how the continuum model is constructed, a simple example of a typical tensegrity module inscribed into a cube of edge length a is presented (Fig. 4).

With the above assumptions, the strain energy of the cube of edge length a, according to the symmetric 3D elasticity theory (ET) [22]:

$$E_{\mathrm{s}}^{\mathrm{ET}} = \frac{1}{2}\int_{V} \boldsymbol{\varepsilon}^{\mathrm{T}}\mathbf{E}\,\boldsymbol{\varepsilon}\,dV = \frac{1}{2}\boldsymbol{\varepsilon}^{\mathrm{T}}\mathbf{E}\,\boldsymbol{\varepsilon}\,a^{3}. \tag{3}$$

To compare the energies and build the equivalent elasticity matrix, the nodal displacements of the structure are expressed by the average mid-values of displacements and their derivatives in the centre of the cube of edge length a, with the use of Taylor series expansion. Nodal coordinates of the analysed tensegrity structure can be expressed using the parameter a, which corresponds to the edge length of the cube: $\{\alpha_{xi}a, \alpha_{yi}a, \alpha_{zi}a\}$. Then, the parameters of the node i (for example nodal displacements) can be described as: $\Delta x_i = \alpha_{xi}a$, $\Delta y_i = \alpha_{yi}a$, $\Delta z_i = \alpha_{zi}a$.

The next step of the analysis is a substitution of the determined nodal displacements in the formula (1). As a result, an expression containing a constant part (independent of a) and terms with a factor a^{n}, $n \in \{1,2,\ldots\}$ is obtained. However, in the case of small values of a, terms with the factor a^{n} can be regarded as higher order terms and should be omitted. Moreover, the mentioned terms contain displacement derivatives greater than the first one, which is beyond the scope of the symmetric theory of elasticity.

Comparison of strain energies (1) and (3) leads to the determination of coefficients of the matrix $\mathbf{E}$. In a general case of an anisotropic structure, the obtained elasticity matrix in Voight's notation has the following form:

$$\mathbf{E} = \begin{bmatrix} e_{11} & e_{12} & e_{13} & e_{14} & e_{15} & e_{16} \\ & e_{22} & e_{23} & e_{24} & e_{25} & e_{26} \\ & & e_{33} & e_{34} & e_{35} & e_{36} \\ & & & e_{44} & e_{45} & e_{46} \\ & & & & e_{55} & e_{56} \\ sym. & & & & & e_{66} \end{bmatrix}. \tag{4}$$

It contains 36 coefficients, including 21 independent ones. The above matrix can take different, particular forms, depending on the type of symmetry within eight possible modes [23].

After integration over the thickness of the shell, the equivalent constitutive coefficients of the 2D shell theory are obtained. The details are presented in the next chapters.

4 Six-Parameter Shell Theory

Continuum model of the tensegrity shell-like structure is based on the linearized 6-parameter shell theory [5]. The subject under consideration is a shell of thickness h. Displacement field is described by three linear displacements u_α, w of middle surface and three rotations ϕ_α, ψ.

Geometric relations, with the use of coordinate system ϑ_1, ϑ_2 are the following:

$$\begin{aligned} \gamma_{\alpha\beta} &= u_{\alpha,\beta} - b_{\alpha\beta} w - \in_{\alpha\beta} \psi, \\ \kappa_{\alpha\beta} &= \varphi_{\alpha,\beta} - \in_{\beta\lambda} b_{\lambda\alpha} \psi, \\ \gamma_{\alpha 3} &= \varphi_\alpha + w_{,\alpha} + b_{\alpha\lambda} u_\lambda, \\ \kappa_{\alpha 3} &= \psi_{,\alpha} - \in_{\lambda\beta} b_{\lambda\alpha} \varphi_\beta, \\ \gamma_{33} &= \psi, \end{aligned} \tag{5}$$

where: $\gamma_{\alpha\beta}, \kappa_{\alpha\beta}, \gamma_{\alpha 3}, \kappa_{\alpha 3}, \gamma_{33}$—strain components.

Linear constitutive relations are crucial from the point of view of the continuum model equivalent to the discrete model:

$$\begin{aligned} N_{\alpha\beta} &= B^0_{\alpha\beta\lambda\mu}\gamma_{\lambda\mu} + B^1_{\alpha\beta\lambda\mu}\kappa_{\lambda\mu}, \\ M_{\alpha\beta} &= \frac{h^2}{12} B^0_{\alpha\beta\lambda\mu}\kappa_{\lambda\mu} + B^1_{\alpha\beta\lambda\mu}\gamma_{\lambda\mu}, \\ N_{\alpha 3} &= k^2 B^0_{\alpha 3\beta 3}\gamma_{\beta 3} + m^2 B^1_{\alpha 3\beta 3}\kappa_{\beta 3}, \\ M_{\alpha 3} &= \frac{h^2}{12} l^2 B^0_{\alpha 3\beta 3}\kappa_{\beta 3} + m^2 B^1_{\alpha 3\beta 3}\gamma_{\beta 3}, \end{aligned} \tag{6}$$

where: $N_{\alpha\beta}$, $M_{\alpha\beta}$, $N_{\alpha 3}$, $M_{\alpha 3}$—internal forces, k^2, l^2, m^2—correction factors. The constitutive coefficients $B^0_{\alpha\beta\lambda\mu}$, $B^1_{\alpha\beta\lambda\mu}$, $B^0_{\alpha 3\beta 3}$, $B^1_{\alpha 3\beta 3}\kappa_{\beta 3}$ for tensegrity-like anisotropic shells depends on elasticity matrix **E** of the continuum model. An example of orthotropic cylindrical shell is introduced in the next chapter.

Equations of equilibrium can be expressed in the form:

$$\begin{aligned}
&N_{\alpha\beta,\alpha} - b_{\alpha\beta}N_{\alpha 3} + f_\beta = 0,\\
&N_{\alpha 3,\alpha} + b_{\alpha\beta}N_{\alpha\beta} + f_3 = 0,\\
&M_{\alpha\beta,\alpha} - N_{\beta 3} - \in_{\lambda\beta} b_{\lambda\alpha}M_{\alpha 3} + m_\beta = 0,\\
&M_{\alpha 3,\alpha} + \in_{\alpha\beta}\left(N_{\alpha\beta} - b_{\alpha\lambda}M_{\lambda\beta}\right) + m_3 = 0.
\end{aligned} \tag{7}$$

The above equations can be used for the analysis of a tensegrity-like shells of any shape. An example of cylindrical shell is presented below.

5 Parametric Study of Cylindrical Tensegrity-like Shell

Let us consider a cylindrical shell of the constant thickness h and radius of curvature R (Fig. 5).

The shell is built of the simplex tensegrity modules (Fig. 6a) adapted to the opening angle of $\pi/48$, with self-equilibrated normal forces presented in Fig. 6b. Module height is equal to the thickness of the shell $a = h$, and its dimensions in the lower surface are $a \times a$.

The shell is composed as a set of four modules oriented to the orthotropic substructure (Fig. 7).

Continuum model applied to the cylindrical substructure provides the following coefficients of the elasticity matrix.

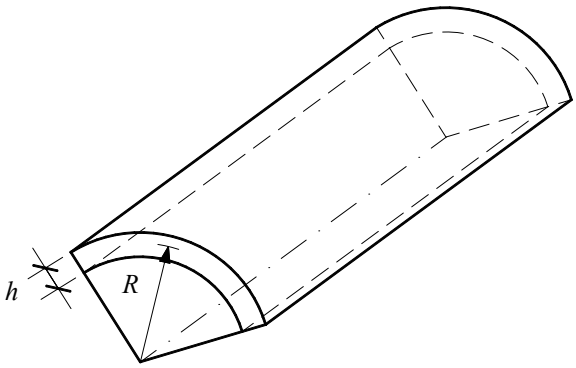

Fig. 5 Cylindrical shell

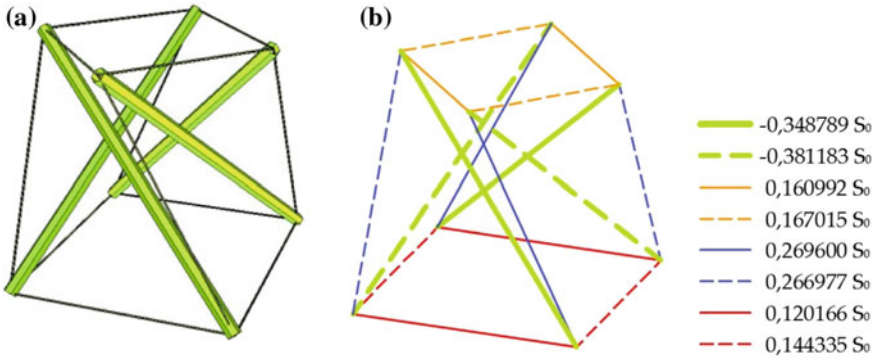

Fig. 6 Simplex module: geometry (**a**), self-equilibrated forces (**b**)

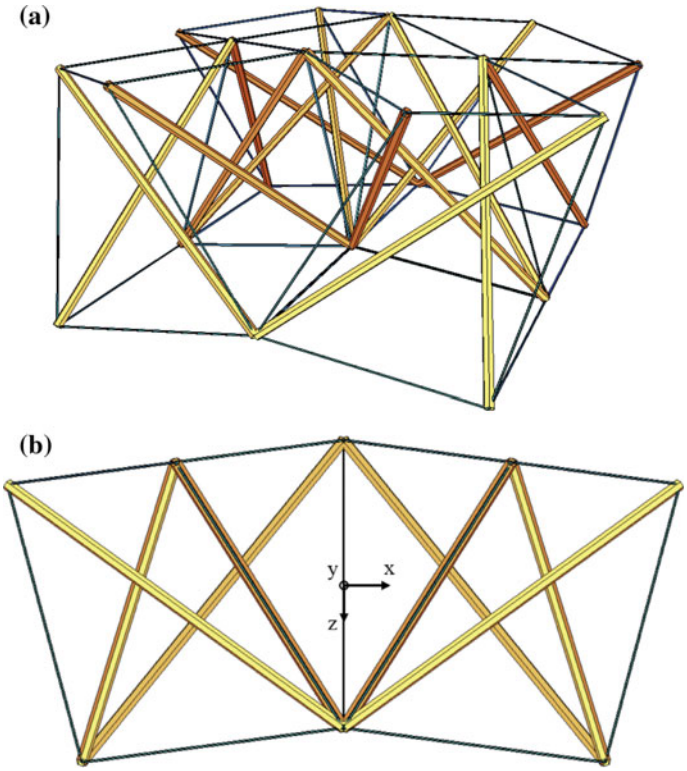

Fig. 7 Orthotropic cylindrical substructure: general view (**a**), side view (**b**)

$$\mathbf{E} = \begin{bmatrix} e_{11} & e_{12} & e_{13} & 0 & 0 & 0 \\ & e_{22} & e_{23} & 0 & 0 & 0 \\ & & e_{33} & 0 & 0 & 0 \\ & & & e_{44} & 0 & 0 \\ & & & & e_{55} & 0 \\ sym. & & & & & e_{66} \end{bmatrix}, \tag{8}$$

$$\begin{aligned}
e_{11} &= \frac{2EA}{a^2}(0,326052 + 1,05578 \cdot k - 0,0740002 \cdot \sigma), \\
e_{12} &= \frac{EA}{a^2}(0,290535 + 0,750993 \cdot k - 0,0181182 \cdot \sigma), \\
e_{13} &= \frac{EA}{a^2}(0,736617 + 0,26907 \cdot k + 0,166119 \cdot \sigma), \\
e_{22} &= \frac{2EA}{a^2}(0,374404 + 1,19171 \cdot k - 0,0692667 \cdot \sigma), \\
e_{23} &= \frac{EA}{a^2}(0,689166 + 0,283706 \cdot k + 0,156652 \cdot \sigma), \\
e_{33} &= \frac{2EA}{a^2}(0,587732 + 1,08399 \cdot k - 0,161385 \cdot \sigma), \\
e_{44} &= \frac{2EA}{a^2}(0,145268 + 0,375496 \cdot k + 0,00264259 \cdot \sigma), \\
e_{55} &= \frac{2EA}{a^2}(0,368309 + 0,134535 \cdot k + 0,0833235 \cdot \sigma), \\
e_{66} &= \frac{2EA}{a^2}(0,344583 + 0,141853 \cdot k + 0,0785901 \cdot \sigma),
\end{aligned} \tag{9}$$

where:

$k = \frac{(EA)_{cable}}{(EA)_{strut}}$, $(EA)_{strut} = EA$, $\sigma = \frac{S}{EA}$, E—Young's modulus of the struts, A—cross-section of the struts.

The above coefficients depends on two important parameters: the cable to strut stiffness relation k and self-equilibrated forces parameter σ. The parameters can be used for the parametric analysis of the shell, for example to study the influence of self-equilibrated forces for the response under static loads. In the theory of tensegrities it is used for active control or diagnosis of the structure.

The components of shell elasticity tensors are the following:

$$\begin{aligned}
&B^0_{1111} = e_{11},\ B^0_{1122} = e_{12}, \\
&B^0_{2222} = e_{22},\ B^0_{2211} = e_{12}, \\
&2B^0_{1212} = e_{44}, \\
&2B^0_{1313} = e_{55},\ 2B^0_{2323} = e_{66}, \\
&B^1_{\alpha\beta\lambda\mu} = \frac{h^2}{12}B^0_{\alpha\beta\lambda\mu},\ B^1_{\alpha 3\beta 3} = \frac{h^2}{12}B^0_{\alpha 3\beta 3}.
\end{aligned} \tag{10}$$

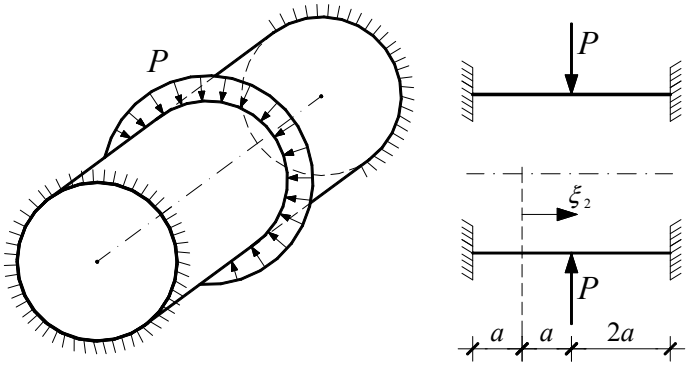

Fig. 8 Cylindrical ring

The numerical example is cylindrical ring of the length $L = 4a$ in coordinate system $\vartheta_1 = \varphi$, $\vartheta_2 = x$, presented in Fig. 8. Symmetry of the cylinder is to be introduced in the analytical solution o differential equations. Only edge load is then applied.

The set of ordinary homogeneous differential equations (with the simplification that $m^2 = 0$ and non-dimensional coordinate $\xi_2 = x/a \in \langle -1, 1\rangle$) for the cylindrical ring is the following:

$$\begin{aligned}
&K u_{2,22} - \hat{\hat{\gamma}}_0 a K^2 w_{,2} + c^2 \varphi_{2,22} = 0,\\
&\quad - K a \hat{\hat{\gamma}}_0 \hat{\hat{\gamma}}_1 u_{2,2} + w_{,22} + K^2 a^2 \hat{\hat{\gamma}}_1 w - a\phi_{2,2} = 0,\\
&K \hat{\hat{\gamma}}_2 u_{2,22} - a K^2 w_{,2} - \hat{\hat{\gamma}}_2 \phi_{2,22} + a^2 K^2 \phi_2 = 0,\\
&l^2 \psi_{,22} - a^2 K^2 \psi = 0,
\end{aligned} \tag{11}$$

where:

$$\hat{\hat{\gamma}}_0 = \frac{B^0_{2211}}{B^0_{2222}},\ \hat{\hat{\gamma}}_1 = \frac{B^0_{2222}}{k^2 B^0_{2323}},\ \hat{\hat{\gamma}}_2 = \frac{h^2}{12R^2}\hat{\hat{\gamma}}_1.$$

The displacement fields can be expresses in the closed form:

$$u_2(\xi_2) = D_5 + D_6 \cdot \xi_2, \tag{12}$$

$$\begin{aligned}
w(\xi_2) = {} & \frac{\hat{\hat{\gamma}}_0}{aK} D_6\\
& + \frac{\hat{\hat{\gamma}}_2}{\hat{\hat{\gamma}}_1 a K^2} \left\{ \begin{array}{l} D_1 \cdot [d_1 \cdot g_3(\xi_2) - d_2 \cdot g_2(\xi_2)] \\ + D_2 \cdot [d_1 \cdot g_4(\xi_2) + d_2 \cdot g_1(\xi_2)] \\ + D_3 \cdot [d_1 \cdot g_1(\xi_2) - d_2 \cdot g_4(\xi_2)] \\ + D_4 \cdot [d_1 \cdot g_2(\xi_2) + d_2 \cdot g_3(\xi_2)] \end{array} \right\},
\end{aligned} \tag{13}$$

$$\phi_2(\xi_2) = D_1 \cdot g_1(\xi_2) + D_2 \cdot g_2(\xi_2) + D_3 \cdot g_3(\xi_2) + D_4 \cdot g_4(\xi_2), \tag{14}$$

$$\psi(\xi_2) = Sinh\left(\frac{aK}{l}\xi_2\right) D_7 + Cosh\left(\frac{aK}{l}\xi_2\right) D_8, \tag{15}$$

where:

$c^2 = \frac{h^2K^2}{12}$,

$g_1(\xi_2) = Sinh(m \cdot \xi_2) \cdot Sin(n \cdot \xi_2)$,

$g_2(\xi_2) = Sinh(m \cdot \xi_2) \cdot Cos(n \cdot \xi_2)$,

$g_3(\xi_2) = Cosh(m \cdot \xi_2) \cdot Sin(n \cdot \xi_2)$,

$g_4(\xi_2) = Cosh(m \cdot \xi_2) \cdot Cos(n \cdot \xi_2)$,

$$m = \frac{aK}{2}\sqrt{\gamma_1\left(1 + \frac{2}{aK}\sqrt{\frac{1}{\hat{\hat{\gamma}}_1\hat{\hat{\gamma}}_2}}\right)},$$

$$n = \frac{\hat{\hat{\gamma}}_1 aK}{2} \frac{\sqrt{\frac{4}{\hat{\hat{\gamma}}_1\hat{\hat{\gamma}}_2 a^2K^2} - 1}}{\sqrt{\hat{\hat{\gamma}}_1\left(1 + \frac{2}{aK}\sqrt{\frac{1}{\hat{\hat{\gamma}}_1\hat{\hat{\gamma}}_2}}\right)}},$$

$d_1 = m\left(m^2 - 3n^2\right)$,

$d_2 = n\left(n^2 - 3m^2\right)$.

The set of eight constants can be defined with the use of boundary conditions according to the Fig. 8:

$$u_2(-1) = 0,\ w(-1) = 0,\ \phi_2(-1) = 0,\ \psi(-1) = 0,$$
$$u_2(1) = 0,\ N_{23}(1) = P,\ \phi_2(1) = 0,\ M_{23}(1) = 0. \tag{16}$$

The solution is obtained with the use of symbolic programming within the *Mathematica* environment. The expressions are too big to present them in the paper in analytical form but it is possible to show them graphically. Two important parameters are important for the analysis the results: cable to strut stiffness ratio

$$k = \frac{(EA)_{cable}}{(EA)_{strut}} \tag{17}$$

and the self-equilibrated normal forces ratio in the tensegrity lattice:

$$\sigma = \frac{S}{EA}. \tag{18}$$

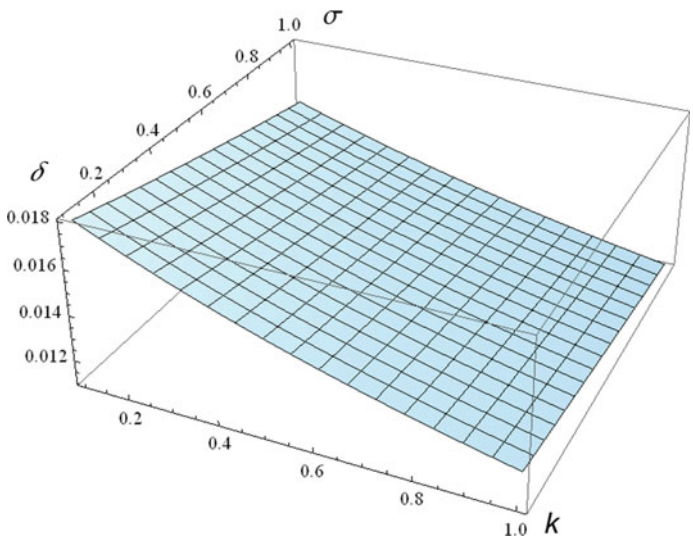

Fig. 9 Parametric study of normalized maximum displacement in the cylindrical ring

The scaled maximum radial displacement $\delta = w_{\max} \frac{EA_{strut}h^3}{PL^3a^2}$ is presented in Fig. 9. The influence of both parameters are on the level of 30% what can be an effective value for active control of the tensegrity-like shell.

6 Conclusion

The six-parameter shell theory, introduced and widely explored by Professor Wojciech Pietraszkiewicz, is applied for tensegrity-like curved structures. Tensegrities are cable-strut lattices of complicated form. The shell model can help to understand their mechanical properties. The preliminary results are promising. Displacements and internal forces of tensegrity-like shells depends on the geometrical properties of the lattice as well as on the self-equilibrated normal forces ratio. The parameters are important for the applications the tensegrity lattices in smart constructions in which active control and self-diagnosis can be applied.

References

1. Pietraszkiewicz, W.: Consistent second approximation to the elastic strain energy in a shell. Z Angew Math. Mech. **59**, 206–208 (1979)
2. Pietraszkiewicz, W.: Finite Rotations and Lagrangean Description in the Non-linear Theory of Shells. Polish Scientific Publishers, Warsaw, Poznań (1979)

3. Pietraszkiewicz, W., Babur, J.: Finite rotations in the description of continuum deformation. Int. J. Eng. Sci. **21**, 1097–1115 (1983)
4. Chróścielewski, J., Makowski, J., Pietraszkiewicz, W.: Nonlinear dynamics of flexible shell structures. Comp. Ass. Mech. Eng. Sci. **9**, 341–357 (2002)
5. Chróścielewski, J., Makowski, J., Pietrasziewicz, W.: Statics and Dynamics of Multifold-shells: Nonlinear Theory and Finite Element Method (in Polish). IFTR Polish Academy of Sciences Press, Warsaw (2004)
6. Eremeyev, V.A., Pietraszkiewicz, W.: The non-linear theory of elastic shells with phase transition. J. Elast. **74**, 67–86 (2004)
7. Eremeyev, V.A., Pietraszkiewicz, W.: Local symmetry group in the general theory of elastic shells. J. Elast. **85**, 125–152 (2006)
8. Chróścielewski, J., Witkowski, W.: Four-node semi-EAS element in six-field nonlinear theory of shells. Int. J. Numer. Meth. Eng. **68**, 1137–1179 (2006)
9. Panasz, P., Wiśniewski, K.: Nine-node shell elements with 6 dofs/node based on two-level approximation. Finite Elem. Anal. Des. **44**, 784–796 (2008)
10. Gilewski, W.: High-precision finite elements on moderately thick shell theory. Ph.D. dissertation. Warsaw University of Technology (1986)
11. Gilewski, W., Al Sabouni-Zawadzka, A., Pełczyński, J.: Physical shape functions in 6-parametre shell theory finite elements. In: Pietraszkiewicz, W., Witkowski, W. (Eds.) Shell Structures: Theory and Applications 4. CRC Press, Boca Raton, London, New York, Leiden (2017)
12. Al Sabouni-Zawadzka, A., Kłosowska, J., Obara, P., Gilewski, W.: Continuum model of orthotropic tensegrity plate-like structures with self-stress included. Engng. Trans. **64**, 501–508 (2016)
13. Obara, P., Gilewski, W.: Discrete and equivalent 6-parameter shell approach to simulate mechanical behavior of tensegrity lattices. Solmech 2018, Warsaw, Poland (2018)
14. Pugh, A.: An Introduction to Tensegrity. University California Press, Berkeley, Los Angeles, London (1976)
15. Motro, R.: Tensegrity: Structural Systems for the Future. Kogan Page, London (2003)
16. Skelton, R.E., de Oliveira, M.C.: Tensegrity Systems. Springer, London (2009)
17. Al Sabouni-Zawadzka, A., Gilewski, W.: Inherent properties of smart tensegrity structures. Appl. Sci. **8**, 787-1-14 (2018)
18. Kasprzak, A., Gilewski, W.: 3D Continuum Model of Tensegrity Modules with the Effect of Self-stress. WCCM XI, ECCM V, Barcelona, Spain (2014)
19. Pellegrino, S., Calladine, C.R.: Matrix analysis of statically and kinematically indeterminate frameworks. Int. J. Solid Struct. **22**, 409–422 (1990)
20. Lewiński, T.: On algebraic equations of elastic trusses, frames and grillages. J. Theor. Appl. Mech. **39**, 307–322 (2001)
21. Pełczyński, J., Gilewski, W.: An extension of algebraic equations of elastic trusses with self-equilibrated system of forces. ECMM 6, Glasgow, UK (2018)
22. Green, A.E., Zerna, W.: Theoretical Elasticity. Press, Oxford, UK, Oxford Uni (1968)
23. Chadwick, P., Vianello, M., Cowin, S.A.: A new proof that the number of linear elastic symmetries is eight. J. Mech. Phys. Solids **49**, 2471–2492 (2001)

On Some Recent Discrete-Continuum Approaches to the Solution of Shell Problems

Ya. M. Grigorenko, A. Ya. Grigorenko and E. Bespalova

Abstract The fundamentals of three new discrete-continuum approaches to the solution of the stationary problems of shell theory are discussed: the discrete Fourier series approach, the spline-collocation method, and the complete systems method. The general idea of the discussed approaches consists in using some sort of transformation to convert the original two-dimensional (or three-dimensional) problems to the corresponding linear one-dimensional boundary-value problems, which are then solved numerically using the method of discrete orthogonalization. The considered problems of elastic deformations of shells employ models of various degree of accuracy: the model of Mushtari-Donnel-Vlasov, the first-order model of Timoshenko-Mindlin, and the model based on three-dimensional theory of elasticity. Combining those models with the proposed solution methods for multi-dimesional problems investigations of the deformation and stress fields in a number of shells, as well as of their free vibration properties, are conducted. The considered shells are described by surface-varying geometrical and physical parameters and it is shown that variation of those parameters on the distribution of their displacement fields, stress fields, and on their dynamic characteristics is significant. Special attention is dedicated to the issue of the accuracy of the obtained numerical solutions.

Keywords Discrete-continuum approaches · Different mechanical models · Anisotropic · Inhomogeneous · Shell structures

1 Introduction

Many constructive elements of modern engineering and building structures have the form of shells of various shapes with a complex inhomogeneous architecture made of modern materials (composite, functionally-gradient, nanomaterials) which reveal anisotropy of physical-mechanical properties. The wide application of the shell systems is attributed to the tendency to satisfy the requirements caused by

Ya. M. Grigorenko · A. Ya. Grigorenko (✉) · E. Bespalova
S. P. Timoshenko Institute of Mechanics, National Academy of Sciences, Nesterova 3, Kiev 03057, Ukraine
e-mail: ayagrigorenko1991@gmail.com

H. Altenbach et al. (eds.), *Recent Developments in the Theory of Shells*,
Advanced Structured Materials 110, https://doi.org/10.1007/978-3-030-17747-8_16

severe operation conditions of various constructive elements of modern engineering as well as to the probability of choice of rational parameters of strength and service reliability under the above conditions. Investigation of the stress-strain state and free vibrations of anisotropic inhomogeneous shells comes up against great difficulties contributed to solving boundary-value problems for partial differential equations with variable coefficients.

In view of wide application of modern computational facilities presented by computers with large memory and high operation speed, the approaches to design various aspects of mechanical performance of shell structures at present are based in main on numerical methods of problem solving. The universal up-to-date numerical methods making it possible to solve various classes of boundary-value problems of the shell theory are developed. These so-called discrete methods are based on the reduction of initial partial differential equations to the systems of high-order algebraic equations. They include such methods as finite-difference, variational-difference, and finite-element ones. The finite-element method, due to its universality and algorhytmicity, today is the first one by use. Based on various modifications of this method, the LIRA, NX NASTRAN, ANSYS, SIMULA Abaqus, PLAXIS, a.o. software packages have been developed which are widely used in solving static and dynamic problems of the shell theory and elasticity.

However, along with the universal discrete approaches to solving problems of the shell theory, the so-called discrete-continual methods are widely applied. The general idea of these methods consists in reduction of original two-dimensional (three-dimensional) problems by making use one or other transformations to linear one-dimensional boundary-value problems, which are solved numerically with the discrete-orthogonalization method, particularly. The discrete-continual approaches can be considered as alternative to the universal numerical methods since they are applied as a rule to analysis of shell objects of a certain class. The solutions obtained with them can occur to be more effective and accurate that makes it possible for these methods to be employed in testing various discrete approaches being modified. The present report proposes three new discrete-continual methods that include the discrete Fourier series, spline-collocation, and complete system ones which can be used in solving stationary problems of the shell theory.

2 Discrete Fourier Series Method in Static Problems for Thick-Walled Shells

The results are presented below, which were obtained in solving the boundary-value stress problems in spatial formulation, using an untraditional approach, for noncircular hollow cylinders with certain boundary conditions on ends. This approach is based on the reduction of a three-dimensional problem to two-dimensional one by

separation of variables along the cylinder length through the use of the Fourier series. The two-dimensional boundary-value problem, by introducing subsidiary functions and separating variables along the directrix, is reduced with the help of the discrete Fourier series to one-dimensional one, which is solved by the numerical discrete-orthogonalization method.

The above approach has been applied to solving the wide class of problems for thick-walled cylindrical shells with different cross-section [10, 11]. Here, to illustrate the discrete Fourier series method, a hollow cylinder with convex corrugated cross-section is considered as an example.

2.1 Problem Statement

Consider elastic hollow cylinders of constant thickness under an external surface load $q = q_0 \sin(\pi s/l)$ ($q_0 = \text{const}$).The cylinders are described in curvilinear orthogonal coordinates $s,\ \psi,\ \gamma$, where s is the longitudinal coordinate, ψ ($0 \le \psi \le 2\pi$) is the azimuth angle, and γ ($\gamma_1 \le \gamma \le \gamma_2$) is the normal (thickness) coordinate.

The cross-section of the reference surface (Fig. 1) is described by epicycloidal arcs [15] and specified parametrically as

$$x = (A + a)\cos\psi - \lambda a \cos\left(\frac{A + a}{a}\psi\right);\ \ y = (A + a)\sin\psi - \lambda a \sin\left(\frac{A + a}{a}\psi\right),$$

where A is the radius of the fixed circle; a ($a > 0$) is the radius of the epicycle; λa ($\lambda < 1$) is the distance to the center of the epicycle.

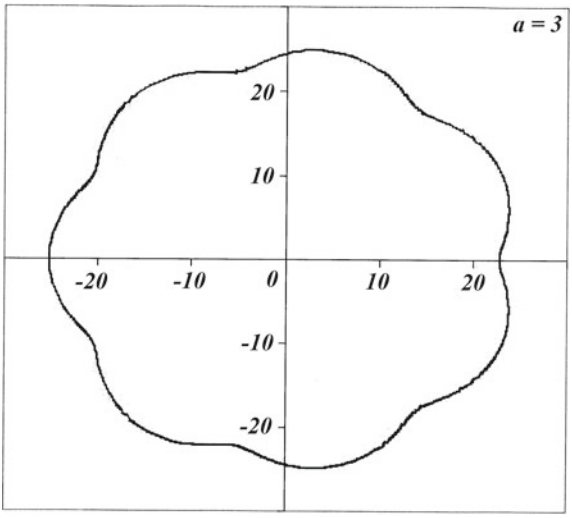

Fig. 1 Cross-section of the reference surface by epicycloidal arcs

The first quadratic form is given by

$$dS^2 = ds^2 + B_2^2(\psi,\gamma)d\psi^2 + d\gamma^2$$

$$B_2 = B_2(\psi,\ \gamma) = H_2(\psi,\ \gamma)\,\omega\,(\psi);\ \ H_2 = H_2(\psi,\ \gamma) = 1 + \frac{\gamma}{R(\psi)};$$

$$\omega = \omega\,(\psi) = \sqrt{\left(\frac{dx}{d\psi}\right)^2 + \left(\frac{dy}{d\psi}\right)^2};\quad R_\psi = R\,(\psi) = \frac{\left(\left(\frac{dx}{d\psi}\right)^2 + \left(\frac{dy}{d\psi}\right)^2\right)^{3/2}}{\frac{dx}{d\psi}\frac{d^2y}{d\psi^2} - \frac{dy}{d\psi}\frac{d^2x}{d\psi^2}};$$

where H_2 is the Lame parameter; R_ψ is the radius of curvature of the cross-section; ω is the transformation coefficient between the longitudinal coordinate and ψ.

We will start with the equations of three-dimensional isotropic elasticity [21]. The boundary conditions at the cylinder ends are as follows:

$$\sigma_s = 0;\quad u_\psi = 0;\quad u_\gamma = 0\,\text{at}\,s = 0,\quad s = l. \tag{1}$$

The boundary conditions on the lateral surfaces are

$$\sigma_\gamma = 0;\quad \tau_{s\gamma} = 0;\quad \tau_{\psi\gamma} = 0\,\text{at}\,\gamma = \gamma_1; \tag{2}$$

$$\sigma_\gamma = q_\gamma;\quad \tau_{s\gamma} = 0;\quad \tau_{\psi\gamma} = 0\,\text{at}\,\gamma = \gamma_2. \tag{3}$$

Choosing the stresses σ_γ, $\tau_{s\gamma}$, $\tau_{\psi\gamma}$ and the displacements u_γ, u_s, u_ψ, as unknown functions and performing some transformations, we arrive at a governing system of partial differential equations of the sixth order with variable coefficients:

$$\begin{aligned}
\frac{\partial\sigma_\gamma}{\partial\gamma} =& -\frac{1}{H_2R_\psi}\sigma_\gamma - \frac{\partial\tau_{s\gamma}}{\partial s} - \frac{1}{B_2}\frac{\partial\tau_{\psi\gamma}}{\partial\psi} + \\
&+ \frac{1}{H_2R_\psi}\left[\frac{E\nu}{1-\nu^2}\frac{\partial u_s}{\partial s} + \frac{\nu}{1-\nu}\sigma_\gamma + \frac{E}{1-\nu^2}\left(\frac{1}{B_2}\frac{\partial u_\psi}{\partial\psi} + \frac{1}{H_2R_\psi}u_\gamma\right)\right];\\
\frac{\partial\tau_{s\gamma}}{\partial\gamma} =& -\frac{1}{H_2}\frac{1}{R_\psi}\tau_{s\gamma} - \frac{\partial}{\partial s}\left[\frac{E}{(1-\nu^2)}\frac{\partial u_s}{\partial s} + \frac{E\nu}{(1-\nu^2)}\frac{1}{H_2}\times\right.\\
&\left.\times\left(\frac{1}{\omega}\frac{\partial u_\psi}{\partial\psi} + \frac{1}{R_\psi}u_\gamma\right) + \frac{\nu}{(1-\nu)}\sigma_\gamma\right] - \frac{1}{B_2}\frac{\partial}{\partial\psi}\left[\frac{E}{2(1+\nu)}\left(\frac{1}{B_2}\frac{\partial u_s}{\partial\psi} + \frac{\partial u_\psi}{\partial s}\right)\right];\\
\frac{\partial\tau_{\psi\gamma}}{\partial\gamma} =& -\frac{2}{H_2R_\psi}\tau_{\psi\gamma} - \frac{1}{B_2}\frac{\partial}{\partial\psi}\left[\frac{E}{1-\nu^2}\left(\nu\frac{\partial u_s}{\partial s} + \frac{1}{B_2}\frac{\partial u_\psi}{\partial\psi} + \frac{1}{H_2R_\psi}u_\gamma\right) + \right.\\
&\left. + \frac{\nu}{(1-\nu)}\sigma_\gamma\right] - \frac{\partial}{\partial s}\left[\frac{E}{2(1+\nu)}\left(\frac{1}{B_2}\frac{\partial u_s}{\partial\psi} + \frac{\partial u_\psi}{\partial s}\right)\right];\\
\frac{\partial u_\gamma}{\partial\gamma} =& -\frac{\nu}{1-\nu}\left(\frac{\partial u_s}{\partial s} + \frac{1}{B_2}\frac{\partial u_\psi}{\partial\psi} - \frac{1}{H_2R_\psi}u_\gamma\right) + \frac{1-\nu-2\nu^2}{E(1-\nu)}\sigma_\gamma;
\end{aligned}$$

$$\frac{\partial u_s}{\partial \gamma} = \frac{2(1+\nu)}{E}\tau_{s\gamma} - \frac{\partial u_\gamma}{\partial s};\ \frac{\partial u_\psi}{\partial \gamma} = \frac{2(1+\nu)}{E}\tau_{\psi\gamma} - \frac{1}{B_2}\frac{\partial u_\gamma}{\partial \psi} + \frac{1}{H_2 R_\psi}u_\psi$$
$$(0 \le s \le l;\quad 0 \le \psi \le 2\pi;\quad \gamma_1 \le \gamma \le \gamma_2) \tag{4}$$

subject to the boundary conditions (1–3).

2.2 Problem-Solving Method

The boundary conditions (1) make it possible to separate the variables with respect to the longitudinal coordinate. To this end, the load components and unknown functions are expanded into Fourier series in s:

$$X(s,\psi,\gamma) = \sum_{n=1}^{N} X_n(\psi,\gamma)\sin\lambda_n s,\ \ Y(s,\psi,\gamma) = \sum_{n=1}^{N} Y_n(\psi,\gamma)\cos\lambda_n s,$$
$$\left(X = \left\{\sigma_\gamma, \tau_{\psi\gamma}, u_\gamma, u_\psi, q_\gamma\right\};\ Y = \left\{\tau_{s\gamma}, u_s\right\};\ \lambda_n = \frac{\pi n}{l} \quad (0 \le s \le l)\right). \tag{5}$$

Substituting series (5) into the governing system (4) and the boundary conditions (2), (3) and separating variables, we derive, for each term in (5), a governing system of partial differential equations with variable coefficients describing a two-dimensional boundary-value problem [12].

The expressions appearing in the governing system of equations and hindering the separation of variables with respect to ψ can be considered as additional functions:

$$\varphi_1^j = \frac{1}{H_2 R_\psi}\left\{\sigma_\gamma; \tau_{s\gamma}; u_\gamma; u_s\right\}\left(j = \overline{1,4}\right);\ \varphi_1^5 = \left(\frac{1}{H_2 R_\psi}\right)^2 u_\gamma;$$
$$\varphi_2^j = \frac{1}{H_2 R_\psi}\left\{\tau_{\psi\gamma}; u_\psi\right\}\ \left(j = \overline{1,2}\right);\quad \varphi_3^j = \frac{1}{B_2}\left\{\frac{\partial \sigma_\gamma}{\partial \psi}; \frac{\partial u_\gamma}{\partial \psi}; \frac{\partial u_s}{\partial \psi}\right\}\ \ \left(j = \overline{1,3}\right);$$
$$\varphi_4^j = \frac{1}{B_2}\left\{\frac{\partial \tau_{\psi\gamma}}{\partial \psi}; \frac{\partial u_\psi}{\partial \psi}; \frac{1}{R_\psi}\frac{\partial u_\psi}{\partial \psi}\right\}\ \ \left(j = \overline{1,3}\right);\ \varphi_5 = \frac{1}{B_2}\frac{\partial}{\partial \psi}\varphi_1^3;$$
$$\varphi_6 = \frac{1}{B_2}\frac{\partial}{\partial \psi}\varphi_3^3;\quad \varphi_7 = \frac{1}{B_2}\frac{\partial}{\partial \psi}\varphi_4^2. \tag{6}$$

These functions allow the governing system of differential equations to be formally represented in such a form that the separation of variables with respect to ψ becomes possible. Expanding the load components and the unknown and additional functions into Fourier series in ψ

$$\tilde{X}(\psi,\gamma)=\sum_{k=0}^{K}\tilde{X}_k(\gamma)\cos k\psi;\quad \tilde{Y}(\psi,\gamma)=\sum_{k=1}^{K}\tilde{Y}_k(\gamma)\sin k\psi;$$

$$\tilde{X}=\left\{\sigma_\gamma,\tau_{s\gamma},u_\gamma,u_s,\varphi_1^j,\varphi_4^j,\varphi_6,q_\gamma\right\};\quad \tilde{Y}=\left\{\tau_{\psi\gamma},u_\psi,\varphi_2^j,\varphi_3^j,\varphi_5,\varphi_7\right\} \tag{7}$$

substituting them into the governing system of equations, and separating variables, we obtain a system of ordinary differential equations for the amplitudes of the Fourier series (7) (the index n being omitted):

$$\begin{aligned}
\frac{d\sigma_{\gamma,k}}{d\gamma}=&\lambda_n\tau_{s\gamma,k}+\left(\frac{\nu}{1-\nu}-1\right)\varphi^{\,1}_{1,k}-\varphi^{\,1}_{4,k}-\frac{E}{1-\nu^2}\left(\lambda_n\varphi^{\,4}_{1,k}+\varphi^{\,3}_{4,k}+\varphi^{\,5}_{1,k}\right);\\
\frac{d\tau_{s\gamma,k}}{d\gamma}=&-\frac{\nu}{1-\nu}\lambda_n\,\sigma_{\gamma,k}+\frac{E}{1-\nu^2}\lambda_n^2\,u_{s,k}-\\
&-\varphi^{\,2}_{1,k}-\left(\frac{E\nu}{1-\nu^2}+\frac{E}{2(1+\nu)}\right)\lambda_n\,\varphi^{\,2}_{4,k}-\frac{E\nu}{1-\nu^2}\lambda_n\,\varphi^{\,3}_{1,k}-\frac{E}{2(1+\nu)}\varphi_{6,k};\\
\frac{d\tau_{\psi\gamma,k}}{d\gamma}=&\frac{E}{2(1+\nu)}\lambda_n^2\,u_{\psi,k}-2\varphi^{\,1}_{2,k}+\left(\frac{E\nu}{1-\nu^2}+\frac{E}{2(1+\nu)}\right)\lambda_n\,\varphi^{\,3}_{3,k}-\\
&-\frac{E}{1-\nu^2}(\varphi_{7,k}+\varphi_{5,k})-\frac{\nu}{1-\nu}\varphi^{\,1}_{3,k};\\
\frac{du_{\gamma,k}}{d\gamma}=&\frac{\left(1-\nu-2\nu^2\right)}{(1-\nu)E}\sigma_{\gamma,k}+\frac{\nu}{1-\nu}\left(\lambda_n\,u_{s,k}-\varphi^{\,2}_{4,k}-\varphi^{\,3}_{1,k}\right)\\
\frac{du_{s,k}}{d\gamma}=&\frac{2(1+\nu)}{E}\tau_{s\gamma,k}-\lambda_n\,u_{\gamma,k};\quad \frac{du_{\psi,k}}{d\gamma}=\frac{2(1+\nu)}{E}\tau_{\psi\gamma,k}-\varphi^{\,2}_{3,k}+\varphi^{\,2}_{2,k}\ \left(k=\overline{0,K}\right),
\end{aligned}\tag{8}$$

subject to the boundary conditions

$$\sigma_{\gamma,k}=0;\quad \tau_{s\gamma,k}=0;\quad \tau_{\psi\gamma,k}=0\ \text{at}\ \gamma=\gamma_1; \tag{9}$$

$$\sigma_{\gamma,k}=q_{\gamma,k};\quad \tau_{s\gamma,k}=0;\quad \tau_{\psi\gamma,k}=0\ \text{at}\ \gamma=\gamma_2. \tag{10}$$

The boundary-value problem (8)–(10) can be solved with the stable numerical discrete-orthogonalization method for all the k harmonics of the Fourier series (7) simultaneously. At each step of integration, the amplitudes of the additional functions are calculated from the current amplitudes of the unknown functions by approximating them by discrete Fourier series [13]. At the beginning of integration, the additional functions are determined from the boundary conditions and the initial values of the unknown functions.

2.3 Analysis of the Numerical Results

Let us analyze the dependence of the stress state of hollow cylinders of the class being considered on their cross-sectional curvature. The input data: the radius of the fixed circle $A = 21$; the radius of the epicycle $a = 3; 7$; the parameter $\lambda = 0.4; 0.5$; the thickness of the cylinder $h = 2$; the length of the cylinder $l = 60$; Young's modulus $E = E_0$; Poisson's ratio $\nu = 0.3$.

The radius of curvature of the reference surface is minimum at the points ($\psi = 0$) where epicycloidal arcs are joined. Table 1 summarizes the values of the radius of curvature and the ratio of the thickness to the radius of curvature for four different cylinders.

It can be seen that the ratio $h/|R_\psi|$ falls between the allowable limits for thick- and medium-walled shells, which justifies the choice of the three-dimensional model for solving problems of this class.

The solution is presented in Figs. 2, 3, and 4 for the mid-length cross-section of the cylinder.

Table 1 The values of the radius of curvature $|R_\psi|$ and the ratio of the thickness to the radius of curvature $h/|R_\psi|$ of reference surface for four different cylinders ($a = 7, a = 3$ and $\lambda = 0.4$, $\lambda = 0.5$)

$A = 21;\ h = 2$				
a	7		3	
The number of epicycloidal arcs	3		7	
λ	0.4	0.5	0.4	0.5
$\lvert R_\psi \rvert$	3.9	2.0	16.8	7.0
$h/\lvert R_\psi \rvert$	0.5	1	0.12	0.29

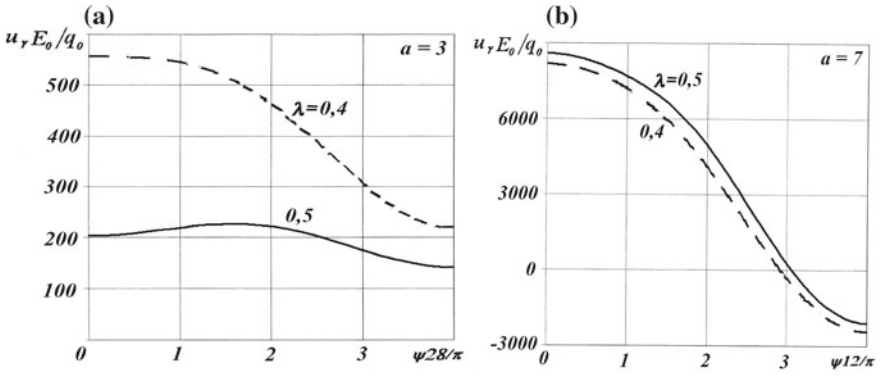

Fig. 2 The circumferential distribution of the displacement u_γ of the mid-surface by $a = 3$ (**a**) and $a = 7$ (**b**)

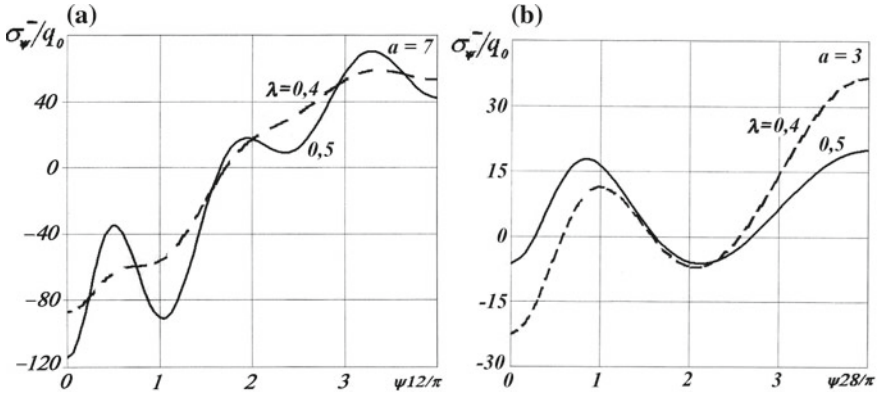

Fig. 3 The circumferential distribution of the stress σ_ψ^- on the inside surface of the cylinder by $a = 7$ (**a**) and $a = 3$ (**b**)

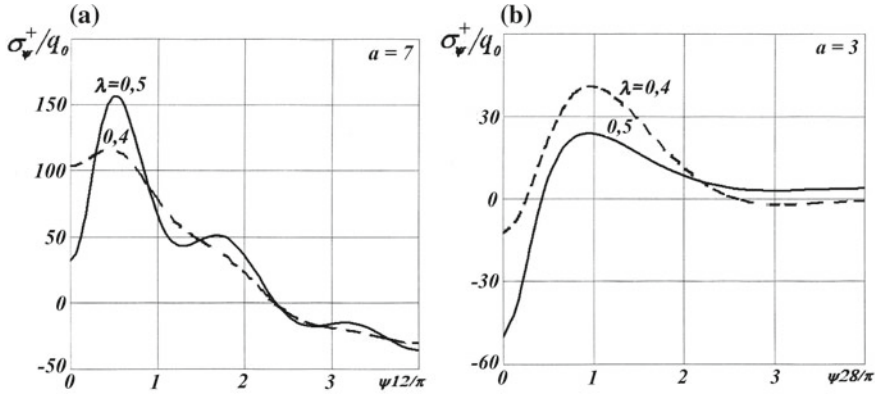

Fig. 4 The circumferential distribution of the stress σ_ψ^+ on the outside surface of the cylinder by $a = 7$ (**a**) and $a = 3$ (**b**)

Figure 2 show the circumferential distribution of the displacement u_γ of the mid-surface. It can be seen from Fig. 2a that as the parameter λ increases, the displacements in the cylinders with three corrugations increase slightly in both sections $\psi = 0$ and $\psi = \pi/3$ The displacements at the junction point are four times larger than and are opposite in sign to the displacements at the corrugation apex.

Figure 2b demonstrates a different pattern for the cylinders with seven corrugations. As the distance to the epicycle center increases, the displacements decrease by a factor of 2.7 for $\psi = 0$ and by factor 1.6 for $\psi = \pi/7$. The more there are corrugations, the higher the stiffness and the smaller the displacements.

The circumferential distribution of the stress σ_ψ^- on the inside surface of the cylinder is shown in Fig. 3, and the circumferential distribution of the stress σ_ψ^+ on the outside surface in Fig. 4.

It follows from Fig. 3a, b that the stress σ_{ψ}^{-} peaks at the junction point when $a = 7$ and $\psi = 0$ and at the corrugation apex when $a = 3$ and $\psi = \pi/7$. The stresses at $\psi = 0$ in the cylinders with seven corrugations are much lower because of higher stiffness.

It can be seen from Fig. 4a that when $a = 7$ the stress σ_{ψ}^{+} peaks at some distance from the section $\psi = 0$ and increases by a factor of 1.2 with increase in λ.

When a =3 (Fig. 4b), the stresses peak at some distance from the junction point if $\lambda = 0.4$ and in the section $\psi = 0$ if $\lambda = 0.5$. The stresses at the apex $\psi = \pi/7$ are nearly zero.

In conclusion, we note the following.

We have solved a three-dimensional problem to find the stress state of corrugated hollow cylinders with cross-section described by epicycloidal arcs. The dependence of the stress state on changes in the curvature caused by variations in the radius of the epicycle and the distance to its center has been analyzed. It has been established that the stiffness of the cylinder increases with variation in the radius of the epicycle and the distance to its center, which strongly affects the displacement and stress fields.

3 Spline-Collocation Method

Noncircular shells with various cross-sections are employed in many areas of modern engineering. Of practical importance is to determine resonance frequencies that depend on the natural frequencies. The scientific literature covers a great many works on the free vibrations of circular cylindrical shells with variable thickness [18]. Because of the complexity of the problem, few studies address the vibrations of noncircular cylindrical shells which are mainly considered to be isotropic and have constant thickness. This problem is considered in Soldatos [18], Suzuki and Leissa [19], Suzuki et al. [20].

Here we will analyze the free vibrations of noncircular cylindrical orthotropic shells of variable thickness using the Timoshenko-Mindlin shell theory [9]. Recently, computational mathematics, mathematical physics, and mechanics have widely employed spline functions to solve such problems. This is due to the following advantages of the spline-approximation method over the other ones: stability of splines against local perturbations, i.e., the behavior of a spline in the neighborhood of a point does not affect the overall behavior of the spline (as polynomial approximation does, for example); better convergence of spline-interpolation compared with polynomial interpolation; and simple and convenient computer implementation of spline algorithms. The use of spline functions in variational, projective, and other discrete–continuous methods allows us to obtain appreciable results as contrasted to the use of classical polynomials, to simplify substantially their numerical implementation, and to obtain a highly accurate solutio The present part analyzes the natural vibrations of noncircular cylindrical shells with elliptical cross-section of variable thickness with different boundary conditions. Since the separation of variables is impossible for this class of shells, it is necessary to employ numerical methods. This

paper proposes an efficient numerical method for studying the natural frequencies of noncircular cylindrical shells of variable thickness thickness. The method involves spline-approximation in one coordinate direction and solution of a boundary-value eigenvalue problem for systems of ordinary differential equations of high order with variable coefficients by stable numerical discrete orthogonalization in combination with step-by-step search [7–9].

3.1 Problem Statement. Basic Equations

We will analyze the free vibrations of noncircular cylindrical shells of arbitrary cross-section and variable thickness (Fig. 5) using the refined Timoshenko shell model based on the straight-normal hypothesis (after small deformation, a straight normal to the initial coordinate surface remains straight and unstretched but does not remain normal). In the coordinate system s, t, fixed to the shell mid-surface (is the normal (to the mid-surface) coordinate $h/2$; s is the circumferential coordinate, $0\ s\ L$; t is the longitudinal coordinate, $t_1 \le t \le t_2$), small displacements can be expressed as

$$u_\gamma(s,t,\gamma,\tau) = w(s,t,\tau);\ u_\theta(s,t,\gamma,\tau) = v(s,t,\tau) + \gamma\psi_\theta(s,t,\tau);\\ u_z(s,t,\gamma,\tau) = u(s,t,\tau) + \gamma\psi_z(s,t,\tau), \tag{11}$$

where τ is time, $u\ (s,\ t,\ \tau\ )$, $v\ (s,\ t,\ \tau\ )$, and $w\ (s,\ t,\ \tau\ )$ are the displacements of the coordinate surface; $\psi_s\ (s,t,\tau\ )$ and $\psi_t\ (s,t,\tau\ )$ are functions defining the total rotation of the normal.

With (1), the expressions for the strains become

$$e_s(s,t,\gamma,\tau) = \varepsilon_s(s,t,\tau) + \gamma\kappa_s(s,t,\tau);\ e_t(s,t,\gamma,\tau) = \varepsilon_t(s,t,\tau) + \gamma\kappa_t(s,t,\tau);\\ e_{st}(s,t,\gamma,\tau) = \varepsilon_{st}(s,t,\tau) + 2\gamma\kappa_{st}(s,t,\tau);\ e_{\gamma s}(s,t,\gamma,\tau) = \gamma_s(s,t,\tau);\\ e_{\gamma t}(s,t,\gamma,\tau) = \gamma_t(s,t,\tau);\ e_{\gamma t}(s,t,\gamma,\tau) = \gamma_t(s,t,\tau)\,. \tag{12}$$

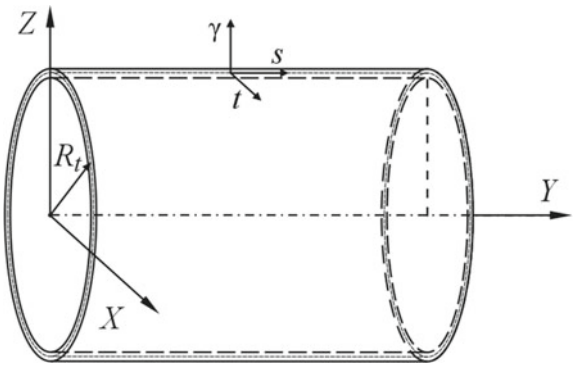

Fig. 5 Noncircular cylindrical shell with elliptical cross-section

where $\varepsilon_s, \varepsilon_t, \varepsilon_{st}$ are the tangential strains of the coordinate surface; $\kappa_s,\ \kappa_t,\ \kappa_{st}$ are flexural strains; $\gamma_s,\ \gamma_t$ are the rotation angles of the normal caused by transversal shears.

The strains and displacements of the shell mid-surface are related by

$$\begin{aligned}
&\varepsilon_s = \frac{\partial u}{\partial s};\ \varepsilon_t = \frac{\partial v}{\partial t} + k(t)w;\ \varepsilon_{st} = \frac{\partial u}{\partial t} + \frac{\partial v}{\partial s};\ \kappa_s = \frac{\partial \psi_s}{\partial s};\\
&\kappa_t = \frac{\partial \psi_t}{\partial t} - k(t)\left(\frac{\partial v}{\partial t} + k(t)w\right);\ 2\kappa_{st} = \frac{\partial \psi_s}{\partial t} + \frac{\partial \psi_t}{\partial s} - k(t)\frac{\partial u}{\partial t};\\
&\gamma_s = \psi_s + \frac{\partial w}{\partial s};\ \gamma_t = \psi_t + \frac{\partial w}{\partial t} - k(t)\, v\,.
\end{aligned} \tag{13}$$

The equations of motion for an element of the coordinate surface are

$$\begin{aligned}
&\frac{\partial N_s}{\partial s} + \frac{\partial N_{st}}{\partial t} = I_0\frac{\partial^2 u}{\partial \tau^2} + I_1\frac{\partial \psi_s}{\partial \tau^2};\ \frac{\partial N_t}{\partial t} + \frac{\partial N_{st}}{\partial s} + k(t)Q_t = I_0\frac{\partial v}{\partial \tau^2} + I_1\frac{\partial^2 \psi_s}{\partial \tau^2};\\
&\frac{\partial Q_s}{\partial s} + \frac{\partial Q_t}{\partial t} - k(t)N_t = I_0\frac{\partial^2 w}{\partial \tau^2};\ \frac{\partial M_s}{\partial s} + \frac{\partial M_{st}}{\partial t} - Q_s = I_1\frac{\partial^2 u}{\partial \tau^2} + I_2\frac{\partial \psi_s}{\partial \tau^2};\\
&\frac{\partial M_t}{\partial t} + \frac{\partial M_{st}}{\partial s} - Q_t = I_1\frac{\partial v}{\partial \tau^2} + I_2\frac{\partial^2 \psi_s}{\partial \tau^2},
\end{aligned} \tag{14}$$

where $N_{st} - k(t)M_{ts} - N_{ts} = 0$, $N_s,\ N_t,\ N_{st},\ N_{ts}$ are tangential forces; $Q_t,\ Q_s$ are shearing forces; $M_t,\ M_s,\ M_{ts},\ M_{st}$ are bending $\rho(s,\ t,\ \gamma)$ is the density of the shell material. The inertial terms I_0, I_1, I_2 in (4) are given by

$$I_0 = \int_{-h/2}^{h/2} \rho(s,t,\gamma)\ d\gamma;\ I_1 = \int_{-h/2}^{h/2} \rho(s,t,\gamma)\,\gamma d\gamma;\ I_2 = \int_{-h/2}^{h/2} \rho(s,t,\gamma)\,\gamma^2 d\gamma\,. \tag{15}$$

If the mechanical properties of the material across the thickness remain constant, then I_0, I_1, I_2 are defined by:

$$I_0 = \rho\, h;\ I_1 = 0;\ I_2 = \rho h^3/12\,.$$

Since the mechanical properties of the material are symmetric about the shell mid-surface, the elasticity relations for orthotropic noncircular cylindrical shells take the form

$$\begin{aligned}
&N_s = C_{11}\varepsilon_s + C_{12}\varepsilon_t;\ N_t = C_{12}\varepsilon_s + C_{22}\varepsilon_t;\ N_{st} = C_{66}\varepsilon_{st} + 2k(t)D_{66}\kappa_{st};\\
&N_{ts} = C_{66}\varepsilon_{ts};\ M_s = K_{11}\kappa_s + K_{12}\kappa_t;\ M_t = K_{12}\kappa_s + K_{12}\kappa_t;\\
&M_{ts} = M_{st} = 2D_{66}\kappa_{ts};\ Q_t = K_2\gamma_t;\ Q_s = K_1\gamma_s\,,
\end{aligned} \tag{16}$$

where the stiffness characteristics of the shell reduced to the coordinate surface are

$$C_{ij} = B_{11}h;\ D_{ij} = B_{ij}h^3/12;\ K_1 = \frac{5}{6}hG_{13};$$
$$K_2 = \frac{5}{6}hG_{23};\ B_{11} = E_1/(1-\nu_1\nu_2);$$
$$B_{22} = E_2/(1-\nu_1\nu_2);\ B_{12} = \nu_2E_1/(1-\nu_1\nu_2) = \nu_1E_{21}/(1-\nu_1\nu_2);\ B_{66} = G_{12}. \tag{17}$$

we have: $E_1 = E_2 = E$; $G_{12} = G_{23} = G_{13} = G$; $\nu_1 = \nu_2 = \nu$.

Assume that all points of the shell undergo harmonic oscillations with circular frequency, i.e., the displacements and total rotation angles can be represtnted as follows (the sign "~" is omitted):

$$\{u(s,t,\tau),\ v(s,t,\tau),\ w(s,t,\tau),\ \psi_s(s,t,\tau),\ \psi_t(s,t,\tau)\} = \\ = \{u(s,t),\ v(s,t), w(s,t),\ \psi_s(s,t),\ \psi_t(s,t)\}\, e^{i\omega t} \tag{18}$$

Selecting the components of the displacement vector and total rotation angles as unknown functions, we can write the governing system of equations as

$$\begin{aligned}
\frac{\partial^2 u}{\partial t^2} =& a_{11}\frac{\partial^2 u}{\partial s^2} + a_{12}\frac{\partial^2 v}{\partial s\partial t} + a_{13}\frac{\partial u}{\partial s} + a_{14}\frac{\partial v}{\partial s} + a_{15}\frac{\partial w}{\partial s} + a_{16}\frac{\partial w}{\partial t} + a_{17}\frac{\partial v}{\partial t} + a_{18}w + a_{19}\omega^2 u;\\
\frac{\partial^2 v}{\partial t^2} =& a_{21}\frac{\partial^2 u}{\partial s\partial t} + a_{22}v + a_{23}\frac{\partial^2 v}{\partial s^2} + a_{24}w + a_{25}\frac{\partial w}{\partial t} + a_{26}\frac{\partial^2 \psi_s}{\partial s\partial t} + a_{27}\psi_t + a_{28}\frac{\partial^2 \psi_t}{\partial s^2} +\\
&+ a_{29}\frac{\partial \psi_t}{\partial s} + a_{2,10}\frac{\partial u}{\partial s} + a_{2,11}\frac{\partial v}{\partial t} + a_{2,12}\frac{\partial u}{\partial t} + a_{2,13}\frac{\partial v}{\partial s} + a_{2,14}\frac{\partial \psi_s}{\partial t} + a_{2,15}\omega^2 v\\
\frac{\partial^2 w}{\partial t^2} =& a_{31}\frac{\partial u}{\partial s} + a_{32}v + a_{33}\frac{\partial v}{\partial t} + a_{34}w + a_{35}\frac{\partial^2 w}{\partial s^2} + a_{36}\frac{\partial \psi_s}{\partial s} + a_{37}\frac{\partial \psi_t}{\partial t} +\\
&+ a_{38}\psi_t + a_{39}\psi_s + a_{3,10}\frac{\partial w}{\partial s} + a_{3,11}\frac{\partial w}{\partial t} + a_{3,12}\omega^2 w;\\
\frac{\partial^2 \psi_s}{\partial t^2} =& a_{41}\frac{\partial u}{\partial t} + a_{42}\frac{\partial^2 u}{\partial s^2} + a_{43}\frac{\partial^2 v}{\partial s\partial t} + a_{44}\frac{\partial w}{\partial s} + a_{45}\Psi_s +\\
&+ a_{46}\frac{\partial^2 \psi_s}{\partial s^2} + a_{47}\frac{\partial^2 \psi_t}{\partial s\partial t} + a_{48}\frac{\partial \psi_t}{\partial s} + a_{49}\frac{\partial u}{\partial s} + a_{4,10}\frac{\partial v}{\partial t} + a_{4,11}w + a_{4,12}\frac{\partial v}{\partial s} + a_{4,13}\frac{\partial \psi_s}{\partial s} + a_{4,14}\frac{\partial \psi_t}{\partial t} +\\
&+ b_{4,15}\frac{\partial \psi_s}{\partial t} + a_{4,16}\omega^2 u + a_{4,17}\omega^2\psi_s;\\
\frac{\partial^2 \psi_t}{\partial t^2} =& a_{51}\frac{\partial^2 u}{\partial s\partial t} + a_{52}v + a_{53}\frac{\partial v}{\partial t} + a_{54}\frac{\partial^2 v}{\partial s^2} + a_{55}w + a_{56}\frac{\partial w}{\partial t} + a_{57}\frac{\partial^2 \psi_s}{\partial s\partial t} +\\
&+ a_{58}\psi_t + a_{59}\frac{\partial^2 \psi_t}{\partial s^2} + a_{5,10}\frac{\partial \psi_t}{\partial t} + a_{5,11}\frac{\partial u}{\partial s} + a_{5,12}\frac{\partial u}{\partial t} + a_{5,13}\frac{\partial v}{\partial s} + a_{5,14}\frac{\partial \psi_s}{\partial t} +\\
&+ a_{5,15}\frac{\partial \psi_t}{\partial s} + +a_{5,16}\frac{\partial \psi_s}{\partial s} + a_{5,17}v + a_{5,18}\psi_t,
\end{aligned} \tag{19}$$

where

$$a_{11}=-\frac{C_{11}}{C_{66}};\ a_{12}=-\frac{C_{12}+C_{66}}{C_{66}};\ a_{13}=-k(t)\frac{C_{12}}{C_{66}};\ a_{14}=-\frac{1}{C_{66}}\frac{\partial C_{66}}{\partial t};$$
$$a_{15}=-\frac{1}{C_{66}}\frac{\partial C_{11}}{\partial s};\ a_{16}=-\frac{1}{C_{66}}\frac{\partial C_{12}}{\partial s};\ a_{17}=-\frac{k(t)}{C_{66}}\frac{\partial C_{12}}{\partial s};\ a_{18}=a_{14};$$
$$a_{19}=-\frac{1}{C_{66}};\ a_{22}=\frac{k^2(t)K_2}{C_{22}};\ a_{23}=-\frac{C_{66}}{C_{22}};\ a_{21}=-\frac{C_{12}+C_{66}-k^2(t)D_{66}}{C_{22}};$$
$$a_{24}=-k'(t)-\frac{k(t)}{C_{22}}\frac{\partial C_{22}}{\partial t};\ a_{25}=-k(t)\frac{C_{22}+K_2}{C_{22}};\ a_{26}=-\frac{k(t)D_{66}}{C_{22}};$$
$$a_{27}=-\frac{k(t)K_2}{C_{22}};\ a_{28}=a_{26};\ a_{29}=-\frac{k(t)}{C_{22}}\frac{\partial D_{66}}{\partial s};\ a_{2,10}=-\frac{1}{C_{22}}\frac{\partial C_{12}}{\partial t};$$
$$a_{2,11}=-\frac{1}{C_{22}}\frac{\partial C_{22}}{\partial t};\ a_{2,12}=-\frac{1}{C_{22}}\Big(\frac{\partial C_{66}}{\partial s}-k^2(t)\frac{\partial D_{66}}{\partial s}\Big);\ a_{2,13}=-\frac{1}{C_{22}}\frac{\partial C_{66}}{\partial s};$$
$$a_{2,14}=a_{29};\ a_{2,15}=-\frac{h\rho}{C_{22}};\ a_{31}=\frac{k(t)C_{12}}{K_2};\ a_{32}=k'(t)+\frac{k(t)}{K_2}\frac{\partial K_2}{\partial t};$$
$$a_{33}=k(t)\frac{K_2+C_{22}}{K_2};\ a_{34}=\frac{k^2(t)C_{22}}{K_2};\ a_{35}=-\frac{K_1}{K_2};\ a_{36}=a_{35};\ a_{37}=-1$$
$$a_{38}=-\frac{1}{K_2}\frac{\partial K_2}{\partial t};\ a_{39}=-\frac{1}{K_2}\frac{\partial K_1}{\partial s};\ a_{3,10}=a_{39};\ a_{3,11}=a_{38};\ a_{3,12}=-\frac{h\rho}{K_2};$$
$$a_{41}=k'(t)-\frac{k(t)}{C_{66}}\frac{\partial C_{66}}{\partial t}+\frac{k(t)}{D_{66}}\frac{\partial D_{66}}{\partial t};\ a_{42}=-k(t)\frac{C_{11}}{C_{66}};\ a_{45}=\frac{K_1}{D_{66}};\ a_{46}=-\frac{D_{11}}{D_{66}};$$
$$a_{43}=k(t)\frac{D_{12}C_{66}-C_{12}D_{66}-C_{66}D_{66}}{C_{66}D_{66}};\ a_{44}=\frac{k^2(t)(D_{12}C_{66}-C_{12}D_{66})+K_1C_{66}}{C_{66}D_{66}};$$
$$a_{47}=-\frac{D_{12}+D_{66}}{D_{66}};\ a_{48}=-\frac{1}{D_{66}}\frac{\partial D_{66}}{\partial t};\ a_{49}=-\frac{k(t)}{C_{66}}\frac{\partial C_{11}}{\partial s};\ a_{4,12}=-\frac{k(t)}{C_{66}}\frac{\partial C_{66}}{\partial t};$$
$$a_{4,10}=\frac{k(t)}{D_{66}}\frac{\partial D_{12}}{\partial s}-\frac{k(t)}{C_{66}}\frac{\partial C_{12}}{\partial s};\ a_{4,11}=\frac{k^2(t)}{D_{66}}\frac{\partial D_{12}}{\partial s}-\frac{k^2(t)}{C_{66}}\frac{\partial C_{12}}{\partial s};\ a_{4,13}=-\frac{1}{D_{66}}\frac{\partial D_{11}}{\partial s};$$
$$a_{4,14}=-\frac{1}{D_{66}}\frac{\partial D_{12}}{\partial s};\ a_{4,15}=a_{48};\ a_{4,16}=-\frac{k(t)h\rho}{C_{66}};\ a_{4,17}=-\frac{k^2(t)h^3\rho}{12D_{66}};$$
$$a_{58}=a_{56};\ a_{51}=k(t)\frac{D_{66}C_{22}-C_{12}D_{22}-C_{66}D_{22}+k^2(t)D_{66}D_{22}}{C_{22}D_{22}};$$
$$a_{52}=k(t)K_2\frac{k^2(t)D_{22}-C_{22}}{C_{22}D_{22}};\ a_{55}=k(t)k'(t)-\frac{k^2(t)}{C_{22}}\frac{\partial C_{22}}{\partial t}+\frac{k^2(t)}{D_{22}}\frac{\partial D_{22}}{\partial t};$$
$$a_{56}=K_2\frac{C_{22}-k^2(t)D_{22}}{C_{22}D_{22}};\ a_{57}=-\frac{k^2(t)D_{22}D_{66}+C_{22}D_{12}+C_{22}D_{66}}{C_{22}D_{22}}$$
$$a_{59}=-\frac{D_{66}(k^2(t)D_{22}+C_{22})}{C_{22}D_{22}};\ a_{5,10}=-\frac{1}{D_{22}}\frac{\partial D_{22}}{\partial t};$$
$$a_{5,11}=-\frac{k(t)}{C_{22}}\frac{\partial C_{12}}{\partial t};\ a_{5,12}=\frac{k^3(t)}{C_{22}}\frac{\partial D_{66}}{\partial s}-\frac{k(t)}{C_{22}}\frac{\partial C_{66}}{\partial s}+\frac{k(t)}{D_{22}}\frac{\partial D_{66}}{\partial s};$$
$$a_{5,13}=-\frac{k(t)}{C_{22}}\frac{\partial C_{66}}{\partial s};\ a_{5,15}=a_{5,14};\ a_{5,14}=-\frac{k^2(t)}{C_{22}}\frac{\partial D_{66}}{\partial s}-\frac{1}{D_{22}}\frac{\partial D_{66}}{\partial s};$$
$$a_{5,16}=-\frac{1}{D_{22}}\frac{\partial D_{12}}{\partial t};\ a_{5,17}=-\frac{k(t)h\rho}{C_{22}};\ a_{5,18}=-\frac{k^2(t)h^3\rho}{12D_{22}}.$$

Let us consider the following boundary conditions on the curvilinear boundaries $s=0$ and $s\ L$:

(i) the boundary is clamped: $u=v=w=0;\ \psi_i=\psi_e=0$
(ii) the boundary is hinged and free along the generatrix: $\partial u\big/\partial s=0;\ v=w=0;$ $\partial\psi_s/\partial s=0;\ \psi_t=0.$

If the shell is open, then the boundaries t_1, t_2 are either clamped ($u=v=w=0;$ $\psi_s=\psi_t=0$) or hinged ($\partial u/\partial t=0;\ v=0;\ \partial w/\partial t=0;\ \partial\psi_s/\partial t=0;\ \psi_t=0$).

If the shell is closed, then the following symmetry conditions on the straight boundaries $t_1=0$ and $t_2=T/2$ (T is the shell length) are $\partial u/\partial t=0;\ v=0;$ $\partial w/\partial t=0;\ \partial\psi_s/\partial t=0;\ \psi_t=0.$

Thus, Eqs. (9) with appropriate boundary conditions on the boundaries $z=0, z=L,$ and t_1, t_2 constitute a two-dimensional boundary-value eigenvalue problem.

3.2 Problem-Solving Technique

If the mid-surface of a shell is cylindrical, then it is convenient to write the equation of the cylinder directrix parametrically: $x = f_1(\theta)$, $y = f_2(\theta)$ or in a polar coordinates: $r = r(\theta)$, where θ is a parameter. Then, the arc element of the directrix is $dt = n(\theta)\,d\theta$, where $n(\theta) = \sqrt{(x'(\theta))^2 + (y'(\theta))^2}$ in the case of the rectangular coordinate system and $n(\theta) = \sqrt{r^2 + r'^2}$ in the case of the polar coordinate system. Derivatives along directrix arc are defined in terms of derivatives with respect to θ

$$\frac{\partial}{\partial t} = \frac{1}{n}\frac{\partial}{\partial \theta};\quad \frac{\partial^2}{\partial t^2} = \frac{1}{n^2}\frac{\partial^2}{\partial \theta^2} - \frac{n'}{n^3}\frac{\partial}{\partial \theta}. \tag{20}$$

With (10), Eqs. (9) become:

$$\begin{aligned}
&\frac{\partial^2 u}{\partial \theta^2} = b_{11}\frac{\partial^2 u}{\partial s^2} + b_{12}\frac{\partial^2 v}{\partial s\partial \theta} + b_{13}\frac{\partial u}{\partial s} + b_{14}\frac{\partial v}{\partial s} + b_{15}\frac{\partial w}{\partial s} + b_{16}\frac{\partial w}{\partial \theta} + b_{17}\frac{\partial v}{\partial \theta} + b_{18}w + b_{19}\omega^2 u;\\
&\frac{\partial^2 v}{\partial \theta^2} = b_{21}\frac{\partial^2 u}{\partial s\partial \theta} + b_{22}v + b_{23}\frac{\partial^2 v}{\partial s^2} + b_{24}w + b_{25}\frac{\partial w}{\partial \theta} + b_{26}\frac{\partial^2 \psi_s}{\partial s\partial \theta} + b_{27}\psi_\theta + b_{28}\frac{\partial^2 \psi_t}{\partial s^2} +\\
&\quad + b_{29}\frac{\partial \psi_t}{\partial s} + b_{2,10}\frac{\partial u}{\partial s} + b_{2,11}\frac{\partial v}{\partial \theta} + b_{2,12}\frac{\partial u}{\partial \theta} + b_{2,13}\frac{\partial v}{\partial s} + b_{2,14}\frac{\partial \psi_s}{\partial \theta} + b_{2,15}\omega^2 v;\\
&\frac{\partial^2 w}{\partial \theta^2} = b_{31}\frac{\partial u}{\partial s} + b_{32}v + b_{33}\frac{\partial v}{\partial \theta} + b_{34}w + b_{35}\frac{\partial^2 w}{\partial s^2} + b_{36}\frac{\partial \psi_s}{\partial s} + b_{37}\frac{\psi_t}{\partial \theta} + b_{38}\psi_t +\\
&\quad + b_{39}\psi_s + b_{3,10}\frac{\partial w}{\partial s} + b_{3,11}\frac{\partial w}{\partial \theta} + b_{3,12}\omega^2 w;\\
&\frac{\partial^2 \psi_s}{\partial \theta^2} = b_{41}\frac{\partial u}{\partial \theta} + b_{42}\frac{\partial^2 u}{\partial s^2} + b_{43}\frac{\partial^2 v}{\partial s\partial \theta} + b_{44}\frac{\partial w}{\partial s} + b_{45}\Psi_s + b_{46}\frac{\partial^2 \psi_s}{\partial s^2} +\\
&\quad + b_{47}\frac{\partial^2 \psi_t}{\partial s\partial \theta} + b_{48}\frac{\partial \psi_t}{\partial s} + b_{49}\frac{\partial u}{\partial s} + b_{4,10}\frac{\partial v}{\partial \theta} + b_{4,11}w + b_{4,12}\frac{\partial v}{\partial s} +\\
&\quad + b_{4,13}\frac{\partial \psi_s}{\partial s} + b_{4,14}\frac{\partial \psi_{t\theta}}{\partial \theta} + b_{4,15}\frac{\partial \psi_s}{\partial \theta} + b_{4,16}\omega^2 u + b_{4,17}\omega^2;\\
&\frac{\partial^2 \psi_t}{\partial \theta^2} = b_{51}\frac{\partial^2 u}{\partial s\partial \theta} + b_{52}v + b_{53}\frac{\partial v}{\partial \theta} + b_{54}\frac{\partial^2 v}{\partial s^2} + b_{55}w + b_{56}\frac{\partial w}{\partial \theta} + b_{57}\frac{\partial^2 \psi_s}{\partial s\partial \theta} +\\
&\quad + b_{58}\psi_t + a_{59}\frac{\partial^2 \psi_t}{\partial s^2} + b_{5,10}\frac{\partial \psi_t}{\partial \theta} + b_{5,11}\frac{\partial u}{\partial s} + b_{5,12}\frac{\partial u}{\partial \theta} + b_{5,13}\frac{\partial v}{\partial s} + b_{5,14}\frac{\partial \psi_s}{\partial \theta} +\\
&\quad + b_{5,14}\frac{\partial \psi_s}{\partial \theta} + b_{5,15}\frac{\partial \psi_t}{\partial s} + b_{5,16}\frac{\partial \psi_s}{\partial s} + b_{5,17}v + b_{5,18}\psi_t,
\end{aligned} \tag{21}$$

where

$$\begin{aligned}
&b_{11} = n^2(\theta)a_{11};\ b_{12} = n(\theta)a_{12};\ b_{13} = -n^2(\theta)k(\theta)\tfrac{C_{12}}{C_{66}};\ b_{14} = -\tfrac{n(\theta)}{C_{66}}\tfrac{\partial C_{66}}{\partial \theta};\\
&b_{16} = n(\theta)a_{16};\ b_{17} = -\tfrac{n^2(\theta)k(\theta)}{C_{66}}\tfrac{\partial C_{12}}{\partial s};\ b_{18} = -\tfrac{n'(\theta)}{n(\theta)} - \tfrac{1}{C_{66}}\tfrac{\partial C_{66}}{\partial \theta};\\
&b_{19} = n^2(\theta)a_{19};\ b_{21} = -n(\theta)\tfrac{C_{12}+C_{66}-k^2(\theta)D_{66}}{C_{22}};\ b_{22} = \tfrac{n^2(\theta)k^2(\theta)K_2}{C_{22}};\\
&b_{23} = n^2(\theta)a_{23};\ b_{24} = -n(\theta)k'(\theta) - \tfrac{n(\theta)k(\theta)}{C_{22}}\tfrac{\partial C_{22}}{\partial \theta};\ b_{25} = -n(\theta)k(\theta)\tfrac{C_{22}+K_2}{C_{22}};\\
&b_{26} = -\tfrac{n(\theta)k(\theta)D_{66}}{C_{22}};\ b_{27} = -\tfrac{n^2(\theta)k(\theta)K_2}{C_{22}};\ b_{28} = n^2(\theta)a_{28};\\
&b_{29} = -\tfrac{n^2(\theta)k(\theta)}{C_{22}}\tfrac{\partial D_{66}}{\partial s};\ b_{2,10} = -\tfrac{n(\theta)}{C_{22}}\tfrac{\partial C_{12}}{\partial \theta};\ b_{2,11} = \tfrac{n'(\theta)}{n(\theta)} - \tfrac{1}{C_{22}}\tfrac{\partial C_{22}}{\partial \theta};\\
&b_{2,12} = -\tfrac{n(\theta)}{C_{22}}\Big(\tfrac{\partial C_{66}}{\partial s} - k^2(\theta)\tfrac{\partial D_{66}}{\partial s}\Big);\ b_{2,13} = n^2(\theta)a_{2,13};\\
&b_{2,14} = n^2(\theta)a_{2,14};\ b_{2,15} = n^2(\theta)a_{2,15};\ b_{31} = \tfrac{n^2(\theta)k(\theta)C_{12}}{K_2};\\
&b_{32} = n(\theta)k'(\theta) + n(\theta)\tfrac{k(\theta)}{K_2}\tfrac{\partial K_2}{\partial \theta};\ b_{33} = n(\theta)k(\theta)\tfrac{K_2+C_{22}}{K_2};\\
&b_{34} = \tfrac{n^2(\theta)k^2(\theta)C_{22}}{K_2};\ b_{35} = n^2 a_{35};\ b_{36} = b_{35};\ b_{37} = -n(\theta);\\
&b_{38} = -n(\theta)\tfrac{1}{K_2}\tfrac{\partial K_2}{\partial \theta};\ b_{39} = n^2(\theta)a_{39};\ b_{3,10} = b_{39};
\end{aligned}$$

$$b_{3,11}=\frac{n'(\theta)}{n(\theta)}-\frac{1}{K_2}\frac{\partial K_2}{\partial\theta};\ b_{3,12}=n^2(\theta)a_{3,12};$$
$$b_{42}=-n^2(\theta)k(\theta)\frac{C_{11}}{C_{66}};\ b_{41}=k'(\theta)-\frac{k(\theta)}{C_{66}}\frac{\partial C_{66}}{\partial\theta}+\frac{k(\theta)}{D_{66}}\frac{\partial D_{66}}{\partial\theta};$$
$$b_{43}=n(\theta)k(\theta)\frac{D_{12}C_{66}-C_{12}D_{66}-C_{66}D_{66}}{C_{66}D_{66}};$$
$$b_{44}=n^2(\theta)\frac{k^2(\theta)(D_{12}C_{66}-C_{12}D_{66})+K_1C_{66}}{C_{66}D_{66}};\ b_{45}=n^2(\theta)a_{45};$$
$$b_{46}=n^2(\theta)a_{46};\ b_{47}=n(\theta)a_{47};\ b_{48}=-\frac{n(\theta)}{D_{66}}\frac{\partial D_{66}}{\partial\theta};$$
$$b_{49}=-\frac{n^2(\theta)k(\theta)}{C_{66}}\frac{\partial C_{11}}{\partial s};\ b_{4,10}=\frac{n(\theta)k(\theta)}{D_{66}}\frac{\partial D_{12}}{\partial s}-\frac{n(\theta)k(\theta)}{C_{66}}\frac{\partial C_{12}}{\partial s};$$
$$b_{4,11}=\frac{n^2(\theta)k^2(\theta)}{D_{66}}\frac{\partial D_{12}}{\partial s}-\frac{n^2(\theta)k^2(\theta)}{C_{66}}\frac{\partial C_{12}}{\partial s};\ b_{4,12}=-\frac{n(\theta)k(\theta)}{C_{66}}\frac{\partial C_{66}}{\partial\theta};$$
$$b_{4,13}=n^2(\theta)a_{4,13};\ b_{4,14}=n(\theta)a_{4,14};\ b_{4,15}=-\frac{n(\theta)}{D_{66}}\frac{\partial D_{66}}{\partial\theta};$$
$$b_{4,16}=n^2(\theta)a_{4,16};\ a_{4,17}=-\frac{n^2(\theta)k^2(\theta)h^3\rho}{12D_{66}};$$
$$b_{51}=n(\theta)k(\theta)\frac{D_{66}C_{22}-C_{12}D_{22}-C_{66}D_{22}+k^2(\theta)D_{66}D_{22}}{C_{22}D_{22}};$$
$$b_{52}=n^2(\theta)k(\theta)K_2\frac{k^2(\theta)D_{22}-C_{22}}{C_{22}D_{22}};\ b_{53}=k'(\theta)-\frac{k(\theta)}{C_{22}}\frac{\partial C_{22}}{\partial\theta}+\frac{k(\theta)}{D_{22}}\frac{\partial D_{22}}{\partial\theta};$$
$$b_{54}=-n^2(\theta)k(\theta)\frac{C_{66}}{\gamma_{22}C_{22}};\ b_{55}=n(\theta)\left(k(\theta)k'(\theta)-\frac{k^2(\theta)}{C_{22}}\frac{\partial C_{22}}{\partial\theta}+\frac{k^2(\theta)}{D_{22}}\frac{\partial D_{22}}{\partial\theta}\right);$$
$$b_{56}=n(\theta)K_2\frac{C_{22}-k^2(\theta)D_{22}}{C_{22}D_{22}};\ b_{57}=-n(\theta)\frac{k^2(\theta)D_{22}D_{66}+C_{22}D_{12}+C_{22}D_{66}}{C_{22}D_{22}};$$
$$b_{58}=n^2(\theta)K_2\frac{C_{22}-k^2(\theta)D_{22}}{C_{22}D_{22}};\ b_{59}=-n^2(\theta)\frac{D_{66}(k^2(\theta)D_{22}+C_{22})}{C_{22}D_{22}};$$
$$b_{5,10}=\frac{n'(\theta)}{n(\theta)}-\frac{1}{D_{22}}\frac{\partial D_{22}}{\partial\theta};\ a_{5,11}=-n^2(\theta)\frac{k(\theta)}{C_{22}}\frac{\partial C_{12}}{\partial\theta};$$
$$b_{5,12}=n(\theta)\left(\frac{k^3(\theta)}{C_{22}}\frac{\partial D_{66}}{\partial s}-\frac{k(\theta)}{C_{22}}\frac{\partial C_{66}}{\partial s}+\frac{k(\theta)}{D_{22}}\frac{\partial D_{66}}{\partial s}\right);\ b_{5,13}=-n^2(\theta)\frac{k(\theta)}{C_{22}}\frac{\partial C_{66}}{\partial s};$$
$$b_{5,14}=-n(\theta)\left(\frac{k^2(\theta)}{C_{22}}\frac{\partial D_{66}}{\partial s}+\frac{1}{D_{22}}\frac{\partial D_{66}}{\partial s}\right);\ b_{5,15}=-n(\theta)\left(\frac{k^2(\theta)}{C_{22}}\frac{\partial D_{66}}{\partial s}+\frac{1}{D_{22}}\frac{\partial D_{66}}{\partial s}\right);$$
$$b_{5,16}=-\frac{n(\theta)}{D_{22}}\frac{\partial D_{12}}{\partial\theta};\ a_{5,17}=-\frac{n^2(\theta)k(t)h\rho}{C_{22}};\ a_{5,18}=-\frac{n^2(\theta)k^2(t)h^3\rho}{12D_{22}}.$$

Problem (21) with appropriate boundary conditions is solved with the spline-collocation method [7]. The unknown functions $u(s,\theta)$,$v(s,\theta)$, $w(s,\theta)$, $\psi_s(s,\theta)$, $\psi_t(s,\theta)$ are expressed as

$$u(s,\theta)=\sum_{i=0}^{N}u_i(\theta)\varphi_{1i}(s),\ v(s,\theta)=\sum_{i=0}^{N}v_i(\theta)\varphi_{2i}(s),\ w(s,\theta)=\sum_{i=0}^{N}w_i(\theta)\varphi_{3i}(s),$$
$$\psi_s(s,\theta)=\sum_{i=0}^{N}\psi_{si}(\theta)\varphi_{5i}(s),\ \psi_t(s,\theta)=\sum_{i=0}^{N}\psi_{ti}(\theta)\varphi_{4i}(s),\tag{22}$$

where $u_i(\theta)$, $v_i(\theta)$, $w_i(\theta)$, $\psi_{si}(\theta)$, $\psi_{ti}(\theta)$ are the required functions of the variable θ, $\varphi_{ji}(s)$ $(j=\overline{1,5};\ i=\overline{0,N})$ are linear combinations of B-splines over a uniform mesh Δ: $0=s_0<s_1<\cdots<s_N=L$ for the boundary conditions at $s=0$ and $s=L$. Since the governing system includes no higher than second-order derivatives of $u(s,\theta)$, $v(s,\theta)$, $w(s,\theta)$, $\psi_s(s,\theta)$, $\psi_t(s,\theta)$ with respect to the coordinate s, we can restrict the approximation to cubic splines. Substituting (22) into (21), we require them to be satisfied at the collocation points $\xi_k\in[0,\ L]$, $k\in\overline{0,N}$.

Let us introduce the following operation of multiplication of a matrix and a vector and of two vectors. Let $P=[p_{ij}]\,(i,\ j=\overline{0,N})$ and $\bar{c}=[c_0,\ c_1,\ldots,c_N]^T$. If $\bar{c}*P=[c_i\,p_{ij}]$. If $\bar{d}=[d_0,d_1,\ldots,d_N]^T$ then $\bar{c}*\bar{d}=[c_0d_0,c_1d_1,\ldots,c_Nd_N]^T$.

Denoting $\Phi_{j\alpha} = \left[\varphi_{ji}^{(\alpha)}(\xi_k)\right](i,\ k = \overline{0,\ N}),\ j = \overline{1,\ 5},\ \alpha = 0,\ 1,\ 2,$ $\bar{u} = [u_0,\ \ldots,\ u_N]^T,\ \bar{v} = [v_0, \ldots,\ v_N]^T,\ \bar{w} = [w_0, \ldots, w_N]^T,\ \bar{\psi}_s = [\psi_{s0}, \ldots, \psi_{sN}]^T,\ \bar{\psi}_t = [\psi_{t0}, \ldots,\ \psi_{tN}]^T,\ \bar{b}_{kl}^T = \{b_{kl}(\theta,\ \xi_0), \ldots,\ b_{kl}(\theta,\ \xi_N)\},\ k = \overline{1,\ 5};\ l = \overline{0,\ N}$ (the collocation points are selected so that the matrices Φ_{j0} are nondegenerated) and constructing the inverse matrices Φ_{j0}^{-1}), we arrive at the following system of differential equations of the second order that describes the free vibrations of a noncircular homogeneous cylindrical shell:

$$
\begin{aligned}
&\bar{u}'' = \Phi_{10}^{-1}(\bar{b}_{11} * \Phi_{12} + \bar{b}_{15} * \Phi_{11} + \rho\omega^2\bar{b}_{19} * \Phi_{10})\bar{u} + \Phi_{10}^{-1}(\bar{b}_{18} * \Phi_{10})\bar{u}' + \\
&\quad + \Phi_{10}^{-1}(\bar{b}_{14} * \Phi_{21})\bar{v} + \Phi_{10}^{-1}(\bar{b}_{12} * \Phi_{21} + \bar{b}_{16} * \Phi_{20})\bar{v}' + \Phi_{10}^{-1}(\bar{b}_{13} * \Phi_{31} + \bar{b}_{17} * \Phi_{30})\bar{w}\,, \\
&\bar{v}'' = \Phi_{20}^{-1}(\bar{b}_{2,10} * \Phi_{11})\bar{u} + \Phi_{20}^{-1}(\bar{b}_{21} * \Phi_{11} + \bar{b}_{2,12} * \Phi_{10})\bar{u}' + \\
&\quad + \Phi_{20}^{-1}(\bar{b}_{22} * \Phi_{20} + \bar{b}_{23} * \Phi_{22} + \bar{b}_{2,13} * \Phi_{21} + \rho\omega^2\bar{b}_{2,15} * \Phi_{20})\bar{v} + \\
&\quad + \Phi_{20}^{-1}(\bar{b}_{2,11} * \Phi_{20})\bar{v}' + \Phi_{20}^{-1}(\bar{b}_{24} * \Phi_{30})\bar{w} + \Phi_{20}^{-1}(\bar{b}_{25} * \Phi_{30})\bar{w}' + \\
&\quad + \Phi_{20}^{-1}(\bar{b}_{25} * \Phi_{41} + \bar{b}_{2,14} * \Phi_{40})\bar{\psi}_s' + \Phi_{20}^{-1}(\bar{b}_{27} * \Phi_{50} + \bar{b}_{28} * \Phi_{52} + \bar{b}_{29} * \Phi_{51})\bar{\psi}_t; \\
&\bar{w}'' = \Phi_{30}^{-1}(\bar{b}_{31} * \Phi_{11})\bar{u} + \Phi_{30}^{-1}(\bar{b}_{32} * \Phi_{20})\bar{v} + \Phi_{30}^{-1}(\bar{b}_{33} * \Phi_{20})\bar{v}' + \\
&\quad + \Phi_{30}^{-1}(\bar{b}_{34} * \Phi_{30} + \bar{b}_{35} * \Phi_{32} + \bar{b}_{3,10} * \Phi_{31} + \rho\omega^2\bar{b}_{3,12} * \Phi_{30})\bar{w} + \Phi_{30}^{-1}(\bar{b}_{3,11} * \Phi_{30})\bar{w}' + \\
&\quad + \Phi_{30}^{-1}\left(\bar{b}_{36} * \Phi_{41} + \bar{b}_{39} * \Phi_{40}\right)\bar{\psi}_x + \Phi_{30}^{-1}\left(\bar{b}_{38} * \Phi_{50}\right)\bar{\psi}_t + \Phi_{30}^{-1}\left(\bar{b}_{37} * \Phi_{50}\right)\bar{\psi}_t'; \\
&\bar{\psi}_s'' = \Phi_{40}^{-1}(\bar{b}_{42} * \Phi_{12} + \bar{b}_{49} * \Phi_{11} + \rho\omega^2\bar{b}_{4,16} * \Phi_{10})\bar{u} + \Phi_{40}^{-1}(\bar{b}_{41} * \Phi_{10})\bar{u}' + \\
&\quad + \Phi_{40}^{-1}(\bar{b}_{4,12} * \Phi_{21})\bar{v} + \Phi_{40}^{-1}(\bar{b}_{43} * \Phi_{21} + \bar{b}_{4,10} * \Phi_{20})\bar{v}' + \\
&\quad + \Phi_{40}^{-1}(\bar{b}_{44} * \Phi_{31} + \bar{b}_{4,11} * \Phi_{30})\bar{w} + \Phi_{40}^{-1}(\bar{b}_{45} * \Phi_{40} + \bar{b}_{46} * \Phi_{42} + \bar{b}_{4,13} * \Phi_{41} + \\
&\quad + \rho\omega^2\bar{b}_{4,17} * \Phi_{40})\bar{\psi}_s + \Phi_{40}^{-1}(\bar{b}_{4,15} * \Phi_{40})\bar{\psi}_s' + \\
&\quad + \Phi_{40}^{-1}(\bar{b}_{48} * \Phi_{51})\bar{\psi}_t + \Phi_{40}^{-1}(\bar{b}_{47} * \Phi_{51} + \bar{b}_{4,14} * \Phi_{50})\bar{\psi}_t'; \\
&\bar{\psi}_t'' = \Phi_{50}^{-1}(\bar{b}_{5,11} * \Phi_{11})\bar{u} + \Phi_{50}^{-1}(\bar{b}_{51} * \Phi_{11} + \bar{b}_{5,12} * \Phi_{10})\ \bar{u}' + \Phi_{50}^{-1}(\bar{b}_{52} * \Phi_{20} + \\
&\quad + \bar{b}_{5,13} * \Phi_{21} + \bar{b}_{54} * \Phi_{22} + \rho\omega^2\bar{b}_{5,17} * \Phi_{20})\bar{v} + \\
&\quad + \Phi_{50}^{-1}(\bar{b}_{53} * \Phi_{20})\bar{v}' + \Phi_{50}^{-1}(\bar{b}_{55} * \Phi_{30})w + \Phi_{50}^{-1}(\bar{b}_{56} * \Phi_{30})\bar{w}' + \\
&\quad + \Phi_{50}^{-1}(\bar{b}_{5,16} * \Phi_{41})\bar{\psi}_s + \Phi_{50}^{-1}(\bar{b}_{57} * \Phi_{41} + \bar{b}_{5,14} * \Phi_{40})\bar{\psi}_s' + \\
&\quad + \Phi_{50}^{-1}(\bar{b}_{58} * \Phi_{50} + \bar{b}_{59} * \Phi_{52} + \bar{b}_{5,15} * \Phi_{51} + \rho\omega^2\bar{b}_{5,18} * \Phi_{50})\bar{\psi}_t + \Phi_{50}^{-1}(\bar{b}_{5,10} * \Phi_{50})\bar{\psi}_t'.
\end{aligned}
\tag{23}
$$

Let us represent system (13) as

$$
\frac{d\bar{Y}}{ds} = A(s, \omega)\,\bar{Y} \quad (0 \le s \le L)\,, \tag{24}
$$

where $A(s, \omega)$ is a square $10(N + 1) \times 10(N + 1)$ matrix. The boundary conditions at $s = 0$ and $s = L$ for this system are

$$
B_1\bar{Y}(\theta_1) = \bar{0};\ \ B_2\bar{Y}(\theta_2) = \bar{0}\,, \tag{25}
$$

where B_1 and B_2 are rectangular $5(N + 1) \times 10(N + 1)$ matrices.

Here $u' = \partial u/\partial s$; $v' = \partial v/\partial s$; $w' = \partial w/\partial s$; $\psi_s' = \partial\psi_s/\partial s$; $\psi_t' = \partial\psi_t/\partial s$;

$$
\begin{aligned}
&\bar{Y} = \{\bar{u},\ \bar{u}',\ \bar{v},\ \bar{v}',\ \bar{w},\ \bar{w}',\ \bar{\psi}_s,\ \bar{\psi}_s',\ \bar{\psi}_t,\ \bar{\psi}_t'\}^T;\ \bar{u} = \{u_0,\ u_1, \ldots,\ u_N\} \\
&\bar{u}' = \left\{u_0',\ u_1', \ldots,\ u_N'\right\};\ \bar{v} = \{v_0,\ v_1, \ldots,\ v_N\};\ \bar{v}' = \left\{v_0',\ v_1', \ldots,\ v_N'\right\}; \\
&\bar{w} = \{w_0,\ w_1, \ldots,\ w_N\};\ \bar{w}' = \left\{w_0',\ w_1', \ldots, w_N'\right\};\ \bar{\psi}_s = \{\psi_{s0}, \psi_{s1}, \ldots,\ \psi_{sN}\}; \\
&\bar{\psi}_s' = \left\{\psi_{s0}',\ \psi_{s1}', \ldots,\ \psi_{sN}'\right\};\ \bar{\psi}_t = \left\{\psi_{t0}, \psi_{t1,} \ldots, \psi_{tN}\right\};\ \bar{\psi}_t' = \left\{\psi_{t0}',\ \psi_{t1}', \ldots, \psi_{tN}'\right\}.
\end{aligned}
$$

To solve the boundary eigenvalue problem (24), (25), we used the discrete-orthogonalization and incremental search methods [9].

3.3 Analysis of the Numerical Results

Let us study how variations in elliptic cross-section of a closed noncircular cylindrical shell affect its natural frequencies in the case where its weight remains constant. Let the shell of length $L = 20l_0$ be made of an isotropic material with Poisson's ratio $\nu = 0,3$. The radius of the corresponding circular cylindrical shell whose weight is equal to that of the noncircular cylindrical shell is $R = 10\,l_0$. The ellipse eccentricity Δ is chosen to be 0, 0.1, 0.2, 0.3, 0.4. The ellipse semi-axes are defined by $a = R(1-\Delta)/f$, $b = R(1+\Delta)/f$, where $f = 1 + \frac{\Delta^2}{4} + \frac{\Delta^4}{64} + \frac{\Delta^6}{256}$.

Let us consider hinged (S–S) and clamped (C–C) boundary conditions. The shell is circumferentially symmetric. The first three natural frequencies $\Omega_i = 2\omega_i l_0\sqrt{\rho/G}$ versus the ellipse eccentricity for different boundary conditions are shown in Fig. 6 (hinged ends) and Fig. 7 (clamped ends).

It can be seen that the frequencies of elliptical cylindrical shells with different cross-sectional aspect ratios differ insignificantly. Moreover, the first and second frequencies decrease with increasing eccentricity for all boundary conditions, while

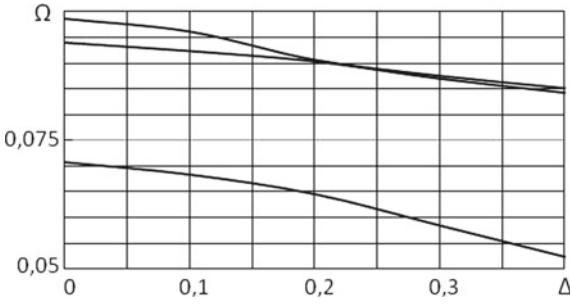

Fig. 6 First three natural frequencies (hinged ends)

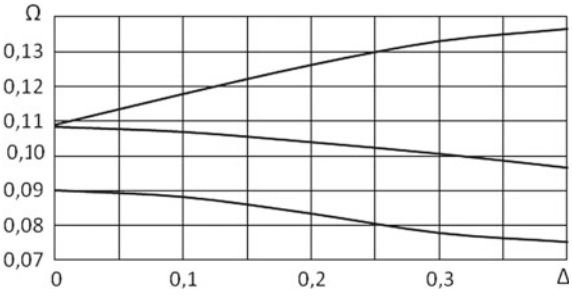

Fig. 7 First three natural frequencies (clamped ends)

the behavior of the third frequency depends on the boundary conditions: it increases if the ends are clamped and decreases if the ends are hinged.

We studied the spectrum of natural frequencies of a closed noncircular cylindrical isotropic shell of variable thickness with length $L = 20l_0$ and Poisson's ratio $\nu = 0, 3$. The radius of the corresponding circular cylindrical shell with weight equal to that of the noncircular cylindrical shell is $R = 10\,l_0$. The ellipse eccentricity $\Delta = 0.1$. The thickness of the noncircular cylindrical shell varies as $H = H_0(1 + \alpha \cos p\theta)$ while its weight remains unchanged, for $p = 2k, k \in N$, $\alpha = 0;\ 0.1;\ 0.2;\ 0.3$ Figure 8a, b, c.

Show the variation in the thickness of the circular shell ($\Delta = 0$) in the circumferential direction at $\alpha = 0.3$ with the parameter p (p =2; 4; 6; 8, respectively) (see Fig. 4).

We also studied the influence of the parameter for $p = 2$, 4, 6 on the natural frequencies of a closed noncircular cylindrical shell symmetric in the circumferential direction and clamped in the longitudinal direction.

Table 2 summarizes the results calculated for the first three values of $\Omega_i = 2\omega_i l_0\sqrt{\rho/G}$ (i is the frequency number) for a closed noncircular cylindrical isotropic shell of variable thickness depending on the parameters p and α.

With increase in for $p = 2$, 4, the first frequency increases by 0.6% and 1.2%, respectively, the second frequency decreases by 3.2 and 6.4%, and the third frequency

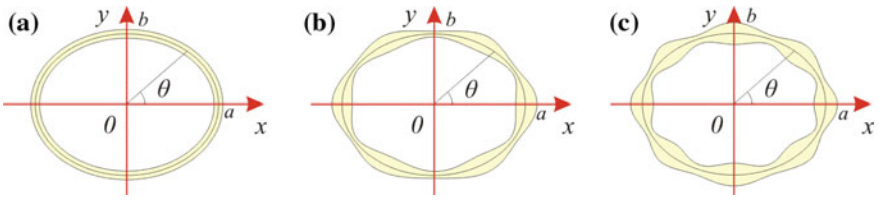

Fig. 8 Cross-section of ellipticall cylinders with different thickness

Table 2 First three natural frequencies closed noncircular isotropic cylindrical shell of variable thickness

p	Ω	$\alpha = 0$	$\alpha = 0.1$	$\alpha = 0.2$	$\alpha = 0.3$
$p = 2$	Ω_1	0.0874	0.0875	0.0877	0.0882
	Ω_2	0.1068	0.1056	0.1044	0.1033
	Ω_3	0.1074	0.1058	0.1051	0.1044
$p = 4$	Ω_1	0.0874	0.0881	0.0885	0.0986
	Ω_2	0.1068	0.1050	0.1026	0.1002
	Ω_3	0.1074	0.1089	0.1089	0.1089
$p = 6$	Ω_1	0.0874	0.0873	0.0872	0.0871
	Ω_2	0.1068	0.1070	0.1071	0.1068
	Ω_3	0.1074	0.1084	0.1080	0.1076

decreases slightly (by up to 1%). At $p = 6$, all the three frequencies decrease with increase in compared with the respective frequencies of constant-thickness shells. The second frequencies undergo maximum changes (up to 7.5%). The parameter p also affects the natural frequency spectrum variable-thickness shells.

The technique proposed makes it possible to determine the natural frequencies of open orthotropic cylindrical shells of circumferentially variable thickness.

We analyzed the behavior of the first frequencies of open orthotropic shells with elliptic cross-section ($\Delta = 0.1$) made of composites. The composite is BM-1 fiberglass plastics with different volume fractions (5:1, 2:1, 1:1) of orthogonally laid up unidirectional layers whose elastic characteristics are presented in Table 3. The boundaries $s = 0$ and $s = L$ of the shell are clamped, and $u = v = w = 0$; $\Psi s = \Psi t = 0$. for $\theta = 0$ and $\theta = \pi$.

The shell thickness varies as

$$H(\theta) = H_0\left(1 + \alpha\left(6\frac{\theta^2}{\pi^2} - 6\frac{\theta}{\pi} + 1\right)\right);\ H_0 = 2l_0.$$

Note that the weight of the shell does not change with variation in the parameter.

The first values of $\Omega_i = 2\omega_i l_0\sqrt{\rho/G_0}$ ($G_0 = 1$ MPa) for different values of are summarized in Table 3 for different orthotropic materials (C1–C3).

Figure 9 shows the values of the first natural frequencies of an open variable-thickness orthotropic cylindrical shells with elliptic cross-section ($\Delta = 0.1$) as functions of the parameter α. The shell thickness varies quadratically.

As follows from Fig. 9, the first three natural frequencies of the shell made of C1 material are the most strongly dependent on the variable thickness. The effect of the α for shells made of this material is 1% (this effect is hardly noticeable for the C2 material and is less than 1% for the C3 material) compared with constant-thickness shells made of the same materials. Therefore, shells made of C1 material should be studied in future.

Table 3 Elastic characteristics of composite materials

Elastic parameters	Fiber fraction		
	C1	C2	C3
	5:1	2:1	1:1
ν_{ts}	0.149	0.105	0.123
ν_{st}	0.0648	0.077	0.110
E_s (10^4 MPa)	4.76	3.68	3.09
E_t (10^4 MPa)	2.07	2.68	2.74
G_{st} (10^4 MPa)	0.531	0.505	0.396
$G_{s\gamma}$ (10^4 MPa)	0.501	0.447	0.366
$G_{\gamma s}$ (10^4 MPa)	0.434	0.414	0.369

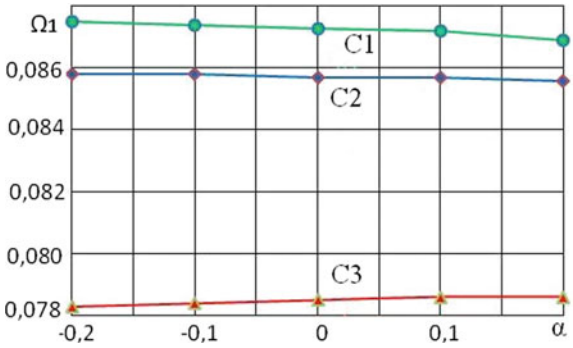

Fig. 9 First three natural frequencies open noncircular orthotropic cylindrical shell of variable thickness

4 Complete Systems Method in Static Problems for Thin-Walled Shells

The ideological fundamentals of the complete systems method (CSM) for solving linear N-dimensional ($N \geq 2$) boundary-value problems of a general form have been outlined in the works [2, 17]. This method has been applied and developed in scalar problems of the heat-mass transfer theory [17], biharmonic problems of the plate theory [3], vector problems of the elasticity theory [5, 6], in problems on free vibrations of anisotropic prismatic bodies, and in nonlinear problems of the shell theory [1, 4]. This method is known as the generalized Kantorovich [3] or Kantorovich-Vlasov method [1, 6] or as complete systems method (CSM) [2, 4, 5]. The present work considers principal ideas of the CSM using, as an example, static problems of shallow shells in variational formulation.

4.1 Problem Statement

Let us consider a shallow shell of the constant thickness h, whose mid-surface occupies the domain $S \cup \partial S = \{x, y : |x| \leq a, |y| \leq b\}$ in projections on the Cartesian coordinate system x, y and has curvatures k_x and k_y aligned with coordinate axes. Inside the domain S, the shell is subject to action of the vector of distributed loads $\bar{q} = \{q_x, q_y, q_n\}$, where the index n indicates the direction perpendicular to the mid-surface. Forces-moments, displacements or their combinations may be given at each point of the boundary ∂S. With this fact, any restrictions, except of their consistency, are not imposed upon conditions of the contour attachment. It is assumed that the shell is made of isotropic linearly elastic material.

The stress-strain state of the shell under the action of distributed loads and contour forces-moments is defined by stationary points of the total deformation

$$G(\bar{U}) = \Pi(\bar{U}) + V(\bar{U}) \tag{26}$$

for the given kinematic restrictions on the separate parts of the domain boundaries.

Here $\Pi(\bar{U}) = \frac{1}{2}\int\limits_S \left(D\bar{U}\right)^T E_0 C D\bar{U} ds$ and $V(\bar{U}) = -W = -\frac{1}{2}\int\limits_S \bar{U}^T \bar{q} ds -$

$$-\left\{\int\limits_{-b}^{b}\left(\tilde{T}_1^{\pm}u + \tilde{S}_1^{\pm}v + \tilde{M}_1^{\pm}w_{,x} + \tilde{Q}_1^{\pm}w\right)dy\right\}_{-a}^{a} - \left\{\int\limits_{-a}^{a}\left(\tilde{T}_2^{\pm}v + \tilde{S}_2^{\pm}u + \tilde{M}_2^{\pm}w_{,y} + \tilde{Q}_2^{\pm}w\right)dx\right\}_{-b}^{b}$$

are the internal deformation energy and potential of the external forces; $D^T = \begin{pmatrix} ()_{,x} & 0 & ()_{,y} & 0 & 0 & 0 \\ 0 & ()_{,y} & ()_{,x} & 0 & 0 & 0 \\ -k_x & -k_y & 0 & -()_{,xx} & -()_{,yy} & -()_{,xy} \end{pmatrix}$—is the matrix differential operator, which relates components of the deformation vector $\bar{\varepsilon} = \{\varepsilon_1, \varepsilon_2, \omega, \kappa_1, \kappa_2, \tau\}$ with components of the displacement vector $\bar{U} = \{u(x, y), v(x, y), w(x, y)\}$, $C = \{c_{ij}\}$, $(i, j = \overline{1, 6})$ is the symmetric matrix of elastic constants of generalized Hooke's law $\bar{N} = C\bar{\varepsilon}$, whose nonzero elements in the isotropic case are: $c_{11} = c_{22} = D_N = \frac{Eh}{1-\mu^2}$, $c_{12} = \mu D_N$; $c_{33} = \frac{1-\mu}{2} D_N$; $c_{44} = c_{55} = D_M = \frac{h^2}{12} D_N$; $c_{45} = \mu D_M$; $c_{66} = \frac{1-\mu}{2} D_M$ (E and μ are the Young modulus and Poisson ratio); $\bar{N} = \{T_1, T_2, S, M_1, M_2, H\}$ is the vector of forces and moments; $E_0 = \{e_{ii}\}(i = \overline{1, 6})$ is the diagonal matrix with elements $e_{ii} = 1(i = \overline{1, 5})$, $e_{66} = 2$; $\tilde{T}_1^{\pm}$, $\tilde{S}_1^{\pm}$, $\tilde{M}_1^{\pm}$, $\tilde{Q}_1^{\pm}$ and $\tilde{T}_2^{\pm}$, $\tilde{S}_2^{\pm}$, $\tilde{M}_2^{\pm}$, $\tilde{Q}_2^{\pm}$ are the contour forces-moments given on the sides $x = \pm a$ and $y = \pm b$, respectively; comma in the lower index denotes differentiation with respect to the above variable; indexes 1, 2, 3 correspond to the coordinate directions x, y, n; all the vectors are considered as vector-columns.

4.2 Solving Method

Principles of construction of the CSM for solving N-dimensional ($N \geq 2$) problems in differential and variational formulations are outlined, as it was noted above, in Bespalova [1, 2], Bespalova and Kitaygorodskiy [3, 4], Bespalova and Urusova [5, 6], Prokopov et al. [17]. Their main point consists in the following moments:

approximating the desired solution in superposition of the functions with separated variables, where all the introduced functions are unknowns (stage 1);
constructing the governing system with respect to the introduced functions of different variables (stage 2);
solving the constructed system and problem (stage 3).

Stage 1. Approximation of the desired stationary points of the given functional.

According to the principal ideas of the CSM, each component of the searched displacement vector $\bar{U} = \{u(x, y), v(x, y), w(x, y)\}$ is accepted as follows:

$$u(x, y) \cong F_{uM}(x, y) = \sum_{i=1}^{M} X_{ui}(x) Y_{ui}(y),$$
$$v(x, y) \cong F_{vM}(x, y) = \sum_{i=1}^{M} X_{vi}(x) Y_{vi}(y),$$
$$w(x, y) \cong F_{wM}(x, y) = \sum_{i=1}^{M} X_{wi}(x) Y_{wi}(y), \tag{27}$$

where M is the number of the series terms retained in approximation, while all the functions $X_{ui}(x)$, $Y_{ui}(y)$, $X_{vi}(x)$, $Y_{vi}(y)$, $X_{wi}(x)$, $Y_{wi}(y)\big(i = \overline{1, M}\big)$ are unknown.

For the sake of convenience, let us present these functions as components of the following two vectors (further they will be called argument vector-functions of the associated argument):

$$\bar{X} = \big\{X_{qi}(x)\big\}_{\substack{q=u,v,w;\\ i=\overline{1,M}}} = \{X_{u1}, X_{u2}, \ldots, X_{uM}, X_{v1}, X_{v2}, \ldots, X_{vM}, X_{w1}, X_{w2}, \ldots, X_{wM}\}$$
$$\bar{Y} = \big\{Y_{qi}(y)\big\}_{\substack{q=u,v,w;\\ i=\overline{1,M}}} = \{Y_{u1}, Y_{u2}, \ldots, Y_{uM}, Y_{v1}, Y_{v2}, \ldots, Y_{vM}, Y_{w1}, Y_{w2}, \ldots, Y_{wM}\}. \tag{28}$$

According to the accepted approximation (27), the desired vector $\bar{U}$ is replaced approximately by the two argument vector-functions $\bar{X}$, $\bar{Y}$, functional (26) is replaced approximately by the functional $G_M\big(\bar{X}, \bar{Y}\big)$, while the stationary condition $\delta G = 0$ by the condition

$$\delta G_M = \delta_{\bar{X}} G_M \delta\bar{X} + \delta_{\bar{Y}} G_M \delta\bar{Y}, \tag{29}$$

where $\delta_{\bar{X}} G_M$, $\delta_{\bar{Y}} G_M$ are the partial variations of the functional G_M with respect to the components of the vectors $\bar{X}$ and $\bar{Y}$, respectively.

Stage 2. Constructing the resolving system with respect to the unknown argument vector-functions $\bar{X}$ and $\bar{Y}$.

Implementation of this stage is based on the known procedure of variational calculus. So, due to independency of the components of the vectors $\bar{X}$ and $\bar{Y}$, condition (29) becomes equivalent to the following system of conditions:

$$\delta_{\bar{X}} G_M = \sum_{k=1}^{M} \left(\delta_{X_{uk}} G_M \delta X_{uk} + \delta_{X_{vk}} G_M \delta X_{vk} + \delta_{X_{wk}} G_M \delta X_{wk}\right) = 0; \tag{30}$$

$$\delta_{\bar{Y}} G_M = \sum_{k=1}^{M} \left(\delta_{Y_{uk}} G_M \delta Y_{uk} + \delta_{Y_{vk}} G_M \delta Y_{vk} + \delta_{Y_{wk}} G_M \delta Y_{wk}\right) = 0. \tag{31}$$

In transitions to the Euler-Lagrange equations, each condition from (30), (31) generates one-dimensional problem with respect to the varied argument vector-function.

Herewith, the argument-functions of another variable, which are unvaried under this condition, appear in the one-dimensional problem as parameters-functionals. So, the one-dimensional problem with respect to the variable x with regard to the functions $\bar{X}$ is equivalent to condition (30), while the functions $\bar{Y}$ enter in it as definite integrals. In contrast, condition (31), gives rise to one-dimensional problem with respect to the variable y with regard to the functions $\bar{Y}$, while the functions X enter in it as definite integrals. Thus, system (30), (31) is reduced to the system of two one-dimensional boundary-value problems with respect to the two argument vector-functions of different variables. This new structure can be written down as follows:

$$\begin{aligned} &L_x\bar{X} + \bar{Q}_x = 0,\ x \in (-a, a) \\ &R_x^{\mp}\bar{X} + \bar{g}_x^{\mp} = 0,\ x = \mp a; \end{aligned} \tag{32}$$

$$\begin{aligned} &L_y\bar{Y} + \bar{Q}_y = 0,\ y \in (-b, b) \\ &R_y^{\mp}\bar{Y} + \bar{g}_y^{\mp} = 0,\ y = \mp b. \end{aligned} \tag{33}$$

where $L_x = \left\{l_{sp}\right\}_{s,p=1,2,3}$ is the block matrix, whose each block $l_{sp} = \left\{l_{ik}^{sp}\right\}_{i,k=\overline{1,M}}$ is the matrix differential operator with respect to the variable x of the second ($s,\ p \neq 3$) or fourth ($s,\ p = 3$) order of the following general form:

$$\begin{aligned} l_{ik}^{sp} &= A_{2ik}^{sp}\frac{d^2}{dx^2} + A_{1ik}^{sp}\frac{d}{dx} + A_{0ik}^{sp};\ (s,\ p \neq 3) \\ l_{ik}^{33} &= A_{4ik}^{sp}\frac{d^4}{dx^4} + A_{3ik}^{sp}\frac{d^3}{dx^3} + A_{2ik}^{sp}\frac{d^2}{dx^2} + A_{1ik}^{sp}\frac{d}{dx} + A_{0ik}^{sp} \quad (s = p = 3); \end{aligned} \tag{34}$$

The matrix operator of boundary conditions $R_x^{\mp}$ has the corresponding form; $\bar{Q}_x = \{q_{pk}\}$ and $\bar{g}_x^{\mp} = \{g_{pk}^{\mp}\}$ are the vectors of free terms in the system of differential equations and boundary conditions.

The coefficients in operators (34) and components of the vectors $\bar{Q}_x$ and $\bar{g}_x^{\mp}$ depend on components of the vector-function $\bar{Y}$. For the sake of clearness, we present expressions for some nonzero coefficients of operators (34):

$$A_{2ik}^{11} = -D_N\int_{-b}^{b} Y_{ui}Y_{uk}dy,\ A_{0ik}^{11} = \frac{1-\nu}{2}D_N\int_{-b}^{b} Y_{ui}^{'}Y_{uk}^{'}dy,$$

$$A_{0ik}^{33} = D_N\left(k_x^2 + 2\nu k_x k_y + k_y^2\right)\int_{-b}^{b} Y_{wi}Y_{wk}dy + D_M\int_{-b}^{b} Y_{wi}^{''}Y_{wk}^{''}dy;$$

$$q_{3k} = -\int_{-b}^{b} q_n(x, y)Y_{wk}dy - \tilde{Q}_2^{\pm}(x)Y_{wk}\Big|_{\pm b} - \tilde{M}_2^{\pm}(x)Y_{wk}^{'}|_{\pm b}. \tag{35}$$

The operators with indexes y in system (2.7) have the same structure differing in that differentiation is conducted only with respect to the variable y in L_y, $R_y^{\mp}$, while

the coefficients in the differential operators depend on components of the vector $\bar{X}$ as follows:

$$A_{2ik}^{11} = -\frac{1-\nu}{2} D_N \int_{-a}^{a} X_{ui} X_{uk} dx,\ A_{0ik}^{11} = D_N \int_{-a}^{a} X_{ui}^{'} X_{uk}^{'} dx,$$

$$A_{0ik}^{33} = D_N \left(k_x^2 + 2\nu k_x k_y + k_y^2\right) \int_{-a}^{a} X_{wi} X_{wk} dx + D_M \int_{-a}^{a} X_{wi}^{''} X_{wk}^{''} dx;$$

$$q_{3k} = -\int_{-a}^{a} q_n(x, y) X_{wk} dx - \tilde{Q}_1^{\pm}(y) X_{wk} \Big|_{\pm a} - \tilde{M}_1^{\pm}(y) X_{wk}^{'} |_{\pm a}. \tag{36}$$

Thus, the interconnection between the one-dimensional problems (32) and (33), which are formulated with respect to the different variables of the domain, is implemented using coefficients in the form (35), (36).

Stage 3. Determining argument functions and problem solving.

To solve the system of two-dimensional problems (32), (33), we will use analog of the sequence substitution method of the linear algebra (Liebmann-Gauss-Seidel's process), whose general scheme is expressed by

$$\begin{aligned} &L_x^{(j-1)} \bar{X}^{(j)} + \bar{Q}_x^{(j-1)} = 0,\ x \in (-a, a), \\ &R_x^{\mp(j-1)} \bar{X}^{(j)} + \bar{g}_x^{\mp(j-1)} = 0,\ x = \mp a; \end{aligned} \tag{37}$$

$$\begin{aligned} &L_y^{(j)} \bar{Y}^{(j)} + \bar{Q}_y^{(j)} = 0,\ y \in (-b, b), \\ &R_y^{\mp} \bar{Y}^{(j)} + \bar{g}_y^{\mp(j)} = 0,\ y = \mp b \end{aligned} \tag{38}$$

where $j = 1, 2, \ldots$ is the iteration parameter.

The intermediate j-th step of the process is realized at the fixed number of the terms M of the approximating relation (27) in the following sequence:

calculating coefficients in the form (35) by using components of the vector-function $\bar{Y}^{(j-1)}$, which are known from the previous $(j-1)$-th step;
determining the vector-function $\bar{X}^{(j)}$ by using solution of the one-dimensional linear boundary-value problem (2.6);
calculating coefficients in the form (2.10) by using components of the defined vector-function $\bar{X}^{(j)}$;
determining the vector-function $\bar{Y}^{(j)}$ by using solution of the one-dimensional linear boundary-value problem (2.7);
checking the calculation accuracy of the argument vector-function $\bar{X}^{(j)}$ and $\bar{Y}^{(j)}$ by the chosen criterion and, if the given accuracy is reached, constructing the desired displacement vector $\bar{U}$ by the accepted approximation (2.1) or transition to the $(j+1)$-th iteration step with repetition of all calculating stages, otherwise.

As the first approximation $\bar{Y}^0 = \{Y_{pi}^{(0)}\}_{\substack{p=u,v,w \\ i=\overline{1,M}}}$, any functions linearly independent of i can be used. The one-dimensional boundary-value problem is solved numerically by the orthogonal sweep method (discrete-orthogonalization method). The required accuracy is provided by increasing the number of the terms M in expression (2.1).

4.3 Calculation Characteristics of the Method

The method developed is substantiated inductively by comparing with solutions obtained either analytically or experimentally or by other methods. The examples of testing the CSM in solving $2D$ and $3D$ problems of mechanics of deformable body (linear, nonlinear, eigenvalue) are outlined in Bespalova [1, 2], Bespalova and Kitaygorodskiy [3, 4], Bespalova and Urusova [5, 6], Prokopov et al. [17]. Here the basic calculating characteristics of the method, which define convergence of Liebmann-Gauss-Seidel's process and stabilization of solving with increasing the number of approximation terms M, is demonstrated by the example of a plate ($2a \times 2a \times h$) with two adjacent sides being clamped and other two being free [16]. The results obtained in the case of uniformly distributed load of intensity q are presented in Table 4.

As is seen, the iterative process of determining the argument-functions (37), (38) converges with sufficient rapidity (3–4 iterations), while the desired solving is stabilized at 4 signs for 4–5 terms of approximating expression. The dissimilarities from the data in Leissa and Niedenfuhr [16] do not exceed 3.5% and are absent practically in the case presented in Huang and Conway [14].

Stable values of the bending moments at two points of the clamped sides $M_1 = -M_x(0, a)/P = -M_y(a, 0)/P$ and $M_2 = -M_x(0, 2a)/P = -M_y(2a, 0)/P$ with the force P concentrated at the free angle are summarized in Table 5.

Table 4 Maximum values of the deflection depending on the parameter j of the iterative process of Liebmann-Gauss-Seidel's type and the number of the approximating terms M

$w_{\max} D_M/qa^4$				
M	$j = 1$	$j = 2$	$j = 3$	$j = 4$
1	0.45683	0.57760	0.57767	0.57768
2	0.51703	0.57840	0.57849	0.57848
3	0.54465	0.57883	0.57887	0.57887
4	0.55656	0.57902	0.57902	0.57902
5	0.55651	0.57904	0.57904	0.57903
6	0.56935	0.57905	0.57905	
Huang				0.57904
Leissa				0.55915

Table 5 Values of the bending moments M_1 and M_2 under action of the concentrated force P at the free angle of the plate

	OKM	(Leissa)	ε, %
M_1	2.4732·10	2.5198·10	1.85
M_2	1.0968	1.0897	0.65

Distinctions between maximum values of the bending moments. which held at angular points at the interfaces of free and fixed sides (M_2) obtained with different methods do not exceed 1%. Such distinctions for the moments at the center of the fixed side (M_1) do not exceed 2%.

In conclusion, we note the following.

The complete systems method (generalized Kantorovich method) differs from the traditional projective Bubnov-Galerkin-Ritz method and Kantorovich-Vlasov method of reduction to ordinary differential equations by the following two principal features:

presentation of the desired solution in the form of combination of the functions with separated variables. where all the components of the approximating expression are considered to be unknowns (it should be noted that as such ones the numerical coefficients in the Bubnov-Galerkin-Ritz method and functions of one variable in the Kantorovich-Vlasov method are accepted);
reduction of the original two-dimensional problem to the new structure in the form of system of two interconnected problems (note that the problem of arbitrary dimensionality in the Bubnov-Galerkin-Ritz method is reduced to the system of algebraic equations. while in the Kantorovich-Vlasov method is reduced to one one-dimensional problem).

The iterative process of solving the system of one-dimensional problems is converged with sufficient rapidity (3–5 iterations). while the desired solution is stabilized at a few number of terms in the approximating expression (for 4–5 terms).

4.4 Employment of the CSM in a Problem on Shell Vibrations

Using rational combination of the CSM and the method of successive approximations in the reverse iteration variant (Rayleigh method). we have developed the technique for determining frequencies and modes of free vibrations of shallow panels with rectangular planform. As an example of application of the technique. we have calculated the minimum natural frequency of the panel depending on the curvature values k_x and k_y in the case of two adjacent sides being clamped and other two being free. The calculated results are shown in Fig. 10a in the form of the plot $\lambda = \lambda(k_y^*) = \omega(k_y^*)/\omega_0$ for fixed curvature values $k_x^* = 0; 20; 50$ and in Fig. 10b as nodal lines of associated vibration modes ($k_y^* \in [-k^*, k^*]$, ω_0—is the frequency of the plate vibrations, $k^* = 50$ is the maximum value of the curvature). Points of inflexion on the curves

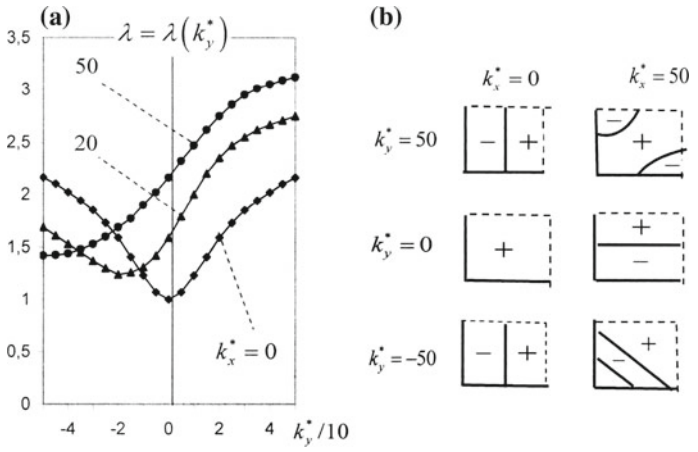

Fig. 10 Dependencies $\lambda = \lambda(k_y^*)$ for curvature values $k_x^* = 0; 20; 50$ (**a**); nodal lines of vibration modes (**b**)

correspond to the change in the vibration modes of the panel on the minimum frequency (Fig. 1b; dashed lines refer to free parts of the contour, solid lines refer to the nodal lines of the vibration mode $w(x, y) = 0$ and clamped parts of the boundary) (Fig. 10).

The curvature sign k_y^*(convexity either upward or downward) for cylindrical panels ($k_y^* \in (-50; 50)$) is of no significance and the dependence $\lambda = \lambda(k_y^*)$ is the symmetric function with respect to $k_y^* = 0$, increasing with the panel curvature (curve $k_x^* = 0$). The curves $\lambda = \lambda(k_y^*)$ for shells with positive Gaussian curvature ($k_y^* \in (0; 50)$) are monotonically increasing functions for all values of k_x^* as well. For shells with negative Gaussian curvature (convexo-concave, $k_y^* \in (-50; 0)$), the dependencies $\lambda = \lambda(k_y^*)$ are presented by nomonotone curves, whose minimum is reached at $k_x^* = -k_y^*$. In this case, the panel mid-surface has diagonal antisymmetry with zero raise at the center. The inflections on the curves correspond to change in the vibration modes of the panel on the minimum frequency (Fig. 1b; the dashed lines refer to the free segments of the contour, the solid lines present the nodal lines of the vibration mode $w(x, y) = 0$ and clamped segments of the boundary).

Thus, change in the frequency properties of the shallow panel may be of qualitatively different nature depending on how its Gaussian curve varies.

5 Conclusions

In the given report we have studied mechanical performance of anisotropic inhomogeneous shells within the framework of models of various severity level such ones as the Mushtari-Donnel-Vlasov and shear first-order Timoshenko-Mindlin ones as well as those in the three-dimensional elasticity theory. To solve stationary prob-

lems of the shell theory, three new discrete-continual methods are proposed. They include the discrete Fourier series, spline-collocation, and complete system ones. The general idea of these methods consists in reducing an original two-dimensional (three-dimensional) problem by use one or other analytical transformations to linear one-dimensional boundary-value problems which are solved numerically by the discrete-orthogonalization method. The mechanical performance of inhomogeneous orthotropic cylindrical shells with arbitrary cross-section both thick- and mid-walled ones and of shallow panels of rectangular plan-form under arbitrary attachment conditions of a boundary contour is analyzed. The stress-strain problem for hollow cylinders with cross-section in the form of convex semi-corrugations that are described by a shortened epicycloid is solved; natural frequencies of non-thin orthotropic cylindrical shells of elliptical cross-section of variable thickness and of shallow shells with various Gaussian curvatures are analyzed depending on the type of boundary conditions. It is noted that variations in the geometrical and physical-mechanical characteristics as well as the attachment conditions of the boundary contour essentially influence the stress-strain state and natural frequencies of the shells. Emphasis is placed on the accuracy of the results of numerical calculations.

References

1. Bespalova, E.I.: Determining the natural frequencies an elastic parallelepiped by the advanced Kantorovich-Vlasov method. Int. Appl. Mech. **47**(4), 410–421 (2011)
2. Bespalova, E.I.: Solution of the problems of the theory of elasticity by the complete systems method. Zhurnal vichislit. Matem. Phys. **9**, 1346–1353 (1989). [in Russian]
3. Bespalova, E.I., Kitaygorodskiy, A.B.: Advanced Kantorovich method for biharmonic problems. J. Eng. Math. **46**, 213–226 (2003)
4. Bespalova, E.I., Kitaygorodskiy, A.B.: The full (complete) systems method in dynamics problems of 3D bodies. Eng. Trans. **48**(4), 395–403 (2000)
5. Bespalova, E., Urusova, G.: Solution of the Lame problems by the complete systems method. Int. J. Comput. Methods Eng. Sci. Mech. **14**(2), 159–167 (2013)
6. Bespalova, E.I., Urusova, G.P.: Solving the torsion problem for an anisotropic prism by the advanced Kantorovich-Vlasov method. Int. Appl. Mech. **46**(2), 149–158 (2010)
7. Budak, V.D., Grigorenko, A.Y., Puzyrov, S.V.: Free vibrations of the non-circular cylindrical shells. in: Proc. 10th Int. Conf. on Modern Building Materials. Structures and Techniques. Lithuania. Vilnius., 874–879 (2010)
8. Grigorenko, A.Y., Puzyrov, S.V., Volchek, E.A.: Investigation of free vibrations of non-circular cylindrical shells by the spline-collocation method. J. Math. Sci. **185**(6), 824–836 (2012)
9. Grigorenko, Y.M., Bespalova, E.I., Kitaigorodskii, A.B., Shinkar A.I.: Free vibrations of elements of shell structures. Naukova Dumka. Kyiv (1986). [in Russian]
10. Grigorenko, Y.M.. Rozhok, L.S.: Applying discrete Fourier series to solve problems of the stress state of hollow noncircular cylinders. Int. Appl. Mech. **50**(2), 105–127 (2014)
11. Grigorenko, Y.M.. Rozhok, L.S.: Effect of orthotropy on the stress state of longitudinally corrugated hollow cylinders. Int. App. Mech. **52**(2), 147–154 (2016)
12. Grigorenko, Y.M.. Rozhok, L.S.: Stress state of hollow cylinders with convex corrugated cross sections. J. Math. Sci. **198**(2), 158–165 (2014)
13. Hamming, R.W.: Numerical Methods for Scientists and Engineers. McGraw-Hill, New York (1962)

14. Huang, M.K., Conway, H.D.: Bending of a uniformly loaded rectangular plate with two adjacent edges clamped the others either simply supported or free. J. Appl. Mech., 451–460 (1952)
15. Korn, G.A., Korn, T.M.: Mathematical Handbook for Scientists and Engineers. McGraw-Hill, New York (1961)
16. Leissa, A.W., Niedenfuhr, F.W.: Bending of a square plate with two adjacent edges free and the others clamped or simply supported. AIAA J. **1**(1), 116–120 (1963)
17. Prokopov, V.G., Bespalova, E.I., Sherenkovskiy, Y.V.: The method of reduction to the ordinary differential equations by L.V. Kantorovich and general method of solving of the heat transfer multidimensional problems. Inzh. Phiz. Zhurnal. **42**(6), 1007–1013 (1982). [in Russian]
18. Soldatos, K.P.: Mechanics of cylindrical shells with non-circular cross-sections (survey). Appl. Mech. Rev. **52**(2), 237–274 (1999)
19. Suzuki, K., Leissa, A.W.: Exact solutions for the free vibrations of open cylindrical shells with circumferentially varying curvature and thickness conditions. J. Sound Vibr. **107**(1), 1–15 (1986)
20. Suzuki, K., Shikanai, G., and A.W. Leissa.: Free vibration of laminated composite non-circular thin cylindrical shells. J. Appl. Mech. **61**(4), 261–271 (1994)
21. Timoshenko, S.P.: Theory of Elasticity. McGraw-Hill, New York (1934)

A Composite Wave Model for a Cylindrical Shell

J. Kaplunov, B. Erbaş and M. Palsü

Abstract A 2D composite wave model is established for a thin elastic cylindrical shell subject to a transverse surface load. It generalises recent authors developments for plate bending, also taking into consideration transverse compression. The long–wave, low–frequency and short–wave, high–frequency limiting behaviours of the composite model correspond to an asymptotic refinement of Kirchhoff Love theory and hyperbolic equations governing Rayleigh wave propagation along shell faces, respectively. In addition, the derived equations of motion enable smoothing a discontinuity at the extension wave front arising in traditional plate and shell theories. At the same time, the proposed approach is not uniformly valid, since it can not be asymptotically justified over the intermediate range, where a typical wavelength is of order shell thickness.

Keywords Elastic · Shell · Plate · Composite model · Asymptotic · Hyperbolic · Transverse compression · Rayleigh wave

1 Introduction

An insightful account of the state of art in mechanics of plates and shells at the end of the 20th century was given in [1], reflecting on the basics of existing models, including most important non-linear considerations, e.g. see [2, 3]. New technological developments, first of all in the area of nanotechnology, resulted in a sort of

J. Kaplunov (✉)
School of Computing and Mathematics, Keele University, Colin Reeves Building, Staffordshire ST5 5BG, UK
e-mail: j.kaplunov@keele.ac.uk

B. Erbaş · M. Palsü
Department of Mathematics, Eskişehir Technical University, Yunus Emre Campus, 26470 Eskişehir, Turkey
e-mail: berbas@eskisehir.edu.tr

M. Palsü
e-mail: mpalsu@eskisehir.edu.tr

H. Altenbach et al. (eds.), *Recent Developments in the Theory of Shells*,
Advanced Structured Materials 110, https://doi.org/10.1007/978-3-030-17747-8_17

renaissance of the theory of thin elastic structures during last two decades. Among recent publications on the subject, we mention [4–13] related to various modern trends.

At the same time, a long–term challenge of deriving consistent 2D wave equations has been addressed only last year for plate bending in [14] also presenting the history of numerous *ad hoc* wave formulation, e.g. see [15–18] for greater detail. The long–wave, low–frequency limit of the composite wave models in [14] corresponds at leading order to the classical Kirchhoff theory, whereas the short–wave high–frequency limit coincides with the 2D hyperbolic equation for Rayleigh waves propagating along plate faces. This equation arises from an asymptotic hyperbolic–elliptic model for surface waves, see [19, 20] and references therein. We remark, however, that the approximations in [14] are not uniformly valid and cannot be asymptotically justified over the intermediate range, where a typical wavelength is of order plate thickness. To this end, we refer to the models proposed in [14] as composite, but not as asymptotic ones, see also [21].

The aim of the consideration below is to extend the framework of [14] to a thin cylindrical shell subject to a surface transverse load. Analysis of the original problem emerges from the preliminary results for plate bending and transverse compression, since the effect of shell curvature is less essential at wavelengths much shorter than midsurface radius [22]. The substantial focus is on the compression problem, which has not been tackled earlier, and is of interest on its own as well. In this case, we establish a composite wave equation predicting both the Rayleigh wave front and quasi–front, i.e. the extension wave front in the theory for plane stress, e.g. see [22] and references therein. The accuracy of this equation is tested in the paper by comparison with the associated exact time-harmonic solution. Obviously, both the Rayleigh wave front and quasi-front are also a feature of the derived shell model involving, in addition, one more composite hyperbolic equation, generalizing that for plate bending.

2 Statement of the Problem

Consider an elastic cylindrical shell of half-thickness h and midsurface radius R ($h \ll R$) composed of a material with Young's modulus E, Poisson's ratio ν, and density ρ. Specify three–orthogonal coordinates α_n, $n = 1, 2, 3$, where α_3 is the distance from the midsurface, and α_1 and α_2 are expressed through cylindrical coordinates as $\alpha_1 = z$ and $\alpha_2 = R\phi$ where z is the distance along the longitudinal axis of the cylinder and ϕ is the polar angle.

Let the shell be subject to transverse load P applied to upper surface $\alpha_3 = h$; in doing so, lower surface $\alpha_3 = -h$ is assumed to be traction free; see Fig. 1 also demonstrating splitting of the load into two parts. The first term in the symbolic sum in this figure corresponds to bending deformation, while the second one is less common in shell theories and is associated with transverse compression. Originally, it was introduced in [23] within the static context. However, the role of transverse

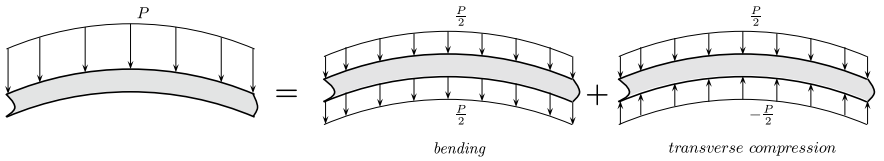

Fig. 1 Decomposition of transverse load

compression appears to be more crucial in dynamics, e.g. see [22, 24]. In particular, at a certain frequency, referred to as the Poisson one in [25], midsurface extension due to transverse compression compensates its membrane deformation.

It is well known that traditional thin shell theory governs only long–wave, low–frequency motions, for which $L \gg h$ and $T \gg h/c$, where L, T and c are typical wavelength, timescale and wave speed, respectively, see [22]. As a result, this theory cannot properly tackle short–wave, high–frequency dynamic phenomena, when $L \lesssim h$ and $T \lesssim h/c$. Below we attempt to complement shell theory with an asymptotic formulation involving their 2D hyperbolic equation along shell faces related to Rayleigh waves, see [20] and references therein. These equations are valid at $T \ll h/c$ and $L \ll h$. From the very beginning we do not expect the proposed approach to be asymptotically justified over the intermediate range, for which $L \sim h$ and $T \sim h/c$.

The equations of motion in thin shell theory can be written as, see [22–24].

$$L_i(u_1, u_2, w) - 2\rho h \frac{\partial^2}{\partial t^2}\left(u_i - \frac{\nu^2 h^2}{3(1-\nu)^2 c_3^2}\frac{\partial^2 u_i}{\partial t^2}\right) = -\frac{\nu h}{2(1-\nu)}\frac{\partial P}{\partial \alpha_i}, \quad i = 1, 2 \tag{1}$$

and

$$L_3(u_1, u_2, w) + 2\rho h \frac{\partial^2 w}{\partial t^2} = P \tag{2}$$

where u_1, u_2 and w are tangential and transverse displacements of upper face $\alpha_3 = h$ of the shell, t is time, $c_3 = \sqrt{\dfrac{E}{(1-\nu^2)\rho}}$ is the speed of the quasi–front (or the extension wave speed in plane stress theory), and L_i and L_3 are differential operators specified in Appendix 1.

This formulation is an asymptotic refinement of the classical Kirchhoff–Love theory incorporating a forcing term in Eq. (1) associated with transverse compression. Also, the term with the fourth order derivative in time in this equation enables smoothing a discontinuity at the quasi–front, see [22] and references therein. Finally, the equations above are written in terms of the upper face displacements, but not midsurface ones as usual. Violation of the long–term tradition is motivated by forthcoming matching with the 2D hyperbollic equation for Rayleigh waves and resulting only in a higher–order asymptotic error. For shorter wave lengths, when $1 \ll L/h \ll \eta^{-1/2}$, but still in the framework of thin shell theory, the equations above coincide at leading order with the equations of plate bending and transverse compression [22], taking

the form

$$D\Delta^2 w + 2\rho\frac{\partial^2 w}{\partial t^2} = P \tag{3}$$

with $D = \dfrac{2Eh^3}{3(1-\nu^2)}$ and

$$E\left(\frac{1}{1+\nu}\Delta u_i + \frac{1}{1-\nu}\frac{\partial}{\partial\alpha_i}\left(\frac{\partial u_1}{\partial\alpha_1} + \frac{\partial u_2}{\partial\alpha_2}\right)\right) - 2\rho\frac{\partial^2}{\partial t^2}\left(u_i - \frac{\nu^2 h^2}{3(1-\nu)^2 c_3^2}\frac{\partial^2 u_i}{\partial t^2}\right) = -\frac{\nu}{1-\nu}\frac{\partial P_i}{\partial\alpha_i} \tag{4}$$

where, to within asymptotically small terms, $\Delta = \dfrac{\partial^2}{\partial\alpha_1^2} + \dfrac{\partial^2}{\partial\alpha_2^2} = \dfrac{\partial^2}{\partial z^2} + \dfrac{1}{R^2}\dfrac{\partial^2}{\partial\theta^2}$.

It is obvious that transverse compression does not cause shear deformation. Thus, $\dfrac{\partial u_1}{\partial\alpha_2} = \dfrac{\partial u_2}{\partial\alpha_1}$, and (4) can be rewritten as

$$\frac{2E}{1-\nu^2}\Delta u_i - 2\rho\frac{\partial^2}{\partial t^2}\left(u_i - \frac{\nu^2 h^2}{3(1-\nu)^2 c_3^2}\frac{\partial^2 u_i}{\partial t^2}\right) = -\frac{\nu}{1-\nu}\frac{\partial P_i}{\partial\alpha_i} \tag{5}$$

or

$$\Delta u_i - \frac{1}{c_3^2}\frac{\partial^2}{\partial t^2}\left(u_i - \frac{\nu^2 h^2}{3(1-\nu)^2 c_3^2}\frac{\partial^2 u_i}{\partial t^2}\right) = -\frac{\nu(1+\nu)}{2E}\frac{\partial P_i}{\partial\alpha_i}. \tag{6}$$

The hyperbolic equation along shell faces for Rayleigh waves expressed through w and u_i, $i = 1, 2$, can be written as, see [20],

$$\Delta w - \frac{1}{c_R^2}\frac{\partial^2 w}{\partial t^2} = -\frac{k_1(1-k_2^2)(1+\nu)}{2EB}\sqrt{-\Delta}P \tag{7}$$

or

$$\Delta u_i - \frac{1}{c_R^2}\frac{\partial^2 u_i}{\partial t^2} = \frac{(1-k_2^4)(1+\nu)}{4EB}\frac{\partial P_i}{\partial\alpha_i} \tag{8}$$

where c_R is the Rayleigh wave speed,

$$k_j = \sqrt{1 - \frac{c_R^2}{c_i^2}}, \quad j = 1, 2, \tag{9}$$

and

$$B = \frac{k_1}{k_2}\left(1-k_1^2\right) + \frac{k_2}{k_1}\left(1-k_2^2\right) - \left(1-k_2^4\right). \tag{10}$$

3 Flat Plate

First, address the composite wave theories for a thin elastic plate. For plate bending they were derived in [14]. At leading order, we have from this paper

$$D\left(\Delta^2 u_3 - \frac{1}{c_R^2}\frac{\partial^2 \Delta u_3}{\partial t^2}\right) + 2\rho h \frac{\partial^2 u_3}{\partial t^2} = \left(1 - h^3 \frac{k_1\left(1-k_2^2\right)}{3B(1-\nu)}\sqrt{-\Delta}\,\Delta\right) P. \quad (11)$$

For plate transverse compression we start from (6) and

$$\frac{\partial^2 \Delta u_i}{\partial t^2} - \frac{1}{c_R^2}\frac{\partial^4 u_i}{\partial t^4} = \frac{(1-k_2^4)(1+\nu)}{4EB}\frac{\partial^3 P}{\partial \alpha_i \partial t^2} \quad (12)$$

obtained from (8) by taking a second order derivative in time. Let us find, then, the sum of (6) and (12) multiplied by γh^2, where γ is so far unknown. The result is

$$\Delta u_i - \frac{1}{c_3^2}\frac{\partial^2 u_i}{\partial t^2} + \gamma h^2 \frac{\partial^2}{\partial t^2}\left(\Delta u_i - \frac{1}{c_R^2}\frac{\partial^2 u_i}{\partial t^2}\right) = \frac{1+\nu}{4E}\left(-2\nu + \gamma h^2 \frac{1-k_2^4}{B}\frac{\partial^2}{\partial t^2}\right)\frac{\partial P}{\partial \alpha_i}. \quad (13)$$

Next, scaling independent variables by

$$\alpha_i = L\xi_i, \quad i = 1, 2, \qquad t = Lc_3^{-1}\tau \quad (14)$$

we have from homogenous equation (13)

$$\Delta_* u_i - \frac{\partial^2 u_i}{\partial \tau^2} + \gamma c_3^2 \eta^2 \frac{\partial^2}{\partial \tau^2}\left(\Delta_* u_i - \frac{c_3^2}{c_R^2}\frac{\partial^2 u_i}{\partial \tau^2}\right) = 0 \quad (15)$$

where $\eta = h/L \ll 1$ is a small geometric parameter, and also $\Delta_* = \partial^2/\partial\xi_1^2 + \partial^2/\partial\xi_2^2$.

It is clear from (15) that at leading order, $\Delta u_i = \dfrac{\partial^2 u_i}{\partial t^2}$. Therefore, to within the same truncation error, it can be reduced to

$$\Delta_* u_i - \frac{\partial^2 u_i}{\partial \tau^2} + \gamma c_3^2 \eta^2 \left(1 - \frac{c_3^2}{c_R^2}\right)\frac{\partial^4 u_i}{\partial \tau^4} = 0. \quad (16)$$

Then, we immediately deduce that (16) coincides with homogenous equation (6) rewritten in scaled variables, provided that

$$\gamma = \frac{\nu^2 c_R^2}{3c_3^2(1-\nu)^2(c_R^2 - c_3^2)}. \quad (17)$$

Thus, the sought for composite equation for plate transverse compression is given by (13) with γ defined by (17). This equation approximates both the quasi–front and the Rayleigh wave front. In fact, as it may easily be verified, the limiting behaviours of (13) are given by (6) and (8) at $\eta \ll 1$ and $\eta \gg 1$, respectively.

4 Numerical Results for Transverse Compression

We begin with testing the accuracy of the dispersion relation associated with homogenous equation (13). For a plane harmonic wave in the form $\exp[\mathrm{i}(k\alpha_1 - \omega t)]$, where k is wavenumber and ω is angular frequency, we have

$$K^2 - \frac{1-\nu}{2}\Omega^2 - \Gamma\Omega^2\left(K^2 - \frac{1}{v_R^2}\Omega^2\right) = 0 \tag{18}$$

with $\Gamma = \gamma c_2^2$, $v_R = \dfrac{c_R}{c_2}$, $\Omega = \dfrac{\omega h}{c_2}$, and $K = kh$, where c_2 is given by (A2.2).

Over the long–wave, low–frequency range ($K \sim \Omega \ll 1$) this dispersion relation can be reduced to

$$K^2 - \frac{1-\nu}{2}\Omega^2 - \Gamma\Omega^4\left(\frac{1-\nu}{2} - \frac{1}{v_R^2}\right) = 0, \tag{19}$$

corresponding to homogenous refined plate equation (6). On other hand, over the short–wave, high–frequency range ($K \sim \Omega \gg 1$) we get from (19)

$$K^2 - \frac{1}{v_R^2}\Omega^2 = 0 \tag{20}$$

associated with the Rayleigh wave.

Numerical data are demonstrated in Figs. 2 and 3, and also Table 1 at $\nu = 0.25$, for which $v_R = 0.9194$. Figure 2 displays the solutions of limiting equations (19) and (20) versus the solution of composite equation (18). The latter is compared with the solution of Rayleigh-Lamb equation (A2.8), presented in Appendix 2, in Fig. 3. Table 1 illustrates the accuracy of the analysed approximations.

Next, consider a plate subject to distributed harmonic load $P = P_0 e^{\mathrm{i}(k\alpha_1 - \omega t)}$ along its upper face $\alpha_3 = h$. Then, we have from (13) for the longitudinal displacement

$$u_1 = \frac{2i(1+\nu)AhP_o}{E} e^{\mathrm{i}(k\alpha_1 - \omega t)} \tag{21}$$

with

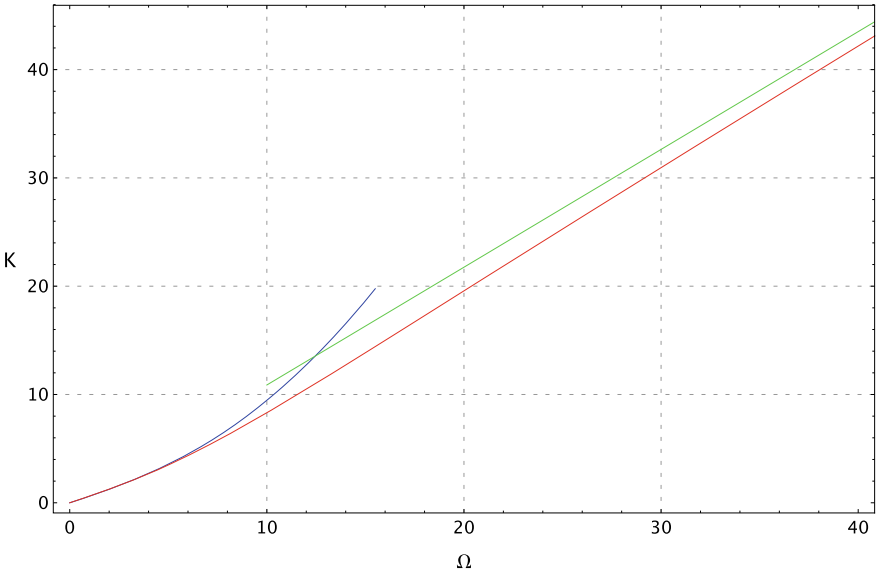

Fig. 2 The dispersion curves for limiting relations (19) (blue line) and (20) (green line) along with composite relation (18) (red line)

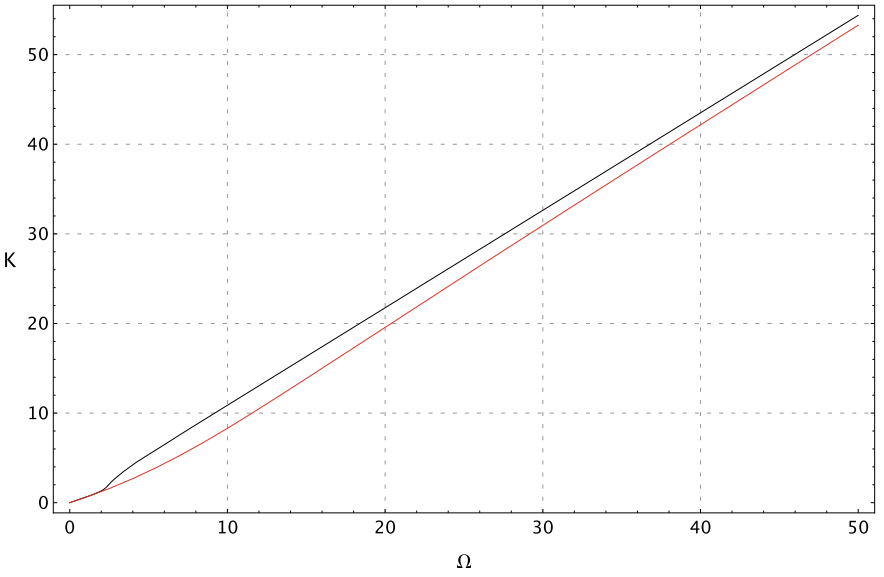

Fig. 3 The dispersion curves for Rayleigh-Lamb relation (A2.8) (black line) and composite relation (18) (red line)

Table 1 Numerical solutions of Rayleigh-Lamb and approximate dispersion relations

Ω	Plate dispersion relation (19)	Rayleigh wave relation (20)	Composite dispersion relation (18)	Rayleigh-Lamb dispersion relation (A2.8)
0.1	0.0612		0.0612	0.0612
0.2	0.1225		0.1225	0.1225
0.3	0.1837		0.1838	0.1838
0.4	0.2449		0.2452	0.2452
0.5	0.3061		0.3067	0.3067
1.	0.6124		0.6166	0.6174
1.5	0.9186		0.9326	0.9411
2.	1.225		1.257	1.321
2.5		2.719	1.594	2.064
3		3.263	1.943	2.902
4		4.351	2.685	4.210
5		5.438	3.490	5.376
6		6.526	4.357	6.496
7		7.614	5.280	7.60
8		8.701	6.253	8.691
9		9.789	7.268	9.787
10		10.88	8.317	10.88
20		21.75	19.57	21.75
30		32.63	30.95	32.63
40		43.51	42.17	43.51

$$A = \frac{1}{8}\frac{K\left(2\nu + \Gamma\Omega^2 B^{-1}(1-k_2^4)\right)}{K^2 - \dfrac{1-\nu}{2}\Omega^2 - \Gamma\Omega^2\left(K^2 - \dfrac{1}{v_R^2}\Omega^2\right)} \tag{22}$$

Numerical examples are presented in Figs. 4 and 5 at $K = (1+\varepsilon)\Omega/v_R$ with $\varepsilon = 0.1$. As above, $\nu = 0.25$ and $v_R = 0.9194$. The solution of plate and Rayleigh equations (A2.9) and (A2.10) are compared with composite solution (22) in Fig. 4. Figure 5 shows comparison of composite and Rayleigh-Lamb solutions given by (22) and (A2.10), respectively.

5 Cylindrical Shell

The relation between 2D shell and plate equations highlighted in Sect. 2 enables formulating a composite wave theory for a cylindrical shell using the results presented in Sect. 3 for a plate. Indeed, we may derive from (1)–(3), (6), (11), and (13)

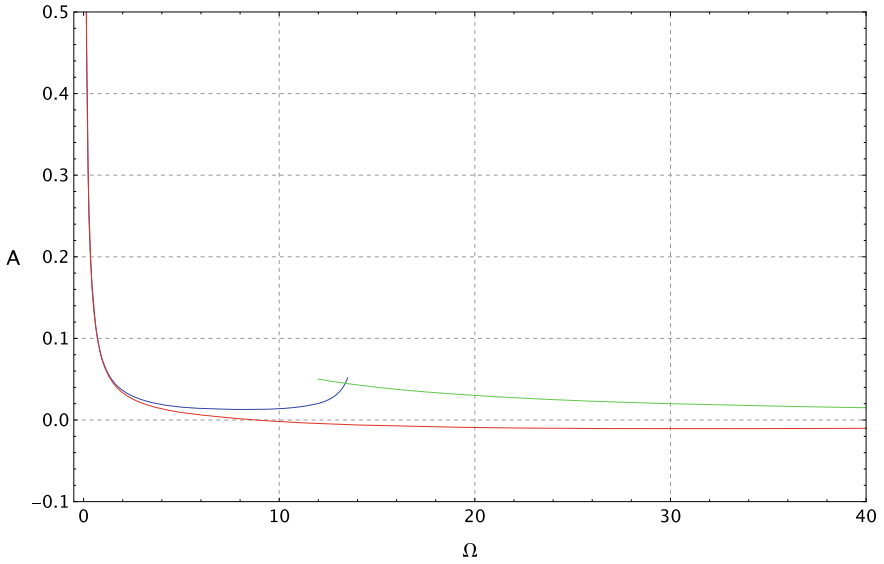

Fig. 4 The displacement amplitudes for plate equation (A2.9) (blue line), Rayleigh equation (A2.10) (green line), and composite equation (22) (red line)

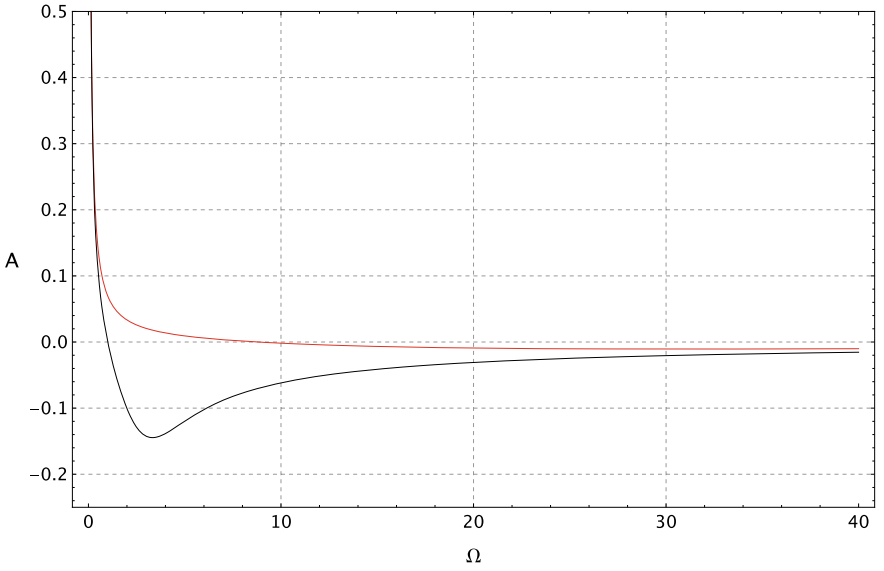

Fig. 5 Comparison of displacement amplitude (22) (red line) with exact solution (A2.6) (black line)

$$L_i(u_1,u_2,w)-2\rho h\frac{\partial^2 u_i}{\partial t^2}+\gamma h^2\frac{\partial^2}{\partial t^2}\left(\Delta u_i-\frac{1}{c_R^2}\frac{\partial^2 u_i}{\partial t^2}\right)=\left(-2\nu+\gamma h^2\frac{1-k_2^4}{B}\frac{\partial^2}{\partial t^2}\right)\frac{\partial P}{\partial \alpha_i}, \tag{23}$$

and

$$L_3(u_1,u_2,w)+2\rho h\frac{\partial^2 w}{\partial t^2}-\frac{D}{c_R^2}\frac{\partial^2 \Delta w}{\partial t^2}=\left(1-h^3\frac{k_1(1-k_2^2)}{3B(1-\nu)}\sqrt{-\Delta}\Delta\right)P. \tag{24}$$

It is worth noting that the Rayleigh wave appears in both equations above. As a result of such superposition, homogeneous boundary conditions are satisfied at traction free lower face $x_3=-h$, see Fig. 1. We also remark that the contribution of the Rayleigh wave itself could be readily deduced by adapting the formulation for surface waves exploited throughout the paper, e.g. see [20], for the original problem for a shell subject to a load applied to its upper face $x_3=h$.

Equations (23) and (24) are similar to those in the so–called "shell theories with modified inertia" [22]. However, the latter are just higher–order, long–wave approximations, whereas the composite model above also governs the short–wave behaviour corresponding to the Rayleigh wave, which appears in both Eqs. (18) and (19). At the same time, the developed asymptotic approach is obviously not uniformly valid, failing, in a sense, over the intermediate range, where a typical wavelength is of order shell thickness.

6 Concluding Remarks

The established model is not uniformly asymptotically valid. Although composite equations (23) and (24) are asymptotically consistent both at $h\ll L$, $T\gg h/c$ and $h\gg L$, $T\ll h/c$, their accuracy at $h\sim L$, $T\sim h/c$ may only be analysed numerically. In this case, full comparison with the 3D exact solution for a hollow cylinder might be the subject of a special consideration. Other limitations of composite formulations are discussed in [14].

The approach proposed for a cylindrical shell makes use the composite equations for plate bending and also for plate transverse compression obtained in Sect. 4. The latter seem to be of an obvious interest themselves, governing both the Rayleigh wave front and quasi–front. They are tested in Sect. 4 by comparison with the solution of a plane time–harmonic problem for a layer.

The developed methodology is not apparently restricted to a circular cylindrical shell studied in the paper. However, further extensions to a shell of more general shape may require an extra insight, in particular, due to presence of pseudodifferential operator $\sqrt{-\Delta}$.

Acknowledgements This work has been supported by the Ministry of Education and Science of the Republic of Kazakhstan, Grant IRN AP05132743. The research was also partly supported

by the grant J2-9224 from the Slovenian Research Agency. MP acknowledges support through Erasmus+EU framework.

Appendix 1. Operators in Shell Theory

The differential operators for a cylindrical shell are given by, cf. [23],

$$L_1 = \frac{\partial T_1}{\partial \alpha_1} + \frac{\partial S}{\partial \alpha_2}, \quad L_2 = \frac{\partial S}{\partial \alpha_1} + \frac{\partial T_2}{\partial \alpha_2} + \frac{N_2}{R}, \quad L_3 = \frac{T_2}{R} - \frac{\partial N_2}{\partial \alpha_1} - \frac{\partial N_2}{\partial \alpha_2} \tag{A1.1}$$

with

$$T_1 = \frac{2Eh}{1-\nu^2}\left(\varepsilon_1 + \nu\varepsilon_2\right), \quad T_2 = \frac{2Eh}{1-\nu^2}\left(\varepsilon_2 + \nu\varepsilon_1\right), \quad S = \frac{Eh}{1+\nu}\delta$$

and

$$N_1 = \frac{\partial G_1}{\partial \alpha_1} + \frac{\partial H}{\partial \alpha_2}, \quad N_2 = \frac{\partial G_2}{\partial \alpha_2} + \frac{\partial H}{\partial \alpha_1} \tag{A1.2}$$

where

$$G_1 = \frac{2Eh^3}{3(1-\nu^2)}(\kappa_1 + \nu\kappa_2), \quad G_2 = \frac{2Eh^3}{3(1-\nu^2)}(\kappa_2 + \nu\kappa_1), \quad H = \frac{2Eh^3}{3(1+\nu)}\theta. \tag{A1.3}$$

In the above

$$\varepsilon_1 = \frac{\partial u_1}{\partial \alpha_1}, \quad \varepsilon_2 = \frac{\partial u_2}{\partial \alpha_2} + \frac{w}{R}, \quad \delta = \frac{\partial u_1}{\partial \alpha_2} + \frac{\partial u_2}{\partial \alpha_1}$$

and

$$\kappa_1 = \frac{\partial^2 w}{\partial \alpha_1^2}, \quad \kappa_2 = -\frac{\partial^2 w}{\partial \alpha_2^2} + \frac{1}{R}\frac{\partial u_2}{\partial \alpha_2}, \quad \theta = -\frac{\partial^2 w}{\partial \alpha_1 \partial \alpha_2} + \frac{1}{R}\frac{\partial u_2}{\partial \alpha_1}. \tag{A1.4}$$

In this formulae $\alpha_1 = z$ and $\alpha_2 = R\phi$, where z and ϕ are cylindrical polars.

Appendix 2. Exact Solution of Plane Time-Harmonic Problem

The governing equations in plane elasticity are given by, e.g. see [26],

$$\Delta\varphi - \frac{1}{c_1^2}\frac{\partial^2\varphi}{\partial t^2} = 0, \quad \Delta\psi - \frac{1}{c_2^2}\frac{\partial^2\psi}{\partial t^2} = 0, \tag{A2.1}$$

where $\varphi(x_1, x_3, t)$ and $\psi(x_1, x_3, t)$ are wave potentials, and c_1 and c_2 are longitudinal and transverse wave speeds given, respectively, by

$$c_1 = \sqrt{\frac{E(1-\nu)}{(1+\nu)(1-2\nu)\rho}} \quad \text{and} \quad c_2 = \sqrt{\frac{E}{2(1+\nu)\rho}}. \tag{A2.2}$$

Consider a layer ($-\infty \le x_1 \le \infty$, $-h \le x_3 \le h$) with boundary conditions on its faces $x_3 = \pm h$ written through wave potentials as

$$\left(\frac{\partial^2\psi}{\partial x_1^2} - \frac{\partial^2\Psi}{\partial x_3^2} + 2\frac{\partial^2\varphi}{\partial x_1\partial x_3}\right)\Big|_{x_3=\pm h} = 0, \tag{A2.3}$$

$$\left(\frac{\nu}{1-\nu}\frac{\partial^2\varphi}{\partial x_1^2} + \frac{\partial^2\varphi}{\partial x_3^2} + 2\chi^2\frac{\partial^2\psi}{\partial x_1\partial x_3}\right)\Big|_{x_3=\pm h} = \frac{(1+\nu)P_0\chi^2}{E}e^{\mathrm{i}(kx_1-\omega t)}, \tag{A2.4}$$

where $\chi = \dfrac{c_2}{c_1} = \sqrt{\dfrac{1-2\nu}{2(1-\nu)}}$.

The solution to the formulated problem for the horizontal displacement at the faces

$$u_1 = \left(\frac{\partial\varphi}{\partial x_1} - \frac{\partial\psi}{\partial x_3}\right)\Big|_{x_3=\pm h}, \tag{A2.5}$$

takes the form $u_1 = \dfrac{2i(1+\nu)\rho h A P_0}{E}e^{\mathrm{i}(kx_1-\omega t)}$ with

$$A = \frac{K}{2D_{RL}}\left(\left(K^2+\beta^2\right)\coth\alpha - 2\alpha\beta\coth\beta\right) \tag{A2.6}$$

where

$$\alpha = \sqrt{K^2 - \chi^2\Omega^2}, \qquad \beta = \sqrt{K^2 - \Omega^2}, \tag{A2.7}$$

and the Rayleigh–Lamb dispersion relation is written as

$$D_{RL}(K, \Omega) = (K^2+\beta^2)^2\coth\alpha - 4K^2\alpha\beta\coth\beta, \tag{A2.8}$$

with Ω and K defined in Sect. 4.

The long–wave, low–frequency expansion of formula (A2.6) at $\Omega \ll 1$ and $K \ll 1$ takes the form

$$A = \frac{\nu K}{2(1-\nu)\left[\Omega^2\left(1+\dfrac{\nu^2}{6(1-\nu)}\Omega^2\right)-\dfrac{2}{1-\nu}K^2\right]} \tag{A2.9}$$

At leading order, we have for the Rayleigh wave contribution at $K \sim \Omega \gg 1$, and $|\Omega/K - v_R| \ll 1$,

$$A = \frac{v_R^3(2-v_R^2)}{2K(c^2-v_R^2)R'(v_R)} \tag{A2.10}$$

where $c = \Omega/K$, $v_R = c_R/c_2$, and the Rayleigh denominator is given by

$$R(c) = (2-c^2)^2 - 4\sqrt{1-\chi^2c^2}\sqrt{1-c^2}, \tag{A2.11}$$

with prime denoting differentiation with respect to the argument of the Rayleigh denominator.

References

1. Simmonds, J.: Some comments on the status of shell theory at the end of the 20th century-complaints and correctives. In: 38th Structures, Structural Dynamics, and Materials Conference, p. 1074 (1998)
2. Pietraszkiewicz, W.: Finite rotations in shells. Theor. Shells **102**, 5–171 (1980)
3. Makowski, J., Pietraszkiewicz, W.: Work-conjugate boundary conditions in the nonlinear theory of thin shells. J. Appl. Mech. **56**(2), 395–402 (1989)
4. Arash, B., Wang, Q.: A review on the application of nonlocal elastic models in modeling of carbon nanotubes and graphenes. Comput. Mater. Sci. **51**(1), 303–313 (2012)
5. Lu, P., Zhang, P.Q., Lee, H.P., Wang, C.M., Reddy, J.N.: Non-local elastic plate theories. Proc. R. Soc. A **463**(2088), 3225–3240 (2007)
6. Jung, W.Y., Han, S.C.: Nonlocal elasticity theory for transient analysis of higher-order shear deformable nanoscale plates. J. Nanomater. **1** (2014)
7. Sajadi, B., Goosen, H., van Keulen, F.: Capturing the effect of thickness on size-dependent behavior of plates with nonlocal theory. Int. J. Solids Struct. **115**, 140–148 (2017)
8. Chebakov, R., Kaplunov, J., Rogerson, G.A.: A non-local asymptotic theory for thin elastic plates. Proc. R. Soc. A **473**(2203), 20170249 (2017)
9. Strozzi, M., Manevitch, L.I., Pellicano, F., Smirnov, V.V., Shepelev, D.S.: Low-frequency linear vibrations of single-walled carbon nanotubes: analytical and numerical models. J. Sound Vib. **333**(13), 2936–2957 (2014)
10. Kaplunov, J., Manevitch, L.I., Smirnov, V.V.: Vibrations of an elastic cylindrical shell near the lowest cut-off frequency. Proc. R. Soc. A **472**(2189), 20150753 (2016)
11. Kaplunov, J., Prikazchikov, D.A., Prikazchikova, L.A.: Dispersion of elastic waves in a strongly inhomogeneous three-layered plate. Int. J. Solids Struct. **113**, 169–179 (2017)
12. Aßmus, M., Nordmann, J., Naumenko, K., Altenbach, H.: A homogeneous substitute material for the core layer of photovoltaic composite structures. Compos. Part B Eng. **112**, 353–372 (2017)
13. Wang, J., Song, Z., Dai, H.H.: On a consistent finite-strain plate theory for incompressible hyperelastic materials. Int. J. Solids Struct. **78**, 101–109 (2016)

14. Erbaş, B., Kaplunov, J., Nolde, E., Palsü, M.: Composite wave models for elastic plates. Proc. R. Soc. A **474**(2214), 20180103 (2018)
15. Grigolyuk, E.I., Selezov, I.T.: Nonclassical theory of vibration of rods, plates, and shells. Rev. Sci. Technol. **5** (1973)
16. Selezov, I.: Some hyperbolic models for wave propagation. In: Hyperbolic Problems: Theory. Numerics, Applications, pp. 833–842. Birkhäuser, Basel (1999)
17. Selezov, I.T.: Hyperbolic models of wave propagation in rods, plates and shells. Mech. Solids (Izv. RAN, Mekhanika Tverdogo Tela) **29**, 64–77 (1994)
18. Le, K.C.: Vibrations of Shells and Rods. Springer Science & Business Media (2012)
19. Kaplunov, J., Prikazchikov, D.A.: Explicit models for surface, interfacial and edge waves. In: Dynamic Localization Phenomena in Elasticity, Acoustics and Electromagnetism, pp. 73–114. Springer, Vienna (2013)
20. Kaplunov, J., Prikazchikov, D.A.: Asymptotic theory for Rayleigh and Rayleigh-type waves. In: Advances in Applied Mechanics, vol. 50, pp. 1–106. Elsevier (2017)
21. Andrianov, I.V., Awrejcewicz, J., Manevitch, L.I.: Asymptotical Mechanics of Thin-Walled Structures. Springer Science & Business Media (2013)
22. Kaplunov, J.D., Kossovitch, L.Y., Nolde, E.V.: Dynamics of Thin Walled Elastic Bodies. Academic Press (1998)
23. Goldenveizer, A.L.: Theory of Elastic Thin Shells: Solid and Structural Mechanics, vol. 2. Elsevier (2014)
24. Belov, A.V., Kaplunov, J.D., Nolde, E.V.: A refined asymptotic model of fluid-structure interaction in scattering by elastic shells. Flow Turbul. Combust. **61**, 255–267 (1998)
25. Norris, A.N., Rebinsky, D.A.: Acoustic coupling to membrane waves on elastic shells. J. Acoust. Soc. Am. **95**(4), 1809–1829 (1994)
26. Achenbach, J.D.: Wave Propagation in Elastic Solids, vol. 16. Elsevier (2012)

A Beam—Just a Beam in Linear Plane Bending

Reinhold Kienzler and Patrick Schneider

Abstract Starting from the equations of the linear, three-dimensional theory of elasticity, the displacements are expanded into power series in the width- and height-coordinates. By invoking the uniform-approximation method in combination with the pseudo-reduction technique, a hierarchy of beam theories of different orders of approximation is established. The first-order approximation coincides with the classical Euler-Bernoulli beam theory, whereas the second-order approximation delivers a Timoshenko-type of shear-deformable beam theory. Differences and implications are discussed.

Keywords TAYLOR-series expansion · Consistent beam theories · Uniform approximation · Pseudo reduction · EULER-BERNOULLI beam · TIMOSHENKO beam

1 Introduction

Although the title of this book is "Recent Developments in the Theory of **Shells**", we would like to contribute to it with a paper on **beams**, a quite classical problem of structural engineering. The reason is threefold. First, beams are a rather special subgroup of shells as they are one-dimensional shells with curvature zero. Second, beam theory evolves from the three-dimensional theory of elasticity by a dimension-reduction technique as shell and also plate do, too. The number of reduced dimensions, however, is two in the former and one in the later case. Third, the honoree took special interest in our work on plate theories over the years and supported us with his eminent knowledge and valuable advice. Therefore, we would like to dedicate our contribution to our friend Wojciech Pietraszkiewicz.

R. Kienzler (✉)
Bremen Institute for Mechanical Engineering (Bime), University of Bremen, Bremen, Germany
e-mail: rkienzler@uni-bremen.de

P. Schneider
Technische Universität Darmstadt, Institute for Lightweight Construction and Design (KLuB), Darmstadt, Germany
e-mail: patrick.schneider@klub.tu-darmstadt.de

H. Altenbach et al. (eds.), *Recent Developments in the Theory of Shells*,
Advanced Structured Materials 110, https://doi.org/10.1007/978-3-030-17747-8_18

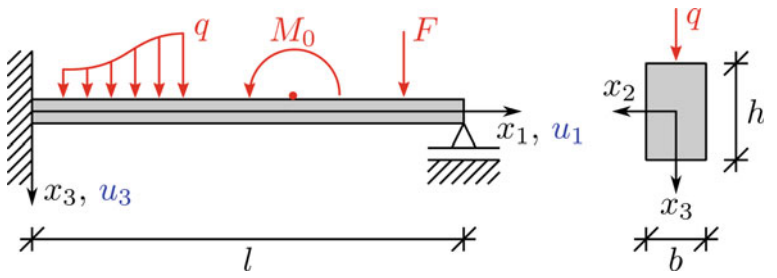

Fig. 1 Beam under distributed load $q(x_1)$, point force F and bending moment M_0 (with rectangular cross section $b \times h$)

Beams are depicted in textbooks on Structural Mechanics as quasi-one-dimensional, somehow supported structural elements loaded by distributed and/or point forces in transversal directions and bending moments (cf. Fig. 1).

The cross sectional dimensions, e.g., height h and width b of rectangular cross-sections, are assumed to be much smaller than the characteristic dimension ℓ in length direction, i.e., $h, b \ll \ell$.

The derivation of the classical, EULER-BERNOULLI beam theory starts with the celebrated kinematical hypotheses: (i) the beam height remains constant during the deformation and the transversal displacement u_3 does not depend on x_3, (ii) plane cross-sections remain plane, i.e., the displacement in length direction u_1 is a linear function in x_3 and constant in x_2, and (iii) cross-cross sections normal to the x_1-axis remain, during bending, normal to the deformed beam axis, which implies no transvers-shear deformations, i.e., shear rigidity is assumed. Further a-priori assumptions are invoked concerning the stress state.

The aim of this contribution is to derive a beam theory form the three-dimensional theory of elasticity without employing any a-priory assumptions.

The first question to be answered is: Under which conditions can the equations of the linear theory of elasticity be applied to describe a beam in plane bending with the transverse displacement in x_3-direction, i.e., bending with respect to the x_2-axis. It turns out that the answer imposes severe restriction on the loading condition, the material law and the geometry of the cross-section.

Let us designate functions which are even (e) or odd (o) in x_2- and in x_3-direction by double indices on the upper right-hand side of the generic symbol, where the first and second index refers to the x_2- and x_3-axis, respectively. Thus $f^{e,o}(x_1, x_2, x_3)$ is an even function in x_2-direction, i.e., $f^{e,o}(x_1, x_2, x_3) = f^{e,o}(x_1, -x_2, x_3)$ and an odd function in x_3-direction, i.e., $f^{e,o}(x_1, x_2, x_3) = -f^{e,o}(x_1, x_2, -x_3)$. Every f has a uniquely determined additive decomposition into four parts as $f(x_1, x_2, x_3) = f^{e,e}(x_1, x_2, x_3) + f^{e,o}(x_1, x_2, x_3) + f^{o,e}(x_1, x_2, x_3) + f^{o,o}(x_1, x_2, x_3)$. It has been shown in [1] that loadings p_i in all three coordinate directions may drive our plane-bending beam problem, as long as the following symmetry/antisymmetry conditions are satisfied

$$p_1 = p_1^{e,o}, \quad p_2 = p_2^{o,o}, \quad p_3 = p_3^{e,e}. \tag{1}$$

One exemplary load distribution for each of the three types $p_1^{e,o}$, $p_2^{o,o}$, $p_3^{e,e}$ is depicted in Fig. 2 for the case of pure boundary tractions, i.e., in the absence of volume forces, for which the same reasoning applies.

Loads in x_3-direction $p_3[N/m^2]$ are the most relevant loading case for engineering applications. In this contribution, we restrict ourselves to the case of tractions that are constant in x_2-direction, applied to the upper and lower beam faces.

Since loads in x_3-direction have to be of type $p_3^{e,e}$, the overall load resultant

$$q(x_1) = \underbrace{\int_{-\frac{b}{2}}^{\frac{b}{2}} \sigma_{33}^*\left(x_1, x_2, +\frac{h}{2}\right) dx_2}_{q^+(x_1)} + \underbrace{\int_{-\frac{b}{2}}^{\frac{b}{2}} \sigma_{33}^*\left(x_1, x_2, -\frac{h}{2}\right) dx_2}_{q^-(x_1)}$$

has to be splitted into a symmetric $q^S = q^{S+} + q^{S-}$ and an anti-symmetric part $q^A = q^{A+} + q^{A-}$ (cf. Fig. 3), where

$$q^{S+} = q^{S-} = \frac{1}{2}(q^+ + q^-),$$
$$q^{A+} = q^{A-} = \frac{1}{2}(q^+ - q^-).$$

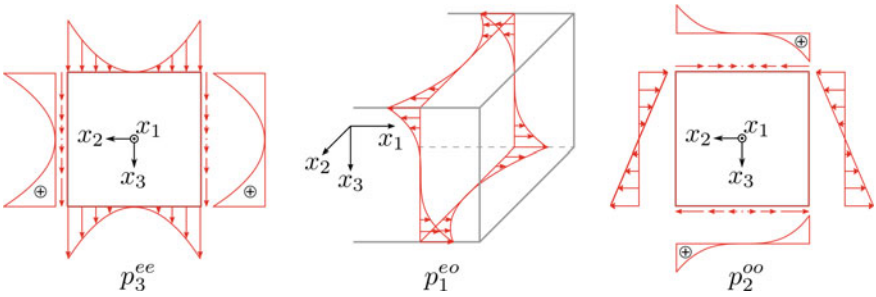

Fig. 2 Exemplary distributions of boundary tractions driving the plane-bending problem

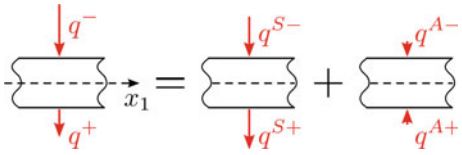

Fig. 3 Splitting of the loads applied to the beam faces $x_3 = \pm h/2$ into symmetric and antisymmetric parts

We see that the classical text-book problem depicted in Fig. 1 is not a pure plane bending problem. While q^S drives the bending problem, q^A which "squeezes" the bar, drives a bar in tension/compression problem. The loading case $q = q^S$ will be treated in the following.

It may be mentioned that loads of the type $p_1^{e,o}$ are represented by the classical distributed bending moments $m(x_1)$ (per unit-length in x_1-direction). However, loads of the type $p_2^{o,o}$ have neither a resulting force nor a resulting moment. One can easily imagine how loads of the type $p_2^{o,o}$ cause "trapezoidal type" cross-section deformations (cf. Fig. 2 right). Beams under bending show cross-section deformation of this type (tension at $x_3 = +h/2$ cause contraction in x_2-direction, compression at $x_3 = -h/2$ cause extension in x_2-direction due to POISSON's ratio and vice versa). Thus loads of the type $p_2^{o,o}$ cause bending.

It has been shown further in [1] that the cross-sectional area has to be double symmetric with respect to the x_2- and x_3-axes in order to arrive at a pure plane bending problem. In addition, the material behavior has to be at least orthotropic with the axes of orthotropy coinciding with the symmetry axes of the cross-section. For simplicity matters, we restrict ourselves further in the following: we consider only surface tractions of the type $q = q^S$, a rectangular cross-section $b \times h$ and isotropic material behavior.

The such defined problem may be studied by a variety of methods. One may interpret it as a general Almansi-Michell problem [2, 3] and study it in the sense of Saint-Venant solutions [4]. Alternatively, one may treat it by means of an asymptotic analysis in the classical sense (as introduced by Ciarlet and Destuynder [5]), or by the method of Γ-convergence (cf. Giorgi [6]), as recently done by Friesecke et al. for plates [7], in order to derive the leading-order approximation. A further approach uses series expansions of the displacements and studies problems arising from a truncation approach, for example by starting with a truncated series expansion, which leads to a Vekua-type hierarchy [8] of approximation theories. Alternatively, one may truncate the elastic energy. An approach leading to a constrained theory was proposed by Steigmann [9] and recently expanded towards refined theories by Pruchnicki [10]. For shell theories, the authors used the so-called consistent approximation, which originates from treatises by Naghdi [11], Koiter [12], Krätzig [13] and Kienzler [14]. It was specialized to plate theories by Kienzler [15] and expanded towards refined theories in [16] and [17]. The analysis in the sense of this approach is presented in the following for beams.

In Sect. 2, we present the elements of the consistent approximation for a beam. In Sects. 3 and 4, the resulting theories for the first- and second-order approximation are discussed, respectively. Some concluding remarks are given in the final Sect. 5.

2 Consistent Approximation

2.1 TAYLOR-*Series Expansion*

We introduce dimensionless coordinates $\xi_i = x_i \big/ \ell$ (i = 1, 2, 3) and employ TAYLOR-series expansions of the displacement field $u_i(\xi_1)$

$$u_i = \ell \sum_{m=0}^{\infty} \sum_{p=0}^{\infty} {}^{mp}u_i(\xi_1)\ \xi_2^m \xi_3^p. \tag{1}$$

The dimensionless coefficients ${}^{mp}u_i(\xi_1)$ are the unknowns of our problem. From the linearized kinematical relations

$$\varepsilon_{ij} = \frac{1}{2}(u_{i,j} + u_{j,i}), \tag{2}$$

the respective strain coefficients

$$\varepsilon_{ij} = \sum_{m=0}^{\infty} \sum_{p=0}^{\infty} {}^{mp}\varepsilon_{ij}(\xi_1)\ \xi_2^m \xi_3^p \tag{3}$$

are obtained by comparing equal coefficients. We compile the strain-energy density W

$$W = \frac{1}{2} E_{ijk\ell} \varepsilon_{ij} \varepsilon_{k\ell}$$

(fourth-order tensor of elasticity $E_{ijk\ell}$, summation over repeated indices) and integrate over the cross-sectional area A to obtain the strain-energy $\overline{W}$ per unit of length

$$\overline{W} = \frac{1}{2} \int_A E_{ijk\ell} \varepsilon_{ij} \varepsilon_{k\ell} dA = \overline{W}\big({}^{mp}u_i(\xi_1), {}^{mp}u_{i,1}(\xi_1)\big) \tag{4}$$

as a function of the dimensionless unknown displacement coefficients ${}^{mp}u_i(\xi_1)$ and their gradients ${}^{mp}u_{i,1} = {}^{mp}u_i'(\xi_1)$. Due to integration over the rectangular cross-section $b \times h$ the "smallness" parameters

$$c^2 = \frac{h^2}{12\ell^2}, \quad d^2 = \frac{b^2}{12\ell^2}, \quad e^2 = c^2, d^2 \tag{5}$$

appear quite naturally and we have

$$\ell^2 \int_{-\frac{h}{2\ell}}^{+\frac{h}{2\ell}} \int_{-\frac{b}{2\ell}}^{+\frac{b}{2\ell}} f(\xi_1)\xi_2^m \xi_3^p d\xi_3 = f(\xi_1)A \begin{cases} 0 & \text{for } m \text{ or } p \text{ odd} \\ 1 & \text{for } m=0,\ p=0, \\ d^2 & \text{for } m=2,\ p=0, \\ c^2 & \text{for } m=0,\ p=2, \\ \frac{9}{5}d^4 & \text{for } m=4,\ p=0, \\ c^2d^2 & \text{for } m=2,\ p=2, \\ \frac{9}{5}c^4 & \text{for } m=0,\ p=4, \\ \vdots & \end{cases} \tag{6}$$

Thus $\overline{W}$ appears as power-series expansion in the squares of the beam parameters. Adopting the shear modulus as characteristic parameter of our isotropic material, we have

$$\begin{aligned} \overline{W} = GA[&(\bullet)1 + (\bullet)\,c^2 + (\bullet)d^2 + (\bullet)c^4 \\ &+ (\bullet)c^2d^2 + (\bullet)d^4 + O\,(e^6)\big]. \end{aligned} \tag{7}$$

Similarly, we obtain for the potential of external forces $\bar{V}$ per unit of length for the special loading case $q = q^{S-} + q^{S+}$ considered here

$$\overline{V} = -\ell \left[\int_{-\frac{b}{2\ell}}^{+\frac{b}{2\ell}} \sigma_{33}^* u_3 d\xi_2 \right] \Bigg|_{\xi_3=-\frac{h}{2\ell}}^{\xi_3=+\frac{h}{2\ell}} = q\ell\big[(\bullet)1 + (\bullet)c^2 + (\bullet)d^2 + O(e^4)\big]. \tag{8}$$

The symbols (•) comprise terms of approximately equal order and are related to the ansatz coefficients and their derivatives. The elastic potential Π

$$\Pi = \ell \int_0^1 \overline{W} + \overline{V} d\xi_1 \tag{9}$$

has thus the same appearance and the variational problem

$$\delta\,\Pi = 0 \tag{10}$$

delivers the EULER-LAGRANGE equations and the stress-boundary conditions (BC). The EULER-LAGRANGE equations, or NAVIER-LAMÉ equations obtained by varying with respect to the TAYLOR-series coefficients of the virtual displacements δu are given as second-order ordinary differential equations (ODE) system in the unknown functions ${}^{mp}u_i(\xi_1)$.It has been shown in [17] that the ODE system in combination with the BC are completely equivalent to the three-dimensional problem, if infinitely

many unknowns are considered. It has further been shown, that the ODE system decouples (also in the boundary conditions) into a:

– rod problem (tension-compression),
– shaft problem (torsion),
– beam problem (bending w.r.t. the ξ_3-axis),
– beam problem (bending w.r.t. the ξ_2-axis).

The latter is the problem of our further considerations, as already sketched in the introduction. The power-law expansion for our bending problem involves coefficients of the following types

$$\begin{aligned} u_1 &= \ell({}^{01}u_1\xi_3 + {}^{03}u_1\xi_3^3 + {}^{21}u_1\xi_2^2\xi_3 + {}^{05}u_1\xi_3^5 \\ &\quad + {}^{23}u_1\xi_2^2\xi_3^3 + {}^{41}u_1\xi_2^4\xi_3 + \ldots), \\ u_2 &= \ell({}^{11}u_2\xi_2\xi_3 + {}^{13}u_2\xi_2\xi_3^3 + {}^{31}u_2\xi_2^3\xi_3 + \ldots), \\ u_3 &= \ell({}^{00}u_3 + {}^{20}u_3\xi_2^2 + {}^{02}u_3\xi_3^2 + {}^{40}u_3\xi_2^4 \\ &\quad + {}^{22}u_3\xi_2^2\xi_3^2 + {}^{04}u_3\xi_3^4 + \ldots), \end{aligned} \tag{11}$$

which have to be calculated from the ODE system. (All other coefficients belong to other sub problems).

2.2 Uniform-Approximation Method

The resulting infinite system of equations, however, is intractable in praxis. The question, therefore, arises where and how to truncate the series expansion. The consistent uniform-approximation method, now, follows the concept that all governing equations of the linear theory of elasticity are approximated to the same degree (order N). This is accomplished by retaining all terms containing factors $d^{2m}c^{2p}$ with $2(m+p) \leq N$ and neglecting all terms with factors of higher order, which we denote by the symbol $O(e^{2(N+1)})$ in the elastic potential. The ODE system of the Nth order approximation of our beam problem involves $(N+1)(3N+4)/2$ differential equations for the same number of unknowns. In this contribution, we concentrate on the zeroth- and first-order approximation and communicate merely results of the second-order approximation. Details of the second-order approximation may be found in the PhD-thesis of Schneider [18] and will be published in a forth-coming paper.

2.3 Pseudo-Reduction Technique

Since the ODE system arising from the uniform-approximation method is linear in the derivatives of the TAYLOR coefficients of the displacements, cf. (19), one is tempted to eliminate all but one, the so-called main variable, from the system by successive insertion of the equations into each other, similar to the basic methods of Linear Algebra. This results in a single higher-order main ODE (which is to be solved) in only the main variable and a set of reduction equations (which express all other displacement coefficients in terms of the main variable). However, special considerations are required, since we are dealing with a truncated power series. All equations are accurate but terms of order $O(e^{2(N+1)})$ and this degree of accuracy is to be preserved by the reduction procedure. Therefore, the factors c^2 and d^2, or, in common, e^2, cannot be treated like normal factors. E.g., division by the factor e^2 would require to calculate the terms with prefactor $e^{2(N+1)}$ in advance. It turns out as most convenient to regard the same displacements multiplied by different powers of e formally as independent variables, e.g., ${}^{oo}u_3$ and $e^{2oo}u_3$. This special pseudo-reduction procedure was introduced and discussed in detail in [19] and has been successfully applied to derive consistent plate theories, cf., e.g., [17, 20–22]. As result, the reduced ODE system (main differential equation and reduction differential equations) and the original one are equivalent despite terms of the order $O(e^{2(N+1)})$.

2.4 Stress and Load Resultants, Equilibrium Conditions

Stress resultants may be either introduced via constitutive relations

$$ {}^{mp}m_{ij}(\xi_1) = \ell^{m+p} \frac{\partial \overline{W}}{\partial\, {}^{mp}\varepsilon_{ij}}, \tag{12} $$

or directly, via integration of moments of the stresses over the cross-sectional area

$$ {}^{mp}m_{ij}(\xi_1) = \ell^{m+p+2} \int_A \sigma_{ij} \xi_2^m \xi_3^p \, d\xi_2 d\xi_3. \tag{13} $$

Similarly, the load resultants follow from

$$ {}^{mp}q_i = -\ell^{m+p-1} \frac{\partial \overline{V}}{\partial^{mp} u_i}, \tag{14} $$

or by integration of the loading-force density over the cross-section under consideration of the tractions along the beam faces $\xi_2 = \pm b/(2\ell), \xi_3 = \pm h/(2\ell)$, $\xi_3 = \pm 1 \big/ 2h \big/ \ell$.

For the here treated load, we simply obtain

$$\begin{aligned} {}^{00}q_3 &= q(\xi_1), \\ {}^{20}q_3 &= \ell^2 d^2 {}^{200}q_3 = \ell^2 d^2 q, \\ {}^{02}q_3 &= \ell^2 3c^2 {}^{200}q_3 = \ell^2 3c^2 q, \\ &\dots \end{aligned} \tag{15}$$

The stress resultants of our plane beam-bending problem are [18]

$$\begin{aligned} m_{11}^{e,o} &: {}^{01}m_{11},\ {}^{21}m_{11},\ {}^{03}m_{11},\ {}^{41}m_{11},\ {}^{23}m_{11},\ {}^{05}m_{11},\ \dots, \\ m_{12}^{o,o} &: {}^{11}m_{12},\ {}^{31}m_{12},\ {}^{13}m_{12},\ \dots, \\ m_{13}^{e,e} &: {}^{00}m_{13},\ {}^{20}m_{13},\ {}^{02}m_{13},\ {}^{40}m_{13},\ {}^{22}m_{13},\ {}^{04}m_{13},\ \dots, \\ m_{22}^{e,o} &: {}^{01}m_{22},\ {}^{21}m_{22},\ {}^{03}m_{22},\ \dots, \\ m_{23}^{o,e} &: {}^{10}m_{23},\ {}^{30}m_{23},\ {}^{12}m_{23},\ \dots, \\ m_{33}^{e,o} &: {}^{01}m_{33},\ {}^{21}m_{33},\ {}^{03}m_{33},\ \dots \end{aligned} \tag{16}$$

The equilibrium equations written in stress resultants follow from the variational principle or, directly, by multiplying the three-dimensional equilibrium equations by $\xi_2^m\, \xi_3^p$ and integration over the cross-section.

As an example, we write down the set of equilibrium equations involving stress and load resultants of the first-order approximation

$$\begin{aligned} \frac{1}{\ell}{}^{00}m'_{13} &= -q, \\ \frac{1}{\ell}{}^{01}m'_{11} - {}^{00}m_{13} &= 0, \\ \frac{1}{\ell}{}^{11}m'_{12} - {}^{01}m_{22} - {}^{10}m_{23} &= 0, \\ \frac{1}{\ell}{}^{02}m'_{13} - 2{}^{01}m_{33} &= -\ell^2 d^2 q, \\ \frac{1}{\ell}{}^{20}m'_{13} - 2{}^{10}m_{23} &= -3\ell^2 c^2 q, \\ \frac{1}{\ell}{}^{03}m'_{11} - 3{}^{02}m_{13} &= 0, \\ \frac{1}{\ell}{}^{21}m'_{11} - 2{}^{11}m_{12} - {}^{20}m_{13} &= 0. \end{aligned} \tag{17}$$

The complete, i.e., infinite equation system, the equations of a second-order approximation, as well as the appropriate boundary conditions are given in [18].

The ODE system for the unknown functions ${}^{mp}u_i(\xi_1)$ are the EULER-LAGRANGE equations of our variational problem that coincide with the equilibrium Eq. (17) after expression of the stresses via HOOKE's law by the strains (3) and replacing the strains via the kinematic relations (2).

3 First-Order Approximation

3.1 ODE System

The first-order approximation involves seven unknown displacement functions

$$ {}^{00}u_3,\ {}^{01}u_1,\ {}^{11}u_2,\ {}^{02}u_3,\ {}^{20}u_3,\ {}^{03}u_1,\ {}^{21}u_1. \tag{18} $$

The displacement quantities are illustrated in Fig. 4

These quantities have to fulfil the following ODE system. With POISSON's ratio ν, the shear modulus G (YOUNG's modulus E with $G = E/(2(1+\nu))$) and the abbreviations

$$ \alpha = 2\frac{1-\nu}{1-2\nu}, \quad \beta = \frac{2\nu}{1-2\nu} \tag{19} $$

we find

	${}^{00}u_3$	${}^{01}u_1$	${}^{11}u_2$	${}^{02}u_3$	${}^{20}u_3$	${}^{03}u_1$	${}^{21}u_1$	RHS
$\delta\,{}^{00}u_3:$	$(\cdot)^{//}$	$(\cdot)^{/}$	0	$c^2(\cdot)^{//}$	$d^2(\cdot)^{//}$	$3c^2(\cdot)^{/}$	$d^2(\cdot)^{/}$	$-\frac{q\ell}{GA}$
$\delta\,{}^{01}u_1:$	$(\cdot)^{/}$	$(\cdot)-\alpha c^2(\cdot)^{//}$	$-\beta c^2(\cdot)^{/}$	$(1-2\beta)c^2(\cdot)^{/}$	$d^2(\cdot)^{/}$	$3c^2(\cdot)$	$d^2(\cdot)$	0
$\delta\,{}^{11}u_2:$	0	$-\beta c^2(\cdot)^{/}$	$-(\alpha c^2+d^2)(\cdot)$	$-2\beta c^2(\cdot)$	$-2d^2(\cdot)$	0	0	0
$\delta\,{}^{02}u_3:$	$c^2(\cdot)^{//}$	$(1-2\beta)c^2(\cdot)^{/}$	$-2\beta c^2(\cdot)$	$-4\alpha c^2(\cdot)$	0	0	0	$-\frac{3c^2q\ell}{GA}$
$\delta\,{}^{20}u_3:$	$d^2(\cdot)^{//}$	$d^2(\cdot)^{/}$	$-2d^2(\cdot)$	0	$-4d^2(\cdot)$	0	0	$-\frac{d^2q\ell}{GA}$
$\delta\,{}^{03}u_1:$	$3c^2(\cdot)^{/}$	$3c^2(\cdot)$	0	0	0	0	0	0
$\delta\,{}^{21}u_1:$	$d^2(\cdot)^{/}$	$d^2(\cdot)$	0	0	0	0	0	0

3.2 Zeroth-Order Approximation

We obtain the ODE-system of the zeroth-order approximation by neglecting all terms in (19) which are multiplied by c^2 or d^2, i.e., e^2. Thus

$$ \begin{aligned} {}^{00}u_3'' + {}^{01}u_1' + O(e^2) &= -\frac{q\ell}{GA}, \\ {}^{00}u_3' + {}^{01}u_1 + O(e^2) &= 0. \end{aligned} \tag{20} $$

This leads to the conclusion that

$$ \frac{q\ell}{GA} = O(e^2). \tag{21} $$

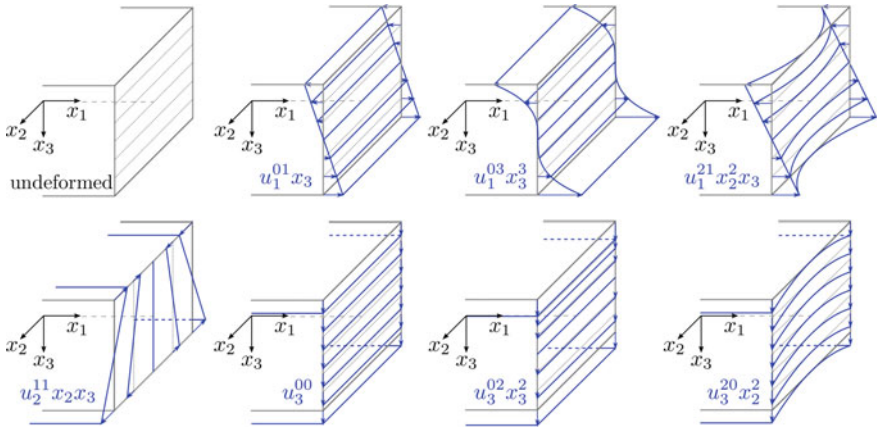

Fig. 4 Displacement quantities involved in the first-order approximation of the plane-bending problem

In turn it follows (19 d, e)

$$\frac{3c^2 q\ell}{GA}, \frac{d^2 q\ell}{GA} = O(e^4), \tag{22}$$

i.e., the right-hand sides of (19 d and e) are to be neglected in the first-order approximation in accordance to (15).

The solutions of (20) are rigid-body motions

$$\begin{aligned} {}^{01}u_1 &= \psi_0, \\ & \quad w_0, \psi_0 = \text{const.}, \\ {}^{00}u_3 &= w_0 - \psi_0 \xi_1, \end{aligned} \tag{23}$$

and the stress resultants are of the order

$${}^{mp}m_{ij} = O(e^2) \quad \text{for all} \quad i, j, m, p \tag{24}$$

as well.

3.3 Pseudo Reduction

For convenience we introduce the description

$$\begin{aligned} w &:= {}^{00}u_3(\xi_1), \\ \psi &:= {}^{01}u_1(\xi_1), \end{aligned} \tag{25}$$

With w, the transverse displacement of the central axis of the beam is designated, whereas the slope of the beam's cross-section is ψ. Both are the classical variables of beams in plane bending. The transverse load q is restricted by the symmetry condition $q = q^{S+} + q^{S-}$, cf. Fig. 3.

Pseudo reduction (cf. [19]) leads to the reduction ODEs

$$\begin{aligned}
&e^2\psi = -e^2 w' + O(e^4),\\
&e^2\,{}^{11}u_2 = \nu e^2 w'' + O(e^4),\\
&e^2\,{}^{02}u_3 = \frac{\nu}{2} e^2 w'' + O(e^4),\\
&e^2\,{}^{20}u_3 = -\frac{\nu}{2} e^2 w'' + O(e^4),\\
&w' + \psi + c^2\,{}^{02}u_3' + d^2\,{}^{20}u_3' + 3c^2\,{}^{03}u_1 + d^2\,{}^{21}u_1 = -2(1+\nu)c^2 w''' + O(e^4)
\end{aligned} \tag{26}$$

and to the main ODE

$$\frac{EI}{\ell^3} w'^{V} = q + O(e^4) \tag{27}$$

with the bending stiffness

$$EI = \frac{Ebh^3}{12}. \tag{28}$$

Equation (27) is the governing differential equation of the classical EULER-BERNOULLI-beam theory!

Insertion of the reduction equations into the displacement ansatz yields

$$\begin{aligned}
u_1 &= \ell\xi_3\big(\psi + {}^{21}u_1\xi_2^2 + {}^{03}u_1\xi_3^2 + O(e^4)\big),\\
u_2 &= \ell\big[\nu\xi_2\xi_3 w'' + O(e^4)\big],\\
u_3 &= \ell\Big[w - \frac{\nu}{2}\xi_2^2 w'' + \frac{\nu}{2}\xi_3^2 w'' + O(e^4)\Big],
\end{aligned} \tag{29}$$

and the remaining reduction ODE (26.e)

$$w' + \psi = -c^2\left(\frac{4+5\nu}{2} w''' + 3\,{}^{03}u_1\right) + d^2\left(\frac{\nu}{2} w''' - {}^{21}u_1\right) + O(e^4). \tag{30}$$

The designation $O(e^4)$ is used also in (29) because $-b/(2\ell) \le \xi_2 \le +b/(2\ell)$ and $-h/(2\ell) < \xi_3 < +h/(2\ell)$. Thus $\xi_2^m \xi_3^p \sim e^{m+p}$.

The displacement coefficients ${}^{03}u_1$ and ${}^{21}u_1$ remain undetermined by the reduction ODEs. They may be chosen arbitrarily, e.g., set to zero, or may be determined either by boundary conditions for the stress state or by equations of a higher-order

(here: second-order) approximation. By using the freedom of choosing those coefficients a posteriori, the governing differential equations are not changed. Anyway, the celebrated normal hypothesis $\psi = -w'$ is not applicable since its deviation is

$$w' + \psi = O(e^2) \tag{31}$$

and has to be considered within a first-order approximation, whereas

$$e^2(w' + \psi) = 0 + O(e^4). \tag{32}$$

For this reason ψ may not be replaced by $-w'$ in (29.a). From (29.c), it follows that the transverse displacement u_3 is not constant, neither in ξ_2- nor in ξ_3-direction, i.e., the transverse strain ε_{33} is not zero, it rather is

$$\varepsilon_{33} = \nu w''\xi_3 + O(e^4). \tag{33}$$

Due to ${}^{03}u_1$ and ${}^{21}u_1$, cross-sections do not remain plane (cf. Fig. 4). If we set ${}^{03}u_1 = {}^{21}u_1 = 0$ for a moment, the extensional strain in length direction becomes

$$\varepsilon_{11} = \psi'\xi_3. \tag{34}$$

With

$$\varepsilon_{22} = \nu w''\xi_3 \tag{35}$$

we see that the out-of-bending-plane stress σ_{22} is

$$\begin{aligned}\sigma_{22} &= \frac{E}{(1+\nu)(1-2\nu)}(\nu\varepsilon_{11} + (1-\nu)\varepsilon_{22} + \nu\varepsilon_{33}) \\ &= \frac{E\xi_3}{(1+\nu)(1-2\nu)}\big(0 + O(e^2)\big),\end{aligned} \tag{36}$$

i.e., we have plane-stress conditions in the (x_1, x_3) bending plane but not a one-dimensional stress state!

3.4 Stress Resultants and Boundary Conditions

Within the first-order theory only two stress resultants remain whereas all others are of order $O(e^4)$. They are the classical bending moment M and the transverse shear force Q

$$M := {}^{01}m_{11} = -\frac{EI}{\ell}w'' + O(e^4),$$
$$Q := {}^{00}m_{13} = -\frac{EI}{\ell^2}w''' + O(e^4),$$
$${}^{mp}m_{ij} = 0 + O(e^4) \text{ else.} \tag{37}$$

The relevant boundary conditions follow to be

$$M = M^* \text{ or } \quad w' = w'^*,$$
$$Q = Q^* \text{ or } \quad w = w^*, \tag{38}$$

with stared quantities prescribed, i.e., given data at the boundaries

$$\xi_1 = 0, 1.$$

In conclusion it may be mentioned that the classical EULER-BERNOULLI beam theory is a consistent first-order approximation of the three-dimensional equations of linear elasticity. The usually introduced a-priori assumptions are not employed but rather disproved.

3.5 Extended Deformation Ansatz

Expansion coefficients not fixed by the reduction equations can be used a posteriori to fulfill boundary conditions along the beam faces $\xi_2 = \pm b \big/ (2\ell)$ and $\xi_3 = \pm h \big/ (2\ell)$, and the local equilibrium conditions written in stresses

$$\sigma_{ij,i} = 0. \tag{39}$$

The analysis is quite involved and will be dealt with in detail in a forthcoming paper. Here we merely sketch some results. As it turns out, the first-order approximation for a beam in plane bending is governed by the generalized plane-stress state in the (x_1, x_3)-plane. Therefore, we have to introduce average quantities for the displacements and stresses by integrating over the ξ_2 coordinate

$$\tilde{u}_i(\xi_1, \xi_3) = \frac{\ell}{b} \int_{-\frac{b}{2\ell}}^{+\frac{b}{2\ell}} u_i(\xi_1, \xi_2, \xi_3) d\xi_2,$$
$$\tilde{\sigma}_{ij}(\xi_1, \xi_3) = \frac{\ell}{b} \int_{-\frac{b}{2\ell}}^{+\frac{b}{2\ell}} \sigma_{ij}(\xi_1, \xi_2, \xi_3) d\xi_2. \tag{40}$$

Finally we find for the displacements

$$\begin{aligned}
\tilde{u}_1 &= \ell\xi_3\left\{-w' + \left[-3(1+\nu)c^2 + \frac{1}{2}\nu d^2 + \frac{1}{6}(2+\nu)\xi_3^2\right]w'''\right\} + \ell O(e^5),\\
\tilde{u}_2 &= 0,\\
\tilde{u}_3 &= \ell\left\{w + \frac{1}{2}\nu\left[\xi_3^2 - d^2\right]w''\right.\\
&\quad\left. + \left[-\frac{1}{24}(1+\nu)\xi_3^4 + \left(\frac{3}{4}(1+\nu)^2c^2 - \frac{1}{4}\nu^2d^2\right)\xi_3^2 + c^4A_1\right]w^{IV} + O(e^6)\right\}
\end{aligned} \tag{41}$$

and for the stresses

$$\begin{aligned}
\tilde{\sigma}_{11} &= -E\left[w''\xi_3 + O(e^3)\right],\\
\tilde{\sigma}_{22} &= E\left[0 + O(e^5)\right],\\
\tilde{\sigma}_{33} &= \frac{1}{6}E\left[w^{IV}\xi_3(9c^2 - \xi_3^2) + O(e^5)\right],\\
\tilde{\sigma}_{23} &= E\left[0 + O(e^5)\right],\\
\tilde{\sigma}_{31} &= -\frac{1}{2}E\left[w'''(3c^2 - \xi_3^2) + O(e^4)\right],\\
\tilde{\sigma}_{12} &= E\left[0 + O(e^5)\right].
\end{aligned} \tag{42}$$

The stress resultants (37) and the boundary conditions at $\xi_1 = 0, 1$ (38) do not change.

We see that the transverse displacements $\tilde{u}_3$ are variable in ξ_3 direction and the strain $\tilde{\varepsilon}_{33}$ is not zero. The constant A_1 has no influence on the stress distribution within the order of magnitude estimate indicated in (42). It can be chosen to coincide with an analytical solution of a three-dimensional beam-like problem available eventually. The longitudinal displacement $\tilde{u}_1$ is not linear, i.e., plane cross-sections do not remain plane during bending and, finally, the normal hypotheses $\tilde{u}_1 = \tilde{u}_3'$ is not satisfied. Thus shear strains and stresses occur. In summary, the celebrated kinematical a-priori hypotheses are not satisfied. Instead, the boundary conditions along the beam faces, cf. Fig. 5, are satisfied.

$$\begin{aligned}
\sigma_{21}|_{\xi_2=\pm\frac{b}{2\ell}} &= 0 + O(e^4)\\
\sigma_{22}|_{\xi_2\pm\frac{b}{2\ell}} &= 0 + O(e^5)\\
\sigma_{23}|_{\xi_2\pm\frac{b}{2\ell}} &= 0 + O(e^5)
\end{aligned} \tag{43}$$

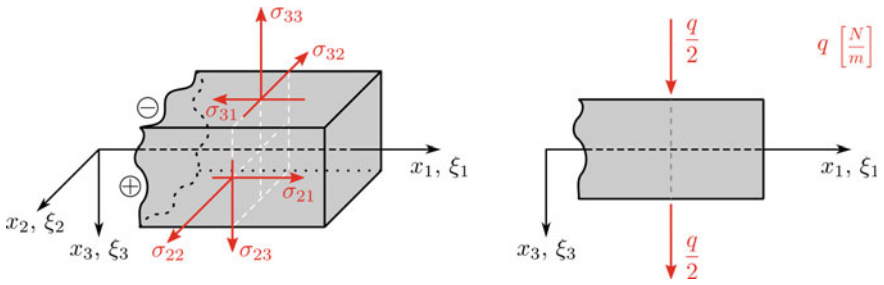

Fig. 5 Boundary conditions along the beam faces $\xi_2 = \pm\frac{b}{2\ell}, \xi_3 = \pm\frac{h}{2\ell}$

$$\begin{aligned}
\sigma_{31}|_{\xi_3=\pm\frac{h}{2\ell}} &= 0 + O(e^4) \\
\sigma_{32}|_{\xi_3=\pm\frac{h}{2\ell}} &= 0 + O(e^5) \\
\sigma_{33}|_{\xi_3=\pm\frac{h}{2\ell}} &= \pm\frac{q}{2b} + O(e^5)
\end{aligned}$$

It may be mentioned that the parabolic distribution of $\tilde{\sigma}_{13}$ (42.c) is the celebrated "Dübel" formula. The stresses $\tilde{\sigma}_{11}$ resemble the classical linear stress distribution of plane bending. With (41) the stress distribution can be consistently extended to

$$\tilde{\sigma}_{11} = -E\xi^3\left[w'' + \frac{1}{6}\left(9(2+\nu)c^2 + 2\xi_3^2\right)w^{IV}\right] + O(e^5). \tag{44}$$

The local equilibrium equations, however, only involve the term (42.a). With (42), we see

$$\begin{aligned}
\tilde{\sigma}_{11,1} + \tilde{\sigma}_{21,2} + \tilde{\sigma}_{31,3} &= 0 + O(e^3), \\
\tilde{\sigma}_{12,1} + \tilde{\sigma}_{22,2} + \tilde{\sigma}_{32,3} &= 0 + O(e^4), \\
\tilde{\sigma}_{13,1} + \tilde{\sigma}_{23,2} + \tilde{\sigma}_{33,3} &= 0 + O(e^4).
\end{aligned} \tag{45}$$

The results confirm the consistent-approximation technique for the first-order approximation.

4 Second-Order Approximation

The second order approximation involves 15 displacement coefficients. The displacement ansatz is

$$
\begin{aligned}
u_1 &= \ell\big({}^{01}u_1\xi_3 + {}^{21}u_1\xi_2^2\xi_3 + {}^{03}u_1\xi^3 + {}^{41}u_1\xi_2^4\xi_3 + {}^{23}u_1\xi_2^2\xi_3^3 + {}^{05}u_1\xi_3^5 + O(e^7)\big)\\
u_2 &= \ell\big({}^{11}u_2\xi_2\xi_3 + {}^{31}u_1\xi_2^3\xi_2 + {}^{13}u\xi_2\xi_3^3 + O(e^6)\big)\\
u_3 &= \ell\big({}^{00}u_3 + {}^{20}u_3\xi_2^2 + {}^{02}u_3\xi_3^2 + {}^{40}u_3\xi_2^4 + {}^{22}u_3\xi_2^2\xi_3^2 + {}^{04}u_3\xi_3^4 + O(e^6)\big). \qquad (46)
\end{aligned}
$$

The ansatz coefficients are governed by 15 ODEs. The pseudo-reduction technique (details may be found in SCHNEIDER [18] and in a forth-coming paper) delivers a TIMOSHENKO-type beam differential equation in the form

$$
\begin{aligned}
\frac{EI}{\ell^3}w^{IV} = q + \Bigg(&-\frac{5}{10}(8+5\nu)c^2 - \frac{1}{2}\nu d^2\\
&+ \frac{2\nu^2}{1+\nu}\frac{d^4}{d^2 5c^2}\Bigg)q'' + O(c^6). \qquad (47)
\end{aligned}
$$

In addition to the classical stress resultants, bending moment $M := {}^{01}m_{11}$ and transverse shear force $Q := {}^{00}m_{13}$, higher-order stress-resultants have to be considered. From pseudo reduction, however, it follows that they are expressible either by M and Q, or by the given external load q. As can be found in [18], we have

$$
\begin{aligned}
{}^{03}m_{11} &= \frac{9}{5}c^2\ell^2 M + O(e^6),\\
{}^{21}m_{11} &= d^2\ell^2 M + O(e^6),\\
{}^{mp}m_{11} &= 0 + O(e^6) \text{ for } m+p > 3,\\
{}^{11}m_{12} &= -\frac{\nu}{1+\nu}d^2\ell^2\frac{d^2}{5c^2+d^2}Q + O(e^6),\\
{}^{mp}m_{12} &= 0 + O(e^6) \text{ for } m+p > 2,\\
{}^{20}m_{13} &= d^2\ell^2\left(1 + \frac{2\nu}{1+\nu}\frac{d^2}{5c^2+d^2}\right)Q + O(e^6),\\
{}^{02}m_{13} &= \frac{3}{5}c^2\ell^2 Q + O(e^6),\\
{}^{mp}m_{13} &= 0 + O(e^6) \text{ for } m+p > 2,\\
{}^{01}m_{22} &= \frac{2\nu}{1+\nu}\frac{d^4\ell^2 q}{5c^2+d^2} + O(e^6),\\
{}^{mp}m_{22} &= 0 + O(e^6) \text{ for } m+p > 1,\\
{}^{10}m_{23} &= -\frac{\nu}{1+\nu}\frac{d^4\ell^2 q}{5c^2+d^2} + O(e^6),\\
{}^{mp}m_{23} &= 0 + O(e^6) \text{ for } m+p > 1,\\
{}^{01}m_{33} &= \frac{6}{5}c^2\ell^2 q + O(e^6),\\
{}^{mp}m_{33} &= 0 + O(e^6) \text{ for } m+p > 1. \qquad (48)
\end{aligned}
$$

In extension to Reissner's approach [23, 24] we introduce energetic averages of the transverse displacement w and the slope ψ as $\tilde{w}$ and $\tilde{\psi}$, respectively, as

$$\frac{1}{2}\ell Q\tilde{w} + \frac{1}{2}M\tilde{\psi} = \frac{\ell^2}{2}\int_{-\frac{b}{2\ell}}^{+\frac{b}{2\ell}}\int_{-\frac{h}{2\ell}}^{+\frac{h}{2\ell}} \sigma_{11}u_1 + \sigma_{12}u_2 + \sigma_{13}u_3 d\xi_2 d\xi_3. \tag{49}$$

With (13), (46), (48) and (26) we find

$$\begin{aligned}\tilde{w} &= w + vw''\left(\frac{3}{10}c^2 - \frac{1}{2}d^2 - 2\frac{v}{1+v}d^2\frac{d^2}{5c^2+d^2}\right) + O(e^4),\\ \tilde{\psi} &= -w' - w'''\left(\frac{3}{10}(8+9v)c^2 - \frac{1}{2}vd^2\right) + O(e^4).\end{aligned} \tag{50}$$

With it, the beam differential Eq. (47) transforms to

$$\frac{EI}{\ell^3}\tilde{w}^{IV} = q - \frac{6}{5}c^2(2+v)q'' + O(e^6), \tag{51}$$

and the classical stress resultants read

$$\begin{aligned}M &= -\frac{EI}{\ell}\tilde{w}'' - \frac{6}{5}(2+v)c^2\ell^2 q,\\ Q &= -\frac{EI}{\ell^2}\tilde{w}''' - \frac{6}{5}(2+v)c^2\ell q'.\end{aligned} \tag{52}$$

The boundary conditions follow to be

$$\begin{aligned}M = M^* \text{ or } \tilde{\psi} = \psi^*,\\ Q = Q^* \text{ or } \tilde{w} = \tilde{w}^*,\end{aligned} \tag{53}$$

where, again stared quantities are prescribed data at the boundaries $\xi_1 = 0, 1$.

The equilibrium conditions of the second-order approximation may be taken, after pseudo reduction, from (17) (cf. [18] for more details)

$$\begin{aligned}&\tfrac{1}{\ell}Q' = -q,\\ &\tfrac{1}{\ell}M' - Q = 0,\\ &\tfrac{1}{\ell}{}^{11}m'_{12} - {}^{01}m_{22} - {}^{10}m_{23} = 0,\\ &\tfrac{1}{\ell}{}^{02}m'_{13} - 2{}^{01}m_{33} = -3c^2\ell^2 q,\\ &\tfrac{1}{\ell}{}^{20}m'_{13} - 2{}^{10}m_{23} = -d^2\ell^2 q,\\ &\tfrac{1}{\ell}{}^{03}m'_{11} - 3{}^{02}m_{13} = 0,\\ &\tfrac{1}{\ell}{}^{21}m'_{11} - 2{}^{11}m_{12} - {}^{20}m_{13} = 0,\\ &\quad \ldots\, O(e^6).\end{aligned} \tag{54}$$

With (48) and (52), it can be seen that the Eqs. (54.b-g) are identically satisfied, whereas (54.a) delivers (51).

So, we have established a consistent second-order approximation of the three-dimensional equations of elasticity without invoking any a priori assumptions.

The factor $6/5$ in (51) reminds us of Timoshenko' shear-correction factor $1/\kappa$. It is interesting to note that

$$\kappa = \frac{5}{6} \tag{55}$$

may not be found in Timoshenko's original contributions [25, 26] (he used rather $\kappa = 2/3$, a static average if the transverse displacement w) but in his textbooks, e.g., [27].

In order to compare our second-order beam equation with that of TIMOSHENKO, we slightly rearrange (51) as

$$\frac{EI}{\ell^3}\tilde{w}^{IV} = q - \frac{6}{5}c^2(2(1+\nu)-\nu)q'' + O(e^6). \tag{56}$$

TIMOSHENDKO's beam equation reads with (55) [27]

$$\frac{EI}{\ell^3}w_{\mathrm{T}} = q - \frac{6}{5}c^2 2(1+\nu)q''. \tag{57}$$

It can be shown that the difference between both equations has its origin in the neglection of the stresses σ_{33} in thickness direction. Therefore, it follows immediately that a shear-correction factor not involving POISSON's ratio cannot lead to a consistent second-order beam theory.

If we further do not assume tacitly that Timoshenko's displacement w is the energetic mean $\tilde{w}$ but the original displacement $w = {}^{00}u_3$, we should compare Timoshenko's beam equation

$$EIw_T = \ell^3\left(q - \frac{2}{\kappa}(1+\nu)c^2q''\right) \tag{58}$$

with (47) leading to

$$\frac{1}{\kappa} = \frac{3}{20}\frac{8+5\nu}{1+\nu} - \beta^2\frac{\nu}{1+\nu}\left[\frac{1}{4} + \frac{\nu}{1+\nu}\frac{\beta^2}{5+\beta^2}\right], \tag{59}$$

involving the width-to-hight ratio

$$\beta = \frac{b}{h} = \frac{d}{c}. \tag{60}$$

If $\beta \ll 1$, the remaining factor

$$\frac{3}{20}\frac{8+5\nu}{1+\nu} \tag{61}$$

was introduced first by Olson [28] in 1938. Nevertheless, a shear correction factor which would lead to a consistent second-order theory has to involve the width-to-hight ratio β. Therefore, Timoshenko's theory is thus inconsistent within three respects. First, it is only applicable for the special loading condition considered here, second, normal stresses in the transverse direction are neglected, and third, trapezoidal displacement components (${}^{11}u_2$) are not considered. The beauty of the consistent second-order approximation is that neither a-priori assumption nor correction factors are necessary.

5 Concluding Remarks

The uniform-approximation technique in combination with the pseudo-reduction method is used to transform the three-dimensional equations of linear elasticity to a hierarchy of beam theories. The equations of the first-order approximation are identical to the classical EULER-BERNOULLI beam theory. A-priori assumptions are not introduced. The method rather disproves the celebrated kinematic a-priori assumptions of the classical beam theory.

Expansion coefficients not fixed by the reduction equations can be used a posteriori to fulfill boundary conditions along the beam faces at $\xi_2 = \pm b\big/(2\ell)$ and $\xi_3 = \pm h\big/(2\ell)$, and the local equilibrium conditions written in stresses. By this procedure, the governing *ODE* is not changed, which also applies for the involved stress resultants.

The second-order approximation leads to a TIMOSHENKO-like beam theory. It turns out that a shear-correction factor introduced a posteriori would depend on POISSON's ratio and the width-to-height ratio β. By this additional terms, effects arising from non-zero transverse normal stresses and a trapezoidal deflection of the cross-section can be considered. Higher-order theories are accurate up to terms of the order $O(e^{2(N+1)})$.

In summary, it may be concluded that it is important to consider a series expansion involving all terms of a desired approximation order. It is not possible to improve a consistent theory by adding displacement terms or assuming stress distributions in an unsystematic manner. If the goal is to improve a consistent second-order beam theory, an ansatz involving 26 coefficients in the displacements would be necessary. The gain of accuracy must be counterbalanced by the increase of complexity.

References

1. Schneider, P., Kienzler, R.: On exact rod/beam/shaft-theories and the coupling among them due to arbitrary material anisotropy. Int. J. Solids Struct. **56–57**, 265–279 (2015)
2. Almansi, E: Sopra la deformazione del cilindri sollicitati lateralmento. Atti Real Accad. Naz. Lincei Rend. Cl sci. fis. mat.e natur. Ser. **5**, 400–408 (1901)
3. Michell, J.: The theory of uniformly loaded beams. Q. J. Math. **32**, 28–42 (1901)
4. Saint-Venant, A. Barré de: Mémoire sur la torsion des prismes: avec des considerations sur leur flexion ainsi que sur l'equilibre interieur des solides élastiques en general: et des furmules practiques pour le calcul de leur résistance á divers efforts s'exerçant simultanément. Imprimiere nationale (1856)
5. Ciarlet, P., Destuynder, P.: A justification of the two-dimensional linear plate model. J. Mech. **18**, 315–344 (1979), Paris
6. Giorgi, E.D.: Sulla convergenza di alcune successioni di integrali del tipo dell'aera. Rud. Mat. Appl. **8**, 279–294 (1975)
7. Friesecke, G., James, R.D., Müller, S.: A theorem on geometric rigidity and the derivation of nonlinear plate theory from three-dimensional elasticity. Commun. Pure Appl. Math. **55**, 1461–1506 (2002)
8. Vekua, I.: Shell theory: general methods of construction. Monographs. Advanced Texts and Surveys in Pure and Applied Mathematics. John Wiley & Sons, New York (1985)
9. Steigmann, D.J.: Two dimensional models for the combined bending and stretching of plates and shells based on three-dimensional linear elasticity. Int. J. Eng. Sci. **46**, 654–676 (2008)
10. Pruchnicki, E.: Two-dimensional model of order h5 for the combined bending, stretching, transverse shearing and transverse normal stress effects of homogeneous plates derived from three-dimensional elasticity. Math. Mech. Solids **19**, 477–490 (2014)
11. Naghdi, P. M.: Foundations of elastic shell theory. Progress in Solid Mechanics IV. North-Holland, Amsterdam (1963)
12. Koiter, W.: On the foundation of the linear theory of thin elastic shells. Koninklije Nederlandse Akademie van Wettenschappen, Proceedings B **73**, 169–195 (1970)
13. Krätzig, W.: On the structure of consistent linear shell theories. In: Koiter, W., Mikhailov, G. (eds.) Theory of plates and shells, pp. 359–368. North-Holland, Amsterdam (1980)
14. Kienzler, R.: Eine Erweiterung der klassischen Schalentheorie; Der Einfluss von Dickenverzerrungen und Querschnittsverwölbungen. Ing. Arch. **52**, 311–322 (1982). Extended version in Ph.D.-Thesis, Technische Hochschule Darmstadt, Darmstadt (1980)
15. Kienzler, R.: On consistent plate theories. Arch. Appl. Mech. **72**, 229–247 (2002)
16. Kienzler, R.: On consistent second-order plate theories. In: Kienzler, R., Ott, I., Altenbach, H. (eds.) Theories of Plates and Shells: Critical Review and New Applications, pp. 85–96. Springer, Berlin (2004)
17. Schneider, P., Kienzler, R., Böhm, M.: Modeling of consistent second-order plate theories for anisotropic materials. Z. Angew. Math. Mech. **94**, 21–42 (2014)
18. Schneider, P.: On the mathematical justification of the consistent-approximation approach and the derivation of a shear-correction-factor free refined beam theory. Dissertation. University Bremen (2015). http://nbn-resolving.de/um:nbn:de:gbv:46-00104458-18
19. Schneider, P., Kienzler, R.: An algorithm for the automatisation of pseudo reduction of PDE systems arising from the uniform-approximation technique. In: Altenbach, H., Eremeyev, V. (Eds.), Shell-like structures. Advanced structural Materials, vol. 15, pp. 377–390. Springer, Berlin (2011)
20. Kienzler, R., Schneider, P.: Consistent theories of isotropic and anisotropic plates. J. Theor. Appl. Mech. **25**, 755–768 (2012)
21. Schneider, P., Kienzler, R.: A Reissner-type plate theory for monoclinic material derived by extending the uniform-approximation technique by orthogonal tensor decomposition of the nth-order gradient. Meccanica **52**, 2143–2167 (2017)
22. Kienzler, R., Schneider, P.: Second-order linear plate theories: Partial differential equations, stress-resultants and displacements. Int. J. Solids Struct. **115–116**, 14–26 (2017)

23. Reissner, E.: On the theory of bending of elastic plates. J. Math. Phys. **23**, 184–191 (1944)
24. Reissner, E.: The effect of transverse shear deformation on the bending of elastic plates. J. Appl. Mech. **12**, 89–77 (1945)
25. Timoshenko, S.: On the correction for shear of the differential equation for transverse vibrations of prismatic bars. Philos. Mag. Ser. **6**(41), 744–746 (1920)
26. Timoshenko, S.: On the transverse vibrations of bars of uniform cross-section. Philos. Mag. Ser. **6**(43), 125–131 (1922)
27. Timoshenko, S., Young, D.H.: Elements of strength of materials, 4th edn. Van Nostrand, Princeton, New Jersey, USA (1962)
28. Olsson, R.G.: Zur Berechnung der Frequenz der Transversalschwingung des prismatischen Stabes. Z. Angew. Math. Mech. **15**, 245 (1935)

Inflation of a Cylindrical Membrane Partially Stretched over a Rigid Cylinder

A. M. Kolesnikov

Abstract We consider the problem of a contact between an initially cylindrical hyperelastic membrane and a rigid rough cylinder. One end of the cylindrical membrane is partially stretched over the rigid cylinder. A uniform internal pressure is applied on that part of the membrane which is not in contact with the cylinder. The membrane is in equilibrium and does not slide off the rigid cylinder due to a friction in the contact area. Is assumed to hold on the contact surface Coulomb's law of friction is assumed to hold in the contact area. The membrane is composed of an incompressible homogeneous, isotropic elastic material possessing a strain energy function. The problem is formulated for arbitrary form of the strain energy function. For the particular case of the Bartenev–Khazanovich (Varga) material, the exact solution is obtained.

1 Introduction

Hyperelastic shells can be found in many nature and engineering structions. In many cases they are subjected by finite strains in the tangential directions and their bending stiffness is vanish. So to model such structures the theories of nonlinear elastic membranes under finite strains are used. Often these thin-walled structures are in contact with massive solid bodies.

Contact problems for elastic membranes is fundamental importance in many applications in the areas of inflatable structures, biological and artificial membranes, design of sensors and actuators. Such models arise in the mathematical descriptions of the thermoforming process used in industry to create polymeric container structures [1, 5, 6, 14, 15, 38]. The mechanical properties of cell and capsule membranes are evaluated by means of a compression experiment between two parallel plates [13, 25, 37] or micropipette technique [39, 41]. The biological processes such as peristaltic propulsion of a solid pellet (bolus) in the gut [26, 27], interaction artery wall,

A. M. Kolesnikov (✉)
Southern Federal University, Milchakova st. 8a, Rostov-on-Don 344090, Russian Federation
e-mail: Alexey.M.Kolesnikov@gmail.com

Don State Technical University, Gagarin square 1, Rostov-on-Don 344000, Russian Federation

H. Altenbach et al. (eds.), *Recent Developments in the Theory of Shells*,
Advanced Structured Materials 110, https://doi.org/10.1007/978-3-030-17747-8_19

atherosclerotic plaque and balloon angioplasty or stent [8, 43] can be modeled in framework contact problems for nonlinear elastic membranes. In the artificial devices the important role plays contact interaction. As a example, in [43] the authors consider mechanical devices of rotational symmetry that can be seen as segments of an artificial worm.

At present some contact problems of elastic membranes and solid bodies have been studied. The works [1, 12, 14, 15, 33, 43] describe the inflation of an incompressible isotropic hyperelastic membrane into solid bodies of revolution. In [12] the rigid body is a tube. In [1, 14, 15] the rigid bodies have complex shapes and contact between the membrane and bodies is arised in several places. The contact between an elastic membrane and an elastic bodies is considered in [33].

In [4, 16] hyperelastic tubes containing a compressible gas or an incompressible liquid and compressed between two rigid surfaces are investigated. In [4] both surfaces are flat. In [16] one surface is a concave or convex circular cylindrical surface.

The paper [2] treats the equilibrium of a thin-walled non-linearly elastic tube that contains a heavy liquid and a weightless compressible gas and that sits upon a rigid horizontal plane.

In [10, 13, 21, 22, 25, 28, 37] the contact problem of an pressurized spherical membrane between two rigid plates is analyzed. The paper [17] treats the equilibrium of a thin-walled hyperelastic sphere that contains a heavy liquid and that sits upon a rigid horizontal plane.

Several researchers have studied the process of the indentation and puncturing of a flat membrane by rigid objects in [29, 30, 34, 40, 44]. In [34] an initially curved membrane is studied too. In [7] the indentation and puncturing of an spherical elastic membrane enclosing an incompressible fluid by a rigid cylindrical indenter are investigated. In [30, 40] the experimental and numerical results are presented.

The works [5, 6, 9, 31, 32, 38, 42] deals with the inflation of elastic flat membranes which are in contact with different solid bodies: horizontal plates, elliptic and circular cylinders and cones. In [6, 9] the nonaxisymmetric contact problem between an inflated membrane and a rigid bodies is considered. In [9] the initially square plane membrane, which is constrained by an elliptic paraboloid indentor, is analyzed. In [6] the inflation of flat elliptical membranes, which are constrained by cylindrical and conical surfaces of elliptical cross-sections and plane horizontal surfaces, is studied. In other papers a circular flat membrane is considered. In [31, 32] the solid bodies which in contact with membrane are elastic. The works [6, 6] also present experimental results. In [42] the plane-strain deformation of a pressurized infinitely long elastic membrane which is in contact with flat surface is considered.

Also the several other contact problems for thin-walled structures have been considered. The paper [45] is devoted to the study of finite inflation of a hyperelastic toroidal membrane on a cylindrical rim. The elastic and rigid rims are considered. In [39, 41] the micropipette aspiration is modeled as a contact problem between a rigid tube and the spherical elastic membrane contained incompressible fluid. A balloon angioplasty model, consisting of the balloon, the atherosclerotic plaque and the artery wall, is presented in [8].

The papers [8, 18–20, 23, 46] treat the equilibrium of a thin-walled non-linearly elastic tube that contains a rigid body. In most studies it assumes that the contact is frictionless, including [23]. I.e. the interaction the solid bodies and the elastic membrane can be describe by a normal surface load. In [4, 22, 31–33, 42] the no-slip or adhesive contacts are considered. The friction contacts are investigated on [18–21, 40, 46].

Usually hyperelastic materials have a high friction coefficient. So the friction can have a significant effect on stresses and strains of thin-walled structures composed of these materials. The steady motion of rigid spherical particles in a thin elastic tube of smaller diameter is considered in [46]. In [18–20] the problems of the equilibrium of the cylindrical the membrane partially stretched over a rigid cylinder or cone are investigated. The friction plays a key role in these problems.

In this paper the contact problem between a hyperelastic cylindrical membrane and a rigid rough cylinder is considered. One end of the membrane is partially stretched over the rigid cylinder. Another part is inflated by an uniform pressure. The membrane does not slide off the rigid cylinder due to a friction in the contact area. The aim of research is to determine the dependence between the size of the contact area, the internal pressure, the friction coefficient and the radii of the membrane and the cylinder.

In Sect. 2 we present the mathematical model of the problem. In our analysis we will use the nonlinear theory of elastic membranes [11, 24, 47]. We introduce two parts of the membrane: in contact with the rigid cylinder and the pressurized part. We derive the equilibrium equations for the both parts of the membrane and formulate conjugation conditions of the solutions. We use the Coulomb law to describe a friction in contact area. In Sect. 3 we present the analytical solution for the membrane composed of Bartenev–Khazanovich (Varga) material [3]. In Sects. 4 and 5 we present results and brief conclusions, respectively.

2 Equilibrium Equations

2.1 Basic Equations

Let us consider a thin-walled tube with a constant thickness h. In the cylindrical coordinates $\{r, \phi, z\}$ we describe the undeformed tube as

$$R = R_0, \quad \Phi \in [0, 2\pi], \quad Z \in [0, +\infty).$$

Let one end of the tube be stretched over a immovable rough rigid cylinder with the radius $r_0 > R_0$ and let tube be inflated by the pressure p_i (Fig. 1). We describe the deformed membrane in the cylindrical coordinates by the functions $r(Z)$ and $z(Z)$. In contact area we have $r(Z) \equiv r_0$, $(Z \in [0, Z_c])$.

Using the Coulomb's law of dry friction in the contact area we consider a limit case of equilibrium. We assume that the tangential traction (due to friction) in whole

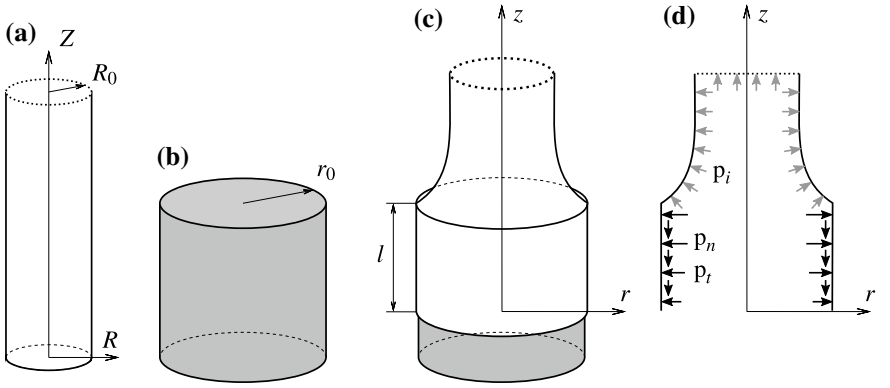

Fig. 1 **a** A cylindrical membrane, **b** a rigid cylinder, **c** the cylindrical membrane stretched over the rigid cylinder, **d** an axial section of the deformed membrane

contact area reaches the limit simultaneously. Another part of membrane is loaded by the uniform pressure p_i. We give the surface loads in the form

$$q_n = \begin{cases} -p_n(Z), & 0 \le Z \le Z_c, \\ -p_i, & Z > Z_c, \end{cases} \qquad q_t = \begin{cases} -f p_n(Z), & 0 \le Z \le Z_c, \\ 0, & Z > Z_c, \end{cases}$$

where $p_n(Z)$ is the normal surface load in the contact area, f is the friction coefficient.

For an axisymmetric deformation of cylindrical membranes the equilibrium equations can be written in the following form

$$\begin{aligned} \frac{d\sigma_1}{dZ} + \frac{\sigma_1 - \sigma_2}{r}\frac{dr}{dZ} + \lambda_1 q_t = 0, \\ \sigma_1\kappa_1 + \sigma_2\kappa_2 + q_n = 0. \end{aligned} \tag{1}$$

Here, κ_1, κ_2 are the principal curvatures

$$\kappa_1 = \begin{cases} 0, & 0 \le Z \le Z_c, \\ \lambda_1^{-1}\psi', & Z > Z_c, \end{cases} \qquad \kappa_2 = \begin{cases} r_0^{-1}, & 0 \le Z \le Z_c, \\ r(Z)^{-1}, & Z > Z_c, \end{cases}$$

and λ_1, λ_2 are the principal stretches

$$\lambda_1(Z) = \begin{cases} z'(Z), & 0 \le Z \le Z_c, \\ \sqrt{r'(Z)^2 + z'(Z)^2}, & Z > Z_c, \end{cases}$$

$$\lambda_2(Z) = \begin{cases} \rho_0 = \dfrac{r_0}{R_0}, & 0 \le Z \le Z_c, \\ \rho(Z) = \dfrac{r(Z)}{R_0}, & Z > Z_c, \end{cases}$$

where $\psi(Z)$ is the slope angle and $()' = \frac{d()}{dZ}$.

For elastic incompressible material using the strain energy density $W(\lambda_1, \lambda_2)$ we have

$$\sigma_1 = \frac{h}{\lambda_2}\frac{\partial W}{\partial \lambda_1}, \quad \sigma_2 = \frac{h}{\lambda_1}\frac{\partial W}{\partial \lambda_2}. \tag{2}$$

2.2 Contact Area

In the contact area the equilibrium equations (1) reduce to

$$\frac{d\sigma_1}{dZ} = \lambda_1 f p_n,$$
$$p_n = \sigma_2 \kappa_2.$$

We obtain

$$\frac{d}{dZ}\left(\frac{h}{\lambda_2}\frac{\partial W}{\partial \lambda_1}\right) = \lambda_1 f \kappa_2 \frac{h}{\lambda_1}\frac{\partial W}{\partial \lambda_2}.$$

Using $h = \text{const}$ and $\lambda_2 = \rho_0 = \text{const}$, we have

$$\frac{\partial^2 W}{\partial \lambda_1^2}\frac{d\lambda_1}{dZ} = \frac{f}{R_0}\frac{\partial W}{\partial \lambda_2}. \tag{3}$$

We can integrate the Eq. (3)

$$Z(\lambda_1) = \frac{R_0}{f}\int_{\lambda_{10}}^{\lambda_1} F(\lambda)d\lambda, \quad F(\lambda_1) = \frac{\partial^2 W(\lambda_1, \lambda_2)}{\partial \lambda_1^2}\left(\frac{\partial W(\lambda_1, \lambda_2)}{\partial \lambda_2}\right)^{-1},$$

where $\lambda_{10} = \lambda_1(0)$. Also we can write the Eq. (3) as the second order differential equation

$$F(z')z'' = \frac{f}{R_0}. \tag{4}$$

Boundary conditions are

$$\sigma_1\Big|_{Z=0} = 0, \quad z(0) = 0. \tag{5}$$

If we known $\lambda_{1c-} = \lambda_1(Z_c)$ then

$$Z_c = \frac{R_0}{f} \int_{\lambda_{10}}^{\lambda_{1c-}} F(\lambda) d\lambda.$$

After that we can calculate the contact length

$$l = z(Z_c).$$

We note that the contact length l is minimum value, which is required to equilibrium of the cylindrical membrane partially stretched over the rigid rough cylinder.

2.3 Inflation Area

At the infinity the cylindrical membrane tends to simple inflation. From the equilibrium equations we have

$$\sigma_1 \to \frac{1}{2} r_\infty p_i, \quad \sigma_2 \to r_\infty p_i \quad \text{at} \quad Z \to \infty. \tag{6}$$

Here, r_∞ is the radius of membrane at the infinity.

For membranes without tangential loads we can use the Pipkin's integral [35]

$$\left(W - \lambda_1 \frac{\partial W}{\partial \lambda_1} \right) \Big|_{Z=Z_{c+}} = \left(W - \lambda_1 \frac{\partial W}{\partial \lambda_1} \right) \Big|_{Z \to \infty}. \tag{7}$$

The equilibrium equation of inflation part of membrane (Fig. 2a) we can write as

$$2\pi r_0 \sigma_{1c+} \sin \psi_{c+} = \pi r_0^2 p_i \tag{8}$$

Using $\lambda_{2c+} = \rho_0$ from Eqs. (6), (7) and (8) we can calculate $\lambda_{1\infty}$, $\lambda_{2\infty} = \rho_\infty$, λ_{1c+} and ψ_{c+}.

2.4 Conjugation Conditions

To solve problem we heed the conjugation conditions. The condition to the functions r: $r(Z_c) = r_0$. So we have

$$\lambda_{2c-} = \lambda_{2c+} = \lambda_{2c} = \rho_0.$$

To solve problem we need determine λ_{1c-} from λ_{1c+}.

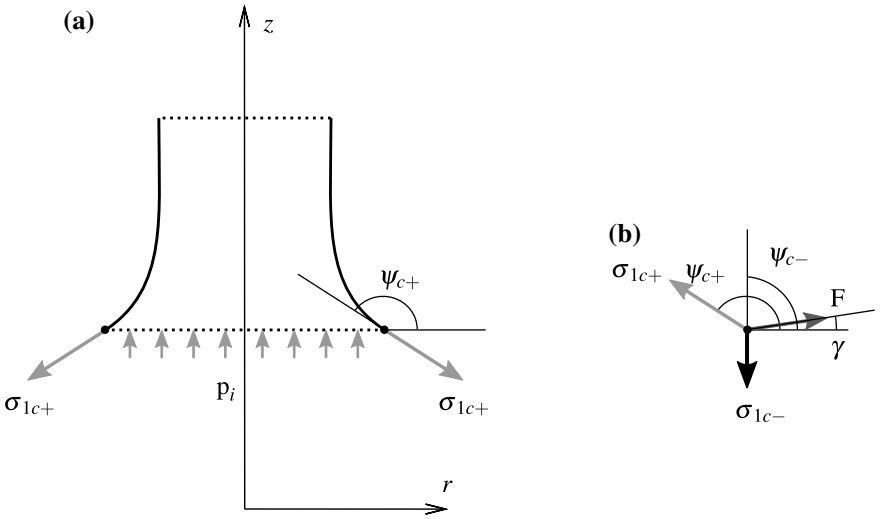

Fig. 2 **a** The inflated part of the membrane, **b** forces applied at the point $Z = Z_c$

At the point Z_c there is the reaction force **F** (Fig. 2b). From one side we can consider its normal and tangential components F_n and F_t. Using Coulomb's law for friction we have

$$\sigma_{1c+} - \sigma_{1c-} = F_t, \quad F_t = f F_n.$$

From another side we have the equilibrium equations in the longitudinal plane at the point Z_c

$$\begin{aligned} -\sigma_{1c-} \cos \psi_{c-} + \sigma_{1c+} \cos \psi_{c+} + F \cos \gamma = 0, \\ -\sigma_{1c-} \sin \psi_{c-} + \sigma_{1c+} \sin \psi_{c+} + F \sin \gamma = 0, \\ F = |\mathbf{F}| = F_n \sqrt{1 + f^2}. \end{aligned}$$

Here, γ is the angle between the force **F** and the axis r.

From the last equations we have

$$\begin{aligned} \sigma_{1c-} = f_e \sigma_{1c+}, \\ f_e = 1 + Cf^2 - f\sqrt{2C + C^2 f^2}, \quad C = 1 - \cos(\psi_{c+} - \psi_{c-}), \end{aligned} \tag{9}$$

where $\psi_{c-} = \frac{\pi}{2}$.

In previously studies [18–20] the continuity of the strains has been used as the conjugation conditions. In another words the edge friction has been neglected. As it will be shown below the edge friction plays important role in the problem. The minimum contact length, required to equilibrium, increases significantly, if we neglect by the edge friction.

3 Bartenev–Khazanovich (Varga) Material

Let us consider the Bartenev–Khazanovich (Varga) material [3]

$$W = 2\mu\left(\lambda_1 + \lambda_2 + \frac{1}{\lambda_1\lambda_2} - 3\right).$$

The stress resultants (2) are written as

$$\sigma_1 = \frac{2\mu h}{\lambda_2}\left(1 - \frac{1}{\lambda_1^2\lambda_2}\right), \quad \sigma_2 = \frac{2\mu h}{\lambda_1}\left(1 - \frac{1}{\lambda_1\lambda_2^2}\right). \tag{10}$$

From the boundary condition (5) we obtain

$$\lambda_1 = \frac{1}{\sqrt{\lambda_2}} = \frac{1}{\sqrt{\rho_0}} \quad \text{at} \quad s = 0.$$

From the conditions (6) we derive the pressure p_i and the principal stretch $\lambda_{1\infty}$ as functions $\lambda_{2\infty} = \rho_\infty$

$$\lambda_{1\infty} = \frac{1}{4\rho_\infty}\left(\rho_\infty^2 + \sqrt{\rho_\infty^4 + 8\rho_\infty}\right),$$
$$p_i = \frac{4\mu h}{R_0\rho_\infty}\left(\frac{1}{\rho_\infty} - \frac{16}{\left(\rho_\infty^2 + \sqrt{\rho_\infty^4 + 8\rho_\infty}\right)^2}\right). \tag{11}$$

From the Pipkin integral (7) we obtain

$$\lambda_{1c+} = \frac{2\left(\rho_\infty^2 + \sqrt{\rho_\infty^4 + 8\rho_\infty}\right)}{\lambda_{2c}\left(8 + \rho_\infty^3 - \rho_\infty^2\lambda_{2c} - (\lambda_{2c} - \rho_\infty)\sqrt{\rho_\infty^4 + 8\rho_\infty}\right)} \tag{12}$$

In the contact area the equilibrium equation (4) reduce to following form [19]

$$t' + \frac{f\rho_0}{2R_0}\cdot\frac{1}{t} - \frac{1}{2R_0\rho_0} = 0, \quad t = \frac{1}{z'(Z)}. \tag{13}$$

This differential equation is the second-kind Abel equation. The solution can be written in the form [36]

$$\begin{aligned} Z(t) &= \frac{2R_0\rho_0}{f}\left(t + \rho_0^2 \ln|\rho_0^2 - t| + c_2\right), \\ z(t) &= \frac{2R_0\rho_0}{f}\left(\ln|\rho_0^2 - t| + c_3\right). \end{aligned} \tag{14}$$

Let denote $t_0 : Z(t_0) = 0$, so we have from (5)

$$\begin{aligned} t_0 = \sqrt{\rho_0}, \quad c_3 = -\ln|\rho_0^2 - \sqrt{\rho_0}|, \\ c_2 = -\sqrt{\rho_0} - \rho_0^2 \ln|\rho_0^2 - \sqrt{\rho_0}|. \end{aligned}$$

From the conjugation condition (9), (10) and (12) we have

$$t_c = \frac{1}{\lambda_{1c-}} = \left(\rho_0\left(1 - f_e\left(1 - \frac{1}{\lambda_{1c+}^2\rho_0}\right)\right)\right)^{\frac{1}{2}}. \tag{15}$$

Subsituding (15) into (14) and we can calculate the contact length

$$l = z(t_c).$$

4 Results

Let us introduce the dimensionless parameters

$$l^* = \frac{l}{R_0}, \quad p^* = \frac{R_0 p_i}{\mu h}.$$

First, we present results for $p_i = 0$ in Fig. 3. The X-axis corresponds to the relative radius ρ_0. The Y-axis corresponds to the value fl^*. The black curves correspond to the friction coefficients $f = 0.1, 0.5, 1$. If we neglect the edge friction then the value fl^* depends only ρ_0 [19]. This result may be obtained from (14) and (15) assuming $f_e = 1$. This case is shown by the gray curve in Fig. 3. We can see that the edge friction has significantly influence on the minimum contact length. The contact length decreases greatly when taking into account the edge friction.

In Figs. 4, 5 and 6 the dependence between the internal pressure p^* and the minimum contact length l^* for the different coefficient frictions $f = 0.1, 0.5, 1$, respectively. The different curves correspond to the different relative radii ρ_0 presented in figures.

As we can see in Figs. 4, 5 and 6 the increasing of the friction coefficient leads to decreasing the minimum contact length. For zero pressure the increasing the

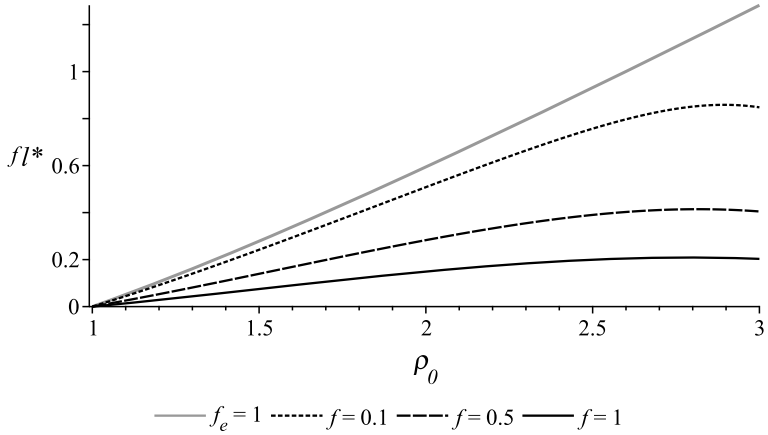

Fig. 3 The minimum contact length fl^* versus the relative radius ρ_0 for $p_i = 0$

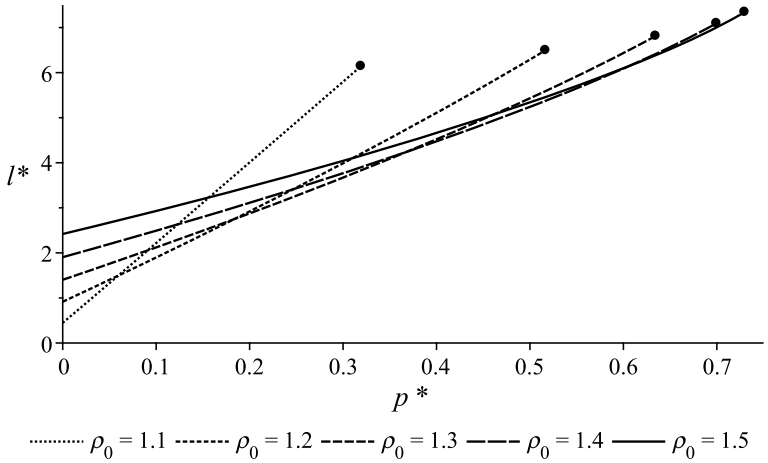

Fig. 4 The minimum contact length l^* versus the internal pressure p^* for the friction coefficient $f = 0.1$ and the different relative radii ρ_0

relative radius leads to increasing the minimum contact length. The minimum contact length increases with increasing the pressure faster for smaller relative radii. The dependences $\ll l - p \gg$ are more nonlinear for higher friction coefficients.

The inflation of cylindrical membrane leads to growth of the radius of a cross–section. There is the pressure $p_{i_{\max}}$ such that if the pressure is more than $p_{i_{\max}}$ then the radius of the inflated cylindircal membrane will more than the radius of the rigid cylinder. It means that membrane will slide off from the rigid cylinder. These cases show by the black dots in Figs. 4, 5 and 6. The pressure $p_{i_{\max}}$ is determined by (11) assuming $\rho_\infty = \rho_0$.

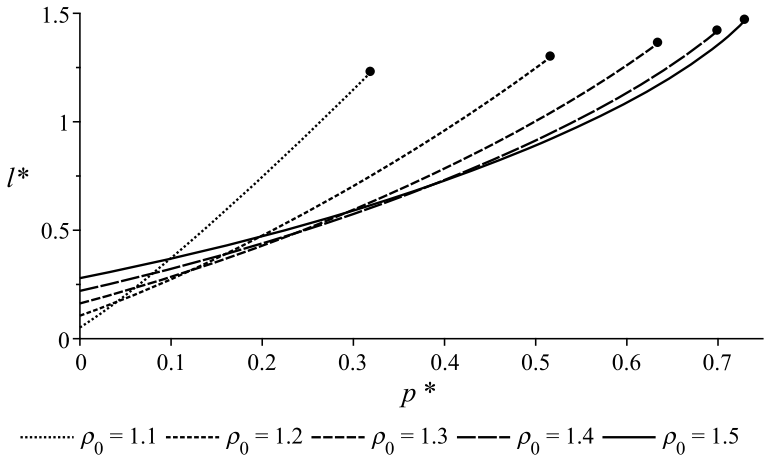

Fig. 5 The minimum contact length l^* versus the internal pressure p^* for the friction coefficient $f = 0.5$ and the different relative radii ρ_0

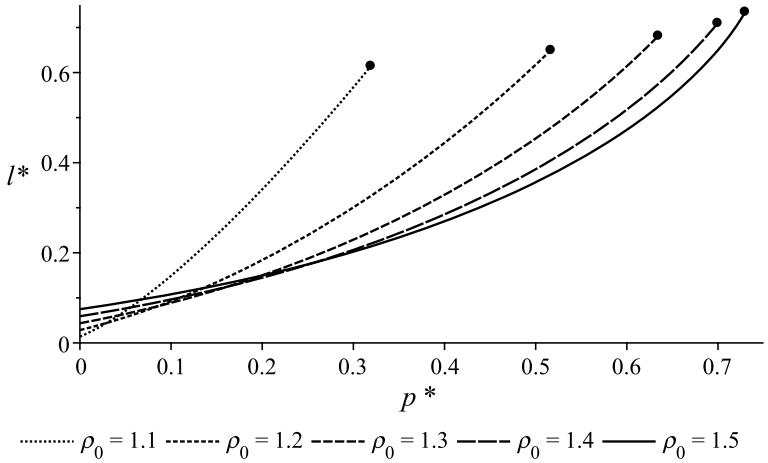

Fig. 6 The minimum contact length l^* versus the internal pressure p^* for the friction coefficient $f = 1$ and the different relative radii ρ_0

In Figs. 4, 5 and 6 we show the results for $\rho_0 \leq 1.5$. The results for $\rho_0 \geq 1.6$ are presented in Fig. 7. In Fig. 7 the curves are not monotonically, ambiguous and they have kinks. This feature is associated with the behavior of this material model under large strains.

Let us consider inflation of a cylindrical membrane. For the simple inflation (6) the function $p^*(\rho)$ has maximum (solid curve in Fig. 8). The maximum pressure is

$$p^*_{\max} = \left(2\sqrt{3} - 3\right) 2^{\frac{2}{3}} \approx 0.7367 \quad \text{at} \quad \rho = 2^{\frac{2}{3}} \approx 1.5874.$$

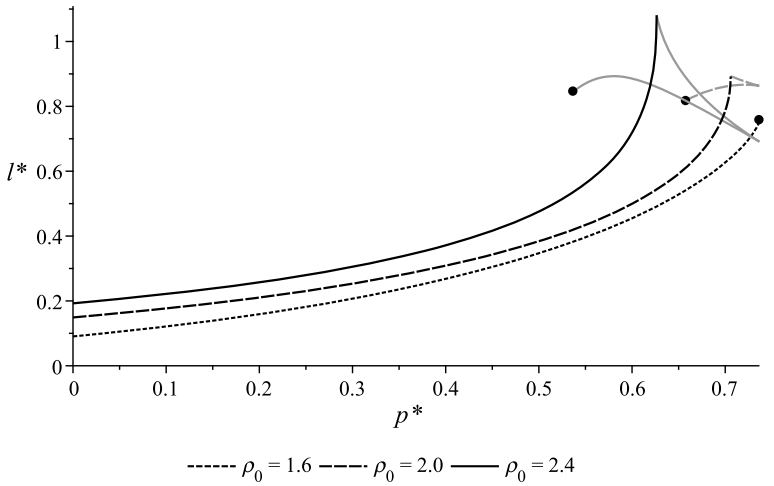

Fig. 7 The minimum contact length l^* versus the internal pressure p^* for the friction coefficient $f = 1$ and the different relative radii ρ_0

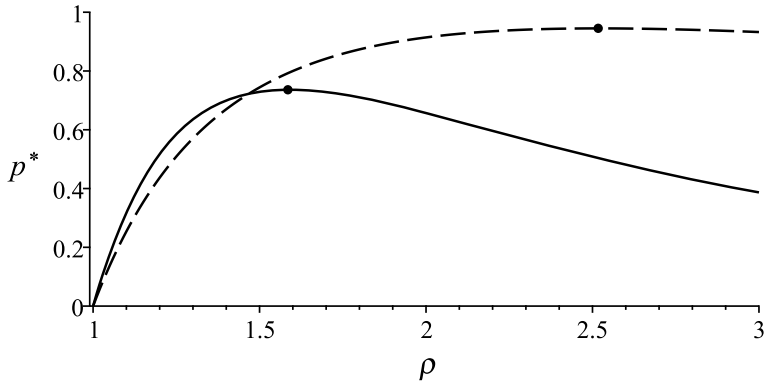

Fig. 8 "Simple" inflations

The dash line in Fig. 8 corresponds to the inflation of tube when $\sigma_1 = 0$ and $\sigma_2 = r_\infty p_i$. In this case the maximum pressure is

$$p^*_{\max} = 3 \cdot 2^{-\frac{5}{3}} \approx 0.9449 \quad \text{at} \quad \rho = 2^{\frac{4}{3}} \approx 2.5198.$$

After maximum pressure the radius of the membrane will increase with decreasing the pressure. Usually it means unstable of an elastic membrane.

In our contact problem for $\rho_0 > 2^{\frac{2}{3}}$ and increasing pressure the membrane reachs a state at the point $Z = Z_c$, corresponded an unstable state under inflation of tube. We suppose that the kink point is the limit case of equilibrium in our problem. But further research is needed to study equilibrium of membrane after a loss of stability.

We note that the Bartenev–Khazanovich model is valid for strains that are less than 0.6 [3]. Thus, huge strains may do not have physical meaning.

5 Conclusion

In this paper the contact problem with a friction is studied for a hyperelastic thin-walled tube and a rigid cylinder. One end of the tube is partially stretched over the cylinder and another part of the tube is loaded by an internal uniform pressure. The friction plays a key role in this problem. The tube does not slide off the cylinder due to only the friction if the contact area is sufficient. If the friction will be absent then the tube will slide off the cylinder even at zero pressure.

The mathematical model of the problem is formulated in the framework of theory nonlinear elastic membrane for an arbitrary isotropic hyperelastic material. The friction is modeled by Coulomb's law. An an example, the problem is solved for Bartenev–Khazanovich (Varga) model of material. The explicit solution is obtained. The dependence between the minimum contract length, which is required to equilibrium, the internal pressure, the friction coefficient and the radii of the tube and the rigid cylinder is derived. The results is illustrated by the plots "the minimum contact length—the internal pressure" for the different parameters of the problem.

Acknowledgements This research was supported by the Government of Russian Federation grant no. 14.Z50.31.0046.

References

1. Andrä, H., Warby, M.K., Whiteman, J.R.: Contact problems of hyperelastic membranes: existence theory. Math. Methods Appl. Sci. **23**(10), 865–895 (2000)
2. Antman, S.S., Schagerl, M.: Slumping instabilities of elastic membranes holding liquids and gases. Int. J. Non-linear Mech. **40**(8), 1112–1138 (2005)
3. Bartenev, G.M., Khazanovich, T.N.: On the high elasticity deformation law of network polymers (in Russian). Vysokomolekulyarnye soedineniya **2**(1), 21–28 (1960)
4. Charrier, J.M.: Air-rubber springs: an analysis. Int. J. Mech. Sci. **15**(6), 435–448 (1973)
5. Charrier, J.M., Shrivastava, S., Wu, R.: Free and constrained inflation of elastic membranes in relation to thermoforming—axisymmetric problems. J. Strain Anal. Eng. Des. **22**(2), 115–125 (1987)
6. Charrier, J.M., Shrivastava, S., Wu, R.: Free and constrained inflation of elastic membranes in relation to thermoforming—non-axisymmetric problems. J. Strain Anal. Eng. Des. **24**(2), 55–74 (1989)
7. Deris, A.H.A., Nadler, B.: Modeling the indentation and puncturing of inflated elastic membranes by rigid indenters. Int. J. Non-linear Mech. **69**, 29–36 (2015)
8. Eftaxiopoulos, D.A., Atkinson, C.: A nonlinear, anisotropic and axisymmetric model for balloon angioplasty. In: Proceedings of the Royal Society of London A: Mathematical, Physical and Engineering Sciences, vol. 461, pp. 1097–1128. The Royal Society (2005)
9. Feng, W.W., Pangnan, H.: On the general contact problem of an inflated nonlinear plane membrane. Int. J. Solids Struct. **11**(4), 437–448 (1975)

10. Feng, W.W., Yang, W.-H.: On the contact problem of an inflated spherical nonlinear membrane. J. Appl. Mech. **40**(1), 209–214 (1973)
11. Green, A.E., Adkins, J.E.: Large Elastic Deformation and Non-linear Continuum Mechanics. Clarendon Press, Oxford (1960)
12. Johnson, W., Soden, P.D.: The discharge characteristics of confined rubber cylinders. Int. J. Mech. Sci. **8**(3), 213–225 (1966)
13. Keller, M.W., Sottos, N.R.: Mechanical properties of microcapsules used in a self-healing polymer. Exp. Mech. **46**(6), 725–733 (2006)
14. Khayat, R.E., Derdouri, A.: Inflation of hyperelastic cylindrical membranes as applied to blow moulding. Part I. Axisymmetric case. Int. J. Numer. Methods Eng. **37**(22), 3773–3791 (1994)
15. Khayat, R.E., Derdouri, A., García-Rejón, A.: Multiple contact and axisymmetric inflation of hyperelastic cylindrical membranes. Proc. Inst. Mech. Eng. Part C J. Mech. Eng. Sci. **207**(3), 175–183 (1993)
16. Kolesnikov, A.M.: Compression of nonlinear elastic membranes between rigid surfaces. In: Shell Structures: Theory and Applications—Proceedings of the 9th SSTA Conference, pp. 71–74 (2010)
17. Kolesnikov, A.M.: Equilibrium of an elastic spherical shell filled with a heavy fluid under pressure. J. Appl. Mech. Tech. Phys. **51**(5), 744–750 (2010)
18. Kolesnikov, A.M.: Cylindrical membrane partially stretched on a rigid cylinder. Int. J. Non-linear Mech. **86**, 15–22 (2016)
19. Kolesnikov, A.M.: Tension of a cylindrical membrane partially stretched over a rigid cylinder. Int. J. Non-linear Mech. **97**, 41–47 (2017)
20. Kolesnikov, A.M., Purtova, I.S.: A cylindrical membrane partially stretched over a rigid cone. In: Shell Structures: Theory and Applications Volume 4: Proceedings of the 11th International Conference "Shell Structures: Theory and Applications", (SSTA 2017), October 11–13, 2017, Gdansk, Poland, pp. 105–108. CRC Press (2017)
21. Kumar, N., DasGupta, A.: On the contact problem of an inflated spherical hyperelastic membrane. Int. J. Non-linear Mech. **57**, 130–139 (2013)
22. Kumar, N., DasGupta, A.: Contact mechanics and induced hysteresis at oscillatory contacts with adhesion. Langmuir **30**(30), 9107–9114 (2014)
23. Kydoniefs, A.D.: Finite axisymmetric deformations of an initially cylindrical elastic membrane enclosing a rigid body. Q. J. Mech. Appl. Math. **22**(3), 319–331 (1969)
24. Libai, A., Simmonds, J.S.: The Nonlinear Theory of Elastic Shells. Academic Press, San Diego (1988)
25. Liu, K.K., Williams, D.R., Briscoe, B.J.: Compressive deformation of a single microcapsule. Phys. Rev. E **54**(6), 6673 (1996)
26. Miftahof, R., Akhmadeev, N.: Dynamics of intestinal propulsion. J. Theor. Biol. **246**(2), 377–393 (2007)
27. Miftahof, R., Fedotov, E.: Intestinal propulsion of a solid non-deformable bolus. J. Theor. Biol. **235**(1), 57–70 (2005)
28. Nadler, B.: On the contact of a spherical membrane enclosing a fluid with rigid parallel planes. Int. J. Non-linear Mech. **45**(3), 294–300 (2010)
29. Nadler, B., Steigmann, D.J.: Modeling the indentation, penetration and cavitation of elastic membranes. J. Mech. Phys. Solids **54**(10), 2005–2029 (2006)
30. Pamplona, D.C., Weber, H.I., Sampaio, G.R.: Analytical, numerical and experimental analysis of continuous indentation of a flat hyperelastic circular membrane by a rigid cylindrical indenter. Int. J. Mech. Sci. **87**, 18–25 (2014)
31. Patil, A., DasGupta, A.: Constrained inflation of a stretched hyperelastic membrane inside an elastic cone. Meccanica **50**(6), 1495–1508 (2015)
32. Patil, A., DasGupta, A., Eriksson, A.: Contact mechanics of a circular membrane inflated against a deformable substrate. Int. J. Solids Struct. **67**, 250–262 (2015)
33. Patil, A., Nordmark, A., Eriksson, A.: Free and constrained inflation of a pre-stretched cylindrical membrane. In: Proceedings of the Royal Society of London A: Mathematical, Physical and Engineering Sciences, vol. 470, p. 20140282. The Royal Society (2014)

34. Pearce, S.P., King, J.R., Holdsworth, M.J.: Axisymmetric indentation of curved elastic membranes by a convex rigid indenter. Int. J. Non-linear Mech. **46**(9), 1128–1138 (2011)
35. Pipkin, A.C.: Integration of an equation in membrane theory. Zeitschrift für Angewandte Mathematik und Physik (ZAMP) **19**(5), 818–819 (1968)
36. Polyanin, A.D., Zaitsev, V.F.: Handbook of Exact Solutions for Ordinary Differential Equations, 2nd edn. Chapman & Hall/CRC (2003)
37. Rachik, M., Barthes-Biesel, D., Carin, M., Edwards-Levy, F.: Identification of the elastic properties of an artificial capsule membrane with the compression test: effect of thickness. J. Colloid Interface Sci. **301**(1), 217–226 (2006)
38. Rasmussen, H.K., Christensen, J.H., Gøttsche, S.: Inflation of polymer melts into elliptic and circular cylinders. J. Non-Newton. Fluid Mech. **93**(2–3), 245–263 (2000)
39. Rudenko, O.V., Kolesnikov, A.M.: Aspiration of a nonlinear elastic spherical membrane. Int. J. Eng. Sci. **80**, 62–73 (2014)
40. Selvadurai, A.P.S.: Deflections of a rubber membrane. J. Mech. Phys. Solids **54**(6), 1093–1119 (2006)
41. Sohail, T., Tang, T., Nadler, B.: Micropipette aspiration of an inflated fluid-filled spherical membrane. Zeitschrift für angewandte Mathematik und Physik **63**(4), 737–757 (2012)
42. Srivastava, A., Hui, C.-Y.: Large deformation contact mechanics of a pressurized long rectangular membrane. II. Adhesive contact. In: Proceeding of the Royal Society A, vol. 469, p. 20130425. The Royal Society (2013)
43. Steigenberger, J., Abeszer, H.: Quasistatic inflation processes within rigid tubes. ZAMM-J. Appl. Math. and Mechanics/Zeitschrift für Angewandte Mathematik und Mechanik **88**(7), 556–572 (2008)
44. Steigmann, D.J.: Puncturing a thin elastic sheet. Int. J. Non-linear Mech. **40**(2–3), 255–270 (2005)
45. Tamadapu, G., DasGupta, A.: Finite inflation of a hyperelastic toroidal membrane over a cylindrical rim. Int. J. Solids Struct. **51**(2), 430–439 (2014)
46. Tözeren, A.: Motion of rigid spheres through elastic tubes. Int. J. Solids Struct. **17**(8), 769–785 (1981)
47. Zubov, L.M.: The Methods of Nonlinear Elasticity in the Shell Theory (In Russian). Rostov University Press, Rostov on Don (1982)

Singular Surface Curves in the Resultant Thermodynamics of Shells

Violetta Konopińska-Zmysłowska and Victor A. Eremeyev

Abstract Within six-parameter shells theory we discuss the governing equations of shells with material or non-material singular curves. By singular curve we mean a surface curve where are discontinuities in some surface fields. As an example we consider shells with junctions and shells undergoing stress-induced phase transitions.

1 Introduction

Singular surfaces play an important role in many cases of three-dimensional (3D) continuum thermodynamics. By singular surface we mean a material or non-material surface across of which some considering fields undergo jumps. A singular surface is a mathematical representation of such discontinuities as shock and acceleration waves, vortex sheets, phase transition fronts, strain localizations, fracture, interfaces between different materials, among other phenomena. The singular surfaces phenomena in the 3D continuum have been described in many publications, see, e.g., [1, 6, 7, 43, 44, 49, 56–58, 74, 78, 80, 81].

However, many singular phenomena occur also in thin-walled structures described within two-dimensional (2D) models such as thin films, membranes, plates and shells. In such cases full analysis using 3D continuum model with singular surface is often impracticable, most likely a 2D shell-like model consisting of a base surface with an additional surface fields, is more convenient in applications. As a result of application of 2D models one get a notion of singular curve as a counterpart of singular surface. The description of a stationary and/or moving surface curve separating shell

V. Konopińska-Zmysłowska (✉) · V. A. Eremeyev
Faculty of Civil and Environmental Engineering, Gdańsk University of Technology, ul. Gabriela Narutowicza 11/12, 80-233 Gdańsk, Poland
e-mail: violetta.konopinska@pg.edu.pl

V. A. Eremeyev
e-mail: eremeyev.victor@gmail.com

H. Altenbach et al. (eds.), *Recent Developments in the Theory of Shells*,
Advanced Structured Materials 110, https://doi.org/10.1007/978-3-030-17747-8_20

areas with different properties allows one to model various singular phenomena in thin structures. Examples of such 1D phenomena in thin solid layers are similar to 2D phenomena occurring in 3D continua: shock and acceleration waves, phase transition fronts, interfaces of different materials, etc. Some singular phenomena in thin solids seems to have no apparent counterparts in 3D thermodynamics and are difficult to handle by 3D models. These are, for example, description of junctions at shell branching and intersections, surface line defects in nanotubes, dislocations in graphen sheets, phase transitions (PT) in some biological membranes, tents and tunnels appearing in martensitic thin films, etc. In such cases jump conditions along singular surface curves form the framework within which some 2D constitutive equations have to be worked out on 2D and 1D level, thus completing the boundary value problem (BVP) of these singular surface phenomena. Additionally, along the singular surface curves there may be given additional 1D fields which can influence the overall singular process.

In engineering applications, thin-walled shell structures often consist of regular shell elements interconnected along curvilinear junctions, which are often briefly called multi-shells or irregular shells. Pressure vessels, silos, liquid and gas storage tanks, tubular towers, complex bridge decks, branching and intersecting pipelines, cars unibody construction, ship hulls, fuselages of aircrafts or rockets are just a few examples of such irregular thin-walled structures from the field of civil and mechanical engineering. In some cases the shell junctions may have additional own mechanical properties allowing the adjacent shell elements to deform (usually rotate) one with respect to another. The junction properties considerably influence behaviour of the whole irregular shell structure. But while the regular shells are discussed in many thousands of papers and are summarized in hundreds books and review papers, description of shell junctions and their influence on the overall behaviour of multi-shell structures are still not well developed and understood. This remark is in sharp contrast to analysis of one-dimensional (1D) steel framed structures with various semi-rigid connections, the design of which was summarized in several books. The description of multifolded shells was presented in [15, 16, 18, 19, 46, 48, 54, 55, 65, 67, 75, 76], see also the review by Pietraszkiewicz and Konopińska [71].

Many singular phenomena mentioned above can be properly modeled by the resultant 2D shell thermodynamics, which provides appropriate jump conditions along the singular surface curves. Within the resultant nonlinear shell theory singular curves were discussed in [27, 29, 30, 53, 55, 68, 72]. In particular, Pietraszkiewicz [64] developed complete resultant 2D thermodynamics of shells, which is an exact implication of 3D rational continuum thermodynamics and provides the most advanced model of a regular shell available in the literature. Completion of this model by appropriate jump conditions along stationary and movable singular curves allowed to model more completely various singular phenomena in shells, like description of various types of shell junctions (deformable, reinforced by beams, with energy and entropy transfer, etc.). It also became possible to develop some advanced 2D thermodynamic constitutive equations in the shell regular parts as well as 1D constitutive equations along the singular curves.

Singular surface curve in resultant 2D thermodynamics may model phase transition interface in shell structure. The stress- and temperature-induced PT are experimentally observed in many thin-walled structural elements made of superelastic shape memory alloys (SMA) and shape memory polymers such as NiTi, NiMnGa, AgCd, AuCd, CuAlNi, polyurethane, etc., which are used in various microelectromechanical systems (MEMS). Thin plates, strips, and tubes made of SMA are used as working elements of such MEMS as micropumps, sensors, actuators, microengines, etc., see e.g. [7–9, 50, 73], or as catheters, superelastic needles, self-expanding stents in medical industry, see [60, 83]. The results of some simple tests of phase transition problems in thin-walled structures are available in the literature, see for example [23, 39, 45, 62]. The 2D model of the shells undergoing stress-induced phase transitions were introduced in [27, 29, 30, 32, 72].

Here we discuss the shells thermomechanics with singular curves considering shells with junctions and shells undergoing phase transitions. We consider the nonlinear resultant theory of shells called also six-parameter theory of shells as the kinematics of the shells is based on six degrees of freedom, which are translation and rotation fields. The foundation of the theory can be found in [16, 24, 34, 51, 52]. Shells with junctions and shells with phase interfaces can be considered as examples of material and non-material singular curves, respectively.

2 Resultant Thermodynamics of Shells with Singular Curves

Within the resultant thermodynamics of shells we assumed that the reference and deformed placements of the shell base surface are regular geometric surfaces, that is without kinks, branchings, self-intersections, etc. Also all surface fields were assumed to be smooth, so the classical form of surface divergence theorem is applicable. Assuming that mass is not created during the process, the resultant 2D balance laws of linear and angular momentum, and energy conservation as well as the entropy inequality were presented by Pietraszkiewicz [64] as exact resultant implications of corresponding laws of 3D rational thermodynamics.

Within the Lagrangian description these local laws are satisfied on any regular part of the shell base surface M and consist of:

Local resultant equilibrium equations

$$Div\mathbf{N} + \rho\mathbf{f} = \dot{\mathbf{l}}, \quad Div\mathbf{M} + ax\left(\mathbf{N}\mathbf{F}^T - \mathbf{F}\mathbf{N}^T\right) + \rho\mathbf{c} = \dot{\mathbf{k}} + \dot{\mathbf{y}} \times \mathbf{l}; \tag{1}$$

local resultant balance of energy

$$\rho\dot{\varepsilon} - (\mathbf{N} \bullet \mathbf{E}^{\circ} + \mathbf{M} \bullet \mathbf{K}^{\circ} + Div\mathbf{w}) - (\rho r - Div\mathbf{q}) = 0; \tag{2}$$

and local resultant entropy inequality

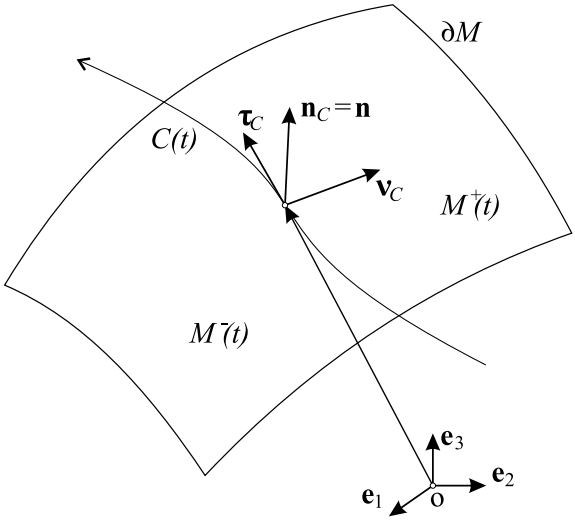

Fig. 1 The regular surface M with moving singular surface curve $C(t)$

$$-\rho\dot{\psi}-\rho\dot{\theta}\eta+\mathbf{N}\bullet\mathbf{E}^{\circ}+\mathbf{M}\bullet\mathbf{K}^{\circ}+Div\mathbf{w}-\rho\theta s-\frac{1}{\theta}\mathbf{q}\cdot\mathbf{g}+\theta Div\mathbf{s}\geqslant 0. \quad (3)$$

In (1)–(3), **N** and **M** are the referential resultant 2D stress and couple-stress tensors of Piola type, **f** and **c** are surface force and couple vectors per unit mass of M, **l** and **k** are surface linear momentum and angular momentum vectors per unit area of M, **y** is the position vector of the base surface $M(t)$ in the current placement, $\mathbf{F}=Grad\mathbf{y}$ is the surface deformation gradient, ε, η, ψ and **q** are the resultant 2D internal energy, entropy, free energy and heat flux vector, $\mathbf{E}^{\circ}$ and $\mathbf{K}^{\circ}$ are the co-rotational time derivatives of 2D strain **E** and bending **K** tensors, **w**, s and **s** are the 2D interstitial working vector, extra surface heat supply and extra surface entropy supply vector, respectively, θ is the mean referential surface temperature, ρ is the surface mass density, Div and $Grad$ are surface divergence and gradient operators, and other surface fields are described as in Pietraszkiewicz [64].

The kinematic structure of the resultant shell thermodynamics is identical with the one of Cosserat surface, see [21, 51, 52], with the position vector **y** of the base surface in current placement (or translation vector **u**) and rotation tensor **Q** fields given on M and treated as independent kinematic variables of the shell motion. The structure of resultant local laws (1)–(3), containing the extra surface field s and divergences of the vector fields **w**, **q** , reminds somewhat the one of local laws of 3D extended thermodynamics, see Müller and Ruggeri [61].

Basic local laws of the resultant shell thermodynamics (1)–(3) were complemented with appropriate 1D jump conditions along stationary and moving singular surface curves. For each balance equations and entropy inequality of (1)–(3) the corresponding 1D jump conditions for linear and angular momentum, and energy as well as

for entropy inequality along the singular curves were formulated by Pietraszkiewicz and Konopińska [47, 68]. In these works authors discussed some geometric and kinematic relations associated with moving and stationary curve on shell base surface, by applying the exact through-the-thickness integration of corresponding 3D balance laws and entropy inequality of 3D rational thermodynamics presented by Truesdell [77]. In order to discuss jumps across singular curves the extended surface transport relation and the extended surface divergence theorems were proposed for the piecewise smooth tensor fields acting on the regular and piecewise regular surface, see Chróścielewski et al. [16] for more details. The so-called patchwork surface divergence theorem has to be used, because in this case the shell base surface M is a piecewise smooth surface being the union of finite number of regular, smooth and connected surface elements M_k, $k = 1, 2, ...$, joined together along spatial curves Γ_a, $a = 1, 2, ...$, forming the complex network of singular spatial curves Γ. This theorem also has to be applied if 2D vector and tensor fields associated with the base surface M are only piecewise smooth ones on some smooth parts of M separated by the movable singular surface curve $C(t)$, see Fig. 1. The resultant, two-dimensionally exact, thermodynamic shell relation formulated by Pietraszkiewicz [64] were complemented by the corresponding jump conditions at the moving (non-material) and stationary (material) singular surface curve, see Pietraszkiewicz and Konopńska [68]. The referential jump conditions for non-material singular thermomechanical processes in shells consist of: local referential dynamic jump conditions across singular curve $C(t)$

$$[\mathbf{N}]\,\boldsymbol{\nu}_C + V\,[\mathbf{l}] = \mathbf{0}, \quad [\mathbf{M}]\,\boldsymbol{\nu}_C + \big[\mathbf{y}\times\mathbf{N}\big]\,\boldsymbol{\nu}_C + V\,\big[\mathbf{k}+\mathbf{y}\times\mathbf{l}\big] = \mathbf{0}; \tag{4}$$

local referential energetic jump condition across $C(t)$

$$V\,[\rho\varepsilon] + \big[\mathbf{w}-\mathbf{q}\big]\cdot\boldsymbol{\nu}_C = 0; \tag{5}$$

and local referential entropic jump inequality across $C(t)$

$$V\,[\rho\eta] - \Big[\frac{\mathbf{q}}{\theta}+\mathbf{s}\Big]\cdot\boldsymbol{\nu}_C \geqslant 0. \tag{6}$$

In (4)–(6) square brackets denote jump of $\boldsymbol{\Phi}$ given by $[\boldsymbol{\Phi}] = \boldsymbol{\Phi}^+ - \boldsymbol{\Phi}^-$, $\boldsymbol{\nu}_C = \boldsymbol{\tau}_C \times \mathbf{n}_C$ is the surface unit vector externally normal to the singular curve $C(t)$ and $V = \mathbf{v}\cdot\boldsymbol{\nu}_C$ is the surface velocity $C(t)$ moving along M.

3 Continuity Conditions along Junctions

The important application of the new jump conditions in structural mechanics is modelling of multi-shells, i.e. complex shell structures composed of regular shell elements interconnected along parts of the boundaries. The problems of shells with

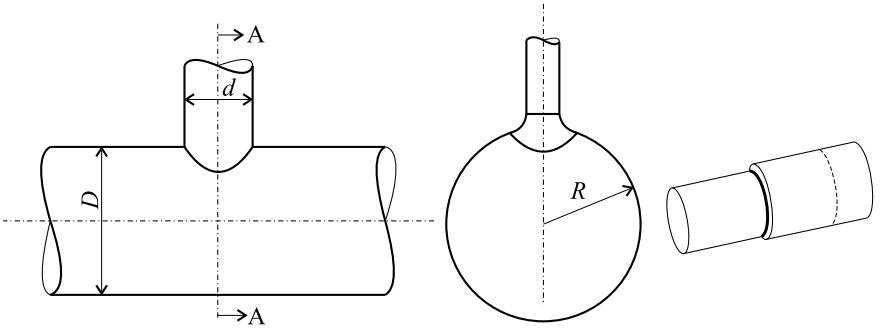

Fig. 2 Junctions in shell structures

junctions were discussed in the literature mainly within the classical, linear, 3-field Kirchhoff-Love thin shell model. Using the linear theory of thin isotropic elastic shells, the axisymmetric junction of two shells of revolution was analyzed in some early papers summarized by Chernykh [13] and Novozhilov et al. [63]. Teng [75, 76] reviewed some recent papers on strength and stability of thin steel shells of revolution composed of cylinders, cones, toroids and plates (Fig. 2).

Pietraszkiewicz and Konopińska [71] presented a review of different theoretical, numerical experimental approaches to modelling, analysis and design of the compound shell structures with junctions. Authors consider many forms of boundary, continuity and/or jump conditions at the singular surface curve modelling junction between regular shell elements. The review contains results for special shell structures like cylinder-cylinder intersections, cone-cylinder and sphere-cylinder junctions, junctions of shells of revolution and tubular joints, as well as for other types of shell junctions. Some books and review papers on junctions in shell structures are also presented.

The non-linear theory of thin irregular shells of Kirchhoff–Love (K-L) type was developed by Makowski et al. [54, 55], where also several forms of static and kinematic jump conditions at the junctions were formulated. Simple forms of non-linear shell relations appropriate for some simplified non-linear models of thin elastic irregular shell structures with junctions were presented in [16]. Chróścielewski et al. [18, 19] developed appropriate two-dimensional (2D) constitutive equations for elasto-plastic behaviour of shell material in order to apply them for numerical analysis of axisymmetric deformations of thin shells of revolution with junctions. Here the complex non-linear industrial examples of compound shell of revolution with account of deformability of the junctions were analyzed.

Within the non-linear resultant six-field shell model, the mechanical theory and numerical analysis by the finite element method (FEM) of multi-shells was developed by Chróścielewski et al. [16], where a number of complex numerical examples of static, stability and dynamic behaviour of elastic multi-shells with rigid junctions in the linear and geometrically non-linear range of deformation were presented. Konopińska and Pietraszkiewicz [46] formulated the exact resultant 2D equilibrium

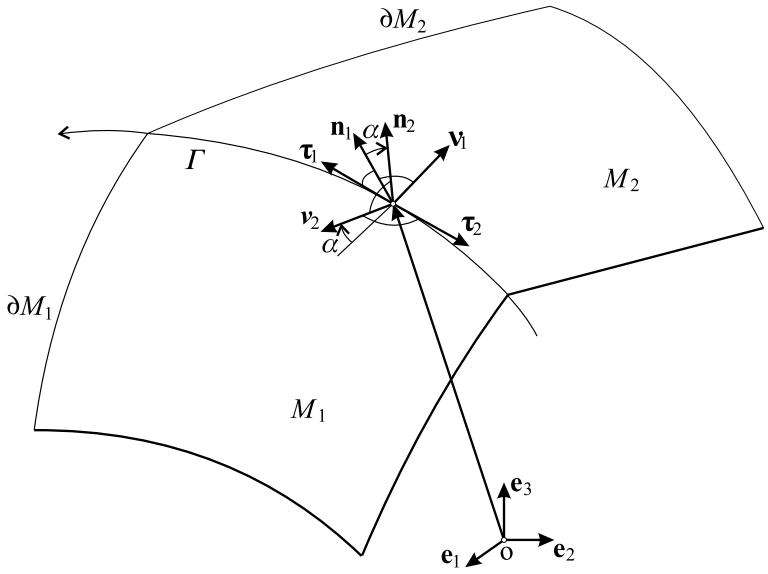

Fig. 3 Junction of two regular shell elements

conditions for the branching and self-intersecting shells, which were later supplemented by an appropriate unique 2D kinematics along the junction of the branching shell by Pietraszkiewicz and Konopińska [67]. This kinematics is work-conjugate to the exact, resultant local equilibrium conditions of the non-linear theory of branching shells. In particular it was shown that the junction behaviour along the stationary singular curve Γ depends on the following shell–junction interaction integral:

$$\text{S–JI} = \int_{\Gamma} ([\mathbf{N}\boldsymbol{\nu} \cdot \delta\mathbf{u}] - [\mathbf{N}\boldsymbol{\nu}] \cdot \delta\mathbf{u}_{\Gamma} + [\mathbf{M}\boldsymbol{\nu} \cdot \boldsymbol{\omega}] - [\mathbf{M}\boldsymbol{\nu}] \cdot \boldsymbol{\omega}_{\Gamma})\, \mathrm{d}s, \tag{7}$$

where $\delta\mathbf{u}, \delta\mathbf{u}_{\Gamma}$ are virtual translations while $\boldsymbol{\omega}, \boldsymbol{\omega}_{\Gamma}$ are virtual rotations near and along Γ, respectively. Pietraszkiewicz and Konopińska [67] took into account different types of junctions, among them are the stiff, entirely simply connected and partly simply supported junctions as well as the elastic, non-local elastic and dissipative junctions. For each type of junction authors proposed the principle of virtual work. It has been shown that the S–JI integral vanishes for the stiff junctions, entirely simply connected and partly simply supported junctions. The natural oscillations of shells with different junctions were consider by Eremeyev et al. [35] using variational approach.

The description of deformable junction within the resultant non-linear shell theory is presented by Pietraszkiewicz [65], where it was assumed that translations across

the junction curve are smooth, so $\left[\mathbf{y}\right] = \mathbf{0}$ across Γ, but rotations $\mathbf{Q}$ are arbitrary. In this paper two regular shell elements joined together along a common boundary are considered, see Fig. 3. In the case of deformable junction 1D relation of constitutive type has been proposed for the junction moments along the junction curve Γ

$$\langle \mathbf{M}\boldsymbol{\nu} \rangle = f\left(\boldsymbol{\kappa}_{\Gamma}\right), \tag{8}$$

where $\langle \mathbf{M}\boldsymbol{\nu} \rangle$ is the average value of $\mathbf{M}\boldsymbol{\nu}$ at Γ, the vector $\boldsymbol{\kappa}_{\Gamma}$ describes the bending resistance of the junction curve Γ during shell deformation and the constitutive function f should be established from appropriate experiments for each particular type of the junction.

From the theory of strength point of view, shell junctions are usually the weakest places of the structure, where large concentrations of stress distributions may take place. To assure their sufficient strength such junctions are usually reinforced by beams. The axially symmetric deformations of a cylindrical shell connected to a circular plate is analyzed by Konopińska-Zmysłowska and Eremeyev [48]. The junction between cylinder and circular plate is reinforced by a ring. The reinforcement along junction is modelled by 1D Cosserat curve which is kinematically consistent with the six-parameter shell theory. The compatibility conditions along the reinforced junction and their influence on the deformations and stress state are analyzed.

As an example of Cosserat curve applications, it is worth to mention the current paper by Miśkiewicz [59], where a refined non-linear six-field theory of beams was developed together with the corresponding numerical algorithm and the computer code, and applied to examples of engineering importance. The 1D beam model developed by Miśkiewicz [59] is compatible with the resultant 1D model of the shell junction discussed here. Presented FEM code was based on the analysis on the non-linear configuration space comprising the rotation group SO(3), which again is similar to the one which should be applied in the six-field shell model with junctions, see Chróścielewski et al. [15, 16].

4 On Constitutive Equations in Six-Parameter Shell Theory

Let us note that the problem of derivation of 2D constitutive equations for refined resultant thermomechanic shell model is quite important, especially for the constitutive equations for the drilling couples. Since no kinematic constraints across the thickness are applied in the resultant approach, see Pietraszkiewicz [64], the 2D constitutive equations cannot be formulated by some degeneration from already known 3D ones. In the special, but important, case of the geometrically non-linear (small-strain) isotropic elastic behaviour, for finding the constitutive equations we have to apply the approach based on the consistent approximation to the 3D complementary energy density of the shell.

The problem of drilling couples and refined constitutive equations in the resultant geometrically non-linear theory of elastic shells was analyzed by Pietraszkiewicz and

Konopińska [69, 70]. Presented approach has been based on the 3D complementary energy density of geometrically non-linear elasticity. New results were obtained 1) explicit definitions of the drilling couples, 2) the consistent 2nd approximation to the 2D complementary energy density of the geometrically non-linear isotropic, elastic shells, 3) the refined constitutive equations for 2D strains and bending strains, 4) the explicit constitutive equations for drilling couples. It has been shown that the drilling couples are much smaller then the stress couples and their influence on the stress and strain state can be omitted in numerical analyzes of regular shell structures.

Pietraszkiewicz [66] formulated the relations of the resultant linear six-field theory of elastic shells by consistent linearization of corresponding relations of the resultant non-linear theory of shells. Contrary to the classical linear three-field Kirchhoff-Love type and five-field Timoshenko-Reissner type shell models, the six-field linear shell model contains the six independent components of the infinitesimal translation and rotation vectors of the shell base surface. The drilling rotation is an independent kinematic variable as well as two surface drilling couples with two work-conjugate surface drilling bending measures. The presence of these additional degrees of freedom is important for analysis of irregular shell structures containing junctions, self-intersections and shell-to-beam transitions.

Another technique to derivate the linear constitutive equations of the six-parameter shells was applied by Altenbach and Eremeyev [3], where through-the-thickness integration procedure was applied to linear plate-like micropolar solid. Further this technique was applied to viscoelastic plates and shells by Altenbach and Eremeyev [2].

The material symmetry group and constitutive equations of anisotropic shells were discussed by Eremeyev and Pietraszkiewicz [28]. This material symmetry group consist of ordered triples of tensors which make the strain energy density invariant under change of the reference placement.The isotropic, hemitropic, orthotropic, transversely isotropic and other types of anisotropy materials are discussed. The group structure is similar to one in the case of micropolar 3D solids, micropolar anisotropic elastic solids are presented by Eremeyev and Pietraszkiewicz [31, 33].

The non-linear BVP of the resultant thermodynamics of shells is non-classical one, because the configuration space of solutions is here an infinite-dimensional Lie group containing rotation group SO(3). This means that in any incremental numerical analysis one should take into account such non-trivial problems as local and global parameterisation of rotations, accumulation of rotations and their increments at each step, C^0 interpolation on SO(3) within each finite element, and many other. Within the six-parameter approach it is possible to construct finite element with the translation vector and rotation tensor at each node. These elements naturally contain the drilling degree of freedom at each node, which is required in proper modelling of the shell junctions and phase transition processes. The 4-node combined shell element with semi-EAS-ANS strain interpolations in six-parameter shell theories with drilling degrees of freedom is presented by Witkowski [82].

Basics on six-parameter shell theory with strain measure of the Cosserat type and the small-strain J_2-type elastoplastic constitutive relations are presented by Burzyński et al. [10]. This formulation can be applied to arbitrary translations and

rotations. In order to demonstrate the correctness of the model and its efficiency to analyze regular and irregular shells, some numerical examples were presented. Burzyński et al. [12] developed the elastic constitutive law for the resultant statically and kinematically exact, non-linear, six-parameter shell theory. Here the Cosserat plane stress equations are integrated through-the-thickness under Reissner-Mindlin kinematics assumption. For constitutive relations within the six-parameter shell theory we refer also to [11, 14, 17, 20].

5 On Phase Transitions in Shells

A phase transition is the transformation of a thermodynamic system from one state of matter to another. In thin-walled shell structures it consists primarily of a diffusionless displacive change of the internal material lattice. Such a process can usually be induced by changing the temperature or/and by applying an external stress. In the resultant models of phase transition in shells proposed by Eremeyev and Pietraszkiewicz [27, 29, 30, 72], some approximations were allowed in the resultant energy balance and entropy inequality.

In the refined resultant shell thermodynamics only one mean referential temperature θ on M was used, because only one resultant energy balance was available, see Pietraszkiewicz [64]. To assure exact correspondence between 2D and 3D 1st and 2nd laws of thermodynamics, three additional 2D fields $\mathbf{w}$, s and $\mathbf{s}$ appeared in the local laws (1)–(3). These additional fields had to be taken into account also in the jump conditions (4)–(6), which are compatible with the refined resultant shell model, see Pietraszkiewicz and Konopińska [68]. Another approach to two-phase thermodynamics was proposed by Eremeyev and Pietraszkiewicz [30] where two surface temperature-related fields and their surface entropy counterparts were introduced.

In phase transition problems, the movable phase interface C can be either coherent or incoherent in rotations. For the coherent interface both kinematic fields $\mathbf{y}$ (or $\mathbf{u}$) and $\mathbf{Q}$ are supposed to be continuous at C and the kinematic compatibility along C become

$$[\![\, \mathbf{v} \,]\!] + V[\![\, \mathbf{F}\boldsymbol{\nu} \,]\!] = \mathbf{0}, \quad [\![\, \boldsymbol{\omega} \,]\!] + V[\![\, \mathbf{K}\boldsymbol{\nu} \,]\!] = \mathbf{0}, \tag{9}$$

where the expression $[\![...]\!] = (...)_B - (...)_A$ means the jump at C dividing two material phases A and B, $\mathbf{v} = \dot{\mathbf{u}}$ is the translational velocity and $\boldsymbol{\omega} = ax\left(\dot{\mathbf{Q}}\mathbf{Q}^T\right)$ the angular velocity vectors, while $V = \dot{\mathbf{x}}_C \cdot \boldsymbol{\nu}$ is the tangent phase interface velocity relative to M. For the interface incoherent in rotations $\mathbf{Q}$ may be discontinuous at C, and the second relation (9) may be violated. In phase transition processes the mean referential temperature θ is assumed to be continuous on the whole M, so that $[\![\, \theta \,]\!] = 0$. The kinetic relations, which describe motion of the phase interface C as a non-material singular curve moving on the shell base surface are presented in [30, 68].

Eremeyev and Pietraszkiewicz [29, 32] considered the phase transitions in thermo-viscoelastic shells. In the case of finite deformations the non-linear thermomechanic boundary value problem for thermoelastic or thermoviscoelastic shells undergoing phase transitions consists of the equilibrium equations with appropriate static and kinematic boundary conditions, the thermoconductivity equations, the compatibility conditions along the interface C and kinetic equations along C all supplemented by proper constitutive equations. The presented in Eremeyev and Pietraszkiewicz [29, 30, 32] kinetic equation describes motion of the phase interface C for all quasi-static processes and allows to find the position of the curvilinear phase interface.

The special case of phase transition problem in shell structure is considered by Eremeyev and Konopińska-Zmysłowska [25], where the phase equilibrium of a two-phase liquid membrane containing a wedge disclination were analyzed within six-parameter shell theory. The model of liquid shell is treated as two-dimensional elastic micropolar fluid which may resist to bending-torsion deformations. Based on variational approach authors formulate the equilibrium conditions at a phase interface. As an example, axial two-phase deformations of an elastic liquid plate with a wedge disclination is studied.

Eremeyev and Pietraszkiewicz [27, 30] introduced the 2D Eshelby tensor as a driving force acting on a phase interface. Eremeyev and Konopińska-Zmysłowska [26] discussed the correspondence between 2D Eshelby tensor and its 3D counterpart introduced by Eshelby [36–38]. We showed that there is a straightforward correspondence between these tensors as for stress resultant tensor and surface energy and their 3D counterparts.

Let us note that a phase interface is only one example of non-material singular curve. For example, other phenomena such as wrinkling, sharp boundary layers found recently in new class of thin structures called pantographic sheets can be modelled through a singular curve motion, see e.g. [22, 40–42, 79].

6 Conclusions

Here we presented a review of recent results within six-parameter shell theory related to the modelling of singular curves. We presented briefly the general compatibility equations along singular curves and discussed two applications of the theory to shells with junctions and shells undergoing stress-induced phase transitions. These two applications are examples of material and non-material singular curves, respectively. The special attention was also paid to 2D constitutive equations. For further applications of the six-parameter shell theory which is one of the main fields of interest of Prof. Wojciech Pietraszkiewicz, we refer to reviews in [4, 5, 24].

Acknowledgements The first author acknowledges financial support from the National Centre of Science of Poland with the grant DEC – 2012/05/D/ST8/02298.

References

1. Abeyaratne, R., Knowles, J.K.: Evolution of Phase Transitions. A Continuum Theory. Cambridge University Press, Cambridge (2006)
2. Altenbach, H., Eremeyev, V.: On the constitutive equations of viscoelastic micropolar plates and shells of differential type. Math. Mech. Complex Syst. **3**(3), 273–283 (2015)
3. Altenbach, H., Eremeyev, V.A.: On the linear theory of micropolar plates. J. Appl. Math. Mech. ZAMM **89**(4), 242–256 (2009)
4. Altenbach, H., Eremeyev, V.A.: Actual developments in the nonlinear shell theorystate of the art and new applications of the six-parameter shell theory. In: Pietraszkiewicz, W., Górski, J. (Eds.) Shell Structures: Theory and Applications, Taylor & Francis Group, London, vol. 3, pp. 3–12 (2014)
5. Altenbach, J., Altenbach, H., Eremeyev, V.A.: On generalized Cosserat-type theories of plates and shells: a short review and bibliography. Arch. Appl. Mech. **80**(1), 73–92 (2010)
6. Berezovski, A., Engelbrecht, J., Maugin, G.A.: Numerical Simulation of Waves and Fronts in Inhomogeneous Solids. World Scientific, New Jersey (2008)
7. Bhattacharya, K.: Microstructure of Martensite: Why It Forms and How It Gives Rise to the Shape-Memory Effect. Oxford University Press, Oxford (2003)
8. Bhattacharya, K., James, R.D.: A theory of thin films of martensitic materials with applications to microactuators. J. Mech. Phys. Solids **47**(3), 531–576 (1999)
9. Bhattacharya, K., James, R.D.: The material is the machine. Science **307**(5706), 53–54 (2005)
10. Burzyński, S., Chróścielewski, J., Witkowski, W.: Elastoplastic law of Cosserat type in shell theory with drilling rotation. Math. Mech. Solids **20**(7), 790–805 (2015)
11. Burzyński, S., Chróścielewski, J., Daszkiewicz, K., Witkowski, W.: Geometrically nonlinear FEM analysis of FGM shells based on neutral physical surface approach in 6-parameter shell theory. Compos. Part B: Eng. **107**, 203–213 (2016)
12. Burzyński, S., Chróścielewski, J., Witkowski, W.: Geometrically nonlinear FEM analysis of 6-parameter resultant shell theory based on 2-D Cosserat constitutive model. J. Appl. Math. Mech. ZAMM **96**(2), 191–204 (2016)
13. Chernykh, K.F.: Linear Theory of Shells (in Russian). University Press, 1968 English Translation by NASA-TT-F-II (1964)
14. Chróścielewski, J., Witkowski, W.: On some constitutive equations for micropolar plates. ZAMM **90**(1), 53–64 (2010)
15. Chróścielewski, J., Makowski, J., Stumpf, H.: Finite element analysis of smooth, folder and multi-shells. Comp. Meth. Appl. Mech. Engrg. **141**, 1–46 (1997)
16. Chróścielewski, J., Makowski, J., Pietraszkiewicz, W.: Statyka i dynamika powłok wielopłatowych: Nieliniowa teoria i metoda elementów skończonych (in Polish). Biblioteka Mechaniki Stosowanej, Wydawnictwo IPPT PAN (2004)
17. Chróścielewski, J., Pietraszkiewicz, W., Witkowski, W.: On shear correction factors in the non-linear theory of elastic shells. Int. J. Solids Struct. **47**(25), 3537–3545 (2010)
18. Chróścielewski, J., Konopińska, V., Pietraszkiewicz, W.: On elasto-plastic analysis of thin shells with deformable junctions. In: Altenbach, H., Eremeyev, V.A. (eds.) Shell-like Structures—Nonclassical Theories and Applications, pp. 441–452. Springer, Berlin (2011)
19. Chróścielewski, J., Konopińska, V., Pietraszkiewicz, W.: On modelling and non-linear elasto-plastic analysis of thin shells with deformable junctions. J. Appl. Math. Mech. ZAMM **91**(6), 477–484 (2011)
20. Chróścielewski, J., Sabik, A., Sobczyk, B., Witkowski, W.: Nonlinear FEM 2D failure onset prediction of composite shells based on 6-parameter shell theory. Thin-Walled Struct. **105**, 207–219 (2016)
21. Cosserat, E., Cosserat, F.: Theorie des corps deformables. Herman et Fils, Paris (1909)
22. Cuomo, M., dell'Isola, F., Greco, L., Rizzi, N.L.: First versus second gradient energies for planar sheets with two families of inextensible fibres: investigation on deformation boundary layers, discontinuities and geometrical instabilities. Compos. Part B: Eng. **115**, 423–448 (2017)

23. Dong, L., Sun, Q.P.: On equilibrium domains in superelastic NiTi tubes - helix versus cylinder. Int. J. Solids Struct. **49**, 1063–1076 (2012)
24. Eremeyev, V., Altenbach, H.: Basics of mechanics of micropolar shells. In: Altenbach, H., Eremeyev, V. (eds.) Shell-like Structures: Advanced Theories and Applications, pp. 63–111. Springer, Cham (2017)
25. Eremeyev, V.A., Konopińska-Zmysłowska, V.: On phase equilibrium of an elastic liquid shell with wedge disclination. In: Pietraszkiewicz W, Witkowski W (eds) Shell Structures: Theory and Applications, vol. 4, Taylor & Francis Group, London, pp. 89–92 (2018)
26. Eremeyev, V.A., Konopińska-Zmysłowska, V.: On the correspondence between two- and three-dimensional Eshelby tensors. Continuum Mechanics and Thermodynamics https://doi.org/10.1007/s00161-019-00754-6 (2019)
27. Eremeyev, V.A., Pietraszkiewicz, W.: The non-linear theory of elastic shells with phase transitions. J. Elast. **74**(1), 67–86 (2004)
28. Eremeyev, V.A., Pietraszkiewicz, W.: Local symmetry group in the general theory of elastic shells. J. Elast. **85**(2), 125–152 (2006)
29. Eremeyev, V.A., Pietraszkiewicz, W.: Phase transitions in thermoelastic and thermoviscoelastic shells. Arch. Mech. **61**(1), 41–67 (2009)
30. Eremeyev, V.A., Pietraszkiewicz, W.: Thermomechanics of shells undergoing phase transition. J. Mech. Phys. Solids **59**(7), 1395–1412 (2011)
31. Eremeyev, V.A., Pietraszkiewicz, W.: Material symmetry group of the non-linear polar-elastic continuum. Int. J. Solids Struct. **49**(14), 1993–2005 (2012)
32. Eremeyev, V.A., Pietraszkiewicz, W.: Phase transitions in thermoviscoelastic shells. In: Hetnarski, R. (ed.) Encyclopedia of Thermal Stresses, pp. 3667–3673. Springer, Berlin (2015)
33. Eremeyev, V.A., Pietraszkiewicz, W.: Material symmetry group and constitutive equations of micropolar anisotropic elastic solids. Math. Mech. Solids **21**(2), 210–221 (2016)
34. Eremeyev, V.A., Lebedev, L.P., Altenbach, H.: Foundations of Micropolar Mechanics. Springer, Heidelberg (2013)
35. Eremeyev, V.A., Lebedev, L.P., Cloud, M.J.: The Rayleigh and Courant variational principles in the six-parameter shell theory. Math. Mech. Solids **20**(7), 806–822 (2015)
36. Eshelby, J.D.: The force on an elastic singularity. Phil. Trans. R Soc. Lond A **244**(877), 87–112 (1951)
37. Eshelby, J.D.: The determination of the elastic field of an ellipsoidal inclusion, and related problems. Proc. Royal Soc. Lond. Ser. A Math. Phys. Sci. **241**(1226), 376–396 (1957)
38. Eshelby, J.D.: The elastic energy-momentum tensor. J. Elast. **5**(3–4), 321–335 (1975)
39. Feng, P., Sun, Q.P.: Experimental investigation on macroscopic domain formation and evolution in polycrystalline NiTi microtubing under mechanical force. J. Mech. Phys. Solids **54**(8), 1568–1603 (2006)
40. Giorgio, I., Grygoruk, R., dellIsola F, Steigmann, D.J.: Pattern formation in the three-dimensional deformations of fibered sheets. Mech. Res. Commun. **69**, 164–171 (2015)
41. Giorgio, I., Harrison, P., dell'Isola, F., Alsayednoor, J., Turco, E.: Wrinkling in engineering fabrics: a comparison between two different comprehensive modelling approaches. In: Proceedings of the Royal Society A: Mathematical, Physical and Engineering Sciences vol. 474(2216), 20180,063 (2018)
42. Giorgio, I., dell'Isola, F., Steigmann, D.J.: Edge effects in hypar nets. Comptes Rendus Mécanique (2019)
43. Gurtin, M.E.: Configurational Forces as Basic Concepts of Continuum Physics. Springer, Berlin (2000)
44. Gurtin, M.E., Fried, E., Anand, L.: The Mechanics and Thermodynamics of Continua. Cambridge University Press, Cambridge (2010)
45. He, Y.J., Sun, Q.P.: Macroscopic equilibrium domain structure and geometric compatibility in elastic phase transition of thin plates. Int. J. Mech. Sci. **52**, 198–211 (2010)
46. Konopińska, V., Pietraszkiewicz, W.: Exact resultant equilibrium conditions in the non-linear theory of branching and self-intersecting shells. Int. J. Solids Struct. **44**(1), 352–369 (2007)

47. Konopińska, V., Pietraszkiewicz, W.: On jump conditions at non-material singular curves in the resultant shell thermomechanics. In: Pietraszkiewicz, W., Górski, J. (Eds.) Shell Structures: Theory and Applications, vol. 3, Taylor & Francis Group, London, pp. 117–120 (2014)
48. Konopińska-Zmysłowska, V., Eremeyev, V.A.: On axially symmetric shell problems with reinforced junctions. In: Owen, R., de Borst, R., Reese, J., Pearce, C. (eds.) ECCM VI-ECFD VII Proceedings, pp. 3681–3688. ECCOMAS, Glasgow (2018)
49. Kosiński, W.: Field Singularities and Wave Analysis in Continuum Mechanics. Ellis Horwood, Chicester and PWN, Warszawa (1986)
50. Lagoudas, D.C. (Ed.): Shape Memory Alloys. Modeling and Engineering Applications, Springer, Berlin (2008)
51. Libai, A., Simmonds, J.G.: Nonlinear elastic shell theory. Adv. Appl. Mech. **23**, 271–371 (1983)
52. Libai, A., Simmonds, J.G.: The Nonlinear Theory of Elastic Shells, 2nd edn. Cambridge University Press, Cambridge (1998)
53. Makowski, J., Pietraszkiewicz, W.: Thermomechanics of Shells with Singular Curves. Wydawnictwo IMP PAN, Gdańsk (2002)
54. Makowski, J., Pietraszkiewicz, W., Stumpf, H.: On the general form of jump conditions for thin irregular shells. Arch. Mech. **50**(2), 483–495 (1998)
55. Makowski, J., Pietraszkiewicz, W., Stumpf, H.: Jump conditions in the non-linear theory of thin irregular shells. J. Elast. **54**(1), 1–26 (1999)
56. Maugin, G.A.: Material Inhomogeneities in Elasticity. Chapman Hall, London (1993)
57. Maugin, G.A.: Nonlinear Waves in Elastic Crystals. Oxford University Press, Oxford (1999)
58. Maugin, G.A.: Configurational Forces: Thermomechanics, Physics, Mathematics, and Numerics. CRC Pressl, Boca Raton (2011)
59. Miśkiewicz, M.: Structural response of existing spatial truss roof construction based on cosserat rod theory. Contin. Mech. Thermodyn. **31**(1), 79–99 (2019)
60. Miyazaki, S., Fu, Y.Q., Huang, W.M. (eds.): Thin Film Shape Memory Alloys: Fundamentals and Device Applications. Cambridge University Press, Cambridge (2009)
61. Müller, I., Ruggeri, T.: Rational Extended Thermodynamics, 2nd edn. Springer, New York (1998)
62. Ng, K.L., Sun, Q.P.: Stress-induced phase transformation and detwinning in NiTi polycrystalline shape memory alloy tubes. Mech. Mater. **38**(1–2), Sp. Iss. SI):41–56 (2006)
63. Novozhilov, V.V., Chernykh, K.F., Mikhailovskii, E.I.: Linear Theory of Thin Shells (in Russian). Politekhnika, Leningrad (1991)
64. Pietraszkiewicz, W.: Refined resultant thermomechanics of shells. Int. J. Eng. Sci. **49**(10), 1112–1124 (2011)
65. Pietraszkiewicz, W.: On a description of deformable junctions in the resultant nonlinear shell theory. In: Advanced Methods of Continuum Mechanics for Materials and Structures, pp. 457–468. Springer (2016)
66. Pietraszkiewicz, W.: The resultant linear six-field theory of elastic shells: what it brings to the classical linear shell models? J. Appl. Math. Mech. ZAMM **96**(8), 899–915 (2016)
67. Pietraszkiewicz, W., Konopińska, V.: On unique two-dimensional kinematics for the branching shells. Int. J. Solids Struct. **48**, 2238–2244 (2011)
68. Pietraszkiewicz, W., Konopińska, V.: Singular curve in the resultant thermomechanics of shells. Int. J. Eng. Sci. **80**, 21–31 (2014)
69. Pietraszkiewicz, W., Konopińska, V.: Drilling couples and refined constitutive equations in the resultant geometrically non-linear theory of elastic shells. Int. J. Solids Struct. **51**, 2133–2143 (2014)
70. Pietraszkiewicz, W., Konopińska, V.: On refined constitutive equations in the six-field theory of elastic shells. In: Pietraszkiewicz, W., Górski, J. (Eds.) Shell Structures: Theory and Applications, vol. 3, Taylor & Francis Group, London, pp. 137–140 (2014)
71. Pietraszkiewicz, W., Konopińska, V.: Junctions in shell structures: a review. Thin-Walled Struct. **95**, 310–334 (2015)
72. Pietraszkiewicz, W., Eremeyev, V.A., Konopińska, V.: Extended non-linear relations of elastic shells undergoing phase transitions. J. Appl. Math. Mech. ZAMM **87**(2), 150–159 (2007)

73. Roytburd, A.L., Slutsker, J.: Theory of multilayer SMA actuators. Mater. Trans. **43**(5), 1023–1029 (2002)
74. Straughan, B.: Stability and Wave Motion in Porous Media, vol. 165. Springer, New York (2008)
75. Teng, J.G.: Intersections in steel shell structures. Prog. Struct. Eng. Mater. **2**, 459–471 (2000)
76. Teng, J.G.: Shell junctions. In: Teng, J.G., Rotter, J.M. (Eds.) Buckling of Thin Metal Shells, pp. 369–408. Spon Press, Taylor & Francis (2004)
77. Truesdell, C.: Rational Termodynamics, 2nd edn. Springer, New York (1984)
78. Truesdell, C., Toupin, R.A.: Encyclopedia of Physics, vol III/1, Springer, Berlin, chap The classical field theories, pp. 226–858 (1961)
79. Turco, E., dell'Isola, F., Cazzani, A., Rizzi, N.L.: Hencky-type discrete model for pantographic structures: numerical comparison with second gradient continuum models. Zeitschrift für angewandte Mathematik und Physik **67**(4), 85 (2016)
80. Šilhavý, M.: The Mechanics and Thermodynamics of Continuum Media. Springer, Berlin (1997)
81. Whitham, G.B.: Linear and Nonlinear Waves. Wiley, New York (1999)
82. Witkowski, W.: 4-node combined shell element with semi-EAS-ANS strain interpolations in 6-parameter shell theories with drilling degrees of freedom. Comput. Mech. **43**, 307–319 (2009)
83. Yoneyama, T., Miyazaki, S. (eds.): Shape Memory Alloys and Biomedical Applications. Woodhead P Ltd, Cambridge (2009)

Hybrid-Mixed Shell Finite Elements and Implicit Dynamic Schemes for Shell Post-buckling

Marko Lavrenčič and Boštjan Brank

Abstract Two topics are addressed: (i) hybrid-mixed formulations for geometrically exact shell models, and (ii) post-buckling analysis of shells by implicit dynamics schemes. As for the hybrid-mixed elements, seven formulations are compared. The one with the assumed-natural-strain interpolation of membrane strains shows very little sensitivity to mesh distortion for curved shells. Another one, which is based on the Hu-Washizu three-field functional, allows for very large solution increments. Hence, a new element is proposed that combines positive features of both mentioned formulations. As for the post-buckling analysis of shells, we use implicit dynamics. In particular, five time-stepping schemes are tested for shell stability problems that include mode jumping. These are trapezoidal rule, schemes with numerical dissipation in the high-frequency range, and energy-momentum conserving method. Numerical examples show that the dissipative schemes are suitable for simulation of complex phenomena that appear in shell stability.

Keywords Geometrically exact shell models · Hybrid-mixed shell elements · Implicit dynamics schemes · Numerical dissipation · Shell stability analysis

1 Introduction

Shell systems are frequent in nature, engineering and technology. The computational methods for simulation, analysis, design and optimization of such systems rely on various shell theoretical models and their finite element approximations. The shell models may be classified according to the adopted basic kinematic assumption. Let us mention several important groups: geometrically exact shell models (without drilling rotation), see e.g. [38, 10]; micropolar shell models (with drilling rotation), see e.g.

M. Lavrenčič (✉) · B. Brank
Faculty of Civil and Geodetic Engineering, University of Ljubljana, Jamova c. 2, 1000 Ljubljana, Slovenia
e-mail: mlavrenc@fgg.uni-lj.si

B. Brank
e-mail: bbrank@fgg.uni-lj.si

H. Altenbach et al. (eds.), *Recent Developments in the Theory of Shells*,
Advanced Structured Materials 110, https://doi.org/10.1007/978-3-030-17747-8_21

[35–37, 47, 48]; rotation-less shell models, see e.g. [42, 30]; shell models that take into account through-the-thickness stretching, see e.g. [9]; and shell models that consider cross-section warping, see e.g. [7].

The finite element formulations for a particular shell model differ with respect to the adopted background variational principle and interpolations. Mixed elements are based on mixed variational principles. When a mixed element condenses the non-displacement-like degrees-of-freedom at the element level, it is called hybrid-mixed or mixed-hybrid, see e.g. [16] (though this terminology is not universally accepted). As for the interpolation of initial and deformed configurations, let us mention classical isoparametric elements and isogeometric shell elements (e.g. [33]); the latter use functions common in the Computer Aided Design.

In this work, we discuss two topics. (i) The first one addresses advanced hybrid-mixed low-order finite elements for the geometrically exact shell models. We consider seven formuations based on: Assumed Natural Strain (ANS) concept; Enhanced Assumed Strain (EAS) concept; Hellinger-Reissner (HR) functional; and Hu-Washizu (HW) functional. For many nonlinear shell problems these elements provide very similar solutions. However, the results may differ considerably for distorted meshes. Moreover, the computations may differ substantially with respect to the allowed load-step length and required time. For some stability problems, the elements may even provide different solutions. We will give a brief assessment of seven hybrid-mixed elements by comparing results of several numerical examples.

(ii) The second topic is stability analysis of shells in the frameworks of implicit structural dynamics and geometrically exact shell model. Inadequacy of path-following static methods has been reported for shells with complex post-critical equilibrium paths, see e.g. [44]. For this reason, the static stability analysis may be replaced by a combined static-dynamic analysis or even by a pure dynamic analysis. In this work, we apply implicit dynamics. To this end, we adopt a family of time-stepping schemes, which are classified as Generalized-energy-momentum (GEM) method, see e.g. [14, 27, 28, 30]. Special cases of GEM are schemes that numerically dissipate in the high-frequency range. An Energy-momentum conserving (EMC) scheme, which conserves energy, angular momentum and linear momentum of an autonomous motion, is also a special case of GEM. Besides GEM, we use Energy-decaying (ED) scheme (see e.g. [8, 2]), which is an extension of the EMC, see e.g. [43, 10]. The ED scheme allows for a controllable numerical dissipation in the high-frequency range. Numerical examples are presented in order to illustrate ability of such an approach to simulate complex shell-buckling processes that include mode jumping.

2 Hybrid-Mixed Shell Finite Elements

2.1 Geometrically Exact Shell Model

We adopt the inextensible-director shell model with Reissner-Mindlin kinematics. An overview of the model is provided below; for a more detailed description, we refer to e.g. [12, 38] and references therein.

Position vectors in the initial and deformed configurations are given as functions of curvilinear coordinates ξ^1, ξ^2, ξ^3

$$X\left(\xi^1, \xi^2, \xi^3\right) = \boldsymbol{X}_0\left(\xi^1, \xi^2\right) + \xi^3 \boldsymbol{D}\left(\xi^1, \xi^2\right), \xi^3 \in [-t/2, t/2], \tag{1}$$

$$x\left(\xi^1, \xi^2, \xi^3\right) = \boldsymbol{x}_0\left(\xi^1, \xi^2\right) + \xi^3 \boldsymbol{d}\left(\xi^1, \xi^2\right), \tag{2}$$

respectively. In what follows, we will omit writing the dependence of functions on curvilinear coordinates. In (1) and (2), $\boldsymbol{D}$ is normal to initial mid-surface, $\boldsymbol{d}$ is deformed (i.e. rotated) shell director described by 2 rotational parameters, $\|\boldsymbol{D}\| = \|\boldsymbol{d}\| = 1$, and t is initial shell thickness. The "in-plane" components of the Green-Lagrange strain tensor are

$$E_{\alpha\beta} = \tfrac{1}{2}\left(\boldsymbol{x}_{,\xi^\alpha} \cdot \boldsymbol{x}_{,\xi^\beta} - \boldsymbol{X}_{,\xi^\alpha} \cdot \boldsymbol{X}_{,\xi^\beta}\right) = \varepsilon_{\alpha\beta} + \xi^3 \kappa_{\alpha\beta} + \left(\xi^3\right)^2 \rho_{\alpha\beta}, \alpha, \beta \in \{1, 2\}, \tag{3}$$

where $\varepsilon_{\alpha\beta} = E_{\alpha\beta}\big|_{\xi^3=0}$ and $\kappa_{\alpha\beta} = \partial E_{\alpha\beta} / \partial \xi^3\big|_{\xi^3=0}$ are membrane and bending strains. The transverse shear strains are

$$E_{\alpha 3} = E_{3\alpha} = \tfrac{1}{2}\left(\boldsymbol{x}_{,\xi^\alpha} \cdot \boldsymbol{d} - \boldsymbol{X}_{,\xi^\alpha} \cdot \boldsymbol{D}\right) = \varepsilon_{\alpha 3} + \xi^3 \kappa_{\alpha 3}. \tag{4}$$

It is reasonable to neglect $\rho_{\alpha\beta}$ in (3) and $\kappa_{\alpha 3}$ in (4) and collect other strains in three vectors: $\boldsymbol{\varepsilon} = [\varepsilon_{11}, \varepsilon_{22}, 2\varepsilon_{12}]^{\mathrm{T}}$, $\boldsymbol{\kappa} = [\kappa_{11}, \kappa_{22}, 2\kappa_{12}]^{\mathrm{T}}$ and $\boldsymbol{\gamma} = [2\varepsilon_{13}, 2\varepsilon_{23}]^{\mathrm{T}}$. Energy-conjugated second Piola-Kirchhoff shell stress resultants are also grouped into vectors of membrane forces, bending moments, and transverse shear forces as $\boldsymbol{N} = [N_{11}, N_{22}, N_{12}]^{\mathrm{T}}$, $\boldsymbol{M} = [M_{11}, M_{22}, M_{12}]^{\mathrm{T}}$ and $\boldsymbol{Q} = [Q_{13}, Q_{23}]^{\mathrm{T}}$, respectively. We adopt the hyperelastic Saint Venant-Kirchhoff shell material model. The following relations between the shell internal forces and the shell strains apply: $\boldsymbol{N} = \boldsymbol{C}^m \boldsymbol{\varepsilon}$, $\boldsymbol{M} = \boldsymbol{C}^b \boldsymbol{\kappa}$, $\boldsymbol{Q} = \boldsymbol{C}^s \boldsymbol{\gamma}$, where $\boldsymbol{C}^m$, $\boldsymbol{C}^b$ and $\boldsymbol{C}^s$ have standard forms for the inextensible-director shell model, see e.g. [38].

Let the shell be loaded by (mid-surface) surface pressure and body loads, which are both included in $\bar{\boldsymbol{b}}$, boundary forces $\bar{\boldsymbol{t}}$, and N point forces $\boldsymbol{F}$. Hence, the potential energy functional reads

$$\Pi(\boldsymbol{u},\boldsymbol{d}) = \Pi_{\text{int}}(\boldsymbol{u},\boldsymbol{d}) - \Pi_{\text{ext}}(\boldsymbol{u},\boldsymbol{d})$$
$$= \int_A \frac{1}{2}\left(\boldsymbol{\varepsilon}^T \boldsymbol{C}^m \boldsymbol{\varepsilon} + \boldsymbol{\kappa}^T \boldsymbol{C}^b \boldsymbol{\kappa} + \boldsymbol{\gamma}^T \boldsymbol{C}^s \boldsymbol{\gamma}\right) dA - \left(\int_A \boldsymbol{u}^T \bar{\boldsymbol{b}} dA + \int_{\Gamma_{\bar{t}}} \boldsymbol{u}^T \bar{\boldsymbol{t}} ds + \sum_{i=1}^{N} \boldsymbol{u}_i^T \boldsymbol{F}\right) \quad (5)$$

where $\boldsymbol{u} = \boldsymbol{x}_0 - \boldsymbol{X}_0$, A is element's area, and $\Gamma_{\bar{t}}$ is part of the boundary where loads are prescribed. The weak form of the boundary value problem corresponds to the minimum of Π

$$\delta\Pi(\boldsymbol{u},\boldsymbol{d};\delta\boldsymbol{u},\delta\boldsymbol{d}) = \int_A \left(\delta\boldsymbol{\varepsilon}^T \boldsymbol{N} + \delta\boldsymbol{\kappa}^T \boldsymbol{M} + \delta\boldsymbol{\gamma}^T \boldsymbol{Q}\right) dA - \delta\,\Pi_{\text{ext}}(\delta\boldsymbol{u},\delta\boldsymbol{d}) = 0, \quad (6)$$

where $\delta\boldsymbol{u}$ and $\delta\boldsymbol{d}$ are kinematically admissible variations, $\delta\,\Pi_{\text{ext}}$ is virtual work of external loading, and $\delta\boldsymbol{\varepsilon}$, $\delta\boldsymbol{\kappa}$ and $\delta\boldsymbol{\gamma}$ are variations of membrane, bending and transverse shear strains, respectively.

Either Eqs. (5) or (6) is the starting point for the finite element discretization, which relies on interpolations of $\boldsymbol{u}$ and $\boldsymbol{d}$ and their variations. As a result, a displacement-based finite element is obtained, which, however, suffers from locking. In Sect. 2.4, we will discuss several discretizations based on mixed interpolations, which provide hybrid-mixed finite elements that are locking-free. After discretization, the linearization needs to be performed in order to apply Newton-Raphson solution method for the resulting system of nonlinear equations. For more details on these topics, see e.g. [12, 39] and references therein.

2.2 Shell Director Description

We adopt two approaches to describe shell director in the deformed configuration. The first one uses large rotations and the second one is rotation-less. As for the former one, either the total rotation vector or the incremental rotation vector is chosen to describe rotation without a drill of the shell director, see e.g. [36, 37, 47]. As for the latter one, presented in Sect. 2.3, we introduce the extensible director.

2.2.1 Total Rotation Vector

The inextensible shell director at deformed configuration can be described as $\boldsymbol{d} = \boldsymbol{\Lambda}_0 \boldsymbol{\Lambda}(\boldsymbol{\vartheta}_G)\boldsymbol{e}_3$, where $\boldsymbol{e}_3 = [0,0,1]^T$, $\boldsymbol{\Lambda}_0$ is known rotation that maps $\boldsymbol{e}_3$ into $\boldsymbol{D}$, and $\boldsymbol{\Lambda}(\boldsymbol{\vartheta}_G)$ is rotation, which is defined in terms of the total rotation vector $\boldsymbol{\vartheta}_G$ (having only two nonzero components, since the drill is zero)

$$\boldsymbol{\Lambda}(\boldsymbol{\vartheta}_G) = \cos\vartheta_G \mathrm{I} + \frac{\sin\vartheta_G}{\vartheta_G}\hat{\boldsymbol{\vartheta}}_G + \frac{1-\cos\vartheta_G}{\vartheta_G^2}(\boldsymbol{\vartheta}_G \otimes \boldsymbol{\vartheta}_G). \quad (8)$$

In (8), $\mathbf{I}$ is identity matrix, $\hat{\boldsymbol{\vartheta}}_G \boldsymbol{b} = \boldsymbol{\vartheta}_G \times \boldsymbol{b}$ for any $\boldsymbol{b}$, and $\vartheta_G = \|\boldsymbol{\vartheta}_G\|$. The expression for the deformed shell director is thus

$$\boldsymbol{d} = \boldsymbol{\Lambda}_0 \Big[\cos\vartheta_G \boldsymbol{e}_3 + \tfrac{\sin\vartheta_G}{\vartheta_G} \boldsymbol{\vartheta}_G \times \boldsymbol{e}_3 \Big]. \tag{9}$$

The variation of (8) is $\delta\boldsymbol{d} = \mathbf{A}(\vartheta_G)\delta\bar{\boldsymbol{\vartheta}}_G$, where $\delta\bar{\boldsymbol{\vartheta}}_G$ is a two-component variation of the total rotation vector. Matrix $\mathbf{A}(\vartheta_G)$ has singularity for $\vartheta_G = k\pi, k = 1, 2, \cdots$, see e.g. [5, 21].

2.2.2 Incremental Rotation Vector

In order to avoid singularity in computations, one can replace $\boldsymbol{\Lambda}_0$ in (9) with $\boldsymbol{\Lambda}_n$. The latter is related to the last converged equilibrium configuration (i.e. to the solution of the last (e.g. n^{th}) increment) as $\boldsymbol{d}_n = \boldsymbol{\Lambda}_n \boldsymbol{e}_3$. The deformed shell director is then described as $\boldsymbol{d} = \boldsymbol{\Lambda}_n \boldsymbol{\Lambda}(\boldsymbol{\vartheta}_I)\boldsymbol{e}_3$, where $\boldsymbol{\vartheta}_I$ is incremental rotation vector. Its variation is $\delta\boldsymbol{d} = \mathbf{A}(\vartheta_I)\delta\bar{\boldsymbol{\vartheta}}_I$, where $\delta\bar{\boldsymbol{\vartheta}}_I$ is a two-component incremental rotation vector. Matrix $\mathbf{A}(\vartheta_I)$ has singularity at $\vartheta_I = \|\boldsymbol{\vartheta}_I\| = k\pi, k = 1, 2, \ldots$ In practice, however, this singularity does not present a problem, since the norm of the incremental rotation vector is always much smaller than π.

2.3 Rotation-Less Shell Model

Let us briefly describe a 6-parameter geometrically exact shell model with only displacement degrees of freedom, which are 3 displacements of shell mid-surface, and 3 components of difference vector. Such model is obtained by a modification of the model from Sect. 2.1.

The shell director is assumed as extensible and its deformed configuration is described as

$$\mathbf{d} = \mathbf{D} + \boldsymbol{w}, \tag{10}$$

where $\boldsymbol{w}$ is the difference vector. Since $\boldsymbol{d}$ is no longer a unit vector, such formulation includes additional (with respect to Sect. 2.1) transverse strain ε_{33} and energy conjugated stress resultant N_{33}. In the same way as in Sect. 2.1, we truncate the strains $E_{\alpha\beta}$ after the linear term and strains $E_{\alpha 3} = E_{3\alpha}$ after the constant term. Thus, we apply an assumption $\kappa_{\alpha 3} = 0$, which has been confirmed numerically to have negligible effect on results. The through-the-thickness normal strain is

$$\varepsilon_{33} = \left(\boldsymbol{x}_{,\xi^3} \cdot \boldsymbol{x}_{,\xi^3} - \boldsymbol{X}_{,\xi^3} \cdot \boldsymbol{X}_{,\xi^3}\right) = d \cdot d - \underbrace{\boldsymbol{D} \cdot \boldsymbol{D}}_{1}. \tag{11}$$

The strains and energy-conjugated second Piola-Kirchoff stress resultants are grouped as $\boldsymbol{\varepsilon} = [\varepsilon_{11}, \varepsilon_{22}, \varepsilon_{33}, 2\varepsilon_{12}]^{\mathrm{T}}$, $\boldsymbol{\kappa} = [\kappa_{11}, \kappa_{22}, 2\kappa_{12}]^{\mathrm{T}}$, $\boldsymbol{\gamma} = [2\varepsilon_{13}, 2\varepsilon_{23}]^{\mathrm{T}}$ and $\boldsymbol{N} = [N_{11}, N_{22}, N_{33}, N_{12}]^{\mathrm{T}}$, $\boldsymbol{M} = [M_{11}, M_{22}, M_{12}]^{\mathrm{T}}$, $\boldsymbol{Q} = [Q_{13}, Q_{23}]^{\mathrm{T}}$, respectively. We adopt the St.Venant-Kirchhoff material model, specialized for the extensible director shell model. The forces $\boldsymbol{N}$ relate to the strains $\boldsymbol{\varepsilon}$ as $\boldsymbol{N} = \boldsymbol{C}^m\boldsymbol{\varepsilon}$, where $\boldsymbol{C}^m = t\boldsymbol{C}$, and $\boldsymbol{C}$ is a part of the standard 3d constitutive matrix. For the moment and transverse shear forces, the constitutive relations remain the same as for the inextensible-director model from Sect. 2.1. The total energy functional depends on $\boldsymbol{u}$ and $\boldsymbol{w}$

$$\Pi(\boldsymbol{u}, \boldsymbol{w}) = \Pi_{\mathrm{int}}(\boldsymbol{u}, \boldsymbol{w}) - \Pi_{\mathrm{ext}}(\boldsymbol{u}, \boldsymbol{w}). \tag{12}$$

By introducing the kinematically admissible variations $\delta\boldsymbol{u}$ and $\delta\boldsymbol{w}$, the virtual work equation can be written as

$$\delta\Pi(\boldsymbol{u}, \boldsymbol{w}; \delta\boldsymbol{u}, \delta\boldsymbol{w}) = \int_A \left(\delta\boldsymbol{\varepsilon}^T\boldsymbol{N} + \delta\boldsymbol{\kappa}^T\boldsymbol{M} + \delta\boldsymbol{\gamma}^T\boldsymbol{Q}\right)dA - \delta\,\Pi_{\mathrm{ext}}(\delta\boldsymbol{u}, \delta\boldsymbol{w}) = 0 \tag{13}$$

Either Eqs. (12) or (13) represent the starting point for the finite element discretization, which relies on interpolations of $\boldsymbol{u}$ and $\boldsymbol{w}$ and their variations. As a result, a displacement-based finite element is obtained, which, however, suffers from locking. In Sect. 2.4, we will describe ANS interpolations, suitable for this model, which eliminate locking.

2.4 Hybrid-Mixed Quadrilateral Finite Elements

Table 1 summarizes seven 4-node quadrilateral finite element formulations. The first six are based on the shell model from Sect. 2.1 and the seventh (i.e. D-ANS) is based on the shell model from Sect. 2.3. These elements are applied for computing numerical examples in Sect. 2.5.

Table 1 Shell hybrid-mixed quadrilaterals. The number of parameters are in parenthesis

FE	Membrane	Thickness stretch	Bending	Shear	References
MITC4	Disp.	/	Disp.	ANS	[17]
MITC4+	ANS	/	Disp.	ANS	[23, 24]
EAS5	EAS (5)	/	Disp.	ANS	[6, 1, 4]
HR-M	HR (5)	/	Disp.	ANS	[39, 34]
HW	HW (5 + 5)	/	HW (5 + 5)	ANS & HW (4 + 4)	[20]
+HW	ANS & HW (5 + 5)	/	HW (5 + 5)	ANS & HW (4 + 4)	/
D-ANS	Disp.	ANS	Disp.	ANS	[3]

Let us briefly describe the first six finite elements from Table 1. They all use the ANS concept [17] for the transverse shear part of shell response. The MITC4+ and + HW elements from Table 1 also use the ANS concept for the membrane part of shell response; for details on this approach see [23, 24, 13, 29]. The basic idea of the ANS concept may be stated as: compute the strains by using (3) and (4) at points where the accuracy is the highest; interpolate those strains over the element in order to obtain the ANS-strains; and finally, replace the displacement-strains by the ANS-strains. One can perceive the ANS concept as the B-bar method or as an interpolation based on a modified Hu-Washizu (HW) principle, see e.g. [41]. The HW principle treats displacements/rotations $\boldsymbol{\Phi} = \{\boldsymbol{u}, \boldsymbol{d}\}$, strains, and stress resultants as independent fields.

The EAS5 element from Table 1 uses the EAS concept [40] for membrane part of shell response; see e.g. [6, 4]. The EAS concept relies on yet another modification of the Hu-Washizu functional. By decomposition of the strains into the displacement-strains (which are computed by using (3) and (4)) and some assumed EAS-strains, and by further applying an orthogonality condition between the EAS-strains and stress resultants, a two-field functional is obtained. This functional depends only on $\boldsymbol{\Phi}$ and EAS-strains and provides an elegant theoretical background for an effective enhancement of standard shell finite elements. The EAS-strains are chosen in such way that they enhance or weaken the displacement-strains.

The HR-M element from Table 1 relies on the Hellinger-Reissner (HR) functional for the membrane part of shell response. The HR functional treats displacements/rotations $\boldsymbol{\Phi} = \{\boldsymbol{u}, \boldsymbol{d}\}$ and stress resultants as independent fields. The HR-M element uses 5-parameter Pian-Sumihara interpolation [34]

$$\begin{Bmatrix} N_{11} \\ N_{22} \\ N_{12} \end{Bmatrix} = \begin{Bmatrix} \beta_1 + (\eta - \bar{\eta})\beta_4 \\ \beta_2 + (\xi - \bar{\xi})\beta_5 \\ \beta_3 \end{Bmatrix} \tag{14}$$

which seems to be the optimal interpolation for the membrane forces for shell quadrilaterals. In (16), β-s are the parameters, $\xi = \xi^1$ and $\eta = \xi^2$ are element coordinates, and $\bar{\xi}$ and $\bar{\eta}$ are the coordinates of the centre of gravity of the element. For further details on HR shell finite elements see e.g. [39, 19, 46].

The HW element from Table 1 relies on Hu-Washizu functional. The element interpolates the displacements, strains and stress resultants. The derivatives of the interpolated displacements provide the displacement-strains (3) and (4), which also take part in the functional. For the membrane part of shell action, the HW element uses 5-parameter Pian-Sumihara interpolation (14) for membrane forces, and 5-parameter interpolation for membrane strains. The same interpolation concept with $5 + 5$ parameters is adopted for the interpolation of moments and bending strains. As for the transverse shear part of the shell response, the following functional is the starting point for the interpolation

$$\Pi_{HW}^{tr.sh.}\left(\boldsymbol{\Phi}, \boldsymbol{Q}, \boldsymbol{\gamma}^{HW}\right) = \int_A \left[\tfrac{1}{2}\boldsymbol{\gamma}^{HW,T}\boldsymbol{C}^s\boldsymbol{\gamma}^{HW} + \boldsymbol{Q}\left(\boldsymbol{\gamma}^{ANS}(\boldsymbol{\Phi}) - \boldsymbol{\gamma}^{HW,T}\right)\right] dA \tag{15}$$

In (15), the displacement-strains $\boldsymbol{\gamma}$ are replaced by the ANS-strains $\boldsymbol{\gamma}^{ANS}(\boldsymbol{\Phi})$. The transverse shear strains $\boldsymbol{\gamma}^{HW}$ are interpolated with 4 parameters, and the transverse shear forces $\boldsymbol{Q}$ are interpolated with 4 parameters as well. For further details on Hu-Washizu shell elements see [20, 22, 46, 48].

The +HW element from Table 1 combines MITC4+ interpolations with those of HW element. We note that all the elements from Table 1, except HW and +HW, use displacement interpolation for the bending part of shell response. The seventh element from Table 1, D-ANS, uses displacement interpolation for the membrane and bending parts of shell response and ANS interpolations for the transverse shear and through-the-thickness parts of shell response. For the former ANS interpolation we apply the proposal from [17] and for the latter the proposal from [3].

2.5 Numerical Examples

The elements from Table 1 were implemented into computer code AceFEM [26]. The numerical examples presented below were computed by an adaptive incremental load factor procedure, which is based on the following function

$$\Delta\lambda_{min} \le \Delta\lambda = B(I_n)\Delta\lambda_n \le \Delta\lambda_{max},\ B = \begin{cases} 2 - \left(\frac{I_n - 1}{I_o - 1}\right)^2, & I_n < I_o \\ 1 - \frac{1}{2}\left(\frac{I_n - I_o}{N - I_o}\right)^2, & I_n \ge I_o \end{cases} \tag{16}$$

Here, $\Delta\lambda$ and $\Delta\lambda_n$ are current and last incremental load factors, respectively; I_n is number of iterations from the last increment; $I_0 = 8$ and $N = 15$ are numbers of desired and maximal allowed incremental iterations, respectively. If convergence is not reached in 15 iterations, the back-step is performed and the increment is re-computed with $\Delta\lambda/2$. The values of this parameters are presented in Table 2 for all the examples. The convergence tolerance was set to 10^{-8}. Large rotation formulation from Sect. 2.2.1 was used for all numerical examples with the exception of example 2.5.4 where formulation from Sect. 2.2.2 was used.

Table 2 Data for adaptive incremental load factor procedure

Example	$\Delta\lambda_{min}$	$\Delta\lambda_{max}$	$\Delta\lambda_{initial}$
2.5.1	10^{-8}	$2 \cdot 10^{-1}$	$5 \cdot 10^{-2}$
2.5.2	10^{-8}	$2 \cdot 10^{-1}$	$5 \cdot 10^{-2}$
2.5.3	10^{-12}	10^{-4}	10^{-4}
2.5.4	10^{-8}	$2 \cdot 10^{-1}$	$5 \cdot 10^{-2}$

2.5.1 Bending of Cylindrical Panel

Cylindrical panel is clamped at one edge and subjected to distributed moment $M = \lambda M_0$ along the opposite edge, see Fig. 1, where λ is load factor. Thus, a pure bending problem is addressed. Regular and distorted meshes from Fig. 1 are used; the ratio $L_{min}/L_{max} = 1/12$. Figure 2 shows the applied load versus displacements u_z and $-u_x$ of point A. Response of all the elements is practically the same for the regular mesh, see Fig. 2a. For the distorted mesh, see Fig. 2b, MITC4 is affected the most, while MITC4+ and +HW give very similar results as for the regular mesh. The results indicate that the hybrid-mixed treatment of membrane part of shell response is beneficial for the bending problems, at least for distorted meshes. Among different possibilities, summarized in Sect. 2.4., the most effective is the ANS treatment, which is applied in MITC4+ and +HW. We note that the superiority of MITC4+ and +HW for distorted meshes is much more exposed in the next example.

Table 3 compares robustness and speed of first six finite elements (FE) from Table 1. With respect to the central process unit (CPU) time, number of required load increments and number of total iterations, HW is superior, and +HW is just behind. Because of 49 back-steps, which reflected in CPU time and number of increments and iterations, HR-M is by far the slowest. We note that the data for adaptive incremental load factor procedure was the same for all elements; see Table 2. We also note that + HW combines good properties of MITC4+ (little sensitivity to mesh distortion) and HW (very large load increments and small number of total iterations).

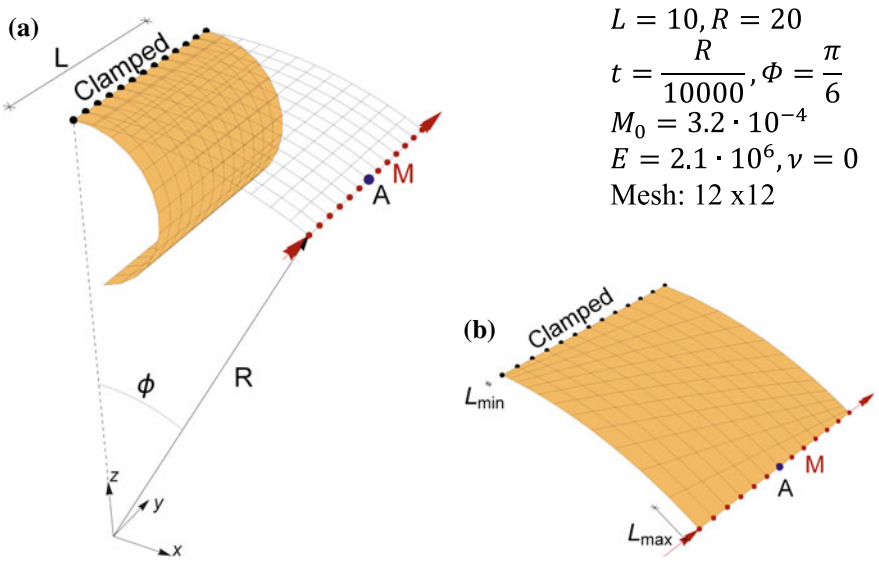

Fig. 1 Cylindrical panel: **a** initial and final deformed configurations for regular mesh; **b** distorted mesh

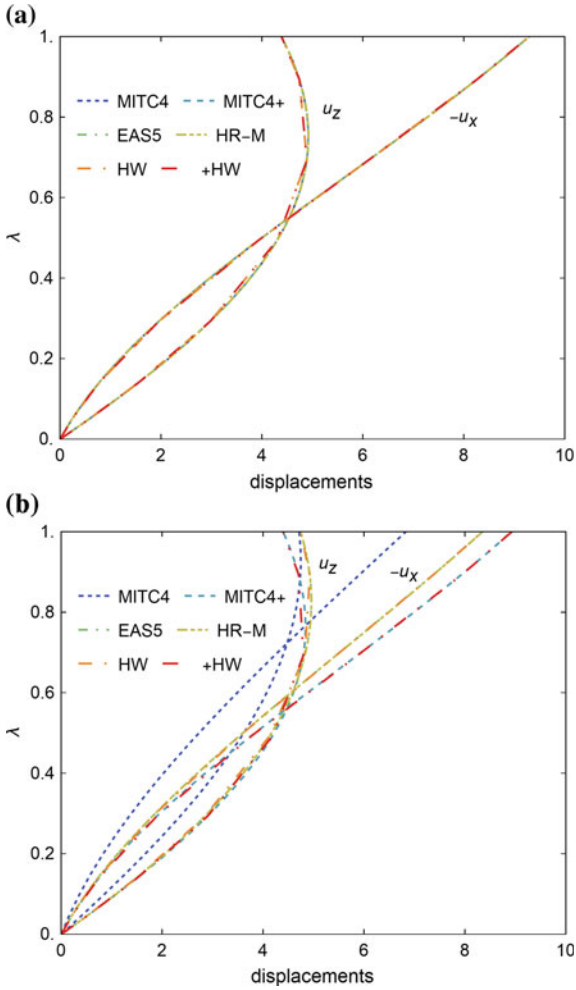

Fig. 2 Cylindrical panel: response for **a** regular mesh and **b** distorted mesh

2.5.2 Twisted Beam

Twisted beam-like shell is clamped at one end and subjected to two end forces $P = \lambda P_y = \lambda P_z$ at the other end, see Fig. 3. The shell undergoes considerable bending, which is followed by stretching, see Fig. 3b. Thus, this is a test for a membrane-bending shell behavior. In Fig. 4, displacements u_z and u_y of nodal point A are shown as functions of P. The reference results were computed by fine mesh of 8×24 HW elements. Regular and distorted mesh are used, with 6×2 and 12×4 elements respectively; the ratio $L_{min}/L_{max} = 1/2$. Despite a coarse regular mesh, there is almost no difference in response between the used elements, see Fig. 4a. For the distorted mesh, see Fig. 4b, MITC4 and D-ANS are affected the most, while MITC4+ and +HW show almost no difference in the response. This demonstrates

Table 3 Cylindrical panel: computational details for $M = M_0$ for regular mesh (top) and distorted mesh (bottom)

FE	MITC4	MITC4+	EAS5	HR-M	HW	+HW
Displacement $-u_x$	9.30	9.30	9.30	9.30	9.30	9.30
Normalized CPU time	1.00	0.89	0.82	8.07	0.23	0.23
Req. no. of load increments	22	22	22	145	7	7
Number of total iterations	205	205	205	1804	41	41
Number of back-steps	0	0	0	49	0	0
Displacement $-u_x$	6.83	8.92	8.35	8.35	8.35	8.93
Normalized CPU time	1.00	0.95	0.62	4.57	0.19	0.33
Req. no. of load increments	22	35	23	105	7	7
Number of total iterations	220	370	232	1165	41	41
Number of back-steps	1	1	0	20	0	0

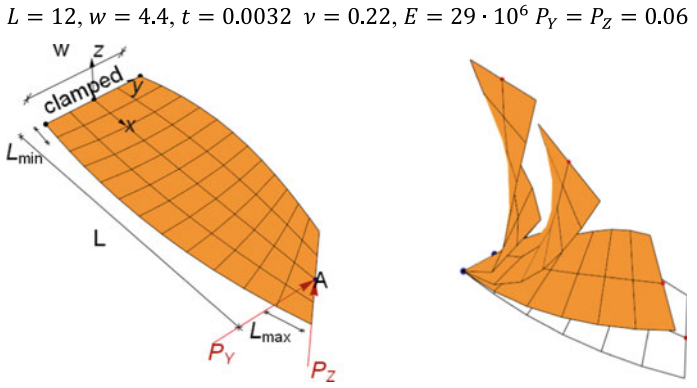

Fig. 3 Twisted beam: problem data; **a** initial configuration and distorted mesh case, **b** deformed configurations for EAS5 and regular mesh

the superior convergence characteristics of membrane ANS for distorted meshes. In Table 4, we compare the elements. The HW and +HW are again the fastest and HR-M is the slowest, needing a number of back-steps.

2.5.3 Deployable Ring

The deployable ring example, see Fig. 4a, was studied in detail in [18]. The reference results in Figs. 6 and 7 were computed by isogeometric Reissner-Mindlin (RM) and Kirchhoff-Love (KL) shell formulations in [33]. The ring is clamped along the bottom cross-section and subjected to imposed rotation $\Phi = \lambda 4\pi$ along the top cross-section. We used meshes of 80×1, 1200×1 and 1200×4 elements. Since our finite elements

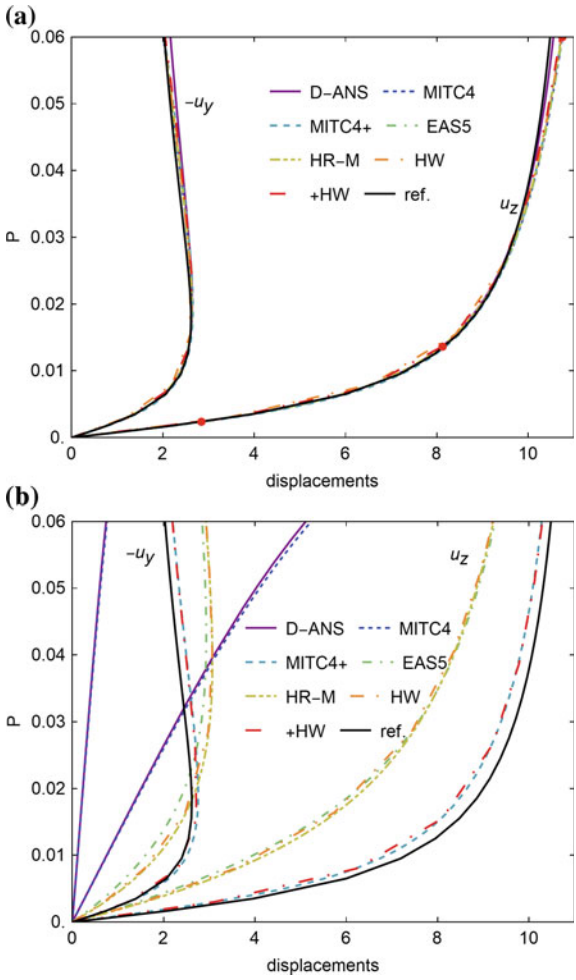

Fig. 4 Twisted beam: force-displacement curves; **a** regular mesh; **b** distorted mesh; red dots mark deformed configurations in Fig. 3b

do not have drilling rotation, the meshes were in the ring's plane. Thus, the elements in the mesh have thickness three times larger than the edge; see Fig. 5a. At $\Phi = 2\pi$, the ring deploys into three circles with radius $R/3$, and its initial shape is regained at $\Phi = 4\pi$ [18]. Thus, the example is a test for coupling of bending and twisting; the latter involves large membrane forces. Moreover, it is also a test for large rotation formulations.

The results are given in Figs. 6 and 7, where load displacement curves are shown; M is the sum of reactions at nodes of imposed rotation. The MITC4 and MITC4+ exhibit severe membrane locking for the coarser mesh and predict completely erroneous solution. Furthermore, it seems that the solution is non-physical, because at $\Phi \approx 2\pi$ the elements move through each other, see Fig. 5b. We note in this respect that the ANS membrane treatment has no effect for flat elements; it seems that this is

Table 4 Twisted beam: computational details for $P = 0.06$ for regular mesh (top) and distorted mesh (bottom)

FE	MITC4	MITC4+	EAS5	HR-M	HW	+HW	D-ANS
Displacement $-u_y$	2.01	2.03	2.01	2.02	2.02	2.05	2.17
Normalized CPU time	1.00	0.94	0.88	1.29	0.09	0.09	1.00
Req. no. of load increments	60	54	58	77	7	7	58
Number of total iterations	651	615	613	836	43	45	615
Number of back-steps	12	9	9	20	0	0	8
Displacement $-u_y$	0.76	2.2	2.84	2.93	2.93	2.19	0.74
Normalized CPU time	1.00	4.50	3.04	6.88	0.39	0.50	0.83
Req. no. of load increments	15	61	40	96	7	7	12
Number of total iterations	145	657	404	1026	41	43	120
Number of back-steps	2	12	3	23	0	0	1

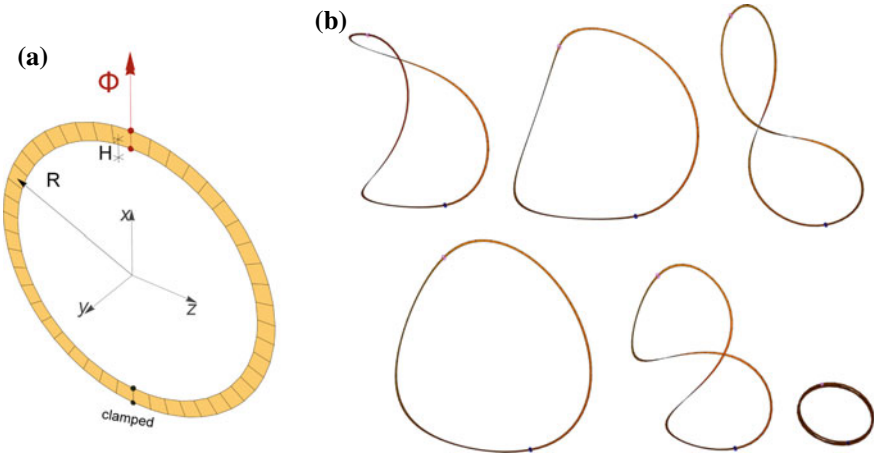

$$R = 20, H = 1/3, t = 1,\ E = 21000, \nu = 0.2, \Phi_{final} = 4\pi, I_1 = 2.778 \cdot 10^{-2}$$

Fig. 5 Deployable ring: **a** problem data, **b** deformed configurations for 80 × 1 mesh for MITC4 (top) and +HW (bottom) at points marked on Fig. 6

the reason that MITC4 and MITC4+ behave the same. It is obvious from the results from Fig. 6 that the elements should be free of membrane locking in order to be able to compute this example.

The other elements predict solutions that are close to the one derived in [18]. An exception is HR-M, which fails to complete the cycle (it fails at $\Phi \approx 1.3\pi$ for coarser mesh and at $\Phi \approx \pi$ for both finer meshes). We note that HW and + HW results change only slightly with mesh refinement. For 1200 × 1 mesh, all the elements provide expected response and the results almost coincide; however, MITC4 and MITC4+ fail at $\Phi \approx 2.6\pi$, see Fig. 7a. For 1200 × 4 mesh, all the

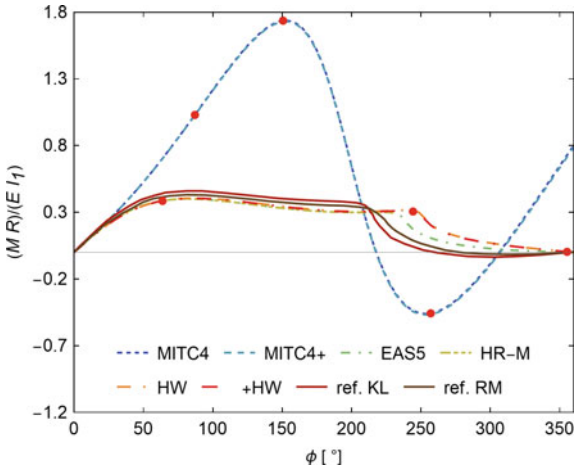

Fig. 6 Deployable ring: load-displacement curve for coarse mesh; red dots mark deformed configurations in Fig. 5b

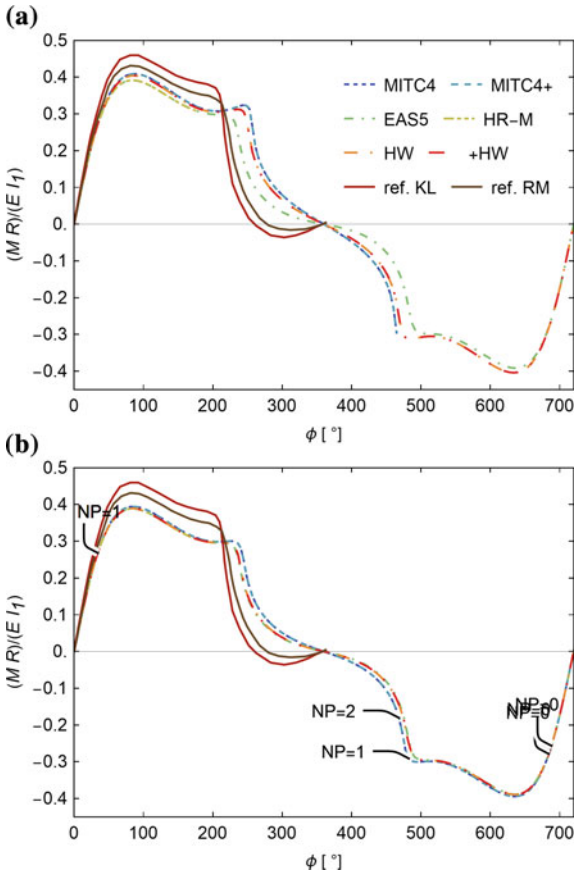

Fig. 7 Deployable ring: load-displacement curves for **a** 1200 × 1 and **b** 1200 × 4 mesh

elements (except HR-M) provide the same response up to the final rotation $\Phi = 4\pi$, see Fig. 7b. We note that our results differ from those provided in [33], which is because of usage of different shell models and adoption of different orientations of meshes. In Fig. 7b, we show the number of negative pivots (NP) on the solution path; a change on NP indicates occurrence of limit/bifurcation point. It is interesting to note that the elements do not predict the critical points at the same configurations; moreover, MITC4 and MITC4+ detect two more than others do.

2.5.4 Pinched Cylinder

Figure 8 shows cylinder with rigid diaphragms at both ends, which restrain the in-plane displacements. The cylinder is pinched by two opposite vertical forces $P = \lambda P_0$. Due to the symmetry, only one eight of the cylinder is modelled and symmetrical boundary conditions are taken into account. Regular and distorted meshes of 48×48 elements are considered, the latter with the elements distorted in the same way as shown in Fig. 1 for the cylindrical panel example; the ratio $L_{min}/L_{max} = 1/4$.

Figure 9 shows the force versus displacements $-u_z$ and u_x at points B and A respectively. Reference solution is taken from [45]. For the regular mesh, the HW, +HW, and HR-M, produce results that differ from the reference solution. The HW fails at $P \approx 10.510^3$, while for +HW and HR-M artificial local buckling occurs, which makes the results deviating from the reference solution, obtained by a very fine mesh. For the distorted mesh, artificial localized buckling does not happen as the mesh is refined around the region of buckling. All elements produce results that coincide

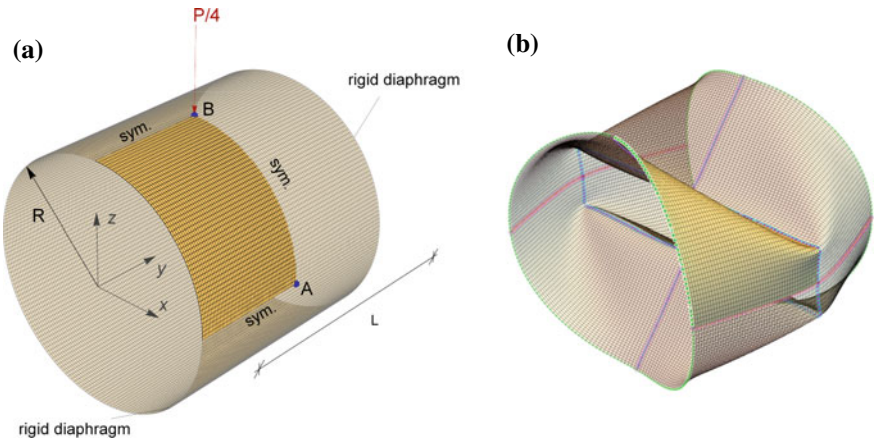

$$R = 100, L = 200, t = 1, P_0 = 12000, E = 30 \cdot 10^3, \nu = 0.3$$

Fig. 8 Pinched cylinder: **a** initial and **b** +HW deformed configuration at point marked on Fig. 9

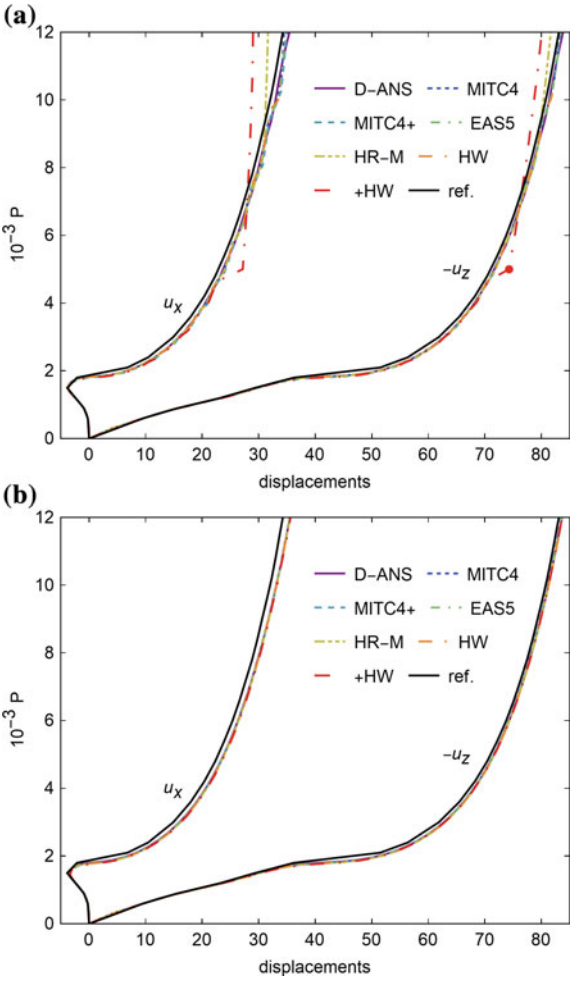

Fig. 9 Pinched cylinder; load-displacement diagram for 48 × 48 mesh; **a** regular mesh; **b** distorted mesh

with the reference solution. It seems from these results that HW and HR elements are more prone to catch a mesh-biased artificial buckling than other elements.

The problem of artificial localized buckling was already reported in [15]. Let us illustrate it clearly for this example by using a coarse mesh of 16 × 16 elements, see Fig. 10. The path-following method [44] was used to compute the complete responses. The force-displacement curves on Fig. 10 indeed show considerable snap-throughs and snap-backs because of artificial buckling; D-ANS curves are the wildest (note that the legend for Fig. 10 is the same as for Fig. 9). Furthermore, the computed results deviate considerable from reference solution. Two deformed configurations for points A and B are also shown on Fig. 10. This example demonstrates that hybrid-mixed formulations do not help avoiding artificial buckling problem for coarse meshes.

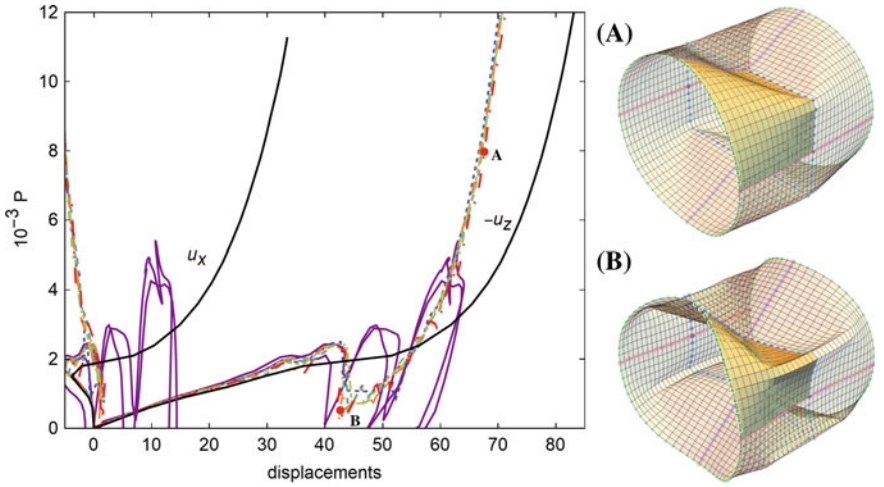

Fig. 10 Pinched cylinder: load-displacement curves for 16×16 mesh and deformed configurations for +HW

Moreover, it seems that they are more prone to it than other formulations. This looks like the only weak spot of +HW element.

3 Shell Stability Analysis with Implicit Dynamics

3.1 Shell Dynamic Formulation

Let us extend the shell model presented in Sect. 2.3 for dynamics. To that end, let us partition the time interval of interest as $[t_0, T] = \bigcup_{n=0}^{N} [t_n, t_{n+1}]$. Hereinafter, $(\cdot)_n$ and $(\cdot)_{n+1}$ will denote the values of $(\cdot)$ at t_n, and t_{n+1}, respectively. Moreover, let α_m and α_f be used to define two time points as $t_{n+\alpha_f} = \alpha_f t_{n+1} + (1-\alpha_f) t_n$ and $t_{n+\alpha_m} = \alpha_m t_{n+1} + (1-\alpha_m) t_n$. Equation (13) is replaced with

$$\delta \Pi_{\text{int}}, n+\alpha_f + \delta \Pi_{\text{dyn}}, n+\alpha_m - \delta \Pi_{\text{ext}}, n+\alpha_f \tag{17}$$

Here,

$$\delta \Pi_{\text{int},n+\alpha_f} = \int_A \left(\delta \boldsymbol{\varepsilon}^T_{n+\alpha_f} \boldsymbol{N}_{n+\alpha_f} + \delta \boldsymbol{\kappa}^T_{n+\alpha_f} \boldsymbol{M}_{n+\alpha_f} + \delta \boldsymbol{\gamma}^T_{n+\alpha_f} \boldsymbol{Q}_{n+\alpha_f} \right) dA, \tag{18}$$

the contribution of inertial forces is

$$\delta \Pi_{\text{dyn},n+\alpha_m} = \int_A \left(A_0 \delta \boldsymbol{u}^T \ddot{\boldsymbol{u}}_{n+\alpha_m} + I_0 \delta \boldsymbol{w}^T \ddot{\boldsymbol{w}}_{n+\alpha_m} \right) dA, \tag{19}$$

where A_0 and I_0 are the mid-surface mass density and inertia of the shell director, respectively, and the external forces part of the potential energy is equipped with Winkler's foundation with stiffness K_S acting in normal direction to the deformed mid-surface $\boldsymbol{n}^{def}$

$$\begin{aligned} \delta \Pi_{\text{ext},n+\alpha_f} = & \int_A \left(\delta \boldsymbol{u}^T \bar{\boldsymbol{b}}_{n+\alpha_f} + \delta \boldsymbol{u}^T \boldsymbol{n}^{def}_{n+\alpha_f} \left(-K_S \boldsymbol{u}^T_{n+\alpha_f} \boldsymbol{n}^{def}_{n+\alpha_f} \right) \right) dA \\ & + \int_{\Gamma_{\bar{t}}} \delta \boldsymbol{u}^T \bar{\boldsymbol{t}}_{n+\alpha_f} ds + \sum_{i=1}^{N} \delta \boldsymbol{u}_i^T \boldsymbol{F}_{i,n+\alpha_f}. \end{aligned} \tag{20}$$

The mid-point values in (17)–(20) are expressed as linear combinations of known values at t_n and unknown values at t_{n+1}

$$\begin{aligned} &\ddot{\boldsymbol{u}}_{n+\alpha_m} = \alpha_m \ddot{\boldsymbol{u}}_{n+1} + (1-\alpha_m)\ddot{\boldsymbol{u}}_n, \ddot{\boldsymbol{w}}_{n+\alpha_m} = \alpha_m \ddot{\boldsymbol{w}}_{n+1} + (1-\alpha_m)\ddot{\boldsymbol{w}}_n, \\ &\boldsymbol{u}_{n+\alpha_f} = \alpha_f \boldsymbol{u}_{n+1} + \left(1-\alpha_f\right)\boldsymbol{u}_n, \boldsymbol{w}_{n+\alpha_f} = \alpha_f \boldsymbol{w}_{n+1} + \left(1-\alpha_f\right)\boldsymbol{w}_n, \\ &\bar{\boldsymbol{b}}_{n+\alpha_f} = \alpha_f \bar{\boldsymbol{b}}_{n+1} + \left(1-\alpha_f\right)\bar{\boldsymbol{b}}_n, \bar{\boldsymbol{t}}_{n+\alpha_f} = \alpha_f \bar{\boldsymbol{t}}_{n+1} + \left(1-\alpha_f\right)\bar{\boldsymbol{t}}_n, \text{etc.} \end{aligned} \tag{21}$$

Motivated by the research on algorithmic conservation of energy, e.g. [43, 10, 27], the same linear combination is used to approximate the internal forces at $t_{n+\alpha_f}$

$$\begin{aligned} \boldsymbol{N}^h_{n+\alpha_f} &= \alpha_f \boldsymbol{N}^h_{n+1} + \left(1-\alpha_f\right)\boldsymbol{N}^h_n = \boldsymbol{C}^m \left[\alpha_f \boldsymbol{\varepsilon}^h_{n+1} + \left(1-\alpha_f\right)\boldsymbol{\varepsilon}^h_n \right], \\ \boldsymbol{M}^h_{n+\alpha_f} &= \alpha_f \boldsymbol{M}^h_{n+1} + \left(1-\alpha_f\right)\boldsymbol{M}^h_n = \boldsymbol{C}^b \left[\alpha_f \boldsymbol{\kappa}^h_{n+1} + \left(1-\alpha_f\right)\boldsymbol{\kappa}^h_n \right], \\ \boldsymbol{Q}^h_{n+\alpha_f} &= \alpha_f \boldsymbol{Q}^h_{n+1} + \left(1-\alpha_f\right)\boldsymbol{Q}^h_n = \boldsymbol{C}^s \left[\alpha_f \boldsymbol{\gamma}^h_{n+1} + \left(1-\alpha_f\right)\boldsymbol{\gamma}^h_n \right]. \end{aligned} \tag{22}$$

Finally, we choose the Newmark approximations [32, 11] to express velocities and accelerations at t_{n+1} with displacements at t_{n+1}

$$\begin{aligned} \dot{\boldsymbol{u}}_{n+1} &= \frac{\gamma}{\beta \Delta t}(\boldsymbol{u}_{n+1} - \boldsymbol{u}_n) - \frac{\gamma-\beta}{\beta}\dot{\boldsymbol{u}}_n - \frac{\gamma-2\beta}{2\beta}\Delta t \ddot{\boldsymbol{u}}_n, \\ \dot{\boldsymbol{w}}_{n+1} &= \frac{\gamma}{\beta \Delta t}(\boldsymbol{w}_{n+1} - \boldsymbol{w}_n) - \frac{\gamma-\beta}{\beta}\dot{\boldsymbol{w}}_n - \frac{\gamma-2\beta}{2\beta}\Delta t \ddot{\boldsymbol{w}}_n, \\ \ddot{\boldsymbol{u}}_{n+1} &= \frac{1}{\beta \Delta t^2}(\boldsymbol{u}_{n+1} - \boldsymbol{u}_n) - \frac{1}{\beta \Delta t}\dot{\boldsymbol{u}}_n - \frac{1-2\beta}{2\beta}\ddot{\boldsymbol{u}}_n, \\ \ddot{\boldsymbol{w}}_{n+1} &= \frac{1}{\beta \Delta t^2}(\boldsymbol{w}_{n+1} - \boldsymbol{w}_n) - \frac{1}{\beta \Delta t}\dot{\boldsymbol{w}}_n - \frac{1-2\beta}{2\beta}\ddot{\boldsymbol{w}}_n, \end{aligned} \tag{23}$$

where β and γ are Newmark's constants. By using (21)–(23) in (20), the functional unknowns become $\boldsymbol{u}_{n+1}$ and $\boldsymbol{w}_{n+1}$.

3.2 Time-Stepping Schemes

The time-stepping scheme adopted in the previous section is called Generalized-energy-momentum (GEM) method, see e.g. [27]. By prescribing α_m and/or α_f, several special cases of implicit time-stepping schemes are obtained; see Table 5. Three schemes from Table 5 are numerically dissipative and two are not. In [14], the remaining parameters of the dissipative schemes are expressed for linear elastodynamics in terms of dissipation parameter $\rho_\infty \in [0, 1]$ such that the dissipation is optimal; i.e. lowest in the low frequency range and highest in the high frequency range. Note that ρ_∞ is spectral radius of the amplification matrix and that larger ρ_∞ indicates smaller dissipation. Special cases in Table 5 are Bossak-Wood-Zienkiewicz (BAM) scheme, modified Hilber-Huges-Taylor (HHT) scheme, modified Generalized-α (GAM) method, Energy-momentum conserving method (EMC), and Newmark's trapezoidal rule (NTR). The term modified indicates that the original versions constructed internal forces in (18) with strains at $t_{n+\alpha_f}$ rather than as adopted in (22).

Besides the schemes from Table 5, we will also use in numerical examples the first-order accurate modification of EMC with high frequency numerical dissipation, called energy-decaying scheme (ED), see e.g. [8, 2]. We refrain from describing ED, but we note that it uses $\alpha_{ED} \in [0, 1]$ and $\beta_{ED} \in [0, 1]$ to control the dissipation of potential and kinetic energy, respectively. Larger α_{ED} and β_{ED} indicate larger dissipation.

Table 5 Considered time-stepping schemes

	α_m	α_f	β	γ	ρ_∞
NTR	1	1	$\frac{1}{(\rho_\infty+1)^2}$	$\frac{3-\rho_\infty}{2\rho_\infty+2}$	$\rho_\infty = 1$
BAM	$\frac{2}{\rho_\infty+1}$	1	$\frac{1}{4}(\alpha_m)^2$	$\alpha_m - 1/2$	$\rho_\infty < 1$
HHT	1	$\frac{2\rho_\infty}{\rho_\infty+1}$	$\frac{1}{4}\left(\alpha_f - 2\right)^2$	$\frac{3}{2} - \alpha_f$	$\rho_\infty < 1$
GAM	$\frac{2-\rho_\infty}{1+\rho_\infty}$	$\frac{1}{1+\rho_\infty}$	$\frac{1}{4}\left(1 - \alpha_f + \alpha_m\right)^2$	$\frac{1}{2} - \alpha_f + \alpha_m$	$\rho_\infty < 1$
EMC	$\frac{2-\rho_\infty}{1+\rho_\infty}$	$\frac{1}{1+\rho_\infty}$	$\frac{1}{4}\left(1 - \alpha_f + \alpha_m\right)^2$	$\frac{1}{2} - \alpha_f + \alpha_m$	$\rho_\infty = 1$

Table 6 Minimal and maximal allowed Δt for dynamic examples

Example	Δt_{min} [s]	Δt_{max} [s]	$\Delta t_{initial}$ [s]
3.3.1	10^{-6}	10^{-2}	$2 \cdot 10^{-3}$
3.3.2	10^{-8}	$2 \cdot 10^{-3}$[a]	10^{-2}
3.3.3 C1	10^{-8}	$2 \cdot 10^{-2}$	10^{-2}
3.3.3 C2	10^{-10}	$2 \cdot 10^{-2}$	10^{-2}

[a]Until $t = 0.28$ s, $\Delta t_{max} = 5 \cdot 10^{-2}$ s

3.3 Numerical Examples

The adaptive procedure (16) is also used for dynamics numerical examples, except that $\Delta\lambda$ in (16) is replaced with the time-step Δt. Table 6 presents data for adaptive time-stepping procedure for all dynamics examples.

3.3.1 Snap-Through of Thin Cylindrical Panel

Dynamic behavior of very thin cylindrical panel ($h/R = 1/4000$), where h is shell thickness, is considered. Figure 11 shows geometry, material and loading data. For the dissipative schemes, the spectral radius was $\rho_\infty = 0.9$. Static analysis with the path-following method [44] was unable to compute the complete response, see [30]. Figure 12 shows that all schemes capture the beginning of buckling and predict a considerable push-back before the snap-through is completed. The push-back is more prominent for EMC (no-damping scheme) and GAM. NTR fails just after the push-back. EMC, which conserves energy for an autonomous motion, does not damp vibrations; thus it is not suitable for this problem. On the other hand, the dissipation

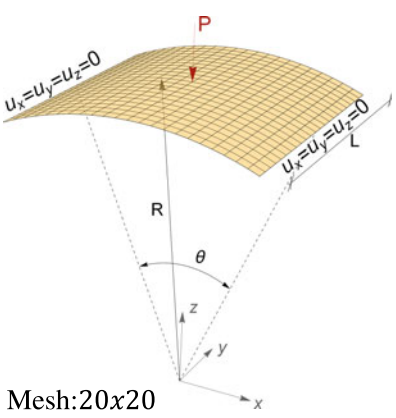

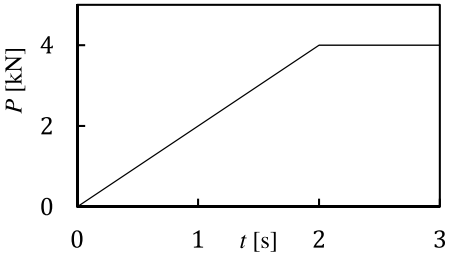

$R = 4000$ mm, $L = 1600$ mm,
$\rho = 7.8\ 10^{-6}$ kg/mm^3, $h = 1$ mm,
$E = 210\ 10^3$ MPa, $\nu = 0.3$,
$\theta = 2 \arcsin[L/(2R)]$

Fig. 11 Thin cylindrical panel: data

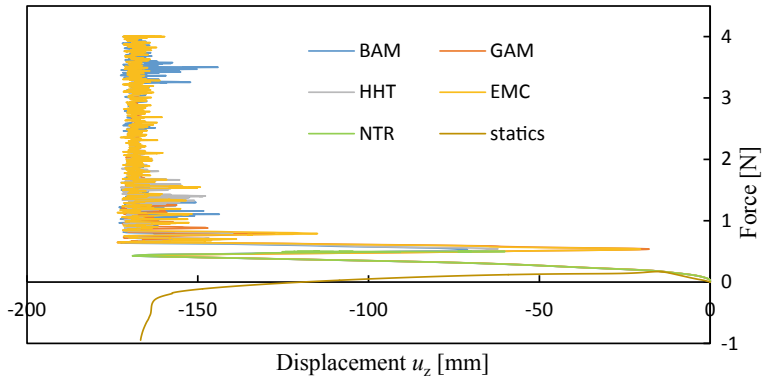

Fig. 12 Thin cylindrical panel: force-displacement curves

in the rest of the schemes damps oscillations during the buckling and in the inverse configuration.

For EMC, NTR, HHT and BAM, oscillations in the total energy are observed, see Fig. 13. Theses oscillations are caused by oscillations of kinetic energy due to insufficient damping. However, for HHT and BAM the oscillations gradually stop, while NTR soon fails. GAM effectively dumps oscillations already from beginning of the buckling. The fact, that EMC is energy conserving for autonomous motion is evident from Fig. 13 where its high-frequency oscillations are visible.

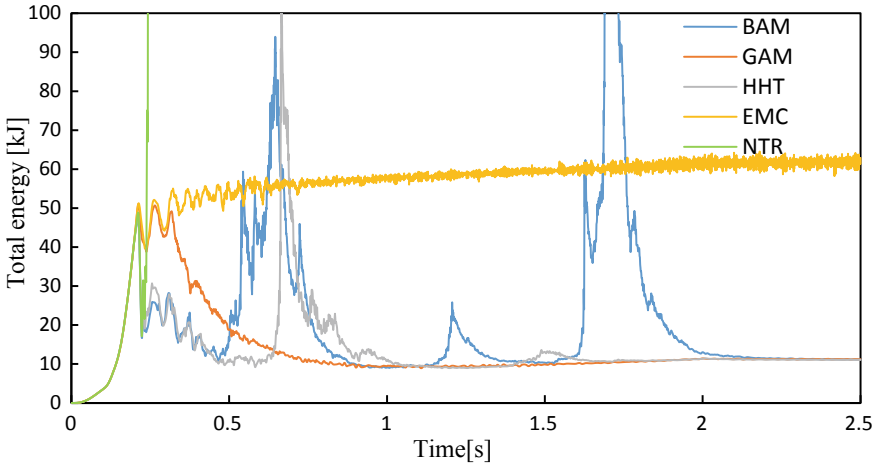

Fig. 13 Thin cylindrical panel: total energy versus time curves

3.3.2 Buckling of Axially Compressed Cylinder

We consider elastic buckling of cylinder under axial compression, see Fig. 14. The data is for the test specimen Z = 500 of Yamaki experiments [50], where displacement was imposed on the upper edge. Different dissipation factors were considered. Figure 15 shows that results are in good agreement with the experiment. The curves labeled as "Asymmetric" were obtained experimentally by increasing and decreasing the imposed axial displacement. The curves labeled as "Symmetric" were obtained experimentally by applying small point-wise disturbance forces, which triggered symmetric buckling mode. This asymmetry/symmetry relates to the shape of buckling mode at the cross-section at the middle-height of the cylinder. The number of axial half-waves is denoted by m and the number of circumferential full waves by n.

Figure 15 show response curves for perfect cylinder. We applied $\rho_\infty = 0.6$ for BAM and $\rho_\infty = 0.8$ for GAM and HHT. For ED, the dissipation factors were $\alpha_{ED} = \beta_{ED} = 0.02$. BAM and HHT results are in very good agreement with the experiment for the post-buckling regime. They predict mode jumping observed in the experiment. Moreover, the wave numbers are exactly the same as experimentally observed. For larger ρ_∞, the HHT and BAM results become polluted by higher frequencies, as seen in Fig. 16, where for larger ρ_∞ energy oscillations are bigger. Consequently, the schemes are not able to catch all the post-buckling modes for small dissipation, see [30]. This kind of pollution is much smaller for GAM, which, however, always misses out one post-buckling mode. For animation of the complete buckling process see [31]. Theoretical critical stress for elastic axially compressed cylinder for axisymmetric buckling mode is $\sigma_{cr} = Eh/\left(R\sqrt{3(1-\nu^2)}\right)$. For the considered cylinder $\sigma_{cr} = 8.31$MPa and the corresponding axial force is $P_{cr,t} = 1290$N. BAM, HHT and GAM schemes predict the critical axial force $P_{cr} = 1327\text{N}\ (103\%\, P_{cr,t})$ and the ED scheme predicts $P_{cr} = 1338\text{N}\ (104\%\, P_{cr,t})$. Because of initial imperfections (not

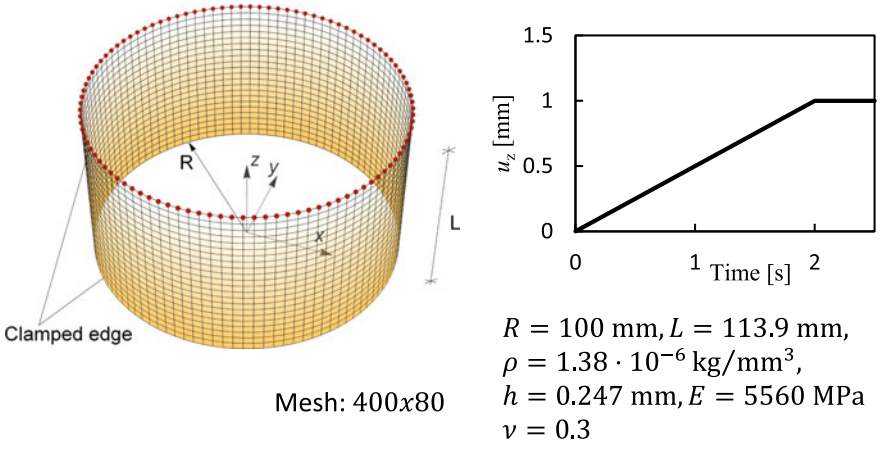

Fig. 14 Axially compressed cylinder: data

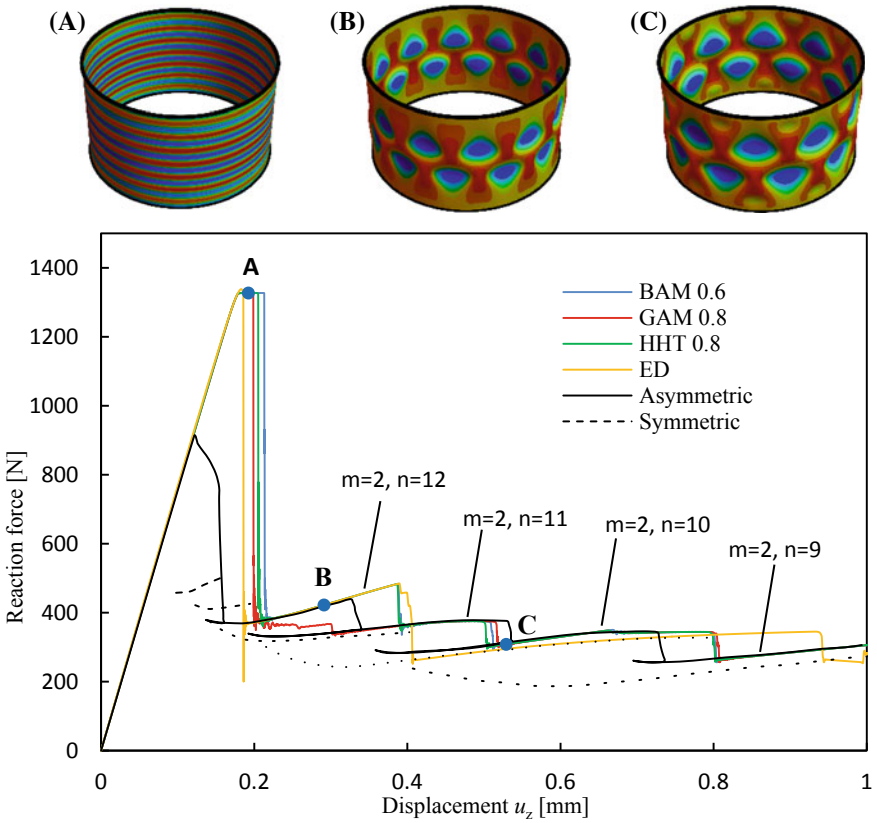

Fig. 15 Axially compressed cylinder with no imperfections: force-displacement curves and deformed configurations for BAM

considered here) the experimental buckling load in Fig. 15 is significantly lower that the computed ones and the theoretical one.

Another analysis was performed with assumed initial geometric imperfections. As proposed in [25], first 18 initial eigenmodes were summed and the amplitude of the sum was amplified by 1% of the thickness to obtain imperfection ΔR. Results are given in Fig. 17. The computed buckling loads reduce significantly and become comparable with the experimental one. The primary buckling pattern changes with respect to the ideal cylinder; compare configuration A in Figs. 15 and 17. However, the post-buckling transition of patterns remains the same as in the experiment. Furthermore, GAM scheme does not miss the post-buckling mode with $n = 12, m = 2$.

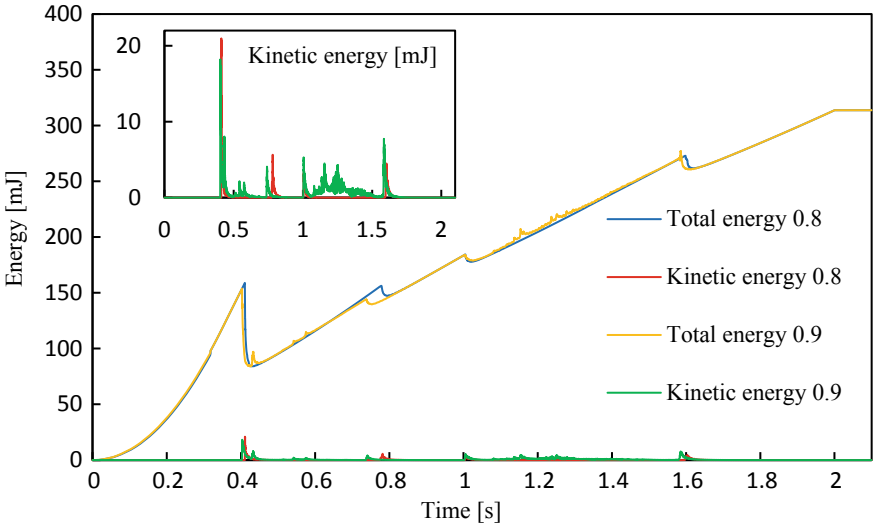

Fig. 16 Axially compressed cylinder with no imperfections: energy curves for HHT

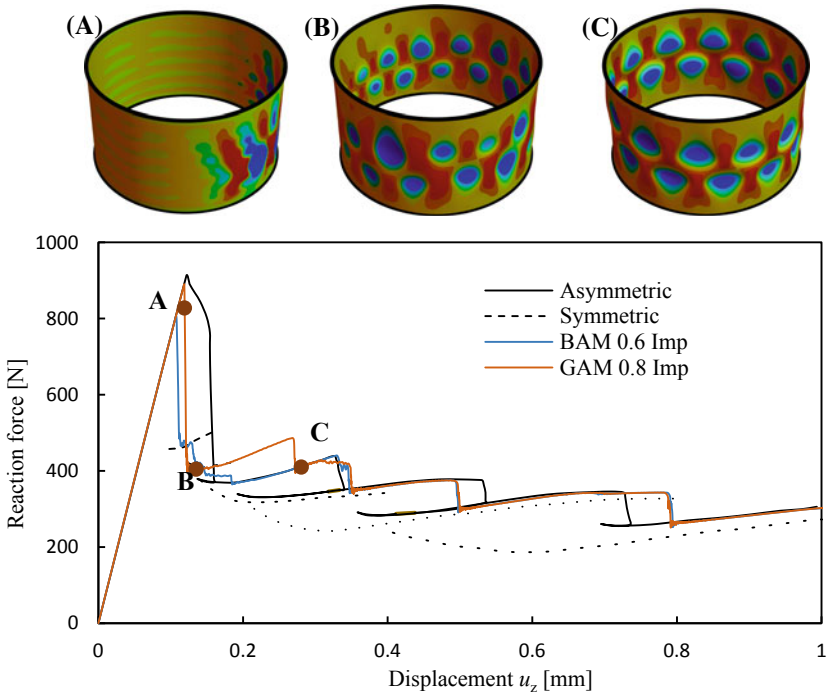

Fig. 17 Axially compressed cylinder with imperfections: force-displacement curves and deformed configurations for GAM

3.3.3 Wrinkling of Cylinder on Elastic Substrate

Buckling of axially compressed cylinders on substrate was studied numerically in [51, 49], where small geometric imperfections and small perturbation force were used, respectively, to trigger the buckling. In our analyses, geometry is perfect and no perturbation force is applied. In [49] a coefficient $C_S = E_s/E_f\left(R/t_f\right)^{3/2}$ is proposed, with the critical value $C_{S,crit} \approx 0.88$. Here, subscripts f and s refer to film (i.e. cylinder) and substrate, respectively. For systems with $C_S < C_{S,crit}$, only axisymmetric wrinkling mode occurs, whereas for $C_S > C_{S,crit}$ the transition from axisymmetric to diamond-like mode is expected. Figure 18 shows two considered data sets; C1 and C2. Compressive axial displacement u_y is imposed at both ends according to presented load function. BAM and GAM with $\rho_\infty = 0.9$ and EMC are used.

Figures 19 and 20 show reaction force at $x = 0$ with respect to axial and radial displacements, together with GAM deformed configurations. Both cylinders initially produce axisymmetric pattern, for all time-stepping schemes. For C1, all schemes capture the transition to the diamond-like pattern. For C2, the transition is captured by GAM and EMC. We may conclude that dissipation has stronger influence on results for cylinders with lower C_S factors.

Theoretical axisymmetric buckling force can be computed as, see [49]

$$f_{cr,el} = E_f\left[\frac{1}{p_0^2} + \frac{t_f^2 p_0^2}{4c^2R^2} + \frac{3R\bar{E}_s}{2c^2 t_f \bar{E}_f p_0}\right] t_f \quad \left[\frac{\mathrm{N}}{\mathrm{mm}}\right], \tag{24}$$

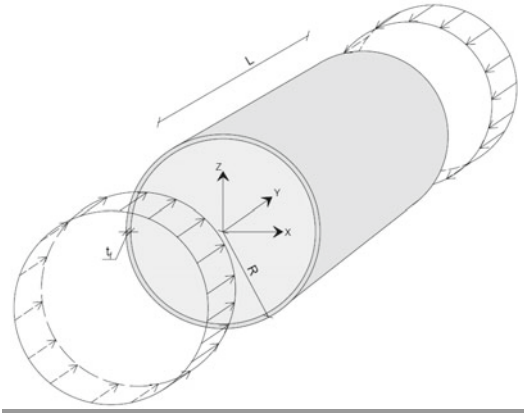

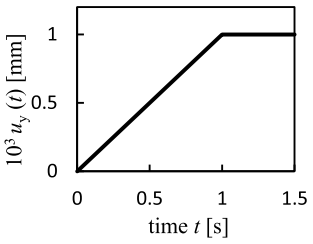

	R [mm]	L [mm]	t_f [mm]	E_f [MPa]	E_f/E_s	K_s [MPa]	ν_f	ν_s	ρ_f $[\frac{\mathrm{g}}{\mathrm{mm}^3}]$	Mesh	C_S
C1	0.3	0.3	10^{-3}	$2.16 \cdot 10^4$	12000	127.6	0.4	0.48	10^{-3}	120×60	0.43
C2	0.113	0.3	10^{-3}	$2.16 \cdot 10^5$	12000	196.3	0.4	0.48	10^{-3}	120×160	0.01

Fig. 18 Cylinder on elastic substrate data

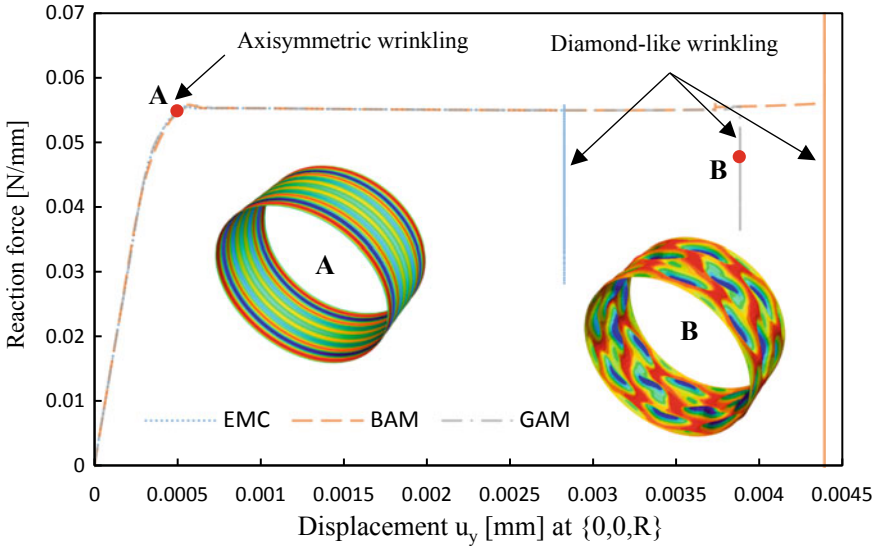

Fig. 19 C1: force-displacement curves and deformed configurations for GAM

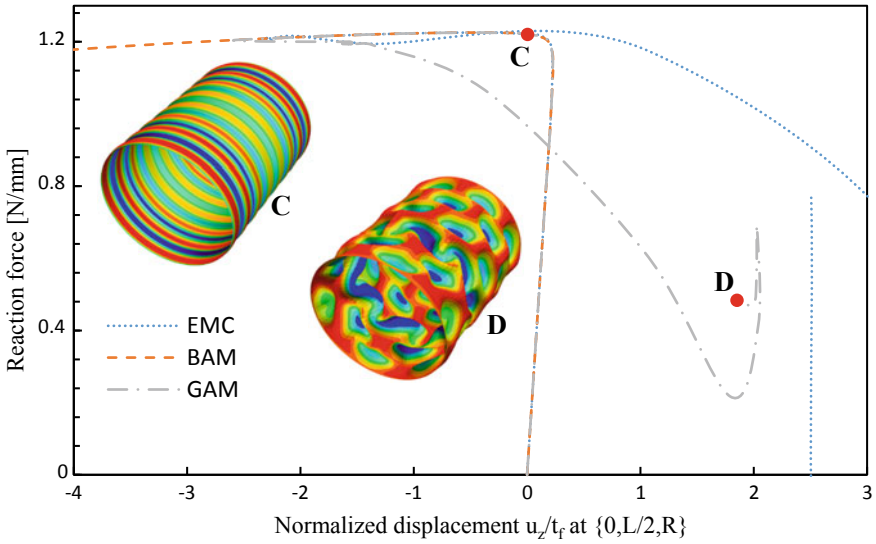

Fig. 20 C2: force-displacement curves and deformed configurations for GAM

Table 7 Computed and theoretical buckling load

Case	C1	C2
$f_{cr,el}$[N/mm]	0, 060	1, 27
f_{cr}[N/mm]$\left(\frac{f_{cr}}{f_{cr,el}}[\%]\right)$	0, 056(93%)	1, 23(97%)

where $c = \sqrt{3\left(1-\nu_f^2\right)}$, $\bar{E}_s = \frac{E_s}{1-\nu_s^2}$, $\bar{E}_f = \frac{E_f}{1-\nu_f^2}$ and p_0 is a critical wave number in the axial direction, obtained by solving

$$-2 + \frac{t_f^2}{6(1-\nu^2)R^2} p_0^4 - \frac{3R}{6(1-\nu^2)t_f} \frac{\bar{E}_s}{\bar{E}_f} p_0 = 0. \tag{25}$$

Numerical results match well with the theoretical critical force, see Table 7, where f_{cr} is computed force, which is the same for all schemes.

4 Conclusions

As for the hybrid-mixed formulations for geometrically exact shell models, the following can be concluded. Numerical examples in [24] and our extensive numerical experiments show that MITC4+ shell element [24] is robust, converges fast, and displays little sensitivity to mesh distortion. However, its weak spot are flat finite element meshes, since the membrane ANS enhancement has no effect on flat elements. Thus, for flat meshes, MITC4+ behaves as MITC4. On the other hand, HW shell element [20] is robust, converges fast, and can take very large solution steps, thus allowing for very fast computations. This was shown in [20] and confirmed by our extensive numerical experiments. However, HW shows sensitivity to mesh distortion. We combined incredible features of MITC4+ and HW and obtained an "optimal" hybrid-mixed finite element, which we call +HW element. The presented numerical examples show that +HW is indeed superior hybrid-mixed element. Its only weak spot might be that it is slightly more prone to predict artificial local buckling for coarse meshes than other types of hybrid-mixed elements.

As for the post-buckling analysis of shells by implicit dynamics schemes, the following conclusions can be drawn. We have briefly discussed application of implicit schemes, with and without numerical dissipation in the high-frequency range, for stability analysis of shells with complex post-buckling equilibrium paths. We can conclude from numerical experiments that this approach is very efficient for some classical shell buckling problems, like post-buckling analysis of axially loaded cylinders.

References

1. Andelfinger, U., Ramm, E.: EAS-elements for two-dimensional, three-dimensional, plate and shell structures and their equivalence to HR-elements. Int. J. Numer. Meth. Eng. **36**, 1311–1337 (1993)
2. Armero, F., Romero, I.: On the formulation of high-frequency dissipative time-stepping algorithms for nonlinear dynamics. Part I: low-order methods for two model problems and nonlinear elastodynamics. Comput. Methods Appl. Mech. Eng. **190**, 2603–2649 (2001)
3. Betsch, P., Stein, E.: An assumed strain approach avoiding artificial thickness straining for a nonlinear 4-node shell element. Commun. Numer. Methods Eng. **11**, 899–909 (1995)
4. Betsch, P., Gruttmann, F., Stein, E.: A 4-node finite shell element for the implementation of general hyperelastic 3D-elsticity at finite strains. Comput. Methods Appl. Mech. Eng. **130**(1–2), 57–79 (1996)
5. Brank, B., Ibrahimbegovic, A.: On the relation between different parametrizations of finite rotations for shells. Eng. Comput. **18**, 950–973 (2001)
6. Brank, B.: Assessment of 4-node EAS-ANS shell elements for large deformation analysis. Comput. Mech. **42**, 39–51 (2008)
7. Brank, B., Carrera, E.: Multilayered shell finite element with interlaminar continuous shear stresses: a refinement of the Reissner-Mindlin formulation. Int. J. Numer. Meth. Eng. **48**(6), 843–874 (2000)
8. Brank, B., Korelc, J., Ibrahimbegovic, A.: Dynamics and time-stepping schemes for elastic shells undergoing finite rotations. Comput. Struct. **81**, 1193–1210 (2003)
9. Brank, B.: Nonlinear shell models with seven kinematic parameters. Comput. Methods Appl. Mech. Eng. **194**, 2336–2362 (2005)
10. Brank, B., Briseghella, L., Tonello, N., Damjanić, F.B.: On non-linear dynamics of shells: Implementation of energy-momentum conserving algorithm for a finite rotation shell model. Int. J. Numer. Meth. Eng. **42**, 409–442 (1998)
11. Brank, B., Mamouri, S., Ibrahimbegović, A.: Constrained finite rotations in dynamics of shells and Newmark implicit time-stepping schemes. Eng. Comput. **22**(5/6), 505–535 (2005)
12. Brank, B., Perić, D., Damjanić, F.B.: On large deformations of thin elasto-plastic shells: Implementation of a finite rotation model for quadrilateral shell element. Int. J. Numer. Meth. Eng. **40**, 689–726 (1997)
13. Choi, C.K., Paik, J.G.: An effective four node degenerated shell element for geometrically nonlinear analysis. Thin-Walled Struct. **24**(3), 261–283 (1996)
14. Chung, J., Hulbert, G.M.: A time integration algorithm for structural dynamics with improved numerical dissipation—the generalized-alpha method. J. Appl. Mech.-Trans. ASME **60**, 371–375 (1993)
15. Crisfield, M.A., Peng, X.: Instabilities induced by coarse meshes for a nonlinear shell problem. Eng. Comput. **13**(6), 110–114 (1996)
16. Crisfield, M.A.: Non-linear Finite Element Analysis of Solids and Structures, Vol. 2, Advanced topics. Wiley (1996)
17. Dvorkin, E.N., Bathe, K.J.: A continuum mechanics based four-node shell element for general nonlinear analysis. Eng. Comput. **1**, 77–88 (1984)
18. Goto, Y., Watanabe, Y., Kasugai, T., Obata, M.: Elastic buckling phenomenon applicable to deployable rings. Int. J. Solids Struct. **29**(7), 893–909 (1992)
19. Gruttmann, F., Wagner, W.: A linear quadrilateral shell element with fast stiffness computation. Comp. Methods Appl. Mech. Eng. **194**, 4279–4300 (2005)
20. Gruttmann, F., Wagner, W.: Structural analysis of composite laminates using a mixed hybrid shell element. Comput. Mech. **37**, 479–497 (2006)
21. Ibrahimbegović, A., Brank, B., Courtois, P.: Stress resultant geometrically exact form of classical shell model and vector-like parameterization of constrained finite rotations. Int. J. Numer. Methods Eng. **52**(11), 1235–1252 (2001)
22. Klinkel, S., Gruttmann, F., Wagner, W.: A mixed shell dormulation accounting for thickness strains and finite strain 3d material models. Int. J. Numer. Meth. Eng. **74**, 945–970 (2008)

23. Ko, Y., Lee, P.S., Bathe, K.J.: A new MITC4+ shell element. Comput. Struct. **182**, 404–418 (2017)
24. Ko, Y., Lee, P.S., Bathe, K.J.: The MITC4+ shell element in geometric nonlinear analysis. Comput. Struct. **185**, 1–14 (2017)
25. Kobayashi, T., Mihara, Y., Fujii, F.: Path-tracing analysis for post-buckling process of elastic cylindrical shells under axial compression. Thin-walled Struct. **61**, 180–187 (2012)
26. Korelc, J., Wriggers, P.: Automation of Finite Element Methods. Springer International Publishing (2016)
27. Kuhl, D., Ramm, E.: Generalized energy–momentum method for non-linear adaptive shell dynamics. Comput. Methods Appl. Mech. Eng. **178**, 343–366 (1999)
28. Kuhl, D., Crisfield, M.A.: Energy-conserving and decaying algorithms in non-linear structural dynamics. Int. J. Numer. Meth. Eng. **45**, 569–599 (1999)
29. Kulikov, G.M., Plotnikova, S.V.: A family of ANS four-node exact geometry shell elements in general convected curvilinear coordinates. Int. J. Numer. Meth. Eng. **83**(10), 1376–1406 (2010)
30. Lavrenčič, M., Brank, B.: Simulation of shell buckling by implicit dynamics and numerically dissipative schemes. Thin-walled Struct. **132**, 682–699 (2018)
31. Lavrenčič, M.: Complete animations of buckling processes available from: http://fgg-web.fgg.uni-lj.si/~/mlavrenc/ (2018)
32. Newmark, N.M.: Method of computation for structural dynamics. Press. Vessel. Piping Des. Anal. **2**, 1235–1264 (1972)
33. Oesterle, B., Sachse, R., Ramm, E., Bischoff, M.: Hierarchic isogeometric large rotation shell elements including linearized transverse shear parametrization. Comput. Methods Appl. Mech. Eng. **321**, 383–405 (2017)
34. Pian, T.H.H., Sumihara, K.: Rational approach for assumed stress finite elements. Int. J. Numer. Meth. Eng. **20**(9), 1685–1695 (1984)
35. Pietraszkiewicz, W.: Lagrangian description and incremental formulation in the non-linear theory of thin shells. Int. J. Non-Linear Mech. **19**(2), 115–140 (1984)
36. Pietraszkiewicz, W., Eremeyev, V.A.: On vectorially parameterized natural strain measures of the nonlinear Cosserat continuum. Int. J. Solids Struct. **46**, 2477–2480 (2009)
37. Schieck, B., Pietraszkiewicz, W., Stumpf, H.: Theory and numerical analysis of shells undergoing large elastic strains. Int. J. Solids Struct. **29**(6), 689–709 (1992)
38. Simo, J.C., Fox D.D.: On a stress resultant geometrically exact shell model. Part I: Formulation and optimal parametrization. Comput. Methods Appl. Mech. Eng. **72**, 267–304 (1989)
39. Simo, J.C., Fox, D.D., Rifai, M.S.: On a stress resultant geometrically exact shell model. Part III: computational aspects of the nonlinear theory. Comput. Methods Appl. Mech. Eng. **79**, 21–70 (1990)
40. Simo, J.C., Rifai, M.S.: A class of mixed assumed strain methods and the method of incompatible modes. Int. J. Numer. Meth. Eng. **29**, 1595–1638 (1990)
41. Simo, J.C., Hughes, T.J.R.: On the variational foundations of assumed strain methods. J. Appl. Mech. **53**(1), 51–54 (1986)
42. Simo, J.C., Rifai, M.S., Fox, D.D.: On a stress resultant geometrically exact shell model. Part IV: variable thickness shells with through-the-thickness stretching. Comput. Methods Appl. Mech. Eng. 81, 91–126 (1990)
43. Simo, J.C., Tarnow, N.: A new energy and momentum conserving algorithm for the nonlinear dynamics of shells. Int. J. Numer. Meth. Eng. **37**, 2527–2549 (1994)
44. Stanić, A., Brank, B., Korelc, J.: On path-following methods for structural failure problems. Comput. Mech. **58**, 281–306 (2016)
45. Sze, K.Y., Liu, X.H., Lo, S.H.: Popular benchmark problems for geometric nonlinear analysis of shells. Finite Elem. Anal. Des. **40**, 1551–1569 (2004)
46. Wagner, W., Gruttmann, F.: A robust non-linear mixed hybrid quadrilateral shell element. Int. J. Numer. Meth. Eng. **64**, 635–666 (2005)
47. Wiśniewski, K.: Finite Rotation Shells, Basic Equations and Finite Elements for Reissner Kinematics. Springer, Netherlands (2010)

48. Wisniewski, K., Turska, E.: Improved 4-node Hu–Washizu elements based on skew coordinates. Comput. Struct. **87**, 407–424 (2009)
49. Xu, F., Potier-Ferry, M.: On axisymmetric/diamond-like mode transitions in axially compressed core-shell cylinders. J. Mech. Phys. Solids **94**, 68–87 (2016)
50. Yamaki, N.: Elastic Stability of Circular Cylindrical Shells. North-Holland, Netherlands (1984)
51. Zhao, Y., Cao, Y.P., Feng, X.Q., Ma, K.: Axial compression-induced wrinkles on a core-shell soft cylinder: theoretical analysis, simulations and experiments. J. Mech. Phys. Solids **73**, 212–227 (2014)

Development of Invariant-Based Triangular Element for Nonlinear Thermoelastic Analysis of Laminated Shells

Stanislav V. Levyakov

Abstract A finite element formulation is proposed for geometrically nonlinear analysis of thermally loaded composite laminated shells taking into account temperature-dependent properties of the material. The laminated shell is modeled by an equivalent single layer under the assumptions of the first-order shear deformation theory. A three-node triangular element is formulated using three natural coordinates directed along the element sides. The study focuses on representation of the total potential thermoelastic energy of anisotropic shell in terms of combined invariants which depend on the natural components of the strain tensor and those of the tensors describing mechanical and physical properties of the material. Based on the resulting expression for the energy, compact and algorithmic relations are derived for computing coefficients of the first and second variations of the strain energy of the finite element which are necessary to formulate the equations for finding equilibrium states and to examine their stability. Some examples are presented to demonstrate the ability of the finite element to deal with postbuckling behavior of thermally loaded laminated shells.

Keywords Laminated shell · Thermal loading · Nonlinear deformation · Temperature dependent properties · Buckling · Stability · Triangular finite element

1 Introduction

In a variety of engineering applications such as oil, chemical, and aerospace industries, shell structures operate in elevated temperature environment. Stringent requirement of high stiffness-to-weight and strength-to-weight ratios calls for advanced composite materials and methods of nonlinear analysis which can accurately describe structural response of composite plates and shells for a wide range of loading conditions.

S. V. Levyakov (✉)
Department of Engineering Mathematics, Novosibirsk State Technical University, 630092 Novosibirsk, Russian Federation
e-mail: stan-levyakov@yandex.ru

H. Altenbach et al. (eds.), *Recent Developments in the Theory of Shells*,
Advanced Structured Materials 110, https://doi.org/10.1007/978-3-030-17747-8_22

In the presence of support conditions that restrain thermal expansion of the material, compressive stresses rapidly develop under increasing temperature, which may result in buckling of thin-walled members. In the absence of mechanical loads, thermal buckling may be not as catastrophic as is the case of combined thermal and mechanical loadings. In most practical situations, plates and shells can withstand postbuckling stresses and carry thermal load beyond the critical temperature. However, a natural question may arise as to how long the plate or shell can remain in a stable state. Further increase in the temperature can lead to secondary buckling resulting in undesirable deflection patterns, high stresses, etc. It is therefore important not only to accurately predict thermal buckling loads but also check stability of postbuckling equilibrium configurations of thin-walled structures designed to operate in severe thermal environment.

There are some points to be taken into consideration in the thermoelastic analysis of composite laminated shells. First, a significant change in the geometry can occur due to heating prior to buckling. In this case, linear buckling analysis based on the assumption of undeformed geometry may lead to overpredicted critical thermal loads. Second, depending on the lamination scheme and boundary conditions, prebuckling stress and strain distributions can be highly nonuniform even for simple shell geometries. Another important point is that mechanical properties of the material degrade with an increase in temperature, which results in reduced stiffness and lower buckling resistance of the shell. In the analysis of structures operating under elevated temperatures, the assumption of temperature-independent properties, which has been commonly used in the literature, can significantly overestimate the thermal buckling loads and strength characteristics.

Mathematical formulation of geometrically nonlinear problems of shells with temperature-dependent properties leads to highly complicated nonlinear equations, which can be solved only by numerical techniques. In the context of the present study, which deals with the finite element modelling, we confine our review of the literature to finite-element formulations proposed for analysis of laminated plates and shells subjected to thermal loading.

Most of the studies on thermoelastic response of thin-walled structures have been carried out under the assumption of temperature-independent material properties. Chen and Chen [1], Thangaratnam et al. [2, 3], and Ounis et al. [4] developed quadrilateral finite elements for solving linear buckling problems of thin rectangular plates using the classical laminate plate theory. It is well known that incorporation of transverse shear deformation is important for more accurate analysis of composite structures characterized by high ratio of in-plane elastic modulus to transverse shear modulus. In this connection, considerable amount of attention has been devoted to shear flexible finite elements. Based on the first order shear deformation theory (FSDT), Chandrashekhara [5] and Prabhu and Dhanaraj [6] presented formulations of nine-node isoparametric elements with 45 degrees of freedom (DOF) for linear buckling analysis of laminated plates subjected to uniform temperature rise. Dawe and Ge [7] developed a spline finite strip method for predicting buckling temperature of rectangular plates. Kabir et al. [8] and Shiau et al. [9] proposed triangular finite elements to solve thermal buckling problems of laminated plates. The above-mentioned

elements were used to evaluate the critical buckling temperature of symmetric and asymmetric laminates where prebuckling bending was ignored. Using the natural-mode approach, Argyris and Tenek [10] developed a three-node triangular element with 18 DOFs for geometrically nonlinear analysis of heated multilayered plates. Ganapathi and Touratier [11] formulated an eight-node isoparametric quadrilateral finite element with 40 DOFs for analysis of postbuckling behavior of composite plates. Finite deflections and failure of laminated shallow shells were studied by Huang and Tauchert [12, 13] who used quadrilateral element with five DOFs per node. Barut et al. [14] developed a triangular element with five DOFs per node for investigating nonlinear structural response of flat and curved laminated panels undergoing large displacements and rotations under nonuniform thermal loading. Patel et al. [15] formulated an eight-node quadrilateral element for nonlinear analysis of laminated cylindrical and conical shells. Based on the calculation results, they showed that prebuckling deformation has a significant effect on the critical buckling temperature. Alijani et al. [16] formulated a semi-analytical finite element of cylindrical shell, where truncated Fourier series were used to approximate displacement and rotation fields in the circumferential direction. Sabik and Kreja [17, 18] performed geometrically nonlinear finite-element analysis of uniformly heated shallow laminated shells and found unsymmetric equilibrium states that refer to solution branches emanating from the first bifurcation point.

Using the higher-order shear deformation theory, Kant and Babu [19], Patel et al. [20] developed more accurate, but more complicated finite-element models for nonlinear analysis of laminated plates and shells subjected to thermal loads. Thermal buckling and postbuckling behavior of plates based on the layerwise theory were studied by Cetkovic [21] and Oh and Lee [22]. It should be noted that refinement in the results that higher order theories provide in the analysis of moderately thick plates and shells is noticeable only in local stress distribution. The global structural response of shells can adequately be predicted by simpler formulations based on the FSDT with considerable computation time savings.

Compared to papers on structures with temperature-independent material properties, there are fewer papers dealing with nonlinear analysis of thermally loaded composite shells with temperature-dependent properties. One of the first studies in this direction was carried out by Chen and Chen [23] who investigated buckling and postbuckling behavior of rectangular plates using the classical laminate plate theory. Thermal postbuckling response of moderately thick laminated plates based on the FSDT was examined by Singha et al. [24] and Srikanth and Kumar [25]. Using the small deflection theory, Chandrashekhara and Bhimaraddi [26] analyzed deformations of laminated doubly curved shallow shells subjected to nonuniform temperature fields. Patel et al. [27, 28] developed a semi-analytical finite element method for thermoelastic analysis of laminated shells of revolution undergoing moderately large rotations. Shariyat [29] proposed a four-node rectangular finite element based on the layerwise theory and studied the effect of boundary conditions, stacking sequence, and geometrical parameters on the buckling temperature of rectangular plates.

It is evident from the literature review that research effort has been focused on thermal buckling and postbuckling of rectangular plates and shells of revolution. There

are few studies dealing with stability analysis of postbuckling states of thermally loaded laminated shells.

The aim of the present study is to formulate a computationally effective triangular finite element for nonlinear analysis of composite laminated shells with temperature dependent material properties. A considerable contribution to the theory of triangular shell finite elements is due to Argyris et al., see e.g. [30–32]. It was shown that, when dealing with a triangular domain, it is advantageous to use three natural coordinate directions along the triangle sides rather than conventional Cartesian coordinates. According to this approach, the components of strains, stresses, stress resultants, etc. related to the natural directions should be determined to evaluate stiffness properties of the element. However, direct derivation of the finite element equations in terms of the natural components involves lengthy manipulations and cumbersome equations connected to coordinate transformations.

To obtain a relatively compact finite element formulation of a triangular shell element, we employ the invariant-based approach. In [33–35], it was shown that the strain energy of a shell composed of isotropic or functionally graded materials can be written as a function of invariants of three normal strains determined in three nonparallel directions on the middle surface of the shell. Based on this result, compact and algorithmic relations were obtained for computing the stiffness matrix of the triangular finite elements. An attempt to extend this approach to composite laminated shells was undertaken in [36]. It was found that the strain energy of the composite shell can be written as a function of so-called combined invariants which depend on the natural components of the strain and stress tensors. As a result, in the derivation of the element stiffness matrix, some computational effort was needed to convert stresses to strains using the constitutive relations. In [37], a method was proposed to express the strain energy density of a laminated shell based on the FSDT in terms of combined invariants which depend on the natural components of the strain tensor and those of the tensor of elastic constants. The expression for the strain energy in terms of invariants leads to straightforward derivation of the element stiffness matrix and thermal load vector. Below, we use the method proposed in [37] to develop a triangular finite element for nonlinear thermoelastic analysis of laminated shells with temperature-dependent material properties.

2 Coordinate Transformation of Tensor Components

We consider a symmetric second-order tensor u_{mn} (m,n = 1,2) and introduce the vector composed of its three independent components in Cartesian coordinates ξ_1 and ξ_2:

$$\boldsymbol{u} = \{u_{11}, u_{22}, u_{12}\}^T. \tag{2.1}$$

Now we consider a triangle on the plane and define three coordinate lines s_i (i = 1,2,3) parallel to the triangle edges (see Fig. 1). Using coordinate

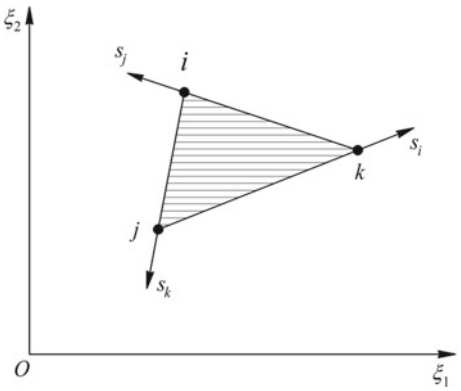

Fig. 1 Cartesian and natural coordinates

transformation, one can determine three components u_i $(i = 1,2,3)$ referred to the coordinates s_i. Following terminology of Argyris [30–32], when dealing with a triangular element we call the quantities u_1, u_2, and u_3 the natural components of the tensor.

Thus, any symmetric two-dimensional tensor u_{mn} can alternatively be represented by the vector comprising three natural components

$$\boldsymbol{u} = \{u_1, u_2, u_3\}^T. \tag{2.2}$$

Relation between Cartesian and natural components is given by (no summation over i)

$$u_i = \alpha_{mni} u_{mn} (i = 1, 2, 3; m, n = 1, 2), \tag{2.3}$$

$$\alpha_{mni} = \lambda_{mi}\lambda_{ni}, \lambda_{1i} = \frac{\xi_{1k} - \xi_{1j}}{l_i}, \lambda_{2i} = \frac{\xi_{2k} - \xi_{2j}}{l_i}, \tag{2.4}$$

where λ_{mi} are the direction cosines of the edge opposite to the ith vertice of the triangle, ξ_{mk} is the mth coordinate of the kth vertice, and l_i is the length of the ith edge. In Eqs. (2.3), (2.4), and below, subscripts i, j, and k run from 1 to 3 and obey the rule of cyclic permutation and summation is performed over repeated subscripts unless otherwise specified.

Relations (2.3) can be inverted to give

$$u_{mn} = \beta_{mni} u_i (i = 1, 2, 3), \tag{2.5}$$

$$\beta_{mni} = \frac{l_1 l_2 l_3 l_i}{8A^2} (\lambda_{mk}\lambda_{nj} + \lambda_{nk}\lambda_{mj} - 2\lambda_{pj}\lambda_{pk}\delta_{mn}) (p = 1, 2), \tag{2.6}$$

where A is the area of the triangle and δ_{mn} is Kronecker's symbol.

Given the lengths of the triangle edges, the area of the triangle can be calculated by the formula

$$A = \frac{1}{4}\sqrt{\Delta}, \quad \Delta = (l_p l_p)^2 - 2l_p^2 l_p^2 (p = 1, 2, 3). \tag{2.7}$$

Note that the coefficients of the coordinate transformations (2.4) and (2.6) satisfy the condition $\alpha_{mni}\beta_{mnj} = \delta_{ij}$.

3 Template Formulas for Invariants

It is well known that the first and second invariants of a two-dimensional tensor u_{mn} are written in terms of Cartesian components as

$$I_u = u_{11} + u_{22}, \quad I_{uu} = u_{11}u_{22} - u_{12}^2. \tag{3.1}$$

Given two symmetric tensors u_{mn} and v_{mn}, the combined invariant is defined as [36]

$$I_{uv} = \frac{1}{2}(u_{11}v_{22} + u_{22}v_{11} - 2u_{12}v_{12}). \tag{3.2}$$

In the particular case where $u_{mn} = v_{mn}$, Eq. (3.2) yields the expression for the second invariant $(3.1)_2$. If $v_{mn} = 2\delta_{mn}$, from Eq. (3.2) one obtains the first invariant $(3.1)_1$.

The invariants mentioned above can be written in terms of three natural components as

$$I_u = 2(aa_p u_p - 2a_p^2 u_p),\ I_{uu} = (a_p u_p)^2 - 2a_p^2 u_p^2,$$

$$I_{uv} = (a_p u_p)(a_q v_q) - 2a_p^2 (uv)_p \ (p, q = 1, 2, 3), \tag{3.3}$$

where a_p and a are nondimensional parameters given by

$$a_p = \frac{(l_p)^2}{\sqrt{\Delta}} (\text{no summation over } p),\ a = \frac{l_q l_q}{\sqrt{\Delta}}. \tag{3.4}$$

In Eq. $(3.3)_3$, we use the notation $(uv)_p = u_p v_p$, in which no summation is carried out over p.

Let us express the invariants in matrix form. To this end, we introduce the matrix notation:

$$\boldsymbol{\tau} = 2\left\{ a_1(a - 2a_1),\ a_2(a - 2a_2),\ a_3(a - 2a_3) \right\}^T, \boldsymbol{a} = \left\{ a_1,\ a_2,\ a_3 \right\}^T,$$

$$\boldsymbol{\rho} = \begin{pmatrix} 2a_1^2 & 0 & 0 \\ & 2a_2^2 & 0 \\ \text{sym} & & 2a_3^2 \end{pmatrix}. \tag{3.5}$$

Using Eq. (3.5), we write Eq. (3.3) as

$$I_u = \boldsymbol{u}^{\mathrm{T}}\boldsymbol{\tau},\ I_{uu} = \boldsymbol{u}^{\mathrm{T}}(\boldsymbol{a}\boldsymbol{a}^{\mathrm{T}} - \boldsymbol{\rho})\boldsymbol{u},\ I_{uv} = \boldsymbol{u}^{\mathrm{T}}(\boldsymbol{a}\boldsymbol{a}^{T} - \boldsymbol{\rho})\boldsymbol{v}, \tag{3.6}$$

where $\boldsymbol{u}$ and $\boldsymbol{v}$ are the 3×1 vectors composed of the natural components of the corresponding tensors.

4 Invariant Representation of the Strain Energy Density of Anisotropic Shell

We consider a shell composed of linear elastic anisotropic materials. Adopting the assumptions of the first order shear deformation theory, we write the strain energy density of the shell as

$$\Pi_V = \Pi_{V1} + \Pi_{V2}, \tag{4.1}$$

where Π_{V1} is the strain energy density due to plane stresses and Π_{V2} is that due to transverse shear stresses. In what follows, we express Π_{V1} and Π_{V2} in terms of the invariants discussed above.

4.1 Representation of Π_{V1} in Terms of Combined Invariants

Under plane-stress conditions, the stress-strain relations can be written as

$$\begin{pmatrix} \sigma_{11} \\ \sigma_{22} \\ \sigma_{12} \end{pmatrix} = \begin{pmatrix} D_{11} & D_{12} & D_{13} \\ & D_{22} & D_{23} \\ sym. & & D_{33} \end{pmatrix} \begin{pmatrix} S_{11} \\ S_{22} \\ 2S_{12} \end{pmatrix}, \tag{4.2}$$

where σ_{mn} and S_{mn} are the Cartesian components of the stress and strain tensors, respectively, and D_{ij} are the elastic constants of the material.

Let us consider three symmetric two-dimensional tensors u_{mn}, v_{mn}, and w_{mn} whose components are so far unknown. Bearing in mind that, for small strains the strain energy density of the shell is a quadratic function of the strains, we assume that

$$\Pi_{V1} = \frac{1}{2}(I_{uS}^2 + I_{vS}^2 + I_{wS}^2), \tag{4.3}$$

where I_{uS}, I_{vS}, and I_{wS} are the combined invariants determined in accordance with the template formula (3.2).

If the strains are known, expression (4.3) contains nine unknown components of the tensors u_{mn}, v_{mn}, and w_{mn}. To find these unknowns, we use the relations

$$\sigma_{11} = \frac{\partial \Pi_{V1}}{\partial S_{11}}, \sigma_{22} = \frac{\partial \Pi_{V1}}{\partial S_{22}}, \sigma_{12} = \frac{\partial \Pi_{V1}}{\partial S_{12}}. \tag{4.4}$$

Equating the coefficients of S_{mn} on the right sides of Eqs. (4.2) and (4.4), we obtain the following nonlinear algebraic equations:

$$\begin{aligned} &u_{22}^2 + v_{22}^2 + w_{22}^2 = 4D_{11}, u_{11}u_{22} + v_{11}v_{22} + w_{11}w_{22} = 4D_{12}, \\ &u_{12}u_{22} + v_{12}v_{22} + w_{12}w_{22} = -4D_{13}, u_{11}^2 + v_{11}^2 + w_{11}^2 = 4D_{22}, \\ &u_{11}u_{12} + v_{11}v_{12} + w_{11}w_{12} = -4D_{23}, u_{12}^2 + v_{12}^2 + w_{12}^2 = 4D_{33}. \end{aligned} \tag{4.5}$$

We have a system of six equations for nine unknowns. Hence, we need three extra equations to remove the indeterminacy of the system. To this end, we employ semi-inverse method. The idea is to prescribe certain values to three unknowns and find the remaining six using Eqs. (4.5). In the process, various guess values of three unknowns can be adopted.

A relatively simple solution of system (4.5) can be obtained by assuming that

$$u_{11} = u_{12} = v_{12} = 0. \tag{4.6}$$

In this case, Eq. (4.5) become

$$\begin{aligned} &u_{22}^2 + v_{22}^2 + w_{22}^2 = 4D_{11}, v_{11}v_{22} + w_{11}w_{22} = 4D_{12}, w_{12}w_{22} = -4D_{13}, \\ &v_{11}^2 + w_{11}^2 = 4D_{22}, w_{11}w_{12} = -4D_{23}, w_{12}^2 = 4D_{33}. \end{aligned} \tag{4.7}$$

Starting with the last equation, one can easily find the solution of system (4.7):

$$\begin{aligned} &u_{22} = 2\sqrt{\frac{\det \boldsymbol{D}}{D_{22}D_{33} - D_{23}^2}}, v_{11} = 2\sqrt{\frac{D_{22}D_{33} - D_{23}^2}{D_{33}}}, \\ &v_{22} = 2\frac{D_{12}D_{33} - D_{13}D_{23}}{\sqrt{D_{33}(D_{22}D_{33} - D_{23}^2)}}, w_{11} = -2\frac{D_{23}}{\sqrt{D_{33}}}, w_{22} = -2\frac{D_{13}}{\sqrt{D_{33}}}, \\ &w_{12} = 2\sqrt{D_{33}}, \end{aligned} \tag{4.8}$$

where $\det \boldsymbol{D}$ is the determinant of the matrix of elastic constants in Eq. (4.2).

As an example, we consider an orthotropic material with the elastic constants

$$D_{11} = \frac{E_{11}}{1 - \nu_{12}\nu_{21}}, D_{12} = \frac{\nu_{21}E_{11}}{1 - \nu_{12}\nu_{21}}, D_{13} = D_{23} = 0, D_{22} = \frac{E_{22}}{1 - \nu_{12}\nu_{21}}, D_{33} = G_{12}, \tag{4.9}$$

where E_{11} and E_{22} are Young's moduli, ν_{12} and ν_{21} are Poisson's ratios satisfying the relation $\nu_{12}E_{22} = \nu_{21}E_{11}$, and G_{12} is the shear modulus. Substituting Eq. (4.9) into Eq. (4.8), we obtain

$$u_{22} = 2\sqrt{\frac{E_{11}(E_{22} - E_{11}\nu_{21}^2)}{E_{22}(1 - \nu_{12}\nu_{21})}}, v_{11} = 2\sqrt{\frac{E_{22}}{1 - \nu_{12}\nu_{21}}}, v_{22} = \frac{2E_{11}\nu_{21}}{\sqrt{E_{22}(1 - \nu_{12}\nu_{21})}},$$
$$w_{11} = w_{22} = 0, w_{12} = 2\sqrt{G_{12}}. \tag{4.10}$$

For isotropic materials, expressions (4.9) become

$$D_{11} = D_{22} = \frac{E}{1 - \nu^2}, D_{12} = \frac{\nu E}{1 - \nu^2}, D_{13} = D_{23} = 0, D_{33} = \frac{E}{2(1 + \nu)}, \tag{4.11}$$

where E is Young's modulus and ν is Poisson's ratio. The components in Eq. (4.10) become

$$u_{22} = 2\sqrt{E}, v_{11} = 2\sqrt{\frac{E}{1 - \nu^2}}, v_{22} = 2\nu\sqrt{\frac{E}{1 - \nu^2}}, w_{11} = w_{22} = 0, w_{12} = \sqrt{\frac{2E}{1 + \nu}}. \tag{4.12}$$

One can easily show that substitution of (4.6) and (4.12) into (4.13) leads to the familiar expression for the strain energy of isotropic material under plane stress.

4.2 Representation of Π_{V2} in Terms of Combined Invariants

We introduce the symmetric tensor [34]

$$\Gamma_{mn} = S_{m3}S_{n3}(m, n = 1, 2), \tag{4.13}$$

where S_{m3} are the transverse shear strains.

The strain energy density of the shell due to transverse shear forces can be written as

$$\Pi_{2V} = \frac{1}{2}g_{mn}\Gamma_{mn}(m, n = 1, 2), \tag{4.14}$$

where g_{mn} are the transverse shear moduli.

The strain energy density (4.14) can also be written in terms of the combined invariants as

$$\Pi_{2V} = \frac{1}{2}(I_g I_\Gamma - 2I_{g\Gamma}). \tag{4.15}$$

Using template formulas (3.6), we write Eq. (4.15) in terms of the natural components of the tensor Γ_{mn}

$$\Pi_{2V} = \frac{1}{2}\boldsymbol{g}^T[\boldsymbol{\tau}\boldsymbol{\tau}^T - 2(\boldsymbol{a}\boldsymbol{a}^T - \boldsymbol{\rho})]\boldsymbol{\Gamma}. \tag{4.16}$$

5 Potential Energy of the Shell as a Function of Natural Strains

According to the first-order shear deformation theory, the strains of the shell are given by

$$S_{mn} = \varepsilon_{mn} + z\kappa_{mn} - \alpha_{mn}\Delta T, \tag{5.1}$$

where ε_{mn} and κ_{mn} are the components of the membrane and bending strains of the shell middle surface, respectively, z is the coordinate measured from the shell middle surface in the transverse direction, α_{mn} are the coefficients of linear thermal expansion, and ΔT is a change in temperature.

Bearing in mind Eq. (3.2) and substituting Eq. (5.1) into Eq. (4.3), we obtain

$$\begin{aligned}\Pi_{1V} = \frac{1}{2}\{&I_{u\varepsilon}^2 + I_{v\varepsilon}^2 + I_{w\varepsilon}^2 + 2z(I_{u\varepsilon}I_{u\kappa} + I_{v\varepsilon}I_{v\kappa} + I_{w\varepsilon}I_{w\kappa}) + z^2(I_{u\kappa}^2 + I_{v\kappa}^2 + I_{w\kappa}^2)\}\\ &- \Delta T(I_{u\alpha}I_{u\varepsilon} + I_{v\alpha}I_{v\varepsilon} + I_{w\alpha}I_{w\varepsilon}) - z\Delta T(I_{u\alpha}I_{u\kappa} + I_{v\alpha}I_{v\kappa} + I_{w\alpha}I_{w\kappa}),\end{aligned} \tag{5.2}$$

where $I_{u\varepsilon}, I_{v\varepsilon}, \ldots, I_{w\kappa}$ are the combined invariants which can be determined in terms of Cartesian components of the tensors using Eq. (3.2) or in terms of natural components using Eq. (3.3).

Integrating the strain energy density given by Eq. (5.2) over the volume of the shell and using Eq. $(3.6)_3$, we write the result of integration in terms of the natural components

$$\Pi_1 = \frac{1}{2}\iint\limits_A \{\boldsymbol{\varepsilon}^T\mathbf{Z}_0\boldsymbol{\varepsilon} + \boldsymbol{\varepsilon}^T\mathbf{Z}_1\boldsymbol{\kappa} + \boldsymbol{\kappa}^T\mathbf{Z}_1\boldsymbol{\varepsilon} + \boldsymbol{\kappa}^T\mathbf{Z}_2\boldsymbol{\kappa} - 2\boldsymbol{\varepsilon}^T\boldsymbol{F}_0 - 2\boldsymbol{\kappa}^T\boldsymbol{F}_1\}dA, \tag{5.3}$$

$$\boldsymbol{\varepsilon} = \{\varepsilon_1, \quad \varepsilon_2, \quad \varepsilon_3\}^T, \boldsymbol{\kappa} = \{\kappa_1, \quad \kappa_2, \quad \kappa_3\}^T, \boldsymbol{\alpha} = \{\alpha_1, \quad \alpha_2, \quad \alpha_3\}^T, \tag{5.4}$$

$$\boldsymbol{Z}_n = (\boldsymbol{a}\boldsymbol{a}^T - \boldsymbol{\rho}) \int_{-h/2}^{h/2} (\boldsymbol{u}\boldsymbol{u}^T + \boldsymbol{v}\boldsymbol{v}^T + \boldsymbol{w}\boldsymbol{w}^T) z^n dz (\boldsymbol{a}\boldsymbol{a}^T - \boldsymbol{\rho}) \quad (n = 0, 1, 2), \tag{5.5}$$

$$\boldsymbol{F}_m = \int_{-h/2}^{h/2} \Delta T z^m (\boldsymbol{a}\boldsymbol{a}^T - \boldsymbol{\rho})(\boldsymbol{u}\boldsymbol{u}^T + \boldsymbol{v}\boldsymbol{v}^T + \boldsymbol{w}\boldsymbol{w}^T)(\boldsymbol{a}\boldsymbol{a}^T - \boldsymbol{\rho})\boldsymbol{\alpha} dz \quad (m = 0, 1). \tag{5.6}$$

Here A is the area of the shell middle surface, h is the shell thickness and ε_i and κ_i are the natural components of the membrane-strain and bending-strain tensors, respectively.

From now on, we confine our attention to laminated composites. Assuming that the temperature change ΔT does not vary in the thickness direction, we write Eqs. (5.5) and (5.6) as

$$\boldsymbol{Z}_n = \frac{1}{n+1} (\boldsymbol{a}\boldsymbol{a}^T - \boldsymbol{\rho}) \sum_{k=1}^{NL} (z_{k+1}^{n+1} - z_k^{n+1})(\boldsymbol{u}\boldsymbol{u}^T + \boldsymbol{v}\boldsymbol{v}^T + \boldsymbol{w}\boldsymbol{w}^T)_k (\boldsymbol{a}\boldsymbol{a}^T - \boldsymbol{\rho}) \quad (n = 0, 1, 2), \tag{5.7}$$

$$\boldsymbol{F}_m = \frac{\Delta T}{m+1} \sum_{k=1}^{NL} (z_{k+1}^{m+1} - z_k^{m+1})(\boldsymbol{a}\boldsymbol{a}^T - \boldsymbol{\rho})(\boldsymbol{u}\boldsymbol{u}^T + \boldsymbol{v}\boldsymbol{v}^T + \boldsymbol{w}\boldsymbol{w}^T)_k (\boldsymbol{a}\boldsymbol{a}^T - \boldsymbol{\rho})\boldsymbol{\alpha}_k, \ (m = 0, 1), \tag{5.8}$$

where NL is the number of layers.

Now we consider the strain energy of the shell due to transverse shear forces. Integrating (4.16), we obtain

$$\Pi_2 = \frac{1}{2} \iint_A \boldsymbol{C}_\Gamma^T \boldsymbol{\Gamma} dA, \boldsymbol{C}_\Gamma = k_s (\boldsymbol{\tau}\boldsymbol{\tau}^T - 2(\boldsymbol{a}\boldsymbol{a}^T - \boldsymbol{\rho})) \int_{-h/2}^{h/2} \boldsymbol{g} dz, \tag{5.9}$$

where k_s is the shear correction factor assumed to be equal to 5/6.

6 Potential Energy of the Shell Finite Element

We consider a three-node triangular shell element. The nodal position vectors are denoted by $\boldsymbol{r}_m$ (m = 1,2,3). At each node, we determine a unit director $\boldsymbol{n}_m$ which is initially normal to the shell middle surface (Fig. 2). According to the FSDT, the unit directors in a deformed state are not necessarily normal to the deformed middle surface of the shell.

We adopt the following expressions for the natural strains ε_i proposed in [33] (no summation over i, j, and k):

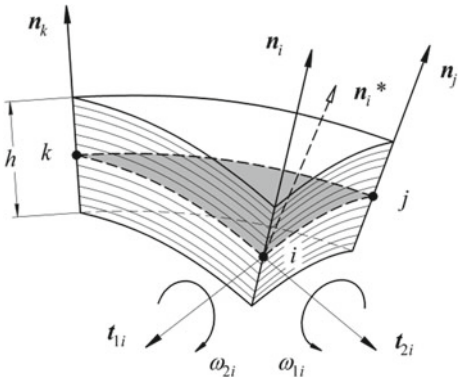

Fig. 2 Shell finite element and nodal rotations

$$\varepsilon_i = \frac{e_i^*}{l_i} \cdot \frac{\arcsin\left(\Delta\chi_i^*\right)}{\Delta\chi_i^*} - 1, \tag{6.1}$$

where

$$\Delta\chi_i^* = \frac{\chi_{2k}^* - \chi_{1j}^*}{2},\ \chi_{2k}^* = \frac{\psi_{2k}^*}{e_i^*},\ \chi_{1j}^* = \frac{\psi_{1j}^*}{e_i^*}, \tag{6.2}$$

$$\Delta\chi_i = \frac{\chi_{2k} - \chi_{1j}}{2},\ \chi_{2k} = \frac{\psi_{2k}}{e_i},\quad \chi_{1j} = \frac{\psi_{1j}}{e_i},\ l_i = e_i \frac{\arcsin(\Delta\chi_i)}{\Delta\chi_i}, \tag{6.3}$$

$$e_i = \sqrt{\left(\boldsymbol{r}_k - \boldsymbol{r}_j\right)^2},\ \psi_{1j} = \boldsymbol{n}_j\left(\boldsymbol{r}_k - \boldsymbol{r}_j\right),\ \psi_{2k} = \boldsymbol{n}_k\left(\boldsymbol{r}_k - \boldsymbol{r}_j\right), \tag{6.4}$$

$$e_i^* = \sqrt{\left(\boldsymbol{r}_k^* - \boldsymbol{r}_j^*\right)^2},\ \psi_{1j}^* = \boldsymbol{n}_j^*\left(\boldsymbol{r}_k^* - \boldsymbol{r}_j^*\right),\ \psi_{2k}^* = \boldsymbol{n}_k^*\left(\boldsymbol{r}_k^* - \boldsymbol{r}_j^*\right). \tag{6.5}$$

In Eqs. (6.1)–(6.5) and below, asterisk refers to a deformed state. It should be noted that relations (6.1) and (6.3) lead to uncertainty of type 0/0 for flat and nearly flat elements. In this case, Taylor series approximations are employed to avoid numerical instability.

Approximate expressions for the natural bending and transverse shear strains κ_m and γ_m are based on the following analytical solution of the bending problem of the Timoshenko beam with prescribed end rotations ϑ_{1j} and ϑ_{2k} (no summation over i, j, and k):

$$\kappa_i = \frac{1}{l_i}\left(\vartheta_{2k} - \vartheta_{1j}\right) + \frac{\eta_{i1}}{l_i}(L_k - L_j)\left(\vartheta_{2k} + \vartheta_{1j}\right), \tag{6.6}$$

$$\gamma_i = \eta_{i2}\left(\vartheta_{2k} + \vartheta_{1j}\right), \tag{6.7}$$

$$\vartheta_{mi} = \arcsin\left(\chi_{mi}^*\right) - \arcsin(\chi_{mi}), \tag{6.8}$$

$$\eta_{i1} = \frac{3}{1+\eta_{i3}}, \eta_{i2} = \frac{1}{6}\eta_{i1}\eta_{i3}, \eta_{i3} = 12\frac{D_i}{C_i l_i^2}. \tag{6.9}$$

$$D_i = \int_{-h/2}^{h/2} E_i dz, C_i = k_s \int_{-h/2}^{h/2} g_i dz, \tag{6.10}$$

$$E_i = D_{11}\lambda_{1i}^4 + D_{22}\lambda_{2i}^4 + (2D_{12} + 4D_{33})\lambda_{1i}^2\lambda_{2i}^2 + 4D_{13}\lambda_{1i}^3\lambda_{2i} + 4D_{23}\lambda_{1i}\lambda_{2i}^3, \tag{6.11}$$

$$g_i = g_{11}\lambda_{1i}^2 + g_{22}\lambda_{2i}^2. \tag{6.12}$$

where L_1, L_2, and L_3 are the area coordinates for the triangular element and k_s is the shear correction factor.

Substituting Eqs. (6.6) and (6.7) into Eq. (5.3) and integrating over the element area, we obtain

$$\Pi_1 = \frac{1}{2}(\boldsymbol{\varepsilon}^T \boldsymbol{K}_\varepsilon \boldsymbol{\varepsilon} + \boldsymbol{\varepsilon}^T \boldsymbol{K}_{\varepsilon\vartheta}\vartheta + \vartheta^T \boldsymbol{K}_{\varepsilon\vartheta}^T \boldsymbol{\varepsilon} + \vartheta^T \boldsymbol{K}_\vartheta \vartheta) - \boldsymbol{\varepsilon}^T \boldsymbol{N}_T - \vartheta^T \boldsymbol{M}_T, \tag{6.13}$$

$$\boldsymbol{K}_\varepsilon = A\boldsymbol{Z}_0, \boldsymbol{K}_{\varepsilon\vartheta} = A\boldsymbol{Z}_1\boldsymbol{C}_A, \boldsymbol{K}_\vartheta = \iint_A \boldsymbol{C}^T \boldsymbol{Z}_2 \boldsymbol{C} dA, \tag{6.14}$$

$$\boldsymbol{N}_T = A\boldsymbol{F}_0, \boldsymbol{M}_T = \boldsymbol{C}_A^T \boldsymbol{F}_1, \tag{6.15}$$

$$\vartheta^T = \{\vartheta_{23}, \quad \vartheta_{12}, \quad \vartheta_{21}, \quad \vartheta_{13}, \quad \vartheta_{22}, \quad \vartheta_{11}\}, \tag{6.16}$$

$$\boldsymbol{C}_A = \begin{bmatrix} l_1^{-1} & -l_1^{-1} & 0 & 0 & 0 & 0 \\ 0 & 0 & l_2^{-1} & -l_2^{-1} & 0 & 0 \\ 0 & 0 & 0 & 0 & l_3^{-1} & -l_3^{-1} \end{bmatrix}, \tag{6.17}$$

Here $\boldsymbol{C}$ is a 3×6 matrix whose nonzero coefficients are given by

$$\begin{aligned} C_{11} &= [1 + \eta_{11}(L_3 - L_2)]l_1^{-1}, C_{12} = -[1 + \eta_{11}(L_2 - L_3)]l_1^{-1}, \\ C_{23} &= [1 + \eta_{21}(L_1 - L_3)]l_2^{-1}, C_{24} = -[1 + \eta_{21}(L_3 - L_1)]l_2^{-1}, \\ C_{35} &= [1 + \eta_{31}(L_2 - L_1)]l_3^{-1}, C_{36} = -[1 + \eta_{31}(L_1 - L_2)]l_3^{-1}. \end{aligned} \tag{6.18}$$

The 6×6 symmetric matrix $\boldsymbol{K}_\vartheta$, not given here explicitly, can easily be evaluated by exact integration using three Gaussian points (see, e.g. [38]).

The strain energy due to transverse shear forces (5.9) can be written as a quadratic function of the deformation parameters (6.16)

$$\Pi_2 = \frac{1}{2}\vartheta^T \boldsymbol{K}_\Gamma \vartheta, \boldsymbol{K}_\Gamma = A\boldsymbol{W}^T \boldsymbol{M}\boldsymbol{W}, \tag{6.19}$$

$$\boldsymbol{M} = \begin{bmatrix} C_{\Gamma 1} & 0 & 0 \\ 0 & C_{\Gamma 2} & 0 \\ 0 & 0 & C_{\Gamma 3} \end{bmatrix}, \boldsymbol{W} = \begin{bmatrix} \eta_{12} & \eta_{12} & 0 & 0 & 0 & 0 \\ 0 & 0 & \eta_{22} & \eta_{22} & 0 & 0 \\ 0 & 0 & 0 & 0 & \eta_{32} & \eta_{32} \end{bmatrix}. \tag{6.20}$$

7 Solution Procedure

To find equilibrium states of the finite-element model of the shell using the Newton-Raphson iterative technique, it is necessary to calculate the coefficients of the first and second variations of the potential energy. Derivation of explicit expressions for the variations is a formidable task because of highly involved expressions for the strains. To avoid the difficulties, we propose a recurrent method for computing the coefficients based on the introduction of three groups (or levels) of variables represented by the vectors

$$\boldsymbol{u}_{(1)} = \left\{ \varepsilon_1,\ \varepsilon_2,\ \varepsilon_3,\ \vartheta_{23},\ \vartheta_{12},\ \vartheta_{21},\ \vartheta_{13},\ \vartheta_{22},\ \vartheta_{11} \right\}^T, \tag{7.1}$$

$$\boldsymbol{u}_{(2)} = \left\{ e_1^*, e_2^*, e_3^*, \psi_{23}^*, \psi_{12}^*, \psi_{21}^*, \psi_{13}^*, \psi_{22}^*, \psi_{11}^* \right\}^T, \tag{7.2}$$

$$\boldsymbol{u}_{(3)} = \left\{ \boldsymbol{q}_1^T,\quad \boldsymbol{q}_2^T,\quad \boldsymbol{q}_3^T \right\}^T,\quad \boldsymbol{q}_i = \left\{ x_{1i}^*, x_{2i}^*, x_{3i}^*, \omega_{1i}, \omega_{2i} \right\}^T \quad (i = 1, 2, 3). \tag{7.3}$$

Here x_{mi} is the mth coordinate of the ith node, ω_{1i} and ω_{2i} are the rotations of the normal vector about orthogonal nodal vectors tangent to the shell middle surface (see Fig. 2). Variations of the vector $\boldsymbol{u}_{(3)}$ comprise the nodal translations and rotations of the nodal unit vectors, a total of 15 independent variations regarded as degrees of freedom of the shell element.

In the absence of external mechanical loads, the total thermoelastic potential energy of the shell element is a sum of Π_1 and Π_2 given by Eqs. (6.13) and (6.19):

$$\Pi = \frac{1}{2}\boldsymbol{u}_{(1)}^T \boldsymbol{K} \boldsymbol{u}_{(1)} - \boldsymbol{u}_{(1)}^T \boldsymbol{P},\ \boldsymbol{K} = \begin{pmatrix} \boldsymbol{K}_\varepsilon & \boldsymbol{K}_{\varepsilon\vartheta} \\ \boldsymbol{K}_{\varepsilon\vartheta}^T & \boldsymbol{K}_\vartheta + \boldsymbol{K}_\Gamma \end{pmatrix},\ \boldsymbol{P} = \begin{pmatrix} \boldsymbol{N}_T \\ \boldsymbol{M}_T \end{pmatrix}, \tag{7.4}$$

where $\boldsymbol{K}$ is the 9×9 symmetric stiffness matrix and $\boldsymbol{P}$ is the 9×1 thermal loading vector.

Using the principle of stationary total potential energy, we obtain a system of nonlinear equations governing equilibrium of the finite element model of a shell with N degrees of freedom

$$\boldsymbol{g}(\boldsymbol{q}, \lambda) = \boldsymbol{0}. \tag{7.5}$$

Here $\boldsymbol{g}$ is the gradient of the total potential energy of the finite-element assemblage, $\boldsymbol{q}$ is the vector comprising the generalized coordinates, and $\lambda = \Delta T$ is the temperature change.

To determine the deformation path which the structure follows under thermal loading, we use the arc-length control method (see e.g. [39]), where the generalized coordinates and the loading factor are unknown functions of a parameter that represents a finite arc length of the solution curve in the space of $(N + 1)$ independent variables. The solution curve is determined in a step-by-step manner starting from the known stress-free configuration of the structure. In the process, Eq. (7.5) are linearized and solved by the iterative Newton-Raphson method. At each solution step, the iterations are performed according to the formula

$$\boldsymbol{H}^{p-1}\delta\boldsymbol{q}^{p} + \boldsymbol{g}^{p-1} + \delta\lambda^{p}\boldsymbol{w}^{p-1} = \boldsymbol{0} \quad (p = 1, 2\ldots), \tag{7.6}$$

where $\boldsymbol{H}$ and $\boldsymbol{g}$ are the Hessian matrix and gradient of the potential energy of the finite-element assemblage, respectively, $\delta\lambda = \delta(\Delta T)$ is the increment in the temperature, $\boldsymbol{w}$ is the vector composed of derivatives of the form $\partial\boldsymbol{g}/\partial\lambda$, $\delta\boldsymbol{q}$ is the $N \times 1$ vector composed of increments in the generalized coordinates (nodal translations and rotations of the directors), and superscript p enumerates iterations. Each continuation step starts with iteration number $p = 1$ after the equilibrium state at previous step has been achieved.

The matrices in Eq. (7.6) are assembled using standard procedure of summation over the finite elements

$$\boldsymbol{H} = \sum_{e} \boldsymbol{H}_{(3)},\ \boldsymbol{g} = \sum_{e} \boldsymbol{g}_{(3)},\ \boldsymbol{w} = \sum_{e} \boldsymbol{w}_{(3)}, \tag{7.7}$$

where contributions of each element are computed using the following recurrent relations (no summation over m):

$$\boldsymbol{g}_{(m+1)} = \boldsymbol{u}'_{(m)}\boldsymbol{g}_{(m)},\ \boldsymbol{w}_{(m+1)} = \boldsymbol{u}'_{(m)}\boldsymbol{w}_{(m)},$$

$$\boldsymbol{H}_{(m+1)} = \boldsymbol{u}'_{(m)}\boldsymbol{H}_{(m)}\boldsymbol{u}'^{T}_{(m)} + g_{(m)s}\boldsymbol{u}''_{(m)s} \quad (m = 1, 2;\ s = 1, \ldots, 9). \tag{7.8}$$

Here $\boldsymbol{u}'_{(m)}$ is the matrix composed of partial derivatives of the components of the vector $\boldsymbol{u}_{(m)}$ with respect to the components of the vector $\boldsymbol{u}_{(m+1)}$, $\boldsymbol{u}''_{(m)s}$ is the symmetric matrix containing second order partial derivatives of the sth component of the vector $\boldsymbol{u}_{(m)}$ with respect to the components of the vector $\boldsymbol{u}_{(m+1)}$, and $g_{(m)s}$ is the sth component of the vector $\boldsymbol{g}_{(m)}$.

To start the recurrent process according to Eqs. (7.8), the following initial values should be used:

$$\boldsymbol{H}_{(1)} = \boldsymbol{K},\ \boldsymbol{g}_{(1)} = \boldsymbol{K}\boldsymbol{u}_{(1)} - \boldsymbol{P},\ \boldsymbol{w}_{(1)} = \partial\boldsymbol{P}/\partial\lambda. \tag{7.9}$$

As pointed out above, the element stiffness matrix $\boldsymbol{K}$ is computed by exact integration. The matrices $\boldsymbol{u}'_{(m)}$ and $\boldsymbol{u}''_{(m)s}$ can be found in [33]. It should be noted that attempts to obtain explicit expression for the vector $\boldsymbol{w}$ lead to extremely involved relations because of the material properties dependent on temperature. For this reason, we have to compute the vector using numerical differentiation

$$\boldsymbol{w} = \frac{1}{2\tau}(\boldsymbol{g}|_{T+\tau} - \boldsymbol{g}|_{T-\tau}) + O(\tau^2), \tag{7.10}$$

where T is the current temperature and τ is a small positive increment in the temperature. In the computations, we set $\tau = 10^{-6}$. Note that in the case where material properties are independent of temperature, the strain-energy functional depends linearly on the temperature change and expression (7.10) gives an exact result.

Equations (7.6) are supplemented by one of the following constraint equations:

$$\begin{gathered}\left(\delta\boldsymbol{q}^1\right)^T\delta\boldsymbol{q}^1 + \left(\delta\lambda^1\right)^2 = (\delta s)^2 \text{for } p = 1,\\ \left(\delta\boldsymbol{q}^p\right)^T\delta\boldsymbol{q}^1 + \delta\lambda^1\cdot\delta\lambda^p = 0 \text{ for } p > 1,\end{gathered} \tag{7.11}$$

in which δs is a specified arc length in the space of $(N+1)$ unknowns.

Solution of Eqs. (7.6) and (7.11) is given by

$$\delta\boldsymbol{q}^p = \delta\lambda^p\boldsymbol{u}^p + \boldsymbol{v}^p, \tag{7.12}$$

$$\delta\lambda^1 = \pm\delta s/\sqrt{1 + \left(\boldsymbol{u}^1\right)^T\boldsymbol{u}^1} \text{ if } p = 1, \tag{7.13}$$

$$\delta\lambda^p = -\left(\boldsymbol{v}^p\right)^T\boldsymbol{u}^1/\sqrt{1 + (\boldsymbol{u}^p)^T\boldsymbol{u}^1} \text{ if } p > 1. \tag{7.14}$$

The sign in Eq. (7.13) determines the tracing direction along the equilibrium path. The vectors $\boldsymbol{u}^p$ and $\boldsymbol{v}^p$ are found by solving the equations

$$\boldsymbol{H}^{p-1}\boldsymbol{u}^p + \boldsymbol{w}^{p-1} = \boldsymbol{0},\ \boldsymbol{H}^{p-1}\boldsymbol{v}^p + \boldsymbol{g}^{p-1} = \boldsymbol{0}. \tag{7.15}$$

After the pth iteration is completed and solution of Eq. (7.6) is found, the nodal vectors are updated using relations [33]

$$\boldsymbol{r}_s^{*(p+1)} = \boldsymbol{r}_s^{*(p)} + \delta\boldsymbol{r}_s^{*(p)},$$

$$\boldsymbol{n}_s^{*(p+1)} = a_1^{(p)}\boldsymbol{n}_s^{*(p)} + a_2^{(p)}\left(\boldsymbol{t}_{1s}^{*(p)}\delta\omega_{1s}^{(p)} + \boldsymbol{t}_{2s}^{*(p)}\delta\omega_{2s}^{(p)}\right),$$

$$\boldsymbol{t}_{ms}^{*(p+1)} = \boldsymbol{t}_{ms}^{*(p)} - \delta\omega_{ms}^{(p)}\left[a_2^{(p)}\boldsymbol{n}_s^{*(p)} + a_3^{(p)}\left(\boldsymbol{t}_{1s}^{*(p)}\delta\omega_{1s}^{(p)} + \boldsymbol{t}_{2s}^{*(p)}\delta\omega_{2s}^{(p)}\right)\right],$$

$$\delta\omega_s^{(p)} = \left(\delta\omega_{1s}^{(p)2} + \delta\omega_{2s}^{(p)2}\right)^{1/2},$$

$$a_1^{(p)} = \cos\delta\omega_s^{(p)},\ a_2^{(p)} = \frac{\sin\delta\omega_s^{(p)}}{\delta\omega_s^{(p)}},\ a_3^{(p)} = \frac{1-\cos\delta\omega_s^{(p)}}{\delta\omega_s^{(p)2}}, \tag{7.16}$$

where s enumerates the nodes.

Iterative computations are performed according to Eq. (7.6) until the solution converges, which requires that the gradient $\boldsymbol{g}$ should vanish. Because of unavoidable numerical errors, however, this condition can be satisfied only approximately. In this work, we use the following convergence criterion: $|\delta u|_{\max}/h \leq 10^{-9}\ldots 10^{-6}$, where $|\delta u|_{\max}$ is the maximum increment in the nodal translation and h is the shell thickness.

Once convergence of the numerical solution is achieved, stability of the corresponding equilibrium configuration of the shell is studied. To infer whether equilibrium state is stable or not, the positive definiteness of the Hessian matrix $\boldsymbol{H}^0$ computed for $p = 1$ is investigated. According to Sylvester's criterion, the equilibrium state is stable if determinants of all upper-left submatrices of $\boldsymbol{H}^0$ are positive definite, otherwise the equilibrium state is unstable. This information can easily be obtained by applying the forward process of the Gauss elimination method to the matrix $\boldsymbol{H}^0$. The change of the sign of the determinants means that a singular point is encountered on the deformation path.

The type of singular point is determined by investigating compatibility of system $(7.15)_1$ for the converged solution. If the system is incompatible, a limit point occurs. In this case, the general solution for $p = 1$ has the form

$$\delta\boldsymbol{q}^1 = \mu\boldsymbol{f},\ \delta\lambda^1 = 0, \tag{7.17}$$

where μ is an arbitrary nonzero factor and $\boldsymbol{f}$ is the nontrivial solution of the homogeneous system $\boldsymbol{H}^0\boldsymbol{f} = \boldsymbol{0}$.

If system $(7.15)_1$ is compatible for the degenerate matrix $\boldsymbol{H}^0$, the singular point is a bifurcation point. In this case, the general solution of the system is given by

$$\delta\boldsymbol{q}^1 = \delta\lambda^1\boldsymbol{u}^1 + \mu\boldsymbol{f}. \tag{7.18}$$

This vector describes the buckling mode and is used to drive the solution to new branches that intersect the equilibrium path at the bifurcation point.

8 Numerical Results and Discussion

In this section we study nonlinear deformation and stability of laminated plates and shells subjected to uniform temperature rise. We assume that the elastic constants

and coefficients of linear thermal expansion of each ply are linear functions of temperature:

$$E_{11}(T) = E^0_{11}(1 + E^1_{11}T),\ E_{22}(T) = E^0_{22}(1 + E^1_{22}T),\ G_{12}(T) = G^0_{12}(1 + G^1_{12}T),$$
$$G_{13}(T) = G^0_{13}(1 + G^1_{13}T),\ G_{23}(T) = G^0_{23}(1 + G^1_{23}T),\ \alpha_{11}(T) = \alpha^0_{11}(1 + \alpha^1_{11}T),$$
$$\alpha_{22}(T) = \alpha^0_{22}(1 + \alpha^1_{22}T), \tag{8.1}$$

where $E^0_{11}, \ldots, \alpha^1_{11}$ are constants. Since Poisson's ratio weakly depends on temperature, it is assumed to be constant.

-NoValue-In all the sample problems considered below, simply supported boundary conditions are imposed in such a manner that all nodal translations are constrained to be equal to zero, but rotations are allowed. The reference temperature is assumed to be zero.

8.1 Thermal Postbuckling Behavior of a Cross-Ply Plate

We consider a simply supported laminated square plate with stacking sequence $(45°/-45°/45°/-45°)$. The side length-to-thickness ratio is $a/h = 30$. The plies are of equal thickness and the material properties are as follows [40]: $E^0_{11}/E^0_{22} = 40$, $G^0_{12}/E^0_{22} = G^0_{13}/E^0_{22} = 0.5$, $G^0_{23}/E^0_{22} = 0.2$, $\alpha^0_{11} = 10^{-6}\ 1/°C$, $\alpha^0_{22} = 10^{-5}\ 1/°C$, $\nu_{12} = 0.25$, $E^1_{11} = -0.5 \times 10^{-3}$, $E^1_{22} = G^1_{12} = G^1_{13} = G^1_{23} = -0.2 \times 10^{-3}$, and $\alpha^1_{11} = \alpha^1_{22} = 0.5 \times 10^{-3}$. The full plate is modeled by a uniform union-jack mesh.

In Fig. 3, we plot temperature versus central deflection of the plate for temperature-independent (TI) and temperature-dependent (TD) material properties. The calculation results show that smooth transition from flat to curved configurations occurs as the temperature increases. The postbuckling curves compare well with the solution of [40] based on Reddy's higher order shear deformation theory. In the temperature range considered, the bent plate is in stable equilibrium.

8.2 Thermal Buckling and Postbuckling of Circular Cylindrical Shells

A simply supported circular cylindrical shell of radius r, wall thickness h, and length L is shown in Fig. 4. The length-to-radius ratio is $L/r = 1$. The shell is composed of orthotropic layers of equal thickness. The material properties of the layers are as follows: $E^0_{11} = 40 \times 10^{10}$ Pa, $E^0_{22} = 1 \times 10^{10}$ Pa, $G^0_{12} = 0.6 \times 10^{10}$ Pa, $G^0_{13} = G^0_{23} = 0.5 \times 10^{10}$ Pa, $\alpha^0_{11} = 10^{-6}$ 1/°C, $\alpha^0_{22} = 10^{-5}$ 1/°C, $E^1_{11} = E^1_{22} = G^1_{12} = G^1_{13} = G^1_{23} = -0.5 \times 10^{-3}$, $\alpha^1_{11} = \alpha^1_{22} = 0.5 \times 10^{-3}$, and $\nu_{12} = 0.25$.

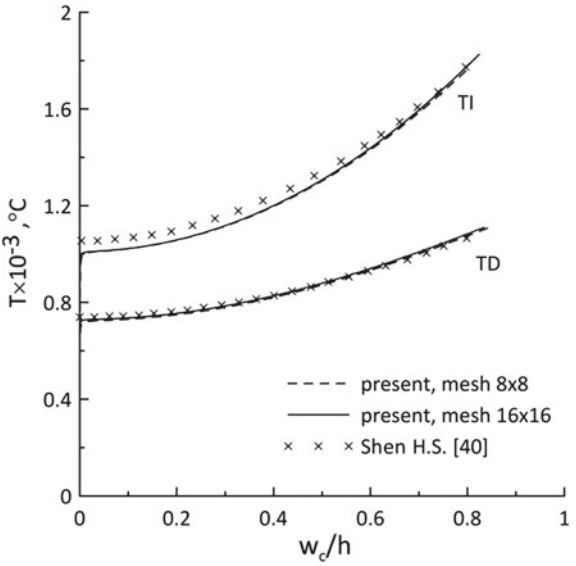

Fig. 3 Temperature versus central deflection of the simply supported square plate with $(\pm 45^{\circ}_2)_T$ lamination scheme

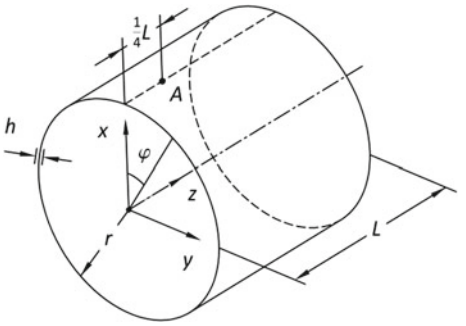

Fig. 4 Geometry of a cylindrical shell

Full shell is discretized using a uniform union-jack mesh obtained by dividing the shell into 160 elements in the circumferential direction and 16 elements in the longitudinal direction. No symmetry conditions are imposed on the shell deformation.

The critical temperatures computed with allowance for nonlinear prebuckling deformations are summarized in Table 1 for various stacking sequences. The ply angle is measured from the longitudinal direction. The first layer is the innermost layer of the shell. As can be seen from Table 1, variation of material properties has a significant effect on the buckling temperature. The analysis based on the assumption of temperature independent properties overestimates the critical temperature by approximately 30%.

Now we study postbuckling response of the shells with $r/h = 100$ using an example of $[(0°/90°)_2]_s$ lamination scheme. In Fig. 5, we show temperature versus outward deflection of point A defined by coordinates $z = L/4$ and $\varphi = 0$. The critical

Table 1 Thermal buckling parameters for simply supported circular cylindrical shells

Stacking sequence		$r/h = 50$		$r/h = 100$	
		$\Delta T_{cr}\alpha_{11}^0 r/h$	Mode shape $(n; m)$	$\Delta T_{cr}\alpha_{11}^0 r/h$	Mode shape $(n; m)$
[0°/90°]	TI	0.06551	(2; 12)	0.06822	(3; 16)
	TD	0.04514	(2; 12)	0.05375	(3; 16)
$[0°/90°]_4$	TI	0.1097	(1; 8)	0.10771	(2; 12)
	TD	0.06604	(1; 8)	0.07760	(2; 12)
$[(0°/90°)_2]_s$	TI	0.1095	(1; 8)	0.11275	(2; 14)
	TD	0.06598	(1; 8)	0.08040	(2; 14)
[90°/0°]	TI	0.09650	(2; 12)	0.08423	(2; 16)
	TD	0.06022	(2; 12)	0.06385	(2; 16)

(n and m are numbers of half-waves in the longitudinal and circumferential directions, respectively)

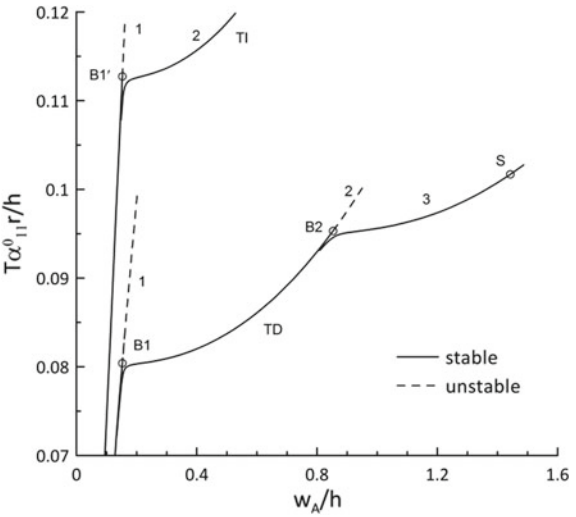

Fig. 5 Temperature versus deflection at point A ($z = L/4$; $\varphi = 0$) of the simply supported cylindrical shells with $[(0°/90°)_2]_s$ lamination scheme: curve 1 refers to $A_1 = A_2 = 0$ (perfect shell), curve 2 to $A_1/r = 10^{-6}$, $m_1 = 14$, $n_1 = 2$, and $A_2 = 0$, and curve 3 to $A_1/r = 10^{-6}$, $m_1 = 14$, $n_1 = 2$, $A_2/r = 10^{-6}$, $m_2 = 10$, and $n_2 = 1$

temperatures are represented by bifurcation points B1 and B1' which correspond to temperature dependent and temperature independent material properties, respectively. The bifurcation points are of multiplicity 2, that is, two distinct solution branches intersect the fundamental deformation path at these points and describe buckling modes of the form $f(z)\cos k\varphi$ and $f(z)\sin k\varphi$, where k is a wave number and $f(z)$ is a certain function satisfying the boundary conditions. Difficulties are encountered when attempts are made to drive the solution to stable postbuckling path beyond the critical temperature. Poor convergence of the solution is observed, which can be attributed to the presence of the two similar solution branches emanating from the same bifurcation point.

To study postbuckling deformation of the shell, we introduce small geometric imperfections using the following two-term approximation for the initial deflection:

$$w_0 = \sum_{i=1}^{2} A_i \cos(m_i \varphi/2) \sin(n_i \pi z/L), \tag{8.2}$$

where A_i are the amplitudes and m_i and n_i are the numbers of half-waves, which are determined based on the computed buckling modes.

Owing to the first term in Eq. (8.2), smooth transition from prebuckling axisymmetric state to asymmetric postbuckling configuration is observed. In the postbuckling regime, the secondary bifurcation point B2 is detected. To study the solution branch that describes stable equilibrium of the shell at higher temperature beyond point B2, the second term in Eq. (8.2) is activated.

To estimate the global structural response of the heated shell, in Fig. 6 we plot the axial reaction force R_z that develops at immovable edges. It is seen that the shell with temperature dependent material properties exhibits pronounced nonlinear behavior at the prebuckling stage and its buckling resistance is much lower compared to shell with temperature independent properties.

Figure 7 shows contour plots of the normalized deflection field $w(z, \varphi)/h$ for the stable equilibrium states labeled B2 and S in Figs. 5 and 6.

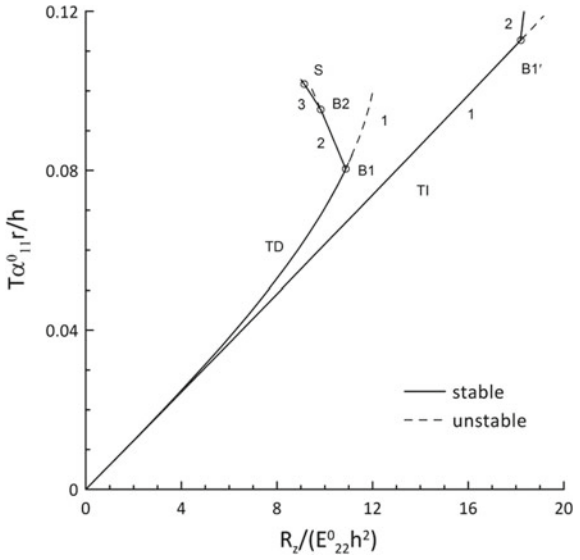

Fig. 6 Temperature versus reaction force R_z for the simply supported cylindrical shells with $[(0°/90°)_2]_s$ lamination scheme: curve 1 refers to $A_1 = A_2 = 0$ (perfect shell), curve 2 to $A_1/r = 10^{-6}$, $m_1 = 14$, $n_1 = 2$, and $A_2 = 0$, and curve 3 to $A_1/r = 10^{-6}$, $m_1 = 14$, $n_1 = 2$, $A_2/r = 10^{-6}$, $m_2 = 10$, and $n_2 = 1$

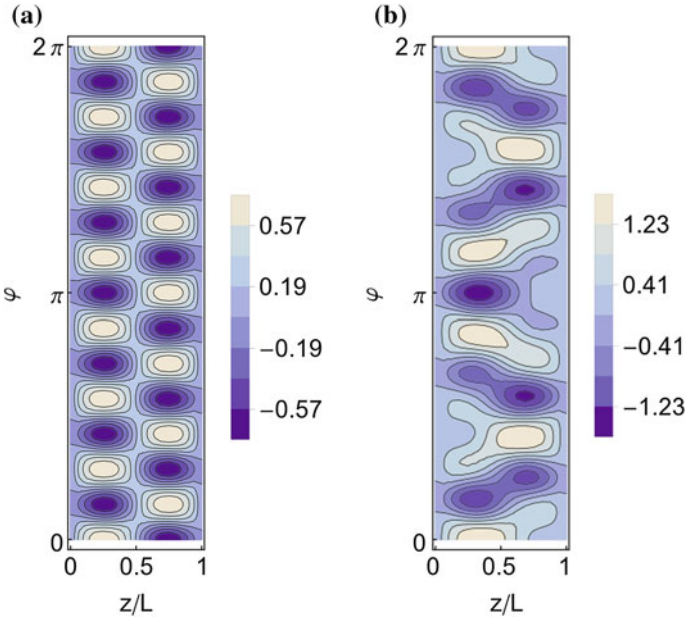

Fig. 7 Contour plots of normalized deflection $w(z,\varphi)/h$ on the developed surface of the cylindrical shell: **a** state B2 and **b** state S

8.3 Thermal Buckling and Postbuckling of Conical Shells

A truncated conical shell of circular cross section is shown in Fig. 8. The shell is composed of identical orthotropic layers with the following properties: $E_{11}^0 = 208 \times 10^9$ Pa, $E_{22}^0 = 5.2 \times 10^9$ Pa, $G_{12}^0 = 2.6 \times 10^9$ Pa, $G_{13}^0 = G_{23}^0 = 1.04 \times 10^9$ Pa, $\alpha_{11}^0 = \alpha_{22}^0 = 10^{-6}$ 1/°C, $E_{11}^1 = -0.5 \times 10^{-3}$, $E_{22}^1 = G_{12}^1 = G_{13}^1 = G_{23}^1 = -0.2 \times 10^{-3}$, $\alpha_{11}^1 = \alpha_{22}^1 = \alpha_0 = 0.5 \times 10^{-3}$, and $\nu_{12} = 0.25$. The shell geometry is characterized by the ratios $a/r = 2$ and $r/h = 100$, where a is the slant length of the truncated cone. Full shell is discretized using a uniform union-jack mesh obtained by dividing the shell into 160 elements in the circumferential direction and 16 elements in the longitudinal direction.

The results of thermal buckling analysis of the truncated conical shells are listed in Table 2 for two lamination schemes. The ply-angle is measured from the meridian. The first layer is the innermost layer. The critical buckling temperature and the number of waves in the buckling modes decrease as the cone angle increases. The critical temperature of the shells with temperature dependent properties is approximately 11–16% lower than that of the shells with the properties independent of temperature. The buckling modes are insensitive to degradation of the material characteristics due to temperature rise. Exception is the case where $\alpha = 30°$ and stacking sequence is symmetric.

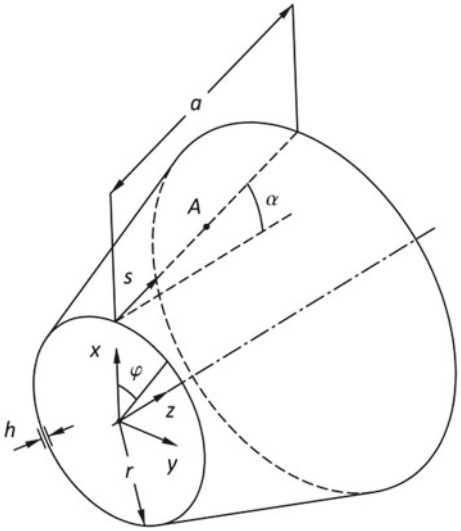

Fig. 8 Geometry of a truncated conical shell

Table 2 Thermal buckling parameters for simply supported truncated conical shells

α, deg		Stacking sequence			
		$[0°/90°]_4$	Mode shape (n; m)	$[(0°/90°)_2]_s$	Mode shape (n; m)
		$\Delta T_{cr}\alpha_{11}^0 r/h$		$\Delta T_{cr}\alpha_{11}^0 r/h$	
15	TI	0.09417	(4; 14)	0.09453	(3; 14)
	TD	0.07947	(4; 14)	0.08012	(3; 14)
30	TI	0.07420	(3; 14)	0.07558	(2; 12)
	TD	0.06350	(3; 14)	0.06506	(3; 14)
45	TI	0.05585	(2; 12)	0.05663	(2; 12)
	TD	0.04916	(2; 12)	0.05009	(2; 12)

(n and m are numbers of half-waves in the longitudinal and circumferential directions, respectively)

In Figs. 9 and 10, we show results of the nonlinear analysis of the conical shell with the angle $\alpha = 30°$ and stacking sequence $[(0°/90°)_2]_s$. The bifurcation points B1 and B1′ represent thermal buckling of the shells with TD and TI material properties, respectively. The critical temperature rise at B1 is 14% lower compared to that at B1′. To study postbuckling deformation, we introduce the initial imperfection pattern

$$w_0 = A\cos(m\varphi/2)\sin(n\pi s/a), \tag{8.3}$$

where $A = r \times 10^{-5}$, $m = 12$ and $n = 2$ for temperature-independent properties and $m = 14$ and $n = 3$ for temperature dependent properties (see Table 2).

Figure 11 shows contour plots of nondimensional deflections computed at states S1 and S2 labeled in Figs. 9 and 10.

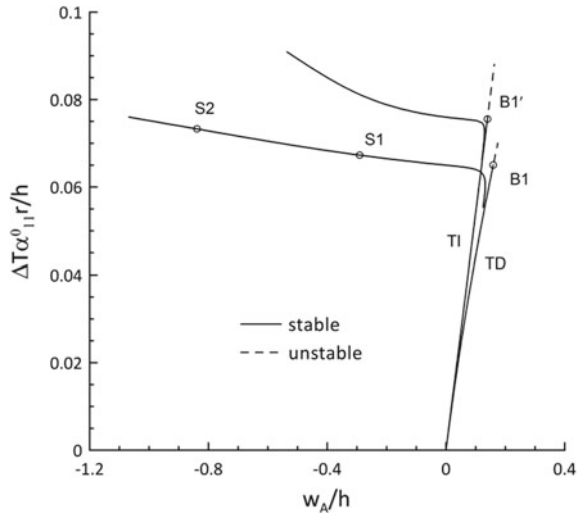

Fig. 9 Temperature rise versus deflection at point A ($s = a/2$ and $\varphi = 0$) for simply supported conical shell ($r/h = 100$, $a/r = 2$, and $\alpha = 30°$) with stacking sequence $[(0°/90°)_2]_s$

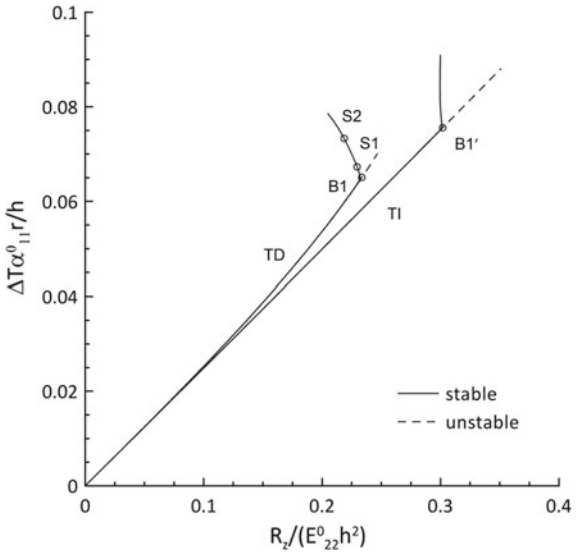

Fig. 10 Temperature rise versus axial reaction force R_z for simply supported conical shell ($r/h = 100$, $a/r = 2$, and $\alpha = 30°$) with stacking sequence $[(0°/90°)_2]_s$

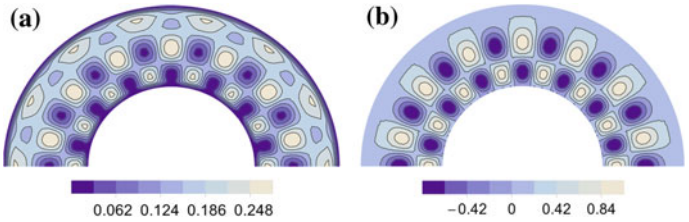

Fig. 11 Contour plot of normalized deflection *w*/*h* on the developed surface of the conical shell: **a** state S1 and **b** state S2

8.4 Large Thermal Deflections of a Laminated Cylindrical Panel

A simply supported cylindrical panel of rectangular plan form is shown in Fig. 12. Dimensions of the panel are $a = b = 1.6$ m, thickness is $h = 0.008$ m, and radius of curvature is $R = 8$ m. The panel is made of fibrous orthotropic material with the following temperature-independent properties: $E_{11} = 138 \times 10^9$ Pa, $E_{22} = 8.28 \times 10^9$ Pa, $G_{12} = G_{13} = G_{23} = 6.9 \times 10^9$ Pa, $\nu_{12} = 0.33$, $\alpha_{11} = 0.18 \times 10^{-6}$ 1/°C, $\alpha_{22} = 27 \times 10^{-6}$ 1/°C.

Large thermal deflections of the panel were examined in [12, 14] under the assumption of double symmetry. Sabik and Kreja [17] considered the problem in a more general statement and found solution branches that describe unsymmetric states of equilibrium. In these studies, however, stability of the equilibrium states was not discussed.

It is of interest to reconsider the problem and investigate stability of equilibrium configurations of the heated panel. The full panel is modeled using 48 × 48 union-

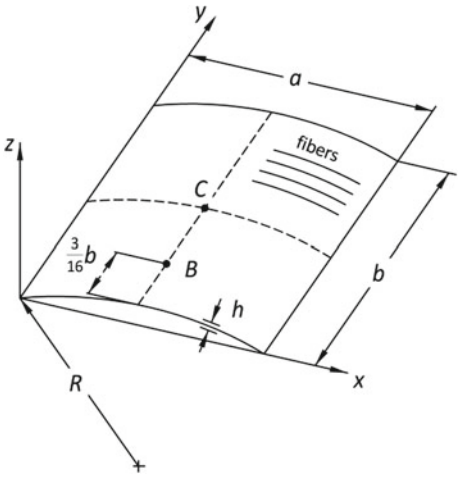

Fig. 12 Geometry of a cylindrical orthotropic panel

jack mesh. The load-deflection curves are shown in Fig. 13 and briefly discussed below.

At the initial stage of loading, the deformed configurations of the panel characterized by double symmetry are stable. Thermal buckling occurs at 80.18 °C, which agrees with the findings of [17]. The accuracy in determining the critical buckling temperature is supported by the mesh convergence analysis (see Table 3). The instability is represented by bifurcation point B1 in Fig. 13. The critical state of the panel and the buckling mode are shown in Figs. 14a and b, respectively, in terms of contour plots. Beyond the point B1, closely spaced bifurcation and limit points are detected on the fundamental deformation path. Symmetric configurations of the panel are found to be unstable beyond the critical buckling temperature.

Investigation of the solution branch departing the bifurcation point B1 shows that this branch refers to unstable states of equilibrium. Using larger perturbations based on the first buckling mode, we find a new, non-adjacent solution branch of unsymmetric equilibrium states containing bifurcation points B7, B8, and B9.

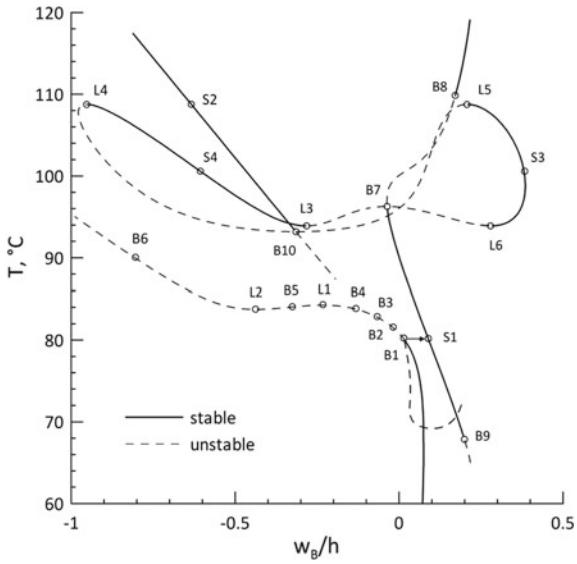

Fig. 13 Temperature rise versus deflection at point B(0; 3*b*/16) of the orthotropic cylindrical panel

Table 3 Critical temperature and central deflection for the cylindrical panel

mesh	T_{cr}, °C	w_C/h
6 × 6	35.77	0.0389
12 × 12	77.63	0.0841
24 × 24	79.52	0.0543
48 × 48	80.18	0.0490

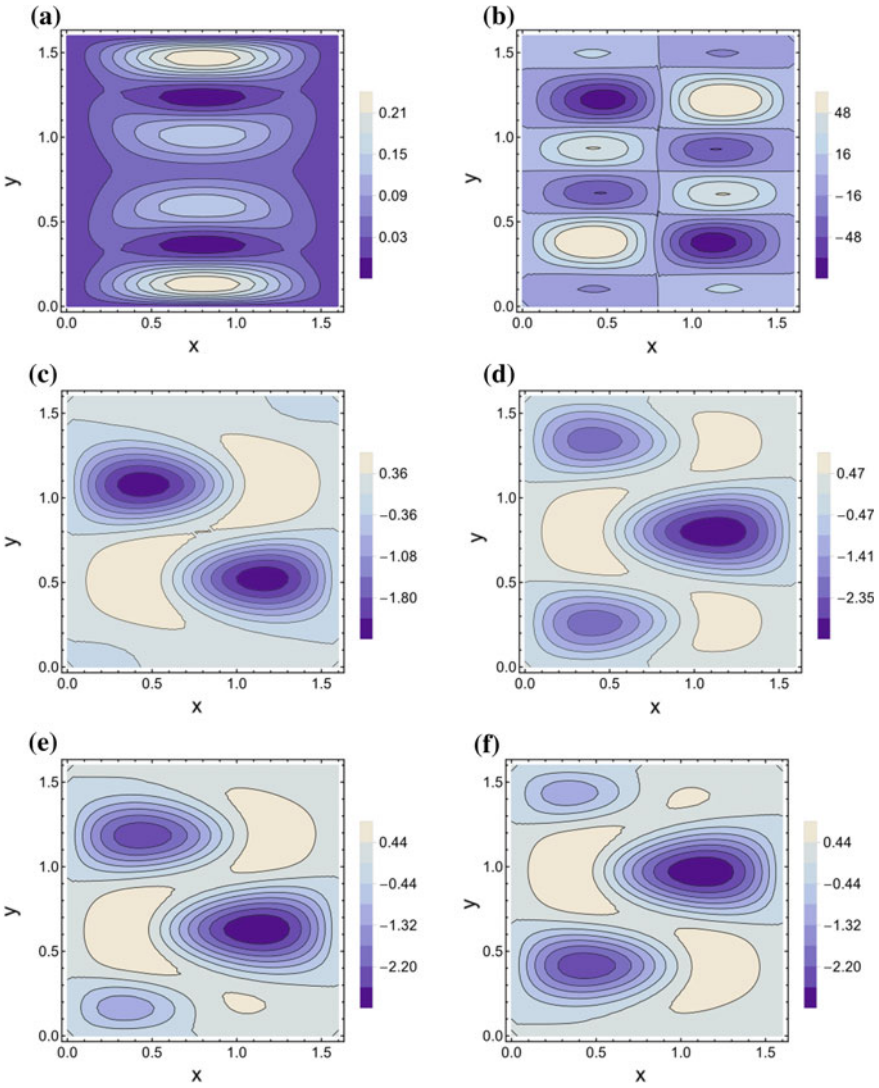

Fig. 14 Contour plots of the normalized deflection *w/h* of the orthotropic cylindrical panel: **a** state B1, **b** buckling mode at B1, **c** state S1, **d** state S2, **e** state S3, and **f** state S4

Contour plots of the normalized deflections that refer to stable states of equilibrium labeled in Fig. 13 are shown in Fig. 14c–f. It is seen that stable equilibrium configurations found in the postbuckling range are unsymmetric.

It should be noted that the above-mentioned bifurcation points define new branches of the nonlinear solution which, in turn, may contain new bifurcation points and so on. It is likely that Fig. 13 represents only a small portion of a big picture of the nonlinear response of the panel.

9 Conclusions

An invariant-based formulation of a triangular finite element has been proposed for nonlinear analysis of laminated shells with temperature dependent properties subjected to thermal loading. The transverse shear flexibility has been taken into account using the first order shear deformation theory. It has been shown that thermoelastic potential energy density of the shell can be written as a quadratic function of combined invariants expressed in terms of the natural strains and components of tensors which characterize mechanical and physical properties of the material. The expression for thermoelastic potential energy has been used as a starting point to formulate the shell finite element. The finite-element relations have been implemented in the author's computer code which has been tested by comparing to results available in the open literature.

A series of problems of thermally loaded laminated shells has been solved in a geometrically nonlinear statement taking into account temperature dependent properties of the material. Stability of the computed equilibrium states beyond the critical buckling temperature have been examined.

Based on the numerical results, the following remarks can be made:

(1) shells with temperature dependent material properties exhibit pronounced nonlinear behavior under heating even in the prebuckling regime;
(2) composite plates and shells with temperature dependent material properties exhibit buckling at lower temperature rise compared to those with temperature independent properties;
(3) care should be taken when using symmetry constraints even for symmetric structures since, under these constraints, stable unsymmetric equilibrium states can be missed in the postbuckling range.

References

1. Chen, L.W., Chen, L.Y.: Thermal buckling behavior of laminated composite plates with temperature-dependent properties. Compos. Struct. **13**(4), 275–287 (1989)
2. Thangaratnam, R.K., Palaninathan, R., Ramachandran, J.: Thermal buckling of laminated composite shells. AIAA J. **28**(5), 859–860 (1990)

3. Thangaratnam, K.R., Palaninathan, R.J.: Thermal buckling of composite laminated plates. Comput. Struct. **32**(5), 1117–1124 (1989)
4. Ounis, H., Tati, A., Benchabane, A.: Thermal buckling behavior of laminated composite plates: a finite-element study. Front. Mech. Eng. **9**(1), 41–49 (2014). https://doi.org/10.1007/s11465-014-0284-z
5. Chandrashekhara, K.: Thermal buckling of laminated plates using a shear flexible finite element. Finite Elem. Anal. Des. **12**, 51–61 (1992)
6. Prabhu, M.R., Dhanaraj, R.: Thermal buckling of laminated composite plates. Comput. Struct. **53**(5), 1193–1204 (1994)
7. Dawe, D.J., Ge, Y.S.: Thermal buckling of shear-deformable composite laminated plates by the spline finite strip method. Comput. Meth. Appl. Mech. Eng. **185**, 347–366 (2000)
8. Kabir, H.R.H., Askar, H., Chaudhuri, R.A.: Thermal buckling response of shear flexible laminated anisotropic plates using a three-node isoparametric element. Compos. Struct. **59**(2), 173–187 (2003)
9. Shiau, L.C., Kuo, S.Y., Chen, C.Y.: Thermal buckling behavior of composite laminated plates. Compos. Struct. **92**(2), 508–514 (2010)
10. Argyris, J., Tenek, L.: High-temperature bending, buckling, and postbuckling of laminated composite plates using the natural mode method. Comput. Methods Appl. Mech. Engrg. **117**, 105–142 (1994)
11. Ganapathi, M., Touratier, M.: A study on thermal postbuckling behaviour of laminated composite plates using a shear-flexible finite element. Finite Elem. Anal. Des. **28**, 115–135 (1997)
12. Huang, N.N., Tauchert, T.R.: Large deflections of laminated cylindrical and doubly-curved panels under thermal loading. Comput. Struct. **41**(2), 303–312 (1991)
13. Huang, N.N., Tauchert, T.R.: Thermal buckling of clamped symmetric laminated plates. Thin-Walled Struct. **13**, 259–273 (1992)
14. Barut, A., Madenci, E., Tessler, A.: Nonlinear thermoelastic analysis of composite panels under non-uniform temperature distribution. Int. J. Solids Struct. **37**, 3681–3713 (2000)
15. Patel, B.P., Shukla, K.K., Nath, Y.: Nonlinear thermoelastic stability characteristics of cross-ply laminated oval cylindrical/conical shells. Finite Elem. Anal. Des. **42**, 1061–1070 (2006)
16. Alijani, A., Darvizeh, M., Darvizeh, A., Ansari, R.: On nonlinear thermal buckling analysis of cylindrical shells. Thin-Walled Struct. **95**, 170–182 (2015)
17. Sabik, A., Kreja, I.: Large thermo-elastic displacement and stability FEM analysis of multilayered plates and shells. Thin-Walled Struct. **71**, 119–133 (2013)
18. Sabik, A., Kreja, I.: Thermo-elastic non-linear analysis of multilayered plates and shells. Compos. Struct. **130**, 37–43 (2015)
19. Kant, T., Babu, C.S.: Thermal buckling analysis of skew fiber-reinforced composite and sandwich plates using shear deformable finite element models. Compos. Struct. **49**, 77–85 (2000)
20. Patel, B.P., Shukla, K.K., Nath, Y.: Thermal buckling of laminated cross-ply oval cylindrical shells. Compos. Struct. **65**, 217–229 (2004)
21. Cetkovic, M.: Thermal buckling of laminated composite plates using layerwise displacement model. Compos. Struct. **142**, 238–253 (2016)
22. Oh, I.-K., Lee, I.: Thermal snapping and vibration characteristics of cylindrical composite panels using layerwise theory. Compos. Struct. **51**, 49–61 (2001)
23. Chen, L.W., Chen, L.Y.: Thermal postbuckling behaviors of laminated composite plates with temperature-dependent properties. Compos. Struct. **19**, 267–283 (1991)
24. Singha, M.K., Ramamachandra, L.S., Bandyopadhyay, J.N.: Thermal postbuckling analysis of laminated composite plates. Compos. Struct. **54**, 453–458 (2001)
25. Srikanth, G., Kumar, A.: Postbuckling response and failure of symmetric laminates under uniform temperature rise. Compos. Struct. **59**, 109–118 (2003)
26. Chandrashekhara, K., Bhimaraddi, A.: Thermal stress analysis of laminated doubly curved shells using a shear flexible finite element. Compute. Struct. **52**(5), 1023–1030 (1994)
27. Patel, B.P., Shukla, K.K., Nath, Y.: Thermal postbuckling characteristics of laminated conical shells with temperature-dependent material properties. AIAA J. **43**(6), 1380–1388 (2005)

28. Patel, B.P., Shukla, K.K., Nath, Y.: Thermal postbuckling analysis of laminated cross-ply truncated circular conical shells. Compos. Struct. **71**, 101–114 (2005)
29. Shariyat, M.: Thermal buckling analysis of rectangular composite plates with temperature-dependent properties based on a layerwise theory. Thin-Walled Struct. **45**, 439–452 (2007)
30. Argyris, J.H., Dunne, P.C., Malejannakis, G.A., Schelkle, E.: A simple triangular facet shell element with applications to linear and non-linear equilibrium and elastic stability problems. Comput. Methods Appl. Mech. Engrg. **10**, 371–403 (1977)
31. Argyris, J., Tenek, L.: Linear and geometrically nonlinear bending of isotropic and multilayered composite plates by the natural mode method. Comput. Methods Appl. Mech. Engrg. **113**, 207–251 (1994)
32. Argyris, J., Tenek, L., Olofsson, L.: TRIC: a simple but sophisticated 3-node triangular element based on 6 rigid-body and 12 straining modes for fast computational simulations of arbitrary isotropic and laminated composite shells. Comput. Methods Appl. Mech. Engrg. **145**, 11–85 (1997)
33. Kuznetsov, V.V., Levyakov, S.V.: Geometrically nonlinear shell finite element based on the geometry of a planar curve. Finite Elem. Anal. Des. **44**, 450–461 (2008)
34. Kuznetsov, V.V., Levyakov, S.V.: Phenomenological invariants and their application to geometrically nonlinear formulation of triangular finite elements of shear deformable shells. Int. J. Solids Struct. **46**, 1019–1032 (2009)
35. Kuznetsov, V.V., Levyakov, S.V.: Nonlinear stability analysis of functionally graded shells using the invariant-based triangular finite element. ZAMM Z. Angew. Math. Mech. **94**(1–2), 101–117 (2013). https://doi.org/10.1002/zamm.201200188
36. Levyakov, S.V., Kuznetsov, V.V.: Complete system of two-dimensional invariants for formulation of triangular finite element of composite shells. Appl. Math. Model. **36**, 5183–5198 (2012)
37. Levyakov, S.V., Kuznetsov, V.V.: Invariant-based formulation of a triangular finite element for geometrically nonlinear thermal analysis of composite shells. Compos. Struct. **177**, 38–53 (2017)
38. Segerlind, L.J.: Applied Finite Element Analysis. Wiley (1984)
39. Yang, Y.-B., Shieh, M.-S.: Solution method for nonlinear problems with multiple critical points. AIAA J. **28**(12), 2110–2116 (1990)
40. Shen, H.S.: Thermal postbuckling behavior of imperfect shear deformable laminated plates with temperature-dependent properties. Comp. Meth. Appl. Mech. Eng. **190**, 5377–5390 (2001)

Interaction of a Spherical Wave with a Rectangular Plate in a Ground

Natalya A. Lokteva and Dmitrii V. Tarlakovskii

Abstract The vibration-absorbing properties of the plate under the action of a spherical harmonic wave propagating in the ground are studied. An elastic isotropic medium is used as a ground model. The main aim of this study is to determine the total vector field of accelerations. The mathematical formulation of the problem includes the assignment of the ingoing wave, the dynamic equations of the ground and the plate, the boundary conditions for the obstacle and the medium, the conditions at infinity for medium, and the conditions of contact of the medium with the obstacle, where we neglect the connection of the plate to the ground. The dynamic equations of the plate is described by the system of equations of V.N. Paimushin. The kinematic parameters of the plate and the parameters of the disturbed stress-strain state of the medium are represented in the form of double trigonometric series satisfying the boundary conditions. After that, the constants of integration, displacement, and vibration acceleration are determined.

1 Introduction

Buildings are often exposed to huge dynamic loads arising from industrial machinery, or transport (such as shallow-depth railroad systems, heavy trucks, railway trains) [10]. Vibration-absorbing barriers placed between the vibration source and the protected object offer an efficient way of foundation protection against ground vibrations as it was shown by [4, 7].

Homogeneous one-layer sound absorption plates are well investigated nowadays. At the same time the study of sandwich plate dynamics requires proper accounting

N. A. Lokteva (✉)
Moscow Aviation Institute National Research University, 125993 Moscow Volokolamskoe Shosse, 4, 125993,, Russian Federation
e-mail: nlok@rambler.ru

D. V. Tarlakovskii
Lomonosov Moscow State University, Moscow, Leninskie Gory, Moscow 119991, Russian Federation
e-mail: tdvhome@email.ru

H. Altenbach et al. (eds.), *Recent Developments in the Theory of Shells*,
Advanced Structured Materials 110, https://doi.org/10.1007/978-3-030-17747-8_23

for both transverse shear and transverse normal stress in the filling layer, otherwise the dynamic stress state can be computed with severe errors. On the other hand, the effect of the ingoing wave shape on the sound absorption properties of plane sandwich barriers must be studied in details to be a basis of further engineering estimates. We study sound absorbing properties of a plate exposed to subsurface spherical harmonic waves on the background of the new improved model of a sandwich plate accounting for all mentioned effects. In practice, such a situation may correspond to vibrations caused by a point source situated nearby the barrier.

2 Problem Statement of Interaction of Harmonic Spherical Wave Propagating in Continuum and a Three-Layered Plate

Let us consider the rectangular plate that consists of three layers, two bearing ones and a honeycomb filling. The origin of the coordinate system is placed in the upper right-handed corner of the plate. Oz-axis is directed normally to the plate surface into the medium "2", Ox and Oy lie in plates plane. Let w be the displacement of points of the medium "2" normal to the plate, and let u be the corresponding tangential displacement. Superscript denotes the media number while the subscript denotes the axis along which the displacement takes place, where 1 coresponds to the coordinate x while 2 to y. The plate divides the medium into 2 parts: media "1" and "2" [11]. Spherical harmonic wave rides on the plate from the medium "1" Fig. 1.

To appreciate vibration absorbing properties of obstacle, term "vibration acceleration" is used. This acceleration is defined in the medium "2" for wave, which

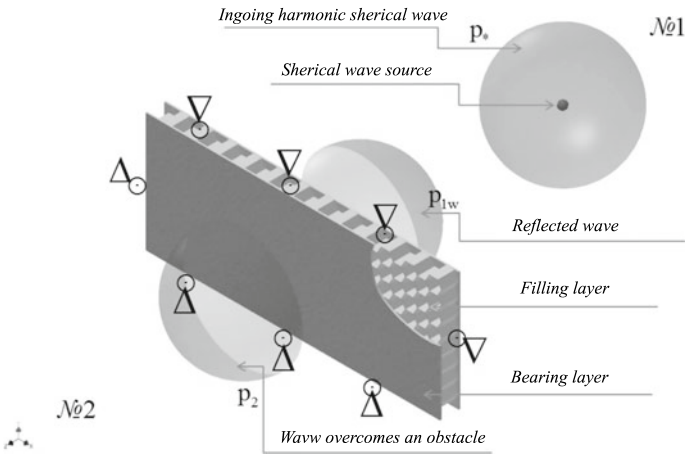

Fig. 1 The interaction of a spherical harmonic wave with a three-layer plate

overcame the obstacle, and it is calculated according to the formulae (1) per axis:

$$a_x = -\omega^2 {u_1}^{(2)}, a_y = -\omega^2 {u_2}^{(2)}, a_z = -\omega^2 w^{(2)}. \tag{1}$$

where ${u_1}^{(2)}$, ${u_2}^{(2)}$ are displacements of the medium "2" anlog the axes x, y; $w^{(2)}$ is the displacement of the second medium normal to the plate surface. The acceleration modulus is calculated using the formula (2).

$$a = \sqrt{a_x^2 + a_y^2 + a_z^2} \tag{2}$$

When undisturbed, the ground is considered to be undeformed. The obstacle is overrun by a harmonic tensile wave of an normal stress amplitude p_* at the front and frequency ω, coming from the negative Oz-axis. The normal vector towards the front of the wave is in the plane Oxy. The main purpose of further study consists in finding the resultant vector field of acceleration (vibration accelerations) in the second half-space as a function of the frequency ω and spatial coordinates x, y, z and depending on the parameters of the plate.

The statement of the problem includes setting the ingoing wave definition, equations of dynamics for the ground and plate, boundary conditions for the plate and ground, condition at infinity, as well as a condition of the ground-to-obstacle contact where the adhesion of the plate with the ground is neglected.

3 Dynamic Equations of Ground

The model of [6] for isotropic elastic medium is used below; the motion is described by the dynamic equations of the elasticity theory (3) together with Cauchy's relations (4) and Hookean law (5) [1].

Dynamic equations:

$$\begin{aligned}
\rho \ddot{u}_1 &= \frac{\partial \sigma_{11}}{\partial x} + \frac{\partial \sigma_{12}}{\partial y} + \frac{\partial \sigma_{13}}{\partial z}, \\
\rho \ddot{u}_2 &= \frac{\partial \sigma_{21}}{\partial x} + \frac{\partial \sigma_{22}}{\partial y} + \frac{\partial \sigma_{23}}{\partial z}, \\
\rho \ddot{w} &= \frac{\partial \sigma_{31}}{\partial x} + \frac{\partial \sigma_{32}}{\partial y} + \frac{\partial \sigma_{33}}{\partial z}.
\end{aligned} \tag{3}$$

Cauchy's equations:

$$\begin{gathered}\varepsilon_{11}=\frac{\partial u_1}{\partial x},\quad \varepsilon_{13}=\frac{1}{2}\left(\frac{\partial u_1}{\partial z}+\frac{\partial w}{\partial x}\right),\quad \varepsilon_{33}=\frac{\partial w}{\partial z},\\ \varepsilon_{22}=\frac{\partial u_2}{\partial y},\quad \varepsilon_{23}=\frac{1}{2}\left(\frac{\partial u_2}{\partial y}+\frac{\partial w}{\partial z}\right),\\ \varepsilon_{12}=\frac{1}{2}\left(\frac{\partial u_2}{\partial x}+\frac{\partial u_1}{\partial y}\right),\quad \theta=\frac{\partial u_1}{\partial x}+\frac{\partial u_2}{\partial y}+\frac{\partial w}{\partial z}.\end{gathered} \tag{4}$$

Constitutive relations:

$$\begin{gathered}\sigma_{11}=\lambda\theta+2\mu\varepsilon_{11},\quad \sigma_{13}=2\mu\varepsilon_{13},\quad \sigma_{33}=\lambda\theta+2\mu\varepsilon_{33},\\ \sigma_{22}=\lambda\theta+2\mu\varepsilon_{22},\quad \sigma_{23}=2\mu\varepsilon_{23}\end{gathered} \tag{5}$$

Here u_1, u_2 and w are displacements along the axes Ox, Oy and Oz; σ_{ij} and ε_{ij} are components of stress and strain tensors; θ is volumetric strain; ρ and λ, μ are mass density and Lame's elastic constants for the ground; dots here and hereinafter denote time derivatives.

The Eqs. (3) can be expressed through the displacements accounting for (4):

$$\begin{gathered}\rho\ddot{u}_1=(\lambda+\mu)\frac{\partial\theta}{\partial x}+\mu\Delta u_1,\quad \rho\ddot{u}_2=(\lambda+\mu)\frac{\partial\theta}{\partial y}+\mu\Delta u_2\\ \rho\ddot{w}=(\lambda+\mu)\frac{\partial\theta}{\partial z}+\mu\Delta w,\quad \Delta=\frac{\partial^2}{\partial x^2}+\frac{\partial^2}{\partial y^2}+\frac{\partial^2}{\partial z^2}\end{gathered} \tag{6}$$

Let us introduce scalar potential φ and vector one ψ, then the (6) can be reduced to:

$$\ddot{\varphi}=c_1^2\Delta\psi,\quad \ddot{\psi}=c_2^2\Delta\psi,\quad c_1^2=\frac{\lambda+2\mu}{\rho},\quad c_2^2=\frac{\mu}{\rho} \tag{7}$$

where the displacments are expressed thru φ and ψ as follows:

$$\begin{aligned}u_1&=\frac{\partial\varphi}{\partial x}+\frac{\partial\psi_3}{\partial y}-\frac{\partial\psi_2}{\partial z},\\ u_2&=\frac{\partial\varphi}{\partial y}+\frac{\partial\psi_1}{\partial z}-\frac{\partial\psi_3}{\partial x},\\ w&=\frac{\partial\varphi}{\partial z}+\frac{\partial\psi_2}{\partial x}-\frac{\partial\psi_1}{\partial y}\end{aligned} \tag{8}$$

Only harmonic waves with the frequency ω are considered below, i.e.

$$\varphi=\varphi_a e^{i\omega t},\ \psi=\psi_a e^{i\omega t}\ldots$$

Here the letter "a" denotes the corresponding amplitude values. In the absence of discrepancies, this index is omitted below.

Assuming the propagating waves be harmonic only, we obtain the following representation for the dynamic equations (4):

$$\begin{gathered}\rho\omega^2 u_1 + (\lambda+\mu)\,\frac{\partial\theta}{\partial x} + \mu\Delta u_1 = 0,\\ \rho\omega^2 u_2 + (\lambda+\mu)\,\frac{\partial\theta}{\partial y} + \mu\Delta u_2 = 0,\\ \rho\omega^2 w\,(\lambda+\mu)\,\frac{\partial\theta}{\partial z} + \mu\Delta w = 0\end{gathered} \tag{9}$$

and finally for the scalar and vector potentials we obtain

$$\Delta\varphi + k_1^2\varphi = 0,\ \Delta\psi + k_2^2\psi = 0,\ \ k_j = \omega/c_j \tag{10}$$

Since the medium "2" is not bounded by the coordinate z, then the Somerfield radiation condition acts as a boundary condition:

$$\frac{\partial\varphi}{\partial r} + ik_1\varphi = o\left(\frac{1}{r}\right),\quad \frac{\partial\psi}{\partial r} + ik_2\psi = o\left(\frac{1}{r}\right),\quad r\to\infty \tag{11}$$

4 Fourier Decomposition of Unknown Functions for both Media

All unknown function for both media are decomposed into trigonometric series and satisfy the simple boundary conditions as it was shown by [8].

$$\begin{gathered}\left[\sigma_{33*},\, w^{(1)},\, w^{(2)},\, \sigma_{33}^{(1)},\, \sigma_{33}^{(2)},\, \varphi^{(l)},\, \varepsilon_{11}^{(l)},\, \varepsilon_{22}^{(l)},\, \varepsilon_{33}^{(l)},\, \sigma_{11}^{(l)},\, \sigma_{13}^{(l)},\, \sigma_{33}^{(l)}\right] =\\ = \sum_{n=1}^{\infty}\sum_{m=1}^{\infty}\left[\sigma_{33*nm},\, {w^{(1)}}_{nm},\, {w^{(2)}}_{nm},\, \sigma_{33nm}^{(1)},\, \sigma_{33nm}^{(2)},\, \varphi_{nm}^{(l)},\, \varepsilon_{11nm}^{(l)},\, \varepsilon_{22nm}^{(l)},\right.\\ \left.\varepsilon_{33nm}^{(l)},\, \sigma_{11nm}^{(l)},\, \sigma_{13nm}^{(l)},\, \sigma_{33nm}^{(l)}\right]\sin(\lambda_{1n}x)\sin(\lambda_{2m}y),\\ \left[u_1,\, {\psi_2}^{(l)},\, \varepsilon_{13}^{(l)},\, u_1^c,\, u_1^a,\, q^1\right] =\\ = \sum_{n=1}^{\infty}\sum_{m=1}^{\infty}\left[u_{1nm},\, \psi_{2nm}^{(l)},\, \varepsilon_{13nm}^{(l)},\, u_{1nm}^c,\, u_{1nm}^a,\, q_{nm}^1\right]\cos(\lambda_{1n}x)\sin(\lambda_{2m}y),\\ \left[u_2,\, {\psi_1}^{(l)},\, \varepsilon_{23}^{(l)},\, \varepsilon_{21}^{(l)},\, u_2^c,\, u_2^a,\, q^2\right] =\\ = \sum_{n=1}^{\infty}\sum_{m=1}^{\infty}\left[u_{2nm},\, {\psi_1}_{nm}^{(l)},\, \varepsilon_{23nm}^{(l)},\, \varepsilon_{21nm}^{(l)},\, u_{2nm}^c,\, u_{2nm}^a,\, q_{nm}^2\right]\sin(\lambda_{1n}x)\cos(\lambda_{2m}y)\\ {\psi_3}^{(l)} = \sum_{n=1}^{\infty}\sum_{m=1}^{\infty}\left[\psi_{3nm}^{(l)}\right]\cos(\lambda_{1n}x)\cos(\lambda_{2m}y).\end{gathered} \tag{12}$$

Accounting for (12), the Cauchy equations (4) and the constitutive equations (5) are represented hence as (13), (14):

$$\begin{gathered}\varepsilon_{11nm}^{(l)} = -\lambda_{1n} u_{1nm}^{(l)},\ \varepsilon_{22nm}^{(l)} = -\lambda_{2m} u_{2nm}^{(l)}, \varepsilon_{33n}^{(l)} = \frac{\partial {w^{(l)}}_{nm}}{\partial z},\ (n, m \geq 1);\\ \varepsilon_{13nm}^{(l)} = \frac{1}{2}\left(\frac{\partial u_{1nm}^{(l)}}{\partial z} + \lambda_{1n} {w^{(l)}}_{nm}\right),\\ \varepsilon_{23nm}^{(l)} = \frac{1}{2}\left(\frac{\partial u_{2nm}^{(l)}}{\partial z} + \lambda_{2m} {w^{(l)}}_{nm}\right),\\ \varepsilon_{21nm}^{(l)} = \frac{1}{2}\left(\lambda_{1n} u_{2nm}^{(l)} + \lambda_{2m} u_{1nm}^{(l)}\right);\\ \theta_{nm}^{(l)} = -\lambda_{1n} u_{1nm}^{(l)} - \lambda_{2m} u_{2nm}^{(l)} + \frac{\partial {w^{(l)}}_{nm}}{\partial z}\ (n, m \geq 1).\end{gathered} \tag{13}$$

$$\begin{gathered}\sigma_{11nm}^{(l)} = \lambda\theta_{nm}^{(l)} + 2\mu\varepsilon_{11nm}^{(l)},\ \sigma_{22nm}^{(l)} = \lambda\theta_{nm}^{(l)} + 2\mu\varepsilon_{22nm}^{(l)},\\ \sigma_{33nm}^{(l)} = \lambda\theta_{nm}^{(l)} + 2\mu\varepsilon_{33nm}^{(l)},\\ \sigma_{13nm}^{(l)} = 2\mu\varepsilon_{13nm}^{(l)}, \sigma_{21nm}^{(l)} = 2\mu\varepsilon_{21nm}^{(l)}, \sigma_{23nm}^{(l)} = 2\mu\varepsilon_{23n}^{(l)}.\end{gathered} \tag{14}$$

Also the equations of dynamics for scalar and vector potentials written as

$$\begin{gathered}-\lambda_{1n}^2 {\varphi^{(l)}}_{nm} - \lambda_{2m}^2 {\varphi^{(l)}}_{nm} + \frac{\partial^2 {\varphi^{(l)}}_{nm}}{\partial z^2} + {k_1}^2 {\varphi^{(l)}}_{nm} = 0,\\ -\lambda_{1n}^2 {\psi^{(l)}}_{inm} - \lambda_{2m}^2 {\psi^{(l)}}_{inm} + \frac{\partial^2 {\psi^{(l)}}_{inm}}{\partial z^2} + {k_1}^2 {\psi^{(l)}}_{inm} = 0.\end{gathered} \tag{15}$$

here:

$$\begin{gathered}{w^{(l)}}_{nm} = \frac{\partial \varphi_{nm}^{(l)}}{\partial z} - \lambda_{1n}\psi_{2nm}^{(l)} + \lambda_{2m}{\psi_1}_{nm}^{(l)}\\ u_{1nm}^{(l)} = \lambda_{1n}\varphi_{nm}^{(l)} - \lambda_{2m}{\psi_3}_{nm}^{(l)} - \frac{\partial {\psi_2}_{nm}^{(l)}}{\partial z}\\ u_{2nm}^{(l)} = \lambda_{2m}\varphi_{nm}^{(l)} + \frac{\partial {\psi_1}_{nm}^{(l)}}{\partial z} + \lambda_{1n}{\psi_3}_{nm}^{(l)}.\end{gathered}$$

5 Ingoing Harmonic Spherical Wave

To describe the ingoing wave, a spherical harmonic wave is considered [1]. The medium motion is described by the Helmholtz equation:

$$\Delta\varphi_a + k^2\varphi_a = 0,\ k = \omega/c_1 \tag{16}$$

While the first boundary condition is the Sommerfeld one, the second corresponds to the boundedness at the infinity:

$$\frac{\partial \varphi_a}{\partial r} + ik\varphi_a = 0\left(\frac{1}{r}\right), \; r \to \infty \tag{17}$$

where r is the radius-vector length.

Let us set the position of the spherical wave source at the point $O_1(x_*, y_*, -d)$ where x_*, y_* are the coordinates of the source, and d is the distance from the source to the obstacle. The radius-vector is defined as

$$r = \sqrt{(x + x_*)^2 + (y + y_*)^2 + (z + d)^2}$$

The Helmholtz equation in the spherical coordinates has the following form:

$$\frac{1}{r^2}(r^2\varphi_a'' + k^2\varphi_a) = 0 \tag{18}$$

Its general solution can be expressed as follows:

$$\varphi_a = \frac{1}{r}(A_\Phi e^{-ikr} + B_\Phi e^{ikr}) \tag{19}$$

Taking into account the boundary conditions, we obtain

$$\varphi_a = \frac{1}{r}A_\Phi e^{-ikr} \tag{20}$$

Let us determine the values of normal displacements and stresses in ingoing wave from the relations (7), (3), and (4), where (21) is the pressure amplitude in the ingoing spherical wave:

$$p_* = \frac{-i\omega\rho_c}{\sqrt{(x - x_*)^2 + (y - y_*)^2 + (z + d)^2}} \tag{21}$$

Then, based on the value $\sigma_{33}|_{t=0,\ z=0} = p_*$ the value A_Φ is determined:

$$\begin{gathered} A_\Phi = \frac{p_* x_*^2 + y_*^2 + d^2}{N}, \\ N = 3\lambda\left(-ie^{-ik\sqrt{x_*^2+y_*^2+d^2}} - \frac{e^{-ik\sqrt{x_*^2+y_*^2+d^2}}}{\sqrt{x_*^2 + y_*^2 + d^2}}\right) + \\ +2\mu\left(-ie^{-ik\sqrt{x_*^2+y_*^2+d^2}} - \frac{e^{-ik\sqrt{x_*^2+y_*^2+d^2}}}{\sqrt{x_*^2 + y_*^2 + d^2}}\right). \end{gathered} \tag{22}$$

Accounting for the potentials definition (10), the dynamic equations (9), and the constitutive relations (5), we can find both displacements and stresses as well in the medium "1" as in the plate.

The displacements and stresses on the plate surface take the following form:

$$\begin{aligned} u_{1*} &= \frac{x_* p_*}{N}\left(-ike^{-ikr_*} - \frac{ke^{-ikr_*}}{r_*}\right), \\ u_{2*} &= \frac{y_* p_*}{N}\left(-ike^{-ikr_*} - \frac{ke^{-ikr_*}}{r_*},\right) \\ w_* &= \frac{d p_*}{N}\left(-ike^{-ikr_*} - \frac{ke^{-ikr_*}}{r_*}\right). \end{aligned} \tag{23}$$

$$\sigma_{11*} = \frac{-i\omega\rho_c}{r_*}, \sigma_{22*} = \frac{-i\omega\rho_c}{r_*}, \sigma_{33*} = \frac{-i\omega\rho_c}{r_*}.$$

Further, all values are also decomposed into trigonometric series. As a result, the values of displacement and stresses at the surface of the plate interacting with the medium "1" in ingoing wave are obtained as follows:

$$\begin{aligned} w_{*nm} &= \frac{di\omega\rho_c}{Nr_*}\left(-ike^{-ikr_*} - \frac{ke^{-ikr_*}}{r_*}\right)\frac{l_1 l_2\left[1-(-1)^n\right]\left[1-(-1)^m\right]}{\pi^2 nm}, \\ \sigma_{33*nm} &= \frac{-i\omega\rho_c}{r_*}\frac{l_1 l_2\left[1-(-1)^n\right]\left[1-(-1)^m\right]}{\pi^2 nm}. \end{aligned} \tag{24}$$

6 The Plate Geometry

The plate consists of three layers, two bearing layers and the filling one (Fig. 2). The plate motion is described by the equation system of [2, 3], which accounts for structural features of the plate.

Bearing layers are isotropic and have thickness $2t$, elasticity modulus E, and Poissons ratio ν. The filling layer of thickness $2h$ is orthotropic and honeycomb structure with the compression modules E_3 and shear modulus G_1, G_2 in axial directions Ox, Oy. The axis Oz is directed from the layer number "1" to the layer number "2". The plate is simply supported on the contour.

A special case of transversally soft filler layer is considered, when $G_1 = G_2 = G$. The normal pressures p_1 and p_2 act on bearing layers. Then the dynamic equations of the plate take the form of [2, 3]:

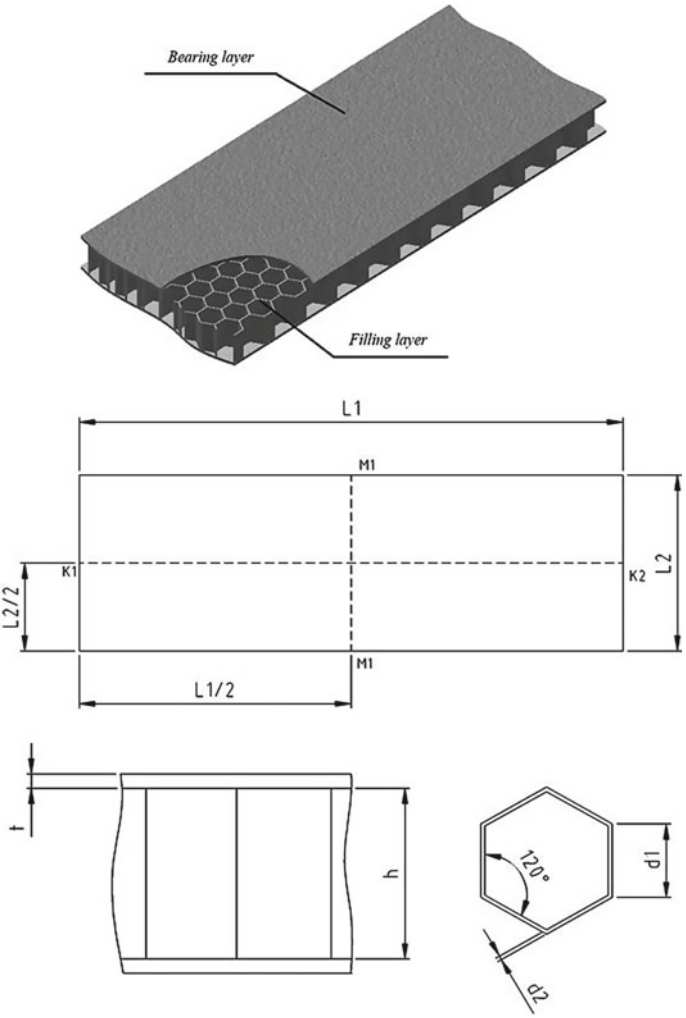

Fig. 2 The geometry of a three-layer plate with honeycomb filling layer. Where $L1$ is the plates' lenght, $L2$ is the plates' width, t is the thickness of bearing layers, $d1$ and $d1$ is the thickness of honeycomd, h is the thickness of filling layer

$$
\begin{aligned}
\rho_c \ddot{u}_1^c &= L_{11}\left(u_1^c\right) + L_{12}\left(u_2^c\right), \\
\rho_c \ddot{u}_2^c &= L_{21}\left(u_1^c\right) + L_{22}\left(u_2^c\right), \\
\rho_a \ddot{u}_1^a &= L_{11}\left(u_1^a\right) + L_{12}\left(u_2^a\right) + 2q^1, \\
\rho_a \ddot{u}_2^a &= L_{21}\left(u_1^a\right) + L_{22}\left(u_2^a\right) + 2q^2, \\
\rho_c \ddot{w}_c - m_c \Delta \ddot{w}_c + \rho_{wq}\left(\ddot{q}_{,x}^1 + \ddot{q}_{,y}^1\right) &= \\
= -D\Delta^2 w_c + 2k_1\left(q_{,x}^1 + q_{,y}^1\right) + p_1 - p_2, & \\
\rho_{aw} \ddot{w}_a - m_a \Delta \ddot{w}_a = -D\Delta^2 w_a - 2c_3 w_a + p_1 + p_2, & \\
\rho_{q1} \ddot{q}^1 - \rho_{wq1} \ddot{w}_{c,x} = u_1^a - k_1 w_{c,x} - k_2\left(q_{,x}^1 + q_{,y}^2\right)_{,x} + k_{31} q^1, & \\
\rho_{q2} \ddot{q}^2 - \rho_{wq2} \ddot{w}_{c,y} = u_2^a - k_1 w_{c,y} - k_2\left(q_{,x}^1 + q_{,y}^2\right)_{,y} + k_{32} q^2, &
\end{aligned}
\tag{25}
$$

where

$$L_{11} = B\left(\frac{\partial^2}{\partial x^2} + \frac{1-\nu}{2}\frac{\partial^2}{\partial y^2}\right),\ L_{12} = L_{21} = B\frac{1+\nu}{2}\frac{\partial^2}{\partial x \partial y},$$
$$L_{22} = B\left(\frac{1-\nu}{2}\frac{\partial^2}{\partial x^2} + \frac{\partial^2}{\partial y^2}\right),\ \Delta = \frac{\partial^2}{\partial x^2} + \frac{\partial^2}{\partial y^2}; \tag{26}$$

$$B = \frac{2Et}{1-\nu^2},\ D = \frac{Bt^2}{3},\ c_3 = \frac{E_3}{2h},\ \rho_a = 2\rho_b t,\ \rho_c = \rho_a + \rho h,$$
$$\rho_{wqi} = \frac{2\rho h^3}{3G_i},\ \rho_{qi} = \frac{2\rho_{wqi}}{G_i},$$
$$k_{3i} = \frac{2h}{G_i}\ (i = 1, 2),\ k_1 = t + h,\ \rho_{aw} = \rho_a + \frac{\rho h}{3}, \tag{27}$$
$$k_2 = \frac{h^2}{3c_3},\ m_c = k_b\rho_b + \frac{\rho h^3}{3},\ m_a = k_b\rho_b + \rho\left(\frac{2h^3}{15} + ht^2 + \frac{2th^2}{3}\right),\ k_b = \frac{2t^3}{3}.$$

In the equation system (22) the further notation is used: w_c, w_a are deflections; q^1, q^2 are transverse shear stresses in the filling along the x-axis and y-axis; ρ, $\rho_{(k)} = \rho_b$ is the mass density of bearing layers and a filling, $u_1^{(k)}$ and $u_2^{(k)}$ are tangential displacements along the x-axis and y-axis respectively in the kth bearing layer, B and D tangent and bending stiffness of the tangent plate, and $w^{(k)}$ is the deflection of k bearing layer, where

$$u_i^c = u_i^{(1)} + u_i^{(2)},\ u_i^a = u_i^{(1)} - u_i^{(2)}\ (i = 1, 2);$$
$$w_c = {w_0}^{(1)} + {w_0}^{(2)},\ w_a = {w_0}^{(1)} - {w_0}^{(2)}. \tag{28}$$

The Eqs. (27) for a transverse soft filler will take the following form:

$$\rho_{wq1} = \rho_{wq2} = \rho_{wq} = \frac{2\rho h^3}{3G},\ \rho_{q1} = \rho_{q2} = \rho_q = \frac{2\rho_{wq}}{G},$$
$$k_{31} = k_{32} = k_3 = \frac{2h}{G}. \tag{29}$$

Following [2, 3], some terms in the system of Eqs. (25) can be neglected:

$$\begin{gathered}
L_{11}\left(u_1^c\right) + L_{12}\left(u_2^c\right) = \rho_c \ddot{u}_1^c,\\
L_{21}\left(u_1^c\right) + L_{22}\left(u_2^c\right) = \rho_c \ddot{u}_2^c,\\
L_{11}\left(u_1^a\right) + L_{12}\left(u_2^a\right) + 2q^1 = \rho_a \ddot{u}_1^a,\\
L_{21}\left(u_1^a\right) + L_{22}\left(u_2^a\right) + 2q^2\rho_a = \ddot{u}_2^a,\\
-D\Delta^2 w_c + 2k_1\left(q_{,x}^1 + q_{,y}^2\right) + p_1 - p_2 = \rho_c \ddot{w}_c,\\
-D\Delta^2 w_a - 2c_3 w_a + p_1 + p_2 = \rho_{aw} \ddot{w}_a,\\
u_1^a - k_1 w_{c,x} - k_2\left(q_{,x}^1 + q_{,y}^2\right)_{,x} + k_{31}q^1 = 0,\\
u_2^a - k_1 w_{c,y} - k_2\left(q_{,x}^1 + q_{,y}^2\right)_{,y} + k_{32}q^2 = 0.
\end{gathered} \tag{30}$$

Finelly, the system of Eqs. (30) taking into account the formulas (26), (27), (28), (29) for harmonic waves is written as follows:

$$\begin{gathered}
B\left(\frac{\partial^2 u_1^c}{\partial x^2}+\frac{1-\nu}{2}\frac{\partial^2 u_1^c}{\partial y^2}+\frac{1+\nu}{2}\frac{\partial^2 u_2^c}{\partial x\partial y}\right)-\rho_c\omega^2 u_1^c=0,\\
B\left(\frac{1+\nu}{2}\frac{\partial^2 u_1^c}{\partial x\partial y}+\frac{1-\nu}{2}\frac{\partial^2 u_2^c}{\partial x^2}+\frac{\partial^2 u_2^c}{\partial y^2}\right)-\rho_c\omega^2 u_2^c=0,\\
B\left(\frac{\partial^2 u_1^a}{\partial x^2}+\frac{1-\nu}{2}\frac{\partial^2 u_1^a}{\partial y^2}+\frac{1+\nu}{2}\frac{\partial^2 u_2^a}{\partial x\partial y}\right)+2q^1-\rho_a\omega^2 u_1^a=0,\\
B\left(\frac{1+\nu}{2}\frac{\partial^2 u_1^a}{\partial x\partial y}+B\frac{1-\nu}{2}\frac{\partial^2 u_2^a}{\partial x^2}+B\frac{\partial^2 u_2^a}{\partial y^2}\right)+2q^2-\rho_a\omega^2 u_2^a=0,\\
-D\left(\frac{\partial^4 w_c}{\partial x^4}+2\frac{\partial^4 w_c}{\partial x^2\partial y^2}+\frac{\partial^4 w_c}{\partial y^4}\right)+2k_1\left(q^1_{,x}+q^2_{,y}\right)+p_1-p_2-\rho_c\omega^2 w_c=0,\\
-D\left(\frac{\partial^4 w_a}{\partial x^4}+2\frac{\partial^4 w_a}{\partial x^2\partial y^2}+\frac{\partial^4}{\partial y^2}w_a\right)-2c_3 w_a+p_1+p_2-\rho_{aw}\omega^2 w_a=0,\\
u_1^a-k_1 w_{c,x}-k_2\left(q^1_{,x}+q^2_{,y}\right)_{,x}+k_3 q^1=0,\\
u_2^a-k_1 w_{c,y}-k_2\left(q^1_{,x}+q^2_{,y}\right)_{,y}+k_3 q^2=0.
\end{gathered}\tag{31}$$

and we have the following boundary conditions on the simply supported contour of the plate:

$$\begin{gathered}
w_c\big|_{x=0,l_1,y=0,l_2}=w_a|_{x=0,l_1,y=0,l_2}=u^a_{1,x}\big|_{x=0,l_1,y=0,l_2}=q^1_{,x}\big|_{x=0,l_1,y=0,l_2}=0\\
w_{c,xx}\big|_{x=0,l_1}=w_{a,xx}\big|_{x=0,l_1}=w_{c,yy}\big|_{y=0,l_2}=w_{c,yy}\big|_{y=0,l_2}=0.
\end{gathered}\tag{32}$$

7 Fourier Decomposition of Unknown Plates' Functions

All unknown function for the plate are decomposed into trigonometric series and satisfy the boundary conditions (32) of the simple support [8].

$$\begin{gathered}
[w,\,p,\,p_1,\,p_2,\,w_*,\,w_a,\,w_c]=\\
=\sum_{n=1}^{\infty}\sum_{m=1}^{\infty}[w_{nm},\,p_{nm},\,p_{1nm},\,p_{2nm},\,w_{*nm},\,w_{anm},\,w_{cnm}]\sin(\lambda_{1n}x)\sin(\lambda_{2m}y),\\
\left[u_1,u_1^c,u_1^a,q^1\right]=\sum_{n=1}^{\infty}\sum_{m=1}^{\infty}\left[u_{1nm},u^c_{1nm},u^a_{1nm},q^1_{nm}\right]\cos(\lambda_{1n}x)\sin(\lambda_{2m}y),\\
\left[u_2,u_2^c,u_2^a,q^2\right]=\sum_{n=1}^{\infty}\sum_{m=1}^{\infty}\left[u_{2nm},u^c_{2nm},u^a_{2nm},q^2_{nm}\right]\sin(\lambda_{1n}x)\cos(\lambda_{2m}y).
\end{gathered}\tag{33}$$

Dynamic equations for the plate are represented hence through the Fourier coefficients. Then, taking into account (33), the equation system (31) for the plate can be solved, and for the normal displacements on the surfaces we have the formulae (34):

$$
\begin{gathered}
(B(\lambda_1^2 - \frac{1-\nu}{2}\lambda_2^2) + \rho_c\omega^2))u_{1nm}^c - B\frac{1+\nu}{2}\lambda_1\lambda_2 u_{2nm}^c = 0, \\
B\frac{1+\nu}{2}\lambda_1\lambda_2 u_{1nm}^c - (B(\frac{1-\nu}{2}\lambda_1^2 + \lambda_2^2) - \rho_c\omega^2))u_{2nm}^c = 0, \\
(-B(\lambda_1^2 + \frac{1-\nu}{2}\lambda_2^2) + \rho_a\omega^2))u_{1nm}^a - B\frac{1+\nu}{2}\lambda_1\lambda_2 u_{2nm}^a + 2q_{nm}{}^1 = 0, \\
B\frac{1+\nu}{2}\lambda_1\lambda_2 u_{1nm}^a - (B(\frac{1-\nu}{2}\lambda_1^2 + \lambda_2^2) - \rho_a\omega^2))u_{2nm}^a + 2q_{nm}{}^2 = 0, \\
(-D(\lambda_1^4 + \lambda_2^4) + \rho_c\omega^2)(w_{nm}{}^{(1)} + w_{nm}{}^{(2)}) - \\
-2k_1(\lambda_1 q_{nm}{}^1 + \lambda_2 q_{nm}{}^2) + p_{1nm} - p_{2nm} = 0, \\
(-D(\lambda_1^4 + \lambda_2^4) + \rho_{aw}\omega^2 - 2c_3)(w_{nm}{}^{(1)} - w_{nm}{}^{(2)}) + p_{1nm} + p_{2nm} = 0, \\
u_{1nm}^a - k_1\lambda_1(w_{nm}{}^{(1)} + w_{nm}{}^{(2)}) - k_2(\lambda_1^2 q_{nm}{}^1 + \lambda_2^2 q_{nm}{}^2) + k_3 q_{nm}{}^1 = 0, \\
u_{2nm}^a - k_1\lambda_2(w_{nm}{}^{(1)} + w_{nm}{}^{(2)}) - k_2(\lambda_1^2 q_{nm}{}^1 + \lambda_2^2 q_{nm}{}^2) + k_3 q_{nm}{}^2 = 0.
\end{gathered} \tag{34}
$$

8 Conditions on the Contact Surface

The pressure amplitude of the wave coming from the medium "1" is equal to the sum of the normal stress in the medium and stress arising as a result of the wave action:

$$
p_1 = \left(\sigma_{33}^{(1)} + \sigma_{33*}\right)\Big|_{z=0}, \quad p_2 = -\sigma_{33}^{(2)}\Big|_{z=0} \tag{35}
$$

In the second medium, the pressure amplitude is the same as the normal stress.

$$
\begin{gathered}
\left(w^{(1)} + w_*\right)\Big|_{z=0} = w_0^{(1)}, \quad w^{(2)}\Big|_{z=0} = w_0^{(2)}, \\
\sigma_{13}^{(1)}\Big|_{z=0} = \sigma_{13}^{(2)}\Big|_{z=0} = 0, \; \sigma_{12}^{(1)}\Big|_{z=0} = \sigma_{12}^{(2)}\Big|_{z=0} = 0, \; \sigma_{23}^{(1)}\Big|_{z=0} = \sigma_{23}^{(2)}\Big|_{z=0} = 0.
\end{gathered} \tag{36}
$$

Medium displacements, summed up with ingoing wave displacements, are equal to the displacement of the first plate bearing layer. The displacement of the second medium is the same as the displacement of the second plate bearing layer. Shear stresses are assumed to be vanishing.

9 Computing of the Fourier Coefficients for the Potentials in Ambient Media

The wave equations in the potentials are also represented through the Fourier coefficients (33):

$$\begin{aligned}\frac{\partial^2 \varphi^{(l)}{}_{nm}}{\partial z^2} + \varphi^{(l)}{}_{nm}\left(k_1{}^2 - \left(\lambda_{1n}^2 + \lambda_{2m}^2\right)\right) = 0,\\ \frac{\partial^2 \psi_i{}^{(l)}{}_{nm}}{\partial z^2} + \psi^{(l)}{}_{inm}\left(k_1{}^2 - \left(\lambda_{1n}^2 + \lambda_{2m}^2\right)\right) = 0,\, i = 1,2,3\end{aligned} \tag{37}$$

Solution of these equations must satisfy the Somerfield condition written in the Fourier coefficients as (33).

$$\begin{aligned}\frac{\partial^2 \varphi_{nm}^{(l)}}{\partial z^2} + \operatorname{sign}\left(k_1 - \left(\lambda_{1n}^2 + \lambda_{2m}^2\right)\right)\kappa_{1nm}^2\left(\omega^2\right)\varphi_{nm}^{(l)} = 0 \;\; (n \geq 1),\\ \frac{\partial^2 \psi_{i\,nm}^{(l)}}{\partial z^2} + \operatorname{sign}\left(k_2 - \left(\lambda_{1n}^2 + \lambda_{2m}^2\right)\right)\kappa_{2nm}^2\left(\omega^2\right)\psi_{inm}^{(l)} = 0 \;\; (n \geq 0),\\ \kappa_{jnm}\left(\omega^2\right) = \kappa_j\left(\lambda_{1n}^2, \lambda_{2m}^2, \omega^2\right) = \sqrt{\left|k_j^2 - \left(\lambda_{1n}^2 + \lambda_{2m}^2\right)^2\right|}.\end{aligned} \tag{38}$$

General solution of the wave equations (38) is given by the following way

$$\begin{aligned}\varphi_{nm}^{(1)}(z,\omega) = C^{(1)}{}_{1nm}(\omega)\left[e^{i\kappa_{1nm}\left(\omega^2\right)z}H\left(k_1 - \left(\lambda_{1n} + \lambda_{2m}\right)\right) + \right.\\ \left. + e^{\kappa_{1nm}\left(\omega^2\right)z}H\left(\left(\lambda_{1n} + \lambda_{2m}\right) - k_1\right)\right],\\ \psi_{inm}^{(1)}(z,\omega) = C^{(1)}{}_{2inm}(\omega)\left[e^{i\kappa_{2nm}\left(\omega^2\right)z}H\left(k_2 - \left(\lambda_{1n} + \lambda_{2m}\right)\right) + \right.\\ \left. + e^{\kappa_{2nm}\left(\omega^2\right)z}H\left(\left(\lambda_{1n} + \lambda_{2m}\right) - k_2\right)\right],\\ \varphi_{n}^{(2)}(z,\omega) = C^{(2)}{}_{1nm}(\omega)\left[e^{-i\kappa_{1nm}\left(\omega^2\right)z}H\left(k_1 - \left(\lambda_{1n} + \lambda_{2m}\right)\right) + \right.\\ \left. + e^{-\kappa_{1nm}\left(\omega^2\right)z}H\left(\lambda_n - \left(\lambda_{1n} + \lambda_{2m}\right)\right)\right],\\ \psi_{inm}^{(2)}(z,\omega) = C^{(2)}{}_{2inm}(\omega)\left[e^{-i\kappa_{2nm}\left(\omega^2\right)z}H\left(k_2 - \left(\lambda_{1n} + \lambda_{2m}\right)\right) + \right.\\ \left. + e^{-\kappa_{2nm}\left(\omega^2\right)z}H\left(\left(\lambda_{1n} + \lambda_{2m}\right) - k_2\right)\right].\end{aligned} \tag{39}$$

To determine the constants $C^{(1)}{}_{1nm}(\omega)$, $C^{(2)}{}_{1nm}(\omega)$, $C^{(1)}{}_{21nm}(\omega)$, $C^{(1)}{}_{22nm}(\omega)$, $C^{(1)}{}_{23nm}(\omega)$,$C^{(2)}{}_{21nm}(\omega)$, $C^{(2)}{}_{22nm}(\omega)$ we have to use the conditions of the contact between the plate and the medium (24), (25). This requires that the stresses, strains, and displacements will be expressed in terms of potentials so that allows one to determine the constants from the boundary conditions. Then the normal and tangential displacements of the medium are found on the basis of the Eqs. (9). The integration constants are determined from the boundary conditions. Further, the vibration acceleration and displacements are determined.

As an example, we considered a plate with the following dimensions, here the plates' parameters are $L1 = 1\,\text{m}$, $L2 = 1\,\text{m}$, $h = 0.015\,\text{m}$, $t = 0.004\,\text{m}$. The bearing layers are made of DIN17100-type steel with density of $\rho_0 = 7859\,\text{kg/m}^3$, Youngs modulus $E_0 = 2 \cdot 10^5\,\text{MPa}$, Poissons ratio of $\nu_0 = 0.28$. Filler material is aluminum of Al-Mn type with density of $\rho_0 = 2730\,\text{kg/m}^3$, Youngs modulus of $E_0 = 0.71 \cdot 10^{-5}\,\text{MPa}$, and Poissons ratio of $\nu_0 = 0.3$. The media 1 and 2 are assumed to be

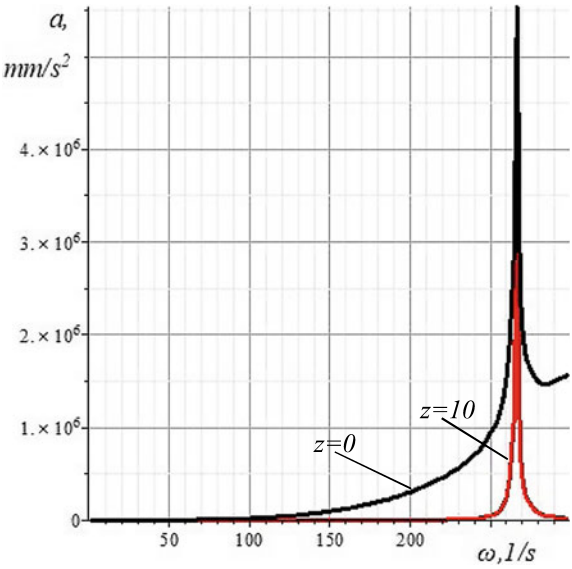

Fig. 3 The figure shows the vibration acceleration module in the different points of medium "2": on the edge of the plate and medium "2" for $z = 0m$; on the medium "2" for $z = 10\,m$

fill-up ground compacted under the humidity degree of 0.5, Youngs modulus of $E = 10^8$ MPa, density of $\rho = 1600\,\mathrm{kg/m^3}$ [9].

The results of calculations of the module of the acceleration field at various points in the medium presented on Fig. 3. The figure shows that a significant decrease in the vibration acceleration module occurs with distance from the plate boundary. It's well known that the low frequencies represent the greatest danger to the foundations of buildings and structures. In accordance with [5, 9], the vibration assessment is carried out in octave bands with geometric mean frequencies of 16, 31.5 and 63 Hz. By plugging the resultant constant values into expressions for displacements, we obtain the expansion factors for the displacements series in the medium 2. Then it became possible to find the vibration acceleration module and its components.

Acknowledgements The reported study was funded by Russian Foundation for Basic Research, according to the research projects Nos. 19-08-00968 A.

References

1. Gorshkov, A.G., Medvedskii, A.L., Rabinskii, L.N., Tarlakovskii, D.V.: Waves in Continuum Media. FIZMATLIT, Moscow (2004)
2. Ivanov, V., Paimushin, V.: Refined formulation of dynamic problems of three-layer shells with a transversally soft filler numerical-analytical method for solving them. Appl. Mech. Eng. Phys. **36**(4), 147–151 (1995a)
3. Ivanov, V., Paimushin, V.: Rrefinement of the equations of the dynamics of multi-layer shells with transversally soft filler. Sol. Mech. **3**, 142–152 (1995b)

4. Kostrov, B.V.: Motion of the rigid massive strip immersed in the elastic medium under the action of the plane wave. Appl. Math. Mech. **28**(1) (1964)
5. Müller, G., Heckl, M.H.: Taschenbuch der Technischen Akustik. Heildelberg, New York, Berlin (2004)
6. Rakhmatulin, K.A.: Elastic and elastoplastic properties of the ground upon dynamic loads on the foundation. Dep in VINITI 4149–4183 (1983)
7. Rylko, M.: On movement of rigid rectangular inclusions in elastic medium affected by flat wave. Mech. Solids (1) (1977)
8. Sheddon, I.: Fourier Transforms. McGraw Hill, New York (1951)
9. SR: Set of Regulations on Design and Construction. SR no. 23-105-2004. Assessing Vibration during Design and Construction and Exploitation of Underground Objects. Moscow (2004)
10. Umek, A.: Dynamic responses of building foundations to incident elastic waves. Ph.D. Thesis, Illinois Institute of Technology, Illinois (1973)
11. Vyalov, S.S.: Problems in the theory of deformability of cohesive soils. Osn Fundam Mekh Gruntov **3**, 1–4 (1966)

Localized Parametric Vibrations of Laminated Cylindrical Shell Under Non-uniform Axial Load Periodically Varying with Time

Gennadi Mikhasev and Rovshen Atayev

Abstract Based on the equivalent single layer model for laminated shells, parametric vibrations of thin laminated non-circular cylindrical shells under non-uniform axial load periodically varying with time are studied. As the governing equations, the non-linear coupled differential equations written in terms of the displacement and stress functions accounting for transverse shears are used. It is assumed that the effective (reduced) shear modulus for an entire laminated package is much less than the reduced Young's modulus. Using the asymptotic method of Tovstik in combination with the multiple scales method with respect to time, solutions of the governing equations are constructed in the form of functions which are exponentially decay far from some generatrix and growing with time in the case of parametric resonance. The system of two differential equations with periodic in time coefficients and accounting for shears is derived to determine the amplitude of parametric vibrations. The main regions of parametric instability taking into account transverse shears were found. An example of parametric vibrations of a sandwich cylinder with the magnetorheological core affected by a magnetic field is considered.

1 Introduction

Parametric vibrations of a mechanical system are vibrations which occur when one or several parameters of a system change as a result of an external influence (boundary conditions, forces, temperature, magnetic or electric field, etc.). The simplest example of parametrically excited vibrations is the dynamic response of a single-degree-of-freedom system—pendulum with an oscillating point of suspension [11, 17, 35]. Thin-walled constructions and their structural elements (beams, plates and shells) are also very sensitive to periodically varying external excitations. Often, parametric vibrations in such members occur when external forces lead to the appearance in a

G. Mikhasev (✉) · R. Atayev
Belarusian State University, 4 Nezavisimosti Avenue, 220030 Minsk, Belarus
e-mail: mikhaseve@bsu.by

R. Atayev
e-mail: at.rovshan@gmail.com

H. Altenbach et al. (eds.), *Recent Developments in the Theory of Shells*,
Advanced Structured Materials 110, https://doi.org/10.1007/978-3-030-17747-8_24

mechanical system of initial stresses having components periodically varying with time [9].

Apparently, for the first time, the problem on parametric vibrations of shells was considered by Chelomey [12]. He studied the dynamic instability of circular cylindrical shells, compressed by the non-stationary forces applied at the shell ends. Later, parametric vibrations of cylindrical shells under periodic axial and radial forces were considered by Markov [22], Oniashvili [32], Wenzke [40], Yao [42, 43], Vijayaraghavan and Evan-Ivanowski [38], Baruch [2] and many others. The general setting of problems on dynamic instability of thin single layer shells under periodic external forces was given by Bolotin [9]. Using equations of membrane and general theories of thin shells, he derived the coupled differential equations in variations describing motion of a thin shell in the neighbourhood of a dynamic membrane stress state. Subsequently, problems on parametric vibrations of thin shells under different loading schemes and various complicating factors (in a nonlinear setting, taking into account energy dissipation, anisotropy, reinforcement, transverse shears, temperature field, initial imperfections etc.) was considered by many authors (s., among many others, [3, 4, 6–8, 10, 18, 19, 31, 33, 39]).

Last decade, the wide use of new composite materials in designing of slender engineering structures stimulated intensive investigations on dynamics of thin-walled laminated and functionally graded elements. However, among an enormous amount of papers on the dynamics of layered structures subjected to external periodic forces, parametrically excited vibrations of layered shells and their dynamic instability are not well understood. This is explained by the complexity of formulation of a non-linear problem for multi-layered thin-walled structures. We shall refer to examples of a very small number of studies on parametric vibrations of thin-walled sandwich elements and multi-layered beams, plates and shells. So, the dynamic stability of thin-walled composite beams, taking into account shear deformation and fiber orientation angle, subjected to axial external force, was studied in Refs. [20, 21]. The parametric vibrations and dynamic instability of laminated composite panels subjected to non-uniform compressive in-plane harmonic edge loading were investigated in [37]. Using the multiple scales method, the authors obtained analytical expressions for the simple and combination resonance instability regions. It was revealed that under localized edge loading, the combination of resonance instability zones are as important as zones of a simple resonance instability. In paper [1], using the variational Ritz method and the R-functions theory, dynamical instability and non-linear parametric vibrations of symmetrically laminated plates of complex shapes and having different cut-outs were considered. The non-linear parametric vibrations of thin laminated composite cylindrical shells subjected to harmonic axial loading were investigated in reference [14]. Considering different lamination schemes, the authors of this paper give a detailed study of parametric resonance of axially stretched and compressed cylinders. Using the Galerkin's technique, in paper [36], parametric vibrations of laminated inhomogeneous orthotropic conical shells under axial load varying with time were investigated. The non-linear dynamic behaviour and parametric vibrations of cylindrical shells functionally graded in the thickness direction under periodic axial loading were studied in Refs. [13, 34].

As a rule, the main methods of studying parametric vibrations of shells are variational ones (e.g., Ritz, Galerkin procedures) which permit to reduce the original equations to the well-known Mathieu-Hill differential equation. The advantage of this approach is that it allows finding all regions of parametric instability. However, it turns out to be computationally very expensive if the problem is two-dimensional and the shell stress state is inhomogeneous. Similar problems arise if, for example, a shell is non-circular and/or loading is inhomogeneous. In such cases, some modes of natural vibrations of a thin shell (for instance eigenmodes of a medium-length cylindrical shell corresponding to a low part of spectrum) can be localized in the vicinity of some line(s), called the weakest one(s), that makes it necessary to account for a large number of terms in the series when using the Ritz or Galerkin procedure or some other technique.

In this paper, we propose the approach based on using the asymptotic method of Tovstik [29] in combination with the multiple scales method with respect to time. This approach allows finding the main regions of parametric instability for the case when excited vibrations are localized in the vicinity of the weakest lines or points [23]. The basic purpose of the paper is to study the influence of transverse shears in a laminated shell with low effective shear modulus on the main region of parametric instability. As an example, the localized parametric vibrations of a sandwich cylindrical shell with magnetorheological core under inhomogeneous axial loading varying with time are considered taking into account shears, with the energy dissipation being ignored.

2 Non-linear Equations

We consider a thin laminated cylindrical shell of length L consisting of N transversely isotropic layers. Each layer is characterized by thickness h_j, Young's modulus E_j, shear modulus G_j, Poisson's ratio ν_j, and density ρ_j, where $j = 1, 2, \ldots, N$ (the numbering of layers begins with the innermost lamina). The middle surface of any fixed layer is taken as the reference surface with the axial and circumferential coordinates α_1 and α_2, respectively, as shown in Fig. 1. In the general case, the cylindrical shell is non-circular with radius of the reference surface equal to $R_2(\alpha_2)$. The shell is under the axial force

$$T_{11}^{\circ} = T_{10}^{\circ}(\alpha_2) + T_{1c}^{\circ}(\alpha_2) \cos \Omega_* t_*, \tag{1}$$

which is non-uniformly distributed along the shell edge and the superposition of static and dynamic components, the last one being the periodic function of time t_* with the excitation frequency Ω_*. Here, T_{11}° is the membrane hoop stress resultant acting in the reference surface. Additional restrictions on this force will be made below.

To predict parametric vibrations of the laminated shell, we shall apply to the equivalent single layer (ESL) theory based on the generalized kinematic hypotheses of Timoshenko [16] (these hypotheses are also listed in paper [25]). In the framework

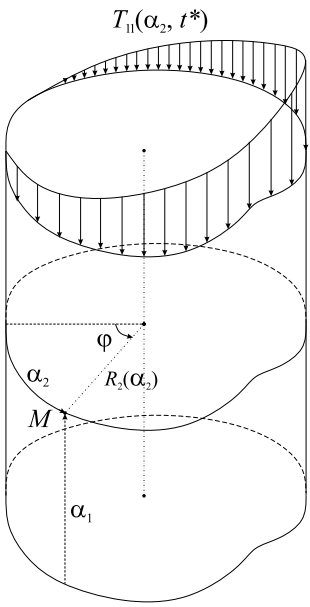

Fig. 1 Coordinate system on the reference surface of laminated non-circular cylindrical shell. Non-uniformly distributed non-stationary axial force

of this theory, Grigoluk and Kulikov [16] have derived the system of five nonlinear differential equations with respect to the five magnitudes, u_i, w, ψ_i, where u_1, u_2, w are displacements of a point on the reference surface in the axial, circumferential and normal directions, respectively, and ψ_1, ψ_2 are shears in the axial and circumferential directions. Because of awkwardness, these equations are not written down here. However, if vibrations occur with formation of a large number of waves although in one direction at the shell surface and $u_i \ll w$, then these equations may be essentially simplified.

Let a, ϕ be the shear functions, and χ is the displacement function such that [16]

$$\psi_1 = \frac{\partial a}{\partial \alpha_1} + \frac{\partial \phi}{\partial \alpha_2}, \quad \psi_2 = \frac{\partial a}{\partial \alpha_2} - \frac{\partial \phi}{\partial \alpha_1}, \tag{2}$$

and

$$a = -\frac{\eta_2}{\eta_1}\frac{h^2}{\beta}\Delta\chi, \quad w = \left(1 - \frac{h^2}{\beta}\Delta\right)\chi. \tag{3}$$

Introduce also the stress function Φ which serves to define the membrane stress resultants in the reference surface:

$$T_{ij} = \delta_{ij}\Delta\,\Phi - \frac{\partial^2 \Phi}{\partial \alpha_i \partial \alpha_j}, \tag{4}$$

where $\Delta = \partial^2/\partial\alpha_1^2 + \partial^2/\partial\alpha_2^2$ is the Laplace operator in the curvilinear coordinates α_1, α_2, and δ_{ij} is Kronecker's symbol ($\delta_{ii} = 1;\ \delta_{ij} = 0, i \neq j$). Then the five coupled equations with respect to u_i, w, ψ_i are reduced to the following compact system of nonlinear differential equations [16]:

$$\begin{aligned} &D\left(1 - \frac{\theta h^2}{\beta}\Delta\right)\Delta^2\chi - \frac{\partial^2\Phi}{\partial\alpha_2^2}\frac{\partial^2 w}{\partial\alpha_1^2} + 2\frac{\partial^2\Phi}{\partial\alpha_1\partial\alpha_2}\frac{\partial^2 w}{\partial\alpha_1\partial\alpha_2} \\ &+ \frac{\partial^2\Phi}{\partial\alpha_1^2}\left(\frac{1}{R_2} - \frac{\partial^2 w}{\partial\alpha_2^2}\right) + \rho_0 h\frac{\partial^2 w}{\partial t^2} = 0, \\ &\Delta^2\Phi - Eh\left[\frac{1}{R_2}\frac{\partial^2 w}{\partial\alpha_1^2} + \left(\frac{\partial^2 w}{\partial\alpha_1\partial\alpha_2}\right)^2 - \frac{\partial^2 w}{\partial\alpha_1^2}\frac{\partial^2 w}{\partial\alpha_2^2}\right] = 0, \end{aligned} \tag{5}$$

$$\frac{1-\nu}{2}\frac{h^2}{\beta}\Delta\phi = \phi, \tag{6}$$

which has to be considered together with the last equation from (3). In the above equations,

$$\begin{aligned} &E = \frac{1-\nu^2}{h}\sum_{j=1}^{N}\frac{E_j h_j}{1-\nu_j^2}, \quad \nu = \sum_{j=1}^{N}\frac{E_j h_j \nu_j}{1-\nu_j^2}\left(\sum_{j=1}^{N}\frac{E_j h_j}{1-\nu_j^2}\right)^{-1}, \\ &D = \frac{Eh^3}{12(1-\nu^2)}\eta_3, \quad \rho_0 = \sum_{k=1}^{N}\rho_k\xi_k, \quad h = \sum_{j=1}^{N}h_j \end{aligned} \tag{7}$$

are the reduced Young's modulus, Poisson's ratio, bending stiffness, density and total thickness of the laminated shell, respectively. These equations contain also parameters $\eta_1, \eta_2, \eta_3, \theta$ and β introduced as follows:

$$\beta = \frac{12(1-\nu^2)}{Eh\eta_1}q_{44}, \quad q_{44} = \frac{\left[\sum_{j=1}^{N}\left(\lambda_j - \frac{\lambda_{jo}^2}{\lambda_{jj}}\right)\right]^2}{\sum_{j=1}^{N}\left(\lambda_j - \frac{\lambda_{jo}^2}{\lambda_{jj}}\right)G_j^{-1}} + \sum_{j=1}^{N}\frac{\lambda_{j0}^2}{\lambda_{jj}}G_j,$$

$$\lambda_j = \int_{\delta_{j-1}}^{\delta_j} f_0^2(z)dz, \quad \lambda_{jn} = \int_{\delta_{j-1}}^{\delta_j} f_j(z)f_n(z)dz \quad (n = 0, j), \quad \theta = 1 - \eta_2^2/(\eta_1\eta_3),$$

$$\eta_1 = \sum_{j=1}^{N}\xi_j^{-1}\pi_{1j}\gamma_j - 3c_{12}^2, \quad \eta_2 = \sum_{j=1}^{N}\xi_j^{-1}\pi_{2j}\gamma_j - 3c_{12}c_{13},$$

$$\eta_3 = 4\sum_{j=1}^{N}(\xi_j^2 + 3\zeta_{j-1}\zeta_j)\gamma_j - 3c_{13}^2, \quad h\xi_j = h_j, \quad h\zeta_n = \delta_n\,(n = 0,\ j),$$
$$\frac{1}{12}h^3\pi_{1j} = \int_{\delta_{j-1}}^{\delta_j} g^2(z)\,dz, \qquad \frac{1}{12}h^3\pi_{2j} = \int_{\delta_{j-1}}^{\delta_j} z\,g(z)\,dz,$$
$$\frac{1}{2}h^2\pi_{3j} = \int_{\delta_{j-1}}^{\delta_j} g(z)\,dz, \quad c_{13} = \sum_{j=1}^{N}(\zeta_{j-1} + \zeta_j)\gamma_j, \quad c_{12} = \sum_{j=1}^{N}\xi_j^{-1}\pi_{3j}\gamma_j, \tag{8}$$
$$\gamma_j = \frac{E_j h_j}{1-\nu_j^2}\left(\sum_{j=1}^{N}\frac{E_j h_j}{1-\nu_j^2}\right)^{-1},$$

where $f_0(z)$, $f_j(z)$, $g(z)$ are continuous functions defined as

$$f_0(z) = \frac{1}{h^2}(z-\delta_0)(\delta_N - z) \quad z \in [\delta_0, \delta_N],$$
$$f_j(z) = \frac{1}{h_j^2}(z-\delta_{j-1})(\delta_j - z) \quad z \in [\delta_{j-1}, \delta_j], \tag{9}$$
$$f_j(z) = 0 \quad z \notin [\delta_{j-1}, \delta_j], \quad g(z) = \int_0^z f_0(x)\mathrm{d}x.$$

Here, $z = \delta_j$ is the coordinate of the upper surface of the jth layer and $z = \delta_0$ is the coordinate of the inner bound of the shell as shown in Fig. 2.

Nonlinear equations (5) are very complicated for the analysis of parametric vibrations and instability. However, it may be simplified by means of linearization of equations in the neighbourhood of the membrane stress state induced by acting axial force (1).

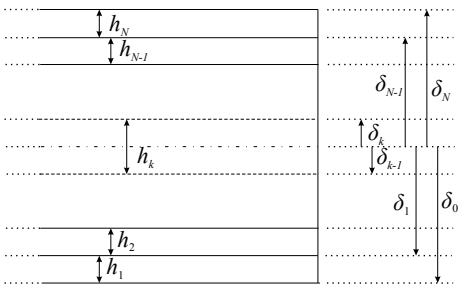

Fig. 2 Cross-section of the laminated shell

3 Linearisation of Governing Equations and Additional Assumptions

Let

$$T_{ij}^{(m)}, \Phi^{(m)}, \chi^{(m)}, w^{(m)}, \phi^{(m)} \tag{10}$$

be functions describing the dynamic membrane stress state $\mathscr{S}^{(m)}$ generated by the periodic axial force (1). The membrane stress resultants $T_{11}^{(m)}$, $T_{12}^{(m)}$, $T_{22}^{(m)}$ are readily found from the membrane stress-strain state equations. If the shell edges are free in the circumferential direction, then $T_{11}^{(m)} = T_{11}^{\circ}(\alpha_2, t_*)$, $\quad T_{22}^{(m)} = T_{12}^{(m)} = 0$ for any α_2 and t_*. The associated in-plane and normal displacements $u_i^{(m)}$, $w^{(m)}$ are easily found from the constitutive equations and strain-displacements correlations [16] which are not written down here.

The problem is to study the shell behaviour in the neighbourhood of the membrane state $\mathscr{S}^{(m)}$ and particularly, to determine the correlation of parameters resulting in the dynamic instability of this state. For this purpose, we shall consider the adjacent stress-strain state $\mathscr{S}$ which is infinitesimally close to the dynamic membrane state $\mathscr{S}^{(m)}$ and characterized by functions $Z^{(m)} + Z$, where $Z^{(m)}$ is any from functions (10), and Z is any of the required associated functions χ, Φ. If Z turns out to bounded for $t_* \to \infty$, then the shell vibrations are called the parametrically stable ones. Otherwise, one says that the state $\mathscr{S}^{(m)}$ is parametrically unstable.

To perform the linearisation of Eq. (5) in the neighborhood of state $\mathscr{S}^{(m)}$, we assume that

$$\frac{\partial T_{11}^{\circ}}{\partial \alpha_2} \sim T_{11}^{\circ} \quad \text{as} \quad h_* \to 0, \tag{11}$$

where $h_* = h/R$, and R is the characteristic dimension which will be introduced below. Condition (11) means that the variability of the axial load in the circumferential direction is small. When taking into account correlations coupling $w^{(m)}$ and T_{11}° [16], one can reveal that

$$\frac{\partial w^{(m)}}{\partial \alpha_2} \sim w^{(m)} \quad \text{as} \quad h_* \to 0. \tag{12}$$

In what follows, we shall study vibrations which are characterized by a large number of short waves in the axial direction. It is assumed that

$$\frac{\partial Z}{\partial \alpha_1} \sim h_*^{-1/4} Z \quad \text{as} \quad h_* \to 0. \tag{13}$$

We note that conditions (12), (13) implies the strong inequality

$$\frac{\partial^2 w^{(m)}}{\partial \alpha_1 \alpha_2} \ll \frac{\partial^2 Z}{\partial \alpha_1 \alpha_2} \quad \text{as} \quad h_* \to 0. \tag{14}$$

for any required function Z.

Let us substitute functions $\Phi^{(m)} + \Phi$, $w^{(m)} + w$, $\chi^{(m)} + \chi$ into Eq. (5). Then, taking into account inequality (14) and performing the linearizion, one arrives at the following equations

$$\frac{Eh^3\eta_3}{12\left(1-\nu^2\right)}\left(1-\frac{\theta h^2}{\beta}\triangle\right)\triangle^2\chi+\frac{1}{R_2(\alpha_2)}\frac{\partial^2\Phi}{\partial\alpha_1^2}+T_{11}^{\circ}(\alpha_2,t_*)\frac{\partial^2}{\partial\alpha_1^2}\left(1-\frac{h^2}{\beta}\triangle\right)\chi$$
$$+\rho_0 h\frac{\partial^2}{\partial t_*^2}\left(1-\frac{h^2}{\beta}\triangle\right)\chi=0,\quad \triangle^2\Phi-\frac{Eh}{R_2(\alpha_2)}\frac{\partial^2}{\partial\alpha_1^2}\left(1-\frac{h^2}{\beta}\triangle\right)\chi=0. \tag{15}$$

Let both edges be simply supported and free of a diaphragm. Then, in terms of the displacement and stress functions, the corresponding conditions read [16]:

$$\chi=\triangle\chi=\triangle^2\chi=\Phi=\triangle\Phi=0,\quad \frac{\partial\phi}{\partial\alpha_1}=0\quad\text{at}\quad\alpha_1=0,L. \tag{16}$$

It is seen that Eq. (15) for χ and Φ are not coupled with Eq. (6) for ϕ, and the boundary condition (16) for ϕ is independent of the residual conditions. Hence, one may set $\phi = 0$. We note that for other variants of boundary conditions (for instance, for simply supported edges with a diaphragm), the function ϕ is not identically zero and serves to take into account shears in a neighbourhood of the shell edges [25].

Equation (15) derived in the framework of ESL theory for laminated shells is the generalization of classical and well-known Mushtari–Donnell–Vlasov type equations [15, 30, 41] for single layer isotropic shells. It is seen that Eq. (15) contain the terms proportional to $\beta^{-1} \sim G^{-1}$, where $G = q_{44}/h$ is so-called the reduced or effective shear modulus for the laminated shell. When $G \to \infty$, Eq. (15) degenerate into the classical equations not accounting for shear effects. We note that if $G \sim E$ then Eq. (15) become asymptotically incorrect because they generate integrals (solutions) with very high index of variation [25]. In what follows, we assume that the laminated shell is shear deformable so that $G \ll E$. The another essential assumption is that the shell is sufficiently thin.

4 Reduction of Equations to Dimensionless Form

Let

$$\mu^4=\frac{h^2\eta_3}{12R^2\left(1-\nu^2\right)} \tag{17}$$

be a small parameter characterizing the shell thickness, where R is the above mentioned characteristic size of the shell. We introduce the dimensionless coordinates, time and counterparts of the required functions:

$$s=\frac{\alpha_1}{R},\quad \varphi=\frac{\alpha_2}{R},\quad t=t_*/T_c,\quad \chi=R\widehat{\chi}(s,\phi),\quad \Phi=\mu^2EhR^2\widehat{\Phi}(s,\phi),$$
$$F(\varphi,t)=\frac{T_{11}^{\circ}(R\phi)}{\mu^2Eh}=f_0(\varphi)+\mu f_1(\varphi)\cos(\Omega t) \tag{18}$$

where $T_c=R\sqrt{\frac{\rho_0}{E}}$ is the characteristic time, and $\Omega=t_c\Omega_*$ is the dimensionless frequency of the periodic axial force. The last equation means that the non-stationary component of the applied force is small when comparing with the static one.

We assume also the following asymptotic estimates:

$$\frac{h^2}{R^2\beta}=\mu^2\kappa,\quad \frac{\theta h^2}{R^2\beta}=\mu^3\tau,\quad \kappa,\tau\sim 1 \text{ as } \mu\to 0, \tag{19}$$

which are valid for sufficiently thin shell containing a "soft" core or several such layers. The last estimation is introduced because of the smallness of a parameter θ; for instance, for a single layer isotropic shell [16], $\theta=1/85$. Correlations (19) imply that the reduced shear modulus G is small when comparing with the reduced Young's modulus E so that $G\sim h_*E$ as $h_*\to 0$.

The substitution of Eqs. (17)–(19) into Eq. (15) results in the differential equations

$$\mu^4\left(1-\mu^3\tau\triangle\right)\triangle^2\widehat{\chi}+\mu^2k(\varphi)\frac{\partial^2\widehat{\Phi}}{\partial s^2}+\mu^2F(\varphi,t)\frac{\partial^2}{\partial s^2}\left(1-\mu^2\kappa\triangle\right)\widehat{\chi}$$
$$+\frac{\partial^2}{\partial t^2}\left(1-\mu^2\kappa\triangle\right)\widehat{\chi}=0,$$
$$\mu^2\triangle^2\widehat{\Phi}-k(\varphi)\frac{\partial^2}{\partial s^2}\left(1-\mu^2\kappa\triangle\right)\widehat{\chi}=0, \tag{20}$$

written in the dimensionless form, where $k(\varphi)=R/R_2(R\varphi)$ is the dimensionless curvature. The corresponding boundary conditions for the functions $\hat{\chi}$, $\hat{\Phi}$ at $s=0$, $l=L/R$ are not changed and expressed by relations (16), where χ, Φ are replaced by their dimensionless counterparts.

5 Asymptotic Approach

Let $\varphi=\varphi_0$ be the "weakest generatrix" in the neighbourhood of which localized parametric vibrations are excited. Following to the approach developed in [29], the formal asymptotic solution of Eq. (20) is sought in the form of series

$$\widehat{\chi}(\phi,t,\mu)=\sin\left(\frac{q_ns}{\mu}\right)\sum_{j=0}^{\infty}\mu^{j/2}\chi_j(\xi,t_0,t_1,\ldots)\exp\left(i\left(\mu^{-1/2}p\xi+\tfrac{1}{2}b\xi^2\right)\right),$$
$$q_n=\mu\pi nl^{-1}\sim 1,\quad n=1,2,\ldots,\quad \xi=\mu^{-\frac{1}{2}}(\varphi-\varphi_0),$$
$$i=\sqrt{-1},\quad t_m=\mu^mt,\quad m=0,1,\ldots, \tag{21}$$

where $\Im b > 0$, χ_j are polynomials in ξ and t_m is "slow time" for $m \geq 1$. The function $\widehat{\Phi}$ is constructed in the same form. It is also assumed that

$$p,\ q_n,\ |b|,\ |y|,\ \left|\frac{\partial y}{\partial x}\right| \sim 1 \text{ as } \mu \to 0, \tag{22}$$

where y is any of functions χ_j, Φ_j and x is any their argument. We fix n and omit this subscript in what follows.

The substitution of Eq. (21) into Eq. (20) results in the sequence of equations

$$\sum_{\varsigma=0}^{j} \mathbf{L}_\varsigma \chi_{j-\varsigma} = 0, \quad j = 0, 1, 2, \ldots, \tag{23}$$

where the operators $\mathbf{L}_\varsigma$ are introduced as follows

$$\begin{gathered}
\mathbf{L}_0 z = \tfrac{\partial^2 z}{\partial t_0^2} + H^2(p, q, \varphi_0)\, z, \\
H(p, q, \phi_0) = \sqrt{\tfrac{\left(p^2+q^2\right)^2}{1+\kappa\left(p^2+q^2\right)} + \tfrac{k^2(\varphi_0) q^4}{\left(p^2+q^2\right)^2} - f_0(\varphi_0) q^2}, \\
\mathbf{L}_1 z = \left(b \tfrac{\partial \mathbf{L}_0}{\partial p} + \tfrac{\partial \mathbf{L}_0}{\partial \varphi_0}\right) \xi z - i \tfrac{\partial \mathbf{L}_0}{\partial p} \tfrac{\partial z}{\partial \xi}, \\
\mathbf{L}_2 z = \tfrac{1}{2}\left(b^2 \tfrac{\partial^2 \mathbf{L}_0}{\partial p^2} + 2b \tfrac{\partial^2 \mathbf{L}_0}{\partial p \partial \varphi_0} + \tfrac{\partial^2 \mathbf{L}_0}{\partial \varphi_0^2}\right) \xi^2 z - \tfrac{1}{2} \tfrac{\partial^2 \mathbf{L}_0}{\partial p \partial \varphi_0} z \\
- \tfrac{1}{2} \tfrac{\partial^2 \mathbf{L}_0}{\partial p^2}\left(i z + \tfrac{\partial^2 z}{\partial \xi^2}\right) - i\left(b \tfrac{\partial^2 \mathbf{L}_0}{\partial p^2} + \tfrac{\partial^2 \mathbf{L}_0}{\partial p \partial \varphi_0}\right) \xi \tfrac{\partial z}{\partial \xi} + \mathbf{N} z, \ldots \\
\mathbf{N} z = 2 \tfrac{\partial^2 z}{\partial t_0 \partial t_1} - q^2 f_1(\varphi_0) \cos(\Omega t_0) z + q^6 \tau z.
\end{gathered} \tag{24}$$

Consider Eq. (23) step by step.

In the zero-order approximation ($j = 0$), one has the homogeneous equation $\mathbf{L}_0 \chi_0 = 0$. Its solution may be written in the form:

$$\begin{gathered}
\chi_0 = P_{0,c}(\xi, t_1, t_2, \ldots) \cos(\omega_0 t_0) + P_{0,s}(\xi, t_1, t_2, \ldots) \sin(\omega_0 t_0), \\
\omega_0 = H(p, q, \varphi_0),
\end{gathered} \tag{25}$$

where $P_{0,c}$, $P_{0,s}$ are polynomials in ξ with coefficients depending on "slow time".

In the first-order approximation ($j = 1$), one obtains the non-homogeneous equation

$$\frac{\partial^2 \chi_1}{\partial t_0^2} + H^2(p, q, \varphi_0)\, \chi_1 = \frac{\partial H^2}{\partial p}\left(i \frac{\partial \chi_0}{\partial \xi} - b \xi \chi_0\right) - \frac{\partial H^2}{\partial \varphi_0} \xi \chi_0. \tag{26}$$

which has unbounded solutions (as $t_0 \to \infty$) called secular terms. To eliminate these terms, one needs to assume

$$\frac{\partial H^2}{\partial p} = 0, \quad \frac{\partial H^2}{\partial \varphi_0} = 0. \tag{27}$$

The above equations serve to determine a wave parameter $p = p^\circ$ and the weakest generatrix $\varphi_0 = \varphi_0^\circ$. There are three different cases:

(case A) $q > z_0$;
(case B) $q < z_0$;
(case C) $q = z_0$,

where z_0 is a root of the equation

$$-2k^2(\varphi_0)\,(1 + \kappa q z)^2 + z^4\,(2 + \kappa q z) = 0. \tag{28}$$

Equation (28) was derived earlier [24] under studying free localized vibrations of an axially pre-stressed laminated non-circular cylindrical shell. It contains a parameter κ accounting for shear in the shell. When $G \to \infty$, then $\kappa \to 0$ (shear is disregarded) and this root $z_0 = 1$ [29].

If $q > z_0$ (case A), then

$$p = 0, \quad \omega_0 = \sqrt{k^2(\varphi_0) - f_0(\varphi_0)q^2 + \frac{q^4}{1 + \kappa q^2}}, \tag{29}$$

and the weakest generatrix φ_0 is found from the equation

$$2k(\varphi_0)k'(\varphi_0) - f_0'(\varphi_0)q^2 = 0, \tag{30}$$

and for $q < z_0$ (case B), one obtains the correlations

$$p = \sqrt{q(z_0 - q)}, \quad \omega_0 = \sqrt{\frac{k^2(\varphi_0)q^2}{z_0^2} - f_0(\varphi_0)q^2 + \frac{q^2 z_0^2}{1 + \kappa q z_0}}, \tag{31}$$

and the following equation

$$2k(\varphi_0)k'(\varphi_0) - f_0'(\varphi_0)z_0^2 = 0 \tag{32}$$

which serves to determine φ_0. In what follows, we consider the magnitude $R = R_2(\varphi_0)$ as the characteristic dimension of the shell.

When $q = z_0$ (case C), Eqs. (29), (30) coincide with Eqs. (31), (32), respectively.

Remark 1 Let

$$f_{cr}^{(1)} = \min_{\varphi_0} \frac{1}{f_0(\varphi_0)} \left[\frac{k^2(\varphi_0)}{q^2} + \frac{q^2}{1 + \kappa q^2} \right] \tag{33}$$

for $q > z_0$ and φ_0 defined from Eq. (30), and

$$f_{cr}^{(2)} = \min_{\varphi_0} \frac{1}{f_0(\varphi_0)} \left[\frac{k^2(\varphi_0)}{z_0^2} + \frac{z_0^2}{1+\kappa z_0^2} \right] \tag{34}$$

for $q \le z_0$ and φ_0 determined from Eq. (32). Then $F_{cr} = \mu^2 Eh \min\left\{f_{cr}^{(1)}, f_{cr}^{(2)}\right\}$ is the critical buckling axial force for a thin laminated circular cylindrical shell [28]. We assume that $f_0(\varphi_0) < \min\left\{f_{cr}^{(1)}, f_{cr}^{(2)}\right\}$ for any φ_0. In other words, the inhomogeneous axial force (1) does not reach the critical buckling value F_{cr} at any generatrix. Then the magnitudes under radicals in Eqs. (29), (31) will be positive for any angle φ_0.

Remark 2 Theoretically, parametric instability is observed in the case when the ratio of the frequency of an external force to the frequency of natural vibrations is equal or close to one of the following values [43]

$$\frac{\Omega}{\omega} = \frac{2}{1}, \quad \frac{2}{2}, \quad \frac{2}{3}, \quad \dots \tag{35}$$

However, there are usually only cases where this ratio is 2/1, 2/2, less often 2/3. At that, the condition $\Omega/\omega = 2/2$ corresponds to usual resonance.

We will consider here the case that is of most interest, where $\Omega \approx 2\omega_0$. Let

$$\Omega = 2\omega_0 + \mu\sigma, \quad \sigma \to 0 \quad \text{when} \quad \mu \to 0, \tag{36}$$

where σ is the frequency detuning parameter.

In the second-order approximation ($j = 2$), one arrives again at the non-homogeneous equation

$$\begin{aligned} \tfrac{\partial^2 \chi_2}{\partial t_0^2} + H^2(p, q, \varphi_0)\chi_2 = -N_c \cos(\omega_0 t_0) - N_s \sin(\omega_0 t_0) + \\ + r\left[P_{0,c} \cos(3\omega_0 t_0 + \sigma t_1) + P_{0,s} \sin(3\omega_0 t_0 + \sigma t_1)\right], \end{aligned} \tag{37}$$

where

$$\begin{aligned} N_c = -\tfrac{1}{2}\tfrac{\partial^2 H^2}{\partial p^2}\tfrac{\partial^2 P_{0,c}}{\partial \xi^2} + a\xi\tfrac{\partial P_{0,c}}{\partial \xi} + \left[c\xi^2 + \tfrac{1}{2}a + \tfrac{\tau(p^2+q^2)^3}{1+\kappa(p^2+q^2)}\right] P_{0,c} + \\ + 2\omega_0 \tfrac{\partial P_{0,s}}{\partial t_1} + r\left[P_{0,s} \sin(\sigma t_1) - P_{0,c} \cos(\sigma t_1)\right] \\ N_s = -\tfrac{1}{2}\tfrac{\partial^2 H^2}{\partial p^2}\tfrac{\partial^2 P_{0,s}}{\partial \xi^2} + a\xi\tfrac{\partial P_{0,s}}{\partial \xi} + \left[c\xi^2 + \tfrac{1}{2}a + \tfrac{\tau(p^2+q^2)^3}{1+\kappa(p^2+q^2)}\right] P_{0,s} - \\ - 2\omega_0 \tfrac{\partial P_{0,c}}{\partial t_1} + r\left[P_{0,s} \cos(\sigma t_1) - P_{0,c} \sin(\sigma t_1)\right], \\ a = -i\left(b\tfrac{\partial^2 H^2}{\partial p^2} + \tfrac{\partial^2 H^2}{\partial p \partial \varphi_0}\right), \quad c = \tfrac{1}{2}\left(b^2\tfrac{\partial^2 H^2}{\partial p^2} + 2b\tfrac{\partial^2 H^2}{\partial p \partial \varphi_0} + \tfrac{\partial^2 H^2}{\partial \varphi_0^2}\right), \quad r = \tfrac{1}{2}q^2 f_1(\varphi_0). \end{aligned} \tag{38}$$

The partial solution of Eq. (37) contains the secular terms generated by the first two components at the right hand of the equation. The conditions for their absence are equality

$$N_c = 0, \quad N_s = 0$$

which results in the differential equation

$$\begin{gathered} -\tfrac{1}{2}\tfrac{\partial^2 H^2}{\partial p^2}\tfrac{\partial^2 \mathbf{X}}{\partial \xi^2} + a\xi\tfrac{\partial \mathbf{X}}{\partial \xi} + \left[c\xi^2 + \tfrac{1}{2}a + \tfrac{\tau(p^2+q^2)^3}{1+\kappa(p^2+q^2)}\right]\mathbf{X} + \\ 2\omega_0 \mathbf{E}_{-1}\tfrac{\partial \mathbf{X}}{\partial t_1} + r(\varphi_0)\mathbf{S}_\sigma \mathbf{X} = \mathbf{O}, \end{gathered} \tag{39}$$

where $\mathbf{X} = (P_{o,s},\, P_{0,c})^{\mathrm{T}}$, $\mathbf{O} = (0,\, 0)^{\mathrm{T}}$ are the two-dimensional vectors, and

$$\mathbf{E}_{-1} = \begin{pmatrix} 0 & -1 \\ 1 & 0 \end{pmatrix}, \quad \mathbf{S}_\sigma = \begin{pmatrix} \cos(\sigma t_1) & \sin(\sigma t_1) \\ \sin(\sigma t_1) & -\cos(\sigma t_1) \end{pmatrix} \tag{40}$$

are the 2×2 matrices.

For the vector equation (39) to have a solution in the form of polynomials in ξ, we have to assume $c = 0$. Hence (see Eq. (38) for c),

$$b = \left\{\frac{\partial^2(H^2)}{\partial p^2}\right\}^{-1} \left\{-\frac{\partial^2(H^2)}{\partial p \partial \varphi_0} \pm i\sqrt{\frac{\partial^2(H^2)}{\partial p^2}\frac{\partial^2(H^2)}{\partial \varphi_0^2} - \left[\frac{\partial^2(H^2)}{\partial p \partial \varphi_0}\right]^2}\right\}. \tag{41}$$

It is seen that $\Im b > 0$ if the inequalities

$$\frac{\partial^2(H^2)}{\partial p^2} > 0, \quad \frac{\partial^2(H^2)}{\partial p^2}\frac{\partial^2(H^2)}{\partial \varphi_0^2} - \left[\frac{\partial^2(H^2)}{\partial p \partial \varphi_0}\right]^2 > 0 \tag{42}$$

hold simultaneously.

If $q > z_0$, then inequalities (42) imply

$$2[(k'(\varphi_0)]^2 + 2k(\varphi_0)k''(\varphi_0) - f_0''(\varphi_0)q^2 > 0, \tag{43}$$

and for $q < z_0$, one has

$$\begin{gathered} \left\{2[k'(\varphi_0)]^2 + 2k(\varphi_0)k''(\phi_0) - f_0''(\varphi_0)z^2\right\}\left[8 + 9\kappa q z + 3(\kappa q z)^2\right] > \\ 4\left[f_0'(\varphi_0)\right]^2 (1 + \kappa q z)^3. \end{gathered} \tag{44}$$

In what follows, we consider the special case when $k \equiv 1$ (a circular cylinder) and $f_0(\varphi)$ is a function. Then Eq. (32) and inequalities (43), (44) result in the conditions

$$f_0'(\varphi_0) = 0, \quad f_0''(\varphi_0) < 0, \tag{45}$$

which mean that the weakest generatrix $\varphi = \varphi_0$ is that which is more stressed by the compressive force. The required parameter b becomes

$$b = i\sqrt{\frac{-q^4(1+\kappa q^2)^2 f_0''(\varphi_0)}{2q^4(2+\kappa q^2) - 4(1+\kappa q^2)^2}} \tag{46}$$

for $q > z_0$ (case A), and

$$b = i\sqrt{\frac{-q(1+\kappa q^2)^3 f_0''(\varphi_0)}{4(z_0 - q)[8 + 9\kappa q z_0 + 3(\kappa q z_0)^2]}} \tag{47}$$

if $q < z_0$ (case B).

Remark 3 It may be seen that $\lim_{q\to z_0} |b| = +\infty$ for both cases (A, B) and requirement (22) for b does not hold if a root q is close to z_0. Thus, the case (C), where q is close to z_0, requires an additional consideration.

We will not consider higher approximations because Eq. (5) are not sufficiently accurate. To construct higher approximations, one needs applying to the full system of governing equations written in terms of displacements u_i, w, ψ_i.

Taking Eq. (41) into account, the vector equation (39) admits a solution in the form

$$\mathbf{X} = \mathscr{H}_m(\theta\xi)\mathbf{Y}_m, \quad \theta^2 = a\left(\frac{\partial^2 H^2}{\partial p^2}\right)^{-1} \tag{48}$$

where $\mathscr{H}_m(x)$ is the Hermit polynomial of the mth degree, and $\mathbf{Y}_m = (S_m(t_1), C_m(t_1))^{\mathrm{T}}$ is the two-dimensional vector with the components depending on "slow time".

The substitution of (48) into Eq. (39) leads to the homogeneous vector differential equation

$$\dot{\mathbf{Y}}_m\ (t_1) = \mathbf{A}_m(t_1)\mathbf{Y}_m(t_1) \tag{49}$$

with the periodic matrix

$$\mathbf{A}_m(t_1) = \begin{pmatrix} -a_0 \sin\sigma t_1 & -a_{2,m} - a_\tau + a_0 \cos\sigma t_1 \\ a_{2,m} + a_\tau + a_0 \cos\sigma t_1 & a_0 \sin\sigma t_1 \end{pmatrix}, \tag{50}$$

where,

$$a_0 = \frac{q^2 f_1(\varphi_0)}{4\omega_0}, \quad a_{2,m} = a\frac{2m+1}{4\omega_0}, \quad a_\tau = \frac{\tau(p^2+q^2)^3}{2\omega_0[1+\kappa(p^2+q^2)]}. \tag{51}$$

The parameters κ, τ appearing in the formula for a_τ depend on the reduced shear modulus G. When $G \to \infty$, then $\kappa, \tau, a_\tau \to 0$ and the matrix $\mathbf{A}_m(t_1)$ coincides with the appropriate matrix (see also Eqs. (24), (25), (38) for H, ω_0 and a, respectively) obtained in [23].

Finally, the parametric response of the shell to applied periodic axial force (1) is given by the formula:

$$\chi = \sin\left(\frac{\pi n s}{l}\right) \exp\left\{i\mu^{-1}\left[p(\varphi-\varphi_0)+\frac{1}{2}b(\varphi-\varphi_0)^2\right]\right\} \times \left\{\mathscr{H}_m\left[\mu^{-\frac{1}{2}}(\varphi-\varphi_0)\theta\right]\left[S_m(\mu t)\sin(\omega_0 t)+C_m(\mu t)\cos(\omega_0 t)\right]+O(\mu^{\frac{1}{2}})\right\}. \quad (52)$$

6 Parametric Instability Domains

Depending on the correlation between parameters $a_0, a_{2,m}, a_\tau, \sigma$, solutions of Eq. (49) are bounded or not. Equation (49) have periodic solutions if and only if their multipliers are equal to one. If the absolute value of all multipliers are more than one, then their solutions growth indefinitely at $t_1 \to \infty$, if less than one, then they decrease [5].

The analysis of Eq. (49) has been performed numerically. We have composed the monodromy matrix and found its eigenvalues, i.e. the required multipliers. It has been revealed that the σa_0—plane is divided by the lines (see Fig. 3)

$$a_0 = \pm\left(a_{2,m} + a_\tau - \frac{\sigma}{2}\right) \quad (53)$$

into the following two domains:

$$\begin{aligned} \mathscr{D}^- &= \left\{(\sigma, a_0) : \left|a_{2,m} + a_\tau - \tfrac{\sigma}{2}\right| < |a_0|\right\}, \\ \mathscr{D}^+ &= \left\{(\sigma, a_0) : \left|a_{2,m} + a_\tau - \tfrac{\sigma}{2}\right| > |a_0|\right\}. \end{aligned} \quad (54)$$

In Fig. 3, each of these domains are shown as the unions of two sub-domains: $\mathscr{D}^\pm = \mathscr{D}_1^\pm \cup \mathscr{D}_2^\pm$. On lines (53), solutions of Eq. (49) are bounded and close to harmonic functions, if a point $M(\sigma, a_0) \in \mathscr{D}^+$, then solutions are decreasing functions, and in the domain $\mathscr{D}^-$ they grow indefinitely. Thus, the domain $\mathscr{D}^-$ corresponds to the parametrically unstable vibrations localized in the neighborhood of the weakest generatrix $\varphi = \varphi_0$. The farther a point $M(\sigma, a_0) \in \mathscr{D}^-$ from lines (53) is situated, the faster the amplitude of the resonance parametric vibrations increases. We note that $\mathscr{D}^-$ is the main region of localized parametric resonance which occurs for $\Omega \approx 2\omega_0$.

Comparing the region $\mathscr{D}^-$ of parametric instability with the analogous domain for a single layer isotropic shell without taking shear into account [23], one can conclude that the incorporation of shear effects into the shell model results in the right shift of the parametric instability domain. If the shell is circular and load (1) is uniformly distributed in the circumferential direction (k, f_0, f_1 are constants), then $b = a = a_{2,m} = 0$ and the domain $\mathscr{D}^-$ corresponds to the parametric resonance of the shear deformable laminated shell where vibrations cover all its surface. If at that shears are ignored, then the region $\mathscr{D}^-$ becomes symmetrical with respect to the σ—and a_0—axes.

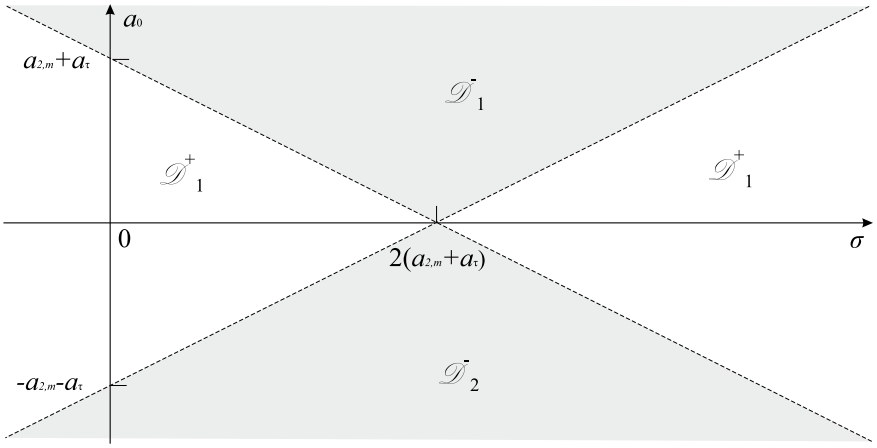

Fig. 3 Main regions of parametric instability

When the axial force (1) is stationary, then Eq. (49) admit the solution in explicit form:

$$\begin{aligned} S_m(\mu t) &= c_1 \sin(\mu a_{2,m} t) + c_2 \cos(\mu a_{2,m} t), \\ C_m(\mu t) &= -c_1 \cos(\mu a_{2,m} t) + c_2 \sin(\mu a_{2,m} t), \end{aligned} \tag{55}$$

where c_1, c_2 are constants. Then, for both cases, (A) and (B), Eq. (52) defines the localized eigenmodes of free vibrations of the axially pre-stressed laminated cylindrical shell with the dimensionless natural frequencies [24]

$$\omega = \omega_0 + \mu a_{2,m} + O\left(\mu^2\right). \tag{56}$$

7 Examples

The aforementioned equations allow us to give the asymptotic estimate of boundaries $\Omega^- \le \Omega \le \Omega^+$ for the dimensionless excitation frequency $\Omega = t_c \Omega_*$ leading to the parametrically unstable vibrations:

$$\Omega^{\pm} = 2\omega_0 + \sqrt[4]{\frac{h^2}{12R^2(1-\nu^2)}}\sigma^{\pm}, \tag{57}$$

where $\sigma^{\pm} = 2\left(a_{2,m} \pm |\alpha_0|\right)$.

Example 1 Not specifying a quantity of layers and a type of material for each layer, as the first example, we shall consider a circular cylindrical shell under the action of the nonuniform axial loading (1), (18), where $f_0 = 0.5(1 + \cos\varphi)$, $f_1 = 1$. Here, the weakest line is the generatrix $\varphi = \varphi_0 \equiv 0$, where the not uniformly distributed axial

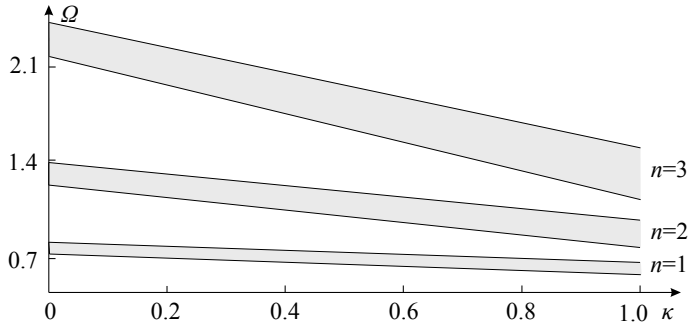

Fig. 4 Main regions for parametric resonance versus the shear parameter κ for $m = 0$ and different number of semi-waves in the axial direction, $n = 1, 2, 3$

forces (1) reach the maximum value. Figure 4 shows the boundaries of main regions for parametric resonance versus the shear parameter κ for $m = 0$ and different number of semi-waves in the axial direction, $n = 1, 2, 3$. It is seen that in the $\kappa\Omega$—plane, the main domains of parametric instability are narrow regions with the width increasing together with the mode number n. The influence of shears on these regions depends also on a number n: for the first mode ($n = 1, m = 0$) corresponding to the lowest natural frequency, the effect of a shear parameter κ turns out to be weak, however it becomes noticeable when a number n grows. It may be also seen that the increase of a shear parameter κ results in the decrease of both the boundary values $\Omega^{\pm}$ for the parametric excitation frequency and the eigenfrequency ω_0. Similar effect of shears on natural frequencies of a thin medium-length laminated cylinder has been recently detected in paper [27].

Example 2 Consider a sandwich circular cylindrical shell of radius $R = 1\,\text{m}$ and length $L = 4\,\text{m}$ with the core of thickness h_2 made of a magnetorheological elastomer (MRE). The face layers having the same thickness $h_1 = h_3$ are fabricated of the ABS-plastic SD-0170 with parameters $E_1 = E_3 = 1.5 \times 10^9\,\text{Pa}$, $\nu_1 = \nu_3 = 0.4$, $\rho_1 = \rho_3 = 1.4 \times 10^3\,\text{kg/m}^3$. Here, the MRE under consideration is treated as an isotropic and elastic material with the Poisson's ratio $\nu_2 = 0.3$, density $\rho_2 = 2.63\,\text{g/sm}^3$ and the shear modulus G_2 which depends on the magnetic field induction B [26]:

$$G_2 = (4.500 + 14.978\,B),\,\text{kPa} \tag{58}$$

The shell is under the non-uniform axial force periodically varying with time and specified in the previous example. In Fig. 5, the boundaries of the main regions of parametric resonance versus the magnetic induction B are shown for different values of the core thickness $h_2 = 6, 9, 12\,\text{mm}$. It is seen that the effect of magnetic field on the main regions of instability depends on the thickness of "soft" core made of MRE: it is weak for small h_2 and becomes noticeable for $h_2 \geq 12\,\text{mm}$ at the interval $0 < B < 50\,\text{mT}$.

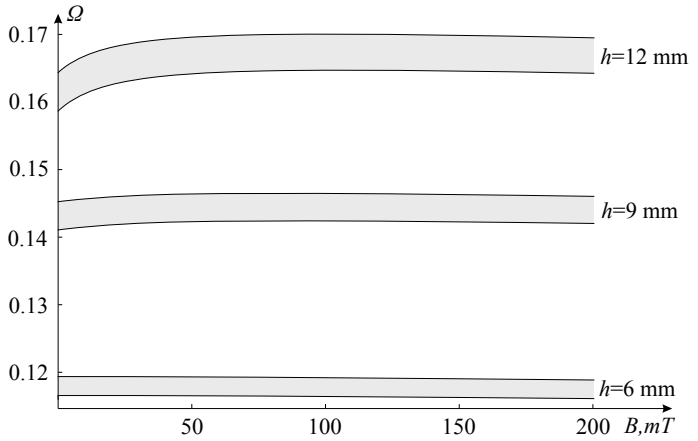

Fig. 5 Main regions of parametric resonance versus the magnetic field induction B for different thickness h_2 of the MRE core

8 Conclusions

Based on the equivalent single layer theory for thin laminated shells, parametric vibrations of laminated non-circular cylindrical shell under non-uniform axial load periodically varying in time were investigates. It was assumed that the reduced shear modulus for a laminated shell is less than the reduced Young's modulus. The non-linear differential equations in terms of displacement and stress functions, taking into account transverse shears, were considered as the governing ones. Using the procedure of linearisation, the non-linear equations were reduced to those describing vibrations of a shell in the neighbourhood of non-stationary membrane stress state.

To study unstable localised parametric vibrations related to the main region of dynamic instability, it was assumed that the excitation frequency is close to one of the natural frequencies corresponding to a localized eigenmode. The asymptotic method of Tovstik in combination with the multiple scales technique was used to predict the dynamic localized response of the shell in the neighbourhood of the weakest generatrix. It was revealed that there exist three different localized modes of parametric vibrations for a thin laminated cylindrical shell subjected to an axial load varying with time. The first type of modes (case A) may be approximated by an exponentially decaying function without any oscillations, the second type of modes (case B) is given by a function which rapidly oscillates and exponentially decreases far away from the weakest line, and the third one (case C) can not be represented by an exponentially decaying function and requires an additional consideration. It was observed that the implementation of one or another form of parametric vibrations of a laminated shell with low reduced shear modulus depends on the ratio of dimensionless shear parameter and wave parameter proportional to a number of waves in the axial direction. Regardless of an expected form of localized parametric vibrations,

we have derived the system of differential equations with periodic coefficients which accounts for transverse shears and is invariant with respect to geometric dimensions, physical parameters, a number of layers and the load distribution law along the shell edge as well. The numerical analysis of this system allowed finding main regions corresponding to both stable and unstable parametric vibrations.

The example considered showed that effect of shear on the main region of parametric resonance depends on both a number of waves on the shell surface and thickness of "soft" layers or core.

References

1. Awrejcewicz, J., Kurpa, L., Mazur, O.: Dynamical instability of laminated plates with external cutout. Int. J. Non-Linear Mech. **81**, 103–114 (2016)
2. Baruch, M.: Parametric instability of stiffened cylindrical shells. Isr. J. Tech. **7**, 297–301 (1969)
3. Bert, C.W., Birman, V.: Parametric instability of thick, orthotropic, circular cylindrical shells. Acta Mech. **71**, 61–76 (1988)
4. Birman, V., Bert, C.W.: Dynamic stability of reinforced composite cylindrical shells in thermal field. J. Sound Vib. **142**(2), 183–190 (1990)
5. Bogdanov, Y., Mazanik, S., Syroid, Y.: Course of differential equations. Universitetskae, Minsk (1996). (in Russia)
6. Bogdanovich, A.E.: Dynamic stability of an elastic orthotropic cylindrical shell with allowance for transverse shears. Polymer Mech. **9**(2), 268–274 (1973)
7. Bogdanovich, A.E.: Dynamic stability of a viscoelastic orthotropic cylindrical shell. Polymer Mech. **9**(4), 626–632 (1973)
8. Bogdanovich, A.E., Feldmane, E.G.: Nonlinear parametric vibrations of viscoelastic orthotropic cylindrical shells. Sov. Appl. Mech. **16**(4), 305–309 (1980)
9. Bolotin, V.V.: Dynamic Stability of Elastic Systems. Gostekhizdat, Moscow. Engl. transl.: Holden-Day, San Francisco 1963, German transi.: Verlag der Wissenshaften, Berlin 1960 (1956). (in Russia)
10. Bondarenko, A.A., Galaka, P.I.: Parametric instability of glass-plastic cylindrical shells. Sov. Appl. Mech. **13**(4), 411–414 (1977)
11. Caughey, T.K.: Subharmonic oscillations of a pendulum. J. Appl. Mech. Trans. ASME **27**(4), 754–755 (1960)
12. Chelomey, V.N.: Dynamic stability of aviation structures. Aeroflot, Moscow (1939). (in Russia)
13. Darabi, M., Darvizeh, M., Darvizeh, A.: Non-linear analysis of dynamic stability for functionally graded cylindrical shells under periodic axial loading. Compos. Struct. **83**(2), 201–211 (2008)
14. Darabi, M., Ganesan, R.: Non-linear dynamic instability analysis of laminated composite cylindrical shells subjected to periodic axial loads. Compos. Struct. **147**, 168–184 (2016)
15. Donnell, L.H.: Beams. Plates and Shells, McGraw-Hill Inc, New York (1976)
16. Grigolyuk, E.I., Kulikov, G.M.: Multilayer Reinforced Shells: Calculation of Pneumatic Tires. Mashinostroenie, Moscow (1988). (in Russian)
17. Kharlamov, S.A.: An example of hetero-parametric excitation of a pendulum by quasi-periodic oscillations of the suspension. Sov. Phys. Dokl. **9**(8), 655–657 (1965). (in Russia)
18. Kochurov, R., Avramov, K.V.: On effect of initial imperfections on parametric vibrations of cylindrical shells with geometrical non-linearity. Int. J. Solids Struct. **49**(3), 537–545 (2012)
19. Kumar, L.R., Datta, P.K., Prabhakara, D.L.: Tension buckling and parametric instability characteristics of doubly curved panels with circular cutout subjected to nonuniform tensile edge loading. Thin-Walled Struct. **42**(7), 947–962 (2004)

20. Machado, S.P., Cortnez, V.H.: Dynamic stability of thin-walled composite beams under periodic transverse excitation. J. Sound Vib. **321**(1), 220–241 (2009)
21. Machado, S.P., Filipich, C.P., Cortnez, V.H.: Parametric vibration of thin-walled composite beams with shear deformation. J. Sound Vib. **305**(4), 563–581 (2007)
22. Markov, A.N.: Dynamic stability of anisotropic cylindrical shells. J. Appl. Math. Mech. **13**(2), 145–150 (1949). (in Russia)
23. Mikhasev, G.I.: Free and parametric vibrations of cylindrical shells under static and periodic axial loads. Tech. Mech. **17**(3), 209–216 (1997)
24. Mikhasev, G.I.: Some problems on localized vibrations and waves in thin shells. In: Altenbah, H., Eremeyev, V.A. (eds.) Shell-Like Structures. Advanced Theories and Applications. CISM International Centre for Mechanical Sciences, vol. 572, pp. 149–209. Springer (2017)
25. Mikhasev, G.I., Botogova, M.G.: Effect of edge shears and diaphragms on buckling of thin laminated medium-length cylindrical shells with low effective shear modulus under external pressure. Acta Mech. **228**, 2119–2140 (2017)
26. Mikhasev, G., Botogova, M., Korobko, E.: Theory of thin adaptive laminated shells based on magnetorheological materials and its application in problems on vibration suppression. In: Altenbach, H., Eremeyev, V. (eds.) Shell-Like Structures. Advanced Structured Materials, vol. 15, pp. 727–740. Springer, Heidelberg (2011)
27. Mikhasev, G., Eremeyev, V., Maevskaya, S., Wilde, K.: Assessment of dynamic characteristics of thin cylindrical sandwich panels with magnetorheological core. Composite Structures (2018). Submitted
28. Mikhasev, G., Mlechka, I.: Localized buckling of laminated cylindrical shells with low reduced shear modulus under non-uniform axial compression. ZAMM **98**(3), 491–508 (2018)
29. Mikhasev, G.I., Tovstik, P.E.: Localized vibrations and waves in thin shells. Asymptotic Methods. FIZMATLIT, Moscow (2009). (in Russia)
30. Mushtari, K., Galimov, K.: Nonlinear theory of thin elastic shells. NSF-NASA, Washington (1961)
31. Ogibalov, P.M., Gribanov, V.F.: Thermostability of plates and shells. Moskov. Universitet, Moscow (1968). (in Russia)
32. Oniashvili, O.D.: On dynamic stability of shells. Soobsch. Akad. Nauk Gruz. **11**(3), 169–175 (1950). (in Russia)
33. Pisarenko, G.S., Chemeris, A.N.: Dynamic stability of a cylindrical shell. In: Dissipation of Energy with the Vibrations of Mechanical Systems (in Russian). Izd. Naukova Dumka, Kiev, pp. 107–114 (1968). (in Russia)
34. Sheng, G.G., Wang, X.: Nonlinear vibrations of FG cylindrical shells subjected to parametric and external excitations. Compos. Struct. **191**, 78–88 (2018)
35. Skalak, R., Yarymovich, M.I.: Sub-harmonic oscillations of a pendulum. J. Appl. Mech. Trans. ASME **27**, 159–164 (1960)
36. Sofiyev, A.H., Kuruoglu, N.: Determination of the excitation frequencies of laminated orthotropic non-homogeneous conical shells. Compos. Part B Eng. **132**, 151–160 (2018)
37. Udar, R.S., Datta, P.K.: Parametric combination resonance instability characteristics of laminated composite curved panels with circular cutout subjected to non-uniform loading with damping. Int. J. Mech. Sci. **49**(3), 317–334 (2007)
38. Vijayaraghavan, A., Evan-Ivanowski, R.M.: Parametric instability of circular cylindrical shells. Trans. ASME E **34**(4), 985–990 (1967)
39. Vol'mir, A.S., Smetanina, L.N.: Dynamic stability of glass-reinforced plastic shells. Polymer Mech. **4**(l), 79–82 (1968)
40. Wenzke, W.: Die dynamische Stabilitat der axialpulsierend belasteten Kreiszylynderschale. Wiss. Z. Techn. Hochschule Otto von Queriscke Magdeburg. Bd. **7**(1), 93–124 (1963)
41. Wlassow, W.S.: Nonlinear Theory of Thin Elastic Shells. Akademie-Verlag, Berlin (1958)
42. Yao, J.C.: Dynamic stability of cylindrical shells and static and periodic axial and radial loads. AIAA J. **1**(6), 1391–1396 (1963)
43. Yao, J.C.: Nonlinear elastic buckling and parametric excitation of a cylinder under axial loads. Trans. ASME **32**(1), 109–115 (1965)

Numerical Analysis of Free Vibration of Laminated Thin-Walled Closed-Section Shell Structures

Bartosz Miller, Barbara Markiewicz and Leonard Ziemiański

Abstract The paper presents dynamic analysis of thin-walled laminated elements with two types of a closed-section: circular and rectangular. The studies are carried out using numerical tube and box shaped shell models with arbitrary laminate stacking sequences. Numerical results in a form of natural frequencies and corresponding mode shapes are obtained to investigate the effects of fiber angle change on the vibration of the structure. Moreover, the influence of boundary conditions, internal diaphragms and slenderness of a structure on natural frequencies and mode shapes of selected cases are also analyzed.

1 Introduction

Civil engineering, like many other engineering fields, e.g. aircraft engineering, is facing the necessity of permanent application of new materials: strong, light and durable. New types of usual and well-known materials like steel or concrete are still being introduced, but it is not enough for the modern engineering and the requirements of engineering structures. On the other hand, composite materials, which exhibit desired high ratio of strength to weight, high durability and the ease of forming various shapes can be answer to those needs.

Although composites have been known and applied for many years in various areas, including civil engineering structures, some of their properties have not been widely investigated. Composite structures are slender and light in comparison to both steel and concrete structures, their dynamic behaviour may be significantly different, its understanding may be crucial in the application of composite materials in structural engineering.

Many researchers studied dynamic behavior of thin-walled closed-section multilayered elements and the influence of various factors on their natural frequencies and corresponding mode shapes [4–7]. Due to the material anisotropy, the composite

B. Miller (✉) · B. Markiewicz · L. Ziemiański
Faculty of Civil and Environmental Engineering and Architecture, Rzeszow University of Technology, ul. Poznanska 2, 35959 Rzeszow, Poland
e-mail: bartosz.miller@prz.edu.pl

H. Altenbach et al. (eds.), *Recent Developments in the Theory of Shells*,
Advanced Structured Materials 110, https://doi.org/10.1007/978-3-030-17747-8_25

elements exhibit axial, flexural and torsional vibrations fully coupled even for doubly symmetric cross-sections [1, 3, 8, 9]. The chapter presents a numerical study of free vibrations of a laminated tube and box shaped elements with different laminate fiber angles and overall element length.

2 Numerical Analysis

2.1 Box Shaped Shell

First calculation case is a shell model of a thin-walled box beam with cross-sectional dimensions 700 × 1000 mm. These dimensions are similar to the composite girders of the existing bridge in Blazowa (Poland). The shell webs consist of four computational 4 mm-thick layers composed of several laminas of the same material characteristics and the same fiber angles (Fig. 1). The material properties are based on [9]: $E_1 = 141.9$ GPa, $E_2 = 9.78$ GPa, $\nu_{12} = 0.42$, $G_{12} = 6.13$ GPa and $\rho = 1445$ kg/m^3.

Three variants of boundary conditions are considered: clamped (cc), pinned (pp) and cantilevered (c) structure, for a span of 12 m and 24 m. The boundary conditions are defined on the shell edges by fixing the translation in all xyz directions of bottom edge while pinned and all the edges for clamped boundary.

The investigated cases of stacking sequences are:

- all the layers have the same fiber angle: 0, 15, 30,45, 60, 75, 90,
- stacking sequences consisted of two layers with 0 and two layers with 45 ply orientation: $[0_2/45_2]$, $[45_2/0_2]$, $[0/45_2/0]$, $[45/0_2/45]$, [0/45/0/45] and [45/0/45/0],
- variants with 0 ply orientation of all the layers in webs and 45 in the flanges and conversely.

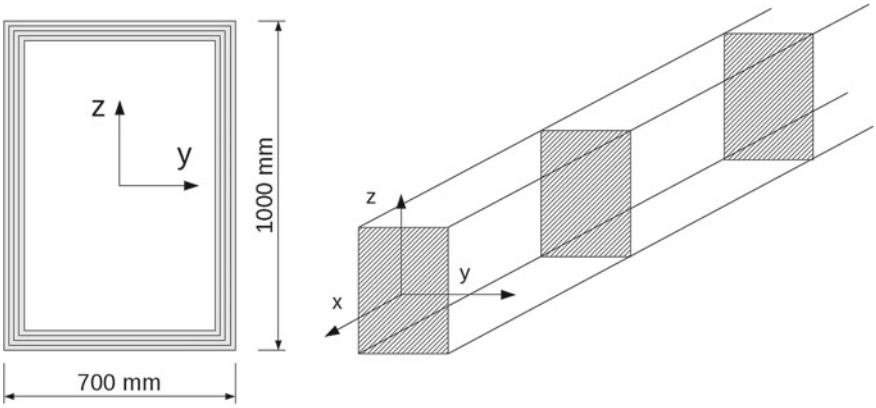

Fig. 1 Box cross-section and shell model of the box with diaphragms

Additional analysis is conducted for a box shell with 16 mm-thick internal diaphragms of [0_4] ply orientation (Fig. 1), located every 2 m along the length of the structure and at its edges. The calculations are also performed for different stiffness of the diaphragm defined by the Young's modulus, whereas their mass is omitted. The influence of diaphragms on the natural frequency and corresponding forms is studied.

2.1.1 Numerical Results

The modal parameters of all the shell models described in this paper were obtained using commercial FE code ADINA [2]. The results are in form of natural frequencies and types of their dominant corresponding mode shapes.

Effect of fiber angle

First, the effect of the fiber angle of all the layers on the natural frequencies of a box shell is analyzed. The mode shapes are coded as follows: BH—horizontal bending, BV—vertical bending and T—twisting. The boundary conditions coding is explained above.

It is worth mentioning that the mode shapes types are determined by the dominant component and each subsequent form of vibrations is more difficult to classify due to appearance of coupling. This phenomenon is stronger in the case of a more stocky beam (with a span of 12 m).

Figure 2 illustrates the result for a 24 m long structure with various boundary conditions. In each mode the natural frequency is normalized with respect to the value

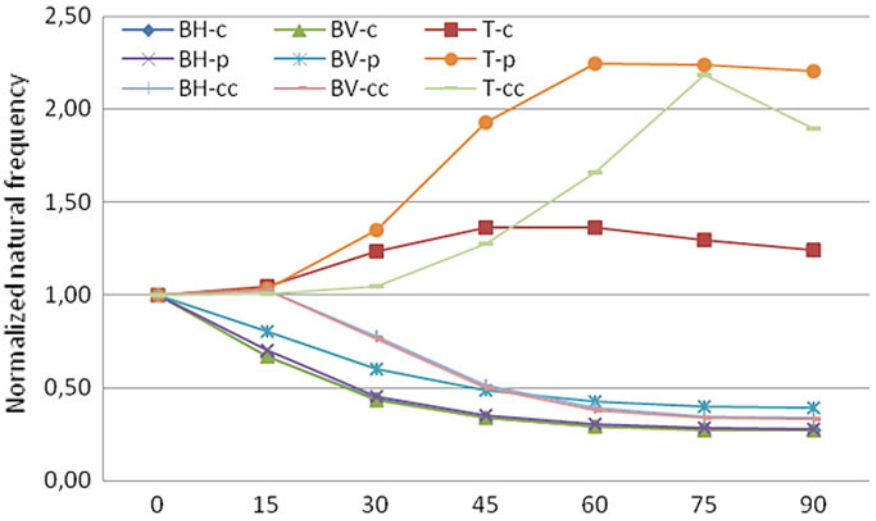

Fig. 2 Variation of the normalized natural frequencies of a 24 m long cantilever (c), pinned (p), clamped (cc), box shell with respect to fiber angle change

for [0] angle for that mode. It can be clearly observed that vertical and horizontal flexural frequencies decrease for a fiber angle from 0 (15 in case of clamped beam) to 60 degrees to about 0.3–0.4 of their initial values. On the other hand, torsional vibration frequencies are not changing monotonically, but at certain values of the fiber angle they reach their extreme. In case of cantilever, the maximum value is reached for 45–60 degrees and it is 1.4 of its initial value. For pinned and clamped shells the value reaches 2.2 for 60 and 75 degrees respectively.

Figure 3 presents comparison of natural frequencies of two cantilever box shells of different slenderness. All the vertical and horizontal flexural frequencies decrease for angle from 0 to 60. In the range of 60–90 degrees no significant changes are visible. Torsional vibration frequencies increase for an angle of 0 to about 60 degrees. In the range of 60–90 degrees they decrease, but in a lower extent. In the case of a 12 m long box shell the torsional vibration frequency is more than twice as big as its initial value, for more slender box the upper value is much smaller.

Another stage of the analysis is the comparison of different stacking sequences consisted of two layers of 0 degrees and two layers of 45 degrees and with so called Circumferentially Uniform Stiffness (CUS).

Identical results are obtained for the fiber orientations $[0/45_2/0]$ and $[45/0_2/45]$ (Tables 1 and 2). Minor differences (up to 0.5 Hz) are noted for the lay-ups [0/45/0/45] versus [45/0/45/0] and $[0_2/45_2]$ versus $[45_2/0_2]$.

In the case of a box shell with a span of 12 m, the first two frequencies do not change significantly for all cases. Symmetrical stacking sequences of the webs and flanges (cases $[0/45_2/0]$ and $[45/0_2/45]$) cause their greater stiffness. The more the layers are differentiated with respect to the webs and flanges local axes, the lower is their stiffness.

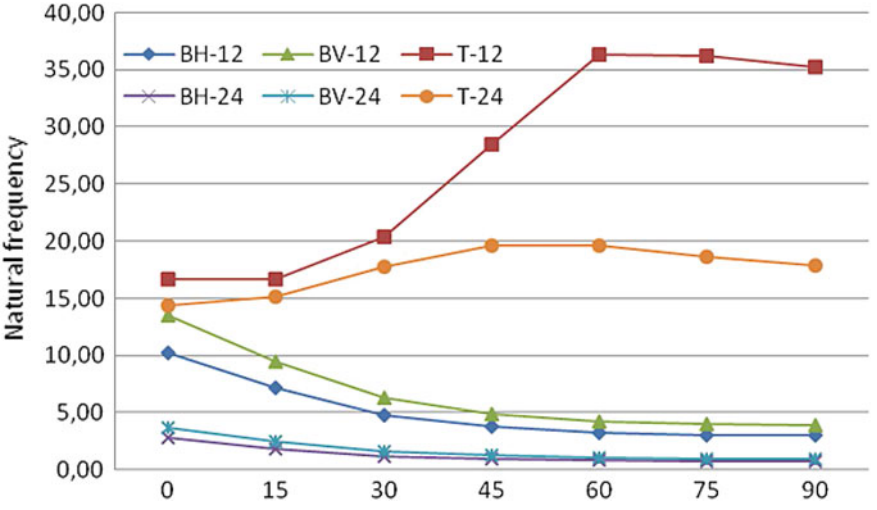

Fig. 3 Variation of the natural frequencies of a 12 m and 24 m long cantilever box shell with respect to fiber angle change

Table 1 Natural frequencies of 12 m long cantilever box shell for different CUS lay-ups [Hz]

Length - 12 m	$[45_2/0_2]$	$[0_2/45_2]$	$[0/45_2/0]$ $[45/0_2/45]$	[0/45/0/45]	[45/0/45/0]
BH1	8.2	8.1	8.3	8.2	8.3
BV1	10.8	10.7	10.9	10.8	10.9
BH2	34.9	34.8	40.0	37	37.4
BV2	20.1	20.1	28.6	23.6	23.6
T1	51.9	52.7	56.1	54.7	54

Table 2 Natural frequencies of 24 m long cantilever box shell for different CUS lay-ups [Hz]

Length - 24 m	$[45_2/0_2]$	$[0_2/45_2]$	$[0/45_2/0]$ $[45/0_2/45]$	[0/45/0/45]	[45/0/45/0]
BH1	2.1	2.1	2.1	2.1	2.1
BV1	2.8	2.8	2.8	2.8	2.8
BH2	12.6	12.4	12.7	12.6	12.7
BV2	16.6	16.4	16.6	16.5	16.6
T1	18.7	18.7	23.0	21.2	21.2

In the case of a slender box shell (24 m) all the analyzed natural frequencies are very similar. The shells with asymmetrical (unbalanced) webs and flanges present lower torsional natural frequencies.

Next, natural frequencies for different fiber angles in the webs and flanges are analyzed. Table 3 compares the results for two stacking sequences and two lengths. Code fλ_1-wλ_2 means λ_1 ply orientation of all the layers in flanges and λ_2 in the webs. When the flanges are stiffer than the webs (f0-w45), horizontal and vertical flexural natural frequencies diverge. When the webs are stiffer (f45-w0), the torsional natural frequencies are lower.

Table 3 Natural frequencies of 12 m and 24 m long cantilever box shells for different stacking sequences in webs and flanges [Hz]

	12 m f0-w45	12 m f45-w0	24 m f0-w45	24 m f45-w0
BH1	5.9	9.8	1.5	2.6
BV1	12.1	9.0	3.1	2.3
BH2	29.5	34.1	9.0	14.5
BV2	55.1	45.1	18.2	13.7
T1	21.1	18.6	19.0	16.6

Effect of diaphragms

The aim of this analysis is to assess the influence of the diaphragms on the natural frequencies of a box shell of variable slenderness and boundary conditions. The (d) columns refer to models stiffened with diaphragms.

The results presented in Tables 4 and 5 show that adding the diaphragms not always causes the increase of natural frequencies. Therefore the analysis was extended to weightless diaphragms of different stiffness defined by the Young's modulus.

The graphs presented in Figs. 4 and 5 (logarithmic scale is used) show that the impact of diaphragms on each next frequency is greater and is much more visible in case of torsional vibration. Not only the boundary conditions and slenderness of the

Table 4 Natural frequencies of 12 m long box shell with $[0_4]$ ply orientation [Hz]

Length - 12 m						
Boundary conditions	cc	cc (d)	pp	pp (d)	c	c (d)
BH1	28.1	35.7	24.2	27.6	10.2	9.7
BV1	43.6	47.3	31.8	32.3	13.5	12.7
BH2	32.4	89.9	32.1	85.3	29.3	38.1
BV2	53.4	109.5	52.6	103.8	46.5	51.9
T1	40.3	68.4	24.8	66.8	16.6	34.8

Table 5 Natural frequencies of 24 m long box shell with $[0_4]$ ply orientation [Hz]

Length - 24 m						
Boundary conditions	cc	cc (d)	pp	pp (d)	c	c (d)
BH1	14.0	13.8	9.9	9.9	2.8	2.6
BV1	18.7	18.0	10.0	9.5	3.6	3.5
BH2	26	30.5	23.5	26.2	14.6	14.4
BV2	38.9	40.2	32.2	32.4	19.6	18.8
T1	18.6	35.0	15.9	34.5	14.3	17.5

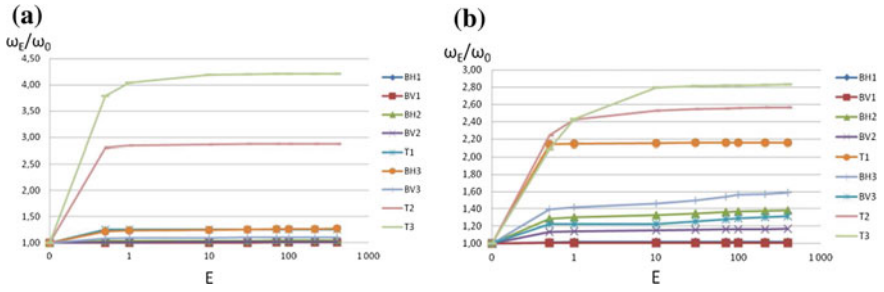

Fig. 4 Variation of the normalized natural frequencies of a **a** 24 m and **b** 12 m long cantilever box shell with $[0_4]$ ply orientation with respect to the Young's modulus of diaphragms material

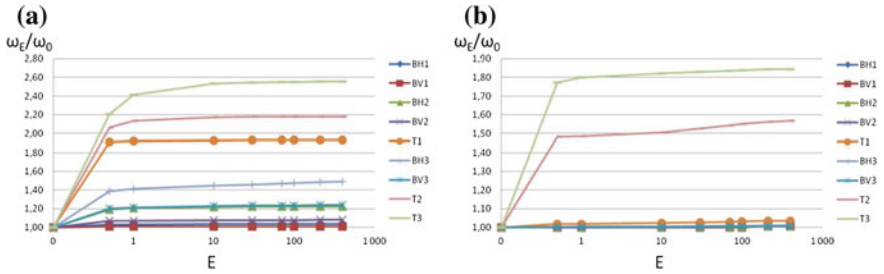

Fig. 5 Variation of the normalized natural frequencies of a 24 m long clamped box shell with $[0_4]$ ply orientation and cantilever with $[45_4]$ ply orientation with respect to the Young's modulus of diaphragms material

element are important, but also the angle of the fibers in the laminate. In the case of 45 degrees ply orientation (Fig. 5b), the impact on the frequency of flexural vibrations is much smaller than for a beam with the same assumptions and fiber positioning along the element. All graphs show the same tendency of initial growth and then independence from diaphragm stiffness.

2.2 Tube Shaped Shell

The second investigated structure is a cantilever tube. Its model is a thin-walled cylindrical shell with a circular cross-section. The diameter of the middle-surface of this circle is R = 0.6103 m. The shell web is 16 mm-thick as before and consists of three or four computational layers of the same thickness (in Fig. 6 exemplary cross-section with four layers is presented). The material properties are same as before. Calculations are performed for three variants of the length of the cantilever: 6, 12 and 24 m.

Three different cases of fiber angles of laminate layers are considered:

- all the layers in all the cross-section quadrants (see red numbers in Fig. 6) are laminated with the same fiber angle, i.e. [30/30/30/30] coded as 30,
- each layer is laminated with a specific fiber angle, the same around the cross-section (CUM), i.e. [0/30/60/90] (starting with the inner layer fiber angle),
- all the layers in the same quadrant show the same lamination fiber angle, but different in next quadrants (described in a quadrants sequence 1,2,3,4); the considered angles are 30/60/-30/-60 (q-30-60), 30/60/-60/-30 (q-60-60) and 45/45/ -45/-45 (q-45-45)

The mode shapes are divided into axial (A), torsional (T), bending (Bm, m = 1, 2, 3,…) and circumferential ones (Cnm, n = 2, 3, 4,…, m = 1, 2, 3,…). Number m means longitudinal mode and n is the number of circumferential wave, see Fig. 6.

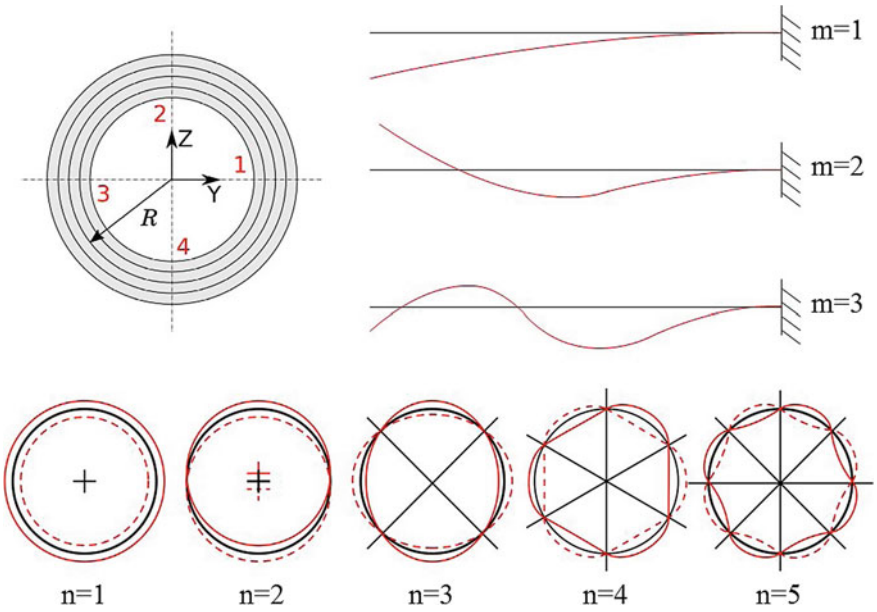

Fig. 6 Tube cross-section and circumferential (n) and longitudinal (m) modes

2.2.1 Numerical Results

Effect of fiber angle

Table 6 presents the changes of the first 11 natural frequencies with respect to different fiber angle of all the layers of 24 m long cantilever.

Figures 7, 8 and 9 present the normalized natural frequencies with respect to

Table 6 Natural frequencies of 24 m long cantilever tube shell for different fiber angles [Hz]

	0	15	30	45	60	75	90
f_1	4.01	2.68	1.74	1.35	1.18	1.11	1.09
f_2	4.01	2.68	1.74	1.35	1.18	1.11	1.09
f_3	14.08	14.93	10.71	8.34	7.27	6.81	6.68
f_4	14.08	14.93	10.71	8.34	7.27	6.81	6.68
f_5	16.13	15.97	19.05	22.79	19.88	18.58	18.21
f_6	16.13	15.97	19.05	22.79	19.88	18.58	18.21
f_7	21.29	16.22	20.90	22.82	22.86	22.08	21.46
f_8	21.29	16.22	20.90	27.45	32.66	28.03	27.10
f_9	21.46	21.60	22.30	27.45	37.73	35.15	34.39
f_{10}	24.92	21.60	23.89	29.54	37.73	35.15	34.39
f_{11}	24.92	21.71	23.89	29.54	38.19	48.11	53.25

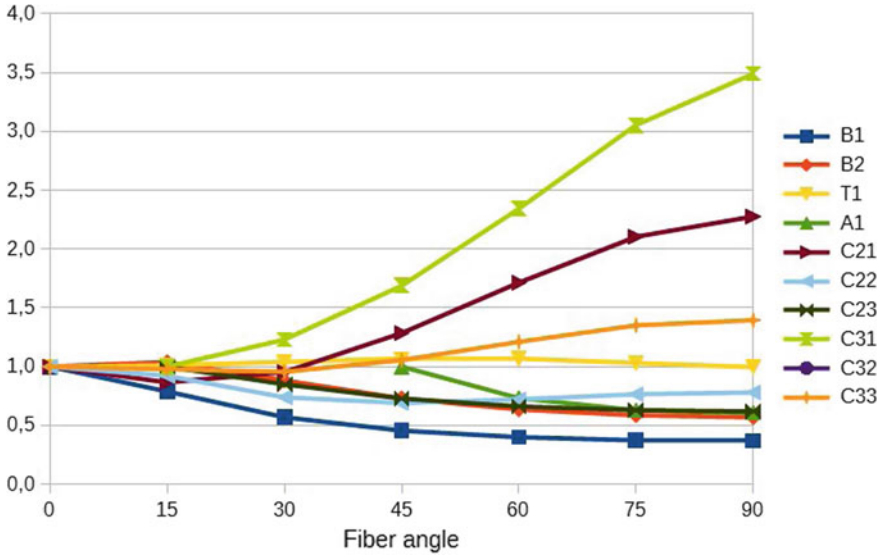

Fig. 7 Variation of the normalized natural frequencies of 6 m long tube with respect to fiber angle change

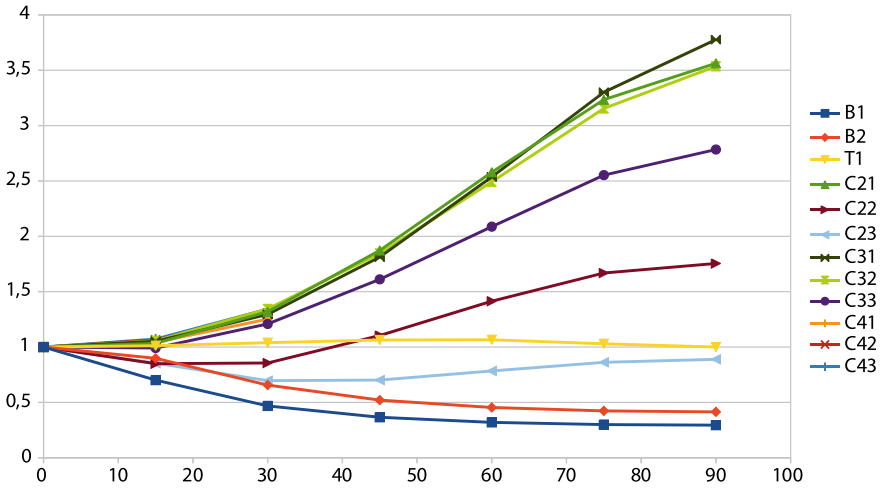

Fig. 8 Variation of the normalized natural frequencies of 12 m long tube with respect to fiber angle change

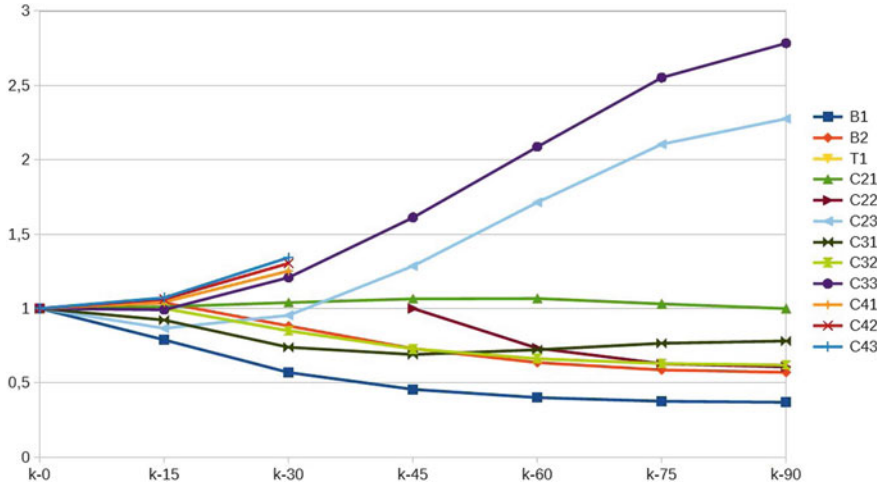

Fig. 9 Variation of the normalized natural frequencies of 24 m long tube with respect to fiber angle change

fiber angle values. The effect of the fiber angle change on the natural frequencies is clearly visible. For the investigated fiber angles some of the natural frequencies change dramatically, i.e. in Fig. 7 (l = 6 m) C31 increases more than three times, even higher is for 12 m long element, see Fig. 8. On the other hand, for 24 m long cantilever C33 increases the most (Fig. 9).

An additional element of the effect of the fiber angle studies is the analysis of the simultaneous variation of fiber angle in two layers for a three-layered tube shell (thickness is still 16 mm).

Figure 10 shows the natural frequencies change according to the fiber angle of two outer layers when ply orientation of the middle one is constant and equals 0. The torsional vibration frequency reaches its maximum for angle 45 and −45 degrees, the difference between extreme values is almost 100 Hz. The natural frequency for bending has its maximum for about 18 degrees fiber angle of outer layers. Shape of the C22 graph looks quite similar to B1, but other three analyzed circumferential vibrations frequencies increase both sides from the value of 0 degrees.

Figure 11 presents the surface graphs of the natural frequencies change of a three layered tube with stacking sequence $[\lambda_1/\lambda_2/\lambda_3]$ with respect to the two different variable fiber angles of two layers and one layer with constant fiber angle, defined above each graph. In case of C21 mode shape (see Fig. 11f–h), the natural frequency is the highest on the edges of the graph surface, what means that 90 degrees is the best possible fiber angle to stiffen tube shell for this type of vibration. What is more, ply orientation of the middle layer has no significant influence in this case (Fig. 11g). Another interesting conclusion is that the surface graph of exemplary other circumferential vibration frequency—C22 (Fig. 11e) looks completely different.

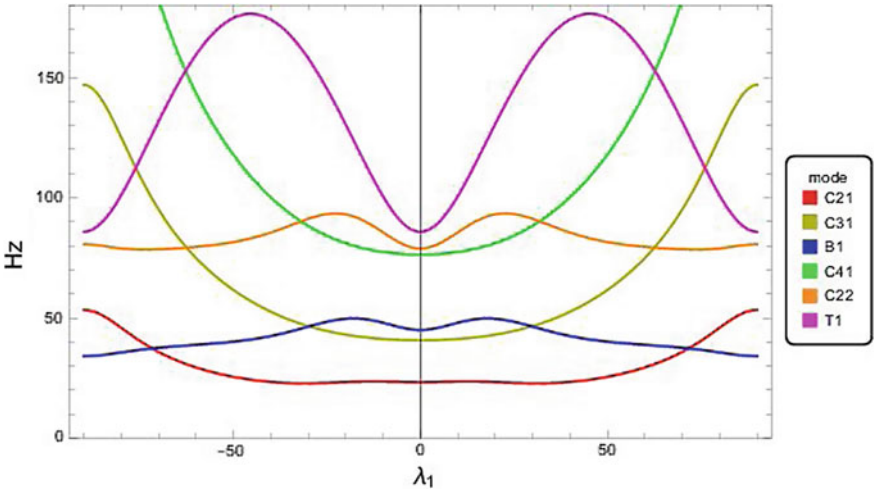

Fig. 10 Variation of the natural frequencies of a three layered, 6 m long tube with stacking sequence $[\lambda_1/0/\lambda_1]$ with respect to changeable fiber angle of two outer layers

Next, the torsional vibration frequency (Fig. 11b, d) reaches its maximum value for fiber angle of 45 degrees. For middle layer of 45 degrees ply orientation it is better to have opposite oriented fibers in outer layers, what gives [-45/45/-45] stacking sequence. And with $\lambda_2 = 0$ the best combinations are [-45/0/45] and [45/0/-45]. And the last discussed case, flexural vibration frequency is the highest for fiber angles near 0 of the opposite sign in Fig. 11a, but when the middle layer is 0 degrees oriented, the maximum value is not reached at 0 degrees (Fig. 11c).

Multiple mode shapes and mode shapes coupling

The mode shapes of cantilever tube shell are multiplied (usually doubled), this phenomenon is illustrated in Table 6 and part of the Table 7 with CUM lay-ups, comparing the 1st and the 2nd natural frequencies, the 3rd with the 4th, and so forth. For quadrants laminations (q-30-60 and q-45-45) these frequencies split due to non-symmetry of the cross-section.

Moreover, some of the free vibration mode shapes are coupled, an example is shown in Fig. 12 presenting coupled circumferential mode with 4th circumferential wave and 1st mode shape in tube axial direction (Fig. 12a) and coupled axial mode shape and circumferential wave (Fig. 12b).

3 Conclusions

As shown in the chapter the lamination fiber angle significantly influences free vibrations of a layered shell.

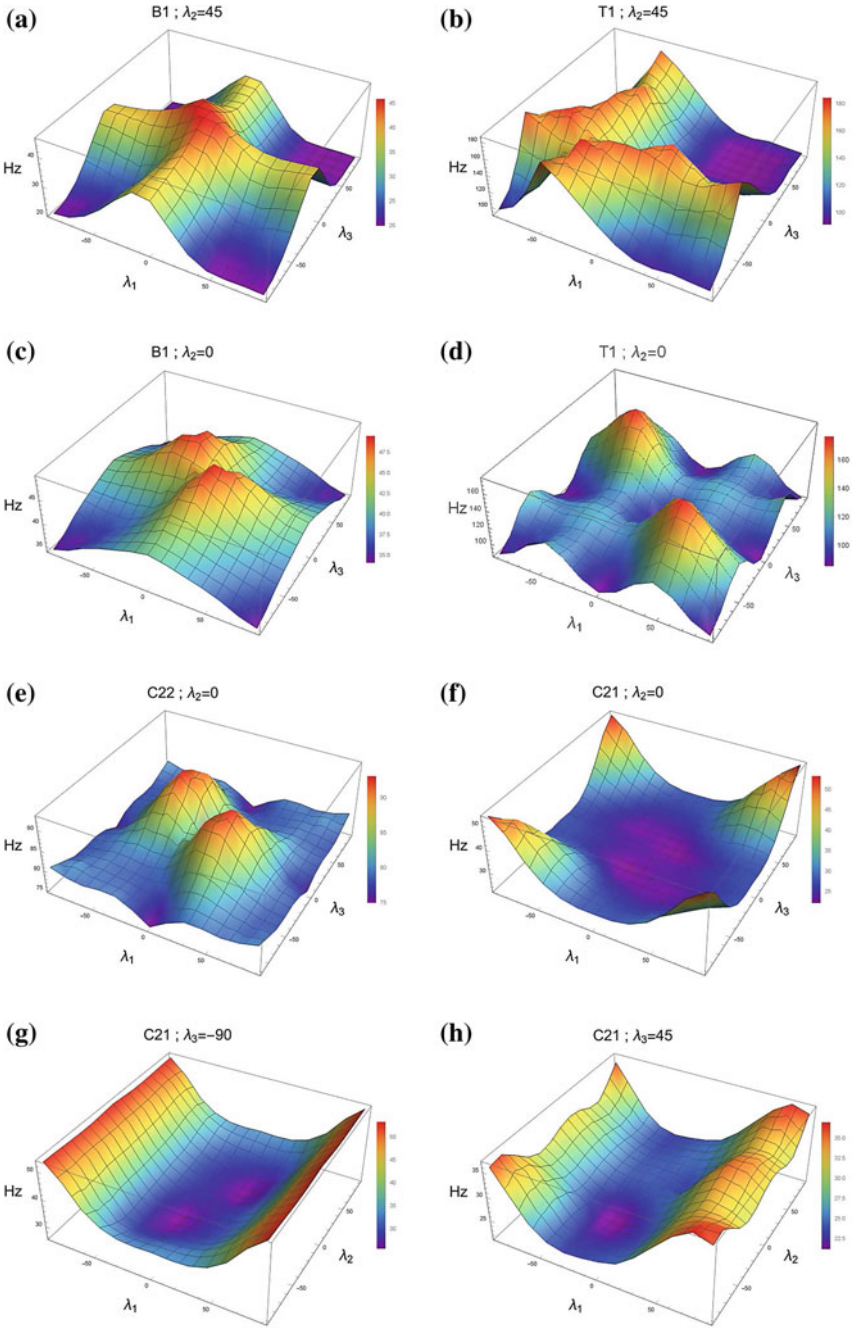

Fig. 11 Variation of the natural frequencies of a three layered tube with stacking sequence $[\lambda_1/\lambda_2/\lambda_3]$ with respect to changeable fiber angle of two layers

Table 7 Natural frequencies splitting due to non-symmetrical lamination fiber angles, l = 12 m

	0	45	90	[0/15/75/90]	[0/30/60/90]	[0/45/45/90]	q-45–45	q-30–60
f_1	14.62	5.35	4.30	10.61	9.72	9.28	5.37	5.20
f_2	14.62	5.35	4.30	10.61	9.72	9.28	5.39	6.55
f_3	14.95	28.00	25.22	25.01	24.19	25.79	29.50	25.27
f_4	14.95	28.00	25.22	25.01	24.19	25.79	29.98	28.70
f_5	30.73	31.71	42.91	31.71	29.69	30.65	31.46	30.36
f_6	30.73	31.71	53.26	31.71	29.69	30.65	31.50	30.69
f_7	40.34	33.93	53.26	49.24	53.80	52.53	32.39	33.14
f_8	40.34	33.93	53.93	54.29	53.80	52.53	32.44	36.45
f_9	42.91	45.64	53.93	54.29	54.56	53.98	43.57	43.81
f_{10}	43.13	45.92	54.20	57.63	54.56	53.98	43.97	44.91
f_{11}	43.13	45.92	58.18	57.63	59.44	63.62	61.35	59.15
f_{12}	54.95	68.90	58.18	70.78	68.51	72.13	65.01	66.05
f_{13}	54.95	68.90	64.66	70.78	68.51	72.13	65.45	67.63

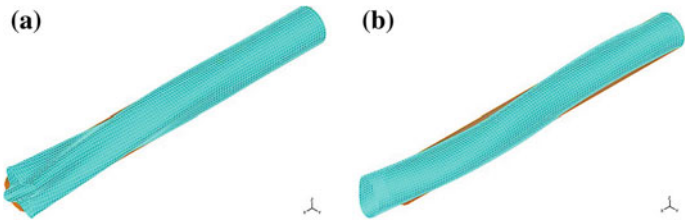

Fig. 12 **a** C41-Circumferential mode with 4th circumferential wave and 1st mode shape in tube axial direction, **b** A1-1rst axial mode with 2nd circumferential wave, l = 12 m

In both considered cases flexural vibration frequencies decrease in the entire range 0–90, regardless of shape, boundary conditions and length, same with axial vibration frequencies for tube-shaped laminate.

On the other hand, torsional vibration frequencies depends on many factors. They do not change in a monotonic manner, but at certain values of the fiber angle they are extreme. They also depend on the lay-up of individual layers in the whole laminate.

Interesting results can be obtained by changing the fiber angle of two layers simultaneously. It gives many possibilities in designing the dynamic response of the element.

The oblique lamination in case of tube-shaped shell implies mode shapes coupling between planes of bending, between flexural and circumferential vibrations (n = 1 and n = 2, 3, 4) and between flexural and axial vibrations.

Circumferential vibration frequencies behave inconsistently, some of the circumferential frequencies increase while the others decrease with the lamination fiber angle increase. Finally, non-symmetrical lamination fiber angles (i.e. q-30-60) causes natural frequencies splitting, see Table 7.

The additional diaphragms in box-shaped laminated shell cause the relatively small increment of flexural and much higher increment of torsional vibration frequencies. The natural frequencies increase rapidly for small Young's modulus and then with further growth of E no significant changes are visible. The impact of diaphragms grows for higher natural frequencies. In some cases the impact of diaphragm stiffeness can be smaller than the impact of its weight (more probable for cantilever).

References

1. Armanios, E., Badir, A.: Free vibration analysis of anisotropic thin-walled closed-section beams. AIAA J. **33**(10), 1905–1910 (1995)
2. Bathe, K.: ADINA: Theory and Modeling Guide Volume I: ADINA Solids & Structures. Watertown: ADINA R&D, Inc (2016)
3. Dancila, D., Armanios, E.: The influence of coupling on the free vibration of anisotropic thin-walled closed-section beams. Int. J. Solids Struct. **35**(23), 3105–3119 (1998)
4. Lopatin, A., Morozov, E.: Fundamental frequency of a cantilever composite cylindrical shell. Compos. Struct. **119**, 638–647 (2015)
5. Nayfeh, A., Pai, P.: Linear and nonlinear structural mechanics. Wiley, Hoboken (2004)
6. Quatu, M.S., Sullivan, R.W., Wang, W.: Recent research advances on the dynamic analysis of composite shells: 200-2009. Compos. Struct. **93**(1), 14–31 (2010)
7. Reddy, J.N.: Mechanics of Laminated Composite Plates and Shells: Theory and Analysis. CRC Press, Boca Raton (2004)
8. Vo, T.P., Lee, J.: Free vibration of thin-walled composite box beams. Compos. Struct. **84**(1), 11–20 (2007)
9. Vo, T.P., Lee, J., Ahn, N.: On six fold coupled vibrations of thin-walled composite box beams. Compos. Struct. **89**(4), 524–535 (2009)

Abnormal Buckling of Thin-Walled Bodies with Shape Memory Effects Under Thermally Induced Phase Transitions

Dmitry V. Nushtaev and Sergey I. Zhavoronok

Abstract Buckling and postbuckling of thin-walled structures made from the Nickel-Titanium shape memory alloy and undergoing non-isothermal direct martensite transitions under varying temperatures are simulated. The once coupled Movchan's model of thermo-elastic shape memory alloy behavior is represented in the incremental formulation for the use within numerical algorithms of nonlinear solid mechanics. The equilibrium state's bifurcation is studied on the background of Lyapunov's stability concept. The physically and geometrically nonlinear solid model allows one to study the martensite phase distribution over the cross-section as well as along the structure during its' buckling and postbuckling deforming. It is shown that the direct martensite transition induced by temperature changes and heterogeneous stress fields in compressed prismatic beams with initial imperfections causes the buckling phenomenon. The obtained results are consistent with the analytical predictions of A.Movchan and L.Silchenko assuming the supplementary phase transform occurring everywhere in accordance with the extended Shenley concept. Thus, the fundamental assumption about decisive contribution of martensite phase transitions in the buckling of thin-walled structures of shape memory alloys is vindicated.

1 Introduction

Shape memory alloys (SMA) undergo phase transitions and structure transforms under varying temperature and stress fields caused by combined mechanical, electrical and thermal excitation [25, 41, 78, 107]. The thermo-elastic phase transitions

D. V. Nushtaev
PAO Severstal, 127299 Klara Zetkin ul. 2, Moscow, Russia
e-mail: nyshtaev.vfb@rambler.ru

S. I. Zhavoronok (✉)
Institute of Applied Mechanics of Russian Academy of Sciences,
125040 Leningradskiy prosp. 7, Moscow, Russia
e-mail: Zhavoronok@iam.ras.ru

H. Altenbach et al. (eds.), *Recent Developments in the Theory of Shells*,
Advanced Structured Materials 110, https://doi.org/10.1007/978-3-030-17747-8_26

[7, 38] of the high-modulus austenite into the low-modulus martensite (direct martensite transform, hereinafter referred to as $A \rightarrow M$) or vice versa (inverse martensite transform, $M \rightarrow A$) and structural transforms of the martensite crystals result in very specific behavior of SMA such as high amplitude reversible strains, high amplitude reaction stresses generated in constrained elements under heating, and the "shape memory" phenomenon proper, i.e. form recovery after inelastic deforming and further heating. One of the most widely used SMA so-called "Nitinol" is based on the Titanium-Nickel system [6, 29]. The unique properties allow one to use NiTi SMA in aeronautics [23, 25, 42], robotics [101], biomedicine [79, 100], etc. as various actuators, bearing elements, dampers, and many other devices (e.g. see [25, 42]). One of applications of SMA consists in the buckling protection of thin-walled composite structures [105] by embedded NiTi fibers [4, 28, 39] or wires [8, 39, 77] as well as in the postbuckling deflections reduction [104] in statics and dynamics [37, 80, 103].

At the same time the buckling of thin-walled SMA elements in itself was almost not studied even though many SMA devices are operating under compressive stresses. Some results were obtained for compressed SMA columns [26, 27, 85–88, 106] in the pseudoelasticity regime (i.e. stress-induced *isothermal* phase transition). Another buckling regime is usually considered as effect of high-level compressive reaction stresses generated in firstly pre-strained and secondly constrained SMA elements under heating; this effect so-called "constrained shape memory" [44] was studied for circular plates [30], for arched beams [31, 44] and for spherical shell segments [32] to investigate their snap-through instability and to develop cutoff valves [33]. On the other hand, the buckling of SMA beams under the *non-isothermal* $A \rightarrow M$ and compressive forces about 0.1…0.2 Eulerian critical forces corresponding to the minimum (i.e. pure martensite) elasticity modulus was observed experimentally by Movchan et al. [60, 72]. It was found that an axially compressed completely austenite SMA beam being cooled through the temperature range of $A \rightarrow M$ buckles before reaching the entirely martensite state. Moreover it was found that the analogous buckling instability exists even for unconstrained completely martensite beams being compressed and heated through the $M \rightarrow A$ temperature range, i.e. during the phase transition resulting in significant raising of elastic moduli (up to pure austenite modulus), nevertheless the critical force remains about 0.15…0.2 Eulerian one corresponding to the martensite modulus (e.g. see [53, 60]).

It was supposed that the phase transition itself initiates the buckling, neither modulus change nor reaction stress. Movchan and Silchenko have proven that the buckling of mechanical systems undergoing thermomechanical phase transitions can be described only by coupled models [61]. Such a theory requires simplifying assumptions to be used together with the linearized bifurcation criteria. It was shown that the known von Kármán and Shenley buckling concepts can be modified to be consistent with shape memory systems undergoing direct transforms [62, 63, 91, 95], inverse transforms [62, 65, 69, 92, 93] or structural transitions [54, 90, 97]. On the one hand the extended von Kármán buckling concept assumes that the only a part of the cross-section undergoes the supplementary phase transition induced by small perturbations of the initial equilibrium form while the cross-section rest undergoes

the elastic unloading [61, 62]. The boundary of the phase transition domain should be found after the constant load condition. This concept so-called "constant load" results in the higher critical stress estimate. On the other hand the extended Shenley concept allowing small variations of the load synchronous with the equilibrium state perturbation results in two extreme cases. The first one consists in the assumption of the "supplementary phase transition occurring everywhere (in the cross-section)" and leads to the lower critical stress estimate whereas the second one results in the trivial situation, i.e. in the absence of the supplementary phase transition synchronous with the equilibrium perturbation. It can be shown that the last concept so-called "assumption of constant phase constitution" leads to the estimate for the critical stress based on the minimum elastic modulus, i.e. it is inconsistent with the obtained experimental results [60]. The mentioned buckling concepts are required to obtain suitable bifurcation criteria based on the linearized SMA statics problem formulation for SMA beams [62, 63, 65, 69, 91–93, 95], shafts [52], plates [64, 66–70, 73, 94, 96], and finally for shells [71, 98]; moreover, they allow one to take into account the rheonomic SMA behavior [34] and to use twice coupled SMA models considering the latent heat absorption (e.g. see [75]).

Strictly speaking, the buckling of thin-walled SMA systems undergoing phase and structure transitions must be analyzed using the appropriate theory of stability of deformation processes and not the static equilibrium criteria. Indeed, the phase and structure transforms occurring in SMA beams, plates, or shells under constant loads and homogeneous temperature fields result in the phase strain accumulation process that can become instable with respect to small perturbations and, finally, in the bifurcation of the equilibrium state. The stability of two-phase states of a solid with respect to phase constitution perturbations was investigated in [18, 20, 89] on the background of the movable sharp phase interface concept of Gibbs [21], the non-uniqueness of solutions was proven and their stability was studied in details. Nevertheless, the effect of phase transforms on the bifurcation of the equilibrium of SMA systems still remains an open question, especially for non-isothermal transitions. An analytical solution based on the Lyapunov theory remains almost impossible whereas the equivalence of static buckling criteria and strong stability theories of deformation processes is not yet proven even for elastic-plastic media, moreover it is not established for SMA. Thus, the numerical analysis of buckling and postbuckling deforming of SMA systems without applying Shenley's or von Kármán's assumptions becomes a possible way of the vindication of analytical estimates using the linearized bifurcation criteria. For instance, the non-linear three-dimensional finite element modelling of axially compressed prismatic SMA beams with initial imperfections being cooled through the $A \rightarrow M$ temperature range [76] resulted in the critical forces close to the predictions based on the extended Shenley concept.

Only a few number of appropriate models of thin-walled structures accounting for diffusionless solid state phase transitions exist nowadays. The first models were developed for thin films and correspond to membrane models with vanishing bending stiffness [5, 24]. One of the first shell theories accounting for the phase transitions based on the sharp phase interface concept [21, 22, 50] was proposed by Eremeyev and Pietraszkiewicz [12] on the background of the statically exact (in terms of stress

and couple resultants) shell model with energetically exact intrinsic kinematics as provided by Simmonds [99], Libai and Simmonds [40], Altenbach and Zhilin [1], Chróścielewski et al. [9]. Only elastic isothermal phase transitions were considered, the dependency of the phase constitution on the temperature was neglected, therefore the problem was formulated as a stationarity condition for the total energy. The continuity conditions at the phase interface curve were obtained in [13, 19], and the strain energy density of the phase interface as well as capillary phenomena at the interface have been taken into account in [84]. The general jump conditions at the interface in two-dimensional solid systems were later defined in [35, 36] on the basis of the resultant shell thermomechanics of Pietraszkiewicz [81] being an extension of Simmonds [99]. The analysis of superelastic behavior of cylindrical shells was performed, and the existence of boundary layers near the interface curves was shown [15]. The proposed approach was extended by considering inelastic thin-walled bodies with propagating sharp phase interfaces [11] were the local balance equations at the interface were deduced for stress-induced phase transforms. The complete theory of viscoelastic two-phase shells was presented in [14, 17] where the homogeneous extension of a material resulted by phase transforms was assumed. The further development consisted in the accounting for the temperature effect in [16] where the temperature field on the base surface was subdivided into the sum of the reference field and its variation; the surface entropy inequality was constructed and the thermodynamic continuity conditions was proposed as well as the kinetic equation defining the quasi-static motion of the phase interface. Analogous approaches based on the sharp interface concept were used earlier to model the buckling instability of systems undergoing the phase transitions of the first kind [111], in particular, for plates [109] and Cosserat's elastic bodies [110].

Let us note nevertheless that the Gibbs concept used in the works cited above assumes the existence of sharp phase interfaces. Strictly speaking, such a model corresponds to single crystal alloys with a single phase interface. In general, two different interfaces should be considered in SMA, the one of the beginning of the phase transition and the other of its' end with mixed phase constitution between them [45, 51, 57, 58] as a result of the diffuse phase transform (so-called "smeared phase transitions", [43]). At the same time the models considering the phase volume ratio $q \in [0, 1]$ as a supplementary field variable (e.g. [56, 73] etc.) lead to the results consistent with the test data, moreover they can be easier implemented in the practice because "…these theories omit the stage in which the interface is explicitly considered which…avoids the need to solve problems with unknown boundaries" [18, p. 62]. It must be also noted that the detailed analysis of the phase transition effect on the buckling of SMA systems requires three-dimensional distributions of stress, strains, and phase concentration parameters at each time point in the environment of the equilibrium bifurcation. Such a solution can be based on higher-order models such as proposed by H. Matsunaga for problems of the buckling of functionally graded plates [46, 49] and shells [47, 48]. Indeed, it was shown that the classical models drastically overestimate the critical forces for thick elastic plates and shells with mechanical properties smoothly varying over their thickness; at the same time it is known that very short SMA beams buckle at compression forces significantly

lower than the ones for many more slender elastic beams [53, 60, 62, 76]; thus, the three-dimensional modelling remains topical. Other solution's approaches may consist in the dimensional reduction proposed by Amosov for beams [2, 3] and thick shells [10, 112–115, 117] or in the use of solid finite elements [76]. It is evident that the consistent finite element simulation of SMA systems is strictly required by engineering applications; thus, we will amount below the solid finite element modeling analogous to [76] to simulate the buckling of prismatic SMA beams and to vindicate the analytical estimates proposed by A. Movchan and L. Silchenko.

2 Equilibrium Stability Problem's Statement

First, let us define the stability concept that is based on the general Lyapunov's definition and could be used within the solid modeling of non-linear deforming of SMA systems under the conditions of non-isothermal martensite phase transitions.

2.1 General Statement of the Problem

Let us consider a solid $V \subset \mathbb{R}^3$, $\partial V = \Sigma_\sigma \oplus \Sigma_u$. Its deforming can be determined within the dynamics equations

$$\rho \ddot{\mathbf{u}} = \nabla \cdot \boldsymbol{\sigma} \tag{1}$$

where $\boldsymbol{\sigma}$ is the Cauchy stress tensor, $\mathbf{u} = \mathbf{R} - \mathbf{r}$ is the displacement between the reference state defined by the position vector $\mathbf{r}$ and the acting state $\tilde{V}$ defined by $\mathbf{R}$, ρ is the mass density, ∇ denotes covariant differentiation referred to the acting state, dots denote differentiation with respect to the time τ. In the quasi-statics we have

$$\|\rho \ddot{\mathbf{u}}\| \to 0 \quad \forall \tau \in (\mathbb{R}_+ \cup \{0\}) \setminus \{\tau^*\}, \quad \mu\left(\tau^*\right) = 0 \tag{2}$$

The boundary conditions can be written as follows:

$$\mathbf{N} \cdot \boldsymbol{\sigma} = \mathbf{P} \tag{3}$$

where $\mathbf{N}$ is the external normal unit in the acting configuration $\tilde{V}$.

The strain state is defined by the tensor $\boldsymbol{\varepsilon}$

$$\boldsymbol{\varepsilon} = \tfrac{1}{2}\left[\hat{\nabla}\mathbf{u} + \hat{\nabla}\mathbf{u}^{\mathrm{T}} + \hat{\nabla}\mathbf{u} \cdot \hat{\nabla}\mathbf{u}^{\mathrm{T}}\right] \tag{4}$$

$\hat{\nabla}$ is the covariant derivative referred to the initial state V and the symbol "$\cdot$" denotes the appropriate scalar product.

In general, the finite constitutive relations $\boldsymbol{\sigma} = \boldsymbol{\sigma}(\boldsymbol{\varepsilon}, T)$ between stresses $\boldsymbol{\sigma}$, strains $\boldsymbol{\varepsilon}$, and the temperature T do not exist, but their incremental form can be established as follows:

$$d\boldsymbol{\sigma} = \mathbf{C} : (d\boldsymbol{\varepsilon} + \mathbf{A}dT) \tag{5}$$

where $\mathbf{C}$ is the "tangent stiffness" tensor defined at the point of the deformation pattern and $\mathbf{A}$ is the thermal dilatation tensor.

Let us consider the homogeneous initial configuration, $\mathbf{r} \equiv 0$, and let $\mathbf{R} = \mathbf{R}(\tau, 0)$ be the corresponding solution of the problem (1), (3)–(5). Applying the Lyapunov concept, we can interpret it as a stable equilibrium if

$$\begin{aligned} &\forall \varepsilon \in \mathbb{R}_+ \quad \exists \delta(\varepsilon) \in \mathbb{R}_+ : \quad \forall \|\delta \mathbf{r}\| < \delta(\varepsilon) \\ &\forall \tau \in \mathbb{R}_+ \quad \|\mathbf{u}(\tau, \delta \mathbf{r})\| < \varepsilon; \end{aligned} \tag{6}$$

moreover the equilibrium is asymptotically stable if

$$\lim \|\mathbf{u}(\tau, \delta \mathbf{r})\| = 0 \quad (\tau \to \infty)$$

where $\| \bullet \|$ denotes an appropriate vector norm.

The further investigation is based on the following assumption. Accounting for (6) we interpret the equilibrium as unstable with respect to the initial excitation $\delta \mathbf{r}$ if the contiguous equilibrium form appears:

$$\exists \tau^* : \quad \forall \tau > \tau^* \quad \exists \mathbf{u}^*(\tau, \delta \mathbf{r}), \quad \left\| \mathbf{u}^* \right\| > \varepsilon^* \tag{7}$$

where ε^* is some representative value and τ^* is the time corresponding to the equilibrium state bifurcation. It can be supposed that the transition from the initial equilibrium state $\mathbf{u}$ to the contiguous one $\mathbf{u}^*$ is followed by the intensive transient process; in other words, the nonzero accelerations $\ddot{\mathbf{u}}$ exist only near the point τ^* (2):

$$\tau^* : \quad \left\| \ddot{\mathbf{u}}(\tau^*) \right\| \neq 0 \tag{8}$$

The kinetic energy maximum can be also used as an bifurcation criterion:

$$\tau^* : \quad \mathrm{T}(\tau^*) \equiv \tfrac{1}{2} \rho \, \dot{\mathbf{u}} \cdot \dot{\mathbf{u}}|_{\tau = \tau^*} = \mathrm{T}_{\max} \tag{9}$$

this criterion could be more stable than the acceleration-based due to smoothness of the kinetic energy dependency on the time parameter as it is shown below.

Thus, if the contiguous equilibrium state (7) occurs, bifurcation load P_{Cr} and temperature T_{Cr} can be found as follows:

$$P_{\mathrm{Cr}} = P(\tau^*), \quad T_{\mathrm{Cr}} = T(\tau^*) \tag{10}$$

where the time value τ^* corresponding to the equilibrium bifurcation point is taken from the condition (8) or (9).

3 Constitutive Equations for the Shape Memory Alloy Undergoing Thermoelastic Phase Transitions

The further investigation is based on the once coupled model of thermo-mechanical behavior of the binary Nickel-Titanium SMA [74]. This model describes the non-isothermal diffusionless smeared phase transitions induced by the combined action of stress and temperature fields; it is based on the phenomenological approach developed by Movchan from 1994 [56] till today [59] (for more details see [55]).

3.1 Basics of the Coupled Phenomonological Model of Non-isothermal SMA Behavior

As usually [55, 56] the phase constitution of SMA is determined by the martensite volume fraction $q \in [0, 1]$ where $q = 0$ corresponds to the entirely austenite phase constitution (A-state) and $q = 1$ to the entirely martensite one (M-state). Let us use hence the smooth approximation proposed by [74] for the phase diagram $q(T, \boldsymbol{\sigma})$:

$$\begin{aligned} q &= \frac{1}{2}\left[1 - \cos(\pi t)\right] \quad (0 \leqslant t \leqslant 1) \\ q &= 0 \quad (t \leqslant 0) \\ q &= 1 \quad (t \geqslant 1) \end{aligned} \tag{11}$$

The formula (11) is unified for both thermally and stress induced $A \to M$ and $M \to A$ phase transitions by introducing the dimensionless temperature t as follows:

$$t = \frac{M_s - T_\sigma}{M_s - M_f} \quad (A \to M) \tag{12}$$

$$t = 1 - \frac{A_s - T_\sigma}{A_s - A_f} \quad (M \to A) \tag{13}$$

where M_s and M_f are the temperatures of the $A \to M$ start and finish, and A_s, A_f are the temperatures of the start and finish of the $M \to A$ transition.

The reduced temperature T_σ accounts for the stress state of the SMA:

$$T_\sigma = T - \frac{\omega_{ij}^{\pm} s^{ij} + Z\left(\sigma_i, \sigma_k^k\right) + \sigma_k^k \varepsilon_0}{\Delta S} \tag{14}$$

where T is the thermodynamic temperature, ε_0 is the volumetric strain effect of the $A \to M$ transition, and ΔS is the difference between the volumetric densities of the entropy of the austenite and martensite phases at the reference temperature;

$$Z\left(\sigma_i, \sigma_k^k\right) = \frac{(\sigma_k^k)^2}{18}\left(\frac{1}{K_M} - \frac{1}{K_A}\right) + \frac{\sigma_i^2}{6}\left(\frac{1}{G_M} - \frac{1}{G_A}\right)$$

$$s^{ij} = \sigma^{ij} - \frac{1}{3}\sigma_k^k g^{ij}; \quad \sigma_i^2 = \frac{2}{3}s^{ij}s_{ij}; \quad e_{ij} = \varepsilon_{ij} - \frac{1}{3}\varepsilon_k^k g_{ij}$$

$$\omega_{ij}^{+} = \frac{3s_{ij}}{2\sigma_i}\rho_D\left[1 - qf^{+}(q)\right]\varphi_1(\sigma_i) + f^{+}(q)e_{ij}^{P} \quad (A \to M)$$

$$\omega_{ij}^{-} = f^{-}(q)\frac{e_{ij}^{P}}{q} \quad (M \to A)$$

Here $f^{\pm}(q) \in [0, q^{-1}]$ is the material function that determines the relationship between the processes of the nucleation and the growing of martensite grains:

$$f^{+}(q) = \frac{1}{2+q} \quad (dq > 0)$$

$$f^{-}(q) = \frac{1}{q} \quad (dq < 0)$$

As a result, we can represent the covariant tensor components $\omega_{ij}^{\pm}$ as follows:

$$\omega_{ij}^{+} = \frac{1}{2+q}\left(e_{ij}^{\pm} + 3\frac{s_{ij}}{\sigma_i}\rho_D\varphi_1(\sigma_i)\right) \quad (A \to M)$$

$$\omega_{ij}^{-} = \frac{e_{ij}^{\pm}}{q} \quad (M \to A)$$

The material function $F_1(\sigma_i)$ is the microstress distribution in a representative volume of the pure austenite,

$$F_1(\sigma) = \sqrt{\frac{2}{\pi}}\int_0^{\sigma}\exp\left(-\frac{\xi^2}{2}\right)d\xi$$

and $\varphi_1(\sigma_i) = F_1(\sigma_i - \sigma_1) + F_1(\sigma_i + \sigma_1) - 1$ where σ_1 denotes the threshold stress of the initiation of the nucleation of oriented martensite grains.

The elastic-temperature strain ε_{ij}^{E}, the phase strain $\varepsilon_{ij}^{\pm}$, and the structure strain ε_{ij}^{S} corresponding to the transformation of the chaotic martensite into oriented one and vice versa are assumed to be additive parts of the summary strain tensor ε_{ij}:

$$\varepsilon_{ij} = \varepsilon_{ij}^{E} + \varepsilon_{ij}^{S} + \varepsilon_{ij}^{\pm} \tag{15}$$

$$\varepsilon_{ij}^{E} = \frac{1}{2G(q)}\left[\sigma_{ij} - \frac{3K(q) - 2G(q)}{9K(q)}\sigma_k^k g_{ij}\right] + \alpha(q)T g_{ij} \tag{16}$$

the bulk modulus $K(q)$ and the shear modulus $G(q)$ as well as thermal expansion ratio $\alpha(q)$ obey the mixture rule:

$$\frac{1}{G(q)} = \frac{q}{G_M} + \frac{1-q}{G_A}; \quad \frac{1}{K(q)} = \frac{q}{K_M} + \frac{1-q}{K_A} \tag{17}$$

$$\alpha(q) = q\alpha_{\mathrm{M}} + (1-q)\alpha_A$$

here $G_M, G_{\mathrm{A}}, K_M, K_{\mathrm{A}}, \alpha_M, \alpha_{\mathrm{A}}$ are shear moduli, bulk moduli, and thermal expansion factors corresponding to the entirely martensite or austenite phase constitution. The increments of the phase and structure strain deviators can be written as follows:

$$de_{ij}^{\pm} = \omega_{ij}^{\pm} dq \tag{18}$$

$$de_{ij}^{S} = \rho_D \frac{3s_{ij}}{2\sigma_i} q\psi_2(\sigma_i)\, d\sigma_i \quad (d\sigma_i > 0)$$

$$de_{ij}^{S} = 0 \quad (d\sigma_i \leqslant 0) \tag{19}$$

ρ_D is the maximum strain intensity of $A \to M$ transition, $p_2(\sigma_i)$ is the density of the microstress distribution $F_1(\sigma_i)$, $\psi_2(\sigma_i) = p_2(\sigma_i - \sigma_2) + p_2(\sigma_i + \sigma_2)$, and σ_2 is the threshold stress value corresponding to the structure transition in the martensite inelasticity regime.

3.2 *Incremental Representation of the Constitutive Equations*

Let us represent all relationships of the used model in the incremental form as it was briefly shown by Nushtaev and Zhavoronok [76]. First, accounting for the phase diagram approximation (11), we obtain the following increments dq^{+}, dq^{-} of the martensite volume ratio q for both direct phase transform, $A \to M$ and for inverse one, $M \to A$, respectively:

$$dq^{+} = \frac{\pi\sqrt{q(1-q)}}{M_s - M_f}\left[\frac{\bar{\omega}_{kl}^{+} + 6\rho_D\varphi_1'(\sigma_i)\, g_{kl}}{\Delta S} d\sigma^{kl} - dT\right] \tag{20}$$

$$dq^{-} = \frac{\pi\sqrt{q(1-q)}}{A_s - A_f}\left[dT - \frac{\omega_{kl}^{-}}{\Delta S} d\sigma^{kl}\right] \tag{21}$$

$$\bar{\omega}_{kl}^{\pm} = \omega_{kl}^{\pm} + \left[\varepsilon_0 + \left(\frac{1}{K_{\mathrm{M}}} - \frac{1}{K_{\mathrm{A}}}\right)\frac{\sigma_k^k}{9}\right] g_{kl} + \left(\frac{1}{G_{\mathrm{M}}} - \frac{1}{G_{\mathrm{A}}}\right)\frac{s_{kl}}{2}$$

while for the strain tensor we can write the Eq. (22):

$$d\varepsilon_{ij}^{\pm} = \left\{ \frac{1}{2}\left(g_{ik}g_{jl} - \frac{1}{3}g_{ij}g_{kl}\right)\left(\frac{q}{G_{\mathrm{M}}} + \frac{1-q}{G_{\mathrm{A}}}\right) + \frac{1}{9}g_{ij}g_{kl}\left(\frac{q}{K_{\mathrm{M}}} + \frac{1-q}{K_{\mathrm{A}}}\right) + \frac{9\rho_D}{8}q\psi_2(\sigma_i)\frac{s_{ij}s_{kl}}{\sigma_i^2}\left[1 + \mathrm{sgn}\left(s_{kl}d\sigma^{kl}\right)\right]\right\} d\sigma^{kl} + g_{ij}\left[q\alpha_{\mathrm{M}} + (1-q)\alpha_{\mathrm{A}}\right]dT + \left[\bar{\omega}_{ij}^{\pm} + (\alpha_{\mathrm{M}} - \alpha_{\mathrm{A}})\,T g_{ij}\right]dq^{\pm} \tag{22}$$

To obtain the formulation useful for further numerical implementation we have to construct the tangent compliance matrix following from the 4D arrays R_{ijkl} and the thermal expansion matrix A_{ij} on the background of (15)–(22) (see also [76]):

$$d\varepsilon_{ij}^{\pm} = R_{ijkl}d\sigma^{kl} + A_{ij}^{\pm}dT, \quad R_{ijkl} = R_{ijkl}^{E} + R_{ijkl}^{S} + R_{ijkl}^{\pm}. \tag{23}$$

The term R_{ijkl}^{E} in (23) corresponds to the elastic strain ε_{ij}^{E}:

$$R_{ijkl}^{E} = \frac{1}{2}\left(g_{ik}g_{jl} - \frac{1}{3}g_{ij}g_{kl}\right)\left(\frac{q}{G_{\mathrm{M}}} - \frac{1-q}{G_{\mathrm{A}}}\right) + \frac{1}{9}g_{ji}g_{kl}\left(\frac{q}{K_{\mathrm{M}}} - \frac{1-q}{K_{\mathrm{A}}}\right) \tag{24}$$

the term R_{ijkl}^{S} corresponds to the strain ε_{ij}^{S} generated by the structure transform:

$$R_{ijkl}^{S} = \frac{9}{4}\rho_D\frac{s_{ij}s_{kl}}{\sigma_i^2}q\psi_2(\sigma_i) \quad (d\sigma_i > 0) \tag{25}$$

$$R_{ijkl}^{S} = 0 \quad (d\sigma_i \leqslant 0) \tag{26}$$

and the third one corresponds to the phase strain for the $A \to M$ transition (27)

$$R_{ijkl}^{+} = \frac{\pi}{\Delta S}\frac{\sqrt{q(1-q)}}{M_s - M_f}\left[\bar{\omega}_{ij}^{+} + (\alpha_{\mathrm{M}} - \alpha_{\mathrm{A}})\,T g_{ij}\right]\left[\bar{\omega}_{kl}^{+} + 3\rho_D\psi_2(q)s_{kl}\right] \tag{27}$$

as for the inverse transition $M \to A$ (28)

$$R_{ijkl}^{-} = -\frac{\pi}{\Delta S}\frac{\sqrt{q(1-q)}}{A_s - A_f}\left[\bar{\omega}_{ij}^{-} + (\alpha_{\mathrm{M}} - \alpha_{\mathrm{A}})\,T g_{ij}\right]\bar{\omega}_{kl}^{-} \tag{28}$$

Finally, we have the following matrices of thermal expansion:

$$A_{ij}^{+} = -\pi\frac{\sqrt{q(1-q)}}{M_s - M_f}\left[(\alpha_{\mathrm{M}} - \alpha_{\mathrm{A}})\,T g_{ij} + \bar{\omega}_{ij}^{+}\right] + \left[q\alpha_{\mathrm{M}} + (1-q)\alpha_{\mathrm{A}}\right]g_{ij} \tag{29}$$

$$A_{ij}^{-} = \pi\frac{\sqrt{q(1-q)}}{A_s - A_f}\left[(\alpha_{\mathrm{M}} - \alpha_{\mathrm{A}})\,T g_{ij} + \bar{\omega}_{ij}^{-}\right] + \left[q\alpha_{\mathrm{M}} + (1-q)\alpha_{\mathrm{A}}\right]g_{ij} \tag{30}$$

The tangent compliances R_{ijkl} defined by (24)–(28) must be inverted to compute the corresponding tangent stiffness:

$$d\sigma^{jikl} = C^{ijkl}\,(d\varepsilon_{kl} - A_{kl}dT)\,. \tag{31}$$

The stiffness matrices corresponding to the stress-strain relations (31) can be implemented hence into finite element software as bump packs. For instance, for the UMAT program block for the SIMULIA Abaqus® complex the input data contain the stresse σ_{ij}, the summary strain ε_{ij}, the phase strain $\varepsilon_{ij}^{\pm}$, the structure strain ε_{ij}^{S}, the temperature T, and finally the martensite volume ratio q.

After computing the dimensionless temperature t (12), (13) the phase transition criterion $t \in [0, 1]$ is considered:

1. If the dimensionless temperature $t \in [0, 1]$ then the increments for the martensite volumetric fraction q, phase strain $\varepsilon_{ij}^{\pm}$ and stress σ_{ij} are computed, and hence the corresponding iteration for the stiffness matrix (31) and the thermal expansion matrix (29), (30) are calculated.
2. If $t \notin [0, 1]$ then the shape memory alloy is considered as elastic material.

Thus, the program block computes only the stiffness matrices C^{ijkl} (31) following from (24)–(30) at a step of the numerical integration algorithm.

This program structure allows one to perform another computations in the standard numerical algorithms of some finite element simulation software including different standard finite element complex.

4 Stability Concepts in the Linearized Buckling Theory for thin-walled SMA structures

The use of the linearized buckling criterium for two-dimensional models of thin-walled SMA systems requires the appropriate system of supplementary assumptions so-called "buckling concepts" as it was shown in [61, 62]. A 2D system such a shell, plate, or a prismatic beam could be defined within its coordinate surface S_0, i.e. $\forall M \in S_0\ \mathbf{R} = \mathbf{r}_0$. The trivial equilibrium configuration $\mathbf{R}$ and the equilibrium perturbation $\delta\mathbf{r}$ leading to the bend state could be hence determined as follows:

$$\mathbf{R} = \mathbf{r}_0 + \zeta\mathbf{n}, \quad \delta\mathbf{r} = w\mathbf{n} + \zeta\chi^{\alpha}\mathbf{r}_{\alpha}, \quad \alpha = 1, 2 \tag{32}$$

where $\mathbf{r}_{\alpha}$ are base in the tangent fibration of S_0 at the point M, $\mathbf{n}$ is the normal unit vector, $\zeta \in [h_-, h_+] \subset \mathbb{R}$ is the normal coordinate, w is the deflection of S_0 while χ_{α} denote components of the rotation vector at $M \in S_0$ (see [82, 83, 113, 116]). Here the deformations corresponding to the pre-buckling equilibrium state are as usually assumed to be infinitely small. Let us also define the set $\mathscr{H} = \{M : \zeta \in [h_-, h_+]\}$.

Let $q_0(T^0, \sigma_i^0)$ be the martensite volume ratio corresponding to the trivial equilibrium $\mathbf{R}$ at the temperature T_0 and stress intensity σ_i^0, and let

$$\delta q^{\Sigma} = \delta q^0 \left(\delta \sigma_i^0\right) + \delta q^* \left(\delta \sigma_i^*\right)$$

be its variation defined by (20), (21); here δq^0 is resulted by the small variations of the pre-buckling stress intensity $\delta \sigma_i^0$ whereas δq^* appears as a result of the kinematic perturbation (32), i.e. $\delta \sigma_i^*$ is defined by the equilibrium (1) of the contagious state. Here and below $\delta \sigma_i^0 \neq \delta \sigma_i^0(\zeta)$. Following [62, 63], two buckling concepts could be introduced hence: the von Kármán one and the Shenley one.

4.1 Extended von Kármán's Buckling Concept for SMA Structures

Let us assume $\delta T^0 = 0$ and let the external load be constant, i.e. $\delta \sigma_i^0 = 0$. The extended von Kármán concept is based on the following hypothesis:

$$\begin{aligned} &\exists \mathscr{H}^0 \neq \emptyset, \ \mathscr{H}^* \neq \emptyset : \quad \mathscr{H} = \mathscr{H}^0 \oplus \mathscr{H}^* \\ &\forall M' \in \mathscr{H}^0 \quad \delta \sigma_i^*(\chi_\alpha, w) \leqslant 0 \quad \Rightarrow \quad \delta q^*(M') = 0 \\ &\forall M'' \in \mathscr{H}^* \quad \delta \sigma_i^*(\chi_\alpha, w) > 0 \quad \Rightarrow \quad \delta q^*(M'') \neq 0 \end{aligned} \tag{33}$$

i.e. the subdomains $\mathscr{H}^*$ of the supplementary phase transition δq^* resulted by the perturbation $\delta \mathbf{r}$ and $\mathscr{H}^0$ of the elastic unloading exist simultaneously. The interface $S^* = \mathscr{H}^* \cap \mathscr{H}^0$ being the front *of the beginning* of the supplementary phase transition is defined by the constant load condition. This concept is also known as "constant load assumption" [62]. It was shown [55] that the extended von Kármán concept leads to the *upper* critical stress estimate consistent with the test data.

4.2 Extended Shenley's Concept for SMA Structures

Let the small variations of the external load leading to $\delta \sigma_i^0 \neq 0$ or of the extended temperature field $\delta T^0 \neq 0$ exist simultaneously with the kinematic perturbation $\delta \mathbf{r}$. As a result, we could consider two limit cases.

$$\exists \delta \sigma_i^0 \neq 0 : \quad \forall M \in \mathscr{H} \ \delta \sigma_i = \delta \sigma_i^0 + \delta \sigma_i^* > 0 \quad \Rightarrow \quad \delta q(M) \neq 0 \tag{34}$$

The limit case defined by (34) (as it is proposed in [62]) leads to $\mathscr{H} = \mathscr{H}^*$, $\mathscr{H}^0 = \emptyset$, i.e. *the supplementary phase transition occurs everywhere*. It was shown that this assumption results in the *lower* critical stress estimate (e.g. see [62, 63]).

$$\exists \delta\sigma_i^0 \neq 0: \quad \forall M \in \mathscr{H}\ \delta\sigma_i = \delta\sigma_i^0 + \delta\sigma_i^* < 0 \quad \Rightarrow \quad \delta q(M) = 0 \tag{35}$$

The limit case defined by (35) leads to $\mathscr{H} = \mathscr{H}^0, \mathscr{H}^* = \emptyset$, i.e. the supplementary phase transition induced by the kinematic perturbation of the equilibrium state *does not occur*. This hypothesis so-called "constant phase constitution assumption" [62] leads to the critical stress estimate based on the minimum modulus E_M of the pure martensite; it is inconsistent with the known experimental results [53, 54, 60, 72].

5 Numerical Simulation of the Buckling and Postbuckling for Thin-Walled SMA Systems

The analytical estimates of Movchan and Silchenko [62], Silchenko [91] for beams as well as the analogous solutions for plates or shells were based on the linearized problem statement for the two-dimensional Kirchhoff-Love's shell theory, therefore the specific assumptions about the coupling effects in SMA, i.e. different concepts of SMA elements buckling [61] were required. As a result, it was supposed that the variation of the phase constitution is the main cause of the bifurcation. Thus, the three-dimensional problem statement that allows one to analyze the phase distribution across the thickness of the shell as well as along the shell axis and in the circumferential direction is required to prove this fundamental assumption. The higher-order shell models such as these of Tarlakovskii and Zhavoronok [102], Zhavoronok [112, 113, 115, 117] etc. can be used for the analysis while the three-dimensional finite element model provides efficient non-linear simulation that can be interpreted as a "numerical experiment" as it was shown by Nushtaev and Zhavoronok [76] where the buckling behavior of the clamped-clamped prismatic SMA beam was investigated.

5.1 Buckling Problem's Statement for a Prismatic SMA Beam

Let us consider a SMA prismatic beam referred to the Cartesian frame $Oxyz$ and bounded by the lateral surface Σ_B and the end faces $\Sigma_{0,l}$ (Fig. 1):

$$\left\{V: x \in \left[-\frac{a}{2}, \frac{a}{2}\right], y \in \left[-\frac{h}{2}, \frac{h}{2}\right], z \in [0, l]\right\}$$
$$\left\{\Sigma_B: \left(x \in \left[-\frac{a}{2}, \frac{a}{2}\right], y = \pm\frac{h}{2}, z \in [0, l]\right) \oplus \left(x = \pm\frac{a}{2}, y \in \left[-\frac{h}{2}, \frac{h}{2}\right], z \in [0, l]\right)\right\}$$
$$\left\{S_{0,l}: x \in \left[-\frac{a}{2}, \frac{a}{2}\right], y \in \left[-\frac{h}{2}, \frac{h}{2}\right], z = 0, l\right\}$$

The beam lateral surface Σ_B is load free:

$$\sigma_{ij} N^j \big|_{\Sigma_B} = 0 \tag{36}$$

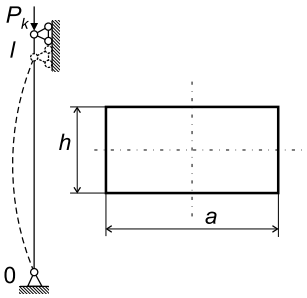

Fig. 1 Loading, trivial equilibrium configuration, and contagious equilibrium configuration of a beam

whereas the boundary conditions on the beam end faces correspond to the simply support conditions applied to the one-dimensional beam model (Fig. 1):

$$
\begin{aligned}
u_z\Big|_{x=y=0}^{z=0} = 0, \quad u_{x,y}\Big|_{x=y=0}^{z=0,l} &= 0 \\
M_x \equiv \int\limits_{S_{0,l}} \sigma_{zz}\Big|_{z=0,l} y\,dF &= 0 \\
M_y \equiv \int\limits_{S_{0,l}} \sigma_{zz}\Big|_{z=0,l} x\,dF &= 0 \\
\int\limits_{S_{0,l}} \sigma_{zz}\Big|_{z=0.l} dF &= -P_k
\end{aligned}
\tag{37}
$$

Thus, the beam is compressed by the axial force P_k at the initial temperature T_0. The temperature field is assumed to be homogeneous, i.e. $T \neq T(x, y, z)$. The phase constitution of the reference configuration is entirely austenite. As provided by the problem statement (1)–(10), the loading process consists in the monotonic cooling of the compressed beam: $T = T_0 - \tau\Delta T$ where the cooling rate ΔT is sufficiently small to uncouple thermal conduction and thermoelasticity problems and to secure the homogeneity of the temperature field over all the volume of the beam.

Let us introduce the perturbation $\delta\mathbf{r}$ corresponding to the beam camber w_0:

$$
\delta\mathbf{r} = w_0(z)\mathbf{i}_2 - x\frac{d}{dz}w_0(z)\mathbf{i}_3 \tag{38}
$$

$\mathbf{i}_i$ are Cartesian unit base vectors. The beam cooling leads to the $A \rightarrow M$ phase transition that can result in the instability of the initial equilibrium state with respect to the perturbation (38) and consequently to the beam buckling at extremely low compression forces as it was found experimentally by Movchan et al. [72] and described theoretically by Movchan and Silchenko [62, 63], Silchenko [91]. The buckling condition (7) will be interpreted using the uniform norm:

$$\|u\| = \max |u_2(0, 0, z, \tau)| \quad (z \in [0, l]) . \tag{39}$$

The bifurcation point τ^* can be found accounting for (8) or (9) as follows:

$$\tau^* : \quad \begin{cases} \ddot{u}_2^* = \max |\ddot{u}_2(0, 0, z, \tau)| \\ T^* = \max [T(\tau)] \end{cases} \quad \tau \in [0, \tau_F], \quad z \in [0, l] . \tag{40}$$

To close the problem statement the constitutive equations (5) must be formulated.

5.2 Solid Finite Element Model and Initial Camber Calibration

The analytical one-dimensional linearized model of beam buckling [62, 63, 91] and the nonlinear three-dimensional finite element model of the nonlinear deformation of the compressed prismatic beam based on the unconditionally stable Newton-Raphson method [108] qualitatively differ. Thus, the last one must be tested to secure the equivalence of three-dimensional boundary conditions and one-dimensional simply support conditions, the consistency of the buckling criterion (39), (40), etc. Moreover the initial camber amplitude effect on the compression force given by (39), (40) and interpreted as buckling one must be studied in details.

Let us consider the prismatic SMA beam of length $l = 0.040\,\text{m}$ and with the cross-section dimensions $a = 0.002\,\text{m}$, $h = 0.001\,\text{m}$. The main thermomechanical properties of the Nickel-Titanium alloy of TN-1 type are given in the Table 1.

Let us use the constant phase constitution concept [62], i.e. the beam is ideally one-phase martensite solid. Thus, the classical Euler formula (41) can be used:

$$P_{\text{Cr}}^{\text{Eu}} = \pi^2 \frac{E J_{\min}}{l^2} \tag{41}$$

First, the one-dimensional model of the simply supported beam consisting in 50 finite elements of beam type was constructed. The beam was loaded by the axial compression force raising up to 100 N. The first eigenvector $\phi(z)$ corresponding to this beam model and obtained from the eigenfrequency problem is used to construct

Table 1 Thermomechanical properties of the NiTi alloy TN-1

Young modulus of the entirely martensite alloy E_{M}, MPa	30000
Young modulus of the entirely austenite alloy E_{A}, MPa	70000
Poisson ratio ν	0.3
Temperature of the A $\rightarrow$ M transition start at $\sigma_i \equiv 0$: M_s, K	316.15
Temperature of the A $\rightarrow$ M transition finish at $\sigma_i \equiv 0$: M_f, K	295.15

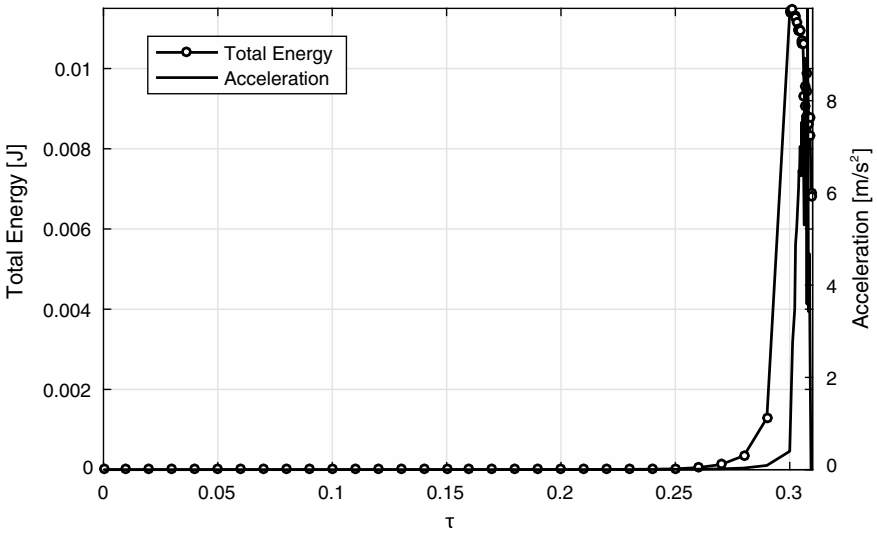

Fig. 2 Lateral acceleration of the central node, m/s^2, and beam total energy, J; pre-buckling state and buckling regime

Table 2 Comparison of the buckling forces obtained numerically and analytically

Camber amplitude $\left\|w_0^{\max}\right\|/h$, %	Buckling force (10), N		Eulerian force (41) P_{Cr}, N	
	Austenite	Martensite	Austenite	Martensite
1.00	71.13	30.34	71.97	30.84
0.50	71.88	30.82		
0.25	71.72	31.01		
0.10	72.02	31.50		

the initial camber $w_0(z)$ (38); here and below the camber amplitude is referred to the cross-section dimension and given by the appropriate dimensionless factor κ. The finite element analogs of the dynamic equations (1) are solved by the Newton-Raphson algorithm [108] for the perturbed system. The obtained inertial forces vanish almost everywhere except the small environment of the bifurcation point (Fig. 2), so that the beam deformation process remains quasi-static.

It can be seen that the maximum kinetic energy and the maximum lateral acceleration of the beam central node are very close (Fig. 3); thus, they are interpreted as lower and upper estimates of the bifurcation point. The buckling force corresponding to (10), (40) and obtained by numerical simulation with various cambers is compared with the critical force (41) (see Table 2).

For the camber amplitude $|w_0^{\max}|/h < 0.05 \ldots 0.10\%$ the contagious equilibrium state does not appears due to the artificial viscosity of the numerical algorithm. The error of the numerical solution does not exceed 1.6% of the exact solution.

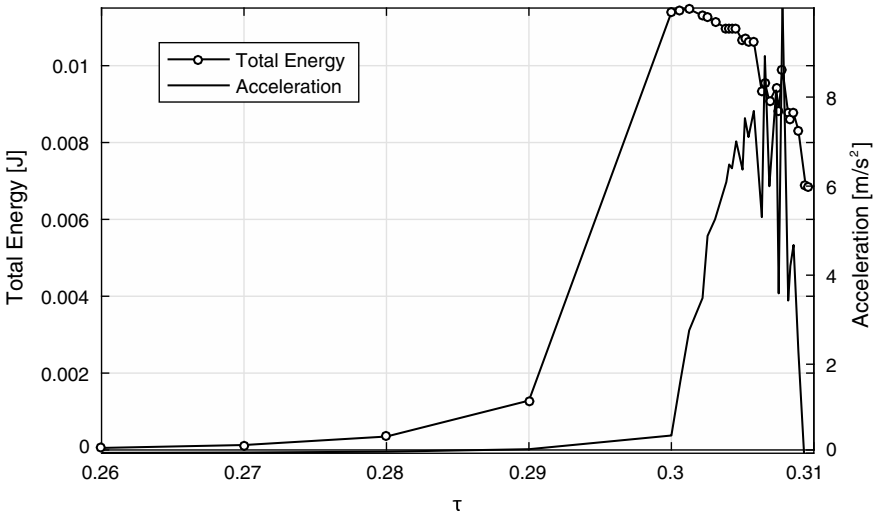

Fig. 3 Lateral acceleration of the central node, m/s^2, and beam total energy, J; bifurcation point environment

The solid finite element model is based on eight-node prismatic finite elements with three degrees of freedom per node. The boundary conditions on the end faces $S_{0,l}$ are formulated to construct the three-dimensional model equivalent to the one-dimensional simply supported beam.

Two rigid planes are normally attached to the beam end faces without friction using the appropriate contact conditions formalism. The planes kinematics obeys the rigid body motion law:

$$\begin{aligned} \mathbf{U}^{0,l} &= U_z^{0,l} - \mathbf{r}_\mathrm{T} \times \boldsymbol{\theta}^{0,l}, \\ \mathbf{r}_\mathrm{T} &= x\mathbf{e}_1 + y\mathbf{e}_2, \quad \boldsymbol{\theta}^{0,l} = \theta_x^{0,l}\mathbf{e}_1 + \theta_y^{0,l}\mathbf{e}_2, \end{aligned} \tag{42}$$

where $\mathbf{U}_z^{0,l}$ is the vertical translation of the rigid plane center and $\boldsymbol{\theta}^{0,l}$ is the rotation of the rigid planes around their centers. Accordingly to (37) $\mathbf{U}_z^0 = 0$, and the vertical force P_k is applied to the upper plane central point. The numerical solution obtained for the unperturbed beam compression (i.e. without camber) with the boundary conditions (42) results in the completely homogeneous stress state.

Applying to the three-dimensional finite element model the initial perturbation (38) with the maximum amplitude $|w_0^{\max}|/h = 1\%$ or $|w_0^{\max}|/l = 0.025\%$ and considering the bifurcation as a transient process (8) or (9), we obtain the numerical estimation of the buckling force. It is compared with the critical force (41) and the one-dimensional finite element model of the simply supported beam in the Table 3.

Thus, the solid finite element model of the SMA beam can be interpreted as completely equivalent to the beam model of Movchan [62, 63], therefore it can be used to validate the analytical results based on the linearized problem statement.

Table 3 Comparison of the buckling forces obtained from beam and solid models

Buckling forces, N	Austenite	Martensite
Analytical solution (41)	71.97	30.84
Beam finite element model	71.13	30.34
Solid finite element model	71.25	30.95

5.3 Simulation of the Buckling and Postbuckling of SMA Beams Under Direct Martensite Transitions

Let us consider the SMA beam with the initial camber $|w_0^{\max}|/l = 0.025\%$ compressed by the axial force P_k. The beam undergoes the $A \to M$ transition described by the constitutive equations (20)–(31) under homogeneous cooling from the initial temperature $T_\sigma^0 > M_s$, $T_0 = 323.15\,\mathrm{K}$. The structure transforms are neglected. The initial force value $P_1 < P_{\mathrm{Cr}}^{\mathrm{E}}(E = E_{\mathrm{M}})$ prevents the beam from the pseudoelastic buckling regime, and the length varies from 0.040 to 0.005 m. The numerical solution based on the three-dimensional finite element model is obtained for the fixed force P_k; if the intensive grooving of the kinetic energy is not obtained before $A \to \mathrm{M}$ finish, then the simulation is repeated for the increased load value $P_{k+1} > P_k$, etc.

Long beam: $l = 0.040\,\mathrm{m}$. Let the beam be loaded by the force $P_k = k$ N, $k = 1 \ldots 4$. The initial camber results in the longitudinal bending and in the stress field heterogeneity. The highest stress. i.e. the minimum reduced temperature T_σ (14) is observed in the central cross-section at the concave beam fiber (Fig. 4).

Thus, the $A \to \mathrm{M}$ transition begins at $T = 315.8\,\mathrm{K}$ in near the maximum stress point, and the phase parameter q is distributed over the beam heterogeneously. As a result, the elasticity moduli (17) vary over beam's cross-sections, and their central axes move from the geometric center to the convex fibers; therefore the initially central compression load becomes eccentric (43), and the bending moment appears:

$$y_0(T, P) = -\frac{\displaystyle\int_{-h/2}^{h/2} \left[\frac{q}{E_M} + \frac{1-q}{E_A}\right]^{-1} y\,dy}{\displaystyle\int_{-h/2}^{h/2} \left[\frac{q}{E_M} + \frac{1-q}{E_A}\right]^{-1} dy} \tag{43}$$

Moreover the phase strain ε_z^+ is approximately proportional to the martensite volume fraction q (27, 28) (Fig. 5), so that results in the raising beam deflection.

Let us consider hence the central node translation w_C (Fig. 6). It can be seen that for $P_k = 1 \ldots 3\,\mathrm{N}$ the contagious equilibrium state appears only for a short time, therefore the initial equilibrium is stable accordingly to the buckling concept (7), moreover it is asymptotically stable. At the same time the load $P_4 = 4\,\mathrm{N}$ results in raising w_C; the stable contagious equilibrium state appears, thus, the beam buckles at $P \in [3, 4]\,\mathrm{N}$. The corresponding acceleration dependency $\ddot{w}_C(\tau)$ it shown on Fig. 7.

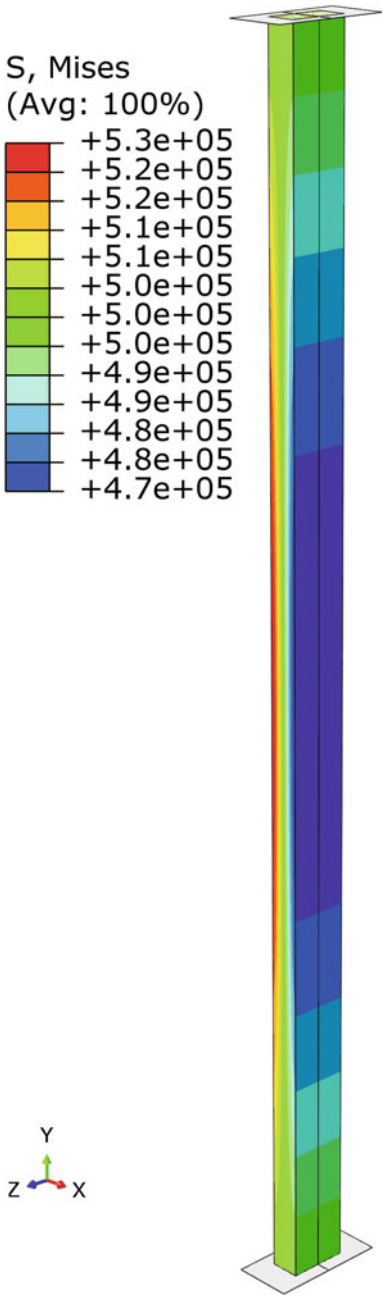

Fig. 4 Equivalent stresses in the austenite beam with the initial camber $|w_0^{\max}|/l = 0.025\%$: $P_0 = 1\,\mathrm{N}$, $P_{\mathrm{Cr}} = 4\,\mathrm{N}$, $T = 323.5\,\mathrm{K}$, $l = 0.040\,\mathrm{m}$

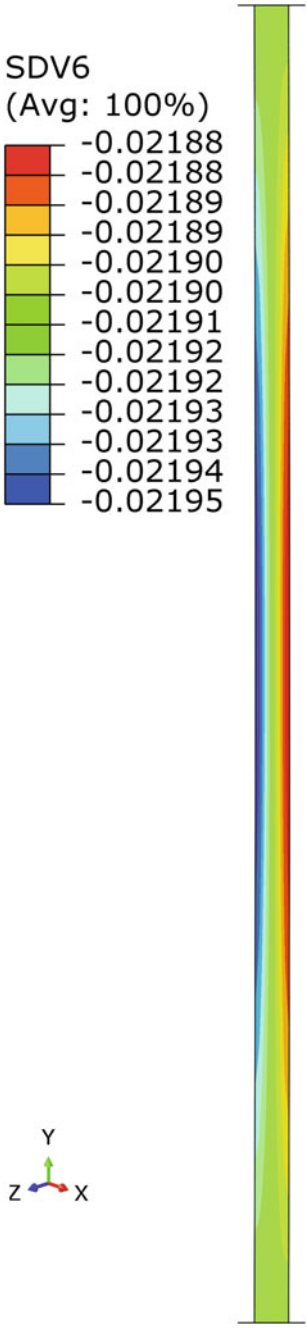

Fig. 5 Phase and structure strains in the beam: $P = 2\,\mathrm{N}$, $T = 305\,\mathrm{K}$

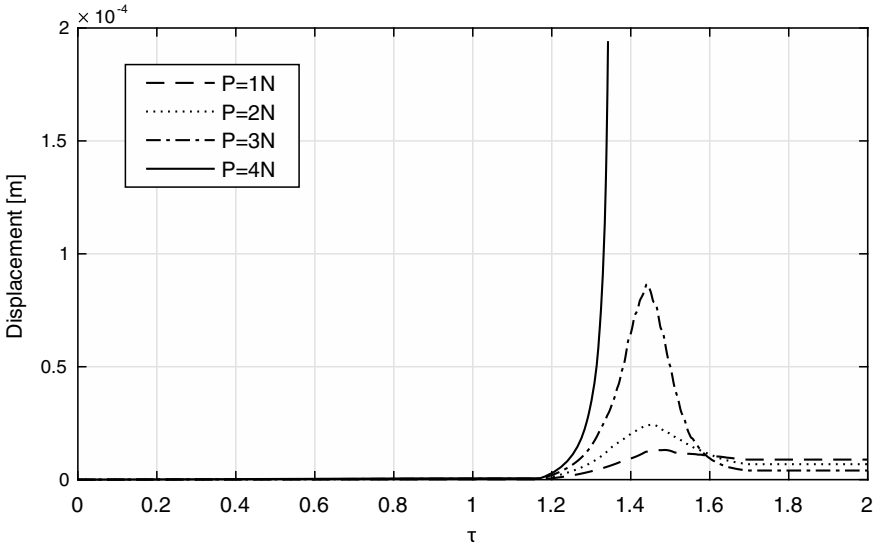

Fig. 6 Lateral translation of the central beam node $w_C(\tau)$, m during the equilibrium bifurcation

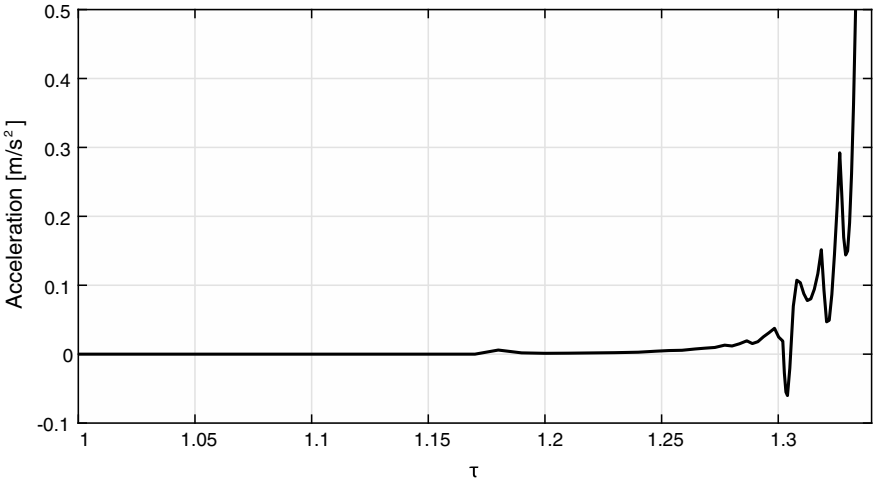

Fig. 7 Lateral acceleration of the central node $\ddot{w}_C(\tau)$, m/s^2 during the equilibrium bifurcation

Finally, the dependency of the kinetic energy on the time parameter τ allows one to find the buckling temperature $T* = T_0 - \tau * \Delta T = 309.86\,\text{K}$.

Middle beam: $l = 0.015\,\text{m}$. The statement of the problem is the same that for the long beam except the compression force range: $P_k = 22; 25; 26\,\text{N}$ whereas the critical force (41) of the entirely martensite beam is estimated as $P_{\text{Cr}}^{\text{E}} = 219.3\,\text{N}$.

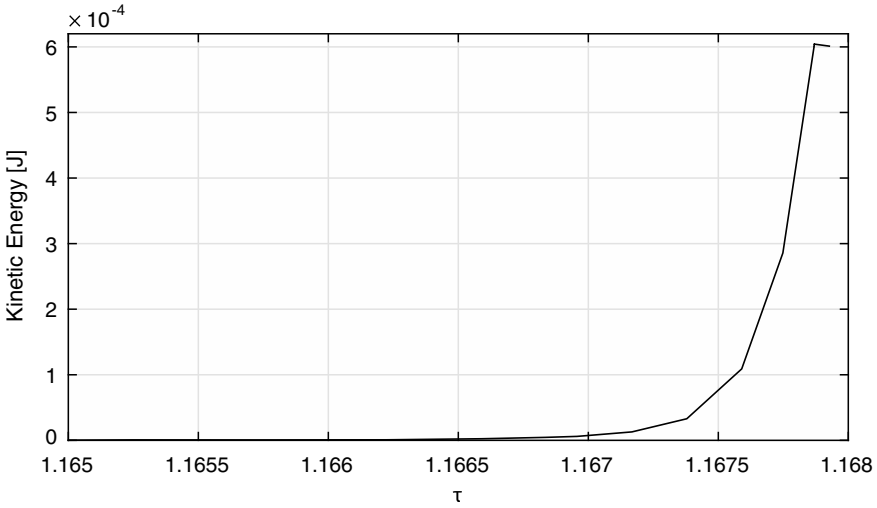

Fig. 8 Kinetic energy near the bifurcation point $\tau^* \approx 1.1678$, compression load $P = 26\,\mathrm{N}$

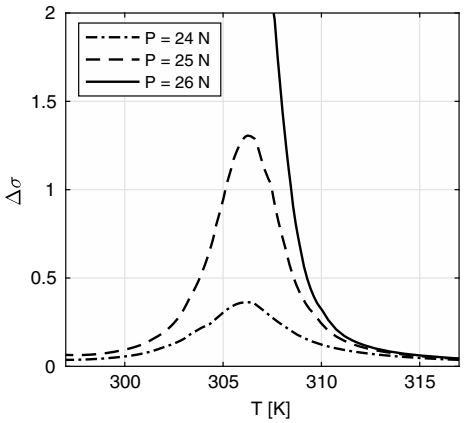

Fig. 9 Dimensionless stress difference $\Delta\sigma$

The intensive kinetic energy growing, i.e. the beam buckling is observed for $P \in [25, 26]\,\mathrm{N}$ (Fig. 8). The critical temperature is estimated as $T(\tau^*) = 316.5\,\mathrm{K}$.

Let us introduce the dimensionless stress difference referred to the compression force (Fig. 9) and the difference of the martensite volume ratio (Fig. 10):

$$\Delta\sigma = \frac{\sigma_z^{\max} - \sigma_z^{\min}}{P_k} F; \quad \Delta q = q_{\max} - q_{\min}. \tag{44}$$

The linear stress distribution over the cross-section leads to the martensite volume ratio distribution $q(x)$ that is very close to the linear one (Fig. 10) except small

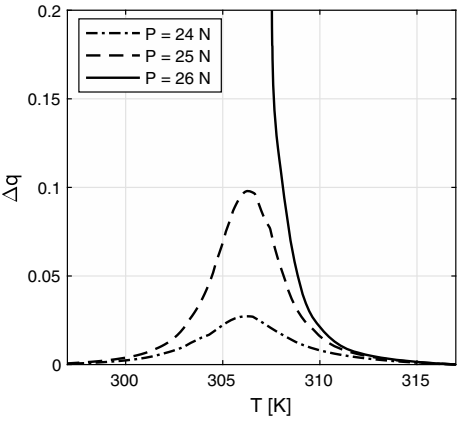

Fig. 10 Martensite volume ratio difference $\Delta q\ (T)$

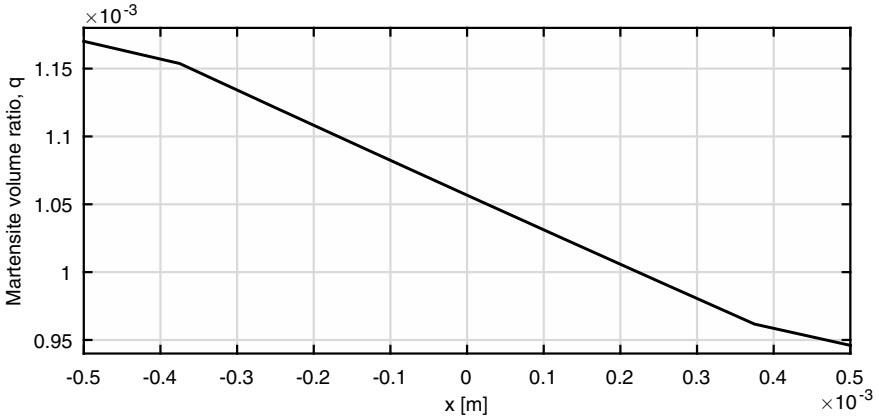

Fig. 11 Martensite volume ratio distribution over cross-section, $T\ (\tau^*) = 316.5\,\mathrm{K}$

boundary layers due to the error of the finite element simulation whereas its distribution $q(z)$ along the beam longitudinal axis is shown on the Fig. 11.

Thus, the bifurcation occurs *after* $A \rightarrow \mathrm{M}$ beginning under conditions of the *martensite transition occurring everywhere:* $dq > 0\,\forall x \in [-a/2, a/2]$ (Figs. 11 and 12) accordingly to the extended Shenley concept (34) (see also [61–63]).

Short beams: The same problem statement is used to study the stability of the SMA beams of length $l = 0.010\,\mathrm{m}$, $l = 0.007\,\mathrm{m}$, and $l = 0.005\,\mathrm{m}$ with the initial load increased up to $P_k = 333.15\,\mathrm{N}$; this value does not result in the pseudoelastic direct martensite transform initiated before the bifurcation of the equilibrium state.

The eccentricities (43) resulted by the changes of the elastic modulus due to the phase transition are presented in the Table 4. The computed buckling forces are

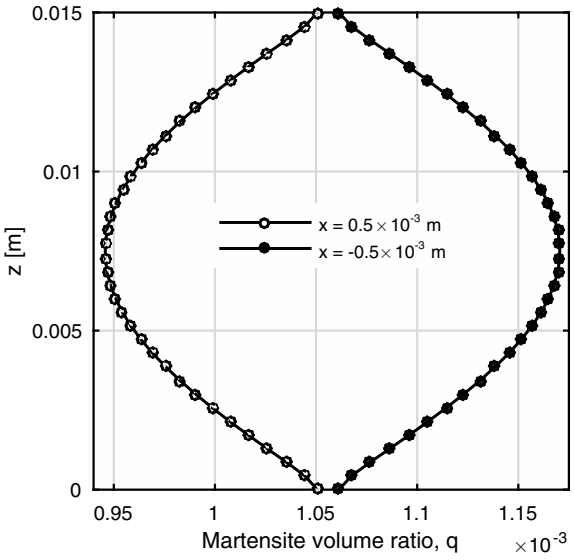

Fig. 12 Martensite volume ratio distribution along the beam, $T\ (\tau*) = 316.5\,\mathrm{K}$

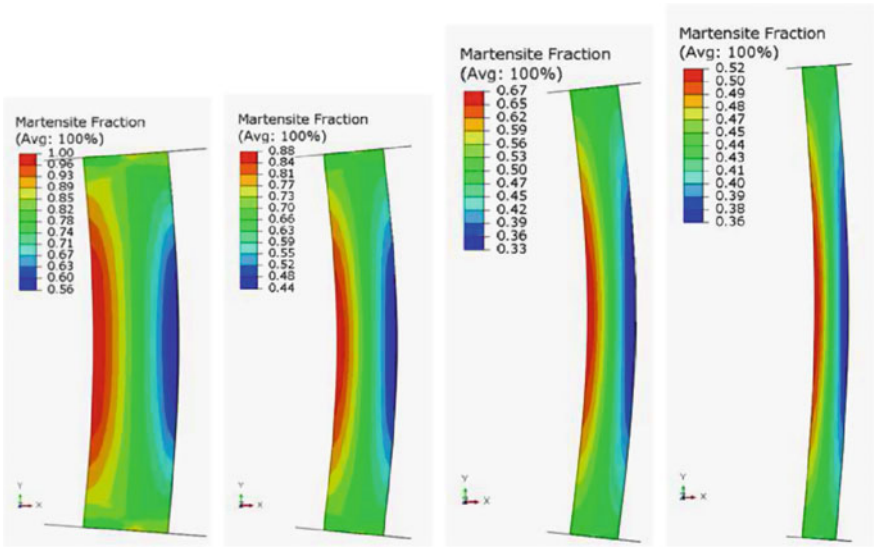

Fig. 13 Distribution of the martensite phase q in beams of various lengths at the bifurcation point

presented in the Table 5 while the typical distributions of the martensite phase over the thickness of the beams at the bifurcation point are shown on the Fig. 13.

Table 4 Compression force eccentricity at the bifurcation point

Beam's length l, m	Relative eccentricity $2y_0/h$, %
0.040	0.36
0.015	2.31
0.010	4.69
0.007	5.40
0.005	4.97

Table 5 Eulerian critical force (41) and the numerically obtained force of beam's buckling under the conditions of the thermally induced A → M phase transition

Length l, m	$P_{\mathrm{Cr}}^{\mathrm{E}}(E_{\mathrm{M}})$, N	$P(\tau^*)$, N	$P(\tau^*)/P_{\mathrm{Cr}}^{\mathrm{E}}(E_{\mathrm{M}})$, %
0.005	1974.00	265…270	14
0.007	1007.00	120…125	12
0.010	493.48	58…59	12
0.015	219.33	25…26	12
0.040	30.84	3…4	11

The computed buckling forces are about 11…14% of the Eulerian force corresponding to the minimum elasticity modulus of entirely martensite SMA. Let us note that the buckling force values correspond to the analytical estimations based on the assumption of the "phase transition occurring everywhere" (34) [62]. The obtained results show that even *very* short beams could buckle under relatively small compression loads; thus, the danger of buckling of thick-walled SMA systems under the conditions of martensite transitions seems to be *drastically underestimated*. The analogous results for the axially compressed clamped-clamped prismatic SMA beam [76] show that the critical forces of the buckling under the conditions of the superelastic transform are about 1.5 times higher than the ones of the thermally induced martensite transition, nevertheless they are significantly lower than the analytical estimates based on the minimum modulus concept (35).

6 Conclusions

The nonlinear deforming of the shape memory alloy beam compressed by the axial force and then cooled through the temperature range of the direct martensite transition was simulated numerically on the basis of the once coupled Movchan's theory of thermoelastic phase transforms and three-dimensional finite element modeling. The initial equilibrium state was perturbed by applying small initial cambers to study the beam buckling instability in terms of Lyapunov's concept. The three-dimensional

problem statement allowed to investigate the phase transition during the beam buckling and the phase constitution effect on the equilibrium stability.

The performed numerical simulations have shown that:

1. The bifurcation of the beam equilibrium state appears after beginning of the direct martensite transform.
2. Beams are stable with respect to the same initial perturbations in the absence of the martensite transitions.
3. The computed buckling forces are about 11–14% of the Eulerian critical forces corresponding to the minimum elastic modulus, i.e. to the entirely martensite state ($q = 1$) whereas the phase constitution is very close to the pure austenite.
4. The obtained buckling forces are consistent with the test data and close to the analytical estimation based on the Shenley concept assuming the phase transition occurring everywhere.
5. The distribution of the martensite volume ratio over the beam cross-section is antisymmetric and almost linear.

These results lead to the following conclusions:

1. The induced by initial perturbations supplementary phase transition in itself causes the buckling of compressed beams.
2. The supplementary phase transition occurs everywhere in the beam, the elastic unloading domains do not appear.

Thus, the fundamental assumption about the decisive phase transition contribution in the buckling instability of thin-walled SMA systems advanced by A. A. Movchan and L. G. Silchenko is vindicated by the numerical simulation on the basis of the exact nonlinear problem statement. Moreover the Shenley concept assuming the supplementary phase transform occurring everywhere gives the lowest critical force estimation that is the closest to the numerical results presented above.

Acknowledgements This investigation was performed under the State Task for Basic Researches (register number AAAA-A19-119012290118-3), state register number AAAA-A17-117032010136-3 and partially supported by the Russian Foundation for Basic Researches under grant Nr. 19-01-00695_a.

References

1. Altenbach, H., Zhilin, P.A.: The theory of elastic thin shells. Adv. Mech. **11**, 107–148 (1988)
2. Amosov, A.A., Zhavoronok, S.I.: Reduction of the plane problem of elasticity theory to a sequence of one-dimensional boundary-value problems. The J of Mekhanika Kompozitsionykh Materialov i Konstruktsii (Composite Mechanics and Design) **3**(1), 69–80 (1997)
3. Amosov, A.A., Knyazev, A.A., Zhavoronok, S.I.: On Solution of 2D-Problem of Stressed Curvilinear Trapezoid. The J of Mekhanika Kompozitsionnykh Materialov i Konstruktsii (Composite Mechanics and Design) **5**(1), 60–72 (1999)
4. Bayat, Y., Toussi, H.E.: Exact solution of thermal buckling and bostbuckling of composite and sma hybrid composite beam by layerwise theory. Aerosp. Sci. Technol. **167**, 484–494 (2017)

5. Bhattacharya, K., James, R.D.: A theory of thin films of martensitic materials with applications to microactuators. J. Mech. Phys. Solids **36**, 531–576 (1999)
6. Buehler, W.J., Gilfrich, J.V., Wiley, R.C.: Effect of low-temperature phase changes on the mechanical properties of alloys near composition TiNi. Appl. Phys. **34**, 1475–1477 (1963)
7. Chang, L.C., Read, T.A.: Behavior of the elastic properties of AuCd. Trans. Metall. Soc. AIME **191**, 47–53 (1951)
8. Choi, S., Lee, J.J., Seo, D.C., Choi, S.W.: The active buckling control of laminate composite beams with embedded shape memory alloy wires. Compos. Struct. **47**, 679–686 (1999)
9. Chróścielewski, J., Makowski, J., Pietraszkiewicz, W.: Statics and Dynamics of Multifold Shells: Nonlinear Theory and Finite Element Methods. Wydawnictwo IPPT PAN, Warszawa (2004). (in Polish)
10. Egorova, O.V., Kurbatov, A.S., Zhavoronok, S.I.: The variational equations of the extended n'th order shell theory and its application to some problems of dynamics. PNPU Mech. Bull. **2**, 36–59 (2015)
11. Eremeyev, V., Pietraszkiewicz, W.: On quasi-static propagation of the phase interface in thin-walled inelastic bodies. In: Nowacki, W.K., Zhao, H. (eds.) EMMC-10 Conference "Multi-Phase and Multi-Component Materials under Dynamic Loading", pp. 99–105. Institute of Fundamental Technological Research of PAS, PASci, Kazimerz Dolny, Poland (2007)
12. Eremeyev, V.A., Pietraszkiewicz, W.: The non-linear theory of elastic shells with phase transformations. J. Elast. **74**(1), 67–86 (2004)
13. Eremeyev, V.A., Pietraszkiewicz, W.: Continuity conditions in elastic shells with phase transformation. In: Gutkowski, W., Kowalewski, I.A. (eds.) Mechanics of the 21st Century: Proceedings of the 21st ICTAM, Springer, Dordrecht, Warsaw, pp. SM19L–10,287 (2005)
14. Eremeyev, V.A., Pietraszkiewicz, W.: Phase transitions in thermoelastic and thermoviscoelastic shells. Arch. Mech. **61**(1), 41–67 (2009)
15. Eremeyev, V.A., Pietraszkiewicz, W.: On tension of a two-phase elastic tube. In: Pietraszkiewicz, W., Kreja, J. (eds.) Shell Structures: Theory and Applications, vol. 2, pp. 63–66 (2010)
16. Eremeyev, V.A., Pietraszkiewicz, W.: Thermomechanics of shells undergoing phase transitions. J. Mech. Phys. Solids **59**, 1395–1412 (2011)
17. Eremeyev, V.A., Pietraszkiewicz, W.: Encyclopedia of thermal stress. In: Phase Transitions in Thermoviscoelastic Shells, pp. 3667–3673. Springer, Berlin (2014)
18. Eremeyev, V.A., Freidin, A.B., Sharipova, L.L.: The stability of the equilibrium of two-phase elastic solids. J. Appl. Math. Mech. **71**, 61–84 (2007)
19. Eremeyev, V.A., Pietraszkiewicz, W., Konopińska, V.: On continuity conditions at the phase interface of two-phase elastic shells. In: Nowacki, W.K., Zhao, H. (eds.) EMMC-10 Conference "Multi-Phase and Multi-Component Materials under Dynamic Loading", pp. 373–379. Institute of Fundamental Technological Research of PAS, PASci, Kazimerz Dolny, Poland (2007)
20. Fu, Y.B., Freidin, A.B.: Characterization ofand stability of two-phase piecewise-homogeneous deformation. Proc. R. Soc. Lond. A **460**, 3065–3094 (2004)
21. Gibbs, J.W.: On the equilibrium of heterogeneous substances. Trans. Connecticut. Acad. Sci. **3**(108–248), 343–524 (1875–1878)
22. Gurtin, M.E.: Thermomechanics of Evolving Phase Boundaries in the Plane. Clarendon Press, Oxford (1993)
23. Hartl, D.J., Lagoudas, D.C.: Aerospace applications of shape memory alloys. Proc. IMechE Part G J. Aerosp. Eng. **221**, 535–552 (2007)
24. James, R.R.R.D.: Pressurized shape memory thin films. J. Elast. **59**, 399–436 (2000)
25. Jani, M.J., Leary, M., Subic, A., Gibson, M.A.: A review of shape memory alloy research, application and opportunities. Mater. Des. **56**, 1078–1113 (2014)
26. Jiang, D., Basle, N.J., Landis, C.M., Kyriakides, C.: Buckling and recovery of NiTi tubes under axial compression. Int. J. Sol. Struct. **80**, 52–63 (2016)
27. Jiang, D., Landis, C.M., Kyriakides, S.: Effects of tension/compression asymmetry on the buckling and recovery of NiTi tube under axial compression. Int. J. Sol. Struct. **100–101**, 41–53 (2016)

28. Kabir, M.Z., Tehrani, B.T.: Closed-form solution for thermal, mechanical and thermo-mechanical buckling and post-buckling of SMA composite beams. Compos. Struct. **168**, 535–548 (2017)
29. Khachin, V.N., Pushin, V.G., Kondratiev, V.V.: Titanium Nickelide: Structure and Properties. Nauka, Moscow (1992)
30. Khusainov, M.A.: Investigation of axisymmetric buckling of round plates. Tech. Phys. J. **67**, 118–120 (1997)
31. Khusainov, M.A., Beliakov, V.N.: Investigation of power characteristics of TiNi arched strip under snap-through buckling. In: Proceedings of the 1st International Workshop "Modern Problems in Strength" named after V.A. Likhachev and 33rd Workshop "Topical Problems in Strength", Novgorod, vol. 2, pp. 139–142 (1997)
32. Khusainov, M.A., Malukhina, O.A.: Buckling analysis of shape memory spherical segments. In: Proceedings of the 3rd International Workshop "Modern Problems in Strength" named after V.A. Likhachev, Novgorod, vol. 2, pp. 185–189 (1999)
33. Khusainov, M.A., Letenkov, O.V., Batalov, A.S.: Thermal cutoff valve with an active element from shape memory alloy TiNi. Vestnik of Yaroslav the Wise Novgorod State University **65**, 40–43 (2011)
34. Klimov, K.Y., Movchan, A.A., Silchenko, T.L.: Influence of rheonomic properties of shape memory alloys on stability of beam from these materials. The J of Mekhanika Kompozitsionnykh Materialov i Konstruktsii (Composite Mechanics and Design) **19**(2), 262–267 (2013)
35. Konopińska, V., Pietraszkiewicz, W.: On jump conditions at non-material singular curves in the resultant shell thermomechanics. In: Pietraszkiewisz, W., Górski, J. (eds.) Shell Structures: Theory and Applications, Balkema, Taylor & Francis Group, London, vol. 3, pp. 117–120 (2014)
36. Konopińska, V., Pietraszkiewicz, W.: Singular curves in the resultant thermomechanics of shells. Int. J. Eng. Sci. **80**, 21–31 (2014)
37. Kuo, S.Y., Shian, L.C., Lai, C.H.: Flutter of buckled shape memory alloy reinforced laminates. Smart Mater. Struct. **21**(11), 035020 (2012)
38. Kurdyumov, G.V., Khandros, L.G.: First reports of the thermoelastic behaviour of the martensitic phase of Au-Cd alloys. Doklady Akademii Nauk SSSR **66**(2), 211–213 (1949)
39. Lee, H.J., Lee, J.J., Huh, J.S.: A simulation study on the thermal buckling behavior of laminate composite shells with embedded shape memory alloy (SMA) wires. Compos. Struct. **47**, 463–469 (1999)
40. Libai, A., Simmonds, J.G.: The Nonlinear Theory of Elastic Shells. Cambridge University Press, Cambridge (1998)
41. Likhachev, V.A.: Shape Memory Effect, Physics. St Petersburg (1997)
42. Likhachev, V.A. (ed.): Materials with Shape Memory Effect. St Petersburg (1999)
43. Malygin, G.A.: Diffuse martensitic transitions and the plasticity of crystals with a shape memory effect. Physics-Uspekhi **44**(2), 173–197 (2001)
44. Malygin, G.A., Khusainov, M.A.: Stability of the mechanical behavior of an arched TiNi strip under the conditions of the constrained shape memory effect. Tech. Phys. J. **49**(10), 1301–1307 (2004)
45. Maovchan, A.A.: Accounting for the variability of elastic moduli and for the effect of stress on the phase constitution of shape memory alloys. Mech. Solids **33**(1), 79–90 (1998)
46. Matsunaga, H.: Free vibration and stability of functionally graded plates according to a 2-D higher-order deformation theory. Compos. Struct. **82**, 499–512 (2008)
47. Matsunaga, H.: Free vibration and stability of functionally graded plates according to a 2-D higher-order deformation theory. Compos. Struct. **84**, 132–146 (2008)
48. Matsunaga, H.: Free vibration and stability of functionally graded circular cylindrical shells according to a 2D higher-order deformation theory. Compos. Struct. **88**, 519–531 (2009)
49. Matsunaga, H.: Thermal buckling of functionally graded plates according to a 2D higher-order deformation theory. Compos. Struct. **90**, 76–86 (2009)
50. Maugin, G.A.: Material Inhomogeneities in Elasticity. Chapman & Hall, London (1993)

51. Mishustin, I.V., Movchan, A.A.: Modeling of phase and structure transformations occurring in shape memory alloys under nonmonotonically varying stresses. Mech. Solids **49**(1), 27–49 (2014)
52. Movchan, A., Silchenko, L.: Stability of a shaft made from a shape memory alloy undergoing martensite phase transitions under the action of torque strength and an axial force. J. Mach. Manuf. Reliab. **38**(2), 154–160 (2009)
53. Movchan, A., Kazarina, S., Silchenko, L., Danilin, A.: Phenomenon of stability loss due to thermoelastic phase transition under a compressive loading. In: Contemporary Research in Theory and Applied Mechanics: Proceedings of 14th US National Congress of Theory and Applied Mechanics, VA, Blacksburg, p. 424 (2002)
54. Movchan, A., Silchenko, L., Kazarina, S., Zhavoronok, S., Silchenko, T.: Stability of titanium nickelide rods loaded in the mode of martensite inelasticity. J. Mach. Manuf. Reliab. **41**(3), 245–251 (2012)
55. Movchan, A., Kazarina, S., Mashikhin, A., Mishustin, I., Saganov, E., Safronov, P.A.: Boundary value problems of mechanics for shape memory alloys. Uchenye Zapiski Kazanskogo Universiteta Seriya Fiziko-Matematicheskie Nauki Memoires Kazan State Univ Phys & Math **157**(3):97–110 (2015)
56. Movchan, A.A.: Micromechanical constitutive equations for shape memory alloys. J. Mach. Manuf. Reliab. **6**, 47–53 (1994)
57. Movchan, A.A.: Coupling effects in bending problems for beams of a shape memory alloy. J. Appl. Mech. Tech. Phys. **39**(1), 143–151 (1998)
58. Movchan, A.A.: Torsion of prismatic beams of shape memory alloys. Mech. Solids **35**(6), 143–154 (2000)
59. Movchan, A.A., Dumansky, S.A.: Solution of the twice-coupled problem of instability of a rod of shape memory alloy caused by a direct thermo-elastic phase transformation. J. Appl. Mech. Tech. Phys. **59**(4), 716–723 (2018)
60. Movchan, A.A., Kazarina, S.A.: Experimental investigation of the buckling resulted by thermoelastic phase transforms under compressive stresses. J. Mach. Manuf. Reliab. **31**(6), 82–89 (2002)
61. Movchan, A.A., Silchenko, L.G.: Stability of the Shenley column under creep or under straight thermoelastic martensite transformation. The J of Mekhanika Kompozitsionnykh Materialov i Konstruktsii (Composite Mechanics and Design) **6**(1), 89–103 (2000)
62. Movchan, A.A., Silchenko, L.G.: Buckling of a rod undergoing direct or reverse martensite transformation under compressive stresses. J. Appl. Mech. Tech. Phys. **44**(3), 442–449 (2003)
63. Movchan, A.A., Silchenko, L.G.: Analysis of buckling induced by the direct thermoelastic transformation under the action of compression stresses. Mech. Solids **39**(2), 104–114 (2004)
64. Movchan, A.A., Silchenko, L.G.: Analytical solution of the coupled buckling problem for a plate from a shape memory alloy subjected to inverse martensite transformation. Mech. Solids **39**(5), 134–139 (2004b)
65. Movchan, A.A., Silchenko, L.G.: Buckling of SMA elements under inverse martensite transforms. In: Proceedings of the 10th International Workshop "Dynamical and Technological Problem of Mechanics of Structures and Continua", MAI, Moscow, vol. 1, pp. 91–93 (2004)
66. Movchan, A.A., Silchenko, L.G.: The stability of a plate of shape memory alloy in a direct thermoelastic phase transition. J. Appl. Math. Mech. **68**(1), 53–64 (2004)
67. Movchan, A.A., Silchenko, L.G.: The stability of a circular plate of shape memory alloy during a direct martensite transformation. J. Appl. Math. Mech. **70**(6), 785–795 (2006)
68. Movchan, A.A., Silchenko, L.G.: Stability of a round shape memory alloy plate at direct martensitic transformation. Phys. Met. Metall. **70**(5), 869–879 (2006)
69. Movchan, A.A., Silchenko, L.G.: Buckling of a circular plate made of a shape memory alloy due to a reverse thermoelastic martensite transformation. Mech. Solids **43**(1), 100–111 (2008)
70. Movchan, A.A., Silchenko, L.G.: Buckling of the cylindrical plate made from the shape memory alloy at thermoelastic martensite transitions in the conditions of compression and shear. The J of Mekhanika Kompozitsionnykh Materialov i Konstruktsii (Composite Mechanics and Design) **15**(2), 221–241 (2009)

71. Movchan, A.A., Silchenko, L.G.: Buckling of the cylindrical shell from the shape memory alloy at compression and torsion. The J of Mekhanika Kompozitsionnykh Materialov i Konstruktsii (Composite Mechanics and Design) **15**(4), 486–496 (2009)
72. Movchan, A.A., Kazarina, S.A., Serov, V.: Experimental investigation of the buckling caused by thermoelastic phase transitions under compressive stresses. In: Proceedings of the 13rd Petersburg Lecturing on Strength Problems, St. Petersburg, pp. 7–9 (2002)
73. Movchan, A.A., Movchan, I.A., Silchenko, L.G.: Stability of an annular plate of a shape memory alloy. J. Appl. Mech. Tech. Phys. **52**(2), 279–287 (2011)
74. Movchan, A.A., Slichenko, L.G., Silchenko, T.L.: Taking account of the martensite inelasticity in the reverse phase transformation in shape memory alloys. Mech. Solids **46**(2), 194–203 (2011b)
75. Movchan, A.A., Kazarina, S.A., Dumanskiy, S.A.: Once and twice coupled buckling problems for shape memory alloys. Russ. Metall. (Metally) **6**, 2–8 (2017)
76. Nushtaev, D.V., Zhavoronok, S.I.: Dynamics of martensite phase transitions in shape memory beams under buckling and postbuckling conditions. IFAC PapersOnLine **51**(2), 873–878 (2018)
77. Ostachowicz, W., Krawczuk, M., Zak, A.: Dynamics and buckling of a multilayer composite plate with embedded SMA wires. Compos. Struct. **48**, 163–167 (2000)
78. Otsuka, K., Wayman, C.M.: Shape Memory Materials. Cambridge University Press, Cambridge (1998)
79. Ovcharenko, E.A., Klyshnikov, K.Y., Vlad, A.R., Sizova, I.N., Kokov, A.N., Nushtaev, D., Yuzhalin, A., Zhuravleva, I.: Computer-aided design of the human aortic root. Comput. Biol. Med. **54**, 109–115 (2014)
80. Park, J.S., Kim, J.H., Moon, S.H.: Thermal postbuckling and flutter characteristics of composite panels embedded with shape memory alloy fibers. Compos. Part B **36**, 627–636 (2005)
81. Pietraszkiewicz, W.: Refined resultant thermomechanics of shells. Int. J. Eng. Sci. **49**, 1112–1124 (2011)
82. Pietraszkiewicz, W.: Encyclopedia of continuum mechanics. Surface Geometry Elements. Springer, Berlin (2018). https://doi.org/10.1007/978-3-662-53605-6_186-1
83. Pietraszkiewicz, W.: Encyclopedia of continuum mechanics. Thin Elastic Shells, Linear Theory. Springer, Berlin (2018). https://doi.org/10.1007/978-3-662-53605-6_187-1
84. Pietraszkiewicz, W., Eremeyev, V.A., Konopińska, V.: Extended non-linear relations of elastic shells undergoing phase transitions. ZAMM—Zeitschr für Angew Math Mech **87**(2), 150–159 (2007)
85. Rahman, M.A., Tani, J.: Buckling of tubular superelastic shape memory alloy shafts. Struct. Eng. Mech. Int. J. **27**, 523–526 (2007)
86. Rahman, M.A., Qiu, J., Tani, J.: Buckling and postbuckling characteristics of the superelastic SMA columns—numerical simulation. J. Intell. Mater. Syst. Struct. **16**, 691–702 (2005)
87. Rahman, M.A., Qiu, J., Tani, J.: Buckling and postbuckling behavior of solid superelastic shape memory alloy shafts. Struct. Eng. Mech. Int. J. **23**, 339–352 (2006)
88. Rahman, M.A., Akanda, S.R., Hossain, M.A.: Effect of cross-section geometry on the response of an SMA column. J. Intell. Mater. Syst. Struct. **19**, 243–252 (2007)
89. Sharipova, L.L., Yeremeyev, V.A., Freidin, A.B.: The stability of an elastic two-phase sphere. Mathematical Modeling, Izv Vuzov Sev-Kavk Region Yestest Nauki Special Issue, pp. 166–168 (2001) (in Russian)
90. Silchenko, L.G.: A phenomenon of the loss of stability in the case of martensite inelasticity. The J of Mekhanika Kompozitsionnykh Materialov i Konstruktsii (Composite Mechanics and Design) **8**(2), 161–171 (2002)
91. Silchenko, L.G.: On stability of a rod made from an alloy with shape memory under direct martensite thermal-elastic phase transformation. The J of Mekhanika Kompozitsionnykh Materialov i Konstruktsii (Composite Mechanics and Design) **9**(4), 457–470 (2003)
92. Silchenko, L.G.: On the loss of stability of rods made of a shape memory alloy caused reactive compressive stress in the reverse martensitic phase transformation. The J of Mekhanika Kompozitsionnykh Materialov i Konstruktsii (Composite Mechanics and Design) **10**(3), 393–406 (2004)

93. Silchenko, L.G.: Stability cramped rods from a shape memory alloy in the reverse martensitic phase transformation. The J of Mekhanika Kompositsionnykh Materialov i Konstruktsii (Composite Mechanics and Design) **10**(4), 566–576 (2004)
94. Silchenko, L.G.: Stability of circular plate of shape memory alloy with the direct martensitic transformation taking into account variable cross-zone size additional phase transformation. The J of Mekhanika Kompozitsionnykh Materialov i Konstruktsii (Composite Mechanics and Design) **11**(3), 451–466 (2005)
95. Silchenko, L.G.: Resistance of rod of shape memory alloy at thermoelastic phase transformations taking into account the transverse shear deformations. The J of Mekhanika Kompozitsionnykh Materialov i Konstruktsii (Composite Mechanics and Design) **12**(4), 458–470 (2006)
96. Silchenko, L.G.: Buckling of rectangular shape memory alloy plates under shear loadings. The J of Mekhanika Kompozitsionnykh Materialov i Konstruktsii (Composite Mechanics and Design) **13**(1), 141–152 (2007)
97. Silchenko, L.G., Silchenko, T.L.: On the buckling of shape memory alloys elements at structural transition taking threshold stresses into account. The J of Mekhanika Kompozitsionnykh Materialov i Konstruktsii (Composite Mechanics and Design) **16**(4), 457–468 (2010)
98. Silchenko, L.G., Movchan, A.A., Silchenko, T.L.: Stability of a cylindrical shell made of a shape memory alloy. Int. Appl. Mech. **19**(2), 262–277 (2014)
99. Simmonds, J.G.: Flexible shells, theory and applications. In: The Nonlinear Thermodynamical Theory of Shells: Descent from 3-Dimensions Without Thickness Expansions, pp. 1–11. Springer, Berlin (1984)
100. Song, C.: History and current situation of shape memory alloys devices for minimally invasive surgery. Open Med. Dev. J. **2**, 24–31 (2010)
101. Sreekumar, M., Nagarajan, T., Singaperumal, M., Zoppi, M., Molfino, R.: Critical review of current trends in shape memory alloy actuators for intelligent robotics. Int. J. Ind. Rob. **34**, 285–294 (2007)
102. Tarlakovskii, D.V., Zhavoronok, S.I.: On the compatibility equations in shell theories considering transverse shear and normal strains. In: Pietraszkiewicz, W., Witkowski, W. (eds.) Shell Structures: Theory and Applications, Balkema, Taylor & Francis Group, London, vol. 4, pp. 173–176 (2018)
103. Tawfik, M., Ro, J.J., Mei, C.: Thermal post-buckling and aeroelastic behavior of shape memory alloy reinforced plate. Smart Mater. Struct. **11**, 297–301 (2002)
104. Thompson, S.P., Laughlan, J.: Adaptive post-buckling response of carbon fibre composite plates employing SMA actuators. Compos. Struct. **38**, 667–678 (1997)
105. Thomson, D., Griffin, O.: Finite element predictions of active buckling control of stiffened panels. J. Intell. Mater. Syst. Struct. **4**, 243–247 (1993)
106. Watkins, R., Shaw, J.: Shape memory alloy column buckling: an experimental study. In: CAST 2013—24th International Conference on Adaptive Structures and Technology (2013)
107. Wei, Z.G., Sandström, R.: Review. Shape-memory materials and hybrid composites for smart systems: part I. shape-memory materials. J. Mater. Sci. **33**, 3743–3762 (1998)
108. Whittaker, E.T., Robinson, G.: The calculus of observations: a treatise of numerical mathematics. In: The Newton-Raphson Method, Dover, New York (1967)
109. Yeremeyev, V.A.: Bulging of a non-linear elastic plate lying on the liquid surface taking phase transitions into account. Appl. Mech. Tech. Phys. **3**, 141–147 (1991)
110. Yeremeyev, V.A.: Equilibrium and stability of micro-inhomogeneous elastic solids undergoing phase transitions. Mat Modelirovanie **9**(2), 68–69 (1997). (in Russian)
111. Yeremeyev, V.A., Zubov, L.M.: The stability of the equilibrium of non-linear elastic solids undergoing phase transitions. Izv AN SSSR, MTT **2**, 58–65 (1991)
112. Zhavoronok, S.I.: Variational formulations of Vekua-type shell theories and some of their applications. In: Pietraszkiewisz, W., Górski, J. (eds.) Shell Structures: Theory and Applications, Balkema, Taylor & Francis Group, London, vol. 3, pp. 341–344 (2014)
113. Zhavoronok, S.I.: A Vekua-type linear theory of thick elastic shells. ZAMM—Zeitschr für Angew Math Mech **94**(1–2), 164–184 (2014)

114. Zhavoronok, S.I.: The generalized Lagrange equations of the second kind for the extended three-dimensional nth order theory of anisotropic shells. The J Of Mekhanika kompozitsionnykh materialov i konstruktsii (Composite Mech Design **21**(3), 370–381 (2015)
115. Zhavoronok, S.I.: On the variational formulation of the extended thick anisotropic shells theory of IN Vekua type. Procedia Eng.**111**, 888–895 (2015)
116. Zhavoronok, S.I.: Encyclopedia of continuum mechanics. In: Elastic Shells, Linear Shear-Deformable Theory, Springer, Berlin (2018). https://doi.org/10.1007/978-3-662-53605-6_194-1
117. Zhavoronok, S.I.: A general higher-order shell theory based on the analytical dynamics of constrained continuum systems. In: Pietraszkiewicz, W., Witkowski, W. (eds.) Shell Structures: Theory and Applications, Balkema, Taylor & Francis Group, London, vol. 4, pp. 189–192 (2018)

On the Homogenization of Nonlinear Shell

Erick Pruchnicki

Abstract In this paper we propose a multiscale finite-strain shell theory for simulating the mechanical response of highly heterogeneous shell with varying thickness. To resolve this issue a higher-order stress-resultant shell formulation based on multiscale homogenization is considered. At the macroscopic scale level, we approximate the displacement field by a fifth-order Taylor-Young expansion in thickness. We take account of the microscale fluctuations by introducing a boundary value problem over the domain of a three-dimensional representative volume element (RVE). The geometrical form and the dimensions of the RVE are determined by the representative microstructure of the heterogeneity. In this way, an in-plane homogenization is directly combined with a through thickness stress integration. As a result the macroscopic stress resultants are the volume averages through RVE of microscopic stress. All microstructural constituents are modeled as first-order continua and three-dimensional continuum, described by the standard equilibrium and the constitutive equations. This type of theory is anxiously awaited.

Keywords Nonlinear elasticity · High-order shell theory · Homogenization · Macro micro Hill-Mandel condition · Thin structure with varying thickness

1 Introduction

Shells are very common structures in engineering, which have inspired extensive research interests on shell theory and its application [1, 2]. Shell theories with small strains can be dated back at least 120 years ago. A recent review of direct theories has been made by Altenbach et al. [3]. Early attempts on shell theories are motivated by engineering intuition which rely on a priori hypotheses of a geometrical or mechanical nature. The classical shell theory, developed by Love [4] is based on Kirchhoff's assumptions [5] and thin shell approximation. Sanders [6] gives the "best" variants of first approximation theory. Further works relaxed some assumptions, these furnish some well-known shell theories [7]. An alternative mathematical approach using

E. Pruchnicki (✉)
Department of Mathematic, University of Lille, 59655 Villeneuve d'Ascq Cedex, France
e-mail: Erick.Pruchnicki@gmail.com

H. Altenbach et al. (eds.), *Recent Developments in the Theory of Shells*,
Advanced Structured Materials 110, https://doi.org/10.1007/978-3-030-17747-8_27

asymptotic expansion method to the three dimensional differential formulation to derive shell theory has been proposed by Gol'denveizer [8]. Ciarlet and Destuynder [9, 10] for plates and Destuynder [11] for shells apply asymptotic method to the three dimensional weak formulation. Convergence results can be obtained for some linear shell theories. For some nonlinear theory, the limiting two-dimensional variational problem of vanishing thickness can also be achieved by Gamma convergence method [12, 13].

Nevertheless these approaches do rely on a priori scalings, assuming applied loads (or deformation) be of certain orders of shell thickness. In reality applied loads are external, which should not be directly related to the thickness in various situations. We obviously meet the same drawback for heterogeneous shells Pruchnicki [14].

Based on more general expansions of displacements, some higher-order refined shell theories have also been derived by three dimensional variational principle method for linear case [15, 16] and for nonlinear case Meroueh [17]. Recently, starting from three dimensional elasticity, Steigmann [18, 19] derives from three-dimensional elasticity a notable shell theory which extends Koiter's shell theory and dictates an optimal third-order approximation for the three-dimensional potential energy. To include the effect of transverse normal stress and transverse shearing, Pruchnicki [20, 21] proposes an optimal fifth-order approximation for the three-dimensional potential energy. We can note that is model satisfy the Legendre–Hadamard condition.

However, theses derivations are restricted to the nearly traction-free case. Thus recently, Song and Dai [22] propose a finite-strain shell theory, which is consistent with the three-dimensional energy principle and with no special restrictions on applied loads.

A new type of general, theoretical framework for the development of comprehensive, nonlinear, multiscale plate theories for laminated structures is presented by Williams [23]. The theoretical framework utilizes a generalized two scale description of the displacement field based on a superposition of global and local effects. The extension to nonlinear shell is only a single scale theory [24]. The zig-zag theories can equally be used to model the behaviour of laminates but they are limited to linear material behaviour [25]. Nevertheless it is not a homogenization method since the computation on the two scales are simultaneously processed. The size of fine scale details in these heterogeneous shells is typically much smaller compared to the dimensions of the structure, thus making direct numerical analyses is prohibitively expensive. To avoid these large-scale computations, it is preferable to model these shells at the macroscale as a homogeneous continuum with effective properties obtained through a homogenization procedure. This method results from solution of two coupled boundary value problems, one at a local scale and other at a global scale. The field of the homogenization of layered composite plates and shells is by now well established for linear material behavior [26]. Sandwich panels consist of a heterogeneous core bonded to two face sheets, the face sheets carry the in-plane loads and the bending moments, whereas the core keeps the face sheets at the desired distance from each other and carries transverse shear loads. The effective properties of the core can be determined by means of classical analytical or numerical

homogenization methods Lewinski and Telega [27]. Next, the whole sandwich structure can be analyzed by application of appropriate laminate composite theory [28]. More recently a coupled two-scale model for layered shell is presented [29, 30, 31].

In the last few years, the masonry community obtained the homogenized flexural characteristics of masonry [32, 33, 34, 35]. These works (except for Mistler et al. [34]) rely on the specific characteristics of masonry (particular geometry and material behavior of constituents), and thus cannot be directly applied to other structural heterogeneous thin structure. In the study of Petracca et al. [36], focused on periodic brick-masonry walls, the macro-scale behavior obeys a Reissner–Mindlin and the local heterogeneous structures is assumed to be transverse isotropic. In many cases, however, the microstructure of heterogeneous shell has a truly three-dimensional character.

Based on asymptotic homogenization concepts, Caillerie [37] and Kohn and Vogelius [38] discussed the homogenization of heterogeneous periodic linear elastic plates. These models are mathematically elegant and rigorous but only related to a simple engineering model (the Kirchhoff plate model). Unfortunately, it is not easy to extend this approach to yield a refined theory (the Reissner-Mindlin model or higher order model) that is capable of capturing transverse shear deformation. The development of this idea are recently proposed by Pruchnicki [39], this issue seems to be restricted to linear elasticity, despite it appears to be a very complicated process even with the transverse isotropy assumption of the local heterogeneous structure.

Geers et al. [40] propose computational homogenization of structured thin sheets and more recently Coenen et al. [41] propose a framework with the same main objectives as in this paper. In these contributions, an inextensible director Kirchhoff–Love shell model for the macroscale is assumed along with a homogenization scheme for the involved stress resultants. The derivation of the homogenization scheme is inspired by multiscale modeling in higher-order continua like second gradient Kouznetsova et al. [42] and Larsson and Diebels [43], where second-order expansions are used to introduce the effect of the macroscopic second-gradient within the RVE. The homogenization procedure is based on the virtual work equivalence between macro and micro fields within a (RVE), Suquet [44] and Miehe et al. [45]. This condition is equivalent to the classical Hill-Mandel condition for macro-homogeneity within the RVE for both first-order and second order homogenization scheme. In the present context of a shell model, the adopted micro–macro transition yields the homogenized stress resultants of the shell in terms of convected coordinates, see also the developments in Grytz and Meschke [46]. In this vein, Larsson and Landervik [47] propose a new model for homogenization of heterogeneous shell based on a second order expansion in thickness of the current position of the shell and finally a simplified asumption on the initial geometry of the shell. The method of homogenization valid for periodic heterogeneous plates and proposed by Lee et al. [48], gives interesting result but it seems to be restricted to small deformations and large rotations and displacements. As a consequence, this approach seems to be intractable in the fully nonlinear setting. This is due to fact that the simplification linked to the application of variational-asymptotic method [49, 50] runs only under the small deformation assumption.

This paper concerns modeling of the mechanical response of heterogeneous shell structures. In order to solve this problem at a microscopic local level we take account of the scale separation in the tangent mid-surface plane of the heterogeneity. This two-scale procedure alleviates computational burden of the truly tridimensional problem. From solving the RVE boundary value problem, the microscopic fluctuations of the deformation field are obtained then we can compute the macro deformation field over the entire shell. This approach do not require any explicit assumptions on the format of the microscopic local constitutive equations. It also enable the incorporation of large deformations and the possibility to introduce the physical and geometrical evolution of the microstructure into the macroscopic analysis and finally allow the use of any modeling technique on the microlevel, the finite element method [51, 52, 53], the boundary element method [54], the Voronoi cell method [55, 56], a crystal plasticity framework [57, 58] or numerical methods based on Fast Fourier Transforms [59, 60, 61] and Transformation Field Analysis [62].

With regard to the processing of macroscopic scale, we note that the topic of bidimensional modelisation of shell has been extensively investigated, in particular, with respect to the capabilities of the shell model to properly describe tridimensional phenomena such as thickness strains.

In the present paper, we employ a fourth-order expansion in the normal direction of the mid-plane leading to an extension for heterogeneous shell of the recent model proposed by Dai and Song [63] for homogeneous plate and for Song and Dai [22] for homogeneous shell. This type of model circumvents the so-called "Poisson locking effect" due to incompatible representation of thickness strains as compared to strains generated by bending action. Thus in this work we remove Love-Kirchoff assumption [41, 64], then we consider a completely general through thickness expansion (up to fourth-order in thickness) of the displacement field. In addition, for Mindlin or Kirchoff models, the constitutive law is two-dimensional, and the thickness change of the plate is not taken into account, and then the finite element formulations suffer many locking problems [65]. In literature, two concepts has been proposed for plate theory with thickness change, for the first one, two extra degrees of freedom are added to the transverse displacements to obtain a quadratic displacement in thickness direction [66], the second one is the enhanced assumed strain concept method proposed by Buechter et al. [67] (an extra degree of freedom is introduced locally). However, these solutions have drawbacks, as for instance if considering an elasto-plastic material law [68]. Because of these drawbacks, a numerical homogenization method with extra degree of freedom, which accounts for the thickness change, either at global [69] or local [70] scales are developed. Also, Fillep et al. [71, 72] modelize technical textile as a Mindlin shell with thickness change.

We obtain the macroscopic bidimensional homogeneous shell from the analysis of a microstructural representative volume element (RVE), representing the full thickness of the shell and an in-plane representative cell of the macroscopic structure. The relevant volume associated with the macroscopic point is represented by a microstructural through thickness RVE (which can be varied over le mid-surface due to the curvature variation). At each macroscopic material point of the shell continuum (for numerical implementation it may be integration point in a finite element

setting) a constitutive relation between the generalized strains (i.e. the directors of expansion displacement field) and the generalized stresses is needed.

Then it is necessary to define the relation between the definitions of the macroscopic generalized strains and stresses for a shell continuum in terms of the microscopic ones. This macro-to-micro scale transition is performed by imposing the macroscopic generalized deformation gradient on the RVE through the essential boundary conditions that may be periodic conditions. At the RVE scale, all microstructural constituents are treated as an ordinary three-dimensional continuum, described by the standard first-order equilibrium and the governing local constitutive equations. Upon solution of the microstructural boundary value problem, the macroscopic generalized stress resultants are expressed by averaging the computed RVE stress field through the use of a generalised Hill-Mandel condition for shell (i.e. an energy condition where the energy in the macroscale is equal to the one in the microscale). In our work, the through thickness dimension is directly combined with the in-plane homogenization. We consider non-zero external forces acting on the top and bottom shell face and body forces. The effect of non-zero external forces acting on the top and bottom shell face is considered in the work of Larsson and Landervik [47] but it is not clear since this load act on simultaneously (twice) on both the local and global scales. This type of procedure is computationally demanding and suitable for parallel processing, Feyel and Chaboche [52]. The paper ends with some concluding remarks.

1.1 Notation

In this section, we provide the main notation and describe in detail the problem we will consider.

Throughout this paper, the summation convention is adopted. The Latin indices take the values 1, 2, 3. The Greek indices run over 1, 2. Boldface letters represent vector-valued functions, tensors or spaces. Ω is an open subset of the Euclidean space $\mathbb{R}^n$ ($n \in \mathbb{N}$). The closure and the boundary of Ω are respectively denoted by $\overline{\Omega}$ and $\partial\Omega$. A domain Ω in $\mathbb{R}^n$ is a bounded, open, connected subset of $\mathbb{R}^n$. Let (e_1, e_2, e_3) denotes an orthonormal basis of the space $\mathbb{R}^3$. The Euclidean scalar product, the exterior product and the tensor product of vectors a, b, $\mathbb{R}^3$ are denoted by a.b, $a \wedge b$ and $a \otimes b$, and the Euclidean norm of the vector $\mathbf{a}$ is denoted by $|\mathbf{a}|$. A double dot between two second-order tensors $\mathbf{A}$, $\mathbf{B}$ is used to denote the standard inner product of their associated matrices: then $\mathbf{A}\mathbf{:}\,\mathbf{B} = \mathrm{tr}(\mathbf{A}^{\mathrm{T}}\,\mathbf{B})$, where tr( ) is the trace and the superscript $^{\mathrm{T}}$ is used to denote the transpose. Subscripts preceded by a comma are used to denote partial derivatives with respect to curvilinear coordinates.

1.2 Description of the Shell Geometry

In the plane $(\mathbf{O}, \mathbf{e}_1, \mathbf{e}_2)$, we consider a domain ω. Let θ: $\omega \to \mathrm{R}^3$ be an injective mapping belonging to $C^\infty(\bar{\omega}, \mathbb{R}^3)$ and such that the two vectors $\mathrm{a}_\alpha(\mathrm{x}') = \theta_{,\alpha}(\mathrm{x}')$ are linearly independent at each $\mathrm{x}' = (x_1, x_2) \in \bar{\omega}$. In other words, x' is the curvilinear coordinates which parametrizes the base surface ω of the shell in the reference configuration, therefore $\hat{x}' := \theta(\mathrm{x}')$ is a generic point of the base surface. We see that $(\mathbf{a}_1(\mathbf{x}'), \mathbf{a}_2(\mathbf{x}'))$ forms the covariant basis of the tangent plane to the mid-surface $S = \theta(\bar{\omega})$ at the point $\hat{\mathbf{x}}'$; the two vectors $\mathrm{a}^\alpha(\mathrm{x}')$ defined by the relation $\mathrm{a}^\alpha(\mathrm{x}').\mathrm{a}_\beta(\mathrm{x}') = \delta^\beta_\alpha$ constitute the *contravariant basis* of the tangent plane. For each $\mathrm{x}' \in \bar{\omega}$, the unit vector
is defined by:

$$\mathrm{a}_3(\mathrm{x}') = \mathrm{a}^3(\mathrm{x}') := \frac{\mathrm{a}_1(\mathrm{x}') \wedge \mathrm{a}_2(\mathrm{x}')}{|\mathrm{a}_1(\mathrm{x}') \wedge \mathrm{a}_2(\mathrm{x}')|}$$

is normal to the mid-surface S at the point x'.

Further, $\kappa = \kappa^\beta_\alpha \, \mathrm{a}_\alpha \otimes \mathrm{a}^\beta = \kappa_{\alpha\beta} \mathrm{a}^\alpha \otimes \mathrm{a}^\beta$ is the second-order curvature tensor of the mid-surface. Then by the Weingarten equations, the variation of a_3 is described by the curvature tensor κ

$$\mathrm{a}_{3,\,\alpha} = -\boldsymbol{\kappa}.\mathrm{a}_\alpha. \tag{1}$$

Then, the mean and Gaussian curvature tensor are defined by

$$H = \frac{1}{2} tr(\boldsymbol{\kappa}) = \frac{1}{2}\kappa^\alpha_\alpha, \quad K = \det(\boldsymbol{\kappa}) = \frac{1}{2}\left[(2H)^2 - \kappa^\beta_\alpha \kappa^\alpha_\beta\right] = \kappa^1_1 \kappa^2_2 - \kappa^2_1 \kappa^1_2.$$

By choosing orthogonal principal directions of the curvature tensor as the base vectors, the non zero components $\kappa^1_1 := \kappa_1$ and $\kappa^2_2 := \kappa_2$ are called the two principal curvatures, and consequently $H = (\kappa_1 + \kappa_2)/2$ and $K = \kappa_1 \kappa_2$.

Now we define the reference or undeformed position of the shell Ω, which is defined through the relation:

$$\hat{x} = \Theta(\mathrm{x}) := \theta(\mathrm{x}') + x_3 \mathrm{a}_3(\mathrm{x}') \quad \text{for} \quad \mathrm{x} \in \overline{\Omega}, \tag{2}$$

with $\mathrm{x} = (x_1, x_2, x_3)$ and $\hat{x} = (\hat{x}_1, \hat{x}_2, \hat{x}_3)$; $\mathbf{x}$ are called the curvilinear coordinates of $\hat{x}$.

Accordingly from formulae (1) and (2), the differential of the reference position is given by:

$$d\hat{x} = d\theta + \mathrm{a}_3 dx_3 + x_3 d\mathrm{a}_3 = \boldsymbol{\mu}.d\theta + \mathrm{a}_3 dx_3,$$

in which $\boldsymbol{\mu} = 1 - x_3\boldsymbol{\kappa}$ and $\mathbf{1} = \mathrm{I} - \mathrm{a}_3 \otimes \mathrm{a}_3 = \mathrm{a}_\alpha \otimes \mathrm{a}^\alpha$ is the second order tensor within the tangent plane to the curved mid-surface S.

Now we define the covariant base vectors at an arbitrary point inside the shell:

$$\mathrm{g}_\alpha(\mathrm{x}) := \Theta_{,\alpha}(\mathrm{x}) \quad \text{and} \quad \mathrm{g}_3\big(\mathrm{x}'\big) := \Theta_{,3}(\mathrm{x}) = \mathrm{a}_3\big(\mathrm{x}'\big), \tag{3}$$

By considering Eqs. (1), (2) and (3), we get the following expressions for both the covariant and contravariant basis inside the shell:

$$\mathrm{g}_\alpha = \boldsymbol{\mu}.\mathrm{a}_\alpha, \quad \mathrm{g}^\alpha = \mathrm{a}^\alpha.\boldsymbol{\mu}^{-1}, \quad \mathrm{g}_3 = \mathrm{g}^3 = \mathrm{a}_3,$$

We can note that g_α and g^α are orthogonal to a_3.

The volume element $d\hat{v}$ at the point $\hat{x} = \Theta(\mathrm{x})$ in the set $\widehat{\Omega} = \Theta(\Omega)$ is calculated in terms of the volume element $d\mathrm{v} = dadx_3$ at the point $\mathbf{x}$ in the set Ω:

$$d\hat{v} = \mu dadx_3$$

in which μ is the two-dimensional determinant of $\boldsymbol{\mu}$, $\mu = 1 - 2Hx_3 + Kx_3^2 = (1 - x_3\kappa_1)(1 - x_3\kappa_2)$ and $da = |\mathrm{a}_1 \wedge \mathrm{a}_2|dx_1dx_2$ is the differential area element of the base surface S. Therefore Θ is one to one and orientation preserving if and only if $\mu > 0$ which is obtained in the region of the space in which

$$|x_3| < \mathrm{Min}(r_1, r_2)$$

where $r_\alpha = |\kappa_\alpha|^{-1}$ are the principal radii of curvature [73, 74].

The current position is written as $\tilde{x}(\mathrm{x})$, then deformation gradient is given by:

$$\mathrm{F} = \tilde{x}_{,i} \otimes \mathrm{g}^i = \nabla\tilde{x}.\boldsymbol{\mu}^{-1} + \tilde{x}_{,3} \otimes \mathrm{a}^3 \tag{4}$$

in which $\nabla\tilde{x} = \tilde{x}_{,\alpha} \otimes \mathrm{a}^\alpha$.

This shell is heterogeneous and the size of the heterogeneities, which is assumed to be of the same order of magnitude of the average thickness (not necessary constant), is very small with regard to the global length-scale x'. For the sake of simplicity, we assume that the heterogeneous microstructure (which is usually made of two materials) of the shell is periodic with respect to the curvilinear coordinate x' and the thickness and the microstructure variations are of the same order of magnitude. Then the microstructure can be defined by a VER.

1.3 The Bidimensional Macroscopic Nonlinear Shell Model

For a hyperelastic material with strain energy function $W(\mathrm{F})$, the first Piola-Kirchoff strain tensor is defined by:

$$\pi = \frac{\partial W}{\partial \mathrm{F}}.$$

For the case of dead loading the potential energy is given by:

$$E = \Psi + V$$

$\Psi = \int_{-\frac{h}{2}}^{\frac{h}{2}} \int_S W(\mathrm{F}) \mu da dx_3$ is the internal energy

$V = \int_{-\frac{h}{2}}^{\frac{h}{2}} \int_{\partial S_t} \bar{t}(s, x_3).\tilde{x}(s, x_3) \psi ds dx_3$ is the work of exterior forces,

in which h is the constant thickness of a fictive homogenized shell which is assumed to be the mean thickness of the shell defined by (the implicit equation with respect to h)

$$\int_S \int_{-\frac{h}{2}}^{\frac{h}{2}} \mu dx_3 da = \int_S \int_{x_3^-(\mathrm{x}')}^{x_3^+(\mathrm{x}')} \mu dx_3 da,$$

the lower (respectively the upper) boundary of the shell are defined by $x_3 = x_3^-(x')$ (respectively $x_3 = x_3^+(x')$), ∂S_t is the part of the boundary of the mid-surface S submitted to a prescribed stress tensor $\bar{t}$. t^- (respectively t^+) denotes the prescribed stress vector on the lower (respectively upper) boundary of the shell. Finally we define ψ, s measures the arc length on the curve ∂S_t with unit tangent τ and unit normal $\nu = \tau \wedge \mathrm{a}_3$ then $\psi = \sqrt{(1 - x_3 \kappa_\tau)^2 + x_3^2 \chi^2}$ in which κ_τ and χ are the normal curvature on the (τ, a_3)-plane and twist of ∂S on the (ν, τ)-axes (defined by the representation $\kappa = \kappa_\nu \nu \otimes \nu + \kappa_\tau \tau \otimes \tau + \chi(\nu \otimes \tau + \tau \otimes \nu)$) (for details see Steigmann [18], Pruchnicki [21], Song and Dai [22]).

Remark On the global macroscale, we do not consider the effect of the load on both upper and lower faces of the shell and the body forces since they act on the basic cell linked to local microscopic scale. Nevertheless, this load act obviously on the macroscopic through the local scale.

The principle of stationary potential energy requires that the variation of the potential energy vanishes:

$$\delta E = \int_{-\frac{h}{2}}^{\frac{h}{2}} \int_S \pi : \delta \mathbf{F} \mu da dx_3 + \int_{-\frac{h}{2}}^{\frac{h}{2}} \int_{\partial S_t} \bar{t}(s, x_3).\delta\tilde{x}(s, x_3) \psi ds dx_3 = 0. \quad (5)$$

Now we suppose that the current position $\tilde{x}(\mathrm{x})$ is C^4 in their arguments. Then, the current position is expanded about the base surface in the form:

$$\tilde{x}(\mathrm{x}) = \tilde{x}^{(0)}(\mathrm{x}') + x_3 \tilde{x}^{(1)}(\mathrm{x}') + \frac{x_3^2}{2} \tilde{x}^{(2)}(\mathrm{x}') + \frac{x_3^3}{6} \tilde{x}^{(3)}(\mathrm{x}') + \frac{x_3^4}{24} \tilde{x}^{(4)}(\mathrm{x}') + O(x_3^5), \quad (6)$$

where $(.)^{(n)} = \partial^n(.)/\partial x_3\big|_{x_3=0}$ $(n = 1, \ldots, 4)$.

Accordingly, the deformation gradient has a similar expansion

$$\mathrm{F}(\mathrm{x}) = \mathrm{F}^{(0)}(\mathrm{x}') + x_3\mathrm{F}^{(1)}(\mathrm{x}') + \frac{x_3^2}{2}\mathrm{F}^{(2)}(\mathrm{x}') + \frac{x_3^3}{6}\mathrm{F}^{(3)}(\mathrm{x}') + \frac{x_3^4}{24}\mathrm{F}^{(4)}(\mathrm{x}') + O(x_3^5). \tag{7}$$

From the definition (4), we see that:

$$\mathrm{F} = \nabla\tilde{x}.\boldsymbol{\mu}^{-1} + \tilde{x}_{,3} \otimes \mathrm{a}^3 = \nabla\tilde{x}.\left(1 + x_3\kappa + x_3^2\kappa^2 + x_3^3\kappa^3 + \ldots\ldots\right) + \tilde{x}_{,3} \otimes \mathrm{a}^3. \tag{8}$$

Combining Eqs. (6)–(8), we obtain the relations:

$$\mathrm{F}^{(0)} = \nabla\tilde{x}^{(0)} + \tilde{x}^{(1)} \otimes \mathrm{a}_3, \tag{9}$$

$$\mathrm{F}^{(1)} = \nabla\tilde{x}^{(0)}.\kappa + \nabla\tilde{x}^{(1)} + \tilde{x}^{(2)} \otimes \mathrm{a}_3, \tag{10}$$

$$\mathrm{F}^{(2)} = 2\left(\nabla\tilde{x}^{(0)}.\kappa^2 + \nabla\tilde{x}^{(1)}.\kappa + \frac{\nabla\tilde{x}^{(2)}}{2}\right) + \tilde{x}^{(3)} \otimes \mathrm{a}_3, \tag{11}$$

$$\mathrm{F}^{(3)} = 6\left(\nabla\tilde{x}^{(0)}.\kappa^3 + \nabla\tilde{x}^{(1)}.\kappa^2 + \frac{\nabla\tilde{x}^{(2)}.\kappa}{2} + \frac{\nabla\tilde{x}^{(3)}}{6}\right) + \tilde{x}^{(4)} \otimes \mathrm{a}_3, \tag{12}$$

$$\mathrm{F}^{(4)} = 24\left(\nabla\tilde{x}^{(0)}.\kappa^4 + \nabla\tilde{x}^{(1)}.\kappa^3 + \frac{\nabla\tilde{x}^{(2)}.\kappa^2}{2} + \frac{\nabla\tilde{x}^{(3)}.\kappa}{6} + \frac{\nabla\tilde{x}^{(4)}}{24}\right) + \tilde{x}^{(5)} \otimes \mathrm{a}_3. \tag{13}$$

By inserting (6) and (9)–(13) into (5), we get:

$$\delta E = \int_S \left(\mathrm{N} : \nabla\delta\tilde{x}^{(0)T} + \sum_{i=1}^{4} \mathrm{M}_i : \nabla\delta\tilde{x}^{(i)T} + \sum_{i=1}^{4} \mathrm{T}_i.\delta\tilde{x}^{(i)}\right)da + \int_{\partial S_t} \mathrm{n}.\delta\tilde{x}^{(0)}(s)ds + \sum_{i=1}^{4}\int_{\partial S_t} \mathrm{m}_i.\delta\tilde{x}^{(i)}(s)ds,$$

in which

$$\mathrm{N} = \int_{-\frac{h}{2}}^{\frac{h}{2}} \pi^T.\left(\sum_{i=0}^{4} x_3^i\kappa^i\right)^T \mu dx_3, \tag{14}$$

$$\mathrm{M}_i = \frac{1}{i!}\int_{-\frac{h}{2}}^{\frac{h}{2}} \pi^T.\left(\sum_{j=i}^{4} x_3^j\kappa^j\right)^T \mu dx_3 \quad \text{for } i = 1, \ldots, 4 \tag{15}$$

$$\mathbf{T}_i = \int_{-\frac{h}{2}}^{\frac{h}{2}} \pi.\mathbf{a}_3\mu dx_3, \tag{16}$$

$$\mathrm{n} = \int_{-\frac{h}{2}}^{\frac{h}{2}} \bar{t}(s, x_3)\psi dx_3,$$

$$\mathrm{m}_i = \frac{1}{i!}\int_{-\frac{h}{2}}^{\frac{h}{2}} \bar{t}(s, x_3)x_3\psi\, dx_3 \quad \text{for}\, i = 1, \ldots., 4$$

1.4 The Transition Law Between Macroscopic and Microscopic Scales and the Microscopic Problem

We assume that the microscopic deformation gradient can be expressed in terms of the macroscopic displacement gradient $\mathbf{F}$ and the microscopic displacement field u^m:

$$\mathrm{F}^m = \mathrm{F} + \mathrm{u}^m_{,i} \otimes \mathrm{g}^i. \tag{17}$$

Thus the microscopic first Piola-Kirchoff tensor is given by:

$$\pi^m = \frac{\partial W(\mathrm{F}^m)}{\partial \mathrm{F}^m}. \tag{18}$$

The equilibrium equation in the VER is:

$$Div\left(\pi^m\right) + \mathrm{f} = 0. \tag{19}$$

in curvilinear coordinates $Div(\pi^m) = \pi^m_{,\alpha}.\mathrm{g}^\alpha + \pi^{m\,(1)}.\mathrm{a}^3$ with $\mathrm{g}^\alpha = \mathrm{a}^\alpha + \kappa.\mathrm{a}^\alpha x_3 + \kappa^2.\mathrm{a}^\alpha x_3 + \ldots\ldots$ [21, 22] and $\mathbf{f}$ is the body force.

The Neumann boundary conditions on both the upper and lower boundaries of the VER are:

$$\pi^m.\mathrm{a}_3\big|_{x_3 = x_3^+(\mathrm{x}')} = \mathrm{t}^+, \quad \text{in} \quad \omega_m \tag{20}$$

$$\pi^m.\mathrm{a}_3\big|_{x_3 = x_3^-(\mathrm{x}')} = -\mathrm{t}^-, \quad \text{in} \quad \omega_m \tag{21}$$

where ω_m is such that $S_m = \theta(\bar{\omega}_m)$, S_m is the mid-surface of the VER.

Now we consider a specific Hill-Mandel condition which expresses the equivalence between both the internal macroscopic (left handside of the following equality) and microscopic energies (right handside of the following equality):

$$\delta E_M = \frac{1}{A_m}[\int_{S_m}\int_{x_3^-(\mathrm{x}')}^{x_3^+(\mathrm{x}')} \pi^m : \delta\mathrm{F}\mu dx_3 da + \int_{S_m}\int_{x_3^-(\mathrm{x}')}^{x_3^+(\mathrm{x}')} \pi^m : \left(\delta\mathrm{u}^m_{,i} \otimes \mathrm{g}^i\right)\mu dx_3 da - \int_{S_m}\int_{x_3^-(\mathrm{x}')}^{x_3^+(\mathrm{x}')} \mathrm{f}.\delta\mathrm{u}^m \mu dx_3 da$$
$$- \int_{S_m}\left(\mathrm{t}^+.\delta\mathrm{u}^m\left(\mathrm{x}', x_3^+(\mathrm{x}')\right)\mu\left(x_3^+(\mathrm{x}')\right) + \mathrm{t}^-.\delta\mathrm{u}^m\left(\mathrm{x}', x_3^-(\mathrm{x}')\right)\mu\left(x_3^-(\mathrm{x}')\right)\right)da], \tag{22}$$

where A_m is the area of the mid-surface S_m and δE_M is the internal macroscopic energy defined by:

$$\delta E_M = \mathrm{N} : \nabla \delta \tilde{x}^{(0)T} + \sum_{i=1}^{4} \mathrm{M}_i : \nabla \delta \tilde{x}^{(i)T} + \sum_{i=0}^{4} \mathrm{T}_i . \delta \tilde{x}^{(i)},$$

and S_m denotes the mid-surface of the VER.

By considering standard argument (divergence theorem and integration by part) and conditions (19)–(21), we see that Hill-Mandel condition (22) is satisfied if and only if:

$$\int_{\partial S_m} \int_{x_3^-(\mathrm{x}')}^{x_3^-(\mathrm{x}')} \mathrm{t}.\delta \mathrm{u}^m(s, x_3) \psi \, ds dx_3 = 0. \tag{23}$$

Condition (23) is satisfied if the condition (C): $\mathbf{t}.\mathbf{u}^m(s, x_3)\psi$ is periodic along $\partial \Gamma_L = \partial S_m \times \left[x_3^-(\mathrm{x}'), x_3^+(\mathrm{x}')\right]$ (lateral boundary of the VER). When the curvature of the shell is constant along the mid-surface (cylindrical or spherical shells) or when the shell is slightly curved (the shell is almost a plate), the condition C reduces to impose the classical periodicity condition of t and u_m on $\partial \Gamma_L$.

Nevertheless in the general case condition (C) can be enforced by using Lagrange multiplier. Therefore the Hill-Mandel condition (22) implies:

$$\mathrm{N} = \frac{1}{A_m} \int_{S_m} \int_{x_3^-(\mathrm{x}')}^{x_3^+(\mathrm{x}')} \pi^{mT} . \left(\sum_{i=0}^{4} x_3^i \kappa^i \right)^T dadx_3, \tag{24}$$

$$\mathrm{M}_i = \frac{1}{i! A_m} \int_{S_m} \int_{x_3^-(\mathrm{x}')}^{x_3^+(\mathrm{x}')} \pi^{mT} . \left(\sum_{j=i}^{4} x_3^j \, \kappa^j \right)^T \mu dadx_3, \quad \text{for } i = 1, \ldots, 4, \tag{25}$$

$$\mathrm{T}_i = \frac{1}{A_m} \int_{S_m} \int_{x_3^-(\mathrm{x}')}^{x_3^+(\mathrm{x}')} \pi^m . \mathrm{a}_3 \mu dadx_3, \quad \text{for } i = 1, \ldots, 4, \tag{26}$$

As the macro-micro transition relations (24)–(26) replace the formulae (14)–(16).

Therefore the microscopic problem is obtained by considering together formulae (18)–(21) and periodicity condition (C). We can observe that this modelization is in accordance with the model presented by Song and Dai [22] for homogeneous shell (u^m vanishes and the model degenerates to a one scale model).

2 Conclusion

We have presented in this paper a multiscale theory for simulating the mechanical response of highly heterogeneous shell based on the concepts of computational homogenization. The concept has been described in terms of the structural description of both the microscopic and macroscopic scales and the resulting boundary value problems.

References

1. Pietraszkiewicz, W., Witkowski, J.: Shell Structures: Theory and Applications, vol. 4. CRC Press (2017)
2. Timoshenko, S., Woinowsky-Krieger, S., Woinowsky-Krieger, S.: Theory of Plates and Shells, vol. 2. McGraw-Hill, New-York, NY (1959)
3. Altenbach, J., Altenbach, H., Eremeyev, V.A.: On generalized cosserat-type theories of plates and shells: a short review and bibliography. Arch. Appl. Mech. **80**(1), 73–92 (2010)
4. Love, A.E.H.: The small free vibrations and deformation of a thin elastic shell. Philos. Trans. R. Soc. London A. **179**, 491–546 (1888)
5. Kirchhoff, G.: Über das gleichgewicht und die bewegung einer elastischen scheibe. Journal für die Reine und Angewandte Mathematik. **40**, 51–88 (1850)
6. Sanders, J.L.: An improved first-approximation theory for thin shells. NASA Report 24 (1959)
7. Koiter, W.T.: On the nonlinear theory of thin elastic shells. Koninklijke Nederlandse Akademie van Wetenschappen. Proc. Ser. B. **69**(1), 1–54 (1966)
8. Gol'denveizer, A.: Derivation of an approximate theory of shells by means of asymptotic integration of the equations of the theory of elasticity. J. Appl. Math. Mech. **27**(4), 903–924 (1963)
9. Ciarlet, P.G., Destuynder, P.: A justification of a nonlinear model in plate theory. Comput. Methods Appl. Mech. Eng. **17**, 227–258 (1979)
10. Ciarlet, P.G., Destuynder, P.: Justification of the 2-dimensional linear plate model. J. Mécanique. **18**(2), 315–344 (1979)
11. Destuynder, P.: Sur une Justification des Modeles de Plaques et de Coques par les Methodes Asymptotiques. Universite Pierre et Marie Curie, Paris Ph.D. thesis, 1980
12. Friesecke, G., James, R.D., Müller, S.: A hierarchy of plate models derived from nonlinear elasticity by Gamma-convergence. Arch. Rat. Mech. Anal. **180**, 183–236 (2006)
13. Le Dret, H., Raoult, A.: The membrane shell model in nonlinear elasticity: a variational asymptotic derivation. J. Nonlinear Sci. **6**(1), 59–84 (1996)
14. Pruchnicki, E.: Nonlinearly elastic membrane model for heterogeneous shells by using a new double scale variational formulation: a formal asymptotic approach. J. Elast. **84**(3), 245–280 (2006)
15. Reddy, J., Liu, C.: A higher-order shear deformation theory of laminated elastic shells. Int. J. Eng. Sci. **23**(3), 319–330 (1985)
16. Reddy, J., Arciniega, R.: Shear deformation plate and shell theories: from stavsky to present. Mech. Adv. Mater. Struct. **11**(6), 535–582 (2004)
17. Meroueh, K.: On a formulation of a nonlinear theory of plates and shells with applications. Comput. Struct. **24**(5), 691–705 (1986)
18. Steigmann, D.J.: Two-dimensional models for the combined bending and stretching of plates and shells based on three-dimensional linear elasticity. Int. J. Eng. Sci. **46**(7), 654–676 (2008)
19. Steigmann, D.J.: Extension of koiter's linear shell theory to materials exhibiting arbitrary symmetry. Int. J. Eng. Sci. **51**, 216–232 (2012)

20. Pruchnicki, E.: Two-dimensional model of order h5 for the combined bending, stretching, transverse shearing and transverse normal stress effect of homogeneous plates derived from three-dimensional elasticity. Math. Mech. Solids. **19**(5), 477–490 (2014)
21. Pruchnicki, E.: A fifth-order model for shells which combines bending, stretching and transverse shearing deduced from three-dimensional elasticity. Math. Mech. Solids. **21**(7), 842–855 (2016)
22. Song, Z., Dai, H.H.: On a consistent finite-strain shell theory based on 3-D nonlinear elasticity. Int. J. Solids Struct. **22**(12), 1557–1570 (2016)
23. Williams, T.O.: A new theoretical framework for the formulation of general, nonlinear, multiscale plate theories. Int. J. Solids Struct. **45**, 2534–2560 (2008)
24. Williams, T.O.: A new, unified, theoretical framework for the formulation of general, nonlinear, single-scale shell theories. Compos. Struct. **107**, 544–558 (2014)
25. Carrera, E.: Theories and finite elements for multilayered, anisotropic, composite plates and shells. Arch. Comput. Methods Eng. **9**(2), 87–140 (2002)
26. Reddy, J.N.: Mechanics of Laminated Composite Plates and Shells: Theory and Analysis (2nd edn). CRC Press, London, L (2004)
27. Lewinski,T., Telega, J. J.: Plates, Laminates and Shells: Asymptotic Analysis and Homogenization. World Scientific, Singapore, New Jersey, London, Hong-Kong, S, N-J, L, H-K (2000)
28. Hohe, J., Becker, W.: Effective stress–strain relations for two dimensional cellular sandwich cores: homogenization, material models, and properties. Appl. Mech. Rev. **55**, 61–87 (2002)
29. Gruttmann, F., Wagner, W.: A coupled two-scale shell model with applications to layered structures. Int. J. Numer. Meth. Engng. **94**, 1233–1254 (2013)
30. Heller, D., Gruttmann, F.: Nonlinear two-scale shell modeling of sandwiches with a comb-like core. Compos. Struct. **144**, 147–155 (2016)
31. Gruttmann, F., Knust, G., Wagner, W.: Theory and numerics of layered shells with variationally embedded interlaminar stresses. Comput. Methods Appl. Mech. Eng. **326**, 713–738 (2017)
32. Cecchi, A., Sab, K.: Out-of-plane model for heterogeneous periodic materials: the case of masonry. Eur. J. Mech. Solids. **21**, 715–746 (2002)
33. Cecchi, A., Milani, G., Tralli, A.: A Reissner-Mindlin limit analysis model for out-of- plane loaded running bond masonry walls. Int. J. Solids and Struct. **44**, 1438–1460 (2007)
34. Mistler, M., Anthoine, A., Butenweg, C.: In-plane and out-of-plane homogenization of masonry. Comput. Struct. **85**, 1321–1330 (2007)
35. Mercatoris, B.C.N., Bouillard, P., Massart, T.J.: Multi-scale detection of failure in planar masonry thin shells using computational homogenization. Eng. Fract. Mech. **76**, 479–499 (2009)
36. Petracca, M., Pela, L., Rossi, R., Oller, S., Guido Camata, G., Spacone, E.: Multiscale computational first order homogenization of thick shells for the analysis of out-of-plane loaded masonry walls. Comput. Methods Appl. Mech. Engrg. **315**, 273–301 (2017)
37. Caillerie, D.: Thin elastic and periodic plates. Math. Models Methods Appl. Sci. **6**, 159–191 (1984)
38. Kohn, R.V., Vogelius, M.: A new model for thin plates with rapidly varying thickness. Int. J. Solids Struct. **20**, 333–350 (1984)
39. Pruchnicki, E.: Homogenization of a second order plate model. Math. Mech. Solids. (2017). https://doi.org/10.1177/1081286517719939
40. Geers, M.G.D., Coenen, E.W., Kouznetsova, V.G.: Multi-scale computational homogenization of structured thin sheets. Model. Simul. Mater. Sci. Eng. **15**, S393–S404 (2007)
41. Coenen, E.W.C., Kouznetsova, V.G., Geers, M.G.D.: Computational homogenization for heterogeneous thin sheets. Int. J. Numer. Methods Eng. **83**, 1180–1205 (2010)
42. Kouznetsova, V.G., Geers, M.G.D., Brekelmans, W.A.A.: Multi-scale constitutive modelling of heterogeneous materials with a gradient-enhanced computational homogenization scheme. Int. J. Numer. Methods Engrg. **54**, 1235–1260 (2002)
43. Larsson, R., Diebels, S.: A second-order homogenization procedure for multi- scale analysis based on micropolar kinematics. Int. J. Numer. Methods Engrg. **69**, 2485–2512 (2007)

44. Suquet, P.M.: Local and global aspects in the mathematical theory of plasticity. In: Sawczuk, A., Bianchi, G. (eds.), Plasticity Today: Modelling, Methods and Applications, pp. 279–310. Elsevier Applied Science Publishers, London (1985)
45. Miehe, C., Schröder, J., Schotte, J.: Computational homogenization analysis in finite plasticity. Simulation of texture development in poly-crystalline materials. Comput. Methods Appl. Mech. Eng. **171**, 387–418 (1999)
46. Grytz, R., Meschke, G.: Consistent micro–macro transitions at large objective strains in curvilinear convective coordinates. Int. J. Numer. Methods Eng. **73**, 805–824 (2008)
47. Larsson, R., Landervik, M.: A stress-resultant shell theory based on multiscale homogenization. Comput. Methods Appl. Mech. Eng. **263**, 1–11 (2013)
48. Lee, C.Y., Yu, W., Hodges, D.H.: Refined modeling of composite plates with in-plane heterogeneity. Z. Angew. Math. Mech. **94**(1–2), 85–100 (2014)
49. Berdichevsky, V.: Variational-asymptotic method of constructing a theory of shells. J. Appl. Math. Mechanics. **43**(4), 664–687 (1979)
50. Sutyrin, V.: Derivation of plate theory accounting asymptotically correct shear deformation. J. Appl. Mech. **64**, 905–915 (1997)
51. Smit, R.J.M., Brekelmans, W.A.M., Meijer, H.E.H.: Prediction of the mechanical behaviour of non-linear heterogeneous systems by multi-level finite element modeling. Comput. Methods Appl. Mech. Eng. **155**, 181–192 (1998)
52. Feyel, F., Chaboche, J.L.: FE2 multiscale approach for modelling the elastoviscoplastic behaviour of long fiber SiC/Ti composite materials. Comput. Methods Appl. Mech. Eng. **183**, 309–330 (2000)
53. Terada, K., Kikuchi, N.: A class of general algorithms for multi-scale analysis of heterogeneous media. Comput. Methods Appl. Mech. Eng. **190**, 5427–5464 (2001)
54. Sfantos, G.K., Aliabadi, M.H.: Multi-scale boundary element modelling of material degradation and fracture. Comput. Methods Appl. Mech. Eng. **196**, 1310–1329 (2007)
55. Ghosh, S., Lee, K., Moorthy, S.: Multiple scale analysis of heterogeneous elastic structures using homogenisation theory and Voronoi cell finite element method. Int. J. Solids Struct. **32**(1), 27–62 (1995)
56. Ghosh, S., Lee, K., Moorthy, S.: Two scale analysis of heterogeneous elastic-plastic materials with asymptotic homogenisation and Voronoi cell finite element model. Comput. Methods Appl. Mech. Eng. **132**, 63–116 (1996)
57. Miehe, C., Schroder, J., Schotte, J.: Computational homogenization analysis in finite plasticity, simulation of texture development in polycrystalline materials. Comput. Methods Appl. Mech. Eng. **171**, 387–418 (1999)
58. Miehe, C., Schotte, J., Schroder, J.: Computational micro–macro transitions and overall moduli in the analysis of polycrystals at large strains. Comput. Mater. Sci. **16**, 372–382 (1999)
59. Pruchnicki, E.: Homogenized nonlinear constitutive law using Fourier series expansion. Int. J. Solids and Struct. **35**(16), 1895–1913 (1998)
60. Michel, J.C., Moulinec, H., Suquet, P.: Effective properties of composite materials with periodic microstructure: a computational approach. Comput. Methods. Appl. Mech. Eng. **172**, 109–143 (1999)
61. Moulinec, H., Suquet, P.: A numerical method for computing the overall response of nonlinear composites with complex microstructure. Comput. Methods. Appl. Mech. Eng. **157**, 69–94 (1998)
62. Oskay, C., Fish, J.: Eigendeformation-based reduced order homogenization for failure analysis of heterogeneous materials. Comput. Methods. Appl. Mech. Eng. **196**, 1216–1243 (2007)
63. Dai, H.H., Song, Z.: On a consistent finite-strain plate theory based on three-dimensional energy principle. Proc. R. Soc. London A. **470**, 20140494 (2014)
64. Cong, Y., Nezamabadi, S., Zahrouni, H., Yvonnet, J.: Multiscale computational homogenization of heterogeneous shells at small strains with extensions to finite displacements and buckling. Int. J. Numer. Meth. Eng. **104**, 235–259 (2015)
65. Buechter, N., Ramm, E.: Shell theory versus degeneration—a comparison in large rotation finite element analysis. Internat. J. Numer. Methods Eng. **34**, 39–59 (1992)

66. Sansour, C.: A theory and finite element formulation of shells at finite deformations involving thickness change: circumventing the use of a rotation tensor. Arch. Appl. Mech. **65**, 194–216 (1995)
67. Buechter, N., Ramm, E., Roehl, D.: Three-dimensional extension of non-linear shell formulation based on the enhanced assumed strain concept. Internat. J. Numer. Methods Eng. **34**, 2551–2568 (1994)
68. Roehl, D., Ramm, E.: Large elasto-plastic finite element analysis of solids and shells with the enhanced assumed strain concept. Int. J. Solids Struct. **33**, 3215–3237 (1996)
69. Helfen, C.E., Diebels, S.: A numerical homogenisation method for sandwich plates based on a plate theory with thickness change. Z. Angew. Math. Mech. **93**(2–3), 113–125 (2013)
70. Helfen, C.E., Diebels, S.: Computational homogenisation of composite plates: consideration of the thickness change with a modified projection strategy. Comput. Math Appl. **67**, 1116–1129 (2014)
71. Fillep, S., Mergheim, J., Steinmann, P.: Computational modelling and homogenization of technical textiles. Eng. Struct. **50**, 68–73 (2013)
72. Fillep, S., Mergheim, J., Steinmann, P.: Towards an efficient two-scale approach to model technical textiles. Comput. Mech. **59**, 385–401 (2017)
73. Naghdi, P.M.: Theory of shells and plates. In: Truesdell, C. (ed.) Handbuch der Physik, vol. VIa/2, pp. 425–640. Springer, Berlin (1972)
74. Dikmen, M.: Theory of thin elastic shells. Pitman, London (1982)

A Non-linear Theory of Thin-Walled Rods of Open Profile Deduced with Incremental Shell Equations

Jakob Scheidl and Yury Vetyukov

Abstract We study the structural behaviour of rods with thin-walled open cross-sections. Such members are best known for their low torsional rigidity and extensive warping deformation when subjected to twisting. Proceeding to large deformations one needs to account for the geometrically non-linear effects in the cross-section, that affect the structural response and prevent a simple generalisation of the linear theory. We here further elaborate a novel approach that utilizes the equations of incremental shell theory to quantify these non-linear effects and incorporate them into an augmented beam theory, which is then put to test on an example of a circularly curved rod. The linear deformation analysis reveals, that arbitrarily curved and straight rods do not share the same asymptotic behaviour. The torsional-flexural buckling loads obtained with the incremental beam theory correspond well to reference computations with shell finite elements, given that subcritical pre-deformations are negligible. The narration concludes with the post-buckling analysis using shell finite elements.

1 Introduction

It is well known, that beams with open, thin-walled cross-sections are particularly vulnerable to twisting and warp significantly. Consequently, potential warping constraints have a major influence on the structural response and complying beam theories need to account for the warping deformations. While many authors have addressed geometrically linear theories in the past, see for example [7, 13, 21], proceeding to arbitrary large deformations is not trivial, as strictly non-linear effects, sometimes referred to as Wagner effects [22], do not allow for a simple generalisation of the theory. More recent studies, like [8], make use of the so called *Method of Hypothesis* to incorporate these effects into the beam theory. This approach involves insertion of a kinematic hypothesis and some further assumptions into the governing

J. Scheidl (✉) · Y. Vetyukov
Institute of Mechanics and Mechatronics, TU Wien, Getreidemarkt 9, 1060 Vienna, Austria
e-mail: jakob.scheidl@tuwien.ac.at

H. Altenbach et al. (eds.), *Recent Developments in the Theory of Shells*,
Advanced Structured Materials 110, https://doi.org/10.1007/978-3-030-17747-8_28

equations of continuum theory. Here, we propose a different strategy, that is free of assumptions and utilizes structural shell theory to deduce a corresponding beam theory. We refer to [17, 19] for the linear asymptotic study, that leads to previously reported linear beam theories, and focus on the analysis of the above mentioned non-linear effects in the framework of the *Direct Approach*, also covered in [16, 19, 20]. Altogether these derivations yield a geometrically non-linear beam theory, that is justified for reasonably large deformations. That is to say, although the equations retain consistency for arbitrarily large deformations, the proof remains valid only for sufficiently small ones.

After having elaborated on the beam theory's derivation and justification in the first sections, we will put it to actual use in Sect. 5, where both the linear deformation behaviour as well as the torsional-flexural-buckling of a circularly curved beam with a semi-circular cross-section are studied. However, in order to demonstrate the importance of the mentioned non-linear effects, we present the results of an even simpler analysis in Fig. 1. It shows different solutions for the evolution of the torsion angle θ_t at the free end of a clamped, straight half-cylinder twisted by a small torque $\boldsymbol{T}$ and pre-stressed by a finite transverse force $\boldsymbol{F}$. The solid blue line corresponds to calculations with the here proposed incremental beam theory, wherein pre-deformations due to the transverse force are neglected, i.e. the beam is assumed to be undeformed but pre-stressed before application of the torque $\boldsymbol{T}$ (*second order theory*). Obviously, this neglect becomes less practical at higher force values, which leads to increasing discrepancies between the beam and the non-linear shell solution obtained with *Abaqus* (hollow dots). Nonetheless, for small force magnitudes shell and beam solution coincide, which is not true for the corresponding beam finite element solution, that was computed using open-section beam elements of the *Abaqus* standard element library. As pointed out by other researchers [8], these elements do not account for the impact of the bending stresses on the effective torsional stiffness and thus only predict the pure constrained torsion case ($F = 0$) correctly. In viewing Fig. 1 as a deformation path of the imperfect system with large imperfection $\boldsymbol{T}$, one recognizes the correspondence to the torsional-flexural buckling problem of the straight beam under a transverse loading $\boldsymbol{F}$. Hence, the above example emphasizes the particular importance of the coupling effects for structural stability problems.

2 Incremental Theory of Rods of Open Profile

As structural stability is an inherently non-linear phenomenon, its investigation requires geometrically non-linear theories to begin with. Here, incremental theories, deduced by linearisation of the full equations in the neighbourhood of a given equilibrium state, provide a convenient way to determine critical points of stability loss [3, 24]. This applies especially to one-dimensional beam theories, where consistent linearisation leads to linear ordinary differential equations. The simplest incremental theory is the so called *theory of second order*, which is, for example, traditionally used to calculate critical forces for the Euler rod-buckling problems.

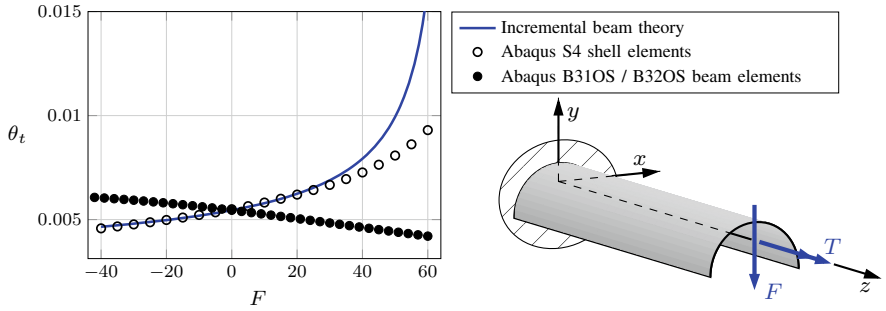

Fig. 1 Constrained torsion of a pre-stressed rod with semi-circular cross-section; comparison of different solutions for the twisting angle θ_t

In contrast to general incremental theories, the theory of second order views the pre-buckling state to be stressed but approximately undeformed. This approach has the main advantage, that the pre-stressed state is much easier to acquire than solutions to the geometrically non-linear deformation problem. Things become even simpler for statically determined systems, where the equilibrium equations suffice to obtain the pre-stresses and solving the linear deformation problem becomes superfluous. Evidently, the reliability of the second order theory diminishes, if large pre-deformations occur before stability loss, compare Fig. 1. Although many structures sustain only little deformations before buckling, this is a major drawback, because the importance of the pre-deformations can only be judged through application of higher order theories. The here derived general incremental theory of curved beams with a thin-walled open cross-section is easily transformed to the second order one as discussed below in Sect. 5 in application to an example problem. Refer to [19] for a more comprehensive review of the chosen theory.

2.1 Beam Kinematic Description

We understand the beam as a one-dimensional material line in space, i.e. successive material points with a certain number of degrees of freedom constituting a solid line. Classically, these material degrees of freedom correspond to the rigid body motion of a designated cross-section. This holds true in the present case, but is not sufficient when attempting to model the kinematics of a beam, whose cross-section is a thin-walled open strip. Such structures require to further account for warping by means of an additional degree of freedom, the *warping amplitude* ψ. Therefore, every single material particle owns a total of seven degrees of freedom, namely: three translations, three rotations and the scalar quantity ψ. In this context, it is important to note, that the particular choice of material degrees of freedom does not fully specify the theory yet, because we may later impose kinematic restrictions concerning, for example,

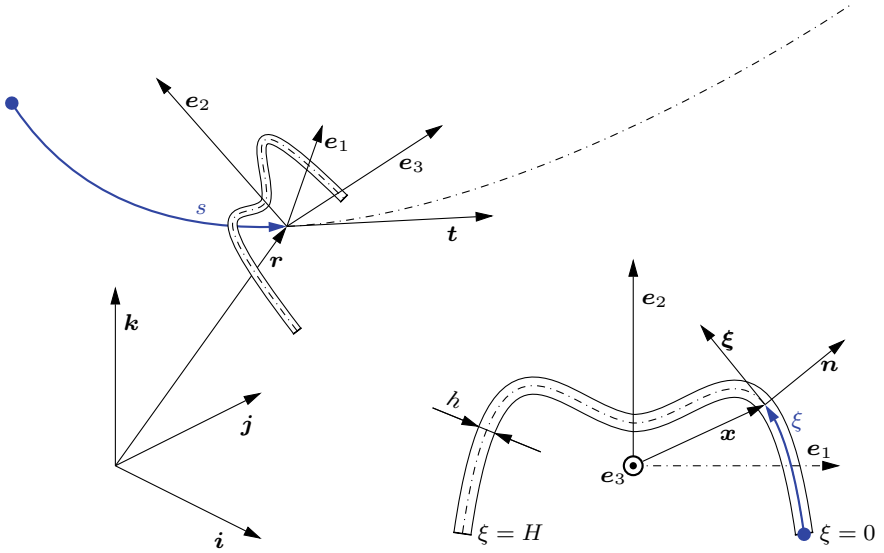

Fig. 2 Beam kinematic description featuring material basis vectors $\boldsymbol{e}_k$ as well as beam axis and cross-section arc coordinates s and ξ respectively

transverse shear or extensibility. Such conditions limit the freedom of movement in the continuum and effectively decide in favour of a specific theory, be it a Bernoulli-, Timoshenko- or other type.

The beam axis $\boldsymbol{r}$ with tangential direction $\boldsymbol{t}$ is a continuous line through the sections' geometric centroids and parametrized with the material arc coordinate s, see Fig. 2. We draw a symmetric cross-section just for convenience, it need not be symmetric in general. The three cross-section rotations are described by the orientation of an orthogonal basis $\boldsymbol{e}_k\,(s)$, where $\boldsymbol{e}_3$ points in the cross-section normal direction and the other two coincide with the section's principal axes. All three meet in the centroid and move together with their designated material point. Usually, vectors or tensors are most conveniently described in this basis. For this reason indexed quantities denote components in $\boldsymbol{e}_k$ exclusively. Lastly, we account for warping by means of the *warping amplitude* ψ in conjunction with the *warping function* $w\,(\xi)$. The latter may in case of a thin-walled open section be approximated by

$$w = -\int \boldsymbol{x}\cdot\boldsymbol{n}\,\mathrm{d}\xi \quad \text{with} \quad \int_0^H w\,\mathrm{d}\xi = 0\,, \tag{1}$$

where the arc coordinate $\xi \in [0,\ H]$, the position vector $\boldsymbol{x}$ and the corresponding unit vectors $\boldsymbol{\xi} = \partial_\xi \boldsymbol{x}$, $\boldsymbol{n} = \boldsymbol{\xi}\times\boldsymbol{e}_3$ are cross-section properties with

$$h\int_0^H \boldsymbol{x}\,\mathrm{d}\xi = 0\,. \tag{2}$$

Therefore, ψ is merely a scaling factor for the warping deformation, which gets distributed over the cross-section according to $w(\xi)$. The condition on the right of (1) determines the integration constant. It ensures that w has no mean value, which would anyway result in just a rigid body deflection of the cross-section.

One can now combine the beam's kinematic abilities to reconstruct the motion of the corresponding shell (summation over repeated indices)

$$\boldsymbol{r}^{\text{shell}}(s,\ \xi) = \boldsymbol{r}(s) + x_\alpha(\xi)\ \boldsymbol{e}_\alpha(s) + w(\xi)\ \psi(s)\ \boldsymbol{e}_3(s)\ . \tag{3}$$

Splitting up the cross-section position vector $\boldsymbol{x}$ into its material components ($\alpha = 1,\ 2$) illustrates, that the material basis describes the section rotations, while a point's position in the section, determined by x_α, remains unchanged.

2.2 Governing Equations of the Incremental Beam Theory

As pointed out previously, an incremental theory relies on small perturbations of quantities, that belong to a previously computed equilibrium state. While the second order incremental theory assumes this state to be pre-stressed but undeformed, here we focus on a general formulation and need to differentiate between the actual configuration of the beam $\boldsymbol{r}$ and the reference one $\mathring{\boldsymbol{r}}$; a small circle will in the following denote quantities of this undeformed and unstrained reference state. Furthermore, we identify quantities of the slightly perturbed, potentially buckled state with an incremental dot $(\ldots)^\cdot$, but assign unique names to some kinematic variables, that describe the incremental deformation. For example, the actual configuration position vector is $\boldsymbol{r}$ and its increment is the infinitesimal displacement $\boldsymbol{r}^\cdot \equiv \boldsymbol{u}$. The same applies to the small rotation vector $\boldsymbol{\theta}$, which accounts for small rotations of the material basis according to $\boldsymbol{e}_k^\cdot = \boldsymbol{\theta} \times \boldsymbol{e}_k$.

Having elaborated on the kinematic mobility of the material particles, i.e. degrees of freedom and their formal representation by $\{\boldsymbol{r},\ \boldsymbol{e}_k,\ \psi\}$ for the actual state and $\left\{\boldsymbol{u},\ \boldsymbol{\theta},\ \psi^\cdot\right\}$ for the incremental one, we now aim at the governing equations of both the non-linear theory for finding the actual state and of the linearised incremental one. To do so, we will develop the non-linear theory starting with the *principle of virtual work* and present the corresponding incremental equations alongside. The latter ones follow from the general formulas by simple linearisation utilizing the incremental dot as a differential operator much like the variational δ, see [1]. Consequently, many variational formulas of the non-linear beam theory reappear in the framework of the incremental theory. However, in contrast to variational properties of a virtual state, incremental values correspond to actual small deformations of the beam. Now, in order to set up the principle of virtual work, we imagine an arbitrary beam segment $s \in [s_1,\ s_2]$, that has been freed from all kinematic boundaries. Then, as pointed

out in [19], the number of distinct work conjugates in the principle of virtual work corresponds to the choice of degrees of freedom, which leads to

$$\int_{s_1}^{s_2} (\boldsymbol{q}\cdot\delta\boldsymbol{r} + \boldsymbol{m}\cdot\delta\boldsymbol{\theta} + b\,\delta\psi - \delta U)\,\mathrm{d}s + (\boldsymbol{Q}\cdot\delta\boldsymbol{r} + \boldsymbol{M}\cdot\delta\boldsymbol{\theta} + B\,\delta\psi)\Big|_{s_1}^{s_2} = 0\,. \quad (4)$$

Here, $\delta\boldsymbol{r}$, $\delta\boldsymbol{\theta}$ and $\delta\psi$ denote small virtual displacements, rotations and warping amplitudes, which force the beam into a virtual, kinematically admissible configuration immediately adjacent to the actual one. The quantity $\delta\boldsymbol{\theta}$ is a stand-alone vector and must not be misconceived as a variation of the small rotation increment vector $\boldsymbol{\theta}$. We further identify externally applied distributed forces $\boldsymbol{q}$, moments $\boldsymbol{m}$ and bimoments b as well as their concentrated counterparts $\boldsymbol{Q}$, $\boldsymbol{M}$ and B at the free edges. The bimoments are self equilibrating, generalised forces, sometimes interpreted as two counteracting bending moments in the cross-section, that yield a torsional moment when differentiated with respect to s. In the framework of the here applied *Direct Approach* they appear naturally as work conjugates for the warping degree of freedom. Lastly, we have accounted for the virtual work of internal forces by means of the negative variation of the *elastic strain energy density* δU, whose general form we are trying to deduce in the following. Uniting all terms under one common integral with partial integration, one may as well omit the integration symbol entirely as the length of the beam segment is arbitrary. Hence, the local form of the principle of virtual work reads

$$\delta U = \big(\boldsymbol{q} + \boldsymbol{Q}'\big)\cdot\delta\boldsymbol{r} + \big(\boldsymbol{m} + \boldsymbol{M}'\big)\cdot\delta\boldsymbol{\theta} + \boldsymbol{Q}\cdot\delta\boldsymbol{r}' + \boldsymbol{M}\cdot\delta\boldsymbol{\theta}' + \big(b + B'\big)\,\delta\psi + B\,\delta\psi'\,, \quad (5)$$

where a prime denotes differentiation with respect to s.

Aiming for the static equilibrium conditions, we state that neither the elastic internal forces produce work ($\delta U = 0$) nor does the cross-section warp ($\delta\psi = 0$) in the case of rigid body motion

$$\delta\boldsymbol{r} = \delta\bar{\boldsymbol{r}} + \delta\bar{\boldsymbol{\theta}}\times\boldsymbol{r} \quad \text{with} \quad \delta\bar{\boldsymbol{r}}\,,\,\delta\bar{\boldsymbol{\theta}} = \text{const.}\,. \quad (6)$$

Evaluating the above principle under these particular circumstances and collecting the coefficients for $\delta\bar{\boldsymbol{r}}$ and $\delta\bar{\boldsymbol{\theta}}$, we obtain the traditional form of equilibrium equations

$$\boldsymbol{Q}' + \boldsymbol{q} = 0\,, \quad \boldsymbol{M}' + \boldsymbol{r}'\times\boldsymbol{Q} + \boldsymbol{m} = 0\,, \quad (7)$$

Further application of the incremental dot as a differential operator, leads to the corresponding incremental formulas

$$\boldsymbol{Q}^{\bullet\prime} + \boldsymbol{q}^{\bullet} = 0\,, \quad \boldsymbol{M}^{\bullet\prime} + \boldsymbol{u}'\times\boldsymbol{Q} + \boldsymbol{r}'\times\boldsymbol{Q}^{\bullet} + \boldsymbol{m}^{\bullet} = 0\,, \quad (8)$$

using the switchability of incrementation and differentiation in $\big(\boldsymbol{r}^{\bullet}\big)' = \big(\boldsymbol{r}'\big)^{\bullet} = \boldsymbol{u}'$. Both sets of Eqs. (7) and (8) must hold independently in order to satisfy the

mechanical equilibrium. Backward substitution in (5) returns a first variational form of the constitutive law

$$\delta U = \boldsymbol{M} \cdot \delta\boldsymbol{\theta}' + \boldsymbol{Q} \cdot \left(\delta\boldsymbol{u}' - \delta\boldsymbol{\theta} \times \boldsymbol{r}'\right) + \left(b + B'\right)\, \delta\psi + B\, \delta\psi' \,. \tag{9}$$

This formulation still lacks the definition of independent variations of strain measures, which may be introduced with the two kinematic formulas of Clebsch [3]

$$\delta\Gamma_k = \left(\delta\boldsymbol{r}' - \delta\boldsymbol{\theta} \times \boldsymbol{r}'\right) \cdot \boldsymbol{e}_k \,, \qquad \delta\kappa_k = \delta\boldsymbol{\theta}' \cdot \boldsymbol{e}_k \tag{10}$$

$$\Gamma_k^{\cdot} = \left(\boldsymbol{u}' - \boldsymbol{\theta} \times \boldsymbol{r}'\right) \cdot \boldsymbol{e}_k \,, \qquad \kappa_k^{\cdot} = \boldsymbol{\theta}' \cdot \boldsymbol{e}_k \,. \tag{11}$$

Once again we have appended the incremental form below. The aforementioned close relationship between variational and incremental formulas is evident. We refer to [19] for an in depth discussion on the strain measures and just define

$$\boldsymbol{\Gamma} = \boldsymbol{r}' - \mathbf{P} \cdot \mathring{\boldsymbol{r}}' \,, \quad \mathbf{P}' = \boldsymbol{\kappa} \times \mathbf{P} \quad \text{with} \quad \mathbf{P} = \boldsymbol{e}_k \mathring{\boldsymbol{e}}_k \,. \tag{12}$$

The vector $\boldsymbol{\Gamma}$ corresponds to axial strains and cross-section shear angles, whereas $\boldsymbol{\kappa}$ accounts for twist and material curvature strains. Both formulas feature the rotation tensor $\mathbf{P}$ that transforms the material basis vectors between the reference and the actual state.

Aiming for a Bernoulli-type of theory we constrain the in-plane part $\boldsymbol{\Gamma}_\perp \equiv \boldsymbol{\Gamma} - \Gamma_3\, \boldsymbol{e}_3$ to zero (*no transverse shear*). This enforces the condition $\boldsymbol{t} = \boldsymbol{e}_3$, meaning that the cross-section remains perpendicular to the deformed beam axis. Hence, the work conjugate of the transverse forces vanishes and we denote the remaining axial strain by $\varepsilon \equiv \boldsymbol{\Gamma} \cdot \boldsymbol{t}$. We further introduce the index t for a more obvious reference to tangential components, e.g. $\kappa_t \equiv \kappa_3$ is the twisting component. As a consequence of the above neglect, the first incremental formula in (11) transforms to

$$\varepsilon^{\cdot}\, \boldsymbol{t} = \boldsymbol{u}' - \boldsymbol{\theta} \times \boldsymbol{r}' \,. \tag{13}$$

Moreover, in analogy to the theory of pure torsion [7, 19], we set the warping amplitude ψ equal to the torsion κ_t, implying

$$\delta\psi = \delta\kappa_t \,, \quad \psi^{\cdot} = \boldsymbol{\theta}' \cdot \boldsymbol{t} \,, \tag{14}$$

where we have used (11) to substitute $\kappa_t^{\cdot}$ in the incremental formula on the right. Imposition of these kinematic constraints effectively defines the strain energy density as a function $U = U\left(\kappa_k,\, \varepsilon,\, \kappa_t'\right)$ with the variation

$$\begin{aligned} \delta U &= \frac{\partial U}{\partial \kappa_k}\, \delta\kappa_k + \frac{\partial U}{\partial \varepsilon}\, \delta\varepsilon + \frac{\partial U}{\partial \kappa_t'}\, \delta\kappa_t' \\ &= \left(\boldsymbol{M} + \left(B' + b\right)\, \boldsymbol{t}\right) \cdot \boldsymbol{e}_k\, \delta\kappa_k + Q_t\, \delta\varepsilon + B\, \delta\kappa_t' \,. \end{aligned} \tag{15}$$

The specific form of the quadratic terms of the strain energy in the non-linear theory is chosen such, that it conforms to the asymptotically justified linear theory. Additional cubic terms account for the non-linear effects:

$$
\begin{aligned}
&U = U\left(\kappa_k,\ \varepsilon,\ \kappa_t'\right) = U^{(2)} + U^{(3)}\\
&U^{(2)} = \frac{1}{2}\,\boldsymbol{\kappa}\cdot\mathbf{a}\cdot\boldsymbol{\kappa} + \frac{1}{2}\,E\,A\,\varepsilon^2 + \frac{1}{2}\,E\,J_0\,\kappa_t'^2 - E\,\boldsymbol{t}\times\boldsymbol{\beta}\cdot\boldsymbol{\kappa}\,\kappa_t'\\
&U^{(3)} = \frac{1}{2}\,\tilde{a}_t\,\kappa_t^2 = \frac{1}{2}\,(\varepsilon\ \mathrm{tr}\,\mathbf{a}_\perp + \boldsymbol{\zeta}\cdot\boldsymbol{\kappa})\ \kappa_t^2\,.
\end{aligned}
\tag{16}
$$

We will elaborate on the origin of the torsional stiffness correction $\tilde{a}_t$ in Sect. 4, which constitutes the cubic part of the strain energy density $U^{(3)}$ together with the square of the twist rate κ_t^2. The constant coefficients in the above law denote in order of appearance: The classic beam stiffness tensor $\mathbf{a}$, the elastic modulus E, the cross-section area A, the warping constant J_0, the planar vector $\boldsymbol{\beta}$, closely related to the position of the shear center in the cross-section, as well as the third order elastic coefficient $\boldsymbol{\zeta}$. The geometric moments appearing in the stiffness coefficients are area integrals over the cross-section, which reduce to line integrals owing to the smallness of the wall-thickness h

$$
\begin{aligned}
&A = h\,H\,,\quad \mathbf{J} = h\int_0^H \boldsymbol{x}\boldsymbol{x}\,\mathrm{d}\xi\,,\quad C = \frac{H\,h^3}{3}\,,\quad \boldsymbol{\gamma} = h\int_0^H \boldsymbol{x}\boldsymbol{x}\cdot\boldsymbol{x}\,\mathrm{d}\xi\\
&J_0 = h\int_0^H w^2\,\mathrm{d}\xi\,,\quad \boldsymbol{\beta} = h\int_0^H \boldsymbol{x}\,w\,\mathrm{d}\xi\,,
\end{aligned}
\tag{17}
$$

with the area moment of inertia tensor $\mathbf{J}$, the classic torsion constant of the thin-walled open profile C as well as a cubic area moment $\boldsymbol{\gamma}$. Introducing the elastic shear modulus as μ, the stiffness coefficients read

$$
\mathbf{a} = -E\,\boldsymbol{t}\times\mathbf{J}\times\boldsymbol{t} + \mu\,C\,\boldsymbol{t}\boldsymbol{t}\,,\quad \boldsymbol{\zeta} = E\,\boldsymbol{\gamma}\times\boldsymbol{t}\,.
\tag{18}
$$

The stiffness tensor $\mathbf{a}$ consists of the classic torsional stiffness $a_t = \mu\,C$ and the planar bending stiffness tensor $\mathbf{a}_\perp = \mathbf{a} - a_t\,\boldsymbol{t}\boldsymbol{t}$. Now, applying partial differentiation with respect to each strain measure to the strain energy density (16), one obtains the constitutive relations for the generalised forces

$$
\begin{aligned}
&\boldsymbol{M} + \left(B' + b\right)\,\boldsymbol{t} = \mathbf{a}\cdot\boldsymbol{\kappa} - E\,\boldsymbol{t}\times\boldsymbol{\beta}\,\kappa_t' + (\varepsilon\ \mathrm{tr}\,\mathbf{a}_\perp + \boldsymbol{\zeta}\cdot\boldsymbol{\kappa})\ \boldsymbol{t}\,\kappa_t + \frac{1}{2}\,\kappa_t^2\,\boldsymbol{\zeta}\\
&Q_t = E\,A\,\varepsilon + \frac{1}{2}\,\kappa_t^2\ \mathrm{tr}\,\mathbf{a}_\perp\,,\qquad B = E\,J_0\,\kappa_t' - E\,\boldsymbol{t}\times\boldsymbol{\beta}\cdot\boldsymbol{\kappa}\,.
\end{aligned}
\tag{19}
$$

Proceeding to the incremental form requires a little more effort this time. With (11) we find

$$\boldsymbol{M}^{\cdot} + \left(B^{\cdot\prime} + b^{\cdot}\right) \boldsymbol{t} = \boldsymbol{\theta} \times \boldsymbol{M} + \mathbf{a} \cdot \boldsymbol{\theta}' - E\, \boldsymbol{t} \times \boldsymbol{\beta}\, \kappa_t^{\cdot\prime} +$$
$$(\varepsilon\ \mathrm{tr}\, \mathbf{a}_\perp + \boldsymbol{\zeta} \cdot \boldsymbol{\kappa})\ \boldsymbol{t}\, \kappa_t^{\cdot} + \left(\varepsilon^{\cdot}\ \mathrm{tr}\, \mathbf{a}_\perp + \zeta_\alpha\, \kappa_\alpha^{\cdot}\right)\ \boldsymbol{t}\, \kappa_t + \kappa_t\, \kappa_t^{\cdot}\, \boldsymbol{\zeta}$$
$$Q_t^{\cdot} = E\, A\, \varepsilon^{\cdot} + \kappa_t\, \kappa_t^{\cdot}\ \mathrm{tr}\, \mathbf{a}_\perp\,, \qquad B^{\cdot} = E\, J_0\, \kappa_t^{\cdot\prime} - E\, \boldsymbol{t} \times \boldsymbol{\beta} \cdot \boldsymbol{\theta}'\,, \tag{20}$$

where $\kappa_\alpha^{\cdot}$ are bending strain increments with summation over $\alpha = 1, 2$. The above constitutive relations conclude the derivation of the governing equations for the incremental theory. The essential relations needed for the upcoming computations are the equilibrium conditions (7) and (8), the kinematic relation (13) and the constitutive formulas (20), accompanied by the section constants (17) and (18). The transition from the incremental theory to the simple linear one is achieved by sheer neglect of all pre-stresses and pre-strains.

3 Shell as a Material Surface

Both the finite element simulations, used for comparison below, as well as the analysis of the varying torsional stiffness of thin-walled rods rest upon the classical Kirchhoff-Love shell theory in the form suggested by Eliseev [3–5], Vetyukov [19]. In the present section we outline the key points of the theory, which are required for the subsequent analytical study.

3.1 Differential Geometry of a Surface

We begin with the necessary notions of differential geometry of a surface in space [2]. The position vector $\boldsymbol{r}(q^\alpha)$ of a particle of a shell is parametrized by two material coordinates q^α, Greek indices run from 1 to 2. Each point on the surface lies on the intersection of two coordinate lines $q^1 = \mathrm{const}$ and $q^2 = \mathrm{const}$. The vectors of derivatives $\boldsymbol{r}_\alpha = \partial \boldsymbol{r} / \partial q^\alpha \equiv \partial_\alpha \boldsymbol{r}$ constitute the natural basis in the tangent plane. The unit normal vector follows as $\boldsymbol{n} = \boldsymbol{r}_1 \times \boldsymbol{r}_2 / |\boldsymbol{r}_1 \times \boldsymbol{r}_2|$. Introducing the cobasis $\boldsymbol{r}^\alpha$ according to $\boldsymbol{r}^\alpha \cdot \boldsymbol{r}_\beta = \delta^\alpha_\beta$, we obtain the representation of an arbitraty vector $\boldsymbol{v}$ and of Hamilton's differential operator

$$\boldsymbol{v} = v^\alpha \boldsymbol{r}_\alpha + v_n \boldsymbol{n}, \quad v^\alpha = \boldsymbol{v} \cdot \boldsymbol{r}^\alpha, \quad \nabla = \boldsymbol{r}^\alpha \partial_\alpha; \tag{21}$$

summation over repeated indices is implied.

The first metric tensor

$$\mathbf{a} = \nabla \boldsymbol{r} = \boldsymbol{r}^\alpha \boldsymbol{r}_\alpha = \mathbf{I} - \boldsymbol{n}\boldsymbol{n} \tag{22}$$

is a projection of the identity tensor $\mathbf{I}$ on the tangent plane. Both covariant and contravariant components

$$a_{\alpha\beta} = \boldsymbol{r}_\alpha \cdot \boldsymbol{r}_\beta, \quad a^{\alpha\beta} = \boldsymbol{r}^\alpha \cdot \boldsymbol{r}^\beta, \quad \mathbf{a} = a_{\alpha\beta}\boldsymbol{r}^\alpha\boldsymbol{r}^\beta = a^{\alpha\beta}\boldsymbol{r}_\alpha\boldsymbol{r}_\beta \tag{23}$$

define lengths and angles on the surface, whose elementary area is

$$\mathrm{d}\Omega = \sqrt{a}\,\mathrm{d}q^1\,\mathrm{d}q^2, \quad a = |\boldsymbol{r}_1 \times \boldsymbol{r}_2|^2 = \det(a_{\alpha\beta}). \tag{24}$$

The second metric tensor

$$\mathbf{b} = -\nabla\boldsymbol{n} = -\boldsymbol{r}^\alpha\partial_\alpha\boldsymbol{n} = b_{\alpha\beta}\boldsymbol{r}^\alpha\boldsymbol{r}^\beta \tag{25}$$

determines the material curvature of the surface. Its symmetry follows from the identity $\partial_\alpha(\boldsymbol{r}_\beta \cdot \boldsymbol{n}) = 0$, and the components result into

$$b_{\alpha\beta} = -\boldsymbol{r}_\alpha \cdot \partial_\beta\boldsymbol{n} = \partial_\alpha\partial_\beta\boldsymbol{r} \cdot \boldsymbol{n}. \tag{26}$$

The components of $\mathbf{a}$ and $\mathbf{b}$ cannot be arbitrary functions of q^α, since they must satisfy the compatibility conditions following from the symmetry of $\partial_\alpha\partial_\beta\partial_\gamma\boldsymbol{r}$ with respect to each pair of indices.

3.2 Kinematics of Deformation

Analysis of finite deformations requires discrimination of two configurations—the reference one (initial) and the deformed one (actual). In the reference state, we accordingly have $\mathring{\boldsymbol{r}}$, $\mathring{\boldsymbol{r}}_\alpha$, $\mathring{\boldsymbol{n}}$, $\mathring{\nabla}$, $\mathring{\mathbf{a}}$, $\mathring{\mathbf{b}}$ and $\mathrm{d}\mathring{\Omega}$ instead of $\boldsymbol{r}$, $\boldsymbol{r}_\alpha$, $\boldsymbol{n}$, ∇, $\mathbf{a}$, $\mathbf{b}$ and $\mathrm{d}\Omega$. A material particle with coordinates q^α moved from the position $\mathring{\boldsymbol{r}}(q^\alpha)$ to $\boldsymbol{r}(q^\alpha)$, and the configuration of the particles in the immediate vicinity of the chosen one is determined by the *deformation gradient*

$$\mathbf{F} = \mathring{\nabla}\boldsymbol{r}^T = \boldsymbol{r}_\alpha\mathring{\boldsymbol{r}}^\alpha. \tag{27}$$

Indeed, it defines the transformation of a material directed line element between the configurations:

$$\mathbf{F} \cdot \mathrm{d}\mathring{\boldsymbol{r}} = \mathbf{F} \cdot \mathring{\boldsymbol{r}}_\alpha q^\alpha = \boldsymbol{r}_\alpha q^\alpha = \mathrm{d}\boldsymbol{r}. \tag{28}$$

The determinant of the tensor $\mathbf{F}$ vanishes, but we introduce a "pseudo-inverse"

$$\begin{aligned} &\mathbf{G} = \nabla\mathring{\boldsymbol{r}}^T = \mathring{\boldsymbol{r}}_\alpha\boldsymbol{r}^\alpha, \quad \mathbf{F} \cdot \mathbf{G} = \mathbf{a}, \quad \mathbf{G} \cdot \mathbf{F} = \mathring{\mathbf{a}}, \\ &\nabla = \mathbf{G}^T \cdot \mathring{\nabla}, \quad \mathring{\nabla} = \mathbf{F}^T \cdot \nabla. \end{aligned} \tag{29}$$

Strains are related to the change of the components of the metric tensors:

$$\begin{aligned} \mathbf{E} &= \frac{1}{2}(\mathbf{F}^T \cdot \mathbf{F} - \mathring{\mathbf{a}}) = E_{\alpha\beta}\mathring{\boldsymbol{r}}^{\alpha}\mathring{\boldsymbol{r}}^{\beta}, \quad E_{\alpha\beta} = \frac{1}{2}(a_{\alpha\beta} - \mathring{a}_{\alpha\beta}); \\ \mathbf{K} &= \mathbf{F}^T \cdot \mathbf{b} \cdot \mathbf{F} - \mathring{\mathbf{b}} = K_{\alpha\beta}\mathring{\boldsymbol{r}}^{\alpha}\mathring{\boldsymbol{r}}^{\beta}, \quad K_{\alpha\beta} = b_{\alpha\beta} - \mathring{b}_{\alpha\beta}. \end{aligned} \tag{30}$$

Both the membrane strain measure $\mathbf{E}$ and the bending measure $\mathbf{K}$ vanish in the absence of deformation. Moreover, according to the laws of differential geometry [2] they remain constant when and only when the shell undergoes a rigid body motion.

3.3 Equations

The complete system of equations follows from a variational principle. We consider a continuum of material normal vectors with five degrees of freedom, namely three translations and two rotations: no work is done on "drilling" rotations about the normal vector. For a two-dimensional domain Ω the principle of virtual work reads as follows:

$$\int_{\Omega} \left(\boldsymbol{q} \cdot \delta\boldsymbol{r} + \boldsymbol{m} \times \boldsymbol{n} \cdot \delta\boldsymbol{n} - J^{-1}\delta U\right) \mathrm{d}\Omega + \oint_{\partial\Omega} (\boldsymbol{P} \cdot \delta\boldsymbol{r} + \boldsymbol{M} \times \boldsymbol{n} \cdot \delta\boldsymbol{n}) \, \mathrm{d}l = 0. \tag{31}$$

The area transformation factor appears as $J = \sqrt{a/\mathring{a}}$; $\mathrm{d}\Omega = J \, \mathrm{d}\mathring{\Omega}$. The force $\boldsymbol{q}$ and the moment $\boldsymbol{m}$ act per unit area in the actual configuration, and $\boldsymbol{P}$ and $\boldsymbol{M}$ are as well referred to the deformed boundary contour $\partial\Omega$. The shell is elastic, and the virtual work of internal forces equals to the variation of the function of the strain energy U, which is counted per unit reference area as it corresponds to a fixed set of material particles.

An additional constraint is introduced in the classical theory of shells. The deformed normal vector remains orthogonal to the deformed surface, and the variation $\delta\boldsymbol{n}$ in the variational equation (31) is not independent:

$$\boldsymbol{r}_{\alpha} \cdot \boldsymbol{n} = 0 \;\Rightarrow\; \delta\boldsymbol{r}_{\alpha} \cdot \boldsymbol{n} + \boldsymbol{r}_{\alpha} \cdot \delta\boldsymbol{n} = 0 \;\Rightarrow\; \delta\boldsymbol{n} + \nabla\delta\boldsymbol{r} \cdot \boldsymbol{n} = 0. \tag{32}$$

This constraint for the motion of neighbouring particles does not influence the degrees of freedom of each of them in the sense of Lagrangian mechanics: internal and external forces produce virtual work on three translations and two rotations.

The stored strain energy remains constant, when the shell undergoes a rigid body motion, that is to say: $\delta U = 0$ if and only if $\delta\mathbf{E} = 0$ and $\delta\mathbf{K} = 0$. Together with (31) and (32), this leads to the common balance equations for the internal force factors: the in-plane tensors of force resultants $\boldsymbol{\tau} = \tau^{\alpha\beta}\boldsymbol{r}_{\alpha}\boldsymbol{r}_{\beta}$ and moment resultants $\boldsymbol{\mu} = \mu^{\alpha\beta}\boldsymbol{r}_{\alpha}\boldsymbol{r}_{\beta}$ as well as the in-plane vector of transverse forces $\boldsymbol{Q}$, which appears in the variational principle as a Lagrange multiplier for the constraint (32) [3, 4]:

$$\begin{aligned} &\nabla\cdot\mathbf{T}+J^{-1}\boldsymbol{q}=0,\quad \mathbf{T}=\boldsymbol{\tau}+\boldsymbol{\mu}\cdot\mathbf{b}+\boldsymbol{Q}\boldsymbol{n};\\ &(\nabla\cdot\boldsymbol{\mu})\cdot\mathbf{a}+\boldsymbol{Q}-J^{-1}\boldsymbol{m}\times\boldsymbol{n}=0. \end{aligned} \tag{33}$$

The linear form of virtual work of internal forces per unit actual area takes the form

$$J^{-1}\delta U=\tau^{\alpha\beta}\delta E_{\alpha\beta}+\mu^{\alpha\beta}\delta K_{\alpha\beta}, \tag{34}$$

which proves that U is actually a function of the selected strain measures. The invariant form of the constitutive relations follows from (34):

$$\boldsymbol{\tau}=J^{-1}\mathbf{F}\cdot\frac{\partial U}{\partial\mathbf{E}}\cdot\mathbf{F}^T,\quad \boldsymbol{\mu}=J^{-1}\mathbf{F}\cdot\frac{\partial U}{\partial\mathbf{K}}\cdot\mathbf{F}^T; \tag{35}$$

no constitutive relation exists for the transverse force $\boldsymbol{Q}$ in a classical shell. At small local strains yet potentially large overall deformations, the strain energy function may be approximated by a quadratic form, which in the isotropic case with no coupling reads

$$U=\frac{1}{2}\left(A_1(\operatorname{tr}\mathbf{E})^2+A_2\mathbf{E}\cdot\cdot\mathbf{E}+D_1(\operatorname{tr}\mathbf{K})^2+D_2\mathbf{K}\cdot\cdot\mathbf{K}\right). \tag{36}$$

The coefficients follow from the linear plate theory:

$$A_1=\frac{Eh\nu}{1-\nu^2},\quad A_2=\frac{Eh}{1+\nu}\quad D_{1,2}=\frac{A_{1,2}h^2}{12}; \tag{37}$$

here E, ν and h are the Young modulus, Poisson ratio and thickness.

3.4 Boundary Conditions

The boundary conditions as well follow from the variational equation (31) and the constraint (32), see [3, 4, 19] for the derivation. The conditions feature the natural basis on the boundary contour $\partial\Omega$, namely the unit normal to the shell surface $\boldsymbol{n}$, the unit tangent vector $\boldsymbol{l}\equiv\partial_l\boldsymbol{r}$ (directional derivative along the contour) and the unit in-plane normal vector to the contour $\boldsymbol{\nu}\equiv\boldsymbol{l}\times\boldsymbol{n}$, see Fig. 3. The direction of the coordinate l is chosen such that $\boldsymbol{\nu}$ points outwards.

On a clamped edge both the position vector and the vector of unit normal are fixed. The dynamic boundary conditions at a part of the boundary free from kinematic constraints, which have been a matter of scientific discussions for decades, follow after formal mathematical transformations to

$$\begin{aligned} &\boldsymbol{\nu}\cdot\mathbf{T}-\partial_l((\boldsymbol{\nu}\cdot\boldsymbol{\mu}\cdot\boldsymbol{l}-\boldsymbol{\nu}\cdot\boldsymbol{M})\boldsymbol{n})=\boldsymbol{P},\\ &\boldsymbol{\nu}\cdot\boldsymbol{\mu}\cdot\boldsymbol{\nu}=-\boldsymbol{l}\cdot\boldsymbol{M}. \end{aligned} \tag{38}$$

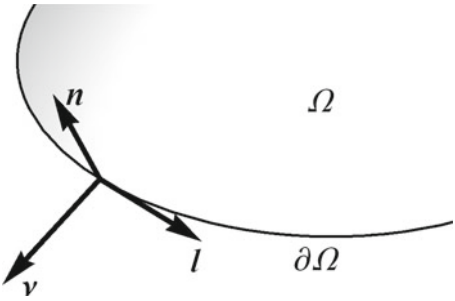

Fig. 3 Local basis at the boundary of the shell. Reprinted from [19] with permission

The fact that the "twisting" component of the external moment $\boldsymbol{\nu} \cdot \boldsymbol{M}$ contributes to the "force" boundary condition is long known from the theory of plates. Jumps in the corners because of discontinuous $\boldsymbol{l}$, $\boldsymbol{\nu}$ result into δ-functions in $\boldsymbol{P}$, which shall be interpreted as concentrated forces [6, 10, 15].

3.5 Transformation to the Reference Configuration with Piola Tensors

Equations of the non-linear three-dimensional theory of elasticity may advantageously be formulated with the differential operator of the reference state and with the Piola tensors. For non-linear shells, a similar procedure was presented by Pietraszkiewicz [10], who applied the index notation and used the expression of the virtual work of internal forces as a starting point. V. Eliseev suggested a novel approach to transforming the equations using the integral form of the equations of balance [3–5, 19].

In elasticity theory, Piola tensors appear with Nanson's formula, which relates directed surface elements of the reference and the actual configuration. Likewise, we consider two differentials on the surface $\mathrm{d}\boldsymbol{r}$, $\mathrm{d}'\boldsymbol{r}$ and their pre-images $\mathrm{d}\mathring{\boldsymbol{r}}$, $\mathrm{d}'\mathring{\boldsymbol{r}}$. We relate surface elements in two configurations:

$$\mathrm{d}\boldsymbol{r} \times \mathrm{d}'\boldsymbol{r} \cdot \boldsymbol{n} = J\, \mathrm{d}\mathring{\boldsymbol{r}} \times \mathrm{d}'\mathring{\boldsymbol{r}} \cdot \mathring{\boldsymbol{n}}. \tag{39}$$

Integrating along a contour on the surface, we deal with a directed line element $\boldsymbol{\nu}\, \mathrm{d}l = \mathrm{d}\boldsymbol{r} \times \boldsymbol{n}$. Now, $\mathrm{d}'\mathring{\boldsymbol{r}} = \mathbf{G} \cdot \mathrm{d}'\boldsymbol{r}$, see (28) and (29), and a cyclic permutation in (39) yields

$$\boldsymbol{\nu}\, \mathrm{d}l = J\, (\boldsymbol{\nu}\, \mathrm{d}l)^{\circ} \cdot \mathbf{G}. \tag{40}$$

The *Piola tensor* of in-plane stress resultants appears now as follows:

$$\boldsymbol{\nu}\, \mathrm{d}l \cdot \boldsymbol{\tau} = (\boldsymbol{\nu}\, \mathrm{d}l)^{\circ} \cdot \mathring{\boldsymbol{\tau}} \quad \Rightarrow \quad \mathring{\boldsymbol{\tau}} = J\mathbf{G} \cdot \boldsymbol{\tau} = \frac{\partial U}{\partial \mathbf{E}} \cdot \mathbf{F}^{T}. \tag{41}$$

Likewise, we introduce

$$\mathring{\boldsymbol{\mu}} = J\mathbf{G}\cdot\boldsymbol{\mu}, \quad \mathring{\boldsymbol{Q}} = J\mathbf{G}\cdot\boldsymbol{Q}, \quad \mathring{\mathbf{T}} = J\mathbf{G}\cdot\mathbf{T} = \mathring{\boldsymbol{\tau}} + \mathring{\boldsymbol{\mu}}\cdot\mathbf{b} + \mathring{\boldsymbol{Q}}\boldsymbol{n}. \tag{42}$$

The equation of balance of forces in (33) can be rewritten in an integral form:

$$\oint \boldsymbol{\nu}\cdot\mathbf{T}\,\mathrm{d}l + \int \boldsymbol{J}^{-1}q\,\mathrm{d}\Omega = 0; \tag{43}$$

the integration is performed over an arbitrary contour and the part of the surface bounded by it. We transform the integrals to the reference configuration with $(\boldsymbol{\nu}\,\mathrm{d}l)^{\circ}$ and $\mathrm{d}\mathring{\Omega}$, which further results in

$$\mathring{\nabla}\cdot\mathring{\mathbf{T}} + \mathring{\boldsymbol{q}} = 0; \tag{44}$$

now it is convenient to consider external force factors per unit area in the reference state:

$$\mathring{\boldsymbol{q}} \equiv J\boldsymbol{q}, \quad \mathring{\boldsymbol{m}} \equiv J\boldsymbol{m}. \tag{45}$$

The equation of equilibrium of moments in (33), transformed to the reference configuration, reads

$$\left(\mathring{\nabla}\cdot\mathring{\boldsymbol{\mu}}\right)\cdot\mathbf{a} + \mathbf{F}\cdot\mathring{\boldsymbol{Q}} - \mathring{\boldsymbol{m}}\times\boldsymbol{n} = 0 \tag{46}$$

and results from an equivalent integral equilibrium condition

$$\oint \boldsymbol{\nu}\cdot(\boldsymbol{\mu}\times\boldsymbol{n} - \mathbf{T}\times\boldsymbol{r})\,\mathrm{d}l + \int (\boldsymbol{m} + \boldsymbol{r}\times\boldsymbol{q})\,\mathrm{d}\Omega = 0. \tag{47}$$

3.6 Linearised Equations of a Pre-stressed Shell

An *incremental formulation* is useful in problems concerning bifurcation of equilibria, small vibrations of loaded structures, etc., see [9, 10]. Denoting small increments of structural entities as $(\cdots)^{\bullet}$, we seek linear equations for the displacement $\boldsymbol{u} \equiv \boldsymbol{r}^{\bullet}$ as a response to the variation of the external force $\mathring{\boldsymbol{q}}^{\bullet}$, see also Sect. 2.2 for a discussion of the incremental theory of rods.

The operations $(\cdots)^{\bullet}$ and ∇ do not commute: $(\nabla\cdot\boldsymbol{r})^{\bullet} = (\mathrm{tr}\,\mathbf{a})^{\bullet} = 0 \neq \nabla\cdot\boldsymbol{u}$, but $\left(\mathring{\nabla}\varphi\right)^{\bullet} = \mathring{\nabla}\varphi^{\bullet}$ for any field φ, and the superposition of an infinitesimal deformation onto a finite one is convenient to study using the above equations for the Piola tensors with $\mathring{\nabla}$. Linearising the equations of equilibrium (44), (46) and assuming $\mathring{\boldsymbol{m}} = 0$ for simplicity, we obtain

$$\begin{aligned}
&\mathring{\nabla}\cdot\mathring{\mathbf{T}}^{\bullet}+\mathring{\boldsymbol{q}}^{\bullet}=0,\\
&\mathbf{G}^{\bullet}\cdot\left(\mathring{\nabla}\cdot\mathring{\boldsymbol{\mu}}\right)+\mathbf{G}\cdot\left(\mathring{\nabla}\cdot\mathring{\boldsymbol{\mu}}^{\bullet}\right)+\mathring{\boldsymbol{Q}}^{\bullet}=0,\\
&\mathring{\mathbf{T}}^{\bullet}=\mathring{\boldsymbol{\tau}}^{\bullet}+\mathring{\boldsymbol{\mu}}^{\bullet}\cdot\mathbf{b}+\mathring{\boldsymbol{\mu}}\cdot\mathbf{b}^{\bullet}+\mathring{\boldsymbol{Q}}^{\bullet}\boldsymbol{n}+\mathring{\boldsymbol{Q}}\boldsymbol{n}^{\bullet}.
\end{aligned}\tag{48}$$

Variations of the deformation gradient and of the unit normal vector:

$$\boldsymbol{r}_{\alpha}^{\bullet}=\partial_{\alpha}\boldsymbol{u}\quad\Rightarrow\quad\mathbf{F}^{\bullet}=\mathring{\nabla}\boldsymbol{u}^{T};\quad\boldsymbol{n}^{\bullet}=-\nabla\boldsymbol{u}\cdot\boldsymbol{n}.\tag{49}$$

The increment of the curvature tensor reads (after some mathematics, see [4, 19])

$$\mathbf{b}^{\bullet}=-2\left(\nabla\boldsymbol{u}\cdot\mathbf{b}\right)^{S}+\boldsymbol{n}\boldsymbol{n}\cdot\nabla\boldsymbol{u}^{T}\cdot\mathbf{b}+\nabla\nabla\boldsymbol{u}\cdot\boldsymbol{n}.\tag{50}$$

Elastic relations for the variations of the Piola tensors:

$$\mathring{\boldsymbol{\tau}}^{\bullet}=\left(\frac{\partial U}{\partial\mathbf{E}}\right)^{\bullet}\cdot\mathbf{F}^{T}+\frac{\partial U}{\partial\mathbf{E}}\cdot\mathbf{F}^{\bullet T},\quad\mathring{\boldsymbol{\mu}}^{\bullet}=\left(\frac{\partial U}{\partial\mathbf{K}}\right)^{\bullet}\cdot\mathbf{F}^{T}+\frac{\partial U}{\partial\mathbf{K}}\cdot\mathbf{F}^{\bullet T};\tag{51}$$

both first terms require variations of the derivatives of the strain energy (36):

$$\left(\frac{\partial U}{\partial\mathbf{E}}\right)^{\bullet}=\left(A_1\mathring{\mathbf{a}}\,\mathrm{tr}\,\mathbf{E}+A_2\mathbf{E}\right)^{\bullet}=A_1\mathring{\mathbf{a}}\,\mathrm{tr}\,\mathbf{E}^{\bullet}+A_2\mathbf{E}^{\bullet},\tag{52}$$

and

$$\begin{aligned}
&\mathbf{E}^{\bullet}=\mathbf{F}^{T}\cdot\nabla\boldsymbol{u}^{S}\cdot\mathbf{F},\\
&\mathbf{K}^{\bullet}=2\left(\mathring{\nabla}\boldsymbol{u}\cdot\mathbf{b}\cdot\mathbf{F}\right)^{S}+\mathbf{F}^{T}\cdot\mathbf{b}^{\bullet}\cdot\mathbf{F}.
\end{aligned}\tag{53}$$

A single vector equation for $\boldsymbol{u}$ follows from (48)–(53). The boundary conditions are simple only when the displacement and the rotation are prescribed or in some special cases, see also discussion by Pietraszkiewicz [10]; for the application to the actual problem of the present contribution see Sect. 4.

A prominent and at the same time simple case is the stability of plates. The in-plane stiffness of the plate $A_{1,2}$ is high, and before variation we presume a plane stress state with negligibly small deformation. The pre-stress $\boldsymbol{\tau}=\partial U/\partial\mathbf{E}$ enters (51), and assuming that the displacement has only the lateral deflection component w, we come up with the known equation

$$\nabla\cdot(\boldsymbol{\tau}\cdot\nabla w)-(D_1+D_2)\Delta\Delta w+q_n^{\bullet}=0;\tag{54}$$

see Reismann [11]; Timoshenko and Gere [14] discussed the case $\boldsymbol{\tau}=\text{const}$.

4 Torsion of a Pre-stressed Cylindrical Panel

The torsional stiffness a_t of a thin-walled open cross-section is much smaller than the stiffness for bending. The local geometrically non-linear effects in the cross-section lead to essential variations of the torsional stiffness depending on the axial force and the bending moment, which is determined by the cubic terms $U^{(3)}$ in the strain energy of the rod model (16). We conclude on these variations solving a problem of torsion of a pre-stressed cylindrical panel using the above incremental formulation of the theory of shells.

4.1 Pre-stressed State

Seeking to find $U^{(3)}$, we consider a straight cylindrical shell with the cross-section as in Fig. 2, the geometry specified as follows:

$$\begin{aligned} &\boldsymbol{r}(\xi, z) = z\boldsymbol{k} + \boldsymbol{x}(\xi), \quad \boldsymbol{x}' \equiv \partial_\xi \boldsymbol{x} = \boldsymbol{\xi}, \\ &\boldsymbol{\xi}' = -\alpha \boldsymbol{n}, \quad \boldsymbol{n}' = \alpha \boldsymbol{\xi}, \quad \boldsymbol{\xi} \times \boldsymbol{k} = \boldsymbol{n}; \end{aligned} \tag{55}$$

z is the axial coordinate and $\boldsymbol{k} = \boldsymbol{e}_3$ is the direction, $\boldsymbol{\xi}$ is the unit tangent vector in the cross-section and $\alpha(\xi)$ is its curvature. Furthermore, we write

$$\nabla = \boldsymbol{\xi}\partial_\xi + \boldsymbol{k}\partial_z, \quad \mathbf{a} = \nabla \boldsymbol{r} = \boldsymbol{\xi}\boldsymbol{\xi} + \boldsymbol{k}\boldsymbol{k}, \quad \mathbf{b} = -\nabla \boldsymbol{n} = -\alpha \boldsymbol{\xi}\boldsymbol{\xi}. \tag{56}$$

The actual state is assigned to coincide with the reference one ($\boldsymbol{r} = \mathring{\boldsymbol{r}}$) and is pre-stressed:

$$\mathring{\boldsymbol{\tau}} = \sigma(\xi)\boldsymbol{k}\boldsymbol{k}, \quad \mathring{\boldsymbol{\mu}} = 0, \quad \sigma(\xi) = \boldsymbol{a} \cdot \boldsymbol{x}(\xi) + b. \tag{57}$$

The linear distribution of the axial stresses resembles a general bending type of loading and is determined by the vector $\boldsymbol{a}$ and the constant term b (which is to be distinguished from the externally applied bi-moments, considered above). With the geometry (56), we easily check the equilibrium conditions (33):

$$\nabla \cdot \mathring{\mathbf{T}} = (\boldsymbol{\xi}\partial_\xi + \boldsymbol{k}\partial_z) \cdot \sigma(\xi)\boldsymbol{k}\boldsymbol{k} = \partial_\xi \sigma \boldsymbol{\xi} \cdot \boldsymbol{k}\boldsymbol{k} + \partial_z \sigma \boldsymbol{k} = 0. \tag{58}$$

The boundary conditions (38) are also fulfilled at the side edges $\xi = 0$ and $\xi = H$, as here $\boldsymbol{\nu} = \mp\boldsymbol{\xi}$, and $\boldsymbol{\nu} \cdot \mathring{\mathbf{T}} = 0$.

Let us now compute the force and the moment, which are produced by these pre-stresses in a cross-section $z = \text{const}$, by mentally separating one part of the shell from another. The contour of integration F consists of the cut $0 < \xi < H$ and of the immediately adjacent points "+" and "–" at the free side edges, which is shown

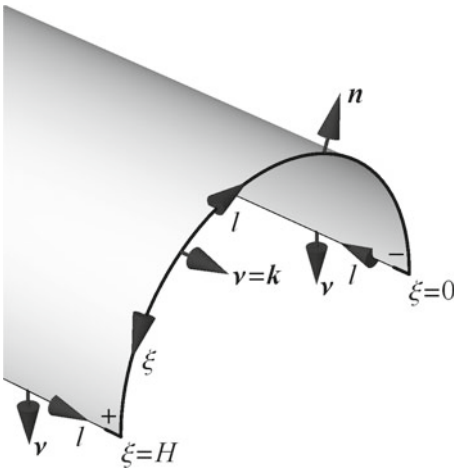

Fig. 4 Separated part of the shell model of a thin-walled rod and the local basis vectors in the cross-section of the cut. Reprinted from [19] with permission

by a thick line in Fig. 4. The directions of the contour coordinate in the shell model l and of the outer normal to the contour $\boldsymbol{\nu}$ are determined by the choice of the unit normal to the shell surface $\boldsymbol{n} = \boldsymbol{\nu} \times \boldsymbol{l}$, see Fig. 3. The coordinate in the cross-section ξ according to the above definition is shown in Fig. 2; $\boldsymbol{n} = \boldsymbol{\xi} \times \boldsymbol{k}$, and on the cut we have

$$\boldsymbol{\nu} = \boldsymbol{k}, \quad \boldsymbol{l} = -\boldsymbol{\xi}, \quad \partial_l = -\partial_\xi. \tag{59}$$

At the free side edges $\xi = 0, H$ we have $\boldsymbol{\nu} = \mp\boldsymbol{\xi}$, $\boldsymbol{l} = \mp\boldsymbol{k}$, $\partial_l = \mp\partial_z$. For the given distribution of the stress resultants of the shell model (57) we intend to determine the force $\boldsymbol{P}$ and the moment $\boldsymbol{M}$, which act at the separated part of the shell from its counterpart and shall be later interpreted in terms of the rod model. It is important, that the contour of integration F spans from one side edge to the other one: the end points of the cut may have concentrated contributions to the integrals because of the jumps of the local basis $\boldsymbol{l}$ and $\boldsymbol{\nu}$ and the derivative with respect to l in the first equality of (38).

As it is often noted in the literature concerning the classical model of Kirchhoff plates [11, 15], the twisting component of the externally applied moment $M_\nu = \boldsymbol{\nu} \cdot \boldsymbol{M}$ is related to the force $\boldsymbol{P}$ through the first of the boundary conditions (38), and the problem of finding the external force factors for a given stressed state in the shell does not possess a unique solution. We will show that indeed arbitrarily chosen $M_\nu(\xi)$ results in different $\boldsymbol{P}(\xi)$, but has no effect on the total force and the total moment in the cross-section.

Proceeding with the actual computation, we first consider $M_\nu = 0$. Now, with (38) we find

$$\boldsymbol{P} = \boldsymbol{k} \cdot \sigma(\xi)\boldsymbol{k}\boldsymbol{k} \tag{60}$$

as $\mathring{\boldsymbol{\mu}} = 0$, and there will be no concentrated forces at the end points. For the total force in the cross-section we write

$$\boldsymbol{Q}^{\mathrm{rod}} = \int_F \boldsymbol{P}\,\mathrm{d}l = \int_0^H \boldsymbol{P}\,\mathrm{d}\xi = bH\boldsymbol{k}; \tag{61}$$

the term with $\boldsymbol{a}$ vanishes because of (2).

Seeking the total moment, we find from the second boundary condition in (38) that $\boldsymbol{M} = 0$, and

$$\boldsymbol{M}^{\mathrm{rod}} = \int_F \boldsymbol{x} \times \boldsymbol{P}\,\mathrm{d}l = \boldsymbol{a} \cdot \int_0^H \boldsymbol{x}\boldsymbol{x} \times \boldsymbol{k}\,\mathrm{d}\xi = h^{-1}\boldsymbol{a} \cdot \mathbf{J} \times \boldsymbol{k}. \tag{62}$$

Returning back to the discussion of the effect of M_ν, we compute its contribution to the total force. The additional term in $\boldsymbol{P}$ equals $\partial_l(M_\nu \boldsymbol{n})$. At the free side edges we have no external actions onto the separated part of the shell, and there $M_\nu = 0$. Integrating the force from one free edge to another one, we find

$$\int_F \partial_l(M_\nu \boldsymbol{n})\,\mathrm{d}l = M_\nu \boldsymbol{n}\big|_+^- = 0 \tag{63}$$

as the external moment M_ν vanishes in the points "+" and "–" of the free side edges. Using integration by parts, it is also easy to ascertain that the twisting moment does not contribute to the total moment in the cross-section:

$$\int_F (M_\nu \boldsymbol{\nu} + \boldsymbol{x} \times \partial_l(M_\nu \boldsymbol{n}))\,\mathrm{d}l = \int_F M_\nu \boldsymbol{\nu}\,\mathrm{d}l + \boldsymbol{x} \times M_\nu \boldsymbol{n}\big|_+^- - \int_F M_\nu \boldsymbol{l} \times \boldsymbol{n}\,\mathrm{d}l = 0. \tag{64}$$

Now we relate the coefficients $\boldsymbol{a}$ and b in the distribution of the pre-stress σ to the equivalent axial extension ε and bending $\boldsymbol{\kappa}_\perp \equiv \boldsymbol{\kappa} - \kappa_t \boldsymbol{t}$. In doing so, we presume the deformation to be small, such that the above consideration of a straight rod remains valid. Indeed, numerical experiments demonstrate that essential changes in the torsional stiffness happen at very small strains. Comparing the axial force Q_t and the bending moment $\boldsymbol{M}$ in (19) at $\kappa_t = 0$ with the values, integrated over the cross-section in (61) and (62), we find

$$\begin{aligned} &bH = EHh\varepsilon \;\;\Rightarrow\;\; b = Eh\varepsilon, \\ &h^{-1}\boldsymbol{a} \cdot \mathbf{J} \times \boldsymbol{k} = -E\boldsymbol{k} \times \mathbf{J} \times \boldsymbol{k} \cdot \boldsymbol{\kappa} \;\;\Rightarrow\;\; \boldsymbol{a} = Eh\boldsymbol{k} \times \boldsymbol{\kappa}; \end{aligned} \tag{65}$$

we have used the relation of the bending stiffness $\mathbf{a}_\perp$ to the tensor of moments of inertia $\mathbf{J}$ from (18) as well as the identity $\boldsymbol{a} \cdot \mathbf{J} = \boldsymbol{k} \times \boldsymbol{a} \cdot \boldsymbol{k} \times \mathbf{J}$.

4.2 Approximate Variational Approach

Now, let us approximate twisting of the shell with the rate κ_t similar to the kinematics of a rod (3). We write the position vector in the deformed configuration as

$$\boldsymbol{r} = \mathring{\boldsymbol{r}} + \kappa_t z \boldsymbol{k} \times \boldsymbol{x} + \kappa_t w(\xi)\boldsymbol{k}. \tag{66}$$

It is questionable whether this state is indeed a solution of the equations of the theory of shells. But we aim at computing the total strain energy of the shell model in the cross-section:

$$U^{\text{rod}} = \int_0^H U^{\text{shell}}\,\mathrm{d}\xi = \frac{1}{2}a_t\kappa_t^2 + \frac{1}{2}\tilde{a}_t\kappa_t^2. \tag{67}$$

The strain energy of the shell U^{shell} includes the conventional quadratic part according to (36), which after integration results in the first term with the known torsional stiffness $a_t = \mu C$, see (18). But the shell is pre-stressed, and its strain energy additionally contains the contraction of the pre-stresses (57) with the corresponding strain measures. This results in an additional quadratic term with respect to κ_t, and the coefficient $\tilde{a}_t$ plays the role of a correction of the torsional stiffness due to bending and axial tension:

$$\frac{1}{2}\tilde{a}_t\kappa_t^2 = \int_0^H \mathring{\boldsymbol{\tau}}\cdot\cdot\,\mathbf{E}\,\mathrm{d}\xi = \int_0^H \sigma(\xi)\boldsymbol{k}\cdot\mathbf{E}\cdot\boldsymbol{k}\,\mathrm{d}\xi. \tag{68}$$

We compute the deformation gradient and the strain

$$\begin{aligned}\mathbf{F} &= \mathring{\nabla}\boldsymbol{r}^T = \mathring{\mathbf{a}} + \kappa_t\boldsymbol{k}\times\boldsymbol{x}\boldsymbol{k} + \kappa_t z\boldsymbol{n}\boldsymbol{\xi} + \kappa_t w'(\xi)\boldsymbol{k}\boldsymbol{\xi},\\ \boldsymbol{k}\cdot\mathbf{E}\cdot\boldsymbol{k} &= \frac{1}{2}\left((\mathbf{F}\cdot\boldsymbol{k})\cdot(\mathbf{F}\cdot\boldsymbol{k}) - 1\right) = \frac{1}{2}\kappa_t^2\boldsymbol{x}\cdot\boldsymbol{x}.\end{aligned} \tag{69}$$

The kinematic relation between the strain measure of the shell and κ_t is quadratic, which is a geometrically non-linear effect.

Thus, the correction of the torsional stiffness is expressed via the second and the third order geometric moments of the cross-section:

$$\tilde{a}_t = \int_0^H \sigma(\xi)\boldsymbol{x}\cdot\boldsymbol{x}\,\mathrm{d}\xi = h^{-1}(\boldsymbol{a}\cdot\boldsymbol{\gamma} + b\,\mathrm{tr}\,\mathbf{J}), \quad \boldsymbol{\gamma} = h\int_0^H \boldsymbol{x}\boldsymbol{x}\cdot\boldsymbol{x}\,\mathrm{d}\xi. \tag{70}$$

Now, $\mathrm{tr}\,\mathbf{J} = E^{-1}\,\mathrm{tr}\,\mathbf{a}_\perp$, we use (65) and arrive at $\tilde{a}_t$ as in (16):

$$\tilde{a}_t = \boldsymbol{\zeta}\cdot\boldsymbol{\kappa} + \varepsilon\,\mathrm{tr}\,\mathbf{a}_\perp, \quad \boldsymbol{\zeta} = E\boldsymbol{\gamma}\times\boldsymbol{k} = Eh\int_0^H \boldsymbol{x}\boldsymbol{x}\cdot\boldsymbol{x}\,\mathrm{d}\xi\times\boldsymbol{k}. \tag{71}$$

The argumentation in the literature [12, 14, 21] is based on similar geometric considerations. Although the developed model corresponds well to the results of numerical analysis of non-reduced problems, a more accurate solution appears to be necessary.

4.3 Exact Solution of the Shell Problem of Torsion

Aiming at the solution of the problem with pre-stresses, let us focus on a simple linear case of torsion of the shell model of a thin-walled rod of open profile. We apply the incremental shell equations from Sect. 3.6 to the undeformed configuration, described by (55), (56). The small strain is sought in the form

$$\mathbf{E}^{\bullet} = 0, \quad \mathbf{K}^{\bullet} = \kappa_{\xi z}(\boldsymbol{\xi}\boldsymbol{k} + \boldsymbol{k}\boldsymbol{\xi}), \quad \kappa_{\xi z} = \text{const}. \tag{72}$$

Instead of checking the conditions of compatibility [3], we simply state that the strains are kinematically admissible [19] and the corresponding field of displacements fulfills

$$\partial_z \boldsymbol{u} = -\kappa_{\xi z}\boldsymbol{k} \times \boldsymbol{x}. \tag{73}$$

We compare to $\boldsymbol{r} - \mathring{\boldsymbol{r}}$ from (66) and identify the rate of twist: $\kappa_t = -\kappa_{\xi z}$. With the constitutive relations (52) the stresses are

$$\mathring{\boldsymbol{\tau}}^{\bullet} = 0, \quad \mathring{\boldsymbol{\mu}}^{\bullet} = D_2\kappa_{\xi z}(\boldsymbol{\xi}\boldsymbol{k} + \boldsymbol{k}\boldsymbol{\xi}). \tag{74}$$

Now we address the equations of equilibrium (48):

$$\begin{aligned} &\mathring{\boldsymbol{\mu}} = 0, \quad \nabla \cdot \mathring{\boldsymbol{\mu}}^{\bullet} = 0 \quad \Rightarrow \quad \mathring{\boldsymbol{Q}}^{\bullet} = 0 \\ &\mathring{\mathbf{T}}^{\bullet} = -\alpha D_2\kappa_{\xi z}\boldsymbol{k}\boldsymbol{\xi} \quad \Rightarrow \quad \nabla \cdot \mathring{\mathbf{T}}^{\bullet} = 0. \end{aligned} \tag{75}$$

Finally, we apply the boundary conditions (38) (updated to the present notation for increments from the undeformed state with dots and circles) and ensure that the side edges are also free from external loading:

$$\boldsymbol{\nu} = \mp\boldsymbol{\xi}, \quad \boldsymbol{l} = \mp\boldsymbol{k}, \quad \boldsymbol{\nu} \cdot \mathring{\mathbf{T}}^{\bullet} = 0, \quad \boldsymbol{\nu} \cdot \mathring{\boldsymbol{\mu}}^{\bullet} \cdot \boldsymbol{l}\boldsymbol{n} = \text{const}, \quad \boldsymbol{\nu} \cdot \mathring{\boldsymbol{\mu}}^{\bullet} \cdot \boldsymbol{\nu} = 0. \tag{76}$$

It proves, that the state (72), (74) is indeed a solution of a problem of statics. It remains yet to find the relation of the rate of twist κ_t to the total twisting moment in the cross-section M_z^{rod}. Moreover, we shall check that both the total force and the total bending moment in the cross-section vanish. The integration is to be performed from one free side edge to another, and concentrated forces need to be considered, as at the free edges we have $\boldsymbol{\nu} \cdot \mathring{\boldsymbol{\mu}}^{\bullet} \cdot \boldsymbol{l} = D_2\kappa_{\xi z}$, while inside the domain $0 < \xi < H$ it will be $\boldsymbol{\nu} \cdot \mathring{\boldsymbol{\mu}}^{\bullet} \cdot \boldsymbol{l} = -D_2\kappa_{\xi z}$ (see (59) and below). As shown above in Sect. 4.1, an arbitrary distribution of the twisting moment along the cut shall not have an effect on the total force and the total moment. The choice

$$M_{\nu}^{\bullet} = -2D_2\kappa_{\xi z} \tag{77}$$

allows avoiding jumps of the expression under the derivative ∂_l in the first of the conditions (38) in the end points $\xi = 0$ and $\xi = H$. Now we use the expression from (75) for $\overset{\circ}{\mathbf{T}}{}^{\bullet}$ and find

$$\boldsymbol{P}^{\bullet} = \boldsymbol{k} \cdot D_2 \kappa_{\xi z} (\boldsymbol{\xi k} + \boldsymbol{k\xi}) \cdot (-\alpha \boldsymbol{\xi\xi}) + \partial_\xi (D_2 \kappa_{\xi z} \boldsymbol{n}) = 0; \tag{78}$$

we have used $\alpha \boldsymbol{\xi} = \boldsymbol{n}'$. This guarantees the absence of the total force in the cross-section. From the second boundary condition in (38) we find $M_l = 0$, and the total moment has just the twisting component:

$$\boldsymbol{M}^{\text{rod}} = \int_0^H M_\nu^{\bullet} \boldsymbol{\nu} \, \mathrm{d}l = -2 D_2 H \kappa_{\xi z} \boldsymbol{k}. \tag{79}$$

It remains to add that a computation with $M_\nu^{\bullet} = 0$ requires more effort as concentrated forces in $\boldsymbol{P}^{\bullet}$ have to be processed in the end points of the cut, but leads to the same conclusions. The classical theory of Kirchhoff-Love shells does not allow to determine, whether the two parts of the shell actually interact by twisting moments or by forces or by a combination of them. This has long been known for plates, see, e.g., the remarks by Timoshenko and Woinowsky-Krieger [15]. Arriving at the same conclusion concerning the equivalence of the distributed twisting moment to a couple of concentrated forces in the corners of a classical plate, Reismann [11] studies the problem further with the Reissner-Mindlin model of a shear deformable plate. This allows to uniquely determine the distributions of the force factors in a cross-section. While the twisting moment is almost constant inside the contour and vanishes near the end points, the transverse force is mainly concentrated near the ends of the domain. This conforms to solution of the Saint-Venant problem of twist of a plate as a three-dimensional body; the importance of the contribution of the transverse shear stresses near the end points of the cross-section of such a plate has been emphasized by Ziegler [23].

Recalling the kinematic formula (73), we relate the rate of twist to the twisting moment and find the classical expression for the torsional rigidity:

$$M_z^{\text{rod}} = 2 D_2 H \kappa_t \quad \Rightarrow \quad a_t = \mu C = 2 D_2 H = \frac{E H h^3}{6(1+\nu)}. \tag{80}$$

4.4 Torsion of a Pre-stressed Shell

Now everything is prepared for a novel and mathematically consistent proof of the expression for the additional torsional rigidity (71). We consider the incremental formulation of the problem of torsion with the account for pre-stresses (57) owing to bending and tension.

The constitutive relations (51) shall now be considered with

$$\frac{\partial U}{\partial \mathbf{E}} = \mathring{\boldsymbol{\tau}}, \quad \frac{\partial U}{\partial \mathbf{K}} = 0. \tag{81}$$

The configuration prior to the linearisation coincides with the reference state; see the discussion before (65). We again seek the strains in the form (72). Then with (51) it follows

$$\mathring{\boldsymbol{\tau}}^{\bullet} = \mathring{\boldsymbol{\tau}} \cdot \mathbf{F}^{\bullet\, T} = \sigma(\xi)\boldsymbol{k}\partial_z \boldsymbol{u}, \quad \mathring{\boldsymbol{\mu}}^{\bullet} = D_2 \kappa_{\xi z}(\boldsymbol{\xi}\boldsymbol{k} + \boldsymbol{k}\boldsymbol{\xi}). \tag{82}$$

The purely kinematical relation of the field of displacements $\boldsymbol{u}$ with the fields of strains does not change in the presence of pre-stresses, and from (73) we find

$$\mathring{\boldsymbol{\tau}}^{\bullet} = -\kappa_{\xi z}\sigma(\xi)\boldsymbol{k}\boldsymbol{k} \times \boldsymbol{x}. \tag{83}$$

We again consider the equilibrium conditions. Additionally to (75), we verify that the new increment of the in-plane stresses is also self-equilibrated:

$$\nabla \cdot \mathring{\boldsymbol{\tau}}^{\bullet} = \boldsymbol{\xi} \cdot \partial_{\xi} \mathring{\boldsymbol{\tau}}^{\bullet} = 0. \tag{84}$$

Let us now address the static boundary conditions, which were not treated in the general incremental formulation in Sect. 3.6; the inherent difficulties have been pointed out by Pietraszkiewicz [10]. In the following we demonstrate that the boundary conditions of the linear formulation shall be augmented by simple correction terms, if the pre-stressed state is a momentless one. Moreover, even these correction terms vanish in the present case.

Consider the first one of the boundary conditions (38) in the general non-linear case. Applying the transformations (41), (42), we rewrite it with the Piola tensors:

$$\mathring{\boldsymbol{\nu}} \cdot \mathring{\mathbf{T}} - \frac{\partial}{\partial \mathring{l}} \left(\mathring{\boldsymbol{\nu}} \cdot \mathring{\boldsymbol{\mu}} \cdot \mathring{\boldsymbol{l}} \mathring{\boldsymbol{n}} \right) = \boldsymbol{P} \left(\frac{\partial l}{\partial \mathring{l}} \right); \tag{85}$$

the torsional moment M_{ν} is ignored owing to the reasons stated above. Here $\mathring{l}$ is the arc coordinate along the boundary in the reference configuration and l is the actual one. Varying this equality from the state

$$\mathring{\boldsymbol{\mu}} = 0, \quad l = \mathring{l}, \quad \boldsymbol{l} = \mathring{\boldsymbol{l}}, \quad \boldsymbol{n} = \mathring{\boldsymbol{n}}, \quad \boldsymbol{\nu} = \mathring{\boldsymbol{\nu}}, \tag{86}$$

we arrive at a linearised boundary condition, which has just one additional term in comparison to the fully linear case:

$$\boldsymbol{\nu} \cdot \mathring{\mathbf{T}}^{\bullet} - \partial_l \left(\boldsymbol{\nu} \cdot \mathring{\boldsymbol{\mu}}^{\bullet} \cdot \boldsymbol{l}\boldsymbol{n} \right) = \boldsymbol{P}^{\bullet} + \boldsymbol{P} \left(\frac{\partial l}{\partial \mathring{l}} \right)^{\bullet}. \tag{87}$$

Now we turn the attention to the moment boundary condition, i.e., to the second equality in (38). We apply the transformation rule (42) twice and find

$$\mathring{\boldsymbol{\nu}} \cdot \frac{\partial U}{\partial \mathbf{K}} \cdot \mathring{\boldsymbol{\nu}} = -J^{-1} M_l \left(\frac{\partial l}{\partial \mathring{l}} \right)^2 . \tag{88}$$

Linearising from the state

$$\mathbf{K} = 0, \quad J = 1, \quad l = \mathring{l}, \quad \boldsymbol{\nu} = \mathring{\boldsymbol{\nu}}, \tag{89}$$

we find

$$\boldsymbol{\nu} \cdot \left(D_1 \mathbf{a} \operatorname{tr} \mathbf{K}^{\bullet} + D_2 \mathbf{K}^{\bullet} \right) \cdot \boldsymbol{\nu} = -M_l^{\bullet} - M_l \left(J^{-1} \left(\frac{\partial l}{\partial \mathring{l}} \right)^2 \right)^{\bullet} . \tag{90}$$

The derived boundary conditions are particularly simple owing to the "pure bending" type of deformation (72), which in the context of shell theory is characterized by $\mathbf{E}^{\bullet} = 0$, i.e. the preservation of the first metric of the surface. Accordingly, the lengths and areas on the surface do not change, and the additional terms in the right-hand sides of (87), (90), which are related to the increments of the geometric elements, vanish.

From (83) we see that the boundary conditions at the free edges $\xi = 0, H$ hold as $\boldsymbol{\nu} \cdot \mathring{\boldsymbol{\tau}}^{\bullet} = 0$. Along with the fulfilled equilibrium and the compatibility conditions inside the domain this means that (72) is an exact solution of the shell problem, linearised in the vicinity of a pre-stressed state.

Computing the twisting moment, we find that the correction term $\widetilde{\boldsymbol{M}}^{\mathrm{rod}}$ in comparison to the linear case will appear only due to the non-vanishing $\boldsymbol{P}^{\bullet}$ because of the new term $\mathring{\boldsymbol{\tau}}^{\bullet}$. Hence, we use (83) and compute

$$\boldsymbol{P}^{\bullet} = \boldsymbol{\nu} \cdot \mathring{\boldsymbol{\tau}}^{\bullet} = -\kappa_{\xi z} \sigma(\xi) \boldsymbol{k} \times \boldsymbol{x} \tag{91}$$

and

$$\widetilde{\boldsymbol{M}}^{\mathrm{rod}} = \int_0^H \boldsymbol{x} \times \boldsymbol{P}^{\bullet} \, \mathrm{d}\xi = -\int_0^H \sigma(\xi) \boldsymbol{x} \times (\kappa_{\xi z} \boldsymbol{k} \times \boldsymbol{x}) \, \mathrm{d}\xi . \tag{92}$$

Transforming the double cross product and recalling the relation to the rate of twist of the shell $\kappa_{\xi z} = -\kappa_t$, we find

$$\widetilde{\boldsymbol{M}}^{\mathrm{rod}} = \kappa_t \boldsymbol{k} \int_0^H \sigma(\xi) \boldsymbol{x} \cdot \boldsymbol{x} \, \mathrm{d}\xi . \tag{93}$$

Comparing with (70), we ensure that the additional torsional stiffness $\tilde{a}_t$ is indeed determined by the expression (71). Continuing the analysis, we compute the increment of the total force in the cross-section:

$$\widetilde{\boldsymbol{Q}}^{\mathrm{rod}} = \int_0^H \boldsymbol{P}^{\cdot}\,\mathrm{d}\xi = -\int_0^H \sigma(\xi)\kappa_{\xi z}\boldsymbol{k}\times\boldsymbol{x}\,\mathrm{d}\xi = -\kappa_t\boldsymbol{M}^{\mathrm{rod}}. \tag{94}$$

Torsion induces a transverse force in a rod, loaded by a bending moment. This seeming contradiction is easy to explain. From the linearised constitutive equations of the rod theory (20) we see that the moment before the linearisation enters the right-hand side as $\boldsymbol{\theta}\times\boldsymbol{M}^{\mathrm{rod}}$. The vector of small rotation is $\boldsymbol{\theta}=\kappa_t z\boldsymbol{k}$, and this term cancels the computed additional force in the cross-section in the equilibrium equations (8):

$$\begin{aligned}\left(\boldsymbol{\theta}\times\boldsymbol{M}^{\mathrm{rod}}\right)' &= \kappa_t\boldsymbol{k}\times\boldsymbol{M}^{\mathrm{rod}},\\ \boldsymbol{r}'\times\widetilde{\boldsymbol{Q}}^{\mathrm{rod}} &= -\kappa_t\boldsymbol{k}\times\boldsymbol{M}^{\mathrm{rod}}.\end{aligned} \tag{95}$$

Two important factors contributed to the simplicity and compactness of the presented analysis. Firstly, the shell is assumed undeformed and being in a membrane stressed state prior to the linearisation. And secondly, the small deformation of the considered form does not change the metric of the surface.

5 Numerical Experiments and Validation

This section focuses on the application of the incremental beam theory to the example problem depicted in Fig. 5. The spatial Cartesian coordinate system with basis $[\boldsymbol{i},\ \boldsymbol{j},\ \boldsymbol{k}]$ has its origin in the centroid of a quadrant, that constitutes the beam axis with material arc coordinate s and radius ρ_1. The statically determined system is clamped at $s=0$ and loaded by a dead force $\boldsymbol{F}$ at the free end $s=L$. The axis connects the geometric centroids of the cross-sections, that consist of semi-circles with arc coordinate $\xi\in[0,\ H]$, radius ρ_2 and thickness h. The first material basis vector $\boldsymbol{e}_1$ points in out-of-plane and the second $\boldsymbol{e}_2$ in radial direction, whereas $\boldsymbol{e}_3$ coincides with the beam axis tangent vector $\boldsymbol{t}$. The specific geometric and material SI-parameters used in the upcoming computations are presented in Table 1.

We will first investigate the linear deformation behaviour of the clamped, curved beam when bent by $\boldsymbol{F}$ both in- and out-of-plane. In comparing the results to reference computations with shell finite elements, one may study the convergence behaviour of the beam theory when proceeding to parameter sets of even slenderer structures. As proved in [19], the applied beam theory is asymptotically correct for straight beams in the geometrically linear setting, as long as the thickness of the open profile remains one order smaller than its length, which itself is presumed to be one order smaller than the size of the beam axis. Using ρ_1, ρ_2 and h as characteristic parameters for

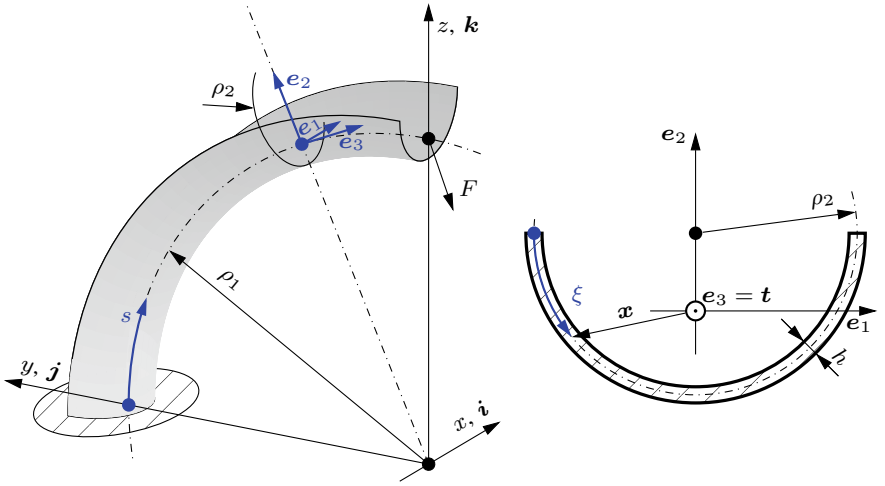

Fig. 5 Circularly curved beam in space with semi-circular cross-section; geometry, spatial system, material basis and parametrisation

Table 1 SI geometric and material parameters of the example problem

ρ_1	ρ_2	L	H	h	E	ν
$\frac{2}{\pi}$	0.02	1	$0.02\,\pi$	0.001	$2.1 \cdot 10^{11}$	0.3

the circular rod, this relation can be expressed with a formal, asymptotically small parameter λ

$$h = \lambda\, \rho_2 = \lambda^2\, \rho_1\,. \tag{96}$$

One may alternatively use L or H instead of ρ_1 or ρ_2 respectively, but the differences vanish when λ tends to zero. Variation of the geometric parameters according to the above rule allows for an empirical check, whether the curved beam conforms to the expected asymptotic behaviour for $\lambda \to 0$. Another interesting aspect is the possible distortion of the shell cross-section in different load cases, which may not be describable by the beam's limited kinematic resources.

Advancing to the incremental theory of second order by simplification of the general incremental equations presented in Sect. 2.2, we aim to calculate the critical forces for torsional-flexural buckling of the beam when loaded by an in-plane either compressive or transverse force $\boldsymbol{F}$. The solutions are again compared to shell finite element computations performed with the in-house software *shellFE* [18, 19] as well as the commercial program *Abaqus*. We conclude the numerical experiments with the post-buckling analysis in the framework of the shell theory, utilizing a geometrically imperfect structure and the finite element code *shellFE*.

For all calculations ahead, we need to provide the section properties according to (17) and (18), starting with the geometric properties of the semi-circular cross-section

$$A = h\,H\,,\quad \mathbf{J} = \left(\frac{\pi}{2}\,h\,\rho_2^3\right)\boldsymbol{e}_1\boldsymbol{e}_1 + \left(\frac{\pi^2-8}{2\,\pi}\,h\,\rho_2^3\right)\boldsymbol{e}_2\boldsymbol{e}_2\,,\quad C = \frac{H\,h^3}{3}$$
$$\boldsymbol{\gamma} = \left(\frac{2\,(\pi^2-8)}{\pi^2}\,h\,\rho_2^4\right)\boldsymbol{e}_2\,,\quad J_0 = \frac{\pi^4-72}{12\,\pi}\,h\,\rho_2^5\,,\quad \boldsymbol{\beta} = -\left(h\,\rho_2^4\right)\boldsymbol{e}_1\,, \tag{97}$$

and the stiffness coefficients read

$$\mathbf{a} = (E\,J_{22})\;\boldsymbol{e}_1\boldsymbol{e}_1 + (E\,J_{11})\;\boldsymbol{e}_2\boldsymbol{e}_2 + \mu\,C\,\boldsymbol{t}\boldsymbol{t}\,,\quad \boldsymbol{\zeta} = (E\,\gamma)\;\boldsymbol{e}_1\,. \tag{98}$$

5.1 Linear Deformation Analysis

The governing equations needed to form the system of differential equations for the linear bending or torsional-bending problem are: the equations of equilibrium (8), the kinematic relation (13) and the constitutive formulas (20). Proceeding to the classic linear formulas we merely neglect all contributions from the pre-stressed state. In contrast to the more general formulation discussed before, we further assume the beam to be inextensible. As a consequence $\boldsymbol{r}' = \boldsymbol{t}$ and the constitutive law for Q_t is replaced by the kinematic condition (13) for $\varepsilon = 0$, which leads to the following system

$$\boldsymbol{Q}' + \boldsymbol{q} = 0\,,\quad \boldsymbol{M}' + \boldsymbol{t}\times\boldsymbol{Q} + \boldsymbol{m} = 0\,, \tag{99a}$$
$$\boldsymbol{M} + \left(B' + b\right)\boldsymbol{t} = \mathbf{a}\cdot\boldsymbol{\theta}' - E\,\boldsymbol{t}\times\boldsymbol{\beta}\,\left(\boldsymbol{\theta}'\cdot\boldsymbol{t}\right)'\,,$$
$$B = E\,J_0\,\left(\boldsymbol{\theta}'\cdot\boldsymbol{t}\right)' - E\,(\boldsymbol{t}\times\boldsymbol{\beta})\cdot\boldsymbol{\theta}'\,, \tag{99b}$$
$$\boldsymbol{u}' - \boldsymbol{\theta}\times\boldsymbol{t} = 0\,, \tag{99c}$$

wherein the incremental dot has been dropped, as there is no more distinction of states necessary. The modified kinematic relation (99c) now includes the condition of no transverse shear as well as the inextensibility constraint. It enables direct integration for the field of displacements $\boldsymbol{u}$ once the solution for the small rotations $\boldsymbol{\theta}$ is available. The remainder of the constitutive law simplifies greatly due to cancellation of all non-linear terms. The effective torsional stiffness stays the traditional one as a consequence.

In the present case there are no distributed forces $\boldsymbol{q}$, $\boldsymbol{m}$ or b, which makes solving the equilibrium equations a trivial task

$$\boldsymbol{Q} = \boldsymbol{F}\qquad \boldsymbol{M} = -\,(\boldsymbol{r} - \rho_1\,\boldsymbol{k})\times\boldsymbol{F}\,, \tag{100}$$

owing to the boundary conditions at the free end $\boldsymbol{Q}\,(s=L)=\boldsymbol{F}$ and $\boldsymbol{M}\,(s=L)=0$. Now, the construction of ODEs in θ_i limits itself to substitution of $\boldsymbol{Q}$, $\boldsymbol{M}$ and B', readily available from (99b), in the first constitutive relation, followed by projection onto each of the three basis vectors $\boldsymbol{e}_k$. For the sake of brevity, we will not cover this process in any more detail, and rather just present the system of differential equations

$$\boldsymbol{e}_1: \qquad a_{11}\theta_1' = M_1\,, \tag{101a}$$

$$\boldsymbol{e}_2: \qquad \boldsymbol{e}_2\cdot\mathbf{a}\cdot\boldsymbol{\theta}' - E\,\beta\,\left(\boldsymbol{\theta}'\cdot\boldsymbol{t}\right)' = M_2\,, \tag{101b}$$

$$\boldsymbol{t}: \qquad -E\,J_0\,\left(\boldsymbol{\theta}'\cdot\boldsymbol{t}\right)'' + E\,\left(\boldsymbol{t}\times\boldsymbol{\beta}\cdot\boldsymbol{\theta}'\right)' + \boldsymbol{t}\cdot\mathbf{a}\cdot\boldsymbol{\theta}' = M_3\,, \tag{101c}$$

accompanied by the boundary conditions

$$\boldsymbol{\theta}\,(s=0)=0\,,\ \theta_t'\,(s=0)=0\,,\ B\,(s=L)=0\,. \tag{102}$$

One might recognize, that the system (101) has each one instance of first, second and third order, but (102) provides only five conditions. This issue can be resolved by transforming (101c) to second order via substitution of $\left(\boldsymbol{\theta}'\cdot\boldsymbol{t}\right)'$ with (101b). It is worth noting, that the first equation decouples from the others and resembles the classic Bernoulli plane bending differential equation.

We consider two load cases: in-plane bending with a radial transverse force $\boldsymbol{F}=F\,\boldsymbol{k}$ and out-of-plane bending with $\boldsymbol{F}=F\,\boldsymbol{i}$. While the first is free of any out-of-plane deformations $\theta_2=\theta_t=0$, the latter induces a combined torsional-bending deformation without in-plane rotations $\theta_1=0$. Though (101a) can be easily integrated in closed form, the two coupled equations are more conveniently solved by numerical integration. Turning to the results, we first take a brief look at the solutions for $\boldsymbol{u}\,(s)$ and $\boldsymbol{\theta}\,(s)$ in Fig. 6 for both load cases. We applied a unit force $F=1$ and plotted non-trivial components only. As the ordinate scale factors indicate, the beam

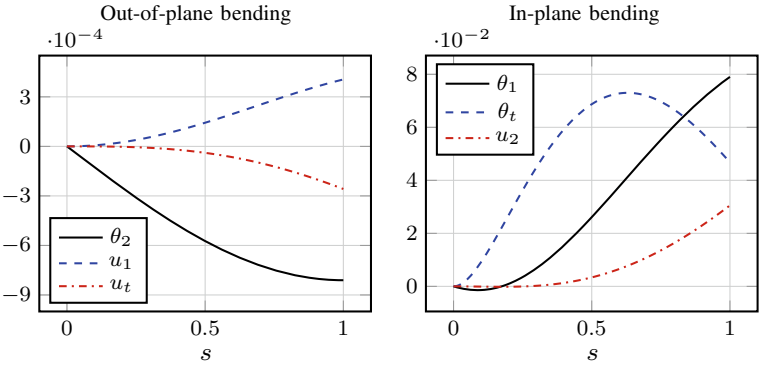

Fig. 6 Linear deformation analysis; distribution of non-trivial components of $\boldsymbol{\theta}$ and $\boldsymbol{u}$ for out-of-plane bending (left), in-plane bending (right)

shows a much softer behaviour when bent out-of-plane than in-plane owing to the low torsional stiffness, which is proportional to h^3 according to (97). Evidently, the considered example is well suited for a buckling analysis, as one can expect pure in-plane deformation paths to become unstable at some critical point. The reason why the displacement vector $\boldsymbol{u}$ has to start with a zero tangent at $s = 0$ is a direct consequence of the clamping boundary conditions (102) in conjunction with the kinematic relation (99c).

In order to compare the results to shell finite element calculations with the program *shellFE*, we first study the cross-section distortion at $s = L/2$ for both load cases in

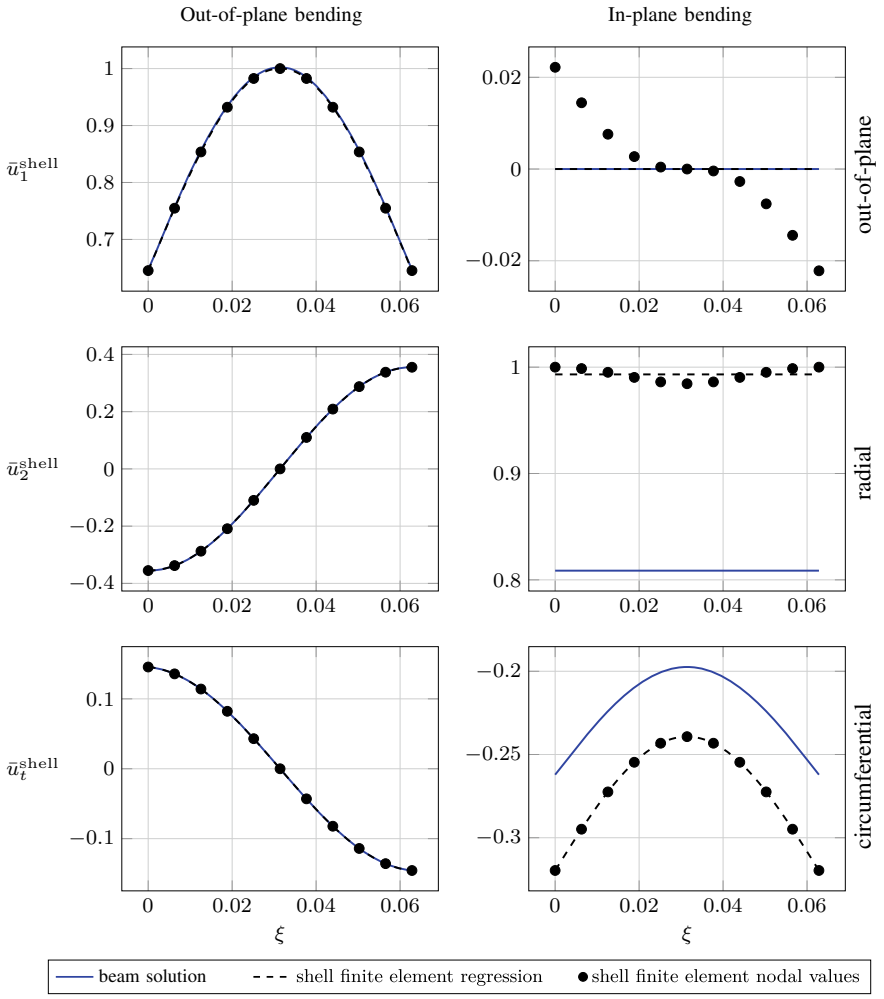

Fig. 7 Comparison of cross-section deformation in beam and shell model for out-of-plane (left) and in-plane bending (right)

Fig. 7. Evaluation at the midpoint of the beam axis helps avoiding possible boundary distractions. We plot the out-of-plane, radial, and circumferential displacements from top to bottom over the arc coordinate in the cross-section ξ, i.e. their distribution in the section as predicted by beam theory and shell finite elements. The shell nodal displacements are marked with thick black dots, whereas the dashed line depicts a regression of these nodal values by means of beam kinematics. That is to say, the regression function used is (3), which has the same seven degrees of freedom to display the cross-section deformation as a single material point of the beam. Lastly, the shell displacements corresponding to the integration of the beam boundary value problem are also reconstructed using (3) and drawn with a blue line. The ordinates of each plot are related to the maximal nodal displacement component occurring for the considered load case according to

$$\bar{u}_i^{\text{shell}} = \frac{u_i^{\text{shell}}}{\max\left\{u_1^{\text{shell}},\ u_2^{\text{shell}},\ u_t^{\text{shell}}\right\}}\,, \tag{103}$$

which allows to distinguish between dominant and less significant components of the shell displacement field $\boldsymbol{u}^{\text{shell}}$.

Analysing the plots, one immediately recognizes that the overall agreement for out-of-plane bending is far better, i.e. the solutions of beam and shell theory are practically congruent. Together radial and normal displacement shift and rotate the cross-section as a rigid body and the axial component accounts for the warping deformation due to torsion. In contrast, the beam in-plane bending solution still delivers only unsatisfactory accuracy. The radial displacements are underestimated in the beam model, although they are reasonably well approximated by the regression of the shell's nodal values. Moreover, the out-of-plane displacements, which correspond to a distortion of the cross-section, cannot be accounted for in the framework of beam theory. This effect, which can be interpreted as the shell struggling to preserve its in-plane metric to avoid membrane strains—see [19] or the paragraph below (90) for a brief discussion on the concept of "pure bending" in shell theory—still has a major influence on the overall deformation and thus limits the reachable accuracy of the beam model.

For the upcoming discussion on the asymptotic behaviour it is however noteworthy, that the effect of cross-sectional contraction or expansion becomes less pronounced for only slightly curved beams and practically irrelevant for straight ones. Therefore, we accompany the following numerical asymptotic analysis with a parameter study, where the standard parameters of Table 1 are preserved, except for ρ_1, which is increased to gradually straighten up the beam and decrease its curvature. In order to preserve the pure in-plane transverse force loading, the direction of $\boldsymbol{F}$ needs to be altered simultaneously. For the asymptotic study we consider an out-of-plane transverse loading $\boldsymbol{F} = F\,\boldsymbol{i}$ and vary the geometric parameters according to (96). The reached accuracy is judged with the relative rotation angle differences ϵ_k defined as

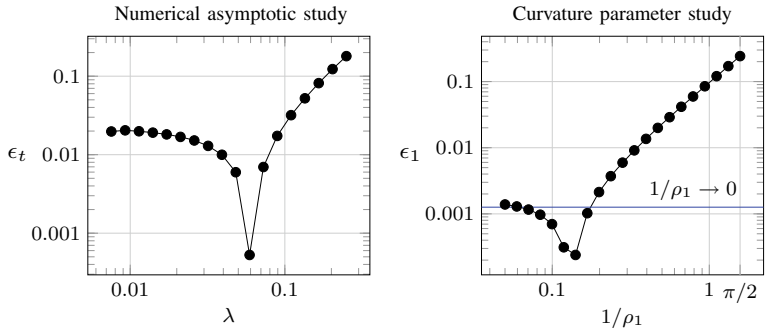

Fig. 8 Numerical asymptotic analysis according to (96) for out-of-plane bending (left) and parameter study for in-plane bending while gradually straightening the beam (right)

$$\epsilon_k = \left| \frac{\theta_k^{\text{shell}}}{\theta_k}\bigg|_{s=L/2} - 1 \right| , \tag{104}$$

where θ_k^{shell} denotes the effective rotation angle of the shell finite element results due to the nodal value regression fit. The results of both studies are presented in Fig. 8. As there is no monotonous convergence for $\lambda \to 0$ in the first picture, we immediately conclude, that the applied theory is not asymptotically correct for curved beams. Therefore, in order to develop a consistent asymptotic theory one would have to include the curvature radius into the set of characteristic parameters. The parameter study in the second picture justifies the statement, that the effect of cross-section distortion diminishes when decreasing the beam's curvature. The graph is however not monotonous and reaches a minimum at a low curvature. From there on the error increases slightly and reaches a distinct value for the straight beam with $1/\rho_1 \to 0$, indicated by a horizontal line in the picture.

5.2 *Stability Analysis: Critical Forces and Post-buckling Behaviour*

In the previous section the beam solution to the in-plane bending problem turned out to be not quite accurate in comparison to reference computations with shell finite elements. At a first glance, this finding does not sound very promising when proceeding to the buckling analysis. Nevertheless, buckling might happen at very small deformations and possible inconsistencies in the approximation of deformations do not necessarily affect the accuracy of the pre-stresses. The latter, namely the moment $\boldsymbol{M}$ and force $\boldsymbol{Q}$, can be taken directly from (100) and are sufficient to describe the influence of the pre-stressed state in the governing equations of the incremental theory of second order. Seeking stability loss for torsional-flexural buckling, we consider a

subcritical state, that is loaded by an in-plane force $\boldsymbol{F}$. The corresponding field of pre-strains is twist free and its out-of-plane components vanish. Hence, $\kappa_2 = \kappa_t = 0$ and the constitutive relations for the pre-stressed state reduce to

$$\boldsymbol{M} = \mathbf{a} \cdot \boldsymbol{\kappa} \qquad Q_t = E\,A\,\varepsilon \qquad B = 0\,. \tag{105}$$

Inversion of the above formulas enables an alternative formulation of the torsional stiffness correction term $\tilde{a}_t$ in (16)

$$\tilde{a}_t = \left(\mathbf{J}^{-1} \cdot (\boldsymbol{t} \times \boldsymbol{M})\right) \cdot \boldsymbol{\gamma} + \frac{Q_t}{A}\,\operatorname{tr}\mathbf{J}\,, \tag{106}$$

which is closely related to (70) and effectively replaces the pre-strains by the pre-stresses in the incremental equations. This allows us to ignore all remaining pre-deformations (both displacements and strains) when proceeding to the incremental equations of second order theory. While this neglect neither changes the equilibrium equations (8) nor the kinematic formula (13) at all, the incremental constitutive relations (20) simplify significantly. We further assume inextensibility $\varepsilon = \varepsilon^\bullet = 0$ which implies $\boldsymbol{r}' = \boldsymbol{t}$ and repeat the whole system of equations for convenience

$$\boldsymbol{Q}^{\bullet\prime} + \boldsymbol{q}^\bullet = 0\,, \qquad \boldsymbol{M}^{\bullet\prime} + \boldsymbol{u}' \times \boldsymbol{Q} + \boldsymbol{t} \times \boldsymbol{Q}^\bullet + \boldsymbol{m}^\bullet = 0 \tag{107a}$$

$$\boldsymbol{M}^\bullet + \left(B^{\bullet\prime} + b^\bullet\right)\boldsymbol{t} = \boldsymbol{\theta} \times \boldsymbol{M} + \mathbf{a} \cdot \boldsymbol{\theta}' - E\,\boldsymbol{t} \times \boldsymbol{\beta}\,\kappa_t^{\bullet\prime} + \tilde{a}_t\,\boldsymbol{t}\,\kappa_t^\bullet$$

$$B^\bullet = E\,J_0\,\kappa_t^{\bullet\prime} - E\,\boldsymbol{t} \times \boldsymbol{\beta} \cdot \boldsymbol{\theta}' \tag{107b}$$

$$\boldsymbol{u}' - \boldsymbol{\theta} \times \boldsymbol{t} = 0\,. \tag{107c}$$

Having related strains to force resultants in (105) in order to construct the strain-free formulation of $\tilde{a}_t$ (106) and now assuming all strain contributions in the above incremental system to be negligible might seem implausible. However, in the course of derivation of $\tilde{a}_t$ in Sect. 4.2 the formulation (106) based on force resultants (actually its equivalent (70)) precedes the strain-related formulation, which itself relies on the assumption of small strains as a result of force resultants of a pre-stressed, yet undeformed state. The necessity to formulate $\tilde{a}_t$ as a function of strains originates from the need to write the strain energy density (16) as a function of independent strain measures.

The stepwise derivation of the system of ODEs follows a slightly different path this time, starting again with the first equation of equilibrium: There were no distributed forces applied before nor are there any increments in these quantities now, thus $\boldsymbol{q}^\bullet = 0$, $\boldsymbol{m}^\bullet = 0$ and $b^\bullet = 0$. Hence, the increment $\boldsymbol{Q}^\bullet$ once more is constant, but as the external concentrated force $\boldsymbol{F}$ is considered a dead force, it follows that $\boldsymbol{Q}^\bullet = \boldsymbol{F}^\bullet = 0$. Again seeking for a system in θ_k we further substitute the kinematic relation (107c) and the constitutive relations (107b) in the second equilibrium equation, each in its proper form, i.e. the required order of derivative in s. Insertion of $\boldsymbol{M}$ and $\boldsymbol{Q}$ from (100) followed by projection onto the material basis vectors $\boldsymbol{e}_k$ concludes the derivation. The differential equation for the in-plane increment θ_1 once

again decouples and has only the trivial solution. As the remaining two equations are rather complicated, they need to be integrated numerically and we forgo writing them down. The boundary conditions for the incremental state read

$$\boldsymbol{\theta}\,(s=0)=0\,,\ \theta_t\,(s=0)=0\,,\ B^{\bullet}\,(s=L)=0\,,\ \boldsymbol{M}^{\bullet}\,(s=L)=0\,, \tag{108}$$

where the last one needs to be included, as we could not solve for the moment $\boldsymbol{M}^{\bullet}$ independently of the incremental deformations in contrast to the linear analysis. Consequently, the differential equations receive a higher order than before. In conjunction with the above boundary conditions the two remaining homogeneous ODEs for the out-of-plane deformations θ_2 and θ_t represent a linear eigenvalue problem with variable coefficients for the critical force value F. As the problem can hardly be solved in a closed form, a suitable numerical method has to be applied; in particular a shooting method for linear systems was used.

We performed the stability analysis for two load cases: loading with a pure transverse force in outward pointing radial direction $\boldsymbol{F}=F\,\boldsymbol{k}$ as well as application of a compressive force $\boldsymbol{F}=F\,\boldsymbol{j}$. The critical values derived with incremental beam theory are compared to shell finite element calculations within the incremental (*Abaqus*) as well as the non-linear shell theory (*shellFE* and *Abaqus*). As illustrated in Fig. 1 the open section beam elements in *Abaqus* do not incorporate the torsional stiffness correction $\tilde{a}_t$ to full extent, which renders them unusable for the present buckling analysis. The results are collected in Table 2 in conjunction with two error measures that quantify both the error between the different structural theories as well as the importance of pre-deformations in the considered load case. Both F_{Beam} and F^{incr}_{Abqs} correspond to computations in the framework of the second order beam and shell theory respectively. Consequently, all subcritical pre-deformations are excluded from these analyses, whereas $F_{shellFE}$ and F^{nl}_{Abqs} are obtained using geometrically non-linear shell finite elements. Therefore, comparison of the two distinct buckling forces obtained with *Abaqus* indicates the importance of pre-deformations for the load case at hand. Evidently, it is negligible for a compressive force loading and has a minor impact on the buckling load when a transverse force is applied. The incremental beam theory yields accurate predictions for the critical forces and the slightly larger discrepancy for the second load case is clearly related to the neglect of pre-deformations.

It remains to study the post-buckling behaviour of the imperfect member, whose undeformed reference configuration is bent out-of-plane just slightly. We plot the out-of-plane deformation paths of the free endpoint computed with *shellFE* in Fig. 9 for compressive force loading and in Fig. 10 for transverse force loading. Each curve corresponds to a different imperfection amplitude and the previously obtained critical force values are marked with vertical grid-lines. The plots are accompanied with 3D-scenes of the member in different stages of the analysis. A stable pitchfork bifurcation can be observed for both load cases, the out-of-plane deformations grow rapidly in the immediate neighbourhood of the bifurcation point. For force values far above the critical point the member gets further twisted and straightened, which may even

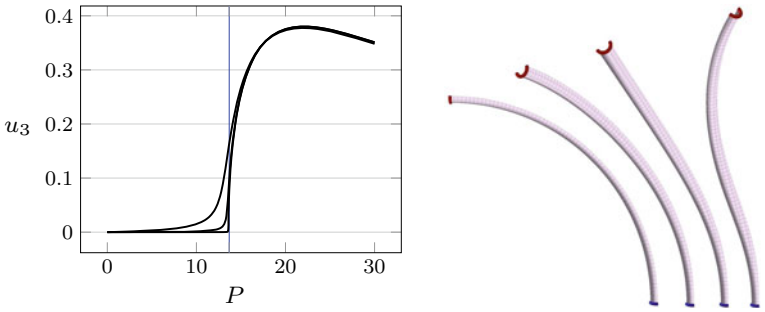

Fig. 9 Out-of-plane deformation paths of the circular rod with different imperfection amplitudes for post-buckling under a *compressive force* loading and illustration of the buckling progress

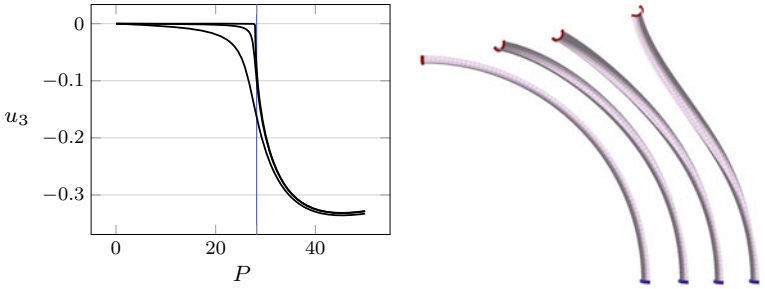

Fig. 10 Out-of-plane deformation paths of the circular rod with different imperfection amplitudes for post-buckling under a *transverse force* loading and illustration of the buckling progress

Table 2 Comparing torsional-flexural buckling loads computed with incremental beam theory to reference computations with shell finite elements performed with *shellFE* and *Abaqus*

	Buckling loads				Error measures	
Load case	F_{Beam}	F^{incr}_{Abqs}	$F_{shellFE}$	F^{nl}_{Abqs}	$\frac{F_{\text{Beam}}}{F^{\text{nl}}_{\text{Abqs}}} - 1$	$\frac{F^{\text{incr}}_{\text{Abqs}}}{F^{\text{nl}}_{\text{Abqs}}} - 1$
Compressive	13.58	13.46	13.59	13.46	0.009	0.000
Transverse	27.10	26.88	27.93	27.72	−0.022	−0.030

result in a decrease of the presented out-of-plane displacements, whereas the vertical component keeps growing.

6 Conclusions

We successfully applied the incremental shell theory to identify specific geometric non-linearities in the theory of curved rods with thin-walled open cross-sections. It turns out, that the effective torsional stiffness in a cross-section depends on its axial

stresses, determined by the normal force Q_t and the bending moments $\boldsymbol{M}_\perp$. Consequently, one has to introduce cubic terms in the strain energy function of beam theory to account for this effect properly. In contrast to alternative strategies that emanate from three-dimensional elasticity theory, the derivation based on incremental shell equations is compact owing to the simplifications already incorporated in the shell theory and, more importantly, free of any further assumptions. This substantiates the developed non-linear, augmented beam theory, that rests upon an asymptotically justified, geometrically linear theory for straight rods of open profile. However, simple numerical experiments show, that curved rods do not share the same asymptotic behaviour, which leaves the development of an asymptotically justified theory for arbitrarily curved rods of open profile for future research.

We further studied the torsional-flexural buckling and the post-buckling behaviour of a circularly curved rod with semi-circular cross-sections. The critical loads obtained with incremental beam theory of second order correspond well to reference computations with different shell finite element methods. This verifies the ability of the beam theory to accurately predict the non-linear structural response of the member. It further demonstrates the appropriate use of the simple second order theory for structural stability analyses, which is limited to cases with negligible subcritical pre-deformations.

References

1. Bonet, J., Wood, R.: Nonlinear Continuum Mechanics for Finite Element Analysis, 2nd edn. Cambridge (2008)
2. Ciarlet, P.: An introduction to differential geometry with applications to elasticity. J. Elast. **1–3**, (78/79), 1–215 (2005)
3. Eliseev, V.: Mechanics of Deformable Solid Bodies. St. Petersburg State Polytechnical University Publishing House, St. Petersburg (2006) (in Russian)
4. Eliseev, V., Vetyukov, Y.: Finite deformation of thin shells in the context of analytical mechanics of material surfaces. Acta Mech. **209**(1–2), 43–57 (2010)
5. Eliseev, V., Vetyukov, Y.: Theory of shells as a product of analytical technologies in elastic body mechanics. In: Pietraszkiewicz, W., Górski, J. (eds.) Shell Structures: Theory and Applications, vol. 3, pp. 81–84. CRC Press/Balkema, Taylor & Francis Group, London (2014)
6. Opoka, S., Pietraszkiewicz, W.: On modified displacement version of the non-linear theory of thin shells. Int. J. Solids Struct. **46**(17), 3103–3110 (2009)
7. Parkus, H.: Mechanik der festen Körper, 2 edn. Springer, Wien, New York (2005)
8. Pi, Y.-L., Bradford, M., Uy, B.: Nonlinear analysis of members curved in space with warping and Wagner effects. Int. J. Solids Struct. **42**, 3147–3169 (2005)
9. Pietraszkiewicz, W.: Lagrangian description and incremental formulation in the non-linear theory of thin shells. Int. J. Nonlinear Mech. **19**, 115–140 (1984)
10. Pietraszkiewicz, W.: Geometrically nonlinear theories of thin elastic shells. Adv. Mech. **12**(1), 51–130 (1989)
11. Reismann, H.: Elastic Plates: Theory and Application. Wiley (1988)
12. Simitses, G.J., Hodges, D.H.: Fundamentals of Structural Stability. Elsevier, New York (2006)
13. Timoshenko, S.: Theory of bending, torsion and buckling of thin-walled members of open cross-section. J. Frankl. Inst. **239**(3,4,5), 201–219, 249–268, 343–361 (1945)
14. Timoshenko, S., Gere, J.: Theory of Elastic Stability, 2nd edn. McGraw-Hill, New-York (1961) (ch. 5)

15. Timoshenko, S., Woinowsky-Krieger, S.: Theory of Plates and Shells, 2nd edn. McGraw-Hill (1959)
16. Vetyukov, Y.: Direct approach to elastic deformations and stability of thin-walled rods of open profile. Acta Mech. **200**(3–4), 167–176 (2008)
17. Vetyukov, Y.: The theory of thin-walled rods of open profile as a result of asymptotic splitting in the problem of deformation of a noncircular cylindrical shell. J. Elast. **98**(2), 141–158 (2010)
18. Vetyukov, Y.: Finite element modeling of Kirchhoff-Love shells as smooth material surfaces. ZAMM **94**(1–2), 150–163 (2014)
19. Vetyukov, Y.: Nonlinear Mechanics of Thin-Walled Structures. Direct Approach and Numerical Analysis. Foundations of Engineering Mechanics. Springer, Vienna, Asymptotics (2014)
20. Vetyukov, Y., Eliseev, V.: Elastic deformations and stability of equilibrium of thin-walled rods of open profile (in Russian). Scientific and Technical Bulletin of St. Petersburg State Polytechnical University 1, pp. 49–53 (2007)
21. Vlasov, V.: Thin-Walled Elastic Beams, 2nd edn. Israel Program for Scientific Translations, Jerusalem (1961)
22. Wagner, H.: Verdrehung und Knickung von offenen Profilen (Torsion and buckling of open sections). NACA Technical Memorandum No. 807, Washington, DC (1936)
23. Ziegler, F.: Mechanics of Solids and Fluids, 2nd edn. Mechanical Engineering Series. Springer, Vienna, New-York (1995)
24. Ziegler, H.: Principles of Structural Stability, 2nd edn. Birkhäuser (1977)

Buckling of Elastic Circular Plate with Surface Stresses

Denis N. Sheydakov

Abstract In the framework of general stability theory for three-dimensional bodies, the buckling analysis has been carried out for a circular plate subjected to the radial compression. It was assumed that the surface stresses are acting on its faces and the behavior of the plate is described by the Gurtin–Murdoch model. For an arbitrary isotropic material, the system of linearized equilibrium equations is derived, which describes the behavior of a plate in a perturbed state. In the case of axisymmetric perturbations, the stability analysis is reduced to solving a linear homogeneous boundary-value problem for a system of three ordinary differential equations. It is shown that for a plate with identical faces, it is sufficient to consider only half of the plate to study its stability. For two specific models of bulk material (Harmonic model and Blatz–Ko model), the buckling analysis has been carried out for a circular plate made of aluminum. It was found, in particular, that the stability of the plate increases with a decrease in its overall size. This effect is due to the influence of surface stresses and is quite significant at the micro- and nanoscale.

1 Introduction

The problem of equilibrium stability for deformable bodies is of major importance because the exhaustion of bearing capacity and the collapse of engineering structures quite often occurs due to the buckling under external loads. Due to the development of modern technologies and the appearance of new materials, the problem of stability analysis while taking into account the various surface phenomena becomes relevant [11]. For example, the deformation pattern of bodies at micro- and nanoscale is often significantly different from the behavior of macro-sized bodies, which can be explained by surface effects [1]. To model surface phenomena, especially in nanomechanics [4, 17], the theory of elasticity with surface stresses has received development. In this theory, in addition to the ordinary stresses distributed in the

D. N. Sheydakov (✉)
South Scientific Center of Russian Academy of Sciences, Chekhova Ave. 41,
344006 Rostov-on-Don, Russia
e-mail: sheidakov@mail.ru

H. Altenbach et al. (eds.), *Recent Developments in the Theory of Shells*,
Advanced Structured Materials 110, https://doi.org/10.1007/978-3-030-17747-8_29

volume, the independent surface stresses are also taken into account at the boundary of the body or its part. These stresses generalize the well-known in hydromechanics scalar surface tension to the case of solids. The introduction of surface stresses allows, in particular, describing the size effect typical for nanomaterials [3, 9, 16].

The present research is dedicated to the buckling analysis of nonlinearly elastic plates with surface stresses. To take into account the influence of the latter, the Gurtin–Murdoch model [6] is used, which from the mechanical point of view is equivalent to a deformable body with a glued elastic membrane. Accounting for surface stresses allows studying the buckling features of micro- and nanosized plates.

2 Governing Equations

In the framework of Gurtin–Murdoch model, the set of static equations for a nonlinearly elastic body with surface stresses in the absence of body forces consists of [14] the equilibrium equations

$$\overset{\circ}{\nabla} \cdot \mathbf{D} = \mathbf{0} \tag{1}$$

the equilibrium conditions on the part of the body surface Ω_s, where the surface stresses are acting

$$\left(\mathbf{n} \cdot \mathbf{D} - \overset{\circ}{\nabla}_s \cdot \mathbf{D}_s \right) \Big|_{\Omega_s} = \mathbf{t} \tag{2}$$

the constitutive equations

$$\mathbf{D} = \mathbf{P} \cdot \mathbf{C}, \qquad \mathbf{P} = 2\frac{\partial W(\mathbf{G})}{\partial \mathbf{G}}, \qquad \mathbf{D}_s = \mathbf{P}_s \cdot \mathbf{C}_s, \qquad \mathbf{P}_s = 2\frac{\partial W_s(\mathbf{G}_s)}{\partial \mathbf{G}_s} \tag{3}$$

and the geometric relations

$$\mathbf{G} = \mathbf{C} \cdot \mathbf{C}^{\mathrm{T}}, \qquad \mathbf{C} = \overset{\circ}{\nabla} \mathbf{R}, \qquad \mathbf{G}_s = \mathbf{C}_s \cdot \mathbf{C}_s^{\mathrm{T}}, \qquad \mathbf{C}_s = \overset{\circ}{\nabla}_s \mathbf{R} \Big|_{\Omega_s} \tag{4}$$

Here $\mathbf{D}$ and $\mathbf{P}$ are the Piola and Kirchhoff stress tensors, respectively; $\overset{\circ}{\nabla}$ is the three-dimensional nabla-operator in Lagrangian coordinates; $\overset{\circ}{\nabla}_s$ is the surface nabla-operator; $\mathbf{D}_s$ and $\mathbf{P}_s$ are the surface stress tensors of the Piola and Kirchhoff type; $\mathbf{n}$ is the unit vector normal to the surface of the undeformed body; $\mathbf{t}$ is the surface loads vector; W and W_s are the bulk and surface strain energy densities, respectively; $\mathbf{G}$ and $\mathbf{G}_s$ are the Cauchy–Green strain tensors in the volume and on the surface of the body; $\mathbf{C}$ and $\mathbf{C}_s$ are the deformation gradients; and $\mathbf{R}$ is the position vector in the actual configuration.

Taking (3) into account, the following relations are valid for the Kirchhoff stress tensor $\mathbf{P}$ in the case of an isotropic body [8, 10]:

$$\mathbf{P} = \sum_{k=1}^{3} \chi_k \mathbf{d}_k \otimes \mathbf{d}_k, \qquad \chi_k = 2\frac{\partial W(G_1, G_2, G_3)}{\partial G_k}, \qquad \mathbf{G} = \sum_{k=1}^{3} G_k \mathbf{d}_k \otimes \mathbf{d}_k \tag{5}$$

where G_k, $\mathbf{d}_k (k = 1, 2, 3)$ are the eigenvalues and eigenvectors of the Cauchy–Green strain tensor $\mathbf{G}$. At the same time, the expression for the surface stress tensor of Kirchhoff type $\mathbf{P}_s$ takes the form [1]:

$$\mathbf{P}_s = \kappa_1 \mathbf{I}_s + 2\kappa_2 \mathbf{G}_s, \qquad \kappa_\theta = 2\frac{\partial W_s(j_1, j_2)}{\partial j_\theta}, \qquad j_\theta = \mathrm{tr}\mathbf{G}_s^\theta, \qquad \theta = 1, 2 \tag{6}$$

Here j_1, j_2 are the invariants of the surface Cauchy–Green strain tensor $\mathbf{G}_s$; $\mathbf{I}$ and $\mathbf{I}_s = \mathbf{I} - \mathbf{n} \otimes \mathbf{n}$ are the three-dimensional and surface unit tensors, respectively.

3 Circular Plate with Surface Stresses

Consider a homogeneous circular plate of radius r_0 and thickness $2h$. We assume that the surface stresses are acting on its top Ω_+ $(z = h)$ and bottom Ω_- $(z = -h)$ faces, i.e. $\Omega_s = \Omega_+ \cup \Omega_-$. In the case of radial compression of the plate, the position vector $\mathbf{R}$ is given by the following relations [13, 18]:

$$\begin{aligned} &\mathbf{R} = \alpha r \mathbf{e}_R + \gamma z \mathbf{e}_Z \\ &R = \alpha r, \qquad \Phi = \varphi, \qquad Z = \gamma z \\ &0 \le r \le r_0, \qquad 0 \le \varphi \le 2\pi, \qquad |z| \le h \end{aligned} \tag{7}$$

where r, φ, z are the cylindrical coordinates in the reference state (Lagrangian coordinates); R, Φ, Z are the Eulerian cylindrical coordinates; $\{\mathbf{e}_r, \mathbf{e}_\varphi, \mathbf{e}_z\}$ and $\{\mathbf{e}_R, \mathbf{e}_\Phi, \mathbf{e}_Z\}$ are the orthonormal vector bases of Lagrangian and Eulerian coordinates, respectively; α is the given ratio of radial compression; and γ is the unknown constant that characterizes the deformation in the thickness direction of the plate.

According to the expressions (4), (7), the deformation gradients in the volume and on the surface are:

$$\mathbf{C} = \alpha(\mathbf{e}_r \otimes \mathbf{e}_R + \mathbf{e}_\varphi \otimes \mathbf{e}_\Phi) + \gamma \mathbf{e}_z \otimes \mathbf{e}_Z, \qquad \mathbf{C}_\pm = \alpha(\mathbf{e}_r \otimes \mathbf{e}_R + \mathbf{e}_\varphi \otimes \mathbf{e}_\Phi) \tag{8}$$

Hereinafter indexes "+" and "–" denote surface quantities related to the top and bottom faces of the circular plate, respectively.

From the relations (4), (8) we obtain the expressions for the corresponding Cauchy–Green strain tensors

$$\mathbf{G} = \alpha^2(\mathbf{e}_r \otimes \mathbf{e}_r + \mathbf{e}_\varphi \otimes \mathbf{e}_\varphi) + \gamma^2 \mathbf{e}_z \otimes \mathbf{e}_z, \qquad \mathbf{G}_\pm = \alpha^2(\mathbf{e}_r \otimes \mathbf{e}_r + \mathbf{e}_\varphi \otimes \mathbf{e}_\varphi) \tag{9}$$

It is obvious that for the considered initial strain state the eigenvectors $\mathbf{d}_k$ $(k = 1, 2, 3)$ of the Cauchy–Green strain tensor coincide with the vector basis of Lagrangian cylindrical coordinates, i.e. $\mathbf{d}_1 = \mathbf{e}_r$, $\mathbf{d}_2 = \mathbf{e}_\varphi$, $\mathbf{d}_3 = \mathbf{e}_z$, and the eigenvalues G_k are: $G_1 = G_2 = \alpha^2$, $G_3 = \gamma^2$. Thus, taking (5), (6) into account, the following relations are valid for the Kirchhoff stress tensors:

$$\begin{aligned} \mathbf{P} &= \chi_1 \mathbf{e}_r \otimes \mathbf{e}_r + \chi_2 \mathbf{e}_\varphi \otimes \mathbf{e}_\varphi + \chi_3 \mathbf{e}_z \otimes \mathbf{e}_z \\ \mathbf{P}_\pm &= \left(\kappa_1^\pm + 2\alpha^2 \kappa_2^\pm\right)(\mathbf{e}_r \otimes \mathbf{e}_r + \mathbf{e}_\varphi \otimes \mathbf{e}_\varphi) \end{aligned} \tag{10}$$

Substituting the above expressions in (3), we find a representation of the Piola stress tensor $\mathbf{D}$ and the surface stress tensors of the Piola type $\mathbf{D}_+$ and $\mathbf{D}_-$ in the case of radial compression of the circular plate

$$\begin{aligned} \mathbf{D} &= \alpha \chi_1 \mathbf{e}_r \otimes \mathbf{e}_R + \alpha \chi_2 \mathbf{e}_\varphi \otimes \mathbf{e}_\Phi + \gamma \chi_3 \mathbf{e}_z \otimes \mathbf{e}_Z \\ \mathbf{D}_\pm &= \alpha \left(\kappa_1^\pm + 2\alpha^2 \kappa_2^\pm\right)(\mathbf{e}_r \otimes \mathbf{e}_R + \mathbf{e}_\varphi \otimes \mathbf{e}_\Phi) \end{aligned} \tag{11}$$

It follows from (11) that the equilibrium equations (1) are automatically satisfied if $\chi_1 = \chi_2$. The equilibrium conditions (2) on the plate faces Ω_+ and Ω_- in the absence of surface loads are written as follows:

$$\chi_3|_{z=\pm h} = 0 \tag{12}$$

By solving the equation (12) at given density W of the bulk strain energy, we find the unknown constant γ.

4 Equations of Neutral Equilibrium

Suppose that in addition to the discussed initial strain state of the circular plate with surface stresses, there is an infinitely close equilibrium state under the same external loads, which is determined by the position vector $\tilde{\mathbf{R}} = \mathbf{R} + \eta \mathbf{v}$. Here η is the small parameter and $\mathbf{v}$ is the vector of additional displacements.

The linearized equilibrium equations for a nonlinearly elastic medium have the form [5, 10]:

$$\overset{\circ}{\nabla} \cdot \mathbf{D}^\bullet = \mathbf{0}, \qquad \mathbf{D}^\bullet = \left[\frac{d}{d\eta}\mathbf{D}(\mathbf{R} + \eta \mathbf{v})\right]_{\eta=0} \tag{13}$$

$$\mathbf{D}^\bullet = \mathbf{P}^\bullet \cdot \mathbf{C} + \mathbf{P} \cdot \overset{\circ}{\nabla} \mathbf{v} \tag{14}$$

Here $\mathbf{D}^\bullet$ and $\mathbf{P}^\bullet$ are the linearized Piola and Kirchhoff stress tensors, respectively. In order to find the expression for the latter, a linearization of the constitutive relations (5) is carried out [12, 14]

$$\begin{aligned}\mathbf{P}^\bullet &= \sum_{k=1}^{3}\left(\chi_k^\bullet \mathbf{d}_k\otimes\mathbf{d}_k+\chi_k\mathbf{d}_k^\bullet\otimes\mathbf{d}_k+\chi_k\mathbf{d}_k\otimes\mathbf{d}_k^\bullet\right)\\ \mathbf{G}^\bullet &= \sum_{k=1}^{3}\left(G_k^\bullet \mathbf{d}_k\otimes\mathbf{d}_k+G_k\mathbf{d}_k^\bullet\otimes\mathbf{d}_k+G_k\mathbf{d}_k\otimes\mathbf{d}_k^\bullet\right)\end{aligned} \tag{15}$$

By taking into account the fact that vectors $\mathbf{d}_k$ and $\mathbf{d}_k^\bullet$ $(k=1,2,3)$ are mutually orthogonal, i.e. $\mathbf{d}_k\cdot\mathbf{d}_k^\bullet=0$, following (15) we obtain $(m,n=1,2,3;\ k\neq m\neq n)$

$$\mathbf{d}_k\cdot\mathbf{P}^\bullet\cdot\mathbf{d}_k=\chi_k^\bullet,\qquad \mathbf{d}_k\cdot\mathbf{P}^\bullet\cdot\mathbf{d}_m=B_n\mathbf{d}_k\cdot\mathbf{G}^\bullet\cdot\mathbf{d}_m,\qquad B_n=\frac{\chi_k-\chi_m}{G_k-G_m} \tag{16}$$

where the relations for $\chi_k^\bullet$ have the form:

$$\chi_k^\bullet=\sum_{n=1}^{3}\chi_{kn}G_n^\bullet,\qquad \chi_{kn}=\frac{\partial\chi_k(G_1,G_2,G_3)}{\partial G_n},\qquad G_n^\bullet=\mathbf{d}_n\cdot\mathbf{G}^\bullet\cdot\mathbf{d}_n$$

Equations (16) represent all components of the linearized Kirchhoff stress tensor $\mathbf{P}^\bullet$ in the basis $\{\mathbf{d}_1,\mathbf{d}_2,\mathbf{d}_3\}$ through the components of the linearized Cauchy–Green strain tensor $\mathbf{G}^\bullet$, while the tensor $\mathbf{G}^\bullet$ itself is

$$\mathbf{G}^\bullet=\overset{\circ}{\nabla}\mathbf{v}\cdot\mathbf{C}^{\mathrm{T}}+\mathbf{C}\cdot\overset{\circ}{\nabla}\mathbf{v}^{\mathrm{T}} \tag{17}$$

According to (2), the linearized equilibrium conditions on the top $(z=h)$ and bottom $(z=-h)$ faces of the plate take the form [1]:

$$\left(\mathbf{e}_z\cdot\mathbf{D}^\bullet\mp\overset{\circ}{\nabla}_\pm\cdot\mathbf{D}_\pm^\bullet\right)\Big|_{z=\pm h}=\mathbf{0} \tag{18}$$

Here $\mathbf{D}_+^\bullet$ and $\mathbf{D}_-^\bullet$ are the linearized surface stress tensors of the Piola type, for which, taking into account the expressions (3), (6), the following relations are valid [15]

$$\mathbf{D}_\pm^\bullet=\mathbf{P}_\pm^\bullet\cdot\mathbf{C}_\pm+\mathbf{P}_\pm\cdot\overset{\circ}{\nabla}_\pm\mathbf{v}_\pm,\qquad \mathbf{P}_\pm^\bullet=\kappa_1^{\pm\bullet}\mathbf{I}_\pm+2\kappa_2^{\pm\bullet}\mathbf{G}_\pm+2\kappa_2^{\pm}\mathbf{G}_\pm^\bullet \tag{19}$$

where $(\theta=1,2)$

$$\begin{aligned}&\kappa_\theta^{\pm\bullet}=\sum_{\tau=1}^{2}\kappa_{\theta\tau}^{\pm}j_\tau^{\pm\bullet},\quad \kappa_{\theta\tau}^{\pm}=\frac{\partial\kappa_\theta^{\pm}(j_1^{\pm},j_2^{\pm})}{\partial j_\tau^{\pm}}\\ &j_1^{\pm\bullet}=\mathrm{tr}\mathbf{G}_\pm^\bullet,\quad j_2^{\pm\bullet}=2\mathrm{tr}\left(\mathbf{G}_\pm\cdot\mathbf{G}_\pm^\bullet\right)\\ &\mathbf{G}_\pm^\bullet=\overset{\circ}{\nabla}_\pm\mathbf{v}_\pm\cdot\mathbf{C}_\pm^{\mathrm{T}}+\mathbf{C}_\pm\cdot\overset{\circ}{\nabla}_\pm\mathbf{v}_\pm^{\mathrm{T}},\qquad \mathbf{v}_\pm=\mathbf{v}|_{z=\pm h}\end{aligned} \tag{20}$$

Here $\mathbf{P}_+^\bullet$ and $\mathbf{P}_-^\bullet$ are the linearized surface stress tensors of the Kirchhoff type; $\mathbf{G}_+^\bullet$ and $\mathbf{G}_-^\bullet$ are the linearized surface strain tensors of the Cauchy-Green type; $\mathbf{v}_+$ and $\mathbf{v}_-$ are the vectors of additional displacements of the plate faces.

We assume that the constant radial displacement is given at the edge of the circular plate ($r = r_0$), the azimuthal displacement is absent, and there is no friction during vertical displacement. This leads to the following linearized edge conditions [13]:

$$\mathbf{e}_r \cdot \mathbf{D}^\bullet \cdot \mathbf{e}_Z|_{r=r_0} = \mathbf{v} \cdot \mathbf{e}_R|_{r=r_0} = \mathbf{v} \cdot \mathbf{e}_\Phi|_{r=r_0} = 0 \tag{21}$$

The vector of additional displacements $\mathbf{v}$ in the basis of Eulerian cylindrical coordinates is written as:

$$\mathbf{v} = v_R \mathbf{e}_R + v_\Phi \mathbf{e}_\Phi + v_Z \mathbf{e}_Z \tag{22}$$

Taking into account the expressions (8), (10), (14), (16), (17), (22) and the fact that in the considered unperturbed state $\mathbf{d}_1 = \mathbf{e}_r$, $\mathbf{d}_2 = \mathbf{e}_\varphi$, $\mathbf{d}_3 = \mathbf{e}_z$, the components of the linearized Piola stress tensor $\mathbf{D}^\bullet$ in the basis of cylindrical coordinates take the form:

$$\begin{aligned}
\mathbf{e}_r \cdot \mathbf{D}^\bullet \cdot \mathbf{e}_R &= \left(\chi_1 + 2\alpha^2 \chi_{11}\right) \frac{\partial v_R}{\partial r} + \frac{2\alpha^2 \chi_{12}}{r} \left(\frac{\partial v_\Phi}{\partial \varphi} + v_R \right) + 2\alpha\gamma \chi_{13} \frac{\partial v_Z}{\partial z} \\
\mathbf{e}_r \cdot \mathbf{D}^\bullet \cdot \mathbf{e}_\Phi &= \left(\chi_1 + \alpha^2 B_3\right) \frac{\partial v_\Phi}{\partial r} + \frac{\alpha^2 B_3}{r} \left(\frac{\partial v_R}{\partial \varphi} - v_\Phi \right) \\
\mathbf{e}_r \cdot \mathbf{D}^\bullet \cdot \mathbf{e}_Z &= \left(\chi_1 + \gamma^2 B_2\right) \frac{\partial v_Z}{\partial r} + \alpha\gamma B_2 \frac{\partial v_R}{\partial z} \\
\mathbf{e}_\varphi \cdot \mathbf{D}^\bullet \cdot \mathbf{e}_R &= \alpha^2 B_3 \frac{\partial v_\Phi}{\partial r} + \frac{\chi_2 + \alpha^2 B_3}{r} \left(\frac{\partial v_R}{\partial \varphi} - v_\Phi \right) \\
\mathbf{e}_\varphi \cdot \mathbf{D}^\bullet \cdot \mathbf{e}_\Phi &= 2\alpha^2 \chi_{12} \frac{\partial v_R}{\partial r} + \frac{\chi_2 + 2\alpha^2 \chi_{22}}{r} \left(\frac{\partial v_\Phi}{\partial \varphi} + v_R \right) + 2\alpha\gamma \chi_{23} \frac{\partial v_Z}{\partial z} \\
\mathbf{e}_\varphi \cdot \mathbf{D}^\bullet \cdot \mathbf{e}_Z &= \frac{\chi_2 + \gamma^2 B_1}{r} \frac{\partial v_Z}{\partial \varphi} + \alpha\gamma B_1 \frac{\partial v_\Phi}{\partial z} \\
\mathbf{e}_z \cdot \mathbf{D}^\bullet \cdot \mathbf{e}_R &= \left(\chi_3 + \alpha^2 B_2\right) \frac{\partial v_R}{\partial z} + \alpha\gamma B_2 \frac{\partial v_Z}{\partial r} \\
\mathbf{e}_z \cdot \mathbf{D}^\bullet \cdot \mathbf{e}_\Phi &= \left(\chi_3 + \alpha^2 B_1\right) \frac{\partial v_\Phi}{\partial z} + \frac{\alpha\gamma B_1}{r} \frac{\partial v_Z}{\partial \varphi} \\
\mathbf{e}_z \cdot \mathbf{D}^\bullet \cdot \mathbf{e}_Z &= 2\alpha\gamma \chi_{13} \frac{\partial v_R}{\partial r} + \frac{2\alpha\gamma \chi_{23}}{r} \left(\frac{\partial v_\Phi}{\partial \varphi} + v_R \right) + \left(\chi_3 + 2\gamma^2 \chi_{33}\right) \frac{\partial v_Z}{\partial z}
\end{aligned} \tag{23}$$

Similarly, according to the relations (8)–(10), (19), (20), (22), the components of the linearized surface stress tensors of the Piola type $\mathbf{D}_+^\bullet$ and $\mathbf{D}_-^\bullet$ are written as follows:

$$
\begin{aligned}
\mathbf{e}_r \cdot \mathbf{D}^{\bullet}_{\pm} \cdot \mathbf{e}_R &= \left(\kappa_1^{\pm} + 6\alpha^2\kappa_2^{\pm} + \xi^{\pm}\right)\frac{\partial v_R^{\pm}}{\partial r} + \frac{\xi^{\pm}}{r}\left(\frac{\partial v_\Phi^{\pm}}{\partial \varphi} + v_R^{\pm}\right)\\
\mathbf{e}_r \cdot \mathbf{D}^{\bullet}_{\pm} \cdot \mathbf{e}_\Phi &= \left(\kappa_1^{\pm} + 4\alpha^2\kappa_2^{\pm}\right)\frac{\partial v_\Phi^{\pm}}{\partial r} + \frac{2\alpha^2\kappa_2^{\pm}}{r}\left(\frac{\partial v_R^{\pm}}{\partial \varphi} - v_\Phi^{\pm}\right)\\
\mathbf{e}_r \cdot \mathbf{D}^{\bullet}_{\pm} \cdot \mathbf{e}_Z &= \left(\kappa_1^{\pm} + 2\alpha^2\kappa_2^{\pm}\right)\frac{\partial v_Z^{\pm}}{\partial r}\\
\mathbf{e}_\varphi \cdot \mathbf{D}^{\bullet}_{\pm} \cdot \mathbf{e}_R &= 2\alpha^2\kappa_2^{\pm}\frac{\partial v_\Phi^{\pm}}{\partial r} + \frac{\kappa_1^{\pm} + 4\alpha^2\kappa_2^{\pm}}{r}\left(\frac{\partial v_R^{\pm}}{\partial \varphi} - v_\Phi^{\pm}\right)\\
\mathbf{e}_\varphi \cdot \mathbf{D}^{\bullet}_{\pm} \cdot \mathbf{e}_\Phi &= \xi^{\pm}\frac{\partial v_R^{\pm}}{\partial r} + \frac{\kappa_1^{\pm} + 6\alpha^2\kappa_2^{\pm} + \xi^{\pm}}{r}\left(\frac{\partial v_\Phi^{\pm}}{\partial \varphi} + v_R^{\pm}\right)\\
\mathbf{e}_\varphi \cdot \mathbf{D}^{\bullet}_{\pm} \cdot \mathbf{e}_Z &= \frac{\kappa_1^{\pm} + 2\alpha^2\kappa_2^{\pm}}{r}\frac{\partial v_Z^{\pm}}{\partial \varphi} \qquad \mathbf{e}_z \cdot \mathbf{D}^{\bullet}_{\pm} = \mathbf{0}
\end{aligned}
\tag{24}
$$

$$
\xi^{\pm} = 2\alpha^2(\kappa_{11}^{\pm} + 4\alpha^2\kappa_{12}^{\pm} + 4\alpha^4\kappa_{22}^{\pm})
$$

$$
v_R^{\pm} = v_R\big|_{z=\pm h}, \qquad v_\Phi^{\pm} = v_\Phi\big|_{z=\pm h}, \qquad v_Z^{\pm} = v_Z\big|_{z=\pm h}
$$

Taking into account the expressions (23), we write the equations of neutral equilibrium (13), describing the perturbed state of the circular plate, in the scalar form:

$$
\begin{aligned}
&\left(\chi_1 + 2\alpha^2\chi_{11}\right)\frac{\partial^2 v_R}{\partial r^2} + \frac{\alpha^2(B_3 + 2\chi_{12})}{r}\frac{\partial^2 v_\Phi}{\partial r\partial\varphi} + \alpha\gamma(B_2 + 2\chi_{13})\frac{\partial^2 v_Z}{\partial r\partial z}\\
&\quad + \frac{\chi_2 + \alpha^2 B_3}{r^2}\frac{\partial^2 v_R}{\partial\varphi^2} + (\chi_3 + \alpha^2 B_2)\frac{\partial^2 v_R}{\partial z^2} + \frac{\chi_1 + 2\alpha^2\chi_{11}}{r}\frac{\partial v_R}{\partial r}\\
&\quad - \frac{2\chi_2 + \alpha^2(B_3 + 2\chi_{22})}{r^2}\frac{\partial v_\Phi}{\partial\varphi} - \frac{\chi_2 + 2\alpha^2\chi_{22}}{r^2}v_R = 0\\
&\left(\chi_1 + \alpha^2 B_3\right)\frac{\partial^2 v_\Phi}{\partial r^2} + \frac{\alpha^2(B_3 + 2\chi_{12})}{r}\frac{\partial^2 v_R}{\partial r\partial\varphi} + \frac{\chi_2 + 2\alpha^2\chi_{22}}{r^2}\frac{\partial^2 v_\Phi}{\partial\varphi^2}\\
&\quad + \frac{\alpha\gamma(B_1 + 2\chi_{23})}{r}\frac{\partial^2 v_Z}{\partial\varphi\partial z} + (\chi_3 + \alpha^2 B_1)\frac{\partial^2 v_\Phi}{\partial z^2} + \frac{\chi_1 + \alpha^2 B_3}{r}\frac{\partial v_\Phi}{\partial r}\\
&\quad + \frac{2\chi_2 + \alpha^2(B_3 + 2\chi_{22})}{r^2}\frac{\partial v_R}{\partial\varphi} - \frac{\chi_2 + \alpha^2 B_3}{r^2}v_\Phi = 0\\
&\left(\chi_1 + \gamma^2 B_2\right)\frac{\partial^2 v_Z}{\partial r^2} + \alpha\gamma(B_2 + 2\chi_{13})\frac{\partial^2 v_R}{\partial r\partial z} + \frac{\chi_2 + \gamma^2 B_1}{r^2}\frac{\partial^2 v_Z}{\partial\varphi^2}\\
&\quad + \frac{\alpha\gamma(B_1 + 2\chi_{23})}{r}\frac{\partial^2 v_\Phi}{\partial\varphi\partial z} + (\chi_3 + 2\gamma^2\chi_{33})\frac{\partial^2 v_Z}{\partial z^2}\\
&\quad + \frac{\chi_1 + \gamma^2 B_2}{r}\frac{\partial v_Z}{\partial r} + \frac{\alpha\gamma(B_2 + 2\chi_{23})}{r}\frac{\partial v_R}{\partial z} = 0
\end{aligned}
\tag{25}
$$

According to the relations (22)–(24), the linearized equilibrium conditions (18) on the plate faces are written as follows ($z = \pm h$):

$$\left(\chi_3 + \alpha^2 B_2\right)\frac{\partial v_R}{\partial z} + \alpha\gamma B_2 \frac{\partial v_Z}{\partial r} \mp (\kappa_1^{\pm} + 6\alpha^2\kappa_2^{\pm} + \xi_{\pm})\left(\frac{\partial^2 v_R}{\partial r^2} + \frac{1}{r}\frac{\partial v_R}{\partial r} - \frac{v_R}{r^2}\right)$$
$$\mp \frac{2\alpha^2\kappa_2^{\pm} + \xi_{\pm}}{r}\left(\frac{\partial^2 v_\Phi}{\partial r \partial \varphi} - \frac{1}{r}\frac{\partial v_\Phi}{\partial \varphi}\right) \mp \frac{\kappa_1^{\pm} + 4\alpha^2\kappa_2^{\pm}}{r^2}\left(\frac{\partial^2 v_R}{\partial \varphi^2} - 2\frac{\partial v_\Phi}{\partial \varphi}\right) = 0$$
$$\left(\chi_3 + \alpha^2 B_1\right)\frac{\partial v_\Phi}{\partial z} + \frac{\alpha\gamma B_1}{r}\frac{\partial v_Z}{\partial \varphi} \mp \frac{2\alpha^2\kappa_2^{\pm} + \xi_{\pm}}{r}\left(\frac{\partial^2 v_R}{\partial r \partial \varphi} + \frac{1}{r}\frac{\partial^2 v_\Phi}{\partial \varphi^2} + \frac{1}{r}\frac{\partial v_R}{\partial \varphi}\right) \quad (26)$$
$$\mp(\kappa_1^{\pm} + 4\alpha^2\kappa_2^{\pm})\left(\frac{\partial^2 v_\Phi}{\partial r^2} + \frac{1}{r}\frac{\partial v_\Phi}{\partial r} - \frac{v_\Phi}{r^2} + \frac{1}{r^2}\frac{\partial^2 v_\Phi}{\partial \varphi^2} + \frac{2}{r^2}\frac{\partial v_R}{\partial \varphi}\right) = 0$$
$$\left(\chi_3 + 2\gamma^2\chi_{33}\right)\frac{\partial v_Z}{\partial z} + 2\alpha\gamma\chi_{13}\frac{\partial v_R}{\partial r} + \frac{2\alpha\gamma\chi_{23}}{r}\left(\frac{\partial v_\Phi}{\partial \varphi} + v_R\right)$$
$$\mp(\kappa_1^{\pm} + 2\alpha^2\kappa_2^{\pm})\left(\frac{\partial^2 v_Z}{\partial r^2} + \frac{1}{r}\frac{\partial v_Z}{\partial r} + \frac{1}{r^2}\frac{\partial^2 v_Z}{\partial \varphi^2}\right) = 0$$

while the linearized edge conditions (21) take the form ($r = r_0$):

$$\left(\chi_1 + \gamma^2 B_2\right)\frac{\partial v_Z}{\partial r} + \alpha\gamma B_2 \frac{\partial v_R}{\partial z} = 0, \qquad v_R = 0, \qquad v_\Phi = 0 \qquad (27)$$

Thus, the stability analysis of a circular plate with surface stresses in the general case is reduced to solving a linear homogeneous boundary-value problem (25)–(27) for the system of three partial differential equations.

5 Axisymmetric Buckling

In the special case of axisymmetric perturbations ($\partial v_R/\partial\varphi = 0$, $\partial v_\Phi/\partial\varphi = 0$, $\partial v_Z/\partial\varphi = 0$), the boundary-value problem (25)–(27) becomes much simpler. The use of substitution [13]

$$v_R = V_R(z)\, J_1(\beta r), \qquad v_\Phi = V_\Phi(z)\, J_1(\beta r) \qquad v_Z = V_Z(z)\, J_0(\beta r) \qquad (28)$$

$$\beta = \zeta_m / r_0, \qquad J_1(\zeta_m) = 0, \qquad m = 1, 2, \ldots$$

leads to the separation of the variable r in the problem and allows to satisfy the linearized boundary conditions (27) at the edge of the plate. Here J_0 and J_1 are the Bessel functions of the first kind.

Given the representation (28), the linearized equilibrium equations (25) are written as follows (hereinafter $'$ denotes the derivative with respect to z):

$$\begin{aligned}(\chi_3+\alpha^2B_2)V_R''-\beta^2\left(\chi_1+2\alpha^2\chi_{11}\right)V_R-\alpha\beta\gamma(B_2+2\chi_{13})V_Z'=0\\(\chi_3+\alpha^2B_1)V_\Phi''-\beta^2\left(\chi_1+\alpha^2B_3\right)V_\Phi=0\\(\chi_3+2\gamma^2\chi_{33})V_Z''-\beta^2\left(\chi_1+\gamma^2B_2\right)V_Z+\alpha\beta\gamma(B_2+2\chi_{13})V_R'=0\end{aligned}\tag{29}$$

Similarly, the linearized equilibrium conditions (26) take the form ($z=\pm h$):

$$\begin{aligned}\left(\chi_3+\alpha^2B_2\right)V_R'\pm\beta^2(\kappa_1^{\pm}+6\alpha^2\kappa_2^{\pm}+\xi_{\pm})V_R-\alpha\beta\gamma B_2V_Z=0\\\left(\chi_3+\alpha^2B_1\right)V_\Phi'\pm\beta^2(\kappa_1^{\pm}+4\alpha^2\kappa_2^{\pm})V_\Phi=0\\\left(\chi_3+2\gamma^2\chi_{33}\right)V_Z'+2\alpha\beta\gamma\chi_{13}V_R\pm\beta^2(\kappa_1^{\pm}+2\alpha^2\kappa_2^{\pm})V_Z=0\end{aligned}\tag{30}$$

As a result, the axisymmetric buckling analysis for the circular plate with surface stresses is reduced to solving a linear homogeneous boundary-value problem (29), (30) for the system of three ordinary differential equations.

If the elastic properties of the top and bottom faces of the plate are the same, i.e. $\kappa_\theta^+=\kappa_\theta^-$ and $\kappa_{\theta\tau}^+=\kappa_{\theta\tau}^-$ ($\theta,\tau=1,2$), then the boundary-value problem (29), (30) has two independent sets of solutions [13, 15]. The **First set** is formed by solutions for which the deflection of a plate is an odd function of z (symmetric buckling):

$$V_R(z)=V_R(-z),\qquad V_\Phi(z)=V_\Phi(-z),\qquad V_Z(z)=-V_Z(-z)$$

For the **Second set** of solutions, the deflection is an even function of z (flexural buckling):

$$V_R(z)=-V_R(-z),\qquad V_\Phi(z)=-V_\Phi(-z),\qquad V_Z(z)=V_Z(-z)$$

Due to this, it is sufficient to consider only half of the plate ($0\le z\le h$) to study its stability. The boundary conditions at the middle surface ($z=0$) follow from the evenness and oddness of the unknown functions V_R, V_Φ, V_Z:

a) for the **First set** of solutions:

$$V_R'(0)=V_\Phi'(0)=V_Z(0)=0\tag{31}$$

b) for the **Second set** of solutions:

$$V_R(0)=V_\Phi(0)=V_Z'(0)=0\tag{32}$$

Thus, the stability analysis of a plate with identical faces can be reduced to solving two linear homogeneous boundary-value problems for the half-plate: (29)–(31) and (29), (30), (32).

6 Numerical Results

As an example, we have studied the stability of a circular plate made of aluminum in the case of axisymmetric perturbations. Two different models of bulk material were considered:

1) Harmonic model [7] (λ_1, λ_2, λ_3 are the principal stretches)

$$W = \frac{1}{2}\lambda\,(\lambda_1+\lambda_2+\lambda_3-3)^2 + 2\mu\left[(\lambda_1-1)^2+(\lambda_2-1)^2+(\lambda_3-1)^2\right]$$

$$\lambda_k = \sqrt{G_k}, \qquad k = 1, 2, 3$$

2) Blatz–Ko model [2] (I_1, I_2, I_3 are the principal invariants of the Cauchy–Green strain tensor)

$$W = \frac{1}{2}\mu b\left(I_1 + \frac{I_3^{-a}-1}{a} - 3\right) + \frac{1}{2}\mu\,(1-b)\left(\frac{I_2}{I_3} + \frac{I_3^{a}-1}{a} - 3\right), \qquad a = \frac{\lambda}{2\mu}$$

$$I_1 = G_1+G_2+G_3, \qquad I_2 = G_1G_2+G_1G_3+G_2G_3, \qquad I_3 = G_1G_2G_3$$

The surface strain energy densities were assumed to be quadratic functions of the invariants $j_1^{\pm}$, $j_2^{\pm}$ [1]:

$$W_{\pm} = \frac{1}{8}\lambda_{\pm}\left(j_1^{\pm}-2\right)^2 + \frac{1}{4}\mu_{\pm}\left(j_2^{\pm}-2j_1^{\pm}+2\right)$$

The following values of bulk λ, μ and surface $\lambda_{\pm}$, $\mu_{\pm}$ elastic moduli were used for the aluminum [4]:

$$\lambda = 52.05\ \text{GPa}, \quad \mu = 34.7\ \text{GPa}, \quad \lambda_{\pm} = -3.49\ \text{Pa}\cdot\text{m}, \quad \mu_{\pm} = 6.22\ \text{Pa}\cdot\text{m}$$

For convenience, the following dimensionless parameters were introduced:

- relative radial compression $\delta = 1-\alpha$,
- radius-to-thickness ratio $r_0^* = r_0/2h$,
- relative thickness $H^* = 2h\mu/\mu_+$.

By numerical solution of the linearized boundary-value problems (29)–(31) and (29), (30), (32) we found the spectra of critical values of the relative radial compression δ, corresponding to the different buckling modes of the circular plate with surface stresses. By analyzing these spectra, the critical radial compression δ_c was obtained for plates of various sizes. It should be noted that we did not study the stability of very thick plates $\left(r_0^* < 5\right)$ in this paper. As a result, it was determined that the flexural buckling occurs at the lowest loads, and the critical radial compression δ_c corresponds to the first flexural mode ($m = 1$).

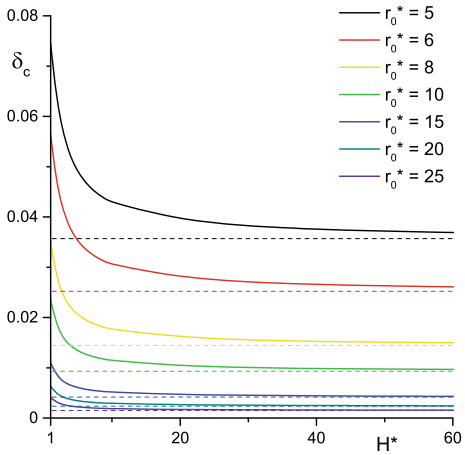

Fig. 1 Size effect on the stability of circular plate with surface stresses. Harmonic model

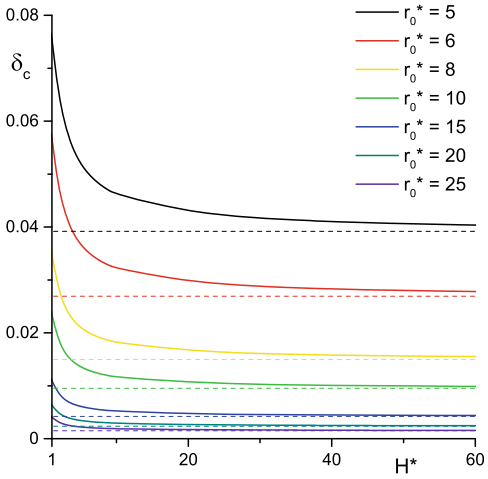

Fig. 2 Size effect on the stability of circular plate with surface stresses. Blatz–Ko model ($b = 0$)

Figures 1 and 2 illustrate the influence of the overall size (scale) of the plate on its stability. The graphs show the dependencies (solid lines) of the critical radial compression δ_c on the relative thickness H^* (size parameter) for plates with the different radius-to-thickness ratio r_0^*. According to the results obtained for both models of bulk material, the stability of the plate increases with a decrease in size. This effect is due to the influence of surface stresses. It is negligible at the macroscale but becomes quite significant at micro- and nanoscale ($H^* \leq 50$). For reference, the graphs also show the results of the stability analysis for plates without surface stresses (dashed lines). As expected, these results do not depend on the overall size of the plate.

Additionally, we have analyzed how the geometric proportions (ratios of linear dimensions) of the circular plate affect its stability. The results are reflected in Figs. 3

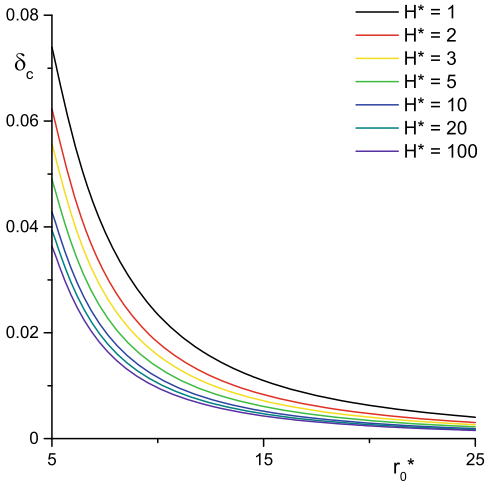

Fig. 3 Effect of plate proportions on its stability. Harmonic model

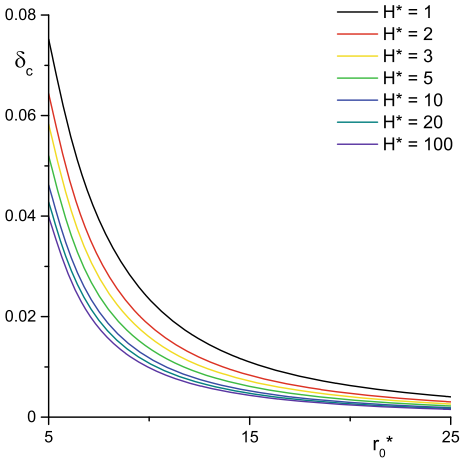

Fig. 4 Effect of plate proportions on its stability. Blatz–Ko model ($b = 0$)

and 4 which show the dependencies of the critical radial compression δ_c on the radius-to-thickness ratio r_0^* for plates of different scale H^*. According to them, the thicker plates are generally more stable, and this fact is more pronounced for smaller plates due to the influence of surface stresses.

7 Conclusion

In the framework of the bifurcation approach, we studied the stability of a nonlinearly elastic circular plate with surface stresses. For an arbitrary isotropic material, the system of linearized equilibrium equations was derived, which describes the behavior

of a plate in a perturbed state. In the case of axisymmetric perturbations, the stability analysis was reduced to solving a linear homogeneous boundary-value problem (29), (30) for a system of three ordinary differential equations. Additionally, it was established that if the elastic properties of the top and bottom faces of the plate are the same, then it is sufficient to consider only half of the plate to study its stability. For two specific models of bulk material (Harmonic model and Blatz–Ko model), the buckling analysis has been carried out for a circular plate made of aluminum in the case of axisymmetric perturbations. As a result, it was found that the stability of the plate increases with a decrease in its overall size. This effect is due to the influence of surface stresses. It is negligible at the macroscale but becomes quite significant at micro- and nanoscale ($H^* \leq 50$).

Acknowledgements This work was supported by the Russian Foundation for Basic Research (grants 16-08-00802-a, 16-01-00647-a, 16-48-230068-r_a) and by the Ministry of Science and Higher Education of the Russian Federation (Project 01201354242).

References

1. Altenbach, H., Morozov, N.F. (eds.): Surface Effects in Solid Mechanics–Models, Simulations, and Applications. Springer, Berlin (2013)
2. Blatz, P.J., Ko, W.L.: Application of finite elastic theory to the deformation of rubbery materials. Trans. Soc. Rheology **6**, 223–251 (1962)
3. Cuenot, S., Fretigny, C., Demoustier-Champagne, S., Nysten, B.: Surface tension effect on the mechanical properties of nanomaterials measured by atomic force microscopy. Phys. Rev. B **69**(16), 165, 410–415 (2004)
4. Duan, H.L., Wang, J., Karihaloo, B.L.: Theory of elasticity at the nanoscale. In: Advances in Applied Mechanics, vol. 42, pp. 1–68. Elsevier, San Diego (2008)
5. Green, A.E., Adkins, J.E.: Large Elastic Deformations and Non-Linear Continuum Mechanics. Clarendon Press, Oxford (1960)
6. Gurtin, M.E., Murdoch, A.I.: A continuum theory of elastic material surfaces. Arch. Ration. Mech. Anal. **57**(4), 291–323 (1975)
7. John, F.: Plane strain problems for a perfectly elastic material of harmonic type. Commun. Pure Appl. Math. **13**, 239–296 (1960)
8. Lurie, A.I.: Non-linear Theory of Elasticity. North-Holland, Amsterdam (1990)
9. Miller, R.E., Shenoy, V.B.: Size-dependent elastic properties of nanosized structural elements. Nanotechnology **11**(3), 139–147 (2000)
10. Ogden, R.W.: Non-Linear Elastic Deformations. Dover, Mineola (1997)
11. Ogden, R.W., Steigmann, D.J., Haughton, D.M.: The effect of elastic surface coating on the finite deformation and bifurcation of a pressurized circular annulus. J. Elast. **47**(2), 121–145 (1997)
12. Sheydakov, D.N.: Stability of a rectangular plate under biaxial tension. J. Appl. Mech. Tech. Phy. **48**(4), 547–555 (2007)
13. Sheydakov, D.N.: Size effect on buckling of non-uniform circular plate made of foam material. Mater. Phys. Mech. **28**(1–2), 26–30 (2016)
14. Sheydakov, D.N.: Effect of surface stresses on stability of elastic circular cylinder. In: dell'Isola, F., Eremeyev, V., Porubov, A. (eds.) Advances in Mechanics of Microstructured Media and Structures, Advanced Structured Materials, vol. 87, pp. 343–355. Springer, Cham (2018)
15. Sheydakov, D.N.: On stability of a nonlinearly elastic rectangular plate with surface stresses. In: Pietraszkiewicz, W., Witkowski, W. (eds.) Shell Structures: Theory and Applications, vol. 4, pp. 271–274. CRC Press, London (2018)

16. Wang, J., Duan, H.L., Huang, Z.P., Karihaloo, B.L.: A scaling law for properties of nanostructured materials. P. Roy. Soc. Lond. A **462**(2069), 1355–1363 (2006)
17. Wang, J., Huang, Z., Duan, H., Yu, S., Feng, X., Wang, G., Zhang, W., Wang, T.: Surface stress effect in mechanics of nanostructured materials. Acta Mech. Solida. Sin. **24**, 52–82 (2011)
18. Zubov, L.M.: Nonlinear Theory of Dislocations and Disclinations in Elastic Bodies. Springer, Berlin (1997)

Asymptotic Derivation of Nonlinear Plate Models from Three-Dimensional Elasticity Theory

Milad Shirani and David J. Steigmann

Abstract A framework for the asymptotic derivation of plate models from three-dimensional elasticity theory is reviewed and extended. This is shown to subsume the pure membrane and bending limits that have been derived via gamma convergence or alternative asymptotic methods, and to incorporate Koiter's model for finite deformations with small midsurface strains. A model that accommodates large midsurface strains and which satisfies the relevant Legendre-Hadamard necessary condition for energy minimizers is also proposed.

1 Introduction

Contemporary research on the theoretical foundation of theories of thin plates and shells emphasizes their relationship to three-dimensional finite elasticity theory. These efforts are typically based on the method of gamma convergence [1], concerned with the limiting variational problem for small thickness, or on asymptotic analysis of the weak forms of the equilibrium equations [2, 3]. However, neither method has generated a model that accommodates bending and stretching in a single framework. The current state of the art in the rigorous derivation of plate theory by gamma convergence is illustrated by [1], which concludes with the observation: "A wide open problem is the question of whether we can rigorously justify theories which are two-dimensional but still involve the small thickness parameter ... A typical case involves boundary conditions that cause part of the shell to stretch, but another part to bend with no stretching." Indeed, such problems are of primary interest in applications. Evidently, then, at present there exists no rigorously derived model for combined bending and stretching. The situation brings to mind Koiter's famous pun [4]: "Extreme rigour in the analysis of physical problems, we are inclined to believe,

M. Shirani · D. J. Steigmann (✉)
Department of Mechanical Engineering, University of California, Berkeley, CA 94720, USA
e-mail: dsteigmann@berkeley.edu

H. Altenbach et al. (eds.), *Recent Developments in the Theory of Shells*,
Advanced Structured Materials 110, https://doi.org/10.1007/978-3-030-17747-8_30

may easily lead to rigor mortis. ...Flexible bodies like thin shells require a flexible approach. ...".

In contrast, the work of Hilgers and Pipkin [5–7], inspired by the need for a regularization of membrane theory for problems in which membrane theory has no solution, furnishes the first careful consideration of the relationship between plate theory and modern three-dimensional nonlinear elasticity in the presence of combined bending and stretching. This work subsumes the models obtained by asymptotic analysis and gamma convergence, and furnishes an extension of Koiter's small-strain model [8, 9] to large midsurface strains. In view of these facts the failure of the community to acknowledge this body of work is discouraging. Perhaps this state of affairs may be attributed to the syndrome to which Koiter alluded.

A parallel approach based on asymptotic expansion of the local differential equations has recently been pursued by Dai and co-workers [10]. An interesting open question, originally posed by Koiter [4], concerns the relationship between the equations generated by this procedure and the Euler-Lagrange equations associated with the energies generated by the present approach.

In the present work we review the Hilgers-Pipkin model from the point of view developed in [11, 12] for thin elastic bodies. In particular, we relax some of the restrictive assumptions imposed in their treatment. Attention is confined to plates. This allows us to illustrate the main ideas as simply as possible while avoiding the less important details associated with the differential geometry of shells. Extensions of these ideas to shells are discussed in [13], and to *materially-uniform* bodies in [14, 15]. The latter framework accommodates a variety of inelastic phenomena.

Standard notation is adopted. Thus, we use bold face for vectors and tensors and indices to denote their Cartesian components. Latin indices take values in $\{1, 2, 3\}$; Greek in $\{1, 2\}$. The latter are associated with surface coordinates and associated vector and tensor components. A dot between bold symbols is used to denote the standard inner product. Thus, if $\mathbf{A}_1$ and $\mathbf{A}_2$ are second-order tensors, then $\mathbf{A}_1 \cdot \mathbf{A}_2 = tr(\mathbf{A}_1\mathbf{A}_2^t)$, where $tr(\cdot)$ is the trace and the superscript ^{t} is used to denote the transpose. The norm of a tensor $\mathbf{A}$ is $|\mathbf{A}| = \sqrt{\mathbf{A} \cdot \mathbf{A}}$. The notation $\otimes$ identifies the standard tensor product of vectors. If $\mathscr{M}$ is a fourth-order tensor, then $\mathscr{M}[\mathbf{A}]$ is the second-order tensor with components $\mathscr{M}_{iAjB}A_{jB}$. We use Div to denote the three-dimensional divergence operator, and div its two-dimensional counterpart. For example, $Div\mathbf{A} = A_{iA,A}\mathbf{e}_i$ and $div\mathbf{A} = A_{i\alpha,\alpha}\mathbf{e}_i$, where $\{\mathbf{e}_i\}$ is an orthonormal basis and subscripts preceded by commas are used to denote partial derivatives with respect to Cartesian coordinates. We also use ∇ to denote the two-dimensional gradient. The unit vector $\mathbf{k} = \mathbf{e}_3$ identifies the orientation of the plate midplane prior to deformation.

In the purely mechanical setting of nonlinear elasticity discussed here, the Piola stress $\tilde{\mathbf{P}}$ of the three-dimensional theory is given by the values of the function

$$\tilde{\mathbf{P}}(\tilde{\mathbf{F}}) = \mathscr{W}_{,\tilde{\mathbf{F}}}, \tag{1}$$

the derivative with respect to the deformation gradient $\tilde{\mathbf{F}}$ of the strain energy $\mathscr{W}(\tilde{\mathbf{F}})$ per unit reference volume. The material is assumed to be uniform for the sake of

simplicity, so that the strain-energy function does *not* depend explicitly on position $\mathbf{x}$ in a reference configuration κ. Superposed tildes are used to denote three-dimensional quantities. The same symbols, without tildes, are used to denote their midplane values.

The force per unit area transmitted across a surface with unit normal $\mathbf{N}$ in κ is

$$\tilde{\mathbf{p}} = \tilde{\mathbf{P}}(\tilde{\mathbf{F}})\mathbf{N}. \tag{2}$$

It is well known that this, together with the equilibrium equation

$$Div\tilde{\mathbf{P}} = 0, \tag{3}$$

are the natural boundary condition and Euler equation for energy-minimizing deformations under conditions of conservative loading without body force, holding on a subset of $\partial\kappa$ and in κ respectively.

A plate is a material body identified with κ, which is generated by the parallel translation of a plane region Ω, with piecewise smooth boundary curve $\partial\Omega$, in the direction orthogonal to Ω. The body itself occupies the volume $\bar{\Omega} \times [-h/2, h/2]$, where $\bar{\Omega} = \Omega \cup \partial\Omega$ and h is the (uniform) thickness. Let l be another length scale such as the diameter of Ω or an interior hole. We assume that $h/l \ll 1$. Further, we regard l as a fixed scale and adopt it as the measure of length. This allows us to put $l = 1$ and thus to simplify the notation.

Our goal is an optimal expression for the term E in the expansion

$$\mathscr{E} = E + o(h^3) \tag{4}$$

of the potential energy $\mathscr{E}$ of the thin three-dimensional body, in which $h \ll 1$. This is shown below to have the form

$$E = hE_1 + h^3E_3, \tag{5}$$

in which E_1 and E_3 are not explicitly dependent on h. We will show that E_1 is the conventional membrane energy, whereas E_3 is associated with bending and strain-gradient effects.

If a particular deformation minimizes the three-dimensional energy; i.e., if it is stable, then the perturbation $\Delta\mathscr{E}$ relative to that deformation satisfies $\Delta\mathscr{E} \geq 0$ for any kinematically possible alternative. This in turn yields $\Delta E_1 + o(h)/h \geq 0$. Passing to the limit, we obtain $\Delta E_1 \geq 0$, and conclude that at leading order in thickness, stable deformations minimize the membrane energy. If attention is restricted to deformations that are strain-free at the midsurface, and if the boundary data are compatible with such deformations, then ΔE_1 vanishes identically and the same argument yields $\Delta E_3 \geq 0$. In this case admissible deformations of the plate correspond to pure bending, and three-dimensional energy minimizers minimize E_3, again at leading order in thickness. These observations underlie the approach to membrane and inextensional bending theory via gamma convergence. However, in the case of combined

bending and stretching of a finite-thickness plate in which terms of order h and h^3 are retained simultaneously, the inequality $\Delta\mathscr{E} \geq 0$ satisfied by equilibria in the three-dimensional theory does *not* imply that $\Delta E \geq 0$. This is the reason why the method of gamma convergence, which is concerned exclusively with the derivation of the limiting minimization problem, has not succeeded in generating a single model for combined bending and stretching, except in the fortuitous circumstance - exemplified by special cases of the linear theory—when the two effects decouple at leading order [16]. Accordingly, we do *not* expect E to be minimized at a stable equilibrium state. One may seek to rectify this situation by expanding the energy to higher orders in h. However, in the nonlinear theory it is impractical to do so, as this requires higher-order three-dimensional elastic moduli [3], which are excessively unwieldy for strain-energy functions commonly used in nonlinear elasticity theory.

An interesting exception to the foregoing observation occurs when $E_1 = O(h^2)$. In this case $\mathscr{E}/h^3 = \bar{E} + o(h^3)/h^3$, where $\bar{E}$ does not depend explicitly on h. Passing to the limit, we conclude that minimizers in the exact theory correspond to minimizers in the approximate theory; that is, if a deformation minimizes $\mathscr{E}$, than it also minimizes $\bar{E}$ at leading order, and vice versa. This situation obtains in the case of wrinkling, in which the energies of stretching and bending are of comparable order [17–19]. We will show that in such circumstances $\bar{E}$ may be identified with Koiter's expression for the energy. This fact lends further support to the widespread view [20] that Koiter's model provides the best 'all-around' theory of plates and shells, despite the fact that it does not emerge as a gamma limit or a formal asymptotic limit.

Of course, there is also a need for a single model of combined stretching and bending when the two contributions to the energy are not comparable in magnitude. This case calls for careful consideration, detailed in Sect. 8.

We assume throughout that equilibrium deformations satisfy the strong-ellipticity condition

$$\mathbf{a}\otimes\mathbf{b}\cdot\mathscr{M}(\tilde{\mathbf{F}})[\mathbf{a}\otimes\mathbf{b}]>0 \quad \text{for all} \quad \mathbf{a}\otimes\mathbf{b}\neq 0, \tag{6}$$

where

$$\mathscr{M}(\tilde{\mathbf{F}}) = \mathscr{W}_{\tilde{\mathbf{F}}\tilde{\mathbf{F}}} \tag{7}$$

is the tensor of elastic moduli. It is well known that this condition must hold pointwise in the body if $\tilde{\mathbf{F}}(\mathbf{x})$ is the gradient of an energy-minimizing deformation.

We shall also make use of the strain-dependent elastic moduli $\mathscr{C}(\tilde{\mathbf{E}})$, where

$$\tilde{\mathbf{E}} = \tfrac{1}{2}(\tilde{\mathbf{F}}^t\tilde{\mathbf{F}} - I) \tag{8}$$

is the strain in which $\mathbf{I}$ is the identity for 3-space, and

$$\mathscr{C}(\tilde{\mathbf{E}}) = \mathscr{U}_{\tilde{\mathbf{E}}\tilde{\mathbf{E}}} \tag{9}$$

in which

$$\mathscr{U}(\tilde{\mathbf{E}}) = \mathscr{W}(\tilde{\mathbf{F}}) \tag{10}$$

is the associated strain-energy function. An application of the chain rule, combined with the minor symmetries of $\mathscr{C}$, furnishes

$$\mathscr{M}(\tilde{\mathbf{F}})[\mathbf{A}] = \mathbf{A}\tilde{\mathbf{S}} + \tilde{\mathbf{F}}\mathscr{C}(\tilde{\mathbf{E}})[\tilde{\mathbf{F}}^t\mathbf{A}] \tag{11}$$

for any tensor $\mathbf{A}$, where

$$\tilde{\mathbf{S}} = \mathscr{U}_{\tilde{\mathbf{E}}} \tag{12}$$

is the symmetric second Piola-Kirchhoff stress, given in terms of the Piola stress by

$$\tilde{\mathbf{P}} = \tilde{\mathbf{F}}\tilde{\mathbf{S}}. \tag{13}$$

We assume $\mathscr{U}(\cdot)$ to be convex in a neighborhood of the origin in strain space, with the origin furnishing an isolated local minimum. Thus $\tilde{\mathbf{S}}$ vanishes at zero strain, and $\mathscr{C}(\mathbf{0})$ is positive definite in the sense that $\mathbf{A}\cdot\mathscr{C}(\mathbf{0})[\mathbf{A}] > 0$ for all non-zero symmetric $\mathbf{A}$. Then,

$$\tilde{\mathbf{S}} = \mathscr{C}(\mathbf{0})[\tilde{\mathbf{E}}] + o(\left|\tilde{\mathbf{E}}\right|). \tag{14}$$

It follows from (11), (14) that

$$\mathscr{M}(\mathbf{I})[\mathbf{A}] = \mathscr{C}(\mathbf{0})[\mathbf{A}] \tag{15}$$

and hence that our hypotheses yields strong ellipticity at zero strain, as in classical linear elasticity theory.

2 Small-Thickness Estimate of the Energy

Position in the reference placement of the plate may be written

$$\mathbf{x} = \mathbf{u} + \varsigma\mathbf{k}, \tag{16}$$

where $\mathbf{u} \in \Omega$ and $\varsigma \in [-h/2, h/2]$. We assume the origin to lie on Ω. The projection

$$\mathbf{1} = \mathbf{I} - \mathbf{k}\otimes\mathbf{k}, \tag{17}$$

is the identity on the translation space Ω' of Ω. The three-dimensional deformation gradient satisfies $d\tilde{\mathbf{y}} = \tilde{\mathbf{F}}d\mathbf{x}$, where $\tilde{\mathbf{y}} = \tilde{\chi}(\mathbf{x})$ is the position after deformation of the material point $\mathbf{x}$ and $\tilde{\boldsymbol{\chi}}$ is the deformation function. Using this with $\tilde{\mathbf{y}} = \hat{\mathbf{y}}(\mathbf{u},\varsigma) = \tilde{\boldsymbol{\chi}}(\mathbf{u}+\varsigma\mathbf{k})$ and $d\mathbf{u} \in \Omega'$ yields the alternative representations

$$(\tilde{\mathbf{F}}\mathbf{1})d\mathbf{u}+\tilde{\mathbf{F}}\mathbf{k}d\varsigma = d\hat{\mathbf{y}} = (\nabla\hat{\mathbf{y}})d\mathbf{u} + (\hat{\mathbf{y}})'d\varsigma, \tag{18}$$

where $\nabla()$ is the (two-dimensional) gradient with respect to $\mathbf{u}$ at fixed ς and the notation $()'$ is used to denote $\partial()/\partial\varsigma$ at fixed $\mathbf{u}$. It follows from $\tilde{\mathbf{F}} = \tilde{\mathbf{F}}\mathbf{1} + \tilde{\mathbf{F}}\mathbf{k} \otimes \mathbf{k}$ that

$$\hat{\mathbf{F}} = \nabla\hat{\mathbf{y}} + \hat{\mathbf{y}}' \otimes \mathbf{k}, \tag{19}$$

where $\hat{\mathbf{F}}(\mathbf{u}, \varsigma) = \tilde{\mathbf{F}}(\mathbf{u} + \varsigma\mathbf{k})$.

The total strain energy in a given deformation is

$$\mathscr{S} = \int_\kappa \mathscr{W}(\tilde{\mathbf{F}}(\mathbf{x}))dv = \int_\Omega \int_{-h/2}^{h/2} \mathscr{W}(\hat{\mathbf{F}}(\mathbf{u}, \varsigma))d\varsigma da. \tag{20}$$

If $\tilde{\boldsymbol{\chi}}(\mathbf{x})$ is sufficiently smooth, then by Leibniz' Rule and Taylor's Theorem, applied to the small parameter h,

$$\int_{-h/2}^{h/2} \mathscr{W}(\hat{\mathbf{F}}(\mathbf{u}, \varsigma))d\varsigma = h\mathscr{W}(\mathbf{F}) + \tfrac{1}{24}h^3\mathscr{W}'' + ..., \tag{21}$$

where, by the chain rule,

$$\mathscr{W}' = \mathbf{P} \cdot \mathbf{F}' \quad \text{and} \quad \mathscr{W}'' = \mathbf{P}' \cdot \mathbf{F}' + \mathbf{P} \cdot \mathbf{F}'' \tag{22}$$

in which

$$\mathbf{F}^{(n)} = \hat{\mathbf{F}}^{(n)}_{|\varsigma=0} \tag{23}$$

and

$$\mathbf{P} = \tilde{\mathbf{P}}(\mathbf{F}), \quad \mathbf{P}' = \mathscr{M}(\mathbf{F})[\mathbf{F}']. \tag{24}$$

From (19) we have

$$\hat{\mathbf{F}}' = \nabla\hat{\mathbf{y}}' + \hat{\mathbf{y}}'' \otimes \mathbf{k} \quad \text{and} \quad \hat{\mathbf{F}}'' = \nabla\hat{\mathbf{y}}'' + \hat{\mathbf{y}}''' \otimes \mathbf{k}. \tag{25}$$

It follows that

$$\mathbf{F} = \nabla\mathbf{r} + \mathbf{d} \otimes \mathbf{k}, \quad \mathbf{F}' = \nabla\mathbf{d} + \mathbf{g} \otimes \mathbf{k}, \quad \text{and} \quad \mathbf{F}'' = \nabla\mathbf{g} + \mathbf{h} \otimes \mathbf{k}, \tag{26}$$

where

$$\mathbf{r} = \mathbf{y}, \quad \mathbf{d} = \mathbf{y}', \quad \mathbf{g} = \mathbf{y}'' \quad \text{and} \quad \mathbf{h} = \mathbf{y}''', \tag{27}$$

in which

$$\mathbf{y}^{(n)} = \hat{\mathbf{y}}^{(n)}_{|\varsigma=0} \tag{28}$$

are *independent* functions of $\mathbf{u} \in \Omega$. These are the coefficient vectors in the order—ς^3 expansion

$$\hat{\mathbf{y}}(\mathbf{u}, \varsigma) = \mathbf{r}(\mathbf{u}) + \varsigma \mathbf{d}(\mathbf{u}) + \tfrac{1}{2}\varsigma^2 \mathbf{g}(\mathbf{u}) + \tfrac{1}{6}\varsigma^3 \mathbf{h}(\mathbf{u}) + \ldots . \tag{29}$$

Here $\mathbf{r}(\mathbf{u})$ is the position of a material point on the deformed image ω of the midsurface Ω; its gradient $\nabla \mathbf{r}$ maps Ω' to the tangent plane T_ω to ω at the material point $\mathbf{u}$. The functions $\mathbf{d}(\mathbf{u})$, $\mathbf{g}(\mathbf{u})$ and $\mathbf{h}(\mathbf{u})$ provide information about the three-dimensional deformation in the vicinity of the midplane.

The regularity of the three-dimensional deformation required by the expansion (29) is not implied by Ball's existence theory for equilibria [21]. Nevertheless, any piecewise C^2 equilibrium deformation, possessing a potential jump in its normal derivative across a smooth surface in κ, is in fact C^2 in the presence of strong ellipticity. It is straightforward to show that it is actually C^n for arbitrary n. Further, in [22] strong ellipticity is used with degree-theoretic arguments to obtain partial existence results for classically smooth (i.e., C^2) equilibria, albeit under pure displacement boundary data. Given our adoption of strong ellipticity, it is thus natural to describe equilibria in terms of Euler equations for a suitable energy functional evaluated on the class of deformations represented by (29).

We write the strain energy as

$$\mathscr{S} = \int_\kappa \mathscr{W}(\tilde{\mathbf{F}}(\mathbf{x}))dv = S + o(h^3), \tag{30}$$

where

$$S = \int_\Omega W(\mathbf{d}, \mathbf{g}, \mathbf{h}, \nabla \mathbf{r}, \nabla \mathbf{d}, \nabla \mathbf{g})da \tag{31}$$

in which

$$W = h\mathscr{W}(\nabla \mathbf{r} + \mathbf{d} \otimes \mathbf{k}) + \tfrac{1}{24}h^3\{\mathbf{P} \cdot (\nabla \mathbf{g} + \mathbf{h} \otimes \mathbf{k}) + \mathbf{P}' \cdot (\nabla \mathbf{d} + \mathbf{g} \otimes \mathbf{k})\} \tag{32}$$

is the order—h^3 strain energy per unit area of Ω. We show below that this formula subsumes the strain energies associated with conventional membrane theory and inextensional bending theory.

We remark that this expression does not furnish the complete strain energy for the order—ς^3 truncation of the three-dimensional deformation. The latter contributes additional terms at higher order in h. However, rather than model a given truncation, our objective here is an accurate order—h^3 expression for the potential energy that is as accurate as possible by the standard of the three-dimensional theory and which yields a meaningful minimization problem in its own right.

In [7] a through-thickness expansion scheme for the three-dimensional deformation is adopted which has the effect of suppressing the term involving $\nabla \mathbf{g}$ in the order—h^3 potential energy. However, the leading-order term in that scheme is not the deformation of the midplane. Instead, it is the average of the deformation through the thickness. In general, the value of ς at which this average is attained depends on the deformation and is not known in advance. Thus, the formulation given in [7] has the inconvenient feature that the surface whose deformation is described by the

theory cannot be identified beforehand. We show here that the present expansion scheme ultimately yields an expression for the energy equivalent to that given in [7], but with the leading-order term given by the deformation $\mathbf{r}(\mathbf{u})$ of the midplane.

To obtain an order—h^3 expansion of the potential energy of the loads, we first consider the simplest case in which $\partial\Omega$ consists of the union of disjoint arcs $\partial\Omega_e$ and $\partial\Omega_n$, where essential and natural boundary conditions, respectively, are specified. For example, suppose three-dimensional position is assigned on $\partial\kappa_{C_e} = \partial\Omega_e \times C$, where $C = [-h/2, h/2]$. We refer to this as a clamped edge. If dead loads are assigned on $\partial\kappa_{C_n} = \partial\Omega_n \times C$, then the potential energy of the three-dimensional body is $\mathscr{E} = \mathscr{S} - \mathscr{L}$, where $\mathscr{S}$ is the total strain energy defined by (20), and

$$\mathscr{L} = \int_{\partial\Omega_n} \Big(\int_{-h/2}^{h/2} \tilde{\mathbf{p}} \cdot \tilde{\boldsymbol{\chi}} \, d\varsigma \Big) da \tag{33}$$

is the load potential, in which $\tilde{\mathbf{p}}(\mathbf{x}) = \hat{\mathbf{p}}(\mathbf{u}, \varsigma)$ is the assigned (three-dimensional) Piola traction. Using a formula like (21), it is straightforward to show that

$$\mathscr{L} = L + o(h^3), \tag{34}$$

where

$$L = \int_{\partial\Omega_n} \chi(\mathbf{r}, \mathbf{d}, \mathbf{g}) da \tag{35}$$

with

$$\chi(\mathbf{r}, \mathbf{d}, \mathbf{g}) = \mathbf{p}_r \cdot \mathbf{r} + \mathbf{p}_d \cdot \mathbf{d} + \mathbf{p}_g \cdot \mathbf{g}, \tag{36}$$

and with

$$\mathbf{p}_r = h\mathbf{p} + \tfrac{1}{24} h^3 \mathbf{p}'', \quad \mathbf{p}_d = \tfrac{1}{12} h^3 \mathbf{p}' \quad \text{and} \quad \mathbf{p}_g = \tfrac{1}{24} h^3 \mathbf{p}, \tag{37}$$

in which $\mathbf{p}_r$, $\mathbf{p}_d$ and $\mathbf{p}_g$ are assigned and the primes identify derivatives of the three-dimensional traction with respect to ς, evaluated at $\varsigma = 0$. The order—h^3 estimate of the potential energy is thus given by

$$E = \int_\Omega W da - L, \tag{38}$$

with

$$L = \int_{\partial\Omega_n} (\mathbf{p}_r \cdot \mathbf{r} + \mathbf{p}_d \cdot \mathbf{d} + \mathbf{p}_g \cdot \mathbf{g}) ds, \tag{39}$$

Comparison with (5) furnishes

$$E_1 = \int_\Omega \mathscr{W}(\nabla \mathbf{r} + \mathbf{d} \otimes \mathbf{k}) da - \int_{\partial\Omega_n} \mathbf{p} \cdot \mathbf{r} ds \tag{40}$$

and

$$24E_3 = \int_\Omega \{\mathscr{M}(\mathbf{F})[\nabla\mathbf{d} + \mathbf{g}\otimes\mathbf{k}]\cdot(\nabla\mathbf{d} + \mathbf{g}\otimes\mathbf{k}) + \mathbf{P}\cdot(\nabla\mathbf{g} + \mathbf{h}\otimes\mathbf{k})\}da$$
$$- \int_{\partial\Omega_n} (\mathbf{p}''\cdot\mathbf{r} + 2\mathbf{p}'\cdot\mathbf{d} + \mathbf{p}\cdot\mathbf{g})ds. \tag{41}$$

We also consider conservative pressure loads. In this case the plate is fixed along the entire edge $\partial\Omega$, and $\partial\Omega_n$ is empty. We suppose a volume of compressible gas to be bounded by the lower lateral surface $\partial\kappa^-$ of the plate together with the walls of a rigid container; the plate is, in effect, a deformable lid. Let $\mathscr{V}^-$ be the enclosed volume; i.e., the volume of the compressible gas. The pressure-volume relation of the gas is given by the function $p^-(\mathscr{V}^-)$. We further assume the upper lateral surface of the plate, $\partial\kappa^+$, to be acted upon by a uniform pressure p^+ of fixed intensity. It is shown in [12] that

$$\mathscr{V}^- = \tfrac{1}{3}\int_{\partial\kappa^-} \tilde{\boldsymbol{\chi}}\cdot\tilde{\mathbf{F}}^*\mathbf{k}da, \tag{42}$$

apart from an unimportant constant, where the superscript * refers to the cofactor. The tractions on the upper and lower lateral surfaces are

$$\tilde{\mathbf{p}}^\pm = \mp p^\pm(\tilde{\mathbf{F}}^\pm)^*\mathbf{k}, \tag{43}$$

where $\mathbf{F}^\pm = \hat{\mathbf{F}}(\mathbf{u}, \pm h/2)$. Further, the load potential is [12]

$$\mathscr{L} = \int_{\mathscr{V}_0^-}^{\mathscr{V}^-} p^-(x)dx - p^+(\mathscr{V} + \mathscr{V}^-), \tag{44}$$

where $\mathscr{V}_0^-$ is an arbitrary constant and

$$\mathscr{V} = \int_\kappa \det\tilde{\mathbf{F}}dv \tag{45}$$

is the volume of the deformed plate.

We suppose that

$$p^\pm = h^n P^\pm + o(h^n), \tag{46}$$

with $P^\pm = O(1)$ and $n = 1$ or $n = 3$. It is then easy to show that

$$\mathscr{L} = L + o(h^n), \tag{47}$$

where

$$L = h^n[\int_{V_0^-}^{V} P^-(x)dx - P^+V] \tag{48}$$

and

$$V = \tfrac{1}{3}\int_{\Omega} \alpha \mathbf{r}\cdot\mathbf{n}da, \tag{49}$$

where $\mathbf{n}$ is the unit normal to the deformed midsurface ω, α is the areal stretch of the midsurface, and Nanson's formula has been used in the form

$$\alpha\mathbf{n} = \mathbf{F}^{*}\mathbf{k} \tag{50}$$

with $\alpha = |\mathbf{F}^{*}\mathbf{k}|$. Using $(26)_1$ with $\mathbf{F}^{*}\mathbf{k} = \mathbf{F}\mathbf{e}_1 \times \mathbf{F}\mathbf{e}_2$, we obtain $\alpha\mathbf{n} = (\nabla\mathbf{r})\mathbf{e}_1 \times (\nabla\mathbf{r})\mathbf{e}_2$ and thus reduce (48) to a functional of the midsurface position field. We note in passing that the determinant of the deformation gradient, evaluated at the midplane, is $J = \mathbf{F}\mathbf{e}_1 \times \mathbf{F}\mathbf{e}_2 \cdot \mathbf{F}\mathbf{k}$. Thus,

$$J = \alpha\mathbf{n}\cdot\mathbf{d}. \tag{51}$$

Accordingly, the requirement $J > 0$ is equivalent to the requirement $\mathbf{d} \in S_+$, where S_+ is the half-space

$$S_+ = \{\mathbf{v} : \mathbf{v}\cdot\mathbf{n} > \mathbf{0}\}. \tag{52}$$

We do not impose bulk incompressibility in the present work, although doing so presents no difficulty.

3 Membrane Limit

Membrane theory is associated with the leading order energy in (5). Thus,

$$\mathscr{E}/h = E_m + o(h)/h, \tag{53}$$

where

$$E_m = \int_{\Omega} \mathscr{W}(\nabla\mathbf{r} + \mathbf{d}\otimes\mathbf{k})da - \int_{\partial\Omega_n} \mathbf{p}\cdot\mathbf{r}ds \tag{54}$$

is the membrane energy in the dead-load boundary-value problem. In the case of pressure loading with $n = 1$ in (48), the relevant energy is

$$E_m = \int_{\Omega} \mathscr{W}(\nabla\mathbf{r} + \mathbf{d}\otimes\mathbf{k})da - [\int_{V_0^-}^{V} P^{-}(x)dx - P^{+}V], \tag{55}$$

where V is defined in (49). In either case the energy is a functional of the midplane deformation field $\mathbf{r}$ and the director field $\mathbf{d}$.

The energy is stationary with respect to $\mathbf{d}$ if and only if the membrane is in a state of plane stress; i.e.,

$$\{\mathscr{W}_{\mathbf{F}}(\nabla\mathbf{r}+\mathbf{d}\otimes\mathbf{k})\}k=0. \tag{56}$$

From (1) and (13) we then have that $\mathbf{Sk}=\mathbf{0}$, which combines with the symmetry of $\mathbf{S}$ to yield

$$\mathbf{S}=S_{\alpha\beta}\mathbf{e}_\alpha\otimes\mathbf{e}_\beta. \tag{57}$$

To prove that (56) may be solved uniquely for $\mathbf{d}$, we first show that any solution, $\bar{\mathbf{d}}$ say, minimizes $\mathscr{W}$ pointwise. To this end we fix $\nabla\mathbf{r}$ and define $M(\mathbf{d})=\mathscr{W}(\nabla\mathbf{r}+\mathbf{d}\otimes\mathbf{k})$. Let $\mathbf{d}(u)$ be a twice-differentiable function. The derivatives of $\sigma(u)=M(\mathbf{d}(u))$ are

$$\dot\sigma=\dot{\mathbf{d}}\cdot\mathbf{P}(\nabla\mathbf{r}+\mathbf{d}\otimes\mathbf{k})k=\dot{\mathbf{d}}\cdot M_{\mathbf{d}} \tag{58}$$

and

$$\begin{aligned}\ddot\sigma&=\ddot{\mathbf{d}}\cdot\mathbf{P}(\nabla\mathbf{r}+\mathbf{d}\otimes\mathbf{k})\mathbf{k}+\dot{\mathbf{d}}\otimes\mathbf{k}\cdot\mathscr{M}(\nabla\mathbf{r}+\mathbf{d}\otimes\mathbf{k})[\dot{\mathbf{d}}\otimes\mathbf{k}]\\&=\ddot{\mathbf{d}}\cdot M_{\mathbf{d}}+\dot{\mathbf{d}}\cdot(M_{\mathbf{dd}})\dot{\mathbf{d}}.\end{aligned} \tag{59}$$

Thus,

$$M_{\mathbf{d}}(\bar{\mathbf{d}})=\mathbf{P}(\nabla\mathbf{r}+\bar{\mathbf{d}}\otimes\mathbf{k})\mathbf{k} \tag{60}$$

vanishes by (56), whereas

$$M_{\mathbf{dd}}(\bar{\mathbf{d}})=\mathscr{A}(\nabla\mathbf{r}+\bar{\mathbf{d}}\otimes\mathbf{k}), \tag{61}$$

where $\mathscr{A}(\mathbf{F})$ is the acoustic tensor defined, for any vector $\mathbf{v}$, by

$$\mathscr{A}(\mathbf{F})\mathbf{v}=\{\mathscr{M}(\mathbf{F})[\mathbf{v}\otimes\mathbf{k}]\}\mathbf{k}. \tag{62}$$

This is positive definite by virtue of the strong ellipticity condition (6).

We conclude that $\ddot\sigma>0$ on straight-line paths defined by $\mathbf{d}(u)=u\mathbf{d}_2+(1-u)\mathbf{d}_1$ with $\mathbf{d}_1,\mathbf{d}_2\in S_+$ fixed and $0\le u\le 1$. These paths are admissible because the domain S_+ of $M(\cdot)$ is convex. Integrating with respect to u yields $\dot\sigma(u)>\dot\sigma(0)$ for $u\in(0,1]$ and $\sigma(1)-\sigma(0)>\dot\sigma(0)$, proving that $M(\mathbf{d})$ is a strictly convex function; i.e.,

$$M(\mathbf{d}_2)-M(\mathbf{d}_1)>M_{\mathbf{d}}(\mathbf{d}_1)\cdot(\mathbf{d}_2-\mathbf{d}_1) \tag{63}$$

for all unequal pairs $\mathbf{d}_1,\mathbf{d}_2$. It follows that M is minimized absolutely at a stationary point and hence that (56) has a unique solution $\bar{\mathbf{d}}(\nabla\mathbf{r})$.

An interesting and heretofore unknown corollary is that for a given midplane deformation, the strain energy is minimized absolutely when the midplane is in a state of plane stress.

With this solution incorporated, the membrane energy reduces to the functional of $\mathbf{r}$ defined by (54) or (55) with their integrands replaced by $\mathscr{W}(\nabla\mathbf{r}+\bar{\mathbf{d}}(\nabla\mathbf{r})\otimes\mathbf{k})$.

However, it transpires that this function fails to satisfy the relevant (two-dimensional) Legendre-Hadamard condition, even if $\mathscr{W}$ is strongly elliptic in the three-dimensional sense. This is due to the presence of compressive stresses in the plane stress-deformation relation, whereas such stresses are precluded by the Legendre-Hadamard condition [23].

To elaborate, we define the membrane strain-energy function

$$W(\nabla\mathbf{r}) = \mathscr{W}(\nabla\mathbf{r} + \bar{\mathbf{d}}(\nabla\mathbf{r}) \otimes \mathbf{k}). \tag{64}$$

Its derivatives are

$$\partial W/\partial r_{i,\alpha} = \partial\mathscr{W}/\partial F_{i\alpha} + (\partial\mathscr{W}/\partial d_j)K_{ji\alpha}, \tag{65}$$

where $K_{ji\alpha} = \partial\bar{d}_j/F_{i\alpha}$ and F_{iA} are the components of $(26)_1$ with $F_{i\alpha} = r_{i,\alpha}$ and $F_{i3} = d_i$. The derivatives $\partial\mathscr{W}/\partial d_j$ vanish identically by (56), yielding

$$\partial W/\partial r_{i,\alpha} = P_{i\alpha}. \tag{66}$$

The associated moduli are

$$E_{i\alpha j\beta} = \partial^2 W/\partial r_{i,\alpha}\partial r_{j,\beta}. \tag{67}$$

The operative Legendre-Hadamard necessary condition for energy minimizers is [24]

$$E_{i\alpha j\beta}x_i x_j y_\alpha y_\beta \geq 0 \quad \text{for all} \quad x_i, y_\alpha. \tag{68}$$

For frame-invariant strain energies, this has the interesting consequence that the symmetric (plane) second Piola-Kirchhoff stress $S_{\alpha\beta}$, defined by $P_{i\alpha} = F_{i\gamma}S_{\gamma\beta}$, satisfies

$$S_{\alpha\beta}y_\alpha y_\beta \geq 0, \tag{69}$$

and is thus positive semi-definite [23].

To see this we observe that by virtue of frame invariance, W is a function, U say, of the surface metric $a_{\alpha\beta} = F_{i\alpha}F_{i\beta}$, or, equivalently, of the surface strain $\epsilon_{\alpha\beta} = \frac{1}{2}(F_{i\alpha}F_{i\beta} - \delta_{\alpha\beta})$, where $\delta_{\alpha\beta}$ is the Kronecker delta. The chain rule then yields

$$S_{\alpha\beta} = \partial U/\partial\epsilon_{\alpha\beta}, \tag{70}$$

in which we understand $\epsilon_{\alpha\beta}$ to be replaced by $\frac{1}{2}(\epsilon_{\alpha\beta} + \epsilon_{\beta\alpha})$ in the function U, with $\epsilon_{\alpha\beta}$ and $\epsilon_{\beta\alpha}$ being regarded as independent when computing the partial derivative. With this it follows by straightforward application of the chain rule that

$$E_{i\alpha j\beta} = \delta_{ij}S_{\alpha\beta} + F_{i\mu}F_{j\lambda}D_{\alpha\mu\beta\lambda}, \tag{71}$$

where

$$D_{\alpha\mu\beta\lambda} = \partial^2 U/\partial\epsilon_{\alpha\mu}\partial\epsilon_{\beta\lambda} \tag{72}$$

are the plane-stress elastic moduli. These possess the usual major and minor symmetries.

The Legendre-Hadamard condition (68) may thus be reduced to

$$x_i x_i S_{\alpha\beta} y_\alpha y_\beta + D_{\alpha\mu\beta\lambda} y_\alpha z_\mu y_\beta z_\lambda \geq 0, \tag{73}$$

where $z_\mu = x_i F_{i\mu}$ is a two-vector on the undeformed midplane. For the choice $x_i = n_i$—the unit normal to the *deformed* midsurface—z_μ vanishes. We then obtain (69) and the conclusion that energy minimizers necessarily yield a stress field that is pointwise positive semi-definite. This severe restriction means that boundary-value problems based on W will generally fail to have energy minimizing solutions. In such circumstances well-posedness may be restored via *relaxation*, in which the function W is replaced by its *quasiconvexification* [25]; i.e., the largest quasiconvex function not exceeding W anywhere on its domain. The latter automatically satisfies the Legendre-Hadamard inequality at all deformations and provides the foundation for the *tension-field theory* of elastic membranes [26]. Precisely the same model emerges directly by the method of gamma convergence [27].

4 Pure Bending

For deformations that generate zero strain at the midplane, our constitutive hypotheses imply that the midplane stress $\mathbf{P}$ and edge traction $\mathbf{p}$ vanish identically, and hence that

$$\mathscr{E}/h^3 = E_b + o(h^3)/h^3, \tag{74}$$

where

$$\begin{aligned} 24E_b = &\int_\Omega \mathscr{M}(\mathbf{F})[\nabla\mathbf{d} + \mathbf{g}\otimes\mathbf{k}]\cdot(\nabla\mathbf{d} + \mathbf{g}\otimes\mathbf{k})da \\ &- \int_{\partial\Omega_n} (\mathbf{p}''\cdot\mathbf{r} + 2\mathbf{p}'\cdot\mathbf{d})ds \end{aligned} \tag{75}$$

in the case of dead loading. Moreover, the midplane value of the deformation gradient is then a rotation, $\mathbf{R}$ say, implying that $\nabla\mathbf{r} = \mathbf{R1}$ and $\mathbf{d} = \mathbf{Rk} = \mathbf{n}$, the unit normal to the deformed midsurface. Thus $\mathbf{d}$ is determined by $\nabla\mathbf{r}$; we write $\mathbf{d} = \bar{\mathbf{d}}(\nabla\mathbf{r})$ as before. It follows that E_b is a functional of the midplane deformation and the vector field $\mathbf{g}$.

This energy is stationary with respect to $\mathbf{g}$ if and only if

$$\{\mathscr{M}(\mathbf{F})[\nabla\bar{\mathbf{d}} + \mathbf{g}\otimes\mathbf{k}]\}\mathbf{k} = \mathbf{0}, \tag{76}$$

or

$$\mathscr{A}(\mathbf{F})\mathbf{g} = -\{\mathscr{M}(\mathbf{F})[\nabla\bar{\mathbf{d}}]\}\mathbf{k}, \tag{77}$$

where $\mathscr{A}(\mathbf{F})$ is the acoustic tensor defined by (62). Thus (76) has the unique solution $g = \bar{\mathbf{g}}(\nabla\mathbf{r}, \nabla\nabla\mathbf{r})$, say.

The solution $\bar{\mathbf{g}}$ also minimizes the strain energy. To see this we fix $\nabla\mathbf{r}$ and define

$$B(\mathbf{g}) = \tfrac{1}{2}\mathscr{M}(\nabla\mathbf{r} + \bar{\mathbf{d}} \otimes \mathbf{k})[\nabla\bar{\mathbf{d}} + \mathbf{g} \otimes \mathbf{k}] \cdot (\nabla\bar{\mathbf{d}} + \mathbf{g} \otimes \mathbf{k}). \tag{78}$$

Consider a parametrized path $\mathbf{g}(u)$. The derivatives of $\sigma(u) = B(\mathbf{g}(u))$ with respect to u are

$$\dot{\sigma} = \dot{\mathbf{g}} \cdot \{\mathscr{M}(\nabla\mathbf{r} + \bar{\mathbf{d}} \otimes \mathbf{k})[\nabla\bar{\mathbf{d}} + \mathbf{g} \otimes \mathbf{k}]\}\mathbf{k} = \dot{\mathbf{g}} \cdot B_{\mathbf{g}} \tag{79}$$

and

$$\begin{aligned}\ddot{\sigma} &= \ddot{\mathbf{g}} \cdot \{\mathscr{M}(\nabla\mathbf{r} + \bar{\mathbf{d}} \otimes \mathbf{k})[\nabla\bar{\mathbf{d}} + \mathbf{g} \otimes \mathbf{k}]\}\mathbf{k} + \dot{\mathbf{g}} \otimes \mathbf{k} \cdot \mathscr{M}(\nabla\mathbf{r} + \bar{\mathbf{d}} \otimes \mathbf{k})[\dot{\mathbf{g}} \otimes k] \\ &= \ddot{\mathbf{g}} \cdot B_{\mathbf{g}} + \dot{\mathbf{g}} \cdot (B_{\mathbf{gg}})\dot{\mathbf{g}},\end{aligned} \tag{80}$$

where we have used the major symmetry of $\mathscr{M}$. Thus,

$$B_{\mathbf{g}}(\bar{\mathbf{g}}) = \{\mathscr{M}(\nabla\mathbf{r} + \bar{\mathbf{d}} \otimes \mathbf{k})[\nabla\bar{\mathbf{d}} + \bar{\mathbf{g}} \otimes \mathbf{k}]\}\mathbf{k} \tag{81}$$

vanishes by (76), and

$$B_{\mathbf{gg}} = \mathscr{A}(\nabla\mathbf{r} + \bar{\mathbf{d}} \otimes \mathbf{k}). \tag{82}$$

Then, $\ddot{\sigma} > 0$ on straight-line paths defined by $\mathbf{g}(u) = u\mathbf{g}_2 + (1-u)\mathbf{g}_1$ with $\mathbf{g}_1, \mathbf{g}_2$ fixed and $0 \le u \le 1$. These paths belong to the convex set E^3, the domain of $B(\cdot)$. Integrating with respect to u yields $\dot{\sigma}(u) > \dot{\sigma}(0)$ for $u \in (0, 1]$ and $\sigma(1) - \sigma(0) > \dot{\sigma}(0)$, proving that the function $B(\mathbf{g})$ is strictly convex; i.e.,

$$B(\mathbf{g}_2) - B(\mathbf{g}_1) > B_{\mathbf{g}}(\mathbf{g}_1) \cdot (\mathbf{g}_2 - \mathbf{g}_1) \tag{83}$$

for all unequal pairs $\mathbf{g}_1, \mathbf{g}_2$. It follows that B is minimized absolutely at a stationary point and thus that the solution $\bar{\mathbf{g}}$ to (77) furnishes the optimal order - h^3 energy.

The explicit energy is obtained from (75) on noting, from (11) with $\mathbf{F} = \mathbf{R}$, that

$$\mathscr{M}(\mathbf{R})[\nabla\mathbf{n} + \bar{\mathbf{g}} \otimes \mathbf{k}] \cdot (\nabla\mathbf{n} + \bar{\mathbf{g}} \otimes \mathbf{k}) = \mathbf{B} \cdot \mathscr{C}(\mathbf{0})[\mathbf{B}], \tag{84}$$

where

$$\mathbf{B} = \mathbf{R}^t[\nabla\mathbf{n} + \bar{\mathbf{g}} \otimes \mathbf{k}] \tag{85}$$

is the bending strain [1, 11].

Further, (74) implies that E_b furnishes the rigorous leading-order energy for isometric deformations of the midplane in the limit as thickness tends to zero. This result is in precise agreement with that obtained by formal asymptotic expansions [3] and the method of gamma convergence [1]. Nevertheless the result is not entirely satisfactory. For, Gauss' *Theorema Egregium* implies that the deformed midsurface is necessarily developable; i.e, that it is a cylinder or a cone. Accordingly E_b does not furnish a model of plates that can be used in general applications. In view of this fact one is forced to conclude, in keeping with Koiter's remark, that its rigorous derivation via gamma convergence is a somewhat overstated achievement as far as applications are concerned.

5 Asymptotic Model for Combined Bending and Stretching

Having derived the order—h^3 expansion of the potential energy for a three-dimensional deformation (cf. (5), (40), (41)), we use it to derive energetically optimal director fields $\mathbf{d}$ and $\mathbf{g}$ for a given midplane deformation $\mathbf{r}$. That is, we minimize the energy with respect to these director fields at a fixed midplane deformation. Accordingly, we impose the stationarity condition

$$h\dot{E}_1 + h^3\dot{E}_3 + o(h^3) = 0, \tag{86}$$

in which the superposed dot refers to the variational (or Gateaux) derivative. We regard this as an asymptotic expansion of the three-dimensional equilibrium statement $\mathscr{E}^{\cdot} = 0$. Accordingly, we require

$$\dot{E}_1 = 0 \quad \text{and} \quad \dot{E}_3 = 0. \tag{87}$$

The first of these follows simply on dividing (86) by h and evaluating the resulting equation in the limit $h \to 0$; the second result then follows on division by h^3 and passage to the same limit.

For a fixed midplane deformation ($\dot{\mathbf{r}} = 0$), Eq. $(87)_1$ reduces to

$$\int_{\Omega} \mathscr{W}_{\mathbf{F}} \cdot \dot{\mathbf{d}} \otimes \mathbf{k} da = 0 \tag{88}$$

in which the variation $\dot{\mathbf{d}}$ is arbitrary in Ω. This is valid under both dead-load and pressure loading conditions, with $n = 3$ in the latter case (cf. (48)). Accordingly, by the Fundamental Lemma,

$$\mathbf{Pk} = \mathbf{0} \quad \text{in} \quad \Omega, \tag{89}$$

where $\mathbf{P} = \tilde{\mathbf{P}}(\nabla\mathbf{r} + \mathbf{d} \otimes \mathbf{k})$. This is precisely the plane-stress condition (56), yielding $\mathbf{d} = \bar{\mathbf{d}}(\nabla\mathbf{r})$ and thus determining $\mathbf{d}$ in terms of the midplane deformation field $\mathbf{r}$. Because we are considering the latter to be fixed, Eq. $(87)_2$ reduces to

$$\int_{\Omega}\{2\mathscr{M}(\mathbf{F})[\nabla\bar{\mathbf{d}}+\mathbf{g}\otimes\mathbf{k}]\cdot\dot{\mathbf{g}}\otimes\mathbf{k}+\mathbf{P}\cdot(\nabla\dot{\mathbf{g}}+\dot{\mathbf{h}}\otimes\mathbf{k})\}da-\int_{\partial\Omega_n}\mathbf{p}\cdot\dot{\mathbf{g}}ds=0, \tag{90}$$

where the major symmetry of $\mathscr{M}$ has been invoked. This also applies in the case of conservative pressure loading with $n=3$ in (48) and with $\partial\Omega_n=\emptyset$. Invoking (89) and integrating the term involving $\nabla\dot{\mathbf{g}}$ by parts, using $\dot{\mathbf{g}}_{|\partial\Omega_e}=\mathbf{0}$, we reduce this to

$$\int_{\Omega}[2\mathbf{P}'\mathbf{k}-div(\mathbf{P1})]\cdot\dot{\mathbf{g}}da+\int_{\partial\Omega_n}(\mathbf{P1}\nu-\mathbf{p})\cdot\dot{\mathbf{g}}ds=0 \tag{91}$$

which implies that

$$2\mathbf{P}'\mathbf{k}=div(\mathbf{P1})\quad\text{in}\quad\Omega\quad\text{and}\quad\mathbf{p}=\mathbf{P1}\nu\quad\text{on}\quad\partial\Omega_n. \tag{92}$$

The second of these results is of course in precise agreement with the three-dimensional theory. However, the first is not. To see this we note that in the three-dimensional theory (3) holds at all points of the plate and hence on the midplane in particular, where it reduces to

$$div(\mathbf{P1})+\mathbf{P}'\mathbf{k}=\mathbf{0}. \tag{93}$$

We attempt to reconcile this with $(92)_1$ by using the three-dimensional theory to relate $\mathbf{P}'\mathbf{k}$ to the tractions $\tilde{\mathbf{p}}^{\pm}$ at the upper and lower lateral surfaces of the plate. With $\mathbf{N}=\pm\mathbf{k}$ as appropriate, a Taylor expansion of (2) furnishes

$$\tilde{\mathbf{p}}^{\pm}=\hat{\mathbf{p}}(\mathbf{u},\pm h/2)=\pm\mathbf{P}\mathbf{k}+(h/2)\mathbf{P}'k\pm(h^2/8)\mathbf{P}''\mathbf{k}+O(h^3). \tag{94}$$

Equivalently,

$$\tilde{\mathbf{p}}^{+}+\tilde{\mathbf{p}}^{-}=h\mathbf{P}'k+O(h^3)\quad\text{and}\quad\tilde{\mathbf{p}}^{+}-\tilde{\mathbf{p}}^{-}=2\mathbf{P}\mathbf{k}+O(h^2). \tag{95}$$

Then, if $\tilde{\mathbf{p}}^{\pm}=O(h^3)$, as in the case of pressure loading with $n=3$ (cf. (43)), we conclude that

$$\mathbf{P}\mathbf{k}=O(h^2)\quad\text{and}\quad\mathbf{P}'k=O(h^2). \tag{96}$$

The first of these is consistent with the prediction (89), whereas the second implies that $(92)_1$ and (93) are consistent with each other in the sense that both yield the estimate $div(\mathbf{P1})=O(h^2)$. With this information we may re-write (41) as

$$\begin{aligned}24E_3=&\int_{\Omega}\{\mathscr{M}(\mathbf{F})[\nabla\mathbf{d}+\mathbf{g}\otimes\mathbf{k}]\cdot(\nabla\mathbf{d}+\mathbf{g}\otimes\mathbf{k})\}da+\int_{\partial\Omega_e}\mathbf{P1}\nu\cdot\mathbf{g}ds\\&-\int_{\partial\Omega_n}(\mathbf{p}''\cdot\mathbf{r}+2\mathbf{p}'\cdot\mathbf{d})ds+O(h^2).\end{aligned} \tag{97}$$

where we have made use $(92)_2$ and (89), the latter implying that $\mathbf{d} = \bar{\mathbf{d}}(\nabla \mathbf{r})$, which we assume to hold on the closure of Ω. Recalling that E_3 is multiplied by h^3 in the expansion (5), we are justified in suppressing terms of order $O(h^2)$ in E_3 as this does not affect the accuracy of the expansion. For consistency we must then suppress $\mathbf{P}'\mathbf{k}$; i.e., we must impose

$$\{\mathscr{M}(\mathbf{F})[\nabla \bar{\mathbf{d}} + \mathbf{g} \otimes \mathbf{k}]\}\mathbf{k} = \mathbf{0}, \tag{98}$$

which, as we have seen in the case of pure bending, uniquely determines $\mathbf{g} = \bar{\mathbf{g}}(\nabla \mathbf{r}, \nabla\nabla \mathbf{r})$ in Ω. With $\mathbf{g}_{|\partial\Omega_e}$ fixed by the data for the three-dimensional parent model, and with $\mathbf{P}$ now determined by $\nabla \mathbf{r}$, we conclude that if the part $\partial\Omega_e$ of the boundary is clamped; i.e., if $\mathbf{r}$ and the normal derivative $\mathbf{r}_{,\nu}$ are assigned thereon, then the full gradient $\nabla \mathbf{r}$, consisting of the normal and tangential derivatives of $\mathbf{r}$, is likewise fixed on $\partial\Omega_e$ and hence that the integral $\int_{\partial\Omega_e} \mathbf{P}\mathbf{1}\nu \cdot \mathbf{g} ds$ is fixed by the data. Accordingly its variational derivative vanishes and the energy may be effectively reduced to

$$24E_3 = \int_\Omega \mathscr{M}(\mathbf{F})[\nabla \bar{\mathbf{d}} + \bar{\mathbf{g}} \otimes \mathbf{k}] \cdot (\nabla \bar{\mathbf{d}} + \bar{\mathbf{g}} \otimes \mathbf{k}) da - \int_{\partial\Omega_n} (\mathbf{p}'' \cdot \mathbf{r} + 2\mathbf{p}' \cdot \bar{\mathbf{d}}) ds, \tag{99}$$

which is a functional of $\mathbf{r}$ alone. Because of (98) we may simplify the first integrand to

$$\mathscr{M}(\mathbf{F})[\nabla \bar{\mathbf{d}} + \bar{\mathbf{g}} \otimes \mathbf{k}] \cdot (\nabla \bar{\mathbf{d}} + \bar{\mathbf{g}} \otimes \mathbf{k}) = \mathbf{P}'\mathbf{1} \cdot \nabla \bar{\mathbf{d}}, \tag{100}$$

but we refrain from doing this so as to preserve the symmetry of the original expression.

With the foregoing results in effect the approximate energy becomes

$$\begin{aligned} E = h \left\{ \int_\Omega \mathscr{W}(\nabla \mathbf{r} + \bar{\mathbf{d}} \otimes \mathbf{k}) da - \int_{\partial\Omega_n} \mathbf{p} \cdot \mathbf{r}\, ds \right\} \\ + \tfrac{1}{24} h^3 \left\{ \int_\Omega \mathscr{M}(\mathbf{F})[\nabla \bar{\mathbf{d}} + \bar{\mathbf{g}} \otimes \mathbf{k}] \cdot (\nabla \bar{\mathbf{d}} + \bar{\mathbf{g}} \otimes \mathbf{k}) da \right. \\ \left. - \int_{\partial\Omega_n} (\mathbf{p}'' \cdot \mathbf{r} + 2\mathbf{p}' \cdot \bar{\mathbf{d}}) ds \right\}, \end{aligned} \tag{101}$$

in the case of dead loading, in which $\mathbf{p}$, $\mathbf{p}'$ and $\mathbf{p}''$ are assigned on $\partial\Omega_n$. In the case of pressure loading with $n = 3$ in (48), the relevant energy is

$$\begin{aligned} E = h \int_\Omega \mathscr{W}(\nabla \mathbf{r} + \bar{\mathbf{d}} \otimes \mathbf{k}) da + \tfrac{1}{24} h^3 \int_\Omega \mathscr{M}(\mathbf{F})[\nabla \bar{\mathbf{d}} + \bar{\mathbf{g}} \otimes \mathbf{k}] \cdot (\nabla \bar{\mathbf{d}} + \bar{\mathbf{g}} \otimes \mathbf{k}) da \\ - h^3 \left[\int_{V_0^-}^{V} P^-(x) dx - P^+ V \right]. \end{aligned} \tag{102}$$

In both cases this energy is a functional of the midplane deformation alone.

The solution $\bar{\mathbf{g}}$ to (98) involves the gradient $\nabla\bar{\mathbf{d}}$ and may thus be expressed in terms of the first and second gradients, $\nabla\mathbf{r}$ and $\nabla\nabla\mathbf{r}$ respectively, of the midsurface deformation function $\mathbf{r}(\mathbf{u})$. To derive the explicit form of this function we observe that the function $\bar{\mathbf{d}}(\nabla\mathbf{r})$ satisfies (56) identically in $\nabla\mathbf{r}$. We write the latter in the form

$$\partial\mathscr{W}/\partial F_{i3} \equiv 0, \tag{103}$$

where $F_{i3} = d_i$, and differentiate with respect to $\nabla\mathbf{r} = r_{i,\alpha}\mathbf{e}_i \otimes \mathbf{e}_\alpha$ (with $\mathbf{e}_3 = \mathbf{k}$), obtaining

$$\mathscr{M}_{i3j\beta} + \mathscr{A}_{ik}K_{kj\beta} = 0, \tag{104}$$

where $\mathscr{A}_{ik}$ are the components of the acoustic tensor defined in (62) and

$$K_{kj\beta} = \partial\bar{d}_k/\partial r_{j,\beta}. \tag{105}$$

Accordingly,

$$K_{kj\beta} = -\mathscr{A}_{ki}^{-1}\mathscr{M}_{i3j\beta}, \tag{106}$$

and the chain rule yields

$$\bar{d}_{i,\alpha} = K_{ij\beta}r_{j,\beta\alpha}. \tag{107}$$

Then, combining (77) in the form

$$\mathscr{A}_{ik}g_k = -\mathscr{M}_{i3j\alpha}\bar{d}_{j,\alpha} \tag{108}$$

with (106), we conclude that

$$\bar{g}_i(\nabla\mathbf{r},\nabla\nabla\mathbf{r}) = K_{ij\alpha}\bar{d}_{j,\alpha} = K_{ij\alpha}K_{jk\beta}r_{k,\alpha\beta} \tag{109}$$

and hence that the second integrand in (101) (or (102)) is a homogeneous quadratic function of the 2nd derivatives $r_{k,\alpha\beta}$. Moreover, as noted in the discussion of pure-bending theory, $\bar{\mathbf{g}}$ minimizes the energy E with respect to $\mathbf{g}$.

The patient reader may well wonder why the midplane deformation $\mathbf{r}$ was held fixed ($\dot{\mathbf{r}} = 0$) in $(87)_{1,2}$. The reason is that $(87)_1$ would otherwise yield the membrane problem which, as we have seen, fails to possess a solution unless the energy is replaced by its relaxation, whereas the purpose of the order—h^3 expansion is to regularize the membrane problem. In this case it is logical to regard E as the operative approximate energy and to render it stationary with respect to $\mathbf{r}$ to derive the relevant equilibrium problem. However, it transpires, rather unexpectedly, that the minimization problem for E is also typically ill-posed.

6 Reflection Symmetry and Ill-Posedness

As we have noted, there is no reason to suppose that minimizers of E, if any, are related to those of the three-dimensional energy $\mathscr{E}$. Nevertheless, it is of interest to determine whether or not E admits minimizers. If a deformation $\mathbf{r}$ minimizes E, then it satisfies the operative Legendre-Hadamard condition pointwise in Ω. In the present context this is the requirement that the part of the energy density that is homogeneous quadratic in the 2nd derivatives $r_{i,\alpha\beta}$ be non-negative definite when the $r_{i,\alpha\beta}$ are replaced by $v_i b_\alpha b_\beta$, with v_i an arbitrary 3-vector and b_α an arbitrary 2-vector [24]. This restriction affects only the 2nd integrand in (101) (or (102)), which has the component form

$$I = \mathscr{M}_{i\alpha j\beta}\bar{d}_{i,\alpha}\bar{d}_{j,\beta} + 2\mathscr{M}_{i\alpha j3}\bar{d}_{i,\alpha}\bar{g}_j + \mathscr{M}_{i3j3}\bar{g}_i\bar{g}_j. \tag{110}$$

Substituting (107) and (106), after some algebra we obtain

$$I = G_{i\alpha j\beta}K_{ik\lambda}K_{jl\mu}r_{k,\lambda\alpha}r_{l,\beta\mu}, \tag{111}$$

where

$$G_{i\alpha j\beta} = \mathscr{M}_{i\alpha j\beta} - A_{kl}K_{ki\alpha}K_{lj\beta}. \tag{112}$$

The relevant Legendre-Hadamard condition is thus given by

$$G_{i\alpha j\beta}a_i a_j b_\alpha b_\beta \geq 0, \quad \text{where} \quad a_i = K_{ij\beta}v_j b_\beta, \tag{113}$$

and this must hold for every v_i and b_α.

It transpires that $G_{i\alpha j\beta} = E_{i\alpha j\beta}$, the moduli for pure membrane theory (cf. (67)). To see this we compute a further derivative of (65), obtaining

$$\begin{aligned} E_{i\alpha j\beta} &= \partial^2\mathscr{W}/\partial F_{i\alpha}\partial F_{j\beta} + (\partial^2\mathscr{W}/\partial F_{i\alpha}\partial d_k)K_{kj\beta} \\ &= \mathscr{M}_{i\alpha j\beta} + \mathscr{M}_{i\alpha k3}K_{kj\beta} \\ &= \mathscr{M}_{i\alpha j\beta} - A_{kl}K_{li\alpha}K_{kj\beta}, \end{aligned} \tag{114}$$

and the claim follows on comparison with (112).

In view of the discussion leading to (73) and (69), we conclude that if a_i can be chosen to be aligned with the normal to the deformed midsurface, then minimizers of E must again deliver a plane 2nd Piola-Kirchhoff stress field that is pointwise positive semi-definite. Hilgers and Pipkin [7] have shown that this situation obtains in the practically important case in which the three-dimensional material possesses reflection symmetry with respect to the midplane Ω; i.e., $\mathscr{U}(\mathbf{E}) = \mathscr{U}(\mathbf{QEQ}^t)$, with $\mathbf{Q} = \mathbf{I} - 2\mathbf{k}\otimes\mathbf{k}$. This severe restriction on the state of stress implies that minimizers of E generally fail to exist and therefore that solution procedures relying on the construction of energy-minimizing sequences of deformations cannot be applied. This is a serious drawback for the practical implementation of the theory.

We conclude that the minimization problem for E is generally ill-posed, despite the fact that the fields $\bar{\mathbf{d}}$ and $\bar{\mathbf{g}}$ minimize the energy for any given midsurface position field. In [7] this is addressed by introducing ad hoc strain-gradient terms which ensure that the Legendre-Hadamard condition is automatically satisfied without qualification. However, these regularizing terms are unrelated to the three-dimensional parent theory. Accordingly, in [7] the existence issue is addressed at the expense of accuracy.

7 Koiter's Model

Another way to cure the problematic ill-posedness of E is simply to suppress the contribution of the stress to the order—h^3 term in the energy. To justify this simplification we may suppose that $S_{\alpha\beta} = O(h)$ at the outset. The constitutive hypotheses discussed in Sect. 1 then imply that the strain $\epsilon_{\alpha\beta} = O(h)$, so that

$$S_{\alpha\mu} = D_{\alpha\mu\beta\lambda}(\mathbf{0})\epsilon_{\beta\lambda} + o(h), \tag{115}$$

where $D_{\alpha\mu\beta\lambda}(\mathbf{0})$ are the classical plane-stress elastic moduli evaluated at zero strain. In view of (11) the stress $\mathbf{S}$ may then be suppressed in the second integral in (101) (or (102)) without affecting the order—h^3 accuracy of E. The operative Legendre-Hadamard condition (113) is then reduced, with the aid of (71), to the inequality

$$D_{\alpha\mu\beta\lambda}(\mathbf{0})y_\alpha w_\mu y_\beta w_\lambda \geq 0, \tag{116}$$

where $w_\mu = a_i F_{i\mu}$ and a_i is given by $(113)_2$. That this inequality is automatically satisfied may be seen on observing that, for any $\mathbf{A}$,

$$0 \leq \mathbf{A} \cdot \mathscr{C}(\mathbf{0})[\mathbf{A}] = D_{\alpha\mu\beta\lambda}(\mathbf{0})A_{\alpha\mu}A_{\beta\lambda} \tag{117}$$

in the present circumstances, and choosing $A_{\alpha\mu} = y_\alpha w_\mu$.

In the present circumstances the midplane strain energy is approximated by $\frac{1}{2}D_{\alpha\mu\beta\lambda}(\mathbf{0})\epsilon_{\alpha\mu}\epsilon_{\beta\lambda} + o(h^2)$. Because this is multiplied by h in (101) (or (102)), we then have that $\mathscr{E}/h^3 = \bar{E} + o(h^3)/h^3$ where $\bar{E}$ involves the sum of the integrals of a homogeneous quadratic function of the surface strain and a homogeneous quadratic function of the bending strain. Thus energy minimizers in the parent theory minimize $\bar{E}$ at leading order in h. Further, the minimization problem for $\bar{E}$ is well posed [20]. Remarkably, $\bar{E}$ is precisely Koiter's energy for combined bending and stretching [9, 13].

The difficulty, of course, is that the magnitude of the stress $S_{\alpha\beta}$ is not known a priori and thus that the assumptions underpinning Koiter's model, if true, can only be justified a posteriori. Fortunately, the feasibility of such a procedure is assured by the existence of minimizers of Koiter's energy.

8 Proposed Model

It is important for the sake of practical analysis to have a well-posed order—h^3 model for combined stretching and bending for use in general applications. This need stems from the availability and utility of robust numerical methods for computing energy minimizers directly and from the fact that it is not possible to exert control over the stress field *a priori*, as required in the establishment of Koiter's energy on the basis of the three-dimensional theory. Further, it is unlikely that the community will accept a much more complex model based on higher-order expansion of the energy, its potential well-posedness notwithstanding.

To secure the desired model we note, with reference to (110) and (113), that the source of ill-posedness stems from the role played by the membrane moduli in the order—h^3 term in the energy functional E. This in turn arises due to the use of the solution $\bar{\mathbf{g}}$ to (98) in the same term. To avoid this, we replace (101) (or (102)) by

$$E'[\mathbf{r}, \mathbf{g}] = \int_\Omega W'(\nabla\mathbf{r}, \nabla\nabla\mathbf{r}, \mathbf{g})da - L, \tag{118}$$

where

$$W' = h\mathscr{W}(\nabla\mathbf{r} + \bar{\mathbf{d}} \otimes \mathbf{k}) + \tfrac{1}{24}h^3\mathscr{M}(\nabla\mathbf{r} + \bar{\mathbf{d}} \otimes \mathbf{k})[\nabla\bar{\mathbf{d}} + \mathbf{g} \otimes \mathbf{k}] \cdot (\nabla\bar{\mathbf{d}} + \mathbf{g} \otimes \mathbf{k}), \tag{119}$$

in which $\mathbf{d} = \bar{\mathbf{d}}(\nabla\mathbf{r})$ is imposed but the fields $\mathbf{r}(\mathbf{u})$ and $\mathbf{g}(\mathbf{u})$ are independent; i.e., we do *not* impose $\mathbf{g} = \bar{\mathbf{g}}$. The Euler equation for $\mathbf{g}$, namely $W'_{\mathbf{g}} = \mathbf{0}$, is equivalent to (98), which furnishes $\mathbf{g} = \bar{\mathbf{g}}$. It follows that, *in equilibrium*, $E'[\mathbf{r}, \mathbf{g}]$ and the order—h^3 plate energy are equivalent insofar as the Euler equations and natural boundary conditions are concerned (see [12] for a derivation). Thus the equilibria of the order—h^3 energy are precisely the equilibria of $E'[\mathbf{r}, \mathbf{g}]$. Moreover, these equilibria render the two functionals equal.

To elaborate, consider the first variation

$$\dot{E}' = \int_\Omega [(\partial W'/\partial r_{i,\alpha})\dot{r}_{i,\alpha} + (\partial W'/\partial r_{i,\alpha\beta})\dot{r}_{i,\alpha\beta} + (\partial W'/\partial g_i)\dot{g}_i]da, \tag{120}$$

in which we have suppressed the load potential, which is not relevant to the present discussion. Equilibria in the approximate theory are, by definition, those states for which $\dot{E}'$ vanishes for all kinematically admissible variations $\dot{r}_i$ and $\dot{g}_i$. This yields $\partial W'/\partial g_i = 0$ in particular, which of course has the unique solution $\mathbf{g} = \bar{\mathbf{g}}(\nabla\mathbf{r}, \nabla\nabla\mathbf{r})$. Accordingly,

$$\tfrac{\partial W'}{\partial g_i}(\nabla\mathbf{r}, \nabla\nabla\mathbf{r}, \bar{\mathbf{g}}(\nabla\mathbf{r}, \nabla\nabla\mathbf{r})) \equiv 0 \tag{121}$$

for all $\nabla\mathbf{r}$ and $\nabla\nabla\mathbf{r}$. Differentiation of this identity yields

$$\partial^2 W'/\partial g_i \partial r_{j,\alpha} = 0 \quad \text{and} \quad \partial^2 W'/\partial g_i \partial r_{j,\alpha\beta} = 0, \tag{122}$$

which may be used to simplify the *equilibrium* expression for the second variation $\ddot{E}'$ accordingly. Thus,

$$\begin{aligned}\ddot{E}' = &\int_\Omega [(\partial W'/\partial r_{i,\alpha})\ddot{r}_{i,\alpha} + (\partial W'/\partial r_{i,\alpha\beta})\ddot{r}_{i,\alpha\beta} + (\partial W'/\partial g_i)\ddot{g}_i]da \\ &+ \int_\Omega [(\partial^2 W'/\partial r_{i,\alpha}\partial r_{j,\beta})\dot{r}_{i,\alpha}\dot{r}_{j,\beta} + (\partial^2 W'/\partial r_{i,\alpha}\partial r_{j,\beta\mu})\dot{r}_{i,\alpha}\dot{r}_{j,\beta\mu} \\ &+(\partial^2 W'/\partial r_{i,\alpha\mu}\partial r_{j,\beta})\dot{r}_{i,\alpha\mu}\dot{r}_{j,\beta} \\ &+(\partial^2 W'/\partial r_{i,\alpha\mu}\partial r_{j,\beta\lambda})\dot{r}_{i,\alpha\mu}\dot{r}_{j,\beta\lambda}]da \\ &+ \int_\Omega (\partial^2 W'/\partial g_i\partial g_j)\dot{g}_i\dot{g}_j da, \end{aligned} \tag{123}$$

in which the first line vanishes due to the stationarity condition $\dot{E}' = 0$ (cf. (120)) and all parenthetical terms are evaluated at the equilibrium state. Thus in equilibrium the second variation is a quadratic functional of $\dot{\mathbf{r}}$ and $\dot{\mathbf{g}}$.

We now fix $\dot{\mathbf{r}}$ and minimize the second variation with respect to $\dot{\mathbf{g}}$. This yields the stationarity condition

$$\int_\Omega (\partial^2 W'/\partial g_i\partial g_j)\dot{g}_j\ddot{g}_i da = 0, \tag{124}$$

which in turn implies that

$$(\partial^2 W'/\partial g_i\partial g_j)\dot{g}_j = 0 \tag{125}$$

pointwise in Ω. The coefficient matrix is seen, with reference to (82), to be $\partial^2 W'/\partial g_i\partial g_j = \frac{1}{12}\mathscr{A}_{ij}$, where $\mathscr{A}$ is the positive definite acoustic tensor defined in (62). Thus the minimizing value is $\dot{\mathbf{g}} = 0$ and the second variation reduces to

$$\begin{aligned}\ddot{E}' = &\int_\Omega [(\partial^2 W'/\partial r_{i,\alpha}\partial r_{j,\beta})\dot{r}_{i,\alpha}\dot{r}_{j,\beta} + (\partial^2 W'/\partial r_{i,\alpha}\partial r_{j,\beta\mu})\dot{r}_{i,\alpha}\dot{r}_{j,\beta\mu} \\ &+(\partial^2 W'/\partial r_{i,\alpha\mu}\partial r_{j,\beta})\dot{r}_{i,\alpha\mu}\dot{r}_{j,\beta} \\ &+(\partial^2 W'/\partial r_{i,\alpha\mu}\partial r_{j,\beta\lambda})\dot{r}_{i,\alpha\mu}\dot{r}_{j,\beta\lambda}]da \end{aligned} \tag{126}$$

at equilibrium. This is non-negative for all kinematically admissible $\dot{\mathbf{r}}$ if the deformation $\mathbf{r}$ is a minimizer of E'.

The operative Legendre-Hadamard necessary condition for minimizers in this case is the requirement that

$$(\partial^2 W'/\partial r_{i,\alpha\mu}\partial r_{j,\beta\lambda})v_i v_j b_\alpha b_\beta b_\mu b_\lambda \geq 0 \tag{127}$$

pointwise in Ω, for all v_i and b_a [24]. With reference to (107) and (119), this is found to be equivalent to

$$\mathscr{M}_{i\alpha j\beta}a_i a_j b_\alpha b_\beta \geq 0, \tag{128}$$

where the a_i are given by $(113)_2$ and $\mathscr{M}$ is evaluated at an equilibrium deformation. That this is so is an immediate consequence of three-dimensional strong ellipticity. Accordingly, the Legendre-Hadamard condition for (118) is automatically satisfied and imposes no a priori restrictions on the stress. This means that $E'[\mathbf{r}, \mathbf{g}]$ meets a fundamental necessary condition for the existence of minimizers without qualification, whereas the order—h^3 energy does so only under restrictive conditions which cannot be verified a priori. It is therefore appropriate to regard equilibria in the order—h^3 model as minimizers of $E'[\mathbf{r}, \mathbf{g}]$, although it remains to be proved that this functional actually possesses a minimizer. This question, which remains open, is addressed to the mathematically inclined reader.

Acknowledgements We gratefully acknowledge the support of the US National Science Foundation through grant CMMI-1538228.

References

1. Friesecke, G., James, R.D., Müller, S.: A hierarchy of plate models derived from nonlinear elasticity by gamma-convergence. Arch. Ration. Mech. Anal. **180**, 183–236 (2006)
2. Ciarlet, P.G.: Mathematical Elasticity, Vol. 3: Theory of Shells. North-Holland, Amsterdam (2000)
3. Fox, D.D., Raoult, A., Simo, J.C.: A justification of nonlinear properly invariant plate theories. Arch. Ration. Mech. Anal. **124**, 157–199 (1993)
4. Koiter, W.T.: Foundations and basic equations of shell theory. A survey of recent progress. In: Niordson, F.I. (Ed.) Theory of Thin Shells, Proceedings IUTAM Symposium, Copenhagen, pp. 93–15. Springer, Berlin (1969)
5. Hilgers, M.G., Pipkin, A.C.: Elastic sheets with bending stiffness. Q. Jl. Mech. Appl. Math. **45**, 57–75 (1992)
6. Hilgers, M.G., Pipkin, A.C.: Bending energy of highly elastic membranes. Quart. Appl. Math. **50**, 389–400 (1992)
7. Hilgers, M.G., Pipkin, A.C.: Bending energy of highly elastic membranes II. Quart. Appl. Math. **54**, 307–316 (1996)
8. Koiter, W.T.: A consistent first approximation in the general theory of thin elastic shells. In: Koiter, W.T. (Ed.) Proceedings IUTAM Symposium on the Theory of Thin Elastic Shells, Delft, pp. 12–33. North-Holland, Amsterdam (1960)
9. Koiter, W.T.: On the nonlinear theory of thin elastic shells. In: Proceedings Knonklijke Nederlandse Akademie van Wetenschappen B69, pp. 1–54 (1966)
10. Song, Z.L., Dai, H.-H.: On a consistent dynamic finite-strain plate theory and its linearization. J. Elast. **125**, 149–183 (2016)
11. Steigmann, D.J.: Thin-plate theory for large elastic deformations. Int. J. Non-linear Mech. **42**, 233–240 (2007)
12. Steigmann, D.J.: Applications of polyconvexity and strong ellipticity to nonlinear elasticity and elastic plate theory. In: Schröder, J., Neff, P. (Eds.) CISM Course on Applications of Poly-, Quasi-, and Rank-One Convexity in Applied Mechanics, vol. 516, pp. 265–299. Springer, Wien and New York (2010)
13. Steigmann, D.J.: Koiter's shell theory from the perspective of three-dimensional nonlinear elasticity. J. Elast. **111**, 91–107 (2013)
14. Steigmann, D.J.: Mechanics of materially-uniform thin films. Math. Mech. Solids **20**, 309–326 (2015)

15. de Feraudy, A., Queguineur, M., Steigmann, D.J.: On the natural shape of a plastically deformed thin sheet. Int. J. Non-lin. Mech. **67**, 378–381 (2014)
16. Paroni, R.: Theory of linearly elastic residually stressed plates. Math. Mech. Solids **11**, 137–159 (2006)
17. Cerda, E., Mahadevan, L.: Geometry and physics of wrinkling. Phys. Rev. Lett. **90**, 1–4 (2003)
18. Healey, T.J., Li, Q., Cheng, R.-B.: Wrinkling behavior of highly stretched rectangular elastic films via parametric global bifurcation. J. Nonlin. Sci. **23**, 777–805 (2013)
19. Taylor, M., Bertoldi, K., Steigmann, D.J.: Spatial resolution of wrinkle patterns in thin elastic sheets at finite strain. J. Mech. Phys. Solids **62**, 163–180 (2014)
20. Ciarlet, P.G.: An Introduction to Differential Geometry with Applications to Elasticity. Springer, Dordrecht (2005)
21. Ball, J.M.: Convexity conditions and existence theorems in nonlinear elasticity. Arch. Ration. Mech. Anal. **63**, 337–403 (1977)
22. Healey, T.J., Rosakis, P.: Unbounded branches of classical injective solutions to the forced displacement problem in nonlinear elastostatics. J. Elast. **49**, 65–78 (1997)
23. Steigmann, D.J.: Proof of a conjecture in elastic membrane theory. ASME J. Appl. Mech. **53**, 955–956 (1986)
24. Hilgers, M.G., Pipkin, A.C.: The Graves condition for variational problems of arbitrary order. IMA. J. Appl. Math. **48**, 265–269 (1992)
25. Dacarogna, B.: Direct Methods in the Calculus of Variations. Springer, Berlin (1989)
26. Steigmann, D.J.: Tension-field theory. Proc. R. Soc. Lond. **A429**, 141–73 (1990)
27. Le Dret, H., Raoult, A.: The membrane shell model in nonlinear elasticity: a variational asymptotic derivation. J. Nonlin. Sci. **6**, 59–84 (1996)

Selected Stability Problems of Thin-Walled Columns and Beams

Czesław Szymczak and Marcin Kujawa

Abstract The article reviews a number of papers in the light of buckling analysis of thin-walled columns and beams. Stability of thin-walled columns and beams are considered a vital engineering science issue in both historical and present-day approaches. The paper refers to the recent authors' works of the 2012–2019 period, published in leading journals. Similar review of stability problems of thin-walled structures developed at Gdansk University of Technology is published in Szymczak (A review of stability problems of thin-walled structures developed at Gdansk University of Technology, 69–78, 2003, [58]), Szymczak (Selected problems of stability of thin-walled columns with bisymmetric cross-section, 111–128, 2012, [59]). This paper is a continuation of the earlier reviews. Only selected references are given.

1 Introduction

Scientists and engineers have studied structural stability since the turn of the 18th and 19th centuries. The classical stability solution of a column under compression was worked by Euler [12] (the solution of critical loads of columns with various end conditions), Lagrange [33] (post-buckling path analysis), Young [75] (the impact of initial curvature imperfections, bending moments and load eccentricity), Kirchhoff [24] (the theory of large deflections) and Engesser [11] (the shear effect in columns of low effective shear stiffness).

In the next step the flexibility method was developed due to frame stability problems by Mises [41], Mises and Ratzersdorfer [42, 43], Chwalla [10] (the flexibility

C. Szymczak
Faculty of Ocean Engineering and Ship Technology, Department of Structural Engineering, Gdansk University of Technology, G. Narutowicza 11/12, 80-233 Gdańsk, Poland
e-mail: szymcze@pg.edu.pl

M. Kujawa (✉)
Faculty of Civil and Environmental Engineering, Department of Structural Mechanics, Gdansk University of Technology, G. Narutowicza 11/12, 80-233 Gdańsk, Poland
e-mail: mark@pg.edu.pl

H. Altenbach et al. (eds.), *Recent Developments in the Theory of Shells*,
Advanced Structured Materials 110, https://doi.org/10.1007/978-3-030-17747-8_31

matrix) the matrix stiffness method was implemented by James [22] (the stiffness matrix), Livesley and Chandler [36]. The historical context of stability methods is included in Timoshenko [67], Kurrer [32], Bažant and Cedolin [3], Todhunter [69]. Since the 1950s up till now the structural stability issue has been regarded in Pflüger [46], Bleich [5], Kollbrunner et al. [25], Gerard [15], Timoshenko and Gere [68], Horne and Merchant [20], Leipholz [34], Chajes [8], Brush [6], Iyengar [21], Waszczyszyn et al. [73], Kowal-Michalska and Mania [26], the review papers [17, 18] and more [47–50]. The increasing column compressive load obviously leads to stability loss whose failure modes may be classified global (flexural, torsional or flexural-torsional), local or distortional with regard to the cross-section, column length and material parameters. Stability loss is naturally a non-linear and quasi-static phenomenon, thus its study brought about a high effort due to its mathematical form, including the classification of post-buckling behaviour (supercritical/post-critical). Further development in the field is bound to caver analytical, experimental and numerical research, in order to expand both theoretical description and phenomenological inquiry on structural stability loss. The body equilibrium stability problem is regarded in a collection of works by Lyapunov [37] as specific case of motion stability of a body, the so-called kinematic stability criterion. If a general criterion for stability loss takes a purely static form without any dynamic elements, it renames to the static stability criterion. Regardless of the criterion, the stability limit is usually achieved within the elastic material performance. Thus the stability problem reduces to the investigation of linear or possibly non-linear, elastic scenarios. The general stability criterion form results from the principle of energy conservation or, more strictly, the principle of relative minimum potential energy. The condition of minimum energy is necessary and sufficient in stability analysis. The total potential energy of a given system, U may be expressed as the sum of the potential energy of elastic deformation and the potential energy linked with external forces (with an opposite sign). The potential energy function is usually expanded in Taylor series with regard to the first nonzero term, decisive for equilibrium stability of the system (the quadratic term is generally the case). The necessary critical state condition (the neutral equilibrium criterion) is usually translated into a zero value of the first variation of U. The state of the system is stable if $\delta U > 0$, critical if $\delta U = 0$ and unstable if $\delta U < 0$ (the cases based on the so-called principle of stationary potential energy). While the n-th variation of the potential energy is zero ($\delta U = \delta^2 U = \delta^n U = 0$), the state of the system is determined by the sign of $\delta^{n+1} U$.

Various approximate methods are incorporated in the analysis of stability. The classical methods are:

- analytical methods: energy (variational) methods [25, 40, 52, 72], orthogonalization methods [72] (overestimating the critical loads), the kernel trace method for integral equations [72] (underestimating the critical loads), the method of assumed exact solutions [72] (the case of elastic-plastic stability analysis), the collocation method [4, 72] and the iterative method [25, 72],
- numerical methods: the finite difference method (FDM) [56], the generalised beam theory (GBT) [1, 7, 16, 54, 55], the finite strip method (FSM) [9, 19, 35, 53] and the finite element method (FEM) [51, 77].

The development in mathematical stability formulation coincides with the experimental research. The research results show that the theoretical prediction may drop beyond the real structural behaviour. Discrepancies typically occur in imperfect. Geometrical and material flaws make the structure to reach the critical state (or limit state) much earlier (in certain specific cases, however, it can be reached much later) than the theory predicts. In engineering practice the influence of initial imperfections structural stability loss cannot be overlooked [14, 23]. A possible engineering solution employs the so-called safety multipliers, said to act as "coefficients of ignorance".

The buckling oriented design is inherent due to thin-walled structural elements, intender to minimize structural dead load for economic reasons. The thin-walled elements are widely applied in various branches of engineering. They are widespread in civil engineering and other fields e.g. aviation and shipbuilding. The controlling means to adjust limit structural dimensions are parameters of structural stability loss in a greater extent than its strength. The stability interest in building industry has recently increased due to permanently growing demands of engineering. In global engineering practice two methods are currently employed in the design of thin-walled structures: the traditional effective width method and the direct strength method (DSM) [31, 45, 76], the latter denoted a constant development up till now.

Advances in computational power and numerical methods (e.g. the finite difference method, finite strip method and finite element method) strongly support the theoretical research in structural stability. Numerical methods, e.g. finite element method, cover non-linear problems, of a high geometric and material complexity. The methods based on incremental formulation and iterative algorithms are commonly employed in stability analysis. However, in order to achieve an acceptable numerical accuracy, a large number of degrees of freedom is required in the problem definition. Thus the numerical analysis cost rises up with regard to computing time, memory and disk space, featuring non-linear, quasi-static problems and no supercomputer power at hand. Thus it is essential to permanently develop numerical methods and pursue new analytical solutions of complex problems, in order to minimize the computational effort. Such a direction fits the stability domain of thin-walled structures in both academic and engineering design fields.

Stability loss of compressed or flexural thin-walled elements in its theoretical background is backed up sufficiently well only in the domain of thin-walled bar structures (showing open or closed cross-sections) fulfilling the classical assumptions of Euler [12] (principal of planar cross-sections) and Vlasov [71] (constrained torsion with possible transverse cross-sectional warping), assuming non-deformable cross-sections (without distortions). The torsion issue deserves a dedicated theoretical background, extending the basic classical matrix theory of beams of Euler and Bernoulli according to the Vlasov proposal.

The recent period has shown a substantial research increase in buckling analysis methodology of thin-walled members (GBT, FSM and DSM). Numerical results complement the experimental studies, however, some papers are purely experimental. These studies are intended to develop and improve numerical buckling modelling,

the attempts based on classical analytical methods are rarely found. Thus the authors' intention is to direct the inquiries on the non-dominant field now, the classical, analytical attempt to stability.

2 Global Buckling of Columns Geometrically Perfect and Imperfect

The paper [27] derives basic stiffness matrices (linearly elastic stiffness matrix and geometric stiffness matrix) dedicated to torsional stability analysis of constrained thin-walled bar structures of open bisymmetric cross-sections. The explicit (close-form) torsional angle functions are solutions of the constrained torsion differential equation of constrained torsion. The matrices are derived by the first Castigliano's theorem [67]. The paper presents the explicit (close-form) solution, i.e. matrices of hyperbolic function components, affected by the FEM mesh density, thus the approach proves unsuitable for a general FEM application, especially in high FE density cases. Hence two variants are proposed to expand the derived functions in power series, paying attention to the mesh density. The first variant is the classical literature "expansion with a deficit", the second one "with an excess" affected by beam discretization density. The latter variant was applied by the author to trigger faster convergence in the coarse grid cases, compared to the former, literature variant.

The progress in computer methods has been accompanied by significant theoretical methodology development of in the field of structural stability. It results from the increasing demands of engineering practice leading to a more rigorous modelling interpretation of the phenomena associated with structural stability loss. The classical problem of initial stability, illustrated by column buckling, is usually analysed by conventional means. The elastic and geometric stiffness matrices are split (see paper [27]) in order to compute their eigenvalues. The development of numerical methods accompanies the ongoing interest in the foundations of non-linear stability theory of elastic structures subjected to conservative loads. The theory regards boundary conditions of the problem and applies the limit state criterion due to a singular tangent stiffness matrix. This approach is straightforward due to a simple determinant computing procedure and incremental limit value procedure. The paper [28] regards torsional mode of stability loss in the case of constrained torsion along with the tangential stiffness matrix derivation by means of the limit state criterion the paper [28] applies the Newton-Raphson iterative algorithm to solve the problem. The analysis was performed by computing packages Mathematica [2, 39, 74].

The paper [61] addresses the impact of global geometrical imperfections on stability loss of bisymmetric I-columns of a constant cross-section (lips possible) subjected to axial compression (conservative loading). The relations are analytically derived of the critical load with respect to initial flexural and torsional imperfections. The impact of initial axis curvature on torsional buckling and the impact of initial column cross-section twist on flexural buckling are addressed here. The classical assumption

of non-deformable cross-section is applied here. Non-linear differential equations of the problem are formulated and solved. The critical load approximation is conducted by Galerkin's method [13, 38, 44, 57]. The proposed analytic solution is confirmed numerically by means of ABAQUS software. The initial equilibrium path and its associated bifurcation points are determined, while subjected to torsional buckling with initial flexural imperfections and flexural buckling with initial torsional imperfections.

The column of a bisymmetric cross-section shows its flexural buckling independent of torsional buckling, due to both bifurcation points the equilibrium paths are symmetric and stable. While flexural imperfections occur critical torsional buckling load is reduced due to given cross-sectional column dimensions, a higher critical load reduction yields from the reduced flange width. On the other hand, initial twist of the column cross-section leads to the flexural buckling load increase. The results and conclusions are significant due to scientific and engineering viewpoints.

3 Local Buckling of Columns and Beams Made of Linearly and Non-linearly Elastic Materials

Both buckling load and mode are fundamentally affected by structural supporting conditions. In real engineering applications the support is elastic of a given stiffness affected by the load. The paper [30] considers the problem of support stiffness in thin-walled purlins of Z-shaped cross-section, screw-fastened to sandwich panels. Joint experimental and numerical research is provided, a simple FEM model based on the experimental results is intended to specify the rotational stiffness of the purlin support without expensive experimental research. Based on numerical and experimental research a number of final conclusions is drawn. First of all, the number and location of fasteners (screws or bolts) are decisive due to rotational stiffness of the purlins. The decisive parameters here are the number of fasteners, their arrangement along the purlin axis and their layout in the flange area in terms of distance from the purlin web. In the considered case the support stiffness rises up with an increasing load. A simplified model of fasteners and an entire system, applied in Kujawa and Szymczak [30], significantly reduce the computational time, while it stays accurate enough to specify the stiffness of purlin supports. The experimental research of Kujawa and Szymczak [30] and the overall, real scale investigation of the purlin constitute the research project aimed at restraining of cold-formed Z-purlins with sandwich panels [70]. An experimental test of roof overload and destruction is provided here. The experiment results in purlin local stability loss leading to distortion of the purlin cross-sections. Thus in real events it is necessary to abort the classical assumptions of Euler and Vlasov of cross-sectional non-deformability.

In real engineering applications the assumptions of Euler and Vlasov are represented by diaphragms arranged at specified intervals along the bar. In the case of diaphragms spaces sparsely or excluded at all the classical assumptions cannot be

made. Such cases point out local or shear buckling loads, with regard character to the element slenderness and the cross-sectional wall thickness.

The paper [62] focuses on distortional stability loss of thin-walled bars of a square cross-section, with or without internal walls. The investigated case states both global and local buckling modes independent. The problem is modelled one-dimensionally, its differential equation is stated and solved by means of the stationary potential energy principle. Analytical model is worked due to critical loads and critical stresses, regarding elastic isotropic simply supported columns. The procedure is shown to determine the half-wave number of the buckling mode incorporating the characteristic column buckling length. The analytical results are compared to the FEM ABAQUS output. The analytical approach leads to critical loads, critical stresses and the related number of half-waves corresponding to minimum critical stresses, accurate enough while compared to the FEM-based results. The proposed analytical solutions determine the optimal shape of thin-walled columns of square cross-section, pointing out the materials of low elasticity and high elastic limit e.g. aluminium alloys or composites.

The paper [60] discusses of thin-walled channel members subjected to compression or bending, regarding the flange-web interaction. The flange deformation is related to angle of twist around the flange-web connection line. Classical differential equation of the problem is taken, similarly to Szymczak and Kujawa [62], incorporating the stationary potential energy principle. Various flange profiles are considered: single, double-bent, single-bent with lips and double-bent with reinforcement. Analytical buckling problem solution is investigated, considering the flange-web interaction, usually neglected in the studies. It is common, however impractical, to assume flange buckling posterior to material yield at the flange-web connecting-edge.

Furthermore, the impact is studied of interaction between flange sheets on critical stress and buckling mode. Both simplified numerical model and FEM procedure are employed introduced. The analytical results are compared with the FSM output, wide in buckling analysis of thin-walled open cross-sections (the CUFSM software [35]), the limitations of both numerical procedures (FEM and FSM) are highlighted.

The paper [29] suggests a complex, entirely non-linear numerical approach, consisting an analytical procedure and a FEM model. This approach is bound to cover the flange-web interaction, the impact of friction between the cross-sectional parts and the impact of material nonlinearity on local stability. Two aluminium alloys were considered here: the heat-treated and the non-heat-treated, both assumed the Ramberg-Osgood material law. The proposed solution may be successfully applied to alloys of stainless and carbon steel as well. The paper is motivated by the growing interest in nonstandard structural solutions for shaping cold-formed members in the context of local buckling analysis. It investigates how material parameters act upon buckling stresses while the problem is nonlinear. Energy method in its quasi-static approach is proposed here, making it possible to specify the critical buckling stresses and structural behaviour due to variable loading in linearly elastic, non-linearly elastic and non-elastic ranges. An attempt is made to relevantly model the interaction of cross-sectional components, to be either in contact initially or to come into contact at buckling. The FEM results are compared to the proposed analytical solution.

Numerical examples confirm correctness of the suggested FEM and the closed-form analytical solutions. Furthermore, numerical research yields a conclusion that initial geometrical imperfections act upon the nature of stability loss and the values of critical stresses, thus stability analysis of cold-formed thin-walled structures is intended to regard initial geometrical imperfections in a general scale. The slightest initial geometrical flaws may trigger large solution variations here, even resembling the chaotic system features.

Local stability is a necessary analytical issue of composite members, pointing out the unidirectional fibre-reinforced laminates. This topic is addressed in Szymczak and Kujawa [63]. The research here concerns local buckling of axially compressed channel columns and the corresponding flange-web interaction. Two parameter homogenization approaches are employed to reflect material orthotropy. The problem differential equation is derived and solved, it analytical results compared to the FEM solution (ABAQUS). The paper shows that the type of material homogenization type acts upon the critical stress. The critical stress increase with the composite reinforcement degree is addressed too. The impact of material homogenization method on characteristic length and the buckling mode is also pointed out.

4 Global and Local Post-buckling of Columns and Beams Made of Linear and Non-linear Elastic Materials

The next article [66] discusses flexural buckling in the pre- and post-buckling ranges of axially compressed aluminium columns. The material is intended to follow the Ramberg-Osgood equation again. A non-linear differential equation of the problem is based on the principle of stationary total potential energy and the assumptions of classical beam theory. An approximate analytical solution of the equation is conducted by means of perturbation approach, it results in buckling loads and the initial post-buckling equilibrium path. Analytical/numerical solutions are achieved in the case of compressed I-columns, either simply supported or both-side clamped sides. The work also regards the impact of material nonlinearity on the critical load and the initial post-buckling behaviour, comparing the results to the linearly elastic material case.

The paper [64] investigates torsional buckling of axially compressed bisymmetric cross-section thin-walled column made of aluminium alloy. The work addresses the loss of torsional stability in initial pre and post-critical ranges. The Ramberg-Osgood nonlinearly elastic law is assumed to model the column material behaviour was applied. The non-linear differential equation of the problem is linked with the principle of stationary total potential energy again. An approximate equation solution of the equation is found by means of the perturbation approach, here the obtained buckling load by the initial post-buckling behaviour pattern (mode). In order to verify the suggested analytical solutions the FEM numerical procedures were run in the ABAQUS environment, proving the solution correctness.

The paper [65] takes continues the topic of two previous articles [64, 66] to investigate the initial post-buckling behaviour of a cold-formed channel member flange due to its local buckling. The member material is assumed to follow a linear stress-strain relationship. The governing non-linear differential equation of the problem is derived upon the minimum total potential energy principle. The perturbation approach leads to an approximate equation solution, to find the critical buckling stress and the initial post-buckling equilibrium path. The bifurcation point is detected symmetric and stable. The proposed analytical solution is compared with the numerical finite element and finite strip method results in order to evaluate the solution validity and assess its applicability range.

5 Conclusions

The article provides a bibliographical review of papers published recently in Gdansk University of Technology in the field of thin-walled structure stability. While a vast research entirety has been focused on stability problems of thin-walled structures up till now, many problems are still open, e.g. complex global-local or global-global buckling modes including multiple bifurcation points, stability of structures made of thin-walled members, e.g. space frames or grids. Moreover, new research issues concern sensitivity analysis of critical loads and buckling modes, they are challenging problems in the case of multiple bifurcation points. Both theoretical and practical viewpoints lead to a challenging field of optimal design of thin-walled columns, beams more complex space frames, including stability constraints of various kinds.

References

1. Abambres, M., Camotim, D., Silvestre, N., Rasmussen, K.: GBT-based structural analysis of elastic-plastic thin-walled members. Comput. Struct. **136**, 1–23 (2014)
2. ABAQUS (2002–2018). http://www.abaqus.com
3. Bažant, Z., Cedolin, L.: Stability of structures: elastic, inelastic, fracture and damage theories. World Scientific Publishing Co. Pte. Ltd (2010)
4. Bellomo, N., Lods, B., Revelli, R., Ridolfi, L.: Generalized Collocation Methods: Solutions to Nonlinear Problems. Modeling and Simulation in Science. Engineering and Technology, Birkhäuser (2007)
5. Bleich, F.: Buckling Strength of Metal Structures. McGraw-Hill (1952)
6. Brush, D., Almroth, B.: Buckling of Bars, Plates and Shells. McGraw-Hill (1975)
7. Camotim, D., Basaglia, C., Silvestre, N.: GBT buckling analysis of thin-walled steel frames: a state-of-the-art report. Thin-Walled Struct. **48**(10), 726–743 (2010)
8. Chajes, A.: Principles of Structural Stability. Prentice-Hall (1974)
9. Cheung, Y., Tham, L.: Finite Strip Method. CRC Press (1998)
10. Chwalla, E.: Die stabilität zentrisch und exzentrisch gedrückter stäbe aus baustahl. Internationale Tagung für Brückenbau und Hochbau, pp. 608–614 (1928)

11. Engesser, F.: Über die knickfestigkeit grader stäbe. Zeitschrift für Architektur und Ingenieurwesen **35**(4), 455–462 (1889)
12. Euler, L.: Sur la force des colonnes. Memoires de l'academie des sciences de Berlin 13, 252–282 (1759)
13. Fletcher, C.: Computational Galerkin Methods. Springer, Berlin (1984)
14. Gambhir, M.: Stability Analysis and Design of Structures. Springer, Berlin (2004)
15. Gerard, G.: Introduction to Structural Stability Theory. McGraw-Hill (1962)
16. Gonçalves, R., Camotim, D.: GBT deformation modes for curved thin-walled cross-sections based on a mid-line polygonal approximation. Thin-Walled Struct. **103**, 231–243 (2016)
17. Hancock, G.: Cold-formed steel structures. J. Constr. Steel Res. **59**, 473–487 (2003)
18. Hancock, G.: Cold-formed steel structures: research review 2013–2014. Adv. Struct. Eng. **19**(3), 393–408 (2016)
19. Hancock, G., Pham, C.: Buckling analysis of thin-walled sections under localized loading using the semi-analytical finite strip method. Thin-Walled Struct. **86**, 35–46 (2015)
20. Horne, M., Merchant, W.: The Stability of Frames. Pergamon (1965)
21. Iyengar, N.: Structural stability of columns and plates. East-West Press Pvt Ltd (1986)
22. James, B.: Principal effects of axial load on moment-distribution analysis of rigid structures. Technical report 534. National Advisory Committee for Aeronautics (1935)
23. Kirby, P., Nethercot, D.: Design for Structural Stability. Wiley (1979)
24. Kirchhoff, G.: Über das gleichgewicht und die bewegung eines unendkich dünnen elastischen stäbes. Journal für Mathematik **56**, 285–313 (1859)
25. Kollbrunner, C., Meister, M.: Knicken, biegedrillknicken, kippen: theorie und berechnung von knickstäben knickvorschrifte. Springer (1961)
26. Kowal-Michalska, K., Mania, R. (eds.): Review and Current Trends in Stability of Structures. A Series of Monographs. Lodz University of Technology (2013)
27. Kujawa, M.: Torsion of restrained thin-walled bars of open constant bisymmetric cross-section. TASK Q. **16**(1), 5–15 (2012a)
28. Kujawa, M.: Torsional buckling of restrained thin-walled bars of open bisymmetric cross-section. TASK Q. **16**(3–4), 301–306 (2012b)
29. Kujawa, M.: Selected local stability problems of channel section flanges made of aluminium alloys. Contin. Mech. Thermodyn. (2018). https://doi.org//10.1007/s00161-018-0705-z
30. Kujawa, M., Szymczak, C.: Numerical and experimental investigation of rotational stiffness of zed-purlins connection with sandwich panels. Thin-Walled Struct. **75**, 43–52 (2014)
31. Kumar, J., Jayachandran, S.: Experimental investigation and evaluation of direct strength method on beam-column behavior of uprights. Thin-Walled Struct. **102**, 165–179 (2016)
32. Kurrer, K.: The history of the theory of structures: from arch analysis to computational mechanics. Ernst and Sohn a Wiley Company (2008)
33. Lagrange, J.: Sur la figure des colonnes. Oeuvres de Lagrange 2, 125–170 (1770–73)
34. Leipholz, H.: Stability Theory. Academic Press (1970)
35. Li, Z., Schafer, B.: CUFSM elastic buckling analysis of thin-walled members with general end boundary conditions (2018). http://www.ce.jhu.edu/bschafer/cufsm
36. Livesley, R., Chandler, D.: Stability Functions for Structural Frameworks. Manchester University Press (1956)
37. Lyapunov, A.: The General Problem of the Stability of Motion. Taylor & Francis (1992)
38. Marchuk, G.: Methods of Numerical Mathematics. Springer, New York (1982)
39. MATLAB (1994–2019). http://www.matlab.com
40. Mikhlin, S.: Variational Methods in Mathematical Physics. Pergamon Press (1964)
41. Mises, R.: Über die stabilitätsprobleme der elastizitätstheorie. Zeitschrift für angewandte Mathematik und Mechanik **3**(6), 406–422 (1923)
42. Mises, R., Ratzersdorfer, J.: Die knicksicherheit von fachwerken. Zeitschrift für angewandte Mathematik und Mechanik **5**(3), 218–235 (1925)
43. Mises, R., Ratzersdorfer, J.: Die knicksicherheit von rahmentragwerken. Zeitschrift für angewandte Mathematik und Mechanik **6**(3), 181–199 (1926)
44. Mitchel, A.: The Finite Element Method in Partial Differential Equations. Wiley (1977)

45. Nguyen, V., Pham, C., Cartwright, B., English, M.: Design of new cold rolled purlins by experimental testing and direct strength method. Thin-Walled Struct. **118**, 105–112 (2017)
46. Pflüger, A.: Stabilitatsprobleme der elastostatik. Springer (1950)
47. Pietraszkiewicz, W., Górski, J. (eds.): Shell Structures: Theory and Applications, vol 3. CRC Press (2014)
48. Pietraszkiewicz, W., Kreja, I. (eds.) Shell Structures: Theory and Applications, vol 2. CRC Press (2010)
49. Pietraszkiewicz, W., Szymczak, C. (eds.): Shell Structures: Theory and Applications, vol 1. Taylor & Francis (2006)
50. Pietraszkiewicz, W., Witkowski, W. (eds.): Shell Structures: Theory and Applications, vol 4. CRC Press (2017)
51. Przemieniecki, J.: Theory of Matrix Structural Analysis. McGraw-Hill (1968)
52. Reedy, J.: Energy and Variational Methods in Applied Mechanics. Willey (1984)
53. Schafer, B., Àdàny, S.: Buckling analysis of cold-formed steel members using CUFSM: conventional and constrained finite strip methods. In: Eighteenth International Specialty Conference on Cold-Formed Steel Structures, Orlando, FL (2006)
54. Schardt, R.: Generalised beam theory-an adequate method for coupled stability problems. Thin-Walled Strct. **19**(2–4), 161–180 (1994)
55. Silvestre, N., Camotim, D.: Second-order generalised beam theory for arbitrary orthotropic materials. Thin-Walled Strct. **40**(9), 791–820 (2002)
56. Smith, G.: Numerical Solution of Partial Differential Equations: Finite Difference Methods. Oxford Applied Mathematics and Computing Science Series (1986)
57. Stoer, J., Bulirsch, R.: Einführung in die numerische mathematik. Springer (1973)
58. Szymczak, C.: A review of stability problems of thin-walled structures developed at Gdansk University of Technology. In: X-th Symposium Stability of Structures, pp. 69–78 (2003)
59. Szymczak, C.: Selected problems of stability of thin-walled columns with bisymmetric cross-section. In: XIII-rd Symposium Stability of Structures, pp. 111–128 (2012)
60. Szymczak, C., Kujawa, M.: On local buckling od cold-formed channel members. Thin-Walled Struct. **106**, 93–101 (2016)
61. Szymczak, C., Kujawa, M.: Buckling of thin-walled columns accounting for initial geometrical imperfections. Int. J. Non-linear Mech. **95**, 1–9 (2017a)
62. Szymczak, C., Kujawa, M.: Distortional buckling of thin-walled columns of closed quadratic cross-section. Thin-walled Struct. **113**, 111–121 (2017b)
63. Szymczak, C., Kujawa, M.: Local buckling of composite channel columns. Contin. Mech. Thermodyn. (2018). https://doi.org/10.1007/s00161-018-0674-2
64. Szymczak, C., Kujawa, M.: Torsional buckling and post-buckling of columns made of aluminium alloy. Appl. Math. Model. **60**, 711–720 (2018b)
65. Szymczak, C., Kujawa, M.: Buckling and initial post-local buckling behaviour of cold-formed channel member flange. Thin-Walled Struct. **137**, 177–184 (2019a)
66. Szymczak, C., Kujawa, M.: Flexural buckling and post-buckling of columns made of aluminium alloy. Eur. J. Mech. A Solids **73**, 420–429 (2019b)
67. Timoshenko, S.: History of Strength of Materials. McGraw-Hill (1953)
68. Timoshenko, S., Gere, J.: Theory of Elastic Stability. McGraw-Hill (1964)
69. Todhunter, I.: A History of the Theory of Elasticity and of the Strength of Materials: Galilei to Saint-Venant, 1639-1850. Franklin Classics (2018)
70. Urbańska-Galewska, E., Werochowski, W., Kujawa, M.: Restraining of the cold-formed Z-purlins with sandwich panels. Technical report. Gdansk University of Technology (2007)
71. Vlasov, V.: Thin-Walled Elastic Beams. Israel Program for Scientific Translations (1961)
72. Waszczyszyn, Z. (ed.): Contemporary methods of structural stability analysis (Współczesne metody analizy stateczności konstrukcji). PAN Ossolineum (1981) (in Polish)
73. Waszczyszyn, Z., Cichoń, C., Radwańska, M.: Stability of Structures by Finite Element Methods. Studies in Applied, vol. 40. Elsevier (1994)
74. Wolfram, S.: Mathematica: a system for doing mathematics by computer. Addison-Wesley (1991)

75. Young, T.: A Course of Lectures on Natural Philosophy and the Mechanical Arts, vol. 2. Printed for Joseph Johnson, St. Paul's Church Yard (1807)
76. Yu, C., Schafer, B.: Simulation of cold-formed steel beams in local and distortional buckling with applications to the direct strength method. J. Constr. Steel Res. **63**, 581–590 (2007)
77. Zienkiewicz, O.: The Finite Element Method in Engineering Science. McGraw-Hill (1971)

Higher-Order Weak Formulation for Arbitrarily Shaped Doubly-Curved Shells

Francesco Tornabene and Michele Bacciocchi

Abstract The aim of this chapter is the development of an efficient and accurate higher-order formulation to solve the weak form of the governing equations that rule the mechanical behavior of doubly-curved shell structures made of composite materials, whose reference domain can be defined by arbitrary shapes. To this aim, a mapping procedure based on Non-Uniform Rational Basis Spline (NURBS) is introduced. It should be specified that the theoretical shell model is based on the Equivalent Single Layer (ESL) approach. In addition, the Generalized Integral Quadrature technique, that is a numerical tool which can guarantee high levels of accuracy with a low computational effort in the structural analysis of the considered shell elements, is introduced. The proposed technique is able to solve numerically the integrals by means of weighted sums of the values that a smooth function assumes in some discrete points placed within the reference domain.

1 Introduction

The peculiar shape of doubly-curved shells allows to identify immediately this kind of structure in everyday life. Cooling towers, long-span roofs, vaults, fluids containers, tanks, nuclear systems, ships, missiles, airplanes, boats are all examples of shell structures that can be easily observed, as specified in the book by Tornabene and Bacciocchi [1]. Thus, it is clear that the study of shell structures could involve various engineering fields and their multidisciplinary feature is easily highlighted.

Their curved shapes define several structural advantages, such as a noticeably efficiency in holding external forces, extraordinary stiffness and resistance, as well as higher values of strength-to-weight ratio. Nevertheless, such positive features are

F. Tornabene (✉)
University of Salento, Via per Monteroni, 73100 Lecce, Italy
e-mail: francesco.tornabene@unisalento.it

M. Bacciocchi
University of Bologna, Viale del Risorgimento 2, 40136 Bologna, Italy
e-mail: michele.bacciocchi@unibo.it

H. Altenbach et al. (eds.), *Recent Developments in the Theory of Shells*,
Advanced Structured Materials 110, https://doi.org/10.1007/978-3-030-17747-8_32

always combined with great difficulties in the analytical description of their curved surfaces. To the best of the author' knowledge, the differential geometry represents one of the most efficient mathematical tools to deal with completely doubly-curved shells, characterized by two different radii of curvature. The book by Kraus [2] and the book by Tornabene and Bacciocchi [1] should be taken as reference to this aim.

The growth of composite materials and their consequent application to shell structures has allowed to further enhance their mechanical features, due to a reduction of the structural weight and an increase of their stiffness and resistance, if compared to classical or isotropic constituents [3–7]. Many papers and researches, in fact, are focused on the study of the structural behavior of shells made of composite materials. Among them, the class of laminated composites should be mentioned. For the sake of completeness, it should be recalled that these structures are defined by an overlapping of many layers characterized by various mechanical properties. These peculiar configurations can affect the mechanical behavior of shell structures and several studies are consequently presented to investigate the effect of the mechanical parameters on their static and dynamic behavior [8–31].

It is well-known that laminates could be affected by some issues, such as delamination, residual stresses and defects at the inter-laminar interfaces. These problems are generally caused by the heterogeneity of the mechanical properties along the thickness of the structures [32–34]. These problems have been solved by defining a continuous gradual variation of the mechanical properties in the thickness direction and the consequent removal of the layer interfaces. Composite materials characterized by this feature are named as Functionally Graded Materials (FGMs) and their application in shells has allowed to obtain even more efficient structures [35–45]. In general, FGMs are obtained by mixing together two phases, such as ceramic and metal. The recent advancements in the nanotechnologies has defined the growth of the so-called nanocomposites in which the reinforcing phase can be made by nanoparticles such as Carbon Nanotubes (CNTs). If these particles are characterized by a through-the-thickness variation of their volume fraction, the class of Functionally Graded Carbon Nanotube-Reinforced Composites is obtained. This topic is extremely investigated in many recently published papers [46–53].

Nevertheless, classical or first-order theories could not be able to model anymore the mechanical behavior of structures made of innovative constituents. Higher-order Shear Deformation Theories (HSDTs) have arisen to this aim in the last decades [54–64]. To the best of the authors' knowledge, the Unified Formulation (UF) represented the turning point in the development of refined structural models, due to its efficiency, compactness and easy computer implementation [1, 65–69]. More general approaches based on this formulation have been also developed during the years, as it can be noted in the following papers [70–75]. It should be mentioned that in general HSDTs are classified as Equivalent Single Layer (ESL) theories if the governing equations are defined in the middle surface of the structure [76–80], but a kinematic expansion along the thickness can be also developed according to the so-called Layer-Wise (LW) approaches [81–85]. Hybrid formulations are also possible, such as an Equivalent Layer-Wise (ELW) model [86].

Once the governing equations are obtained, two formulations can be solved, which are respectively the strong and weak forms. The first approach provides a system of partial differential equations, whereas an integral formulation is given by the second one [87]. In general, the fundamental system of equations cannot be solved analytically and a numerical solution has to be pursued. If the strong formulation is chosen, a numerical tool able to approximate the derivatives should be used. On the other hand, the integrals have to be solved numerically if the weak formulation is developed. The Generalized Differential Quadrature (GDQ) and Generalized Integral Quadrature (GIQ) methods could be efficiently employed to this aim, as specified in the review paper by Tornabene et al. [88]. For the sake of completeness, it should be mentioned that the fundamental aspects of these techniques have been presented by Shu [89].

2 Definition of the Geometry

The current section is focused on the analytical description of doubly-curved surfaces, which are taken as the middle surfaces of the shell structures under consideration. A brief illustration of the main principles of differential geometry is presented to this aim, since an accurate and precise definition of these surfaces is required [1, 2].

In general, each shell can be considered as an elastic body defined by two curved surfaces. The distance between the two surfaces, which denotes the thickness of the structure, is small if compared to the other sizes. An orthogonal and principal coordinate system is defined within the shell middle surface. If α_1 and α_2 represent the curvilinear coordinates at issue, the local reference system is denoted by $O'\alpha_1\alpha_2\zeta$, in which $\zeta \equiv \alpha_3$ is the normal direction. For the sake of clarity, a generic shell element of thickness h is depicted in Fig. 1. In the same figure, it can be easily noted also the global reference system $Ox_1x_2x_3$. Each global direction is identified by the corresponding unit vector denoted by $\mathbf{e}_i$, for $i = 1, 2, 3$.

A closed domain should be identified, therefore the following limitations are required

$$\alpha_1 \in \left[\alpha_1^0, \alpha_1^1\right], \quad \alpha_2 \in \left[\alpha_2^0, \alpha_2^1\right], \quad \zeta \in [-h/2, h/2] \tag{1}$$

in which α_1^0, α_2^0 and α_1^1, α_2^1 stand for the minimum and maximum values of the curvilinear coordinates, respectively.

A generic point P of the three-dimensional solid is specified by the position vector $\mathbf{R}(\alpha_1, \alpha_2, \zeta)$, which assumes the aspect shown below

$$\mathbf{R}(\alpha_1, \alpha_2, \zeta) = \mathbf{r}(\alpha_1, \alpha_2) + \zeta\, \mathbf{n}(\alpha_1, \alpha_2) \tag{2}$$

where $\mathbf{r}(\alpha_1, \alpha_2)$ denotes the position vector of each point P' laying on the shell middle surface. On the other hand, $\mathbf{n}(\alpha_1, \alpha_2)$ represents the outward unit normal vector, which can be computed by means of the following vector product

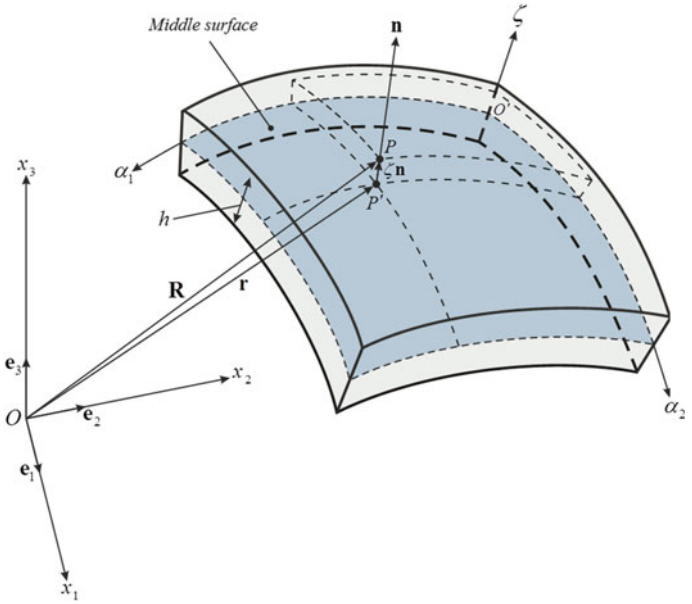

Fig. 1 Doubly-curved shell element. Representation of the local and global reference systems

$$\mathbf{n}\left(\alpha_1, \alpha_2\right) = \frac{\mathbf{r}_{,1} \times \mathbf{r}_{,2}}{\left|\mathbf{r}_{,1} \times \mathbf{r}_{,2}\right|} \tag{3}$$

where $\mathbf{r}_{,i} = \partial \mathbf{r} / \partial \alpha_i$, for $i = 1, 2$. It is important to specify that the shape of the structure is well-defined once the position vector $\mathbf{r}\left(\alpha_1, \alpha_2\right)$ is introduced. At this point, the Lamè parameters of the curved surface can be specified. The following dot products are needed to this aim

$$A_1\left(\alpha_1, \alpha_2\right) = \sqrt{\mathbf{r}_{,1} \cdot \mathbf{r}_{,1}}, \quad A_2\left(\alpha_1, \alpha_2\right) = \sqrt{\mathbf{r}_{,2} \cdot \mathbf{r}_{,2}} \tag{4}$$

By using the second-order derivatives of the position vector $\mathbf{r}$, which are denoted by $r_{,ii} = \partial^2 \mathbf{r} / \partial \alpha_i^2$ for $i = 1, 2$, it is possible to evaluate the main radii of curvature of the structure $R_1\left(\alpha_1, \alpha_2\right)$, $R_2\left(\alpha_1, \alpha_2\right)$ having in mind the definitions shown below

$$R_1\left(\alpha_1, \alpha_2\right) = -\frac{A_1^2}{\mathbf{r}_{,11} \cdot \mathbf{n}}, \quad R_2\left(\alpha_1, \alpha_2\right) = -\frac{A_2^2}{\mathbf{r}_{,22} \cdot \mathbf{n}} \tag{5}$$

It is important to specify that these quantities assume different values in each point of the middle surface, if a completely doubly-curved surface is analyzed. The effect of curvature is included also in the following geometric parameters

$$H_1\left(\alpha_1, \alpha_2\right) = 1 + \frac{\zeta}{R_1}, \quad H_2\left(\alpha_1, \alpha_2\right) = 1 + \frac{\zeta}{R_2} \tag{6}$$

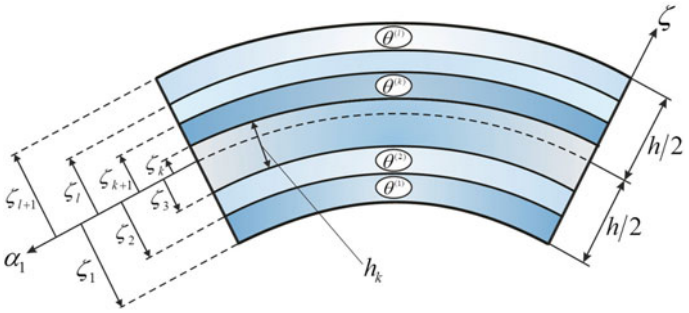

Fig. 2 Schematic representation of a laminated composite shell. Identification of the thickness coordinate of the various layers that compose the structure

Finally, if the structure is made of several layers (or plies), it should be recalled that the overall thickness h is given by

$$h = \sum_{k=1}^{l} h_k \tag{7}$$

where h_k represents the thickness of the k-th layer, whose definition is written below

$$h_k = \zeta_{k+1} - \zeta_k \tag{8}$$

The meaning of ζ_{k+1} and ζ_k can be easily deducted in Fig. 2. In particular, the coordinates ζ_{k+1}, ζ_k are required to identify the lower and upper boundaries of the k-th ply.

2.1 Numerical Remarks

A numerical solution of the corresponding governing equations will be carried out in the following sections. To this aim, the middle surface of the structure must be discretized by defining the position of I_N, I_M gridpoints along the principal directions α_1, α_2, respectively. From the mathematical point of view, the following notations are used to identify the discrete points in hand

$$\begin{aligned} \alpha_1^0 &= \alpha_{11},\ \alpha_{12},\ \ldots,\ \alpha_{1f}, \ldots,\ \ldots,\ \alpha_{1I_N} = \alpha_1^1 \\ \alpha_2^0 &= \alpha_{21},\ \alpha_{22},\ \ldots,\ \alpha_{2g},\ \ldots,\ \ldots,\ \alpha_{2I_M} = \alpha_2^1 \end{aligned} \tag{9}$$

where α_{1f} and α_{2g} stand for the coordinates of a generic node on the middle surface, which can be defined as follows

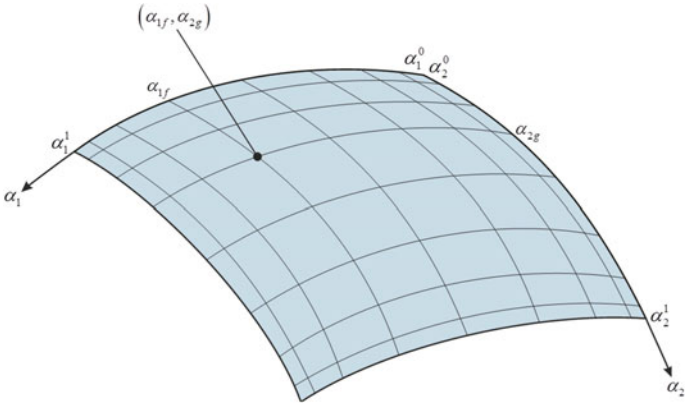

Fig. 3 Location of a generic discrete point of coordinates α_{1f} and α_{2g} on the shell middle surface

$$\begin{aligned} \alpha_{1f} &= \frac{\alpha_1^1 - \alpha_1^0}{r_{I_N} - r_1}\left(r_f - r_1\right) + \alpha_1^0 \\ \alpha_{2g} &= \frac{\alpha_2^1 - \alpha_2^0}{r_{I_M} - r_1}\left(r_g - r_1\right) + \alpha_2^0 \end{aligned} \tag{10}$$

for $f = 1, 2, \ldots, I_N$ and $g = 1, 2, \ldots, I_M$. For the sake of completeness, a generic two-dimensional discrete surface is depicted in Fig. 3. The meaning of r_f, r_g depends on the kind of distribution used to define the positions of the gridpoints. Several grid point distributions that can be used to this aim are defined and illustrated in depth in the review paper by Tornabene et al. [88]. It is important to specify that the discrete domain just defined denotes a rectangular domain from the computational point of view.

At this point, a coordinate transformation, named mapping, can be introduced to define arbitrarily shaped curved surfaces, as the one depicted in Fig. 4 [90–95]. Analytically speaking, the mapping procedure in hand is given by the following expressions

$$\alpha_1 = \alpha_1\left(\xi_1, \xi_2\right), \quad \alpha_2 = \alpha_2\left(\xi_1, \xi_2\right) \tag{11}$$

where $\xi_1 \in [-1, +1]$ and $\xi_2 \in [-1, +1]$ are the natural coordinates of the computational domain.

The coordinate transformation can be obtained by using the so-called blending functions, due to the versatility of Computer-Aided Design (CAD) software. The mapping transformation assumes the following aspect

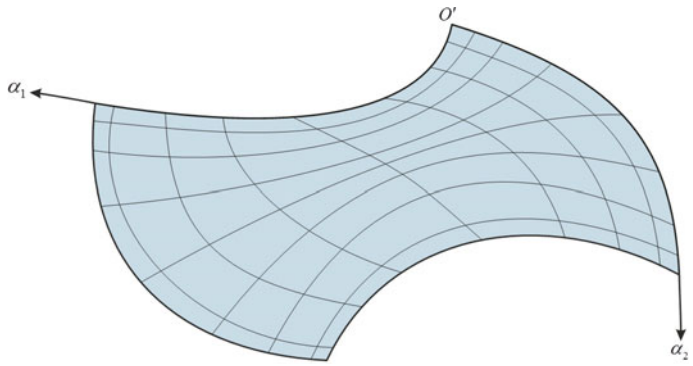

Fig. 4 Example of an arbitrarily shaped doubly-curved surface

$$\begin{aligned}\alpha_1(\xi_1,\xi_2) = &\frac{1}{2}\left((1-\xi_2)\,\bar{\alpha}_{1(1)}(\xi_1) + (1+\xi_1)\,\bar{\alpha}_{1(2)}(\xi_2) + \right.\\ &+ \left.(1+\xi_2)\,\bar{\alpha}_{1(3)}(\xi_1) + (1-\xi_1)\,\bar{\alpha}_{1(4)}(\xi_2)\right) + \\ &- \frac{1}{4}\left((1-\xi_1)(1-\xi_2)\,\alpha_{1(1)} + (1+\xi_1)(1-\xi_2)\,\alpha_{1(2)} + \right.\\ &+ \left.(1+\xi_1)(1+\xi_2)\,\alpha_{1(3)} + (1-\xi_1)(1+\xi_2)\,\alpha_{1(4)}\right)\end{aligned} \tag{12}$$

$$\begin{aligned}\alpha_2(\xi_1,\xi_2) = &\frac{1}{2}\left((1-\xi_2)\,\bar{\alpha}_{2(1)}(\xi_1) + (1+\xi_1)\,\bar{\alpha}_{2(2)}(\xi_2) + \right.\\ &+ \left.(1+\xi_2)\,\bar{\alpha}_{2(3)}(\xi_1) + (1-\xi_1)\,\bar{\alpha}_{2(4)}(\xi_2)\right) + \\ &- \frac{1}{4}\left((1-\xi_1)(1-\xi_2)\,\alpha_{2(1)} + (1+\xi_1)(1-\xi_2)\,\alpha_{2(2)} + \right.\\ &+ \left.(1+\xi_1)(1+\xi_2)\,\alpha_{2(3)} + (1-\xi_1)(1+\xi_2)\,\alpha_{2(4)}\right)\end{aligned} \tag{13}$$

where $\bar{\alpha}_{1(1)}, \bar{\alpha}_{1(2)}, \bar{\alpha}_{1(3)}, \bar{\alpha}_{1(4)}$ and $\bar{\alpha}_{2(1)}, \bar{\alpha}_{2(2)}, \bar{\alpha}_{2(3)}, \bar{\alpha}_{2(4)}$ are the parametric curves that describe the shape of every edge of the arbitrarily shaped domain, whereas $\alpha_{1(1)}, \alpha_{2(1)}, \alpha_{1(2)}, \alpha_{2(2)}, \alpha_{1(3)}, \alpha_{2(3)}, \alpha_{1(4)}, \alpha_{2(4)}$ stand for the coordinates of the four corners of the domain in hand. It should be recalled that the curvilinear edges are obtained by means of the so-called Non-Uniform Rational Basis Splines (NURBS).

The spatial derivatives must be written in the coordinate system ξ_1, ξ_2. As far as the first-order derivatives are concerned, the following result is obtained by means of the chain rule of differentiation

$$\begin{bmatrix} \frac{\partial}{\partial \xi_1} \\ \frac{\partial}{\partial \xi_2} \end{bmatrix} = \begin{bmatrix} \frac{\partial \alpha_1}{\partial \xi_1} & \frac{\partial \alpha_2}{\partial \xi_1} \\ \frac{\partial \alpha_1}{\partial \xi_2} & \frac{\partial \alpha_2}{\partial \xi_2} \end{bmatrix} \begin{bmatrix} \frac{\partial}{\partial \alpha_1} \\ \frac{\partial}{\partial \alpha_2} \end{bmatrix} = \mathbf{J} \begin{bmatrix} \frac{\partial}{\partial \alpha_1} \\ \frac{\partial}{\partial \alpha_2} \end{bmatrix} \tag{14}$$

in which the Jacobian matrix $\mathbf{J}$ has been introduced. For the sake of completeness, the mapping procedure based on NURBS is presented graphically in Fig. 5. This procedure is known also as Isogeometric mapping [96–99].

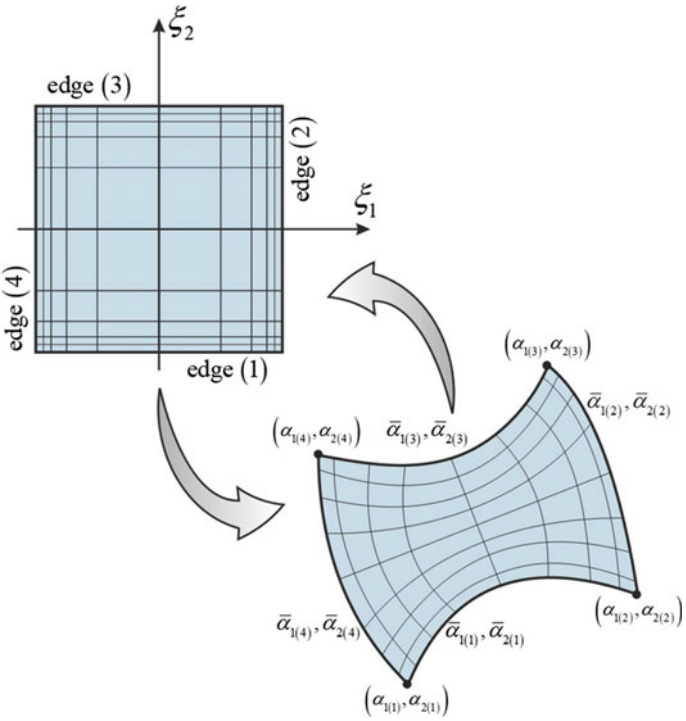

Fig. 5 Graphical illustration of the isogeometric mapping

3 Shell Structural Model

The structural model is based on an Equivalent Single Layer (ESL) approach. Therefore, the shell middle surface, described analytically in the previous section, represents the reference domain of the problem in hand. As a consequence, all the geometric and mechanical quantities involved in the governing equations are evaluated on this surface.

The displacement field is described in terms of three-dimensional displacement components U_1, U_2, U_3 by means of the following expressions

$$U_1 = \sum_{\tau=0}^{N+1} F_\tau^{\alpha_1} u_1^{(\tau)}, \quad U_2 = \sum_{\tau=0}^{N+1} F_\tau^{\alpha_2} u_2^{(\tau)}, \quad U_3 = \sum_{\tau=0}^{N+1} F_\tau^{\alpha_3} u_3^{(\tau)} \tag{15}$$

in which $F_\tau^{\alpha_1} = F_\tau^{\alpha_1}(\zeta)$, $F_\tau^{\alpha_2} = F_\tau^{\alpha_2}(\zeta)$, $F_\tau^{\alpha_3} = F_\tau^{\alpha_3}(\zeta)$ are the so called thickness functions. On the other hand, $u_1^{(\tau)} = u_1^{(\tau)}(\alpha_1, \alpha_2, t)$, $u_2^{(\tau)} = u_2^{(\tau)}(\alpha_1, \alpha_2, t)$, $u_3^{(\tau)} = u_3^{(\tau)}(\alpha_1, \alpha_2, t)$ represent the generalized displacements of the model, which can be collected conveniently in the corresponding vector $\mathbf{u}^{(\tau)} = \mathbf{u}^{(\tau)}(\alpha_1, \alpha_2, t)$

$$\mathbf{u}^{(\tau)} = \left[u_1^{(\tau)}(\alpha_1, \alpha_2, t) \quad u_2^{(\tau)}(\alpha_1, \alpha_2, t) \quad u_3^{(\tau)}(\alpha_1, \alpha_2, t) \right]^T \tag{16}$$

The kinematic model just introduced can be used to define several Higher-order Shear Deformation Theories (HSDTs) by defining the maximum order of expansion N and the thickness functions. It is important to specify that several functions can be used as thickness functions. Nevertheless, the easiest choice consists in the following one

$$\begin{aligned} F_\tau^{\alpha_i} &= \zeta^\tau, \quad \text{for} \quad \tau = 0, 1, 2, ..., N \\ F_{N+1}^{\alpha_i} &= (-1)^k \left(\frac{2}{\zeta_{k+1} - \zeta_k} \zeta - \frac{\zeta_{k+1} + \zeta_k}{\zeta_{k+1} - \zeta_k} \right) \end{aligned} \tag{17}$$

for $i = 1, 2, 3$. It can be easily deducted that the $(N + 1)$-th order of kinematic expansion is always linked to the Murakami's function, which is required to capture the so-called zig-zag effect [30]. Each theory can be defined in a compact manner by using the acronyms EDN and EDZN, neglecting or including the Murakami's function [87]. Some examples are listed below for the kinematic expansion up to the fourth-order

$$\begin{aligned} N = 1 \quad &\rightarrow \quad \begin{cases} \text{ED1} \\ \text{EDZ1} \end{cases} \qquad N = 2 \quad \rightarrow \quad \begin{cases} \text{ED2} \\ \text{EDZ2} \end{cases} \\ N = 3 \quad &\rightarrow \quad \begin{cases} \text{ED3} \\ \text{EDZ3} \end{cases} \qquad N = 4 \quad \rightarrow \quad \begin{cases} \text{ED4} \\ \text{EDZ4} \end{cases} \end{aligned} \tag{18}$$

3.1 Displacement Interpolation Using Lagrange Polynomials

The generalized displacements included in the corresponding vector $\mathbf{u}^{(\tau)}$ must be written as a function of the nodal displacements in order to develop the weak formulation of the governing equations. A higher-order polynomial interpolation obtained through the use of the Lagrange polynomials is employed to this aim. The generalized displacements assume the following aspect

$$\begin{bmatrix} u_1^{(\tau)} \\ u_2^{(\tau)} \\ u_3^{(\tau)} \end{bmatrix} = \sum_{f=1}^{I_N} \sum_{g=1}^{I_M} \begin{bmatrix} l_f(\alpha_1) l_g(\alpha_2) & 0 & 0 \\ 0 & l_f(\alpha_1) l_g(\alpha_2) & 0 \\ 0 & 0 & l_f(\alpha_1) l_g(\alpha_2) \end{bmatrix} \begin{bmatrix} u_{1(fg)}^{(\tau)} \\ u_{2(fg)}^{(\tau)} \\ u_{3(fg)}^{(\tau)} \end{bmatrix} \tag{19}$$

in which $l_f(\alpha_1)$, $l_g(\alpha_2)$ represent the f-th and g-th Lagrange polynomials of degree $I_N - 1$ and $I_M - 1$ defined below

$$
\begin{aligned}
l_f(\alpha_1) &= \frac{\prod_{i=1}^{I_N}(\alpha_1 - \alpha_{1f})}{(\alpha_1 - \alpha_{1f})\prod_{i=1,\, i\neq f}^{I_N}(\alpha_{1f} - \alpha_{1i})} \\
l_g(\alpha_2) &= \frac{\prod_{j=1}^{I_M}(\alpha_2 - \alpha_{2j})}{(\alpha_2 - \alpha_{2g})\prod_{j=1,\, j\neq g}^{I_M}(\alpha_{2g} - \alpha_{2j})}
\end{aligned}
\tag{20}
$$

They can be conveniently collected in the corresponding vector as follows

$$
\begin{aligned}
\boldsymbol{l}_{\alpha_1} &= \left[l_1(\alpha_1) \cdots l_f(\alpha_1) \cdots l_{I_N}(\alpha_1) \right] \\
\boldsymbol{l}_{\alpha_2} &= \left[l_1(\alpha_2) \cdots l_g(\alpha_2) \cdots l_{I_M}(\alpha_2) \right]
\end{aligned}
\tag{21}
$$

It is important to specify that the coordinates α_{1f} and α_{2g} can be defined by using Eq. (10). The vector $\bar{\mathbf{u}}^{(\tau)} = \bar{\mathbf{u}}^{(\tau)}(\alpha_{1f}, \alpha_{2g}, t)$ can be conveniently introduced to collect the nodal displacements just presented. It assumes the following form

$$
\bar{\mathbf{u}}^{(\tau)} = \left[\bar{\mathbf{u}}_1^{(\tau)} \; \bar{\mathbf{u}}_2^{(\tau)} \; \bar{\mathbf{u}}_3^{(\tau)} \right]^T \tag{22}
$$

where

$$
\begin{aligned}
\bar{\mathbf{u}}_1^{(\tau)} &= \left[\left| u_{1(11)}^{(\tau)} \cdots u_{1(I_N 1)}^{(\tau)} \right| u_{1(12)}^{(\tau)} \cdots u_{1(I_N 2)}^{(\tau)} \left| \cdots \right| u_{1(1 I_M)}^{(\tau)} \cdots u_{1(I_N I_M)}^{(\tau)} \right]^T \\
\bar{\mathbf{u}}_2^{(\tau)} &= \left[\left| u_{2(11)}^{(\tau)} \cdots u_{2(I_N 1)}^{(\tau)} \right| u_{2(12)}^{(\tau)} \cdots u_{2(I_N 2)}^{(\tau)} \left| \cdots \right| u_{2(1 I_M)}^{(\tau)} \cdots u_{2(I_N I_M)}^{(\tau)} \right]^T \\
\bar{\mathbf{u}}_3^{(\tau)} &= \left[\left| u_{3(11)}^{(\tau)} \cdots u_{3(I_N 1)}^{(\tau)} \right| u_{3(12)}^{(\tau)} \cdots u_{3(I_N 2)}^{(\tau)} \left| \cdots \right| u_{3(1 I_M)}^{(\tau)} \cdots u_{3(I_N I_M)}^{(\tau)} \right]^T
\end{aligned}
\tag{23}
$$

It can be observed that these nodal quantities are collected following the order denoted by the arrow in Fig. 6. Equation (19) can be conveniently written in compact matrix form as follows

$$
\mathbf{u}^{(\tau)} = \mathbf{N}^T \bar{\mathbf{u}}^{(\tau)} \tag{24}
$$

for $\tau = 0, 1, 2, ..., N, N+1$, where

$$
\mathbf{N}^T = \begin{bmatrix} \bar{\mathbf{N}}^T & 0 & 0 \\ 0 & \bar{\mathbf{N}}^T & 0 \\ 0 & 0 & \bar{\mathbf{N}}^T \end{bmatrix} \tag{25}
$$

If the symbol $\otimes_k$ denotes the so-called Kronecker product, the quantities $\bar{\mathbf{N}}^T$ can be defined as shown below

$$
\bar{\mathbf{N}}^T = \boldsymbol{l}_{\alpha_2} \otimes_k \boldsymbol{l}_{\alpha_1} \tag{26}
$$

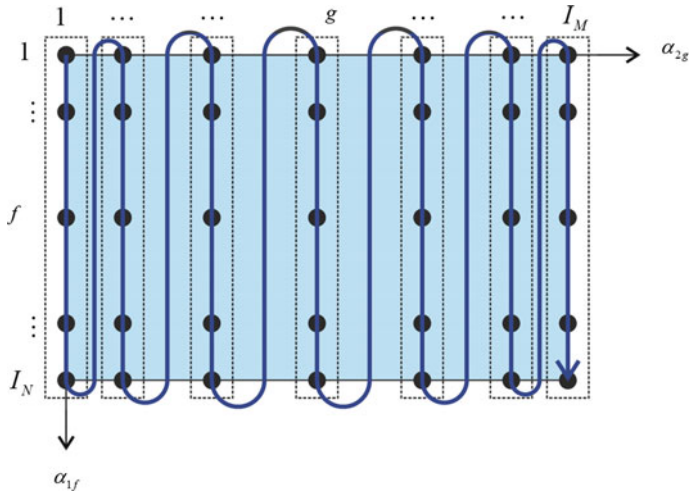

Fig. 6 Organization of the nodal displacements in the corresponding vectors

3.2 Kinematic Equations

Once the displacement field and the interpolation of the generalized displacements are defined, it is possible to introduce the generalized strains $\boldsymbol{\varepsilon}^{(\tau)\alpha_i} = \boldsymbol{\varepsilon}^{(\tau)\alpha_i}(\alpha_1, \alpha_2, t)$ defined below

$$\boldsymbol{\varepsilon}^{(\tau)\alpha_i} = \left[\varepsilon_1^{(\tau)\alpha_i} \ \varepsilon_2^{(\tau)\alpha_i} \ \gamma_1^{(\tau)\alpha_i} \ \gamma_2^{(\tau)\alpha_i} \ \gamma_{13}^{(\tau)\alpha_i} \ \gamma_{23}^{(\tau)\alpha_i} \ \omega_{13}^{(\tau)\alpha_i} \ \omega_{23}^{(\tau)\alpha_i} \ \varepsilon_3^{(\tau)\alpha_i} \right]^T \tag{27}$$

for $\tau = 0, 1, 2, ..., N, N+1$ and $i = 1, 2, 3$. The definition of the generalized strains can be given as a function of the nodal displacements as follows

$$\boldsymbol{\varepsilon}^{(\tau)\alpha_i} = \mathbf{B}^{\alpha_i} \bar{\mathbf{u}}^{(\tau)} \tag{28}$$

for $i = 1, 2, 3$, in which the operators $\mathbf{B}^{\alpha_i}$ are defined below

$$\mathbf{B}^{\alpha_1} = \begin{bmatrix} \frac{1}{A_1} \boldsymbol{l}_{\alpha_2} \otimes_k \boldsymbol{l}_{\alpha_1}^{(1)} \\ \frac{1}{A_1 A_2} \frac{\partial A_2}{\partial \alpha_1} \boldsymbol{l}_{\alpha_2} \otimes_k \boldsymbol{l}_{\alpha_1} \\ -\frac{1}{A_1 A_2} \frac{\partial A_1}{\partial \alpha_2} \boldsymbol{l}_{\alpha_2} \otimes_k \boldsymbol{l}_{\alpha_1} \\ \frac{1}{A_2} \boldsymbol{l}_{\alpha_2}^{(1)} \otimes_k \boldsymbol{l}_{\alpha_1} \\ -\frac{1}{R_1} \boldsymbol{l}_{\alpha_2} \otimes_k \boldsymbol{l}_{\alpha_1} \\ \mathbf{0} \\ \boldsymbol{l}_{\alpha_2} \otimes_k \boldsymbol{l}_{\alpha_1} \\ \mathbf{0} \\ \mathbf{0} \end{bmatrix} \tag{29}$$

$$\mathbf{B}^{\alpha_2} = \begin{bmatrix} \frac{1}{A_1 A_2}\frac{\partial A_1}{\partial \alpha_2}\boldsymbol{l}_{\alpha_2}\otimes_k \boldsymbol{l}_{\alpha_1} \\ \frac{1}{A_2}\boldsymbol{l}^{(1)}_{\alpha_2}\otimes_k \boldsymbol{l}_{\alpha_1} \\ \frac{1}{A_1}\boldsymbol{l}_{\alpha_2}\otimes_k \boldsymbol{l}^{(1)}_{\alpha_1} \\ -\frac{1}{A_1 A_2}\frac{\partial A_2}{\partial \alpha_1}\boldsymbol{l}_{\alpha_2}\otimes_k \boldsymbol{l}_{\alpha_1} \\ \mathbf{0} \\ -\frac{1}{R_2}\boldsymbol{l}_{\alpha_2}\otimes_k \boldsymbol{l}_{\alpha_1} \\ \mathbf{0} \\ \boldsymbol{l}_{\alpha_2}\otimes_k \boldsymbol{l}_{\alpha_1} \\ \mathbf{0} \end{bmatrix} \tag{30}$$

$$\mathbf{B}^{\alpha_3} = \begin{bmatrix} \frac{1}{R_1}\boldsymbol{l}_{\alpha_2}\otimes_k \boldsymbol{l}_{\alpha_1} \\ \frac{1}{R_2}\boldsymbol{l}_{\alpha_2}\otimes_k \boldsymbol{l}_{\alpha_1} \\ \mathbf{0} \\ \mathbf{0} \\ \frac{1}{A_1}\boldsymbol{l}_{\alpha_2}\otimes_k \boldsymbol{l}^{(1)}_{\alpha_1} \\ \frac{1}{A_2}\boldsymbol{l}^{(1)}_{\alpha_2}\otimes_k \boldsymbol{l}_{\alpha_1} \\ \mathbf{0} \\ \mathbf{0} \\ \boldsymbol{l}_{\alpha_2}\otimes_k \boldsymbol{l}_{\alpha_1} \end{bmatrix} \tag{31}$$

It can be easily noted that the following quantities are required in the definitions of the operators $\mathbf{B}^{\alpha_i}$

$$\begin{aligned} \boldsymbol{l}^{(1)}_{\alpha_1} &= \left[\frac{\partial l_1(\alpha_1)}{\partial \alpha_1} \cdots \frac{\partial l_f(\alpha_1)}{\partial \alpha_1} \cdots \frac{\partial l_{I_N}(\alpha_1)}{\partial \alpha_1} \right] \\ \boldsymbol{l}^{(1)}_{\alpha_2} &= \left[\frac{\partial l_1(\alpha_2)}{\partial \alpha_2} \cdots \frac{\partial l_g(\alpha_2)}{\partial \alpha_2} \cdots \frac{\partial l_{I_M}(\alpha_2)}{\partial \alpha_2} \right] \end{aligned} \tag{32}$$

In other words, the vectors $\boldsymbol{l}^{(1)}_{\alpha_1}$ and $\boldsymbol{l}^{(1)}_{\alpha_2}$ collects the first-order derivatives with respect to the principal coordinates of the Lagrange interpolation polynomials.

3.3 Constitutive Equations

The resultants of the internal forces or stresses can be collected in the vector $\mathbf{S}^{(\tau)\alpha_i} = \mathbf{S}^{(\tau)\alpha_i}(\alpha_1, \alpha_2, t)$, which represents the τ-th order generalized stress resultant vector. Its components are given below

$$\mathbf{S}^{(\tau)\alpha_i} = \left[N_1^{(\tau)\alpha_i} \;\; N_2^{(\tau)\alpha_i} \;\; N_{12}^{(\tau)\alpha_i} \;\; N_{21}^{(\tau)\alpha_i} \;\; T_1^{(\tau)\alpha_i} \;\; T_2^{(\tau)\alpha_i} \;\; P_1^{(\tau)\alpha_i} \;\; P_2^{(\tau)\alpha_i} \;\; S_3^{(\tau)\alpha_i} \right]^T \tag{33}$$

for $\tau = 0, 1, 2, ..., N, N+1$ and $i = 1, 2, 3$. By definition, the stress resultants at issue can be evaluated as a function of the nodal displacements introduced in the previous paragraphs as follows

$$\mathbf{S}^{(\tau)\alpha_i} = \sum_{\eta=0}^{N+1} \sum_{j=1}^{3} \mathbf{A}^{(\tau\eta)\alpha_i\alpha_j} \mathbf{B}^{\alpha_j} \bar{\mathbf{u}}^{(\eta)} \tag{34}$$

where $\mathbf{A}^{(\tau\eta)\alpha_i\alpha_j}$ stands for the constitutive operator of the model. If the structure is made of orthotropic layers it assumes the following matrix form

$$\mathbf{A}^{(\tau\eta)\alpha_i\alpha_j} = \begin{bmatrix}
A_{11(20)}^{(\tau\eta)\alpha_i\alpha_j} & A_{12(11)}^{(\tau\eta)\alpha_i\alpha_j} & A_{16(20)}^{(\tau\eta)\alpha_i\alpha_j} & A_{16(11)}^{(\tau\eta)\alpha_i\alpha_j} & 0 & 0 & 0 & 0 & A_{13(10)}^{(\tau\tilde{\eta})\alpha_i\alpha_j} \\
A_{12(11)}^{(\tau\eta)\alpha_i\alpha_j} & A_{22(02)}^{(\tau\eta)\alpha_i\alpha_j} & A_{26(11)}^{(\tau\eta)\alpha_i\alpha_j} & A_{26(02)}^{(\tau\eta)\alpha_i\alpha_j} & 0 & 0 & 0 & 0 & A_{23(01)}^{(\tau\tilde{\eta})\alpha_i\alpha_j} \\
A_{16(20)}^{(\tau\eta)\alpha_i\alpha_j} & A_{26(11)}^{(\tau\eta)\alpha_i\alpha_j} & A_{66(20)}^{(\tau\eta)\alpha_i\alpha_j} & A_{66(11)}^{(\tau\eta)\alpha_i\alpha_j} & 0 & 0 & 0 & 0 & A_{36(10)}^{(\tau\tilde{\eta})\alpha_i\alpha_j} \\
A_{16(11)}^{(\tau\eta)\alpha_i\alpha_j} & A_{26(02)}^{(\tau\eta)\alpha_i\alpha_j} & A_{66(11)}^{(\tau\eta)\alpha_i\alpha_j} & A_{66(02)}^{(\tau\eta)\alpha_i\alpha_j} & 0 & 0 & 0 & 0 & A_{36(01)}^{(\tau\tilde{\eta})\alpha_i\alpha_j} \\
0 & 0 & 0 & 0 & A_{44(20)}^{(\tau\eta)\alpha_i\alpha_j} & A_{45(11)}^{(\tau\eta)\alpha_i\alpha_j} & A_{44(10)}^{(\tau\tilde{\eta})\alpha_i\alpha_j} & A_{45(10)}^{(\tau\tilde{\eta})\alpha_i\alpha_j} & 0 \\
0 & 0 & 0 & 0 & A_{45(11)}^{(\tau\eta)\alpha_i\alpha_j} & A_{55(02)}^{(\tau\eta)\alpha_i\alpha_j} & A_{45(01)}^{(\tau\tilde{\eta})\alpha_i\alpha_j} & A_{55(01)}^{(\tau\tilde{\eta})\alpha_i\alpha_j} & 0 \\
0 & 0 & 0 & 0 & A_{44(10)}^{(\tilde{\tau}\eta)\alpha_i\alpha_j} & A_{45(01)}^{(\tilde{\tau}\eta)\alpha_i\alpha_j} & A_{44(00)}^{(\tilde{\tau}\tilde{\eta})\alpha_i\alpha_j} & A_{45(00)}^{(\tilde{\tau}\tilde{\eta})\alpha_i\alpha_j} & 0 \\
0 & 0 & 0 & 0 & A_{45(10)}^{(\tilde{\tau}\eta)\alpha_i\alpha_j} & A_{55(01)}^{(\tilde{\tau}\eta)\alpha_i\alpha_j} & A_{45(00)}^{(\tilde{\tau}\tilde{\eta})\alpha_i\alpha_j} & A_{55(00)}^{(\tilde{\tau}\tilde{\eta})\alpha_i\alpha_j} & 0 \\
A_{13(10)}^{(\tilde{\tau}\eta)\alpha_i\alpha_j} & A_{23(01)}^{(\tilde{\tau}\eta)\alpha_i\alpha_j} & A_{36(10)}^{(\tilde{\tau}\eta)\alpha_i\alpha_j} & A_{36(01)}^{(\tilde{\tau}\eta)\alpha_i\alpha_j} & 0 & 0 & 0 & 0 & A_{33(00)}^{(\tilde{\tau}\tilde{\eta})\alpha_i\alpha_j}
\end{bmatrix} \tag{35}$$

where the definitions below are required

$$\begin{aligned}
A_{nm\,(pq)}^{(\tau\eta)\alpha_i\alpha_j} &= \sum_{k=1}^{l} \int_{\zeta_k}^{\zeta_{k+1}} \bar{B}_{nm}^{(k)} F_{\eta}^{\alpha_j} F_{\tau}^{\alpha_i} \frac{H_1 H_2}{H_1^p H_2^q} d\zeta \\
A_{nm\,(pq)}^{(\tilde{\tau}\eta)\alpha_i\alpha_j} &= \sum_{k=1}^{l} \int_{\zeta_k}^{\zeta_{k+1}} \bar{B}_{nm}^{(k)} F_{\eta}^{\alpha_j} \frac{\partial F_{\tau}^{\alpha_i}}{\partial \zeta} \frac{H_1 H_2}{H_1^p H_2^q} d\zeta \\
A_{nm\,(pq)}^{(\tau\tilde{\eta})\alpha_i\alpha_j} &= \sum_{k=1}^{l} \int_{\zeta_k}^{\zeta_{k+1}} \bar{B}_{nm}^{(k)} \frac{\partial F_{\eta}^{\alpha_j}}{\partial \zeta} F_{\tau}^{\alpha_i} \frac{H_1 H_2}{H_1^p H_2^q} d\zeta \\
A_{nm\,(pq)}^{(\tilde{\tau}\tilde{\eta})\alpha_i\alpha_j} &= \sum_{k=1}^{l} \int_{\zeta_k}^{\zeta_{k+1}} \bar{B}_{nm}^{(k)} \frac{\partial F_{\eta}^{\alpha_j}}{\partial \zeta} \frac{\partial F_{\tau}^{\alpha_i}}{\partial \zeta} \frac{H_1 H_2}{H_1^p H_2^q} d\zeta
\end{aligned} \tag{36}$$

for $\tau, \eta = 0, 1, 2, ..., N, N+1, n, m = 1, 2, ..., 6, p, q = 0, 1, 2$ and $i, j = 1, 2, 3$. The mechanical properties of the constituents are all included in the coefficients $\bar{B}_{nm}^{(k)}$ for the k-th layer, which are defined below to give the possibility to include the shear correction factor κ if required by the structural model

$$\begin{aligned} \bar{B}_{nm}^{(k)} &= \bar{E}_{nm}^{(k)} \quad \text{for} \quad n, m = 1, 2, 3, 6 \\ \bar{B}_{nm}^{(k)} &= \kappa \bar{E}_{nm}^{(k)} \quad \text{for} \quad n, m = 4, 5 \end{aligned} \tag{37}$$

The symbol $\bar{E}_{nm}^{(k)}$ is introduced to denote the elastic coefficients of the materials. This notation is used to specify if the structural model at issue needs the plane stress hypothesis. In this circumstance, one gets

$$\bar{E}_{nm}^{(k)} = \bar{Q}_{nm}^{(k)} \tag{38}$$

where $\bar{Q}_{nm}^{(k)}$ represents the plane stress reduced elastic coefficients. Otherwise, the following relation is assumed

$$\bar{E}_{nm}^{(k)} = \bar{C}_{nm}^{(k)} \tag{39}$$

in which $\bar{C}_{nm}^{(k)}$ stands for the non-reduced elastic coefficients. It is well-known that these quantities can be evaluated as a function of the engineering constants of the various constituents, which are the Young's moduli, Poisson's ratios and shear moduli. Finally, it is important to specify that this constitutive model is able to deal with different kinds of laminated composites, in which the orientation of each layer is completely arbitrary. In particular, for a laminated made of l plies, the following notation is employed to denote univocally the stacking sequence

$$\left(\theta^{(1)}/\theta^{(2)}/\ldots/\theta^{(k)}/\ldots/\theta^{(l)}\right) \tag{40}$$

where $\theta^{(k)}$ stands for the orientation of the k-th layer.

3.4 Equations of Motion

The weak formulation of the equations of motion for a laminated composite doubly-curved shell can be carried out by means of the Hamilton's variational principle. For the sake of conciseness, only the final system of equation is presented here. In particular, the fundamental equations are given below in terms of nodal displacements

$$\sum_{\eta=0}^{N+1} \mathbf{K}^{(\tau\eta)} \bar{\mathbf{u}}^{(\eta)} + \sum_{\eta=0}^{N+1} \bar{\mathbf{M}}^{(\tau\eta)} \ddot{\bar{\mathbf{u}}}^{(\eta)} = \mathbf{Q}^{(\tau)} \tag{41}$$

for $\tau = 0, 1, 2, ..., N, N+1$. It can be noted that the system in Eq. (41) provides three equations for each order of kinematic expansion. The various terms in Eq. (41) are now illustrated in compact form for an arbitrarily shaped domain. It should be recalled that the determinant of the Jacobian matrix defined in Eq. (14) is needed to this aim. The operator $\mathbf{K}^{(\tau\eta)}$ is the stiffness matrix of the structure, whose definition is shown below

$$\mathbf{K}^{(\tau\eta)} = \int_{-1}^{1}\int_{-1}^{1} \begin{bmatrix} \mathbf{K}_{11} & \mathbf{K}_{12} & \mathbf{K}_{13} \\ \mathbf{K}_{21} & \mathbf{K}_{22} & \mathbf{K}_{23} \\ \mathbf{K}_{31} & \mathbf{K}_{32} & \mathbf{K}_{33} \end{bmatrix} A_1 A_2 \det(\mathbf{J})\, d\xi_1 d\xi_2 \tag{42}$$

with $\mathbf{K}_{ij} = (\mathbf{B}^{\alpha_i})^T \mathbf{A}^{(\tau\eta)\alpha_i\alpha_j} \mathbf{B}^{\alpha_j}$, for $i, j = 1, 2, 3$. The mass matrix, instead, is denoted by $\bar{\mathbf{M}}^{(\tau\eta)}$ and its definition is shown below

$$\bar{\mathbf{M}}^{(\tau\eta)} = \int_{-1}^{1}\int_{-1}^{1} \begin{bmatrix} \mathbf{M}_{11} & \mathbf{0} & \mathbf{0} \\ \mathbf{0} & \mathbf{M}_{22} & \mathbf{0} \\ \mathbf{0} & \mathbf{0} & \mathbf{M}_{33} \end{bmatrix} A_1 A_2 \det(\mathbf{J})\, d\xi_1 d\xi_2 \tag{43}$$

with $\mathbf{M}_{ij} = \bar{\mathbf{N}}\, I_0^{(\tau\eta)\alpha_i\alpha_j} \bar{\mathbf{N}}^T$, in which $I^{(\tau\eta)\alpha_i\alpha_i}$, for $i, j = 1, 2, 3$, are the inertia masses of the laminate that depend on the mass density $\rho^{(k)}$ of each layer defined below

$$I_0^{(\tau\eta)\alpha_i\alpha_i} = \sum_{k=1}^{l} \int_{\zeta_k}^{\zeta_{k+1}} \rho^{(k)} F_\tau^{\alpha_i} F_\eta^{\alpha_i} H_1 H_2 d\zeta \tag{44}$$

On the other hand, $\ddot{\mathbf{u}}^{(\eta)}$ includes the second-order time derivatives of the nodal displacements defined in Eq. (22). Finally, $\mathbf{Q}^{(\tau)}$ represents the external load vector and it can take into account the effect of both surface $\mathbf{Q}_{sa}^{(\tau)}$ and volume $\mathbf{Q}_{va}^{(\tau)}$ loads, as $\mathbf{Q}^{(\tau)} = \mathbf{Q}_{sa}^{(\tau)} + \mathbf{Q}_{va}^{(\tau)}$. As far as the surface forces are concerned, one gets

$$\mathbf{Q}_{sa}^{(\tau)} = \int_{-1}^{1}\int_{-1}^{1} \begin{bmatrix} \bar{\mathbf{N}} q_{1sa}^{(\tau)} \\ \bar{\mathbf{N}} q_{2sa}^{(\tau)} \\ \bar{\mathbf{N}} q_{3sa}^{(\tau)} \end{bmatrix} A_1 A_2 \det(\mathbf{J})\, d\xi_1 d\xi_2 \tag{45}$$

where the values of the generalized load components $q_{1sa}^{(\tau)}$, $q_{2sa}^{(\tau)}$, $q_{3sa}^{(\tau)}$ applied on the shell middle surface can be obtained by means of the principle of static equivalence shown below, starting from the pressures applied on the lower surface $q_{1a}^{(-)}$, $q_{2a}^{(-)}$, $q_{3a}^{(-)}$ and on the upper surface $q_{1a}^{(+)}$, $q_{2a}^{(+)}$, $q_{3a}^{(+)}$ of the shell

$$\begin{aligned} q_{1sa}^{(\tau)} &= q_{1a}^{(-)} F_\tau^{\alpha_1(-)} H_1^{(-)} H_2^{(-)} + q_{1a}^{(+)} F_\tau^{\alpha_1(+)} H_1^{(+)} H_2^{(+)} \\ q_{2sa}^{(\tau)} &= q_{2a}^{(-)} F_\tau^{\alpha_2(-)} H_1^{(-)} H_2^{(-)} + q_{2a}^{(+)} F_\tau^{\alpha_2(+)} H_1^{(+)} H_2^{(+)} \\ q_{3sa}^{(\tau)} &= q_{3a}^{(-)} F_\tau^{\alpha_3(-)} H_1^{(-)} H_2^{(-)} + q_{3a}^{(+)} F_\tau^{\alpha_3(+)} H_1^{(+)} H_2^{(+)} \end{aligned} \tag{46}$$

where $F_\tau^{\alpha_i(-)}$, $F_\tau^{\alpha_i(+)}$, for $i = 1, 2, 3$, represent the values of the thickness functions evaluated at the external surfaces of the shell, whereas the geometric parameters $H_1^{(\pm)}$, $H_2^{(\pm)}$ are given below

$$H_1^{(\pm)} = 1 \pm \frac{h}{2R_1}, \quad H_2^{(\pm)} = 1 \pm \frac{h}{2R_2} \tag{47}$$

On the other hand, the volume load vector can be defined as follows

$$\mathbf{Q}_{va}^{(\tau)} = \int_{-1}^{1}\int_{-1}^{1} \begin{bmatrix} \bar{\mathbf{N}} q_{1va}^{(\tau)} \\ \bar{\mathbf{N}} q_{2va}^{(\tau)} \\ \bar{\mathbf{N}} q_{3va}^{(\tau)} \end{bmatrix} A_1 A_2 \det(\mathbf{J})\, d\xi_1 d\xi_2 \tag{48}$$

with $q_{iva}^{(\tau)} = I_0^{(\tau)\alpha_i} g_i$, for $i = 1, 2, 3$, and

$$I_0^{(\tau)\alpha_i} = \sum_{k=1}^{l} \int_{\zeta_k}^{\zeta_{k+1}} \rho^{(k)} F_\tau^{\alpha_i} H_1 H_2 d\zeta \tag{49}$$

assuming that g_i is the gravitational acceleration in the local reference system.

3.4.1 Boundary Conditions

In general, these kinds of structural problems can be solved once a set of boundary conditions (natural or essential) are applied. In particular, an external edge can be fully clamped (C), free (F), or simply-supported (S). In the following, the corresponding conditions are illustrated for the various types of restraints. To this aim, since distorted domains are considered, it is convenient to introduce the outward unit vectors $\mathbf{n}_n, \mathbf{n}_s, \mathbf{n}_\zeta$ depicted in Fig. 7. The components of each vector are given by the direction cosines of the three corresponding directions, as specified below

$$\begin{aligned} \mathbf{n}_n &= \begin{bmatrix} n_{n1} & n_{n2} & n_{n3} \end{bmatrix}^T \\ \mathbf{n}_s &= \begin{bmatrix} n_{s1} & n_{s2} & n_{s3} \end{bmatrix}^T \\ \mathbf{n}_\zeta &= \begin{bmatrix} n_{\zeta 1} & n_{\zeta 2} & n_{\zeta 3} \end{bmatrix}^T \end{aligned} \tag{50}$$

These quantities are needed to computed the generalized displacements and the stress resultants involved in the boundary conditions along a generic edge of the structure. As far as the generalized displacements are concerned, one gets

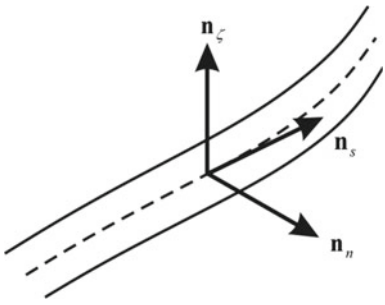

Fig. 7 Definition of the outward unit normal vectors along an arbitrarily shaped external edge

$$\begin{aligned} u_n^{(\tau)} &= n_{n1} u_1^{(\tau)} + n_{n2} u_2^{(\tau)} \\ u_s^{(\tau)} &= n_{s1} u_1^{(\tau)} + n_{s2} u_2^{(\tau)} \\ u_\zeta^{(\tau)} &= u_3^{(\tau)} \end{aligned} \tag{51}$$

whereas the corresponding stress resultant components are given by

$$\begin{aligned} N_n^{(\tau)\alpha_1} &= N_1^{(\tau)\alpha_1} n_{n1}^2 + N_2^{(\tau)\alpha_1} n_{n2}^2 + N_{12}^{(\tau)\alpha_1} n_{n1} n_{n2} + N_{21}^{(\tau)\alpha_1} n_{n1} n_{n2} \\ N_{ns}^{(\tau)\alpha_2} &= N_1^{(\tau)\alpha_2} n_{n1} n_{s1} + N_2^{(\tau)\alpha_2} n_{n2} n_{s2} + N_{12}^{(\tau)\alpha_2} n_{n1} n_{s2} + N_{21}^{(\tau)\alpha_2} n_{n2} n_{s1} \\ T_\zeta^{(\tau)\alpha_3} &= T_1^{(\tau)\alpha_3} n_{n1} + T_2^{(\tau)\alpha_3} n_{n2} \end{aligned} \tag{52}$$

At this point, the boundary conditions for each external edge can be written analytically

$$\begin{aligned} &\text{(C)} \quad \rightarrow \quad u_n^{(\tau)} = u_s^{(\tau)} = u_\zeta^{(\tau)} = 0 \\ &\text{(S)} \quad \rightarrow \quad N_n^{(\tau)\alpha_1} = 0, \quad u_s^{(\tau)} = u_\zeta^{(\tau)} = 0 \\ &\text{(F)} \quad \rightarrow \quad N_n^{(\tau)\alpha_1} = N_{ns}^{(\tau)\alpha_2} = T_\zeta^{(\tau)\alpha_3} = 0 \end{aligned} \tag{53}$$

It should be recalled that the boundary conditions should be enforced only in terms of generalized displacements of the weak formulation of the governing equations is solved, since a C^0 approach is developed. Nevertheless, it is possible also to apply the boundary conditions in terms of stress resultants in order to obtain the corresponding weak formulation with C^1 continuity requirements, as typically done by those methodologies based on the strong form of the governing equations. In the current research, both the C^1 and C^0 approaches are considered.

4 Numerical Technique

In general, a closed-form solution is not available for the structural models just presented. Therefore, a numerical technique must be used to achieve an approximate solution of the governing equations. In particular, it is easy to note that a numerical approach able to approximate integrals is required. The Generalized Integral Quadrature (GIQ) method can be employed to this aim. In the following, only the basis aspects of this technique are presented.

Let us consider a two-dimensional smooth function $f(x, y)$, with $x \in [a, b]$ and $y \in [c, d]$. As specified in the previous sections, the domain under consideration must be discretized by defining respectively I_N, I_M discrete points along each principal direction, so that x_k, y_l define the coordinates of a generic node. By definition, the GIQ provides the following result

$$I = \int_c^d \int_a^b f(x, y)\, dxdy \cong \sum_{k=1}^{I_N} \sum_{l=1}^{I_M} w_k^{1I_N} w_l^{1I_M} f(x_k, y_l) \tag{54}$$

where $w_i^{1I_N}$, $w_j^{1I_M}$ represent the weighting coefficients for the summation in hand. As specified in the paper [88] and in the book by Tornabene and Bacciocchi [1], these coefficients can be evaluated starting from the definitions of the corresponding weighting coefficients used for the approximation of first-order derivatives.

The definitions presented in the previous section must be written in discrete form and evaluated in each point of the reference domain by means of the GIQ technique. Both the mechanical and geometric properties of the structures must be computed in each discrete point of the reference domain, as well.

4.1 Discrete Form of the Governing Equations

By means of the GIQ method, the two-dimensional integral that defines the stiffness matrix $\mathbf{K}^{(\tau\eta)}$ can be written in the corresponding discrete form as shown below

$$\mathbf{K}^{(\tau\eta)} = \sum_{f=1}^{I_N} \sum_{g=1}^{I_M} w_f^{1I_N} w_g^{1I_M} A_{1(fg)} A_{2(fg)} \begin{bmatrix} \mathbf{K}_{11} & \mathbf{K}_{12} & \mathbf{K}_{13} \\ \mathbf{K}_{21} & \mathbf{K}_{22} & \mathbf{K}_{23} \\ \mathbf{K}_{31} & \mathbf{K}_{32} & \mathbf{K}_{33} \end{bmatrix}_{(fg)} \tag{55}$$

for $\tau, \eta = 0, 1, 2, ..., N, N+1$, in which $A_{1(fg)}$, $A_{2(fg)}$ represent the Lamè parameters evaluated in each point of the domain. In the same manner, the mass matrix $\bar{\mathbf{M}}^{(\tau\eta)}$ can be evaluated numerically by means of the same approach. In this circumstance, one gets

$$\bar{\mathbf{M}}^{(\tau\eta)} = \sum_{f=1}^{I_N} \sum_{g=1}^{I_M} w_f^{1I_N} w_g^{1I_M} A_{1(fg)} A_{2(fg)} \begin{bmatrix} \mathbf{M}_{11} & \mathbf{0} & \mathbf{0} \\ \mathbf{0} & \mathbf{M}_{22} & \mathbf{0} \\ \mathbf{0} & \mathbf{0} & \mathbf{M}_{33} \end{bmatrix}_{(fg)} \tag{56}$$

for $\tau, \eta = 0, 1, 2, ..., N, N+1$. Analogously, the discrete vectors of the surface loads and the volume forces can be accomplished following the same approach. As far as the surface forces, one gets

$$\mathbf{Q}_{sa}^{(\tau)} = \sum_{f=1}^{I_N} \sum_{g=1}^{I_M} w_f^{1I_N} w_g^{1I_M} A_{1(fg)} A_{2(fg)} \begin{bmatrix} \bar{\mathbf{N}} q_{1sa}^{(\tau)} \\ \bar{\mathbf{N}} q_{2sa}^{(\tau)} \\ \bar{\mathbf{N}} q_{3sa}^{(\tau)} \end{bmatrix}_{(fg)} \tag{57}$$

for $\tau = 0, 1, 2, ..., N, N+1$. On the other hand, the discrete vector of the volume forces is given below

$$\mathbf{Q}_{va}^{(\tau)} = \sum_{f=1}^{I_N} \sum_{g=1}^{I_M} w_f^{1I_N} w_g^{1I_M} A_{1(fg)} A_{2(fg)} \begin{bmatrix} \bar{\mathbf{N}} q_{1va}^{(\tau)} \\ \bar{\mathbf{N}} q_{2va}^{(\tau)} \\ \bar{\mathbf{N}} q_{3va}^{(\tau)} \end{bmatrix}_{(fg)} \tag{58}$$

for $\tau = 0, 1, 2, ..., N, N+1$. It should be recalled that these quantities must be computed in each grid point of the domain, characterized by the coordinates α_{1f}, α_{2g}.

5 Free Vibration Analysis

In this section, the procedure needed to investigate the natural frequencies, as well as the corresponding mode shapes, of arbitrarily shaped structures is presented. The weak form of the governing equations for the problem at issue can be obtained by Eq. (41), by setting the external load vector equal to zero. In other words, the vibrational behavior is ruled by the following system of equations

$$\sum_{\eta=0}^{N+1} \mathbf{K}^{(\tau\eta)} \bar{\mathbf{u}}^{(\eta)} + \sum_{\eta=0}^{N+1} \bar{\mathbf{M}}^{(\tau\eta)} \ddot{\bar{\mathbf{u}}}^{(\eta)} = \mathbf{0} \tag{59}$$

The solution of the dynamic problem considered in hand can be achieved by using the separation of variables as shown below

$$\bar{\mathbf{u}}^{(\tau)} \left(\alpha_{1f}, \alpha_{2g}, t\right) = \bar{\mathbf{U}}^{(\tau)} \left(\alpha_{1f}, \alpha_{2g}\right) e^{i\omega t} \tag{60}$$

for each order of kinematic expansion τ. The vector $\bar{\mathbf{U}}^{(\tau)}$ collects the modal displacements for each circular frequency ω of the structure. The modal amplitudes are included in the corresponding vector following the same scheme used in the previous paragraphs to collect the generalized displacements.

The second-order derivatives with respect to the time variable t provide the following result

$$\sum_{\eta=0}^{N+1} \mathbf{K}^{(\tau\eta)} \bar{\mathbf{U}}^{(\eta)} = \omega^2 \sum_{\eta=0}^{N+1} \bar{\mathbf{M}}^{(\tau\eta)} \bar{\mathbf{U}}^{(\eta)} \tag{61}$$

The discrete global system of governing equations can be obtained at this point by evaluating the stiffness matrix and the mass matrix by means of the GIQ method. As a result, one gets

$$\mathbf{K}\boldsymbol{\delta} = \omega^2 \mathbf{M}\boldsymbol{\delta} \tag{62}$$

in which $\mathbf{K}$, $\mathbf{M}$ denote respectively the discrete global stiffness and mass matrices, whereas $\boldsymbol{\delta}$ represents the discrete vector of mode shapes.

The dynamic problem at issue can be solved more efficiently by means of the so-called kinematic condensation principle. In other words, it is convenient to separate

the modal displacements related to the internal points of the domain from the ones placed along the external edges. Mathematically speaking, one gets

$$\boldsymbol{\delta} = \left[\boldsymbol{\delta}_b \ \boldsymbol{\delta}_d \right]^T \tag{63}$$

where the subscript b and d are used to specify the quantities related to the boundary and domain points, respectively. The stiffness and mass matrices are consequently partitioned as shown below

$$\begin{bmatrix} \mathbf{K}_{bb} & \mathbf{K}_{bd} \\ \mathbf{K}_{db} & \mathbf{K}_{dd} \end{bmatrix} \begin{bmatrix} \boldsymbol{\delta}_b \\ \boldsymbol{\delta}_d \end{bmatrix} = \omega^2 \begin{bmatrix} \mathbf{0} & \mathbf{0} \\ \mathbf{0} & \mathbf{M}_{dd} \end{bmatrix} \begin{bmatrix} \boldsymbol{\delta}_b \\ \boldsymbol{\delta}_d \end{bmatrix} \tag{64}$$

It is clear that the operators $\mathbf{K}_{bb}$, $\mathbf{K}_{bd}$, $\mathbf{K}_{db}$ are related to the application of boundary conditions along the boundary points, whereas $\mathbf{K}_{dd}$, $\mathbf{M}_{dd}$ denote the stiffness and inertia matrices linked to the internal points of the domain.

After some easy manipulations, a generalized eigenvalue problem is obtained as results

$$\left(\mathbf{M}_{dd}^{-1} \left(\mathbf{K}_{dd} - \mathbf{K}_{db} \mathbf{K}_{bb}^{-1} \mathbf{K}_{bd} \right) - \omega^2 \mathbf{I} \right) \delta_d = \mathbf{0} \tag{65}$$

in which $\mathbf{I}$ stands for the identity matrix. The solution of the motion equations in Eq. (65) provides the values of the circular frequencies ω_k, which are related to the corresponding natural frequencies as $f_k = \omega_k / 2\pi$.

6 Applications

The numerical solutions of some numerical tests and applications are presented at this point. The aim of this section is to prove that the theoretical framework based on the weak formulation and the numerical approach based on the GIQ method can be efficiently and accurately used to deal with these kinds of structural problems [100].

6.1 Convergence Features

The accuracy of the proposed approach is proven firstly by considering a simply-supported square plate. The length of the edges is $L_x = L_y = 1$ m and the thickness is given by $h = 0.1$ m. The accuracy is investigated in terms of the relative error for the first natural frequency ε_1, which is defined as follows

$$\varepsilon_1 = \frac{f_1}{f_{1,\,exact}} - 1 \tag{66}$$

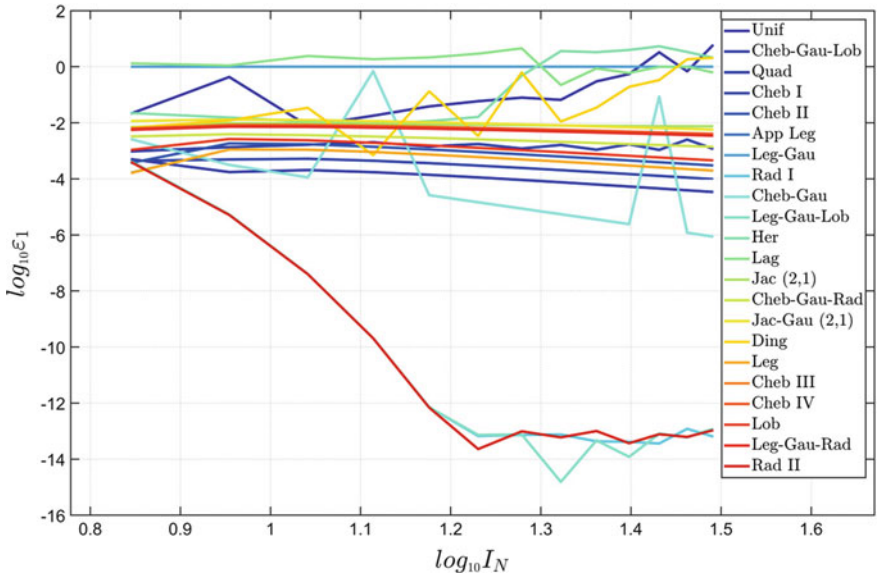

Fig. 8 Convergence behavior of the first natural frequency for a SSSS isotropic square plate in the framework of the Reissner-Mindlin theory (FSDT): weak formulation with C^1 boundary conditions

where f_1 is the numerical value of the first frequency, whereas the corresponding exact value is given by $f_{1,\,exact}$ and can be computed as shown in the book by Reddy [6]. Both the solutions are computed in the theoretical framework provided by the FSDT.

Two different mechanical configurations are considered. Firstly, the plate is made of one single isotropic layer ($E = 70\,\text{GPa}$, $\nu = 0.3$, $\rho = 2707\,\text{kg/m}^3$). Then, a laminated plate is taken into account with (0/90/90/0) as stacking sequence ($E_1 = 137.9$ GPa, $E_2 = E_3 = 8.96$ GPa, $G_{12} = G_{13} = 7.1$ GPa, $G_{23} = 6.21$ GPa, $\nu_{12} = \nu_{13} = 0.3$, $\nu_{23} = 0.49$, $\rho = 1450\ \text{kg/m}^3$).

The solutions are obtained by means of the weak formulation with C^1 and C^0 boundary conditions, for several grid point distributions and increasing number of discrete points $I_N = I_M$. The corresponding convergence graphs in logarithmic scale are depicted respectively in Figs. 8 and 9.

In general, it can be observed that better results can be obtained by setting properly the discrete grid distribution. For instance, only few distributions, including the Legendre-Gauss-Lobatto distribution, are accurate. In particular, a noticeably level of accuracy ($\approx 10^{-13} \div 10^{-14}$ in logarithmic scale) can be reached quickly for a reduced number of grid points ($I_N = I_M = 15$), if the weak formulation is solved together with C^1 boundary conditions (Fig. 8). In this circumstance, the curves oscillate randomly about the most accurate value of the solution once the machine epsilon is reached and the so-called "Roundoff Plateau" can be easily identified.

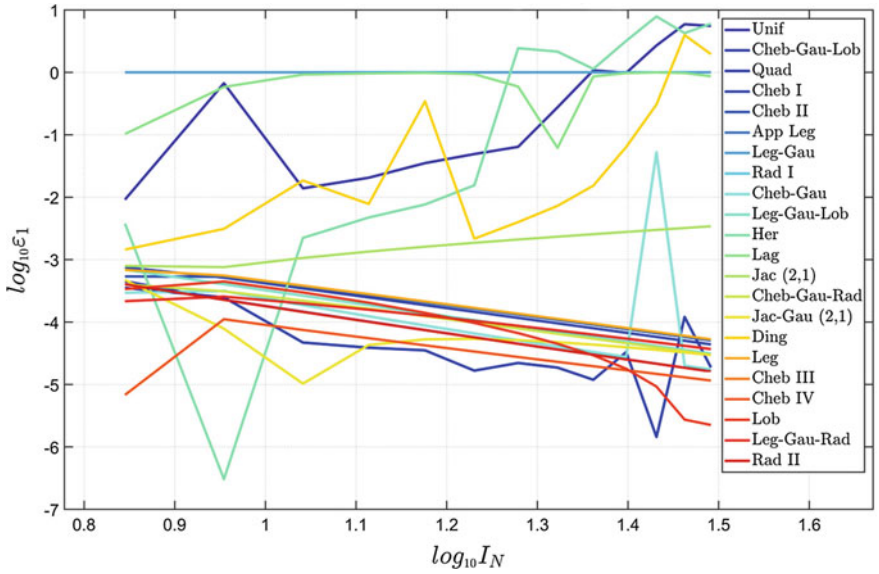

Fig. 9 Convergence behavior of the first natural frequency for a SSSS isotropic square plate in the framework of the Reissner-Mindlin theory (FSDT): weak formulation with C^0 boundary conditions

On the other hand, if the boundary conditions are characterized by a C^0 requirement, the solution is characterized by a linear convergence and the accuracy that can be achieved is extremely lower than the other approach, independently from the choice of the grid distributions. Due to the linear convergence behavior, the same accuracy of the previous approach could be obtained by increasing excessively the number of discrete points (Fig. 9). The same behavior can be observed for both the isotropic and laminated plates.

6.2 Arbitrarily Shaped Domains

In this section, the natural frequencies of some structures characterized by distorted domains are obtained by solving the weak formulation of the corresponding governing equations.

Firstly, a fully clamped isotropic circular plate (radius R and thickness h) is analyzed (Fig. 10). Its geometry can be applied from the one that characterize a square plate, whose middle surface is described by the following position vector

$$\mathbf{r}(x, y) = x\,\mathbf{e}_1 + y\,\mathbf{e}_2 \tag{67}$$

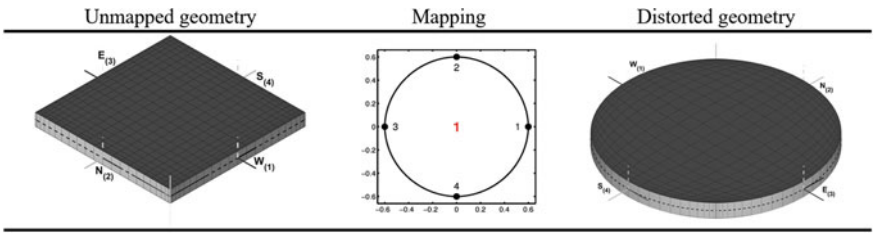

Fig. 10 Circular plate: definition of the distorted domain starting from a rectangular plate

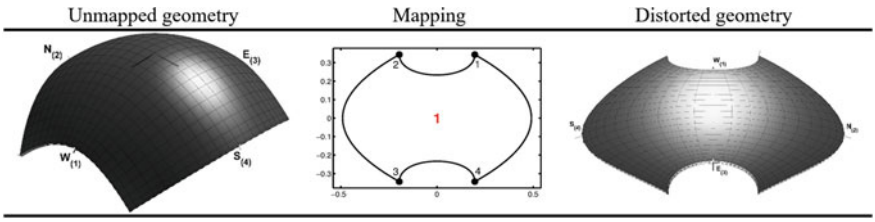

Fig. 11 Arbitrarily shaped shell structure: definition of the distorted domain starting from a doubly-curved shell of translation

The mapping procedure presented in the previous sections is used to define the circular shape depicted in Fig. 10. It is important to specify that four circular arches are used to this aim, since the determinant of the Jacobian matrix must be different from zero. The natural frequencies are presented in dimensionless form as follows

$$\lambda = 2\pi f R^2 \sqrt{\rho h / D} \tag{68}$$

in which D is the flexural stiffness given by $D = Eh^3/12\left(1-\nu^2\right)$.

This test aims to validate the theoretical and numerical frameworks presented in the previous sections. In particular, the solutions given by the GIQ method are compared with the semi-analytical ones proposed by Liew et al. [101]. The natural frequencies for the considered structure are presented in Table 1, for several HSDTs and different ratios h/R. It can be easily observed that the HSDTs provide results that tend to detach from the reference ones for higher value of thickness, as predictable, since the reference solution is based on a first-order shear deformation theory. In addition, the two weak formulations (C^0 and C^1) provide the same solutions, since only the displacements are involved in the fully clamped boundary conditions.

An arbitrary shaped doubly-curved shell is considered now. The reference domain (both regular and mapped) is shown in Fig. 11. In particular, a laminated composite doubly-curved panel of translation characterized by the following position vector is considered

$$\begin{aligned}\mathbf{r}\left(\alpha_1,\alpha_2\right) = &\left(2\tan\left(\alpha_1\right) - \sin\left(\alpha_2\right)\tan^2\left(\alpha_2\right)\right)\mathbf{e}_1 - 2\tan\left(\alpha_2\right)\mathbf{e}_2 + \\ &+\left(\tan^2\left(\alpha_1\right)\cos\left(\alpha_1\right)\tan^2\left(\alpha_2\right)\right)\mathbf{e}_3\end{aligned} \tag{69}$$

Table 1 Comparison of the frequency parameter λ of a fully clamped isotropic circular plate of radius R, for different HSDTs. The discrete solution is obtained by setting $I_N = I_M = 25$ as total number of points

Mode	FSDT	ED2	ED3	ED4	Ref. [101]
$h/R = 0.05$					
1	10.270	10.282	10.285	10.284	10.145
2	21.227	21.252	21.265	21.263	21.002
3	34.408	34.449	34.484	34.479	34.258
4	39.322	39.368	39.411	39.406	38.885
5	50.107	50.164	50.235	50.228	49.782
6	59.502	59.570	59.664	59.656	58.827
7	67.707	67.783	67.909	67.898	67.420
8	81.440	81.534	81.709	81.694	80.933
9	86.001	86.098	86.288	86.275	84.995
10	87.350	87.446	87.649	87.635	87.022
$h/R = 0.10$					
1	10.061	10.085	10.099	10.095	9.941
2	20.413	20.460	20.512	20.504	20.232
3	32.448	32.518	32.643	32.628	32.406
4	36.892	36.971	37.125	37.107	36.479
5	46.280	46.371	46.612	46.588	46.178
6	54.442	54.550	54.865	54.835	53.890
7	61.254	61.365	61.765	61.731	61.272
8	72.725	72.859	73.394	73.348	72.368
9	76.473	76.613	77.197	77.148	75.664
10	77.399	77.528	78.137	78.088	77.454
$h/R = 0.20$					
1	9.344	9.384	9.430	9.422	9.240
2	17.944	18.007	18.163	18.143	17.834
3	27.175	27.251	27.576	27.541	27.214
4	30.505	30.591	30.982	30.939	30.211
5	37.104	37.186	37.739	37.684	37.109
6	42.767	42.860	43.559	43.488	42.409
7	47.309	47.391	48.218	48.137	47.340
8	54.785	54.877	55.389	55.389	54.557
9	57.183	57.278	58.416	58.297	56.682
10	57.830	57.911	59.057	58.944	57.793
$h/R = 0.25$					
1	8.902	8.945	9.010	8.999	8.807
2	16.61	16.671	16.873	16.849	16.521
3	24.634	24.701	25.099	25.056	24.670
4	27.501	27.576	28.050	27.997	27.253

(continued)

Table 1 (continued)

Mode	FSDT	ED2	ED3	ED4	Ref. [101]
5	33.102	33.167	33.814	33.746	33.083
6	37.848	37.920	38.728	38.639	37.550
7	41.694	41.754	42.574	42.565	41.657
8	47.853	47.917	49.095	48.962	47.650
9	49.829	49.895	51.155	51.008	49.420

Table 2 First ten natural frequencies of an arbitrarily shaped laminated doubly-curved panel of translation. The discrete solution is obtained by setting $I_N = I_M = 25$ as total number of points

f [Hz]	FSDT	FSDTZ	ED2	EDZ2	ED3	EDZ3	ED4	EDZ4	
Weak formulation C^1									3D-FEM
1	115.916	115.899	115.302	115.237	115.213	115.173	116.115	116.212	113.816
2	122.155	122.140	121.684	121.616	121.744	121.747	122.184	122.225	120.808
3	194.165	194.136	193.449	193.364	193.425	193.373	193.516	193.448	193.623
4	196.277	196.235	195.415	195.406	195.854	195.395	195.864	195.684	194.692
5	353.920	353.857	352.402	352.277	353.407	353.282	353.648	353.575	350.881
6	355.113	355.074	353.751	353.590	354.083	353.937	354.695	354.763	352.397
7	507.457	507.382	505.614	505.426	506.269	505.939	505.544	505.498	505.891
8	509.924	509.852	508.126	508.008	509.064	508.433	507.802	507.583	508.220
9	536.163	536.133	534.208	533.960	534.567	534.140	533.520	533.532	534.428
10	542.467	542.430	540.408	540.172	540.811	540.707	541.451	541.512	540.991
Weak formulation C^0									3D-FEM
1	115.806	115.795	115.583	115.522	115.553	115.493	115.389	115.379	113.816
2	122.809	122.803	122.652	122.593	122.628	122.570	122.466	122.455	120.808
3	195.416	195.395	194.966	194.886	195.092	195.010	194.857	194.845	193.623
4	196.492	196.470	196.036	195.953	196.168	196.085	195.926	195.916	194.692
5	355.348	355.317	354.196	354.036	354.400	354.246	353.931	353.905	350.881
6	356.718	356.688	355.605	355.451	355.806	355.657	355.350	355.325	352.397
7	509.441	509.389	507.816	507.636	508.175	507.987	507.620	507.600	505.891
8	512.044	511.993	510.459	510.266	510.881	510.685	510.300	510.280	508.220
9	537.872	537.850	536.189	535.915	536.715	536.466	535.914	535.875	534.428
10	545.104	545.083	543.281	543.021	543.617	543.377	542.831	542.788	540.991

with $\alpha_1 \in [-\pi/4, \pi/4]$, $\alpha_2 \in [-\pi/4, \pi/4]$, and $h = 0.05\,\text{m}$. As it can be easily noted from Fig. 11, a completely curvilinear transformation is taken into account as far as the nonlinear mapping is concerned. The lamination scheme is given by (0/30/60/90), and all the layers have the same thickness ($h_1 = h_2 = h_3 = h_4 = 0.0125\,\text{m}$) and mechanical properties ($E_1 = 137.9\,\text{GPa}$, $E_2 = E_3 = 8.96\,\text{GPa}$, $G_{12} = G_{13} = 7.1\,\text{GPa}$, $G_{23} = 6.21\,\text{GPa}$, $\nu_{12} = \nu_{13} = 0.3$, $\nu_{23} = 0.49$, $\rho = 1450$

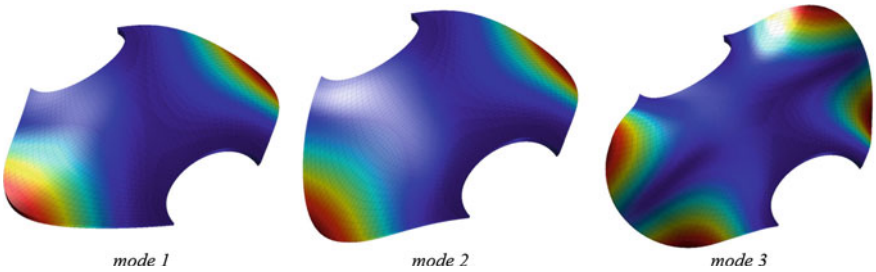

Fig. 12 First three mode shapes of the laminated composite shell structure characterized by an arbitrarily shaped domain

kg/m^3). The discrete solution is obtained by setting $I_N = I_M = 25$ as total number of points. With reference to Fig. 11, it should be specified that the edges denoted by W and E are clamped, whereas the other two are set as free. Thus, the two different formulations are both considered in this circumstance, as it can be noted from Table 2. Here, the natural frequencies are shown for various HSDTs, including also the Murakami's function to capture the zig-zag effect.

A three-dimensional model solved by the well-known Finite Element Method (3D-FEM) is also considered and defined in the commercial software Strand7 (9248 brick elements with 20 nodes). From the results shown in Table 2, the solutions obtained by means of higher-order models are closer to the 3D-FEM results. If compared to the three-dimensional models, the present two-dimensional approaches are able to get the same results with an extremely lower number of degrees of freedom. A 20-node element model is introduced, in fact, for the 3D-FEM solutions. Thus, there is a huge advantage in terms of computational time. In fact, it should be recalled that the considered structures can be modeled by using one sole element, even if the domain is highly distorted. For the sake of completeness, the first three mode shapes of the laminated composite shell structure are depicted in Fig. 12, from wich it can be easily noted that also the boundary conditions are well-enforced for distorted domains.

These applications prove that the mapping procedure shown in the previous sections represents an efficient tool to deal with arbitrarily shaped geometries, when the weak formulation of the governing equation is solved.

7 Final Remarks

A weak formulation has been developed for the mechanical analysis of doubly-curved shell structures made of composite materials. For this purpose, the Lagrange polynomials of high degree have been used for the interpolation of the nodal displacements. The governing equations have been obtained in the framework of Higher-order Shear Deformation Theories (HSDTs). In general, an outstanding degree of accuracy is reached for a small number of discrete grid points.

References

1. Tornabene, F., Bacciocchi, M.: Anisotropic doubly-curved shells. Higher-Order Strong and Weak Formulations for Arbitrarily Shaped Shell Structures. Esculapio, Bologna (2018)
2. Kraus, H.: Thin Elastic Shells. Wiley, New York (1967)
3. Vinson, J.R.: The Behavior of Shells Composed of Isotropic and Composite Materials. Springer, Berlin (1993)
4. Jones, R.M.: Mechanics of Composite Materials, 2nd edn. Taylor & Francis, London (1999)
5. Vasiliev, V.V., Morozov, E.V.: Mechanics and Analysis of Composite Materials. Elsevier, Oxford (2001)
6. Reddy, J.N.: Mechanics of Laminated Composite Plates and Shells, 2nd edn. CRC Press, Boca Raton (2004)
7. Barbero, E.J.: Introduction to Composite Materials Design. CRC Press, Boca Raton (2011)
8. Tornabene, F.: Free vibrations of anisotropic doubly-curved shells and panels of revolution with a free-form meridian resting on Winkler-Pasternak elastic foundations. Compos. Struct. **94**, 186–206 (2011)
9. Tornabene, F.: Free vibrations of laminated composite doubly-curved shells and panels of revolution via the GDQ method. Comput. Method. Appl. M **200**, 931–952 (2011)
10. Tornabene, F., Fantuzzi, N., Viola, E., Reddy, J.N.: Winkler-Pasternak foundation effect on the static and dynamic analyses of laminated doubly-curved and degenerate shells and panels. Compos. Part B Eng. **57**, 269–296 (2014)
11. Tornabene, F., Fantuzzi, N., Bacciocchi, M.: The local GDQ method applied to general higher-order theories of doubly-curved laminated composite shells and panels: the free vibration analysis. Compos. Struct. **116**, 637–660 (2014)
12. Tornabene, F., Fantuzzi, N., Bacciocchi, M., Viola, E.: A new approach for treating concentrated loads in doubly-curved composite deep shells with variable radii of curvature. Compos. Struct. **131**, 433–452 (2015)
13. Tornabene, F., Fantuzzi, N., Bacciocchi, M., Viola, E.: Higher-order theories for the free vibration of doubly-curved laminated panels with curvilinear reinforcing fibers by means of a local version of the GDQ method. Compos. Part B Eng. **81**, 196–230 (2015)
14. Tornabene, F., Fantuzzi, N., Bacciocchi, M.: Higher-order structural theories for the static analysis of doubly-curved laminated composite panels reinforced by curvilinear fibers. Thin Wall. Struct. **102**, 222–245 (2016)
15. Tornabene, F., Fantuzzi, N., Bacciocchi, M.: The local GDQ method for the natural frequencies of doubly-curved shells with variable thickness: a general formulation. Compos. Part B Eng. **92**, 265–289 (2016)
16. Tornabene, F., Fantuzzi, N., Bacciocchi, M., Neves, A.M.A., Ferreira, A.J.M.: MLSDQ based on RBFs for the free vibrations of laminated composite doubly-curved shells. Compos. Part B Eng. **99**, 30–47 (2016)
17. Tornabene, F., Fantuzzi, N., Bacciocchi, M.: On the mechanics of laminated doubly-curved shells subjected to point and line loads. Int. J. Eng. Sci. **109**, 115–164 (2016)
18. Bacciocchi, M., Eisenberger, M., Fantuzzi, N., Tornabene, F., Viola, E.: Vibration analysis of variable thickness plates and shells by the generalized differential quadrature method. Compos. Struct. **156**, 218–237 (2016)
19. Brischetto, S., Tornabene, F., Fantuzzi, N., Bacciocchi, M.: Interpretation of boundary conditions in the analytical and numerical shell solutions for mode analysis of multilayered structures. Int. J. Mech. Sci. **122**, 18–28 (2017)
20. Tornabene, F., Fantuzzi, N., Bacciocchi, M., Reddy, J.N.: A posteriori stress and strain recovery procedure for the static analysis of laminated shells resting on nonlinear elastic foundation. Compos. Part B Eng. **126**, 162–191 (2017)
21. Fantuzzi, N., Tornabene, F., Bacciocchi, M., Neves, A.M.A., Ferreira, A.J.M.: Stability and accuracy of three fourier expansion-based strong form finite elements for the free vibration analysis of laminated composite plates. Int. J. Numer. Meth. Eng. **111**, 354–382 (2017)

22. Tornabene, F., Fantuzzi, N., Bacciocchi, M.: Linear static behavior of damaged laminated composite plates and shells. Materials **10**(811), 1–52 (2017)
23. Jouneghani, F.Z., Mohammadi Dashtaki, P., Dimitri, R., Bacciocchi, M., Tornabene, F.: First-order shear deformation theory for orthotropic doubly-curved shells based on a modified couple stress elasticity. Aerosp. Sci. Technol. **73**, 129–147 (2018)
24. Tornabene, F., Dimitri, R.: A numerical study of the seismic response of arched and vaulted structures made of isotropic or composite materials. Eng. Struct. **159**, 332–366 (2018)
25. Tornabene, F., Fantuzzi, N., Bacciocchi, M., Viola, E.: Mechanical behavior of damaged laminated composites plates and shells: higher-order shear deformation theories. Compos. Struct. **189**, 304–329 (2018)
26. Tornabene, F., Bacciocchi, M.: Effect of curvilinear reinforcing fibers on the linear static behavior of soft-core sandwich structures. J. Compos. Sci. **2**(14), 1–43 (2018)
27. Brischetto, S., Tornabene, F.: Advanced GDQ models and 3D stress recovery in multi-layered plates, spherical and double-curved panels subjected to transverse shear loads. Compos. Part B Eng. **146**, 244–269 (2018)
28. Tornabene, F., Brischetto, S.: 3D capability of refined GDQ models for the bending analysis of composite and sandwich plates, spherical and doubly-curved shells. Thin Wall. Struct. **129**, 94–124 (2018)
29. Tornabene, F., Bacciocchi, M.: Dynamic stability of doubly-curved multilayered shells subjected to arbitrarily oriented angular velocities: numerical evaluation of the critical speed. Compos. Struct. **201**, 1031–1055 (2018)
30. Tornabene, F., Fantuzzi, F., Bacciocchi, M.: Foam core composite sandwich plates and shells with variable stiffness: effect of curvilinear fiber path on the modal response. J. Sandw. Struct. Mater. **21**, 320–365 (2019)
31. Tornabene, F., Fantuzzi, N., Bacciocchi, M.: Refined shear deformation theories for laminated composite arches and beams with variable thickness: natural frequency analysis. Eng. Anal Bound Elem.**100**, 24–47 (2019)
32. Tornabene, F., Viola, E.: Free vibration analysis of functionally graded panels and shells of revolution. Meccanica **44**, 255–281 (2009)
33. Tornabene, F., Viola, E., Inman, D.J.: 2-D differential quadrature solution for vibration analysis of functionally graded conical, cylindrical shell and annular plate structures. J. Sound Vib. **328**, 259–290 (2009)
34. Tornabene, F.: Free vibration analysis of functionally graded conical, cylindrical shell and annular plate structures with a four-parameter power-law distribution. Comput. Method Appl. M **198**, 2911–2935 (2009)
35. Tornabene, F., Viola, E.: Free vibrations of four-parameter functionally graded parabolic panels and shells of revolution. Eur. J. Mech. A Solid **28**, 991–1013 (2009)
36. Viola, E., Tornabene, F.: Free vibrations of three parameter functionally graded parabolic panels of revolution. Mech. Res. Commun. **36**, 587–594 (2009)
37. Tornabene, F., Viola, E.: Static analysis of functionally graded doubly-curved shells and panels of revolution. Meccanica **48**, 901–930 (2013)
38. Tornabene, F., Fantuzzi, N., Bacciocchi, M.: Free vibrations of free-form doubly-curved shells made of functionally graded materials using higher-order equivalent single layer theories. Compos. Part B Eng. **67**, 490–509 (2014)
39. Tornabene, F., Fantuzzi, N., Viola, E., Batra, R.C.: Stress and strain recovery for functionally graded free-form and doubly-curved sandwich shells using higher-order equivalent single layer theory. Compos. Struct. **119**, 67–89 (2015)
40. Fantuzzi, N., Tornabene, F., Viola, E.: Four-parameter functionally graded cracked plates of arbitrary shape: a GDQFEM solution for free vibrations. Mech. Adv. Mater. Struct. **23**, 89–107 (2016)
41. Brischetto, S., Tornabene, F., Fantuzzi, N., Viola, E.: 3D exact and 2D generalized differential quadrature models for free vibration analysis of functionally graded plates and cylinders. Meccanica **51**, 2059–2098 (2016)

42. Fantuzzi, N., Brischetto, S., Tornabene, F., Viola, E.: 2D and 3D shell models for the free vibration investigation of functionally graded cylindrical and spherical panels. Compos. Struct. **154**, 573–590 (2016)
43. Tornabene, F., Brischetto, S., Fantuzzi, N., Bacciocchi, M.: Boundary conditions in 2D numerical and 3D exact models for cylindrical bending analysis of functionally graded structures. Shock Vib. **2373862**, 1–17 (2016)
44. Tornabene, F., Fantuzzi, N., Bacciocchi, M., Viola, E., Reddy, J.N.: A numerical investigation on the natural frequencies of FGM sandwich shells with variable thickness by the local generalized differential quadrature method. Appl. Sci. **7**(131), 1–39 (2017)
45. Jouneghani, F.Z., Dimitri, R., Bacciocchi, M., Tornabene, F.: Free vibration analysis of functionally graded porous doubly-curved shells based on the first-order shear deformation theory. Appl. Sci. **7**(1252), 1–20 (2017)
46. Tornabene, F., Fantuzzi, N., Bacciocchi, M., Viola, E.: Effect of agglomeration on the natural frequencies of functionally graded carbon nanotube-reinforced laminated composite doubly-curved shells. Compos. Part B Eng. **89**, 187–218 (2016)
47. Kamarian, S., Salim, M., Dimitri, R., Tornabene, F.: Free vibration analysis of conical shells reinforced with agglomerated carbon nanotubes. Int. J. Mech. Sci. **108–109**, 157–165 (2016)
48. Fantuzzi, N., Tornabene, F., Bacciocchi, M., Dimitri, R.: Free vibration analysis of arbitrarily shaped functionally graded carbon nanotube-reinforced plates. Compos. Part B Eng. **115**, 384–408 (2017)
49. Tornabene, F., Fantuzzi, N., Bacciocchi, M.: Linear static response of nanocomposite plates and shells reinforced by agglomerated carbon nanotubes. Compos. Part B Eng. **115**, 449–476 (2017)
50. Nejati, M., Asanjarani, A., Dimitri, R., Tornabene, F.: Static and free vibration analysis of functionally graded conical shells reinforced by carbon nanotubes. Int. J. Mech. Sci. **130**, 383–398 (2017)
51. Nejati, M., Dimitri, R., Tornabene, F., Yas, M.H.: Thermal buckling of nanocomposite stiffened cylindrical shells reinforced by functionally graded wavy carbon nano-tubes with temperature-dependent properties. Appl. Sci. **7**(1223), 1–24 (2017)
52. Banić, D., Bacciocchi, M., Tornabene, F., Ferreira, A.J.M.: Influence of Winkler-Pasternak foundation on the vibrational behavior of plates and shells reinforced by agglomerated carbon nanotubes. Appl. Sci. **7**(1228), 1–55 (2017)
53. Tornabene, F., Bacciocchi, M., Fantuzzi, N., Reddy, J.N.: Multiscale approach for three-phase CNT/polymer/fiber laminated nanocomposite structures. Polym. Compos. **40**, E102–E126 (2019)
54. Whitney, J.M., Pagano, N.J.: Shear deformation in heterogeneous anisotropic plates. J. Appl. Mech. T ASME **37**, 1031–1036 (1970)
55. Whitney, J.M., Sun, C.T.: A higher order theory for extensional motion of laminated composites. J. Sound Vib. **30**, 85–97 (1973)
56. Reissner, E.: On transverse bending of plates, including the effect of transverse shear deformation. Int. J. Solids Struct. **11**, 569–573 (1975)
57. Green, A.E., Naghdi, P.M.: A theory of composite laminated plates. IMA J. Appl. Math. **29**, 1–23 (1982)
58. Reddy, J.N.: A simple higher-order theory for laminated composite plates. J. Appl. Mech. T ASME **51**, 745–752 (1984)
59. Bert, C.W.: A critical evaluation of new plate theories applied to laminated composites. Compos. Struct. **2**, 329–347 (1984)
60. Reddy, J.N., Liu, C.F.: A higher-order shear deformation theory for laminated elastic shells. Int. J. Eng. Sci. **23**, 319–330 (1985)
61. Reddy, J.N.: A generalization of the two-dimensional theories of laminated composite plates. Commun. Appl. Numer. M **3**, 173–180 (1987)
62. Librescu, L., Reddy, J.N.: A few remarks concerning several refined theories of anisotropic composite laminated plates. Int. J. Eng. Sci. **27**, 515–527 (1989)
63. Reddy, J.N.: On refined theories of composite laminates. Meccanica **25**, 230–238 (1990)

64. Robbins, D.H., Reddy, J.N.: Modeling of thick composites using a layer-wise laminate theory. Int. J. Numer. Meth. Eng. **36**, 655–677 (1993)
65. Carrera, E.: A refined multi-layered finite-element model applied to linear and non-linear analysis of sandwich plates. Compos. Sci. Technol. **58**, 1553–1569 (1998)
66. Carrera, E.: Theories and finite elements for multilayered, anisotropic, composite plates and shells. Arch. Comput. Methods Eng. **9**, 87–140 (2002)
67. Carrera, E.: Theories and finite elements for multilayered plates and shells: a unified compact formulation with numerical assessment and benchmarking. Arch. Comput. Methods Eng. **10**, 215–296 (2003)
68. Carrera, E.: Historical review of zig-zag theories for multilayered plates and shells. Appl. Mech. Rev. **56**, 287–308 (2003)
69. Carrera, E.: On the use of the Murakami's zig-zag function in the modeling of layered plates and shells. Comput. Struct. **82**, 541–554 (2004)
70. Dozio, L.: A hierarchical formulation of the state-space Levy's method for vibration analysis of thin and thick multilayered shells. Compos. Part B Eng. **98**, 97–107 (2016)
71. Dozio, L., Alimonti, L.: Variable kinematic finite element models of multilayered composite plates coupled with acoustic fluid. Mech. Adv. Mater. Struct. **23**, 981–996 (2016)
72. Vescovini, R., Dozio, L.: A variable-kinematic model for variable stiffness plates: vibration and buckling analysis. Compos. Struct. **142**, 15–26 (2016)
73. Wenzel, C., D'Ottavio, M., Polit, O., Vidal, P.: Assessment of free-edge singularities in composite laminates using higher-order plate elements. Mech. Adv. Mat. Struct. **23**, 948–959 (2016)
74. Demasi, L.: ∞^3 hierarchy plate theories for thick and thin composite plates: the generalized unified formulation. Compos. Struct. **84**, 256–270 (2008)
75. D'Ottavio, M.: A sublaminate generalized unified formulation for the analysis of composite structures. Compos. Struct. **142**, 187–199 (2016)
76. Viola, E., Tornabene, F., Fantuzzi, N.: Static analysis of completely doubly-curved laminated shells and panels using general higher-order shear deformation theories. Compos. Struct. **101**, 59–93 (2013)
77. Viola, E., Tornabene, F., Fantuzzi, N.: General higher-order shear deformation theories for the free vibration analysis of completely doubly-curved laminated shells and panels. Compos. Struct. **95**, 639–666 (2013)
78. Tornabene, F., Viola, E., Fantuzzi, N.: General higher-order equivalent single layer theory for free vibrations of doubly-curved laminated composite shells and panels. Compos. Struct. **104**, 94–117 (2013)
79. Tornabene, F., Fantuzzi, N., Viola, E., Ferreira, A.J.M.: Radial basis function method applied to doubly-curved laminated composite shells and panels with a general higher-order equivalent single layer formulation. Compos. Part B Eng. **55**, 642–659 (2013)
80. Tornabene, F., Fantuzzi, N., Viola, E., Carrera, E.: Static analysis of doubly-curved anisotropic shells and panels using CUF approach, differential geometry and differential quadrature method. Compos. Struct. **107**, 675–697 (2014)
81. Tornabene, F., Fantuzzi, N., Bacciocchi, M., Viola, E.: Accurate inter-laminar recovery for plates and doubly-curved shells with variable radii of curvature using layer-wise theories. Compos. Struct. **124**, 368–393 (2015)
82. Tornabene, F., Fantuzzi, N., Bacciocchi, M., Dimitri, R.: Dynamic analysis of thick and thin elliptic shell structures made of laminated composite materials. Compos. Struct. **133**, 278–299 (2015)
83. Tornabene, F., Fantuzzi, N., Bacciocchi, M., Dimitri, R.: Free vibrations of composite oval and elliptic cylinders by the generalized differential quadrature method. Thin Wall. Struct. **97**, 114–129 (2015)
84. Tornabene, F., Fantuzzi, N., Viola, E.: Inter-laminar stress recovery procedure for doubly-curved, singly-curved, revolution shells with variable radii of curvature and plates using generalized higher-order theories and the local GDQ method. Mech. Adv. Mater. Struct. **23**, 1019–1045 (2016)

85. Tornabene, F.: General higher order layer-wise theory for free vibrations of doubly-curved laminated composite shells and panels. Mech. Adv. Mater. Struct. **23**, 1046–1067 (2016)
86. Tornabene, F., Fantuzzi, N., Bacciocchi, M., Reddy, J.N.: An equivalent layer-wise approach for the free vibration analysis of thick and thin laminated sandwich shells. Appl. Sci. **7**(17), 1–34 (2017)
87. Tornabene, F., Fantuzzi, N., Bacciocchi, M.: Strong and weak formulations based on differential and integral quadrature methods for the free vibration analysis of composite plates and shells: convergence and accuracy. Eng. Anal. Bound Elem. **92**, 3–37 (2018)
88. Tornabene, F., Fantuzzi, N., Ubertini, F., Viola, E.: Strong formulation finite element method based on differential quadrature: a survey. Appl. Mech. Rev. **67**, 020801 (2015)
89. Shu, C.: Differential Quadrature and Its Application in Engineering. Springer, Berlin (2000)
90. Fantuzzi, N., Tornabene, F., Viola, E., Ferreira, A.J.M.: A strong formulation finite element method (SFEM) based on RBF and GDQ techniques for the static and dynamic analyses of laminated plates of arbitrary shape. Meccanica **49**, 2503–2542 (2014)
91. Fantuzzi, N.: New insights into the strong formulation finite element method for solving elastostatic and elastodynamic problems. Curved Layer Struct. **1**, 93–126 (2014)
92. Fantuzzi, N., Bacciocchi, M., Tornabene, F., Viola, E., Ferreira, A.J.M.: Radial basis functions based on differential quadrature method for the free vibration of laminated composite arbitrary shaped plates. Compos. Part B Eng. **78**, 65–78 (2015)
93. Tornabene, F., Fantuzzi, N., Bacciocchi, M.: Mechanical behaviour of composite cosserat solids in elastic problems with holes and discontinuities. Compos. Struct. **179**, 468–481 (2017)
94. Fantuzzi, N., Leonetti, L., Trovalusci, P., Tornabene, F.: Some novel numerical applications of cosserat continua. Int. J. Comp. Meth. **15**, 1850054 (2018)
95. Fantuzzi, N., Tornabene, F., Bacciocchi, M., Ferreira, A.J.M.: On the convergence of laminated composite plates of arbitrary shape through finite element models. J. Compos. Sci. **2**(16), 1–50 (2018)
96. Fantuzzi, N., Tornabene, F.: Strong formulation isogeometric analysis (SFIGA) for laminated composite arbitrarily shaped plates. Compos. Part B Eng. **96**, 173–203 (2016)
97. Tornabene, F., Fantuzzi, N., Bacciocchi, M.: The GDQ method for the free vibration analysis of arbitrarily shaped laminated composite shells using a NURBS-based isogeometric approach. Compos. Struct. **154**, 190–218 (2016)
98. Fantuzzi, N., Puppa, G.D., Tornabene, F., Trautz, M.: Strong formulation isogeometric analysis for the vibration of thin membranes of general shape. Int. J. Mech. Sci. **120**, 322–340 (2017)
99. Tornabene, F., Fantuzzi, N., Bacciocchi, M.: A new doubly-curved shell element for the free vibrations of arbitrarily shaped laminated structures based on weak formulation isogeometric analysis. Compos. Struct. **171**, 429–461 (2017)
100. Tornabene, F., Fantuzzi, N., Bacciocchi, M.: DiQuMASPAB: Differential Quadrature for Mechanics of Anisotropic Shells, Plates, Arches and Beams. User Manual. Esculapio, Bologna. https://DiQuMASPAB.editrice-esculapio.com (2018)
101. Liew, K.M., Wang, C.M., Xiang, Y., Kitipornchai, S.: Vibration of Mindlin Plates. Elsevier, London (1998)

Strong Formulation: A Powerful Way for Solving Doubly Curved Shell Structures

Francesco Tornabene and Nicholas Fantuzzi

Abstract A theoretical framework based on an Equivalent Single Layer (ESL) approach is proposed in this chapter to develop several Higher-order Shear Deformation Theories (HSDTs) in a unified and compact manner. In particular, the maximum order of kinematic expansion can be arbitrarily chosen in order to define more refined displacement fields. The Murakami's function can be also included in the model to take into account the so-called zig-zag effect. The proposed theory is employed to describe the mechanical behavior of doubly-curved shell structures made of composite materials. In particular, the differential geometry is used to define accurately the curved surfaces at issue. The strong formulation of the governing equation is solved by means of a numerical approach based on the Generalized Differential Quadrature (GDQ) method. The accuracy of both the theoretical model and the numerical method is shown through some applications, in which the solutions are compared with the results obtained by means of a three-dimensional finite element model.

1 Introduction

It is well-known that a system of differential equations can be introduced to model a physical phenomenon from the mathematical point of view. In general, various parameters are involved in these systems, according to the kind of phenomenon that has to be investigated [1–4]. The displacement field, the static and dynamic responses, the internal stresses and the natural frequencies are some mechanical parameters that have to be considered and evaluated for instance, when the structural analysis of doubly-curved shells is performed. Such quantities can be accomplished once the corresponding differential governing equations are solved, by enforcing also the proper boundary conditions [5].

F. Tornabene (✉)
University of Salento, Via per Monteroni, 73100 Lecce, Italy
e-mail: francesco.tornabene@unisalento.it

N. Fantuzzi
University of Bologna, Viale del Risorgimento 2, 40136 Bologna, Italy
e-mail: nicholas.fantuzzi@unibo.it

H. Altenbach et al. (eds.), *Recent Developments in the Theory of Shells*,
Advanced Structured Materials 110, https://doi.org/10.1007/978-3-030-17747-8_33

In general, the system of governing equations cannot be solved from the analytical point of view. Therefore, a numerical solution, which approximates the effective one, is often pursued. Several numerical techniques have been proposed in the last decades to this aim, as illustrated in the review paper by Tornabene et al. [6]. Two different approaches can be used for this purpose, which are respectively based on the strong and weak formulations of the same equations. When the strong formulation is considered, the differential system is directly written in its discrete form. On the other hand, an integral form is developed if the corresponding weak formulation is taken into account. It is clear that these two approaches require a different numerical tool to be solved. In particular, the first one need a methodology able to approximate the derivatives, whereas the second one requires a technique able to solve integrals. For examples, the Generalized Differential Quadrature (GDQ) and the Generalized Integral Quadrature (GIQ) methods could be employed to this aim [6]. The basis of these techniques can be found also in the book by Shu [7] and in the book by Tornabene and Bacciocchi [1]. In this chapter, a numerical approach based on the GDQ method is presented to deal with the mechanical analysis of doubly-curved laminated composite shells [8, 9].

It should be recalled that the use of composite materials in shell structures is becoming more and more popular due to the great advantages in terms of structural efficiency that can be achieved, as illustrated in [10–16]. This topic is investigated in many papers available in literature, especially as far as laminated composites [17–36] and functionally graded materials [37–56] are concerned.

This peculiar mechanical configurations could not be investigated accurately if first-order theories, such as the well-known Reissner-Mindlin approach, are employed. To this aim, many authors proposed more refined approaches able to model the structural response so that it becomes closer to the effective one. This is one of the main reasons that has led to the growth of the so-called Higher-Order Shear Deformation Theories (HSDTs), as specified in the papers [57–67]. This topic has been studied and developed in depth in the last decades and several efficient approaches have been proposed. Among them, the unified formulation, known as Unified Formulation (UF), should be mentioned [1, 68–72]. To the best of the authors' knowledge, the UF represents an efficient methodology to study the mechanical behavior of beams, plates and shells made of composite materials, as proven in the papers [73–88]. In particular, the researches just mentioned are based on an Equivalent Single Layer (ESL) approach, since the kinematic expansion of the displacement field is developed within the shell middle surface, which represents the reference domain of the structural problem at issue. Nevertheless, a different methodology which performs the kinematic expansion along the shell thickness could be used. This method, which is particularly efficient when laminated composites are investigated, is known as Layer-Wise (LW) approach [89–93]. Finally, it should be mentioned that some authors proposed also more general formulations based on the UF [94–99].

2 Principles of Differential Geometry

The differential geometry is an extremely efficient tool to describe in an accurate manner the geometry of a doubly-curved shell [1, 8]. In particular, it provides the analytical description of those curved surfaces which can be taken as the middle surface of the structures at issue. The present formulation, in fact, is developed within the shell middle surface, which represents the reference domain of the governing equations, since an Equivalent Single Layer (ESL) approach is pursued.

A generic doubly-curved surface can be identified in a Cartesian coordinate reference system $Ox_1x_2x_3$ by the corresponding position vector $\mathbf{r}\,(\alpha_1, \alpha_2)$. The parameters α_1, α_2 denote the orthogonal and principal coordinates of the shell middle surface, which have to follow the limitations values shown below

$$\alpha_1 \in \left[\alpha_1^0, \alpha_1^1\right], \quad \alpha_2 \in \left[\alpha_2^0, \alpha_2^1\right] \tag{1}$$

where α_1^0, α_2^0 and α_1^1, α_2^1 are the boundary values of the curvilinear coordinates. In general, each point within the three-dimensional shell can be identified by the vector $\mathbf{R}\,(\alpha_1, \alpha_2, \zeta)$ defined below

$$\mathbf{R}\,(\alpha_1, \alpha_2, \zeta) = r\,(\alpha_1, \alpha_2) + \zeta \mathbf{n}\,(\alpha_1, \alpha_2) \tag{2}$$

in which $\mathbf{n}\,(\alpha_1, \alpha_2)$ stands for the outward unit normal vector. On the other hand, ζ represents the thickness coordinate. At this point, the local reference system $O'\alpha_1\alpha_2\zeta$ can be defined on the shell middle surface, as shown in Fig. 1.

It is important to specify that the overall thickness of the shell h takes into account the size of each layer, if a laminated composite structure made of l plies is considered. The following relation is required to this aim

$$h = \sum_{k=1}^{l} h_k \tag{3}$$

in which h_k denotes the thickness of the k-th layer. For the sake of clarity, it should be specified that the index k is introduced to specify all the geometric and mechanical properties of the corresponding layer. At this point, it is clear also that the thickness coordinate ζ is defined within the following interval

$$\zeta \in [-h/2, h/2] \tag{4}$$

A complete characterization of a doubly-curved surface can be performed by introducing the fundamental forms provided by the differential geometry, once the position vector of the shell middle surface is introduced. The first fundamental coefficients $\mathrm{E}\,(\alpha_1, \alpha_2)$, $\mathrm{F}\,(\alpha_1, \alpha_2)$, $\mathrm{G}\,(\alpha_1, \alpha_2)$ can be conveniently collected in the matrix $\mathbf{I}_P$ defined below

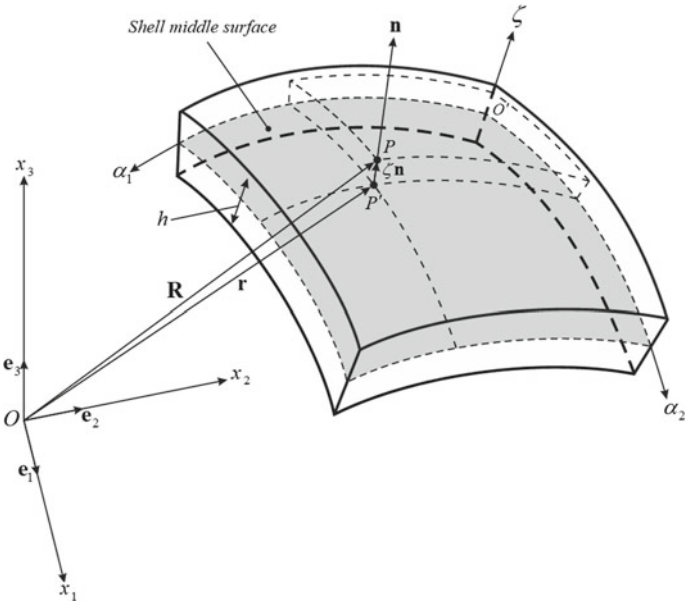

Fig. 1 Definition of a generic shell element and local and global reference systems representation

$$\mathbf{I}_P = \begin{bmatrix} \mathrm{E} & \mathrm{F} \\ \mathrm{F} & \mathrm{G} \end{bmatrix} = \begin{bmatrix} \mathbf{r}_{,1} \cdot \mathbf{r}_{,1} & \mathbf{r}_{,1} \cdot \mathbf{r}_{,2} \\ \mathbf{r}_{,1} \cdot \mathbf{r}_{,2} & \mathbf{r}_{,2} \cdot \mathbf{r}_{,2} \end{bmatrix} \tag{5}$$

in which $\mathbf{r}_{,i} = \partial \mathbf{r} / \partial \alpha_i$, for $i = 1, 2$, whereas the symbol "$\cdot$" is used to denote the dot product. The outward unit normal vector $\mathbf{n}\,(\alpha_1, \alpha_2)$, instead, assume the following form

$$\mathbf{n} = \frac{\mathbf{r}_{,1} \times \mathbf{r}_{,2}}{\left| \mathbf{r}_{,1} \times \mathbf{r}_{,2} \right|} \tag{6}$$

in which the symbol "$\times$" is used to denote the vector product. Once the outward unit normal vector is defined, it is possible to evaluate the so-called second fundamental coefficients $\mathrm{L}\,(\alpha_1, \alpha_2)$, $\mathrm{M}\,(\alpha_1, \alpha_2)$, $\mathrm{N}\,(\alpha_1, \alpha_2)$, which can be collected in the corresponding matrix $\mathbf{II}_P$ defined below

$$\mathbf{II}_P = \begin{bmatrix} \mathrm{L} & \mathrm{M} \\ \mathrm{M} & \mathrm{N} \end{bmatrix} = \begin{bmatrix} -\mathbf{r}_{,11} \cdot \mathbf{n} & -\mathbf{r}_{,12} \cdot \mathbf{n} \\ -\mathbf{r}_{,12} \cdot \mathbf{n} & -\mathbf{r}_{,22} \cdot \mathbf{n} \end{bmatrix} \tag{7}$$

where $\mathbf{r}_{,ij} = \partial^2 \mathbf{r} / \partial \alpha_i \partial \alpha_j$, for $i, j = 1, 2$. A new matrix denoted by $\mathbf{S}_P$ can be conveniently introduced as shown below

$$\mathbf{S}_P = \mathbf{I}_P^{-1} \mathbf{II}_P = \frac{1}{\mathrm{EG} - \mathrm{F}^2} \begin{bmatrix} \mathrm{LG} - \mathrm{FM} & \mathrm{GM} - \mathrm{FN} \\ \mathrm{EM} - \mathrm{FL} & \mathrm{EN} - \mathrm{FM} \end{bmatrix} \tag{8}$$

This operator allows to compute the Gaussian curvature Γ_G and the mean curvature Γ_M of a doubly-curved surface. In particular, one gets

$$\Gamma_G = \det(\mathbf{S}_P) = \frac{\mathrm{LN} - \mathrm{M}^2}{\mathrm{EG} - \mathrm{F}^2} = \frac{1}{R_1 R_2} \tag{9}$$

$$\Gamma_M = \frac{1}{2}\mathrm{tr}\,(\mathbf{S}_P) = \frac{1}{2}\frac{\mathrm{LG} - 2\mathrm{FM} + \mathrm{EN}}{\mathrm{EG} - \mathrm{F}^2} = \frac{1}{2}\left(\frac{1}{R_1} + \frac{1}{R_2}\right) \tag{10}$$

where $R_1 = R_1(\alpha_1, \alpha_2)$ and $R_2 = R_2(\alpha_1, \alpha_2)$ are the main radii of curvature defined below

$$R_1 = \frac{1}{\Gamma_M - \sqrt{\Gamma_M^2 - \Gamma_G}}, \quad R_2 = \frac{1}{\Gamma_M + \sqrt{\Gamma_M^2 - \Gamma_G}} \tag{11}$$

Since α_1, α_2 are principal and orthogonal by hypothesis ($\mathrm{F} = \mathrm{M} = 0$), the following simplified definitions can be used to define the radii of curvature

$$R_1 = \frac{\mathrm{E}}{\mathrm{L}}, \quad R_2 = \frac{\mathrm{G}}{\mathrm{N}} \tag{12}$$

The curvature effect is taken into account also in the following geometric parameters

$$H_1(\alpha_1, \alpha_2) = 1 + \frac{\zeta}{R_1}, \quad H_2(\alpha_1, \alpha_2) = 1 + \frac{\zeta}{R_2} \tag{13}$$

Finally, the well-known Lamé parameters $A_1 = A_1(\alpha_1, \alpha_2)$, $A_2 = A_2(\alpha_1, \alpha_2)$ can be easily evaluated as shown below

$$A_1 = \sqrt{\mathrm{E}}, \quad A_2 = \sqrt{\mathrm{G}} \tag{14}$$

where the meaning of E, G can be deducted in the previous relations.

3 Shell Fundamental Equations

A two-dimensional model is introduced in this section to analyze the mechanical behavior of laminated composite doubly-curved shell structures, in the framework provided by a unified formulation based on the ESL approach. Various Higher-order Shear Deformation Theories (HSDTs) can be developed to this aim. Each theory can be characterized by a different maximum order of kinematic expansion N. The three-dimensional displacement field assumes the following form

$$\begin{aligned} U_1 &= F_0 u_1^{(0)} + F_1 u_1^{(1)} + F_2 u_1^{(2)} + F_3 u_1^{(3)} + ... + F_N u_1^{(N)} + F_{N+1} u_1^{(N+1)} \\ U_2 &= F_0 u_2^{(0)} + F_1 u_2^{(1)} + F_2 u_2^{(2)} + F_3 u_2^{(3)} + ... + F_N u_2^{(N)} + F_{N+1} u_2^{(N+1)} \\ U_3 &= F_0 u_3^{(0)} + F_1 u_3^{(1)} + F_2 u_3^{(2)} + F_3 u_3^{(3)} + ... + F_N u_3^{(N)} + F_{N+1} u_3^{(N+1)} \end{aligned} \tag{15}$$

where $U_i\,(\alpha_1, \alpha_2, \zeta, t)$ is the i-th displacement component, whereas $u_i^{(\tau)}\,(\alpha_1, \alpha_2, t)$ is the i-th generalized displacement defined on the shell middle surface for each order of kinematic expansion $\tau = 0, 1, 2, ..., N, N+1$. On the other hand, $F_\tau = F_\tau\,(\zeta)$ represents the so-called thickness functions that allow to characterize the displacement field in hand. A possible choice consists in the following one

$$\begin{aligned} F_\tau &= \zeta^{\,\tau}, \quad \text{for} \;\; \tau = 0, 1, 2, ..., N \\ F_{N+1} &= (-1)^k \left(\frac{2}{\zeta_{k+1} - \zeta_k} \zeta - \frac{\zeta_{k+1} + \zeta_k}{\zeta_{k+1} - \zeta_k} \right) \end{aligned} \tag{16}$$

where the parameters ζ_{k+1}, ζ_k are needed to identify the lower and upper boundaries of the k-th layer along the thickness direction. In particular, the expression of F_{N+1} stands for the so-called Murakami's function, which can be efficiently included in the model to capture the zig-zag effect, when laminated and sandwich structures are analyzed.

For the sake of conciseness, a compact nomenclature can be introduced to denote univocally a higher-order structural model. The following theories can be defined, by neglecting or including the zig-zag effect [1, 71, 72]

$$\begin{array}{ll} N = 1 \rightarrow \text{ED1} & N = 1 \rightarrow \text{EDZ1} \\ N = 2 \rightarrow \text{ED2} & N = 2 \rightarrow \text{EDZ2} \\ N = 3 \rightarrow \text{ED3} & N = 3 \rightarrow \text{EDZ3} \\ N = 4 \rightarrow \text{ED4} & N = 4 \rightarrow \text{EDZ4} \end{array} \tag{17}$$

It should be specified that the Reissner-Mindlin model or First-order Shear Deformation Theory (FSDT) can be also developed in the framework of the proposed unified formulation.

The generalized displacements $u_i^{(\tau)}\,(\alpha_1, \alpha_2, t)$ represent the degrees of freedom of the model and can be conveniently collected in the corresponding vector $\mathbf{u}^{(\tau)} = \mathbf{u}^{(\tau)}\,(\alpha_1, \alpha_2, t)$ defined below

$$\mathbf{u}^{(\tau)} = \left[u_1^{(\tau)} \quad u_2^{(\tau)} \quad u_3^{(\tau)} \right]^T \tag{18}$$

At this point, the generalized strain components defined on the shell middle surface could be defined and written for each order τ of kinematic expansion. For the sake of conciseness, the vector $\boldsymbol{\varepsilon}^{(\tau)} = \boldsymbol{\varepsilon}^{(\tau)}\,(\alpha_1, \alpha_2, t)$ is introduced for this reason. It assumes the following form

$$\boldsymbol{\varepsilon}^{(\tau)} = \left[\varepsilon_1^{(\tau)} \;\; \varepsilon_2^{(\tau)} \;\; \gamma_1^{(\tau)} \;\; \gamma_2^{(\tau)} \;\; \gamma_{13}^{(\tau)} \;\; \gamma_{23}^{(\tau)} \;\; \omega_{13}^{(\tau)} \;\; \omega_{23}^{(\tau)} \;\; \varepsilon_3^{(\tau)} \right]^T \tag{19}$$

for $\tau = 0, 1, 2, ..., N, N+1$. If the differential operator $\mathbf{D}_\Omega$ is defined as follows

$$\mathbf{D}_\Omega = \begin{bmatrix} \frac{1}{A_1}\frac{\partial}{\partial\alpha_1} & \frac{1}{A_1A_2}\frac{\partial A_2}{\partial\alpha_1} & -\frac{1}{A_1A_2}\frac{\partial A_1}{\partial\alpha_2} & \frac{1}{A_2}\frac{\partial}{\partial\alpha_2} & -\frac{1}{R_1} & 0 & 1\,0\,0 \\ \frac{1}{A_1A_2}\frac{\partial A_1}{\partial\alpha_2} & \frac{1}{A_2}\frac{\partial}{\partial\alpha_2} & \frac{1}{A_1}\frac{\partial}{\partial\alpha_1} & -\frac{1}{A_1A_2}\frac{\partial A_2}{\partial\alpha_1} & 0 & -\frac{1}{R_2} & 0\,1\,0 \\ \frac{1}{R_1} & \frac{1}{R_2} & 0 & 0 & \frac{1}{A_1}\frac{\partial}{\partial\alpha_1} & \frac{1}{A_2}\frac{\partial}{\partial\alpha_2} & 0\,0\,1 \end{bmatrix}^T \tag{20}$$

the kinematic equations shown below in compact matrix form can be used to define the generalized strain component vector

$$\boldsymbol{\varepsilon}^{(\tau)} = \mathbf{D}_\Omega \mathbf{u}^{(\tau)} \tag{21}$$

for each order of kinematic expansion τ.

The constitutive relations are needed at this point to relate the strains and the corresponding stress components, by introducing also the mechanical features of the materials of the various layers [1, 13]. The following assumptions are valid for a laminated composite structure made of l orthotropic plies

1. Each lamina is defined by neglecting discontinuities and voids, since it is modeled as a continuous medium.
2. Each layer is made of a linear-elastic constituent.
3. From the macroscopic point of view, the layer is an homogeneous medium. In particular, the following properties should be taken into account for a fiber-reinforced layer:
   a. The matrix and the fibers, which make up the layer, are perfectly bonded.
   b. The fibers are continuous and parallel and their placement is defined by a constant orientation angle $\theta^{(k)}$. For a laminated composite structure made of l plies, the notation $\left(\theta^{(1)}/\theta^{(2)}/\ldots/\theta^{(k)}/\ldots/\theta^{(l)}\right)$ is used to specify univocally the stacking sequence.
   c. The fibers and the matrix can be modeled as isotropic constituents.
   d. The presence of voids, micro cracks, and residual stresses in the matrix is not allowed.

The current hypotheses allow to introduce the following three-dimensional constitutive equations

$$\boldsymbol{\sigma}^{(k)} = \bar{\mathbf{C}}^{(k)} \boldsymbol{\varepsilon}^{(k)} \tag{22}$$

where $\boldsymbol{\sigma}^{(k)} = \boldsymbol{\sigma}^{(k)}(\alpha_1, \alpha_2, \zeta, t)$ stands for the stress component vector, whereas $\boldsymbol{\varepsilon}^{(k)} = \boldsymbol{\varepsilon}^{(k)}(\alpha_1, \alpha_2, \zeta, t)$ collects the three dimensional strain components. They assume the aspect shown below for the k-th layer

$$\boldsymbol{\sigma}^{(k)} = \left[\, \sigma_1^{(k)} \;\; \sigma_2^{(k)} \;\; \tau_{12}^{(k)} \;\; \tau_{13}^{(k)} \;\; \tau_{23}^{(k)} \;\; \sigma_3^{(k)} \,\right]^T \tag{23}$$

$$\boldsymbol{\varepsilon}^{(k)} = \left[\, \varepsilon_1^{(k)} \;\; \varepsilon_2^{(k)} \;\; \gamma_{12}^{(k)} \;\; \gamma_{13}^{(k)} \;\; \gamma_{23}^{(k)} \;\; \varepsilon_3^{(k)} \,\right]^T \tag{24}$$

On the other hand, the constitutive operator $\bar{\mathbf{C}}^{(k)}$ for the k-th orthotropic layer can be defined as follows

$$\bar{\mathbf{C}}^{(k)} = \begin{bmatrix} \bar{E}_{11}^{(k)} & \bar{E}_{12}^{(k)} & \bar{E}_{16}^{(k)} & 0 & 0 & \bar{E}_{13}^{(k)} \\ \bar{E}_{12}^{(k)} & \bar{E}_{22}^{(k)} & \bar{E}_{26}^{(k)} & 0 & 0 & \bar{E}_{23}^{(k)} \\ \bar{E}_{16}^{(k)} & \bar{E}_{26}^{(k)} & \bar{E}_{66}^{(k)} & 0 & 0 & \bar{E}_{36}^{(k)} \\ 0 & 0 & 0 & \bar{E}_{44}^{(k)} & \bar{E}_{45}^{(k)} & 0 \\ 0 & 0 & 0 & \bar{E}_{45}^{(k)} & \bar{E}_{55}^{(k)} & 0 \\ \bar{E}_{13}^{(k)} & \bar{E}_{23}^{(k)} & \bar{E}_{36}^{(k)} & 0 & 0 & \bar{E}_{33}^{(k)} \end{bmatrix} \tag{25}$$

in which $\bar{E}_{nm}^{(k)}$ stands for the elastic constants of the material, which can be computed through the engineering constants of the medium (Young's moduli, shear moduli, Poisson's ratios). This nomencalture is used to introduce the plane stress-reduced elastic coefficients $\bar{E}_{nm}^{(k)} = \bar{Q}_{nm}^{(k)}$ or the non-reduced ones $\bar{E}_{nm}^{(k)} = \bar{C}_{nm}^{(k)}$, according to requirements of the structural theory under consideration.

For the sake of completeness, it should be remarked that the three-dimensional strains defined in Eq. (24) can be related to the generalized displacement components as shown below

$$\varepsilon^{(k)} = \sum_{\tau=0}^{N+1} \mathbf{Z}^{(\tau)} \mathbf{D}_{\Omega} \mathbf{u}^{(\tau)} \tag{26}$$

where the matrix $\mathbf{Z}^{(\tau)}$ assumes the following aspect

$$\mathbf{Z}^{(\tau)} = \begin{bmatrix} \frac{F_\tau}{H_1} & 0 & 0 & 0 & 0 & 0 & 0 & 0 & 0 \\ 0 & \frac{F_\tau}{H_2} & 0 & 0 & 0 & 0 & 0 & 0 & 0 \\ 0 & 0 & \frac{F_\tau}{H_1} & \frac{F_\tau}{H_2} & 0 & 0 & 0 & 0 & 0 \\ 0 & 0 & 0 & 0 & \frac{F_\tau}{H_1} & 0 & \frac{\partial F_\tau}{\partial \zeta} & 0 & 0 \\ 0 & 0 & 0 & 0 & 0 & \frac{F_\tau}{H_2} & 0 & \frac{\partial F_\tau}{\partial \zeta} & 0 \\ 0 & 0 & 0 & 0 & 0 & 0 & 0 & 0 & \frac{\partial F_\tau}{\partial \zeta} \end{bmatrix} \tag{27}$$

The internal stresses can be conveniently expressed in terms of stress resultants, which can be included in the corresponding vector $\mathbf{S}^{(\tau)} = \mathbf{S}^{(\tau)}(\alpha_1, \alpha_2, t)$ defined below

$$\mathbf{S}^{(\tau)} = \left[N_1^{(\tau)} \; N_2^{(\tau)} \; N_{12}^{(\tau)} \; N_{21}^{(\tau)} \; T_1^{(\tau)} \; T_2^{(\tau)} \; P_1^{(\tau)} \; P_2^{(\tau)} \; S_3^{(\tau)} \right]^T \tag{28}$$

for each order of kinematic expansion τ. The τ-th order generalized stress resultant vector assumes the following definition

$$\mathbf{S}^{(\tau)} = \sum_{k=1}^{l} \int_{\zeta_k}^{\zeta_{k+1}} \left(\mathbf{Z}^{(\tau)} \right)^T \sigma^{(k)} H_1 H_2 d\zeta = \sum_{\eta=0}^{N+1} \mathbf{A}^{(\tau\eta)} \mathbf{D}_{\Omega} \mathbf{u}^{(\eta)} \tag{29}$$

in which $\mathbf{A}^{(\tau\eta)}$ is the constitutive operator given by

$$\mathbf{A}^{(\tau\eta)} = \begin{bmatrix} A^{(\tau\eta)}_{11(20)} & A^{(\tau\eta)}_{12(11)} & A^{(\tau\eta)}_{16(20)} & A^{(\tau\eta)}_{16(11)} & 0 & 0 & 0 & 0 & A^{(\tau\tilde{\eta})}_{13(10)} \\ A^{(\tau\eta)}_{12(11)} & A^{(\tau\eta)}_{22(02)} & A^{(\tau\eta)}_{26(11)} & A^{(\tau\eta)}_{26(02)} & 0 & 0 & 0 & 0 & A^{(\tau\tilde{\eta})}_{23(01)} \\ A^{(\tau\eta)}_{16(20)} & A^{(\tau\eta)}_{26(11)} & A^{(\tau\eta)}_{66(20)} & A^{(\tau\eta)}_{66(11)} & 0 & 0 & 0 & 0 & A^{(\tau\tilde{\eta})}_{36(10)} \\ A^{(\tau\eta)}_{16(11)} & A^{(\tau\eta)}_{26(02)} & A^{(\tau\eta)}_{66(11)} & A^{(\tau\eta)}_{66(02)} & 0 & 0 & 0 & 0 & A^{(\tau\tilde{\eta})}_{36(01)} \\ 0 & 0 & 0 & 0 & A^{(\tau\eta)}_{44(20)} & A^{(\tau\eta)}_{45(11)} & A^{(\tau\tilde{\eta})}_{44(10)} & A^{(\tau\tilde{\eta})}_{45(10)} & 0 \\ 0 & 0 & 0 & 0 & A^{(\tau\eta)}_{45(11)} & A^{(\tau\eta)}_{55(02)} & A^{(\tau\tilde{\eta})}_{45(01)} & A^{(\tau\tilde{\eta})}_{55(01)} & 0 \\ 0 & 0 & 0 & 0 & A^{(\tilde{\tau}\eta)}_{44(10)} & A^{(\tilde{\tau}\eta)}_{45(01)} & A^{(\tilde{\tau}\tilde{\eta})}_{44(00)} & A^{(\tilde{\tau}\tilde{\eta})}_{45(00)} & 0 \\ 0 & 0 & 0 & 0 & A^{(\tilde{\tau}\eta)}_{45(10)} & A^{(\tilde{\tau}\eta)}_{55(01)} & A^{(\tilde{\tau}\tilde{\eta})}_{45(00)} & A^{(\tilde{\tau}\tilde{\eta})}_{55(00)} & 0 \\ A^{(\tilde{\tau}\eta)}_{13(10)} & A^{(\tilde{\tau}\eta)}_{23(01)} & A^{(\tilde{\tau}\eta)}_{36(10)} & A^{(\tilde{\tau}\eta)}_{36(01)} & 0 & 0 & 0 & 0 & A^{(\tilde{\tau}\tilde{\eta})}_{33(00)} \end{bmatrix} \tag{30}$$

The following definitions are required to evaluate the elastic coefficients included in the constitutive operator

$$\begin{aligned} A^{(\tau\eta)}_{nm\,(pq)} &= \sum_{k=1}^{l} \int_{\zeta_k}^{\zeta_{k+1}} \bar{B}^{(k)}_{nm} F_\eta F_\tau \frac{H_1 H_2}{H_1^p H_2^q} d\zeta \\ A^{(\tilde{\tau}\eta)}_{nm\,(pq)} &= \sum_{k=1}^{l} \int_{\zeta_k}^{\zeta_{k+1}} \bar{B}^{(k)}_{nm} F_\eta \frac{\partial F_\tau}{\partial \zeta} \frac{H_1 H_2}{H_1^p H_2^q} d\zeta \\ A^{(\tau\tilde{\eta})}_{nm\,(pq)} &= \sum_{k=1}^{l} \int_{\zeta_k}^{\zeta_{k+1}} \bar{B}^{(k)}_{nm} \frac{\partial F_\eta}{\partial \zeta} F_\tau \frac{H_1 H_2}{H_1^p H_2^q} d\zeta \\ A^{(\tilde{\tau}\tilde{\eta})}_{nm\,(pq)} &= \sum_{k=1}^{l} \int_{\zeta_k}^{\zeta_{k+1}} \bar{B}^{(k)}_{nm} \frac{\partial F_\eta}{\partial \zeta} \frac{\partial F_\tau}{\partial \zeta} \frac{H_1 H_2}{H_1^p H_2^q} d\zeta \end{aligned} \tag{31}$$

for $\tau, \eta = 0, 1, 2, ..., N, N+1, n, m = 1, 2, 3, 4, 5, 6$ and $p, q = 0, 1, 2$. The symbol $\bar{B}^{(k)}_{nm}$ is used to introduce the shear correction factor $\kappa = 1/\chi$, if needed, as it can be noted by its definition

$$\begin{aligned} \bar{B}^{(k)}_{nm} &= \bar{E}^{(k)}_{nm} \quad \text{for} \quad n, m = 1, 2, 3, 6 \\ \bar{B}^{(k)}_{nm} &= \kappa \bar{E}^{(k)}_{nm} \quad \text{for} \quad n, m = 4, 5 \end{aligned} \tag{32}$$

In general, if required, the shear correction factor is assumed equal to the constant value of $5/6$ (or $\chi = 1.2$). It should be specified that this coefficient is commonly used in the structural theories up to the second order of kinematic expansion.

On the other hand, the equations of motion and the corresponding boundary conditions can be deducted by applying the well-known Hamilton's principle [1].

In particular, three partial differential equations are carried out for each order of kinematic expansion τ and can be included in the following system in compact matrix form

$$\mathbf{D}_{\Omega}^{*}\mathbf{S}^{(\tau)} + \mathbf{q}^{(\tau)} = \sum_{\eta=0}^{N+1} \mathbf{M}^{(\tau\eta)}\ddot{\mathbf{u}}^{(\eta)} \tag{33}$$

in which the equilibrium differential operator $\mathbf{D}_{\Omega}^{*}$ assumes the following aspect

$$\mathbf{D}_{\Omega}^{*} = \begin{bmatrix} \frac{1}{A_1}\frac{\partial}{\partial\alpha_1} + \frac{1}{A_1A_2}\frac{\partial A_2}{\partial\alpha_1} & -\frac{1}{A_1A_2}\frac{\partial A_1}{\partial\alpha_2} & -\frac{1}{R_1} \\ -\frac{1}{A_1A_2}\frac{\partial A_2}{\partial\alpha_1} & \frac{1}{A_2}\frac{\partial}{\partial\alpha_2} + \frac{1}{A_1A_2}\frac{\partial A_1}{\partial\alpha_2} & -\frac{1}{R_2} \\ \frac{1}{A_1A_2}\frac{\partial A_1}{\partial\alpha_2} & \frac{1}{A_1}\frac{\partial}{\partial\alpha_1} + \frac{1}{A_1A_2}\frac{\partial A_2}{\partial\alpha_1} & 0 \\ \frac{1}{A_2}\frac{\partial}{\partial\alpha_2} + \frac{1}{A_1A_2}\frac{\partial A_1}{\partial\alpha_2} & \frac{1}{A_1A_2}\frac{\partial A_2}{\partial\alpha_1} & 0 \\ \frac{1}{R_1} & 0 & \frac{1}{A_1}\frac{\partial}{\partial\alpha_1} + \frac{1}{A_1A_2}\frac{\partial A_2}{\partial\alpha_1} \\ 0 & \frac{1}{R_2} & \frac{1}{A_2}\frac{\partial}{\partial\alpha_2} + \frac{1}{A_1A_2}\frac{\partial A_1}{\partial\alpha_2} \\ -1 & 0 & 0 \\ 0 & -1 & 0 \\ 0 & 0 & -1 \end{bmatrix}^{T} \tag{34}$$

On the other hand, the mass matrix $\mathbf{M}^{(\tau\eta)}$ is given by

$$\mathbf{M}^{(\tau\eta)} = \begin{bmatrix} I^{(\tau\eta)} & 0 & 0 \\ 0 & I^{(\tau\eta)} & 0 \\ 0 & 0 & I^{(\tau\eta)} \end{bmatrix} \tag{35}$$

in which $I^{(\tau\eta)}$ stands for the inertia terms, which depend on the mass density of the k-th layer $\rho^{(k)}$ as shown below

$$I^{(\tau\eta)} = \sum_{k=1}^{l} \int_{\zeta_k}^{\zeta_{k+1}} \rho^{(k)} F_\tau F_\eta H_1 H_2 \, d\zeta \tag{36}$$

The generalized acceleration components, instead, are included in the corresponding vector $\ddot{\mathbf{u}}^{(\eta)} = \ddot{\mathbf{u}}^{(\eta)}(\alpha_1, \alpha_2, t)$ given by

$$\ddot{\mathbf{u}}^{(\tau)} = \begin{bmatrix} \ddot{u}_1^{(\tau)} & \ddot{u}_2^{(\tau)} & \ddot{u}_3^{(\tau)} \end{bmatrix}^{T} \tag{37}$$

Finally, the static load vector $\mathbf{q}^{(\tau)}$ collects three load components for each order of kinematic expansion τ. It assumes the aspect shown below

$$\mathbf{q}^{(\tau)} = \begin{bmatrix} q_1^{(\tau)} & q_2^{(\tau)} & q_n^{(\tau)} \end{bmatrix}^{T} \tag{38}$$

in which the various load components applied on the shell middle surface can be evaluated as a function of the load applied on the top surface $q_1^{(+)},\ q_2^{(+)},\ q_n^{(+)}$ and on the bottom surface $q_1^{(-)},\ q_2^{(-)},\ q_n^{(-)}$, according to the definitions shown below

$$\begin{aligned} q_1^{(\tau)} &= q_1^{(-)} F_\tau^{(-)} H_1^{(-)} H_2^{(-)} + q_1^{(+)} F_\tau^{(+)} H_1^{(+)} H_2^{(+)} \\ q_2^{(\tau)} &= q_2^{(-)} F_\tau^{(-)} H_1^{(-)} H_2^{(-)} + q_2^{(+)} F_\tau^{(+)} H_1^{(+)} H_2^{(+)} \\ q_n^{(\tau)} &= q_n^{(-)} F_\tau^{(-)} H_1^{(-)} H_2^{(-)} + q_n^{(+)} F_\tau^{(+)} H_1^{(+)} H_2^{(+)} \end{aligned} \tag{39}$$

for $\tau = 0, 1, 2, ..., N, N+1$. It should be noted that $H_1^{(\pm)}$, $H_2^{(\pm)}$ and $F_\tau^{(\pm)}$ are respectively the values of the curvature parameters and of the thickness functions evaluated on the external surfaces of the shell ($\zeta = \pm h/2$).

The various aspects of the structural problem just presented, which are the kinematic, the constitutive laws, and the equilibrium, can be included in a sole system known as fundamental system of equations. In particular, for each order of kinematic expansion τ, the following system is accomplished

$$\sum_{\eta=0}^{N+1} \mathbf{L}^{(\tau\eta)} \mathbf{u}^{(\eta)} + \mathbf{q}^{(\tau)} = \sum_{\eta=0}^{N+1} \mathbf{M}^{(\tau\eta)} \ddot{\mathbf{u}}^{(\eta)} \tag{40}$$

where $\mathbf{L}^{(\tau\eta)} = \mathbf{D}_\Omega^* \mathbf{A}^{(\tau\eta)} \mathbf{D}_\Omega$ denotes the fundamental operator. It should be noted that Eq. (40) describes both the static and dynamic problem of laminated doubly-curved shells. In particular, the inertia terms must be neglected to investigate their static behavior, whereas the load vector must be set equal to zero to analyze the free vibrations.

Nevertheless, these problems cannot be solved without the proper boundary conditions, which are also obtained by means of the Hamilton's principle. In particular, it should be recalled that a generic edge can be completely clamped (C), simply-supported (S) or free (F). The following conditions are required for the external edges characterized by $\alpha_1 = \alpha_1^0$ or $\alpha_1 = \alpha_1^1$, and $\alpha_2^0 \leq \alpha_2 \leq \alpha_2^1$

$$\begin{aligned} \text{C} &\rightarrow u_1^{(\tau)} = u_2^{(\tau)} = u_3^{(\tau)} = 0 \\ \text{S} &\rightarrow N_1^{(\tau)} = 0, \quad u_2^{(\tau)} = u_3^{(\tau)} = 0 \\ \text{F} &\rightarrow N_1^{(\tau)} = N_{12}^{(\tau)} = T_1^{(\tau)} = 0 \end{aligned} \tag{41}$$

for $\tau = 0, 1, 2, ..., N, N+1$. On the other hand, the following relations are needed for $\alpha_2 = \alpha_2^0$ or $\alpha_2 = \alpha_2^1$, and $\alpha_1^0 \leq \alpha_1 \leq \alpha_1^1$

$$\begin{aligned} \text{C} &\rightarrow u_1^{(\tau)} = u_2^{(\tau)} = u_3^{(\tau)} = 0 \\ \text{S} &\rightarrow N_2^{(\tau)} = 0, \quad u_1^{(\tau)} = u_3^{(\tau)} = 0 \\ \text{F} &\rightarrow N_{21}^{(\tau)} = N_2^{(\tau)} = T_2^{(\tau)} = 0 \end{aligned} \tag{42}$$

In addition, when complete shells of revolution or toroids are analyzed, which denote structures with a closing meridian or parallel, the two coincident sides are affected by the conditions required to enforce the structural compatibility. If the common edge is denoted by $\alpha_1 = \alpha_1^0$ and $\alpha_1 = \alpha_1^1$, the equations in hand assume the following aspect

$$\begin{aligned} N_1^{(\tau)}\left(\alpha_1^0, \alpha_2, t\right) &= N_1^{(\tau)}\left(\alpha_1^1, \alpha_2, t\right), \quad u_1^{(\tau)}\left(\alpha_1^0, \alpha_2, t\right) = u_1^{(\tau)}\left(\alpha_1^1, \alpha_2, t\right) \\ N_{12}^{(\tau)}\left(\alpha_1^0, \alpha_2, t\right) &= N_{12}^{(\tau)}\left(\alpha_1^1, \alpha_2, t\right), \quad u_2^{(\tau)}\left(\alpha_1^0, \alpha_2, t\right) = u_2^{(\tau)}\left(\alpha_1^1, \alpha_2, t\right) \\ T_1^{(\tau)}\left(\alpha_1^0, \alpha_2, t\right) &= T_1^{(\tau)}\left(\alpha_1^1, \alpha_2, t\right), \quad u_3^{(\tau)}\left(\alpha_1^0, \alpha_2, t\right) = u_3^{(\tau)}\left(\alpha_1^1, \alpha_2, t\right) \end{aligned} \tag{43}$$

for $\alpha_2^0 \leq \alpha_2 \leq \alpha_2^1$ and $\tau = 0, 1, 2, ..., N, N+1$. On the other hand, one gets the following relations along $\alpha_2 = \alpha_2^0$ and $\alpha_2 = \alpha_2^1$

$$\begin{aligned} N_{21}^{(\tau)}\left(\alpha_1, \alpha_2^0, t\right) &= N_{21}^{(\tau)}\left(\alpha_1, \alpha_2^1, t\right), \quad u_1^{(\tau)}\left(\alpha_1, \alpha_2^0, t\right) = u_1^{(\tau)}\left(\alpha_1, \alpha_2^1, t\right) \\ N_2^{(\tau)}\left(\alpha_1, \alpha_2^0, t\right) &= N_2^{(\tau)}\left(\alpha_1, \alpha_2^1, t\right), \quad u_2^{(\tau)}\left(\alpha_1, \alpha_2^0, t\right) = u_2^{(\tau)}\left(\alpha_1, \alpha_2^1, t\right) \\ T_2^{(\tau)}\left(\alpha_1, \alpha_2^0, t\right) &= T_2^{(\tau)}\left(\alpha_1, \alpha_2^1, t\right), \quad u_3^{(\tau)}\left(\alpha_1, \alpha_2^0, t\right) = u_3^{(\tau)}\left(\alpha_1, \alpha_2^1, t\right) \end{aligned} \tag{44}$$

for $\alpha_1^0 \leq \alpha_1 \leq \alpha_1^1$ and $\tau = 0, 1, 2, ..., N, N+1$. Finally, it should be specified that the sequence WSEN is employed to facilitate the identification of each edge. In particular, one gets the following coordinates

$$\begin{aligned} \text{West edge (W)} &\rightarrow \alpha_1^0 \leq \alpha_1 \leq \alpha_1^1, \ \alpha_2 = \alpha_2^0 \\ \text{South edge (S)} &\rightarrow \alpha_1 = \alpha_1^1, \ \alpha_2^0 \leq \alpha_2 \leq \alpha_2^1 \\ \text{East edge (E)} &\rightarrow \alpha_1^0 \leq \alpha_1 \leq \alpha_1^1, \ \alpha_2 = \alpha_2^1 \\ \text{North edge (N)} &\rightarrow \alpha_1 = \alpha_1^0, \ \alpha_2^0 \leq \alpha_2 \leq \alpha_2^1 \end{aligned} \tag{45}$$

4 Numerical Procedure

It is well-known that a closed-form solution cannot be obtained for the mathematical model presented in the previous section. Therefore, the systems of differential equations at issue cannot be solved analytically and a numerical method should be employed to get an approximate solution. In general, two formulations of the same fundamental system can be carried out, which are respectively the strong and weak formulations. If the strong formulation is considered, a numerical tool able to approximate derivatives is required, in order to transform directly these equations into the corresponding discrete system. On the other hand, the governing system of differential equations is replaced by a set of integral equations if the weak formulation is taken into account. The main aim of this section is the illustration of a numerical methodology able to evaluate numerically the derivatives of a generic function, since

the strong formulation has to be developed. The differential quadrature method is discussed for this purpose [1, 6].

Let us consider a smooth function $f(x)$ defined in a one-dimensional closed domain, for $x \in [a, b]$. By definition, the derivatives of the considered function are evaluated in specific discrete points defined in the reference domain. If I_N denotes the number of discrete nodes, the following points are introduced within the reference interval

$$a = x_1, \; x_2, \; ..., \; x_k, \; ..., \; x_{I_N-1}, \; x_{I_N} = b \tag{46}$$

in which the position of a generic point x_k is given by

$$x_k = \frac{b-a}{d-c}\left(\frac{r_k - r_1}{r_{I_N} - r_1} - c\right) + a \tag{47}$$

where r_k, for $k = 1, 2, ..., I_N$, stands for the position of the k-th node according to the discrete distributions defined in the interval $[c, d]$, which can be used to this aim. It should be recalled that various discrete distributions can be employed for this purpose. One of the most common choice is given by the Chebyshev–Gauss–Lobatto distribution, which provides the following definitions

$$r_k = \cos\left(\frac{I_N - k}{I_N - 1}\pi\right) \tag{48}$$

for $k = 1, 2, ..., I_N$ and $r_k \in [-1, 1]$.

A set of basis functions $\psi_j\,(x)$, for $j = 1, 2, ..., I_N$, is required for the polynomial approximation $f(x)$ within the reference domain, as shown below

$$f(x) \approx \sum_{j=1}^{I_N} \lambda_j \psi_j\,(x) \tag{49}$$

in which λ_j stands for some unknown coefficients that have to be computed. At this point, it is convenient to include the values that the function assumes in each discrete point $f(x_k)$ in the corresponding vector $\mathbf{f}$, which is given by

$$\mathbf{f} = \left[\, f(x_1) \cdots f(x_k) \cdots f(x_{I_N}) \,\right]^T \tag{50}$$

For the sake of clarity, the definition of the discrete grid points within the reference domain and the representation of the functional values are graphically depicted in Fig. 2.

The approximation introduced in Eq. (49) can be written also in compact matrix form as follows

$$\mathbf{f} \approx \mathbf{A}\boldsymbol{\lambda} \tag{51}$$

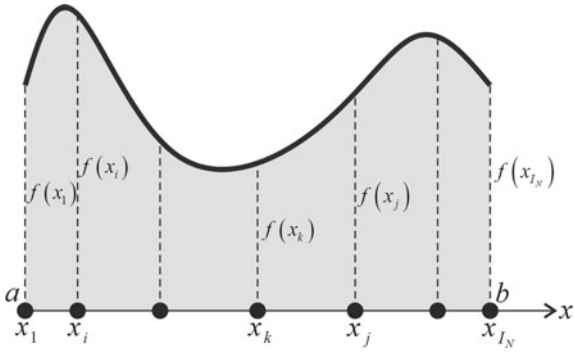

Fig. 2 Discrete point distribution for a one-dimensional scheme

where

$$\boldsymbol{\lambda} = \left[\lambda_1 \cdots \lambda_k \cdots \lambda_{I_N} \right]^T \tag{52}$$

On the other hand, $\mathbf{A}$ is known as the coefficient matrix of size $I_N \times I_N$, whose elements are given by A_{ij}. In other words, A_{ij} represents the value that the j-th basis function assumes in the i-th point of the reference domain.

$$A_{ij} = \psi_j (x_i) \tag{53}$$

At this point, Eq. (51) provides the definition of the coefficient vector $\boldsymbol{\lambda}$, by simply inverting the operator $\mathbf{A}$

$$\lambda = \mathbf{A}^{-1}\mathbf{f} \tag{54}$$

By definition, the n-th order derivative of the function $f(x)$ assumes the following aspect

$$\frac{d^n f(x)}{dx^n} = \sum_{j=1}^{I_N} \lambda_j \frac{d^n \psi_j (x)}{dx^n} \tag{55}$$

for $n = 1, 2, ..., I_N - 1$. It should be noted that the coefficients λ_j do not depend on x and the derivative procedure affects only the basis functions. If the values of the n-th derivative are evaluated in each discrete point, the following vector can be conveniently introduced

$$\mathbf{f}^{(n)} = \left[\left. \frac{d^n f(x)}{dx^n} \right|_{x_1} \cdots \left. \frac{d^n f(x)}{dx^n} \right|_{x_k} \cdots \left. \frac{d^n f(x)}{dx^n} \right|_{x_{I_N}} \right]^T \tag{56}$$

so that one gets

$$\mathbf{f}^{(n)} = \mathbf{A}^{(n)}\boldsymbol{\lambda} \tag{57}$$

in which the generic element $A_{ij}^{(n)}$ of the matrix $\mathbf{A}^{(n)}$ is defined as follows

$$A_{ij}^{(n)} = \left. \frac{d^n \psi_j(x)}{dx^n} \right|_{x_i} \tag{58}$$

Recalling the definition shown in Eq. (54), the vector $\mathbf{f}^{(n)}$ shown in Eq. (57) becomes

$$\mathbf{f}^{(n)} = \mathbf{A}^{(n)} \mathbf{A}^{-1} \mathbf{f} \tag{59}$$

If the differential operator $\mathbf{D}^{(n)} = \mathbf{A}^{(n)} \mathbf{A}^{-1}$ of size $I_N \times I_N$ is introduced, one gets the following definition

$$\mathbf{f}^{(n)} = \mathbf{D}^{(n)} \mathbf{f} \tag{60}$$

in which the generic element $D_{ij}^{(n)}$ of the corresponding matrix denotes the weighting coefficients for the n-th order derivative.

It is quite evident that this procedure could be inaccurate if the matrix $\mathbf{A}$ turns out to be ill-conditioned, since its inverse is required. This issue could be avoided if the Lagrange polynomials are used as basis functions, since this choice provides the following result

$$\mathbf{A} = \mathbf{I} \tag{61}$$

in which $\mathbf{I}$ stands for the identity matrix. As a consequence, one gets

$$D_{ij}^{(n)} = \left(\mathbf{A}^{(n)} \mathbf{A}^{-1}\right)_{ij} = \left(\mathbf{A}^{(n)} \mathbf{I}\right)_{ij} = A_{ij}^{(n)} = l_j^{(n)}(x_i) \tag{62}$$

where $l_j^{(n)}(x_i)$ stands for the n-th order derivative of the polynomial $l_j(x)$ defined below, evaluated in the point x_i

$$l_j(x_i) = \frac{\prod_{k=1}^{I_N} (x_i - x_k)}{\left(x_i - x_j\right) \prod_{k=1, i \neq k}^{I_N} (x_i - x_k)} \tag{63}$$

The recursive procedure proposed by Shu [7] can be conveniently followed to define the weighting coefficients for the n-th order derivatives, starting from the weighting coefficients for the first-order derivatives $D_{ij}^{(1)}$ given by

$$D_{ij}^{(1)} = \frac{\prod_{k=1, i \neq k}^{I_N} (x_i - x_k)}{\left(x_i - x_j\right) \prod_{k=1, j \neq k}^{I_N} \left(x_j - x_k\right)} \tag{64}$$

The methodology in hand is shown below. Thus, the weighting coefficients $D_{ij}^{(n)}$ can be computed as follows

$$D_{ij}^{(n)} = n\left(D_{ij}^{(1)} D_{ii}^{(n-1)} - \frac{D_{ij}^{(n-1)}}{x_i - x_j}\right) \tag{65}$$

for $i \neq j$ and

$$D_{ij}^{(n)} = -\sum_{j=1, j\neq i}^{I_N} D_{ij}^{(n)} \tag{66}$$

This numerical recursive approach based on the use of Lagrange polynomials as basis functions is known in the literature as Generalized Differential Quadrature (GDQ) method. Further details concerning this methodology can be found in the review paper by Tornabene et al. [6], in the book by Tornabene and Bacciocchi [1] and in the book by Shu [7].

It should be noted that this numerical method is illustrated here only for one-dimensional domains, but it can be easily extended also to multi-dimensional domain by defining the discrete grid distribution along each principal direction. In the case under consideration, the number of points along α_1, α_2 are denoted by I_N, I_M, respectively.

Once the GDQ method is applied, the governing system of equations defined in Eq. (40) can be written in its discrete form. If a static problem is solved, the following discrete sistem is carried out

$$\mathbf{K}\boldsymbol{\delta}_S = \mathbf{F} \tag{67}$$

where $\mathbf{K}$ denotes the stiffness matrix, $\boldsymbol{\delta}_S$ the displacement vector, and $\mathbf{F}$ the load vector. On the other hand, if the free vibration problem is solved, the following discrete system is obtained

$$\mathbf{K}\delta_D = \omega^2 \mathbf{M}\delta_D \tag{68}$$

where $\mathbf{M}$ represents the mass matrix, δ_D the mode shape vector, and ω the circular frequency, which easily provides the value of the corresponding natural frequency as $f = \omega/2\pi$. A proper condensation procedure could be developed to reduce the size of the problems under consideration.

5 Applications and Results

In this section, the natural frequencies of some laminated shell structures are computed numerically by means of the GDQ method [100]. The results are evaluated by varying the maximum order of kinematic expansion. Therefore, the analyses are carried out for several HSDTs. In addition, the natural frequencies related to the

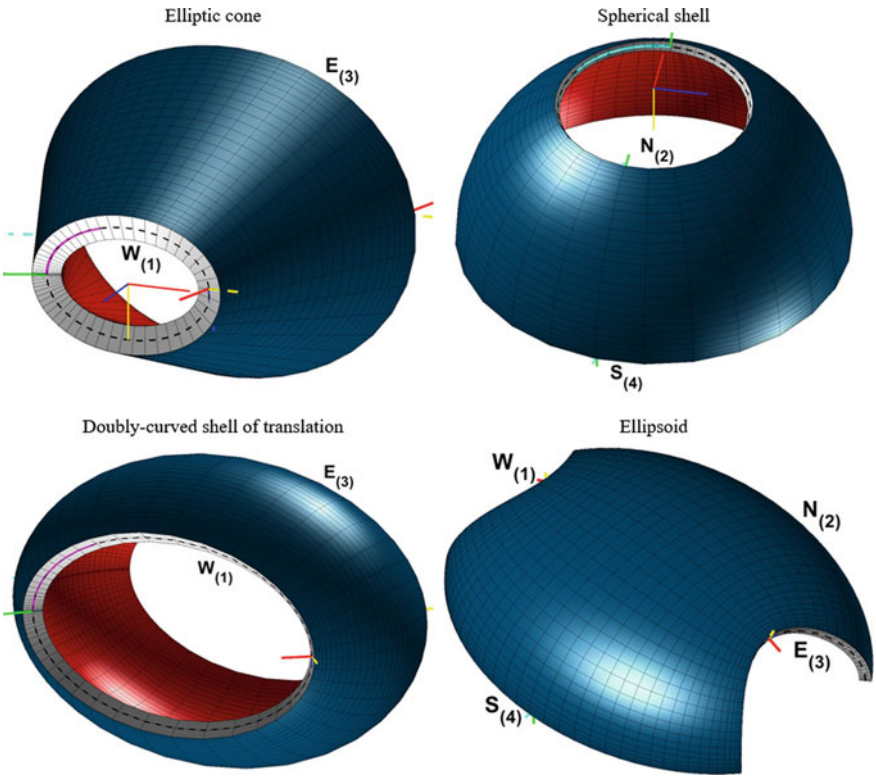

Fig. 3 Laminated composite shells structures: discrete representation and edge identification

FSDT (or FSDTZ including the Murakami's function) are presented for the sake of completeness. Finally, the procedure is validated by means of the comparison with the frequencies obtained by the commercial code Abaqus. A three-dimensional finite element (3D-FEM) model is built to this aim by using the "C3D20" brick elements embedded in Abaqus.

The shell structures under consideration are depicted in Fig. 3. In particular, an elliptic cone, a spherical shell, a doubly-curved shell of translation obtained by sliding an ellipse over another ellipse, and an ellipsoid are investigated. Their position vectors and geometric features are listed in Table 1, in which $\mathbf{e}_i$, for $i = 1, 2, 3$ denotes the unit vectors of the corresponding directions of the global reference system $Ox_1x_2x_3$, as depicted in Fig. 1. The number of discrete points (I_N, I_M) is also specified in the same table.

The elliptic cone is made of one single layer of orthotropic material with (30) as lamination scheme. The mechanical properties of the layer are given by $E_1 = 137.9$ GPa, $E_2 = E_3 = 8.96$ GPa, $G_{12} = G_{13} = 7.1$ GPa, $G_{23} = 6.21$ GPa, $\nu_{12} = \nu_{13} = 0.3$, $\nu_{23} = 0.49$, $\rho = 1450$ kg/ m^3. Since only one layer is considered, the various theories do not include the Murakami's function. In fact, the Murakami's

Table 1 Position vectors and geometric features of the shell structures depicted in Fig. 3

Elliptic cone ($I_N = 41$, $I_M = 21$)
$\mathbf{r}(\alpha_1, y) = (a\cos\alpha_1 + y\sin\alpha\sin\varphi)\ \mathbf{e}_1 - y\cos\alpha\,\mathbf{e}_2 + (b\sin\alpha_1 - y\sin\alpha\cos\varphi)\ \mathbf{e}_3$
$\varphi(\alpha_1) = \arctan\left(-\frac{b\cos\alpha_1}{a\sqrt{1-\cos^2\alpha_1}}\right)$, $a = 3\,\text{m}$, $b = 2\,\text{m}$, $\alpha_1 \in [0, 2\pi]$,
$y \in [0, 10\,\text{m}]$, $\alpha = \pi/9$, $h = 1\,\text{m}$
Spherical shell ($I_N = 31$, $I_M = 31$)
$\mathbf{r}(\alpha_1, \alpha_2) = R\sin\alpha_1\cos\alpha_2\mathbf{e}_1 - R\sin\alpha_1\sin\alpha_2\mathbf{e}_2 + R\cos\alpha_1\mathbf{e}_3$
$R = 2\,\text{m}$, $\alpha_1 \in [\pi/6, \pi/2]$, $\alpha_2 \in [0, 2\pi]$, $h = 0.1\,\text{m}$, $h_1 = h_2 = 0.05\,\text{m}$
Doubly-curved shell of translation ($I_N = 51$, $I_M = 21$)
$\mathbf{r}(\alpha_1, \alpha_2) = \left(\frac{a^2\tan\alpha_1}{\sqrt{b^2+a^2\tan^2\alpha_1}} - d\left(1 - \sqrt{1 - \frac{c^2\tan^2\alpha_2}{d^2+c^2\tan^2\alpha_2}}\right)\sin\alpha_1\right)\mathbf{e}_1 - \frac{c^2\tan\alpha_2}{\sqrt{d^2+c^2\tan^2\alpha_2}}\mathbf{e}_2 +$ $+\left(b\left(1 - \sqrt{1 - \frac{a^2\tan^2\alpha_1}{b^2+a^2\tan^2\alpha_1}}\right) + d\left(1 - \sqrt{1 - \frac{c^2\tan^2\alpha_2}{d^2+c^2\tan^2\alpha_2}}\right)\cos\alpha_1\right)\mathbf{e}_3$
$a = d = 10\,\text{m}$, $b = c = 7\,\text{m}$, $\alpha_1 \in [0, 2\pi]$, $\alpha_2 \in [-5\pi/18, 5\pi/18]$, $h = 1\,\text{m}$, $h_1 = h_2 = 0.5\,\text{m}$
Ellipsoid ($I_N = 31$, $I_M = 31$)
$\mathbf{r}(\alpha_1, \alpha_2) = \left(\frac{a\sqrt{a^2-b^2\sin^2\alpha_1-c^2\cos^2\alpha_1}}{\sqrt{a^2-c^2}}\cos\alpha_2\right)\mathbf{e}_1 + (b\cos\alpha_1\sin\alpha_2)\ \mathbf{e}_2 +$ $+\left(-\frac{c\sqrt{a^2\sin^2\alpha_2+b^2\cos^2\alpha_2-c^2}}{\sqrt{a^2-c^2}}\sin\alpha_1\right)\mathbf{e}_3$
$\alpha_1 \in [0, \pi]$, $\alpha_2 \in [\pi/6, 5\pi/6]$, $a = 2\,\text{m}$, $b = 1.5\,\text{m}$,
$c = 1\,\text{m}, a \geq b \geq c$, $h_1 = h_3 = 0.025\,\text{m}$, $h_2 = 0.05\,\text{m}$

function should be embedded only for laminated composites, when there is an interlaminar interface to be analyzed. The first ten natural frequencies are shown in Table 2, considering FC as boundary conditions.

The next structure is a FC spherical shell made of two layers with (30/45) as stacking sequence. The mechanical features of the two plies are the same of the previous application. Since the structure is made of two layers, in this circumstance the results are provided also for the corresponding zig-zag models. Table 3 shows the first ten natural frequencies for the considered geometry.

Then, a doubly-curved shell of translation is analyzed. This peculiar geometry is obtained by sliding an elliptic arch over another ellipse, by using the corresponding geometric parameters listed in Table 1. The lamination scheme and the mechanical features are the same employed in the previous application. Even in this circumstance, the HSDTs are developed by neglecting and considering the zig-zag effect. As far as the boundary conditions are concerned, the sequence FC is required. The first ten natural frequencies are shown in Table 4.

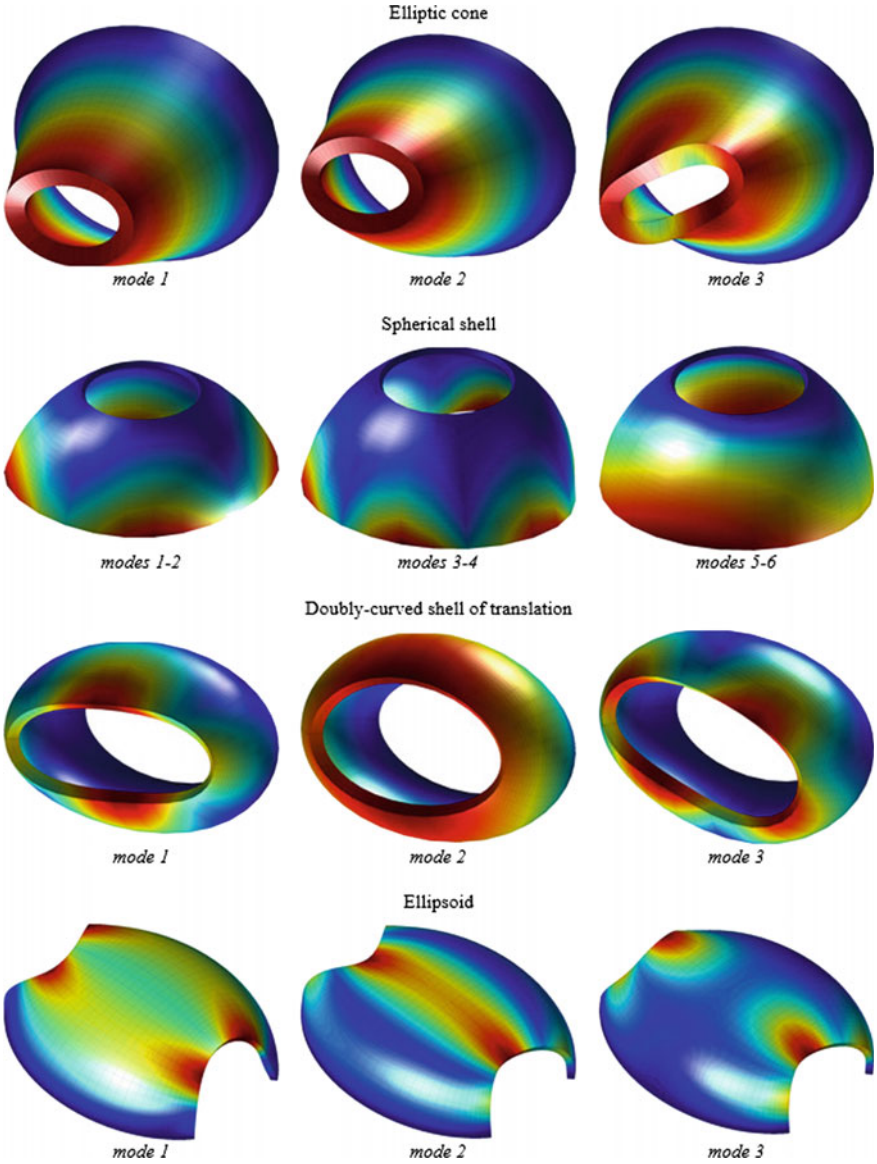

Fig. 4 First three mode shapes of the laminated composite shell structures

Finally, a FCFC sandwich ellipsoid with an inner soft-core is considered. The structure is made of three layers and the stacking sequence is given by (0/core/90). The two external skins are made of the same orthotropic medium ($E_1 = 53.78$ GPa, $E_2 = E_3 = 17.93$ GPa, $G_{12} = G_{13} = 8.96$ GPa, $G_{23} = 3.45$ GPa, $\nu_{12} = \nu_{13} = 0.25$, $\nu_{23} = 0.34$, $\rho = 1900\,\text{kg/m}^3$), whereas the core is isotropic ($E = 0.232$ GPa,

Table 2 First ten natural frequencies [Hz] for a FC orthotropic elliptic cone for various higher-order shear deformation theories

f [Hz]	FSDT	ED2	ED3	ED4	3D-FEM
1	45.529	45.374	45.391	45.376	45.345
2	49.715	49.483	49.502	49.491	49.493
3	66.081	66.954	66.970	66.939	66.917
4	72.474	72.404	72.459	72.400	72.330
5	74.483	74.732	74.802	74.756	74.721
6	98.668	98.006	98.115	98.089	98.080
7	104.622	104.034	104.169	104.135	104.140
8	104.823	104.683	104.814	104.791	104.780
9	110.597	110.278	110.545	110.505	110.460
10	112.681	112.447	112.676	112.630	112.580

Table 3 First ten natural frequencies [Hz] for a FC laminated composite spherical shell for various higher-order shear deformation theories

f [Hz]	FSDT	ED2	ED3	ED4	3D-FEM
1	43.020	42.870	42.979	42.860	42.922
2	43.020	42.870	42.979	42.860	42.922
3	60.477	60.568	60.610	60.542	60.564
4	60.477	60.568	60.610	60.542	60.564
5	82.542	82.527	82.633	82.551	82.584
6	82.542	82.527	82.633	82.551	82.584
7	98.939	99.185	99.213	99.159	99.168
8	98.939	99.185	99.213	99.159	99.168
9	143.964	144.283	144.321	144.266	144.280
10	143.964	144.283	144.321	144.266	144.280
f [Hz]	FSDTZ	EDZ2	EDZ3	EDZ4	3D-FEM
1	43.011	42.854	42.929	42.852	42.922
2	43.011	42.854	42.929	42.852	42.922
3	60.455	60.558	60.580	60.539	60.564
4	60.455	60.558	60.580	60.539	60.564
5	82.533	82.515	82.598	82.544	82.584
6	82.533	82.515	82.598	82.544	82.584
7	98.892	99.173	99.187	99.158	99.168
8	98.892	99.173	99.187	99.158	99.168
9	143.884	144.266	144.294	144.265	144.280
10	143.884	144.266	144.294	144.265	144.280

Table 4 First ten natural frequencies [Hz] for a FC laminated composite doubly-curved shell of translation for various higher-order shear deformation theories

f [Hz]	FSDTZ	EDZ2	EDZ3	EDZ4	3D-FEM
1	21.843	21.828	21.872	21.839	21.833
2	22.317	22.179	22.213	22.197	22.214
3	22.598	22.575	22.613	22.579	22.590
4	33.061	32.833	32.875	32.860	32.852
5	43.253	43.070	43.105	43.109	43.065
6	44.719	44.811	44.828	44.801	45.006
7	45.647	45.757	45.830	45.795	45.817
8	52.433	52.233	52.269	52.267	52.272
9	54.176	54.570	54.574	54.562	54.561
10	64.237	64.009	64.038	64.035	64.012
f [Hz]	FSDTZ	EDZ2	EDZ3	EDZ4	3D-FEM
1	21.829	21.824	21.856	21.841	21.833
2	22.315	22.175	22.207	22.195	22.214
3	22.584	22.571	22.597	22.581	22.590
4	33.057	32.828	32.869	32.859	32.852
5	43.246	43.066	43.107	43.108	43.065
6	44.680	44.806	44.814	44.803	45.006
7	45.601	45.751	45.812	45.798	45.817
8	52.418	52.230	52.267	52.267	52.272
9	54.173	54.567	54.569	54.561	54.561
10	64.232	64.005	64.036	64.034	64.012

Table 5 First ten natural frequencies [Hz] for a FCFC sandwich ellipsoid with an inner soft-core for various higher-order shear deformation theories

f [Hz]	FSDTZ	EDZ2	EDZ3	EDZ4	3D-FEM
1	118.538	117.785	117.774	117.414	117.388
2	143.203	141.791	141.780	141.317	141.253
3	146.529	145.210	145.187	144.678	144.464
4	190.667	189.652	189.629	189.019	188.798
5	218.887	217.144	217.125	216.441	216.305
6	246.935	246.318	246.297	245.946	245.851
7	250.336	250.109	250.099	249.938	249.844
8	256.984	256.281	256.252	255.566	255.512
9	263.792	262.386	262.364	261.534	261.393
10	285.299	284.256	284.224	283.158	282.904

$\nu = 0.2$, $\rho = 320\,\text{kg/m}^3$). It should be noted that the mechanical properties of the soft-core are extremely lower than the ones of the external sheets. Therefore, a sandwich structure is considered and its mechanical behavior can be accurately described only by the zig-zag theories. The natural frequencies are shown in Table 5.

Finally, the first three mode shapes for the laminated composite shells considered in this section are depicted in Fig. 4 for the sake of completeness.

6 Final Remarks

The results presented in the previous section prove that an excellent agreement can obtained between the proposed solutions and the reference ones carried out through a three-dimensional FEM model (3D-FEM), independently from the structural model. Nevertheless, it can be observed that higher-order theories provide closer results to the reference ones for thicker structures. In particular, higher-order theories, as the ED3, ED4, and their corresponding zig-zag approaches, should be used since they can provide closer results the three-dimensional FEM solution. Finally, it should be recalled that the three-dimensional FEM models require a greater number of degrees of freedom to obtain the solutions, whereas the GDQ is able to reach the same level of accuracy with a reduced number of degrees of freedom. It should be specified, in fact, that the considered doubly-curved shells have been modeled and analyzed by using a sole element. Thus, the proposed approach represents a powerful, accurate and efficient way for investigating the mechanical behavior of doubly-curved laminated composites shell structures.

References

1. Tornabene, F., Bacciocchi, M.: Anisotropic doubly-curved shells. higher-order strong and weak formulations for arbitrarily shaped shell structures, Esculapio, Bologna (2018)
2. Tornabene, F., Fantuzzi, N., Bacciocchi, M.: The GDQ method for the free vibration analysis of arbitrarily shaped laminated composite shells using a NURBS-based isogeometric approach. Compos. Struct. **154**, 190–218 (2016)
3. Tornabene, F., Fantuzzi, N., Bacciocchi, M.: A New Doubly-Curved Shell Element for the Free Vibrations of Arbitrarily Shaped Laminated Structures Based on Weak Formulation IsoGeometric Analysis. Compos. Struct. **171**, 429–461 (2017)
4. Fantuzzi, N., Della Puppa, G., Tornabene, F., Trautz, M.: Strong formulation isogeometric analysis for the vibration of thin membranes of general shape. Int. J. Mech. Sci. **120**, 322–340 (2017)
5. Tornabene, F., Fantuzzi, N., Bacciocchi, M.: Strong and weak formulations based on differential and integral quadrature methods for the free vibration analysis of composite plates and shells: convergence and accuracy. Eng. Anal. Bound Elem. **92**, 3–37 (2018)
6. Tornabene, F., Fantuzzi, N., Ubertini, F., Viola, E.: Strong formulation finite element method based on differential quadrature: a survey. Appl. Mech. Rev. **67**, 020801-1–55 (2015)
7. Shu, C.: Differential Quadrature and its Application in Engineering. Springer, London (2000)
8. Kraus, H.: Thin Elastic Shells. Wiley, New York (1967)

9. Fantuzzi, N., Tornabene, F.: Strong formulation isogeometric analysis (SFIGA) for laminated composite arbitrarily shaped plates. Compos. Part B-Eng. **96**, 173–203 (2016)
10. Vinson, J.R.: The Behavior of Shells Composed of Isotropic and Composite Materials. Springer, London (1993)
11. Jones, R.M.: Mechanics of Composite Materials, 2nd edn. Taylor & Francis, London (1999)
12. Vasiliev, V.V., Morozov, E.V.: Mechanics and Analysis of Composite Materials. Elsevier, Oxford (2001)
13. Reddy, J.N.: Mechanics of Laminated Composite Plates and Shells, 2nc edn. CRC Press, Boca Raton (2004)
14. Barbero, E.J.: Introduction to Composite Materials Design. CRC Press, Boca Raton (2011)
15. Tornabene, F., Fantuzzi, N., Bacciocchi, M.: Mechanical behaviour of composite cosserat solids in elastic problems with holes and discontinuities. Compos. Struct. **179**, 468–481 (2017)
16. Fantuzzi, N., Leonetti, L., Trovalusci, P., Tornabene, F.: Some novel numerical applications of cosserat continua. Int. J. Comp. Method **15**(06), 1850054-1 (2018)
17. Tornabene, F.: Free vibrations of anisotropic doubly-curved shells and panels of revolution with a free-form meridian resting on Winkler-Pasternak elastic foundations. Compos. Struct. **94**, 186–206 (2011)
18. Tornabene, F.: Free vibrations of laminated composite doubly-curved shells and panels of revolution via the GDQ method. Comput. Method Appl. Mech. Eng. **200**, 931–952 (2011)
19. Tornabene, F., Fantuzzi, N., Viola, E., Reddy, J.N.: Winkler-Pasternak foundation effect on the static and dynamic analyses of laminated doubly-curved and degenerate shells and panels. Compos. Part B-Eng. **57**, 269–296 (2014)
20. Fantuzzi, N., Tornabene, F., Viola, E., Ferreira, A.J.M.: A strong formulation finite element method (SFEM) based on RBF and GDQ techniques for the static and dynamic analyses of laminated plates of arbitrary shape. Meccanica **49**, 2503–2542 (2014)
21. Fantuzzi, N.: New insights into the strong formulation finite element method for solving elastostatic and elastodynamic problems. Curved Layer. Struct. **1**, 93–126 (2014)
22. Tornabene, F., Fantuzzi, N., Bacciocchi, M.: The local GDQ method applied to general higher-order theories of doubly-curved laminated composite shells and panels: the free vibration analysis. Compos. Struct. **116**, 637–660 (2014)
23. Fantuzzi, N., Bacciocchi, M., Tornabene, F., Viola, E., Ferreira, A.J.M.: Radial basis functions based on differential quadrature method for the free vibration of laminated composite arbitrary shaped plates. Compos. Part B-Eng. **78**, 65–78 (2015)
24. Tornabene, F., Fantuzzi, N., Bacciocchi, M., Viola, E.: A new approach for treating concentrated loads in doubly-curved composite deep shells with variable radii of curvature. Compos. Struct. **131**, 433–452 (2015)
25. Tornabene, F., Fantuzzi, N., Bacciocchi, M., Neves, A.M.A., Ferreira, A.J.M.: MLSDQ based on RBFs for the free vibrations of laminated composite doubly-curved shells. Compos. Part B-Eng. **99**, 30–47 (2016)
26. Tornabene, F., Fantuzzi, N., Bacciocchi, M.: On the mechanics of laminated doubly-curved shells subjected to point and line loads. Int. J. Eng. Sci. **109**, 115–164 (2016)
27. Bacciocchi, M., Eisenberger, M., Fantuzzi, N., Tornabene, F., Viola, E.: Vibration analysis of variable thickness plates and shells by the generalized differential quadrature method. Compos. Struct. **156**, 218–237 (2016)
28. Brischetto, S., Tornabene, F., Fantuzzi, N., Bacciocchi, M.: Interpretation of boundary conditions in the analytical and numerical shell solutions for mode analysis of multilayered structures. Int. J. Mech. Sci. **122**, 18–28 (2017)
29. Tornabene, F., Fantuzzi, N., Bacciocchi, M., Reddy, J.N.: A posteriori stress and strain recovery procedure for the static analysis of laminated shells resting on nonlinear elastic foundation. Compos. Part B- Eng. **126**, 162–191 (2017)
30. Fantuzzi, N., Tornabene, F., Bacciocchi, M., Neves, A.M.A., Ferreira, A.J.M.: Stability and accuracy of three fourier expansion-based strong form finite elements for the free vibration analysis of laminated composite plates. Int. J. Numer. Method Eng. **111**, 354–382 (2017)

31. Tornabene, F., Fantuzzi, N., Bacciocchi, M.: Linear static behavior of damaged laminated composite plates and shells. Materials **10**(811), 1–52 (2017)
32. Tornabene, F., Fantuzzi, N., Bacciocchi, M., Reddy, J.N.: An equivalent layer-wise approach for the free vibration analysis of thick and thin laminated sandwich shells. Appl. Sci. **7**(17), 1–34 (2017)
33. Zare Jouneghani, F., Mohammadi Dashtaki, P., Dimitri, R., Bacciocchi, M., Tornabene, F.: First-order shear deformation theory for orthotropic doubly-curved shells based on a modified couple stress elasticity. Aerosp. Sci. Technol. **73**, 129–147 (2018)
34. Tornabene, F., Bacciocchi, M.: Effect of curvilinear reinforcing fibers on the linear static behavior of soft-core sandwich structures. J. Compos. Sci. **2**(14), 1–43 (2018)
35. Tornabene, F., Bacciocchi, M.: Dynamic stability of doubly-curved multilayered shells subjected to arbitrarily oriented angular velocities: numerical evaluation of the critical speed. Compos. Struct. **201**, 1031–1055 (2018)
36. Fantuzzi, N., Tornabene, F., Bacciocchi, M., Ferreira, A.J.M.: On the convergence of laminated composite plates of arbitrary shape through finite element models. J. Compos. Sci. **2**(16), 1–50 (2018)
37. Tornabene, F., Viola, E.: Free vibration analysis of functionally graded panels and shells of revolution. Meccanica **44**, 255–281 (2009)
38. Tornabene, F., Viola, E., Inman, D.J.: 2-D differential quadrature solution for vibration analysis of functionally graded conical, cylindrical shell and annular plate structures. J. Sound Vib. **328**, 259–290 (2009)
39. Tornabene, F.: Free vibration analysis of functionally graded conical, cylindrical shell and annular plate structures with a four-parameter power-law distribution. Comput. Method Appl. Mech. Eng. **198**, 2911–2935 (2009)
40. Tornabene, F., Viola, E.: Free vibrations of four-parameter functionally graded parabolic panels and shells of revolution. Eur. J. Mech. A-Solid **28**, 991–1013 (2009)
41. Viola, E., Tornabene, F.: Free vibrations of three parameter functionally graded parabolic panels of revolution. Mech. Res. Commun. **36**, 587–594 (2009)
42. Tornabene, F., Viola, E.: Static analysis of functionally graded doubly-curved shells and panels of revolution. Meccanica **48**, 901–930 (2013)
43. Fantuzzi, N., Tornabene, F., Viola, E.: Four-parameter functionally graded cracked plates of arbitrary shape: a GDQFEM solution for free vibrations. Mech. Adv. Mater. Struct. **23**, 89–107 (2016)
44. Brischetto, S., Tornabene, F., Fantuzzi, N., Viola, E.: 3D exact and 2D generalized differential quadrature models for free vibration analysis of functionally graded plates and cylinders. Meccanica **51**, 2059–2098 (2016)
45. Fantuzzi, N., Brischetto, S., Tornabene, F., Viola, E.: 2D and 3D shell models for the free vibration investigation of functionally graded cylindrical and spherical panels. Compos. Struct. **154**, 573–590 (2016)
46. Tornabene, F., Brischetto, S., Fantuzzi, N., Bacciocchi, M.: Boundary conditions in 2D numerical and 3D exact models for cylindrical bending analysis of functionally graded structures. Shock Vib. **2373862**, 1–17 (2016)
47. Tornabene, F., Fantuzzi, N., Bacciocchi, M., Viola, E., Reddy, J.N.: A numerical investigation on the natural frequencies of FGM sandwich shells with variable thickness by the local generalized differential quadrature method. Appl. Sci. **7**(131), 1–39 (2017)
48. Zare Jouneghani, F., Dimitri, R., Bacciocchi, M., Tornabene, F.: Free vibration analysis of functionally graded porous doubly-curved shells based on the first-order shear deformation theory. Appl. Sci. **7**(1252), 1–20 (2017)
49. Tornabene, F., Fantuzzi, N., Bacciocchi, M., Viola, E.: Effect of agglomeration on the natural frequencies of functionally graded carbon nanotube-reinforced laminated composite doubly-curved shells. Compos. Part B-Eng. **89**, 187–218 (2016)
50. Kamarian, S., Salim, M., Dimitri, R., Tornabene, F.: Free vibration analysis of conical shells reinforced with agglomerated carbon nanotubes. Int. J. Mech. Sci. **108–109**, 157–165 (2016)

51. Fantuzzi, N., Tornabene, F., Bacciocchi, M., Dimitri, R.: Free vibration analysis of arbitrarily shaped functionally graded carbon nanotube-reinforced plates. Compos. Part B-Eng. **115**, 384–408 (2017)
52. Tornabene, F., Fantuzzi, N., Bacciocchi, M.: Linear static response of nanocomposite plates and shells reinforced by agglomerated carbon nanotubes. Compos. Part B-Eng. **115**, 449–476 (2017)
53. Nejati, M., Asanjarani, A., Dimitri, R., Tornabene, F.: Static and free vibration analysis of functionally graded conical shells reinforced by carbon nanotubes. Int. J. Mech. Sci. **130**, 383–398 (2017)
54. Nejati, M., Dimitri, R., Tornabene, F., Hossein Yas, M.: Thermal buckling of nanocomposite stiffened cylindrical shells reinforced by functionally graded wavy carbon nano-tubes with temperature-dependent properties. Appl. Sci. **7**(1223), 1–24 (2017)
55. Banić, D., Bacciocchi, M., Tornabene, F., Ferreira, A.J.M.: Influence of Winkler-Pasternak foundation on the vibrational behavior of plates and shells reinforced by agglomerated carbon nanotubes. Appl. Sci. **7**(1228), 1–55 (2017)
56. Tornabene, F., Bacciocchi, M., Fantuzzi, N., Reddy, J.N.: Multiscale approach for three-phase CNT/Polymer/Fiber laminated nanocomposite structures. Polym Composite **40**, E102–E126 (2019)
57. Whitney, J.M., Pagano, N.J.: Shear deformation in heterogeneous anisotropic plates. J. Appl. Mech-T ASME **37**, 1031–1036 (1970)
58. Whitney, J.M., Sun, C.T.: A higher order theory for extensional motion of laminated composites. J. Sound Vib. **30**, 85–97 (1973)
59. Reissner, E.: On transverse bending of plates, including the effect of transverse shear deformation. Int. J. Solids Struct. **11**, 569–573 (1975)
60. Green, A.E., Naghdi, P.M.: A theory of composite laminated plates. IMA J. Appl. Math. **29**, 1–23 (1982)
61. Reddy, J.N.: A simple higher-order theory for laminated composite plates. J. Appl. Mech-T ASME **51**, 745–752 (1984)
62. Bert, C.W.: A critical evaluation of new plate theories applied to laminated composites. Compos. Struct. **2**, 329–347 (1984)
63. Reddy, J.N., Liu, C.F.: A higher-order shear deformation theory for laminated elastic shells. Int. J. Eng. Sci. **23**, 319–330 (1985)
64. Reddy, J.N.: A generalization of the two-dimensional theories of laminated composite plates. Commun. Appl. Numer. Method **3**, 173–180 (1987)
65. Librescu, L., Reddy, J.N.: A few remarks concerning several refined theories of anisotropic composite laminated plates. Int. J. Eng. Sci. **27**, 515–527 (1989)
66. Reddy, J.N.: On refined theories of composite laminates. Meccanica **25**, 230–238 (1990)
67. Robbins, D.H., Reddy, J.N.: Modeling of thick composites using a layer-wise laminate theory. Int. J. Numer. Method Eng. **36**, 655–677 (1993)
68. Carrera, E.: A refined multi-layered finite-element model applied to linear and non-linear analysis of sandwich plates. Compos. Sci. Technol. **58**, 1553–1569 (1998)
69. Carrera, E.: Theories and finite elements for multilayered, anisotropic, composite plates and shells. Arch. Comput. Methods Eng. **9**, 87–140 (2002)
70. Carrera, E.: Theories and finite elements for multilayered plates and shells: a unified compact formulation with numerical assessment and benchmarking. Arch. Comput. Methods Eng. **10**, 215–296 (2003)
71. Carrera, E.: Historical review of zig-zag theories for multilayered plates and shells. Appl. Mech. Rev. **56**, 287–308 (2003)
72. Carrera, E.: On the use of the Murakami's zig-zag function in the modeling of layered plates and shells. Comput. Struct. **82**, 541–554 (2004)
73. Viola, E., Tornabene, F., Fantuzzi, N.: Static analysis of completely doubly-curved laminated shells and panels using general higher-order shear deformation theories. Compos. Struct. **101**, 59–93 (2013)

74. Viola, E., Tornabene, F., Fantuzzi, N.: General higher-order shear deformation theories for the free vibration analysis of completely doubly-curved laminated shells and panels. Compos. Struct. **95**, 639–666 (2013)
75. Tornabene, F., Viola, E., Fantuzzi, N.: General higher-order equivalent single layer theory for free vibrations of doubly-curved laminated composite shells and panels. Compos. Struct. **104**, 94–117 (2013)
76. Tornabene, F., Fantuzzi, N., Viola, E., Ferreira, A.J.M.: Radial basis function method applied to doubly-curved laminated composite shells and panels with a general higher-order equivalent single layer formulation. Compos. Part B-Eng. **55**, 642–659 (2013)
77. Tornabene, F., Fantuzzi, N., Viola, E., Carrera, E.: Static analysis of doubly-curved anisotropic shells and panels using CUF approach, differential geometry and differential quadrature method. Compos. Struct. **107**, 675–697 (2014)
78. Tornabene, F., Fantuzzi, N., Bacciocchi, M.: Free vibrations of free-form doubly-curved shells made of functionally graded materials using higher-order equivalent single layer theories. Compos. Part B-Eng. **67**, 490–509 (2014)
79. Tornabene, F., Fantuzzi, N., Viola, E., Batra, R.C.: Stress and strain recovery for functionally graded free-form and doubly-curved sandwich shells using higher-order equivalent single layer theory. Compos. Struct. **119**, 67–89 (2015)
80. Tornabene, F., Fantuzzi, N., Bacciocchi, M., Viola, E.: Higher-order theories for the free vibration of doubly-curved laminated panels with curvilinear reinforcing fibers by means of a local version of the GDQ method. Compos. Part B-Eng. **81**, 196–230 (2015)
81. Tornabene, F., Fantuzzi, N., Bacciocchi, M.: Higher-order structural theories for the static analysis of doubly-curved laminated composite panels reinforced by curvilinear fibers. Thin Wall. Struct. **102**, 222–245 (2016)
82. Tornabene, F., Fantuzzi, N., Bacciocchi, M.: The local GDQ method for the natural frequencies of doubly-curved shells with variable thickness: a general formulation. Compos. Part B-Eng. **92**, 265–289 (2016)
83. Tornabene, F., Dimitri, R.: A numerical study of the seismic response of arched and vaulted structures made of isotropic or composite materials. Eng. Struct. **159**, 332–366 (2018)
84. Tornabene, F., Fantuzzi, N., Bacciocchi, M., Viola, E.: Mechanical behavior of damaged laminated composites plates and shells: higher-order shear deformation theories. Compos. Struct. **189**, 304–329 (2018)
85. Brischetto, S., Tornabene, F.: Advanced GDQ models and 3D stress recovery in multi-layered plates, spherical and double-curved panels subjected to transverse shear loads. Compos. Part B-Eng. **146**, 244–269 (2018)
86. Tornabene, F., Brischetto, S.: 3D capability of refined GDQ models for the bending analysis of composite and sandwich plates, spherical and doubly-curved shells. Thin Wall. Struct. **129**, 94–124 (2018)
87. Tornabene, F., Fantuzzi, F., Bacciocchi, M.: Foam core composite sandwich plates and shells with variable stiffness: effect of curvilinear fiber path on the modal response. J. Sandw. Struct. Mater. **21**, 320–365 (2019)
88. Tornabene, F., Fantuzzi, N., Bacciocchi, M.: Refined shear deformation theories for laminated composite arches and beams with variable thickness: natural frequency analysis. Eng. Anal. Bound Elem **100**, 24–47 (2019)
89. Tornabene, F., Fantuzzi, N., Bacciocchi, M., Viola, E.: accurate inter-laminar recovery for plates and doubly-curved shells with variable radii of curvature using layer-wise theories. Compos. Struct. **124**, 368–393 (2015)
90. Tornabene, F., Fantuzzi, N., Bacciocchi, M., Dimitri, R.: Dynamic analysis of thick and thin elliptic shell structures made of laminated composite materials. Compos. Struct. **133**, 278–299 (2015)
91. Tornabene, F., Fantuzzi, N., Bacciocchi, M., Dimitri, R.: Free vibrations of composite oval and elliptic cylinders by the generalized differential quadrature method. Thin Wall Struct. **97**, 114–129 (2015)

92. Tornabene, F., Fantuzzi, N., Viola, E.: Inter-laminar stress recovery procedure for doubly-curved. singly-curved, Revolution shells with variable radii of curvature and plates using generalized higher-order theories and the local GDQ method. Mech. Adv. Mater. Struc. **23**, 1019–1045 (2016)
93. Tornabene, F.: General higher order layer-wise theory for free vibrations of doubly-curved laminated composite shells and panels. Mech. Adv. Mater. Struct. **23**, 1046–1067 (2016)
94. Dozio, L.: A hierarchical formulation of the state-space Levy's method for vibration analysis of thin and thick multilayered shells. Compos. Part B-Eng. **98**, 97–107 (2016)
95. Dozio, L., Alimonti, L.: Variable kinematic finite element models of multilayered composite plates coupled with acoustic fluid. Mech. Adv. Mater. Struct. **23**, 981–996 (2016)
96. Vescovini, R., Dozio, L.: A variable-kinematic model for variable stiffness plates: vibration and buckling analysis. Compos. Struct. **142**, 15–26 (2016)
97. Wenzel, C., D'Ottavio, M., Polit, O., Vidal, P.: Assessment of free-edge singularities in composite laminates using higher-order plate elements. Mech. Adv. Mater. Stuct. **23**, 948–959 (2016)
98. Demasi, L.: ∞^3 Hierarchy plate theories for thick and thin composite plates: the generalized unified formulation. Compos. Struct. **84**, 256–270 (2008)
99. D'Ottavio, M.: A sublaminate generalized unified formulation for the analysis of composite structures. Compos. Struct. **142**, 187–199 (2016)
100. Tornabene, F., Fantuzzi, N., Bacciocchi, M.: DiQuMASPAB: Differential Quadrature for Mechanics of Anisotropic Shells, Plates, Arches and Beams. User Manual. Esculapio, Bologna. https://DiQuMASPAB.editrice-esculapio.com (2018)

On a Simple Shell Model for Thin Structures with Functionally Graded Materials

Werner Wagner and Friedrich Gruttmann

1 Introduction

Traditional composites consisting of different materials have been widely used to design structures with high performance demands. However, due to the mismatch of material parameters such composites tend to stress singularities, which may occur at the interface between different materials. This holds especially when the composite is exposed to high temperature gradients. A mismatch of thermal expansion coefficients will induce considerable residual stresses and may lead to cracking and debonding. Therefore, the concept of functionally graded material (FGM) was introduced to avoid stress singularities along with an ultra-high temperature environment, e.g. [19]. Multi-phase materials are prepared by continuously changing the volume fraction of the constituents [16, 20]. The FGM is suitable for various applications, such as thermal coatings of barrier for ceramic engines, gas turbines, nuclear fusions, optical thin layers, and other engineering applications. To describe the variation of material properties often power-law functions, exponential functions or sigmoid functions are used, e.g. [6, 13, 26].

A review on theories for the modeling and analysis of functionally graded plates and shells is given in [23]. Due to the extensive growth of literature on approximation techniques for FGM structures only a limited selection can be given. The papers [1, 4, 7, 8, 15, 17, 18, 21] among many others deal with plate models.

W. Wagner (✉)
Institut für Baustatik, Karlsruher Institut für Technologie, Kaiserstr. 12,
76131 Karlsruhe, Germany
e-mail: w.wagner@kit.edu

F. Gruttmann
Fachgebiet Festkörpermechanik, Technische Universität Darmstadt, Franziska-Braun-Str. 7,
64287 Darmstadt, Germany
e-mail: gruttmann@mechanik.tu-darmstadt.de

H. Altenbach et al. (eds.), *Recent Developments in the Theory of Shells*,
Advanced Structured Materials 110, https://doi.org/10.1007/978-3-030-17747-8_34

In our previous paper [12] a shell model for layered structures with *N physical* layers is presented. The parameters for orthotropic material behaviour along with zero normal stress condition in thickness direction are different for each individual layer due to variable fiber angles in laminates. The displacements of the Reissner-Mindlin kinematics are enriched by so–called warping displacements which are interpolated with layer-wise cubic functions through the thickness. Based on a multi-field functional the interpolation of the independent quantities is performed in representative volume elements (RVEs) in a proper way. For layer-wise constant material parameters—as is the case for linear elasticity—the transverse shear stresses are quadratic functions of the thickness coordinate. These stresses are described continuously at the boundaries of the physical layers and the zero stress boundary conditions at the outer surfaces are automatically fulfilled without further constraints.

Present formulation is characterized by the following features.

- The theory and finite element formulation [12] is adapted to FGM shells. A power law for the shape of the elastic constants in thickness direction is implemented. The shell is subdivided in *N numerical* layers. Hence the layer-wise cubic interpolation for the warping displacements and the quadratic shape of transverse shear stresses provides an approximation. As consequence one obtains jumps for the transverse shear stresses at the boundaries of the numerical layers and the stress boundary conditions are only approximately fulfilled. Warping parameters and Lagrange parameters are eliminated by static condensation. In this context shear correction factors are obtained.
- The jumps at the layer boundaries vanish and the zero stress boundary conditions at the outer surfaces are progressively better fulfilled with an increase of numerical layers. Furthermore the integral of the transverse shear stresses converges against the shear force obtained from the material law for the stress resultants. The investigations show, that only a small number of numerical layers are necessary to obtain converged results.
- For linear elasticity the computation of the condensed material matrix can be done once as a pre–processing, which reduces the computing time significantly. Reference solutions are computed using solid shell element [14] with implemented power law for the material constants. As standard nodal degrees are used, the elements can be applied to shell intersection problems. The extension of the theory to geometrical nonlinear problems is straight forward. The essential advantage of the formulation is its inherent simplicity in theory and finite element implementation.

The paper is organized as follows. In Sect. 2 a brief summary of the essential equations according to Ref. [12] with necessary modifications for FGM shells are given. Several examples are presented in Sect. 3. The evaluated displacements and stresses are compared with 3D reference solutions, which are computed with solid shell elements.

2 Variational Formulation

2.1 Kinematics

Let $\mathscr{B}_0$ be the three–dimensional Euclidean space occupied by the shell in the undeformed configuration with boundary $\partial\mathscr{B}_0$. The position vector $\boldsymbol{\Phi}$ of any point $P \in \mathscr{B}_0$ reads

$$\boldsymbol{\Phi}(\xi^1, \xi^2, \xi^3) = \mathbf{X}(\xi^1, \xi^2) + \xi^3\, \mathbf{N}(\xi^1, \xi^2) \qquad |\mathbf{N}(\xi^1, \xi^2)| = 1\,, \tag{1}$$

where the position vector $\mathbf{X}$ and the normal vector $\mathbf{N}$ of the shell mid–surface Ω are parametrized with convected coordinates ξ^α. Furthermore, ξ^3 and h denote the thickness coordinate defined in the range $-\frac{h}{2} \le \xi^3 \le \frac{h}{2}$ and the shell thickness, respectively. The coordinate on the boundary $\Gamma = \Gamma_u \cup \Gamma_\sigma$ is denoted by s. The usual summation convention is used, where Latin indices range from 1 to 3 and Greek indices range from 1 to 2. Commas denote partial differentiation with respect to the coordinates ξ^i.

Hence, the geometry of the deformed shell space $\mathscr{B}$ is described by

$$\boldsymbol{\phi}(\xi^1, \xi^2, \xi^3) = \mathbf{x}(\xi^1, \xi^2) + \xi^3\, \mathbf{d}(\xi^1, \xi^2) \qquad \mathbf{d} = \mathbf{N} + \Delta\mathbf{d}\,. \tag{2}$$

The vector $\mathbf{d}(\boldsymbol{\varphi})$ is not directed perpendicular to the deformed shell mid–surface, thus shear deformations are accounted for. Hence, the vector field $\mathbf{v}(\xi^1, \xi^2) = [\mathbf{u}, \boldsymbol{\varphi}]^T$ is introduced, where $\mathbf{u} = \mathbf{x} - \mathbf{X}$ and $\boldsymbol{\varphi}$ denote the displacements and rotations of the mid-surface, respectively.

Inserting the position vector (1) and kinematic assumption (2) into the linear strain tensor $\bar{\boldsymbol{\varepsilon}}$ leads to

$$\bar{\boldsymbol{\varepsilon}} = \bar{\varepsilon}_{ij}\, \mathbf{G}^i \otimes \mathbf{G}^j \qquad \bar{\varepsilon}_{\alpha\beta} = \varepsilon_{\alpha\beta} + \xi^3\, \kappa_{\alpha\beta} \qquad 2\,\bar{\varepsilon}_{\alpha 3} = \gamma_\alpha \qquad \bar{\varepsilon}_{33} = 0\,, \tag{3}$$

where $\mathbf{G}^i$ denote contravariant base vectors.

The membrane strains $\varepsilon_{\alpha\beta}$, curvatures $\kappa_{\alpha\beta}$ and shear strains γ_α read

$$\begin{aligned} \varepsilon_{\alpha\beta} &= \frac{1}{2}(\mathbf{u}_{,\alpha} \cdot \mathbf{X}_{,\beta} + \mathbf{u}_{,\beta} \cdot \mathbf{X}_{,\alpha}) \\ \kappa_{\alpha\beta} &= \frac{1}{2}(\mathbf{u}_{,\alpha} \cdot \mathbf{N}_{,\beta} + \mathbf{u}_{,\beta} \cdot \mathbf{N}_{,\alpha} + \Delta\mathbf{d}_{,\alpha} \cdot \mathbf{X}_{,\beta} + \Delta\mathbf{d}_{,\beta} \cdot \mathbf{X}_{,\alpha}) \\ \gamma_\alpha &= \mathbf{u}_{,\alpha} \cdot \mathbf{N} + \Delta\mathbf{d} \cdot \mathbf{X}_{,\alpha} \end{aligned} \tag{4}$$

and are arranged in the vector

$$\boldsymbol{\varepsilon}(\mathbf{v}) = [\varepsilon_{11}, \varepsilon_{22}, 2\varepsilon_{12}, \kappa_{11}, \kappa_{22}, 2\kappa_{12}, \gamma_1, \gamma_2]^T\,. \tag{5}$$

So-called warping displacements $\tilde{\mathbf{u}}$ are superposed on the displacement field following from Eqs. (1) and (2). The shape for $\tilde{\mathbf{u}} = [\tilde{u}_1, \tilde{u}_2]^T$ with components referring to a local Cartesian coordinate system is chosen as in Ref. [11]

$$\tilde{\mathbf{u}}(\xi^3) = \boldsymbol{\Phi}(\xi^3)\,\boldsymbol{\alpha}\,. \tag{6}$$

The vector $\boldsymbol{\alpha}$ is constant throughout RVEs introduced below, and contains alternating values in 1– and 2–direction at nodes in thickness direction. For this purpose the shell is subdivided in thickness direction into N numerical layers. The matrix $\boldsymbol{\Phi}$ is formulated with layer-wise cubic hierarchic functions

$$\begin{aligned} &\boldsymbol{\Phi}(\xi^3) = \left[\, \phi_1\,\mathbf{1}_2\ \phi_2\,\mathbf{1}_2\ \phi_3\,\mathbf{1}_2\ \phi_4\,\mathbf{1}_2 \,\right] \mathbf{a}^i \\ &\phi_1 = \frac{1}{2}\,(1-\zeta) \qquad \phi_2 = 1-\zeta^2 \qquad \phi_3 = \frac{8}{3}\,\zeta\,(1-\zeta^2) \qquad \phi_4 = \frac{1}{2}\,(1+\zeta)\,, \end{aligned} \tag{7}$$

and $\mathbf{a}^i$ is an assembly matrix, which relates the 8 degrees of freedom of layer i to the M components of $\boldsymbol{\alpha}$. For N layers this leads to $M = 6 \cdot N + 2$ components in $\boldsymbol{\alpha}$. Furthermore, ζ is a normalized coordinate of layer i defined in the range $-1 \le \zeta \le 1$ and $\mathbf{1}_n$ denotes a unit matrix of order n.

The strains $\mathbf{E} = [E_{11}, E_{22}, 2E_{12}, 2E_{13}, 2E_{23}]^T$ of a point in shell space with coordinate ξ^3 are obtained with

$$\begin{aligned} \mathbf{E} &= \mathbf{A}_1\,\boldsymbol{\varepsilon} + \mathbf{A}_2\,\boldsymbol{\alpha} \\ \mathbf{A}_1 &= \begin{bmatrix} \mathbf{1}_3 & \xi^3\,\mathbf{1}_3 & \mathbf{0} \\ \mathbf{0} & \mathbf{0} & \mathbf{1}_2 \end{bmatrix} \qquad A_2 = \begin{bmatrix} \mathbf{0}_{3\times 8} \\ \mathbf{A}_{2s} \end{bmatrix} \mathbf{a}^i \\ \mathbf{A}_{2s} &= \left[\, \phi_1'\,\mathbf{1}_2\ \phi_2'\,\mathbf{1}_2\ \phi_3'\,\mathbf{1}_2\ \phi_4'\,\mathbf{1}_2 \,\right] \quad \phi_j' = \frac{\mathrm{d}\phi_j}{\mathrm{d}\zeta}\,\frac{2}{h^i}\,. \end{aligned} \tag{8}$$

Here, h^i denotes the thickness of layer i. The in-plane strains $\{E_{11}, E_{22}, 2E_{12}\}$ are linear functions of ξ^3. As long as the shell is not too thick this is a good approximation. The shell strains $\boldsymbol{\varepsilon}$ are transformed to the local Cartesian coordinate system of below introduced RVE before adding the two parts in Eq. (8). The transformations are standard and therefore are not displayed here. All stress and strain components of the following subsections refer to the local orthonormal coordinate system.

2.2 *Constitutive Equations for the Stress Resultants*

Assuming linear elastic isotropic material behaviour the constitutive equations are introduced with $S^{33} = 0$ in the following standard manner

$$\begin{bmatrix} S^{11} \\ S^{22} \\ S^{12} \\ S^{13} \\ S^{23} \end{bmatrix} = \begin{bmatrix} C_{11} & C_{12} & 0 & 0 & 0 \\ C_{21} & C_{22} & 0 & 0 & 0 \\ 0 & 0 & C_{33} & 0 & 0 \\ 0 & 0 & 0 & C_{44} & 0 \\ 0 & 0 & 0 & 0 & C_{55} \end{bmatrix} \begin{bmatrix} E_{11} \\ E_{22} \\ 2E_{12} \\ 2E_{13} \\ 2E_{23} \end{bmatrix} \tag{9}$$
$$\mathbf{S} = \mathbf{C}\,\mathbf{E}\,.$$

The material constants C_{ij} are functions of Young's modulus $E(\xi^3)$ and Poisson's ratio $\nu(\xi^3)$.

$$\begin{aligned} C_{11} = C_{22} &= \frac{E}{1-\nu^2} \\ C_{12} = C_{21} &= \frac{E\,\nu}{1-\nu^2} \\ C_{33} = C_{44} = C_{55} &= \frac{E}{2\,(1+\nu)} \end{aligned} \tag{10}$$

Different types of FGM-models were introduced. These are power-law functions (P-FGM), exponential functions (E-FGM), or sigmoid functions (S-FGM), see e.g. [7], for the definition of the volume fractions. Here we use the indices 1 and 2 for the constituents. The formulae for the P-FGM model [3] are

$$V_1 = \left(\frac{1}{2} + \frac{\xi^3}{h}\right)^p, \quad V_2 = 1 - V_1 \tag{11}$$

$$E(\xi^3) = E_1\,V_1(\xi^3) + E_2\,V_2(\xi^3), \quad \nu(\xi^3) = \nu_1\,V_1(\xi^3) + \nu_2\,V_2(\xi^3)\,, \tag{12}$$

the E-FGM model [9] is defined by

$$\begin{aligned} E(\xi^3) &= E_1\,e^{B_E(\xi^3+h/2)} \quad B_E = \frac{1}{h}\ln(\frac{E_1}{E_2}) \\ \nu(\xi^3) &= \nu_1\,e^{B_\nu(\xi^3+h/2)} \quad B_\nu = \frac{1}{h}\ln(\frac{\nu_1}{\nu_2})\,, \end{aligned} \tag{13}$$

and the S-FGM [5] model

$$\begin{aligned} V_1 = \quad & \frac{1}{2}\left(1 + \frac{2\,\xi^3}{h}\right)^p \quad V_2 = 1 - V_1 \quad \text{for } [-\frac{h}{2} \le \xi^3 \le 0] \\ V_1 = 1 - & \frac{1}{2}\left(1 - \frac{2\,\xi^3}{h}\right)^p \quad V_2 = 1 - V_1 \quad \text{for } [0 \le \xi^3 \le \frac{h}{2}] \end{aligned} \tag{14}$$

$$E(\xi^3) = E_1\,V_1(\xi^3) + E_2\,V_2(\xi^3), \quad \nu(\xi^3) = \nu_1\,V_1(\xi^3) + \nu_2\,V_2(\xi^3)\,. \tag{15}$$

The relation of the stress resultants to $\mathbf{S}$ is defined by thickness integration of the specific internal virtual work and $\delta\mathbf{E} = \mathbf{A}_1\,\delta\boldsymbol{\varepsilon} + \mathbf{A}_2\,\delta\boldsymbol{\alpha}$. This yields

$$\int_{-h/2}^{+h/2} \delta \mathbf{E}^T \mathbf{S}\, \bar{\mu}\, \mathrm{d}\xi^3 = \delta \boldsymbol{\varepsilon}^T \boldsymbol{\sigma}_1 + \delta \boldsymbol{\alpha}^T \boldsymbol{\sigma}_2 \quad \boldsymbol{\sigma}_1 := \int_{-h/2}^{+h/2} \mathbf{A}_1^T \mathbf{S}\, \bar{\mu}\, \mathrm{d}\xi^3 \quad \boldsymbol{\sigma}_2 := \int_{-h/2}^{+h/2} \mathbf{A}_2^T \mathbf{S}\, \bar{\mu}\, \mathrm{d}\xi^3 \,, \tag{16}$$

where $\bar{\mu}$ denotes the determinant of the shifter tensor. The components of

$$\boldsymbol{\sigma}_1 = [n^{11}, n^{22}, n^{12}, m^{11}, m^{22}, m^{12}, q^1, q^2]^T \tag{17}$$

are membrane forces $n^{\alpha\beta} = n^{\beta\alpha}$, bending moments $m^{\alpha\beta} = m^{\beta\alpha}$ and shear forces q^α. The components of $\boldsymbol{\sigma}_2$ are higher order stress resultants. They are work conjugate to the components of $\boldsymbol{\alpha}$.

Now, inserting (9) with (8) into $(16)_2$ and $(16)_3$ yields the constitutive equations for the stress resultants

$$\begin{bmatrix} \boldsymbol{\sigma}_1 \\ \boldsymbol{\sigma}_2 \end{bmatrix} = \begin{bmatrix} \mathbf{D}_{11} & \mathbf{D}_{12} \\ \mathbf{D}_{21} & \mathbf{D}_{22} \end{bmatrix} \begin{bmatrix} \boldsymbol{\varepsilon} \\ \boldsymbol{\alpha} \end{bmatrix} \qquad \mathbf{D}_{\alpha\beta} = \int_{-h/2}^{+h/2} \mathbf{A}_\alpha^T \mathbf{C}\, \mathbf{A}_\beta\, \bar{\mu}\, \mathrm{d}\xi^3 = \mathbf{D}_{\beta\alpha}^T \,. \tag{18}$$

The integration for $\mathbf{D}_{\alpha\beta}$ is approximately performed by summation over N numerical layers and three point Gauss integration for each layer. With consideration of $\mathrm{d}\xi^3 = \frac{h^i}{2}\, \mathrm{d}\zeta$ it holds

$$\mathbf{D}_{\alpha\beta} \approx \sum_{i=1}^{N} \sum_{j=1}^{3} \mathbf{A}_\alpha^T(\zeta_j)\, \mathbf{C}(\zeta_j)\, \mathbf{A}_\beta(\zeta_j)\, \bar{\mu}\, \frac{h^i}{2}\, W_j \,. \tag{19}$$

Here, ζ_j and W_j denote the normalized thickness coordinate and weighting factor of the particular Gauss point, respectively. The integrals are computed in a RVE with rectangular shape, thus $\bar{\mu} = 1$ holds.

At first, $\mathbf{D}_{11}$ yields

$$\mathbf{D}_{11} = \int_{-h/2}^{+h/2} \mathbf{A}_1^T \mathbf{C}\, \mathbf{A}_1\, \bar{\mu}\, \mathrm{d}\xi^3 = \begin{bmatrix} \mathbf{D}_m & \mathbf{D}_{mb} & \mathbf{0} \\ \mathbf{D}_{mb}^T & \mathbf{D}_b & \mathbf{0} \\ \mathbf{0} & \mathbf{0} & \mathbf{D}_s \end{bmatrix}_{(8\times 8)} \tag{20}$$

with submatrices for membrane, bending and shear. The submatrix $\mathbf{D}_{mb}$ refers to coupling of membrane and bending behaviour. Due to the assumed isotropy for the constitutive behaviour $\mathbf{D}_s = D_s\, \mathbf{1}_2$ is a diagonal matrix.

In an analogous way the matrices $\mathbf{D}_{22}$ and $\mathbf{D}_{21}$ are assembled with the contributions of the layers using (8) and (9) in (19). Due to the interpolation functions with local layer-wise support it follows that $\mathbf{D}_{22}$ is banded and thus is sparse. In $\mathbf{D}_{21}$ only the last two columns are populated.

2.3 Equilibrium Equations and a Constraint

Neglecting body forces the equilibrium equations for the in–plane directions read

$$\begin{bmatrix} S^{11}{}_{,1} + S^{12}{}_{,2} + S^{13}{}_{,3} \\ S^{12}{}_{,1} + S^{22}{}_{,2} + S^{23}{}_{,3} \end{bmatrix} := \mathbf{f} = \mathbf{0}\,. \tag{21}$$

In Eq. (21) the in-plane stresses $S^{\alpha\beta}$ as well as transverse shear stresses $S^{\alpha 3}$ enter. As the stress components refer to below introduced constant orthonormal coordinate system partial derivatives instead of covariant derivatives can be used. For the in-plane stresses holds with (8) and (9)

$$\begin{bmatrix} S^{11} \\ S^{22} \\ S^{12} \end{bmatrix} = \begin{bmatrix} C_{11} & C_{12} & 0 \\ C_{21} & C_{22} & 0 \\ 0 & 0 & C_{33} \end{bmatrix} \begin{bmatrix} \varepsilon_{11} + \xi^3 \kappa_{11} \\ \varepsilon_{22} + \xi^3 \kappa_{22} \\ 2\varepsilon_{12} + \xi^3 2\kappa_{12} \end{bmatrix}. \tag{22}$$

Introducing

$$\bar{\mathbf{C}}_{23} = \begin{bmatrix} C_{11} & C_{12} & 0 & 0 & 0 & C_{33} \\ 0 & 0 & C_{33} & C_{21} & C_{22} & 0 \end{bmatrix} \qquad \boldsymbol{\lambda}_\varepsilon = \begin{bmatrix} \varepsilon_{11,1} \\ \varepsilon_{22,1} \\ 2\varepsilon_{12,1} \\ \varepsilon_{11,2} \\ \varepsilon_{22,2} \\ 2\varepsilon_{12,2} \end{bmatrix} \qquad \boldsymbol{\lambda}_\kappa = \begin{bmatrix} \kappa_{11,1} \\ \kappa_{22,1} \\ 2\kappa_{12,1} \\ \kappa_{11,2} \\ \kappa_{22,2} \\ 2\kappa_{12,2} \end{bmatrix} \tag{23}$$

the derivatives of the in-plane stresses yield

$$\begin{bmatrix} S^{11}{}_{,1} + S^{12}{}_{,2} \\ S^{12}{}_{,1} + S^{22}{}_{,2} \end{bmatrix} = \begin{bmatrix} \bar{\mathbf{C}}_{23} & \xi^3 \bar{\mathbf{C}}_{23} \end{bmatrix} \begin{bmatrix} \boldsymbol{\lambda}_\varepsilon \\ \boldsymbol{\lambda}_\kappa \end{bmatrix} \tag{24}$$
$$\mathbf{f}_1 = \mathbf{C}_{23}\,\boldsymbol{\lambda}\,.$$

Furthermore we introduce

$$\boldsymbol{\sigma}_2 = -\int_{-h/2}^{+h/2} \boldsymbol{\Phi}^T \begin{bmatrix} S^{13}{}_{,3} \\ S^{23}{}_{,3} \end{bmatrix} \bar{\mu}\; \mathrm{d}\xi^3 \qquad\qquad \mathbf{D}_{23} := -\int_{-h/2}^{+h/2} \boldsymbol{\Phi}^T \mathbf{C}_{23}\, \bar{\mu}\; \mathrm{d}\xi^3\,, \tag{25}$$

where the reformulation of $(16)_3$ to $(25)_1$ is obtained with $\bar{\mu} = 1$ and integration by parts as well as consideration of stress boundary conditions $S^{\alpha 3}(-h/2) = S^{\alpha 3}(+h/2) = 0$. The integration for $\mathbf{D}_{23}$ is performed in an analogous way to Eq. (19).

Now the integral form of $\mathbf{f} = \mathbf{0}$ according to Eq. (21) is formulated with $\delta\tilde{\mathbf{u}} = \boldsymbol{\Phi}\,\delta\boldsymbol{\alpha}$. Considering (24) and (25) it follows

$$\int_{-h/2}^{+h/2} \delta\tilde{\mathbf{u}}^T \mathbf{f}\, \bar{\mu}\, \mathrm{d}\xi^3 = -\delta\boldsymbol{\alpha}^T (\boldsymbol{\sigma}_2 + \mathbf{D}_{23}\, \boldsymbol{\lambda}) = 0 \tag{26}$$

and one obtains with $\delta\boldsymbol{\alpha} \neq \mathbf{0}$

$$\boldsymbol{\sigma}_2 + \mathbf{D}_{23}\, \boldsymbol{\lambda} = \mathbf{0}\,. \tag{27}$$

This equation describes equilibrium of higher order stress resultants.

The warping displacements have to fulfill an orthogonality condition. To specify this constraint we introduce the equilibrium of virtual in-plane stresses considering (24)

$$\begin{bmatrix} \delta S^{11}{}_{,1} + \delta S^{12}{}_{,2} \\ \delta S^{12}{}_{,1} + \delta S^{22}{}_{,2} \end{bmatrix} = \mathbf{C}_{23}\, \delta\boldsymbol{\lambda} = \delta\mathbf{f}_1 = \mathbf{0}\,. \tag{28}$$

The integral form of $\delta\mathbf{f}_1 = \mathbf{0}$ yields with $\tilde{\mathbf{u}} = \boldsymbol{\Phi}\, \boldsymbol{\alpha}$

$$\int_{-h/2}^{+h/2} \delta\mathbf{f}_1^T \tilde{\mathbf{u}}\, \bar{\mu}\, \mathrm{d}\xi^3 = \delta\boldsymbol{\lambda}^T \int_{-h/2}^{+h/2} \mathbf{C}_{23}^T \boldsymbol{\Phi}\, \bar{\mu}\, \mathrm{d}\xi^3\, \boldsymbol{\alpha} = 0\,. \tag{29}$$

Introducing $\mathbf{D}_{32} = -\int_{-h/2}^{+h/2} \mathbf{C}_{23}^T\, \boldsymbol{\Phi}\, \bar{\mu}\, \mathrm{d}\xi^3 = \mathbf{D}_{23}^T$ Eq. (29) reads $-\delta\boldsymbol{\lambda}^T \mathbf{D}_{32}\, \boldsymbol{\alpha} = 0$, where $\delta\boldsymbol{\lambda} \neq \mathbf{0}$. Thus, the orthogonality condition reads

$$\mathbf{g}(\boldsymbol{\alpha}) = \mathbf{D}_{32}\, \boldsymbol{\alpha} = \mathbf{0}\,. \tag{30}$$

The constraint (30) enforces the correct shape of the warping displacements through the thickness and no additional membrane forces and bending moments are associated with $\tilde{\mathbf{u}}$.

2.4 Constrained Optimization Problem

We introduce the constrained optimization problem

$$\Pi(\boldsymbol{\theta}) = \int_{\Omega} [W(\boldsymbol{\varepsilon}, \boldsymbol{\alpha}) + \boldsymbol{\lambda}^T\, \mathbf{g}(\boldsymbol{\alpha})]\, \mathrm{d}A + \Pi_{ext}(\mathbf{u}) \quad \rightarrow \quad \text{stat.} \tag{31}$$

with independent quantities $\boldsymbol{\theta} := [\mathbf{v}, \boldsymbol{\alpha}, \boldsymbol{\lambda}]^T$. The strain energy density $W(\boldsymbol{\varepsilon}, \boldsymbol{\alpha})$ per area element $\mathrm{d}A$ is obtained with thickness integration of $W(\mathbf{E}) = \frac{1}{2} \int_{-h/2}^{+h/2} \mathbf{E}^T\, \mathbf{C}\, \mathbf{E}\, \bar{\mu}\, \mathrm{d}\xi^3$ and leads with $\mathbf{E} = \mathbf{A}_1\, \boldsymbol{\varepsilon} + \mathbf{A}_2\, \boldsymbol{\alpha}$ and $(18)_2$ to the quadratic form

$$W(\boldsymbol{\varepsilon}, \boldsymbol{\alpha}) = \frac{1}{2} \begin{bmatrix} \boldsymbol{\varepsilon} \\ \boldsymbol{\alpha} \end{bmatrix}^T \begin{bmatrix} \mathbf{D}_{11} & \mathbf{D}_{12} \\ \mathbf{D}_{21} & \mathbf{D}_{22} \end{bmatrix} \begin{bmatrix} \boldsymbol{\varepsilon} \\ \boldsymbol{\alpha} \end{bmatrix}. \tag{32}$$

In order to account for the constraint (30) the Lagrange term $\boldsymbol{\lambda}^T \mathbf{g}(\boldsymbol{\alpha})$ is incorporated in Eq. (31) with the vector of Lagrange multipliers $\boldsymbol{\lambda}$.

The shell is loaded statically by surface loads $\bar{\mathbf{p}}$ in Ω and by boundary forces $\bar{\mathbf{t}}$ on boundary Γ_σ. Hence, the potential of the external forces is expressed as

$$\Pi_{ext}(\mathbf{u}) = -\int_{\Omega} \mathbf{u}^T \bar{\mathbf{p}}\, \mathrm{d}A - \int_{\Gamma_\sigma} \mathbf{u}^T \bar{\mathbf{t}}\, \mathrm{d}s\,. \tag{33}$$

Furthermore, the area element of the reference surface is given with $\mathrm{d}A = |\mathbf{X}_{,1} \times \mathbf{X}_{,2}|\, \mathrm{d}\xi^1\, \mathrm{d}\xi^2$.

With admissible variations $\delta\boldsymbol{\theta} = [\delta\mathbf{v}, \delta\boldsymbol{\alpha}, \delta\boldsymbol{\lambda}]^T$ and $\delta\mathbf{v} = [\delta\mathbf{u}, \delta\boldsymbol{\varphi}]^T$ the stationary condition associated with functional (31) reads

$$\begin{aligned} \delta\Pi(\boldsymbol{\theta}, \delta\boldsymbol{\theta}) &= \int_{\Omega} \begin{bmatrix} \delta\boldsymbol{\varepsilon} \\ \delta\boldsymbol{\alpha} \\ \delta\boldsymbol{\lambda} \end{bmatrix}^T \begin{bmatrix} \mathbf{D}_{11} & \mathbf{D}_{12} & \mathbf{0} \\ \mathbf{D}_{21} & \mathbf{D}_{22} & \mathbf{D}_{23} \\ \mathbf{0} & \mathbf{D}_{32} & \mathbf{0} \end{bmatrix} \begin{bmatrix} \boldsymbol{\varepsilon} \\ \boldsymbol{\alpha} \\ \boldsymbol{\lambda} \end{bmatrix} \mathrm{d}A + \delta\Pi_{ext} = 0 \\ \delta\Pi_{ext} &= -\int_{\Omega} \delta\mathbf{u}^T \bar{\mathbf{p}}\, \mathrm{d}A - \int_{\Gamma_\sigma} \delta\mathbf{u}^T\, \bar{\mathbf{t}}\, \mathrm{d}s\,. \end{aligned} \tag{34}$$

The virtual shell strains $\delta\boldsymbol{\varepsilon} = [\delta\varepsilon_{11}, \delta\varepsilon_{22}, 2\delta\varepsilon_{12}, \delta\kappa_{11}, \delta\kappa_{22}, 2\delta\kappa_{12}, \delta\gamma_1, \delta\gamma_2]^T$ yield

$$\begin{aligned} \delta\varepsilon_{\alpha\beta} &= \frac{1}{2}(\delta\mathbf{u}_{,\alpha} \cdot \mathbf{X}_{,\beta} + \delta\mathbf{u}_{,\beta} \cdot \mathbf{X}_{,\alpha}) \\ \delta\kappa_{\alpha\beta} &= \frac{1}{2}(\delta\mathbf{u}_{,\alpha} \cdot \mathbf{N}_{,\beta} + \delta\mathbf{u}_{,\beta} \cdot \mathbf{N}_{,\alpha} + \delta\mathbf{d}_{,\alpha} \cdot \mathbf{X}_{,\beta} + \delta\mathbf{d}_{,\beta} \cdot \mathbf{X}_{,\alpha}) \\ \delta\gamma_\alpha &= \delta\mathbf{u}_{,\alpha} \cdot \mathbf{N} + \delta\mathbf{d} \cdot \mathbf{X}_{,\alpha}\,. \end{aligned} \tag{35}$$

Concerning the associated Euler-Lagrange equations we refer to Ref. [12]. One obtains the equilibrium of stress resultants and stress couple resultants, the constraint (30) and the equilibrium of higher order stress resultants (27) in Ω as well as static boundary conditions on Γ_σ.

2.5 *Representative Volume Element*

The evaluation of above defined matrices is carried out in RVEs which are located at the integration points of the mid-surface Ω, see Fig. 1. For linear elasticity the computation can be done in advance for one RVE only. An orthonormal coordinate system is introduced in the center of the square reference surface Ω_i with edge length ℓ. Investigations in [12] prove that in a wide range around $\ell = 100\,h$ the results are independent of ℓ.

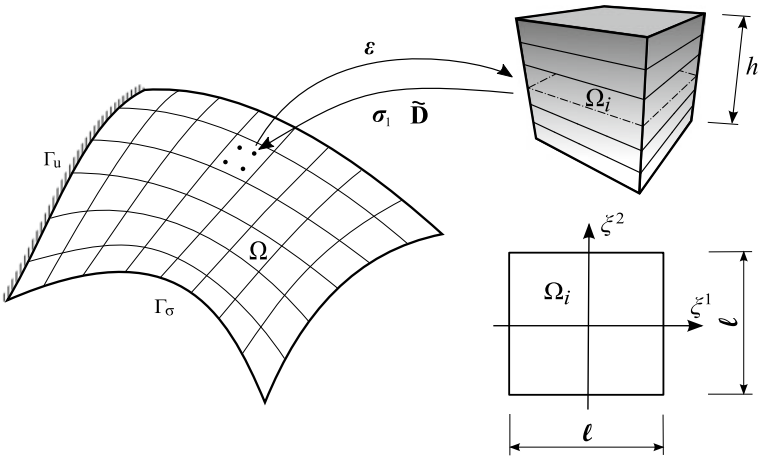

Fig. 1 RVE at an integration point of a shell and reference surface of the RVE

Normalized coordinates $-1 \le \xi \le 1$ and $-1 \le \eta \le 1$ are defined with $\xi = \frac{2}{\ell}\,\xi^1$ and $\eta = \frac{2}{\ell}\,\xi^2$, which yields a constant Jacobian matrix

$$\mathbf{J} = \begin{bmatrix} \frac{\partial \xi^1}{\partial \xi} & \frac{\partial \xi^2}{\partial \xi} \\ \frac{\partial \xi^1}{\partial \eta} & \frac{\partial \xi^2}{\partial \eta} \end{bmatrix} = \begin{bmatrix} \frac{\ell}{2} & 0 \\ 0 & \frac{\ell}{2} \end{bmatrix}. \tag{36}$$

The approximation for $\boldsymbol{\theta}^h := [\boldsymbol{\varepsilon}^h, \boldsymbol{\alpha}^h, \boldsymbol{\lambda}^h]^T$ in Ω_i is chosen as

$$\begin{bmatrix} \boldsymbol{\varepsilon}^h \\ \boldsymbol{\alpha}^h \\ \boldsymbol{\lambda}^h \end{bmatrix} = \begin{bmatrix} \mathbf{N}_\varepsilon^1 & \mathbf{N}_\varepsilon^2 & \mathbf{0} & \mathbf{0} & \mathbf{N}_\varepsilon^3 \\ \mathbf{0} & \mathbf{0} & \mathbf{0} & \mathbf{N}_\alpha & \mathbf{0} \\ \mathbf{0} & \mathbf{N}_\lambda^1 & \mathbf{N}_\lambda^2 & \mathbf{0} & \mathbf{N}_\lambda^3 \end{bmatrix} \begin{bmatrix} \hat{\boldsymbol{\varepsilon}} \\ \hat{\boldsymbol{\lambda}}_1 \\ \hat{\boldsymbol{\lambda}}_2 \\ \hat{\boldsymbol{\alpha}} \\ \hat{\boldsymbol{\lambda}}_3 \end{bmatrix} \qquad \boldsymbol{\theta}^h = \mathbf{N}_\theta\, \hat{\boldsymbol{\theta}}\,, \tag{37}$$

where $\hat{\boldsymbol{\varepsilon}} \in \mathbb{R}^8$, $\hat{\boldsymbol{\lambda}}_1 \in \mathbb{R}^6$, $\hat{\boldsymbol{\lambda}}_2 \in \mathbb{R}^4$, $\hat{\boldsymbol{\lambda}}_3 \in \mathbb{R}^8$ and $\hat{\boldsymbol{\alpha}} \in \mathbb{R}^M$. The interpolation matrices $\mathbf{N}_\varepsilon^1 = \mathbf{1}_8$, $\mathbf{N}_\varepsilon^2$ and $\mathbf{N}_\varepsilon^3$ are adapted from Ref. [10]

$$\begin{aligned} \mathbf{N}_\varepsilon^2 &= \begin{bmatrix} \mathbf{N}_\varepsilon^{m2} & \mathbf{0} & \mathbf{0} \\ \mathbf{0} & \mathbf{N}_\varepsilon^{b2} & \mathbf{0} \\ \mathbf{0} & \mathbf{0} & \mathbf{N}_\varepsilon^{s2} \end{bmatrix}_{8\times 6} \quad \mathbf{N}_\varepsilon^{m2} = \mathbf{N}_\varepsilon^{b2} = \begin{bmatrix} \eta & 0 \\ 0 & \xi \\ 0 & 0 \end{bmatrix} \qquad \mathbf{N}_\varepsilon^{s2} = \begin{bmatrix} \eta & 0 \\ 0 & \xi \end{bmatrix} \\ \mathbf{N}_\varepsilon^3 &= \begin{bmatrix} \mathbf{N}_\varepsilon^{m3} & \mathbf{0} \\ \mathbf{0} & \mathbf{N}_\varepsilon^{b3} \\ \mathbf{0} & \mathbf{0} \end{bmatrix}_{8\times 8} \quad \mathbf{N}_\varepsilon^{m3} = \mathbf{N}_\varepsilon^{b3} = \begin{bmatrix} \xi & 0 & 0 & 0 \\ 0 & \eta & 0 & 0 \\ 0 & 0 & \xi & \eta \end{bmatrix}. \end{aligned} \tag{38}$$

Due to the rectangular shape of Ω_i the coefficient matrices $\mathbf{T}_\varepsilon^0$, $(\mathbf{T}_\sigma^0)^{-1}$ and the quantities $\bar{\xi}$, $\bar{\eta}$, j_0/j, as are used in Ref. [10], can be discarded.

With $\mathbf{N}_\alpha = \mathbf{1}_M$ the warping displacements $\boldsymbol{\alpha}^h$ are constant in Ω_i. This also holds for the derivatives of membrane strains and curvatures $\boldsymbol{\lambda}^h = [\boldsymbol{\lambda}_\varepsilon^h, \boldsymbol{\lambda}_\kappa^h]^T$ with

$$\begin{aligned}
\mathbf{N}_\lambda^1 &= \begin{bmatrix} \mathbf{N}_\lambda^{11} & \mathbf{0} & \mathbf{0} \\ \mathbf{0} & \mathbf{N}_\lambda^{11} & \mathbf{0} \end{bmatrix} \qquad \mathbf{N}_\lambda^{11} = \frac{2}{\ell} \begin{bmatrix} 0 & 0 \\ 0 & 1 \\ 0 & 0 \\ 1 & 0 \\ 0 & 0 \\ 0 & 0 \end{bmatrix} \\
\mathbf{N}_\lambda^2 &= \begin{bmatrix} \mathbf{N}_\lambda^{21} & \mathbf{0} \\ \mathbf{0} & \mathbf{N}_\lambda^{21} \end{bmatrix} \qquad \mathbf{N}_\lambda^{21} = \begin{bmatrix} 1 & 0 \\ 1 & 0 \\ 0 & 1 \\ 0 & 1 \\ 0 & 1 \\ 1 & 0 \end{bmatrix} \\
\mathbf{N}_\lambda^3 &= \begin{bmatrix} \mathbf{N}_\lambda^{31} & \mathbf{0} \\ \mathbf{0} & \mathbf{N}_\lambda^{31} \end{bmatrix} \qquad \mathbf{N}_\lambda^{31} = \frac{2}{\ell} \begin{bmatrix} 1 & 0 & 0 & 0 \\ 0 & 0 & 0 & 0 \\ 0 & 0 & 1 & 0 \\ 0 & 0 & 0 & 0 \\ 0 & 1 & 0 & 0 \\ 0 & 0 & 0 & 1 \end{bmatrix}.
\end{aligned} \tag{39}$$

The components of $\mathbf{N}_\lambda^1$ and $\mathbf{N}_\lambda^3$ are obtained computing the derivatives of the membrane strains and curvatures in (37) with respect to ξ^α considering (36). When multiplying $\bar{\mathbf{C}}_{23}$ from (23) with $\mathbf{N}_\lambda^{21}$, one obtains a reduced form of $\bar{\mathbf{C}}_{23}$ as is used in [11] as approximation to avoid singular matrices. Here, $\mathbf{N}_\lambda^2\,\hat{\boldsymbol{\lambda}}_2$ describes an independent part of the interpolation.

We insert $\boldsymbol{\theta}^h = \mathbf{N}_\theta\,\hat{\boldsymbol{\theta}}$ according to Eq. (37) and the corresponding equation for the virtual quantities $\delta\boldsymbol{\theta}^h = \mathbf{N}_\theta\,\delta\hat{\boldsymbol{\theta}}$ in stationary condition (34), which now reads

$$\delta\Pi(\boldsymbol{\theta}^h, \delta\boldsymbol{\theta}^h) = \int_\Omega \frac{1}{\ell^2} \int_{\Omega_i} \delta\boldsymbol{\theta}^{hT}\,\mathbf{D}\,\boldsymbol{\theta}^h\,\mathrm{d}A_i\,\mathrm{d}A + \delta\Pi_{ext} = 0 \qquad \mathbf{D} = \begin{bmatrix} \mathbf{D}_{11} & \mathbf{D}_{12} & \mathbf{0} \\ \mathbf{D}_{21} & \mathbf{D}_{22} & \mathbf{D}_{23} \\ \mathbf{0} & \mathbf{D}_{32} & \mathbf{0} \end{bmatrix} \tag{40}$$

or

$$\delta\Pi(\boldsymbol{\theta}^h, \delta\boldsymbol{\theta}^h) = \int_\Omega \delta\hat{\boldsymbol{\theta}}^T\,\mathbf{H}\,\hat{\boldsymbol{\theta}}\,\mathrm{d}A + \delta\Pi_{ext} = 0 \qquad \mathbf{H} = \frac{1}{\ell^2} \int_{\Omega_i} \mathbf{N}_\theta^T\,\mathbf{D}\,\mathbf{N}_\theta\,\mathrm{d}A_i\,. \tag{41}$$

The constant and symmetric Matrix $\mathbf{D}$ is of order $J = 20 + M$. The integration for $\mathbf{H}_{K\times K}$, where $K = 26 + M$, can be carried out analytically. A 2×2 Gauss integration also leads to exact results. It is important to note, that although $\mathbf{D}$ is singular, $\mathbf{H}$ is regular.

The parameters $\hat{\boldsymbol{\beta}} := [\hat{\boldsymbol{\lambda}}_1, \hat{\boldsymbol{\lambda}}_2, \hat{\boldsymbol{\alpha}}, \hat{\boldsymbol{\lambda}}_3]^T$ in $\hat{\boldsymbol{\theta}} = [\hat{\boldsymbol{\varepsilon}}, \hat{\boldsymbol{\beta}}]^T$ are independent quantities in the RVEs, and thus are not continuous in Ω. Furthermore $\delta\Pi_{ext}$ does not depend on $\hat{\boldsymbol{\beta}}$. For this reason elimination of $\hat{\boldsymbol{\beta}}$ from the set of equations

$$\begin{bmatrix} \mathbf{H}_{11} & \mathbf{H}_{12} \\ \mathbf{H}_{21} & \mathbf{H}_{22} \end{bmatrix} \begin{bmatrix} \hat{\boldsymbol{\varepsilon}} \\ \hat{\boldsymbol{\beta}} \end{bmatrix} = \begin{bmatrix} \boldsymbol{\sigma}_1 \\ \mathbf{0} \end{bmatrix} \tag{42}$$

is possible. Here, $\mathbf{H}_{\alpha\beta}$ are submatrices of $\mathbf{H}$, where $\mathbf{H}_{11} = \mathbf{D}_{11}$. The right hand side of Eq. (42) contains the vector of stress resultants, since the lateral surfaces of the RVEs are not stress free. Static condensation yields $\hat{\boldsymbol{\beta}} = -\mathbf{H}_{22}^{-1}\,\mathbf{H}_{21}\,\hat{\boldsymbol{\varepsilon}}$ and the material law for the stress resultants

$$\boldsymbol{\sigma}_1 = \tilde{\mathbf{D}}\,\hat{\boldsymbol{\varepsilon}} \qquad \tilde{\mathbf{D}} = \mathbf{H}_{11} - \mathbf{H}_{12}\,\mathbf{H}_{22}^{-1}\,\mathbf{H}_{21}\,. \tag{43}$$

Due to the interpolation with layer-wise shape functions $\mathbf{H}_{22}$ is sparse, which means a comparatively limited effort for the static condensation.

The condensed matrix $\tilde{\mathbf{D}}_{8\times 8}$ possesses the same structure as $\mathbf{D}_{11}$, see Eq. (20).

$$\tilde{\mathbf{D}} = \begin{bmatrix} \tilde{\mathbf{D}}_m & \tilde{\mathbf{D}}_{mb} & \mathbf{0} \\ \tilde{\mathbf{D}}_{mb}^T & \tilde{\mathbf{D}}_b & \mathbf{0} \\ \mathbf{0} & \mathbf{0} & \tilde{\mathbf{D}}_s \end{bmatrix} \qquad \begin{matrix} \tilde{\mathbf{D}}_m = \mathbf{D}_m \\ \tilde{\mathbf{D}}_b = \mathbf{D}_b \\ \tilde{\mathbf{D}}_{mb} = \mathbf{D}_{mb} \end{matrix} \qquad \tilde{\mathbf{D}}_s = \tilde{D}_s\,\mathbf{1}_2 \tag{44}$$

Only the submatrix $\mathbf{D}_s = D_s\,\mathbf{1}_2$ is affected by the static condensation. In this context a shear correction factor is defined as normalized shear stiffness

$$k = \frac{\tilde{D}_s}{D_s}\,. \tag{45}$$

The notion of a shear correction factor was first introduced by Timoshenko [25]. For a homogeneous shell one obtains the well-known value $k = 5/6$, as is given in [2, 22]. The computations show, that k is independent of the total thickness h. This means that $\tilde{\mathbf{D}}$ can be computed only from $\mathbf{D}_{11}$ and k for shells with variable thickness.

Identifying the parameters $\hat{\boldsymbol{\varepsilon}}$ in the RVEs with the shell strains $\boldsymbol{\varepsilon}$ according to (5), variational equation (41) yields with static condensation (43)

$$\delta\Pi(\boldsymbol{\varepsilon}, \delta\boldsymbol{\varepsilon}) = \int_\Omega \delta\boldsymbol{\varepsilon}^T\,\tilde{\mathbf{D}}\,\boldsymbol{\varepsilon}\,\mathrm{d}A + \delta\Pi_{ext} = 0\,. \tag{46}$$

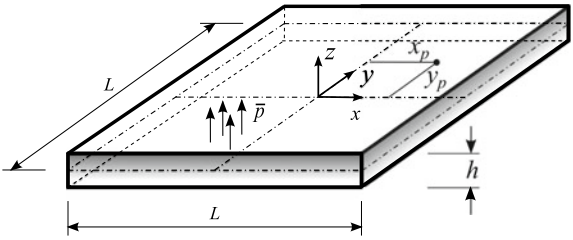

Fig. 2 Simply supported square plate under uniform load

Equation (46) represents the principle of virtual work as variational basis for geometrical linear shell elements based on the displacement method. The displacement boundary conditions $\mathbf{u} = \bar{\mathbf{u}}$ on Γ_u have to be fulfilled as constraints.

Concerning a finite element formulation for quadrilaterals we refer to Ref. [10]. The elements possess 5 or 6 degrees of freedom (dofs) at the nodes. At nodes on intersections 6 dofs (3 global displacements and 3 global rotations) and at the remaining nodes 5 dofs (3 global displacements and 2 local rotations) are present. The evaluation of the stresses at any point of the shell is performed via material law (9) along with the layer strains (8). This requires knowledge of the vector $\boldsymbol{\alpha}$ and thus a back substitution of the parameters $\hat{\boldsymbol{\beta}}$. For this purpose the necessary submatrices of $\mathbf{H}$ have to be stored.

3 Examples

The derived shell model together with the FGM materials are implemented in an extended version of the general finite element program FEAP [24]. Two plate examples and one shell example are presented to show the efficiency and quality of the derived theory.

3.1 Simply Supported Square Plate Under Uniform Load

The behavior of a simply supported square plate with uniform load, see Fig. 2, is studied as first example.

The geometrical data are the length $L_x = L_y = L = 1000$ mm and different thicknesses $h = 10/20/40/100$ mm. Thus plates with aspect ratios of $L/h = 100/50/25/10$ are analyzed along with an uniform load $\bar{p} = 1\ \text{N/mm}^2$. The material parameters for SiC-AL FGM material are chosen as follows

$$\begin{aligned} E_1 = E_c &= 380000\ \text{N/mm}^2 \quad \nu_1 = \nu_c = 0.3 \\ E_2 = E_m &= 70000\ \ \text{N/mm}^2 \quad \nu_2 = \nu_m = 0.3\,. \end{aligned} \tag{47}$$

Table 1 Center displacement

FE-Mesh	$w_c(3D)$ (mm)	$w_c(2D)$ (mm)
4×4	45.49	45.56
8×8	45.78	45.78
16×16	46.04	46.04
32×32	46.24	46.25
64×64	46.34	46.34
128×128	46.37	46.37

Table 2 Shear correction factors k for different values of p

p	k
0	0.833333
1	0.830398
2	0.769281
4	0.690095
6	0.674322
8	0.679216
10	0.689889
20	0.741394

The p-volume fraction model, see Eq. (11), is used with p=1,2,6,10. An application of other fraction models does not change the results significantly. The boundary conditions are set as follows: $u_z(\pm L/2, y) = u_z(x, \pm L/2) = 0$. Furthermore statically determined in-plane boundary conditions are chosen via $u_x(-L/2, -L/2) = u_y(-L/2, -L/2) = u_y(L/2, -L/2) = 0$. This is substituted in case of symmetry by $u_x(0, y) = \varphi_y(0, y) = 0$ and $u_y(x, 0) = \varphi_x(x, 0) = 0$. Results of the present formulation are compared to 3D-results obtained with the solid shell element [14].

3.1.1 Center Displacement, Shear Correction Factors and Bending Stresses

The center displacement is evaluated for $h = 20$ mm (L/h=50) and $p = 6$. Different FE-meshes are chosen for one quarter of the plate, taken symmetry into account. 16 elements are used in thickness direction for the 3D-case, whereas 8 layers are used in the 2D-case. The results in Table 1 show excellent agreement for all discretizations.

Next we compute shear correction factors. They are not used in the present formulation, but are available as a by-product, see Eq. (45). The FE-mesh has 32×32 elements in-plane and 8 layers for one quarter of the plate, taken symmetry into account. Results for different values of p are presented in Table 2.

The results for bending stresses of the present formulation are compared to 3D-results. Again $h = 20$ mm ($L/h = 50$), $p = 6$ and 8 layers are chosen. In the

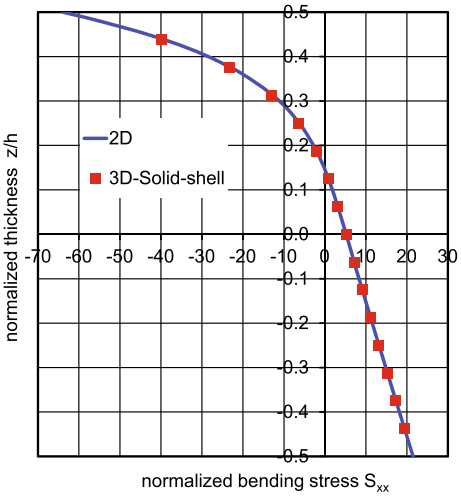

Fig. 3 Bending stresses S_{xx} at (0, 0)

2D-case a center of a shell element and in the 3D-case a node of a solid shell element is used for the examination. Thus, a 65 × 65 2D-mesh and a 64 × 64 3D-mesh for the full system are used. The results in Fig. 3 for the normalized bending stresses $S_{xx} = \frac{S^{11}}{\bar{p}}(\frac{h}{L_x})^2 100$ show excellent agreement.

3.1.2 Shear Stresses

Here, the results for shear stresses of the present formulation are compared to 3D-results. In detail shear stresses are calculated at position $x_p = 9/21L$, $y_p = 0$. Thus, the finite element discretization is chosen to a 35 × 35 2D-mesh and a 42 × 42 3D-mesh for the full system; symmetry is not taken into account. These discretizations are used in the following. Normalized shear stresses $S_{xz} = \frac{|S^{13}|}{\bar{p}}(\frac{h}{L_x})^2 1000$ are presented through the plate thickness with respect to normalized thickness values z/h.

Before going into details we discuss three additional aspects. At first a convergence study on the necessary number of numerical layers N in thickness direction is presented. Again $h = 20$ mm $(L/h = 50)$, $p = 6$ are chosen. Figure 4 shows results for N=2,4,6,8. It can be seen clearly that for N = 2 no stress continuity is found at the layer border at $z/h = 0$ and the top of the plate. Results for N=4 leads only to small differences at borders, whereas the discontinuities are neglectable for N>4. In the following all calculations were done with N=8.

Secondly we investigate the influence of the warping displacements on the results for shear stresses S_{xz}. Again $h = 20$ mm $(L/h = 50)$, $p = 6$ are chosen. Figure 5 demonstrate the large errors neglecting this in case of a pure Reissner-Mindlin (RM) formulation.

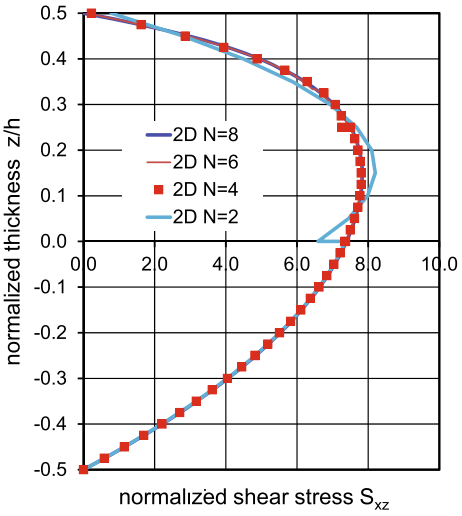

Fig. 4 Shear stresses S_{xz} at $(9/21L, 0)$ for different number of layers N

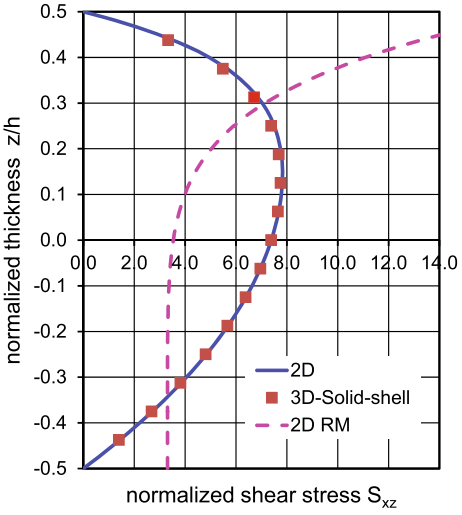

Fig. 5 Shear stresses S_{xz} at $(9/21L, 0)$ for different theories

Finally, the influence of boundary conditions on the results for shear stresses S_{xz} is demonstrated. Compared are results based on the boundary conditions described above with more restrictive conditions. In addition boundary conditions are set (in the sense of a hard support) as follows: $u_y(\pm L/2, y) = u_x(x, \pm L/2) = 0$ and $\varphi_x(\pm L/2, y) = \varphi_y(x, \pm L/2) = 0$. $h = 100$ mm $(L/h = 10)$, $p = 6$ are chosen. Figure 6 depicts the differences with respect to the boundary conditions in case of moderately thick plates. Similar differences occur for other values like displacements and bending stresses.

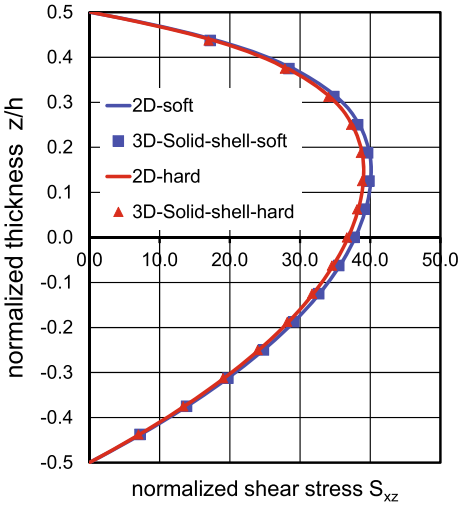

Fig. 6 Shear stresses S_{xz} at $(9/21L, 0)$ for different boundary conditions

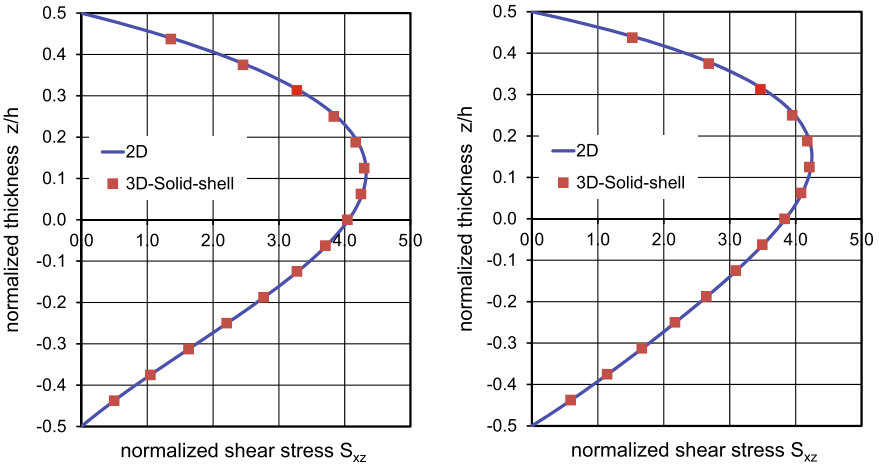

Fig. 7 Shear stresses S_{xz} at $(9/21L, 0)$ for $h = 10$ mm and $p = 1, 2$

3.1.3 Shear Stresses for Different L/h and p-Values

In this section we compare results of the present formulation with a 3D solution as described above. We choose thicknesses $h = 10/20/40/100$ mm with aspect ratios $L/h = 100/50/25/10$ and as example power-law functions $p = 1, 2, 4, 6, 10$. As a result it can be noticed that for all thickness values and for all values of p an excellent agreement between the 2D and 3D solution can be observed. Thus, only selected results for shear stresses are presented. Figures 7, 8 and 9, 10 depict solutions

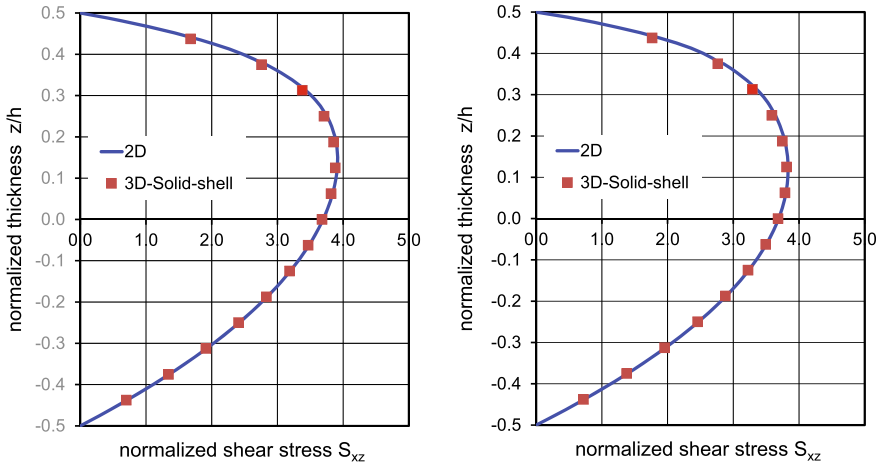

Fig. 8 Shear stresses S_{xz} at $(9/21L, 0)$ for $h = 10$ mm and $p = 6, 10$

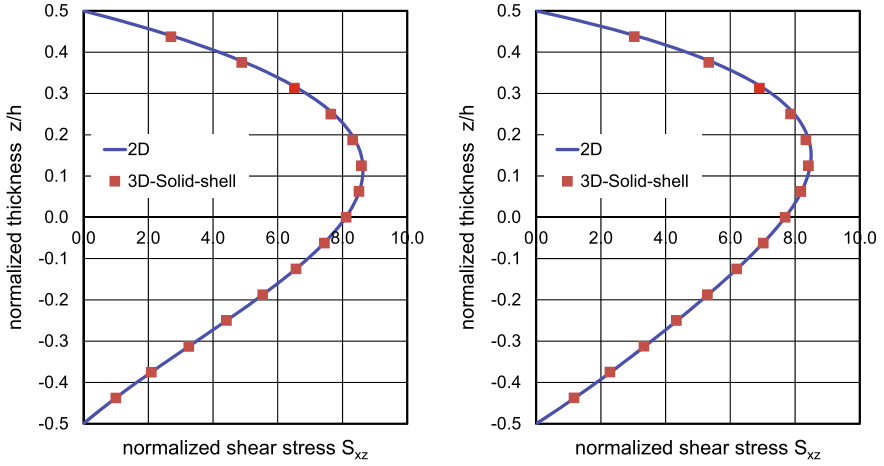

Fig. 9 Shear stresses S_{xz} at $(9/21L, 0)$ for $h = 20$ mm and $p = 1, 2$

for a thin plate, whereas Figs. 11 and 12 show stress curves for a moderately thick plate.

Finally, we present shear stresses for thickness $h = 10$ mm and power-law parameters $p = 1, 2, 4, 6, 10$ in Fig. 13. The influence of p on the distribution of S_{xz} can be seen clearly.

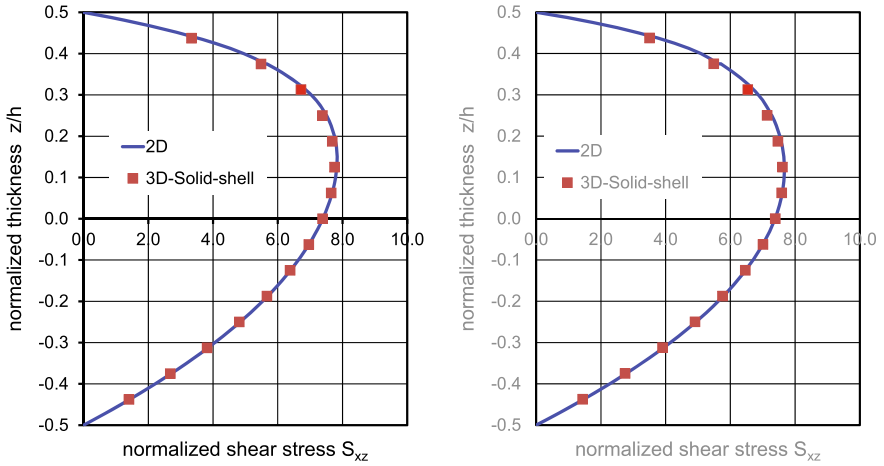

Fig. 10 Shear stresses S_{xz} at $(9/21L, 0)$ for $h = 20$ mm and $p = 6, 10$

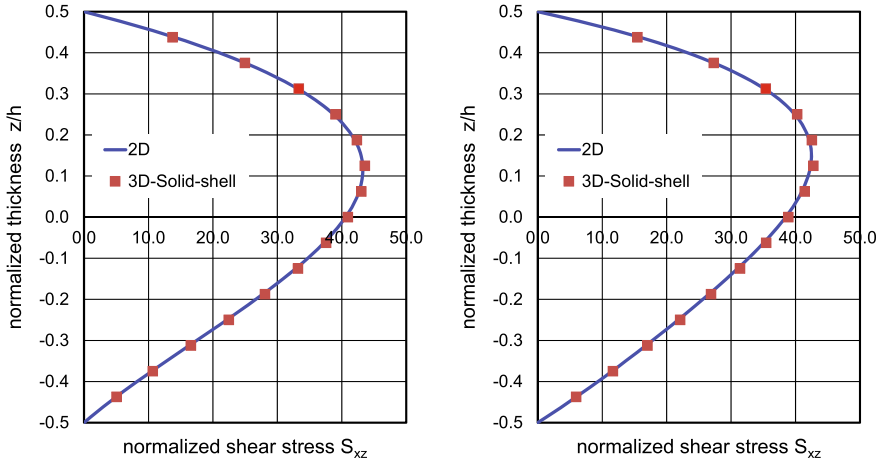

Fig. 11 Shear stresses S_{xz} at $(9/21L, 0)$ for $h = 100$ mm and $p = 1, 2$

3.2 *Simply Supported Square Sandwich Plate Under Uniform Load*

Consider a sandwich plate composed of three layers as shown in Fig. 14. Geometry, loading, boundary conditions and FE-discretizations are chosen according to the first example. In detail a thickness of $h = 100$ mm and a value $p = 6$ are chosen. Two FGM face sheets ($h_f = h/3$) are made from a mixture of a metal and a ceramic, while a core ($h_c = h/3$) is made of an isotropic homogeneous material. We apply N = 4 numerical layers(2D) and 6 elements(3D) within the FE-discretization for

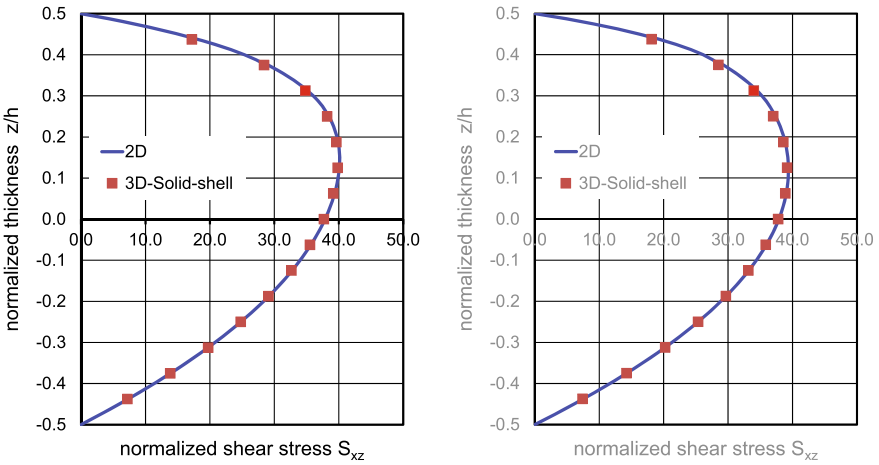

Fig. 12 Shear stresses S_{xz} at $(9/21L, 0)$ for $h = 100$ mm and $p = 6, 10$

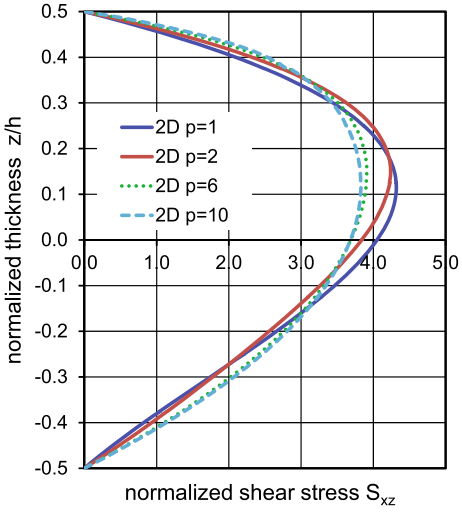

Fig. 13 Shear stresses S_{xz} at $(9/21L, 0)$ for $h = 10$ mm and $p = 1, 2, 4, 6, 10$

face sheet and core. Material data for metal and ceramic are according to the first example. We investigate the cases CMMC with a metallic core and MCCM with a ceramic core. The material properties are assumed to vary continuously through the plate thickness by a power-law distribution as $E(z) = E_m + (E_c - E_m)V(z)$, where V is the volume fraction of the ceramic part, see Table 3. A graphical interpretation is presented in Fig. 15. Figure 16 depicts solutions for normalized shear stresses in the cases CMMC with a metallic core and MCCM with a ceramic core. Again excellent agreement with the 3D-solution can be observed.

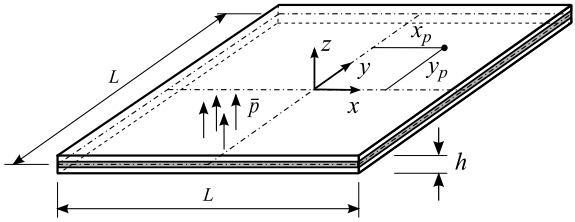

Fig. 14 Sandwich plate

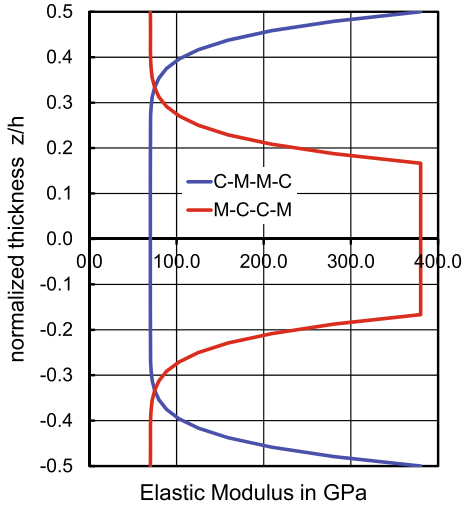

Fig. 15 Thickness distribution of elastic modulus in GPa for sandwich plate

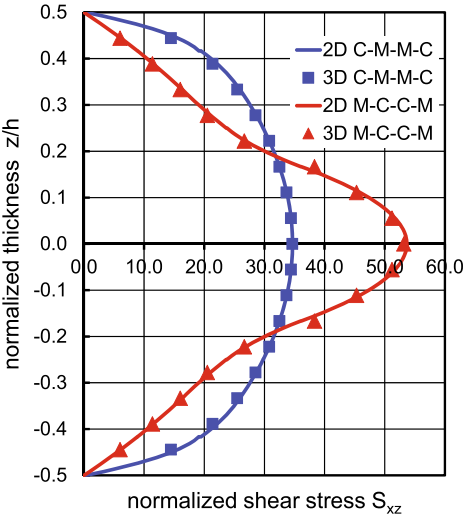

Fig. 16 Shear stresses S_{xz} at $(9/21L, 0)$ for 2 configurations

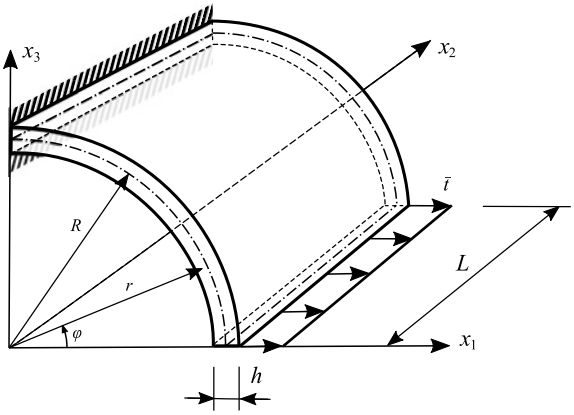

Fig. 17 Bending of a clamped circular shell

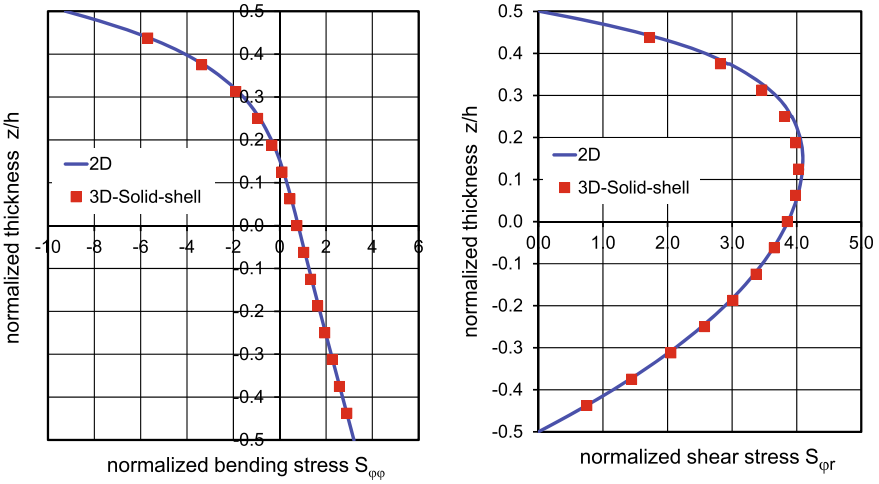

Fig. 18 Stresses $\sigma_{\varphi\varphi}$ and $\sigma_{\varphi r}$ in a circular shell at $\varphi = \pi/4$

Table 3 Chosen volume fraction of the ceramic part for CMMC and MCCM cases

$V(z)$	CMMC	MCCM	Domain
$V_b(z)$	$(-0.5-3\frac{z}{h})^p$	$(1.5+3\frac{z}{h})^p$	$z \in [-h/2, -h/6]$
$V_m(z)$	0	1	$z \in [-h/6,\ h/6]$
$V_t(z)$	$(-0.5+3\frac{z}{h})^p$	$(1.5-3\frac{z}{h})^p$	$z \in [\ h/6,\ h/2]$

3.3 Clamped Circular Shell

In Fig. 17 a clamped circular shell is depicted. The curved boundaries at $x_2 = 0$ and $x_2 = L$ are free of stresses. At the boundary $x_1 = R$ a constant load $\bar{t} = 100$ N/mm is applied. The geometrical data are defined by $R = 1000$ mm , $h = 40$ mm , $L = 1000$ mm . The material parameters for SiC-AL FGM material are chosen according to the first example. The problem is computed using the developed element formulations and a mesh of 41 elements in circumferential direction. In thickness direction again 8 layers are used. The p-volume fraction model, see Eq. (11) is used with p = 1, 2, 6. The solutions for the normalized bending stresses $S_{\varphi\varphi} = \frac{S^{11}}{\bar{t}}(\frac{h}{R})^2 1000$ and the normalized shear stresses $S_{\varphi r} = \frac{S^{13}}{\bar{t}}(\frac{h}{R})^2 10^5$ at an angle $\varphi = \pi/4$ are plotted as function of the coordinate $z = r - R$. The results of the present formulation in Fig. 18 are again compared to a 3D-solution (40×16) [14] and show very good agreement.

4 Conclusions

The kinematics of shells is extended as warping displacements are superposed on the displacement field of the Reissner–Mindlin theory. Power-law functions describe the elastic constants as function of the thickness coordinate. The investigations show that only a small number of numerical layers ($N \approx 5 - 8$) have to be used to obtain converged results for the shape of the displacements and transverse shear stresses in thickness direction. In all computed examples the parameters associated with $\mathbf{N}_{\varepsilon}^{s2}$ are zero, such that this matrix and the associated parameters could be taken out. Furthermore, matrix $\mathbf{N}_{\lambda}^{1}$ has negligible influence on the results, see Eqs. (37) and (39). Present formulation can easily be implemented in a shell element based on the Reissner-Mindlin theory.

References

1. Altenbach, H., Eremeyev, V.A.: Direct approach-based analysis of plates composed of functionally graded materials. Arch. Appl. Mech. **78**, 775–794 (2008)
2. Bach, C., Baumann, R.: Elastizität und Festigkeit, 9th edn. Springer, Berlin (1924)
3. Bao, G., Wang, L.: Multiple cracking in functionally graded ceramic/metal coatings. Int. J. Solids Struct. **32**, 2853–2871 (1995)
4. Carrera, E., Brischetto, S., Robaldo, A.: Variable kinematic model for the analysis of functionally graded material plates. AIAA J. **46**(1), 194–203 (2008)
5. Chung, Y.L., Chi, S.H.: The residual stress of functionally graded materials. J. Chin. Inst. Civil Hydraul. Eng. **13**, 1–9 (2001)
6. Chi, S.H., Chung, Y.L.: Cracking in coating-substrate composites of multi-layered and sigmoid FGM coatings. Eng. Fract. Mech. **70**, 1227–1243 (2003)

7. Chi, S.-H., Chung, Y.-L.: Mechanical behavior of functionally graded material plates under transverse load—Part I: analysis. Int. J. Solids Struct. **43**, 3657–3674 (2006)
8. Chi, S.-H., Chung, Y.-L.: Mechanical behavior of functionally graded material plates under transverse load—Part II: Numerical results. Int. J. Solids Struct. **43**, 3675–3691 (2006)
9. Delale, F., Erdogan, F.: The crack problem for a nonhomogeneous plane. ASME J. Appl. Mech. **50**, 609–614 (1983)
10. Gruttmann, F., Wagner, W.: Structural analysis of composite laminates using a mixed hybrid shell element. Comput. Mech. **37**, 479–497 (2006)
11. Gruttmann, F., Wagner, W., Knust, G.: A coupled global-local shell model with continuous interlaminar shear stresses. Comput. Mech. **57**, 237–255 (2016)
12. Gruttmann, F., Wagner, W.: Shear correction factors for layered plates and shells. Comput. Mech. **59**(1), 129–146 (2017)
13. Gu, P., Asaro, R.J.: Crack deflection in functionally graded materials. Int. J. Solids Struct. **34**, 3085–3098 (1997)
14. Klinkel, S., Gruttmann, F., Wagner, W.: A continuum based 3D-shell element for laminated structures. Comput. Struct. **71**, 43–62 (1999)
15. Kulikov, G.M., Plotnikova, S.V.: A sampling surfaces method and its implementation for 3D thermal stress analysis of functionally graded plates. Compos. Struct. **120**, 315–325 (2015)
16. Kwon, P., Crimp, M.: Automating the design process and powder processing of functionally gradient materials. In: Srivatsan, T.S., et al. (Eds.) Composites and Functionally Graded Materials, vol. 80, pp. 73–88 (1997)
17. Nguyen, T.K., Sab, K., Bonnet, G.: First-order shear deformation plate models for functionally graded materials. Compos. Struct. **83**, 25–36 (2008)
18. Nguyen, T.N., Ngo, T.D., Nguyen-Xuan, H.: A novel three-variable shear deformation plate formulation: theory and Isogeometric implementation. Comput. Methods Appl. Mech. Engrg. **326**, 376–401 (2017)
19. Niino, A., Maeda, S.: Recent development status of functionally gradient materials. ISIJ Int. **30**, 699–703 (1990)
20. Nogata, F.: Learning about design concepts from natural functionally graded materials. In: Srivatsan, T.S., et al. (Eds.) Composites and Functionally Graded Materials, vol. 80, pp. 11–18 (1997)
21. Reddy, J.N.: Analysis of functionally graded plates. Int. J. Numer Meth. Engng. **47**, 663–684 (2000)
22. Reissner, E.: On bending of elastic plates. Quart. Appl. Math. **5**, 55–68 (1947)
23. Thai, H.T., Kim, S.-E.: A review of theories for the modeling and analysis of functionally graded plates and shells. Compos. Struct. **128**, 70–86 (2015)
24. Taylor, R.L.: FEAP. http://www.ce.berkeley.edu/projects/feap/ (2019)
25. Timoshenko, S.P.: On the correction for shear of the differential equation for transverse vibrations of prismatic bars. Phil. Mag. Ser. **6**, 41:245, 744–746 (1921)
26. Yung, Y.Y., Munz, D.: Stress analysis in a two materials joint with a functionally graded material. In: Shiota, T., Miyamoto, M.Y. (Eds.) Functionally Graded Material, pp. 41–46 (1996)

On Performance of Nine-Node Quadrilateral Shell Elements 9-EAS11 and MITC9i

K. Wiśniewski and E. Turska

Abstract The chapter concerns nine-node quadrilateral shell elements derived for the Reissner-Mindlin kinematics and Green strain. They are based on the potential energy functional extended to include drilling rotations. A standard element of this class suffers from locking and over-stiffening; several special techniques are needed to improve its performance. We developed three nine-node shell elements with the membrane strains enhanced by the EAS11 representation of Bischoff and Ramm (Int. J. Num. Meth. Eng. 40:4427–4449, 1997 [2]). The transverse shear strains are treated either by the ANS method of Jang and Pinsky (Int. J. Num. Meth. Eng. 24:2389–2411, 1987 [6]), or are enhanced by the EAS6 representation of Sansour and Kollmann (Comput. Mech. 24:435–447, 2000 [17]), or remain unmodified. We also modify the EAS transformation rule, extending the idea put forward in Park and Lee (Comput. Mech. 15:473–484, 1995 [15]) for curved shells. Several numerical examples provide comparison of three 9-EAS11 elements to our MITC9i shell element of Wisniewski and Turska (Comput. Mech. 62, 499–523, 2018 [20]).

1 Introduction

The chapter concerns nine-node quadrilateral shell elements derived for the Reissner-Mindlin kinematics and Green strain. They are based on the potential energy functional extended to include the drilling rotation. The standard element of this class suffers from locking and over-stiffening, and several special techniques are needed to improve its performance. Our best MITC9i shell element described in [20] is based on the method of *improved two-level approximations* of covariant strains (MITCi),

K. Wiśniewski (✉)
Institute of Fundamental Technological Research, Polish Academy of Sciences, Warsaw, Poland
e-mail: kwisn@ippt.pan.pl

E. Turska
Polish Japanese Academy of Information Technology, Warsaw, Poland
e-mail: eturska@pjwstk.edu.pl

H. Altenbach et al. (eds.), *Recent Developments in the Theory of Shells*,
Advanced Structured Materials 110, https://doi.org/10.1007/978-3-030-17747-8_35

and was gradually developed in [13, 14, 21]. The other important features of this element are as follows:

1. To reduce shape distortion effects, the so-called Corrected Shape Functions (CSF) of [3] are extended to shells and used instead of the standard ones. In effect, all patch tests are also passed for shifts of the midside nodes along straight element sides and for arbitrary shifts of the central node.
2. Several extensions of the CSF are proposed to enable computations of non-flat shells. In particular, a criterion is put forward to determine the shift parameters associated with the central node for non-flat elements. Additionally, a method is presented to construct a parabolic side for a shifted midside node, which improves accuracy for symmetric curved edges.
3. Drilling rotations are included by using the drilling Rotation Constraint equation, in a way consistent with the additive/multiplicative rotation update scheme for large rotations. It is shown that the CSF reduce the sensitivity of a solution to the regularization parameter γ of the penalty method for this constraint.

In the current chapter, we compare the MITC9i shell element to the nine-node shell elements with the membrane strains enhanced by the EAS11 representation of [2]. The transverse shear strains are treated either by the ANS method of [6], or are enhanced by the EAS6 representation of [17], or remain unmodified. We also modify the EAS transformation rule extending the idea put forward in [15]. Several numerical examples provide comparison of three 9-EAS11 elements to our MITC9i shell element.

2 Basic Shell Equations with Drilling Rotation

Two-field functional In the present work, we use a two-field extended shell functional depending on displacements and three-parameter rotations,

$$F_2(\boldsymbol{\chi}, \mathbf{Q}_0) \doteq \int_B \mathscr{W}(\mathbf{C})\, \mathrm{d}V + F_{\text{ext}} + F_{\text{drill}}(\boldsymbol{\chi}, \mathbf{Q}_0), \tag{1}$$

where $\boldsymbol{\chi}$ is the deformation function and $\mathbf{Q}_0 \in SO(3)$ is the rotation tensor. The strain energy density $\mathscr{W}$ depends on the right Cauchy-Green deformation tensor $\mathbf{C} \doteq \mathbf{F}^T\mathbf{F}$, where $\mathbf{F} \doteq \nabla\boldsymbol{\chi}$ is the deformation gradient. F_{ext} is the potential of external loads. The last component in Eq. (1) is added to incorporate the drilling rotation using the penalty method,

$$F_{\text{drill}} \doteq \frac{1}{2}\int_M \gamma\, c^2\, \mathrm{d}A, \qquad c \doteq \frac{1}{2}\left[(\mathbf{F}_0\mathbf{t}_2)\cdot(\mathbf{Q}_0\mathbf{t}_1) - (\mathbf{F}_0\mathbf{t}_1)\cdot(\mathbf{Q}_0\mathbf{t}_2)\right], \tag{2}$$

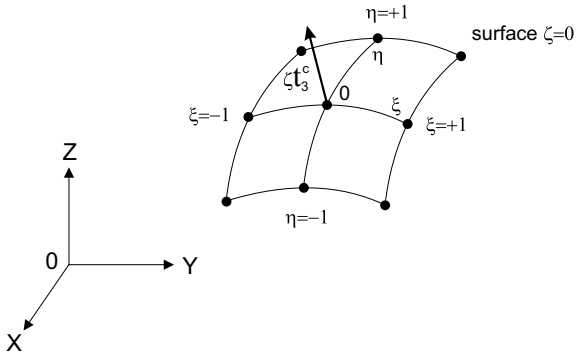

Fig. 1 The reference surface ($\zeta = 0$) of nine-node shell element

where c is the l.h.s. of the (1, 2) component of the Rotation Constraint (RC) equation, $\text{skew}(\mathbf{Q}_0^T \mathbf{F}_0) = \mathbf{0}$, and $\gamma \in (0, \infty)$ is the regularization parameter; the importance of this constraint was already noticed in [1] though it was used for a different purpose. Note that $\mathbf{F}_0$ and $\mathbf{Q}_0$ are associated with the reference (middle) shell surface for the initial configuration, and $\mathbf{t}_1$ and $\mathbf{t}_2$ are the tangent vectors of the local Cartesian basis on this surface.

Reissner-Mindlin kinematics The initial configuration of the shell is parameterized by the natural coordinates $\xi, \eta \in [-1, +1]$ on the reference (middle) surface, and the normal coordinate $\zeta \in [-h/2, +h/2]$, where h is the initial shell thickness, see Fig. 1. For the deformed configuration, we use the Reissner-Mindlin kinematical assumptions,

$$\mathbf{x}(\xi, \eta, \zeta) = \mathbf{x}_0(\xi, \eta) + \zeta\, \mathbf{Q}_0(\xi, \eta)\, \mathbf{t}_3(\xi, \eta), \tag{3}$$

where $\mathbf{x}$ is a position vector at an arbitrary ζ and $\mathbf{x}_0$ at $\zeta = 0$. Besides, $\mathbf{t}_3$ is the unit normal vector in the initial configuration. The rotation tensor $\mathbf{Q}_0$ is parameterized by the canonical rotation vector $\boldsymbol{\psi}$,

$$\mathbf{Q}_0(\boldsymbol{\psi}) \doteq \mathbf{I} + \frac{\sin\omega}{\omega}\tilde{\boldsymbol{\psi}} + \frac{1 - \cos\omega}{\omega^2}\tilde{\boldsymbol{\psi}}^2, \tag{4}$$

where $\omega = \|\boldsymbol{\psi}\| = \sqrt{\boldsymbol{\psi} \cdot \boldsymbol{\psi}} \geq 0$ and $\tilde{\boldsymbol{\psi}} \doteq \boldsymbol{\psi} \times \mathbf{I}$. This parametrization is used within the load step, and is a part of the rotation update scheme based on quaternions, to handle unrestricted rotations.

The deformation function $\boldsymbol{\chi} : \mathbf{x} = \boldsymbol{\chi}(\mathbf{X})$ maps the initial (non-deformed) configuration of a shell onto the current (deformed) one. Let us write the deformation gradient as follows:

$$\mathbf{F} \doteq \frac{\partial \mathbf{x}}{\partial \mathbf{X}} = \frac{\partial \mathbf{x}}{\partial \boldsymbol{\xi}}\, \mathbf{J}^{-1}, \tag{5}$$

where $\boldsymbol{\xi} \doteq \{\xi, \eta, \zeta\}$ and the Jacobian matrix $\mathbf{J} \doteq \partial \mathbf{X}/\partial \boldsymbol{\xi}$. The right Cauchy-Green deformation tensor is $\mathbf{C} \doteq \mathbf{F}^T\mathbf{F}$ and the Green strain is defined as $\mathbf{E} \doteq \frac{1}{2}(\mathbf{C} - \mathbf{C}_0)$, where $\mathbf{C}_0 \doteq \mathbf{C}|_{\mathbf{x}=\mathbf{X}} = \mathbf{I}$. The Green strain can be linearized in ζ,

$$\mathbf{E}(\zeta) \approx \mathbf{E}_0 + \zeta \mathbf{E}_1, \tag{6}$$

where the *0th order* strain $\mathbf{E}_0$ includes the membrane components $\boldsymbol{\varepsilon}$ and the transverse shear components $\boldsymbol{\gamma}/2$ while the *1st order* strain $\mathbf{E}_1$ includes the bending/twisting components $\boldsymbol{\kappa}$. The transverse shear part of $\mathbf{E}_1$ is typically neglected, i.e. $\kappa_{\alpha 3} \approx 0$ ($\alpha = 1, 2$). By Eq. (3), the normal strains ε_{33} and κ_{33} are equal to zero and must be either recovered from an auxiliary condition, such as the plane stress condition used in the current chapter, or be introduced by the EAS method.

3 Corrected Shape Functions for Nine-Node Shell Element

The standard isoparametric shape functions for a nine-node element are derived assuming that the midside nodes (5, 6, 7, 8) are located at the middle positions between the corner nodes, and that the central node 9 is located at the element center, see Fig. 2a. When these nodes are shifted from the middle positions then the physical space parameterized by the standard shape functions is distorted, see e.g. Figs. 13a and 20 in [14].

To alleviate this problem, in [3] the Corrected Shape Functions (CSF) were proposed with six additional parameters $\alpha, \beta, \gamma, \varepsilon, \theta, \kappa \in [-1, +1]$, see Fig. 2b, which define shifts of the midside nodes and the central node from the middle positions in the local coordinates space. The CSF for the nine-node element are defined in two steps. First, the CSF of the eight-node (serendipity) element are defined,

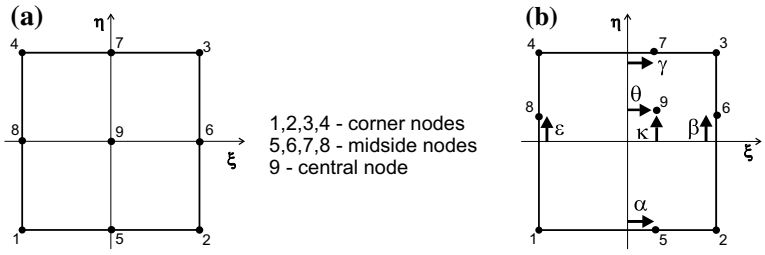

Fig. 2 Nine-node element: **a** Numbering and naming of nodes, **b** Shift parameters

$$
\begin{aligned}
\bar{N}_1 &\doteq \frac{1}{4}(1-\xi)(1-\eta)\frac{(1+\alpha)(1+\varepsilon)-(1+\alpha)(1+\eta)-(1+\varepsilon)(1+\xi)}{(1+\alpha)(1+\varepsilon)},\\
\bar{N}_2 &\doteq \frac{1}{4}(1+\xi)(1-\eta)\frac{(1-\alpha)(1+\beta)-(1-\alpha)(1+\eta)-(1+\beta)(1-\xi)}{(1-\alpha)(1+\beta)},\\
\bar{N}_3 &\doteq \frac{1}{4}(1+\xi)(1+\eta)\frac{(1-\gamma)(1-\beta)-(1-\gamma)(1-\eta)-(1-\beta)(1-\xi)}{(1-\gamma)(1-\beta)},\\
\bar{N}_4 &\doteq \frac{1}{4}(1-\xi)(1+\eta)\frac{(1+\gamma)(1-\varepsilon)-(1+\gamma)(1-\eta)-(1-\varepsilon)(1+\xi)}{(1+\gamma)(1-\varepsilon)},\\
\bar{N}_5 &\doteq \frac{(\xi^2-1)(1-\eta)}{2(\alpha^2-1)}, \qquad \bar{N}_6 \doteq \frac{(1+\xi)(\eta^2-1)}{2(\beta^2-1)},\\
\bar{N}_7 &\doteq \frac{(\xi^2-1)(1+\eta)}{2(\gamma^2-1)}, \qquad \bar{N}_8 \doteq \frac{(1-\xi)(\eta^2-1)}{2(\varepsilon^2-1)},
\end{aligned}
\tag{7}
$$

which account for shifts of the midside nodes from the middle positions. Next, the basis function for the central node 9 is added hierarchically to them. The obtained CSF for the nine-node element are as follows:

$$
\begin{aligned}
&N_i(\xi,\eta) = \bar{N}_i(\xi,\eta) - \bar{N}_i(\theta,\kappa)\, N_9(\xi,\eta), \qquad i = 1,\ldots,8,\\
&N_9 \doteq \frac{(\xi^2-1)(\eta^2-1)}{(\theta^2-1)(\kappa^2-1)},
\end{aligned}
\tag{8}
$$

where $\bar{N}_i(\theta,\kappa) \doteq \bar{N}_i(\xi=\theta,\eta=\kappa)$, see [3], Eq. (20). When the shift parameters are equal to zero, then the CSF of Eq. (8) reduce to the standard shape functions.

These six parameters are computed as proportional to the distance in the physical space, and to determine them, several nonlinear equations must be solved: 4 equations with 1 unknown for the midside nodes and 2 equations with 2 unknowns for the central node. This is done only once, so the time overhead is insignificant.

In [20], several extensions of the method of calculating the shift parameters are presented, which enable the use of the CSF for nine-node shell elements located in 3D space. They provide an improved accuracy of a solution for non-flat shell elements. Besides a method of constructing symmetric side curves for shifted midside nodes is described; we refer a reader interested in details to this paper. The so-extended CSF can also be applied to the 9-EAS11 shell elements, and, as our tests prove, they can be very beneficial, e.g. they are needed to pass the bending patch test for some types of nodal shifts.

4 Characteristics of 9-EAS11 Shell Elements

In the current chapter, we consider the class of nine-node shell elements with the *Enhanced Assumed Strain* (EAS) method applied to membrane strains. The EAS method was introduced in [18] for four-node elements; in this method, the compatible

strains $\mathbf{E}^{\mathrm{c}}$ are enhanced additively, i.e. $\mathbf{E} = \mathbf{E}^{\mathrm{c}} + \mathbf{E}^{\mathrm{enh}}$, where $\mathbf{E}^{\mathrm{enh}}$ is obtained from covariant components in a basis at the element center ("c").

Enhancement of membrane strains The EAS enhancement of the membrane strains $\boldsymbol{\varepsilon}$ is constructed at a Gauss Point "g" as follows:

$$\mathbf{E}_g^{\mathrm{enh}} = \mathbf{J}_c^{-T}\, \mathbf{E}_{\xi g}\, \mathbf{J}_c^{-1} \left(\frac{j_c}{j_g}\right), \qquad \mathbf{E}_\xi \doteq \begin{bmatrix} E_{11} & E_{12} & 0 \\ E_{12} & E_{22} & 0 \\ 0 & 0 & 0 \end{bmatrix}, \tag{9}$$

where the Jacobian is $\mathbf{J}_c \doteq [\ \mathbf{g}_1^c \mid \mathbf{g}_2^c \mid \frac{h}{2}\mathbf{t}_3^c\ ]$ and $\mathbf{g}_1^c, \mathbf{g}_2^c$ are natural vectors at the element center. Note that a general rule to transform the covariant components $\mathbf{E}_\xi$ to the Cartesian ones is $\mathbf{E}^{\mathrm{CART}} = \mathbf{J}^{-T}\, \mathbf{E}_\xi\, \mathbf{J}^{-1}$, see [19] Eq. (2.24) or [22] Eq. (7).

In the 9-EAS11 shell elements, the membrane strains $\boldsymbol{\varepsilon}$ are enhanced by the representation with 11 multipliers q_i, as in [2] Eq. (30),

$$\begin{aligned} E_{11} &= P_\xi\ (q_1 + \eta q_2 + \eta^2 q_3), \\ E_{22} &= P_\eta\ (q_9 + \xi q_{10} + \xi^2 q_{11}), \\ E_{12} &= P_\xi (q_4 + \eta q_5) + P_\eta (q_6 + \xi q_7) + P_\xi P_\eta q_8, \end{aligned} \tag{10}$$

where $P_\xi \doteq 1 - 3\xi^2$ and $P_\eta \doteq 1 - 3\eta^2$. This representation uses the following polynomial bases:

$$\begin{aligned} E_{11}:&\quad \{P_\xi,\ P_\xi\eta,\ P_\xi\eta^2\}, \\ E_{22}:&\quad \{P_\eta,\ P_\eta\xi,\ P_\eta\xi^2\}, \\ E_{12}:&\quad \{P_\xi,\ P_\eta,\ P_\xi\eta,\ P_\eta\xi,\ P_\xi P_\eta\}. \end{aligned} \tag{11}$$

We applied to each of these bases, the Gram-Schmidt orthogonalization with respect to the inner product function $\int_{-1}^{+1}\int_{-1}^{+1} f_i\, f_k\, \mathrm{d}\xi\, \mathrm{d}\eta$, where f_i, f_k are terms of the basis considered, and obtained

$$\begin{aligned} E_{11}:&\quad \{A\ P_\xi,\ B\ P_\xi\eta,\ -C\ P_\xi\eta^2\}, \\ E_{22}:&\quad \{A\ P_\eta,\ B\ P_\eta\xi,\ -C\ P_\eta\xi^2\}, \\ E_{12}:&\quad \{A\ P_\xi,\ A\ P_\eta,\ B\ P_\xi\eta,\ B\ P_\eta\xi,\ C\ P_\xi P_\eta\}, \end{aligned} \tag{12}$$

where $A \doteq \sqrt{5}/4$, $B \doteq \sqrt{15}/4$ and $C \doteq 5/8$. Hence, the bases of Eq. (11) are orthogonal and this procedure only renormalized them. When the bases of Eq. (12) are used in Eq. (10), then A, B and C only affect values of multipliers q_i. We have checked on the example of Sect. 5.3 that the use of Eq. (12) does not change the solution indeed.

The EAS transformation rule for curved shells A Jacobian at the element center is used in Eq. (9), hence, this transformation can be inadequate for curved shells. To account for a shell curvature but to retain the original form of Eq. (9) for flat shells,

we modified the idea of [15], which uses at Gauss points, the Cartesian basis for the element center properly rotated forward; it is designated *Local coordinate system 2*, see p. 478 therein. Because we need to determine the Jacobian $\mathbf{J} \doteq [\, \mathbf{g}_1 \mid \mathbf{g}_2 \mid \frac{h}{2}\mathbf{t}_3 \,]$ at a Gauss point, we apply this idea to the vectors $\mathbf{g}_1$ and $\mathbf{g}_2$ as follows:

1. The normal vectors, $\mathbf{t}_3^c$ at the element center and $\mathbf{t}_3^g$ at a Gauss point, are computed in a standard manner.
2. $\mathbf{t}_3^c$ is rotated into $\mathbf{t}_3^g$ by the canonical rotation vector $\mathbf{v} \doteq \theta \mathbf{n}$, where

$$\mathbf{n} = \mathbf{t}_3^c \times \mathbf{t}_3^g / \|\mathbf{t}_3^c \times \mathbf{t}_3^g\|, \qquad \theta \doteq \arccos(\mathbf{t}_3^c \cdot \mathbf{t}_3^g). \tag{13}$$

   Here the vector $\mathbf{n}$ defines an axis of rotation and θ is the rotation angle. A corresponding rotation tensor $\mathbf{R}(\mathbf{v})$ is defined by Eq. (4), where $\boldsymbol{\psi}$ is replaced by $\mathbf{v}$. Note that $\mathbf{t}_3^g = \mathbf{R}(\mathbf{v})\, \mathbf{t}_3^c$ by definition.
3. The natural basis vectors at the element center are forward-rotated to the Gauss point as follows:

$$\mathbf{g}_1^* = \mathbf{R}(\mathbf{v})\, \mathbf{g}_1^c, \qquad \mathbf{g}_2^* = \mathbf{R}(\mathbf{v})\, \mathbf{g}_2^c. \tag{14}$$

   Alternatively, we can re-write Eq. (14) using Eq. (8.6) of [19] as follows:

$$\begin{aligned} \mathbf{g}_1^* &= \mathbf{g}_1^c + s\, (\mathbf{n} \times \mathbf{g}_1^c) + (1 - c)[\mathbf{n} \times (\mathbf{n} \times \mathbf{g}_1^c)], \\ \mathbf{g}_2^* &= \mathbf{g}_2^c + s\, (\mathbf{n} \times \mathbf{g}_2^c) + (1 - c)[\mathbf{n} \times (\mathbf{n} \times \mathbf{g}_2^c)], \end{aligned} \tag{15}$$

   where $c \doteq \cos\theta = \mathbf{t}_3^c \cdot \mathbf{t}_3^g$ and $s \doteq \sin\theta = \sin(\arccos(c))$. Note that these formulas are different than those of [15] Eq. (31).
4. Using Eq. (14) or (15), we can define the modified Jacobian $\mathbf{J}^* \doteq [\, \mathbf{g}_1^* \mid \mathbf{g}_2^* \mid \frac{h}{2}\mathbf{t}_3^g \,]$. Note that $\mathbf{J}^* = \mathbf{R}(\mathbf{v})\, \mathbf{J}_c$, and we can use its inverse $(\mathbf{J}^*)^{-1} = \mathbf{J}_c^{-1}\mathbf{R}^T(\mathbf{v})$ instead of ${\mathbf{J}_c}^{-1}$ in Eq. (9). For flat shells, $\mathbf{v} = \mathbf{0}$, hence, $\mathbf{R}(\mathbf{v}) = \mathbf{I}$ and $(\mathbf{J}^*)^{-1} = \mathbf{J}_c^{-1}$, as required.

Remark. The forward-rotated Cartesian basis of [15] was proposed to obtain invariant *Assumed Strain* elements, which can pass both the patch and locking tests. (The *Assumed Strain* method in this paper does not use the *two-level interpolations* of strains; hence, it is different than a method of the same name of [4]). The independent strain fields are assumed with respect to a local coordinate system defined at the element centroid, e.g. for the shell with six degrees of freedom per node, 52 terms are assumed. The numerical results of [15] indicate that their elements perform well, but effects of the new *Local coordinate system 2* on accuracy for curved shells and distorted meshes are mixed; e.g. in the "Pinched ring" example accuracy worsens.

The modified EAS transformation rule for curved shells of Eq. (14) was implemented in our 9-EAS11 shell elements and tested in Sect. 5.2; no improved accuracy was obtained in this test, but, undoubtedly, more tests are necessary to draw a final conclusion.

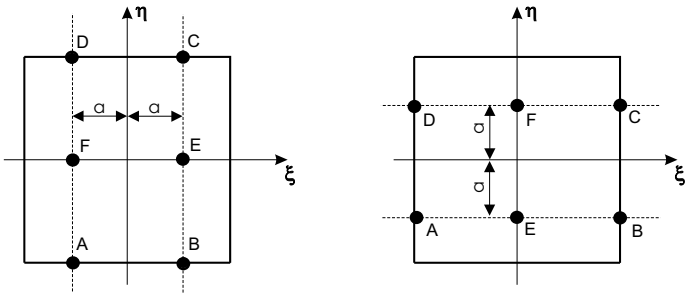

Fig. 3 Sampling points used in [6] for: **a** γ_{31} and **b** γ_{32}. $a = \sqrt{1/3}$

Treatment of transverse shear strains The transverse shear strains $\boldsymbol{\gamma}$ are treated in the 9-EAS11 shell elements in three ways:

1. By using the ANS of [6], where the two-level approximations are applied to the covariant (COV) components, which involves the 2×3 and 3×2 tying point schemes of Fig. 3 and the following interpolation functions:

$$\gamma_{31}: \qquad \bar{N}_1 = \frac{\eta(\eta-1)}{2}, \quad \bar{N}_2 = 1-\eta^2, \quad \bar{N}_3 = \frac{\eta(\eta+1)}{2}, \tag{16}$$

$$\gamma_{32}: \qquad \bar{S}_1 = \frac{\xi(\xi-1)}{2}, \quad \bar{S}_2 = 1-\xi^2, \quad \bar{S}_3 = \frac{\xi(\xi+1)}{2}. \tag{17}$$

   The same locations of the tying points were used earlier in [5].
2. By using the EAS method, with the transformation rule of Eq. (9) and the matrix

$$\mathbf{E}_\xi \doteq \begin{bmatrix} 0 & 0 & E_{13} \\ 0 & 0 & E_{23} \\ E_{13} & E_{23} & 0 \end{bmatrix}. \tag{18}$$

   The covariant transverse shear components of the enhancement are assumed as in [17], Eqs. (127) and (128),

$$E_{13} = P_\xi\,(q_1 + \eta q_2 + \eta^2 q_3), \qquad E_{23} = P_\eta\,(q_4 + \xi q_5 + \xi^2 q_6), \tag{19}$$

   where 6 parameters are used—this variant is designated EAS6.
3. By using unmodified transverse shear strains.

Finally, the bending/twisting strain $\boldsymbol{\kappa}$ is unmodified in the tested 9-EAS11 elements.

Table 1 Tested 9-EAS11 shell elements with drilling rotation

Element	CSF	Strains		
		Membrane $\boldsymbol{\varepsilon}$	Bending $\boldsymbol{\kappa}$	Transverse shear $\boldsymbol{\gamma}$
Tested elements				
9-EAS11/DISP/ANS [2]	No	EAS11	DISP	ANS of [6]
9-EAS11/DISP/EAS6 [17]	No	EAS11	DISP	EAS6 of [17], Eqs. (127) and (128)
9-EAS11/DISP/DISP [own]	No	EAS11	DISP	DISP
Reference element				
MITC9i [20]	Yes	MITCi	MITCi	MITCi
16-DISP, 4 × 4 GP [own]	No	DISP	DISP	DISP

5 Numerical Examples

In this section, we present numerical tests of three nine-node 9-EAS11 shell elements described in Sect. 4 and listed in Table 1, where "DISP" means that the strain is not modified.

All the tested and reference shell elements are of the Reissner-Mindlin type and have 6 dofs/node; the drilling rotation is incorporated as specified in Eqs. (1) and (2), for more details see Sects. 2 and 5 of [20]. Note that in all these elements:

1. the CSF are implemented in the version extended for shells of [20], Sect. 4, which enables calculation of shift parameters for non-flat elements.
2. the 3 × 3 Gauss integration is used in all nine-node elements, and they all have a correct rank.

All these FEs were derived by ourselves using the automatic differentiation program AceGen described in [8], and were tested within the finite element program FEAP developed by Taylor [23]. The use of these programs is gratefully acknowledged. Our parallel multithreaded (OMP) version of FEAP is described in [7].

5.1 Patch Tests

The standard five-element patch of elements was proposed in [16] and we run this test also for the mesh distorted by shifts of nodes shown in Fig. 4. The membrane and bending patch tests are performed as described in [12]; the transverse shear test is performed for the load case defined for a nine-node plate in [5], see "Shearing case" in Fig. 2b therein.

Four cases of nodal shifts are considered, see Fig. 4: (A) zero shifts (regular mesh), (B) arbitrary shifts of node 25, (C) parallel shifts of nodes 21–24, and (D)

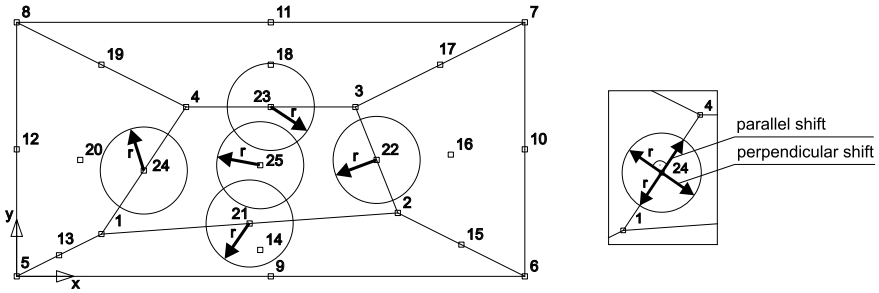

Fig. 4 Five-element patch test for the mesh distorted by shifts of some nodes (circles not to scale)

perpendicular shifts nodes 21–24, for which edges of the central element are curved. For more details on these tests see [20]. The conclusions are as follows:

1. For the 9-EAS11 elements, the membrane patch test is passed for all cases of nodal shifts for the standard shape functions. As the CSF are not needed, we can say that 9-EAS11 performs better than MITC9i, which needs the CSF to pass Case B and C, and, even with the CSF, fails for Case D.
2. For the method 1 and 2 of treating the transverse shear described in Sect. 4, and for the standard shape functions (no CSF), the bending patch test is passed for Case A but is failed for Cases B, C and D.

   Therefore, we implemented the CSF also in the 9-EAS11 elements sand found that then they pass Case B and C but fail for Case D. The level of errors is similar to that for MITC9i. We see that the CSF are indispensable though they also do not solve the problem of curved edges (Case D).
3. The transverse shear patch test is passed for the standard shape functions (no CSF) for all cases of shifts.

5.2 Curved Cantilever

The curved cantilever is fixed at one end and loaded by a moment M_z at the other, see Fig. 5. The data is as follows: $E = 2 \times 10^5$, $\nu = 0$, width $b = 0.025$ and radius of curvature $R = 0.1$. The FE mesh consists of 6 nine-node elements, which have either regular (Fig. 5a) or distorted shape (Fig. 5b); a definition of distortions is given in [9] p. 245. For the distorted mesh, this test is very demanding.

The shell thickness h is varied in the range $[10^{-2}, 10^{-6}]$, and the moment is assumed as $M_z = (R/h)^{-3}$, so the solution of a linear problem should remain constant. The analytical solution for the curved beam subjected to uniform bending is $u_y = M_z R^2/(EI) = 0.024$, where I is the moment of inertia.

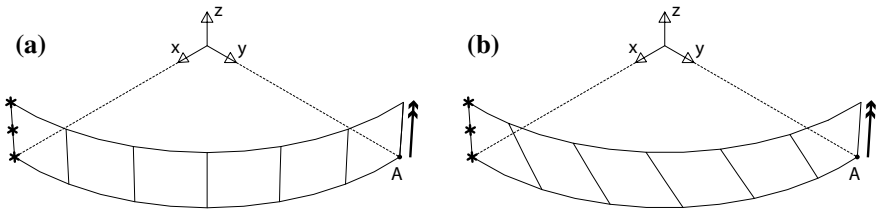

Fig. 5 Curved cantilever and two meshes: **a** regular and **b** distorted

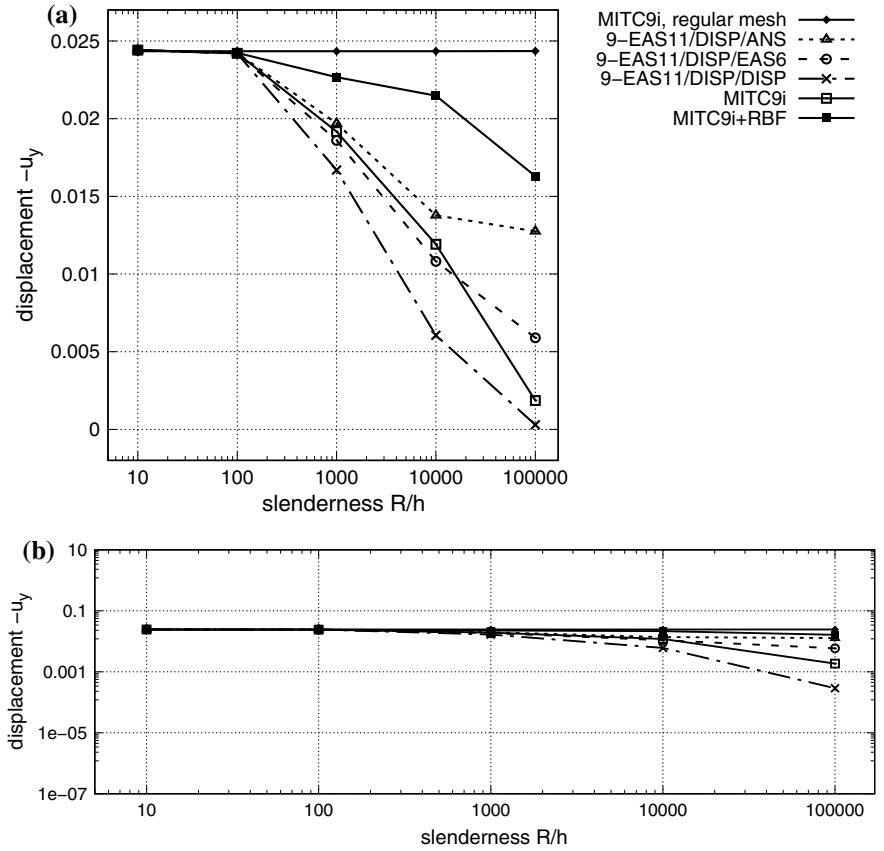

Fig. 6 Curved cantilever. Displacement u_y at point A for the distorted mesh and diminishing thickness. $\gamma = G$. **a** log-standard scale, **b** log-log scale to enable comparisons with Fig. 6 of [9]

The displacement u_y at point A obtained by a linear analysis are shown in Fig. 6, where, for the vertical axis, we use either (a) the standard scale or (b) the logscale, to enable comparisons with Fig. 6 of [9]. We conclude this test as follows:

1. For the regular mesh, the solutions for all tested elements are represented by the horizontal line, which is close to the analytical value. Neither one of the tested elements locks for this mesh despite its curvature. The basic element '9-DISP' severely locks for this mesh; this solution is not shown in these figures.
2. For the distorted mesh, all the tested elements lock for the $R/h > 100$. The most accurate is 9-EAS11/DISP/ANS, then MITC9i, 9-EAS11/DISP/EAS6 and 9-EAS11/DISP/DISP. The CSF are not important for this test.

We performed several additional tests to shed some light on the locking for the distorted mesh, and we found that:

1. The 9-URI2×2 element does not lock for the distorted mesh; this curve is not shown in Fig. 6. (It is the nine-node Uniformly Reduced Integration (2×2 Gauss points) element, which has 7 spurious zero eigenvalues).
2. The Residual Bending Flexibility (RBF) correction, which is a means to handle the sinusoidal bending and an extreme slenderness, significantly improves the results of this test; compare curves for MITC9i and MITC9i+RBF in Fig. 6.

For the nine-node elements, the implementation of the RBF correction must be slightly different than for the four-node elements of [10]. Assuming an isotropic elastic material, the transverse shear strain energy for a single element is defined as follows:

$$\mathscr{W}_\gamma = 2h \int_{-1}^{+1} \int_{-1}^{+1} \left(G_1^* \, \varepsilon_{13}^2 + G_2^* \, \varepsilon_{23}^2 \right) \, J \, \mathrm{d}\xi \, \mathrm{d}\eta, \tag{20}$$

where the corrected shear moduli are defined separately for each direction, i.e.

$$G_1^* = \left(\frac{1}{G} + \frac{l_1^2}{h^2 E} \right)^{-1}, \qquad G_2^* = \left(\frac{1}{G} + \frac{l_2^2}{h^2 E} \right)^{-1}. \tag{21}$$

Here l_1 and l_2 are the lengths of vectors connecting opposite mid-side points. To avoid an excessive twist, the full RBF correction is applied to the value at center and only a fraction of it to the remaining part. An integrand of Eq. (20) is modified as follows:

$$G_1^* \, \varepsilon_{13}^2 \approx G_1^* \, (\bar{\varepsilon}_{13}^c)^2 + G_{1c}^* \left[\varepsilon_{13}^2 - (\bar{\varepsilon}_{13}^c)^2 \right], \tag{22}$$

where

$$G_{1c}^* \doteq \left(\frac{1}{G} + a \, \frac{l_1^2}{h^2 E} \right)^{-1}, \qquad a \doteq \frac{c}{c + (1-c) \, (l_1/l_2)^2}, \tag{23}$$

and $c = 0.04$, as suggested in [11]. Similar formulas are used for $G_2^* \, \varepsilon_{23}^2$. For more details on our implementation of the RBF method, see [19] Sect. 13.2.3.

3. Comparing the displacements u_y of our Fig. 6b and Fig. 6 of [9] (in both figures the log-log scale is used, but actually for this scale, the differences are not clearly visible), we conclude that the elements 9-EAS11/DISP/ANS and MITC9i perform in this test slightly better than Q2-ANS/EAS. If we use the RBF correction then MITC9i performs similarly to the Q2-DSG/DSG element of [9].

5.3 *Pinched Hemispherical Shell with Hole*

A hemispherical shell with an 18° hole is loaded by two pairs of equal but opposite external forces P applied along the 0X and 0Y axes, see Fig. 7. Because of a double symmetry, a quarter of the hemisphere is modeled. In this test, the shell undergoes an

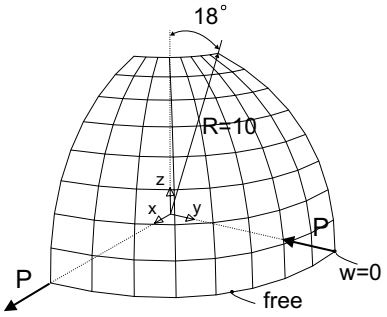

Fig. 7 Pinched hemispherical shell with hole. Geometry and load

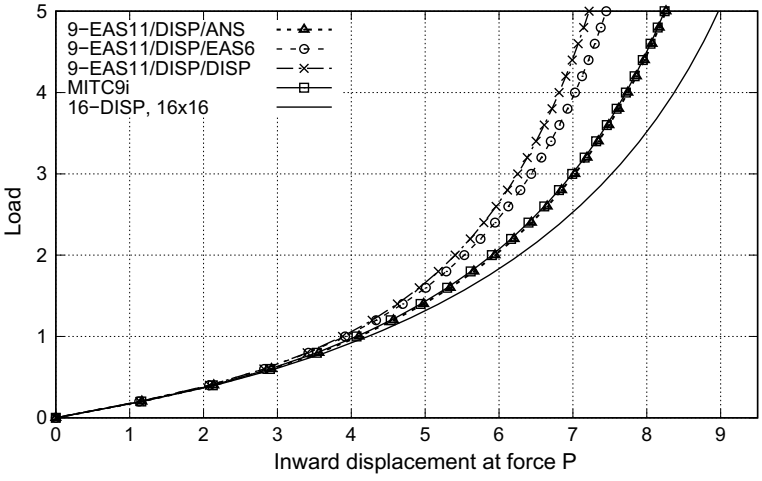

Fig. 8 Pinched hemispherical shell with hole. Nonlinear solutions. 8×8 mesh, $\mu = G/1000$

almost inextensional deformation and, because it is very thin (thickness $h = 0.01$), the membrane locking can manifest itself strongly.

The non-linear analyses are performed using the Newton method and $\Delta P = 0.2$. The solution curves for the 8×8-element mesh are shown in Fig. 8, where the inward displacement under the force is presented.

We see that the solutions for 9-EAS11/DISP/ANS and MITC9i coincide, while for 9-EAS11/DISP/EAS6 and 9-EAS11/DISP/DISP are stiffer. For the 16×16-element mesh, the solutions for 9-EAS11/DISP/ANS and MITC9i coincide with that for the reference element 16-DISP.

6 Final Remarks

We have developed three nine-node quadrilateral shell elements with the membrane part enhanced by the EAS method; they are designated 9-EAS11 because the strain enhancement uses 11 parameters. The preliminary conclusions are as follows:

1. Using the EAS11 enhancement, the membrane patch test is passed for all types of shifts of nodes, even these for which the element's edges are curved. The modified EAS transformation rule was also implemented, but further tests are needed to draw a conclusion on its usefulness.
2. For the transverse shear part of the 9-EAS11 element, the ANS method is more accurate than the EAS6 enhancement and the unmodified strains. Accuracy of the 9-EAS11/DISP/ANS element is similar or slightly higher than of the MITC9i element, but MITC9i with the RBF correction is more accurate.
3. The Corrected Shape Functions (CSF) are not needed for the 9-EAS11 elements to pass the membrane patch test, but are beneficial for the bending patch test, like for the MITC9i element.

Generally, the preliminary results indicate that the 9-EAS11/DISP/ANS element compares very well with our MITC9i element.

References

1. Badur, J., Pietraszkiewicz, W.: On geometrically non-linear theory of elastic shells derived from pseudo-Cosserat continuum with constrained micro-rotations. In: Pietraszkiewicz, W. (ed.) Finite Rotations in Structural Mechanics, pp. 19–32. Springer, Berlin (1986)
2. Bischoff, M., Ramm, E.: Shear deformable shell elements for large strains and rotations. Int. J. Num. Meth. Eng. **40**, 4427–4449 (1997)
3. Celia, M.A., Gray, W.G.: An improved isoparametric transformation for finite element analysis. Int. J. Num. Meth. Eng. **20**, 1447–1459 (1984)
4. Huang, H-Ch.: Static and Dynamic Analyses of Plates and Shells. Springer, Berlin (1989)
5. Huang, H.C., Hinton, E.: A nine node Lagrangian Mindlin plate element with enhanced shear interpolation. Eng. Comput. **1**, 369–379 (1984)

6. Jang, J., Pinsky, P.M.: An assumed covariant strain based 9-node shell element. Int. J. Num. Meth. Eng. **24**, 2389–2411 (1987)
7. Jarzebski, P., Wisniewski, K., Taylor, R.L.: On parallelization of the loop over elements in FEAP. Comput. Mech. **56**(1), 77–86 (2015)
8. Korelc, J.: Multi-language and multi-environment generation of nonlinear finite element codes. Eng. Comput. **18**, 312–327 (2002)
9. Koschnick, F., Bischoff, G.A., Camprubi, N., Bletzinger, K.U.: The discrete strain gap method and membrane locking. Comput. Methods Appl. Mech. Eng. **194**, 2444–2463 (2005)
10. MacNeal, R.H.: A simple quadrilateral shell element. Comput. Struct. **8**(2), 175–183 (1978)
11. MacNeal, R.H.: Finite Elements: Their Design and Performance. Mechanical Engineering, vol. 89. Marcel Dekker Inc., New York (1994)
12. MacNeal, R.H., Harder, R.L.: A proposed standard set of problems to test finite element accuracy. Finite Elem. Anal. Des. **1**, 3–20 (1985)
13. Panasz, P., Wisniewski, K.: Nine-node shell elements with 6 dofs/node based on two-level approximations. Part I: theory and linear tests. Finite Elem. Anal. Des. **44**, 784–796 (2008)
14. Panasz, P., Wisniewski, K., Turska, E.: Reduction of mesh distortion effects for nine-node elements using corrected shape functions. Finite Elem. Anal. Des. **66**, 83–95 (2013)
15. Park, H.C., Lee, S.W.: A local coordinate system for assumed strain shell element formulation. Comput. Mech. **15**, 473–484 (1995)
16. Robinson, J., Blackham, S.: An evaluation of lower order membranes as contained in MSC. NASTRAN, ASA and PAFEC FEM Systems, Robinson and Associates, Dorset, England (1979)
17. Sansour, C., Kollmann, F.G.: Families of 4-node and 9-node finite elements for a finite deformation shell theory. An assessment of hybrid stress, hybrid strain and enhanced strain elements. Comput. Mech. **24**, 435–447 (2000)
18. Simo, J.C., Rifai, M.S.: A class of mixed assumed strain methods and the method of incompatible modes. Int. J. Num. Meth. Eng. **29**, 1595–1638 (1990)
19. Wisniewski, K.: Finite rotation shells. Basic Equations and Finite Elements for Reissner Kinematics. Springer, Berlin (2010)
20. Wisniewski, K., Turska, E.: Improved nine-node shell element MITC9i with reduced distortion sensitivity. Comput. Mech. **62**, 499–523 (2018)
21. Wisniewski, K., Panasz, P.: Two improvements in formulation of nine-node element MITC9. Int. J. Num. Meth. Eng. **93**, 612–634 (2013)
22. Wisniewski, K., Wagner, W., Turska, E., Gruttmann, F.: Four-node Hu-Washizu elements based on skew coordinates and contravariant assumed strain. Comput. Struct. **88**, 1278–1284 (2010)
23. Zienkiewicz, O.C., Taylor, R.L.: The finite element method. In: Basic Formulation and Linear Problems, vol. 1, 4th edn. McGraw-Hill (1989)

Higher Order Theory of Electro-Magneto-Elastic Plates and Shells

V. V. Zozulya

Abstract New higher order models of the electro-magneto-elastic plates and shells have been developed here. The 3-D equations of the linear electro-magneto-elasticity have been presented in an orthogonal system of coordinates. For the creation of 2-D models of plates and shells the curvilinear system of coordinates related to the middle surface of the shell has been used along with special hypothesis based on assumptions that take into account the fact that the considered plates and shells are thin. Higher order theory is based on the expansion of the 3-D equations of the linear theory of the electro-magneto-elasticity into Fourier series in terms of Legendre polynomials. All equations for higher order theory of the electro-magneto-elastic plates in Cartesian and polar coordinates as well as for cylindrical and spherical shells in coordinates related to the shells geometry have been developed and presented here in detail. The obtained equations can be used for calculating the stress-strain and for modelling thin walled structures in macro, micro and nano scale when taking into account coupled electro-magneto-elastic effects.

Keywords Plates · Shell · Electro-magneto-elasticity · Legendre polynomial · Higher order theory

1 Introduction

In the era of nanotechnology and bioengineering, much of the attention of scientists and engineers has been focused on study multiphysical phenomena in materials, structures and devices, where mechanical deformation, polarization and magnetization are simultaneously coupled. The materials with such properties have broad applications in science and engineering, for example in the energy traducers that convert electrical energy to mechanical energy or vice versa, the sensors technologies of actuators, micro-electro-mechanical (MEMS) and nano-electro-mechanical

V. V. Zozulya (✉)
Centro de Investigacion Cientifica de Yucatan, A.C., Calle 43, No 130, Colonia: Chuburna de Hidalgo, 97200 Mérida, Yucatan, Mexico
e-mail: zozulya@cicy.mx

H. Altenbach et al. (eds.), *Recent Developments in the Theory of Shells*,
Advanced Structured Materials 110, https://doi.org/10.1007/978-3-030-17747-8_36

(NEMS) structures, imaging devices, smart and self-adaptive structures, artificial muscles, etc. [6, 17, 18, 21, 28–30, 36, 46, 60, 61, 64, 69, 71].

The study of piezoelectricity was initiated by bothers J. Curie and P. Curie in 1880. They found that certain crystalline materials generate an electric charge proportional to a mechanical stress. Since that time many other coupled electro-magneto-elastic phenomena have been discovered, investigated and applied in sciences and engineering. These achievements and other obtained theoretical and practical results have been reported in a numerous publications including journal papers (among others see [3, 4, 11, 12, 24, 33, 34, 45, 50–53, 58, 67]), books and monographs [14, 16, 26, 30, 32, 40, 43, 44, 47, 49, 54, 60, 61, 71].

Due to the application of the piezoelectric and piezomagnetic couplings effects in civil, mechanical, aerospace, biomedical and engineering, electro-magneto-elastic theories of solids become an important topic for researchers in the field of theoretical and applied mechanics. Theoretical mechanics can provide effective tools for electro-magneto-elastic material behavior modeling. For example, the one- and two-dimensional theories of electro-magneto-elastic beams, plates, and shells are effective tools for the design and optimization of the materials, structures and devices subjected to the electro-magneto-elastic impact.

Many different models of beams, plates, and shells that consider effects of electro-magneto-elastic coupling have been developed so far. For further information and references we mention here the following books [7–10, 15, 21, 30, 54, 60, 61, 63, 68]. Based on the information presented in those books and on the Refs. [1, 2, 5, 13, 19, 20, 25, 27, 31, 35, 37–39, 41, 42, 48, 55–57, 62, 65, 66, 70, 77, 80] most known models of electro-magneto-elastic beams, plates, and shells can be classified the following way:

- Models based on classical Euler–Bernoulli, Timoshenko, Mindlin and higher order shear deformation theories.
- Models based on the so called direct approach, which consists of considering the shell as a 2-D deformable continua enhanced by sets of deformable directors.
- Models based on 3-D equations of elasticity and exploration of the polynomial series expansion in term of thickness.

Classical theories are very popular among the engineering community because of their relative simplicity and physical clarity. Numerous books and monographs have been written on the subject, some of them are referred above. Unfortunately, classical theories have some shortcomings and logical contradictions such as their proximity and inaccuracy, for this reason in some cases there is no congruency with the results obtained by using the 3-D approach and experiments. Thus, there is demand to develop new more accurate theories.

As an alternative to classical methods, the direct approach can be used by considering a deformable surface endowed with a certain microstructure, as a model for plates and shells. The direct approach, which is well-known since Euler, was summarized for the first time in the monograph of the Cosserat brothers presenting the kinematical model of a continuum with material points which behave like rigid bodies (having 6 degrees of freedom, instead of 3 in the classical continuum mechanics).

The main difficulty in any direct approach is the determination of the effective stiffness coefficients appearing in the two-dimensional constitutive equations in terms of the three-dimensional elasticity constants. For further information one can see [6, 7, 59] and references there.

The third approach consists in the expansion of the stress-strain field components into polynomials series in terms of thickness. It was proposed by Cauchy and Poisson but was not popular than. Significant expansion and development of that method was done by Kil'chevskii [39]. Vekua has used Legendre's polynomials for the expansion of the equations of elasticity and reduction of the 3-D problem to 2-D one [70]. An approach based on the expansion of the equations of elasticity into Fourier series in terms of Legendre's polynomials has been widely used for the development of the mathematically consistent high order theories of beams, rods, plates and shells Such an approach has a significant advantage because Legendre's polynomials are orthogonal and as result the obtained equations are simpler. This approach has been significantly extended in a large number of publications, among them we have to mention the Carrera unified approach [19–23] and the following books [38, 55–57, 70].

In our previous publications [72–87] the approach based on the use of Legendre's polynomials series expansion has been applied to the development of the high order models of rods, plates and shells. More specifically, the developed approach has been applied to the plates and shells thermoelastic contact problems where mechanical and thermal conditions are changed during deformation in [72–75, 79, 81, etc.]. The mathematical formulation, differential equations and mechanical and thermal contact conditions for the cases of two parallel plates have been reported in [72]. Extension to nonstationary proses has been done in [73]. A more general approach was introduced in [77], where methodology of all coefficients of the differential equations, contact and boundary conditions calculation are explained in detail and their analytical expressions for the case of n-order approximation and shells of arbitrary geometry is presented. Then, the approach was further developed and applied to the problem of plates and shells thermos-mechanical contact with rigid bodies through a heat conducting layer, thermoelasticity of the laminated composite materials with the possibility of delamination and mechanical and thermal contact between laminas in the temperature field [74], the pencil-thin nuclear fuel rods modeling in [75], functionally graded shells in [76, 78, 82] and modeling of MEMS and NEMS in [79, 81]. Developments of the high order theories and their comparison with Euler-Bernoulli and Timoshnko's theories for micropolar, couple stress and nonlocal curved elastic rods have been done in [83–85], respectively. In [86, 87] micropolar and couple stress theories are extended for the cases of plates and shells. An analysis and comparison with the classical theory of elastic and thermoelastic plates and shells has been done in [77, 80].

In this paper 2-D higher order models of elastic plates and shells that are based on 3-D linear electro-magneto-elastic theories have been developed. All the equations of the 3-D linear electro-magneto-elasticity have been presented in a special orthogonal curvilinear system of coordinates related to the middle surface of the shell and a special hypothesis based on assumptions that take into account the fact that the plates and shells that have been considered are thin. The higher order models are

based on the expansion of the equations of the 3-D linear electro-magneto-elasticity into Fourier series in terms of Legendre polynomials with respect to thickness. All the equations of the 2-D higher order models of plates in Cartesian and polar coordinates and of the cylindrical and spherical shells have been developed and presented here. The obtained equations can be used to calculate stress-strain and to model thin walled structures in macro-, micro- and nano-scales by taking into account electro-magneto-elastic coupling effects. The proposed models can be efficient in MEMS and NEMS modeling as well as in computer simulation.

2 3-D Electro-Magneto-Elasticity in Orthogonal Coordinates

In this study we are developing an approach based on the expansion of the 3-D equations of electro-magneto-elasticity into Fourier series in terms of Legendre polynomials and are applying it to create higher order theories of plates and shells. Let us consider a shell of arbitrary geometry in a 3-D Euclidian space, which occupies the domain $V = \Omega \times [-h, h]$ with a smooth boundary ∂V. Here $2h$ is thickness, Ω is the middle surface of the shell. The boundary of the shell ∂V can be presented in the form $\partial V = S \cup \Omega^+ \cup \Omega^-$, where Ω^+ and Ω^- are the upper and lower sides and S denotes lateral sides.

In the linear theory of electro-magneto-elasticity in order to study the mechanical state of the continuum media we introduce the stress $\boldsymbol{\sigma}(\mathbf{x})$ and strain $\boldsymbol{\varepsilon}(\mathbf{x})$ tensors and the displacement $\mathbf{u}(\mathbf{x})$, traction $\mathbf{p}(\mathbf{x})$ vectors. In order to study the electro-magnetic state of the continuum media we introduce vectors of electric $\mathbf{E}(\mathbf{x})$ and magnetic $\mathbf{M}(\mathbf{x})$ field and electric $\mathbf{D}(\mathbf{x})$ and magnetic $\mathbf{B}(\mathbf{x})$ displacements, respectively. They can be presented in the form

$$\boldsymbol{\sigma} = \begin{vmatrix} \sigma_{11} & \sigma_{21} & \sigma_{31} \\ \sigma_{12} & \sigma_{22} & \sigma_{32} \\ \sigma_{13} & \sigma_{23} & \sigma_{33} \end{vmatrix}, \boldsymbol{\varepsilon} = \begin{vmatrix} \varepsilon_{11} & \varepsilon_{21} & \varepsilon_{31} \\ \varepsilon_{12} & \varepsilon_{22} & \varepsilon_{32} \\ \varepsilon_{13} & \varepsilon_{23} & \varepsilon_{33} \end{vmatrix}, \mathbf{u} = \begin{vmatrix} u_1 \\ u_2 \\ u_3 \end{vmatrix}, \mathbf{p} = \begin{vmatrix} p_1 \\ p_2 \\ p_3 \end{vmatrix}, \mathbf{E} = \begin{vmatrix} E_1 \\ E_2 \\ E_3 \end{vmatrix},$$
$$\mathbf{M} = \begin{vmatrix} M_1 \\ M_2 \\ M_3 \end{vmatrix}, \mathbf{D} = \begin{vmatrix} D_1 \\ D_2 \\ D_3 \end{vmatrix}, \mathbf{B} = \begin{vmatrix} B_1 \\ B_2 \\ B_3 \end{vmatrix} \tag{2.1}$$

For the purpose of the theories developed here we introduce an orthogonal curvilinear system of coordinates $\mathbf{x} = (x_1, x_2, x_3)$, such that position vector of an arbitrary point is equal to $\mathbf{R}(x_1, x_2, x_3) = \mathbf{e}_i x_i$. Unit orthogonal basic vectors and their derivatives with respect to space coordinates are equal to

$$\mathbf{e}_i = \frac{1}{H_i}\frac{\partial \mathbf{R}}{\partial x_i}, \frac{\partial \mathbf{e}_i}{\partial x_j} = \Gamma_{ij}^k \mathbf{e}_k \tag{2.2}$$

where H_i are Lamé coefficients and Γ_{ij}^k are Christophel symbols. They are calculated by the equations

$$H_i = \left|\frac{\partial \mathbf{R}}{\partial x_i}\right| = \sqrt{\frac{\partial \mathbf{R}}{\partial x_i} \cdot \frac{\partial \mathbf{R}}{\partial x_i}} \tag{2.3}$$

$$\Gamma_{ij}^k = -\frac{1}{H_i}\frac{\partial H_i}{\partial x_j}\delta_{ik} + \frac{1}{2H_iH_k}\left(\delta_{jk}\frac{\partial H_jH_k}{\partial x_i} + \delta_{ik}\frac{\partial H_iH_k}{\partial x_j} - \delta_{ij}\frac{\partial H_iH_j}{\partial x_k}\right) \tag{2.4}$$

From the last equation it follows that $\Gamma_{ij}^k = 0$ for $i \neq j \neq k$ and

$$\Gamma_{ii}^k = -\frac{1}{H_k}\frac{\partial H_i}{\partial x_k}, \quad \Gamma_{ik}^k = -\frac{1}{H_i}\frac{\partial H_k}{\partial x_i} \quad \text{for} \quad i \neq k \tag{2.5}$$

In the introduced system of coordinates the equations of equilibrium and the Maxwell equations under the assumptions of static electro-magnetic fields are given by

$$\nabla_j \sigma_{ji} + b_i = 0, \quad \nabla_i D_i = b_e, \quad \nabla_i B_i = b_m \tag{2.6}$$

where $b_i(\mathbf{x})$ are the body forces, $f_e(\mathbf{x})$ is the electric charge density and $f_m(\mathbf{x})$ is the heat source the electric current density, respectively.

Divergences of the stress tensor and the electric and magnetic displacement vectors in the curvilinear orthogonal system of coordinates have the form

$$\nabla_j \sigma_{ji} = \frac{1}{H_1H_2H_3}\sum_{j=1}^{3}\left(\frac{\partial}{\partial x_i}\left(\frac{H_1H_2H_3}{H_i}\sigma_{ij}\right) + \frac{H_1H_2H_3}{H_iH_j}\left(\sigma_{ij}\frac{\partial H_j}{\partial x_i} - \sigma_{ii}\frac{\partial H_i}{\partial x_j}\right)\right),$$

$$\nabla_i D_i = \frac{1}{H_1H_2H_3}\sum_{i=1}^{3}\frac{\partial}{\partial x_i}\left(\frac{H_1H_2H_3D_i}{H_i}\right), \quad \nabla_i B_i = \frac{1}{H_1H_2H_3}\sum_{i=1}^{3}\frac{\partial}{\partial x_i}\left(\frac{H_1H_2H_3B_i}{H_i}\right) \tag{2.7}$$

The infinitesimal strain tensor ε_{ij} , the electric field E_i and the magnetic field H_i are defined as

$$\varepsilon_{ij} = \frac{1}{2}\left(\nabla_j u_i + \nabla_i u_j\right), \quad E_i = \nabla_i \phi, \quad M_i = \nabla_i \varphi \tag{2.8}$$

where $\phi(\mathbf{x})$ and $\varphi(\mathbf{x})$ are the electric and magnetic potentials, respectively.

Gradients of the displacement vector and the electric and magnetic potentials in the curvilinear orthogonal system of coordinates have the form

$$\nabla_j u_i = \left(\frac{1}{H_i}\frac{\partial u_i}{\partial x_j} - \frac{u_j}{H_iH_j}\frac{\partial H_j}{\partial x_i} + \delta_{ij}\sum_{k=1}^{3}\frac{u_k}{H_iH_k}\frac{\partial H_i}{\partial x_k}\right),$$

$$\nabla_i \phi = \frac{1}{H_i}\frac{\partial \phi}{\partial x_i}, \quad \nabla_i \varphi = \frac{1}{H_i}\frac{\partial \varphi}{\partial x_i} \tag{2.9}$$

The mathematical model of the linear electro-magneto-elasticity is based on the constitutive relation between components of an elastic field, such as $\sigma_{ij}(\mathbf{x})$ and $\varepsilon_{ij}(\mathbf{x})$ stress and strain tensors, $E_k(\mathbf{x})$ electric displacement and magnetic induction $B_i(\mathbf{x})$ vectors. Due to the coupling of elastic, electric and magnetic behaviors, the constitutive equations for a homogeneous, linear anisotropic electro-magneto-elastic solid are

$$\begin{aligned} \sigma_{ij} &= c_{ijkl}\varepsilon_{kl} - e_{lij}E_l - h_{lij}M_l \\ D_i &= e_{ikl}\varepsilon_{kl} + \epsilon_{ik}E_k + \beta_{il}M_l \\ B_i &= h_{ikl}\varepsilon_{kl} + \beta_{il}E_l + \gamma_{il}M_l \end{aligned} \tag{2.10}$$

where c_{ijkl}, ϵ_{ik} and γ_{il} denote the elastic stiffness tensor, dielectric permitivities and magnetic permeabi-lities, respectively, e_{ikl}, h_{lij} and β_{il} are the piezoelectric, piezomagnetic and electro-magnetic coupling coefficients, respectively.

The material constants in (2.10) satisfy the following symmetry conditions

$$\begin{aligned} &c_{ijkl} = c_{jikl} = c_{ijlk} = c_{klij}, \quad e_{lij} = e_{lji}, \quad h_{lij} = h_{lji} \\ &\epsilon_{ik} = \epsilon_{ki}, \quad \beta_{ik} = \beta_{ki}, \quad \gamma_{ik} = \gamma_{ki} \end{aligned} \tag{2.11}$$

Moreover, the elastic constant, dielectric permittivities and magnetic permeabilities tensors are positive definite, i.e.

$$c_{ijkl}\varepsilon_{ij}\varepsilon_{kl} > 0, \quad \epsilon_{ij}E_iE_j > 0, \quad \gamma_{ij}M_iM_j > 0, \quad \forall \varepsilon_{ij} \neq 0, \quad \forall E_i \neq 0, \quad \forall M_i \neq 0 \tag{2.12}$$

By substituting the constitutive relations (2.10) in (2.8) and abtained result in (2.6) one can find the coupled system of differential equations of the linear electro-magneto-elasticity for the displacement vector, electric and magnetic potentials in the form

$$\begin{vmatrix} \mathbf{L}_{uu} & \mathbf{L}_{ue} & \mathbf{L}_{um} \\ \mathbf{L}_{eu} & L_{ee} & L_{em} \\ \mathbf{L}_{mu} & L_{me} & L_{mm} \end{vmatrix} \cdot \begin{vmatrix} \mathbf{u} \\ \phi \\ \varphi \end{vmatrix} = \begin{vmatrix} \mathbf{b} \\ b_e \\ b_m \end{vmatrix}, \tag{2.13}$$

where

$$\begin{aligned} \mathbf{L}_{uu} &= \begin{vmatrix} L_{11} & L_{12} & L_{13} \\ L_{21} & L_{22} & L_{23} \\ L_{33} & L_{32} & L_{33} \end{vmatrix}, \quad \mathbf{L}_{eu} = \begin{vmatrix} L_{e1} \\ L_{e2} \\ L_{e3} \end{vmatrix}, \quad \mathbf{L}_{mu} = \begin{vmatrix} L_{m1} \\ L_{m2} \\ L_{m3} \end{vmatrix}, \quad \mathbf{b} = \begin{vmatrix} b_1 \\ b_2 \\ b_3 \end{vmatrix}, \\ \mathbf{L}_{ue} &= \begin{vmatrix} L_{1e} & L_{2e} & L_{3e} \end{vmatrix}, \quad \mathbf{L}_{ue} = \begin{vmatrix} L_{1m} & L_{2m} & L_{3m} \end{vmatrix} \end{aligned} \tag{2.14}$$

The differential operators in (2.14) for the homogeneous generally anisotropic medium have the form

$$\mathbf{L}_{uu}\cdot\mathbf{u}=\frac{\mathbf{e}_i}{2H_1H_2H_3}\sum_{k,l=1}^{3}\left(\sum_{j=1}^{3}\left(c_{ijkl}\left(\frac{\partial}{\partial x_i}\left(\frac{H_1H_2H_3}{H_i}(\nabla_l u_k+\nabla_k u_l)\right)\right.\right.\right.$$
$$\left.\left.\left.+\frac{H_1H_2H_3}{H_iH_j}\frac{\partial H_j}{\partial x_i}(\nabla_l u_k+\nabla_k u_l)\right)-c_{iikl}\frac{H_1H_2H_3}{H_iH_j}\frac{\partial H_i}{\partial x_j}(\nabla_l u_k+\nabla_k u_l)\right)\right),$$

$$\mathbf{L}_{ue}\phi=\frac{\mathbf{e}_i}{2H_1H_2H_3}\sum_{l=1}^{3}\left(\sum_{j=1}^{3}\left(e_{lij}\left(\frac{\partial}{\partial x_i}\left(\frac{H_1H_2H_3}{H_i}\nabla_l\phi\right)+\frac{H_1H_2H_3}{H_iH_j}\frac{\partial H_j}{\partial x_i}\nabla_l\phi\right)\right.\right.$$
$$\left.\left.-e_{lii}\left(\frac{H_1H_2H_3}{H_iH_j}\frac{\partial H_i}{\partial x_j}\nabla_l\phi\right)\right)\right)$$

$$\mathbf{L}_{um}\varphi=\frac{\mathbf{e}_i}{2H_1H_2H_3}\sum_{l=1}^{3}\left(\sum_{j=1}^{3}\left(h_{lij}\left(\frac{\partial}{\partial x_i}\left(\frac{H_1H_2H_3}{H_i}\nabla_l\varphi\right)+\frac{H_1H_2H_3}{H_iH_j}\frac{\partial H_j}{\partial x_i}\nabla_l\varphi\right)\right.\right.$$
$$\left.\left.-h_{lii}\left(\frac{H_1H_2H_3}{H_iH_j}\frac{\partial H_i}{\partial x_j}\nabla_l\varphi\right)\right)\right)$$

$$\mathbf{L}_{eu}\cdot\mathbf{u}=\frac{1}{2H_1H_2H_3}\sum_{k,l=1}^{3}\sum_{i=1}^{3}e_{ikl}\frac{\partial}{\partial x_i}\left(\frac{H_1H_2H_3}{H_i}(\nabla_l u_k+\nabla_k u_l)\right),$$

$$L_{ee}\phi=\frac{1}{H_1H_2H_3}\sum_{k,i=1}^{3}\epsilon_{ik}\frac{\partial}{\partial x_i}\left(\frac{H_1H_2H_3}{H_i}\nabla_k\phi\right),$$

$$L_{em}\varphi=\frac{1}{H_1H_2H_3}\sum_{k,i=1}^{3}\beta_{ik}\frac{\partial}{\partial x_i}\left(\frac{H_1H_2H_3}{H_i}\nabla_k\varphi\right)$$

$$\mathbf{L}_{mu}\cdot\mathbf{u}=\frac{1}{2H_1H_2H_3}\sum_{k,l=1}^{3}h_{ikl}\sum_{i=1}^{3}\frac{\partial}{\partial x_i}\left(\frac{H_1H_2H_3}{H_i}(\nabla_l u_k+\nabla_k u_l)\right),$$

$$L_{me}\phi=\frac{1}{H_1H_2H_3}\sum_{k,i=1}^{3}\beta_{ik}\frac{\partial}{\partial x_i}\left(\frac{H_1H_2H_3}{H_i}\nabla_k\phi\right),$$

$$L_{mm}\varphi=\frac{1}{H_1H_2H_3}\sum_{k,i=1}^{3}\gamma_{ik}\frac{\partial}{\partial x_i}\left(\frac{H_1H_2H_3}{H_i}\nabla_k\phi\right)\tag{2.15}$$

For a correct formulation of the linear electro-magneto-elasticity problems it is necessary to assign boundary conditions. Here we consider the mixed boundary conditions for the Eqs. (2.13) in the following form.

For prescribing mixed mechanical boundary condition, the boundary of the body is presented as $\partial V=\partial V_u\cup\partial V_p$, where vectors of displacement $\mathbf{u}^u(\mathbf{x})$ and traction $\mathbf{p}^u(\mathbf{x})$ are given as

$$\mathbf{u}(\mathbf{x}) = \mathbf{u}^u(\mathbf{x}), \quad \forall \mathbf{x} \in \partial V_u, \quad \mathbf{p}(\mathbf{x}) = \boldsymbol{\sigma}(\mathbf{x}) \cdot \mathbf{n}(\mathbf{x}) = \mathbf{p}^u(\mathbf{x}), \quad \forall \mathbf{x} \in \partial V_p, \quad (2.16)$$

For prescribing a mixed electrical boundary condition, the boundary of the body is presented as $\partial V = \partial V_\phi \cup \partial V_e$, where electrical potential $\phi^u(\mathbf{x})$ and surface charge $D^e(\mathbf{x})$ are defined as

$$\phi(\mathbf{x}) = \phi^u(\mathbf{x}), \quad \forall \mathbf{x} \in \partial V_\phi, \quad \mathbf{D}(\mathbf{x}) \cdot \mathbf{n}(\mathbf{x}) = D^e(\mathbf{x}), \quad \forall \mathbf{x} \in \partial V_e \quad (2.17)$$

For prescribing a mixed magnetic boundary condition boundary of the body is presented as $\partial V = \partial V_\varphi \cup \partial V_h$, where magnetic potential $\varphi^u(\mathbf{x})$ and surface charge $B^e(\mathbf{x})$ are defined as

$$\varphi(\mathbf{x}) = \varphi^u(\mathbf{x}), \quad \forall \mathbf{x} \in \partial V_\varphi, \quad \mathbf{B}(\mathbf{x}) \cdot \mathbf{n}(\mathbf{x}) = B^e(\mathbf{x}), \quad \forall \mathbf{x} \in \partial V_h \quad (2.18)$$

Thus, the linear electro-magneto-elasticity problem consists of a system of partial differential equations (2.13) with differential operators of the form (2.15), and boundary (2.16)–(2.18) conditions. They are formulated in an arbitrary orthogonal coordinates form. In order to solve any specific problem we have to introduce any specific system of coordinates and represent all parameters (2.1) as functions of those coordinates and all operators in a corresponding coordinate form.

In solving specific problems it is convenient and customary to rewrite constitutive relations (2.10) in matrix form. Since the stress and strain tensors are symmetric, each component can be specified by one subscript rather than two. These are defined according to the scheme

$$\begin{aligned} \tilde{\boldsymbol{\sigma}} &= (\sigma_{11}, \sigma_{22}, \sigma_{33}, \sigma_{23}, \sigma_{13}, \sigma_{12}) \\ \tilde{\boldsymbol{\varepsilon}} &= (\varepsilon_{11}, \varepsilon_{22}, \varepsilon_{33}, \varepsilon_{23}, \varepsilon_{13}, \varepsilon_{12}) \end{aligned} \quad (2.19)$$

The tensor of elastic modulus c_{ijkl} is symmetrical by the first two (i and j) and the last two (k and l) indexes so we can write it as

$$c_{ijkl} = c_{IJ}, \quad i, j, k, l = 1, 2, 3; I, J = 1, 2, \ldots, 6 \quad (2.20)$$

Consequently, the coefficients $c_{I,J}$, $I, J = 1, 2, \ldots, 6$ (a, ß = 1, 2,..., 6) form a square matrix (6×6).

Taking into account the symmetry of the tensors e_{lij} and h_{lij} by the pair of the last two indexes it possible to define two three-by-six matrices

$$e_{lij} = e_{lI}, \quad h_{lij} = h_{lI}, \quad l = 1, 2, 3; I = 1, 2, \ldots, 6 \quad (2.21)$$

for electro- magnetic constants. In the new notation constitutive relations (2.10) may be rewritten in the form

$$\tilde{\boldsymbol{\sigma}} = \widetilde{\mathbf{C}} \cdot \tilde{\boldsymbol{\varepsilon}} - \widetilde{\mathbf{D}} \cdot \mathbf{E} - \tilde{\mathbf{Q}} \cdot \mathbf{M},$$
$$\mathbf{D} = \widetilde{\mathbf{D}} \cdot \tilde{\boldsymbol{\varepsilon}} + \boldsymbol{\Sigma} \cdot \mathbf{E} + \mathbf{B} \cdot \mathbf{M},$$
$$\mathbf{B} = \widetilde{\mathbf{Q}} \cdot \tilde{\boldsymbol{\varepsilon}} + \mathbf{B} \cdot \mathbf{E} + \Gamma \cdot \mathbf{M}. \tag{2.22}$$

where matrix coefficients in the case of a homogeneous generally anisotropic body have the form

$$\tilde{\mathbf{C}} = \begin{vmatrix} c_{11} & c_{12} & c_{13} & c_{14} & c_{15} & c_{16} \\ c_{12} & c_{22} & c_{23} & c_{24} & c_{25} & c_{26} \\ c_{13} & c_{23} & c_{33} & c_{34} & c_{35} & c_{36} \\ c_{14} & c_{24} & c_{34} & c_{44} & c_{45} & c_{46} \\ c_{15} & c_{25} & c_{35} & c_{45} & c_{55} & c_{56} \\ c_{16} & c_{26} & c_{36} & c_{46} & c_{56} & c_{66} \end{vmatrix}, \quad \tilde{\mathbf{D}} = \begin{vmatrix} d_{11} & d_{12} & d_{13} \\ d_{21} & d_{22} & d_{23} \\ d_{31} & d_{32} & d_{33} \\ d_{41} & d_{42} & d_{43} \\ d_{51} & d_{52} & d_{53} \\ d_{61} & d_{62} & d_{63} \end{vmatrix}, \quad \tilde{\mathbf{Q}} = \begin{vmatrix} q_{11} & q_{12} & q_{13} \\ q_{21} & q_{22} & q_{23} \\ q_{31} & q_{32} & q_{33} \\ q_{41} & q_{42} & q_{43} \\ q_{51} & q_{52} & q_{53} \\ q_{61} & q_{62} & q_{63} \end{vmatrix}, \tag{2.23}$$

$$\boldsymbol{\Sigma} = \begin{vmatrix} \epsilon_{11} & \epsilon_{12} & \epsilon_{13} \\ \epsilon_{21} & \epsilon_{22} & \epsilon_{23} \\ \epsilon_{31} & \epsilon_{32} & \epsilon_{33} \end{vmatrix}, \quad \mathbf{B} = \begin{vmatrix} \beta_{11} & \beta_{12} & \beta_{13} \\ \beta_{21} & \beta_{22} & \beta_{23} \\ \beta_{31} & \beta_{32} & \beta_{33} \end{vmatrix}, \quad \Gamma = \begin{vmatrix} \gamma_{11} & \gamma_{12} & \gamma_{13} \\ \gamma_{21} & \gamma_{22} & \gamma_{23} \\ \gamma_{31} & \gamma_{32} & \gamma_{33} \end{vmatrix}$$

It should be noted that the number of independent coefficients in (2.23) (i.e., the number of material constants) depends on the symmetry of the crystal. In the general case of the triclinic system in (2.23) matrix $\tilde{\mathbf{C}}$ contains 21 elastic constants, matrices $\tilde{\mathbf{D}}$ and 18 electric while $\tilde{\mathbf{Q}}$ contains 18 magnetic constants and finally matrices $\boldsymbol{\Sigma}$, $\mathbf{B}$ and Γ each contain 6 electro-magnetic constants. The crystallographic symmetry (relating to chosen coordinate axes) in the deformed electro-magneto-elastic body decreases substantially the number of independent constants in the equations above. For further information see [17, 30, 40, 46, 47, 54].

Taking into account that 3-D equations of the electro-magneto-elasticity presented here are the basis, for the development of the higher order theory of plates and shells it is convenient to write them in the curvilinear orthogonal system of coordinates related to the middle surface of the shell.

3 3-D Electro-Magneto-Elasticity in Coordinates Related to the Middle Surface

For convenience and the simplification of the higher order theory of plates and shells creation we are introducing here a new curvilinear system of coordinates related to the middle surface of the shell. In this case coordinates $\mathbf{x}_\alpha(x_1, x_2)$ are associated with the main curvatures k_1 and k_2 of the middle surface of the shell and coordinate x_3 is perpendicular to it. The position vector $\mathbf{R}(\mathbf{x})$ of any point in domain V, occupied by material points of the shell may be presented as

$$\mathbf{R}(\mathbf{x}) = \mathbf{r}(\mathbf{x}_\alpha) + x_3 \mathbf{n}(\mathbf{x}_\alpha) \tag{3.1}$$

where $\mathbf{r}(\mathbf{x}_\alpha)$ is the position vector of the points located in the middle line of the rod, and $\mathbf{n}(\mathbf{x}_\alpha)$ is a unit vector normal to the middle surface of the shell.

In this case the 3-D equations of the linear electro-magneto-elasticity presented here can be simplified by taking into account that Lamé coefficients and their derivatives have the form

$$H_\alpha = A_\alpha(1 + k_\alpha x_3) \quad \text{for } \alpha = 1, 2 \text{ and } H_3 = 1$$
$$\frac{\partial H_\beta}{\partial x_\alpha} = \frac{\partial A_\beta}{\partial x_\alpha}(1 + k_\alpha x_3), \ \frac{\partial H_\beta}{\partial x_3} = k_\beta A_\beta, \ \frac{\partial H_3}{\partial x_i} = 0 \tag{3.2}$$

Here $A_\alpha(x_1, x_2) = \sqrt{\mathbf{r}(x_1, x_2) \cdot \mathbf{r}(x_1, x_2)}$ are coefficients of the first quadratic form of a surface.

The equations of equilibrium and the Maxwell equations after simplification have the same form as it is presented in (2.6), but divergence of the stress tensor $\sigma_{ij}(\mathbf{x})$ and the electric $D_i(\mathbf{x})$ and magnetic $B_i(\mathbf{x})$ displacements take the form

$$\begin{aligned}
\nabla_j \sigma_{j\alpha} &= \frac{1}{A_1 A_2}\frac{\partial(A_2\sigma_{1\alpha})}{\partial x_1} + \frac{1}{A_1 A_2}\frac{\partial(A_1\sigma_{2\alpha})}{\partial x_2} + \frac{\partial \sigma_{3\alpha}}{\partial x_3} + \frac{\sigma_{\alpha\beta}}{A_1 A_2}\frac{\partial A_\alpha}{\partial x_\beta} - \frac{\sigma_{\beta\beta}}{A_1 A_2}\frac{\partial A_\beta}{\partial x_1} \\
&\quad + (k_1 + k_2)\sigma_{3\alpha} + k_\alpha \sigma_{\alpha 3} \\
\nabla_j \sigma_{j3} &= \frac{1}{A_1 A_2}\frac{\partial(A_2\sigma_{13})}{\partial x_1} + \frac{1}{A_1 A_2}\frac{\partial(A_1\sigma_{23})}{\partial x_2} + \frac{\partial \sigma_{33}}{\partial x_3} + (k_1 + k_2)\sigma_{33} - \frac{k_1}{A_1}\sigma_{11} - \frac{k_2}{A_2}\sigma_{22} \\
\nabla_i D_i &= \frac{1}{A_1}\frac{\partial D_1}{\partial x_1} + \frac{D_1}{A_1 A_2}\frac{\partial A_2}{\partial x_1} + \frac{1}{A_2}\frac{\partial D_2}{\partial x_2} + \frac{D_2}{A_1 A_2}\frac{\partial A_1}{\partial x_2} + (k_1 + k_2)D_3 + \frac{\partial D_3}{\partial x_3} \\
\nabla_i B_i &= \frac{1}{A_1}\frac{\partial B_1}{\partial x_1} + \frac{B_1}{A_1 A_2}\frac{\partial A_2}{\partial x_1} + \frac{1}{A_2}\frac{\partial B_2}{\partial x_2} + \frac{B_2}{A_1 A_2}\frac{\partial A_1}{\partial x_2} + (k_1 + k_2)B_3 + \frac{\partial B_3}{\partial x_3}
\end{aligned} \tag{3.3}$$

The infinitesimal strain tensor ε_{ij}, the electric field E_i and the magnetic field after simplification have the same form as it is presented in (2.8), but gradients of the displacement vector and the electric and magnetic potentials take the form

$$\begin{aligned}
\nabla_\beta u_\alpha &= \frac{1}{A_\alpha}\frac{\partial u_\alpha}{\partial x_\beta} - \frac{u_\beta}{A_\alpha A_\beta}\frac{\partial A_\beta}{\partial x_\alpha} + \delta_{\alpha\beta}\left(\sum_{\gamma=1}^{2}\frac{u_\gamma}{A_\alpha A_\gamma}\frac{\partial A_\alpha}{\partial x_\gamma} + k_\alpha u_3\right), \\
\nabla_\beta u_3 &= \frac{1}{H_\beta}\frac{\partial u_3}{\partial x_\beta} - k_\beta u_\beta, \quad \nabla_3 u_i = \frac{\partial u_i}{\partial x_3}, \quad \alpha, \beta = 1, 2, \quad i = 1, 2, 3, \\
\nabla_\alpha \phi &= \frac{1}{A_\alpha}\frac{\partial \phi}{\partial x_\alpha}, \quad \nabla_\alpha \varphi = \frac{1}{H_\alpha}\frac{\partial \varphi}{\partial x_\alpha}, \quad \nabla_3 \phi = \frac{\partial \phi}{\partial x_3}, \quad \nabla_3 \varphi = \frac{\partial \varphi}{\partial x_3}
\end{aligned} \tag{3.4}$$

After substituting (3.4) into relations (2.8) the infinitesimal strain tensor ε_{ij}, the electric field E_i and the magnetic field H_i are defined as

$$\begin{aligned}
&\varepsilon_{11} = \frac{1}{A_1}\frac{\partial u_1}{\partial x_1} + \frac{u_2}{A_1 A_2}\frac{\partial A_1}{\partial x_2} + k_1 u_3, \varepsilon_{12} = \frac{1}{2}\left(\frac{1}{A_1}\frac{\partial u_2}{\partial x_1} - \frac{u_1}{A_1 A_2}\frac{\partial A_1}{\partial x_2} + \frac{1}{A_2}\frac{\partial u_1}{\partial x_2} - \frac{u_2}{A_1 A_2}\frac{\partial A_2}{\partial x_1}\right), \varepsilon_{33} = \frac{\partial u_3}{\partial x_3}, \\
&\varepsilon_{13} = \frac{1}{2}\left(\frac{1}{A_1}\frac{\partial u_3}{\partial x_1} - k_1 u_1 + \frac{\partial u_1}{\partial x_3}\right), \varepsilon_{22} = \frac{1}{A_2}\frac{\partial u_2}{\partial x_2} + \frac{u_1}{A_1 A_2}\frac{\partial A_2}{\partial x_1} + k_2 u_3, \varepsilon_{23} = \frac{1}{2}\left(\frac{1}{A_2}\frac{\partial u_3}{\partial x_2} - k_2 u_2 + \frac{\partial u_2}{\partial x_3}\right) \\
&E_\alpha = \frac{1}{A_\alpha}\frac{\partial \phi}{\partial x_\alpha}, \quad E_3 = \frac{\partial \phi}{\partial x_3}, \quad M_\alpha = \frac{1}{A_\alpha}\frac{\partial \varphi}{\partial x_\alpha}, \quad M_3 = \frac{\partial \varphi}{\partial x_3}, \quad \alpha = 1, 2
\end{aligned} \tag{3.5}$$

The coupled system of differential equations of the linear electro-magneto-elasticity for the displacement vector as well as the electric and magnetic potentials has the form (2.13) and differential operators for a homogeneous generally anisotropic medium have the form

$$
\begin{aligned}
\mathbf{L}_{uu}\cdot\mathbf{u} &= \frac{\mathbf{e}_\alpha}{2A_1A_2}\sum_{k,l=1}^{3}\left(\sum_{j=1}^{3}\left(c_{\alpha jkl}\left(\frac{\partial}{\partial x_\alpha}\left(\frac{A_1A_2}{A_\alpha}\left(\nabla_l u_k+\nabla_k u_l\right)\right)+\frac{A_1A_2}{A_\alpha A_j}\frac{\partial A_j}{\partial x_\alpha}\left(\nabla_l u_k+\nabla_k u_l\right)\right)\right.\right.\\
&\quad\left.\left.-c_{\alpha\alpha kl}\frac{A_1A_2}{A_\alpha A_j}\frac{\partial A_\alpha}{\partial x_j}\left(\nabla_l u_k+\nabla_k u_l\right)\right)\right),\\
\mathbf{L}_{uu}\cdot\mathbf{u} &= \frac{\mathbf{e}_3}{2A_1A_2}\sum_{k,l=1}^{3}\left(\sum_{\beta=1}^{2}c_{3\beta kl}\left(\frac{\partial\left(\nabla_l u_k+\nabla_k u_l\right)}{\partial x_3}+(k_1+k_2)\left(\nabla_l u_k+\nabla_k u_l\right)+\frac{A_1A_2k_\beta}{A_\beta}\left(\nabla_l u_k+\nabla_k u_l\right)\right)\right.\\
&\quad\left.+c_{33kl}\left(\frac{\partial\left(\nabla_l u_k+\nabla_k u_l\right)}{\partial x_3}+(k_1+k_2)\left(\nabla_l u_k+\nabla_k u_l\right)\right)\right)\\
\mathbf{L}_{ue}\phi &= \frac{\mathbf{e}_\alpha}{2A_1A_2}\sum_{l=1}^{3}\left(\sum_{\beta=1}^{2}\left(e_{l\alpha j}\left(\frac{\partial}{\partial x_\alpha}\left(\frac{A_1A_2}{A_\alpha}\nabla_l\phi\right)+\frac{A_1A_2}{A_\alpha A_\beta}\frac{\partial A_\beta}{\partial x_\alpha}\nabla_l\phi\right)-e_{l\alpha\alpha}\left(\frac{A_1A_2}{A_\alpha A_\beta}\frac{\partial A_\alpha}{\partial x_\beta}\nabla_l\phi\right)\right)\right.\\
&\quad\left.+e_{l\alpha3}\frac{\partial}{\partial x_\alpha}\left(\frac{A_1A_2}{A_\alpha}\nabla_l\phi\right)-e_{l\alpha\alpha}\frac{A_1A_2k_\alpha}{A_\alpha}\nabla_l\phi\right)\\
\mathbf{L}_{ue}\phi &= \frac{\mathbf{e}_3}{2A_1A_2}\sum_{l=1}^{3}\left(\sum_{\beta=1}^{2}\left(e_{l3\beta}\left(\frac{\partial\nabla_l\phi}{\partial x_3}+(k_1+k_2)\nabla_l\phi+\frac{A_1A_2k_\beta}{A_\beta}\nabla_l\phi\right)+e_{l33}\left(\frac{\partial\nabla_l\phi}{\partial x_3}+(k_1+k_2)\nabla_l\phi\right)\right)\right.
\end{aligned}
\tag{3.6}
$$

$$
\begin{aligned}
\mathbf{L}_{um}\varphi &= \frac{\mathbf{e}_\alpha}{2A_1A_2}\sum_{l=1}^{3}\left(\sum_{\beta=1}^{2}\left(h_{l\alpha j}\left(\frac{\partial}{\partial x_\alpha}\left(\frac{A_1A_2}{A_\alpha}\nabla_l\varphi\right)+\frac{A_1A_2}{A_\alpha A_\beta}\frac{\partial A_\beta}{\partial x_\alpha}\nabla_l\varphi\right)-h_{l\alpha\alpha}\left(\frac{A_1A_2}{A_\alpha A_\beta}\frac{\partial A_\alpha}{\partial x_\beta}\nabla_l\varphi\right)\right)\right.\\
&\quad\left.+h_{l\alpha3}\frac{\partial}{\partial x_\alpha}\left(\frac{A_1A_2}{A_\alpha}\nabla_l\varphi\right)-h_{l\alpha\alpha}\frac{A_1A_2k_\alpha}{A_\alpha}\nabla_l\varphi\right)\\
\mathbf{L}_{um}\varphi &= \frac{\mathbf{e}_3}{2A_1A_2}\sum_{l=1}^{3}\left(\sum_{\beta=1}^{2}\left(h_{l3\beta}\left(\frac{\partial\nabla_l\varphi}{\partial x_3}+(k_1+k_2)\nabla_l\varphi+\frac{A_1A_2k_\beta}{A_\beta}\nabla_l\varphi\right)+h_{l33}\left(\frac{\partial\nabla_l\varphi}{\partial x_3}+(k_1+k_2)\nabla_l\varphi\right)\right)\right)\\
\mathbf{L}_{eu}\cdot\mathbf{u} &= \frac{1}{2A_1A_2}\sum_{k,l=1}^{3}\left(\sum_{\alpha=1}^{2}e_{\alpha kl}\frac{\partial}{\partial x_\alpha}\left(\frac{A_1A_2}{A_\alpha}\left(\nabla_l u_k+\nabla_k u_l\right)\right)+e_{3kl}\left((k_1+k_2)\left(\nabla_l u_k+\nabla_k u_l\right)+\frac{\partial}{\partial x_3}\left(\nabla_l u_k+\nabla_k u_l\right)\right)\right),\\
L_{ee}\phi &= \frac{1}{A_1A_2}\sum_{\beta,\alpha=1}^{2}\epsilon_{\alpha\beta}\frac{\partial}{\partial x_\alpha}\left(\frac{A_1A_2}{A_\alpha}\nabla_\beta\phi\right)+\frac{1}{A_1A_2}\sum_{\alpha=1}^{2}\epsilon_{\alpha3}\frac{\partial}{\partial x_\alpha}\left(\frac{A_1A_2}{A_\alpha}\frac{\partial\phi}{\partial x_3}\right)+\frac{1}{A_1A_2}\sum_{\beta=1}^{2}\epsilon_{3\beta}\frac{\partial}{\partial x_3}\left(A_1A_2\nabla_\beta\phi\right)\\
L_{em}\varphi &= \frac{1}{A_1A_2}\sum_{\beta,\alpha=1}^{2}\beta_{\alpha\beta}\frac{\partial}{\partial x_\alpha}\left(\frac{A_1A_2}{A_\alpha}\nabla_\beta\varphi\right)+\frac{1}{A_1A_2}\sum_{\alpha=1}^{2}\beta_{\alpha3}\frac{\partial}{\partial x_\alpha}\left(\frac{A_1A_2}{A_\alpha}\frac{\partial\varphi}{\partial x_3}\right)+\frac{1}{A_1A_2}\sum_{\beta=1}^{2}\beta_{3\beta}\frac{\partial}{\partial x_3}\left(A_1A_2\nabla_\beta\varphi\right)\\
\mathbf{L}_{mu}\cdot\mathbf{u} &= \frac{1}{2A_1A_2}\sum_{k,l=1}^{3}\left(\sum_{\alpha=1}^{2}h_{\alpha kl}\frac{\partial}{\partial x_\alpha}\left(\frac{H_1H_2}{H_\alpha}\left(\nabla_l u_k+\nabla_k u_l\right)\right)+h_{3kl}\left((k_1+k_2)\left(\nabla_l u_k+\nabla_k u_l\right)+\frac{\partial}{\partial x_3}\left(\nabla_l u_k+\nabla_k u_l\right)\right)\right),\\
L_{me}\phi &= \frac{1}{A_1A_2}\sum_{\beta,\alpha=1}^{2}\beta_{\alpha\beta}\frac{\partial}{\partial x_\alpha}\left(\frac{A_1A_2}{A_\alpha}\nabla_\beta\phi\right)+\frac{1}{A_1A_2}\sum_{\alpha=1}^{2}\beta_{\alpha3}\frac{\partial}{\partial x_\alpha}\left(\frac{A_1A_2}{A_\alpha}\frac{\partial\phi}{\partial x_3}\right)+\frac{1}{A_1A_2}\sum_{\beta=1}^{2}\beta_{3\beta}\frac{\partial}{\partial x_3}\left(A_1A_2\nabla_\beta\phi\right)\\
L_{mm}\varphi &= \frac{1}{A_1A_2}\sum_{\beta,\alpha=1}^{2}\gamma_{\alpha\beta}\frac{\partial}{\partial x_\alpha}\left(\frac{A_1A_2}{A_\alpha}\nabla_\beta\varphi\right)+\frac{1}{A_1A_2}\sum_{\alpha=1}^{2}\gamma_{\alpha3}\frac{\partial}{\partial x_\alpha}\left(\frac{A_1A_2}{A_\alpha}\frac{\partial\varphi}{\partial x_3}\right)+\frac{1}{A_1A_2}\sum_{\beta=1}^{2}\gamma_{3\beta}\frac{\partial}{\partial x_3}\left(A_1A_2\nabla_\beta\varphi\right)
\end{aligned}
$$

In this section, the system of differential equations of the 3-D linear electro-magneto-elasticity in a special system of coordinates related to the middle surface of the shell is considered in detail. These equations will be used in the next sections for the development of the approximate 2-D theories of plates and shells.

4 2-D Formulation of the Problem

We expand the physical parameters, that describe the thermodynamic state of the electro-magneto-elastic body into the Legendre polynomials series along the coordinate x_3. Such expansion can be done because of any function $f(p)$, which is defined in domain $-1 \le p \le 1$ and satisfies Dirichlet's conditions (continuous, monotonous, and having a finite set of discontinuity points), can be expanded into Legendre's series according to formulas

$$f(p) = \sum_{k=0}^{\infty} a_k P_k(p) \quad \text{where} \quad a_n = \frac{2k+1}{2} \int_{-1}^{1} f(p) P_k(p) dp \tag{4.1}$$

Any function of more than one independent variable can also be expanded into Legendre's series with respect to for example, variable $x_3 \in [-1, 1]$, but first the new normalized variable $\omega = x_3/h \in [-1, 1]$ has to be introduced.

Taking into account (4.1) we transform the 3-D electro-magneto-elastic problem into a 2-D one, by expanding all the parameters that describe stress-strain of the shell in the Legendre polynomials series along the coordinate x_3.

For electrical field parameters we have

$$\begin{aligned}
\phi(\mathbf{x}) &= \sum_{k=0}^{\infty} \phi^k(\mathbf{x}_\alpha) P_k(\varpi), \quad \phi^k(\mathbf{x}_\alpha) = \frac{2k+1}{2h} \int_{-h}^{h} \phi(\mathbf{x}_\alpha, x_3) P_k(\varpi) dx_3, \\
E_i(\mathbf{x}) &= \sum_{k=0}^{\infty} E_i^k(\mathbf{x}_\alpha) P_k(\varpi), \quad E_i^k(\mathbf{x}_\alpha) = \frac{2k+1}{2h} \int_{-h}^{h} E_i(\mathbf{x}_\alpha, x_3) P_k(\varpi) dx_3, \\
D_i(\mathbf{x}) &= \sum_{k=0}^{\infty} D_i^k(\mathbf{x}_\alpha) P_k \varpi), \quad D_i^k(\mathbf{x}_\alpha) = \frac{2k+1}{2h} \int_{-h}^{h} D_i(\mathbf{x}_\alpha, x_3) P_k(\varpi) dx_3,
\end{aligned} \tag{4.2}$$

For magnetical field parameters we have

$$\begin{aligned}
\varphi(\mathbf{x}) &= \sum_{k=0}^{\infty} \varphi^k(\mathbf{x}_\alpha) P_k(\varpi), \quad \varphi^k(\mathbf{x}_\alpha) = \frac{2k+1}{2h} \int_{-h}^{h} \varphi(\mathbf{x}_\alpha, x_3) P_k(\varpi) dx_3, \\
M_i(\mathbf{x}) &= \sum_{k=0}^{\infty} M_i^k(\mathbf{x}_\alpha) P_k(\varpi), \quad M_i^k(\mathbf{x}_\alpha) = \frac{2k+1}{2h} \int_{-h}^{h} M_i(\mathbf{x}_\alpha, x_3) P_k(\varpi) dx_3, \\
B_i(\mathbf{x}) &= \sum_{k=0}^{\infty} B_i^k(\mathbf{x}_\alpha) P_k \varpi), \quad B_i^k(\mathbf{x}_\alpha) = \frac{2k+1}{2h} \int_{-h}^{h} B_i(\mathbf{x}_\alpha, x_3) P_k(\varpi) dx_3,
\end{aligned} \tag{4.3}$$

For stress-strain field we have

$$u_i(\mathbf{x}) = \sum_{k=0}^{\infty} u_i^k(\mathbf{x}_\alpha) P_k(\varpi), \quad u_i^k(\mathbf{x}_\alpha) = \frac{2k+1}{2h} \int_{-h}^{h} u_i(\mathbf{x}_\alpha, x_3) P_k(\varpi) dx_3,$$
$$\sigma_{ij}(\mathbf{x}) = \sum_{k=0}^{\infty} \sigma_{ij}^k(\mathbf{x}_\alpha) P_k(\varpi), \quad \sigma_{ij}^k(\mathbf{x}_\alpha) = \frac{2k+1}{2h} \int_{-h}^{h} \sigma_{ij}(\mathbf{x}_\alpha, x_3) P_k(\varpi) dx_{33},$$
$$\varepsilon_{ij}(\mathbf{x}) = \sum_{k=0}^{\infty} \varepsilon_{ij}^k(\mathbf{x}_\alpha) P_k(\varpi), \quad \varepsilon_{ij}^k(\mathbf{x}_\alpha) = \frac{2k+1}{2h} \int_{-h}^{h} \varepsilon_{ij}(\mathbf{x}_\alpha, x_3) P_k(\varpi) dx_3, \quad (4.4)$$

For derivatives with respect to coordinates $\boldsymbol{x}_\alpha$, the following relations take place

$$\frac{2k+1}{2h} \int_{-h}^{h} \frac{\partial u_i(\mathbf{x}_\alpha, x_3, t)}{\partial x_\alpha} P_k(\varpi) dx_3 = \frac{\partial u_i^k(\mathbf{x}_\alpha, t)}{\partial x_\alpha}, \quad \frac{2k+1}{2h} \int_{-h}^{h} \frac{\partial \sigma_{ij}(\mathbf{x}_\alpha, x_3, t)}{\partial x_\alpha} P_k(\varpi) dx_3 = \frac{\partial \sigma_{ij}^k(\mathbf{x}_\alpha, t)}{\partial x_\alpha},$$
$$\frac{2k+1}{2h} \int_{-h}^{h} \frac{\partial \phi(\mathbf{x}_\alpha, x_3, t)}{\partial x_\alpha} P_k(\varpi) dx_2 = \frac{\partial \phi^k(\mathbf{x}_\alpha, t)}{\partial x_\alpha}, \quad \frac{2k+1}{2h} \int_{-h}^{h} \frac{\partial \varphi(\mathbf{x}_\alpha, x_3, t)}{\partial x_\alpha} P_k(\varpi) dx_2 = \frac{\partial \varphi^k(\mathbf{x}_\alpha, t)}{\partial x_\alpha},$$
$$\frac{2k+1}{2h} \int_{-h}^{h} \frac{\partial E_i(\mathbf{x}_\alpha, x_3, t)}{\partial x_\alpha} P_k(\varpi) dx_3 = \frac{\partial E_i^k(\mathbf{x}_\alpha, t)}{\partial x_\alpha}, \quad \frac{2k+1}{2h} \int_{-h}^{h} \frac{\partial M_i(\mathbf{x}_\alpha, x_3, t)}{\partial x_\alpha} P_k(\varpi) dx_3 = \frac{\partial M_i^k(\mathbf{x}_\alpha, t)}{\partial x_\alpha} \quad (4.5)$$

Derivatives of the displacements, electrical and magnetic potentials with respect to x_3 following [66, 84] can be represented in the form

$$\frac{2k+1}{2h} \int_{-h}^{h} \frac{\partial u_i(\mathbf{x}_\alpha, x_3)}{\partial x_3} P_k(\varpi) dx_3 = \underline{u_i^k}(\mathbf{x}_\alpha),$$
$$\frac{2k+1}{2h} \int_{-h}^{h} \frac{\partial \phi(\mathbf{x}_\alpha, x_3)}{\partial x_3} P_k(\varpi) dx_3 = \underline{\phi^k}(\mathbf{x}_\alpha),$$
$$\frac{2k+1}{2h} \int_{-h}^{h} \frac{\partial \varphi(\mathbf{x}_\alpha, x_3)}{\partial x_3} P_k(\varpi) dx_3 = \underline{\varphi^k}(\mathbf{x}_\alpha) \quad (4.6)$$

where

$$\underline{u_i^k}(\mathbf{x}_\alpha) = \frac{2k+1}{h} \left(u_i^{k+1}(\mathbf{x}_\alpha) + u_i^{k+3}(\mathbf{x}_\alpha) + \ldots \right),$$
$$\underline{\phi^k}(\mathbf{x}_\alpha) = \frac{2k+1}{h} \left(\phi^{k+1}(\mathbf{x}_\alpha) + \phi^{k+3}(\mathbf{x}_\alpha) + \ldots \right),$$
$$\underline{\varphi^k}(\mathbf{x}_\alpha) = \frac{2k+1}{h} \left(\varphi^{k+1}(\mathbf{x}_\alpha) + \varphi^{k+3}(\mathbf{x}_\alpha) + \ldots \right), \quad (4.7)$$

In the Eqs. (4.6) for the derivative of functions $u_i(\mathbf{x}_\alpha, x_3)$, $\phi(\mathbf{x}_\alpha, x_3)$ and $\varphi(\mathbf{x}_\alpha, x_3)$ the following representations have been used

$$\frac{\partial u_i(\mathbf{x}_\alpha, x_3)}{\partial x_3} = \frac{1}{h}\sum_{k=0}^{\infty} u_i^k(\mathbf{x}_\alpha)\frac{\partial P_k(\varpi)}{\partial x_3}, \quad \frac{\partial \phi(\mathbf{x}_\alpha, x_3)}{\partial x_3} = \frac{1}{h}\sum_{k=0}^{\infty} \phi_i^k(\mathbf{x}_\alpha)\frac{\partial P_k(\varpi)}{\partial x_3},$$
$$\frac{\partial \varphi(\mathbf{x}_\alpha, x_3)}{\partial x_3} = \frac{1}{h}\sum_{k=0}^{\infty} \varphi_i^k(\mathbf{x}_\alpha)\frac{\partial P_k(\varpi)}{\partial x_3} \tag{4.8}$$

and the following relation between Legendre polynomials and their derivatives [50, 73]

$$\frac{\partial P_k(\varpi)}{\partial \varpi} = ((2k-1)P_{k-1}(\varpi) + (2k-5)P_{k-3}(\varpi) + \dots) \tag{4.9}$$

Derivatives of electric and magnetic displacement vectors and the stress tensor with respect to x_3 can be transformed using integration by parts and formulas (4.9). Finally, they can be represented in the form

$$\frac{2k+1}{2h}\int_{-h}^{h}\frac{\partial D_3(\mathbf{x}_\alpha, x_3)}{\partial x_3}P_k(\varpi)dx_3 = \frac{2k+1}{h}\left[D_3^+(\mathbf{x}_\alpha) - (-1)^k D_3^-(\mathbf{x}_\alpha)\right] - \underline{D_3^k}(\mathbf{x}_\alpha),$$
$$\frac{2k+1}{2h}\int_{-h}^{h}\frac{\partial B_3(\mathbf{x}_\alpha, x_3)}{\partial x_3}P_k(\varpi)dx_3 = \frac{2k+1}{h}\left[B_3^+(\mathbf{x}_\alpha) - (-1)^k B_3^-(\mathbf{x}_\alpha)\right] - \underline{B_3^k}(\mathbf{x}_\alpha),$$
$$\frac{2k+1}{2h}\int_{-h}^{h}\frac{\partial \sigma_{3i}(\mathbf{x}_\alpha, x_3)}{\partial x_3}P_k(\varpi)dx_3 = \frac{2k+1}{h}\left[\sigma_{3i}^+(\mathbf{x}_\alpha) - (-1)^k \sigma_{3i}^-(\mathbf{x}_\alpha)\right] - \underline{\sigma_{3i}^k}(\mathbf{x}_\alpha), \tag{4.10}$$

where

$$\underline{D_3^k} = \frac{2k+1}{h}\left(D_3^{k-1} + D_3^{k-3} + \dots\right), \underline{B_3^k} = \frac{2k+1}{h}\left(B_3^{k-1} + B_3^{k-3} + \dots\right), \underline{\sigma_{3i}^k} = \frac{2k+1}{h}\left(\sigma_{3i}^{k-1} + \sigma_{3i}^{k-3} + \dots\right) \tag{4.11}$$

Now, by substituting the Legendre's polynomial coefficients of the stress tensor (4.4), electric (4.2) and magnetic (4.3) displacements into the equations of equilibrium and the Maxwell equations (2.6), and taking into account (3.3) and (4.10) we obtain 2-D equations of equilibrium and Maxwell equations in the form

$$\tilde{\nabla}_j \sigma_{ji}^k + \tilde{b}_i^k = 0, \quad \tilde{\nabla}_i D_i^k = \tilde{b}_e^k, \quad \tilde{\nabla}_i B_i^k = \tilde{b}_m^k = 0 \tag{4.12}$$

where divergences of the corresponding tensor and vector components have the form

$$\begin{aligned}
\tilde{\nabla}_j\sigma^k_{j\alpha} &= \frac{1}{A_1A_2}\frac{\partial(A_2\sigma^k_{1\alpha})}{\partial x_1} + \frac{1}{A_1A_2}\frac{\partial(A_1\sigma^k_{2\alpha})}{\partial x_2} + \frac{\sigma^k_{\alpha\beta}}{A_1A_2}\frac{\partial A_\alpha}{\partial x_\beta} - \frac{\sigma^k_{\beta\beta}}{A_1A_2}\frac{\partial A_\beta}{\partial x_1} \\
&\quad + (k_1+k_2)\sigma^k_{3\alpha} + k_\alpha\sigma^k_{\alpha 3} - \underline{\sigma^k_{3\alpha}} \\
\tilde{\nabla}_j\sigma^k_{j3} &= \frac{1}{A_1A_2}\frac{\partial(A_2\sigma^k_{13})}{\partial x_1} + \frac{1}{A_1A_2}\frac{\partial(A_1\sigma^k_{23})}{\partial x_2} + (k_1+k_2)\sigma^k_{33} - \frac{k_1}{A_1}\sigma^k_{11} - \frac{k_2}{A_2}\sigma^k_{22} - \underline{\sigma^k_{33}} \\
\tilde{\nabla}_i D^k_i &= \frac{1}{A_1}\frac{\partial D^k_1}{\partial x_1} + \frac{D^k_1}{A_1A_2}\frac{\partial A_2}{\partial x_1} + \frac{1}{A_2}\frac{\partial D^k_2}{\partial x_2} + \frac{D^k_2}{A_1A_2}\frac{\partial A_1}{\partial x_2} + (k_1+k_2)D^k_3 - \underline{D^k_3} \\
\tilde{\nabla}_i B^k_i &= \frac{1}{A_1}\frac{\partial B^k_1}{\partial x_1} + \frac{B^k_1}{A_1A_2}\frac{\partial A_2}{\partial x_1} + \frac{1}{A_2}\frac{\partial B^k_2}{\partial x_2} + \frac{B^k_2}{A_1A_2}\frac{\partial A_1}{\partial x_2} + (k_1+k_2)B^k_3 - \underline{B^k_3}
\end{aligned} \tag{4.13}$$

where

$$\begin{aligned}
&\tilde{b}^k_i = b^k_i + \frac{2k+1}{h}\left(\sigma^+_{3i} - (-1)^k\sigma^-_{3i}\right),\ \tilde{b}^k_e = b^k_e + \frac{2k+1}{h}\left(D^+_3 - (-1)^k D^-_3\right), \\
&\tilde{b}^k_m = b^k_m + \frac{2k+1}{h}\left(B^+_3 - (-1)^k B^-_3\right)
\end{aligned} \tag{4.14}$$

In the same way, by substituting the Legendre's polynomial coefficients for displacement vector (4.4), electric (4.2) and magnetic potentials in (3.5) and taking into account (4.5) and (4.6) the 2-D expressions for the Cauchy strain tensor, electric field and the magnetic field vectors can be found in the form

$$\begin{aligned}
&\varepsilon^k_{11} = \frac{1}{A_1}\frac{\partial u^k_1}{\partial x_1} + \frac{u^k_2}{A_1A_2}\frac{\partial A_1}{\partial x_2} + k_1u^k_3,\quad \varepsilon^k_{12} = \frac{1}{2}\left(\frac{1}{A_1}\frac{\partial u^k_2}{\partial x_1} - \frac{u^k_1}{A_1A_2}\frac{\partial A_1}{\partial x_2} + \frac{1}{A_2}\frac{\partial u^k_1}{\partial x_2} - \frac{u^k_2}{A_1A_2}\frac{\partial A_2}{\partial x_1}\right),\quad \varepsilon_{33} = \underline{u^k_3}, \\
&\varepsilon^k_{13} = \frac{1}{2}\left(\frac{1}{A_1}\frac{\partial u^k_3}{\partial x_1} - k_1u^k_1 + \underline{u^k_1}\right),\quad \varepsilon^k_{22} = \frac{1}{A_2}\frac{\partial u^k_2}{\partial x_2} + \frac{u^k_1}{A_1A_2}\frac{\partial A_2}{\partial x_1} + k_2u^k_3,\quad \varepsilon^k_{23} = \frac{1}{2}\left(\frac{1}{A_2}\frac{\partial u^k_3}{\partial x_2} - k_2u^k_2 + \underline{u^k_2}\right), \\
&E^k_\alpha = \frac{1}{A_\alpha}\frac{\partial\phi^k}{\partial x_\alpha},\quad E^k_3 = \underline{\phi^k},\quad M^k_\alpha = \frac{1}{A_\alpha}\frac{\partial\varphi^k}{\partial x_\alpha},\quad M^k_3 = \underline{\varphi^k},\quad \alpha = 1,2
\end{aligned} \tag{4.15}$$

The constitutive relations for electro-magneto-elasticity following customary engineering applications notations (2.22) for the Legendre's polynomial coefficients (4.2)–(4.4) have the form

$$\begin{aligned}
\tilde{\boldsymbol{\sigma}}^k &= \tilde{\mathbf{C}}\cdot\tilde{\boldsymbol{\varepsilon}}^k - \tilde{\mathbf{D}}\cdot\mathbf{E}^k - \tilde{\mathbf{Q}}\cdot\mathbf{M}^k, \\
\mathbf{D}^k &= \tilde{\mathbf{D}}\cdot\tilde{\boldsymbol{\varepsilon}}^k + \boldsymbol{\Sigma}\cdot\mathbf{E}^k + \mathbf{B}\cdot\mathbf{M}^k, \\
\mathbf{B}^k &= \tilde{\mathbf{Q}}\cdot\tilde{\boldsymbol{\varepsilon}}^k + \mathbf{B}\cdot\mathbf{E}^k + \Gamma\cdot\mathbf{M}^k.
\end{aligned} \tag{4.16}$$

In the same way as in the 3-D case, by substituting relations (4.15) into constitutive relations (4.16) and the obtained result into the equations of equilibrium and Maxwell equations (4.12) the couples differential equations of the electro-magneto-elasticity in form of the Legendre's polynomial coefficients of displacement vector, electric and magnetic potentials can be obtained.

As result of the performed transformations instead of the 3-D system of the differential equations in (2.13) with coefficients (3.6) we have an infinite system of 2-D differential equations for coefficients of the Legendre's polynomial series expansion. In order to simplify the problem an approximate theory has to be developed where only a finite number of members have to be taken into account in the (4.2)–(4.4) and in all of the relations above. For example, if we consider the n-order approximate shell theory, only $n+1$ members in the expansion (4.2)–(4.4) are taken into account

$$\begin{aligned}
&\phi(\mathbf{x}) = \sum_{k=0}^{n} \phi^k(\mathbf{x}_\alpha) P_k(\varpi), \quad E_i(\mathbf{x}) = \sum_{k=0}^{n} E_i^k(\mathbf{x}_\alpha) P_k(\varpi), \quad D_i(\mathbf{x}) = \sum_{k=0}^{n} D_i^k(\mathbf{x}_\alpha) P_k \varpi),\\
&\varphi(\mathbf{x}) = \sum_{k=0}^{n} \varphi^k(\mathbf{x}_\alpha) P_k(\varpi), \quad M_i(\mathbf{x}) = \sum_{k=0}^{n} M_i^k(\mathbf{x}_\alpha) P_k(\varpi), \quad B_i(\mathbf{x}) = \sum_{k=0}^{n} B_i^k(\mathbf{x}_\alpha) P_k \varpi),\\
&u_i(\mathbf{x}) = \sum_{k=0}^{n} u_i^k(\mathbf{x}_\alpha) P_k(\varpi), \quad \sigma_{ij}(\mathbf{x}) = \sum_{k=0}^{n} \sigma_{ij}^k(\mathbf{x}_\alpha) P_k(\varpi), \quad \varepsilon_{ij}(\mathbf{x}) = \sum_{k=0}^{n} \varepsilon_{ij}^k(\mathbf{x}_\alpha) P_k(\varpi),
\end{aligned} \tag{4.17}$$

In this case we consider that $u_i^k = 0$, $\omega_i^k = 0$, $\sigma_{ij}^k = 0$, $\mu_i^k = 0$, $\boldsymbol{\varepsilon}^k = 0$ and $\kappa_i^k = 0$ for $k < 0$ and for $k > n$.

Then, the 2-D system of differential equations of the electro-magneto-elasticity for n-order theory of shells can be presented in the matrix form. It has the same form like 3-D system of differential equations (2.13), but differential operators $\mathbf{L}_{uu}, \ldots, L_{mm}$ are block matrices of the form

$$\begin{aligned}
\mathbf{L}_{uu} &= \begin{vmatrix} \mathbf{L}_{uu}^{00} & \cdots & \mathbf{L}_{uu}^{0n} \\ \vdots & \ddots & \vdots \\ \mathbf{L}_{uu}^{n0} & \cdots & \mathbf{L}_{uu}^{nn} \end{vmatrix}, \quad \mathbf{L}_{ue} = \begin{vmatrix} \mathbf{L}_{ue}^{00} & \cdots & \mathbf{L}_{ue}^{0n} \\ \vdots & \ddots & \vdots \\ \mathbf{L}_{ue}^{n0} & \cdots & \mathbf{L}_{ue}^{nn} \end{vmatrix}, \quad \mathbf{L}_{um} = \begin{vmatrix} \mathbf{L}_{um}^{00} & \cdots & \mathbf{L}_{um}^{0n} \\ \vdots & \ddots & \vdots \\ \mathbf{L}_{um}^{n0} & \cdots & \mathbf{L}_{um}^{nn} \end{vmatrix},\\
\mathbf{L}_{eu} &= \begin{vmatrix} \mathbf{L}_{eu}^{00} & \cdots & \mathbf{L}_{eu}^{0n} \\ \vdots & \ddots & \vdots \\ \mathbf{L}_{eu}^{n0} & \cdots & \mathbf{L}_{eu}^{nn} \end{vmatrix}, \quad L_{ee} = \begin{vmatrix} L_{ee}^{00} & \cdots & L_{ee}^{0n} \\ \vdots & \ddots & \vdots \\ L_{ee}^{n0} & \cdots & L_{ee}^{nn} \end{vmatrix}, \quad L_{em} = \begin{vmatrix} L_{em}^{00} & \cdots & L_{em}^{0n} \\ \vdots & \ddots & \vdots \\ L_{em}^{n0} & \cdots & L_{em}^{nn} \end{vmatrix}\\
\mathbf{L}_{mu} &= \begin{vmatrix} \mathbf{L}_{mu}^{00} & \cdots & \mathbf{L}_{mu}^{0n} \\ \vdots & \ddots & \vdots \\ \mathbf{L}_{mu}^{n0} & \cdots & \mathbf{L}_{mu}^{nn} \end{vmatrix}, \quad L_{me} = \begin{vmatrix} L_{me}^{00} & \cdots & L_{me}^{0n} \\ \vdots & \ddots & \vdots \\ L_{me}^{n0} & \cdots & L_{me}^{nn} \end{vmatrix}, \quad L_{mm} = \begin{vmatrix} L_{mm}^{00} & \cdots & L_{mm}^{0n} \\ \vdots & \ddots & \vdots \\ L_{mm}^{n0} & \cdots & L_{mm}^{nn} \end{vmatrix}
\end{aligned} \tag{4.18}$$

and $\mathbf{u}$, ϕ, φ, $\mathbf{b}$, b_e and b_m are block vectors of the form

$$\mathbf{u} = \begin{vmatrix} \mathbf{u}^0 \\ \vdots \\ \mathbf{u}^n \end{vmatrix}, \phi = \begin{vmatrix} \phi^0 \\ \vdots \\ \phi^n \end{vmatrix}, \varphi = \begin{vmatrix} \varphi^0 \\ \vdots \\ \varphi^n \end{vmatrix}, \mathbf{b} = \begin{vmatrix} \mathbf{b}^0 \\ \vdots \\ \mathbf{b}^n \end{vmatrix}, b_e = \begin{vmatrix} b_e^0 \\ \vdots \\ b_e^n \end{vmatrix}, b_m = \begin{vmatrix} b_m^0 \\ \vdots \\ b_m^n \end{vmatrix} \tag{4.19}$$

The block matrices $\mathbf{L}_{uu}$, $\mathbf{L}_{ue}$,$\mathbf{L}_{um}$, $\mathbf{L}_{eu}$, $\mathbf{L}_{mu}$ in (4.18) can be represented in the form of 3-D matrix differential operators

$$\mathbf{L}_{uu}^{rk} = \begin{vmatrix} L_{11}^{rk} & L_{12}^{rk} & L_{13}^{rk} \\ L_{21}^{rk} & L_{22}^{rk} & L_{23}^{rk} \\ L_{31}^{rk} & L_{32}^{rk} & L_{33}^{rk} \end{vmatrix}, \quad \mathbf{L}_{eu}^{rk} = \begin{vmatrix} L_{e1}^{rk} \\ L_{e2}^{rk} \\ L_{e2}^{rk} \end{vmatrix}, \quad \mathbf{L}_{mu}^{rk} = \begin{vmatrix} L_{m1}^{rk} \\ L_{m2}^{rk} \\ L_{m2}^{rk} \end{vmatrix},$$
$$\mathbf{L}_{ue}^{rk} = \begin{vmatrix} L_{1e}^{rk} & L_{2e}^{rk} & L_{3e}^{rk} \end{vmatrix}, \quad \mathbf{L}_{um}^{rk} = \begin{vmatrix} L_{1m}^{rk} & L_{2m}^{rk} & L_{3m}^{rk} \end{vmatrix} \tag{4.20}$$

and block vectors $\mathbf{u}$ and $\mathbf{b}$ in (4.19) as 3-D vectors

$$\mathbf{u}^{k} = \begin{vmatrix} u_1^k \\ u_2^k \\ u_3^k \end{vmatrix}, \quad \mathbf{b}^{k} = \begin{vmatrix} b_1^k \\ b_2^k \\ b_3^k \end{vmatrix} \tag{4.21}$$

The order of the system of differential equations depends on the assumption regarding thickness distribution of the stress-strain and electro-magnetic parameters of the shell. The higher the order of approximation, the better accuracy of the result obtained using the proposed theory. The complete system of linear differential equations of the electro-magneto-elasticity of any order can be obtained using the equations presented here. For the first order approximation block matrices (4.18) have the form

$$\mathbf{L}_{uu} = \begin{vmatrix} \mathbf{L}_{uu}^{00} & \mathbf{L}_{uu}^{01} \\ \mathbf{L}_{uu}^{10} & \mathbf{L}_{uu}^{11} \end{vmatrix}, \quad \mathbf{L}_{ue} = \begin{vmatrix} \mathbf{L}_{ue}^{00} & \mathbf{L}_{ue}^{01} \\ \mathbf{L}_{ue}^{10} & \mathbf{L}_{ue}^{11} \end{vmatrix}, \quad \mathbf{L}_{um} = \begin{vmatrix} \mathbf{L}_{um}^{00} & \mathbf{L}_{um}^{01} \\ \mathbf{L}_{um}^{10} & \mathbf{L}_{um}^{11} \end{vmatrix},$$
$$\mathbf{L}_{eu} = \begin{vmatrix} \mathbf{L}_{eu}^{00} & \mathbf{L}_{eu}^{01} \\ \mathbf{L}_{eu}^{10} & \mathbf{L}_{eu}^{11} \end{vmatrix}, \quad L_{ee} = \begin{vmatrix} L_{ee}^{00} & L_{ee}^{01} \\ L_{ee}^{10} & L_{ee}^{11} \end{vmatrix}, \quad L_{em} = \begin{vmatrix} L_{em}^{00} & L_{em}^{01} \\ L_{em}^{10} & L_{em}^{11} \end{vmatrix},$$
$$\mathbf{L}_{mu} = \begin{vmatrix} \mathbf{L}_{mu}^{00} & \mathbf{L}_{mu}^{01} \\ \mathbf{L}_{mu}^{10} & \mathbf{L}_{mu}^{11} \end{vmatrix}, \quad L_{me} = \begin{vmatrix} L_{me}^{00} & L_{me}^{01} \\ L_{me}^{10} & L_{me}^{11} \end{vmatrix}, \quad L_{mm} = \begin{vmatrix} L_{mm}^{00} & L_{mm}^{01} \\ L_{mm}^{10} & L_{mm}^{11} \end{vmatrix}, \tag{4.22}$$

and block vectors

$$\mathbf{u} = \begin{vmatrix} \mathbf{u}^0 \\ \mathbf{u}^1 \end{vmatrix}, \quad \phi = \begin{vmatrix} \phi^0 \\ \phi^1 \end{vmatrix}, \quad \varphi = \begin{vmatrix} \varphi^0 \\ \varphi^1 \end{vmatrix}, \quad \mathbf{b} = \begin{vmatrix} \mathbf{b}^0 \\ \mathbf{b}^1 \end{vmatrix}, \quad b_e == \begin{vmatrix} b_e^0 \\ b_e^1 \end{vmatrix}, \quad b_m = \begin{vmatrix} b_m^0 \\ b_m^1 \end{vmatrix} \tag{4.23}$$

In the next sections, we will consider the applications of the approach developed here to the plates in Cartesian and polar coordinates as well as for cylindrical and spherical shells. The first order approximation theory will be considered in more detail.

5 Higher Order Theory of Electro-Magneto-Elastic Plates in Cartesian Coordinates

All of the above equations of the electro-magneto-elastic theory become much simpler for the case plates. Let us first consider the plate in Cartesian coordinates. In order to simplify and present the corresponding equations in the traditional form we introduce the Cartesian coordinates $x_1 = x$, $x_2 = y$ and $x_3 = z$. In this case, coefficients of the first quadratic form of a surface and main curvatures are equal to $A_1 = 1, A_2 = 1, k_1 = k_2 = 0$. After the substitution of those parameters in all of the above equations, the equations that correspond to the higher order theory of linear electro-magneto-elasticity of the plates in Cartesian coordinates will be obtained.

The equations of equilibrium and the Maxwell equations for Legendre's polynomial coefficients in this case have the form (4.12) but the operator of divergence of the stress tensor and the electric and magnetic displacement vectors in the Cartesian system of coordinates have the form

$$\tilde{\nabla}_\alpha \sigma^k_{\alpha x} = \frac{\partial \sigma^k_{xx}}{\partial x} + \frac{\partial \sigma^k_{yx}}{\partial y} - \underline{\sigma^k_{zx}}, \quad \tilde{\nabla}_\alpha \sigma^k_{\alpha y} = \frac{\partial \sigma^k_{xy}}{\partial x} + \frac{\partial \sigma^k_{yy}}{\partial y} - \underline{\sigma^k_{zy}}, \quad \tilde{\nabla}_\alpha \sigma^k_{\alpha z} = \frac{\partial \sigma^k_{xz}}{\partial x} + \frac{\partial \sigma^k_{yz}}{\partial y} - \underline{\sigma^k_{zz}},$$
$$\tilde{\nabla}_\alpha D^k_\alpha = \frac{\partial D^k_x}{\partial x} + \frac{\partial D^k_y}{\partial y} - \underline{D^k_z}, \quad \tilde{\nabla}_\alpha B^k_\alpha = \frac{\partial B^k_x}{\partial x} + \frac{\partial B^k_y}{\partial y} - \underline{B^k_z}, \quad \alpha = x, y. \tag{5.1}$$

where

$$\underline{\sigma^k_{zi}} = \frac{2k+1}{h}\left(\sigma^{k-1}_{zi} + \sigma^{k-3}_{zi} + \ldots\right), i = x, y, z,$$
$$\underline{D^k_z} = \frac{2k+1}{h}\left(D^{k-1}_z + D^{k-3}_z + \ldots\right), \underline{B^k_z} = \frac{2k+1}{h}\left(B^{k-1}_z + B^{k-3}_z + \ldots\right) \tag{5.2}$$

Expressions for the Legendre's polynomial coefficients of the Cauchy strain tensor, electric field and the magnetic field vectors in this case have the form

$$\varepsilon^k_{xx} = \frac{\partial u^k_x}{\partial x}, \quad \varepsilon^k_{xy} = \frac{1}{2}\left(\frac{\partial u^k_y}{\partial x} + \frac{\partial u^k_x}{\partial y}\right), \quad \varepsilon_{zz} = \underline{u^k_z},$$
$$\varepsilon^k_{xz} = \frac{1}{2}\left(\frac{\partial u^k_z}{\partial x} + \underline{u^k_x}\right), \quad \varepsilon^k_{yy} = \frac{\partial u^k_y}{\partial y}, \quad \varepsilon^k_{yz} = \frac{1}{2}\left(\frac{\partial u^k_z}{\partial y} + \underline{u^k_y}\right)$$
$$E^k_x = \frac{\partial \phi^k}{\partial x}, \quad E^k_y = \frac{\partial \phi^k}{\partial y}, \quad E^k_z = \underline{\phi^k}, \quad M^k_x = \frac{\partial \varphi^k}{\partial x}, \quad M^k_y = \frac{\partial \varphi^k}{\partial y}, \quad M^k_z = \underline{\varphi^k} \tag{5.3}$$

where $\underline{\phi^k}$ and $\underline{\varphi^k}$ are defined in (4.7) and $\underline{u^k_i}$ is presented as

$$\underline{u^k_i} = \frac{2k+1}{h}\left(u^{k+1}_i + u^{k+3}_i + \ldots\right), \quad i = x, y, z. \tag{5.4}$$

Presented above equations of the electro-magneto-elasticity for the general case of homogeneous anisotropic material are very complicate. In order to simplify them and present here important for applications examples following [17, 30, 46, 54] we consider material with hexagonal crystal structure (class 6 mm), which is polarized in the direction of the axis z. In this case the electro-magneto-elastic constants become significantly simplified and have the form

$$\tilde{\mathbf{C}} = \begin{vmatrix} c_{11} & c_{12} & c_{13} & 0 & 0 & 0 \\ c_{12} & c_{11} & c_{13} & 0 & 0 & 0 \\ c_{13} & c_{13} & c_{33} & 0 & 0 & 0 \\ 0 & 0 & 0 & c_{44} & 0 & 0 \\ 0 & 0 & 0 & 0 & c_{44} & 0 \\ 0 & 0 & 0 & 0 & 0 & (c_{11}-c_{12})/2 \end{vmatrix}, \quad \tilde{\mathbf{D}} = \begin{vmatrix} 0 & 0 & d_{13} \\ 0 & 0 & d_{13} \\ 0 & 0 & d_{33} \\ 0 & d_{51} & 0 \\ d_{51} & 0 & 0 \\ 0 & 0 & 0 \end{vmatrix},$$

$$\tilde{\mathbf{Q}} = \begin{vmatrix} 0 & 0 & q_{13} \\ 0 & 0 & q_{13} \\ 0 & 0 & q_{33} \\ 0 & q_{51} & 0 \\ q_{51} & 0 & 0 \\ 0 & 0 & 0 \end{vmatrix}, \quad \tilde{\mathbf{\Sigma}} = \begin{vmatrix} \epsilon_{11} & 0 & 0 \\ 0 & \epsilon_{11} & 0 \\ 0 & 0 & \epsilon_{33} \end{vmatrix},$$

$$\tilde{\mathbf{B}} = \begin{vmatrix} \beta_{11} & 0 & 0 \\ 0 & \beta_{11} & 0 \\ 0 & 0 & \beta_{33} \end{vmatrix}, \quad \tilde{\mathbf{\Gamma}} = \begin{vmatrix} \gamma_{11} & 0 & 0 \\ 0 & \gamma_{11} & 0 \\ 0 & 0 & \gamma_{33} \end{vmatrix} \tag{5.5}$$

The Legendre's polynomial coefficients of the stress and strain tensor for material polarized in the direction of axis z direction in matrix notations (2.19) are defined as the following

$$\begin{aligned} \tilde{\boldsymbol{\sigma}}^k &= (\sigma^k_{xx}, \sigma^k_{yy}, \sigma^k_{zz}, \sigma^k_{yz}, \sigma^k_{xz}, \sigma^k_{xy}) \\ \tilde{\boldsymbol{\varepsilon}}^k &= (\varepsilon^k_{xx}, \varepsilon^k_{yy}, \varepsilon^k_{zz}, \varepsilon^k_{yz}, \varepsilon^k_{xz}, \varepsilon^k_{xy}) \end{aligned} \tag{5.6}$$

By substituting matric relations for electro-magneto-elastic constants (5.5) and vectorial representations for stress and strain tensors (5.6) in the electro-magneto-elastic constitutive relations for the Legendre's polynomial coefficients (4.16) we represent them in the form

$$\begin{aligned} \sigma^k_{xx} &= c_{11}\varepsilon^k_{xx} + c_{12}\varepsilon^k_{yy} + c_{13}\varepsilon^k_{zz} - d_{13}E^k_z - q_{13}M^k_z, \\ \sigma^k_{yy} &= c_{12}\varepsilon^k_{xx} + c_{11}\varepsilon^k_{yy} + c_{13}\varepsilon^k_{zz} - d_{13}E^k_z - q_{13}M^k_z, \\ \sigma^k_{zz} &= c_{13}(\varepsilon^k_{xx} + \varepsilon^k_{yy}) + c_{33}\varepsilon^k_{zz} - d_{33}E^k_z - q_{33}M^k_z, \quad \sigma^k_{xy} = \tfrac{1}{2}(c_{11}-c_{12})\varepsilon^k_{xy}, \\ \sigma^k_{xz} &= c_{44}\varepsilon^k_{xz} - d_{51}E^k_x - q_{51}M^k_x, \quad \sigma^k_{yz} = c_{44}\varepsilon^k_{yz} - d_{51}E^k_y - q_{51}M^k_y, \\ D^k_x &= d_{51}\varepsilon^k_{xz} + \epsilon_{11}E^k_x + \beta_{11}M^k_x, \quad D^k_y = d_{51}\varepsilon^k_{yz} + \epsilon_{11}E^k_y + \beta_{11}M^k_y, \end{aligned}$$

$$
\begin{aligned}
D_z^k &= d_{13}(\varepsilon_{xx}^k + \varepsilon_{yy}^k) + d_{33}\varepsilon_{zz}^k + \epsilon_{33}E_z^k + \beta_{33}M_z^k,\\
B_x^k &= q_{51}\varepsilon_{xz}^k + \beta_{11}E_x^k + \gamma_{11}M_x^k, \quad B_y^k = q_{51}\varepsilon_{yz}^k + \beta_{11}E_y^k + \gamma_{11}M_y^k,\\
B_z^k &= q_{13}(\varepsilon_{xx}^k + \varepsilon_{yy}^k) + q_{33}\varepsilon_{zz}^k + \beta_{33}E_z^k + \gamma_{33}M_z^k,
\end{aligned} \tag{5.7}
$$

By substituting equations for the Legendre's polynomial coefficients of the strain tensor, electric and magnetic field vectors (5.3) into the constitutive equations for the Legendre's polynomial coefficients (5.7) we obtain equations for the Legendre's polynomial coefficients, the stress tensor and the electric and magnetic displacement vectors expressed in the form of the Legendre's polynomial coefficients of the displacement vector and electro and magnetic potentials components in the form

$$
\begin{aligned}
&\sigma_{xx}^k = c_{11}\frac{\partial u_x^k}{\partial x} + c_{12}\frac{\partial u_y^k}{\partial y} + c_{13}\underline{u_z^k} - d_{13}\underline{\phi^k} - q_{13}\underline{\varphi^k}, \sigma_{yy}^k = c_{11}\frac{\partial u_y^k}{\partial y} + c_{12}\frac{\partial u_x^k}{\partial x} + c_{13}\underline{u_z^k} - d_{13}\underline{\phi^k} - q_{13}\underline{\varphi^k},\\
&\sigma_{zz}^k = c_{13}\left(\frac{\partial u_x^k}{\partial x} + \frac{\partial u_y^k}{\partial y}\right) - d_{33}\underline{\phi^k} - q_{33}\underline{\varphi^k}, \sigma_{yz}^k = \frac{c_{44}}{2}\left(\frac{\partial u_z^k}{\partial y} + \underline{u_y^k}\right) - d_{51}\frac{\partial \phi^k}{\partial y} - q_{51}\frac{\partial \varphi^k}{\partial y},\\
&\sigma_{xz}^k = \frac{c_{44}}{2}\left(\frac{\partial u_z^k}{\partial x} + \underline{u_x^k}\right) - d_{51}\frac{\partial \phi^k}{\partial x} - q_{51}\frac{\partial \varphi^k}{\partial x}, \sigma_{xy}^k = \frac{c_{11}-c_{12}}{4}\left(\frac{\partial u_x^k}{\partial y} + \frac{\partial u_y^k}{\partial x}\right)\\
&D_x = \frac{d_{51}}{2}\left(\frac{\partial u_z^k}{\partial x} + \underline{u_x^k}\right) + \epsilon_{11}\frac{\partial \phi^k}{\partial x} + \beta_{11}\frac{\partial \varphi^k}{\partial x}, D_x = \frac{d_{51}}{2}\left(\frac{\partial u_z^k}{\partial x} + \underline{u_x^k}\right) + \epsilon_{11}\frac{\partial \phi^k}{\partial x} + \beta_{11}\frac{\partial \varphi^k}{\partial x},\\
&D_z = d_{13}\left(\frac{\partial u_x^k}{\partial x} + \frac{\partial u_y^k}{\partial y}\right), B_x = \frac{q_{51}}{2}\left(\frac{\partial u_z^k}{\partial x} + \underline{u_x^k}\right) + \beta_{11}\frac{\partial \phi^k}{\partial x} + \gamma_{11}\frac{\partial \varphi^k}{\partial x},\\
&B_x = \frac{q_{51}}{2}\left(\frac{\partial u_z^k}{\partial x} + \underline{u_x^k}\right) + \beta_{11}\frac{\partial \phi^k}{\partial x} + \gamma_{11}\frac{\partial \varphi^k}{\partial x}, B_z = q_{13}\left(\frac{\partial u_x^k}{\partial x} + \frac{\partial u_y^k}{\partial y}\right)
\end{aligned} \tag{5.8}
$$

By substituting the Eqs. (5.8) into the equations of equilibrium (4.12) and taking into account that the divergence operator for the Legendre's polynomial coefficients of the stress tensor and the electric and magnetic displacement vectors has form (5.1), we obtain the coupled system of differential equations of the linear electro-magneto-elasticity for the displacement vector as well as electric and magnetic potentials in the form (2.13) where elements of the block matrices and block vectors (4.20) have the form

$$
\mathbf{L}_{uu}^{rk} = \begin{vmatrix} L_{xx}^{rk} & L_{xy}^{rk} & L_{xz}^{rk} \\ L_{yx}^{rk} & L_{yy}^{rk} & L_{yz}^{rk} \\ L_{zx}^{rk} & L_{zy}^{rk} & L_{zz}^{rk} \end{vmatrix}, \quad \mathbf{L}_{eu}^{rk} = \begin{vmatrix} L_{ex}^{rk} \\ L_{ey}^{rk} \\ L_{ez}^{rk} \end{vmatrix}, \quad \mathbf{L}_{mu}^{rk} = \begin{vmatrix} L_{mx}^{rk} \\ L_{my}^{rk} \\ L_{mz}^{rk} \end{vmatrix}, \quad \mathbf{u}^k = \begin{vmatrix} u_x^k \\ u_y^k \\ u_z^k \end{vmatrix}, \quad \mathbf{b}^k = \begin{vmatrix} b_x^k \\ b_y^k \\ b_z^k \end{vmatrix}
$$

$$
\mathbf{L}_{ue}^{rk} = \begin{vmatrix} L_{xe}^{rk} & L_{ye}^{rk} & L_{ze}^{rk} \end{vmatrix}, \quad \mathbf{L}_{um}^{rk} = \begin{vmatrix} L_{xm}^{rk} & L_{ym}^{rk} & L_{zm}^{rk} \end{vmatrix}, \tag{5.9}
$$

Some elements of these matrices are differential operators, some are constants and some are equal to zero.

Below, all elements of the matrices (5.9) for the case of the first order theory of the linear couple electro-magneto-elastic theory of plates in Cartesian coordinates are presented in the form

$$L_{xx}^{00} = c_{11}\frac{\partial^2}{\partial x^2} + \frac{c_{11}-c_{12}}{4}\frac{\partial^2}{\partial y^2}, \quad L_{xy}^{00} = \frac{c_{11}+3c_{12}}{4}\frac{\partial^2}{\partial x \partial y}, \quad L_{xz}^{00} = 0, \quad L_{xx}^{01} = 0,$$

$$L_{xy}^{01} = 0, \quad L_{xz}^{01} = \frac{c_{13}}{h}\frac{\partial}{\partial x}, L_{xe}^{00} = 0, \quad L_{xe}^{01} = -\frac{d_{13}}{h}\frac{\partial}{\partial x}, \quad L_{xm}^{00} = 0, \quad L_{xm}^{01} = -\frac{q_{13}}{h}\frac{\partial}{\partial x},$$

$$L_{yx}^{00} = \frac{c_{11}+3c_{12}}{4}\frac{\partial^2}{\partial x \partial y}, \quad L_{yy}^{00} = c_{11}\frac{\partial^2}{\partial y^2} + \frac{c_{11}-c_{12}}{4}\frac{\partial^2}{\partial x^2}, \quad L_{yz}^{00} = 0, \quad L_{yx}^{01} = 0,$$

$$L_{yy}^{01} = 0, \quad L_{yz}^{01} = \frac{c_{13}}{h}\frac{\partial}{\partial x}, L_{ye}^{00} = 0, \quad L_{ye}^{01} = -\frac{d_{13}}{h}\frac{\partial}{\partial y}, \quad L_{ym}^{00} = 0, \quad L_{ym}^{01} = -\frac{q_{13}}{h}\frac{\partial}{\partial y},$$

$$L_{zx}^{00} = 0, \quad L_{zy}^{00} = 0, \quad L_{zz}^{00} = \frac{c_{44}}{2}\left(\frac{\partial^2}{\partial x^2} + \frac{\partial^2}{\partial y^2}\right), \quad L_{zx}^{01} = \frac{c_{44}}{2h}\frac{\partial}{\partial x},$$

$$L_{zy}^{01} = \frac{c_{44}}{2h}\frac{\partial}{\partial y}, \quad L_{zz}^{01} = 0, L_{ze}^{00} = -d_{51}\left(\frac{\partial^2}{\partial x^2} + \frac{\partial^2}{\partial y^2}\right),$$

$$L_{ze}^{01} = 0, \quad L_{zm}^{00} = -q_{51}\left(\frac{\partial^2}{\partial x^2} + \frac{\partial^2}{\partial y^2}\right), \quad L_{zm}^{01} = 0, L_{xx}^{10} = 0,$$

$$L_{xy}^{10} = 0, \quad L_{xz}^{10} = -\frac{3c_{44}}{2h}\frac{\partial}{\partial x}, \quad L_{xx}^{11} = c_{11}\frac{\partial^2}{\partial x^2} + \frac{c_{11}-c_{12}}{4}\frac{\partial^2}{\partial y^2} - \frac{3c_{44}}{2h^2},$$

$$L_{xy}^{11} = \frac{c_{11}+3c_{12}}{4}\frac{\partial^2}{\partial x \partial y}, \quad L_{xz}^{11} = 0, L_{xe}^{10} = \frac{3d_{51}}{h}\frac{\partial}{\partial x}, \quad L_{xe}^{11} = 0,$$

$$L_{xm}^{10} = \frac{3q_{51}}{h}\frac{\partial}{\partial x}, \quad L_{xm}^{11} = 0, L_{yx}^{10} = 0, \quad L_{yy}^{10} = 0,$$

$$L_{yz}^{10} = -\frac{3c_{44}}{2h}\frac{\partial}{\partial y}, \quad L_{yx}^{11} = \frac{c_{11}+3c_{12}}{4}\frac{\partial^2}{\partial x \partial y},$$

$$L_{yy}^{11} = c_{11}\frac{\partial^2}{\partial x^2} + \frac{c_{11}-c_{12}}{4}\frac{\partial^2}{\partial y^2} - \frac{3c_{44}}{2h^2}, \quad L_{yz}^{11} = 0, L_{ye}^{10} = \frac{3d_{51}}{h}\frac{\partial}{\partial y},$$

$$L_{ye}^{11} = 0, \quad L_{ym}^{10} = \frac{3q_{51}}{h}\frac{\partial}{\partial y}, \quad L_{ym}^{11} = 0, L_{zx}^{10} = \frac{3c_{13}}{h}\frac{\partial}{\partial x},$$

$$L_{zy}^{10} = \frac{3c_{13}}{h}\frac{\partial}{\partial y}, \quad L_{zz}^{10} = 0, \quad L_{zx}^{11} = 0, \quad L_{zy}^{11} = 0,$$

$$L_{zz}^{11} = \frac{c_{44}}{2}\left(\frac{\partial^2}{\partial x^2} + \frac{\partial^2}{\partial y^2}\right) + \frac{3c_{33}}{h^2}, L_{ze}^{10} = 0,$$

$$L_{ze}^{11} = -d_{51}\left(\frac{\partial^2}{\partial x^2} + \frac{\partial^2}{\partial y^2}\right) + \frac{3d_{33}}{h^2}, \quad L_{zm}^{10} = 0,$$

$$L_{zm}^{11} = -q_{51}\left(\frac{\partial^2}{\partial x^2} + \frac{\partial^2}{\partial y^2}\right) + \frac{3q_{33}}{h^2}, \quad L_{ex}^{00} = 0, \quad L_{ey}^{00} = 0,$$

$$L_{ez}^{00} = \frac{d_{51}}{2}\left(\frac{\partial^2}{\partial x^2} + \frac{\partial^2}{\partial y^2}\right), \quad L_{ex}^{01} = \frac{d_{51}}{2h}\frac{\partial}{\partial x}, \quad L_{ey}^{01} = \frac{d_{51}}{2h}\frac{\partial}{\partial y}, \quad L_{ez}^{01} = 0,$$

$$L_{ee}^{00} = \epsilon_{11}\left(\frac{\partial^2}{\partial x^2} + \frac{\partial^2}{\partial y^2}\right), \quad L_{ee}^{01} = 0, \quad L_{em}^{10} = \beta_{11}\left(\frac{\partial^2}{\partial x^2} + \frac{\partial^2}{\partial y^2}\right), \quad L_{em}^{11} = 0, \tag{5.10}$$

$$L^{00}_{mx}=0,\quad L^{00}_{my}=0,\quad L^{00}_{mz}=\frac{q_{51}}{2}\left(\frac{\partial^2}{\partial x^2}+\frac{\partial^2}{\partial y^2}\right),\quad L^{01}_{mx}=\frac{q_{51}}{2h}\frac{\partial}{\partial x},$$

$$L^{01}_{my}=\frac{q_{51}}{2h}\frac{\partial}{\partial y},\quad L^{01}_{mz}=0, L^{00}_{me}=\beta_{11}\left(\frac{\partial^2}{\partial x^2}+\frac{\partial^2}{\partial y^2}\right),\quad L^{01}_{me}=0,$$

$$L^{10}_{mm}=\gamma_{11}\left(\frac{\partial^2}{\partial x^2}+\frac{\partial^2}{\partial y^2}\right),\quad L^{11}_{mm}=0, L^{10}_{ex}=-\frac{3d_{13}}{h}\frac{\partial}{\partial x},$$

$$L^{10}_{ey}=-\frac{3d_{13}}{h}\frac{\partial}{\partial y},\quad L^{10}_{ez}=0,\quad L^{11}_{ex}=0,\quad L^{11}_{ey}=0,$$

$$L^{11}_{ez}=\frac{d_{51}}{2}\left(\frac{\partial^2}{\partial x^2}+\frac{\partial^2}{\partial y^2}\right)-\frac{3d_{33}}{h^2}, L^{10}_{ee}=0,\quad L^{11}_{ee}=\epsilon_{11}\left(\frac{\partial^2}{\partial x^2}+\frac{\partial^2}{\partial y^2}\right)-\frac{3\epsilon_{33}}{h^2},$$

$$L^{10}_{em}=0,\quad L^{11}_{em}=\beta_{11}\left(\frac{\partial^2}{\partial x^2}+\frac{\partial^2}{\partial y^2}\right)-\frac{3\beta_{33}}{h^2}, L^{10}_{mx}=-\frac{3q_{13}}{h}\frac{\partial}{\partial x},$$

$$L^{10}_{my}=-\frac{3q_{13}}{h}\frac{\partial}{\partial y},\quad L^{10}_{mz}=0,\quad L^{11}_{mx}=0,\quad L^{11}_{my}=0,$$

$$L^{11}_{mz}=\frac{q_{51}}{2}\left(\frac{\partial^2}{\partial x^2}+\frac{\partial^2}{\partial y^2}\right)-\frac{3q_{33}}{h^2}, L^{10}_{me}=0,$$

$$L^{11}_{me}=\beta_{11}\left(\frac{\partial^2}{\partial x^2}+\frac{\partial^2}{\partial y^2}\right)-\frac{3\beta_{33}}{h^2},\quad L^{10}_{mm}=0,\quad L^{11}_{mm}=\gamma_{11}\left(\frac{\partial^2}{\partial x^2}+\frac{\partial^2}{\partial y^2}\right)-\frac{3\gamma_{33}}{h^2},$$

A complete 2-D system of the differential equations for the higher order theory of the electro-magneto-elastic plates in the Cartesian system of coordinates is presented in this section. Explicit expressions for divergences of the Legendre's polynomial coefficients of stress tensor and the electric and magnetic displacement vectors (5.1), for the Legendre's polynomial coefficients of strain tensor and electric field and the magnetic field vectors (5.3) and for the Legendre's polynomial coefficients of stress tensor and the electric and magnetic displacement vectors (5.8) as functions of the Legendre's polynomial coefficients of displacements and electric and magnetic potentials for higher order theory of plates are presented here. For the case of the first order approximation theory, elements of matrix differential operators (5.9), that are included in the equations of equilibrium (5.13) are also presented in the explicit form (5.10). They can be used for theoretical analysis, as well as analytical and numerical solutions of the problems arising in science and engineering.

6 Higher Order Theory of Electro-Magneto-Elastic Plates in Polar Coordinates

Sometimes polar coordinates are preferred for theoretical analysis as well for analytical and numerical computations, especially in the case of radially polarized materials. Therefore, let us develop equations for the high theory of the linear electro-magneto-elastic plates in polar coordinates. In this case we have notations $x_1=\rho$, $x_2=\varphi$ and $x_3=z$. Coefficients of the first quadratic form of a surface and main curvatures

are equal to $A_1 = 1$, $A_2 = \rho$, and $k_1 = k_2 = 0$ respectively. After the substitution of those parameters in all of the above equations, the equations that correspond to the higher order theory of linear electro-magneto-elasticity of the plates in polar coordinates will be obtained.

The equations of equilibrium and Maxwell equations for Legendre's polynomial coefficients in this case have the form (3.12) but the operator of divergence of the stress tensor and the electric and magnetic displacement vectors in the polar system of coordinates have the form

$$\begin{aligned}
\tilde{\nabla}_\alpha \sigma^k_{\alpha\rho} &= \frac{\partial \sigma^k_{\rho\rho}}{\partial \rho} + \frac{1}{\rho}\frac{\partial \sigma^k_{\varphi\rho}}{\partial \varphi} + \frac{\sigma^k_{\rho\rho} - \sigma^k_{\varphi\varphi}}{\rho} - \underline{\sigma^k_{z\rho}},\\
\tilde{\nabla}_\alpha \sigma^k_{\alpha\varphi} &= \frac{\partial \sigma^k_{\rho\varphi}}{\partial \rho} + \frac{\partial \sigma^k_{\varphi\varphi}}{\partial \varphi}\frac{1}{\rho} + \frac{\sigma^k_{\rho\varphi} - \sigma^k_{\varphi\rho}}{\rho} - \underline{\sigma^k_{z\varphi}},\\
\tilde{\nabla}_\alpha \sigma^k_{\alpha x} &= \frac{\partial \sigma^k_{\rho z}}{\partial \rho} + \frac{1}{\rho}\frac{\partial \sigma^k_{\varphi z}}{\partial \varphi} + \frac{1}{\rho}\sigma^k_{\rho z} - \underline{\sigma^k_{zz}}\\
\tilde{\nabla}_\alpha D^k_\alpha &= \frac{\partial D^k_\rho}{\partial \rho} + \frac{D^k_\rho}{\rho} + \frac{1}{\rho}\frac{\partial D^k_\varphi}{\partial \varphi} - \underline{D^k_z},\\
\tilde{\nabla}_\alpha B^k_i &= \frac{\partial B^k_\rho}{\partial \rho} + \frac{B^k_\rho}{\rho} + \frac{1}{\rho}\frac{\partial B^k_\varphi}{\partial \varphi} - \underline{B^k_z}, \quad \alpha = \rho, \varphi.
\end{aligned} \tag{6.1}$$

where

$$\begin{aligned}
&\underline{\sigma^k_{zi}} = \frac{2k+1}{h}\left(\sigma^{k-1}_{zi} + \sigma^{k-3}_{zi} + \ldots\right), i = \alpha = \rho, \varphi, z,\\
&\underline{D^k_z} = \frac{2k+1}{h}\left(D^{k-1}_z + D^{k-3}_z + \ldots\right), \underline{B^k_z} = \frac{2k+1}{h}\left(B^{k-1}_z + B^{k-3}_z + \ldots\right)
\end{aligned} \tag{6.2}$$

Expressions for the Legendre's polynomial coefficients of the Cauchy strain tensor, electric field and the magnetic field vectors in this case have the form

$$\begin{aligned}
&\varepsilon^k_{\rho\rho} = \frac{\partial u^k_\rho}{\partial \rho}, \quad \varepsilon^k_{\rho\varphi} = \frac{1}{2}\left(\frac{\partial u^k_\varphi}{\partial \rho} + \frac{1}{\rho}\frac{\partial u^k_\rho}{\partial \varphi} - \frac{u^k_\varphi}{\rho}\right), \quad \varepsilon_{zz} = \underline{u^k_z},\\
&\varepsilon^k_{\rho z} = \frac{1}{2}\left(\frac{\partial u^k_z}{\partial \rho} + \underline{u^k_\rho}\right), \quad \varepsilon^k_{\varphi\varphi} = \frac{1}{\rho}\frac{\partial u^k_\varphi}{\partial \varphi} + \frac{u^k_\rho}{\rho}, \quad \varepsilon^k_{\varphi z} = \frac{1}{2}\left(\frac{1}{\rho}\frac{\partial u^k_z}{\partial \varphi} + \underline{u^k_\varphi}\right)\\
&E^k_\pi = \frac{\partial \phi^k}{\partial \rho}, \quad E^k_\varphi = \frac{1}{\rho}\frac{\partial \phi^k}{\partial \varphi}, \quad E^k_z = \underline{\phi^k}, \quad M^k_\rho = \frac{\partial \varphi^k}{\partial \rho}, \quad M^k_y = \frac{1}{\rho}\frac{\partial \varphi^k}{\partial \varphi}, \quad M^k_z = \underline{\varphi^k}
\end{aligned} \tag{6.3}$$

where $\underline{\phi^k}$ and $\underline{\varphi^k}$ are defined in (4.7) and $\underline{u^k_i}$ is presented as

$$\underline{u^k_i} = \frac{2k+1}{h}\left(u^{k+1}_i + u^{k+3}_i + \ldots\right), \quad i = \rho, \varphi, z. \tag{6.4}$$

For the same reason as in the previous section we consider a material with a hexagonal crystal structure (class 6 mm), but polarized in the radial axis ρ . In this case the constitutive relations have the same form (5.5), but the Legendre's polynomial coefficients of the stress and strain tensor in matrix notations (2.19) are defined as the following

$$\begin{aligned}\tilde{\boldsymbol{\sigma}}^k &= (\sigma^k_{zz}, \sigma^k_{\varphi\varphi}, \sigma^k_{\rho\rho}, \sigma^k_{\rho\varphi}, \sigma^k_{\rho z}, \sigma^k_{\varphi z})\\ \tilde{\boldsymbol{\varepsilon}}^k &= (\varepsilon^k_{zz}, \varepsilon^k_{\varphi\varphi}, \varepsilon^k_{\rho\rho}, \varepsilon^k_{\rho\varphi}, \varepsilon^k_{\rho z}, \varepsilon^k_{\varphi z})\end{aligned} \tag{6.5}$$

By substituting matric relations for electro-magneto-elastic constants (5.5) and vectorial representations for stress and strain tensors (6.5) in the electro-magneto-elastic constitutive relations for the Legendre's polynomial coefficients (4.16) we represent them in the form

$$\begin{aligned}\sigma^k_{\rho\rho} &= c_{33}\varepsilon^k_{\rho\rho} + c_{13}(\varepsilon^k_{\varphi\varphi} + \varepsilon^k_{zz}) - d_{33}E^k_\rho - q_{33}M^k_\rho,\\ \sigma^k_{\varphi\varphi} &= c_{13}\varepsilon^k_{\rho\rho} + c_{11}\varepsilon^k_{\varphi\varphi} + c_{12}\varepsilon^k_{zz} - d_{13}E^k_\rho - q_{13}M^k_\rho,\\ \sigma^k_{zz} &= c_{13}\varepsilon^k_{\rho\rho} + c_{12}\varepsilon^k_{\varphi\varphi} + c_{11}\varepsilon^k_{zz} - d_{13}E^k_\rho - q_{13}M^k_\rho,\\ \sigma^k_{\rho\varphi} &= c_{44}\varepsilon^k_{\rho\varphi} - d_{51}E^k_\varphi - q_{51}M^k_\varphi,\\ \sigma^k_{\rho z} &= c_{44}\varepsilon^k_{\rho z} - d_{51}E^k_z - q_{51}M^k_z,\\ \sigma^k_{\varphi z} &= \tfrac{1}{2}(c_{11} - c_{12})\varepsilon^k_{\varphi z},\\ D^k_\rho &= d_{13}(\varepsilon^k_{\varphi\varphi} + \varepsilon^k_{zz}) + d_{33}\varepsilon^k_{\rho\rho} + \epsilon_{33}E^k_\rho + \beta_{33}M^k_\rho,\\ D^k_\varphi &= d_{51}\varepsilon^k_{\rho\varphi} + \epsilon_{11}E^k_\varphi + \beta_{11}M^k_\varphi,\\ D^k_z &= d_{51}\varepsilon^k_{\rho z} + \epsilon_{11}E^k_z + \beta_{11}M^k_z,\\ B^k_\rho &= q_{13}(\varepsilon^k_{\varphi\varphi} + \varepsilon^k_{zz}) + q_{33}\varepsilon^k_{\rho\rho} + \beta_{33}E^k_\rho + \gamma_{33}M^k_\rho,\\ B^k_\varphi &= q_{51}\varepsilon^k_{\rho\varphi} + \beta_{11}E^k_\varphi + \gamma_{11}M^k_\varphi,\\ B^k_z &= q_{51}\varepsilon^k_{\rho z} + \beta_{11}E^k_z + \gamma_{11}M^k_z\end{aligned} \tag{6.6}$$

By substituting equations for the Legendre's polynomial coefficients of the strain tensor, electric and magnetic field vectors (6.3) into the constitutive equations for the Legendre's polynomial coefficients (6.6) we obtain equations for the Legendre's polynomial coefficients the stress tensor and the electric and magnetic displacement vectors expressed in the form of the Legendre's polynomial coefficients of the displacement vector and electro and magnetic potentials components in the form

$$\sigma^k_{\rho\rho} = c_{33}\frac{\partial u^k_\rho}{\partial\rho} + c_{13}\left(\frac{1}{\rho}\frac{\partial u^k_\varphi}{\partial\varphi} + \frac{u^k_\rho}{\rho} + 2\underline{u^k_z}\right) - d_{33}\underline{\phi^k} - q_{33}\underline{\varphi^k},$$

$$\sigma^k_{\varphi\varphi} = c_{11}\left(\frac{1}{\rho}\frac{\partial u^k_\varphi}{\partial\varphi} + \frac{u^k_\rho}{\rho}\right) + c_{13}\frac{\partial u^k_\rho}{\partial\rho} + c_{12}\underline{u^k_z} - d_{13}\underline{\phi^k} - q_{13}\underline{\varphi^k},$$

$$\sigma_{zz}^k = c_{13}\frac{\partial u_\rho^k}{\partial \rho} + c_{12}\left(\frac{1}{\rho}\frac{\partial u_\varphi^k}{\partial \varphi} + \frac{u_\rho^k}{\rho}\right) + c_{11}\underline{u_z^k} - d_{13}\underline{\phi^k} - q_{13}\underline{\varphi^k},$$

$$\sigma_{\rho\varphi}^k = \frac{c_{44}}{2}\left(\frac{\partial u_\varphi^k}{\partial \rho} + \frac{1}{\rho}\frac{\partial u_\rho^k}{\partial \varphi} - \frac{u_\varphi^k}{\rho}\right) - d_{51}\frac{1}{\rho}\frac{\partial \phi^k}{\partial \varphi} - \frac{1}{\rho}q_{51}\frac{\partial \varphi^k}{\partial \varphi},$$

$$\sigma_{\rho z}^k = \frac{c_{44}}{2}\left(\frac{\partial u_z^k}{\partial \rho} + \underline{u_\rho^k}\right) - d_{51}\frac{\partial \phi^k}{\partial \rho} - q_{51}\frac{\partial \varphi^k}{\partial \rho}, \quad \sigma_{\varphi z}^k = \frac{c_{11}-c_{12}}{4}\left(\frac{1}{\rho}\frac{\partial u_z^k}{\partial \varphi} + \underline{u_\varphi^k}\right)$$

$$D_\rho = d_{33}\frac{\partial u_\rho^k}{\partial \rho} + d_{13}\left(\frac{1}{\rho}\frac{\partial u_\varphi^k}{\partial \varphi} + \frac{u_\rho^k}{\rho} + \underline{u_z^k}\right) + \epsilon_{33}\frac{\partial \phi^k}{\partial \rho} + \beta_{33}\frac{\partial \varphi^k}{\partial \rho},$$

$$D_\varphi = \frac{d_{51}}{2}\left(\frac{\partial u_\varphi^k}{\partial \rho} + \frac{1}{\rho}\frac{\partial u_\rho^k}{\partial \varphi} - \frac{u_\varphi^k}{\rho}\right) + \epsilon_{11}\frac{1}{\rho}\frac{\partial \phi^k}{\partial \varphi} + \beta_{11}\frac{1}{\rho}\frac{\partial \varphi^k}{\partial \varphi},$$

$$D_z = \frac{d_{52}}{2}\left(\frac{\partial u_z^k}{\partial \rho} + \underline{u_\rho^k}\right) + \epsilon_{11}\underline{\phi^k} + \beta_{11}\underline{\varphi^k},$$

$$B_\rho = q_{33}\frac{\partial u_\rho^k}{\partial \rho} + d_{13}\left(\frac{1}{\rho}\frac{\partial u_\varphi^k}{\partial \varphi} + \frac{u_\rho^k}{\rho} + \underline{u_z^k}\right) + \beta_{33}\frac{\partial \phi^k}{\partial \rho} + \gamma_{33}\frac{\partial \varphi^k}{\partial \rho},$$

$$B_\varphi = \frac{q_{51}}{2}\left(\frac{\partial u_\varphi^k}{\partial \rho} + \frac{1}{\rho}\frac{\partial u_\rho^k}{\partial \varphi} - \frac{u_\varphi^k}{\rho}\right) + \beta_{11}\frac{1}{\rho}\frac{\partial \phi^k}{\partial \varphi} + \gamma_{11}\frac{1}{\rho}\frac{\partial \varphi^k}{\partial \varphi},$$

$$B_z = \frac{q_{52}}{2}\left(\frac{\partial u_z^k}{\partial \rho} + \underline{u_\rho^k}\right) + \beta_{11}\underline{\phi^k} + \gamma_{11}\underline{\varphi^k}, \tag{6.7}$$

By substituting the Eqs. (5.8) into the equations of equilibrium (4.12) and taking into account that the divergence operator for the Legendre's polynomial coefficients of the stress tensor and the electric and magnetic displacement vectors has form (5.1), we obtain the coupled system of differential equations of the linear electro-magneto-elasticity for the displacement vector as well as electric and magnetic potentials in the form (2.13) where elements of the block matrices and block vectors (4.20) have the form

$$\mathbf{L}_{uu}^{rk} = \begin{vmatrix} L_{\rho\rho}^{rk} & L_{\rho\varphi}^{rk} & L_{\rho z}^{rk} \\ L_{\varphi\rho}^{rk} & L_{\varphi\varphi}^{rk} & L_{\varphi z}^{rk} \\ L_{z\rho}^{rk} & L_{z\varphi}^{rk} & L_{zz}^{rk} \end{vmatrix}, \quad \mathbf{L}_{eu}^{rk} = \begin{vmatrix} L_{e\rho}^{rk} \\ L_{e\varphi}^{rk} \\ L_{ez}^{rk} \end{vmatrix}, \quad \mathbf{L}_{mu}^{rk} = \begin{vmatrix} L_{m\rho}^{rk} \\ L_{m\varphi}^{rk} \\ L_{mz}^{rk} \end{vmatrix}, \quad \mathbf{u}^k = \begin{vmatrix} u_\rho^k \\ u_\varphi^k \\ u_z^k \end{vmatrix}, \quad \mathbf{b}^k = \begin{vmatrix} b_\rho^k \\ b_\varphi^k \\ b_z^k \end{vmatrix}$$

$$\mathbf{L}_{ue}^{rk} = \begin{vmatrix} L_{\rho e}^{rk} & L_{\varphi e}^{rk} & L_{ze}^{rk} \end{vmatrix}, \quad \mathbf{L}_{um}^{rk} = \begin{vmatrix} L_{\rho m}^{rk} & L_{\varphi m}^{rk} & L_{zm}^{rk} \end{vmatrix}, \tag{6.8}$$

Some elements of these matrices are differential operators, some are constants and some are equal to zero.

Below, all elements of the matrices (5.9) for the case of the first order theory of the linear couple electro-magneto-elastic theory of plates in Cartesian coordinates are presented in the form

$$L^{00}_{\rho\rho} = c_{33}\left(\frac{\partial^2}{\partial\rho^2} + \frac{1}{\rho}\frac{\partial}{\partial\rho}\right) + \frac{c_{44}}{2\rho^2}\frac{\partial^2}{\partial\varphi^2} - \frac{c_{11}}{\rho^2},$$

$$L^{00}_{\rho\varphi} = \frac{c_{44}+2c_{13}}{2\rho}\frac{\partial^2}{\partial\rho\partial\varphi} - \frac{c_{44}+2c_{11}}{2\rho}\frac{\partial}{\partial\varphi},$$

$$L^{00}_{xz} = 0, \quad L^{01}_{xx} = 0, \quad L^{01}_{xy} = 0, \quad L^{01}_{\rho z} = \frac{c_{13}}{h}\frac{\partial}{\partial\rho} + \frac{c_{13}-c_{12}}{\rho h},$$

$$L^{01}_{\rho e} = 0, \quad L^{01}_{\rho m} = 0, L^{00}_{\rho e} = -d_{33}\left(\frac{\partial^2}{\partial\rho^2} + \frac{1}{\rho}\frac{\partial}{\partial\rho}\right) + \frac{d_{13}}{\rho}\frac{\partial}{\partial\rho} - \frac{d_{51}}{\rho^2}\frac{\partial^2}{\partial\varphi^2},$$

$$L^{00}_{\rho m} = -q_{33}\left(\frac{\partial^2}{\partial\rho^2} + \frac{1}{\rho}\frac{\partial}{\partial\rho}\right) + \frac{q_{13}}{\rho}\frac{\partial}{\partial\rho} - \frac{q_{51}}{\rho^2}\frac{\partial^2}{\partial\varphi^2},$$

$$L^{00}_{\varphi\rho} = \frac{c_{44}+2c_{13}}{2\rho}\frac{\partial^2}{\partial\rho\partial\varphi} + \frac{c_{44}+2c_{11}}{2\rho}\frac{\partial}{\partial\varphi},$$

$$L^{00}_{\varphi\varphi} = \frac{c_{44}}{2}\left(\frac{\partial^2}{\partial\rho^2} + \frac{1}{\rho}\frac{\partial}{\partial\rho} - \frac{1}{\rho^2}\right) + \frac{c_{11}}{\rho^2}\frac{\partial^2}{\partial\varphi^2}, \quad L^{00}_{\rho z} = 0,$$

$$L^{01}_{\varphi\rho} = 0, \quad L^{01}_{\varphi\varphi} = 0, \quad L^{01}_{\varphi z} = \frac{c_{12}}{\rho h}\varphi,$$

$$L^{00}_{\varphi e} = -\frac{d_{13}+d_{51}}{\rho}\frac{\partial^2}{\partial\rho\partial\varphi} - \frac{d_{51}}{\rho^2}\frac{\partial}{\partial\varphi}, \quad L^{01}_{\varphi e} = 0,$$

$$L^{00}_{\varphi m} = -\frac{q_{13}+q_{51}}{\rho}\frac{\partial^2}{\partial\rho\partial\varphi} - \frac{q_{51}}{\rho^2}\frac{\partial}{\partial\varphi}, \quad L^{01}_{\varphi m} = 0,$$

$$L^{00}_{z\rho} = 0, \quad L^{00}_{z\varphi} = 0, \quad L^{00}_{zz} = \frac{c_{44}}{2}\left(\frac{\partial^2}{\partial\rho^2} + \frac{1}{\rho}\frac{\partial}{\partial\rho}\right) + \frac{c_{11}-c_{12}}{4\rho^2}\frac{\partial^2}{\partial\varphi^2},$$

$$L^{01}_{z\rho} = \frac{c_{44}}{2h}\left(\frac{\partial}{\partial\rho} + \frac{1}{\rho}\right), \quad L^{01}_{z\varphi} = \frac{c_{11}-c_{12}}{4\rho h}\frac{\partial}{\partial\varphi}, \quad L^{01}_{zz} = 0,$$

$$L^{00}_{ze} = 0, \quad L^{01}_{ze} = -\frac{d_{13}}{h}\left(\frac{\partial}{\partial\rho} + \frac{1}{\rho}\right), \quad L^{00}_{zm} = 0, \quad L^{01}_{zm} = -\frac{q_{13}}{h}\left(\frac{\partial}{\partial\rho} + \frac{1}{\rho}\right),$$

$$L^{10}_{\rho\rho} = 0, \quad L^{10}_{\rho\varphi} = 0, \quad L^{10}_{\rho z} = -\frac{3c_{44}}{2h}\frac{\partial}{\partial\rho}, \quad L^{11}_{\rho\rho} = c_{33}\left(\frac{\partial^2}{\partial\rho^2} + \frac{1}{\rho}\frac{\partial}{\partial\rho}\right) + \frac{c_{44}}{2\rho^2}\frac{\partial^2}{\partial\varphi^2} - \frac{3c_{44}}{2h^2} - \frac{c_{11}}{\rho^2},$$

$$L^{11}_{\rho\varphi}\frac{c_{44}+2c_{13}}{2\rho}\frac{\partial^2}{\partial\rho\partial\varphi} - \frac{c_{44}+2c_{11}}{2\rho}\frac{\partial}{\partial\varphi}, \quad L^{11}_{xz} = 0,$$

$$L^{11}_{\rho e} = -d_{33}\left(\frac{\partial^2}{\partial\rho^2} + \frac{1}{\rho}\frac{\partial}{\partial\rho}\right) - d_{51}\left(\frac{1}{\rho^2}\frac{\partial^2}{\partial\varphi^2} - \frac{3}{h^2}\right) + d_{13}\frac{1}{\rho}\frac{\partial}{\partial\rho}, \quad L^{10}_{\rho e} = 0,$$

$$L^{11}_{xm} = -d_{33}\left(\frac{\partial^2}{\partial\rho^2} + \frac{1}{\rho}\frac{\partial}{\partial\rho}\right) - d_{51}\left(\frac{1}{\rho^2}\frac{\partial^2}{\partial\varphi^2} - \frac{3}{h^2}\right) + d_{13}\frac{1}{\rho}\frac{\partial}{\partial\rho}, \quad L^{10}_{xm} = 0,$$

$$L^{10}_{\varphi x} = 0, \quad L^{10}_{\varphi\varphi} = 0, \quad L^{10}_{\varphi z} = -\frac{3(c_{11}-c_{12})}{4\rho h}\frac{\partial}{\partial\varphi}, \quad L^{11}_{\varphi x} = \frac{c_{44}+2c_{13}}{4\rho}\frac{\partial^2}{\partial\rho\partial\varphi} + \frac{c_{44}+2c_{11}}{2\rho^2}\frac{\partial}{\partial\varphi},$$

$$L^{11}_{\varphi\varphi} = \frac{c_{44}}{2}\left(\frac{\partial^2}{\partial\rho^2} + \frac{1}{\rho}\frac{\partial}{\partial\rho} - \frac{1}{\rho}\right) + c_{11}\left(\frac{1}{\rho^2}\frac{\partial^2}{\partial\varphi^2} - \frac{3}{4h^2}\right) - \frac{3c_{12}}{4h^2}, \quad L^{11}_{\varphi z} = 0,$$

$$L^{10}_{\varphi e} = 0, \quad L^{11}_{\varphi e} = -\frac{d_{13}+d_{51}}{\rho}\frac{\partial^2}{\partial\rho\partial\varphi} - \frac{d_{51}}{\rho^2}\frac{\partial}{\partial\varphi}, \quad L^{10}_{\varphi m} = 0, \quad L^{11}_{\varphi m} = -\frac{q_{13}+q_{51}}{\rho}\frac{\partial^2}{\partial\rho\partial\varphi} - \frac{q_{51}}{\rho^2}\frac{\partial}{\partial\varphi},$$

$$L_{z\rho}^{10}=-\frac{3c_{13}}{h}\left(\frac{\partial}{\partial\rho}+\frac{1}{\rho}\right),\quad L_{zy}^{10}=-\frac{3c_{12}}{\rho h}\frac{\partial}{\partial\varphi},\quad L_{zz}^{10}=0,\quad L_{zx}^{11}=0,\quad L_{zy}^{11}=0,\quad L_{ze}^{11}=0,L_{zm}^{11}=0,$$

$$L_{zz}^{11}=\frac{c_{44}}{2}\left(\frac{\partial^2}{\partial\rho^2}+\frac{1}{\rho}\frac{\partial}{\partial\rho}\right)+\frac{c_{11}-c_{12}}{4\rho^2}\frac{\partial^2}{\partial\varphi^2}-\frac{3c_{11}}{h^2},\quad L_{ze}^{10}=\frac{3d_{13}}{h^2}\frac{\partial}{\partial\rho},\quad L_{zm}^{10}=\frac{3q_{13}}{h^2}\frac{\partial}{\partial\rho},$$

$$L_{e\rho}^{00}=d_{33}\left(\frac{\partial^2}{\partial\rho^2}+\frac{1}{\rho}\frac{\partial}{\partial\rho}\right)+\frac{d_{13}}{\rho}\frac{\partial}{\partial\rho}+\frac{d_{51}}{2\rho^2}\frac{\partial^2}{\partial\varphi^2},$$

$$L_{e\varphi}^{00}=\frac{d_{51}+2d_{13}}{2\rho}\frac{\partial^2}{\partial\rho\partial\varphi}-\frac{d_{51}}{2\rho^2}\varphi,$$

$$L_{ez}^{00}=\frac{d_{13}}{h}\left(\frac{\partial}{\partial\rho}+\frac{1}{\rho}\right),L_{e\rho}^{01}=0,\quad L_{e\varphi}^{01}=0,\quad L_{ez}^{01}=0,$$

$$L_{ee}^{00}=\epsilon_{33}\left(\frac{\partial^2}{\partial\rho^2}+\frac{1}{\rho}\frac{\partial}{\partial\rho}\right)+\frac{\epsilon_{11}}{\rho^2}\frac{\partial^2}{\partial\varphi^2},\quad L_{ee}^{01}=0,$$

$$L_{em}^{10}=\beta_{33}\left(\frac{\partial^2}{\partial\rho^2}+\frac{1}{\rho}\frac{\partial}{\partial\rho}\right)+\frac{\beta_{11}}{\rho^2}\frac{\partial^2}{\partial\varphi^2},\quad L_{em}^{11}=0,$$

$$L_{m\rho}^{00}=q_{33}\left(\frac{\partial^2}{\partial\rho^2}+\frac{1}{\rho}\frac{\partial}{\partial\rho}\right)+\frac{q_{13}}{\rho}\frac{\partial}{\partial\rho}+\frac{q_{51}}{2\rho^2}\frac{\partial^2}{\partial\varphi^2},$$

$$L_{m\varphi}^{00}=\frac{q_{51}+2q_{13}}{2\rho}\frac{\partial^2}{\partial\rho\partial\varphi}-\frac{d_{51}}{2\rho^2}\varphi,\quad L_{mz}^{00}=q\frac{d_{13}}{h}\left(\frac{\partial}{\partial\rho}+\frac{1}{\rho}\right),$$

$$L_{m\rho}^{01}=0,\quad L_{m\varphi}^{01}=0,\quad L_{mz}^{01}=0,$$

$$L_{me}^{00}=\beta_{33}\left(\frac{\partial^2}{\partial\rho^2}+\frac{1}{\rho}\frac{\partial}{\partial\rho}\right)+\frac{\gamma_{11}}{\rho^2}\frac{\partial^2}{\partial\varphi^2},\quad L_{me}^{01}=0,$$

$$L_{mm}^{10}=\gamma_{33}\left(\frac{\partial^2}{\partial\rho^2}+\frac{1}{\rho}\frac{\partial}{\partial\rho}\right)+\frac{\gamma_{11}}{\rho^2}\frac{\partial^2}{\partial\varphi^2},\quad L_{mm}^{11}=0,$$

$$L_{e\rho}^{10}=0,\quad L_{e\varphi}^{10}=0,\quad L_{ez}^{00}=-\frac{3d_{51}}{2h}\frac{\partial}{\partial\rho},$$

$$L_{e\rho}^{11}=d_{33}\left(\frac{\partial^2}{\partial\rho^2}+\frac{1}{\rho}\frac{\partial}{\partial\rho}\right)+\frac{d_{51}}{2\rho^2}\frac{\partial^2}{\partial\varphi^2}+\frac{d_{13}}{\rho}\frac{\partial}{\partial\rho}-\frac{3d_{51}}{2h^2},$$

$$L_{e\varphi}^{11}=\frac{d_{51}+2d_{13}}{2\rho}\frac{\partial^2}{\partial\rho\partial\varphi}-\frac{d_{51}}{2\rho^2}\frac{\partial}{\partial\rho}\varphi,\quad L_{ez}^{11}=0,$$

$$L_{ee}^{10}=0,\quad L_{ee}^{11}=\epsilon_{33}\left(\frac{\partial^2}{\partial\rho^2}+\frac{1}{\rho}\frac{\partial}{\partial\rho}\right)+\frac{\epsilon_{11}}{\rho^2}\frac{\partial^2}{\partial\varphi^2}-\frac{3\epsilon_{11}}{h^2},$$

$$L_{em}^{10}=0,\quad L_{em}^{11}=\beta_{33}\left(\frac{\partial^2}{\partial\rho^2}+\frac{1}{\rho}\frac{\partial}{\partial\rho}\right)+\frac{\beta_{11}}{\rho^2}\frac{\partial^2}{\partial\varphi^2}-\frac{3\beta_{11}}{h^2},$$

$$L_{m\rho}^{10}=0,\quad L_{m\varphi}^{10}=0,\quad L_{mz}^{10}=-\frac{3q_{51}}{2h}\frac{\partial}{\partial\rho},$$

$$L_{m\rho}^{11}=q_{33}\left(\frac{\partial^2}{\partial\rho^2}+\frac{1}{\rho}\frac{\partial}{\partial\rho}\right)+\frac{q_{51}}{2\rho^2}\frac{\partial^2}{\partial\varphi^2}+\frac{q_{13}}{\rho}\frac{\partial}{\partial\rho}-\frac{3q_{51}}{2h^2},$$

$$L^{11}_{m\varphi} = \frac{q_{51}+2q_{13}}{2\rho}\frac{\partial^2}{\partial\rho\partial\varphi} - \frac{d_{51}}{2\rho^2}\frac{\partial}{\partial\rho}\varphi, \quad L^{11}_{mz} = 0,$$
$$L^{10}_{me} = 0, \quad L^{11}_{me} = \beta_{33}\left(\frac{\partial^2}{\partial\rho^2} + \frac{1}{\rho}\frac{\partial}{\partial\rho}\right) + \frac{\beta_{11}}{\rho^2}\frac{\partial^2}{\partial\varphi^2} - \frac{3\beta_{11}}{h^2},$$
$$L^{10}_{mm} = 0, \quad L^{11}_{mm} = \gamma_{33}\left(\frac{\partial^2}{\partial\rho^2} + \frac{1}{\rho}\frac{\partial}{\partial\rho}\right) + \frac{\gamma_{11}}{\rho^2}\frac{\partial^2}{\partial\varphi^2} - \frac{3\gamma_{11}}{h^2}. \tag{6.9}$$

A complete 2-D system of the differential equations for the higher order theory of the electro-magneto-elastic plates in the polar system of coordinates is presented in this section. Explicit expressions for divergences of the Legendre's polynomial coefficients of stress tensor and the electric and magnetic displacement vectors (6.1), for the Legendre's polynomial coefficients of strain tensor and electric field and the magnetic field vectors (6.3) and for the Legendre's polynomial coefficients of stress tensor and the electric and magnetic displacement vectors (6.7) as functions of the Legendre's polynomial coefficients of displacements and electric and magnetic potentials for higher order theory of plates are presented here. For the case of the first order approximation theory, elements of matrix differential operators (6.8), that are included in the equations of equilibrium (2.13) are also presented in the explicit form (6.9). They can be used for theoretical analysis, as well as analytical and numerical solutions of the problems arising in science and engineering.

7 Higher Order Theory of Electro-Magneto-Elastic Cylindrical Shell

Models of the electro-magneto-elastic shells of cylindrical geometry are very important and often used in theoretical analysis as well as applied in sciences and engineering. Therefore, we will develop equations for the higher order theory of linear elastic cylindrical shells here. Let us introduce cylindrical coordinates and such that $x_1 = x$, $x_2 = \varphi$ and $x_3 = r$, $r \in [R-h, R+h]$. Coefficients of the first quadratic form of a surface and main curvatures are equal to $A_1 = 1$, $A_2 = R$, and $k_1 = 0$, $k_2 = \frac{1}{R}$, respectively. After the substitution of those parameters in the Eqs. (4.12)–(4.16), the equations that correspond to the higher order theory of linear electro-magneto-elasticity of the of cylindrical shell will be obtained.

The equations of equilibrium and Maxwell equations for Legendre's polynomial coefficients in this case have the form (4.12) but the operator of divergence of the stress tensor and the electric and magnetic displacement vectors in the cylindrical system of coordinates have the form

$$\tilde{\nabla}_\alpha \sigma^k_{\alpha x} = \frac{\partial\sigma^k_{xx}}{\partial x} + \frac{1}{R}\frac{\partial\sigma^k_{\varphi x}}{\partial\varphi} + \frac{\sigma^k_{rx}}{R} - \frac{\sigma^k_{rx}}{R}, \quad \tilde{\nabla}_\alpha \sigma^k_{\alpha\varphi} = \frac{\partial\sigma^k_{x\varphi}}{\partial x} + \frac{1}{R}\frac{\partial\sigma^k_{\varphi\varphi}}{\partial\varphi} + \frac{2\sigma^k_{\varphi r}}{R} - \frac{\sigma^k_{r\varphi}}{R},$$
$$\tilde{\nabla}_\alpha \sigma^k_{\alpha r} = \frac{\partial\sigma^k_{xr}}{\partial x} + \frac{1}{R}\frac{\partial\sigma^k_{\varphi r}}{\partial\varphi} + \frac{\sigma^k_{\varphi\varphi}+\sigma^k_{rr}}{R} - \frac{\sigma^k_{rr}}{R},$$

$$\tilde{\nabla}_\alpha D_\alpha^k = \frac{\partial D_x^k}{\partial x} + \frac{1}{R}\frac{\partial D_\varphi^k}{\partial \varphi} + \frac{D_r^k}{2R} - \underline{D_r^k}, \quad \tilde{\nabla}_\alpha B_\alpha^k = \frac{\partial B_x^k}{\partial x} + \frac{1}{R}\frac{\partial B_\varphi^k}{\partial \varphi} + \frac{B_r^k}{2R} - \underline{B_r^k}, \quad \alpha = x, \varphi. \tag{7.1}$$

where

$$\underline{\sigma_{ri}^k} = \frac{2k+1}{h}\left(\sigma_{ri}^{k-1} + \sigma_{ri}^{k-3} + \ldots\right), i = x, \varphi, r, \quad \underline{D_r^k} = \frac{2k+1}{h}\left(D_r^{k-1} + D_r^{k-3} + \ldots\right), \underline{B_r^k} = \frac{2k+1}{h}\left(B_r^{k-1} + B_r^{k-3} + \ldots\right) \tag{7.2}$$

Expressions for the Legendre's polynomial coefficients of the Cauchy strain tensor, electric field and the magnetic field vectors in this case have the form

$$\begin{gathered}
\varepsilon_{xx}^k = \frac{\partial u_x^k}{\partial x}, \quad \varepsilon_{x\varphi}^k = \frac{1}{2}\left(\frac{\partial u_\varphi^k}{\partial x} + \frac{1}{R}\frac{\partial u_x^k}{\partial \varphi}\right), \quad \varepsilon_{rr} = \underline{u_r^k}, \\
\varepsilon_{xr}^k = \frac{1}{2}\left(\frac{\partial u_r^k}{\partial x} + \underline{u_x^k}\right), \quad \varepsilon_{\varphi\varphi}^k = \frac{1}{R}\frac{\partial u_\varphi^k}{\partial \varphi} + \frac{u_r^k}{R}, \quad \varepsilon_{\varphi r}^k = \frac{1}{2}\left(\frac{\partial u_r^k}{\partial \varphi} - \frac{u_\varphi^k}{R} + \underline{u_y^k}\right) \\
E_x^k = \frac{\partial \phi^k}{\partial x}, \quad E_\varphi^k = \frac{1}{R}\frac{\partial \phi^k}{\partial \varphi}, \quad E_r^k = \underline{\phi^k}, \quad M_x^k = \frac{\partial \varphi^k}{\partial x}, \quad M_\varphi^k = \frac{1}{R}\frac{\partial \varphi^k}{\partial \varphi}, \quad M_r^k = \underline{\varphi^k}
\end{gathered} \tag{7.3}$$

where $\underline{\phi^k}$ and $\underline{\varphi^k}$ are defined in (4.7) and $\underline{u_i^k}$ is presented as

$$\underline{u_i^k} = \frac{2k+1}{h}\left(u_i^{k+1} + u_i^{k+3} + \ldots\right), \quad i = x, \varphi, r. \tag{7.4}$$

For the same reason as in the previous section, in order to simplify future consideration following [30, 54] we consider a material with a hexagonal crystal structure (class 6 mm material). For a cylindrical shell we can consider axial, radial and circular polarization of the shell material. In all of these cases the constitutive relations can be considered in the form (5.5), but the Legendre's polynomial coefficients of the stress and strain tensor in matrix notations (2.19) are defined in a different way for each case of polarization.

For materials polarized in the axial direction, related to axis x they are defined as the following

$$\begin{aligned}
\tilde{\boldsymbol{\sigma}}^k &= (\sigma_{rr}^k, \sigma_{\varphi\varphi}^k, \sigma_{xx}^k, \sigma_{x\varphi}^k, \sigma_{xr}^k, \sigma_{\varphi r}^k) \\
\tilde{\boldsymbol{\varepsilon}}^k &= (\varepsilon_{rr}^k, \varepsilon_{\varphi\varphi}^k, \varepsilon_{xx}^k, \varepsilon_{x\varphi}^k, \varepsilon_{xr}^k, \varepsilon_{\varphi r}^k)
\end{aligned}, \tag{7.5}$$

and constitutive relations (4.16) have the form

$$\begin{aligned}
\sigma_{xx}^k &= c_{33}\varepsilon_{xx}^k + c_{13}(\varepsilon_{\varphi\varphi}^k + \varepsilon_{rr}^k) - d_{33}E_x^k - q_{33}M_x^k, \\
\sigma_{\varphi\varphi}^k &= c_{13}\varepsilon_{xx}^k + c_{11}\varepsilon_{\varphi\varphi}^k + c_{13}\varepsilon_{rr}^k - d_{13}E_x^k - q_{13}M_x^k, \\
\sigma_{rr}^k &= c_{13}\varepsilon_{xx}^k + c_{12}\varepsilon_{\varphi\varphi}^k + c_{11}\varepsilon_{rr}^k - d_{13}E_x^k - q_{13}M_x^k, \\
\sigma_{x\varphi}^k &= c_{44}\varepsilon_{x\varphi}^k - d_{51}E_\varphi^k - q_{51}M_\varphi^k, \\
\sigma_{xr}^k &= c_{44}\varepsilon_{xr}^k - d_{51}E_r^k - q_{51}M_r^k, \quad \sigma_{\varphi r}^k = \tfrac{1}{2}(c_{11} - c_{12})\varepsilon_{\varphi r}^k,
\end{aligned}$$

$$
\begin{aligned}
D_x^k &= d_{13}(\varepsilon_{\varphi\varphi}^k + \varepsilon_{rr}^k) + d_{33}\varepsilon_{xx}^k + \epsilon_{33}E_x^k + \beta_{33}M_x^k \\
D_\varphi^k &= d_{51}\varepsilon_{x\varphi}^k + \epsilon_{11}E_\varphi^k + \beta_{11}M_\varphi^k, \quad D_r^k = d_{51}\varepsilon_{xr}^k + \epsilon_{11}E_r^k + \beta_{11}M_r^k, \\
B_x^k &= q_{13}(\varepsilon_{\varphi\varphi}^k + \varepsilon_{rr}^k) + q_{33}\varepsilon_{xx}^k + \beta_{33}E_x^k + \gamma_{33}M_x^k \\
B_\varphi^k &= q_{51}\varepsilon_{x\varphi}^k + \beta_{11}E_\varphi^k + \gamma_{11}M_\varphi^k, \quad B_r^k = q_{51}\varepsilon_{xr}^k + \beta_{11}E_r^k + \gamma_{11}M_r^k,
\end{aligned} \tag{7.6}
$$

For materials polarized in the radial direction, related to axis r they are defined as the following

$$
\begin{aligned}
\tilde{\boldsymbol{\sigma}}^k &= (\sigma_{xx}^k, \sigma_{\varphi\varphi}^k, \sigma_{rr}^k, \sigma_{\varphi r}^k, \sigma_{xr}^k, \sigma_{r\varphi}^k) \\
\tilde{\boldsymbol{\varepsilon}}^k &= (\varepsilon_{xx}^k, \varepsilon_{\varphi\varphi}^k, \varepsilon_{rr}^k, \varepsilon_{\varphi r}^k, \varepsilon_{xr}^k, \varepsilon_{r\varphi}^k)
\end{aligned}, \tag{7.7}
$$

and constitutive relations (4.16) have the form

$$
\begin{aligned}
\sigma_{xx}^k &= c_{11}\varepsilon_{xx}^k + c_{12}\varepsilon_{\varphi\varphi}^k + c_{13}\varepsilon_{rr}^k - d_{13}E_r^k - q_{13}M_r^k, \\
\sigma_{\varphi\varphi}^k &= c_{12}\varepsilon_{xx}^k + c_{11}\varepsilon_{\varphi\varphi}^k + c_{13}\varepsilon_{rr}^k - d_{13}E_r^k - q_{13}M_r^k, \\
\sigma_{rr}^k &= c_{13}(\varepsilon_{xx}^k + \varepsilon_{\varphi\varphi}^k) + c_{33}\varepsilon_{rr}^k - d_{33}E_r^k - q_{33}M_r^k, \\
\sigma_{x\varphi}^k &= \tfrac{1}{2}(c_{11} - c_{12})\varepsilon_{x\varphi}^k, \\
\sigma_{xr}^k &= c_{44}\varepsilon_{xr}^k - d_{51}E_x^k - q_{51}M_x^k, \quad \sigma_{\varphi r}^k = c_{44}\varepsilon_{\varphi r}^k - d_{51}E_\varphi^k - q_{51}M_\varphi^k, \\
D_x^k &= d_{51}\varepsilon_{xr}^k + \epsilon_{11}E_x^k + \beta_{11}M_x^k, \quad D_\varphi^k = d_{51}\varepsilon_{\varphi r}^k + \epsilon_{11}E_\varphi^k + \beta_{11}M_\varphi^k, \\
D_r^k &= d_{13}(\varepsilon_{xx}^k + \varepsilon_{\varphi\varphi}^k) + d_{33}\varepsilon_{rr}^k + \epsilon_{33}E_r^k + \beta_{33}M_r^k, \\
B_x^k &= q_{51}\varepsilon_{xr}^k + \beta_{11}E_x^k + \gamma_{11}M_x^k, \quad B_\varphi^k = q_{51}\varepsilon_{\varphi r}^k + \beta_{11}E_\varphi^k + \gamma_{11}M_\varphi^k, \\
B_r^k &= q_{13}(\varepsilon_{xx}^k + \varepsilon_{\varphi\varphi}^k) + q_{33}\varepsilon_{rr}^k + \beta_{33}E_r^k + \gamma_{33}M_r^k,
\end{aligned} \tag{7.8}
$$

For material polarized in the circular direction, related to axis φ they are defined as the following

$$
\begin{aligned}
\tilde{\boldsymbol{\sigma}}^k &= (\sigma_{xx}^k, \sigma_{rr}^k, \sigma_{\varphi\varphi}^k, \sigma_{r\varphi}^k, \sigma_{\varphi r}^k, \sigma_{xr}^k) \\
\tilde{\boldsymbol{\varepsilon}}^k &= (\varepsilon_{xx}^k, \varepsilon_{rr}^k, \varepsilon_{\varphi\varphi}^k, \varepsilon_{r\varphi}^k, \varepsilon_{\varphi r}^k, \varepsilon_{xr}^k)
\end{aligned}, \tag{7.9}
$$

and constitutive relations (4.16) have the form

$$
\begin{aligned}
\sigma_{xx}^k &= c_{11}\varepsilon_{xx}^k + c_{13}\varepsilon_{\varphi\varphi}^k + c_{12}\varepsilon_{rr}^k - d_{13}E_\varphi^k - q_{13}M_\varphi^k, \\
\sigma_{\varphi\varphi}^k &= c_{13}\varepsilon_{xx}^k + c_{11}\varepsilon_{\varphi\varphi}^k + c_{13}\varepsilon_{rr}^k - d_{13}E_\varphi^k - q_{13}M_\varphi^k, \\
\sigma_{rr}^k &= c_{13}(\varepsilon_{xx}^k + \varepsilon_{rr}^k) + c_{33}\varepsilon_{\varphi\varphi}^k - d_{33}E_\varphi^k - q_{33}M_\varphi^k, \\
\sigma_{x\varphi}^k &= c_{44}\varepsilon_{x\varphi}^k - d_{51}E_x^k - q_{51}M_x^k, \\
\sigma_{xr}^k &= \tfrac{1}{2}(c_{11} - c_{12})\varepsilon_{xr}^k, \quad \sigma_{\varphi r}^k = c_{44}\varepsilon_{\varphi r}^k - d_{51}E_r^k - q_{51}M_r^k, \\
D_x^k &= d_{51}\varepsilon_{x\varphi}^k + \epsilon_{11}E_x^k + \beta_{11}M_x^k, \quad D_r^k = d_{51}\varepsilon_{\varphi r}^k + \epsilon_{11}E_r^k + \beta_{11}M_r^k,
\end{aligned}
$$

$$
\begin{aligned}
D_{\varphi}^{k} &= d_{13}(\varepsilon_{xx}^{k}+\varepsilon_{rr}^{k})+d_{33}\varepsilon_{\varphi\varphi}^{k}+\epsilon_{33}E_{\varphi}^{k}+\beta_{33}M_{\varphi}^{k},\\
B_{x}^{k} &= q_{51}\varepsilon_{x\varphi}^{k}+\beta_{11}E_{x}^{k}+\gamma_{11}M_{x}^{k},\quad B_{r}^{k}=q_{51}\varepsilon_{\varphi r}^{k}+\beta_{11}E_{r}^{k}+\gamma_{11}M_{r}^{k},\\
B_{\varphi}^{k} &= q_{13}(\varepsilon_{xx}^{k}+\varepsilon_{rr}^{k})+q_{33}\varepsilon_{\varphi\varphi}^{k}+\beta_{33}E_{\varphi}^{k}+\gamma_{33}M_{\varphi}^{k}.
\end{aligned}
\tag{7.10}
$$

By substituting equations for the Legendre's polynomial coefficients of the strain tensor, electric and magnetic field vectors (7.3) into the constitutive equations for the Legendre's polynomial coefficients (7.6), (7.8) or (7.10) we obtain equations for the Legendre's polynomial coefficients the stress tensor and the electric and magnetic displacement vectors expressed in the form of the Legendre's polynomial coefficients of the displacement vector and electro and magnetic potentials components.

Here, we consider in more detail the case of axial polarization (7.5). In this case the Legendre's polynomial coefficients, the stress tensor and the electric and magnetic displacement vectors expressed are presented in the form of the Legendre's polynomial coefficients of the displacement vector and electro and magnetic potentials components as the following

$$
\begin{aligned}
\sigma_{xx}^{k} &= c_{33}\frac{\partial u_{x}^{k}}{\partial x}+c_{13}\left(\frac{1}{R}\frac{\partial u_{\varphi}^{k}}{\partial\varphi}+\frac{u_{r}^{k}}{R}+\underline{u_{r}^{k}}\right)-d_{33}\frac{\partial\phi^{k}}{\partial x}-q_{33}\frac{\partial\varphi^{k}}{\partial x},\\
\sigma_{\varphi\varphi}^{k} &= c_{13}\frac{\partial u_{x}^{k}}{\partial x}+c_{11}\left(\frac{1}{R}\frac{\partial u_{\varphi}^{k}}{\partial\varphi}+\frac{u_{r}^{k}}{R}\right)+c_{13}\underline{u_{r}^{k}}-d_{13}\frac{\partial\phi^{k}}{\partial x}-q_{13}\frac{\partial\varphi^{k}}{\partial x},\\
\sigma_{rr}^{k} &= c_{13}\frac{\partial u_{x}^{k}}{\partial x}+c_{12}\left(\frac{1}{R}\frac{\partial u_{\varphi}^{k}}{\partial\varphi}+\frac{u_{r}^{k}}{R}\right)+c_{11}\underline{u_{r}^{k}}-d_{13}\frac{\partial\phi^{k}}{\partial x}-q_{13}\frac{\partial\varphi^{k}}{\partial x},\\
\sigma_{x\varphi}^{k} &= \frac{c_{44}}{2}\left(\frac{\partial u_{\varphi}^{k}}{\partial x}+\frac{1}{R}\frac{\partial u_{x}^{k}}{\partial\varphi}\right)-\frac{d_{51}}{R}\frac{\partial\phi^{k}}{\partial\varphi}-\frac{q_{51}}{R}\frac{\partial\varphi^{k}}{\partial\varphi},\\
\sigma_{xr}^{k} &= \frac{c_{44}}{2}\left(\frac{\partial u_{r}^{k}}{\partial x}+\underline{u_{x}^{k}}\right)-d_{51}\underline{\phi^{k}}-q_{51}\underline{\varphi^{k}}\quad \sigma_{\varphi r}^{k}=\frac{c_{11}-c_{12}}{4}\left(\frac{\partial u_{r}^{k}}{\partial\varphi}-\frac{u_{\varphi}^{k}}{R}+\underline{u_{y}^{k}}\right),\\
D_{x}^{k} &= d_{13}\left(\frac{1}{R}\frac{\partial u_{\varphi}^{k}}{\partial\varphi}+\frac{u_{r}^{k}}{R}+\underline{u_{r}^{k}}\right)+d_{33}\frac{\partial u_{x}^{k}}{\partial x}+\epsilon_{33}\frac{\partial\phi^{k}}{\partial x}+\beta_{33}\frac{\partial\varphi^{k}}{\partial x}\\
D_{\varphi}^{k} &= \frac{d_{51}}{2}\left(\frac{\partial u_{\varphi}^{k}}{\partial x}+\frac{1}{R}\frac{\partial u_{x}^{k}}{\partial\varphi}\right)+\frac{\epsilon_{11}}{R}\frac{\partial\phi^{k}}{\partial\varphi}+\frac{\beta_{11}}{R}\frac{\partial\varphi^{k}}{\partial\varphi},\quad D_{r}^{k}=\frac{d_{51}}{2}\left(\frac{\partial u_{r}^{k}}{\partial x}+\underline{u_{x}^{k}}\right)+\epsilon_{11}\underline{\phi^{k}}+\beta_{11}\underline{\varphi^{k}},\\
B_{x}^{k} &= q_{13}\left(\frac{1}{R}\frac{\partial u_{\varphi}^{k}}{\partial\varphi}+\frac{u_{r}^{k}}{R}+\underline{u_{r}^{k}}\right)+q_{33}\frac{\partial u_{x}^{k}}{\partial x}+\beta_{33}\frac{\partial\phi^{k}}{\partial x}+\gamma_{33}\frac{\partial\varphi^{k}}{\partial x}\\
B_{\varphi}^{k} &= \frac{q_{51}}{2}\left(\frac{\partial u_{\varphi}^{k}}{\partial x}+\frac{1}{R}\frac{\partial u_{x}^{k}}{\partial\varphi}\right)+\frac{\beta_{11}}{R}\frac{\partial\phi^{k}}{\partial\varphi}+\frac{\gamma_{11}}{R}\frac{\partial\varphi^{k}}{\partial\varphi},\quad B_{r}^{k}=\frac{q_{51}}{2}\left(\frac{\partial u_{r}^{k}}{\partial x}+\underline{u_{x}^{k}}\right)+\beta_{11}\underline{\phi^{k}}+\gamma_{11}\underline{\varphi^{k}},
\end{aligned}
\tag{7.11}
$$

By substituting the Eqs. (7.11) into the equations of equilibrium (4.12) and taking into account that the divergence operator for the Legendre's polynomial coefficients of the stress tensor and the electric and magnetic displacement vectors have form (7.1), we obtain the coupled system of differential equations of the linear electro-magneto-elasticity for the displacement vector as well as electric and magnetic

potentials in the form (2.13) where elements of the block matrices and block vectors (4.20) have the form

$$\mathbf{L}^{rk}_{uu}=\begin{vmatrix} L^{rk}_{xx} & L^{rk}_{x\varphi} & L^{rk}_{xr}\\ L^{rk}_{\varphi x} & L^{rk}_{\varphi\varphi} & L^{rk}_{\varphi r}\\ L^{rk}_{rx} & L^{rk}_{r\varphi} & L^{rk}_{rr}\end{vmatrix},\quad \mathbf{L}^{rk}_{eu}=\begin{vmatrix} L^{rk}_{ex}\\ L^{rk}_{e\varphi}\\ L^{rk}_{er}\end{vmatrix},\quad \mathbf{L}^{rk}_{mu}=\begin{vmatrix} L^{rk}_{mx}\\ L^{rk}_{m\varphi}\\ L^{rk}_{mr}\end{vmatrix},\quad \mathbf{u}^{k}=\begin{vmatrix} u^{k}_{x}\\ u^{k}_{\varphi}\\ u^{k}_{r}\end{vmatrix},\quad \mathbf{b}^{k}=\begin{vmatrix} b^{k}_{x}\\ b^{k}_{\varphi}\\ b^{k}_{r}\end{vmatrix}$$

$$\mathbf{L}^{rk}_{ue}=\begin{vmatrix} L^{rk}_{xe} & L^{rk}_{\varphi e} & L^{rk}_{re}\end{vmatrix},\quad \mathbf{L}^{rk}_{um}=\begin{vmatrix} L^{rk}_{xm} & L^{rk}_{\varphi m} & L^{rk}_{rm}\end{vmatrix}, \tag{7.12}$$

Some elements of these matrices are differential operators, some are constants and some are equal to zero.

Below, all elements of the matrices (5.9) for the case of the first order theory of the linear couple electro-magneto-elastic theory of plates in Cartesian coordinates are presented in the form

$$L^{00}_{xx}=c_{11}\frac{\partial^2}{\partial x^2}+\frac{c_{11}-c_{12}}{4}\frac{\partial^2}{\partial y^2},\quad L^{00}_{xy}=\frac{c_{11}+3c_{12}}{4}\frac{\partial^2}{\partial x\partial y},$$

$$L^{00}_{xz}=0,\quad L^{01}_{xx}=0,\quad L^{01}_{xy}=0,\quad L^{01}_{xz}=\frac{c_{13}}{h}\frac{\partial}{\partial x},$$

$$L^{00}_{xe}=0,\quad L^{01}_{xe}=-\frac{d_{13}}{h}\frac{\partial}{\partial x},\quad L^{00}_{xm}=0,\quad L^{01}_{xm}=-\frac{q_{13}}{h}\frac{\partial}{\partial x},$$

$$L^{00}_{yx}=\frac{c_{11}+3c_{12}}{4}\frac{\partial^2}{\partial x\partial y},\quad L^{00}_{yy}=c_{11}\frac{\partial^2}{\partial y^2}+\frac{c_{11}-c_{12}}{4}\frac{\partial^2}{\partial x^2},$$

$$L^{00}_{yz}=0,\quad L^{01}_{yx}=0,\quad L^{01}_{yy}=0,\quad L^{01}_{yz}=\frac{c_{13}}{h}\frac{\partial}{\partial x},$$

$$L^{00}_{ye}=0,\quad L^{01}_{ye}=-\frac{d_{13}}{h}\frac{\partial}{\partial y},\quad L^{00}_{ym}=0,\quad L^{01}_{ym}=-\frac{q_{13}}{h}\frac{\partial}{\partial y},$$

$$L^{00}_{zx}=0,\quad L^{00}_{zy}=0,\quad L^{00}_{zz}=\frac{c_{44}}{2}\left(\frac{\partial^2}{\partial x^2}+\frac{\partial^2}{\partial y^2}\right),$$

$$L^{01}_{zx}=\frac{c_{44}}{2h}\frac{\partial}{\partial x},\quad L^{01}_{zy}=\frac{c_{44}}{2h}\frac{\partial}{\partial y},\quad L^{01}_{zz}=0,$$

$$L^{00}_{ze}=-d_{51}\left(\frac{\partial^2}{\partial x^2}+\frac{\partial^2}{\partial y^2}\right),\quad L^{01}_{ze}=0,$$

$$L^{00}_{zm}=-q_{51}\left(\frac{\partial^2}{\partial x^2}+\frac{\partial^2}{\partial y^2}\right),\quad L^{01}_{zm}=0,$$

$$L^{10}_{xx}=0,\quad L^{10}_{xy}=0,\quad L^{10}_{xz}=-\frac{3c_{44}}{2h}\frac{\partial}{\partial x},\quad L^{11}_{xx}=c_{11}\frac{\partial^2}{\partial x^2}+\frac{c_{11}-c_{12}}{4}\frac{\partial^2}{\partial y^2}-\frac{3c_{44}}{2h^2},$$

$$L^{11}_{xy}=\frac{c_{11}+3c_{12}}{4}\frac{\partial^2}{\partial x\partial y},\quad L^{11}_{xz}=0,\ L^{10}_{xe}=\frac{3d_{51}}{h}\frac{\partial}{\partial x},\quad L^{11}_{xe}=0,\quad L^{10}_{xm}=\frac{3q_{51}}{h}\frac{\partial}{\partial x},$$

$$L^{11}_{xm}=0,\quad L^{10}_{yx}=0,\quad L^{10}_{yy}=0,\quad L^{10}_{yz}=-\frac{3c_{44}}{2h}\frac{\partial}{\partial y},\quad L^{11}_{yx}=\frac{c_{11}+3c_{12}}{4}\frac{\partial^2}{\partial x\partial y},$$

$$L^{11}_{yy}=c_{11}\frac{\partial^2}{\partial x^2}+\frac{c_{11}-c_{12}}{4}\frac{\partial^2}{\partial y^2}-\frac{3c_{44}}{2h^2},\quad L^{11}_{yz}=0,\ L^{10}_{ye}=\frac{3d_{51}}{h}\frac{\partial}{\partial y},$$

$$
\begin{aligned}
&L_{ye}^{11}=0,\quad L_{ym}^{10}=\frac{3q_{51}}{h}\frac{\partial}{\partial y},\quad L_{ym}^{11}=0, L_{zx}^{10}=\frac{3c_{13}}{h}\frac{\partial}{\partial x},\quad L_{zy}^{10}=\frac{3c_{13}}{h}\frac{\partial}{\partial y},\\
&L_{zz}^{10}=0,\quad L_{zx}^{11}=0,\quad L_{zy}^{11}=0,\quad L_{zz}^{11}=\frac{c_{44}}{2}\left(\frac{\partial^2}{\partial x^2}+\frac{\partial^2}{\partial y^2}\right)+\frac{3c_{33}}{h^2},\\
&L_{ze}^{10}=0,\quad L_{ze}^{11}=-d_{51}\left(\frac{\partial^2}{\partial x^2}+\frac{\partial^2}{\partial y^2}\right)+\frac{3d_{33}}{h^2},\quad L_{zm}^{10}=0,\\
&L_{zm}^{11}=-q_{51}\left(\frac{\partial^2}{\partial x^2}+\frac{\partial^2}{\partial y^2}\right)+\frac{3q_{33}}{h^2},\\
&L_{ex}^{00}=0,\quad L_{ey}^{00}=0,\quad L_{ez}^{00}=\frac{d_{51}}{2}\left(\frac{\partial^2}{\partial x^2}+\frac{\partial^2}{\partial y^2}\right),\quad L_{ex}^{01}=\frac{d_{51}}{2h}\frac{\partial}{\partial x},\quad L_{ey}^{01}=\frac{d_{51}}{2h}\frac{\partial}{\partial y},\\
&L_{ez}^{01}=0, L_{ee}^{00}=\epsilon_{11}\left(\frac{\partial^2}{\partial x^2}+\frac{\partial^2}{\partial y^2}\right),\quad L_{ee}^{01}=0,\quad L_{em}^{10}=\beta_{11}\left(\frac{\partial^2}{\partial x^2}+\frac{\partial^2}{\partial y^2}\right),\\
&L_{em}^{11}=0, L_{mx}^{00}=0,\quad L_{my}^{00}=0,\quad L_{mz}^{00}=\frac{q_{51}}{2}\left(\frac{\partial^2}{\partial x^2}+\frac{\partial^2}{\partial y^2}\right),\quad L_{mx}^{01}=\frac{q_{51}}{2h}\frac{\partial}{\partial x},\\
&L_{my}^{01}=\frac{q_{51}}{2h}\frac{\partial}{\partial y},\quad L_{mz}^{01}=0, L_{me}^{00}=\beta_{11}\left(\frac{\partial^2}{\partial x^2}+\frac{\partial^2}{\partial y^2}\right),\quad L_{me}^{01}=0,\\
&L_{mm}^{10}=\gamma_{11}\left(\frac{\partial^2}{\partial x^2}+\frac{\partial^2}{\partial y^2}\right),\quad L_{mm}^{11}=0, L_{ex}^{10}=-\frac{3d_{13}}{h}\frac{\partial}{\partial x},\quad L_{ey}^{10}=-\frac{3d_{13}}{h}\frac{\partial}{\partial y},\\
&L_{ez}^{10}=0,\quad L_{ex}^{11}=0,\quad L_{ey}^{11}=0,\quad L_{ez}^{11}=\frac{d_{51}}{2}\left(\frac{\partial^2}{\partial x^2}+\frac{\partial^2}{\partial y^2}\right)-\frac{3d_{33}}{h^2},\\
&L_{ee}^{10}=0,\quad L_{ee}^{11}=\epsilon_{11}\left(\frac{\partial^2}{\partial x^2}+\frac{\partial^2}{\partial y^2}\right)-\frac{3\epsilon_{33}}{h^2},\quad L_{em}^{10}=0,\\
&L_{em}^{11}=\beta_{11}\left(\frac{\partial^2}{\partial x^2}+\frac{\partial^2}{\partial y^2}\right)-\frac{3\beta_{33}}{h^2}, L_{mx}^{10}=-\frac{3q_{13}}{h}\frac{\partial}{\partial x},\quad L_{my}^{10}=-\frac{3q_{13}}{h}\frac{\partial}{\partial y},\\
&L_{mz}^{10}=0,\quad L_{mx}^{11}=0,\quad L_{my}^{11}=0,\quad L_{mz}^{11}=\frac{q_{51}}{2}\left(\frac{\partial^2}{\partial x^2}+\frac{\partial^2}{\partial y^2}\right)-\frac{3q_{33}}{h^2},\\
&L_{me}^{10}=0,\quad L_{me}^{11}=\beta_{11}\left(\frac{\partial^2}{\partial x^2}+\frac{\partial^2}{\partial y^2}\right)-\frac{3\beta_{33}}{h^2},\quad L_{mm}^{10}=0,\\
&L_{mm}^{11}=\gamma_{11}\left(\frac{\partial^2}{\partial x^2}+\frac{\partial^2}{\partial y^2}\right)-\frac{3\gamma_{33}}{h^2},
\end{aligned}
\tag{7.13}
$$

A complete 2-D system of the differential equations for the higher order theory of the electro-magneto-elastic plates in the Cartesian system of coordinates is presented in this section. Explicit expressions for divergences of the Legendre's polynomial coefficients of stress tensor and the electric and magnetic displacement vectors (7.1), for the Legendre's polynomial coefficients of strain tensor and electric field and the magnetic field vectors (7.3) and for the Legendre's polynomial coefficients of stress tensor and the electric and magnetic displacement vectors (7.11) as functions of the Legendre's polynomial coefficients of displacements and electric and magnetic potentials for higher order theory of plates are presented here. For the case of the first order approximation theory, elements of matrix differential operators (5.9), that are

included in the equations of equilibrium (2.13) are also presented in the explicit form (7.13). They can be used for theoretical analysis, as well as analytical and numerical solutions of the problems arising in science and engineering.

8 Higher Order Theory of Electro-Magneto-Elastic Spherical Shell

Let us consider the higher order model of the electro-magneto-elastic elastic shells of the spherical geometry, which is very important and often used in theoretical analysis as well as applied in sciences and engineering. Let us introduce spherical coordinates such that $x_1 = \varphi, x_2 = \psi$ and $x_3 = r, r \in [R-h, R+h]$. Coefficients of the first quadratic form of a surface and main curvatures are equal to $A_1 = R,\ A_2 = R\sin(\psi)$, and $k_1 = \frac{1}{R}, k_2 = \frac{1}{R}$, respectively. By substituting these parameters in the Eqs. (4.12)–(4.16), the equations that correspond to the higher order theory of linear electro-magneto-elasticity of the of cylindrical shell will be obtained.

The equations of equilibrium and Maxwell equations for Legendre's polynomial coefficients in this case have the form (4.12) but the operator of divergence of the stress tensor and the electric and magnetic displacement vectors in the system of coordinates introduced here have the form

$$
\begin{aligned}
\tilde{\nabla}_\alpha \sigma^k_{\alpha\varphi} &= \frac{1}{R}\frac{\partial \sigma^k_{\varphi\varphi}}{\partial\varphi} + \frac{1}{R}\frac{\partial \sigma^k_{\psi\varphi}}{\sin(\psi)\partial\psi} + \frac{2\sigma^k_{r\varphi}}{R} - \frac{\underline{\underline{\sigma^k_{r\varphi}}}}{R},\\
\tilde{\nabla}_\alpha \sigma^k_{\alpha\psi} &= \frac{1}{R}\frac{\partial \sigma^k_{\varphi\psi}}{\partial\varphi} + \frac{1}{R}\frac{\partial \sigma^k_{\psi\psi}}{\sin(\psi)\partial\psi} + \frac{\sigma^k_{\psi r}}{R} + \frac{2\sigma^k_{r\psi}}{R} - \frac{\underline{\underline{\sigma^k_{r\psi}}}}{R},\\
\tilde{\nabla}_\alpha \sigma^k_{\alpha r} &= \frac{1}{R}\frac{\partial \sigma^k_{\varphi r}}{\partial\varphi} + \frac{\partial \sigma^k_{\psi r}}{\sin(\psi)\partial\psi} - \frac{\sigma^k_{\varphi\varphi} + \sigma^k_{\psi\psi} - 2\sigma^k_{rr}}{R} - \frac{\underline{\underline{\sigma^k_{rr}}}}{R}\\
\tilde{\nabla}_\alpha D^k_\alpha &= \frac{1}{R}\frac{\partial D^k_\varphi}{\partial\varphi} + \frac{1}{R}\frac{\partial D^k_\psi}{\sin(\psi)\partial\psi} + \frac{D^k_r}{2R} - \underline{D^k_r},\\
\tilde{\nabla}_\alpha B^k_\alpha &= \frac{1}{R}\frac{\partial B^k_\varphi}{\partial\varphi} + \frac{1}{R}\frac{\partial B^k_\psi}{\sin(\psi)\partial\psi} + \frac{B^k_r}{2R} - \underline{B^k_r}, \quad \alpha = \varphi, \psi.
\end{aligned}
\tag{8.1}
$$

where

$$
\underline{\sigma^k_{ri}} = \frac{2k+1}{h}\left(\sigma^{k-1}_{ri} + \sigma^{k-3}_{ri} + \ldots\right), i = x, \varphi, r, \quad \underline{D^k_r} = \frac{2k+1}{h}\left(D^{k-1}_r + D^{k-3}_r + \ldots\right), \underline{B^k_r} = \frac{2k+1}{h}\left(B^{k-1}_r + B^{k-3}_r + \ldots\right)
\tag{8.2}
$$

Expressions for the Legendre's polynomial coefficients of the Cauchy strain tensor, electric field and the magnetic field vectors in this case have the form

$$\varepsilon^k_{\varphi\varphi} = \frac{1}{R}\left(\frac{\partial u^k_\varphi}{\partial\varphi} + u^k_r\right), \quad \varepsilon^k_{\varphi\psi} = \frac{1}{2R}\left(\frac{\partial u^k_\varphi}{\sin(\psi)\partial\psi} + \frac{\partial u^k_\psi}{\partial\varphi}\right), \quad \varepsilon_{rr} = \underline{u^k_r},$$
$$\varepsilon^k_{\varphi r} = \frac{1}{2}\left(\frac{1}{R}\left(\frac{\partial u^k_r}{\partial\varphi} - u^k_\varphi\right) + \underline{u^k_\varphi}\right), \quad \varepsilon^k_{\psi\psi} = \frac{1}{R}\left(\frac{\partial u^k_\psi}{\sin(\psi)\partial\psi} + u^k_r\right),$$
$$\varepsilon^k_{\psi r} = \frac{1}{2}\left(\frac{1}{R}\left(\frac{\partial u^k_r}{\sin(\psi)\partial\psi} - u^k_\psi\right) + \underline{u^k_\psi}\right) E^k_\varphi = \frac{1}{R}\frac{\partial\phi^k}{\partial\varphi},$$
$$E^k_\psi = \frac{1}{R}\frac{\partial\phi^k}{\sin(\psi)\partial\psi}, \quad E^k_r = \underline{\phi^k}, \quad M^k_\varphi = \frac{1}{R}\frac{\partial\varphi^k}{\partial\varphi},$$
$$M^k_\psi = \frac{1}{R}\frac{\partial\varphi^k}{\sin(\psi)\partial\psi}, \quad M^k_r = \underline{\varphi^k} \tag{8.3}$$

where $\underline{\phi^k}$ and $\underline{\varphi^k}$ are defined in (4.7) and $\underline{u^k_i}$ is presented as

$$\underline{u^k_i} = \frac{2k+1}{h}\left(u^{k+1}_i + u^{k+3}_i + \ldots\right), \quad i = x, \varphi, r. \tag{8.4}$$

For the same reason as in the previous section, in order to simplify future consideration following [30, 54] we consider a material with a hexagonal crystal structure (class 6 mm). For a spherical shell we can consider axial, radial and circular polarization of the shell material. In all of these cases the constitutive relations can be considered in the form (5.5), but the Legendre's polynomial coefficients of the stress and strain tensor in matrix notations (2.19) are defined in a different way for each case of polarization.

For materials polarized in the radial direction, related to axis r they are defined as the following

$$\begin{aligned}\tilde{\boldsymbol{\sigma}}^k &= (\sigma^k_{\psi\psi}, \sigma^k_{\varphi\varphi}, \sigma^k_{rr}, \sigma^k_{\varphi r}, \sigma^k_{\psi r}, \sigma^k_{\varphi\psi})\\ \tilde{\boldsymbol{\varepsilon}}^k &= (\varepsilon^k_{\psi\psi}, \varepsilon^k_{\varphi\varphi}, \varepsilon^k_{rr}, \varepsilon^k_{\varphi r}, \varepsilon^k_{\psi r}, \varepsilon^k_{\varphi\psi})\end{aligned}, \tag{8.5}$$

When substituting matrix relations for electro-magneto-elastic constants (5.5) and vectorial representations for stress and strain tensors (8.5) in the electro-magneto-elastic constitutive relations for the Legendre's polynomial coefficients (4.16) we represent them in the form

$$\begin{aligned}\sigma^k_{\varphi\varphi} &= c_{11}\varepsilon^k_{\varphi\varphi} + c_{12}\varepsilon^k_{\psi\psi} + c_{13}\varepsilon^k_{rr} - d_{13}E^k_r - q_{13}M^k_r,\\ \sigma^k_{\psi\psi} &= c_{12}\varepsilon^k_{\varphi\varphi} + c_{11}\varepsilon^k_{\psi\psi} + c_{13}\varepsilon^k_{rr} - d_{13}E^k_r - q_{13}M^k_r,\\ \sigma^k_{rr} &= c_{13}(\varepsilon^k_{\varphi\varphi} + \varepsilon^k_{\psi\psi}) + c_{33}\varepsilon^k_{rr} - d_{33}E^k_r - q_{33}M^k_r,\\ \sigma^k_{\varphi\psi} &= \tfrac{1}{2}(c_{11} - c_{12})\varepsilon^k_{\varphi\psi}, \sigma^k_{\varphi r} = c_{44}\varepsilon^k_{\varphi r} - d_{51}E^k_\varphi - q_{51}M^k_\varphi,\\ \sigma^k_{\psi r} &= c_{44}\varepsilon^k_{\psi r} - d_{51}E^k_\psi - q_{51}M^k_\psi,\\ D^k_\varphi &= d_{51}\varepsilon^k_{\varphi r} + \epsilon_{11}E^k_\varphi + \beta_{11}M^k_\varphi, D^k_\psi = d_{51}\varepsilon^k_{\psi r} + \epsilon_{11}E^k_\psi + \beta_{11}M^k_\psi,\end{aligned}$$

$$
\begin{aligned}
D_r^k &= d_{13}(\varepsilon_{\varphi\varphi}^k + \varepsilon_{\psi\psi}^k) + d_{33}\varepsilon_{rr}^k + \epsilon_{33}E_r^k + \beta_{33}M_r^k,\\
B_\varphi^k &= q_{51}\varepsilon_{\varphi r}^k + \beta_{11}E_\varphi^k + \gamma_{11}M_\varphi^k, \quad B_\psi^k = q_{51}\varepsilon_{\psi r}^k + \beta_{11}E_\psi^k + \gamma_{11}M_\psi^k,\\
B_r^k &= q_{13}(\varepsilon_{\varphi\varphi}^k + \varepsilon_{\psi\psi}^k) + q_{33}\varepsilon_{rr}^k + \beta_{33}E_r^k + \gamma_{33}M_r^k,
\end{aligned} \tag{8.6}
$$

By substituting equations for the Legendre's polynomial coefficients of the strain tensor, electric and magnetic field vectors (8.3) into the constitutive equations for the Legendre's polynomial coefficients (8.6), we obtain equations for the Legendre's polynomial coefficients, the stress tensor and the electric and magnetic displacement vectors expressed in the form of the Legendre's polynomial coefficients of the displacement vector as well aselectro and magnetic potentials components in the form

$$
\begin{aligned}
\sigma_{\varphi\varphi}^k &= \frac{c_{11}}{R}\left(\frac{\partial u_\varphi^k}{\partial\varphi} + u_r^k\right) + \frac{c_{12}}{R}\left(\frac{\partial u_\psi^k}{\sin(\psi)\partial\psi} + u_r^k\right) + c_{13}\underline{u_r^k} - d_{13}\underline{\phi^k} - q_{13}\underline{\varphi^k},\\
\sigma_{\psi\psi}^k &= \frac{c_{12}}{R}\left(\frac{\partial u_\varphi^k}{\partial\varphi} + u_r^k\right) + c_{11}\frac{1}{R}\left(\frac{\partial u_\psi^k}{\sin(\psi)\partial\psi} + u_r^k\right) + c_{13}\underline{u_r^k} - d_{13}\underline{\phi^k} - q_{13}\underline{\varphi^k},\\
\sigma_{rr}^k &= \frac{c_{13}}{R}\left(\frac{\partial u_\varphi^k}{\partial\varphi} + \frac{\partial u_\psi^k}{\sin(\psi)\partial\psi} + 2u_r^k\right) + c_{33}\underline{u_r^k} - d_{33}\underline{\phi^k} - q_{33}\underline{\varphi^k},\\
\sigma_{\varphi\psi}^k &= \frac{c_{11}-c_{12}}{4R}\left(\frac{\partial u_\varphi^k}{\sin(\psi)\partial\psi} + \frac{\partial u_\psi^k}{\partial\varphi}\right)\\
\sigma_{\varphi r}^k &= \frac{c_{44}}{2}\left(\frac{1}{R}\left(\frac{\partial u_r^k}{\partial\varphi} - u_\varphi^k\right) + \underline{u_\varphi^k}\right) - \frac{d_{51}}{R}\frac{\partial\phi^k}{\partial\varphi} - \frac{q_{51}}{R}\frac{\partial\varphi^k}{\partial\varphi},\\
\sigma_{\psi r}^k &= \frac{c_{44}}{R}\left(\frac{\partial u_\psi^k}{\sin(\psi)\partial\psi} + u_r^k\right) - \frac{d_{51}}{R}\frac{\partial\phi^k}{\sin(\psi)\partial\psi} - \frac{q_{51}}{R}\frac{\partial\varphi^k}{\sin(\psi)\partial\psi},\\
D_\varphi^k &= \frac{d_{51}}{2}\left(\frac{1}{R}\left(\frac{\partial u_r^k}{\partial\varphi} - u_\varphi^k\right) + \underline{u_\varphi^k}\right) + \frac{\epsilon_{11}}{R}\frac{\partial\phi^k}{\partial\varphi} + \frac{\beta_{11}}{R}\frac{\partial\varphi^k}{\partial\varphi},\\
D_\psi^k &= \frac{d_{51}}{R}\left(\frac{\partial u_\psi^k}{\sin(\psi)\partial\psi} + u_r^k\right) + \frac{\epsilon_{11}}{R}\frac{\partial\phi^k}{\sin(\psi)\partial\psi} + \frac{\beta_{11}}{R}\frac{\partial\varphi^k}{\sin(\psi)\partial\psi},\\
D_r^k &= d_{13}\frac{1}{R}\left(\frac{\partial u_\varphi^k}{\partial\varphi} + \frac{\partial u_\psi^k}{\sin(\psi)\partial\psi} + 2u_r^k\right) + d_{33}\underline{u_r^k} + \epsilon_{33}\underline{\phi^k} + \beta_{33}\underline{\varphi^k},\\
B_\varphi^k &= \frac{q_{51}}{2}\left(\frac{1}{R}\left(\frac{\partial u_r^k}{\partial\varphi} - u_\varphi^k\right) + \underline{u_\varphi^k}\right) + \frac{\beta_{11}}{R}\frac{\partial\phi^k}{\partial\varphi} + \frac{\gamma_{11}}{R}\frac{\partial\varphi^k}{\partial\varphi},\\
B_\psi^k &= \frac{q_{51}}{R}\left(\frac{\partial u_\psi^k}{\sin(\psi)\partial\psi} + u_r^k\right) + \frac{\beta_{11}}{R}\frac{\partial\phi^k}{\sin(\psi)\partial\psi}E_\psi^k + \frac{\gamma_{11}}{R}\frac{\partial\varphi^k}{\sin(\psi)\partial\psi},\\
B_r^k &= q_{13}\frac{1}{R}\left(\frac{\partial u_\varphi^k}{\partial\varphi} + \frac{\partial u_\psi^k}{\sin(\psi)\partial\psi} + 2u_r^k\right) + q_{33}\underline{u_r^k} + \beta_{33}\underline{\phi^k} + \gamma_{33}\underline{\varphi^k},
\end{aligned} \tag{8.7}
$$

By substituting the Eqs. (7.11) into the equations of equilibrium (4.12) and taking into account that the divergence operator for the Legendre's polynomial coefficients of the stress tensor and the electric and magnetic displacement vectors has form (7.1), we obtain the coupled system of differential equations of the linear electro-magneto-elasticity for the displacement vector, electric and magnetic potentials in the form (2.13) where elements of the block matrices and block vectors (4.20) have the form

$$\mathbf{L}^{rk}_{uu} = \begin{vmatrix} L^{rk}_{\varphi\varphi} & L^{rk}_{\varphi\psi} & L^{rk}_{\varphi r} \\ L^{rk}_{\psi\varphi} & L^{rk}_{\psi\psi} & L^{rk}_{\psi r} \\ L^{rk}_{r\varphi} & L^{rk}_{r\psi} & L^{rk}_{rr} \end{vmatrix}, \quad \mathbf{L}^{rk}_{eu} = \begin{vmatrix} L^{rk}_{e\varphi} \\ L^{rk}_{e\psi} \\ L^{rk}_{er} \end{vmatrix}, \quad \mathbf{L}^{rk}_{mu} = \begin{vmatrix} L^{rk}_{m\varphi} \\ L^{rk}_{m\psi} \\ L^{rk}_{mr} \end{vmatrix}, \quad \mathbf{u}^{k} = \begin{vmatrix} u^{k}_{\varphi} \\ u^{k}_{\psi} \\ u^{k}_{r} \end{vmatrix}, \quad \mathbf{b}^{k} = \begin{vmatrix} b^{k}_{\varphi} \\ b^{k}_{\psi} \\ b^{k}_{r} \end{vmatrix}$$

$$\mathbf{L}^{rk}_{ue} = \begin{vmatrix} L^{rk}_{\varphi e} & L^{rk}_{\psi e} & L^{rk}_{re} \end{vmatrix}, \quad \mathbf{L}^{rk}_{um} = \begin{vmatrix} L^{rk}_{\varphi m} & L^{rk}_{\psi m} & L^{rk}_{rm} \end{vmatrix}, \tag{8.8}$$

Some elements of these matrices are differential operators, some are constants and some are equal to zero.

Below, all elements of the matrices (5.9) for the case of the first order theory of the linear couple electro-magneto-elastic theory of plates in Cartesian coordinates are presented in the form

$$L^{00}_{\varphi\varphi} = \frac{c_{11}}{R^2}\frac{\partial^2}{\partial\varphi^2} + \frac{3c_{44}}{R^2}, \quad L^{00}_{\varphi\psi} = \frac{(c_{11}+c_{12})\csc(\psi)}{2R^2}\frac{\partial^2}{\partial\varphi\partial\psi}, \quad L^{00}_{\varphi r} = \frac{c_{11}+c_{12}+3c_{44}}{R^2}\frac{\partial}{\partial\varphi},$$

$$L^{01}_{\varphi\varphi} = 0, \quad L^{01}_{\varphi\psi} = 0, L^{01}_{\varphi r} = \frac{c_{13}}{hR}\frac{\partial}{\partial\varphi}, \quad L^{00}_{\varphi e} = -\frac{3d_{51}}{R^2}\frac{\partial}{\partial\varphi}, \quad L^{01}_{\varphi e} = -\frac{d_{13}}{hR}\frac{\partial}{\partial\varphi},$$

$$L^{00}_{\varphi m} = -\frac{3q_{51}}{R^2}\frac{\partial}{\partial\varphi}, \quad L^{01}_{\varphi m} = -\frac{q_{13}}{hR}\frac{\partial}{\partial\varphi}, L^{00}_{\psi\varphi} = \frac{c_{12}\csc(\psi)}{2R}\frac{\partial^2}{\partial\varphi\partial\psi},$$

$$L^{00}_{\psi\psi} = \frac{c_{11}-c_{12}}{2R^2}\frac{\partial^2}{\partial\varphi^2} + \frac{c_{11}\csc(\psi)^2}{R^2}\frac{\partial^2}{\partial\psi^2} - \frac{c_{11}\csc(\psi)^2\cot(\psi)}{R^2}\frac{\partial}{\partial\psi} - \frac{3c_{44}}{R^2},$$

$$L^{00}_{\psi r} = \frac{(c_{11}+c_{12}+3c_{44})\csc(\psi)}{R^2}\frac{\partial}{\partial\psi}, \quad L^{01}_{\psi\varphi} = 0, \quad L^{01}_{\psi\psi} = \frac{c_{11}-c_{12}}{2Rh},$$

$$L^{01}_{\psi r} = \frac{c_{13}\csc(\psi)}{hR}\frac{\partial}{\partial\psi}, L^{00}_{\psi e} = -\frac{d_{51}\csc(\psi)}{R^2}\frac{\partial}{\partial\psi}, \quad L^{01}_{\psi e} = -\frac{d_{13}\csc(\psi)}{R^2}\frac{\partial}{\partial\psi},$$

$$L^{00}_{\psi m} = -\frac{q_{51}\csc(\psi)}{R^2}\frac{\partial}{\partial\psi}, \quad L^{01}_{\psi m} = -\frac{q_{51}\csc(\psi)}{R^2}\frac{\partial}{\partial\psi},$$

$$L^{00}_{r\varphi} = -\frac{c_{11}+c_{12}+c_{44}-2c_{13}}{R^2}\frac{\partial}{\partial\varphi}, \quad L^{00}_{r\psi} = -\frac{(c_{11}+c_{12}+c_{44}-2c_{13})\csc(\psi)}{R^2}\frac{\partial}{\partial\psi},$$

$$L^{00}_{rr} = \frac{c_{44}}{R^2}\frac{\partial^2}{\partial\varphi^2} + \frac{c_{44}\csc(\psi)^2}{R^2}\frac{\partial^2}{\partial\psi^2} - \frac{c_{44}\csc(\psi)^2\cot(\psi)}{R^2}\frac{\partial}{\partial\psi} - \frac{2c_{11}+2c_{12}-4c_{13}}{R^2},$$

$$L^{01}_{r\varphi} = 0, \quad L^{01}_{r\psi} = 0, \quad L^{01}_{rr} = \frac{2(c_{33}-c_{13})}{hR},$$

$$L^{00}_{re} = -\frac{d_{51}}{R^2}\frac{\partial^2}{\partial\varphi^2} - \frac{d_{51}\csc(\psi)^2}{R^2}\frac{\partial^2}{\partial\psi^2} - \frac{d_{51}\csc(\psi)^2\cot(\psi)}{R^2}\frac{\partial}{\partial\psi}, \quad L^{01}_{re} = -\frac{2(d_{33}-d_{13})}{hR},$$

$$L^{00}_{rm} = -\frac{q_{51}}{R^2}\frac{\partial^2}{\partial\varphi^2} - \frac{q_{51}\csc(\psi)^2}{R^2}\frac{\partial^2}{\partial\psi^2} - \frac{q_{51}\csc(\psi)^2\cot(\psi)}{R^2}\frac{\partial}{\partial\psi}, \quad L^{01}_{rm} = -\frac{2(q_{33}-q_{13})}{hR},$$

$$L^{10}_{\varphi\varphi} = \frac{3c_{44}}{hR}, \quad L^{10}_{\varphi\psi} = 0, \quad L^{10}_{\varphi r} = -\frac{3c_{44}}{hR}\frac{\partial}{\partial\varphi}, \quad L^{11}_{\varphi\varphi} = \frac{c_{11}}{R^2}\frac{\partial^2}{\partial\varphi^2} - \frac{3c_{44}}{R^2},$$

$$
\begin{aligned}
&L^{11}_{\varphi\psi} = \frac{(c_{11}+c_{12})\csc(\psi)}{2R^2}\frac{\partial^2}{\partial\varphi\partial\psi}, L^{11}_{\varphi r} = \frac{c_{11}+c_{12}+3c_{44}}{R^2}\frac{\partial}{\partial\varphi},\\
&L^{10}_{\varphi e} = \frac{3d_{51}}{hR}\frac{\partial}{\partial\varphi}, \quad L^{11}_{\varphi e} = -\frac{3d_{51}}{R^2}\frac{\partial}{\partial\varphi}, \quad L^{10}_{\varphi m} = \frac{3q_{51}}{hR}\frac{\partial}{\partial\varphi}, \quad L^{11}_{\varphi m} = -\frac{3q_{51}}{R^2}\frac{\partial}{\partial\varphi},\\
&L^{10}_{\psi\varphi} = 0, \quad L^{10}_{\psi\psi} = \frac{3c_{44}}{hR}, \quad L^{10}_{\psi r} = -\frac{3c_{44}\csc(\psi)}{hR}\frac{\partial}{\partial\psi}, \quad L^{11}_{\psi\varphi} = \frac{c_{11}\csc(\psi)}{R^2}\frac{\partial^2}{\partial\varphi\partial\psi},\\
&L^{11}_{\psi\psi} = \frac{c_{11}-c_{12}}{2R^2}\frac{\partial^2}{\partial\varphi^2} + \frac{c_{11}\csc(\psi)^2}{R^2}\frac{\partial^2}{\partial\psi^2} - \frac{c_{11}\csc(\psi)^2\cot(\psi)}{R^2}\frac{\partial}{\partial\psi} - \frac{3c_{44}}{R^2},\\
&L^{11}_{\psi r} = \frac{(c_{11}+c_{12}+3c_{44})\csc(\psi)}{R^2}\frac{\partial}{\partial\psi}, L^{10}_{\psi e} = \frac{3d_{51}\csc(\psi)}{hR}\frac{\partial}{\partial\psi},\\
&L^{11}_{\psi e} = -\frac{3d_{51}\csc(\psi)}{hR}\frac{\partial}{\partial\psi}, \quad L^{10}_{\psi m} = \frac{3q_{51}\csc(\psi)}{hR}\frac{\partial}{\partial\psi},\\
&L^{11}_{\psi m} = -\frac{3q_{51}\csc(\psi)}{hR}\frac{\partial}{\partial\psi}, \quad L^{10}_{r\varphi} = -\frac{3c_{13}}{hR}\frac{\partial}{\partial\varphi},\\
&L^{10}_{r\psi} = -\frac{3c_{13}\csc(\psi)}{hR}\frac{\partial}{\partial\psi}, \quad L^{10}_{rr} = -\frac{6c_{13}}{hR}, \quad L^{11}_{r\varphi} = -\frac{c_{11}+c_{12}-2c_{13}+c_{44}}{R^2}\frac{\partial}{\partial\varphi},\\
&L^{11}_{r\psi} = -\frac{(c_{11}+c_{12}-2c_{13}+c_{44})\csc(\psi)}{R^2}\frac{\partial}{\partial\varphi},\\
&L^{11}_{rr} = \frac{c_{44}}{R^2}\frac{\partial^2}{\partial\varphi^2} + \frac{c_{44}\csc(\psi)^2}{R^2}\frac{\partial^2}{\partial\psi^2} - \frac{c_{44}\csc(\psi)^2\cot(\psi)}{R^2}\frac{\partial}{\partial\psi} - \frac{2c_{11}+2c_{12}-4c_{13}+3c_{33}}{R^2},\\
&L^{10}_{re} = 0, \quad L^{11}_{re} = -\frac{d_{51}}{R^2}\frac{\partial^2}{\partial\varphi^2} - \frac{d_{51}\csc(\psi)^2}{R^2}\frac{\partial^2}{\partial\psi^2} - \frac{d_{51}\csc(\psi)^2\cot(\psi)}{R^2}\frac{\partial}{\partial\psi} + \frac{3d_{33}}{h^2},\\
&L^{10}_{rm} = 0, \quad L^{11}_{rm} = -\frac{q_{51}}{R^2}\frac{\partial^2}{\partial\varphi^2} - \frac{q_{51}\csc(\psi)^2}{R^2}\frac{\partial^2}{\partial\psi^2} - \frac{q_{51}\csc(\psi)^2\cot(\psi)}{R^2}\frac{\partial}{\partial\psi} + \frac{3q_{33}}{h^2},\\
&L^{00}_{e\varphi} = -\frac{d_{51}-2d_{13}}{R^2}\frac{\partial}{\partial\varphi}, \quad L^{00}_{e\psi} = -\frac{(d_{51}-2d_{13})\csc(\psi)}{R^2}\frac{\partial}{\partial\psi}, \quad L^{01}_{e\varphi} = 0, \quad L^{01}_{e\psi}0,\\
&L^{01}_{er} = \frac{2d_{33}}{hR}, L^{00}_{er} = \frac{d_{51}}{R^2}\frac{\partial^2}{\partial\varphi^2} + \frac{d_{51}\csc(\psi)^2}{R^2}\frac{\partial^2}{\partial\psi^2} - \frac{d_{51}\csc(\psi)^2\cot(\psi)}{R^2}\frac{\partial}{\partial\psi} + \frac{4d_{13}}{R^2},\\
&L^{00}_{ee} = \frac{\epsilon_{11}}{R^2}\frac{\partial^2}{\partial\varphi^2} + \frac{\epsilon_{11}\csc(\psi)^2}{R^2}\frac{\partial^2}{\partial\psi^2} - \frac{\epsilon_{11}\csc(\psi)^2\cot(\psi)}{R^2}\frac{\partial}{\partial\psi}, \quad L^{01}_{ee} = \frac{2\epsilon_{33}}{hR},\\
&L^{10}_{em} = \frac{\beta_{11}}{R^2}\frac{\partial^2}{\partial\varphi^2} + \frac{\beta_{11}\csc(\psi)^2}{R^2}\frac{\partial^2}{\partial\psi^2} - \frac{\beta_{11}\csc(\psi)^2\cot(\psi)}{R^2}\frac{\partial}{\partial\psi}, \quad L^{01}_{em} = \frac{2\beta_{33}}{hR},\\
&L^{00}_{m\varphi} = -\frac{q_{51}-2q_{13}}{R^2}\frac{\partial}{\partial\varphi}, \quad L^{00}_{m\psi} = -\frac{(q_{51}-2q_{13})\csc(\psi)}{R^2}\frac{\partial}{\partial\psi}, \quad L^{01}_{m\varphi} = 0, \quad L^{01}_{m\psi}0,\\
&L^{01}_{mr} = \frac{2q_{33}}{hR}, L^{00}_{mr} = \frac{q_{51}}{R^2}\frac{\partial^2}{\partial\varphi^2} + \frac{q_{51}\csc(\psi)^2}{R^2}\frac{\partial^2}{\partial\psi^2} - \frac{q_{51}\csc(\psi)^2\cot(\psi)}{R^2}\frac{\partial}{\partial\psi} + \frac{4q_{13}}{R^2},\\
&L^{00}_{me} = \frac{\beta_{11}}{R^2}\frac{\partial^2}{\partial\varphi^2} + \frac{\beta_{11}\csc(\psi)^2}{R^2}\frac{\partial^2}{\partial\psi^2} - \frac{\beta_{11}\csc(\psi)^2\cot(\psi)}{R^2}\frac{\partial}{\partial\psi}, \quad L^{01}_{ee} = \frac{2\beta_{33}}{hR},\\
&L^{10}_{mm} = \frac{\gamma_{11}}{R^2}\frac{\partial^2}{\partial\varphi^2} + \frac{\gamma_{11}\csc(\psi)^2}{R^2}\frac{\partial^2}{\partial\psi^2} - \frac{\gamma_{11}\csc(\psi)^2\cot(\psi)}{R^2}\frac{\partial}{\partial\psi}, \quad L^{01}_{mm} = \frac{2\gamma_{33}}{hR}, \qquad (8.9)\\
&L^{10}_{e\varphi} = -\frac{3d_{13}}{hR}\frac{\partial}{\partial\varphi}, \quad L^{10}_{e\psi} = -\frac{3d_{13}\csc(\psi)}{hR}\frac{\partial}{\partial\psi}, \quad L^{10}_{er} = -\frac{6d_{13}}{hR}, \quad L^{11}_{e\varphi} = -\frac{d_{51}-2d_{13}}{R^2}\frac{\partial}{\partial\varphi},\\
&L^{11}_{e\psi} = -\frac{d_{51}-2d_{13}}{R^2}\frac{\partial}{\partial\psi}, \quad L^{11}_{er} = \frac{d_{51}}{R^2}\frac{\partial^2}{\partial\varphi^2} + \frac{d_{51}\csc(\psi)^2}{R^2}\frac{\partial^2}{\partial\psi^2} - \frac{d_{51}\csc(\psi)^2\cot(\psi)}{R^2}\frac{\partial}{\partial\psi} + \frac{4d_{13}}{R^2} - \frac{3d_{33}}{h^2},\\
&L^{10}_{ee} = 0, \quad L^{11}_{ee} = \frac{\epsilon_{11}}{R^2}\frac{\partial^2}{\partial\varphi^2} + \frac{\epsilon_{11}\csc(\psi)^2}{R^2}\frac{\partial^2}{\partial\psi^2} - \frac{\epsilon_{11}\csc(\psi)^2\cot(\psi)}{R^2}\frac{\partial}{\partial\psi} - \frac{3\epsilon_{33}}{h^2},
\end{aligned}
$$

$$L_{me}^{10}=0,\quad L_{me}^{11}=\frac{\beta_{11}}{R^2}\frac{\partial^2}{\partial\varphi^2}+\frac{\beta_{11}\csc(\psi)^2}{R^2}\frac{\partial^2}{\partial\psi^2}-\frac{\beta_{11}\csc(\psi)^2\cot(\psi)}{R^2}\frac{\partial}{\partial\psi}-\frac{3\beta_{33}}{h^2},$$

$$L_{m\varphi}^{10}=-\frac{3q_{13}}{hR}\frac{\partial}{\partial\varphi},\quad L_{m\psi}^{10}=-\frac{3q_{13}\csc(\psi)}{hR}\frac{\partial}{\partial\psi},\quad L_{mr}^{10}=-\frac{6q_{13}}{hR},\quad L_{m\varphi}^{11}=-\frac{q_{51}-2q_{13}}{R^2}\frac{\partial}{\partial\varphi},$$

$$L_{m\psi}^{11}=-\frac{q_{51}-2q_{13}}{R^2}\frac{\partial}{\partial\psi},\quad L_{mr}^{11}=\frac{q_{51}}{R^2}\frac{\partial^2}{\partial\varphi^2}+\frac{q_{51}\csc(\psi)^2}{R^2}\frac{\partial^2}{\partial\psi^2}-\frac{q_{51}\csc(\psi)^2\cot(\psi)}{R^2}\frac{\partial}{\partial\psi}+\frac{4q_{13}}{R^2}-\frac{3q_{33}}{h^2},$$

$$L_{me}^{10}=0,\quad L_{me}^{11}=\frac{\beta_{11}}{R^2}\frac{\partial^2}{\partial\varphi^2}+\frac{\beta_{11}\csc(\psi)^2}{R^2}\frac{\partial^2}{\partial\psi^2}-\frac{\beta_{11}\csc(\psi)^2\cot(\psi)}{R^2}\frac{\partial}{\partial\psi}-\frac{3\beta_{33}}{h^2},$$

$$L_{mm}^{10}=0,\quad L_{mm}^{11}=\frac{\gamma_{11}}{R^2}\frac{\partial^2}{\partial\varphi^2}+\frac{\gamma_{11}\csc(\psi)^2}{R^2}\frac{\partial^2}{\partial\psi^2}-\frac{\gamma_{11}\csc(\psi)^2\cot(\psi)}{R^2}\frac{\partial}{\partial\psi}-\frac{3\gamma_{33}}{h^2},$$

A complete 2-D system of the differential equations for the higher order theory of the electro-magneto-elastic plates in the Cartesian system of coordinates is presented in this section. Explicit expressions for divergences of the Legendre's polynomial coefficients of stress tensor and the electric and magnetic displacement vectors (8.1), for the Legendre's polynomial coefficients of strain tensor and electric field and the magnetic field vectors (8.3) and for the Legendre's polynomial coefficients of stress tensor and the electric and magnetic displacement vectors (8.7) as functions of the Legendre's polynomial coefficients of displacements and electric and magnetic potentials for higher order theory of plates are presented here. For the case of the first order approximation theory, elements of matrix differential operators (5.9), that are included in the equations of equilibrium (2.13) are also presented in the explicit form (8.9). They can be used for theoretical analysis, as well as analytical and numerical solutions of the problems arising in science and engineering.

9 Conclusions

In this paper new higher order theories for plates and shells, which are based on the linear electro-magneto-elasticity, have been developed. The 2-D theory is developed from general 3-D equations of the electro-magneto-elasticity in the special curvilinear system of coordinates related to the middle surface of the shell and assuming that the shell is thin. The higher order theory is based on the expansion of the equations of electro-magneto-elasticity into Fourier series in terms of Legendre polynomials with respect to a thickness coordinate. All the functions that define the physical state of the shell including stress and strain tensors, vectors of mechanical, electrical and magnetic displacements, electric and magnetic fields, body forces, electric and magnetic charge density have been expanded into Fourier series in terms of Legendre polynomials with respect to a thickness coordinate. Thereby, all equations of the electro-magneto-elasticity including generalized constitutive law have been transformed to the corresponding equations for Fourier coefficients of the expansion. Then, for Fourier coefficients, the system of differential equations of equilibrium in terms of displacements and electro-magnetic potentials has been obtained in the same way as in the classical theory of elasticity.

A complete 2-D system of the differential equations for the higher order theory of electro-magneto-elastic plates in Cartesian and polar coordinates and of the electro-magneto-elastic cylindrical and spherical shells in cylindrical and spherical system of coordinates related to the geometry of the shell are presented here. Explicit expressions for divergences of the Legendre's polynomial coefficients of the stress tensor and electric and magnetic displacement vectors, for the Legendre's polynomial coefficients of strain tensor and electric field and for the Legendre's polynomial coefficients of the stress tensor and electric and magnetic displacement vectors as functions of the Legendre's polynomial coefficients of displacements vector and electrical and magnetic potentials for higher order theory of plates and shells are presented here. For the case of the first order approximation theory, elements of matrix differential operators, which are included in the equations of equilibrium, are also presented in explicit form.

The obtained equations can be used for physical strain calculation as well as for modeling thin walled structures in macro, micro and nano scales by taking into account coupled electro-magneto-elastic effects. Specially proposed models can be efficient in MEMS and NEMS modeling as well as computer simulation.

Acknowledgements The work presented in this paper was supported by the Committee of Science and Technology of Mexico (CONACYT) by the Research Grant, (Ciencia Basica, Reference No **256458**), which is gratefully acknowledged.

References

1. Albarody, T.M.B., Al-Kayiem, H.H., Faris, W.: The transverse shear deformation behaviour of magneto-electro-elastic shell. J. Mech. Sci. Technol. **30**(1), 77–87 (2016)
2. Altay, G., Dökmeci, M.C.: Some comments on the higher order theories of piezoelectric, piezo-thermo-elastic and thermos-piezoelectric rods and shells. Int. J. Solids Struct. **40**, 4699–4706 (2003)
3. Altay, G., Dökmeci, M.C.: Variational principles for piezoelectric, thermos-piezoelectric, and hygro-thermo-piezoelectric continua revisited. Mech. Adv. Mater. Struct. **14**(7), 549–562 (2007)
4. Altay, G., Dökmeci, M.C.: On the fundamental equations of electro-magneto-elastic media in variational form with an application to shell-laminae equations. Int. J. Solids Struct. **47**, 466–492 (2010)
5. Altenbach, H., Brigadnov, I., Eremeyev, V.A.: Oscillations of amagneto-sensitive elastic sphere. J. Appl. Math. Mech. (ZAMM) **88**(6), 497–506 (2008)
6. Altenbach, H., Carrera, E., Kulikov, G.. (eds.) Analysis and Modelling of Advanced Structures and Smart Systems, p. 380. Springer, New York (2018)
7. Altenbach, H., Eremeyev, V.A.: Shell Like Structures. Non Classical Theories and Applications, p. 761. Springer, New York (2011)
8. Ambartsumyan, S.A., Baghdasaryan, G.Y.: Electroconductive Plates and Shells in Magnetic Field, p. 243. Nauka, Moscow (1996)
9. Ambartsumyan, S.A., Baghdasaryan, G.Y., Belubekyan, M.V.: Magneto-elasticity of Thin Shells and Plates, p. 272. Nauka, Moscow (1977)
10. Ambrartsumian, S.A., Belubekian, M.B.: Some Problems of Electromagnetic Elastic Plates, p. 143. Yerevan State University Publisher, Yerevan (1991)

11. Aouadi, M.: On the coupled theory of thermo-magneto-electro-elasticity. Q. J. Mech. Appl. Mech. **60**(4), 443–456 (2007)
12. Aouadi, M.: The Generalized theory of thermo-magneto-electro-elasticity. Technische Mechanik **27**(2), 133–146 (2007)
13. Badri T. M., Al-Kayiem H. H., Dynamic analysis of laminated composite thermo-magneto-electro-elastic shells. J. Mech. Sci. Technol. **9**(28) (2014)
14. Baghdasaryan, G., Danoyan, Z.: Magneto-Elastic Waves, p. 265. Springer, Singapore (2018)
15. Baghdasaryan, G., Mikilyan, M.: Effects of Magneto-elastic Interactions in Conductive Plates and Shells, p. 294. Springer, New York (2016)
16. Bardzokas, D.I., Filshtinsky, M.L., Filshtinsky, L.A.: Mathematical Methods in Electro-Magneto-Elasticity, p. 541. Springer, New York (2007)
17. Berlineourt, D., Kerran, D., Jaffe, H.: Piezoelectric and piezomagnetic materials and their function in transducers. In: Mason, W.P. (ed.) Physical Acoustics. Principles and Methods, pp. 169–270. Academic, New York (1964)
18. Brown, W.F.: Magneto-Elastic Interactions, p. 163. Springer, New York (1966)
19. Carrera, E.: Theories and finite elements for multilayered plates and shells: a unified compact formulation with numerical assessment and benchmarking. Arch. Comput. Methods Eng. **10**(3), 215–296 (2003)
20. Carrera, E., Brischetto, S., Nali, P.: Variational statements and computational models for multi field problems and multilayered structures. Mech. Adv. Mater. Struct. **15**, 182–198 (2008)
21. Carrera E., Brischetto S., Nali P.: Plates and Shells for Smart Structures. Classical and Advanced Theories for Modeling and Analysis, p. 316. A John Wiley & Sons, Ltd., New Delhi (2011)
22. Carrera, E., Cinefra, M., Petrolo, M., Zappino, M.: Finite Element Analysis of Structures Through Unified Formulation, p. 412. New Delhi, A John Wiley & Sons Ltd (2014)
23. Carrera, E., Fazzolari, F.A., Cinefra, M.: Thermal Stress Analysis of Composite Beams, Plates and Shells. Computational Modelling and Applications, p. 416. Academic, New York (2017)
24. Eremeev, V.A., Nasedkin, A.V.: Natural vibrations of nanodimensional piezoelectric bodies with contact-type boundary conditions. Mech. Solids **50**(5), 495–507 (2015)
25. Eremeev, V.A., Pietraszkiewicz, W.: Local symmetry group in the general theory of elastic shells. J. Elast. **85**(2), 125–152 (2006)
26. Eringen, A.C.: On the foundations of electro-elastostatics. Int. J. Eng. Sci. **1**(1), 127–153 (1963)
27. Eringen, A.C.: Theory of electromagnetic elastic plate. Int. J. Eng. Sci. **27**(4), 363–375 (1989)
28. Girchenko, A.A., Eremeev, V.A., Altenbach, H.: On the coupled electromechanical behavior of artificial materials with chiral-shell elements. Int. J. Mech. Aerosp. Ind. Mech. Manuf. Eng. **7**(5), 840–856 (2013)
29. Girchenko, A.A., Eremeyev, V.A., Morozov, N.F.: Modelling of spriral nanofilms with piezo-electric properties. Phys. Mesomech. **14**, 10–15 (2011)
30. Grinchenko, V.T., Ulitko, A.F., Shulga, N.A.: Electro-elasticity, p. 280. Naukova, Dumka, Kiev (1989)
31. Gülay, A., Dokmeci, C.M.: On the fundamental equations of electro-magneto-elasticity-media in variational form with an application to shell/lamina equations. Int. J. Solids Struct. **47**, 466–492 (2010)
32. Guz, A.N., Makhort, F.G.: Acousto-Electro-Magneto-Elasticity, p. 288. Naukova, Dumka, Kiev (1988)
33. He, J.-H.: Coupled variational principles of piezoelectricity. Int. J. Eng. Sci. **39**, 323–341 (2001)
34. He, J.-H.: Variational theory for linear magneto-electro-elasticity. Int. J. Nonlinear Sci. Numer. Simul. **2**(4), 309–316 (2001)
35. Heyliger, P.R., Pan, E.: Static fields in magneto-electro-elastic laminates. AIAA J. **42**, 1435–1443 (2004)
36. Heywang, W., Lubitz, K., Wersing, W.: Piezoelectricity. Evolution and Future of a Technology, p. 576. Springer, Berlin (2008)
37. Jiang, A., Ding, H.: Analytical solutions to magneto-electro-elastic beams. Struct. Eng. Mech. **18**, 195–209 (2004)
38. Khoma, I.Y.: Generalized Theory of Anisotropic Shells, p. 172. Naukova Dumka, Kiev (1987)

39. Kil'chevskiy, N.A.: Fundamentals of the Analytical Mechanics of Shells, NASA TT, F-292, p. 361. Washington, D.C. (1965)
40. Korotkina, M.R.: Electro-Magneto-Elasticity, p. 304. Moscow State University Publisher, Moscow (1988)
41. Kuang, Z.B.: Physical variational principle and thin plate theory in electro-magneto-elastic analysis. Int. J. Solids Struct. **48**, 317–325 (2011)
42. Kuang, Z.-B.: An applied electro-magneto-elastic thin plate theory. Acta Mech. **225**, 1153–1166 (2014)
43. Kuang, Z.-B.: Theory of Electro-Elasticity, p. 438. Springer, Berlin (2014)
44. Landau, L.D., Lifshitz, E.: Electrodynamics of Continuous Media. Addison Wesley, New York (1960)
45. Li, J.Y.: Uniqueness and reciprocity theorems for linear thermo-electro-magneto-elasticity. Q. J. Mech. Appl. Mech. **56**(1), 35–43 (2003)
46. Mason W.P.: Piezoelectric Crystals and their Application to Ultrasonics, p. 508. Princeton, New Jersey (1950)
47. Maugin, G.A.: Continuum Mechanics of Electromagnetic Solids, p. 606. North-Holland, Amsterdam (1988)
48. Moita, J.M.S., Soares, C.M.M., Soares, C.A.M.: Analyses of magneto-electro-elastic plates using a higher order finite element model. Compos. Struct. **91**, 421–426 (2009)
49. Moon, F.C.: Magneto-Solid Mechanics, p. 436. Wiley, New York (1984)
50. Nasedkin, A.V., Eremeyev, V.A.: Spectral Properties of Piezoelectric Bodies with Surface Effects. In: Altenbach, H., Morozov, N.F. (eds.) Surface Effects in Solid Mechanics, pp. 105–121. Models, Simulations and Applications, Springer, Berlin (2013)
51. Nasedkin, A.V., Eremeyev, V.A.: Harmonic vibrations of nanosized piezoelectric bodies with surface effects. J. Appl. Math. Mech. (ZAMM) **94**, 878–892 (2014)
52. Nasedkin, A.V., Eremeyev, V.A.: Some models for nanosized magnetoelectric bodies with surface effects. In: Parinov, I.A., Chang, S.-H., Topolov, V.Yu. (eds.) Advanced Materials Manufacturing, Physics, Mechanics and Applications, pp. 373–391. Springer, Berlin (2016)
53. Pan, E.: Exact solution for simply supported and multilayered magneto-electro-elastic plates. J. Appl. Mech. **68**(4), 608–618 (2001)
54. Parton, V.Z., Kudryavtsev, B.A.: Electro-Magneto-Elasticity, Piezo-Electrics and-Electrically Conductive Solids, p. 526. Gordon & Breach, New York (1988)
55. Pelekh, B.L., Sukhorol'skii, M.A.: Contact Problems of the Theory of Elastic Anisotropic Shells, p. 216. Naukova Dumka, Kiev (1980)
56. Pelekh, B.L., Lazko, V.A.: Laminated Anisotropic Plates and Shells with Stress Concentrators, p. 296. Naukova Dumka, Kiev (1982)
57. Pelekh, B.L., Maksimuk, A.V., Korovaychuk, I.M.: Contact Problems for Layered Structural Elements with Coatings, p. 280. Naukova Dumka, Kiev (1988)
58. Perez-Fernandez, L.D., Bravo-Castillero, J., Rodriguez-Ramos, R., Sabina, F.J.: On the constitutive relations and energy potentials of linear thermo-magneto-electro-elasticity. Mech. Res. Commun. **36**, 343–350 (2009)
59. Pietraszkiewicz, W.: The resultant linear six-feld theory of elastic shells. What it brings to the classical linear shell models? J Appl Math Mech (ZAMM) **96**, 899–915 (2016)
60. Podstrigach, Ya.S., Burak Ya.I., Gachkevich A.R. Chernyavskaya L.V.: Termo-Elasticity of Electroconductive Bodies, p. 248. Naukova Dumka, Kiev (1977)
61. Podstrigach Ya.S., Burak Ya.I., Kondrat V.F.: Magneto-Thermo-Elasticity of Electroconductive Bodies, p. 296. Naukova Dumka, Kiev (1981)
62. Razavi, S.: Magneto-Electro-Thermo-Mechanical Response of a Multiferroic Doubly-Curved Nano-Shell. J. Solid Mech. **10**(1), 130–141 (2018)
63. Rogacheva, N.N.: The Theory of Piezoelectric Shells and Plates, p. 266. CRC Press, Boca Raton (1994)
64. Rupitsch, S.J.: Piezoelectric Sensors and Actuators. Fundamentals and Applications, p. 566. Springer, Berlin (2019)

65. Shooshtari, A., Razavi, S.: Vibration analysis of a magneto-electro-elastic rectangular plate based on a higher-order shear deformation theory. Lat. Am. J. Solids Struct. **13**, 554–572 (2016)
66. Shooshtari, A., Razavi, S.: Vibration of a multiphase magneto-electro-elastic simply supported rectangular plate subjected to harmonic forces. J. Intell. Mater. Syst. Struct. **28**(4), 451–467 (2017)
67. Soh, A.K., Liu, J.X.: On the constitutive equations of magneto-electro-elastic solids. J. Intell. Mater. Syst. Struct. **16**(4), 597–602 (2005)
68. Tiersten, H.F.: Linear Piezoelectric Plate Vibrations, p. 216. Springer, New York (1969)
69. Tzou, H.S.: Piezoelectric Shells. Distributed Sensing and Control of Continua, p. 492. Springer, New York (1993)
70. Vekua, I.N.: Shell Theory, General Methods of Construction, p. 287. Pitman Advanced Publishing Program, Boston (1986)
71. Yang, J.: The Mechanics of Piezoelectric Structures, p. 327. World Scientific Publishing Co. Pte. Ltd., Singapore (2006)
72. Zozulya, V.V.: The combines problem of thermoelastic contact between two plates through a heat conducting layer. J. Appl. Math. Mech. **53**(5), 622–627 (1989)
73. Zozulya, V.V.: Contact cylindrical shell with a rigid body through the heat-conducting layer in transitional temperature field. Mech. Solids **2**, 160–165 (1991)
74. Zozulya, V.V.: Laminated shells with debonding between laminas in temperature field. Int. Appl. Mech. **42**(7), 842–848 (2006)
75. Zozulya, V.V.: Mathematical modeling of pencil-thin nuclear fuel rods. In: Gupta, A. (ed.) Structural Mechanics in Reactor Technology, p. C04–C12. Toronto, Canada (2007)
76. Zozulya, V.V., Zhang, Ch.: A high order theory for functionally graded axisymmetric cylindrical shells. Int. J. Mech. Sci. **60**(1), 12–22 (2012)
77. Zozulya, V.V.: A high order theory for linear thermoelastic shells: comparison with classical theories. J. Eng. Article ID 590480, 19 (2013)
78. Zozulya, V.V.: A high-order theory for functionally graded axially symmetric cylindrical shells. Arch. Appl. Mech. **83**(3), 331–343 (2013)
79. Zozulya, V.V., Saez, A.: High-order theory for arched structures and its application for the study of the electrostatically actuated MEMS devices. Arch. Appl. Mech. **84**(7), 1037–1055 (2014)
80. Zozulya, V.V.: A higher order theory for shells, plates and rods. Int. J. Mech. Sci. **103**, 40–54 (2015)
81. Zozulya, V.V., Saez, A.: A high order theory of a thermo elastic beams and its application to the MEMS/NEMS analysis and simulations. Arch. Appl. Mech. **86**(7), 1255–1272 (2016)
82. Zozulya, V.V.: A higher order theory for functionally graded beams based on Legendre's polynomial expansion. Mech. Adv. Mater. Struct. **24**(9), 745–760 (2017)
83. Zozulya, V.V.: Micropolar curved rods. 2-D, high order, Timoshenko's and Euler-Bernoulli models. Curved Layer. Struct. **4**, 104–118 (2017)
84. Zozulya, V.V.: Couple stress theory of curved rods. 2-D, high order, Timoshenko's and Euler-Bernoulli models. Curved Layer. Struct. **4**, 119–132 (2017)
85. Zozulya, V.V.: Nonlocal theory of curved rods. 2-D, high order, Timoshenko's and Euler-Bernoulli models. Curved Layer. Struct. **4**, 221–236 (2017)
86. Zozulya, V.V.: Higher order theory of micropolar plates and shells. J. Appl. Math. Mech. (ZAMM) **98**, 886–918 (2018)
87. Zozulya, V.V.: Higher order couple stress theory of plates and shells. J. Appl. Math. Mech. (ZAMM) **98**, 1834–1863 (2018). https://doi.org/10.1002/zamm.201800022

Exact Solutions of Nonlinear Micropolar Elastic Theory for Compressible Solids

L. M. Zubov, A. M. Kolesnikov and O. V. Rudenko

Abstract In this article we obtain exact solutions of finite inhomogeneous deformations of three-dimensional micropolar elastic bodies. We consider a model of the physically linear isotropic compressible material with six material parameters. The obtained solutions describe following types of finite deformations: cylindrical bending of a rectangular plate, straightening of a cylindrical sector, double cylindrical bending, pure bending of a circular cylinder sector, inflation and reversing of a hollow sphere. The results can be used to verify two-dimensional models of micropolar elastic shells.

1 Introduction

In this paper we derive exact solutions for problems of large inhomogeneous deformations of compressible isotropic micropolar elastic bodies. By a micropolar body we mean a continuous medium with couple stresses and rotational interactions of material particles. This model is also called the Cosserat continuum. The basics of the nonlinear theory of the Cosserat elastic continuum had been given in [5, 8–11, 14, 16]. The model of a micropolar medium is used to describe granular polycrystalline bodies, polymers, composites, suspensions, liquid crystals, geophysical structures, biological tissues, metamaterials, nanostructured materials, etc. The exact solutions can be used to a experimental determination of material parameters in the constitutive relations of the medium. Also they can be used to control the accuracy of calculations in numerical solution of nonlinear equilibrium equations for micropolar bodies.

The derived solutions are special cases of one-dimensional deformations of micropolar elastic bodies. Those are such deformations for which the system of partial

L. M. Zubov · A. M. Kolesnikov (✉) · O. V. Rudenko
Southern Federal University, Milchakova st. 8a, Rostov-on-Don 344090, Russian Federation
e-mail: Alexey.M.Kolesnikov@gmail.com

L. M. Zubov
e-mail: zubovl@yandex.ru

O. V. Rudenko
e-mail: Rudenko-Olga-Sfedu@yandex.ru

H. Altenbach et al. (eds.), *Recent Developments in the Theory of Shells*,
Advanced Structured Materials 110, https://doi.org/10.1007/978-3-030-17747-8_37

differential equations of equilibrium reduces to a system of ordinary differential equations. A general method of constructing a class of one-dimensional deformations of a non-linear elastic Cosserat continuum is presented in [12]. In this paper the exact solutions describe the following types of one-dimensional deformations of a micropolar elastic medium: cylindrical bending of a rectangular plate, straightening of a circular cylinder sector, inflation and reversing of a cylindrical tube, pure bending of a circular cylinder sector, double cylindrical bending, inflation and reversing of a hollow sphere. These types of deformations correspond to universal solutions of equilibrium equations for the incompressible isotropic micropolar bodies which were obtained in the earlier paper [18]. In the case of compressed bodies, exact solutions in explicit analytic form for large deformations can be obtain only for some specific constitutive relations of an elastic material. In the present paper we use a model of the physically linear isotropic compressible micropolar body with six material parameters.

The micropolar shell model is two-dimensional analogue of the Cosserat continuum [1, 3, 4, 6, 13]. It is also called the Cosserat surface. In this model, by a shell we mean a material surface or a two-dimensional material continuum. Each point (particle) of this continuum has six degrees of freedom of an absolutely rigid body. The rotational degrees of freedom of a surface particle are kinetically independent of its displacement field. Solutions of problems of stretching, bending, inflation and reversing of cylindrical and spherical Cosserat surfaces, and bending of flat plates were obtained in the paper [17] for finite deformations. The solutions [17] describe nonlinear deformations of the shells, similar to the deformations corresponding to represented here solutions of three-dimensional micropolar theory of elasticity. Comparison of solutions obtained within the theory of shells and solutions obtained within the three-dimensional theory can be used to verify relations of the theory of micropolar shells.

2 Initial Relations of Nonlinear Micropolar Elasticity

The deformation of the elastic medium is described by a mapping of the reference configuration to the current configuration. In the case of a micropolar continuum, it is determined by two kinematically independent fields of displacement and rotation

$$\mathbf{R} = \mathbf{R}(\mathbf{r}) = \mathbf{r} + \mathbf{u}(\mathbf{r}), \quad \mathbf{H} = \mathbf{H}(\mathbf{r}),$$

where $\mathbf{r} = x_s\mathbf{i}_s$, $\mathbf{R} = X_k\mathbf{i}_k$, $(s, k = 1, 2, 3)$, x_s and X_k are Cartesian coordinates of the reference and current configurations, respectively, $\mathbf{i}_k$ are the unit vectors of the Cartesian coordinates, $\mathbf{u}$ is a displacement vector field, $\mathbf{H}$ is a proper orthogonal tensor, which describes the rotational degrees of freedom of the micropolar medium. It is called the microrotation tensor (or turntensor).

Below we use the following gradient, divergence, and rotor operators in the reference configuration coordinates

$$\operatorname{grad}\boldsymbol{\Psi} = \mathbf{r}^n \otimes \frac{\partial \boldsymbol{\Psi}}{\partial q^n}, \quad \operatorname{div}\boldsymbol{\Psi} = \mathbf{r}^n \cdot \frac{\partial \boldsymbol{\Psi}}{\partial q^n},$$
$$\operatorname{rot}\boldsymbol{\Psi} = \mathbf{r}^n \times \frac{\partial \boldsymbol{\Psi}}{\partial q^n}, \quad \mathbf{r}^n = \mathbf{i}_k \frac{\partial q^n}{\partial x_k},$$

where $\boldsymbol{\Psi}$ is an arbitrary differentiable tensor field of any order, $q^n = q^n(x_1, x_2, x_3)$ are curvilinear coordinates (the Lagrangian coordinates).

The system of equations of a micropolar elastic medium in the absence of mass forces and moments includes the following equations [5, 8–11, 14, 16]:

Equilibrium equations

$$\operatorname{div}\mathbf{D} = 0, \quad \operatorname{div}\mathbf{G} + \left(\mathbf{F}^{\mathrm{T}} \cdot \mathbf{D}\right)_{\times} = 0. \tag{1}$$

Constitutive relations

$$\mathbf{D} = \mathbf{P} \cdot \mathbf{H}, \quad \mathbf{G} = \mathbf{K} \cdot \mathbf{H},$$
$$\mathbf{P} = \frac{\partial W}{\partial \mathbf{E}}, \quad \mathbf{K} = \frac{\partial W}{\partial \mathbf{L}}, \quad W = W(\mathbf{E}, \mathbf{L}). \tag{2}$$

Geometric relations

$$\mathbf{F} = \operatorname{grad}\mathbf{R}, \quad \mathbf{E} = \mathbf{F} \cdot \mathbf{H}^{\mathrm{T}},$$
$$\mathbf{L} = \frac{1}{2}\mathbf{r}^n \otimes \left(\frac{\partial \mathbf{H}}{\partial q^n} \cdot \mathbf{H}^{\mathrm{T}}\right)_{\times} = \frac{1}{2}\mathbf{I}\operatorname{tr}\left[\mathbf{H} \cdot (\operatorname{rot}\mathbf{H})^{\mathrm{T}}\right] - \mathbf{H} \cdot (\operatorname{rot}\mathbf{H})^{\mathrm{T}}. \tag{3}$$

Here $\mathbf{D}$, $\mathbf{G}$ are the stress and couple stress tensors of the first Piola-Kirchhoff type, $\mathbf{P}$, $\mathbf{K}$ are a stress and a couple stress tensors of the second Piola-Kirchhoff type, $\mathbf{E}$, $\mathbf{L}$ are deformations tensors of a nonlinear micropolar continuum called stretch and wryness tensors, respectively [5, 8–11, 14], $\mathbf{I}$ is a unit tensor, W is a strain energy density. Symbol $\boldsymbol{\Phi}_{\times}$ means the vector invariant of a second-order tensor $\boldsymbol{\Phi}$:

$$\boldsymbol{\Phi}_{\times} = (\Phi_{mn}\mathbf{r}_m \otimes \mathbf{r}_n)_{\times} = \Phi_{mn}\mathbf{r}_m \times \mathbf{r}_n.$$

Below we will use the model of the compressible isotropic physically linear micropolar continuum [10]. This model is determined by the quadratic function of the strain energy density

$$2W = \lambda \operatorname{tr}^2(\mathbf{E} - \mathbf{I}) + (\mu + \beta)\operatorname{tr}\left[(\mathbf{E} - \mathbf{I}) \cdot (\mathbf{E} - \mathbf{I})^{\mathrm{T}}\right]$$
$$+ (\mu - \beta)\operatorname{tr}(\mathbf{E} - \mathbf{I})^2 + \delta \operatorname{tr}^2\mathbf{L} + (\gamma + \eta)\operatorname{tr}\left(\mathbf{L} \cdot \mathbf{L}^{\mathrm{T}}\right) + (\gamma - \eta)\operatorname{tr}\mathbf{L}^2. \tag{4}$$

where λ, μ, β, δ, γ, η are material constants. Also we will use the Poisson's ratio, which is expressed as

$$\nu = \frac{\lambda}{2(\lambda + \mu)}.$$

For this material model the stress tensor $\mathbf{P}$ is a linear function of the tensor $(\mathbf{E}-\mathbf{I})$, and the couple stress tensor $\mathbf{K}$ is a linear function of the wryness tensor $\mathbf{L}$:

$$\begin{aligned}\mathbf{P} &= \lambda\mathbf{I}\,(\mathrm{tr}\mathbf{E}-3)+(\mu+\beta)\,(\mathbf{E}-\mathbf{I})+(\mu-\beta)\left(\mathbf{E}^{\mathrm{T}}-\mathbf{I}\right),\\ \mathbf{K} &= \delta\mathbf{I}\mathrm{tr}\mathbf{L}+(\gamma+\eta)\,\mathbf{L}+(\gamma-\eta)\,\mathbf{L}^{\mathrm{T}}.\end{aligned} \tag{5}$$

Let us consider a special case of deformation of the micropolar medium such that $\mathbf{H}=\mathbf{A}$, where $\mathbf{A}$ a proper orthogonal macrorotation tensor. I.e. it is the orthogonal multiplier in the polar expansion of the strain gradient [7]

$$\mathbf{F}=\mathbf{U}\cdot\mathbf{A}. \tag{6}$$

Here $\mathbf{U}$ is a symmetric positive definite stretch tensor [7]. In this case, according to (3) and (6), we have

$$\mathbf{E}=\mathbf{E}^{\mathrm{T}}=\mathbf{U}.$$

Let us suppose that material constants δ, γ and η are zero. Then it follows from (5) that the couple stresses are absence: $\mathbf{K}=\mathbf{0}$, and the stress tensor $\mathbf{P}$ is symmetric and is expressed by the formula

$$\mathbf{P}=\lambda\mathbf{I}\mathrm{tr}(\mathbf{U}-\mathbf{I})+2\mu\,(\mathbf{U}-\mathbf{I}), \tag{7}$$

and the strain energy density has the form

$$W=\frac{1}{2}\lambda\mathrm{tr}^2(\mathbf{U}-\mathbf{E})+\mu\mathrm{tr}\mathbf{U}^2. \tag{8}$$

The relations (7), (8) correspond to the model of the harmonic or the semi-linear material which is well-known in the theory of elasticity of simple materials [7]. Thus the model of the physically linear micropolar body reduces to the model of the simple harmonic material when $\delta=\gamma=\eta=0$ and $\mathbf{H}=\mathbf{A}$. In other words, the physically linear micropolar material (4) can be considered as a generalization of the harmonic material model to the moment elastic medium.

In the nonlinear theory of elasticity of simple materials, a number of exact solutions are known for finite deformations [7]. These solutions belong to the class of isotropic incompressible bodies. The list of models of compressible nonlinear elastic bodies, that allow explicit exact solutions, is quite small. Most of these exact solutions was found for semi-linear material [7]. As it shows below, the model of the physically linear micropolar body also allows to obtain several exact solutions about inhomogeneous finite deformations.

When the equilibrium problems are solving by the semi-inverse method, we give the finite deformations of a medium by the mapping $Q^M=Q^M(q^s)$, where q^s $(s=1,2,3)$ are curvilinear coordinates in the reference configuration (the Lagrangian coordinates), and Q^M $(M=1,2,3)$ are curvilinear coordinates in the

current configuration (the Eulerian coordinates). Further, we use the following coordinate systems:

Cartesian:

$$q^1 = x_1, \quad q^2 = x_2, \quad q^3 = x_3,$$
$$Q^1 = X_1, \quad Q^2 = X_2, \quad Q^3 = X_3.$$

Cylindrical:

$$q^1 = r, \quad q^2 = \varphi, \quad q^3 = z,$$
$$Q^1 = R, \quad Q^2 = \Phi, \quad Q^3 = Z,$$
$$x_1 = r\cos\varphi, \quad x_2 = r\sin\varphi, \quad x_3 = z,$$
$$X_1 = R\cos\Phi, \quad X_2 = R\sin\Phi, \quad X_3 = Z.$$

Spherical:

$$q^1 = r, \quad q^2 = \varphi, \quad q^3 = \theta,$$
$$Q^1 = R, \quad Q^2 = \Phi, \quad Q^3 = \Theta,$$
$$x_1 = r\cos\varphi\cos\theta, \quad x_2 = r\sin\varphi\cos\theta, \quad x_3 = r\sin\theta,$$
$$X_1 = R\cos\Phi\cos\Theta, \quad X_2 = R\sin\Phi\cos\Theta, \quad X_3 = R\sin\Theta.$$

Note, $\theta = \pm\frac{\pi}{2}$ at the sphere poles.

For these orthogonal coordinates we use the orthonormalized base vectors tangent to curvilinear coordinate curves. As above, $\mathbf{i}_1, \mathbf{i}_2, \mathbf{i}_3$ are the unit vectors of the Cartesian coordinates. The basis vectors $\mathbf{e}_r$, $\mathbf{e}_\varphi$, $\mathbf{e}_z$ and $\mathbf{e}_R$, $\mathbf{e}_\Phi$, $\mathbf{e}_Z$ associated with cylindrical coordinates are expressed as

$$\mathbf{e}_r = \mathbf{i}_1\cos\phi + \mathbf{i}_2\sin\phi, \quad \mathbf{e}_\phi = -\mathbf{i}_1\sin\phi + \mathbf{i}_2\cos\phi, \quad \mathbf{e}_z = \mathbf{i}_3,$$
$$\mathbf{e}_R = \mathbf{i}_1\cos\Phi + \mathbf{i}_2\sin\Phi, \quad \mathbf{e}_\Phi = -\mathbf{i}_1\sin\Phi + \mathbf{i}_2\cos\Phi, \quad \mathbf{e}_Z = \mathbf{i}_3.$$

The basis vectors associated with the spherical coordinates are presented as

$$\mathbf{e}_r = (\mathbf{i}_1\cos\varphi + \mathbf{i}_2\sin\varphi)\cos\theta + \mathbf{i}_3\sin\theta,$$
$$\mathbf{e}_\varphi = -\mathbf{i}_1\sin\varphi + \mathbf{i}_2\cos\varphi,$$
$$\mathbf{e}_\theta = -(\mathbf{i}_1\cos\varphi + \mathbf{i}_2\sin\varphi)\sin\theta + \mathbf{i}_3\cos\theta,$$
$$\mathbf{e}_R = (\mathbf{i}_1\cos\Phi + \mathbf{i}_2\sin\Phi)\cos\Theta + \mathbf{i}_3\sin\Theta,$$
$$\mathbf{e}_\Phi = -\mathbf{i}_1\sin\Phi + \mathbf{i}_2\cos\Phi,$$
$$\mathbf{e}_\Theta = -(\mathbf{i}_1\cos\Phi + \mathbf{i}_2\sin\Phi)\sin\Theta + \mathbf{i}_3\cos\Theta.$$

In this paper we present the exact solution for six families of finite deformations of the micropolar theory of elasticity. Each family is characterized by a mapping $Q^M = Q^M(q^s)$. This mapping gives the field of displacement of the medium and contains

one unknown function of one variable. Microrotation in a micropolar medium is kinematically independent of displacements. Thus the mapping $Q^M(q^s)$ have to supplemented by a set of orthogonal tensor fields $\mathbf{H}(q^s)$ to complete the description of the deformation. Each of the six families of the inhomogeneous deformations contains several subfamilies that differ in microrotation fields. For each subfamily, the expressions for the tensors $\mathbf{E}$ and $\mathbf{L}$ are obtained using the formula (3). The expression for the deformation gradient $\mathbf{F}$ is identical for all solutions from one family.

3 Cylindrical Bending of Rectangular Plate

A mapping $Q^M = Q^M(q^s)$ has the form

$$R = R(x_1), \quad \Phi = kx_2, \quad Z = \alpha x_3. \tag{9}$$

where k, α are constants. Considering that $\mathbf{R} = R\mathbf{e}_R + Z\mathbf{e}_Z$, we obtain the deformation gradient

$$\mathbf{F} = R'\mathbf{i}_1 \otimes \mathbf{e}_R + kR\mathbf{i}_2 \otimes \mathbf{e}_\Phi + \alpha\mathbf{i}_3 \otimes \mathbf{e}_Z, \quad R' = \frac{dR}{dx_1}.$$

The mapping (9) is supplemented by four subfamilies of microrotation.

3.1 Subfamily 1A

$$\begin{aligned} \mathbf{H} &= \mathbf{i}_1 \otimes \mathbf{e}_R + \mathbf{i}_2 \otimes \mathbf{e}_\Phi + \mathbf{i}_3 \otimes \mathbf{e}_Z, \\ \mathbf{E} &= R'\mathbf{i}_1 \otimes \mathbf{i}_1 + kR\mathbf{i}_2 \otimes \mathbf{i}_2 + \alpha\mathbf{i}_3 \otimes \mathbf{i}_3, \\ \mathbf{L} &= k\mathbf{i}_2 \otimes \mathbf{i}_3. \end{aligned} \tag{10}$$

According to (2), (5), (10) the stress and couple stress Piola type tensors are defined as

$$\begin{aligned} \mathbf{D} &= D_{1R}\mathbf{i}_1 \otimes \mathbf{e}_R + D_{2\Phi}\mathbf{i}_2 \otimes \mathbf{e}_\Phi + D_{3Z}\mathbf{i}_3 \otimes \mathbf{e}_Z, \\ D_{1R} &= (\lambda + 2\mu)\, R' + \lambda k R + \lambda\alpha - (2\mu + 3\lambda)\,, \\ D_{2\Phi} &= \lambda R' + (\lambda + 2\mu)\, kR + \lambda\alpha - (2\mu + 3\lambda)\,, \\ D_{3Z} &= \lambda R' + \lambda k R + (\lambda + 2\mu)\, \alpha - (2\mu + 3\lambda)\,. \end{aligned} \tag{11}$$

$$\begin{aligned} \mathbf{G} &= G_{2Z}\mathbf{i}_2 \otimes \mathbf{e}_Z + G_{3\Phi}\mathbf{i}_3 \otimes \mathbf{e}_\Phi, \\ G_{2Z} &= k\,(\gamma + \eta)\,, \quad G_{3\Phi} = k\,(\gamma - \eta)\,. \end{aligned}$$

The equilibrium equation $(1)_2$ is satisfied identically for the considered deformation. The equilibrium equation $(1)_1$ is reduced to a scalar equation

$$\frac{\partial D_{1R}}{\partial x_1} - kD_{2\Phi} = 0. \tag{12}$$

From (11) the Eq. (12) is reduced to a ordinary differential equation in the unknown function $R(x_1)$:

$$R'' - k^2 R = -\frac{k\left(1-\nu\left(\alpha-1\right)\right)}{1-\nu}. \tag{13}$$

The solution of this differential equation is

$$R(x_1) = c_1 e^{-kx_1} + c_2 e^{kx_1} + \frac{\left(1-\nu\left(\alpha-1\right)\right)}{k\left(1-\nu\right)}. \tag{14}$$

In view of $0 \le x_1 \le h$, where h is a plate thickness, we can write the boundary conditions of the absence of external loads on the faces of the plate

$$D_{1R}\Big|_{x_1=0,h} = 0. \tag{15}$$

The constants of integration are determined from (11), (13), (14) and (15) as

$$c_1 = -\frac{\left(1-\nu\left(\alpha-1\right)\right)\mathrm{e}^{kh}}{k\left(1-\nu\right)\left(1+\mathrm{e}^{kh}\right)},$$
$$c_2 = \frac{\left(1-\nu\left(\alpha-1\right)\right)\left(1-2\nu\right)}{k\left(1-\nu\right)\left(1+\mathrm{e}^{kh}\right)}.$$

3.2 Subfamily 1B

$$\mathbf{H} = -\mathbf{i}_1 \otimes \mathbf{e}_R + \mathbf{i}_2 \otimes \mathbf{e}_\Phi - \mathbf{i}_3 \otimes \mathbf{e}_Z,$$
$$\mathbf{E} = -R'\mathbf{i}_1 \otimes \mathbf{i}_1 + kR\mathbf{i}_2 \otimes \mathbf{i}_2 - \alpha\mathbf{i}_3 \otimes \mathbf{i}_3,$$
$$\mathbf{L} = -k\mathbf{i}_2 \otimes \mathbf{i}_3.$$

So we have

$$D_{1R} = \left(\lambda+2\mu\right)R' - \lambda kR + \lambda\alpha + \left(2\mu+3\lambda\right),$$
$$D_{2\Phi} = -\lambda R' + \left(\lambda+2\mu\right)kR - \lambda\alpha - \left(2\mu+3\lambda\right),$$
$$D_{3Z} = \lambda R' - \lambda kR + \left(\lambda+2\mu\right)\alpha + \left(2\mu+3\lambda\right),$$
$$G_{2Z} = k\left(\gamma+\eta\right), \quad G_{3\Phi} = -k\left(\gamma-\eta\right).$$

The equation for the unknown function $R(x_1)$ differs from the case of 1A:

$$R'' - k^2 R = \frac{k\,(1+\nu\,(1+\alpha))}{1-\nu}.$$

The solution of this differential equation is

$$R(x_1) = c_1 e^{-kx_1} + c_2 e^{kx_1} + \frac{(1+\nu\,(\alpha+1))}{k\,(1-\nu)}.$$

The integrations constants are determined from (15) as

$$c_1 = \frac{(1-2\nu)\,(1+\nu\,(\alpha+1))\,\mathrm{e}^{kh}}{k\,(1-\nu)\left(1+\mathrm{e}^{kh}\right)},$$
$$c_2 = -\frac{1+\nu\,(\alpha+1)}{k\,(1-\nu)\left(1+\mathrm{e}^{kh}\right)}.$$

3.3 Subfamily 1C

$$\mathbf{H} = \mathbf{i}_1 \otimes \mathbf{e}_R - \mathbf{i}_2 \otimes \mathbf{e}_\Phi - \mathbf{i}_3 \otimes \mathbf{e}_Z,$$
$$\mathbf{E} = R'\mathbf{i}_1 \otimes \mathbf{i}_1 - kR\mathbf{i}_2 \otimes \mathbf{i}_2 - \alpha\mathbf{i}_3 \otimes \mathbf{i}_3,$$
$$\mathbf{L} = -k\mathbf{i}_2 \otimes \mathbf{i}_3.$$

The stress and couple stress tensors have components

$$D_{1R} = (\lambda+2\mu)\,R' - \lambda k R - \lambda\alpha - (2\mu+3\lambda)\,,$$
$$D_{2\Phi} = -\lambda R' + (\lambda+2\mu)\,kR + \lambda\alpha + (2\mu+3\lambda)\,,$$
$$D_{3Z} = -\lambda R' + \lambda k R + (\lambda+2\mu)\,\alpha + (2\mu+3\lambda)\,,$$
$$G_{2Z} = k\,(\gamma+\eta)\,, \quad G_{3\Phi} = k\,(\gamma-\eta)\,.$$

The equation for the unknown function $R(x_1)$ is written as

$$R'' - k^2 R = \frac{k\,(1+\nu\,(\alpha+1))}{1-\nu}.$$

The solution of this differential equation is

$$R(x_1) = c_1 e^{-kx_1} + c_2 e^{kx_1} - \frac{1+\nu\,(\alpha+1)}{k\,(1-\nu)}.$$

From (15) we obtain

$$c_1 = -\frac{(1-2\nu)\,(1+\nu\,(\alpha+1))\,\mathrm{e}^{kh}}{k\,(1-\nu)\left(1+\mathrm{e}^{kh}\right)},$$
$$c_2 = \frac{1+\nu\,(\alpha+1)}{k\,(1-\nu)\left(1+\mathrm{e}^{kh}\right)}.$$

3.4 Subfamily 1D

$$\mathbf{H} = -\mathbf{i}_1 \otimes \mathbf{e}_R - \mathbf{i}_2 \otimes \mathbf{e}_\Phi + \mathbf{i}_3 \otimes \mathbf{e}_Z,$$
$$\mathbf{E} = -R'\mathbf{i}_1 \otimes \mathbf{i}_1 - kR\mathbf{i}_2 \otimes \mathbf{i}_2 + \alpha\mathbf{i}_3 \otimes \mathbf{i}_3,$$
$$\mathbf{L} = k\mathbf{i}_2 \otimes \mathbf{i}_3.$$

We have

$$D_{1R} = (\lambda+2\mu)\,R' + \lambda kR - \lambda\alpha + (2\mu+3\lambda)\,,$$
$$D_{2\Phi} = \lambda R' + (\lambda+2\mu)\,kR - \lambda\alpha + (2\mu+3\lambda)\,,$$
$$D_{3Z} = -\lambda R' - \lambda kR + (\lambda+2\mu)\,\alpha - (2\mu+3\lambda)\,,$$
$$G_{2Z} = k\,(\gamma+\eta)\,, \quad G_{3\Phi} = -k\,(\gamma-\eta)\,.$$

The equation for the unknown function $R(x_1)$ has the form

$$R'' - k^2 R = \frac{k\,(1-\nu\,(\alpha-1))}{1-\nu}.$$

The solution of this differential equation is

$$R(x_1) = c_1 e^{-kx_1} + c_2 e^{kx_1} - \frac{(1-\nu\,(\alpha-1))}{1-\nu}.$$

Using (15) we have

$$c_1 = \frac{(1-\nu\,(\alpha-1))\,\mathrm{e}^{kh}}{k\,(1-\nu)\left(1+\mathrm{e}^{kh}\right)},$$
$$c_2 = -\frac{(1-2\nu)\,(1-\nu\,(\alpha-1))}{k\,(1-\nu)\left(1+\mathrm{e}^{kh}\right)}.$$

It can be shown that resultant force vector acting in sections of a deformable body $\Phi = \mathrm{const}$ is equal to zero for all subfamilies 3A – 3D. The resultant moment has direction of the vector $\mathbf{e}_Z$ and value

$$M = l \int_0^h \left(R D_{\phi\Phi} + G_{\phi Z} \right) dr,$$

where l is length of the sector of the cylinder along the coordinate z ($0 \le z \le l$).

The constant κ can be computed from given bending moment M. And constant α can be calculated from given longitudinal force acting in sections $Z = \text{const}$

$$F = \phi_1 \int_{r_0}^{r_1} D_{zZ} r dr.$$

Here ϕ_1 is a sector angle ($0 \le \phi \le \phi_1$).

4 Straightening of a Circular Hollow–Cylinder Sector

A mapping $Q^M = Q^M(q^s)$ is described by

$$X_1 = X_1(r), \quad X_2 = \xi\phi, \quad X_3 = \alpha z, \tag{16}$$

where ξ, α are constants. In view of

$$\mathbf{R} = X_1 \mathbf{i}_1 + X_2 \mathbf{i}_2 + X_3 \mathbf{i}_3,$$

we find the deformation gradient

$$\mathbf{F} = X_1' \mathbf{e}_r \otimes \mathbf{i}_1 + \frac{\xi}{r} \mathbf{e}_\phi \otimes \mathbf{i}_2 + \alpha \mathbf{e}_z \otimes \mathbf{i}_3, \quad X_1' = \frac{dX_1}{dr}.$$

The mapping (16) is supplemented by four subfamilies of microrotations.

4.1 Subfamily 2A

$$\begin{aligned} \mathbf{H} &= \mathbf{e}_r \otimes \mathbf{i}_1 + \mathbf{e}_\phi \otimes \mathbf{i}_2 + \mathbf{e}_z \otimes \mathbf{i}_3, \\ \mathbf{E} &= X_1' \mathbf{e}_r \otimes \mathbf{e}_r + \frac{\xi}{r} \mathbf{e}_\phi \otimes \mathbf{e}_\phi + \alpha \mathbf{e}_z \otimes \mathbf{e}_z, \\ \mathbf{L} &= -\frac{1}{r} \mathbf{e}_\phi \otimes \mathbf{e}_z. \end{aligned} \tag{17}$$

From (2), (5) and (17) the stress and couple stress tensors have the form

$$\begin{aligned}
\mathbf{D} &= D_{r1}\mathbf{e}_r \otimes \mathbf{i}_1 + D_{\phi 2}\mathbf{e}_\phi \otimes \mathbf{i}_2 + D_{z3}\mathbf{e}_z \otimes \mathbf{i}_3,\\
D_{r1} &= (\lambda + 2\mu)\, X_1' + \lambda\frac{\xi}{r} + \lambda\alpha - (2\mu + 3\lambda)\,,\\
D_{\phi 2} &= \lambda X_1' + (\lambda + 2\mu)\,\frac{\xi}{r} + \lambda\alpha - (2\mu + 3\lambda)\,,\\
D_{z3} &= \lambda X_1' + \lambda\frac{\xi}{r} + (\lambda + 2\mu)\,\alpha - (2\mu + 3\lambda)\,,\\
\mathbf{G} &= G_{\phi 3}\mathbf{e}_\phi \otimes \mathbf{i}_3 + G_{z2}\mathbf{e}_z \otimes \mathbf{i}_2,\\
G_{\phi 3} &= -(\gamma + \eta)\,\frac{1}{r}, \quad G_{z2} = -(\gamma - \eta)\,\frac{1}{r}.
\end{aligned} \tag{18}$$

The equilibrium equation $(1)_2$ is satisfied identically for the considered deformation. The equilibrium equation $(1)_1$ is reduced to a scalar ordinary differential equation

$$\frac{1}{r}\frac{\partial}{\partial r}\left(r D_{r1}\right) = 0. \tag{19}$$

In view of $r_0 \le r \le r_1$, where r_0, r_1 are inner and outer radii, respectively, the boundary conditions for the absence of external loads on the lateral surfaces of the cylinder sector are written as

$$D_{r1}\Big|_{r=r_0,r_1} = 0. \tag{20}$$

In view of (19), (20), we obtain

$$D_{r1} \equiv 0. \tag{21}$$

The identity (21) is reduced to an ordinary differential equation in the unknown function $X_1(r)$, namely

$$X_1' + \frac{\xi\nu}{(1-\nu)\,r} = \frac{1 + (1-\alpha)\,\nu}{1-\nu}.$$

The solution of this differential equation has the form

$$X_1(r) = \frac{1 + (1-\alpha)\,\nu}{1-\nu}\,r - \frac{\xi\nu}{1-\nu}\ln r + \text{const}.$$

The integration constant corresponds to a rigid displacement and could assume any value, including zero.

4.2 Subfamily 2B

$$\mathbf{H} = -\mathbf{e}_r \otimes \mathbf{i}_1 + \mathbf{e}_\phi \otimes \mathbf{i}_2 - \mathbf{e}_z \otimes \mathbf{i}_3,$$
$$\mathbf{E} = k_1 X_1' \mathbf{e}_r \otimes \mathbf{e}_r + k_2 \frac{\xi}{r} \mathbf{e}_\phi \otimes \mathbf{e}_\phi + k_3 \alpha \mathbf{e}_z \otimes \mathbf{e}_z,$$
$$\mathbf{L} = -\frac{1}{r} \mathbf{e}_\phi \otimes \mathbf{e}_z.$$

We have

$$D_{r1} = (\lambda + 2\mu) X_1' - \lambda \frac{\xi}{r} + \lambda\alpha + (2\mu + 3\lambda),$$
$$D_{\phi 2} = -\lambda X_1' + (\lambda + 2\mu) \frac{\xi}{r} - \lambda\alpha - (2\mu + 3\lambda),$$
$$D_{z3} = \lambda X_1' - \lambda \frac{\xi}{r} + (\lambda + 2\mu)\alpha + (2\mu + 3\lambda).$$
$$G_{\phi 3} = (\gamma + \eta) \frac{1}{r}, \quad G_{z2} = -(\gamma - \eta) \frac{1}{r}.$$

The equation for the unknown function $X_1(r)$ differs from the case 2A:

$$X_1' - \frac{\xi\nu}{(1-\nu) r} = -\frac{1 + (1+\alpha)\nu}{1-\nu}.$$

The solution of this differential equation is

$$X_1(r) = -\frac{1 + (1+\alpha)\nu}{1-\nu} r + \frac{\xi\nu}{1-\nu} \ln r + \text{const}.$$

4.3 Subfamily 2C

$$\mathbf{H} = \mathbf{e}_r \otimes \mathbf{i}_1 - \mathbf{e}_\phi \otimes \mathbf{i}_2 - \mathbf{e}_z \otimes \mathbf{i}_3,$$
$$\mathbf{E} = X_1' \mathbf{e}_r \otimes \mathbf{e}_r - \frac{\xi}{r} \mathbf{e}_\phi \otimes \mathbf{e}_\phi - \alpha \mathbf{e}_z \otimes \mathbf{e}_z,$$
$$\mathbf{L} = -\frac{1}{r} \mathbf{e}_\phi \otimes \mathbf{e}_z.$$

The components of the stress and couple stress tensors are expressed as

$$D_{r1} = (\lambda + 2\mu)\, X_1' - \lambda\frac{\xi}{r} - \lambda\alpha - (2\mu + 3\lambda)\,,$$
$$D_{\phi 2} = -\lambda X_1' + (\lambda + 2\mu)\,\frac{\xi}{r} + \lambda\alpha + (2\mu + 3\lambda)\,,$$
$$D_{z3} = -\lambda X_1' + \lambda\frac{\xi}{r} + (\lambda + 2\mu)\,\alpha + (2\mu + 3\lambda)\,,$$
$$G_{\phi 3} = (\gamma + \eta)\,\frac{1}{r}, \quad G_{z2} = (\gamma - \eta)\,\frac{1}{r}.$$

The equation in the unknown function $X_1(r)$ is

$$X_1' - \frac{\xi\nu}{(1-\nu)\,r} = \frac{1 + (1+\alpha)\,\nu}{1-\nu}.$$

The solution of this differential equation is given by

$$X_1(r) = \frac{1 + (1+\alpha)\,\nu}{1-\nu} r + \frac{\xi\nu}{1-\nu}\ln r + \text{const}.$$

4.4 Subfamily 2D

$$\mathbf{H} = -\mathbf{e}_r \otimes \mathbf{i}_1 - \mathbf{e}_\phi \otimes \mathbf{i}_2 + \mathbf{e}_z \otimes \mathbf{i}_3,$$
$$\mathbf{E} = -X_1'\mathbf{e}_r \otimes \mathbf{e}_r - \frac{\xi}{r}\mathbf{e}_\phi \otimes \mathbf{e}_\phi + \alpha\mathbf{e}_z \otimes \mathbf{e}_z,$$
$$\mathbf{L} = -\frac{1}{r}\mathbf{e}_\phi \otimes \mathbf{e}_z.$$

We have

$$D_{r1} = (\lambda + 2\mu)\, X_1' + \lambda\frac{\xi}{r} - \lambda\alpha + (2\mu + 3\lambda)\,,$$
$$D_{\phi 2} = \lambda X_1' + (\lambda + 2\mu)\,\frac{\xi}{r} - \lambda\alpha + (2\mu + 3\lambda)\,,$$
$$D_{z3} = -\lambda X_1' - \lambda\frac{\xi}{r} + (\lambda + 2\mu)\,\alpha - (2\mu + 3\lambda)\,,$$
$$G_{\phi 3} = -\,(\gamma + \eta)\,\frac{1}{r}, \quad G_{z2} = (\gamma - \eta)\,\frac{1}{r}.$$

The equation for the unknown function $X_1(r)$ has the form

$$X_1' + \frac{\xi\nu}{(1-\nu)\,r} = -\frac{1 + (1-\alpha)\,\nu}{1-\nu}.$$

The solution of this differential equation is

$$X_1(r) = -\frac{1+(1-\alpha)\,\nu}{1-\nu} r - \frac{\xi\nu}{1-\nu} \ln r + \text{const}.$$

It can be shown that resultant force vector acting in sections of a deformable body $X_2 = \text{const}$ has the direction of the vector $\mathbf{i}_2$ and value

$$F_2 = l \int_{r_0}^{r_1} D_{\phi 2} dr,$$

where l is a cylinder sector length ($0 \le z \le l$).

The resultant force vector acting in sections of a deformable body $X_3 = \text{const}$ has the direction of the vector $\mathbf{i}_3$ and value

$$F_3 = \phi_1 \int_{r_0}^{r_1} D_{z3} r dr,$$

where ϕ_1 is a cylinder sector angle ($0 \le \phi \le \phi_1$).

The constants ξ and α can be computed from given forces F_2 and F_3. And we can compute the bending moment which is required for straightening a circular hollow-cylinder sector. The resultant moment acts in sections of a deformable body $X_2 = \text{const}$, and has the direction of the vector $\mathbf{i}_3$ and value

$$M = l \int_{r_0}^{r_1} \left(X_1 D_{\phi 2} + G_{z3}\right) dr.$$

5 Pure Bending and Reversing of a Circular Hollow–Cylinder Sector

We set up a mapping $Q^M = Q^M(q^s)$ by defining

$$R = R(r), \quad \Phi = \kappa\phi, \quad Z = \alpha z. \tag{22}$$

where κ and α are constants. In view of

$$\mathbf{r} = r\mathbf{e}_r + z\mathbf{e}_z, \quad \mathbf{R} = R\mathbf{e}_R + Z\mathbf{e}_Z,$$

we find the deformation gradient

$$\mathbf{F} = R'\mathbf{e}_r \otimes \mathbf{e}_R + \frac{\kappa R}{r}\mathbf{e}_\phi \otimes \mathbf{e}_\Phi + \alpha \mathbf{e}_z \otimes \mathbf{e}_Z, \quad R' = \frac{dR}{dr}.$$

The mapping (22) is supplemented by four subfamilies of microrotations.

5.1 Subfamily 3A

$$\begin{aligned} \mathbf{H} &= \mathbf{e}_r \otimes \mathbf{e}_R + \mathbf{e}_\phi \otimes \mathbf{e}_\Phi + \mathbf{e}_z \otimes \mathbf{e}_Z, \\ \mathbf{E} &= R'\mathbf{e}_r \otimes \mathbf{e}_r + \frac{\kappa R}{r}\mathbf{e}_\phi \otimes \mathbf{e}_\phi + \alpha \mathbf{e}_z \otimes \mathbf{e}_z, \\ \mathbf{L} &= \frac{\kappa - 1}{r}\mathbf{e}_\phi \otimes \mathbf{e}_z. \end{aligned} \tag{23}$$

Using (2), (5), (23) stress and couple stress tensors are given by

$$\begin{aligned} \mathbf{D} &= D_{rR}\mathbf{e}_r \otimes \mathbf{e}_R + D_{\phi\Phi}\mathbf{e}_\phi \otimes \mathbf{e}_\Phi + D_{zZ}\mathbf{e}_z \otimes \mathbf{e}_Z, \\ D_{rR} &= (\lambda + 2\mu) R' + \lambda\frac{\kappa R}{r} + \lambda\alpha - (2\mu + 3\lambda), \\ D_{\phi\Phi} &= \lambda R' + (\lambda + 2\mu)\frac{\kappa R}{r} + \lambda\alpha - (2\mu + 3\lambda), \\ D_{zZ} &= \lambda R' + \lambda\frac{\kappa R}{r} + (\lambda + 2\mu)\alpha - (2\mu + 3\lambda), \\ \mathbf{G} &= G_{\phi Z}\mathbf{e}_\phi \otimes \mathbf{e}_Z + G_{z\Phi}\mathbf{e}_z \otimes \mathbf{e}_\Phi, \\ G_{\phi Z} &= (\gamma + \eta)\frac{\kappa - 1}{r}, \quad G_{z\Phi} = (\gamma - \eta)\frac{\kappa - 1}{r}. \end{aligned} \tag{24}$$

The equilibrium equation $(1)_2$ is satisfied identically for the considered deformation. The equilibrium equation $(1)_1$ is reduced to a scalar equation

$$\frac{\partial D_{rR}}{\partial r} + \frac{D_{rR} - \kappa D_{\phi\Phi}}{r} = 0. \tag{25}$$

Using (24), the Eq. (25) is reduced to an ordinary differential equation in the unknown function $R(r)$:

$$R'' + \frac{R'}{r} - \kappa^2\frac{R}{r^2} = \frac{(\kappa - 1)((\alpha - 1)\nu - 1)}{(1 - \nu)r}.$$

The solution for this differential equation is

$$R(r) = c_1 r^{\kappa} + c_2 r^{-\kappa} + \frac{(\kappa - 1)\left((\alpha - 1)\nu - 1\right)}{\left(1 - \kappa^2\right)(1 - \nu)} r.$$

In view of $r_0 \le r \le r_1$, where r_0, r_1 are inner and outer radii, respectively, the boundary conditions for the absence of external loads on the lateral surfaces of the cylinder sector are written in the form

$$D_{rR}\Big|_{r=r_0,r_1} = 0. \tag{26}$$

The constants of integration c_1 and c_2 can be obtained from the boundary conditions (26). Their expressions are cumbersome enough to write them explicit here.

5.2 Subfamily 3B

$$\mathbf{H} = -\mathbf{e}_r \otimes \mathbf{e}_R + \mathbf{e}_\phi \otimes \mathbf{e}_\Phi - \mathbf{e}_z \otimes \mathbf{e}_Z,$$
$$\mathbf{E} = k_1 R' \mathbf{e}_r \otimes \mathbf{e}_r + k_2 \frac{\kappa R}{r} \mathbf{e}_\phi \otimes \mathbf{e}_\phi + k_3 \alpha \mathbf{e}_z \otimes \mathbf{e}_z,$$
$$\mathbf{L} = -\frac{\kappa + 1}{r} \mathbf{e}_\phi \otimes \mathbf{e}_z.$$

Now we have

$$D_{rR} = (\lambda + 2\mu) R' - \lambda \frac{\kappa R}{r} + \lambda\alpha + (2\mu + 3\lambda),$$
$$D_{\phi\Phi} = -\lambda R' + (\lambda + 2\mu) \frac{\kappa R}{r} - \lambda\alpha - (2\mu + 3\lambda),$$
$$D_{zZ} = \lambda R' - \lambda \frac{\kappa R}{r} + (\lambda + 2\mu)\alpha + (2\mu + 3\lambda).$$
$$G_{\phi Z} = (\gamma + \eta) \frac{\kappa + 1}{r}, \quad G_{z\Phi} = -(\gamma - \eta) \frac{\kappa + 1}{r}.$$

The equation in the unknown $R(r)$ differs from the case 3 :

$$R'' + \frac{R'}{r} - \kappa^2 \frac{R}{r^2} = -\frac{(\kappa + 1)\left((\alpha + 1)\nu + 1\right)}{(1 - \nu) r}.$$

The solution of this differential equation is given by

$$R(r) = c_1 r^{\kappa} + c_2 r^{-\kappa} - \frac{(\kappa + 1)\left((\alpha + 1)\nu + 1\right)}{\left(1 - \kappa^2\right)(1 - \nu)} r.$$

5.3 Subfamily 3C

$$\mathbf{H} = \mathbf{e}_r \otimes \mathbf{e}_R - \mathbf{e}_\phi \otimes \mathbf{e}_\Phi - \mathbf{e}_z \otimes \mathbf{e}_Z,$$
$$\mathbf{E} = R'\mathbf{e}_r \otimes \mathbf{e}_r - \frac{\kappa R}{r}\mathbf{e}_\phi \otimes \mathbf{e}_\phi - \alpha \mathbf{e}_z \otimes \mathbf{e}_z,$$
$$\mathbf{L} = -\frac{\kappa + 1}{r}\mathbf{e}_\phi \otimes \mathbf{e}_z.$$

The components of the stress and couple stress tensors are expressed as

$$D_{rR} = (\lambda + 2\mu) R' - \lambda\frac{\kappa R}{r} - \lambda\alpha - (2\mu + 3\lambda),$$
$$D_{\phi\Phi} = -\lambda R' + (\lambda + 2\mu)\frac{\kappa R}{r} + \lambda\alpha + (2\mu + 3\lambda),$$
$$D_{zZ} = -\lambda R' + \lambda\frac{\kappa R}{r} + (\lambda + 2\mu)\alpha + (2\mu + 3\lambda),$$
$$G_{\phi Z} = (\gamma + \eta)\frac{\kappa + 1}{r}, \quad G_{z\Phi} = (\gamma - \eta)\frac{\kappa - 1}{r}.$$

The equation in the unknown $R(r)$ is written as

$$R'' + \frac{R'}{r} - \kappa^2\frac{R}{r^2} = \frac{(\kappa + 1)((\alpha + 1)\nu + 1)}{(1 - \nu) r}.$$

The solution of this differential equation is given by

$$R(r) = c_1 r^\kappa + c_2 r^{-\kappa} + \frac{(\kappa + 1)((\alpha + 1)\nu + 1)}{\left(1 - \kappa^2\right)(1 - \nu)} r.$$

5.4 Subfamily 3D

$$\mathbf{H} = -\mathbf{e}_r \otimes \mathbf{e}_R - \mathbf{e}_\phi \otimes \mathbf{e}_\Phi + \mathbf{e}_z \otimes \mathbf{e}_Z,$$
$$\mathbf{E} = -R'\mathbf{e}_r \otimes \mathbf{e}_r - \frac{\kappa R}{r}\mathbf{e}_\phi \otimes \mathbf{e}_\phi + \alpha \mathbf{e}_z \otimes \mathbf{e}_z,$$
$$\mathbf{L} = \frac{\kappa - 1}{r}\mathbf{e}_\phi \otimes \mathbf{e}_z.$$

Now we have

$$D_{rR} = (\lambda + 2\mu) R' + \lambda\frac{\kappa R}{r} - \lambda\alpha + (2\mu + 3\lambda),$$

$$D_{\phi\Phi} = \lambda R' + (\lambda + 2\mu)\frac{\kappa R}{r} - \lambda\alpha + (2\mu + 3\lambda),$$

$$D_{zZ} = -\lambda R' - \lambda\frac{\kappa R}{r} + (\lambda + 2\mu)\alpha - (2\mu + 3\lambda),$$

$$G_{\phi Z} = (\gamma + \eta)\frac{\kappa - 1}{r}, \quad G_{z\Phi} = -(\gamma - \eta)\frac{\kappa + 1}{r}.$$

The equation in the unknown $R(r)$ is written as

$$R'' + \frac{R'}{r} - \kappa^2\frac{R}{r^2} = -\frac{(\kappa - 1)((\alpha - 1)\nu - 1)}{(1 - \nu)r}.$$

The solution of this differential equation is

$$R(r) = c_1 r^{\kappa} + c_2 r^{-\kappa} - \frac{(\kappa - 1)((\alpha - 1)\nu - 1)}{\left(1 - \kappa^2\right)(1 - \nu)}r.$$

It can be shown that the resultant force vector acting in sections of a deformable body $\Phi = \text{const}$ equals zero for all subfamilies 3A – 3D. And the resultant moment has the direction of the vector $\mathbf{e}_Z$ and value

$$M = l\int_0^h \left(RD_{\phi\Phi} + G_{\phi Z}\right)dr,$$

where l is a length of cylinder sector along the coordinate z ($0 \le z \le l$).

The constant κ can be computed from given bending moment M. The constant α can be calculated from given longitudinal force acting in sections $Z = \text{const}$,

$$F = \phi_1\int_{r_0}^{r_1} D_{zZ}rdr.$$

Here ϕ_1 is sector angle ($0 \le \phi \le \phi_1$).

6 Double Cylindrical Bending of a Circular Hollow–Cylinder Sector

A mapping $Q^M = Q^M(q^s)$ is described by

$$R = R(r), \quad \Phi = sz, \quad Z = t\phi, \tag{27}$$

where s, t are constants. Since

$$\mathbf{r} = R\mathbf{e}_r + z\mathbf{e}_z, \quad \mathbf{R} = R\mathbf{e}_R + Z\mathbf{e}_Z,$$

the deformation gradient is found

$$\mathbf{F} = R'\mathbf{e}_r \otimes \mathbf{e}_R + \frac{t}{r}\mathbf{e}_\phi \otimes \mathbf{e}_Z + sR\mathbf{e}_z \otimes \mathbf{e}_\Phi, \quad R' = \frac{dR}{dr}.$$

The mapping (27) is supplemented by four subfamilies of microrotations.

6.1 Subfamily 4A

$$\begin{aligned} \mathbf{H} &= \mathbf{e}_r \otimes \mathbf{e}_R + \mathbf{e}_\phi \otimes \mathbf{e}_Z - \mathbf{e}_z \otimes \mathbf{e}_\Phi, \\ \mathbf{E} &= R'\mathbf{e}_r \otimes \mathbf{e}_r + \frac{t}{r}\mathbf{e}_\phi \otimes \mathbf{e}_\phi + sR\mathbf{e}_z \otimes \mathbf{e}_z, \\ \mathbf{L} &= -\frac{1}{r}\mathbf{e}_\phi \otimes \mathbf{e}_z + s\mathbf{e}_z\mathbf{e}_\phi. \end{aligned} \tag{28}$$

Using (2), (5), (28) the stress and couple stress tensors are determined as

$$\begin{aligned} \mathbf{D} &= D_{rR}\mathbf{e}_r \otimes \mathbf{e}_R + D_{\phi Z}\mathbf{e}_\phi \otimes \mathbf{e}_Z + D_{z\Phi}\mathbf{e}_z \otimes \mathbf{e}_\Phi, \\ D_{rR} &= (\lambda + 2\mu)\, R' + \lambda\frac{t}{r} - \lambda sR - (2\mu + 3\lambda), \\ D_{\phi Z} &= \lambda R' + (\lambda + 2\mu)\,\frac{t}{r} - \lambda sR - (2\mu + 3\lambda), \\ D_{z\Phi} &= -\lambda R' - \lambda\frac{t}{r} + (\lambda + 2\mu)\, sR + (2\mu + 3\lambda), \\ \mathbf{G} &= G_{\phi\Phi}\mathbf{e}_\phi \otimes \mathbf{e}_\Phi + G_{zZ}\mathbf{e}_z \otimes \mathbf{e}_Z, \\ G_{\phi\Phi} &= -s\,(\gamma - \eta) + \frac{1}{r}\,(\gamma + \eta), \\ G_{zZ} &= s\,(\gamma + \eta) - \frac{1}{r}\,(\gamma - \eta). \end{aligned} \tag{29}$$

The equilibrium equation $(1)_2$ is satisfied identically for the considered deformation. The equilibrium equation $(1)_1$ is reduced to a scalar equation

$$\frac{\partial D_{rR}}{\partial r} + \frac{D_{rR}}{r} - sD_{z\Phi} = 0. \tag{30}$$

From (29), the Eq. (30) is reduced to an ordinary differential equations in the unknown $R(r)$:

$$R'' + \frac{1}{r}R' + \left(a_1 + \frac{a_2}{r}\right)R = a_3 + \frac{a_4}{r}, \tag{31}$$

$$a_1 = -s^2, \quad a_2 = -\frac{s\nu}{1-\nu},$$
$$a_3 = \frac{s\,(1+\nu)}{1-\nu}, \quad a_4 = \frac{1+(1-st)\,\nu}{1-\nu}.$$

The Eq. (31) is a particular case of the extended confluent hypergeometric equation [2]. Its solution can be represented by Kummer's functions.

We suppose $r_0 \le r \le r_1$, where r_0, r_1 are inner and outer radii, respectively. The boundary conditions for the absence of external loads on the lateral surfaces of the cylinder sector are written as

$$D_{rR}\Big|_{r=r_0,r_1} = 0. \tag{32}$$

6.2 Subfamily 4B

$$\mathbf{H} = \mathbf{e}_r \otimes \mathbf{e}_R - \mathbf{e}_\phi \otimes \mathbf{e}_Z + \mathbf{e}_z \otimes \mathbf{e}_\Phi,$$
$$\mathbf{E} = R'\mathbf{e}_r \otimes \mathbf{e}_r - \frac{t}{r}\mathbf{e}_\phi \otimes \mathbf{e}_\phi + sR\mathbf{e}_z \otimes \mathbf{e}_z,$$
$$\mathbf{L} = -\frac{1}{r}\mathbf{e}_\phi \otimes \mathbf{e}_z - s\mathbf{e}_z\mathbf{e}_\phi.$$

Now we have

$$D_{rR} = (\lambda+2\mu)\,R' - \lambda\frac{t}{r} + \lambda sR - (2\mu+3\lambda)\,,$$
$$D_{\phi Z} = -\lambda R' + (\lambda+2\mu)\,\frac{t}{r} - \lambda sR + (2\mu+3\lambda)\,,$$
$$D_{z\Phi} = \lambda R' - \lambda\frac{t}{r} + (\lambda+2\mu)\,sR - (2\mu+3\lambda)\,,$$
$$G_{\phi\Phi} = -s\,(\gamma-\eta) - \frac{1}{r}\,(\gamma+\eta)\,,$$
$$G_{zZ} = s\,(\gamma+\eta) + \frac{1}{r}\,(\gamma-\eta)\,.$$

The equation in the unknown $R(r)$ differs from the case 4:

$$R'' + \frac{1}{r}R' + \left(a_1 + \frac{a_2}{r}\right)R = a_3 + \frac{a_4}{r},$$
$$a_1 = -s^2, \quad a_2 = \frac{s\nu}{1-\nu},$$
$$a_3 = -\frac{s\,(1+\nu)}{1-\nu}, \quad a_4 = \frac{k_1\,(1+(1+st)\,\nu)}{1-\nu}.$$

6.3 Subfamily 4C

$$\mathbf{H} = -\mathbf{e}_r \otimes \mathbf{e}_R - \mathbf{e}_\phi \otimes \mathbf{e}_Z - \mathbf{e}_z \otimes \mathbf{e}_\Phi,$$
$$\mathbf{E} = -R'\mathbf{e}_r \otimes \mathbf{e}_r - \frac{t}{r}\mathbf{e}_\phi \otimes \mathbf{e}_\phi - sR\mathbf{e}_z \otimes \mathbf{e}_z,$$
$$\mathbf{L} = -\frac{1}{r}\mathbf{e}_\phi \otimes \mathbf{e}_z - s\mathbf{e}_z\mathbf{e}_\phi.$$

The components of the stress and couple stress tensors are expressed as

$$D_{rR} = (\lambda + 2\mu)\, R' + \lambda\frac{t}{r} + \lambda s R + (2\mu + 3\lambda)\,,$$
$$D_{\phi Z} = \lambda R' + (\lambda + 2\mu)\,\frac{t}{r} + \lambda s R + (2\mu + 3\lambda)\,,$$
$$D_{z\Phi} = \lambda R' + \lambda\frac{t}{r} + (\lambda + 2\mu)\, s R + (2\mu + 3\lambda)\,,$$
$$G_{\phi\Phi} = s\,(\gamma - \eta) + \frac{1}{r}\,(\gamma + \eta)\,,$$
$$G_{zZ} = s\,(\gamma + \eta) + \frac{1}{r}\,(\gamma - \eta)\,.$$

The equation in the unknown $R(r)$ has the form

$$R'' + \frac{1}{r}R' + \left(a_1 + \frac{a_2}{r}\right) R = a_3 + \frac{a_4}{r},$$
$$a_1 = -s^2, \quad a_2 = \frac{s\nu}{1-\nu},$$
$$a_3 = \frac{s\,(1+\nu)}{1-\nu}, \quad a_4 = -\frac{(1 + (1 - st)\,\nu)}{1-\nu}.$$

6.4 Subfamily 4D

$$\mathbf{H} = -\mathbf{e}_r \otimes \mathbf{e}_R + \mathbf{e}_\phi \otimes \mathbf{e}_Z + \mathbf{e}_z \otimes \mathbf{e}_\Phi,$$
$$\mathbf{E} = -R'\mathbf{e}_r \otimes \mathbf{e}_r + \frac{t}{r}\mathbf{e}_\phi \otimes \mathbf{e}_\phi + sR\mathbf{e}_z \otimes \mathbf{e}_z,$$
$$\mathbf{L} = -\frac{1}{r}\mathbf{e}_\phi \otimes \mathbf{e}_z + s\mathbf{e}_z\mathbf{e}_\phi.$$

Now we obtain

$$D_{rR} = (\lambda + 2\mu)\, R' - \lambda \frac{t}{r} - \lambda s R + (2\mu + 3\lambda)\,,$$
$$D_{\phi Z} = -\lambda R' + (\lambda + 2\mu)\, \frac{t}{r} + \lambda s R - (2\mu + 3\lambda)\,,$$
$$D_{z\Phi} = -\lambda R' + \lambda \frac{t}{r} + (\lambda + 2\mu)\, s R - (2\mu + 3\lambda)\,,$$
$$G_{\phi\Phi} = s\,(\gamma - \eta) - \frac{1}{r}\,(\gamma + \eta)\,,$$
$$G_{zZ} = s\,(\gamma + \eta) - \frac{1}{r}\,(\gamma - \eta)\,.$$

The equation in the unknown $R(r)$ is written as

$$R'' + \frac{1}{r} R' + \left(a_1 + \frac{a_2}{r}\right) R = a_3 + \frac{a_4}{r}, \tag{33}$$

$$a_1 = -s^2, \quad a_2 = -\frac{s\nu}{1-\nu},$$
$$a_3 = -\frac{s\,(1+\nu)}{1-\nu}, \quad a_4 = -\frac{(1+(1-st)\,\nu)}{1-\nu}.$$

Let us consider the deformation (27) of the cylinder sector such that the ends $z = 0$ and $z = l$ are joined. Here l is a length of the cylinder sector. In this case the deformed body is a circular hollow cylinder in the current configuration. Then we have the conditions

$$\Phi\Big|_{z=0} = 0, \quad \Phi\Big|_{z=l} = 2\pi.$$

And we find that $s = \frac{2\pi}{l}$.

It can be shown that the resultant moment acting in sections of a deformable body $Z = \text{const}$ equal zero for all subfamilies 4A – 4D. And the resultant force vector has the direction of the vector $\mathbf{e}_Z$ and its value is

$$F = l \int_{r_0}^{r_1} D_{\phi Z} dr.$$

The deformation parameter t can be computed from given force F.

7 Radially Symmetric Deformation of a Hollow Sphere

We give a mapping $Q^M = Q^M(q^s)$ in the form

$$R = R(r), \quad \Phi = \phi, \quad \Theta = \theta. \tag{34}$$

In view of

$$\mathbf{r} = R\mathbf{e}_r, \quad \mathbf{R} = R\mathbf{e}_R, \tag{35}$$

the deformation gradient has the form

$$\mathbf{F} = R'\mathbf{e}_r \otimes \mathbf{e}_R + \frac{R}{r}\mathbf{e}_\phi \otimes \mathbf{e}_\Phi + \frac{R}{r}\mathbf{e}_\theta \otimes \mathbf{e}_\Theta, \quad R' = \frac{dR}{dr}.$$

The mapping (34) is supplemented by four subfamilies of microrotation.

7.1 Subfamily 5A

$$\begin{aligned} \mathbf{H} &= \mathbf{e}_r \otimes \mathbf{e}_R + \mathbf{e}_\phi \otimes \mathbf{e}_\Phi + \mathbf{e}_\theta \otimes \mathbf{e}_\Theta, \\ \mathbf{E} &= R'\mathbf{e}_r \otimes \mathbf{e}_r + \frac{R}{r}\mathbf{e}_\phi \otimes \mathbf{e}_\phi + \frac{R}{r}\mathbf{e}_\theta \otimes \mathbf{e}_\theta. \end{aligned} \tag{36}$$

From (2), (5) and (36), the stress and couple stress tensors have the form

$$\begin{aligned} \mathbf{D} &= D_{rR}\mathbf{e}_r \otimes \mathbf{e}_R + D_{\phi\Phi}\mathbf{e}_\phi \otimes \mathbf{e}_\Phi + D_{\theta\Theta}\mathbf{e}_\theta \otimes \mathbf{e}_\Theta, \\ D_{rR} &= (\lambda + 2\mu)\, R' + 2\lambda\frac{\kappa R}{r} - (3\lambda + 2\mu)\,, \\ D_{\phi\Phi} &= D_{\theta\Theta} = \lambda R' + 2\,(\lambda + \mu)\,\frac{R}{r} - (3\lambda + 2\mu)\,. \end{aligned} \tag{37}$$

The wryness tensor $\mathbf{L}$ and couple stress tensor $\mathbf{G}$ are zero tensors.

The equilibrium equation $(1)_2$ is satisfied identically for the considered deformation. The equilibrium equation $(1)_1$ is reduced to a scalar equation

$$\frac{\partial D_{rR}}{\partial r} + 2\frac{D_{rR} - D_{\phi\Phi}}{r} = 0. \tag{38}$$

In consequence of (37), the Eq. (38) is reduced to an ordinary differential equation in the unknown function $R(r)$, namely

$$R'' + 2\frac{R'}{r} - 2\frac{R}{r^2} = 0. \tag{39}$$

The solution for this differential equation is

$$R(r) = c_1 r + \frac{c_2}{r}. \tag{40}$$

We give the boundary conditions in the form

$$D_{rR}\Big|_{r=r_0} = -p_0, \quad D_{rR}\Big|_{r=r_1} = -p_1. \tag{41}$$

Here r_0 and r_1 are inner and outer radii, respectively, p_0 and p_1 are pressures per unit area in the reference configuration in the inner and outer surfaces, respectively.

Using (37), (40) and (41) the integration constants are presented as

$$c_1 = 1 - \frac{(1-2\nu)\left(r_1^3 p_1 - r_0^3 p_0\right)}{2\mu(1+\nu)\left(r_1^3 - r_0^3\right)}, \quad c_2 = -\frac{(p_1 - p_0)\, r_1^3 r_0^3}{4\mu\left(r_1^3 - r_0^3\right)}.$$

7.2 Subfamily 5B

$$\mathbf{H} = \mathbf{e}_r \otimes \mathbf{e}_R - \mathbf{e}_\phi \otimes \mathbf{e}_\Phi - \mathbf{e}_\theta \otimes \mathbf{e}_\Theta,$$
$$\mathbf{E} = R'\mathbf{e}_r \otimes \mathbf{e}_r - \frac{R}{r}\mathbf{e}_\phi \otimes \mathbf{e}_\phi - \frac{R}{r}\mathbf{e}_\theta \otimes \mathbf{e}_\theta,$$
$$\mathbf{L} = -\frac{2}{r}\mathbf{e}_\phi \otimes \mathbf{e}_\theta + \frac{2}{r}\mathbf{e}_\theta \otimes \mathbf{e}_\phi.$$

Now we obtain

$$D_{rR} = (\lambda + 2\mu)\, R' - 2\lambda\frac{R}{r} - (3\lambda + 2\mu),$$
$$D_{\phi\Phi} = D_{\theta\Theta} = -\lambda R' + 2(\lambda + \mu)\frac{R}{r} + (3\lambda + 2\mu),$$

$$\mathbf{G} = \frac{4\eta}{r}\mathbf{e}_\phi \otimes \mathbf{e}_\Theta - \frac{4\eta}{r}\mathbf{e}_\theta \otimes \mathbf{e}_\Phi.$$

The equation in the unknown function $R(r)$ differs from the case 5A:

$$R'' + \frac{2R'}{r} - \frac{2aR}{r^2} = \frac{4a}{r}, \quad a = \frac{1+\nu}{1-\nu}.$$

The solution of this equation is given by

$$R(r) = c_1 r^{-\frac{1-b}{2}} + c_2 r^{-\frac{1+b}{2}} - \frac{1+\nu}{\nu}r, \quad b = \sqrt{\frac{9+7\nu}{1-\nu}}.$$

The integration constants c_1 and c_2 are determined by the boundary conditions (41). Their expressions are cumbersome enough to write them explicit here.

8 Reversing of a Hollow Sphere

A mapping $Q^M = Q^M(q^s)$ has the form

$$R = R(r), \quad \Phi = \phi, \quad \Theta = -\theta. \tag{42}$$

In view of (35), the deformation gradient is defined by

$$\mathbf{F} = R'\mathbf{e}_r \otimes \mathbf{e}_R + \frac{R}{r}\mathbf{e}_\phi \otimes \mathbf{e}_\Phi - \frac{R}{r}\mathbf{e}_\theta \otimes \mathbf{e}_\Theta, \quad R' = \frac{dR}{dr}.$$

The mapping (42) is supplemented by four subfamilies of microrotations.

8.1 Subfamily 6A

$$\mathbf{H} = -\mathbf{e}_r \otimes \mathbf{e}_R + \mathbf{e}_\phi \otimes \mathbf{e}_\Phi - \mathbf{e}_\theta \otimes \mathbf{e}_\Theta, \tag{43}$$

$$\mathbf{E} = -R'\mathbf{e}_r \otimes \mathbf{e}_r + \frac{R}{r}\mathbf{e}_\phi \otimes \mathbf{e}_\phi - \frac{R}{r}\mathbf{e}_\theta \otimes \mathbf{e}_\theta, \tag{44}$$

$$\mathbf{L} = -\frac{2}{r}\mathbf{e}_\phi \otimes \mathbf{e}_\theta + \frac{2}{r}\mathbf{e}_\theta \otimes \mathbf{e}_\phi. \tag{45}$$

In view of (2), (5) and (43), the stress and couple stress tensors are defined as

$$\begin{aligned} \mathbf{D} &= D_{rR}\mathbf{e}_r \otimes \mathbf{e}_R + D_{\phi\Phi}\mathbf{e}_\phi \otimes \mathbf{e}_\Phi + D_{\theta\Theta}\mathbf{e}_\theta \otimes \mathbf{e}_\Theta, \\ D_{rR} &= (\lambda + 2\mu)\, R' - 2\lambda\frac{R}{r} + (2\mu + 3\lambda), \\ D_{\phi\Phi} &= -\lambda R' + 2(\lambda + \mu)\frac{R}{r} - (2\mu + 3\lambda), \\ D_{\theta\Theta} &= \lambda R' - 2(\lambda + \mu)\frac{R}{r} + (2\mu + 3\lambda), \end{aligned} \tag{46}$$

$$\begin{aligned} \mathbf{G} &= G_{\phi\Theta}\mathbf{e}_\phi \otimes \mathbf{e}_\Theta + G_{\theta\Phi}\mathbf{e}_\theta \otimes \mathbf{e}_\Phi, \\ G_{\phi\Theta} &= \frac{4\eta}{r}, \quad G_{\theta\Phi} = \frac{4\eta}{r}. \end{aligned} \tag{47}$$

The equilibrium equation $(1)_2$ is satisfied identically for the considered deformation. The equilibrium equation $(1)_1$ is written in the form . Using (46) the equilibrium equation is reduced to an ordinary differential equation in the unknown function $R(r)$:

$$R'' + \frac{2R'}{r} - \frac{2aR}{r^2} = -\frac{4a}{r}, \quad a = \frac{1+\nu}{1-\nu}.$$

The solution of this differential equation has the form

$$R(r) = c_1 r^{-\frac{1+b}{2}} + c_2 r^{-\frac{1-b}{2}} + \frac{1+\nu}{\nu} r, \quad b = \sqrt{\frac{9+7\nu}{1-\nu}}.$$

The integration constants c_1 and c_2 are determined by the boundary conditions (41). Their expressions are cumbersome enough to write them explicit here.

8.2 *Subfamily 6B*

$$\mathbf{H} = -\mathbf{e}_r \otimes \mathbf{e}_R - \mathbf{e}_\phi \otimes \mathbf{e}_\Phi + \mathbf{e}_\theta \otimes \mathbf{e}_\Theta,$$
$$\mathbf{E} = -R'\mathbf{e}_r \otimes \mathbf{e}_r - \frac{R}{r}\mathbf{e}_\phi \otimes \mathbf{e}_\phi - \frac{R}{r}\mathbf{e}_\theta \otimes \mathbf{e}_\theta.$$

Now we have

$$D_{rR} = (\lambda + 2\mu) R' - (2\mu + 3\lambda),$$
$$D_{\phi\Phi} = -\lambda R' + 2\mu \frac{R}{r} + (2\mu + 3\lambda),$$
$$D_{\theta\Theta} = -\lambda R' - 2\mu \frac{R}{r} + (2\mu + 3\lambda).$$

The wryness tensor $\mathbf{L}$ and the couple stress tensor $\mathbf{G}$ are zero tensors.

The equation in the unknown function $R(r)$ is same as Eq. (39). Its solution has the form (40). From the boundary conditions (41) we determine the constants c_1 and c_2 as

$$c_1 = -1 - \frac{(1-2\nu)\left(r_1^3 p_1 - r_0^3 p_0\right)}{\mu(1+\nu)\left(r_1^3 - r_0^3\right)}, \quad c_2 = -\frac{(p_1 - p_0) r_1^3 r_0^3}{4\mu\left(r_1^3 - r_0^3\right)}.$$

9 Conclusion

In this paper, several families of finite deformations of a micropolar body had been considered. Following the semi-inverse method, we reduced the original system of differential equilibrium equations with three independent variables to a system of ordinary differential equations. In the present paper we used the model of the physically linear isotropic compressible micropolar body with six material parameters. Its strain energy density is quadratic form of stretch and wryness tensors.

We consider arbitrary large strains and rotations in spite of this, the ordinary differential equations obtained in solving problems are linear. This allowed us to construct the exact solutions for the problems of strong cylindrical bending of a rectangular plate, straightening of a cylindrical layer, inflation and reversing of a cylindrical tube, pure bending of a circular cylinder sector, double cylindrical bending, inflation and reversing of a hollow sphere.

The solutions obtained in this paper within the three-dimensional non-linear micropolar elasticity theory can be used to verify the two-dimensional theory of micropolar shells. Also these solutions can be used for establishing the connection of material constants in the constitutive relations of the two-dimensional shell model with the material constants of the three-dimensional micropolar medium. To do this we can use the formulae obtained in the paper [15]. These formulae express the resultant stresses and the resultant couple stresses in a shell by the stresses and the couple stresses of a three-dimensional medium averaging through a thickness.

Acknowledgements The research was supported by Russian Foundation for Basic Research (grant 16-08-00802 A).

References

1. Altenbach, J., Altenbach, H., Eremeyev, V.A.: On generalized cosserat-type theories of plates and shells: a short review and bibliography. Arch. Appl. Mech. **80**(1), 73–92 (2010)
2. Campos, L.M.B.C.: On some solutions of the extended confluent hypergeometric differential equation. J. Comput. Appl. Math. **137**(1), 177–200 (2001)
3. Chróścielewski, J., Makowski, J., Pietraszkiewicz, W.: Statyka i dynamika powłok wielopłatowych. Nieliniowa teoria i metoda elementów skończonych (In Polish). Wydawnictwo IPPT PAN, Warszawa (2004)
4. Eremeyev, V.A., Zubov, L.M.: Mechanics of elastic shells, Nauka, Moscow (2008). (In Russian)
5. Eringen, A.C.: Theory of micropolar elasticity. In: Microcontinuum Field Theories, pp. 101–248. Springer (1999)
6. Libai, A., Simmonds, J.G.: The Nonlinear Theory of Elastic Shells, 2 edn. Cambridge University Press (1998)
7. Lurie, A.I.: Non-linear theory of elasticity, North-Holland (1990)
8. Nikitin, E., Zubov, L.M.: Conservation laws and conjugate solutions in the elasticity of simple materials and materials with couple stress. J. Elast. **51**(1), 1–22 (1998)
9. Pietraszkiewicz, W., Eremeyev, V.A.: On natural strain measures of the non-linear micropolar continuum. Int. J. Solids Struct. **46**(3–4), 774–787 (2009)
10. Shkutin, L.I.: Mechanics of deformations of flexible bodies (In Russian). Nauka, Novosibirsk (1988)
11. Toupin, R.A.: Theories of elasticity with couple-stress. Arch. Rational Mech. Anal. **17**(2), 85–112 (1964)
12. Zelenina, A.A., Zubov, L.M.: One-dimensional deformations of nonlinearly elastic micropolar bodies. Mech. Solids **45**(4), 575–582 (2010)
13. Zhilin, P.A.: Mechanics of deformable directed surfaces. Int. J. Solids Struct. **12**(9–10), 635–648 (1976)
14. Zubov, L.M.: Nonlinear Theory of Dislocations and Disclinations in Elastic Bodies, vol. 47. Springer Science & Business Media (1997)
15. Zubov, L.M.: Micropolar-shell equilibrium equations. Dokl. Phys. **54**(6), 290–293 (2009)

16. Zubov, L.M.: Continuum theory of dislocations and disclinations in nonlinearly elastic micropolar media. Mech. Solids **46**(3), 348 (2011)
17. Zubov, L.M.: On universal deformations of nonlinear isotropic elastic shells. In: Shell-Like Structures, pp. 279–294. Springer (2011)
18. Zubov, L.M.: Universal deformations of micropolar isotropic elastic solids. Math. Mech. Solids **21**(2), 152–167 (2016)